VETERINARY PHARMACOLOGY, ION-CHANNELS AND ANTHELMINTICS

RICHARD JOHN MARTIN

Department of Preclinical Veterinary Sciences, R.(D.) S.V.S., University of Edinburgh

Thesis submitted for the degree of Doctor of Science, The University of Edinburgh

1997

EX BIBL UNIV. EDINBURGH

THE UNIVERSITY OF EDINBURGH

ABSTRACT OF SUBMISSION FOR HIGHER DEGREE

(Postgraduate Regulation 1.1.3)

Richard J. Martin

Name of Candidate .....

Department of Preclinical Veterinary Sciences, R.(D.)S.V.S., Summerhall, University of Edinburgh

Address .....

D.Sc. March 1997

Degree in view ..... *Date* .....

Veterinary Pharmacology, Ion-channels and Anthelmintics.

Title of Submission .....

.....

In this collection of papers modes of action of anthelmintic and anaesthetic drugs used in Veterinary Practice are investigated using electrophysiological techniques. New preparations and analytical techniques for investigation are described along with properties of ion-channel target sites. The pharmacology of piperazine, levamisole, pyrantel, morantel, oxantel, avermectins, cyclic depsipeptides, ketamine, metomidate, alphaxalone and xylazine are studied. This information is reviewed in formats suitable for graduate and undergraduate study.

Two-micropipette current-clamp and voltage-clamp techniques for recording effects of GABA agonists and antagonists on nematode muscle are developed using *Ascaris suum*. Piperazine, an anthelmintic, is shown to act as a GABA agonist of low potency and, like GABA, to mediate an increase in Cl conductance by an action on extrasynaptic receptors. Diethylcarbamazine, a piperazine derivative, did not to act as a GABA agonist but blocked a voltage-activated K current. The agonist profile of the *Ascaris* GABA receptor was similar to vertebrate $GABA_A$ receptors but the antagonist profile was very different, indicating the presence of a distinctive type of receptor ($GABA_N$). Novel arylaminopyridazine derivatives were synthesised and tested as competitive antagonists on the $GABA_N$ receptor. The K_B for NCS 281-93, was 4.7 μM. A preparation suitable for patch-clamp studies was developed and GABA receptors activated by GABA and piperazine. Both agonists activated channels with a mean single-channel conductance of 22 pS but GABA mean open-times were longer (32 ms) than those of piperazine (14 ms).

The effects of ivermectin on muscle GABA receptors in *Ascaris* and on 19 pS Cl channels were observed using cell-attached and isolated inside-out patches. Ivermectin locked open the small Cl channels when applied to the outside membrane. A novel fluorescent and active bodipy ivermectin analogue was synthesised and the movement of the probe followed in vesicle membranes using the FRAP (fluorescence recovery after photobleaching) technique. Quenching experiments showed that the ivermectin probe did not move through the cell membrane in the time scale of the experiment (30 min). A novel two-microelectrode current-clamp preparation of the *Ascaris* pharynx was used to show that an ivermectin analogue potentiated a glutamate gated Cl channel at low concentrations and produced and increase in the Cl conductance at a higher concentration. The actions of potent and novel potential anthelmintic cyclic depsipeptides were investigated using conventional parasitological techniques and the mode of action investigated in *Ascaris* muscle using current-clamp. It was found that these compounds did not act directly as a GABA agonist or acetylcholine antagonist. The actions of the anthelmintic praziquantel are reviewed and a tegumental preparation of *Schistosoma mansoni* developed for single-channel recording.

Extrasynaptic nicotinic acetylcholine receptors were found to be located on the bag region of *Ascaris suum* muscle with iontophoresis experiments. Acetylcholine gated non-selective cation channels which were blocked by high concentrations of diethylcarbamazine. A novel muscle vesicle preparation was developed and used to record single-channel currents activated by acetylcholine, and the anthelmintics levamisole, pyrantel, oxantel and morantel. Mean open-times of the channels opened by these agonist were in the range 0.5 to 3ms and channels with two different conductances were detected. The anthelmintics levamisole, pyrantel, oxantel and morantel all produced open-channel block. Morantel was the most effective blocker and its action modelled using a novel two-ion block model. Effects of levamisole on another parasitic nematode, *Oesophagostomum dentatum,* were studied using the muscle vesicle preparation. The different conductances and mean open-times of channels showed that levamisole receptors were not homogeneous but that there are at least two major types, *G35* and *G45.*

During patch-clamp experiments on *Ascaris* muscle, a novel high-conductance Ca-dependent Cl channel was observed. The channel was found to be permeable to mono-carboxylic and di-carboxylic acids with a pore size estimated to be 6.6A°. The channel was sensitive to intracellular pH and is hypothesised to be involved in the excretion of carboxylic acids from anaerobic metabolism. The distinctive features of the channel suggest it plays a role in regulating the membrane potential of the cell and is a possible drug target site. A two microelectrode voltage-clamp was used to identify a voltage-activated Ca current and two K currents in somatic muscle of the *Ascaris.* A Kostyuk voltage-clamp preparation to record from an isolated bag preparation was developed. A slow non-selective cation current was identified which was increased in amplitude by acetylcholine through a non-nicotinic receptor. The FaRP peptide PF1 had an inhibitory effect on the current showing that there were peptide receptors on the isolated muscle.

Properties of zona-free oocytes and voltage-activated Na and K currents in a human neuroblastoma cell line and K and Cl currents in rat bone marrow derived mast cells were examined by using the patch-clamp technique. New analytical techniques for single ion-channel current behaviour were developed. To detect periods of non-stationary - drift in experimental conditions - a cusum technique was used to separate out stationary periods. Multiple channel openings of in a single patch recording could be described by a generalized binomial of Poisson.

CONTENTS

	Page
Abstract	1
Declaration	3
Introduction	4
Acknowledgments	7
Section 1: GABA ligand-gated ion-channels on *Ascaris suum* muscle and the action of piperazine, diethylcarbamazine and novel arylaminopyridazine antagonists.	8
References (Section 1)	17
Section 2: Preparations for examination of effects of ketamine, metomidate, pentobarbitone and alphaxalone on GABA, glycine and glutamate responses and xylazine	20
References (Section 2)	21
Section 3: Effects of ivermectin, cyclic depsipeptides and praziquantel	23
References (Section 3)	29
Section 4: Single-channel studies on the nicotinic acetylcholine receptors of nematode parasites and the action of levamisole, pyrantel, oxantel and morantel	31
References (Section 4)	35
Section 5: *Ascaris* muscle membrane channel currents	37
References (Section 5)	42
Section 6: Voltage-activated Na, K and Cl currents in mammalian preparations	44
References (Section 6)	46
Section 7: Reviews, Book Chapter and Books	47
References (Section 7)	47
Publications in support of candidature	

DECLARATION

Responsibility for publications

75 papers, 7 book chapters and 2 books are presented in this Thesis identified by Arabic numerals with decimal points (*e.g.* 3.2 and 8.1.7) in the Reference list of each Section (1-7). In Sections 1 to 6, the first number relates to the Section number and the second number to the sequence of the publication in that Section. Section 7 contains reviews, book chapters and books. I was sole author in 19 papers (1.1, 1.2, 1.3, 1.4, 1.5, 1.6, 1.7, 1.8, 1.11, 1.17, 2.1, 2.2, 2.3, 3.7, 3.8, 4.4, 5.10, 5.11, 7.2 and senior author on 17 papers (1.16, 1.19, 3.1, 3.2, 3.3, 3.4, 3.5, 3.6, 3.11, 4.1, 4.4, 4.15, 5.1, 5.4, 5.9, 5.13, 7.1. In the remaining papers I was a major contributor and responsibility for authorship was shared. I was the sole author of the book chapters 8.1.1, 8.1.2, 8.1.3, 8.1.4, 8.1.5, 8.1.6, 8.1.7 and sole author of the books 9.1 and 9.2.

Supervision of research

The following information on my research workers indicates the nature of the involvement which resulted in the publications.

1. Post-Doctoral Research Fellows
   - Anne Pennington
   - Panos Georgiou
   - Mark Evans
   - Diane Dixon
   - Momtchil Valkanov
2. PhD candidates at Edinburgh University
   - Catherine Cullen
   - Peter Thorn
   - Chas Bountra
   - Anne Duittoz
   - Sue Robertson
   - Alan Robertson
   - Vivienne Dale
   - Peter Hill
3. Candidate for MSc
   - Iain Murray
4. Scientific collaborators
   - Keith Bland
   - Randall House
   - Chris Glasbey
   - Bernard Ginsborg
   - Lesley Patmore
   - Jean-Marie Sitamze
   - Camille Wermuth
   - Achim Harder
   - John Kusel
   - Jean-Marie Sitamze
   - Henrik Bjorn
   - Michael Londerhausen
   - Peter Jeschke
   - Nicholas Sangster
   - A. Minta
   - Richard Haughland
   - Chris Redman
   - P. Fallon
   - Jay Modha
   - Michael Doenhoff

Signature:.... ..... Date.....17/March 1997.....

INTRODUCTION.

This Thesis brings together a collection of research papers and texts which review effects of pharmacological agents which may be used in Veterinary Practice and biophysical properties of target ion-channels. The techniques used in the investigations are electrophysiological and are aided by computer analysis. This approach to the investigation in Veterinary Pharmacology evolved as a result of influences on me by a number of individuals. A key early influence was a physics school teacher of mine at Loughborough Grammar School, Harry Bowen, a man with a ruddy nose and enthusiasm for his subject. He taught me during the years 1960-1965. At that stage it seemed that all things scientific were 'deterministic' and governed by simple rules like Ohms law that predict the relationship between current and voltage. I opted for study at a Veterinary School because my father was a vet and I grew up on a farm. After I started my veterinary degree, at Liverpool University in 1968, the undergraduate teachings of 'Tony' King seemed to confirm again, that logic and simple rules could predict outcomes: his teachings covered Neuroanatomy and included the use of simple 'wiring diagrammes' connecting input (sensory) with output (motor) responses. He taught 'Functional Anatomy' where physiological explanations were regarded with high status. Although I came from an agricultural background, growing up on a farm in Leicestershire, I became more interested in 'Science' and in particular the 'Nervous System'. It became obvious in 1972, when I was near completion of my BVSc, that I did not want a career in 'Practice' but in 'Science' and that I would require a PhD to continue. Even at that stage it was clear that technical skills were an important aspect of science and that an intermediate degree was required before embarking on a PhD. I saw an advertisement in the journal Nature for a 'Diploma in Neurophysiology' run in Professor A. Iggo's department and so spent one year taking the course in Edinburgh. One of the most enjoyable periods of the Diploma study were the practicals spent with Randall House

who showed me the beauty of isolated preparations in perspex chambers, intracellular micropipettes and the use of 'Biophysics' to describe responses of cells to drugs. I have used this approach in my research. After my PhD, Alan Knifton encouraged me to apply for a Lectureship in the Department of Veterinary Pharmacology in 1975 with Professor Frank Alexander as Head of Department. As a result my interest in drugs used in Veterinary Practice was encouraged.

Chronologically I first developed a simple vertebrate (lamprey) preparation for recording conductance changes in central neurones due to GABA and glycine gating of Cl channels and then investigated the effects of injectable anaesthetic agents (pentobarbitone, metomidate, ketamine and alphaxalone) showing that there was not a universal mechanism of anaesthesia but that there were specific effects on transmitter responses by anaesthetic agents. These studies related to my interest in the nervous system. I then took the line that I would investigate the actions of anthelmintics that were 'obviously connected' with Veterinary Pharmacology and used by Vets in practice.

Investigations on the action of anthelmintics followed, initially with piperazine showing it acted as a GABA agonist at extrasynaptic muscle receptors in nematodes. During these early studies, Neher and Sakmann developed the patch-clamp technique for single-channel recording. I wanted to apply this exciting technique to the study of anthelmintics and so went to Nottingham University to learn how to make patch recordings from Peter Usherwood. Soon after my studies on piperazine, ivermectin appeared on the market as a very potent broad spectrum anthelmintic and there was an increased interest in the *Ascaris* preparation I had developed for looking at Cl conductance changes. It was fairly easy to apply the techniques I had developed for looking at GABA and piperazine to the investigation of the action of ivermectin.

The extrasynaptic nicotinic receptors on *Ascaris* muscle were first detected during my investigations of the action of diethylcarbamazine, a piperazine derivative that had no direct action on the *Ascaris* GABA receptor but in high concentrations antagonized the action of acetylcholine. The extrasynaptic nicotinic receptors I had observed on the *Ascaris* muscle were shown to be important because of the action of the nicotinic anthelmintic pyrantel. Single-channel studies of nicotinic channels as sites of action of the nicotinic anthelmintics followed with the recognition of channel-block and the heterogeneous nature of the receptors on muscle. One particularly novel analytical model that was developed and applied to the action of morantel was the 'sequential double block model' where two molecules of morantel are proposed to enter the pore of the ion-channel sequentially and thus to produce a cooperative block. In developing this analytical approach the influence and encouragement of Bernard Ginsborg was of great importance. "Data is hard enough to get so you may as well analyze it thoroughly." "Explanation of phenomena is more important than just gathering data." "Matrix analysis - I'll give you a tutorial."

All of my experimental studies seem to have combined an interest in using simple Physics or Biophysics usually to describe the actions of drugs which may be used in Veterinary Practice and that have effects on excitable membranes. Interestingly the simple deterministic view has had to be revised and now includes a stochastic element. This Thesis combines these studies by collecting together the research papers and reviews of the actions of the drugs (anthelmintics and anaesthetics) and properties of potential sites of action (ion-channels). The observations have been presented in formats suitable for undergraduate (books) and post-graduate (research papers and reviews) study.

ACKNOWLEDGMENTS.

I have commented on some of the individuals who have had a big influence on my approach but I have also had the opportunity (and pleasure) to work with and be influenced by others in the laboratory including: Catherine Cullen, Peter Thorn, Anne Pennington, Susan Robertson, Chris Glasbey, Anne Duittoz, Mark Evans, Jean-Marie Sitamze, Camille Wermuth, Diane Dixon, Momtchil Valkanov, Lesley Patmore, Vivienne Dale, Alan Robertson, Peter Hill, Nick Sangster, Iain Murray, Henrik Bjorn and John Kusel.

Financial support has also been very important to keep these studies going. The Wellcome Trust has been the main contributor but support has also come from the Agricultural Research Council, Science and Engineering Research council, Pfizer Central Research, Merck USA, Pharmacia/Upjohn and the Faculty of Veterinary Medicine at Edinburgh.

SECTION 1: GABA LIGAND-GATED ION-CHANNELS ON *ASCARIS SUUM* MUSCLE AND THE ACTION OF PIPERAZINE, DIETHYLCARBAMAZINE AND NOVEL ARYLAMINOPYRIDAZINE ANTAGONISTS.

Ascaris suum is a worm-like nematode parasite that is found in its mature adult form in the small intestine of the pig. It is a large nematode and can be over 30 cm in length. Because it is a large size and because it can be recovered from the local abattoir on a weekly basis at Edinburgh, it became a useful model for examining the electrophysiological properties of the muscle cells and the unique pharmacology of nematode parasites. The large size of the parasite and its somatic muscle cell allowed two micropipettes to be placed in the same muscle cell and permitted the development of a two-microelectrode current-clamp and voltage-clamp technique for the study of drug action (Martin, 1979; Martin, 1980a;b;c).

The somatic muscle cells of *Ascaris* are composed of three parts: i) the contractile spindle region which is oriented longitudinally; ii) the enlarged balloon shaped structure called the bag which contains the nucleus; and iii) the arm, a process of the muscle that passes to one of the longitudinally running nerve cords where it receives synaptic contacts.

The two microelectrode current-clamp and voltage-clamp preparation

A body-flap preparation was used and it was shown (Martin, 1979; Martin, 1980a) that two micropipettes could be placed simultaneously in the bag region of the muscle for current injection through one electrode and recording through the other. Under cool conditions (22°C) to abolish spontaneous movement, it was found that the resting membrane potential was -31 ± 1 mV (mean ± S.E., N= 17) and that the input conductance was 2.4 ± 0.2 µS (mean ± S.E., N= 12).

GABA receptors on the bag

It was found (Martin, 1979; Martin, 1980a) that the bath application of GABA produced a large reversible and dose-dependent hyperpolarization and an increase in the input conductance of the muscle membrane. Ion-substitution experiments and the measurement of the reversal potential under voltage-clamp showed that GABA mediated an increase in Cl ion conductance. Iontophoresis experiments showed that the receptors mediating this increase in Cl conductance included extrasynaptic receptors located on the bag region of the muscle. The ED_{50} of GABA was 13μM and picrotoxin was weak antagonist. The antagonist action of benzylpenicillin was investigated (Martin, 1980b) under voltage-clamp and found to decrease with hyperpolarization. Interestingly during these experiments the GABA induced current was found to relax following a depolarizing step with a time constant of 32.3 ms (Martin, 1980b) a value that was later found to very similar to the mean open-time of the GABA single-channels currents (Martin, 1985). Importantly none of the conventional $GABA_A$ antagonists were found to be a potent antagonist at the *Ascaris* GABA receptor, showing that the receptor was pharmacologically different.

Piperazine

Piperazine, and a derivative diethylcarbamazine are used as anthelmintics for the control of nematode infestations but their modes of action were not clear at the beginning of the investigation because it had been reported that iontophoretic application of piperazine to the bag region of *Ascaris* muscle produced no effect despite the demonstration of extrasynaptic GABA receptors there. Added to this, diethylcarbamazine, had been reported to have an excitatory effect on *Ascaris* muscle not an inhibitory effect. In the paper (Martin, 1982) it was found and reported that piperazine was less potent than GABA but mimicked the action of GABA by producing a dose-dependent increase in the Cl conductance of the bag

membrane when bath-applied and ionophoretically applied to the bag under both current-clamp and voltage-clamp conditions. Simultaneous iontophoretic application of piperazine and GABA from two separate micropipettes with the bag held under voltage-clamp showed that the two agonists produced less that additive current responses and settled any debate, demonstrating conclusively that both compounds acted as an agonist on the same extrasynaptic GABA receptors of the bag membrane.

Diethylcarbamazine

The bath application of diethylcarbamazine did not produce a hyperpolarization but instead produced a dose-dependent depolarization (Martin, 1982). This excitatory effect was investigated further. Diethylcarbamazine is unlikely to mediate its effects on *Ascaris* muscle via histamine receptors because histamine is without effect on the muscle (Martin, 1982). The action of diethylcarbamazine as a GABA agonist was investigated under voltage-clamp: it was found that diethylcarbamazine has no agonist action on the GABA receptors and that it did not act as a GABA antagonist. But it was shown for the first time that there were extrasynaptic nicotinic acetylcholine receptors on the bag membrane that were antagonized by tubocurarine and very high concentrations of diethylcarbamazine. The reversal potentials of the acetylcholine currents observed under voltage-clamp were in the region of -5 mV, consistent with the opening of a non-selective cation channels. Diethylcarbamazine did not mimic the actions of acetylcholine by opening the non-selective cation channels but rather acted as an antagonist at high concentrations. Piperazine has no effect on the action of the acetylcholine currents. Interestingly, it was found that diethylcarbamazine reversibly and in a dose-dependent manner blocked a voltage-dependent K current in the bag when applied in concentrations greater that 100µM and this was mimicked by the K channel blocker 4-aminopyridine. Thus the excitatory depolarizing

effect of diethylcarbamazine in *Ascaris* was explained and related to a blocking effect of voltage-activated K channels.

Significance of extrasynaptic nicotinic acetylcholine receptors

The significance of the extrasynaptic acetylcholine receptor (Martin, 1982) was discussed and it was pointed out that that nicotinic anthelmintics act as agonists at these extrasynaptic receptors and that pyrantel was a potent agonist. As a result of this observation, Harrow and Gration, (1985) tested the effects of other nicotinic anthelmintics including levamisole, pyrantel and morantel and (Robertson and Martin, 1993a; Robertson *et al.,* 1994; Evans and Martin, 1996) subsequently investigated the effects of these compounds at the single-channel level as ion-channels and receptors as targets.

GABA and piperazine single-channel currents

A preparation suitable for recording GABA and piperazine single-channel currents was developed (Martin, 1983; Martin, 1984; Martin, 1985). At the time there were no commercial patch-clamp amplifiers so an amplifier built by myself and based on a Teledyne Philbrick 1035 op-amp and a 1GΩ (Welwyn) feedback resistor was required. The preparation developed used a body-flap preparation pinned onto Sylgard and used collagenase (1 mg ml^{-1}) to prepare clean membranes. Giga-seal recordings were produced after suction on the patch-pipette and GABA- and piperazine-activated channels recorded using cell-attached and outside-out patches. It was found that GABA activated channels have a mean slope conductance of 22 ± 1 pS (mean ± S.E., N=11) and that piperazine activated channels had a mean slope conductance of 21 ± 2 pS (mean ± S.E., N=11). The conductance of the channels opened by the two agonists could not be distinguished and corresponded to a single channel permeability of $4x10^{14}cm^3$ s^{-1} for the mainstate permeability. This corresponds to the movement of about 5 million Cl ions every

second at the resting membrane potential of -35 mV and if the Cl ions are separated by a minimum distance of twice the Pauling radius of 3.9 A° moving in single file, the ions would have a mean velocity of 4 mm s^{-1}. At low concentrations of GABA the mean open-times of the channels was in the region of 32 ms; at low concentrations of piperazine the mean open times were shorter and in the region of 14 ms. The distribution of the open-times was examined using a specially developed maximum likelihood estimation which was written in FORTRAN 77 and utilized the NAG E04CCF subroutine. Two exponential components were required to describe the distribution of the open-times of both GABA and piperazine activated channels. This analysis showed that there are at least two open-states which may be referred to a brief open state and a longer open state. The brief open-state could be explained as an opening due to a single bound agonist molecule and the longer open-state could be explained as due to a double bound agonist receptor opening. The fact that the proportion of brief openings increased as the concentration of the agonist was increased is consistent with this explanation. The probability of the channels being in the open-state also increased with agonist concentration before the onset of desensitization that was seen with high concentrations of agonist in the patch pipette and appeared as an increase in the very long closed-times separating openings. The lower potency of piperazine compared to GABA was explained by the fact that piperazine required a higher concentration to initiate the same frequency of opening and the fact that the piperazine open-times were on average shorter. Although piperazine was some 10 -100 less potent than GABA in these studies, the fact that piperazine was still an agonist showed that an adequate interaction of the amine moiety with the presumed anionic sub-site of the receptor is enough to permit channel opening. Piperazine lacks the carboxyl group of GABA. The GABA receptor of nematodes is therefore a target site for anthelmintic therapy (Gration *et al.,* 1986; Martin, 1987).

Cusum, Q-Q and P-P plots for analysis of single-channel currents

One of the problems in looking at single channel currents over a long period of time is that some drifts in experimental conditions may occur despite all attempts by the experimenter to maintain constant conditions. It is also a problem to determine at what point (when) in the recording was there a change in conditions. The cusum technique was applied to single channel recordings (Glasbey and Martin, 1986) for the first time to detect changes in stationarity and to localize the point of change. In addition, *Q-Q* plots and *P-P* plots, to look at the exponential distribution and best fitting models were used for the first time on single-channel currents. The advantages of these techniques, is that they produce a relatively simple visual display of the structure of the channel data before exponential fitting and allow subsequent confirmation after fitting of exponentials.

The $GABA_N$ receptor and arylaminopyridazine-GABA derivatives as Ascaris GABA receptor antagonists

The pharmacology of the *Ascaris* GABA receptor was studied using the two microelectrode current-clamp technique to examine dose-response relationships and the action of agonists described using the modified Hill equation to determine the EC_{50}s (Martin *et al.,* 1991). The agonist profile of the *Ascaris* receptor is similar but not identical to that of the vertebrate $GABA_A$ receptor with potent $GABA_A$ agonists being potent at the *Ascaris* receptor. However the potency of the sulphonic acid GABA derivatives (3APS and P4S) as well as muscimol and isoguvacine (table 2 [Martin *et al.*, 1991]) is less than that at a vertebrate $GABA_A$ type. In addition piperazine acts as a GABA agonist in *Ascaris* (Martin, 1982; 1985).

There are however major differences between *Ascaris* GABA receptors and the vertebrate $GABA_A$ type of receptor. The antagonists bicuculline and pictrotoxin (Martin, 1980a; b) SR95531 (Duittoz and Martin, 1989; 1991a; b; c), and the most potent $GABA_A$ steroid antagonist RU5135 act as weak GABA antagonists in *Ascaris* (Martin *et al.*, 1991; Martin, 1993). The concentration of RU5135 required to block GABA responses in *Ascaris* (IC_{50} = 117μM) were much higher than found at the vertebrate $GABA_A$ type of receptors (IC50 = 5 nM). The insensitivity to all the $GABA_A$ receptor antagonists distinguishes the *Ascaris* GABA receptor pharmacologically from the vertebrate receptor and identifies a pharmacologically separate $GABA_N$ receptor (Martin, 1987; Martin *et al.*, 1991). The $GABA_N$ nomenclature was suggested with N denoting Not antagonized by picrotoxin and N = Nematode.

The actions of arylaminopyridazine-GABA derivatives were investigated. Initially, in current-clamp studies, it was found that SR95531, a potent vertebrate $GABA_A$ receptor antagonist was inactive but that SR95103 did show some activity in *Ascaris* (Duittoz and Martin, 1989). The potency order in *Ascaris* contrasted with vertebrate $GABA_A$ receptors. SR95103 behaved like a competitive antagonist in *Ascaris*: the data was described by a model in which 2 molecules of GABA but one molecule of antagonist interacted with the receptor with a dissociation constant, K_B of 64μM. The actions of SR95103 were then investigated (Duittoz and Martin, 1991b) using single-channel recording techniques and outside-out patch recordings. It was reported again that the main conductance state of the GABA channels was 22 pS but that channels with lower conductance states of 16 pS and 6.5 pS were also seen. In multi-channels patches it was found that the distribution of the numbers of channels open was adequately described by the binomial distribution. SR95103 reduced the frequency of channel opening but not the channel amplitudes.

When the inhibition of SR95103 on the Popen values of the GABA channels was examined and fitted with a modified Hill equation, it was found that the Hill coefficient was 0.98 suggesting again that only one molecule of antagonist combined with the receptor. The IC_{50} was 24μM. When the burst distribution was analyzed it was found that the effect of SR95103 was to produce a reduction in the burst durations of the openings. The effect on the distribution of closed times was to increase the duration of the intermediate and long closed time components but there was no effect on the brief closed time components. From the kinetic changes observed it was concluded that SR95103 acts like a competitive antagonist at low concentrations but at higher concentrations there is an additional non-competitive element to the antagonism

A range of arylaminopyridazine GABA derivatives were then investigated using the current-clamp technique to examine their effects on GABA dose-response relationships (Duittoz and Martin, 1991c). In a previous study (Duittoz and Martin, 1991a) it was found that SR95531 and SR95103 had a different potency sequence when compared to the sequence at the vertebrate $GABA_A$ receptor. SR95531 was a very weak antagonist in *Ascaris* but SR95103, approximately 20 times less potent than SR95531 in vertebrate preparations was more potent than SR95531 in *Ascaris.* These results suggested the existence of different accessory binding sites at the *Ascaris* $GABA_N$ receptor contrasting with $GABA_A$ receptors. To test this hypothesis, a series of arylaminopyridazine derivatives of GABA were investigated in *Ascaris* (Duittoz and Martin, 1991c). The results showed that SR42627, a potent antagonist at the $GABA_A$ receptor was one of the weakest analogues in *Ascaris.* In contrast SR95132, virtually inactive in vertebrate preparations, was equipotent to SR95103, at this stage of the investigation the most potent antagonist available in *Ascaris.* The 3 most potent analogues, SR95103, SR95132, and SR42666, behaved like competitive antagonists with one molecule of antagonist acting on the receptor. The dissociation

constants, K_bs, were 64, 65 and 105 µM respectively. The structure-activity relationships for this series of compounds were examined in *Ascaris* and compared to vertebrates. It was found that substitution of the pyridazine ring in the 4-position, while detrimental to the antagonist potency at the vertebrate $GABA_A$ receptor was a prerequisite for antagonistic potency on the *Ascaris* receptor. These results can be interpreted in terms of the accessory binding site theory of Ariëns suggesting the presence of different accessory binding sites on the *Ascaris* receptor.

Novel arylaminopyridazine compounds

Novel arylaminopyridazine derivatives were then synthesized and tested as GABA antagonists in *Ascaris* using the current-clamp technique to measure the conductance changes and the structure-activity relationship explored further (Sitamze, *et al.,* 1994; Martin *et al.,* 1994).

The structure-activity relationship showed that substitution of the carboxylic group on the GABA side chain with sulphonic (NCS 248-90, NCS 249-90 and NCS 250-91), phosphonic (NCS 283-93) and tetrazole (NCS 274-93) demonstrated that substitution resulted in reduction of the potency of the compound consistent with the GABA side chain binding to the same site as GABA. Lengthening the side chain of the 2-position moiety with comparison of NCS 194-83 with SR95103 showed that increasing the length of the GABA side chain also reduced the potency of the antagonist. Comparison of the potency of NCS 260-91 with that of NCS 263-91 and comparison of NCS 276-93 with SR95103 showed that omission of the GABA side chain also resulted in loss of antagonist activity. These observations demonstrated that an intact GABA sequence is optimal for receptor recognition by the antagonist and suggests that it is the 2-position moiety of the antagonist that binds to the *Ascaris* GABA binding site. A distance of 5A° between the acidic and

basic function is likely to pertain since more extended antagonists were less potent. Complete removal of the 2-position moiety (NCS 259-91, NCS 260-91) did not lead to abolition of GABA receptor antagonist activity suggesting that the remaining molecule can still recognize part of the GABA receptor site.

At the $GABA_N$ receptor it was found that replacement of the 3-amino group by a neutral group in the compounds NCS 270-92, NCS 271-92 and NCS 273-92 still showed antagonist activity at the GABA receptor, although reduced in activity. This correlates with the structure of the anthelmintic piperazine which is a selective GABA agonist in *Ascaris* and also lacks an amidinic or guanidinic system delocalizing charge, showing that delocalization is not an absolute requirement at the $GABA_N$ receptor.

Substitution in the 4-position was found to lead to an increase in the potency of the $GABA_N$ antagonists and to be a prerequisite (Martin *et al.,* 1994) for antagonist potency. A free access zone between the anionic and cationic binding sites at $GABA_A$ receptors is required for receptor recognition in vertebrates but not in *Ascaris.* In the novel compounds that were synthesized (Martin *et al.,* 1994) it was found that introduction of more lipophilic groups increased the potency of the antagonist compounds. NCS 281-93 had a 4-phenylpropyl group present and gave rise to a K_B of 4.7μM. These pharmacological studies clearly demonstrate the presence of distinctive GABA receptors present in the nematode and suggest them as potential target sites for new anthelmintics (Martin, 1987; Martin *et al.,* 1991; Martin 1993).

REFERENCES

1.1. Martin, R J. (1979). The effect of GABA on the conductance of Ascarid muscle. *British Journal of Pharmacology*. **70**, 129p

1.2. Martin, R J. (1980a). The effect of GABA on the membrane potential and input conductance of *Ascaris suum* muscle. *British Journal of Pharmacology*. **71**, 99-106.

1.3. Martin, R. J. (1980b). The voltage sensitivity of GABA antagonist at the bag region of *Ascaris suum* muscle. *British Journal of Pharmacology.* **70**, 139P

1.4. Martin, R. J. (1980c) The action of benzylpenicillin at the bag region of *Ascaris suum* muscle. *Journal of Physiology* **313,** 58-59P.

1.5. Martin, R J. (1982). Electrophysiological effects of piperazine and diethylcarbamazine on *Ascaris suum* somatic muscle. *British Journal of Pharmacology*. **77**, 255-265.

1.6. Martin, R J. (1983). GABA single channel currents from *Ascaris* muscle. *Journal of Physiol*. **336**, 36-37p.

1.7. Martin, R. J. (1984). GABA and piperazine activated single-channels in *Ascaris* muscle. In: The electropharmacology of the in vitro synapse; 9th International Congress of Pharmacology, St Andrews, August 1984. Ed: G A Cottrell. p61-64.

1.8. Martin, R. J. (1985). GABA and piperazine activated single-channel currents from *Ascaris suum* body muscle. *British Journal of Pharmacology*. **84**, 445-461.

1.9. Glasbey, C. A, and Martin, R. J. (1986). Exploratory and confirmatory plots of single-channel records. *Journal of Neuroscience Methods*. **16**, 239-294.

1.10. Gration, K. A. F., Harrow, I. D., and Martin, R. J. (1986). GABA receptors in parasites of veterinary importance. In: Pesticide action; Ed: Ford, M G, Lunt, G G., Rey, R C and Usherwood, P. N. R., V C H Cirencester, Horwood. p415-422.

1.11. Martin, R. J. (1987). The γ-aminobutyric acid receptor of *Ascaris* as a target site for anthelmintics. *Transactions of the Biochemical Society.* **15,** 61-65.

1.12. Duittoz, A. H. and Martin R J (1989). SR95103 acts as a GABA antagonist in *Ascaris suum* muscle. *British Journal of Pharmacology*, **97,** 490P.

1.13. Duittoz, A. H. and Martin, R. J. (1991a) Effects of the arylaminopyridazine-GABA derivatives, SR95103 and SR95531 on the *Ascaris* muscle GABA receptor: the relative potency of the antagonists, in *Ascaris*, is different to that at the vertebrate GABAa receptor. *Comparative Biochemistry and Physiology,* **98**C, 417-422.

1.14. Duittoz, A H and Martin R J (1991b). Effects of SR95103 on GABA activated single-channel currents from *Ascaris suum* muscle. *Comparative Biochemistry and Physiology*, **98**C, 423-432.

1.15. Duittoz, A.H. and Martin, R. J. (1991c) Antagonists properties of arylaminopyridazine GABA derivatives at the *Ascaris* muscle GABA receptor. *Journal of Experimental Biology,* **159**, 149-164.

1.16. Martin, R J, Pennington, A J, Duittoz, A H, Robertson, S. and Kusel, J.R.(1991) The physiology and pharmacology of neuromuscular transmission in the nematode parasite *Ascaris suum*. *Parasitology,* **102**, S41-S58.

1.17. Martin, R. J. (1993). Electrophysiology of *Ascaris* muscle. *Journal of Cell Biochemistry.* **S17C**, 21P.

1.18. Sitamze, J.-M., Wermuth, C.G. and Martin, R.J. (1994). The arylaminopyridazine-GABA derivative NCS 281-93 is a potent GABA antagonist in *Ascaris suum. British Journal of Pharmacology*. **112**, 518P.

1.19. Martin, R.J., Sitamze, J-M., Duittoz, A.H., and Wermuth, C.G. (1994). Novel arylaminopyridazine-GABA receptor antagonists examined electrophysiologically in *Ascaris suum. European Journal of Pharmacology.* **276**, 9-19.

SECTION 2: PREPARATIONS FOR EXAMINATION OF EFFECTS OF KETAMINE, METOMIDATE, PENTOBARBITONE AND ALPHAXALONE ON GABA, GLYCINE AND GLUTAMATE RESPONSES AND XYLAZINE

A series of experiments were initiated with anatomical observations on large reticulo-spinal neurons that are found in the brainstem of the lamprey (Martin, 1979a). The experimental advantage of this preparation at the time was that brain neurones from the lamprey were visible with trans-illumination under the dissecting microscope because of the lack of myelin. These neurones were large enough to permit stable intracellular recordings to be made from them during the bath application of pharmacological agents (Martin, 1978 and 1979a). It was found that there were two inhibitory receptors present in the cells that could be separated out by the agonist actions of glycine, GABA and the antagonist action of strychnine, bicuculline and picrotoxin (Martin, 1979b). The two receptor types fitted the profile of vertebrate $GABA_A$ and glycine ligand-gated channels, although it is now appreciated that the assumption that there is only one $GABA_A$ and one glycine subtype is oversimplified. It was possible to estimate the dissociation constants of strychnine and thebaine as competitive antagonists of the glycine receptor using the Schild equation. The dissociation constant for strychnine was 0.6 µM and the dissociation constant for thebaine was 5.6 µM. The dissociation constant for bicuculline was 2.6 µM at the GABA receptor.

The effects of the injectable anaesthetic agents, pentobarbitone, ketamine, metomidate and alphaxalone/alphadolone on the responses to iontophoretic application of GABA and glycine were examined (Cullen and Martin 1982). The GABA responses were prolonged by pentobarbitone and prolonged by ketamine but depressed by high concentrations of all the drugs as well as by anaesthetic concentrations of ketamine. The glycine responses were depressed by alphaxalone and by supra-anaesthetic concentrations of ketamine and

metomidate. No drugs were found to potentiate glycine responses. In the absence of an effect common to the 4 anaesthetic agents, it was concluded that neither potentiation nor inhibition of all GABA or glycine responses is an essential feature of all anaesthetics. However the effects observed may contribute to the overall clinical picture during anaesthesia in higher vertebrates. The view that there is a single mechanism for all anaesthetics was not supported by these observations.

The effect of the same injectable anaesthetics on the responses of the same neurones to iontophoretic application of glutamate and on the spontaneous synaptic potentials was also examined (Cullen and Martin 1984). Of all the anaesthetics examined only pentobarbitone has a consistent dose-dependent depressant effect on glutamate responses. The inhibitory post-synaptic potentials were diminished in frequency by high concentrations of all anaesthetics. The most striking feature of the experiments was the lesser effect of anaesthetics on glutamate than on GABA and glycine responses. This contrast was particularly dramatic for metomidate.

Xylazine.

The effects of xylazine on a number of isolated preparations including the sciatic nerve preparation of a from were investigated and the α-agonist action of the compound described (Aziz and Martin, 1978).

REFERENCES

2.1. Martin, R. J. (1978) Glycine and GABA receptors of lamprey bulbar reticulo-spinal neurones. *Comparative Biochemistry and Physiology*. **6IC**, 37-40.

2.2. Martin, R. J. (1979a). A study of the morphology of the large reticulo-spinal neurones of the lamprey ammocoete by intracellular injection of Procion Yellow. *Brain Behaviour and Evolution.* **16,** 1-18.

2.3. Martin, R. J. (1979b). Glycine and GABA induced conductance changes in the lamprey reticulo-spinal neurones and their antagonism by strychnine, Thebaine,

Bicuculline, and Picrotoxin. *Comparative Biochemistry and Physiology*. **63C**, 109-115.

2.4. Cullen, K. D. and Martin, R. J. (1982). Dissimilar influences of some injectable anaesthetics on the responses of reticulo-spinal neurones to inhibitory transmitters in the lamprey. *British Journal of Pharmacology*. **77**, 493-504.

2.5. Cullen, K. D. and Martin, R. J. (1984). Effects of injectable anaesthetics on responses to L-glutamate and on spontaneous synaptic activity in lamprey reticulo-spinal neurones. *British Journal of Pharmacology*. **82**, 659-666.

2.6. Aziz, M. A, Martin, R. J. (1978). α Agonist and local anaesthetic properties of xylazine. *Zbl. Vet. Med. A.* **25,** 191-188.

SECTION 3: EFFECTS OF IVERMECTIN, CYCLIC DEPSIPEPTIDES AND PRAZIQUANTEL

Ivermectin

Ivermectin was an anthelmintic introduced by Merck as a novel potent agent with biological activity against parasitic nematodes and insects but not against tape worms and flukes. It was derived from a family of highly lipid soluble macrocylic lactones from *Streptomyces avermitilis.* At the time of initiation of the investigation it was known that ivermectin increased the opening of Cl channels in a number of vertebrate preparations and it was suggested to act a GABA agonist.

Dihydroavermectin was tested as a GABA agonist by application to outside-out patches (Martin and Pennington 1988; 1989a; 1989b). Dihydroavermectin failed to open characteristic GABA channels even when high concentrations were used. The high concentrations also failed to potentiate openings of GABA channels already activated by application of 3-4μM GABA. Interestingly dihydroavermectin acted as an antagonist at this concentration by depressing the probability of GABA channel opening and reducing the mean channel conductance. In outside-out patches (but not inside-out patches) low concentrations of dihydroavermectin produced opening of channels and because of the progressive opening of the channels which then remained open, the effect was know as a 'staircase' effect. The conductance of the channels was 9-15 pS and open-times were long and greater that 100 ms. There was a long delay between bath-application of the dihydroavermectin and the onset of opening. The long delay and the lipophilic nature of dihydroavermectin suggested a site of action in the lipid phase of the membrane. It was concluded from this study that dihydroavermectin opens non-GABA-gated Cl channels.

The Muscle vesicle preparation.

During experiments on collagenase treated flap preparations it was noticed that small membrane vesicle often budded off from the bag and that they were frequently easier to for a giga-seal with. A result a membrane vesicle preparation was developed (Martin *et al.,* 1990) which involved incubating the flap preparation of *Ascaris* in collagenase for 10 min. and then washing the preparation in saline and on further incubation for a period of up to 1 hour, membrane vesicle were produced as outgrowths of the bag region of the original. The vesicles were harvested by suction using a Pasteur pipette. The vesicle preparation was examined using transmission electron microscopy and found to contain cytoplasm and glycogen, like the original bags. The vesicles were suitable for patch-clamp recording and produced giga-seal recording more easily than the original collagenase treated flap preparations. In addition FRAP (fluorescence recovery after photobleaching) was used to measure the mobility of the phospholipid membrane. The lateral diffusion coefficient of a lipid probe (5-N [octadecanoyl]-aminofluorescein) was $8.1x\ 10^{-9}cm^2\ sec^{-1}$ but only an average of 68% of the membrane was mobile. Ivermectin had no effect on the lateral diffusion coefficient or on the proportion of the mobile phase.

FRAP experiments

A fluorescent ivermectin derivative (4" 5,7 dimethyl bodipy proprionylivermectin) was prepared by substitution of the florescent bodipy molecule in the 4" position on the oleandrosyl disaccharide residue of ivermectin producing a fluorescent compound that was still active but could be detected with FITC fluorescence (Martin *et al.,* 1992). The fluorescent compound when injected into adult *Ascaris suum* in doses greater than 0.1 µg per worm produced a dose-dependent immobilization. The distribution of the fluorescent compound after injection was examined in frozen sections. It was found that the fluorescent compound was concentrated in the nerve cords and septa surrounding the

longitudinally running nerves. The hypodermal chalice which contains the nerve cords was found to concentrate the fluorescent ivermectin. It was also found that the bodipy compound concentrated in the area directly in contact with the peri-enteric fluid in the region of the lateral line. The hypodermal layers were found to take up the bodipy ivermectin. Florescence in isolated muscle cells was examined and found to occur in 'beads' interpreted as the result of lipophilic pinocytotic vesicles. The accumulation of the bodipy ivermectin within the nerve cord and in muscles is consistent with an action of ivermectin in muscle and nerve-cord membranes of nematode parasites.

The distribution of 4" 5,7 dimethyl bodipy proprionylivermectin was studied in the muscle vesicle preparation (Martin and Kusel 1992) were it was found that the fluorescent probe in concentrations > 1 ng ml^{-1} produced a dose-dependent fluorescence that was not reduced by prior incubation with 1 µM ivermectin. This was interpreted as indicating that the fluorescent probe was free in the lipid phase of the membrane and not associated with the receptor in the membrane. The lateral diffusion coefficient of the probe was examined using FRAP and found to be $14x10^{-10}cm^2\ s^{-1}$ nearly three times faster than the lipid probe octadecanoyl-aminofluorescein in the same membranes. Calculation showed that on average the probe would move 7.5 µm in 100 s. Only 46% of the probe was mobile because the membrane was not homogeneous with 64% of the membrane in a non-mobile (non-fluid) condition. Trypan blue quenching showed that the ivermectin probe was only distributed in the outer bilayer of the membrane after a period of 30 min. and it did not cross into the inner bilayer over the time scale of the experiment. A model of the mode of action of ivermectin was proposed (Martin and Kusel 1992; Martin 1992) in which it acts by binding and gating open a Cl channel in the outer bilayer of the membrane. It was also concluded that ivermectin would not 'flip-flop' across the membrane and because of this its action is inconsistent with it acting as an ionophore to carry ions across the membrane.

An electrophysiological preparation for recording a glutamate gated Cl channel from a nematode parasite.

Molecular experiment using the *lacZ* marker had shown that a glutamate-gated Cl channel was expressed in the pharynx of the model nematode *Caenorhabditis* elegans in the pM4 muscle. But the location of a glutamate gated channel sensitive to avermectins had not been determined in parasitic nematodes, nor had an electrophysiological preparation been developed to study this receptor. The studies (Martin and Pennington, 1989b) had described effects on somatic muscle but glutamate has little effect on the membrane conductance when applied in bath. The nature of the somatic muscle Cl channel gated by dihydroavermectin (Martin and Pennington, 1989b) remains to be further characterized.

Consequently an electrophysiological preparation of *Ascaris suum* pharyngeal muscle suitable for recording changes of input conductance using a two-microelectrode current clamp and pharmacological study was developed (Martin, 1996). The preparation was shown to contain a glutamate gated Cl ion-channel sensitive to the avermectin analogue, milbemycin D. The application of glutamate produced a dose-dependent increase in Cl conductance and the effect of glutamate was potentiated by milbemycin D. Milbemycin D also produced a dose-dependent increase in input conductance of the pharyngeal muscle. These observations show that one of the sites of action of the avermectins is the pharyngeal muscle and that the drugs inhibit feeding. This preparation offers the possibility of studying the pharmacology of the glutamate-gated Cl channels in a parasitic nematode and the properties of the properties of these ion-channels.

Interestingly the pharyngeal preparation of *Ascaris suum* also responds to aspartate in addition to glutamate (Murray and Martin, 1996) by hyperpolarization and an increase in

membrane conductance. This effect contrasts with the effect of aspartate on expressed glutamate-gated Cl channels from *C. elegans* and suggest the possibility that the 'real' ivermectin glutamate-gated receptors are more complex and may be gated by more than glutamate and avermectins. Future study of the pharmacology of these ion-channels offers an approach for the future development of therapeutic compounds.

Cyclic depsipeptides

The 24-membered cyclic depsipeptide, PF 1022A is a fermentation product of the strain PF 1022 of *Myclia sterilia* that was isolated from the microflora on the leaf of the plant *Camellia japonica* collected from the Ibaragi Prefecture in Japan. Previously, it had been reported that this compound had potent antinematodal properties against *Toxocare canis* and *Toxocara cati*, intestinal nematodes of dogs and cats. It was found (Martin *et al.,* 1996) that when PF1022A was given orally to mice it also showed good activity against *Heligmosomoides polygyrus* and *Heterakis spumosa* and in vivo it also had a good action against *Trichinella spiralis.* AN 18-membered enniatin analogue, JES 1798 showed good activity against *Nippostrongylus braziliensis* (Martin *et al.,* 1996a). The optical antipode of PF 1022A was inactive.

The effects of the active anthelmintic cyclic depsipeptides, PF1022A, and JES 1798 on the membrane potential and input conductance of somatic muscle of *Ascaris suum* was examined using a two-microelectrode current-clamp technique. The aim of the experiments was to determine if the compounds behaved as a nicotinic antagonist or as a GABA agonist in a nematode preparation because previous reports had suggested that PF 1022A may act as a GABA agonist in nematodes. Neither PF 1022a nor JES 1798 antagonized the effects of the selective nicotinic agonist, levamisole. The effect of PF1022a, and JES 1798, but not PF 1022a antipode was to produce a small time-dependent increase in input conductance

associated with little or no potential change. The increase in input conductance did not occur in the Cl-free bathing solution suggesting that the increase in input conductance was mediated by Cl ions. The addition of high concentrations of Ca to the preparation after the addition of PF 1022a did not lead to activation of Ca activated Cl channels suggesting that its mode of action was not that of a Ca ionophore. It was concluded that these novel potent anthelmintics do not act as direct GABA agonists nor do they have a nicotinic antagonist effect.

Praziquantel

Praziquantel is an anthelmintic active against tape worms and schistosomes. In a review of the mode of action of praziquantel (Redman *et al.,* 1996) it became clear that one site of action of this compound is the tegument of the parasite. The effect on the tegument of the parasite is to increase the Ca permeability of the outer membrane by an unknown mechanism.

In order to study the ion-channels of the tegument and in the future study the effect of praziquantel, a vesicle preparation was developed that allows resolution of low conductance single ion-channel currents from adult male *Schistosoma mansoni* (Robertson *et al.,* 1996; Robertson *et al.,* 1997). Adult male schistosomes were exposed to a low pH (3.75) medium for a period of approximately 30 minutes at 37°C. During this period smooth vesicles formed from the tegument. Fluorescence microscopy following staining of the tegument with the dye, 5-N-[octadecanoyl]aminofluorescien (AF-18), transmission electron microscopy and scanning electron microscopy revealed that the vesicles were produced from the outer tegumental membrane. The fluorescence studies showed the presence of the double bilayer structure of the outer membrane in > 41% of the vesicles. These studies suggested that the preparation is suitable for single-channel recording with the patch-clamp technique.

Cell-attached and isolated inside-out patch recordings of ion channel activity were obtained with giga-ohm resistance seals. Different types of ion-channel were recorded from tegumental vesicles from male schistosomes, illustrating the potential of the technique. The channels observed included: a non-selective cation channel (360 pS); a K^+ channel (with a conductance of 114 pS in high bath-K conditions); and a Cl^- selective channel (20 pS). The currents of these ion-channels may cross the double bilayer of the outer tegumental membrane. The preparation developed will permit the effects of praziquantel on ion-channels to be studied in with greater resolution and an explanation for the increased Ca permeability to be sought.

REFERENCES

3.1 Martin, R. J. and Pennington, A. J. (1988) Effect of dihydroavermectin B1a on Cl single-channel currents in *Ascaris*. *Pesticide. Science.,* **24**, 90-91.

3.2. Martin, R. J. and Pennington, A. J. (1989a). Ivermectin induces cation channels in isolated patches of *Ascaris* muscle. *Journal of Physiology.* **410**, 83P.

3.3. Martin, R. J. and Pennington, A. J. (1989b). A patch-clamp study of effects of dihydroavermectin on *Ascaris* muscle. *British Journal of Pharmacology.* **98**, 747-756.

3.4. Martin, R. J, Kusel, J. R. and Pennington, A. J. (1990). Surface properties of membrane vesicles prepared from muscle cells of *Ascaris suum*. *Journal of Parasitology*, **76**, 340-348.

3.5. Martin, R. J., Kusel, J. R. Robertson, S. J. Minta, A. and Haugland, R. (1992) Distribution of a fluorescent ivermectin derivative, bodipy ivermectin, in tissues of the nematode parasite *Ascaris suum*. *Parasitology Research*. **78**, 341-348.

3.6. Martin. R. J. and Kusel, J. R. (1992). On the distribution of a fluorescent ivermectin probe (4" 5,7 dimethylpropionic bodipy ivermectin) in membranes of *Ascaris suum*. *Parasitology,* **104**, 549-555.

3.7. Martin R. J. (1992). Electrophysiological effects of Anthelmintics in the Parasitic Nematode *Ascaris suum*. *Asia Pacific Journal of Pharmacology*, **7** 115-192.

3.8. Martin, R. J. (1996). An electrophysiological preparation of *Ascaris suum* pharyngeal muscle reveals a glutamate-gated chloride channel sensitive to the avermectin analogue milbemycin D. *Parasitology*, **112**, 247-252.

3.9. Murray, I. A. and Martin, R. J. (1996). L-glutamate and L-aspartate increase input conductance of *Ascaris suum* pharyngeal muscle. *Journal of Physiology*. **495P**, 33p

3.10. Robertson, A. P., Martin, R. J. and Kusel, J. R. (1996). Single-channel recordings from tegument-derived vesicles of *Schistosoma mansoni.* J. Physiol. **495P**. 33-34.

3.11. Redman, C. A., Robertson, A., Fallon, P. G., Modha, J., Kusel, J. R., Doenhoeff, M. J. and Martin, R. J. (1996). Praziquantel: An urgent and Exciting Challenge. *Parasitology Today*, **12**, 14-20.

3.12. Martin, R. J. and Harder, A. Londerhausen, M. and Jeschke, P. (1996) Effects of the cyclic depsipeptide, PF1022A, on the membrane potential and input conductance of the somatic muscle cell of *Ascaris suum*. *Pesticide. Science* **48,** 343-349.

SECTION 4: SINGLE-CHANNEL STUDIES ON THE NICOTINIC ACETYLCHOLINE RECEPTORS OF NEMATODE PARASITES AND THE ACTION OF LEVAMISOLE, PYRANTEL, OXANTEL AND MORANTEL

Acetylcholine-activated single-channel currents from Ascaris suum.

In earlier experiments using a two-microelectrode voltage-clamp an extrasynaptic nicotinic acetylcholine receptor had been located on the bag region of the somatic muscle cells of *Ascaris* which was also activated by the anthelmintic pyrantel (Martin, 1982).

Consequently the muscle vesicle preparation was used to record acetylcholine-activated single-channel currents from cell-attached and isolated inside-out patches (Martin and Pennington, 1990; Pennington and Martin, 1990). It was observed that acetylcholine activated channels of two amplitudes: 40-50 pS and 25-35 pS. The open-times of the larger conductance channel had a distribution that was described by two components suggesting the presence of at least two open-states. The brief open-time component had a mean duration of 1.18 ms and the longer component had a mean duration of 4.89 ms when 1-10μM acetylcholine was used as the agonist.

Levamisole-activated channel currents

When similar experiments were carried out with the imidazothiazole, levamisole, as the agonist (Robertson and Martin, 1993a) channels with conductances ranging between 19-46 pS were observed and mean open-times ranging between 0.8 - 2.85 ms. Two components to the open-time distribution was also observed, again suggesting the presence of two detectable open-states. The main difference between acetylcholine and levamisole was that levamisole produced an open-channel block which was seen as 'a flickering channel-block' at concentrations above 30μM at negative membrane potentials. The dissociation

constant for the block was measured as 123µM at -50mV and 46µM at -75mV and 9.4µM at -100 mV. At higher concentrations levamisole produced openings in 'clusters'. Thus for the first time levamisole was observed to act as an agonist and as an antagonist at the site of action in nematodes. Another interesting aspect of the action of levamisole was its ability to open the channels when applied to the inside (cytoplasmic) membrane of isolated inside-out patches (Robertson and Martin, 1993b). The explanation for this phenomena, was not that there are levamisole binding sites present on the inside of the nicotinic channels, but that levamisole has a pKa of 8.0 and about 10% it is in an unionized state and able to pass through the lipid membrane of the patch and reach the extracellular receptor binding sites of the channel. Because of the proportion of the unionized moiety, levamisole for the same reason, may be applied to the skin of the back of cattle (pour-on preparations) and enter the body for therapeutic action.

Pyrantel

Pyrantel is one of a group of tetrahydropyrimidines produced by *Pfizer* for anthelmintic use against nematode parasites. Its action at the single-channel level was explored using the vesicle preparations derived form *Ascaris* muscle (Martin, 1993; Robertson *et al.,* 1994). Pyrantel in concentrations between 0.03-100µM activated non-selective cation channel currents with at least two conductance levels being present. There was a smaller conductance channel with a conductance 22.4±0.3 pS (mean ± S.E., n=8) and a larger conductance channel with a mean conductance of 41 ± 2 pS (mean ± S.E.>, n= 28). Detailed kinetic analysis showed that there was again at least 2 distinguishable open-states and at least 3 closed states. The mean open-time duration of the larger conductance channel was 1.5 ms. With high concentrations of pyrantel (100µM) there were sequences of openings and closings of the channel at negative membrane potentials indicating the

presence of open-channel block. The dissociation constant for the channel block was 37 μM at -50mV and 20 μM at -75mV.

Oxantel

Oxantel is an *m*-oxyphenol analogue of pyrantel and was developed from pyrantel for its activity against whipworms (*Trichuris* species). Despite the fact that pyrantel is an effective anthelmintic against many gastro-intestinal nematodes, it has little effect against whipworms. Interestingly oxantel has little action against *Ascaris suum* despite its close structural relationship to these drugs. Oxantel has a benzene ring present which means that it is more lipophilic in nature. The actions of oxantel were investigate using the same procedures and techniques as described for levamisole and pyrantel (Dale and Martin, 1994). Oxantel throughout the concentration range 10-100 μM activated single-channel currents. At 10μM the mean open-time was 1.34 ms. Oxantel like levamisole and pyrantel produced open-channel block, but at lower concentrations. The dissociation constant for channel block at -50mV was 18.5 μM and 6.9 μM at -75 mV. It can be seen that oxantel is 2- 3 times more potent than pyrantel as an open-channel blocker and this action may contribute to the reduced potency of oxantel in *Ascaris.* One explanation of the different potencies of pyrantel and oxantel against the nematode species may relate to the detailed amino-acid sequence structure of the nicotinic receptors and differences between species.

Morantel

The tetrahydropyrimidine anthelmintic, morantel, was also investigated using the muscle vesicle preparation and the patch-clamp technique (Evans and Martin, 1991; 1993a; 1993b; 1993c; 1993d; 1996). Morantel in the pipette (6nM to 600μM), activated single nicotinic acetylcholine currents. The kinetic properties of the main-conductance state of morantel-

activated currents were investigated throughout the concentration range, 0.6μM to 600μM. Open-time distributions were best fitted by a single exponential. Mean open-times were slightly voltage-dependent, increasing from 0.9 ms at +75mV to 1.74 ms at -75mV in the presence of 0.6μM morantel. At low concentrations, closed-time distributions were best fitted by the sum of two or three exponential components. As the concentration of morantel was increased (100-600μM), a fast-flickering open channel-block was observed at positive potentials, even though morantel, a cation, was only present at the extracellular surface of the membrane. The block rate was dependent on morantel concentration and both block rate and duration of block increased as the potential became less positive. A simple channel-block mechanism did not explain properties of this block. At negative potentials, as the morantel concentration increased, a complex block was observed. With increases in morantel concentration, two additional gap components appeared in closed-time distributions: one was short with a duration (~13 ms) independent of morantel concentration; the other was long with a duration that increased with morantel concentration (up to many minutes). In combination, these two components produced a marked reduction in probability of channel opening (*Po*) with increasing morantel concentration. The relationship between the degree of block and morantel concentration had a Hill coefficient of 1.6, suggesting the involvement of at least two blocking molecules. The data was analysed using a novel simple sequential double block kinetic model using matrix analysis and a maximum likelihood fitting procedure.

Levamisole receptors in Oesophagostomum dentatum

A muscle vesicle preparation from the nematode parasite *Oesophagostomum dentatum* was developed in order to examine changes in the channel properties of the levamisole receptors associated with resistance (Robertson *et al.*, 1996; Martin *et al.*, 1997). Properties of nicotinic acetylcholine receptors (*nAChRs)* activated by the anthelmintic

levamisole (10μM) were investigated using cell-attached and isolated inside-out patches. The current-voltage relationships of the single-channel currents were linear with conductances in the range 24.6-57.7 pS with a mean of 39.5 pS. The distribution of open-times were fitted with a single exponential and mean open-times were in the range 0.98-4.43 ms with an average of 2.2 ms. The distributions of conductances and open-times of the channels showed that the receptors could not be described as single homogeneous. There were at least two channel subtypes: one type, *G35,* had a mean conductance of 35 pS and open-time of 1.6 ms; another subtype, *G45,* had a mean conductance of 44.6 pS and open-time of 2.7 ms. In addition a channel with a conductance near 25 pS and a channel with conductance near 55 pS were observed. A model of the heterogeneic population of *nAChRs* is suggested and related to the development of levamisole resistance in nematodes (Martin *et al.,* 1997).

REFERENCES

4.1. Martin, R. J. and Pennington, A. J. (1990). Acetylcholine-activated single channel currents from isolated *Ascaris suum* muscle. *Journal of Physiology.* **420,** 91P.

4.2. Pennington, A. J. and Martin, R. J. (1990). A patch clamp study of acetylcholine-activated ion channels in *Ascaris suum* muscle. *Journal of Experimental Biology*, **154**, 201-221.

4.3. Evans, A. M. and Martin, R. J. (1991). Morantel an agonist and a slowly dissociating blocker of nicotinic-acetylcholine channels from *Ascaris suum. British Journal of Pharmacology.* **107,** 21P.

4.4. Martin, R. J. (1993). Neuromuscular transmission in nematodes and anthelmintic drug action. *Pharmacology and Therapeutics.* **58**, 13-50.

4.5. Robertson S. J. and Martin R. J. (1993a). Levamisole activated single-channel currents from muscle of the nematode parasite. *British Journal of Pharmacology,* **108,** 170-178.

4.6. Robertson, S. J. and Martin, R. J. (1993b). The Activation of Nicotinic Acetylcholine Receptors in the Nematode Parasite *Ascaris suum* by the Application of Levamisole to the Cytoplasmic Surface of Muscle Membrane. *Pesticide Science,* **37**, 293-299.

4.7. Robertson, S. J., Pennington, A. J., Evans, A. M. and Martin, R. J. (1994). The action of pyrantel as an agonist and open-channel blocker at acetylcholine receptors in isolated *Ascaris suum* muscle vesicles. *European Journal of Pharmacology.* **271**, 273-282

4.8. Dale, V. E. M. and Martin, R.J. (1994). Oxantel activated single-channel currents in *Ascaris* muscle membrane. *Parasitology*. **110**, 437-448.

4.9. Evans, A. M. and Martin, R. J. (1993a). At positive potentials the cationic agonist morantel blocks nicotinic-acetylcholine channels in muscle membrane vesicles isolated from *Ascaris suum. Journal of Physiology.* **459,** 394P.

4.10. Evans, A. M. and Martin, R. J. (1993b). Morantel may bind to more than one site within the nicotinic acetylcholine channel from *Ascaris suum*. *Journal of Physiology*. **459**, 489P.

4.11. Evans, A. M. and Martin, R. J. (1993c). On the block by morantel of nicotinic acetylcholine channels isolated from *Ascaris suum:* positive co-operativity between at least two blocking molecules. *Journal of Physiology*. **467**, 171P.

4.12. Evans, A.M. and Martin, R.J. (1993d). On the block by morantel of nicotinic acetylcholine channels isolated from *Ascaris suum*: Rate constants for multi-ion block estimated by maximum likelihood. *Journal of Physiology*. **467,** 254P.

4.13. Evans, A.M. and Martin, R.J. (1996). Activation and Cooperative multi-ion block of single nicotinic-acetylcholine channel currents of muscle by the tetrahydropyrimidine anthelmintic, morantel. *British Journal of Pharmacology.* **118**, 1127-1140.

4.14. Robertson, A. P., Bjorn, H., Sangster, N.C. and Martin, R.J. (1996). Levamisole-activated single channel currents form isolated muscle vesicles of *Oesphagostomum dentatum. Journal of Physiology*. **495P** 83-84P.

4.15. Martin, R. J. Robertson, A. P. Bjorn, H. and Sangster, N. C. (1997). Heterogeneous levamisole receptors: a single-channel study of nicotinic acetylcholine receptors from *Oesphagostomum dentatum. European Journal of Pharmacology.* (In Press).

SECTION 5: *ASCARIS* MUSCLE MEMBRANE CHANNEL CURRENTS

Ca-dependent Cl channel and excretion of carboxylic acids

During experiments on the GABA and piperazine single channel currents (Martin 1985) it was regularly observed that a large conductance channel was active spontaneously in many of the patches formed from the bag region of the *Ascaris* muscle cell (Martin and Thorn, 1984). When the properties of this channel were investigated further (Thorn and Martin, 1987) it was found to have a conductance of around 200 pS, to be permeable to Cl ions, to be dependent and activated by Ca at the cytoplasmic membrane and the probability of channel opening decreased when the membrane was depolarized. The channel also possessed a number of unique properties: there were subconductance states that were present only when the membrane patch was depolarized; the binomial distribution did not describe the proportion of time different numbers of channels were open and suggested that adjacent channels in the same patch could have different open probabilities. The function of the channel was not determined at this stage but it was noted that the voltage sensitivity was incompatible with it acting to repolarize the membrane after depolarization. One suggestion was that it may contribute to the resting membrane potential of the cell because of its large conductance and frequency of occurrence in the membrane.

In a subsequent investigation (Dixon and Martin, 1993) the permeabilities of halide anions and NO_3 were determined. The channel displayed a permeability sequence of I > Br = No_3 > Cl > F which differed for the corresponding conductance sequence which was Cl > No_3 = Br = I > F. The ionic environment within the channel pore was investigated using the Reuter Stevens plots to describe the selectivity and fluidity of the channel pore. The channel was found to have a high fluidity near that of water with a coefficients, a_1, of 9.1 $kJA^{o}mol^{-1}$. In addition the approach of Wright and Diamond was employed to estimate the

number of cationic binding sites within the pore which was found to vary inversely with the ionic radius of the anion and was 2.15 for F but was 0.89 for NO_3.

Subsequent papers (Dixon *et al.,* 1993; Dixon and Martin, 1993; Valkanov, Martin and Dixon, 1994;) explored the permeability of the channels to mono- and di-carboxylic acids. The P_{anion}/P_{Cl} ratios were determined. The relationship between permeability of the anion and the Stokes diameter was inverse and approximately linear with limiting pore diameter of $6.55A^0$ Calculation of the transition state energy required to transfer a single methyl group from the aqueous phase to the binding site in the channel gave a low value of about -0.6 $kJmol^{-1}$ and indicated again that there was a cationic binding site of low field strength. The permeability of oxalate, succinate, oxaloacetate, and malate were also studied with the result that it was found that all but malate was conducted through the channel. The relative conductivity of all anions could be predicted from the component structure of the anion. The failure to conduct malate prevents an energy drain of the muscle cell because it is present in significant quantities in the cytoplasm. The study on the di-carboxylic anions (Valkanov and Martin, 1995) further supported the hypothesis that the Cl channel functions to transport organic waste anions across the membrane. The channel has the advantage of providing a transport system driven by the membrane potential of the cell.

Effects of pH on the Ca-dependent Cl channel

Respiration in *Ascaris* results in the production of protons and long-chain fatty acyl waste products. It had been shown that the Ca-dependent Cl channel was permeable to mono-carboxylic and di-carboxylic acids so it was of interest to examine the effect of pH on the gating of the channel to get a clearer insight into the physiology of this ion-channel (Robertson and Martin, 1996). Under control conditions, the channel had the highest probability of opening at -35mV, the resting membrane potential of the cell. At positive

membrane potentials, the probability of channel opening decreased. A Boltzmann equation was used to describe the relationship between membrane potential and channel opening and to calculate the effective gating change. A reduction of the external pH produced an increase in channel opening at hyperpolarized potentials; an increase in internal pH caused an increase in the probability of channel opening and made the effective gating charge less negative. The most marked effect was produced by a reduction of the internal pH which produced a change in the polarity of the effective gating charge from -3.0e to +1.8e: the effect was to reverse the voltage-sensitivity of channel opening. A simple model was proposed to explain these observations. In the model a 'selectivity filter' is not affected by the pH change and a 'voltage-sensitive gate' that was exposed to the cytoplasm has had imidazolium side chain of histidine molecules which resulted in a change in charge on the gate as the pH was changed.

The physiological significance of the pH sensitivity relates to the normal pH of *Ascaris* cytoplasm (7.4) and the fact that waste carboxylic acids are 99.2% ionized suggesting that passive diffusion of the uncharged acid across the muscle membrane is an unlikely method of excretion. The presence of an active proton pump would be required to exclude protons produced during anaerobic respiration. An increase in the activity of this pump would lead to an increased internal pH and increase in ionized: unionized carboxylic acid ratio. In turn, the raised internal pH would favour opening of the Ca-dependent Cl channel and facilitate excretion of the waste anions (Robertson and Martin, 1996).

Distribution of numbers of open channels in multi-ion channel patches

It was pointed out earlier (Thorn and Martin, 1987) that the distribution of the numbers of channels open in patches, where the activity of Ca-activated Cl channels were being recorded, that the distribution of the number of open channels was not described by a

binomial distribution. Assumptions inherent in the use of the binomial distribution have then to be relaxed (Glasbey and Martin, 1988). The important assumptions of the binomial distribution are i) all channels have the same probability, *p*, of being open; and ii) the channels behave independently of one another; and iii) the value. *p*, remains constant over the experiment. It is possible to consider relaxation of all of these. If some of the channels have differing probabilities of being open then the distribution of the numbers of channels open will be described by the generalized distribution of Poisson. If channels interact so that opening of one channel increases the opening of another adjacent channel, then this will be described by the additive generalization of the binomial distribution. If *p* varies, mathematically the simples assumption is that *p* follows a beta distribution and would produce a beta-binomial distribution.

Voltage-activated currents in somatic muscle of Ascaris.

Previous electrophysiological study of *Ascaris* muscle by other workers found that there were three types of depolarizing potential recorded in the bag region of the muscle. The three potentials were: i) the spike potentials; ii) the slow waves; iii) the modulation waves. The two-microelectrode voltage-clamp technique with voltage-steps was used (Martin *et al.,* 1992) to dissect out a voltage-dependent inactivating Ca current and voltage sensitive K currents. The Ca current-voltage relationship was U-shaped with a threshold around -15 mV and peak at +5 mV. Two voltage-dependent inactivating K currents were dissected out. One of these currents, sensitive to 5 mM 4-amimopyridine and fast inactivating was fitted to a Boltzmann curve with a half-maximal activation voltage of +14 mV; it was I_A-like. The other K current, resistant to 4-aminopyridine was slowly inactivating and had a half-maximal activation voltage of +29 mV and was I_K-like. The Ca current had some but not all of the properties of the two major types (LVA and HVA) of Ca current described in other preparations. It was not inactivated at a potential of -35 mV. The report (Martin *et al.,*

1992) along with the effects of Ca channel blockers (Wann, 1985) suggested that the *Ascaris* Ca channel may be distinctive and a possible target site. The properties of the K channel currents with slow recovery from inactivation may permit the K currents to contribute to the slow waves and modulation waves.

Kostyuk technique for recording from isolated muscle bags and the a non-nicotinic acetylcholine receptor

Isolated muscle bags from the parasitic nematode *Ascaris suum* were prepared by collagenase treatment and dissection (Martin and Valkanov, 1996a; Martin and Valkanov 1996b). Single bags were mounted in a V-shaped plastic pipette for voltage-clamp and intra-cellular and extra-cellular perfusion. With 'physiological' intra- and extra-cellular solutions, depolarizing voltage-steps from near the normal resting membrane potential, -40 mV, produced in leak-corrected currents, a slowly activating outward current at potentials more positive than -20 mV. At the end of the depolarizing pulse there was a slow inward tail-current with a reversal potential near -20 mV. Hyperpolarizing voltage-steps produced an outward current relaxation and an outward tail current with the same reversal potential. The observations can be explained by the presence in the bag, of a non-selective cation-channel current, $I_{bcat,}$ that opens spontaneously at the holding potential: depolarization increases opening of the channel and hyperpolarization decreases opening.

Bath-applied acetylcholine in concentrations greater that 10^{-7}M produced an increase in the amplitude of I_{bcat}. The effect of acetylcholine was not antagonized or prevented by 100μM mecamylamine or 100μM tubocurarine, suggesting the presence of a non-nicotinic acetylcholine receptor. 100μM atropine had no detectable effect on the effect of acetylcholine but the FMRFamide peptide, PF_1, in concentrations > 1μM, reduced the

amplitude of I_{bcat}. I_{bcat} was maintained when Cs was used to replace intracellular and extracellular cations, showing that the channels were permeable to Cs.

It is concluded that the bag membrane possesses a slow voltage-activated non-selective cation channel current, I_{bcat}. The effect of acetylcholine in the presence of nicotinic antagonists indicates the presence of non-nicotinic acetylcholine receptors on the bag membrane. The effect of PF_1 indicates the presence of PF_1 receptors on the bag membrane.

REFERENCES

5.1. Martin, R. J. and Thorn, P. (1984). A high conductance anion channel from *Ascaris suum* muscle. *Journal of Physiology*. **345**, 46P.

5.2. Thorn, P. and Martin, R. J. (1987). A high conductance Ca-dependent anion channel in *Ascaris suum* muscle. *Quarterly Journal of Experimental Physiology* **72,** 31-49.

5.3. Glasbey, C A, and Martin, R J. (1988). The distribution of number of open channels in multi-channel patches. *Journal of Neuroscience Methods*, **24**, 283-287.

5.4. Martin, R. J., Thorn, P. Gration, K.A.F. and Harrow. I. D. (1992). Voltage-activated currents in somatic muscle of the nematode parasite *Ascaris suum. Journal of Experimental Biology.* **173,** 75-90.

5.5. Dixon, D. M., Valkanov, M.A. and Martin, R. J. (1993). A Patch-Clamp Study of the Ionic Selectivity of the Large Conductance, Ca-activated Chloride Channel in Muscle Vesicles Prepared from *Ascaris suum*. *Journal of Membrane Biology,* **131**, 143-149.

5.6. Dixon, D. M. and Martin, R.J. (1993). Patch-clamp and Chloride channels in *Ascaris suum. Parasitology Today,* **9**, 41-344.

5.7. Valkanov, M. A., Martin, R.J. and Dixon, D.M. (1994) The Ca-activated Chloride Channel of *Ascaris suum* Conducts the Volatile Fatty acids Produced by Anaerobic Respiration: A patch-clamp Study. *Journal of Membrane Biology*, **138,** 133-141.

5.8. Valkanov, M.A. and Martin, R.J. (1995) A Cl channel in *Ascaris suum* selectively conducts dicarboxylic products from anaerobic glucose metabolism and indicates a role in the transmembrane transport of waste organic anions. *Journal of Membrane Biology,* **148**, 41-49.

5.9. Robertson, A. R. and Martin, R. J. (1996). Effects of pH on the large-conductance Ca-dependent Cl channel of *Ascaris* muscle. *Parasitology*. **113**, 191-198.

5.10.. Martin, R. J.(1994). A non-nicotinic receptor in muscle of *Ascaris suum. Journal of Physiology*. **447,** 63P.

5.11. Martin, R. J. (1994). Non-nicotinic acetylcholine receptors on nematode muscle may allow recovery of parasites from levamisole treatment. *Proceedings of the 6th international congress of the European Association of Veterinary Pharmacology and Toxicology*. P253.

5.12. Martin, R. J. and Valkanov, M. A. (1996a). The Kostyuk technique for recording currents from isolated muscle bags of *Ascaris suum. Journal of Physiology..* **491P** 105-106p.

5.13. Martin, R. J. and Valkanov, M. A. (1996b). Effects of acetylcholine on a slow voltage-activated non-selective cation current mediated by non-nicotinic receptors on isolated *Ascaris* muscle bags. *Journal of Experimental Physiology.* **81.** 909-925.

SECTION 6: VOLTAGE-ACTIVATED Na, K AND Cl CURRENTS IN MAMMALIAN PREPARATIONS

During experiments on the nematode preparation and the learning of the patch-clamp technique, opportunities to explore voltage-activated ion-channels in mammalian cell arose. The opportunities took advantage of the fact that the techniques used are the same.

Single-channel currents from zona-free mouse eggs

Cell-attached patch recordings were made from zona-free unfertilized mouse eggs and single channel currents recorded (Bland *et al.,* 1984; Bountra and Martin 1987). Difficulties in obtaining high resistance giga-seals were encountered because of the microvilli on the surface of the membrane. Despite these difficulties a high-conductance K channel was recorded and Ca channel current activated by depolarization. .

Na and K currents in a human neuroblastoma cell line.

One of the opportunities was to examine the Na and K currents present in a human neuroblastoma cell line, IMR-32 (Ginsborg, Martin and Patmore, 1987; 1991). These cell were examined using the whole-cell voltage-clamp technique which allowed the estimation of the membrane potential of the cell and a description of the Na current in these cell using the Hogkin Huxley kinetic analysis. A Boltzmann fit to the activation curve gave a half-maximal activation voltage of -41.6 mV and a 'slope' of 3.9 mV. The steady state inactivation curve had a half-maximal inactivation voltage of -81 mV and a slope of 9.7 mV. The time constants T_m and T_h of 0.16 and 0.63 ms were calculated for a voltage jump from -80 mV to -10 mV. Outward K currents were examined by using voltage pulses which depolarized the cell to -20 mV or more positive values, from a holding potential of -80 mV and by depolarizing pulses to 0 mV or to positive values from a holding potential of -30 mV.

A Boltzmann fit to the K currents gave a half-maximal activation voltage of 10 mV and a 'slope' of 14 mV. The time course for the activation of the whole cell K current was described by a single exponential equation with a time constant varying between 4 and 27 ms depending on the destination potential. The properties of K single channel currents were investigated and their open-time described by single exponential distribution and the closed-times were described by a double exponential distribution. The probability density function of the open- and closed-times were used to successfully predict the whole cell K current following a voltage step.

K and Cl currents in mucosal and connective tissue rat mast cell

Mast cells accumulate and were known to be involved in the reaction of host animals to nematode parasite rejection, particularly in the elimination of gastro-intestinal nematodes. Mast cell types were recognised to be heterogeneous and in the rat there are two types: the connective tissue type represented by the peritoneal mast cell; and the connective tissue type represented by the bone marrow derived mast cell. Before our studies commenced, rat mucosal mast cells were thought to possess only a K-selective inwardly rectifying (IR_k) current in the resting state. In our studies the rat bone marrow cells were used as a model for the mucosal mast cell type and whole-cell currents were recorded with the perforated amphotericin B patch-technique (Hill, Martin and Miller, 1996a; 1996b; 1996c). An inwardly rectifying K current was recognized that was activated by hyperpolarizing membrane potential steps and an outwardly rectifying Cl current that was activated by positive membrane potentials. This outwardly rectifying current was more frequently observed in cell that had been warmed above $25C^0$ and when the integrity of the cell cytoplasm was preserved by using the perforated-patch technique. It was seen less frequently with the conventional

whole-cell technique. The outwardly rectifying Cl current was also seen in peritoneal mast cells when recorded from with the perforated-patch technique and when the temperature was raised above $25C^0$. The suggested function of the outwardly rectifying current was i) to regulate the resting membrane potential and ii) to counteract the depolarization of the cell during degranulation, thus maintaining the driving force for Ca entry. It follows from the second suggested function that pharmacological antagonism of the Cl current would antagonize the repolarization process required for the entry of Ca and degranulation: the effect of Cl channel block would then be to limit degranulation. The blocking of degranulation with Cl channel blockers offers one novel approach to the control of inappropriate degranulation that occurs with allergic reactions.

REFERENCES

6.1. Bland , K. P., Bountra, C., Georgiou, P., House., C. R., and Martin, R. J. (1984). Single-channel currents in fertilised mouse eggs. *J. Physiol.* **353,** 84p.

6.2. Bountra, C. and Martin, R J. (1987). Single-channel currents from Zona-free hamster eggs. *Quarterly Journal of Experimental Physiology* **72**, 483-492.

6.3. Ginsborg, B L, Martin, R J, and Patmore, L. (1987). On the electrical properties of a human neuroblastoma cell-line (IMR-32). *Journal of Physiology.* **386,** 111P.

6.4. Ginsborg, B. L., Martin R. J. and Patmore, L. (1991). On the inward and outward voltage-activated currents of the human neuroblastoma cell line (IMR-32). *Journal of Physiology*. **434,** 121-149.

6.5. Hill, P. B., Martin, R. J. and Miller, H. R. P. (1996a). Effects of temperature and cytoplasmic disruption on whole-cell membrane currents of rat bone marrow-derived mast cells. *Journal of Physiology* **491P** 90.

6.6. Hill, P. B., Martin, R. J. and Miller, H. R. P. (1996b). A comparison of whole-cell currents in mucosal and connective tissue rat mast cells. *Journal of Physiology*. **495P**. 84p.

6.7. Hill, P. B., Martin, R. J., Miller, H. R. P. (1996c). Characterisation of whole-cell currents in mucosal and connective tissue rat mast cells using amphotericin-B-perforated patches and temperature control. *European Journal of Physiology.* **432.** 986-994.

SECTION 7: REVIEWS, BOOK CHAPTERS and BOOKS

The work carried out in these experiment has also been presented in reviews suitable for postgraduates (Martin *et al.,* 1996; Martin, 1997a and b) and undergraduates (Martin, 1985a; 1985b; 1985c; 1985d; 1985f; 1985g; Martin 1988a and Martin 1985g). The aim of the reviews was simply to further disseminate the result of the studies and to put them in context with the work of others.

REFERENCES

7.1. Martin, R.J., Valkanov, M.A., Dale, M.V.E, Robertson, A.R. and Murray, I. (1996) Electrophysiology of *Ascaris* muscle and anti-nematodal drug action. *Parasitology* **113S.** S137-S156.

7.2. Martin, R.J. (1997a). Modes of action of Anthelmintic Drugs. *British Veterinary Journal.* (In Press)

7.3. Martin, R.J. Robertson, A. P. and Bjorn, H. (1997b). Target sites of anthelmintics. *Parasitology.* **114S.** (In Press).

8.1.1. Martin, R. J. (1985a). Depressants of the central nervous system; narcotics, anticonvulsants, analgesics. p130-155. In: *Introduction to Veterinary Pharmacology* Ed: Alexander F. A., Longman, 1985.

8.1.2. Martin, R. J. (1985b). Depressants of the central nervous system; General anaesthetics. p156-173. In: *Introduction to Veterinary* Pharmacology. Ed: Alexander F. A., Longman, 1985.

8.1.3. Martin, R. J. (1985c). Stimulants of the central nervous system. p174-179. In: *Introduction to Veterinary Pharmacology.* Ed: Alexander F. A., Longman, 1985.

8.1.4. Martin, R. J. (1985d). Local analgesics agents. p180-184. In: *Introduction to Veterinary Pharmacology.* Ed: Alexander F. A, Longman, 1985.

8.1.5. Martin, R. J. (1985e). Drugs acting on the heart. p203-211. In: Introduction to Veterinary Pharmacology. Ed: Alexander F A, Longman, 1985.

8.1.6. Martin, R. J. (1985f). Chemotherapy of helminth infections: Taeniacides. p347-354. In: *Introduction to Veterinary Pharmacology.* Ed: Alexander F A Longman, 1985.

8.1.7. Martin, R. J. (1985g). Chemotherapy of helminth infections: Nematocides, Fasciolacides. In: *Introduction to Veterinary Pharmacology*: Ed: Alexander F A Longman, 1985.

9.1. Martin, R J. (1988). ***Small Animal Therapeutics***. Wright, Bristol, London and Boston.

9.1.1. Chapter I: General principles of drug distribution and dosage. p1-19.
9.1.2. Chapter II: Antibiotics. p20-50.
9.1.3. Chapter III: Glucocorticoids. p51-66.
9.1.4. Chapter IV: Vaccination. p67-79.
9.1.5. Chapter V: Analgesia. p80-90.
9.1.6. Chapter VI: Tranquilizers, sedatives, anaesthetics and local anaesthetics. 91-111.
9.1.7. Chapter VII: Epilepsy. p112-118.
9.1.8. Chapter VIII: Endoparasite therapeutics. p119-128.
9.1.9. Chapter IX: Ectoparasite therapeutics. p129-145.
9.1.10. Chapter X: Fluid therapy. p146-158.
9.1.11. Chapter XI: The gastrointestinal tract. p159-175.
9.1.12. Chapter XII: The cardiovascular system. p176-193.
9.1.13. Chapter XIII: The respiratory tract. p194-204.
9.1.14. Chapter XIV: The reproductive system. p205-217.
9.1.15. Chapter XV: The urinary tract. p218-234.
9.1.16. Chapter XVI: The endocrine system. p235-249.
9.1.17. Chapter XVII: The eye. p250-264.
9.1.18. Chapter XVIII: Cancer chemotherapy. p265-274.
9.1.19. Chapter XIX: Vitamins and minerals. p275-287.
9.1.20. Chapter XX: Poisons. p288-303.
9.1.21. Chapter XXI: The law and medicines. p304-312.

9.2. Martin R.J. (1991) ***Terapeutica de pequenos animales***. Interamericana McGraw-Hill. Madrid, pp1-280.

9.2.1. Capitulo 1I: Principios generales de la distibution y dosification de farmacos. p1-19.
9.2.2. Capitulo 2: Antibioticos. p19-44.
9.2.3. Capitulo 3: Glucocorticoids. p45-58.
9.2.4. Capitulo 4: Vacunacion. p59-70.
9.2.5. Capitulo 5: Analgesia. p71-80.
9.2.6. Capitulo 6: Tranquilizantes, sedantes, y anestesicos y locales. p81-98.
9.2.7. Capitulo 7: Epilepsia. p99-104.
9.2. 8. Capitulo 8: Terapeutica frente a endoparasitos. p105-114.
9.2. 9. Capitulo 9: Terapeutica frente a ectoparasitos. p115-1128.
9.2.10. Capitulo 10: Sueroterapia. p129-140.
9.2.11. Capitulo 11: El aparato gastrointestinal. p141-154.
9.2.12. Capitulo 12: El sistema cardiovascular. p155-170.
9.2.13. Capitulo 13: El aparato respiratorio. p171-180.
9.2.14. Capitulo 14: El sistema reproductor. p181-192.
9.2.15. Capitulo 15: El aparato urinario. p193-206.
9.2.16. Capitulo 16: El sistema endocrino. p207-218.
9.2.17. Capitulo 17: El ojo. p219-232.
9.2.18. Capitulo 18: Quimioterapia del Cancer. p233-242.
9.2.19. Capitulo 19: Vitaminas y minerales. p243-245.
9.2.20. Capitulo 20: Toxicos. p255-267.

1 μg) contracted rabbit aorta, dog saphenous vein and guinea-pig lung strip, but had little or no effect on the other preparations.

PGH_2 was a potent agonist on all the preparations examined; these effects, may have been mediated either directly or indirectly by conversion to other biologically active prostanoids (Bunting, Gryglewski, Moncada & Vane, 1976). In contrast TXA_2 and U-46619 were potent agonists on rabbit aorta, dog saphenous vein and guinea-pig lung only. U-46619 therefore appears to be a selective TXA_2-like agonist; if this is so it could prove to be valuable in the study of the biological actions of TXA_2 since, unlike TXA_2, U-46619 is stable.

PGH_2 and sheep platelet microsomes were supplied by Dr. P.J. McCabe of the Biochemistry Department, Glaxo Group Research, Ware Division.

References

VAN ALPHEN, G.W.H.M. & ANGEL, M.A. (1975). Activity of prostaglandin E, F, A and B on sphincter, dilator and ciliary muscle preparations of the cat eye. *Prostaglandins*, **9**, 157–166.

APPERLEY, EIRA, HUMPHREY, P.P.A. & LEVY, G.P. (1976). Receptors for 5-hydroxytryptamine and noradrenaline in rabbit isolated ear artery and aorta. *Br. J. Pharmac.*, **58**, 211–221.

BUNDY, G.L. (1975). The synthesis of prostaglandin endoperoxide analogs. *Tetrahedron Lett.*, **24**, 1957–1960.

BUNTING, S., GRYGLEWSKI, R., MONCADA, S. & VANE, J.R. (1976). Arterial walls generate from prostaglandin endoperoxides a substance (prostaglandin X) which relaxes strips of mesenteric and coeliac arteries and inhibits platelet aggregation. *Prostaglandins*, **12**, 897–911.

FURCHGOTT, R.F. & BHADRAKOM, S. (1953). Reactions of rabbit aorta to epinephrine, isopropylarterenol, sodium nitrite and other drugs. *J. Pharmac. exp. Ther.*, **108**, 129–143.

GORMAN, R.R., SUN, F.F., MILLER, O.V. & JOHNSON, R.A. (1977). Prostaglandins H_1 and H_2. Convenient biochemical synthesis and isolation. Further biological and spectroscopic characterisation. *Prostaglandins*, **13**, 1043–105.

HAMBERG, M., SVENSSON, J. & SAMUELSSON, B. (1975). Thromboxanes: a new group of biologically active compounds derived from prostaglandin endoperoxides. *Proc. nat. Acad. Sci. USA*, **72**, 2994–2998.

HORTON, E.W. & MAIN, I.H.M. (1963). A comparison of the actions of prostaglandin $F_2\alpha$ and E_1 on smooth muscle. *Br. J. Pharmac. Chemother.*, **24**, 470–476.

HUMPHREY, P.P.A. (1978). The effects of Uptake$_1$ on α-adrenoceptor antagonist potency in dog saphenous vein. *Br. J. Pharmac.*, **63**, 665–669.

LULICH, K.M., MITCHELL, H.W. & SPARROW, M.P. (1976). The cat lung strip as an *in vitro* preparation of peripheral airways: a comparison of β-adrenoceptor agonists, autacoids and anaphylactic challenge on the lung strip and trachea. *Br. J. Pharmac.*, **58**, 71–79.

MALMSTEN, C. (1976). Some biological effects of prostaglandin endoperoxide analogs. *Life Sci.*, **18**, 169–176.

MONCADA, S., BUNTING, S., MULLANE, K., THOROGOOD, P., VANE, J.R., RAZ, A. & NEEDLEMAN, P. (1977). Imidazole: A selective inhibitor of thromboxane synthetase. *Prostaglandins*, **13**, 611–618.

VANE, J.R. (1957). A sensitive method for the assay of 5-hydroxytryptamine. *Br. J. Pharmac. Chemother.*, **12**, 344–349.

VANE, J.R. (1964). The use of isolated organs for detecting active substances in the circulating blood. *Br. J. Pharmac. Chemother.*, **23**, 360–37.

The effect of GABA on the conductance of Ascar' uscle

R.J. MARTIN (introduced by F. ALEXANDER)

Department of Veterinary Pharmacology, Royal (Dick) School of Veterinary Studies, University of Edinburgh

Del Castillo, De Mello & Morales (1964a) have described the hyperpolarizing effect of γ-aminobutyric acid (GABA) on the membrane potential of *Ascaris* muscle. The aim of the present experiments was to describe the effect of GABA on the conductance of *Ascaris* muscle.

Recordings were made from the bag region of the *Ascaris* muscle cells using two potassium-acetate filled microelectrodes for separate current injection and voltage recording. The preparation was perfused constantly with cool (22°C) Ringer (Del Castillo *et al.*, 1964b) to abolish spontaneous depolarizations of the pacemaker and permit the recording of stable resting potentials. The effect on the input conductance was measured from the slope of the current voltage plots observed in the different concentrations of GABA.

The resting membrane potential recorded in the bag region was 31 ± 1 mV, mean ± s.e. mean ($n = 17$). The resting conductance was 2.4 ± 0.2 M Ω^{-1}, mean ± s.e. mean ($n = 12$). The application of GABA in concentrations greater than 3 μM was followed by a hyperpolarizing potential and an increase in input conductance. These effects were reversible and dose-dependant. Conductance log dose-response relationships were obtained from 6 preparations. The dose-response relationships were described by a form of the Hill equation (1), where Δg is the conductance change produced by the concentration of GABA, A.

$$\Delta g = \frac{\Delta g_{max}}{1 + \left(\frac{K_{\frac{1}{2}}}{A}\right)^{n_H}} \qquad (1)$$

$K_{\frac{1}{2}}$ is the concentration of GABA producing the half maximum conductance change, Δg_{max} is the maximum conductance change, and n_H is the Hill coefficient. A least squares estimate of the values of n_H, $K_{\frac{1}{2}}$ and Δg_{max} was made using an iterative procedure for each of the 6 bags. The size of the responses did not appear to depend upon the location of the bags. The mean ± s.e. mean of n_H was 3.1 ± 0.6 ($n = 6$). The mean ± s.e. mean of $K_{\frac{1}{2}}$ was 18 ± 3 μM ($n = 6$). The mean ± s.e. mean of Δg_{max} was 4.5 ± 0.9 M Ω^{-1} ($n = 6$).

It was also possible to estimate the reversal potentials of the GABA responses by extrapolation. The mean ± s.e. mean was 29.5 ± 2 mV ($n = 7$) more negative than the resting potential at 10^{-5} M GABA.

References

DEL CASTILLO, J., DE MELLO, W.C., & MORALES, T. (1964a). Inhibitory action of γ-aminobutyric acid (GABA) on Ascaris muscle. *Experientia*, **20**, 141–145.

DEL CASTILLO, J., DE MELLO, W. C. & MORALES, T. (1964b). Mechanism of the paralysing action of piperazine on Ascaris muscle. *Br. J. Pharmac.*, **22**, 463–477.

Induction of analgesia and morphine potentiation by irreversible inhibitors of GABA-transaminase

W.R. BUCKETT

Centre de Recherche Merrell International, 16, rue d'Ankara 67084-Strasbourg Cedex, France

Attempts have been made to ascribe a role for GABA in analgesia, but the results have been controversial. For example, the GABA agonist muscimol enhances morphine analgesia (Biggio, Della Bella, Frigeni & Guidotti, 1977), whereas the GABA-transaminase inhibitor aminooxyacetic acid has been reported to antagonize morphine analgesia (Ho, Loh & Way, 1976). The recent availability of two irreversible inhibitors of GABA-transaminase, γ-vinyl GABA (GVG; DL-4-aminohex-5-enoic acid; RMI 71754) and γ-acetylenic GABA (GAG; DL-4-aminohex-5-ynoic acid; RMI 71645) led to this study of their analgesic properties, their effects upon morphine analgesia and their utilization during morphine-withdrawal to detect any change in sensitivity of the GABA system.

Analgesia was tested using groups of ten CD_1 mice (20–25 g) on a 52°C hot-plate. GVG (ED_{50} 770 (670–870) mg/kg i.p.) and GAG (ED_{50} 51 (46–56) mg/kg i.p.) were active, but at higher doses than morphine HCl (ED_{50} 6.9 (6.1–7.7) mg/kg s.c.). Analgesia was maximal 4 to 6 h after GVG or GAG (ED_{50} dose i.p.), correlating with the rise in mouse brain GABA levels (Jung *et al.*, 1977a, b). Analgesia could be demonstrated with the (+)-isomer of GVG, the form active as a GABA-transaminase inhibitor; none was detectable after the inactive (−)-isomer of GVG up to 800 mg/kg i.p. GVG and GAG-induced analgesia was not preventable by naloxone HCl (1 mg kg), nor did these compounds inhibit (up to 10^{-4} M) the contractions of the isolated transmurally-stimulated guinea pig ileum, indicating lack of opioid involvement. In the rat, analgesia was shown using the tail-stimulation test (Hoffmeister, 1968) using groups of six male Sprague-Dawley rats (140–170 g). Although GVG (ED_{50} 1100 (960–1240) mg/kg i.p.) and GAG (ED_{50} 61 (50–72) mg/kg i.p.) were less active than morphine HCl (ED_{50} 1.60 (1.40–1.90) mg/kg s.c.), they also inhibited both vocalization and vocalization after-discharge.

The analgesic activity of morphine HCl in mice on the 56°C hot-plate was potentiated by a factor of three after GVG (800 mg/kg i.p.), with GVG itself being inactive. Lower doses of GVG did not potentiate morphine, suggesting a large increase in GABA levels (Jung *et al.*, 1977b) is necessary for this action. In rats withdrawn from morphine (60–840 mg/kg i.p. through 14 days), the hypothermia elicited by GVG (800 mg/kg i.p.) and GAG (100 mg/kg i.p.) did not differ significantly from that in controls, indicating that no change in sensitivity in the GABA system occurs during withdrawal.

It is concluded that the administration of GVG and GAG can result in analgesia, with a temporal relationship between analgesia and increased brain GABA levels. Only the GVG isomer which is active as a GABA-transaminase inhibitor has analgesic properties. There is enhancement of morphine analgesia by elevated GABA levels, although changes in sensitivity of the GABA system on morphine-withdrawal are not evident. These results support a causal relationship between increased brain GABA levels and analgesia, although the active sites remain to be explored.

Br. J. Pharmac. (1980), **71**, 99–106

THE EFFECT OF γ-AMINOBUTYRIC ACID ON THE INPUT CONDUCTANCE AND MEMBRANE POTENTIAL OF ASCARIS MUSCLE

R.J. MARTIN

Department of Veterinary Pharmacology, Royal (Dick) School of Veterinary Studies, University of Edinburgh, Edinburgh EH9 1QH

1 Twin intracellular recordings were made from the bag region of *Ascaris* muscle in order to make conductance measurements. The preparation was bathed in a cool (22°C) Ringer solution to abolish the large spontaneous depolarizing potentials and to improve stability for recording.

2 The resting membrane potential was -31 ± 1 mV, mean ± s.e. mean ($n = 17$). The current–voltage plots were linear in the hyperpolarizing direction but showed evidence of delayed rectification during the application of depolarizing currents. The input conductance of the bag was measured from the slope of these plots during the application of hyperpolarizing current. The resting conductance of the bags was 2.4 ± 0.2 μS, mean ± s.e. mean ($n = 12$).

3 When the preparation was perfused with γ-aminobutyric acid (GABA) in concentrations greater than 3 μM, a dose-dependent increase in conductance associated with a hyperpolarizing potential was recorded. The log dose-response relationship obtained from 6 preparations was sigmoidal and had an ED_{50} of 13 μM.

4 When Cl^- in the Ringer was replaced by SO_4^{2-}, the GABA-induced conductance changes decreased and were associated with depolarizing potentials.

5 Voltage responses were recorded in the bag region during the iontophoretic application of GABA to different regions of the muscle cell. The largest responses were recorded when GABA was applied to the bag region. Smaller responses were recorded when GABA was applied to the arms and syncytial regions. The responses of the bags were dose dependent and were antagonized by bath applied picrotoxin.

6 An extrapolation method using 10^{-5} M GABA suggested that the GABA reversal potential was about 30 mV more negative than the resting membrane potential. This was confirmed by means of a two microelectrode voltage clamp technique. The reversal potential was thus estimated as -61.2 ± 2.2 mV mean ± s.e. mean ($n = 27$).

Introduction

Ascaris suum is a worm-like intestinal parasite of the pig. The muscle cells of *Ascaris* are composed of three parts called, the spindle, the bag and the arm (Figure 1a). The spindle is the elongated fibrillar part which is the contractile region. It lies under the hypodermis and is arranged longitudinally. The nucleus of the cell is located in the bag region of the muscle. The bag is balloon shaped, about 200 μm in diameter and fills the body cavity. The arm, a thin process, reaches transversely from the bag to one of the longitudinally running nerve cords. The arms come together to form a syncytium over the nerve cord and are electrically coupled in this region (De Bell, Del Castillo & Sanchez, 1963). Spontaneous depolarizing potentials of 2 to 10 mV amplitude superimposed on a resting potential of −30 mV can be recorded in the bag region (Jarman, 1959). Acetylcholine depolarizes these cells (Del Castillo, De Mello & Morales, 1963), while piperazine and γ-aminobutyric acid (GABA) hyperpolarize them (Del Castillo, De Mello & Morales 1964a, b). The inhibitory receptors responsible for the hyperpolarization were believed to be located exclusively at the syncytium because hyperpolarizing responses to bath applied piperazine were reported to be largest in bags located near the nerve cord. It was also reported that iontophoretic application of piperazine only produced responses when applied near the region of the syncytium (Del Castillo *et al.*, 1964a). However, Brading & Caldwell (1971) sectioned the arms of muscle cells and still recorded GABA-induced

07-1188/80/130099-08 $01.00

© Macmillan Publishers Ltd 1980

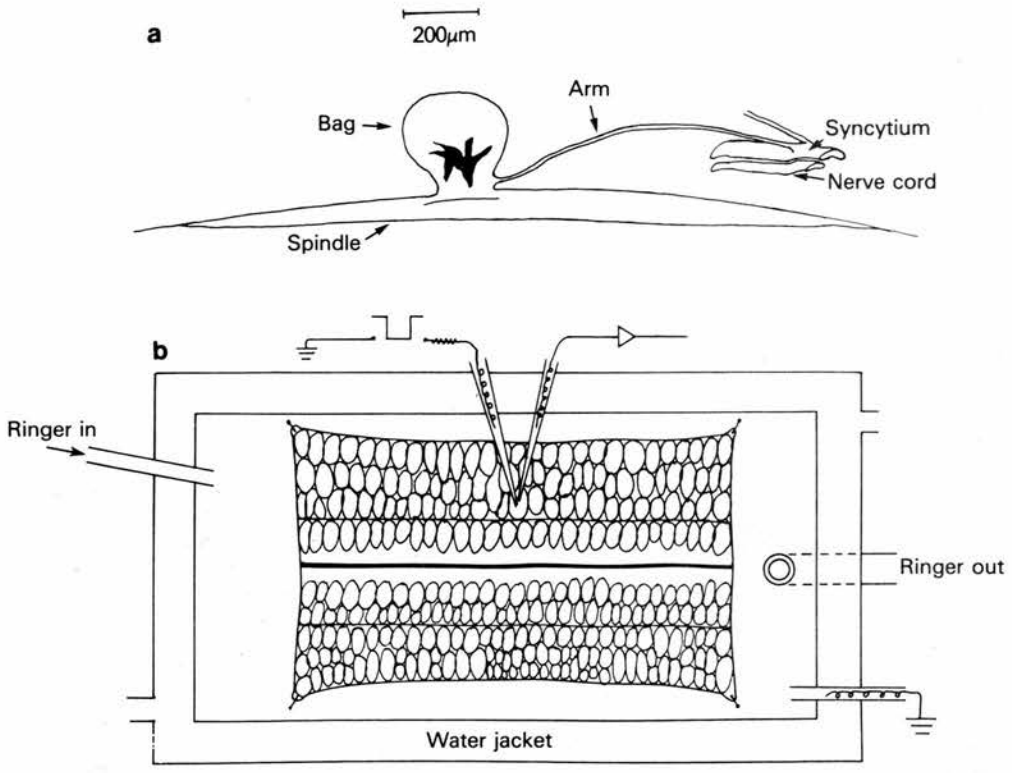


Figure 1 (a) Diagram of the *Ascaris* muscle cell illustrating its anatomical features. (b) Experimental chamber and preparation. A section of *Ascaris* is pinned, cuticle side down, onto Sylgard in a chamber containing 1.5 ml Ringer solution and perfused at a rate of 6 ml/min. The chamber is fitted with a water jacket to maintain the preparation at 22°C. Two potassium acetate filled micropipettes are illustrated, inserted into the bag region of the muscle cell. One pipette was used for current injection, the other was used for recording voltage responses. During the iontophoresis of γ-aminobutyric acid to different parts of the muscle cell, one pipette was used for iontophoresis and one was placed in the bag for recording voltage responses. During the voltage clamp-experiments a third GABA filled pipette was placed over the bag, between the voltage and current electrodes.

hyperpolarizations in the bags. They suggested that the bags may also possess GABA receptors. These studies have been reviewed by Gerschenfeld (1973). The present paper describes the effects of bath-applied GABA on the conductance of single muscle cells and the results of GABA iontophoretic experiments which show that there are inhibitory receptors sensitive to GABA located on the bag region of the muscle cells. A preliminary account of some of these observations has been presented to the British Pharmacological Society (Martin 1980).

Methods

Specimens of *Ascaris suum* were obtained from the local slaughter house and transported to the laboratory in warm Locke solution. The worms were then placed in fresh Locke solution which was replaced daily and maintained at 37°C in a water bath. Experience with different media suggested that this solution was most satisfactory for maintaining the *Ascaris* in a healthy condition. The *Ascaris* survived for over 1 week under these conditions but were used for experiments within 4 days.

In most experiments a cylindrical section of the worm, about 2 cm long was obtained from 6 cm behind the head. These sections were cut along the lateral line and the intestine removed. The preparation was then pinned, cuticle side down, onto Sylgard in a chamber containing 1.5 ml of Ringer solution (Figure 1b). The chamber was surrounded by a water jacket which maintained the preparation at about 22°C. A caudal 2 cm section was used during the iontophoretic experiments because the anatomy of the muscle in this region more readily permitted the application of GABA to different regions of the muscle cell.

The preparation was perfused at a constant rate of 6 ml/min with Ringer solution. This rate was temporarily increased during the initial application of GABA and during washing. The Ringer contained (mM): NaCl 135, KCl 3.0, $CaCl_2$ 3.0, $MgCl_2$ 15.7 and glucose 3, buffered to pH 7.6 with 5mM Tris-maleate. Although this solution contains higher Cl^- than *Ascaris* haemolymph (Brading & Caldwell, 1964), it has proved satisfactory for electrical recording. In experiments on the effects of the removal of Cl^-, Cl^- salts were replaced by SO_4^{2-} salts and the osmolarity maintained by the addition of sucrose.

Micropipettes were placed under the visual control with a dissecting microscope and micromanipulators. For conductance measurements, two potassium acetate (2 M) filled micropipettes with resistances of 15 to 25 MΩ were used, one for recording voltage and the other for current injection.

They were connected via Ag/AgCl wires to high input impedance preamplifiers. Similar micropipettes were filled with 2 M GABA, pH 2.5, for the iontophoresis experiments. GABA was then applied as a cation by a micro-iontophoresis programmer, Model 160 (W-P instruments Inc.). Retaining currents of about 10 nA were used. A 1GΩ resistor was used as a constant current source for the current micropipette, while the current flowing was measured from the voltage applied to the 1GΩ resistor. The bath electrode was an Agar-KCl bridge. In order to estimate the GABA reversal potentials directly, a two microelectrode voltage clamp technique was used with the iontophoretic application of GABA to the bag. The micropipettes were made and filled as described previously except that the current micropipettes had resistances of 4 to 6 MΩ. The gain of the control amplifier was usually set at 1000. The current injected into the cell was measured from the voltage drop across a 500 KΩ resistor connected in series with the current electrode. No correction was made for the resistance (Rs) in series with the membrane capacity. Rs is partly due to the experimental bath and agar bridge. It was estimated to be approximately 10 KΩ, so that when a transmembrane current (Im) of 200 nA was passed a potential error of 2 mV (Im·Rs) in the voltage recording would have been produced. A maximum of 200 nA was passed as the holding current when clamping the bag at −80 mV (it was uaually much less at −80 mV). The efficiency of the clamp was tested by placing a second voltage measuring electrode in the bag on the opposite side to the first. The difference in potential recorded by these two pipettes was less than 5% in preparations undamaged by the electrode penetration. Voltage clamp studies were only carried out on bags with resting input conductances less than 4 μS.

The drugs used were GABA (Sigma) and picrotoxin (Sigma). GABA was applied to the bath via the Ringer during experiments on conductance changes. Picrotoxin was applied in a similar manner during the iontophoresis experiments.

Responses were monitored on a cathode ray oscilloscope and on a 2 channel pen recorder.

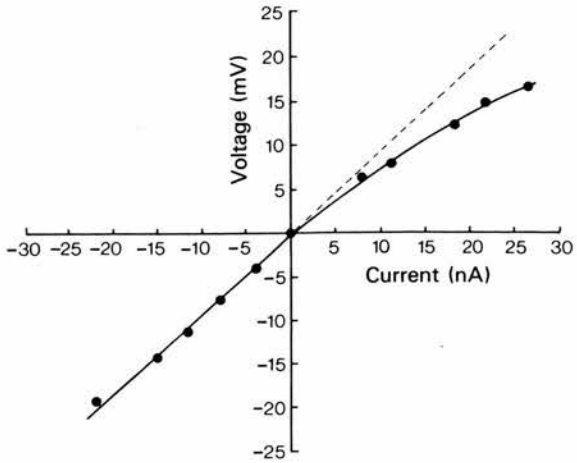


Figure 2 Current-voltage relationship observed in the bag region. Ordinate scale: voltage responses; abscissa scale; transmembrane current. The relationship is linear during the application of hyperpolarizing current but shows evidence of delayed rectification during the application of depolarizing current.

Results

The experiments described here were conducted on muscle cells of 50 preparations. At temperatures of 37°C, large spontaneous depolarizing potentials associated with pacemaker activity at the syncytium were recorded in the bag region. The large depolarizing potentials were therefore abolished by cooling the preparation to 22°C. This procedure had the added advantage of improving the stability of the muscle preparation. Under these conditions the membrane potential was stable and measured -31 ± 1 mV, mean ± s.e. mean ($n = 17$).

To determine current-voltage relationships, two micropipettes were placed in the bag, one for current injection and one for recording voltage responses (Figure 2). These plots showed evidence of delayed rectification when depolarizing currents were injected but there was a linear current-voltage relationship when hyperpolarizing currents were injected. The time constant of the bag was about 6 ms. The input conductance was therefore measured from the slope of the current-voltage plots obtained during the injection of hyperpolarizing current pulses of 250 ms duration. The resting input conductance of the bags measured 2.4 ± 0.2 μS, mean ± s.e. mean ($n = 12$).

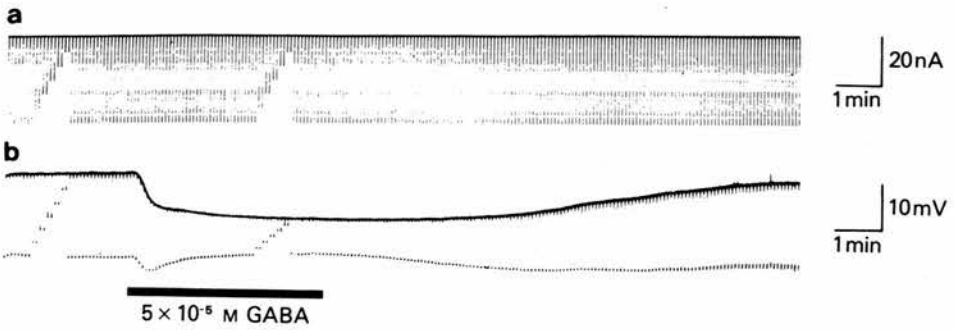


Figure 3 Effect of γ-aminobutyric acid (GABA) on input conductance. The top trace (a) represents hyperpolarizing current pulses of 250 ms (downward deflections) duration; (b) represents the hyperpolarizing voltage responses (downward deflections). The application of 5×10^{-5} M GABA increased the resting input conductance from 2.1 μS to 4.9 μS.

γ-Aminobutyric acid-induced conductance changes

Bath-applied GABA in concentrations greater than 3 μM caused a reversible increase in conductance, which was associated with a hyperpolarizing potential (Figure 3). Various concentrations of GABA were applied separately in ascending concentrations to 6 cells from 6 preparations and ΔG measured in bags located at different distances from the nerve cord. The dose-dependent nature of the response is illustrated by the sigmoidal log dose-response relationship shown in Figure 4. The concentration of GABA producing the half maximal effect (the ED_{50}) was 13 μM. No consistent signs of desensitization were observed even during the application of high doses of GABA.

Ionic mechanism

Cl^- is known to be involved in the hyperpolarizing response to piperazine and GABA (Del Castillo *et al.*, 1964a; Brading & Caldwell, 1971). The effect of low Cl^- on the GABA conductances was tested in 5 experiments. The resting input conductances of the bags decreased slightly in the low Cl^- Ringer, indicating a small Cl^- permeability in the absence of GABA. The GABA-induced conductance changes decreased when the preparations were perfused with low Cl^- Ringer in all experiments and were associated with depolarizing potentials. These GABA-induced conductance changes continued to decline in the low Cl^- Ringer over a period of 20 to 30 min. For example, in one experiment 2×10^{-5}M GABA produced a change in input conductance of 3.2 μS in normal Ringer but after perfusing the preparation with low Cl^- Ringer solution for 8 min, 2×10^{-5} M GABA produced a smaller conductance change of 2.8 μS. After 17 min the GABA-induced conductance change fell to 0.8 μS. The GABA conductances returned to near control levels after perfusing the preparations with the normal

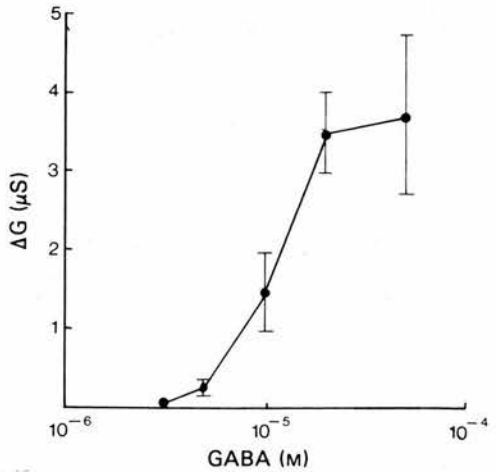


Figure 4 The log dose-response relationship for the change in input conductance of the bags produced by different molar concentrations of γ-aminobutyric acid (GABA). This relationship was obtained from 6 preparations and each point represents the mean of 5 or 6 observations; vertical lines show s.e. means. The ED_{50} was 13 μM.

Ringer. In the crayfish, Takeuchi & Takeuchi (1967) attributed the progressive reduction of GABA conductances in low Cl^- Ringer to the gradual removal of intracellular Cl^-.

γ-Aminobutyric acid iontophoresis

The bath-applied GABA experiments showed that large conductance changes could be observed in bags located well away from the nerve cord. It seemed unlikely that these conductance changes could be explained by inhibitory receptors exclusively located at the syncytium as suggested by Del Castillo *et al.* (1964a). The resistance of the arm should have limited

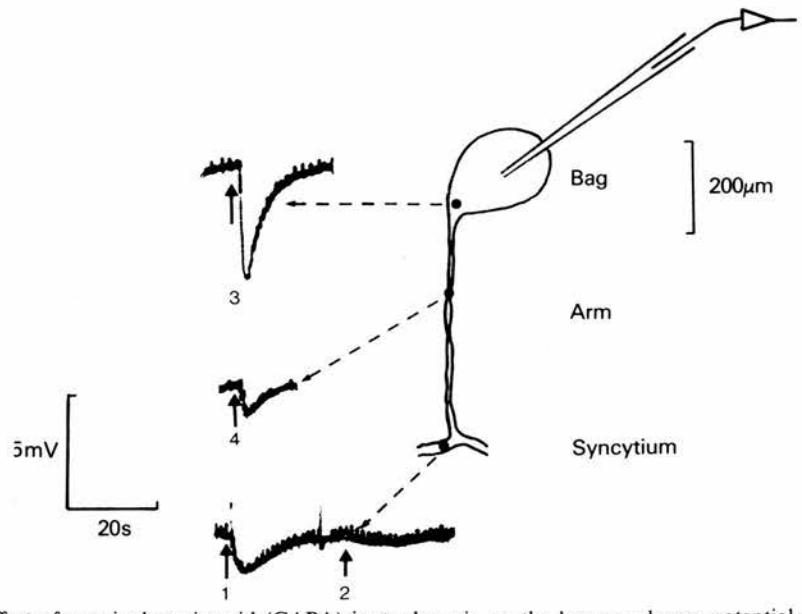


Figure 5 Effect of γ-aminobutyric acid (GABA) iontophoresis on the bag membrane potential when GABA is applied to different regions of the muscle cell. This preparation was made from a caudal section of *Ascaris*. A standard current pulse of 0.4 μC (at the vertical arrow) was used to deliver GABA to the different regions marked (●). Even though this preparation was at 22°C, small depolarizing potentials were still observed. The effect of GABA release over the syncytium was tested first (1). The GABA pipette was raised 50 μm but then only caused a small response (2). Application of GABA to the bag produced the largest response (3). No response to GABA iontophoresis was observed when the GABA pipette was placed 100 μm from the edge of the bag, except for small responses observed over the arm (4).

the size of the conductance changes observed in bags located at a distance from the nerve cord. GABA was therefore applied iontophoretically to the bags to detect the presence of GABA receptors on the bag. When GABA was released from a micropipette placed over the bags of muscle cells, a dose-dependent hyperpolarization was invariably recorded even when the bags were located 2 mm from the nerve cords.

Figure 5 illustrates the results of a typical experiment in which GABA was applied to different regions of the muscle cell of a caudal section of *Ascaris*. In this particular experiment a standard current pulse of 0.4 μC was used to deliver the GABA to the different regions of the muscle cell. The response at the syncytium was tested first (Figure 5 (1)). When the GABA pipette was raised 50 μm only a small response was observed (Figure 5 (2)). The response at the bag was tested next (Figure 5 (3)). Typically it was larger than at the syncytium. No response was observed when the GABA pipette was removed 100 μm from the bag except for small responses over the arm (Figure 5 (4)).

Picrotoxin antagonism

Picrotoxin was used in order to confirm that the above responses were due to the action of GABA and not due to the direct action of the iontophoretic current. The effects of bath-applied picrotoxin were tested on 4 preparations. The results of one of these experiments is illustrated in Figure 6. In all these preparations picrotoxin antagonized the actions of GABA when applied in concentrations of 50 to 500 μM. The antagonism of picrotoxin was dose-dependent but was not easily washed off. The reduction of the slope of the dose-response curves indicated that picrotoxin acted as a non-competitive antagonist.

Reversal potential

Extrapolation of current voltage plots like those shown in Figure 7 using bath-applied 10^{-5}M GABA suggested that the reversal potential was about 30 mV more negative than the resting membrane potential. However, this method of estimating the reversal potential assumes that conductance values are independent of the membrane potential. The reversal potential was therefore estimated directly. GABA was applied iontophoretically to the bag and the potential of the bag altered by means of a two microelectrode voltage clamp system. The results of a typical experiment are shown in Figure 8a and b. It can be seen that the peak of the outward GABA-induced current

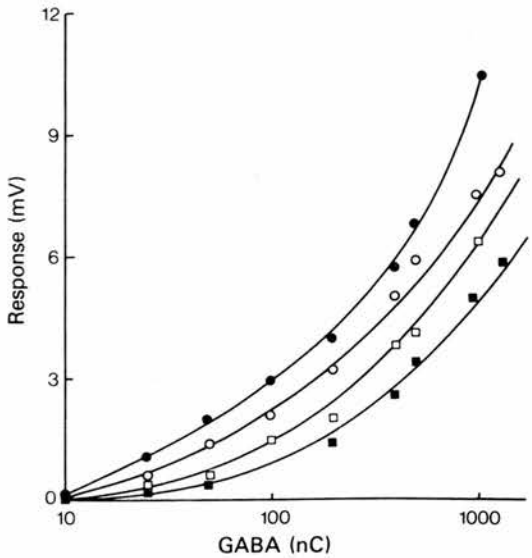


Figure 6 Antagonism of γ-aminobutyric acid (GABA) by picrotoxin. Peak hyperpolarizations recorded in the bag (ordinate scale) are plotted against the iontophoretic current (log scale abscissa). The GABA pipette was placed over the bag. The control responses (●) were observed initially. Picrotoxin 5×10^{-5} M (○) was then applied in the bath and the responses re-determined. Picrotoxin 5×10^{-4} M (■) was then applied and the responses determined. Finally the preparation was washed for 20 min and the responses again determined (□). Picrotoxin antagonized the GABA responses in a dose-dependent manner. The antagonism was only partially reversed by 20 min washing.

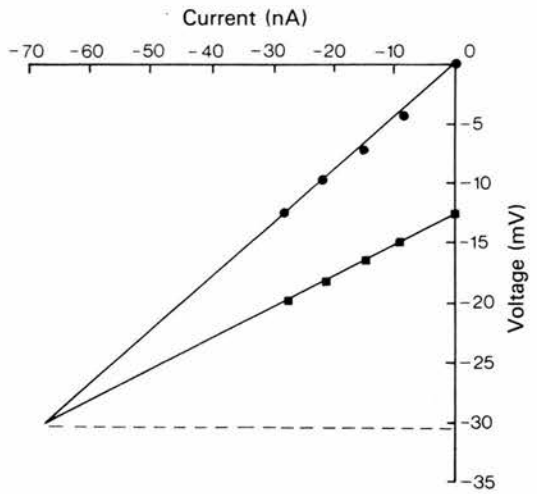


Figure 7 Estimation of the reversal potential by extrapolation. The current-voltage relationships were determined without γ-aminobutyric acid (GABA, ●) and then in the presence of 10^{-5} M GABA (■). The resting membrane potential (−30 mV) was plotted as zero on the ordinate scale with negative potentials indicating hyperpolarization. The hyperpolarizing current is plotted on the abscissa scale. GABA 10^{-5} M hyperpolarized the bag by 13 mV and increased the resting conductance from 2.3 μS to 4.2 μS. The intersection of the two current voltage slopes gives an estimate of 31 mV for the reversal potential.

at −35 mV declines in amplitude as the membrane potential is increased and is reversed in direction near −55 mV. The estimated value of the GABA reversal potential from 27 such experiments was −61.2 mV ± 2.2 mV mean ± s.e. mean. The speed of the response is also interesting since there was several seconds between the iontophoretic pulse and the peak of the GABA current (Figure 8a). This delay occurred even though the GABA pipette was placed directly over the bags and was measured in 27 experiments as 3.6 ± 0.3 s (mean ± s.e. mean).

Discussion

Conductance changes

The experiments described in this paper show that GABA produces a dose-dependent and reversible increase in input conductances associated with a hyperpolarizing potential. The involvement of Cl^- was confirmed by the effect of low Cl^- Ringer on the GABA-induced conductance changes and membrane potential. Brading & Caldwell (1971) have suggested that the main action of GABA may be to inhibit an electrogenic transport system. However, this suggestion was made following an analysis of the membrane potential using KCl filled micropipettes for recording. The inhibition of an electrogenic transport system by GABA does not explain the marked effects of low Cl^- Ringer on the conductance changes, nor the fact that the value (−61.2 ± 2.2 mV) of the reversal potential estimated in the present experiments was close to the value predicted by a Nernst Cl^- electrode (−64.8 mV) with an intracellular Cl^- concentration of 13.7 mM (Brading & Caldwell 1971).

Iontophoresis of γ-aminobutyric acid

The iontophoresis of GABA on the bag region confirmed the presence of inhibitory receptors on the bag. The results contrast with the experiments of Del Castillo *et al.* (1964a) which suggested that there were no inhibitory receptors on the bag. However, they applied piperazine not GABA iontophoretically. Piperazine is less potent (about 100 times) than GABA (Del Castillo *et al.*, 1964b) and may act more slowly (Constanti & Nistri, 1976).

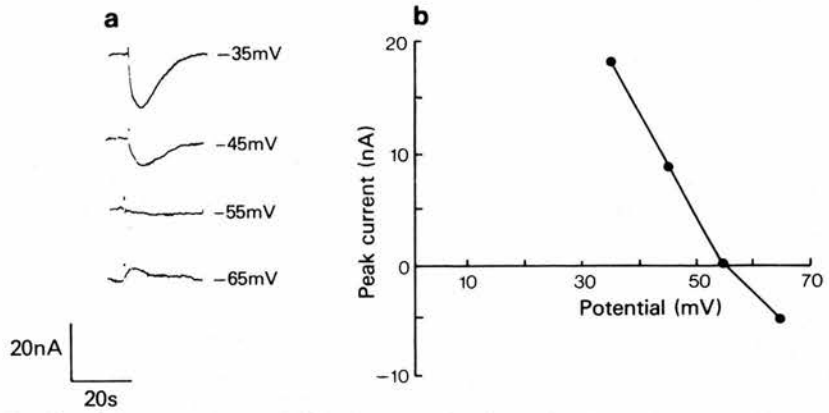


Figure 8 Estimation of the reversal potential by the two microelectrode voltage clamp technique. (a) γ-Aminobutyric acid (GABA) was applied directly over the bag using an iontophoretic current of 1 μA for 500 ms (during the artefact) and the GABA-induced current was observed at different holding potentials. A downward deflection indicates an outward GABA-induced current. Note that the peak of the GABA current occurred several seconds after the application of GABA and that the reversal potential is near −55 mV. (b) Graph of the peak GABA current (positive values indicate an outward current on the ordinate scale) against the membrane potential (positive values on the abscissa scale indicate increased hyperpolarization).

The physiological significance of the presence of GABA receptors on the bag is obscure since it is a region devoid of synapses. However this observation sets no precedent since there are other examples in invertebrates where somatic membranes possess receptors without synapses (Tauc & Gerschenfeld, 1962; Kerkut, Pitman & Walker, 1969). The GABA responses produced by iontophoresis at the syncytium were usually smaller than those produced at the bag. This observation may be explained in part by shielding of inhibitory receptors at the synctium as suggested by Del Castillo *et al.* (1964) as well as the decrement between the syncytium and bag associated with electronic spread.

The slow response following γ-aminobutyric acid iontophoresis

The peak of the GABA-induced voltage or current responses occurred several seconds after the iontophoretic GABA pulse, even though the GABA pipette was placed directly over the bag. The membrane of the bag region of *Ascaris* muscle is covered by several other thin membranes (Ellory, 1967). One explanation for the delay of several seconds between the GABA pulse and the peak of the response might be due to diffusion across this layer. However, without further analysis it is not possible to exclude other factors such as uptake , slow dissociation of GABA from receptors or rate limiting intermediate steps between receptor activation and membrane conductance increases. (Diamond & Roper, 1973).

The author wishes to acknowledge the generous support of the Agricultural Research Council.

References

BRADING, A.F. & CALDWELL, P.C. (1964) The effect of ions on the resting potentials of muscle cells in *Ascaris lumbricoides*. *J. Physiol.*, **173**, 36P.

BRADING A.F. & CALDWELL, P.C. (1971). The resting membrane potential of somatic muscle cells of *Ascaris lumbricoides*. *J. Physiol.*, **217**, 605–624.

CONSTANTI, A. & NISTRI, A. (1976). A comparative study of the action of γ-aminobutyric acid and piperazine on the lobster muscle fibre and the frog spinal cord. *Br. J. Pharmac.* **57**, 347–358.

DE BELL, J., DEL CASTILLO, J. & SANCHEZ, V. (1963). Electrophysiology of the somatic muscle cells of *Ascaris lumbricoides*. *J. Cell. comp. Physiol.*, **62**, 159–177.

DEL CASTILLO, J., DE MELLO, W.C. & MORALES, T., (1963). The physiological role of acetylcholine in the neuromuscular system of *Ascaris lumbricoides*. *Archs. int. Physiol.* **71**, 741–757.

DEL CASTILLO, J., DE MELLO, W.C., & MORALES, T. (1964a). Mechanism of the paralysing action of piperazine on *Ascaris* muscle. *Br. J.. Pharmac.*, **22**, 463–477.

DEL CASTILLO, J., DE MELLO, W.C. & MORALES, T. (1964b). Inhibitory action of γ-aminobutyric acid (GABA) on Ascaris Muscle. *Experientia*, **20**, 145–145.

DIAMOND, J. & ROPER, S. (1973) Analysis of Mauthner cell responses to iontophoretically delivered pulses of GABA, glycine and L-glutamate. *J. Physiol*, **232**, 113–128.

ELLORY, J.C. (1967). Ion movements in muscle cells of *Ascaris lumbricoides. PhD. Thesis, University of Bristol.*

GERSCHENFELD, H.M. (1973). Chemical transmission in invertebrate central nervous systems and neuromuscular junctions. *Physiol. Rev.*, **53**, 1–112.

JARMAN, M., (1959) Electrical activity in the muscle cells of *Ascaris. Nature*, **184**, 1244.

KERKUT, G.A., PITMAN, R.M. & WALKER R.J. (1969). Iontophoretic application of acetylcholine and GABA onto insect central neurones. *Comp. Biochem. Physiol.*, **31**, 611–633.

MARTIN, R.J. (1980). The effect of GABA on the conductance of Ascarid muscle. *Br. J. Pharmac.*, **68**, 128–129 p.

TAKEUCHI, A. & TAKEUCHI, N. (1967). Anion permeability of the inhibitory post-synaptic membrane of the crayfish neuromuscular junction. *J. Physiol.* **191**, 575–590.

TAUC, L. & GERSCHENFELD, H.M., (1962). A cholinergic mechanism of inhibitory synaptic transmission in a molluscan nervous system. *J. Neurophysiol.*, **25**, 236–262.

(Received October 9, 1979
Revised February 11, 1980.)

ne voltage sensitivity of GABA antagonists at e bag region of Ascaris muscle

J. MARTIN (introduced by F. ALEXANDER)

partment of Veterinary Pharmacology, Royal (Dick) hool of Veterinary Studies, University of Edinburgh

ne voltage sensitive blocking action of a number of olinoceptor antagonists has been described (e.g. scher, Large & Rang, 1979). This report describes me observations on the voltage sensitivity of the ABA block produced by bicuculline, benzylpenicillin d picrotoxin.

Recordings were made from the bag region of *scaris suum* muscle using a 2 microelectrode voltage mp technique. The voltage recording pipette was ed with 4 M K acetate (adjusted to pH 7.6), while e current injection pipette was filled with 0.5 M $_2SO_4$. GABA was applied iontophoretically to the g with a third pipette placed over the bag between e other two pipettes. The preparation was perfused nstantly with cool (25°C) Ringer (NaCl, 135 mM; Cl, 3.0 mM; $CaCl_2$, 3.0 mM; $MgCl_2$, 15.7 mM; glu-se 3 mM; buffered to pH 7.6 with 5 mM tris-aleate). This abolished spontaneous depolarizing tentials.

Iontophoresis of GABA produced an outward flow current when the bag was clamped near its resting tential (−30 mV). The current peaks slowly about s after the GABA pulse. The amplitude of this cur-nt declines and will reverse in direction on hyper-larization.

The effects of bath-applied antagonists on the mplitude of the peak of the GABA currents was observed. The degree of block can be defined as $A1-1$ where $A1$ is the ratio of the GABA current before and during the application of antagonists (Ascher, Large and Rang, 1979). The voltage sensitivity of the block produced by each antagonist was expressed as $(A1_h - 1)/(A1_L - 1)$ where $A1_L - 1$ is the block produced at a low membrane potential (−30 to −40 mV) and $A1_h - 1$ is the block produced on hyperpolarization of the membrane potential by 30 mV (−60 to −70 mV). The values obtained for bicuculline (20 μM), picrotoxin (0.5 mM) and benzylpenicillin (2 mM) were respectively 1.48 ± 0.15 ($n = 7$), 0.80 ± 0.11 ($n = 4$), and 0.54 ± 0.11 ($n = 6$), means ± s.e. mean. Thus the degree of block produced by bicuculline increased slightly on hyperpolarization, while the results obtained with picrotoxin suggest little voltage sensitivity. The degree of block produced by benzylpenicillin decreased on hyperpolarization.

It is easy to correlate the direction of the voltage sensitivity of the antagonists with their ionic charges but there may be several reasons, including channel block, why antagonists show voltage sensitivity (Colquhoun, Dreyer & Sheridan, 1979).

This work was supported by a grant from the A.R.C.

References

ASCHER, P., LARGE, W.A. & RANG, H.P. (1979). Studies on the mechanism of action of acetylcholine antagonists on rat parasympathetic ganglion cells. *J. Physiol.*, **295**, 139–170.

COLQUHOUN, D., DREYER, F. & SHERIDAN, R.E. (1979). The actions of tubocurarine at the frog neuromuscular junction. *J. Physiol.*, **293**, 247–284.

[*From the Proceedings of the Physiological Society*, 12–13 *December* 1980
Journal of Physiology, **313**, 58–59*P*]

The action of sodium benzylpenicillin at the bag region of *Ascaris suum* muscle

By R. J. Martin. *Department of Veterinary Pharmacology, Royal (Dick) School of Veterinary Studies, University of Edinburgh*

Benzylpenicillin may antagonize the action of GABA by blocking Cl ion channels (Hochner, Spira & Werman, 1976). During studies on the bag region of *Ascaris* muscle using a two micro-electrode clamp technique, it was found that the GABA block produced by 2 mM-benzylpenicillin showed a moderate decrease on hyperpolarization (Martin, 1980). If benzylpenicillin acts by channel block the degree of block should increase with agonist concentration. This was tested by applying increasing amounts of GABA ionophoretically to the bag region of the muscle at a holding potential of −35 mV. The slope of the dose–response curves was reduced with the degree of block increasing with higher levels of GABA application.

Kinetic studies were carried out using a voltage-jump technique. A holding potential of approximately −70 mV was used with a depolarizing step in membrane potential of 30 mV, lasting 1–2 sec. The net GABA current observed during the depolarization step showed an outward relaxation which was described by a single exponential. The time constant at −35 to −40 mV was estimated as $32{\cdot}3 \pm 3{\cdot}9$ msec at 20 °C ($n = 6$). However, the relaxation in the presence of benzylpenicillin could not be described by a single exponential. In high concentrations of benzylpenicillin (4–7 mM) the net GABA current showed a fast outward relaxation just after the depolarization step. This outward relaxation was then followed by a small but slower inward relaxation.

Thus the blocking action of benzylpenicillin at the bag region of *Ascaris* muscle was characterized by voltage sensitivity, increased with agonist concentration and showed characteristic relaxations. These properties suggest a channel blocking action.

This work was supported by the A.R.C.

REFERENCES

Hochner, B., Spira, M. E. & Werman, R. (1976). *Brain Res.* **107**, 85–103.
Martin, R. J. (1980). *Br. J. Pharmacol. Chemother.* **70**, 139*P*.

[*From the Proceedings of the Physiological Society*, 12–13 *November* 1982
Journal of Physiology, **336**, 36–37*P*]

GABA single channel currents from *Ascaris* muscle

By R. J. Martin. *Department of Veterinary Pharmacology, Royal (Dick) School of Veterinary Studies, Summerhall, University of Edinburgh EH9 1QH*

The properties of GABA receptors of nematode muscle are of interest since they appear to be the site of action of important anthelmintics. This report describes initial results of a patch-clamp study.

GABA-induced single-channel currents were recorded in *Ascaris* Ringer (Martin, 1980) from the muscle bag region of the parasite *Ascaris suum*. Clean membranes were prepared using collagenase (1 mg/ml. for 1 hr) and giga-seal recordings (filtered at 900 Hz) made using outside-out and extracellular cell-attached patch-clamp techniques (Hamill, Marty, Neher, Sakmann & Sigworth, 1981). The patch electrode contained 140 mM-CsCl as the main electrolyte to reduce K but allow Cl currents. The GABA concentrations used were 10–100 μM. Fig. 1 shows a typical recording of GABA channels obtained with an outside-out patch during the bath application of 25 μM-GABA. The single-channel conductances from the outside-out and cell-attached patches were similar. The mean channel conductance measured from three outside-out patches and four cell-attached patches was $25{\cdot}6 \pm 1{\cdot}3$ pS (mean $\pm$S.E. $n = 7$).

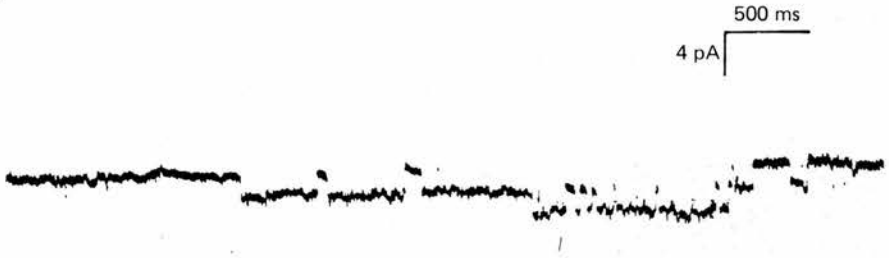


Fig. 1. Single channel currents (inwards, downwards) produced by the bath application of 25 μM-GABA. An outside-out patch with a pipette potential of -70 mV was used. In this patch there are up to two channels open. The average single channel current was 1·9 pA. The mean open time was 71 ms. Since the reversal potential was near 0 mV the single channel conductance was estimated as 27 pS (17 °C).

I thank Professor P. N. R. Usherwood and Dr R. Ramsey of Nottingham University for instruction and the A.R.C. for financial support.

REFERENCES

Hamill, O. P., Marty, A., Neher, E., Sakmann, B. & Sigworth, F. J. (1981). *Pflügers Arch.* **391**, 85–100.

Martin, R. J. (1980). *Brit. J. Pharmacol.* **71**, 99–106.

Br. J. Pharmac. (1982), **77**, 255–265

ELECTROPHYSIOLOGICAL EFFECTS OF PIPERAZINE AND DIETHYLCARBAMAZINE ON *Ascaris suum* SOMATIC MUSCLE

R.J. MARTIN

Department of Veterinary Pharmacology, Royal (Dick) School of Veterinary Studies, Summerhall, University of Edinburgh

1 Electrophysiological recordings were made from the bag region of *Ascaris suum* muscle. Membrane potential and input conductance or membrane current under voltage clamp were measured.

2 In high-Cl^- Ringer, bath-applied piperazine, at concentrations greater than 10^{-4} M, produced a dose-dependent and reversible increase in input conductance associated with a hyperpolarizing potential. The increase in input conductance was reduced when the preparations were bathed in low-Cl^- Ringer. γ-Aminobutyric acid (GABA) and piperazine reversal potentials were measured with a voltage clamp on the same cells using iontophoretic application of the agonists. The reversal potentials were the same and close to the predicted Nernst Cl^- potential (−65 mV). When GABA and piperazine were applied simultaneously piperazine reversibly reduced the amplitude of the control outward GABA current response. It was concluded that piperazine acts as a GABA agonist of low potency on the extra-synaptic GABA receptors of the bag, mediating an increase in Cl^- conductance.

3 Acetylcholine was applied iontophoretically within 100 μm of the bag region while the preparation was bathed in a low-Ca^{2+}, low-Cl^- Ringer. The response under voltage clamp was a dose-dependent inward current associated with an increase in input conductance. This response was reversibly antagonized by 3×10^{-5} M tubocurarine, high concentrations of diethylcarbamazine (10^{-3} to 10^{-2} M) but not high concentrations of piperazine (10^{-3} to 10^{-2} M). It was concluded that there are extra-synaptic acetylcholine receptors on the bag region of *Ascaris* muscle and that diethylcarbamazine but not piperazine acts as an antagonist.

4 Bath-applied diethylcarbamazine (10^{-4} to 2×10^{-3} M) produced a reversible dose-dependent depolarization of the membrane potential which was associated with an increase in the amplitude and frequency of spontaneous depolarizing potentials in active preparations at 32°C to 35°C in high-Cl^- Ringer. The excitatory action of diethylcarbamazine was not blocked by 3×10^{-5} M tubocurarine. Diethylcarbamazine (10^{-4} to 10^{-3} M) had no effect on the outward current response to GABA iontophoresis. Diethylcarbamazine (10^{-4} to 10^{-2} M) reversibly antagonized in a dose-dependent manner the delayed rectification of the bag membrane. In a low-Ca^{2+}, low-Cl^- Ringer, diethylcarbamazine (10^{-4} to 2×10^{-3} M) reversibly antagonized the voltage-sensitive outward current of the bag. This effect was mimicked by high-K^+ Ringer or perfusion with 4-aminopyridine (10^{-3} to 2×10^{-3} M). It was concluded that diethylcarbamazine did not react with the GABA receptor but antagonized a voltage-sensitive K^+ conductance.

Introduction

Nematode infections of intestinal parasites are common in both man and animals. For example, Standen (1975) estimated that 1 in 4 to 1 in 6 of the world's human population are infected with intestinal nematodes. In domestic animals infestations are so common that routine treatment with anthelmintics is required.

Piperazine and a derivative diethylcarbamazine are commonly used for the control of nematode infestations but their mode of action is not clear. It has been reported that piperazine mimics the action of γ-aminobutyric acid (GABA) and brings about hyperpolarization of *Ascaric* somatic muscle cells and that this is associated with relaxation (Del Castillo, De Mello & Morales, 1964a,b; Aubry, Cowell, Davey & Shevde, 1970). Despite these observations the exact mode of action of piperazine in *Ascaris* is still unknown. For example, it has been reported that iontophoretic application of piperazine on to the bag region of *Ascaris* muscle has no effect on membrane

0007-1188/82/100255-11 $01.00

© The Macmillan Press Ltd 1982

potential (Del Castillo *et al.*, 1964a) but this region is known to contain extra-synaptic GABA receptors (Martin, 1980). Aubry *et al.* (1970) were unable to further the argument as to whether piperazine should best be considered to act as an inhibitory transmitter or as a cholinoceptor antagonist as originally suggested by Norton & De Beer (1956). Further, Phillips, Sturman & West (1976) have suggested that piperazine acts by increasing the absorption of histamine by the parasite and that histamine may be an inhibitory transmitter. Added to this, Broome (1962) has reported that the piperazine derivative, diethylcarbamazine, has an excitatory not an inhibitory action on the contractility of the *Ascaris* nerve muscle preparation. In a recent review of the actions of diethylcarbamazine, Hawking (1979) reported little new information on the mode of action in nematodes but suggested that the mode of action in *Ascaris* may be due to the piperazine ring of diethylcarbamazine.

It was therefore decided to examine the electrophysiological effects of piperazine and diethylcarbamazine in the large nematode intestinal parasite of the pig, *Ascaris suum*, and particularly to examine possible interactions with GABA and acetylcholine receptors. This paper describes the results of these experiments which show that piperazine but not diethylcarbamazine has a GABA agonist action increasing Cl^- conductance; piperazine did not produce a curariform block: diethylcarbamazine antagonized a voltage-sensitive K^+ conductance.

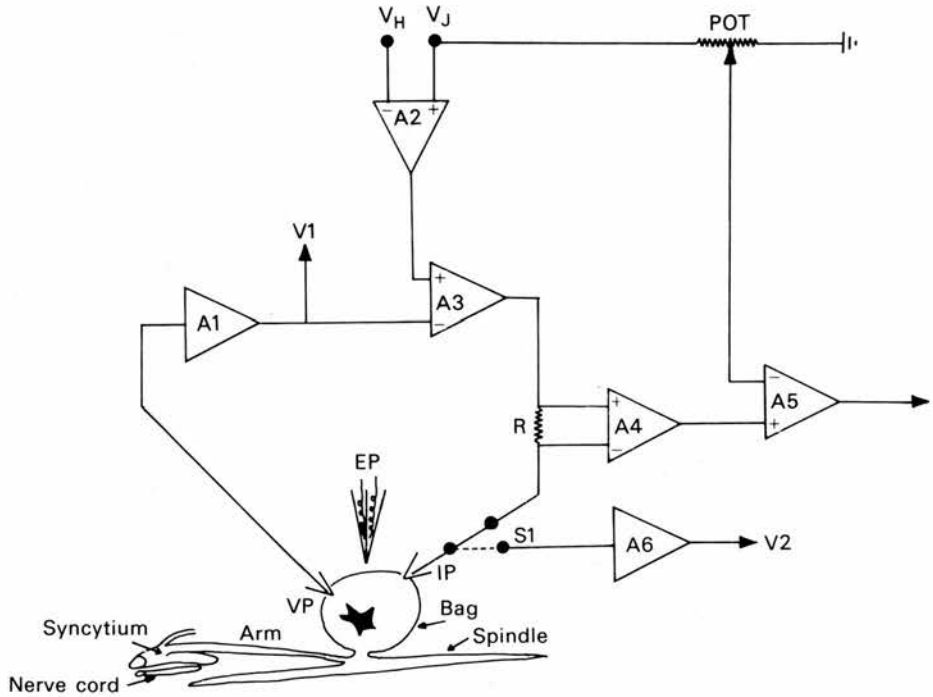


Figure 1 Diagram of preparation and recording system. Two 5 mΩ micropipettes (K^+ acetate filled) were placed intracellularly in the bag region of *Ascaris* muscle. The voltage pipette (VP) was connected to a high input impedance amplifier (A1) and the intracellular potential recorded at V1. A differential amplifier (A2) was used to determine the command potential. This allowed separate adjustment of the holding potential and voltage steps by applying different voltages to V_H for the holding potential and the V_J for the voltage steps. The control amplifier (A3) had a gain of 500. The current passed through the current pipette (IP) was determined by measuring the voltage drop across a 500 K resistor (R) using a differential amplifier (A4) with a high input impedance. A differential amplifier (A5) was used to subtract a rectangular current pulse during the voltage jumps because of the large voltage-insensitive leakage resistance of the bag. The level of the current subtraction was adjusted by using the potentiometer (POT) only at the beginning of the experiment and this was then left unaltered thereafter. The transmembrane current was recorded at the output of A5. The current pipette was placed intracellularly with the aid of a high input impedance amplifier (A6) when the switch S1 was suitably positioned to record the potential ofV_2. This amplifier (A6) was provided with a constant current injection facility. The iontophoretic pipettes (EP) were placed close (within 100 μm) to the bag membrane between the pipettes VP and IP.

Methods

The preparation

Specimens of *Ascaris suum* were collected from the local slaughter house and maintained in Locke solution (replaced daily), at 37°C in a water bath. The *Ascaris* were used for experiments within 4 days. A 2 cm flap preparation, made from the anterior region of the worm, was pinned on to sylgard in an experimental chamber and surrounded by a water jacket. The temperature of the preparation was maintained at 22° to 25°C except for experiments on the effects of diethylcarbamazine on the membrane potential where the temperature was raised to 32° to 35°C to permit spontaneous electrical activity. The anatomy of the muscle cell is illustrated in Figure 1. Further details of the preparation are available (Martin, 1980).

Ringer solution

The preparation was perfused at a constant rate of 5 ml/min. Four types of Ringer were used. A high-Cl^- Ringer containing (mM): NaCl 135, KCl 3.0, $CaCl_2$ 3.0, $MgCl_2$ 15.7, glucose 3.0 and Tris 5.0, adjusted to pH 7.6 with maleic acid, was used for the examination of Cl^- mediated events. A low-Cl^- Ringer (as above but in which the Cl^- was replaced isotonically with acetate) was used to examine the effects of Cl^- removal on the piperazine-induced conductances. A low-Ca^{2+}, low-Cl^- Ringer (in which the Ca^{2+} was omitted and the Cl^- replaced isotonically with acetate) was used to reduce the Cl^- currents and the voltage-sensitive Ca^{2+} spikes (Weisblat, Byerly & Russel, 1976). The low Ca^{2+}:Mg^{2+} ratio of this Ringer also blocks chemical synaptic transmission. A high-K^+ Ringer containing, either 19 or 35 mM K^+ was prepared by the addition of K^+ acetate to the low-Ca^{2+}, low-Cl^- Ringer.

Recording

Two micropipettes filled with 4 M K^+ acetate (pH 7.6) and 5 MΩ resistance were placed in the bag region of the muscle cell for conductance measurements or voltage clamping, Figure 1. One micropipette was used for voltage recording and the other for current injection. They were connected via Ag/AgCl wires to high input impedance amplifiers. This system permitted the selection of either current clamp (using a 1GΩ resistor as a constant source) or voltage clamp facilities. The time constant of the bag was about 6 ms so that under current clamp rectangular current pulses of greater than 250 ms were used. Under voltage clamp the gain of the control amplifier was set at × 500. During the voltage steps, the bag potential changed rapidly to the new potential in less than 1 ms but the transmembrane current took longer (less than 3 ms) before adjusting to a new level because of the capacitance currents of the membrane. The voltage-insensitive leakage current of the bags was relatively large compared to the voltage-sensitive current or agonist-induced currents. Its effect was reduced by subracting the rectangular current pulse of up to 90 nA with a differential amplifier, see Figure 1. The amplitude of the subtracted current pulse was adjusted using a potentiometer at the beginning of the experiment and this then remained unaltered afterwards. The effect of the series resistance (about 10 K) was expected to be small during the voltage clamp studies.

Responses were monitored on a Tectronix 5103N oscilloscope. Permanent records were made either by photographing the oscilloscope or on a Devices MX212 two channel pen recorder.

Iontophoresis

A third single or double barrelled micropipette was usually placed over the bag, extracellularly between the intracellular voltage and current micropipettes. This pipette was placed within 100 μm of the bag but positioned so that the use of large ejection currents did not cause a d.c. artefact on the electrical responses of the bag. Pipettes were filled appropriately with 0.5 M GABA pH 2.5, 0.5 M piperazine citrate, 0.5 M diethylcarbamazine citrate or 2 M acetylcholine chloride. The agonists were ejected as cations by micro-iontophoresis programmers Model 160 (W-P instruments INC). Retaining currents of 5–10 nA were used. The effect of ejection currents of the opposite polarity were routinely checked as a control but were found to be without effect.

Drugs

The drugs used were GABA (Sigma), piperazine citrate (Sigma), piperazine hexahydrate (Sigma), diethylcarbamazine citrate (Wellcome), acetylcholine chloride (BDH), diethylcarbamazine base and tubocurarine (Sigma). Bath applications of piperazine hexahydrate were used for the study on conductance changes. Diethylcarbamazine base was prepared from the citrate salt by dissolving it in a small volume of 2.5 M NaOH and extraction in chloroform followed by evaporation under vacuum.

Results

The following experiments were carried out to determine the effects of piperazine and diethylcaramazine on the electrical responses of *Ascaris*

muscle. The experiments described here were carried out on the muscle cells of 70 preparations. Except where stated, each experiment was carried out on at least 4 preparations with essentially similar results. Except for experiments on the depolarizing action of diethylcarbamazine on the membrane potential the experiments were carried out at a temperature of 22° to 25°C to block the spontaneous depolarizing potentials and to allow the recording of stable membrane potentials. Recordings were made from the bag region of the muscle cells with a conductance of less than 4 μS and resting membrane potentials of 35–40 mV.

Action of piperazine on bag input conductance

In a high-Cl^- Ringer, bath applications of piperazine in concentrations greater than 10^{-4} M resulted in a reversible increase in the input conductance of the bag together with a hyperpolarization of the membrane potential. This is illustrated in Figure 2a and b where it can be seen that 5×10^{-3} M piperazine reduces the amplitude of the electronic potential produced by the injection of a constant rectangular current pulse. There is an increase in the resting conductance (determined from the amplitude of the electrotonic potential) from 3.6 μS to 5.3 μS. The piperazine induced conductance change was dose-dependent. This is illustrated by dose-response relationship seen in Figure 2c, obtained by the application of increasing concentrations of piperazine with washing between applications. No desensitization was apparent.

Del Castillo *et al.* (1964a) have already illustrated the involvement of Cl^- in the effect of piperazine on membrane potential. The same effect on the piperazine-induced conductance change was examined when the preparations were perfused with a low-Cl^- Ringer. The conductance increases produced by piperazine (10^{-3} M) were dramatically and reversibly reduced to less than 15% of the control levels after perfusing the preparation with low-Cl^- Ringer for 30 min and were undetectable after 1.5 h (not shown). The piperazine conductance changes returned to near control levels after replacement of the Cl^-.

Iontophoresis of piperazine

It has already been pointed out that extra-synaptic GABA receptors are located on the bag region of *Ascaris* muscle cells (Martin 1980). It seemed reasonable to expect that these same receptors would be stimulated during the bath-application of piperazine to produce the recorded increase in input conductance in the bag. Piperazine was therefore applied iontophoretically to the bag region and the transmembrane current responses recorded under voltage clamp. It was found that the application of piperazine within 100 μm of the bag region (and in regions further than 1 mm from the syncytium) produced a dose-dependent outward current at −35 mV in high-Cl^- Ringer. This observation contrasts with the earlier observations of Del Castillo *et al.* (1964a) and shows that piperazine does in fact stimulate extra-synaptic receptors. The results of an iontophoresis experiment is shown in Figure 3. GABA

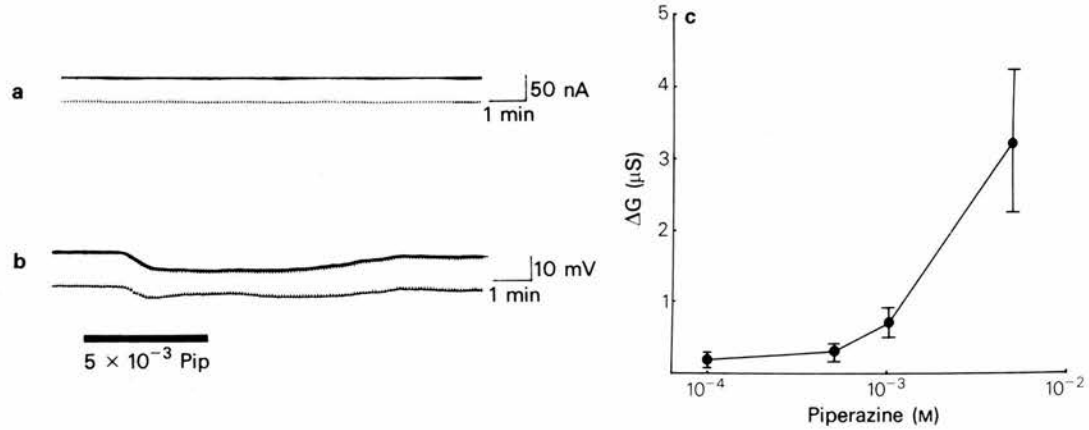


Figure 2 Effect of piperazine on bag input conductance in high Cl^- Ringer: (a) and (b) show a recording of a piperazine-induced conductance change. (a) Constant hyperpolarizing rectangular current pulses of 500 ms. (b) voltage recording during current injection and bath application of 5×10^{-3} M piperazine during the period indicated by the horizontal bar. The piperazine produced a reversible increase in input conductance of 1.7 μS associated with a hyperpolarizing potential. (c) Piperazine dose-response relationship. Ordinate scale: increase in input conductance. Abscissa scale: piperazine molar concentration. Each point shows the mean of 4 observations; vertical lines indicate s.e.mean.

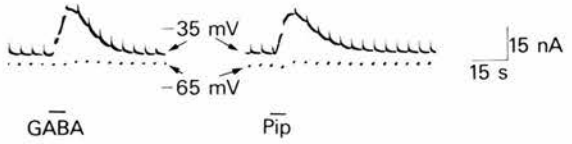


Figure 3 γ-Aminobutyric acid (GABA) and piperazine reversal potentials determined under voltage clamp conditions. The record shows the transmembrane currents (outward currents displayed upwards). The bag was held at −35 mV while hyperpolarizing steps to −65 mV of 1 s duration were made. GABA and piperazine were applied iontophoretically to the same preparation during the period indicated by the horizontal bar. 50nA was used for the ejection of GABA; 800 nA was used for the ejection of piperazine. The transmembrane current record shows that at −35 mV, GABA and piperazine produced an outward current. The envelope of this current record shows that there is little current at −65 mV, which is known to be near the GABA reversal potential. The current steps increase during the application of GABA and piperazine, indicating an increase in conductance of the bag membrane.



Figure 4 Simultaneous application of γ-aminobutyric acid (GABA) and piperazine. A control GABA outward current response following a brief ejection pulse (at ●, 1 μA for 400 ms) was reversibly reduced during the continuous application of piperazine (300 nA during the period indicated by the horizontal bar). Notice also that the total outward current at the peak of the GABA response during the application of piperazine is less than the control.

was first applied to the bag from a single barrelled micropipette using an ejection current of 50 nA during the period indicated by the horizontal bar. It can be seen that at −35 mV a peak outward current of 20 nA was produced. When the GABA pipette was replaced by a piperazine pipette located in the same position near the bag (and well away from the syncytium) an ejection current of 800 nA during the same time-period was required to elicit a similar response. The increase in the ejection current required for piperazine is consistent with its lower potency. Step changes in membrane potential from −35 to −65 mV, lasting 1 s were made throughout the application of the agonists to allow the simultaneous measurement of the induced currents at both potentials by using the envelope of the current record. It can be seen that at −65 mV there is little or no GABA or piperazine-induced current and that this is close to the reversal potential for GABA and piperazine. The estimations of the reversal potentials in other preparations were also similar and close to the predicted Nernst Cl^- potential of *Ascaris* muscle (Martin, 1980).

Picrotoxin will antagonize the response to GABA iontophoresis on the bag of *Ascaris* muscle (Martin, 1980). Picrotoxin in concentrations of 5×10^{-5} to 5×10^{-4} M reversibly and in a dose-dependant manner also antagonized the outward current responses to piperazine iontophoresis.

Simultaneous iontophoresis of γ-aminobutyric acid and piperazine

It is apparent from the previous experiment that piperazine mimics the actions of GABA and increases the Cl^- conductance of the bag membrane. It was decided to test the logical conclusion that piperazine and GABA act on the same receptors. This was carried out using the simultaneous iontophoretic application of piperazine and GABA from a double-barrelled pipette placed over the bag and observing the transmembrane currents at a holding potential of −35 mV. If piperazine and GABA occupy the same receptors then the amplitude of a control GABA response should be reduced during the application of piperazine. The result of a typical experiment is shown in Figure 4. A control GABA response with a peak current of 18 nA was reversibly reduced to 15 nA, then 13.5 nA during the continuous application of piperazine. In this and other preparations it was observed that the level of depression of the GABA response was dose-dependent and increased with the amount of piperazine applied iontophoretically. Notice also that the total outward current at the peak produced by piperazine and GABA in Figure 4 is less than the control. This result was only observed in this and other preparations at the higher levels of piperazine application. Such an action is expected if piperazine is a partial agonist (Iravani, 1965). Alternatively, piperazine iontophoresis at higher levels might produce an inward current due to a non-specific depolarizing effect (Del Castillo *et al.*, 1964a) in addition to the outward Cl^- current. The total piperazine current would then underestimate the activation of GABA receptors. A further study of this was not made.

Iontophoresis of acetylcholine

Bath-applied acetylcholine depolarizes *Ascaris* muscle causing contraction. The acetylcholine receptors responsible for the depolarization were believed to be exclusively located at the syncytium, the position of the neuromuscular synapse (Del Castillo *et al.*, 1963). However, Brading & Caldwell (1971) cut the

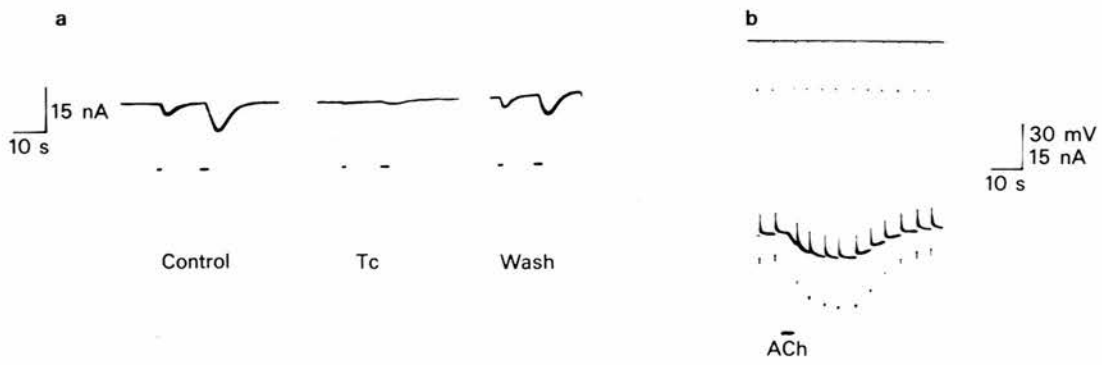


Figure 5 Effect of acetylcholine (ACh) on the transmembrane current under voltage clamp. (a) Iontophoresis of acetylcholine (500 nA for 0.5 s at the short bar and 500 nA for 2 s at the longer bar) produces a dose-dependent inward current at −35 mV when applied within 100 μm of the bag. This response was reversibly antagonized by 3×10^{-5} M tubocurarine (Tc) applied in the bath for 2 min. This antagonism was removed by washing for 3 min. (b) Iontophoresis of acetylcholine (500 nA for 2 s at the horizontal bar) during voltage steps (500 ms duration) from a holding potential of −35 mV to −65 mV. Top trace shows the voltage record and the lower trace shows the transmembrane current. Note that acetylcholine increases the current required for the voltage steps, illustrating that acetylcholine increases the input conductance of the bag membrane.

arms of the muscle cells, to separate the bag region from the syncytium and still observed the depolarizing response to bath-applied acetylcholine. It seemed likely therefore that there were extra-synaptic acetylcholine receptors on the bag. In order to test this hypothesis acetylcholine was applied iontophoretically while measuring the transmembrane current under voltage clamp at −35 mV. In most preparations a low-Ca^{2+}, low-Cl^- Ringer was used during these experiments. This had several advantages including increasing the input resistance of the bags and facilitating successful recording. The low-Ca^{2+}, high-Mg^{2+} ratio was also used to reduce the tonically released acetylcholine and its interaction with bath-applied tubocurarine (Del Castillo *et al.*, 1963). Figure 5a shows the results of a typical experiment. It was found that application of acetylcholine (within 100 μm of the bag) caused a dose-dependent inward current which was reversibly blocked by 3×10^{-5} M tubocurarine. No responses were obtained when the iontophoretic pipette was placed at greater distances from the bag (except over the arms and syncytium). Figure 5b shows that the action of acetylcholine was associated with an increase in bag conductance. Repeated voltage steps from the holding potential of −35 mV to −65 mV lasting 500 ms were made during the application of acetylcholine. It can be seen that there is an increase in the size of the transmembrane current steps during the response due to the conductance increase. Estimates of the acetylcholine-induced currents at −35 and −65 mV were made from the change in the envelope of the current records. In Figure 5b, for example, the peak of the inward acetylcholine current at −35 mV was 8.5 nA, at −65 mV it was 17 nA. Simple extrapolation suggested that the acetylcholine reversal potential was in the region of −5 mV. However, it should be pointed out that a linear current-voltage relationship was assumed for this estimation. This assumption does not hold universally.

Piperazine and diethylcarbamazine antagonism of acetylcholine

Norton & De Beer (1956) first suggested that piperazine has a tubocurarine like action in *Ascaris* and this was not ruled out by Aubry *et al.* (1976). It was possible to test this hypothesis using the response of the extra-synaptic acetylcholine receptors of the bag and observing the effect of bath-applied piperazine on preparations in which the Cl^- mediated responses had been eliminated. To eliminate the Cl^- mediated responses and tonic transmitter release the preparations were perfused as before in a low-Ca^{2+}, low-Cl^- Ringer for at least 1.5 h. After this no piperazine- or GABA-induced conductance increases were detectable. Acetylcholine was then applied iontophoretically as before while the bag was held at −35 mV. It was found that high concentrations of piperazine (10^{-3} to 10^{-2} M) had little effect on the amplitude of the acetylcholine induced current. Figure 6a shows the results of a typical experiment. This illustrates that the action of piperazine was unlike that of tubocurarine in *Ascaris* and that it did not act as a cholinergic antagonist as has been previously suggested (compare Figures 5a and 6a).

It was also of interest to examine the effects of

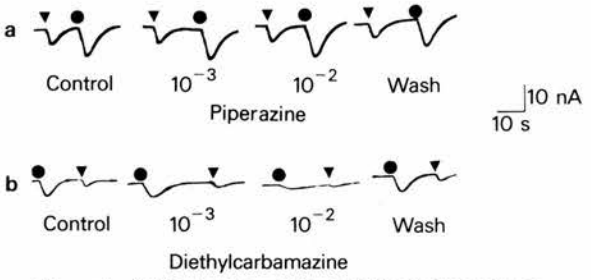


Figure 6 Diethylcarbamazine and piperazine antagonism of acetylcholine. Acetylcholine applied iontophoretically produces a dose-dependent inward current (applied with 400 nA for 0.5 s at (▼) and with 400 nA for 2.5 s at (●), bag voltage clamped at −35 mV, low-Ca^{2+}, low-Cl^- Ringer). (a) Piperazine in high concentrations up to 10^{-2} M failed to antagonize the response. Each concentration was applied for 2 min and then washed for 3 min before the final test. (b) Another preparation, diethylcarbamazine in concentrations greater than 10^{-3} M reversibly antagonized the acetylcholine responses. Each concentration was applied for 2 min and then washed for 3 min before the final test.

diethylcarbamazine under the same conditions. Bath-applied diethylcarbamazine (10^{-3} to 10^{-2} M as citrate) was used. In concentrations greater than 10^{-3} M, diethylcarbamazine produced a reversible and dose-dependent antagonism of the acetylcholine responses. Figure 6b illustrates the results of a typical experiment. It was concluded that diethylcarbamazine but not piperazine has a weak cholinoceptor antagonist action.

Effect of histamine on membrane potential and input conductance

Phillips *et al.* (1976) have reported that piperazine affects the uptake of histamine by the parasite and that histamine may be an inhibitory transmitter. Histamine was therefore applied iontophoretically to the bag and in the bath in concentrations up to 10^{-3} M with little or no effect on the membrane potential or input conductance. This was despite perfusing the preparation in a high-Cl^- Ringer in conditions under which stimulation of inhibitory nerves produces hyperpolarization (Del Castillo *et al.*, 1964a). The lack of effect of histamine does not support the suggestion that histamine is a natural inhibitory transmitter.

Effect of bath-applied diethylcarbamazine on membrane potential

Broome (1962) has described an excitatory effect of diethylcarbamazine producing bigger waves of contraction and relaxation in the *Ascaris* nerve muscle preparation. Its action was not like that of acetylcholine which produced a simple sustained contraction. Unlike acetylcholine its action was not blocked by tubocurarine. The effect of bath-applied diethylcarbamazine on membrane potential was therefore examined. A high-Cl^- Ringer was used initially to permit detection of possible interactions with GABA receptors. It was found that diethylcarbamazine (10^{-4} to 2×10^{-3} M as citrate) in active preparations at 32° to 35°C produced a reversible dose-dependent depolarization associated with an increase in the spontaneous depolarizing potentials. These potentials are produced by pacemaker activity at the syncytium. However, the effect on membrane potential at the lower temperatures of 22° to 25°C was variable and often absent. Diethylcarbamazine base (10^{-4} to 2×10^{-3} M) was also used at 32° to 35°C to test this effect further and to eliminate possible effects of citrate. Figure 7a illustrates a typical depolarizing response to diethylcarbamazine base which was associated with an increase in frequency and amplitude of the spontaneous depolarizing potentials. The effect of diethylcarbamazine base was essentially similar to that of the citrate. The dose-response relationship shown in Figure 7b was determined by applying increasing concentrations and washing between applications. At high concentrations the preparation began to contract making recording more difficult.

Broome (1962) has reported that tubocurarine has no blocking action on the excitatory effect on contraction induced by diethylcarbamazine. The effect of 3×10^{-5}M tubocurarine on the depolarizing action of diethylcarbamazine (10^{-3} to 2×10^{-3} M base) was also examined in three preparations. This concentration of tubocurarine which blocked the responses to acetylcholine iontophoresis had no antagonistic action on the diethylcarbamazine responses. From these observations it was concluded that diethylcarbamazine has a depolarizing action which is not due to a cholinergic action.

Effect of diethylcarbamazine on γ-aminobutyric acid responses

Diethylcarbamazine is a piperazine derivative and piperazine has been shown to be a GABA agonist in this preparation. A possible explanation therefore of the depolarizing action of diethylcarbamazine was that it might be acting on the same receptor as piperazine but as a GABA antagonist. To test for this, GABA responses were elicited by iontophoresis at the bag in a high-Cl^- Ringer while the effect of simultaneous iontophoresis of diethylcarbamazine or bath-application of diethylcarbamazine (10^{-4} to 10^{-3} M as citrate) on transmembrane currents was observed. It was found that neither iontophoresis nor bath-application of diethylcarbamazine had a detect-

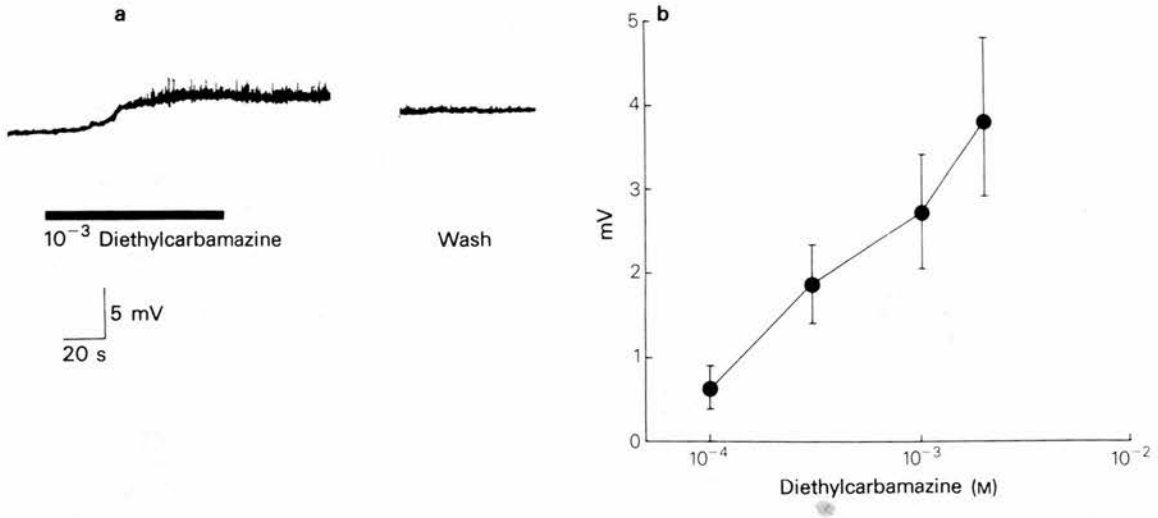


Figure 7 Depolarizing effect of diethylcarbamazine. Diethylcarbamazine base was bath-applied to preparations bathed in high-Cl^- Ringer and its effect on bag membrane potential recorded at a temperature of 32° to 35°C. (a) Diethylcarbamazine (10^{-3} M) produced depolarization associated with an increase in the frequency and amplitude of spontaneous depolarizing potentials. The membrane potential returned to the resting level after washing for 10 min, temperature 32°C. (b) Diethylcarbamazine log-dose response relationship obtained in high-Cl^- Ringer. Ordinate scale: membrane depolarization. Abscissa scale: molar concentration of diethylcarbamazine base applied in the bath. Each point shows the mean of 8 or 11 observations; vertical lines indicate s.e.mean.

able effect on the GABA currents. The result of a typical experiment is shown in Figure 8. It was concluded from these observations that diethylcarbamazine did not act as a GABA antagonist.

Effect of diethylcarbamazine on delayed rectification

The bag current-voltage relationship is characterized by the existence of delayed rectification (Martin, 1980). It was noticed during the previous experiments that diethylcarbamazine (10^{-4} to 2×10^{-3} M as base or citrate) antagonized this delayed rectification in a reversible and dose-dependant manner. This same effect was also observed at 22° to 25°C. Figure 9 shows the effects of perfusing a preparation with diethylcarbamazine base on the current-voltage relationship at 25°C.

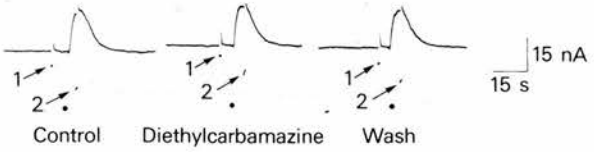


Figure 8 Effect of diethylcarbamazine on γ-aminobutyric acid (GABA) responses. In a high-Cl^- Ringer, GABA applied iontophoretically (at (●) using 1 μA for 400 ms) produced an outward transmembrane current response when the bag membrane potential was held at −40 mV. Two hyperpolarizing steps to −70 mV lasting 1 s at (1) and (2) were made. It was thus possible to estimate the GABA-induced conductance from the change in the transmembrane current steps required to hyperpolarize the bag to −70 mV. Iontophoresis of GABA (control) produced an outward current response of 20 nA at −40 mV and an increase in input conductance of 1 μS. Bath-application of 10^{-3} M diethylcarbamazine citrate had little effect on the GABA response. Occasionally, as in this preparation, there was a small increase in the resting membrane conductance during the application of diethylcarbamazine citrate.

The effect of diethylcarbamazine on the voltage-sensitive outward current in *Ascaris* was examined in a low-Ca^{2+}, low-Cl^- Ringer using depolarizing steps from −35 to −20 mV. This Ringer was used to reduce Cl^- and voltage-sensitive Ca^{2+} currents. It was found that diethylcarbamazine (as base, citrate was not used) in concentrations greater than 10^{-4} M reversibly antagonized the voltage-sensitive outward current. In addition to this effect, there was sometimes a small steady inward current during its application. The level of antagonism was dose-dependent and increased with the concentration of diethylcarbamazine within the range tested (10^{-4} to 2×10^{-3} M). Figure 10a and b shows the effects of bath-applied diethylcarbamazine. Delayed rectification in other preparations is mediated via an outward K^+ current (Hodgkin & Huxley, 1952). In order to confirm this in *Ascaris* the effects of a high-K^+ Ringer (19 mM and 35 mM) to reduce the K^+ electrochemical gradient and 4-aminopyridine (10^{-3} and 2×10^{-3} M) as a K^+ blocker were tested. It was found

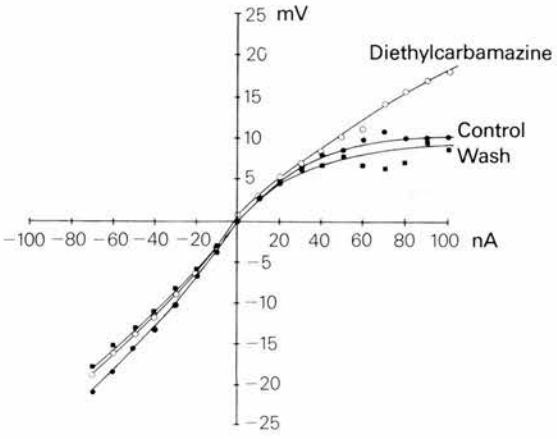


Figure 9 Effect of diethylcarbamazine in the current-voltage relationship. The current-voltage relationship was determined in a high Cl^- Ringer using constant rectangular current pulses of 500 ms duration and the change in membrane potential produced by the current measured at the end of the pulse. The control current-voltage relationship showed delayed rectification during the injection of depolarizing current. Diethylcarbamazine base 10^{-3} M bath-applied (for 5 min) produced a reversible depolarization of 2 mV and a reversible antagonism of the delayed rectification (after washing for 5 min). Temperature 25°C.

that they mimicked the action of diethylcarbamazine by decreasing the voltage-sensitive outward current. Attempts to separate effects on different voltage-sensitive K^+ currents were not made in this study. It was concluded that diethylcarbamazine has an antagonistic action on the voltage-sensitive K^+ conductance of the *Ascaris* membrane.

Discussion

Piperazine as a γ-aminobutyric acid agonist

The experiments described in this paper show that piperazine acts as a GABA agonist of low potency on extra-synaptic receptors on *Ascaris* muscle giving rise to hyperpolarization mediated by an increase in Cl^- conductance. No cholinergic antagonistic action of piperazine was detected despite the application of high concentrations. Thus no evidence was found to support the hypothesis of a curariform block as originally suggested by Norton & De Beer (1957) and reiterated by Sheth (1975). It is now reasonable to explain the piperazine-induced reversible paralysis of nematodes and their expulsion from the intestine during therapy (Desowitz, 1971) by its GABA mimetic action. The site of action of piperazine is not necessarily limited to the region of the neuromuscular synapse as originally described by Del Castillo *et al.* (1964a). It is clear from this study that extra-synaptic GABA receptors may also be stimulated by piperazine during therapy.

It is interesting that piperazine also acts as a GABA agonist on crayfish muscle (Iravani, 1965) and lobster muscle (Constanti & Nistri, 1976) but not on rat sympathetic neurones (Connor, Constanti, Dunn, Forward & Nistri, 1981). In fact, Nistri & Constanti (1979) have suggested the existence of at least two separate types of GABA receptor in some invertebrates and some vertebrate preparations with piperazine as a selective agonist in invertebrates. However, piperazine does have a GABA mimetic action in some areas of the vertebrate central nervous system (Perkins & Stone, 1982).

Extra-synaptic cholinoceptors

The iontophoresis of acetylcholine on to the bag region of the muscle confirms the presence of extra-synaptic receptors on the bag in addition to those already reported to be present at the syncytium (Del Castillo *et al.*, 1963). The extra-synaptic receptors were antagonized by tubocurarine and their activation increased the membrane conductance and gives rise to an inward current under voltage clamp conditions. The physiological significance of these receptors is not known since it is a region devoid of synapses. However, treatment of the host with a cholinomimetic anthelmintic may stimulate these extra-syaptic receptors, as well as the synaptic ones. For example, pyrantel tartrate, a nicotinic anthelmintic (Aubry *et al.*, 1976) is a potent agonist and acts on the acetylcholine receptors of the bag when applied iontophoretically (unpublished observations). It may have a similar action during therapy.

Effect of diethylcarbamazine on K^+ conductance

In this study it was shown that diethylcarbamazine did not mimic the actions of piperazine but antagonized a voltage-sensitive K^+ current in *Ascaris*. Diethylcarbamazine also depolarized the membrane in active preparations at 32° to 35°C, but this effect was variable and often absent at 22° to 25°C. The effect of K^+ on the resting membrane potential in *Ascaris* has been reported to be small (Brading & Caldwell, 1971). It is likely that the depolarizing action in active preparations results mainly from an action on the voltage-sensitive K^+ conductance rather than from any effect on the resting K^+ conductance. This in turn could give rise to an excitatory effect on contractility as observed by Broome (1962). The absence of any nicotinic agonist action or GABA antagonism in *Ascaris* is consistent with such a mechanism. The absence of a nicotinic action con-

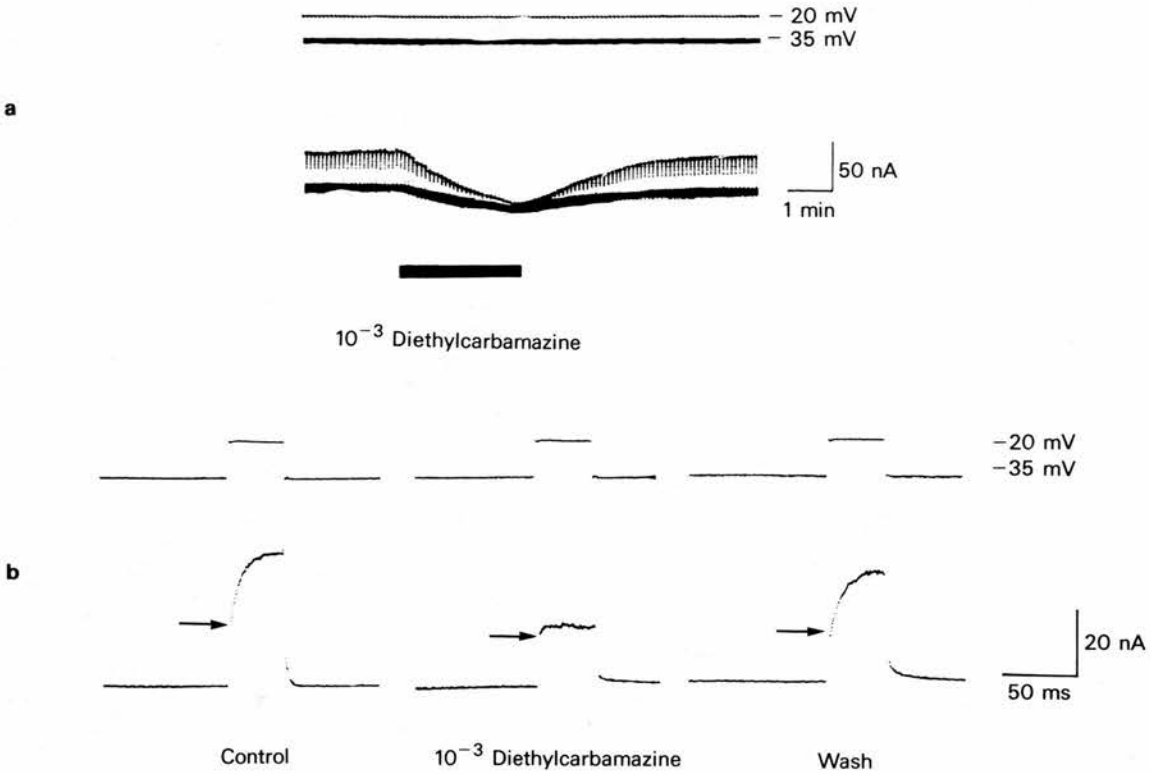


Figure 10 Effect of diethylcarbamazine antagonism on the voltage-sensitive outward current: (a) and (b) are recordings from two separate preparations bathed in low-Ca^{2+}, low-Cl^- Ringer at 25°C. Both illustrate the effect of bath-applied diethylcarbamazine base (10^{-3} M) on transmembrane currents. Bag membrane potentials were held at −35 mV with depolarizing steps to −20 mV lasting 150 ms in (a) but 50 ms in (b). The top traces display membrane potentials while the lower traces display the transmembrane currents. (a) Diethylcarbamazine applied during the horizontal bar produced a steady inward current at −35 mV and reduced the inward current required to depolarize the cell. (b) Similar conditions as (a) except that the recordings were made on a faster time scale. After the depolarizing step there was a voltage-independent step in the transmembrane current (up to arrow) due to the leakage resistance of the bag. The capacitance currents were too fast to be seen on this photograph. This current step was then followed only in the control and post-wash records by an approximately exponential increase in the outward current. The early part of the control and wash voltage-sensitive currents were retouched with dots. Note that diethylcarbamazine reversibly antagonized the voltage-sensitive outward current.

trasts with the effects of diethylcarbamazine reported in some mammalian preparations (Abaitey & Parratt, 1976; 1977). However, the interpretation of the mechanism of action of diethylcarbamazine in whole animal studies is complicated by the rapid appearance of metabolites (Hawking, 1979).

The author wishes to thank the Agricultural Research Council for financial support and Dr S. Watts of the Wellcome Foundation for the gift of diethylcarbamazine citrate.

References

ABAITEY, A.K. & PARRATT, J.R. (1976). Cardiovascular effects of diethylcarbamazine citrate. *Br. J. Pharmac.*, **55,** 219–227.

ABAITEY, A.K. & PARRATT, J.R. (1977). The effects of diethylcarbamazine citrate on smooth muscle. *J. Pharm. Pharmac.*, **29,** 428–432.

AUBRY, M.L., COWELL, P., DAVEY, M.J. & SHEVDE, G. (1970). Aspects of the pharmacology of a new anthelmintic: pyrantel. *Br. J. Pharmac.*, **38,** 332–344.

BRADING, A.F. & CALDWELL, P.C. (1971). The resting membrane potential of the somatic muscle cells of *Ascaris lumbricoides*. *J. Physiol.*, **217,** 605–624.

BROOME, A.W.J. (1962). Mechanisms of anthelmintic action with particular reference to drugs affecting neuromuscular activity. In *Drugs Parasites and Hosts* ed. Goodwin, L.G. & Nimmo-Smith, R.H. pp. 43–61. London: Churchill.

CONNOR, J.D., CONSTANTI, A., DUNN, P.M., FORWARD, A. & NISTRI, A. (1981). The efffects of piperazine on rat sympathetic neurones. *Br. J. Pharmac.*, **74,** 445–454.

CONSTANTI, A. & NISTRI, A. (1976). A comparative study of the action of γ-aminobutyric acid and piperazine on the lobster muscle fibre and the frog spinal cord. *Br. J. Pharmac.*, **57,** 347–358.

DEL CASTILLO, J., DE MELLO, W.C. & MORALES, T. (1963). The physiological role of acetylcholine in the neuromuscular system of *Ascaris lumbricoides. Archs Int. Physiol.*, **71,** 741–757.

DEL CASTILLO, J., DE MELLO, W.C. & MORALES, T. (1964a). Mechanism of the paralysing action of piperazine on *Ascaris* muscle. *Br. J. Pharmac.*, **22,** 463–477.

DEL CASTILLO, J., DE MELLO, W.C. & MORALES, T. (1964b). Inhibitory action of γ-aminobutyric acid (GABA) on Ascaris muscle. *Experientia.*, **20,** 145–146.

DESOWITZ, R.S. (1971). Antiparasite chemotherapy. *A. Rev. Pharmac.*, ***11,*** *351–368.*

HAWKING, F. (1979). Diethylcarbamazine and new compounds for treatment of filariasis. *Adv. Pharmac. Chem.*, **16,** 130–194.

HODGKIN, A.L. & HUXLEY, A.F. (1952). Currents carried by sodium and potassium ions through the membrane of the giant axon of *Loligo. J. Physiol.*, **116,** 449–472.

IRAVANI, J. (1965). Wechselbeziehung von Barbituraten und Piperazin mit GABA an der Membran des Krebsmuskels. *Naunyn-Schmeidebergs Arch. exp. Path. Pharmak.*, **251,** 265–274.

MARTIN, R.J. (1980). The effect of γ-aminobutyric acid on the input conductance and membrane potential of *Ascaris* muscle. *Br. J. Pharmac.*, **71,** 99–106.

NISTRI, A. & CONSTANTI, A. (1979). Pharmacological characterization of different types of GABA and glutamate receptors in vertebrates and invertebrates. *Prog. Neurobiol.*, **13,** 117–235.

NORTON,S. & DE BEER, E.J. (1957). Investigations on the action of piperazine on *Ascaris lumbricoides. Am. J. trop. Med.*, **6,** 898–905.

PERKINS, M.N. & STONE, T.W. (1982). Comparison of the effects of ethylinediamine analogues and γ-animobutyric acid on cortical and pallidal neurones. *Br. J. Pharmac.*, **75,** 93–99.

PHILLIPS, J.L., STURMAN, G. & WEST, G.B. (1976). The interaction between anthelmintic drugs and histamine in *Ascaris suum. Br. J. Pharmac.*, **57,** 417–420.

SHETH, U.K. (1975). Mechanisms of anthelmintic action. *Prog. Drug. Res.*, **19,** 147–157.

STANDEN, O.D. (1975). Chemotherapy of intestinal helminthiasis. *Prog. Drug. Res.*, **19,** 158–165.

WEISBLAT, D.A., BYERLY, L. & RUSSELL, R.L. (1976). Ionic mechanisms of electrical activity in somatic muscle of the nematode *Ascaris lumbricoides. J. comp. Physiol.*, **111,** 93–113.

(*Received February 5, 1982.*)

REFERENCES

ALGER, B.E. and TEYLER, T.J. (1976) Brain Res. 110, 463-480.

COLLINGRIDGE, G.L., KEHL, S.J. and McLENNAN, H. (1984) Can. J. Physiol. Pharmacol. in Press.

CRUNELLI, V., FORDA, S. and KELLY, J.S. (1983) J. Phyusiol. 341, 627-640.

CURTIS, D.R., FELIX, D. and McLENNAN, H. (1970) Br. J. Pharmac. 40, 881-883.

HICKS, T.P. and McLENNAN, H. (1979) Can. J. Physiol. Pharmacol 57, 973-978.

KEHL, S.J. and McLENNAN, H. (1983) Brain Res. 279, 278-281.

KEHL, S.J., McLENNAN, H. and COLLINGRIDGE, G.L. (1984) Neuroscience 11, 111-124.

KOERNER, J.F. and COTMAN, C.W. (1981) Brain Res. 216, 192-198.

McLENNAN, H. (1983) Prog. Neurobiol. 20, 251-271.

NEWBERRY, N.R. and NICOLL, R.A. J. Physiol. (1984) 348, 239-25

OLNEY, J.W., FULLER, T.A., deGUBAREFF, T. and LABRUYERE, J. (1981) Neurosci. Lett. 25, 185-191.

McLENNAN, H. and LIU, J.R. (1982) Exp. Brain Res. 45, 151-156.

TEICHBERG, V.I., TAL, N., GOLDBERG, O. and LUINI, A. (1984) Brain Res. 291, 285-292.

WATKINS, J.C. and EVANS, R.H. (1981) Ann. Rev. Pharmacol. Toxicol. 21, 165-204.

WHEAL, H.V. and MILLER, J.J. (1980) Brain Res. 182, 145-155.

GABA AND PIPERAZINE ACTIVATED SINGLE CHANNELS IN ASCARIS MUSCLE

By R.J. Martin. Department of Veterinary Pharmacology, Royal (Dick) School of Veterinary Studies, Summerhall, University of Edinburgh, Edinburgh.

GABA and piperazine activated single channel currents were recorded from the bag region of the somatic muscle of the nematode parasite Ascaris suum. Cell-attached and outside-out patch clamp techniques were used. Clean membranes were routinely prepared using collagenase.

GABA (concentrations greater than 1 uM) or piperazine (concentrations greater than 200 uM) applied to the extra-celllular surface of the patches brought about the opening of channels producing rectangular shaped current pulses of varying duration but essentially constant amplitude. The IV relationships of the single channel currents for both agonists were linear and had conductances in the region of 21 pS. The reversal potential was near 0 mV when Cl^- was equally distributed on both sides of the membrane.

At low concentrations of GABA (3 to 4 uM), the effective mean channel open time was in the region of 32 msec (-75 mV, 22C, cell-attached patches). At low

concentrations of piperazine (500 uM) the effective mean open channel lifetime was shorter, in the region of 14 msec (-75 mV, 22 C, cell-attached patches). The open and closed time distributions were described by the sum of a number of exponentials. A negative log-likelihood procedure was used to make best estimates of the number of components, their weighting, and their mean values. For each agonist at these concentrations the channel open lifetime distributions were best described by the sum of two exponentials. With 3 uM GABA as the agonist the fast component had a mean value of 2.7 msec while the slow component had a mean value of 44 msec. With 500 uM piperazine the mean value of the fast component was 7.6 msec while the mean value of the slow component was 28 msec. 35% of the GABA and 47% of the piperazine openings were of the brief type while the remainder were of the longer type. As a consequence the brief openings for GABA carried only 3% of the total current; for piperazine 19% of the current was carried by the brief openings. During these recordings no simultaneous openings were observed suggesting that these double exponentials were not due to activation of two types of channel but were due to two open mainstates.

The channel openings of these low agonist concentrations occurred as single events or in bursts and clusters of bursts. It was found that the channel closed

times at these concentrations were best described by the sum of up to three exponentials suggesting the presence of three closed mainstates.

Piperazine is known to be 10 to 100 times less potent than GABA in the Ascaris preparation (Martin 1982). The mainstate channel conductances of both agonists were the same so that any conductance differences could not explain the magnitude of the observed differences in potency. The difference in potency may be explained by the fact that piperazine required a high concentration to achieve a similar opening rate to GABA. In addition the effective mean open time for piperazine was generally shorter than that of GABA.

Increases in agonist concentration produced an increase in the probability of the channel being open. This increase was also associated with an increase in the frequency of the channel opening, an increase in the number of openings per burst and an increase in the effective mean channel open time together with a reduction in the proportion of brief openings.

These observations on the channel open times are inconsistent with a simple two step KM Model of agonist action (Del Castillo and Katz 1957; Katz and Miledi 1972)

which involves binding of a single agonist molecule for channel opening. However, one attractive model in which two agonist molecules can combine with two sub-units of the receptor channel complex to produce opening is the Monod-Wyman-Chaugeau model (Colquhoun & Hawkes 1977 and 1982). It can account by a plausible physical mechanism for: the changes in mean open time observed in these experiments with agonist concentration: double exponential distribution of the open times and the change in the proportion of the fast and slow openings.

REFERENCES

COLQUHOUN, D. and HAWKES, A.G. (1977). Proceedings of the Royal Society Series B 199, 231-262.

COLQUHOUN, D. and HAWKES, A.G. (1982). Philosophical transactions of the Royal Society Series B 300, 1-59.

DEL CASTILLO, J. and KATZ, B. (1957). Proceedings of the Royal Society Series B 146, 369-381.

HAMILL, P., MARTY, A., NEHER, E., SAKMANN, B. and SIGWORTH, F.J. Pfluger Arch. 391, 85-100.

KATZ, B. and MILEDI R. (1972). J. Physiol. 244 665-699.

MARTIN, R.J. (1982). British Journal of Pharmacology 77, 255-265.

VOLTAGE-CLAMP ANALYSIS OF EXCITATORY AMINO ACID RESPONSES IN MOUSE SPINAL NEURONES IN CULTURE.

By Mark L. Mayer and Gary L. Westbrook. Laboratory of Developmental Neurobiology, NICHD, Bldg.36 Room 2A21, NIH, Bethesda, Md.20205, USA.

The interpretation of experiments designed to analyse the mechanism of action of L-glutamate and related acidic amino acids in the vertebrate CNS is complicated by the failure of a number of laboratories to record a consistent action of L-glutamate on neuronal input resistance. Some recent advances in physiology and pharmacology, when combined, provide a simple explanation for much of the controversy surrounding the mode of action of excitatory amino acids.

The first breakthrough was due to the development by Jeff Watkins and his colleagues of a series of agonists and antagonists which differentiate excitatory amino acid receptors into 3 subpopulations selectively activated by N-methyl-D-aspartic acid (NMDA), quisqualic acid and kainic acid respectively. A second advance came with the discovery, by Phillip Ascher's team in Paris and by Gary Westbrook and myself at NIH, that the voltage-senstive action of NMDA is due to a membrane potential dependent channel block by Mg^{2+} of inward current flow through ion channels linked to NMDA receptors. Thus NMDA receptors do not appear to be linked to a potential sensitive gating mechanism of the type first described by Hodgkin & Huxley, and the voltage-dependent blocking action of Mg^{2+} provides an alternative to suggestions that NMDA modulates sodium or calcium currents.

Our experiments were performed under voltage-clamp on mouse spinal cord neurones in culture. In solutions containing physiological concentrations of Mg^{2+} ($\sim$1 mM) current-voltage plots of amino acid responses show 3 types of behaviour. NMDA and L-aspartate have a negative slope conductance at membrane potentials more negative than -30 mV, and current-voltage plots of NMDA and L-aspartate responses are J-shaped, with a null potential of 0 mV. Kainate and quisqualate behave as classical excitatory agonists and have a near linear current-voltage plot over a wide range of membrane potentials. Responses evoked by other amino acids, especially L-glutamate and L-homocysteate have a very characteristic current voltage plot: over the potential range -70 to -30mV the slope of the plot is close to zero; at more depolarized membrane potentials the slope becomes steeply positive and as a consequence the current-voltage plot has a nearly rectangular shape.

The reversal potential of responses evoked by all acidic amino acids is similar and close to 0 mV. Since intracellular injection of Cs^{+} does not alter the reversal potential it is probable that the ion channels linked to both NMDA and kainate/quisqualate receptors are similar in their permeability to those activated by acetylcholine at the end-plate, which do not discriminate well between Na^{+}, K^{+} and Cs^{+}. The permeability of amino acid activated ion channels to divalent cations, especially Ca^{2+} remains to be accurately determined.

Plots of the membrane potential - chord conductance relationship of amino acid responses, derived using the

Br. J. Pharmac. (1985), **84**, 445–461

γ-Aminobutyric acid- and piperazine-activated single-channel currents from *Ascaris suum* body muscle

R.J. Martin

Department of Veterinary Pharmacology, Royal (Dick) School of Veterinary Studies, Summerhall, University of Edinburgh, Edinburgh, EH9 1QH

1 γ-Aminobutyric acid (GABA)- and piperazine-activated single-channel currents were recorded from the bag region of the somatic muscle of the nematode parasite *Ascaris suum*. Cell-attached and outside-out patch-clamp techniques were used. Clean membranes were routinely prepared using collagenase.

2 GABA (concentrations greater than 1 μM) or piperazine (concentrations greater than 200 μM) applied to the extracellular surface of the patches brought about the opening of channels producing rectangular shaped current pulses of varying duration but essentially constant amplitude. The I/V relationships of the single-channel currents for both agonists were linear and had conductances in the region of 22 pS (in symmetrical 170 mM Cl^-). The reversal potential was near 0 mV when Cl^- was equally distributed on both sides of the membrane. Occasionally two subconductance states were seen. The mainstate single-channel permeability was estimated to be 4×10^{-14} $cm^3 s^{-1}$.

3 At low concentrations of GABA (3–4 μM), the effective mean channel open time was in the region of 32 ms (−75 mV, 22°C, cell-attached patches). At low concentrations of piperazine (500 μM) the effective mean open channel lifetime was shorter, in the region of 14 ms (−75 mV, 22°C cell-attached patches). For each agonist the channel open lifetime distributions were best described by the sum of two exponentials suggesting two open mainstates. Channel openings occurred as single events and in bursts with brief closed periods within bursts. The channel closed time histograms at these concentrations were best described by the sum of up to three exponentials, suggesting the presence of three closed states. Channel open times showed no appreciable voltage sensitivity.

4 Before desensitization, increases in agonist concentration produced an increase in the probability of the channel being open. The increased probability was associated with an increase in the frequency of channel opening, an increase in the effective mean channel open time, an increase in burst duration, an increase in the number of openings per burst, together with a reduction in the proportion of brief openings.

5 Desensitization was seen as a decline in the probability of the channel being opened during prolonged applications of agonist. It was associated with the appearance of very long (seconds) closed periods. The distributions of the closed channel times were then best described by up to four exponentials.

Introduction

Nematode parasites continue to inflict much suffering on human and animal hosts. Approximately one in five of the world's human population is infected with intestinal nematodes (Standen, 1975), while infestations in domestic animals are a major source of economic loss. Anthelmintics make a substantial contribution to the control of these parasites.

The electrophysiological effects of anthelmintics on nematodes can be studied in the parasite *Ascaris suum*. This is because this pig parasite has large muscle cells which have allowed easy intracellular recording (e.g. Jarman, 1959). The muscle cells of *Ascaris suum* are composed of four parts: the bag, spindle, arm and syncytium, (Figure 1). The bag contains the nucleus; the spindle is the contractile portion; the arm conducts action potentials from the neuromuscular junction at the syncytium (De Bell *et al.*, 1963).

It has been shown that the important anthelmintic, piperazine, acts as a low potency agonist at extrasynaptic γ-aminobutyric acid (GABA) receptors on

© The Macmillan Press Ltd 1985

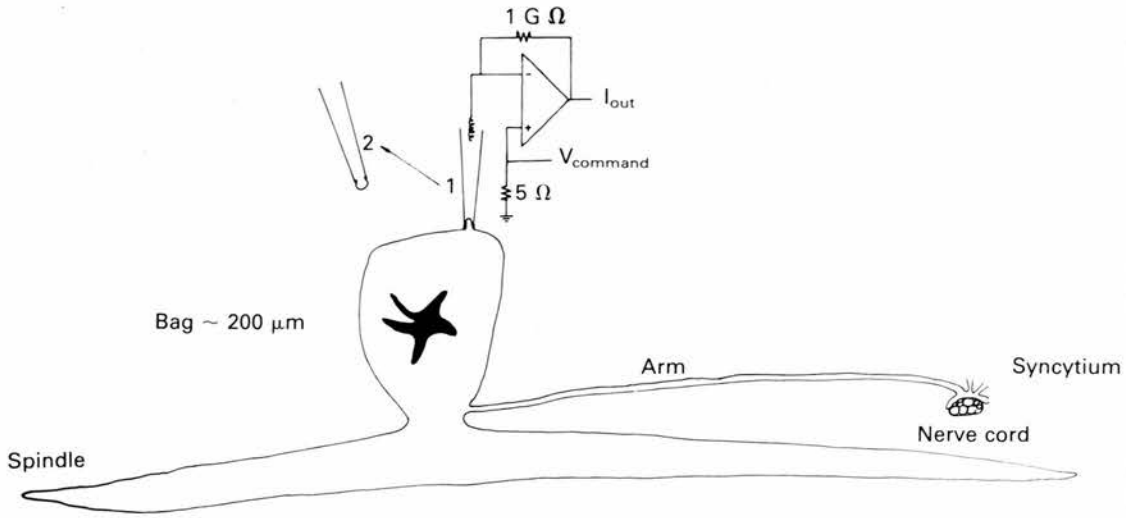


Figure 1 Diagram of *Ascaris* muscle cell and recording technique. An electrode recording from a cell-attached patch (1) is seen applied to the bag region of the muscle cell. An outside-out patch (2) is also shown. The transpatch current was monitored at 'I out'. The potential of the patch electrode was controlled at 'V command'.

the bag region of the muscle and that activation of the receptors gives rise to an increase in Cl^- conductance (Martin, 1982). As a further study of effects of agonists on these extra-synaptic receptor operated channels it was decided to carry out a patch-clamp study in the manner of Hamill *et al.* (1981). This paper describes observations which allow a description of the unitary conductance and the kinetic behaviour of single extra-synaptic receptor operated channels opened by GABA and piperazine. An initial account has already appeared (Martin 1983).

Methods

In general the methods of Hamill *et al.* (1981) were followed but the application to *Ascaris* is described below.

The preparation

Specimens of *Ascaris suum* were collected from the local slaughter house and maintained in Locke solution (replaced daily) at 32°C in a water bath. The *Ascaris* were used for experiments within four days. A 2 cm flap preparation made from the anterior region of the worm was pinned on to Sylgard in an experimental chamber which was surrounded by a water jacket to maintain the temperature at 22–25°C. Generally the smaller parasites (about 10 cm) were used rather than the larger ones.

Enzyme treatment

The preparations were routinely treated with collagenase (1 mg ml^{-1}) for 1 h to remove the superficial connective tissue and extracellular matrix which normally cover the bag membrane. Electron microscopy confirmed that this enzyme treatment was sufficient to prepare 'clean' membranes. The addition of this enzyme at 22–25°C to the preparation was associated with a decline in the bag resting membrane potential from about −35 mV to less than −7 mV. There was also a small increase in the bag input conductance. Despite this, it was shown using intracellular recording techniques that bath application of GABA still produced large reversible increases in bag input conductance as in the control period before enzyme treatment. However, as a result GABA produced little or no hyperpolarization of the bag membrane. Estimation of the GABA reversal potential using current pulse injections (Martin, 1980) showed that this had declined from −65 mV to between −7 mV and 0 mV. This observation indicated an increase in the intracellular Cl^- concentration to near extracellular levels. During patch experiments membrane potentials were checked using the whole-cell recording mode. However, it was not possible to clamp the cell effectively in this way because of the high input conductance of the cell (2–3 μS).

The effect of collagenase on membrane potential has not been described in other muscle preparations under similar circumstances. As a further examination

of the action of collagenase, the time and temperature dependency of the effect on potential was examined using intracellular recording electrodes. It was found at 22–25°C that the membrane potential declined gradually to less than −7 mV within 20 min of applying the collagenase. The membrane potential did not recover at 22–25°C during further periods of examination (up to 6 h). When the temperature of the preparation was raised to 32–37°C it was found that there was a partial recovery of the resting membrane potential within 30 min. These observations could be explained by the increase in the effective surface area of the membrane exposed to Ringer solution as a result of collagenase action together with the suppression at 22–25°C of an active transport mechanism which is implicated in maintaining the resting membrane potential (Brading & Caldwell, 1971). It was not advantageous to record from preparations at higher temperatures since spontaneous depolarizing potentials and movement can be present (Martin, 1980); further details of the flap preparation are available (Martin, 1980).

Ringer solution

The preparation was maintained in a low-Ca^{2+} Ringer solution containing (mM): NaCl 135, KCl 3.0, $MgCl_2$ 15.7, glucose 3.0 and Tris 5.0 adjusted to pH 7.6 with maleic acid. A low-Ca^{2+} Ringer was used for two reasons: firstly, to reduce spontaneous muscle contraction; secondly, to reduce spontaneous Ca^{2+} activated ion channels. Initial experiments showed that spontaneous high conductance (> 100 pS) channels were frequently present in membrane patches taken from the bag. These channels were abolished when the preparation was perfused with low- Ca^{2+} Ringer solution.

Patch electrode solution

The patch electrode was filled with a solution containing (mM): CsCl 140, $MgCl_2$ 15.7 and Tris 5.0 adjusted to pH 7.6 with maleic acid. The Cs^+-rich solution was used to suppress any K^+ currents. EGTA was not included as a Ca^{2+} buffer because its chemical structure suggested the possibility of an interaction with the GABA receptors: this was not examined systematically.

Recording

Patch electrodes were made from Hawksley microhaematocrit capillary tubes (cat. no. 1604) and had a resistance of 1 MΩ with an outside tip diameter of 1 μm. They were connected by a Clarke's electromedical suction pipette holder to the input of the current-voltage converter. The current-voltage converter was laboratory made and based on a Teledyne Philbrick 1035 op-amp and a 1 GΩ (Welwyn) feedback resistor. Recordings were amplified and filtered at 1 kHz (−3 dB). The patch electrodes were coated to near the tip with Sylgard to improve the frequency response of the recording system.

A cell-attached patch was formed when a patch electrode was pushed gently against the bag membrane and suction was applied to the pipette. After suction the seal resistance between the pipette tip and membrane patch gradually increased to greater than 1 GΩ. It was then possible to alter the transpatch potential by altering the patch electrode potential. Outside-out patches were prepared by rupturing the cell- attached patch by applying a high transpatch potential (> 150 mV) and then gently withdrawing the patch electrode from the bag. Under favourable circumstances the patch resealed in the outside-out conformation (Hamill *et al.*, 1981).

Data processing

Responses were monitored on an oscilloscope and recorded on a Racal Thermionic Store Four FM tape recorder (slowest frequency response 1.25 kHz, −1 dB). Initially single-channel current responses were played back from the tape at one quarter the original speed on to a Devices MX212 two channel pen recorder. The channel open and closed times were then analysed by hand with the aid of a Reichert Jung videoplan. Subsequently recordings on tape were analysed with the aid of a Cromenco microcomputer programmed to measure channel open and closed times. The data were played back from the tape, sampled and digitized every 200 or 400 μs and continually monitored and adjusted for slow d.c. drifts. An increase in current of greater than about 70% of the unit channel current was recorded as a channel opening. After an opening, a decrease in the current to less than about 50% of the single channel current was recorded as channel closing. The programme then determined and stored the durations of each open and closed interval in order of their occurrence (as the integer number of sample intervals). For each patch record mean values, frequency histograms and their semi-log plots of open and closed times were displayed and plotted by the microcomputer programme. The numbers representing open and closed times were transferred over the local area network to a mainframe computer for further analysis. Effective mean open times are here quoted as the observed values without correction for unresolved short intervals. Analysis of the data by hand or computer gave essentially the same estimates for effective mean open and closed times. However, these values were affected by the threshold settings since measurement of open times is affected by the number of rapid brief closings or 'flickerings' that

are detected by this analysis. Measurements of open times in the presence of GABA or piperazine were therefore made using very similar threshold settings for both sets of data.

Statistics

It was assumed that the channel open or closed times were distributed as a mixture of m exponentials. The probability density function for the open or closed time of T ms is then

$$f(T) = \sum_{i=1}^{m} \frac{K_i}{U_i} e^{-T/Ui} \qquad -(1)$$

Where the ith exponential has a mean U (>0) and is present in the proportion K_i ($1 \geq K_i \geq 0$) and

$$\sum_{i=1}^{m} K_i = 1$$

When sampling frequency is δ ms the probability that an open or closed interval of T ms duration is recorded as an opening or closing of j intervals (where j is an integer) is

$$\begin{aligned} p(j|T) &= [T/\delta] + 1 - T/\delta && \text{if } j = [T/\delta] \\ &= T/\delta - [T/\delta] && \text{if } j = [T/\delta] + 1 \\ &= 0 && \text{otherwise} \end{aligned} \qquad -(2)$$

where [z] denotes 'the integer part of z'.

Combining (1) and (2) the probability that an opening or closing is recorded as being between j and k intervals (inclusively) is

$$P(j,k) = \int_0^{\infty} \sum_{l=j}^{k} p(l|T)\, f(T)\, dT$$

$$= \sum_{i=1}^{m} K_i\, U_i/\delta\, (e^{-\delta j/Ui} - e^{-\delta(k+1)/Uj})\, (e^{-\delta/Ui} - 1) \qquad -(3)$$

If open or closed times less than T_0 ms or greater than T_1 ms are (partially) censored that it is not observed, then (3) holds between the limits j_0 and k_0 where

$$j_0 = |T_0/\delta - \sum| + 2$$

and

$$k_0 = |T_1/\delta + \sum| - 2$$

and $\sum$ is an arbitrarily small positive number.

Conditional on the observed intervals being between j_0 and k_0

$$P(j,k) = \frac{\sum_{i=1}^{m} K_i\, U_i/\delta\, (e^{-\delta j/Ui} - e^{-\delta(k+1)/Ui})\, (e^{-\delta/Ui} - 1)}{\sum_{i=1}^{m} K_i\, U_i/\delta\, (e^{-\delta j0/Ui} - e^{-\delta(k0+1)/Ui})\, (e^{-\delta/Ui} - 1)}$$

which has the property that

$P(j_0, k_0) = 1$.

Examination of the open and closed time histograms show that openings less than 1 ms were not well detected and measured. Therefore, during the analysis T_0 was taken as 1 ms (Colquhoun & Sigworth 1983). When δ equals 0.2 ms j_0 was 6 and when δ equals 0.4 ms j_0 was 4. The selection of periods of observation inevitably led to censoring of long open or closed times so k_0 was set to 30,000.

If the observations are independent then the negative log-likelihood is

$$L = -\sum_{l=1}^{n} l_n P(Y_l, Y_l)$$

where P is given in (4), and Y_l is a sample of open or closed times. Parameters K and U in P were estimated from Y by minimizing L. This was carried out numerically by iterative refinement from initial guesses at the parameter values. Parameters were estimated for m = 1, 2, 3 for open times and m = 1, 2, 3, 4, 5 for closed times. It was taken that a decrease in the negative log-likelihoods of 3.0 or more for each addition of one extra exponential component indicated a significant improvement in fit.

The parameter estimates for best fitting models were then determined together with approximate standard errors based on a quadratic approximation to L. The goodness of fit of the best fit models was tested by calculating the chi-squared statistic and found to be adequate. It is pointed out that the fitting of exponentials in this way ignores time sequencing in the data which ought to carry important information when fitting compartmental models.

Drugs

The drugs used were GABA and piperazine hexahydrate. The enzyme used was collagenase (C-0130). All drugs were obtained from Sigma.

Results

The following experiments were carried out on muscle cells from 45 preparations. GABA- or piperazine-activated channels were recorded from 45 cell-attached patches and 15 outside-out patches. GABA- or

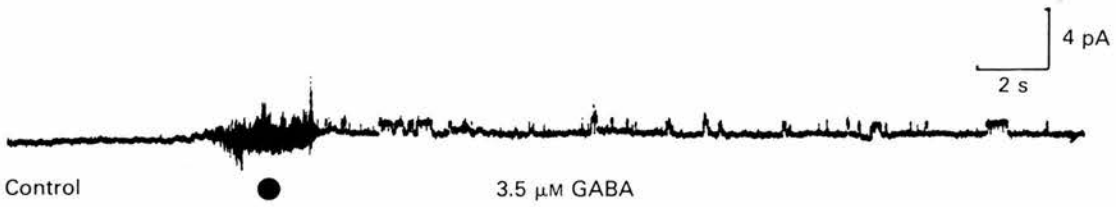


Figure 2 Effect of GABA bath-application on an outside-out patch: GABA 3.5 μM was bath-applied during the artefact marked (●). It produced rectangular outward (upward) currents of about 1 pA amplitude but of varying duration (mean open time 32 ms). Up to two channels were present in this patch. After a period of about 5 min the channel activity became quiet presumably due to desensitization (not shown). Transpatch potential + 40 mV, 170 mM Cl^- on both sides of the membrane. Although GABA 3.5 μM was also present in the patch electrode, no channels were observed prior to bath-application.

piperazine-induced channels were recorded in about 15% of cell-attached patches forming giga-seals. Single-channels with similar conductances and open times to GABA or piperazine channels were not recorded when the agonists were omitted from the patch electrode in 56 consecutive cell-attached patches, although other spontaneous ion channels were very occasionally seen. The formation of outside-out patches was generally more difficult; only 8% of cell-attached patches with giga-seals led to the production of successful outside-out patches. Observations on GABA and piperazine channel open times and conductances from the two patch types were not detectably different.

Channel activation

Figure 2 shows the typical effect of bath-application of 3.5 μM GABA to an outside-out patch with a transmembrane potential of + 40 mV. Following application of the agonist there appeared up to two rectangular outward current pulses which lasted for varying durations. The amplitude of the channel currents was essentially constant at the fixed transmembrane potential.

In the experiment illustrated in Figure 2, GABA (3.5 μM) was also present in the patch electrode (on the intracellular side of the outside- out patch) but no channel currents were observed prior to the external

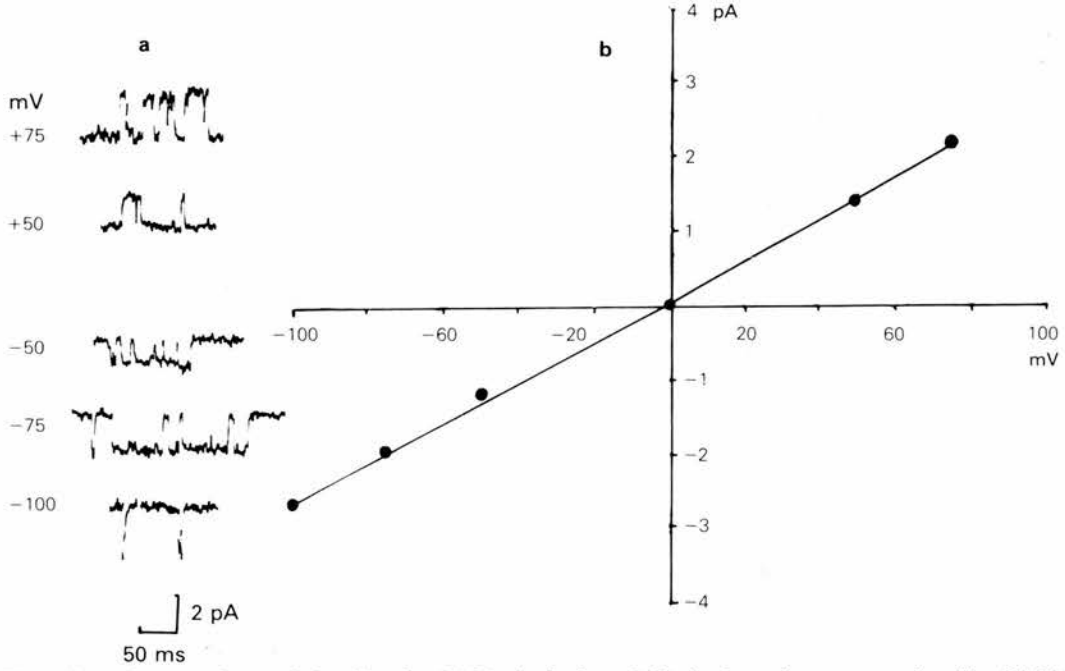


Figure 3 Current-voltage relationship of a GABA single channel. Single channel currents produced by GABA 7.5 μM using an isolated outside-out patch recording are seen at different transpatch potentials in (a). The current-voltage relationship (linear slope G = 26 pS) is plotted in (b): ordinate scale, single-channel current amplitude; abscissa scale, transpatch potential. The reversal potential was near 0 mV.

application of the agonist, so this observation is consistent with the receptor binding site only being present on the external surface of the membrane.

Channel conductance

In order to determine the channel conductance the amplitudes of the current steps at different transpatch potentials were measured. The conductance was then determined from the slope of the current voltage relationship. Figure 3 shows a typical (linear) current voltage relationship obtained between + 75 and − 100 mV from an isolated outside-out patch with GABA as the agonist. The reversal potential with Cs^+ as the main cation in the patch electrode and symmetrical Cl^- across the patch was near 0 mV. Reversal potentials close to 0 mV were also observed with cell-attached patch recordings (not shown) and enzyme-treated preparations (see Methods) where the intracellular Cl^- concentrations were found to approach extracellular concentrations. These observations on the reversal potential are consistent with the channel currents being carried by Cl^- ions. The slope of the current-voltage relationship shown in Figure 3 gave a value of 26 pS for the channel conductance. The mean estimates for the channel conductance using isolated-patches were GABA 22.0 ± 1.2 pS (mean ± s.e., $n = 11$) and in two piperazine experiments 19.0 pS: the mean estimates from cell-attached patches were GABA 21.7 ± 1.2 pS (mean ± s.e., $n = 11$) and piperazine 21.4 ± 1.5 pS (mean ± s.e., $n = 11$). There was no significant difference (t test) between any of these values. It was concluded from these observations that the channels opened by GABA and piperazine have the same mainstate conductance.

Subconductance states

Occasionally with GABA or piperazine the amplitudes of the single channel currents did not reach their full level during opening or closing but found levels approximately 30% or 70% of the full levels, (Figure 4). This was interpreted as indicating the presence of two subconductance states. However, openings of reduced amplitude comprised only a small fraction of the total open time. For example, in one experiment with 20 μM GABA as the agonist (− 75 mV cell-attached patch) less than 2% of the total open time was in any of the subconductance states. It was unlikely that the reduced conductance states arose from simultaneous opening of separate channels of opposite polarity since they were never observed at these potentials in isolation. Hamill *et al.* (1983) have also described multiple conductance states in cultured mouse spinal cord neurones for GABA and glycine channels.

Single channel permeability

Although channel conductances of around 22 pS were observed this quantity does not take account of the Cl^- concentration on each side of the membrane; channel conductances with more physiological Cl^- concentrations present are expected to be lower (Sakmann *et al.*, 1983). However, if constant field conditions were assumed, it was possible to estimate the single channel permeability. For example, a channel current of 1.57 pA was observed to flow with a driving force of − 70 mV (G = 22 pS) across the patch. An equal Cl^- distribution of 170 mM gives rise to an estimate of around 4×10^{-14} cm^3 s^{-1} for the mainstate

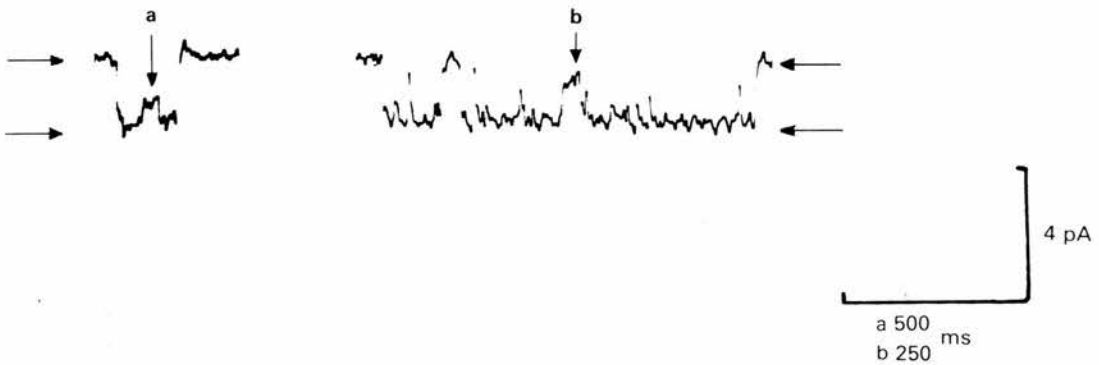


Figure 4 Subconductance states. Two cell-attached patch recordings (inward currents downwards, transpatch potential − 75 mV) are shown. (a) GABA 3 μM as agonist shows a subconductance state marked with the vertical arrow of about 70% of the mainstate. (b) Piperazine 1 mM as agonist shows a subconductance state marked with a vertical arrow which is about 30% of the mainstate. Horizontal arrows mark the main open state amplitude.

single channel permeability. The current of 1.57 pA corresponds to the movement of 10 million Cl^- ions every second through the ion channel. If the Cl^- ions pass in single file separated by a minimum distance of twice the Pauling radii (3.9 Å) a mean velocity through the membrane of around 4 mm s^{-1} would be required. Bormann *et al.* (1983) have estimated the permeability of GABA activated channels in cultured rat hippocampal neurones to be 6.4×10^{-14} cm^3 s^{-1}.

The duration of channel open times

Figure 5a shows a typical example of a cell-attached patch recording with 3 μM GABA as the agonist; the transpatch potential was − 75 mV. In this experiment the effective mean open time was found to be 34 ms. The distribution of channel open times for the experiment illustrated in Figure 5 is shown in the histogram of Figure 6a. The overall mean estimate from other experiments under the same conditions of concentration and potential for the GABA open times was 30.5 ± 2.7 ms (mean ± s.e., $n = 6$). When 500 μM piperazine was used as the agonist instead of GABA, shorter mean open channel times were observed. Figure 5b shows a typical recording using a cell-attached patch at − 75 mV. The effective mean channel open time in this experiment was 18 ms. Figure 7a shows the distribution of the piperazine open channel times observed for the experiment illustrated in Figure 5b. The mean estimate for the piperazine channel open times obtained from experiments under the same conditions of concentration and potential was

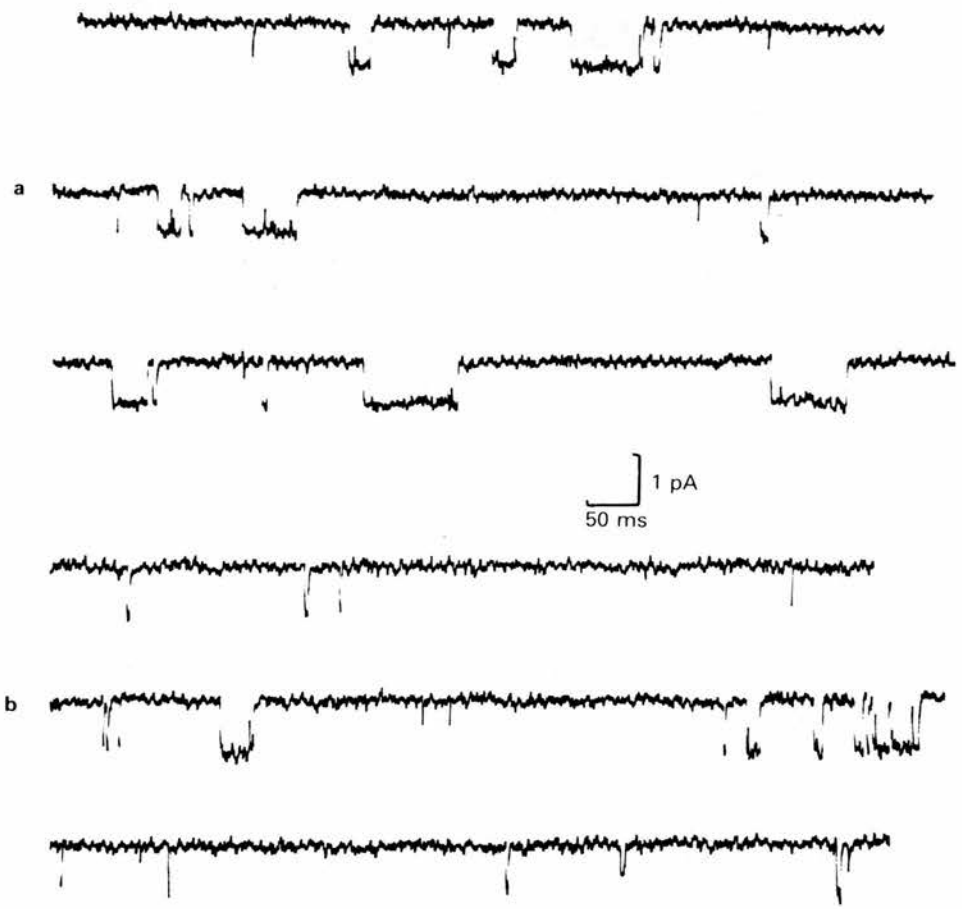


Figure 5 Continuous single-channel recordings using low agonist concentrations, cell-attached patches, transpatch potential − 75 mV, Cl^- concentration equal on both sides of membrane. Brief and longer openings are seen (downwards, inward current). Some brief closings giving rise to bursts are seen: (a) three traces GABA 3 μM as agonist; (b) three traces piperazine 500 μM as agonist. Effective channel open times: GABA, 33 ms; piperazine, 18 ms. Measured burst durations: GABA 39 ms; piperazine 24 ms.

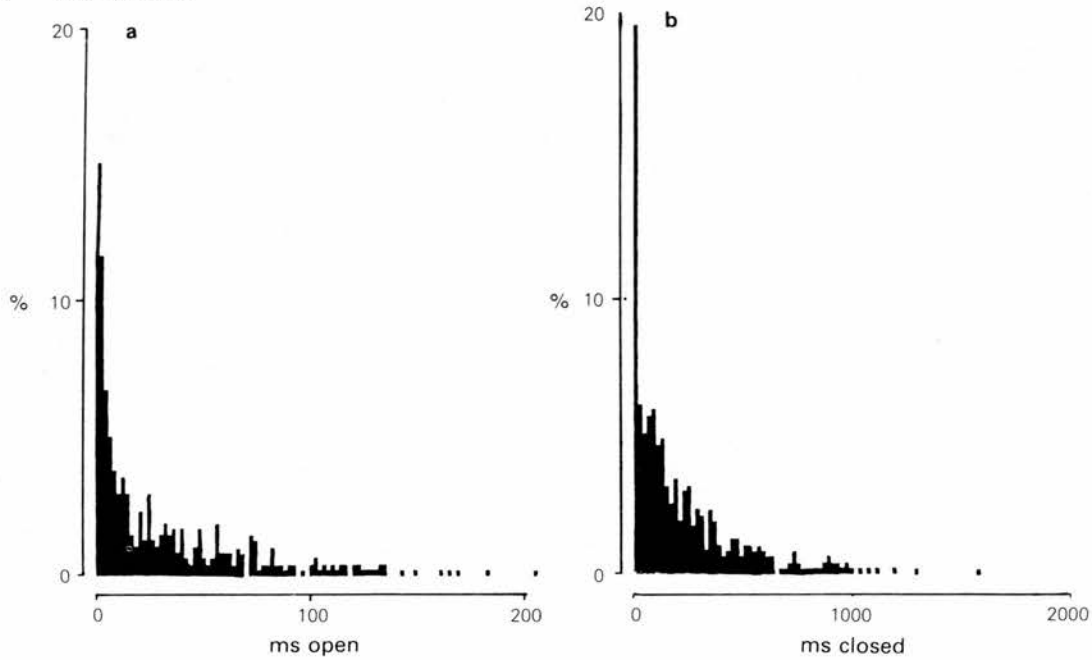


Figure 6 Distributions of GABA open and closed times. A cell-attached patch with GABA 3 μM as agonist and transpatch potential of − 75 mV was used (Figure 5a was part of the recording). (a) Histogram of GABA effective mean open times, mean ± s.d. = 32.6 ± 41.8 ms, 2 ms binwidths. (b) GABA effective closed times, mean ± s.d. = 221 ± 252 ms, 20 ms binwidths. $n = 471$, ordinate scale: frequency (%).

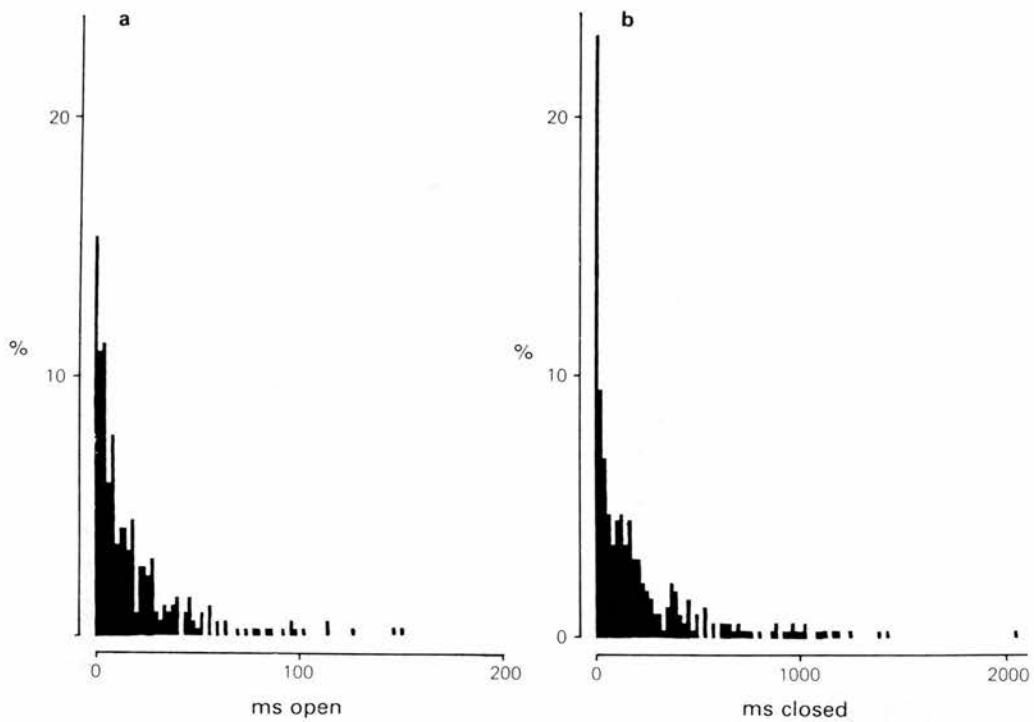


Figure 7 Distributions of piperazine open and closed times. A cell-attached patch with piperazine 500 μM as agonist and transpatch potential of − 75 mV was used (Figure 5b was part of the recording). (a) Histogram of piperazine channel effective open times, mean ± s.d. = 18.7 ± 4.0 ms, 2 ms binwidths. (b) Histogram of piperazine channel effective closed times, mean ± s.d. = 258 + 664 ms, 20 ms binwidths. $n = 337$, ordinate scale: frequency (%).

13.8 ± 2.4 ms, (mean $\pm$ s.e., $n = 4$). Similar results with the same concentrations of agonists were obtained with outside-out patches.

Effect of membrane potential on open time

The effect of membrane potential on channel open times for 3–4 μM GABA and 500 μM piperazine was examined using cell-attached patches. It was found for GABA, using the available observations between -100 mV and -40 mV, that there was no significant correlation between the membrane potential and mean channel open times ($r = 0.26, n = 12, P < 0.05$). It was also found for piperazine that there was no significant correlation using the observations between -150 mV and -75 mV ($r = 0.6$, $n = 10$, $P < 0.05$). These results suggest that the channel open times were not appreciably voltage sensitive.

The distribution of channel open times

The histograms of Figures 6a and 7a illustrate typical distributions of channel open times for GABA (3 μM) and piperazine (500 μM) recorded under the same patch potential of -75 mV. It was found that these distributions could not be described with a single exponential but were best described by a double exponential. Table 1 summarises the values of the parameters estimated for these double exponentials. In the experiment with GABA as the agonist the fast component had a mean value of 2.1 ms while the slow component had a mean value of 46 ms. For piperazine the mean value of the fast component was 7.6 ms while the mean value of the slow component was 28 ms. After the double exponential had been fitted it was possible to estimate the relative number of fast openings and slow openings for both GABA and piperazine. It can be seen from Table 1 that 36% GABA and 47% piperazine openings were of the fast type while the remainder were of the slow type. As a consequence the brief openings for GABA carried only 3% of the total current but for piperazine 19% of the current was carried by the brief openings. During both of these recordings no simultaneous openings were observed. Simultaneous double openings would be expected if there were two channel types activated by the GABA agonists. The lack of simultaneous openings then implies that there are at least two open channel states rather than two separate channel populations. (Colquhoun & Hawkes, 1981; 1982). Similar observations have been made with acetylcholine channels (Colquhoun & Sakmann, 1981) and glutamate channels (Cull-Candy & Parker, 1982). Dudel (1979) has observed two components in noise analysis and relaxation studies for GABA activated channels, while Jackson *et al.* (1982) have observed a double exponential in the distribution of GABA channel open times obtained from cultured mouse spinal cord cells.

The distribution of channel closed times

In both cell-attached and outside-out patches with low concentrations of GABA or piperazine as the agonist, opening often occurred in bursts, see for example Figure 2 and 5. The existence of this bursting behaviour was due to brief (1–6 ms) closed periods occurring in sequence between brief or long openings. These brief closings gave rise to the fast components of the exponentials which were required to describe the distribution of the channel closed times (Figures 6b, 7b and Table 2). When the length of the burst was defined

Table 1 Estimates of parameters of open probability density functions

Open distributions	*No of components*	*means* $\pm$ s.e. (ms)		
Low agonist concentration	m	U_1	U_2	K_1
3 μM GABA	2	2.1 ± 0.6	46 ± 5	0.36 ± 0.05
500 μM piperazine	2	7.6 ± 3.6	28 ± 6	0.47 ± 0.17
High agonist concentration	m	U_1	U_2	K_1
20 μM GABA	2	4.0 ± 1.4	101 ± 17	0.09 ± 0.04
1 mM piperazine	1	—	53 ± 2	0

The probability density functions of channel open times were described by a mixture of m exponentials.

$$f(T) = \sum_{i=1}^{m} \frac{Ki}{Ui} e^{-T/Ui}$$

, where the i th exponential has a mean value Ui ms and is present in the proportion K_i ($1 > K_i > 0$). The best estimates $\pm$ s.e. for the parameters -75 mV, cell-attached patches, typical K_i & U_i from single patch recordings.

T is ms and $\sum_{i=1}^{m} K_i = 1$

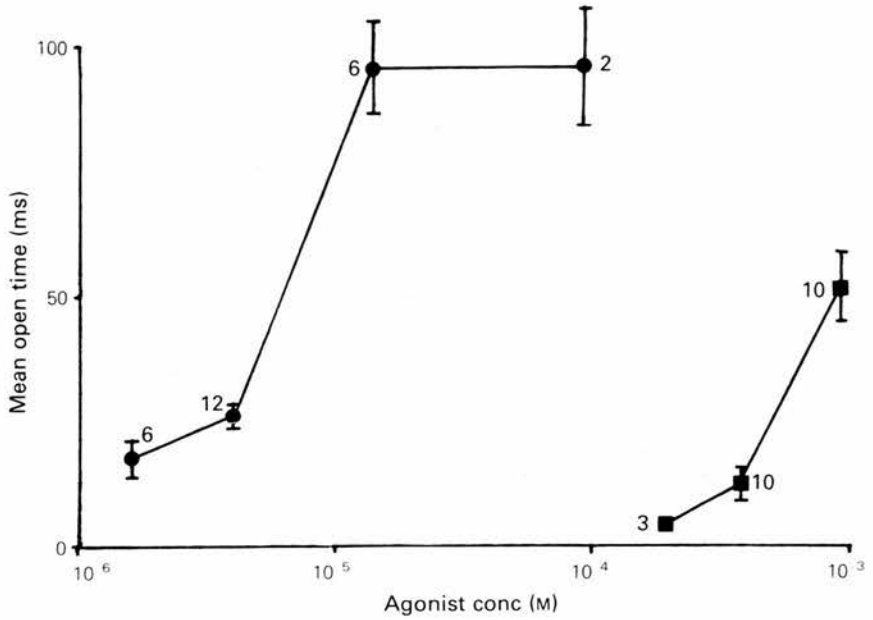


Figure 8 Effective mean open time-agonist concentration relationship. Ordinate scale: effective mean channel open time. Abscissa scale: agonist concentration. GABA (●); piperazine (■). Cell-attached patches were used with transpatch potentials between − 50 and − 100 mV. The numbers of recordings, each with 70–900 openings, together with the standard error bars are shown.

as the duration of a single opening or sequence of openings separated by closings less than 7.5 ms it was found that the mean burst length depended on the nature of the agonist. The mean burst duration for 3 μM GABA was always longer (39 ms in the experiment illustrated in Figure 5) than for 500 μM piperazine (24 ms in the experiment in Figure 5). This bursting behaviour was observed in outside-out patches soon after the bath-application of low agonist concentrations (e.g. Figures 2 and 10) and this suggests that the phenomenon is not due to desensitization (Sakmann *et al.*, 1980). Another possible explanation for the bursting behaviour could have been that the agonists were acting in addition as channel blockers (Neher & Steinbach, 1978). Agonist channel block was thought unlikely since it was found that the effective mean channel open time actually increased rather than decreased with agonist concentration (Figures 8, 9 and 10). A channel block mechanism would be expected to produce a decrease in open time with an increase in agonist concentration. It was also found that the mean channel open times were not appreciably voltage sensitive, unlike a channel block mechanism. The distributions of the closed times at

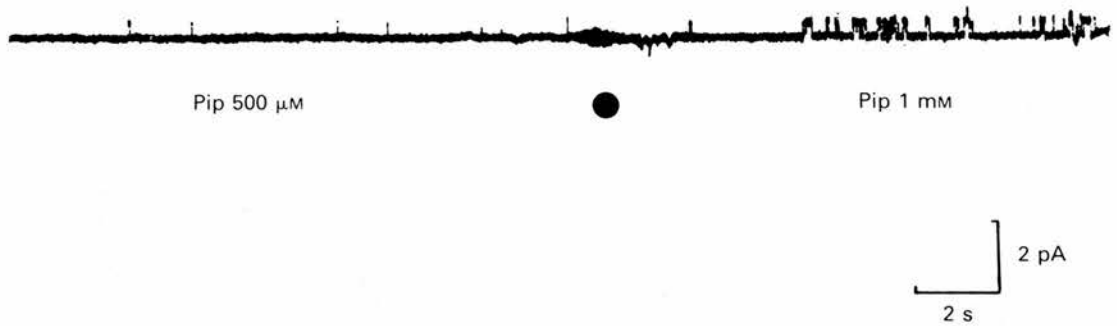


Figure 9 Effect of increasing agonist (piperazine) concentration on an outside-out patch. An outside-out patch recording is shown with a transpatch potential of + 50 mV. At the artefact marked (●) the concentration of piperazine was increased from 500 μM to 1 mM. The probability of the channel being open increased from less than 0.1 to 0.3. There was also an associated increase in effective mean channel open time from 12 ms to 38 ms. The channel activity became quiet after 1 min in the 1 mM piperazine, presumably due to desensitization (not shown).

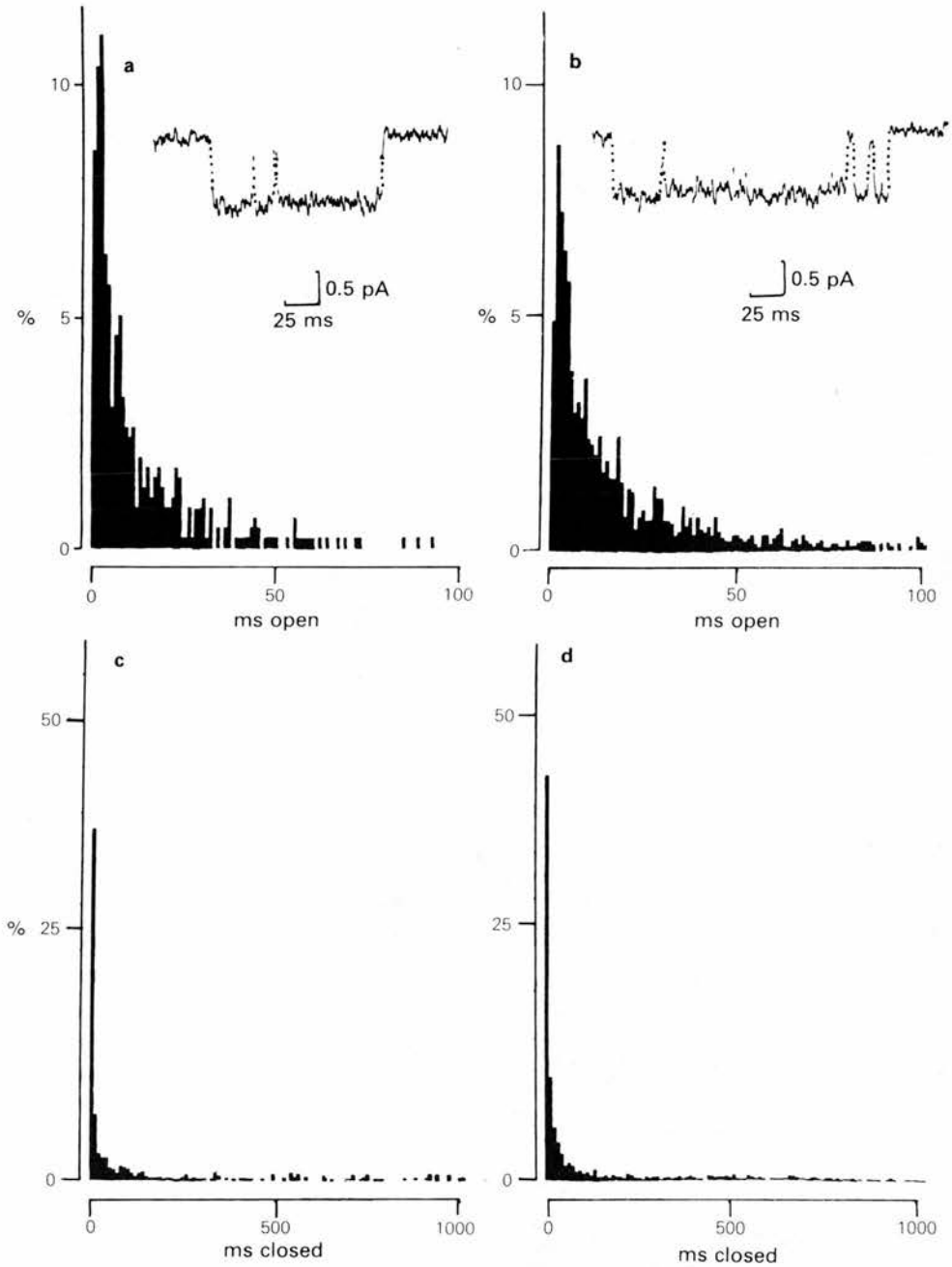


Figure 10 Histograms of the open and closed time distributions at two GABA concentrations: isolated outside-out patch − 75 mV (inset, openings inward currents shown downwards, retouched), temperature 22°C. (a) GABA 2.5 μM; sample recording and histogram of open times; 1 ms binwidths; $n = 452$; ordinate scale: frequency percentage; effective mean open time ± s.d. 14.4 ± 19.5 ms. (b) GABA 4.5 μM; sample recording and histogram of open times; 1 ms binwidths; $n = 1532$; ordinate scale: frequency percentage; effective mean open time ± s.d. 24.4 ± 49.7 ms; note the decrease in the proportion of fast openings. (c) GABA 2.5 μM; histogram of closed times; 10 ms binwidths; $n = 452$; ordinate scale frequency percentage; mean closed time ± s.d. 535.1 ± 1044.7 ms. (d) GABA 4.5 μM; histogram of closed times; 10 ms binwidths; $n = 1532$; ordinate scale frequency percentage; mean closed time ± s.d. 281.2 ± 952.4 ms; note the increase in the proportion of brief closings which was associated with a mean increase in the number of rapid closings per burst from 0.64 to 1.4. No desensitization was evident during the application of the higher agonist concentration.

low agonist concentrations were best described by up to three exponentials. The second component in the distribution was due to the tendency of bursts to be separated by longer closed periods (5–150 ms) giving rise to clusters. The third component was due to much longer closed periods which separated the clusters. Table 2 shows the values estimated for the parameters of the exponentials used to describe the distributions of closed times for the experiments illustrated in Figure 5, 6b and 7b. These observations suggest that there are up to three closed states at these agonist concentrations.

Effect of increased agonist concentration

Figure 9 illustrates with an outside-out patch recording effects of increasing the agonist concentration from 500 μM piperazine to 1 mM piperazine. In this experiment the probability of the channel being open increased from less than 0.1 with 500 μM piperazine to 0.3 with 1 mM piperazine. This was associated with an increase in the effective mean channel open time from 12 ms to 38 ms. The number of openings per bursts increased from about 1 to a mean of 3.2; the burst duration increased from a mean of 12 ms to a mean of 122 ms. After a period of 30 s at this higher concentration of piperazine the channel became quiet, presumably due to desensitization (not shown).

Figure 10 illustrates some representative recordings and the distributions of open and closed times from another outside-out patch experiment where the GABA concentration was increased from 2.5 μM to 4.5 μM. The probability of the channel being open increased from 0.03 to 0.09; the effective mean channel open time increased from 14 ms to 24 ms. Comparison of Figure 10a and b shows that the proportion of brief openings declined with increased agonist concentration. In contrast the proportion of brief closings increased (Figures 10c and d). The number of brief closings per burst increased from a mean of 0.64 to 1.4; the mean burst duration increased from 24 ms to 58 ms. When the distributions of the open times were described by the sum of two exponentials it was found that: the proportion of brief openings declined from 48% to 23% (both with a mean of 4.0 ms); in contrast the proportion of longer openings increased from 52% (mean 22 ms) to 77% (mean 46 ms). When the distributions of the closed times were described by the sum of exponentials it was found that: the proportion of brief closings forming bursts increased from 39% (mean 4.5 ms) to 58% (mean 3 ms); the second closed component separating the bursts and forming clusters became shorter and reduced from a mean of 50 ms (20% of closings) to 28 ms (19% of closings); the third component separating clusters also became shorter and decreased from a mean of 1,180 ms (41% of closings) to 740 ms (23% of closings).

Table 2 Estimates of parameters of closed probability density functions

Closed distributions	*No. of components*	*means* ± s.e. (ms)							
Low agonist concentration	m	U_1	U_2	U_3		K_1	K_2		
3 μM GABA	3	1.6 ± 0.5	40 ± 20	1320 ± 130		0.13 ± 0.06	0.07 ± 0.03		
500 μM piperazine	3	1.8 ± 0.6	130 ± 30	510 ± 100		0.20 ± 0.03	0.51 ± 0.09		
High agonist concentration	m	U_1	U_2	U_3	U_4	K_1	K_2	K_3	
20 μM GABA	4	5.6 ± 1.1	34 ± 14	310 ± 170	1950 ± 60	0.49 ± 0.07	0.19 ± 0.07	0.13 ± 0.04	
1 mM piperazine	4	2.7 ± 0.2	13 ± 2	230 ± 80	2760 ± 70	0.69 ± 0.04	0.23 ± 0.04	0.04 ± 0.01	

The probability density functions of channel closed times were described by a mixture of m exponentials.

$$f(T) = \sum_{i=1}^{m} \frac{Ki}{Ui} e^{-T/Ui}$$

, where the i th exponential has a mean value U_i ms and is present in the proportion K_i ($1 > K_i > 0$).
The best estimates ± s.e. for the parameters − 75 mV, cell-attached patches, typical K_i & U_i from single patch recordings.

T is ms and $\sum_{i=1}^{m} K_i = 1$

The effect of agonist concentration over a wider range was examined using cell-attached patches. Figures 8 and 12c and d show the effect of concentration on effective mean open times for GABA and piperazine. It can be seen that the log-dose response relationship for piperazine resembles that of GABA but it is shifted along the concentration axis. Tables 1 and 2 show some typical probability density functions estimated for channel open and closed times at 20 μM GABA and 1 mM piperazine; part of the recordings are shown in Figure 12. It can be seen as before that there is a decrease in the proportion of brief openings and an increase in the proportion of brief closings with increasing agonist concentration. For example, at 3 μM GABA, 36% of the openings were of the brief type but at 20 μM, only 9% were of the brief type (Table 1); at 3 μM GABA, 13% of the closings were of the brief type while at 20 μM, 49% were of the brief type (Table 2). A similar change in the proportion of brief events were also seen with piperazine (Tables 1 and 2). Increases in channel open time with an increase in ligand concentration have not been observed with acetylcholine (Sakmann *et al.*, 1980) but they have been observed for the glutamate receptor (Gration *et al.*, 1981) and for Ca^{2+} activated K^+ channels (Barret *et al.*, 1982).

Desensitization

Desensitization was often seen after prolonged application of higher agonist concentrations. It was interpreted as the cause of the decline, sometimes abrupt, in the probability of the channel being open. It was associated with long closed periods (seconds) between normal periods of activity giving rise to grouping of channel activity. This behaviour is illustrated in Figure 11 with an outside-out patch following application of 4.6 μM GABA. Following channel activation for 60 s there was a long quiescent period. After 90 s channel opening recommenced and contin-

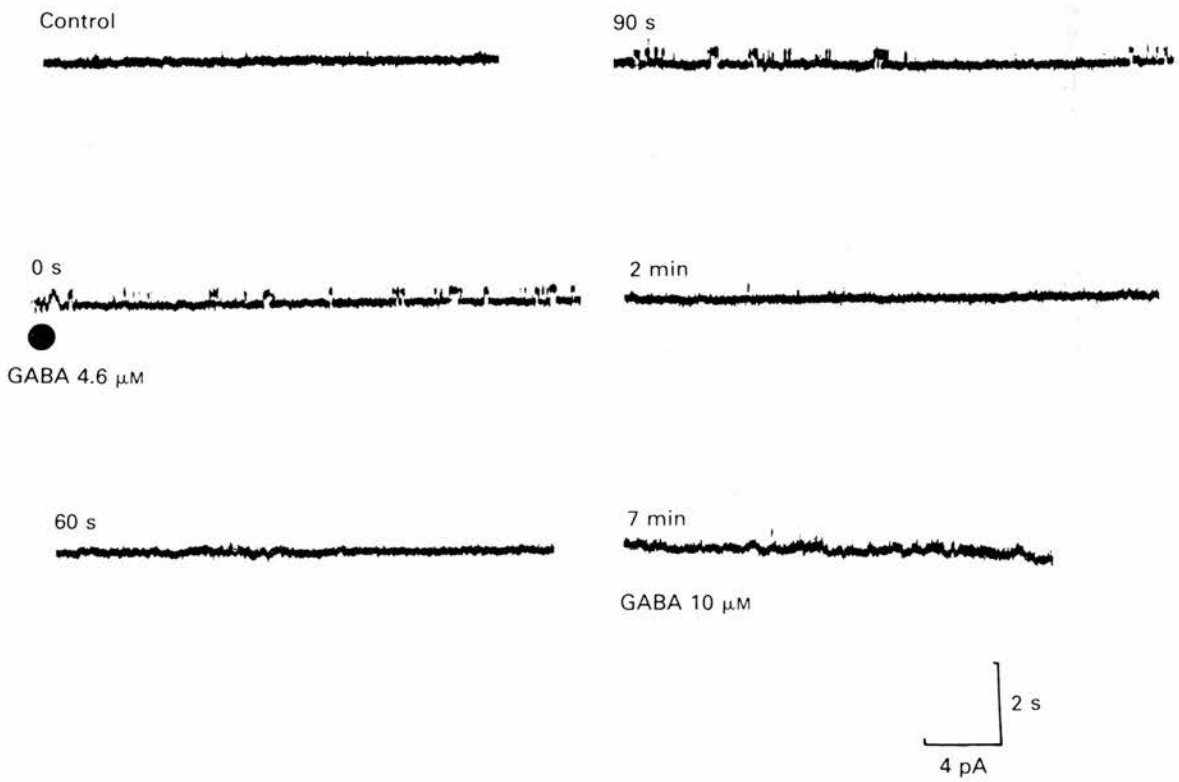


Figure 11 Desensitization: an outside-out patch recording is shown, transpatch potential + 40 mV. During the control period no channel openings were observed. At the artefact marked (●) GABA 4.6 μM was added to the bath and produced channel openings (outward currents, upward). After 60 s a quiescent period followed and after a further 90 s channel opening recommenced. The channel openings then continued until a period marked 2 min when the recordings again became very quiet. During this period marked 2 min, only two openings were observed. The preparation remained quiet and after a period of 7 min a concentration of GABA 10 μM was added to the bath and produced no increase in the probability of the channel being open.

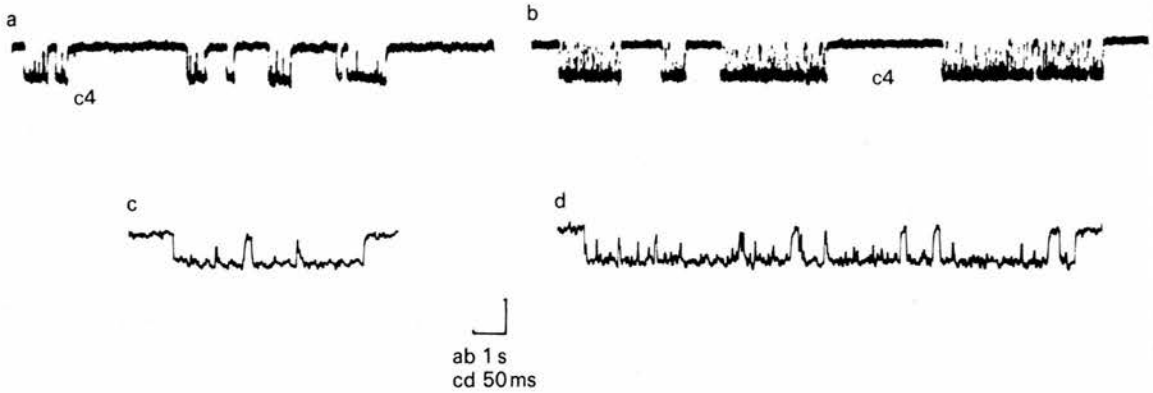


Figure 12 Single channel currents recorded using high agonist concentrations, cell-attached patches, transpatch potential − 75 mV. (a) GABA 20 μM as agonist. (b) Piperazine 1 mM as agonist. Note the presence of the long closed periods (c4) seen with the slow recording speeds. (c) Part of the recording of (a) but at a higher time resolution; GABA effective mean open time 95 ms. (d) Part of recording of (b) but at higher time resolution; piperazine effective mean open time 54 ms.

ued until 2 min after application when the recording again became quiet. Channel activity was then not further stimulated by the addition of a higher (10 μM) concentration of GABA. Similar very long closed periods between opening or grouping activity were also seen with cell-attached patches and with piperazine as the agonist. Table 2 shows the values for the probability density functions which were used to best describe the distribution of the closed periods with 20 μM GABA and 1 mM piperazine as agonists with cell-attached patches at − 75 mV; parts of the recordings used for the analysis are shown in Figure 12. Up to four exponentials were required to best describe the distributions suggesting that there are up to four closed mainstates at higher agonist concentrations. The longest component was not present at lower concentrations and presumably corresponded to the desensitized state. Figures 12a and b show examples of the grouping of clusters which was observed using 20 μM GABA and 1 mM piperazine as agonist. Note the appearance of long closed periods lasting several seconds.

Discussion

The primary aim of this series of experiments was to examine the behaviour of the single channel currents produced by activation of membrane receptors with GABA and piperazine. It had already been shown that these agonists will activate extra-synaptic receptors found on the bag region of the *Ascaris* muscle cell and that they give rise to an increase in Cl^- conductance (Martin, 1982).

Distribution of channel open times

The distribution of the channel open times produced by piperazine and GABA were usually described by the sum of two exponentials. At least 35% of the openings were found, at low agonist concentrations, to be due to the brief openings. The remainder were estimated to be due to the slower openings. Double exponential distributions have been implied or observed in single channel studies with acetylcholine (Colquhoun & Sakmann, 1981), glutamate (Cull-Candy & Parker, 1982), calcium activated potassium channels (Barret *et al.*, 1982) and GABA channels in cultured cells (Jackson *et al.*, 1982). The lack of simultaneous double openings observed suggests that the double exponential distribution cannot be explained by more than one channel population but implies the existence of more than one open channel mainstate. It has been suggested (Colquhoun & Sakmann, 1981; Cull-Candy & Parker, 1982) that the brief openings correspond to openings of receptor channels occupied only by one agonist molecule and that the longer opening state corresponds to receptor-operated channels occupied by two agonist molecules. These observations on the channel open times are inconsistent with a simple two step KM model (Del Castillo & Katz, 1957; Katz & Miledi, 1972), which involves the binding of a single agonist molecule for channel opening.

Increases in agonist concentration in this study were associated with increases in effective mean open time and decreases in the proportion of brief openings. One possibility is that this might be due to the failure to resolve brief intervening closings (Neher, 1983) due to

the limited frequency response of the amplifier; the observations in this paper were carried out under conditions which did not always permit good resolution of events less than 1 ms. However, it is pointed out that Gration *et al.* (1981) have previously observed concentration-dependent increases in mean open time of glutamate-activated channels.

One attractive model of agonist action in which two agonist molecules can combine to two subunits of the receptor-channel complex to produce opening is the Monod-Wyman-Changeux model (Colquhoun & Hawkes, 1977; 1982). It can account by a plausible physical mechanism for: the changes in mean open time observed in these experiments with agonist concentration: the double exponential distribution of the open times and the change in the proportion of fast and slow openings: the greater than linear relationship between the probability of the channel being open and the agonist concentration.

The distribution of channel closed times

The distribution of channel closed times for piperazine and GABA could not be described by a single exponential but required up to three exponentials with low agonist concentrations; the brief components corresponding to the rapid closings during bursts. Channel block by the agonist was thought unlikely, because of the observed increase in the mean open times associated with an increase in agonist concentration, and no voltage sensitivity (Neher & Steinbach, 1978). One explanation of this phenomenon is the 'Nachschlag' effect (Colquhoun & Sakmann, 1981). This is the isomerization of the channel to the open configuration after closing without dissociation of agonist molecules. The existence of the three exponentials in the probability density functions which best describe the distributions of the closed times at low agonist concentrations suggest the presence of three closed states.

At high agonist concentrations and after an initial period of a high probability of channel opening, long closed periods appeared separating openings into groupings of clusters. The distribution of channel closed times at these higher agonist concentrations were best described by up to four exponentials suggesting the existence of at least four closed states. The extra component at the higher concentrations was interpreted as due to the appearance of the desensitized state. Sakmann *et al.* (1980) have noted long closed states at high agonist concentrations and interpreted them as due to desensitization. However, desensitization has not been noted before during briefer bath applications of GABA and piperazine (Martin, 1980; 1982).

Differences between piperazine and GABA

Piperazine is some 10 to 100 times less potent than GABA in the *Ascaris* preparation (Martin, 1982). The mainstate channel conductances of both agonists were similar so that any conductance differences could not explain the magnitude of the observed differences in potency. This difference in potency may be explained by the fact that piperazine required a higher concentration to achieve a similar opening rate to GABA. In addition, the effective mean open time for piperazine was generally shorter than that of GABA. Thus, for example, 3.5 μM GABA in one typical experiment produced a mean opening rate of 3.9 s^{-1} with an effective mean open time of 33 ms and a probability of the channel being open of 0.14. On the other hand, another typical experiment using 500 μM piperazine as the agonist produced a channel opening rate of 3.6 s^{-1}, and an effective mean open time of 19 ms giving a probability of 0.08 for the channel being open. Lambert *et al.* (1983) have already suggested that in general, less potent agonists have shorter open channel lifetimes.

The observation that piperazine is an agonist suggests that an adequate interaction of the amine moiety with the presumed anionic sub-site of the receptor is enough to permit channel opening. Piperazine has a heterocyclic ring structure and lacks a carboxyl group like that of GABA. The fact that the effective mean open time of GABA is generally longer than that of piperazine suggests that some interaction between the carboxyl group of GABA and the receptor may be important in delaying channel closure in addition to facilitating channel opening. It is interesting that Auerbach *et al.* (1983) have reported analogous results with acetylcholine agonists. They have suggested that the continued presence of the agonist in the transmitter binding site affects the stability of the open channel.

It was found in these studies that piperazine mimics the action of GABA in that they are both able to open channels of the same mainstate conductance. Evidence was found for both compounds producing two open mainstates and up to three closed states as well as an additional desensitized state. The lower potency of piperazine could be accounted for if higher concentrations of this drug were required to produce channel openings which generally had shorter mean open times.

The density of extra-synaptic GABA receptors

A peak current of about 20 nA can be generated by iontophoretic application of GABA to the bag under voltage clamp with a driving force of 30 mV (Martin,

1982). Thus each channel would carry a current of 0.66 pA (G = 22 pS) and require the activation of about 29,000 receptors. The bag membrane surface exposed to GABA is approximately 70,000 μm^2 and this suggests an average area occupied by each receptor of about 2.4 μm^2. On this basis each typical cell-attached patch of 5–10 μm^2 (Sakmann & Neher, 1983) would be expected to contain approximately 2–4 receptor-operated channels. However, only about 1 in 7 of the patches created in these experiments showed any (one or more channels per patch) recordable GABA-activated channel activity. The explanation for the much lower observed success rate is not known. One possibility is that desensitization might have occurred during patch formation.

I particularly thank the following who made this work possible: Professor P.N.R. Usherwood and Dr R. Ramsay, Department of Zoology, Nottingham University, for instruction on the patch-clamp technique: Dr A.D. Short, Department of Veterinary Physiology, Edinburgh University, for writing computer programmes: Mr C.A. Glasbey, AFRC Unit of Statistics, University of Edinburgh, for the exponential distribution theory and analysis.

References

AUERBACH, A., DEL CASTILLO, J. SPECHT, P.C. & TITMUS, M. (1983). Correlation of agonist structure with acetylcholine receptor kinetics: studies on the frog end-plate and on chick embryo muscle. *J. Physiol.*, **343,** 551–568.

BARRETT, J.N., MAGELBY, K.L. & PALLOTTA, B.S. (1982). Properties of single calcium-activated potassium channels in cultured rat muscle. *J. Physiol.*, **331,** 211–230.

BORMANN, J., SAKMANN, B. & SEIFERT, W. (1983). Isolation of GABA-activated single-channel Cl^- currents in the soma membrane of rat hippocampal neurones. *J. Physiol.*, **341,** 10P.

BRADING, A.F. & CALDWELL, P.C. (1971). The resting membrane potential of the somatic muscle cells of *Ascaris lumbricoides*. *J. Physiol.*, **271,** 605–624.

COLQUHOUN, D. & HAWKES, A.G. (1977). Relaxation and fluctuations of membrane currents that flow through drug-operated channels. *Proc. R. Soc. Series B*, **199,** 231–262.

COLQUHOUN, D. & HAWKES, A.G. (1981). On the stochastic properties of single ion channels. *Proc. R. Soc. Series B*, **211,** 205–235.

COLQUHOUN, D. & HAWKES, A.G. (1982). On the stochastic properties of bursts of single ion channel openings and of clusters of bursts. *Phil. Trans. R. Soc. Series B*, **300,** 1–59.

COLQUHOUN, D. & SAKMANN. (1981). Fluctuations in the microsecond time range of the current through single acetylcholine channel receptor ion channels. *Nature*, **294,** 464.

COLQUHOUN, D. & SIGWORTH, F.J. (1983). Fitting and statistical analysis of single-channel records. In *Single-Channel Recording*. ed. Sakmann, B. & Neher, E. pp. 191–263. New York & London; Plenum.

CULL-CANDY, S.G. & PARKER, I. (1982). Rapid kinetics of single glutamate-receptor channels. *Nature*, **295,** 410–412.

DE BELL, J., DEL CASTILLO, J. & SANCHEZ, V. (1963). Electrophysiology of the somatic muscle cells of *Ascaris lumbricoides*. *J. cell. Comp. Physiol.*, **62,** 159–177.

DEL CASTILLO, J. & KATZ, B. (1957). Interaction at end-plate receptors between different choline derivatives. *Proc. R. Soc. Series B*, **146,** 369–381.

DUDEL, J. (1979). Voltage dependance of amplitude and time course of inhibitory synaptic current in crayfish muscle. *Pflugers arch. ges. Physiol.*, **371,** 167–174.

GRATION, K.A.F., LAMBERT, J.J., RAMSEY, R.R. & USHERWOOD, P.N.R. (1981). Non-random openings and concentration-dependent life times of glutamate-gated channels in muscle membrane. *Nature*, **291,** 423–425.

HAMILL, O.P., BORMANN, J. & SAKMANN, B. (1983). Activation of multiple-conductance state chloride channels in spinal neurones by glycine and GABA. *Nature*, **305,** 805–808.

HAMILL, O.P., MARTY, A., NEHER, E., SAKMANN, B. & SIGWORTH, F.J. (1981). Improved patch-clamp techniques for high-resolution current recording from cells and cell-free membrane patches. *Pflugers arch. ges. Physiol.*, **391,** 85–100.

JACKSON, M.B., LECAR, H., MATHERS, D.A. & BARKER J.L. (1982). Single channel currents activated by γ-aminobutyric acid, muscimol, and (−)-pentobarbital in cultured mouse spinal neurons. *J. Neurosci.*, **2,** 889–894.

JARMAN, M. (1959). Electrical activity in the muscle cells of *Ascaris*. *Nature*, **184,** 1244.

KATZ, B. & MILEDI, R. (1972). The statistical nature of the acetylcholine potential and its molecular components. *J. Physiol.*, **224,** 665–699.

LAMBERT, J.J., DURANT, N.N. & HENDERSON, E.G. (1983). Drug-induced modification of ionic conductance at the neuromuscular junction. *Am. Rev. Pharmac. Tox.*, **23,** 505–539.

MARTIN, R.J. (1980). The effect of γ-aminobutyric acid on the input conductance and membrane potential of *Ascaris* muscle. *Br. J. Pharmac.*, **71,** 99–106.

MARTIN, R.J. (1982). Electrophysiological effects of piperazine and diethylcarbamazine on *Ascaris suum* somatic muscle. *Br. J. Pharmac.*, **77,** 255–265.

MARTIN, R.J. (1983). GABA single channel currents from *Ascaris* muscle. *J. Physiol.*, **336,** 36–37P.

NEHER, E. (1983). The charge carried by single-channel currents of rat cultured muscle cells in the presence of local anaesthetics. *J. Physiol.*, **339,** 663–678.

NEHER, E. & STEINBACH, J.H. (1978). Local anaesthetics transiently block currents through single acetylcholine receptor channels. *J. Physiol.*, **277,** 153–176.

SAKMANN, B., HAMILL, O.P. & BORMANN, J. (1983). Patch-clamp measurements of elementary chloride currents activated by the putative inhibitory transmitters GABA and glycine in mammalian spinal cord. *J. Neur. Trans. Supp.*, **18,** 83–95.

SAKMANN, B. & NEHER, E. (1983). Geometric parameters of

pipettes and membrane patches. In *Single-Channel Recording*. ed. New York & London: Plenum.

SAKMANN, B., PATLAK, J. & NEHER, E. (1980). Single acetylcholine-activated channels show burst-kinetics in presence of desensitizing concentrations of agonist. *Nature*, **286,** 71–73.

STANDEN, D.D. (1975). Chemotherapy of intestinal helminthiasis. *Prog. Drug Res.*, **19,** 158–165.

(*Received June 29, 1984.*
Revised September 11, 1984.
Accepted October 8, 1984.)

Journal of Neuroscience Methods, 16 (1986) 239–249
Elsevier

NSM 00577

Exploratory and confirmatory plots of single-channel records

C.A. Glasbey [1] and R.J. Martin [2]

[1] *AFRC Unit of Statistics, University of Edinburgh, King's Buildings, and*
[2] *Department of Veterinary Pharmacology, Royal (Dick) School of Veterinary Studies, Summerhall, University of Edinburgh, Edinburgh (U.K.)*

(Received November 22nd, 1985)
(Revised February 13th, 1986)
(Accepted February 18th, 1986)

Key words: CUSUM plot – exponential distribution – Kolmogorov–Smirnov type test – non-stationarity – $P-P$ plot – $Q-Q$ plot

Graphical displays are used to study open- and closed-time durations of a single ion-channel. CUSUM plots, in conjunction with Kolmogorov–Smirnov type tests, provide checks for changes in channel behaviour. Distributional properties are examined by means of $Q-Q$ and $P-P$ plots. The methods are illustrated using GABA-activated channel records from *Ascaris suum*.

Introduction

Graphical displays of data can be very informative, both before and after any statistical analyses. Exploratory plots can suggest an appropriate model or reveal unexpected features of a data set. After a model has been fitted, confirmatory, or diagnostic, plots can provide better general assessments of goodness-of-fit than can be achieved by specific tests.

In this paper cumulative sum (CUSUM) plots are defined and illustrated; they are used to check for changes in behaviour of a single ion-channel. Quantile ($Q-Q$) plots and probability ($P-P$) plots are used to investigate the appropriateness of mixtures of exponential distributions for durations of open- and closed-times. $Q-Q$ plots are used to see whether the data have the form of a single exponential or a mixture of exponentials. $P-P$ plots are used to confirm the goodness-of-fit of estimated mixtures of exponential distributions.

These methods are illustrated using a particular data set, which showed evidence of non-stationarity, from GABA-activated channel records from *Ascaris suum*. A

Correspondence, C.A. Glasbey, AFRC Unit of Statistics, University of Edinburgh, King's Buildings, Edinburgh, EH9 3JZ, U.K.

0165-0270/86/$03.50 © 1986 Elsevier Science Publishers B.V. (Biomedical Division)

cell-attached patch-clamp technique was used with 3 μM GABA in the pipette; the data come from one of the experiments reported by Martin (1985).

Methods

CUSUM plots

CUSUM plots have been described by Woodward and Goldsmith (1964). A CUSUM plot of a series of observations $x_1, x_2, \ldots, x_n$ can be obtained as follows:

(a) Calculate the mean value of the x's, that is

$$\bar{x} = \frac{1}{n} \sum_{i=1}^{n} x_i;$$

(b) Calculate the cumulative sum

$$S_j = \sum_{i=1}^{j} (x_i - \bar{x}) \qquad \text{for } j = 1, \ldots, n;$$

(this may be obtained recursively by

$$S_0 = 0$$

$$S_j = S_{j-1} + (x_j - \bar{x}) \qquad \text{for } j = 1, \ldots, n;)$$

(c) Plot S_j against j for $j = 1, \ldots, n$.

If the x's are a permutation of the integers 1 to n then the hypothesis that these are in a random order can be tested using a Kolmogorov–Smirnov (K–S) type test, see for example Pettitt (1979). The standard K–S test statistic is the maximum deviation of the CUSUM from zero. This is particularly sensitive to systematic differences between the first and second halves of the series, but will often fail to detect non-randomness near the start or finish of the series. However, other K–S type statistics exist which can be used to test for non-randomness at the ends of the series. For the theory see Hajek and Sidak (1967, p. 182). For any positive value of α there exists a test statistic

$$D_\alpha = \text{maximum value of} \left[\frac{|S_j|}{1 + (\alpha - 1)\, j/n} \right] \qquad \text{for } j = 1, \ldots, n,$$

where $|S_j|$ denotes the absolute value of S_j. (The value $\alpha = 1$ gives the standard K–S statistic.) The probability of obtaining a D_α-value greater than this if the x's are the integers 1 to n in a random order is approximately

$$2 \exp\left[\frac{-24\alpha D_\alpha^2}{n^2(n+1)} \right],$$

or 1 if this is smaller. A small probability for a particular value of α indicates that it is unlikely that the x's are in a random order.

Q–Q plots

If observations $x_1, x_2, \ldots, x_n$ are a random sample from an exponential distribution with a mean of unity, then the ith smallest value has an expected value close to the ith quantile which is $-\log_e(1-(i-\frac{1}{2})/n)$. Even when the exponential distribution has a mean value other than unity, or a censoring boundary because observations below a certain threshold are not recorded, the ith smallest observed value will still be approximately linearly related to this ith quantile. Therefore, if the ordered observations are plotted against the quantiles and lie approximately in a straight line, then this is evidence for the x's being exponentially distributed. The slope corresponds to the mean of the uncensored distribution and the intercept is the censoring threshold. This is an example of a quantile (Q–Q) plot (Wilk and Gnanadesikan, 1968).

P–P plots

When a distribution has been fitted to data the goodness-of-fit can be assessed using a probability (P–P) plot (Wilk and Gnanadesikan, 1968). The estimated probabilities of observations being less than certain values are plotted against the proportions of data that are less than these same values. The points should lie approximately on a 45° line between (0,0) and (1,1). If the distribution is discrete on an integer scale and m distinct values are observed:

$x_{(1)} < x_{(2)} \ldots < x_{(m)}$,

with respective frequencies $N_1, N_2, \ldots, N_m$ summing to n, then the P–P plot for a particular fitted distribution simplifies to a plot of

$$P(x \le x_{(i)}) \text{ and } P(x \le x_{(i+1)} - 1) \text{ against } \frac{1}{n}\sum_{j=1}^{i} N_j \qquad \text{for } i = 1, \ldots, m.$$

The significance of any departure from the 45° line can be tested using a K–S statistic. (See, for example, Siegel, 1956, pp. 47–52.) The test will be conservative, that is it will reject the fit less often than it should, because parameters in the distribution have been estimated using the data that are being tested. The test statistic D is the maximum vertical displacement of the slope-corrected P–P plot from the 45° line. The probability of a more extreme value if the distribution is correct is approximately

$2 \exp[-2nD^2]$,

or 1, whichever is less.

Results

CUSUM plots

Fig. 1A shows the log-duration plotted against observation number for 185 consecutive open-times from the GABA-activated channel record. Times have been log-transformed to enable short and long times to be viewed on the same scale.

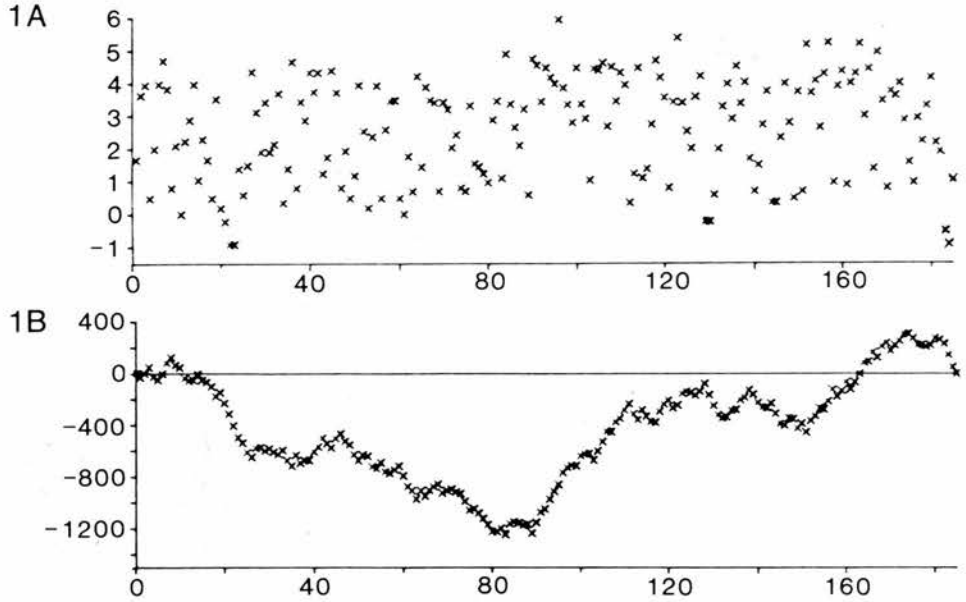


Fig. 1. A: log-transformed open-times plotted in observed order. Ordinate, $\log_e$ times (ms); abscissa, observation number. B: CUSUM of ranks of open-times. Ordinate, CUSUM; abscissa, observation number.

Similarly, Fig. 2A is a plot of the log-transformed closed-times which interlace with the open-times in Fig. 1A. If the behaviour of the ion-channel has remained constant then we would not expect either plot to have any striking features such as a drift in mean value or a grouping of very long or short times. Examination of Figs. 1A and 2A does not reveal any strong evidence for non-stationarity.

Fig. 2B shows the CUSUM plot of closed-times with the zero line marked on for reference. Some features of the data are shown more clearly in this figure than they were in Fig. 2A. The downward slope over the first 25 observations indicates that on average they are less than the mean closed-time. The large upward jump about observation 88 is caused by 3 long closed periods. This is followed by a run of below-average closed-times up to observation 125. There are two long closed-times about observation 170 which are again followed by below-average times. By its definition the CUSUM ends back at zero because $S_n = 0$.

To reduce the dominance of a few long times, CUSUM plots could be obtained using log-transformed times, or any other transformation for that matter. An alternative approach is to rank the data, so that for instance the duration of the ith open-time O_i is replaced by k if O_i is the kth largest open-time. Figs. 1B and 2C show the CUSUM plots of the ranks of the open- and closed-times respectively. In Fig. 1B it can be seen that the first 80 or 90 open-times tend to be shorter than those which follow. The most distinctive feature of Fig. 2C is the sequence of short closed-times between observations 90 and 100 which cause the CUSUMs to de-

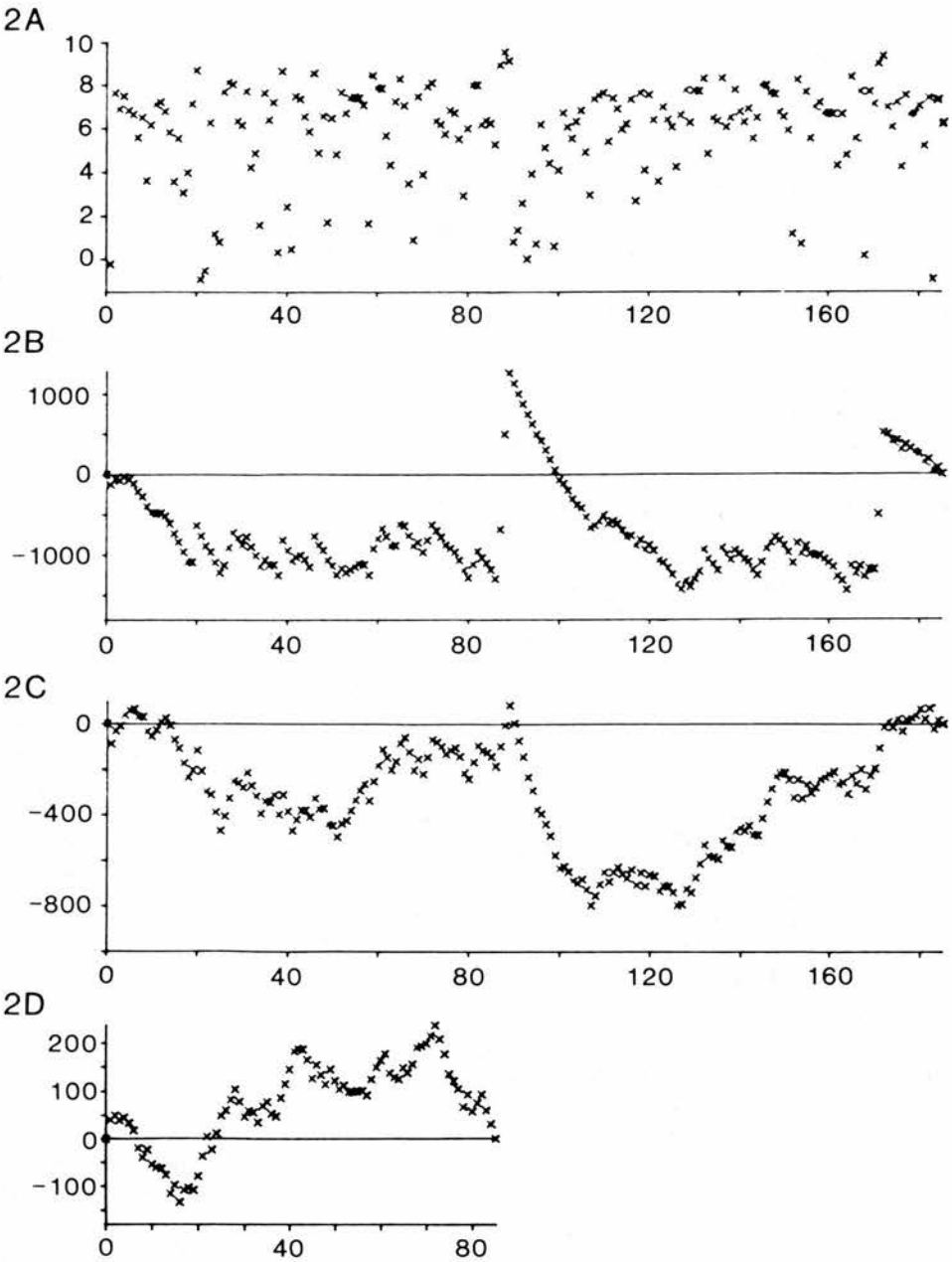


Fig. 2. A: log-transformed closed-times plotted in observed order. Ordinate, $\log_e$ times (ms); abscissa, observation number. B: CUSUM of closed-times. Ordinate, CUSUM; abscissa, observation number. C: CUSUM of ranks of closed-times. Ordinate, CUSUM; abscissa, observation number. D: CUSUM of ranks of deviations of log-transformed closed-times from their mean value. First-half of data only. Ordinate, CUSUM; abscissa, observation number.

crease rapidly. It is informative to compare Figs. 2B and 2C; Fig. 2B emphasises the long times whereas Fig. 2C emphasises the sequence of short times.

Although a lot of useful qualitative information can be extracted from CUSUM plots it is difficult to assess whether the fluctuations are arising by chance or because of some change in behaviour of the ion-channel. This is where ranks prove very useful because the hypothesis that they are in a random order can be tested using a K–S type test, as described in the previous section. If the ranks are in a random order then the process is stationary. However, the converse is not true because if a stationary process has correlation between successive observations then the ranks will not be in a random order. This is precisely the situation encountered with some ion-channel recordings, for example a channel may make slow transitions between two modes of gating. Therefore the durations of successive openings or closings may be positively correlated, but the correlation is often small. The rank correlation coefficients for the open- and closed-times are 0.19 and 0.05 respectively for this data set. So, although the test may be used to give some indication of non-stationarity it should be interpreted with caution.

The probabilities obtained for the CUSUM of the ranks of the open-times plotted in Fig. 1B were 0.08, 0.006 and 0.28 respectively for $\alpha = 9$, 1 and $1/9$. In order, these values of α provide tests for non-stationarity at the start, middle and finish of the recording period. The value of 9 was chosen rather arbitrarily to measure departures from zero in the first few observations, and the value of $1/9$ produces the equivalent statistic for the last few observations. Therefore, there is strong evidence, even bearing in mind that consecutive times are correlated, that the behaviour of the ion-channel changes, and this appears to be between observations 80 and 90. The probabilities for test statistics based on the closed-times are 0.36, 0.18 and 0.35 using the same values for α. This result shows that the CUSUMs plotted in Fig. 2C do not depart significantly from the zero-line. However this should not preclude examination of more local details in the CUSUM plots. As has already been commented on, there are three closed-times of long duration about observation 88 followed by a sequence of short times up to observation 100. Before this event the open-times are on average shorter than afterwards. Combining these pieces of evidence together, there are grounds for believing that the behaviour of the ion-channel changes between observations 85 and 100. Therefore, for further analysis, we propose to divide the data set in two, taking the first-half up to observation 85, the second-half after observation 100 and discarding the centre portion. However it is important to realise that the change in channel behaviour may not be permanent, and if the record had been longer then the channel may have reverted to its original mode of gating. Short-term, apparent non-stationarity may simply be a local feature of a stationary process.

The CUSUMs so far discussed have been used to detect changes in mean duration times. They can also be used to detect other departures from assumptions, such as non-constant variability in durations. For example, Fig. 2D is a plot of the CUSUM of the ranks of $|\log C_i - \overline{\log C}|$ for the first-half of the data, where $\overline{\log C}$ is the mean value of $\log C_i$ for $i = 1, \ldots, n$, C_i is the duration of the ith closed time, n is now 85, and $| \; |$ denotes absolute value. The downward slopes at the start and

finish of the series are evidence for the closed-times being more variable in the middle of the series than at the ends. The probabilities associated with K–S type tests are 0.74, 0.22 and 0.04. Therefore there is some evidence for less variability after the 70th observation. However, it should be borne in mind that correlations in the data make the 0.04 probability less significant than it appears and there are risks of data-dredging, because if enough tests are performed on a set of data then something unusual will always be found. Therefore, we will take no action to rectify this possible flaw.

Q–Q plots

Fig. 3A is a Q–Q plot of the open-times in the first-half of the data. Times of less than 1 ms have been omitted because the response time of the recording equipment meant that some short openings were missed. A notable, and sometimes notorious, feature of *Q–Q* plots is that they emphasise tails of distributions at the expense of the centre portion. On occasions this can be useful, although not in this instance. Although the plot looks linear it is dominated by the largest few open-times and tells us only that these are approximately exponentially distributed. To examine the distribution of shorter open-times we have to magnify the lower part of Fig. 3A. This is plotted in Fig. 3B and displays very marked curvature. Therefore there is clear evidence that the open-times are not distributed as a single-exponential.

No comparable *Q–Q* plots exist for identifying mixtures of exponential distributions unless some of their parameters are known. However some information can be extracted from the *Q–Q* plot for a single-exponential distribution. If the trend in the data is anywhere concave, that is has a negative second derivative, then it cannot be a sample from a mixture of exponentials because *Q–Q* plots for mixtures of exponentials are convex. Further, if the exponentials have sufficiently different mean values then the *Q–Q* plot will be piecewise-linear, that is a series of straight lines joined together, one for each distribution in the mixture. In particular, for a mixture of two well-separated exponential distributions the single-exponential *Q–Q* plot will be bilinear. We conclude from Figs. 3A and 3B that the open-times are not inconsistent with a sample from a mixture of exponential distributions, but at least two exponentials are required. The general slope in Fig. 3A of about 30 ms is an indication of the mean open-time in the slowest exponential component in the mixture distribution.

Figs. 3C and 3D show comparable *Q–Q* plots of the closed-times in the first-half of the data. Once again there is evidence that there are at least two exponential distributions present in the mixture.

P–P plots

The observed times were on a discrete, rather than a continuous, scale, so discrete analogues of mixtures of exponential distributions have been used. These were fitted to the open- and closed-times in the first- and second-halves of the data by maximum likelihood estimation, as described by Martin (1985). The best-fitting single exponential distribution for the open-times in the first-half of the data has a mean value of 22 ms. Fig. 4A shows the corresponding *P–P* plot which has been

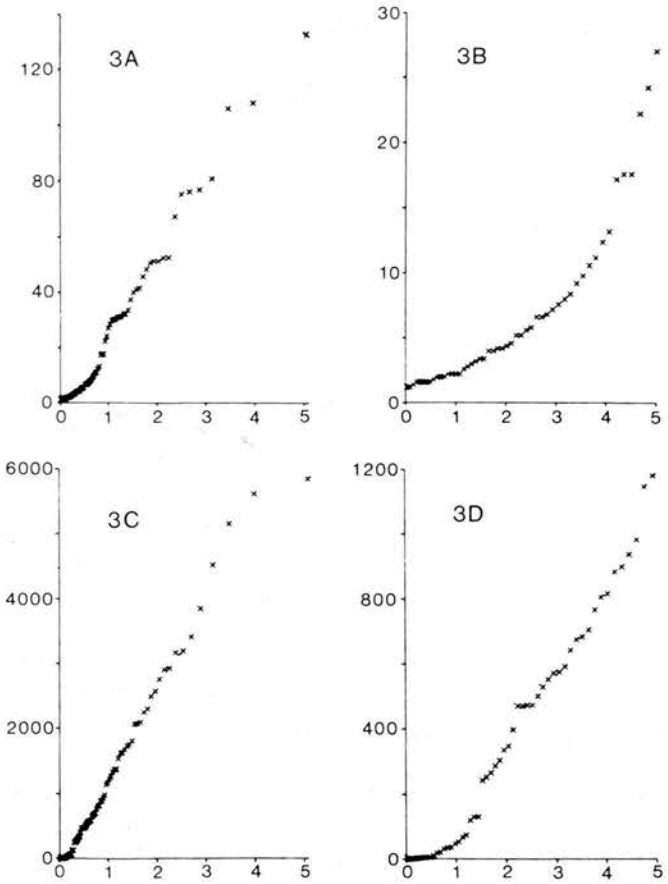


Fig. 3. A: Q–Q plot of open-times. First-half of data. Ordinate, open-times (ms); abscissa, quantiles of exponential distribution. B: lower portion of Fig. 3A. Ordinate, open-times (ms); abscissa, quantiles of exponential distribution. C: Q–Q plot of closed-times. First-half of data. Ordinate, closed-times (ms); abscissa, quantiles of exponential distribution. D: Lower portion of Fig. 3C. Ordinate, closed-times (ms): abscissa, quantiles of exponential distribution.

modified by subtracting the 45° slope. Therefore, if the distribution fits well, the points should lie close to the zero-line which is also shown. The large negative departures up to a probability of 0.6 show that the fit to the first 60% of the data is poor, essentially because the single exponential distribution is fitting the longer open-times. There are more very small times observed than would be expected from an exponential distribution. In compensation, between probabilities 0.4 and 0.6 there are fewer observations than expected. For Fig. 4A the K–S type test gave a probability of 0.002. We conclude that a single-exponential distribution gives an inadequate fit to the open-times in the first-half of the data. This confirms the visual impression we had already drawn from Fig. 4A, and also from the curvature in the Q–Q plot in Fig. 3B.

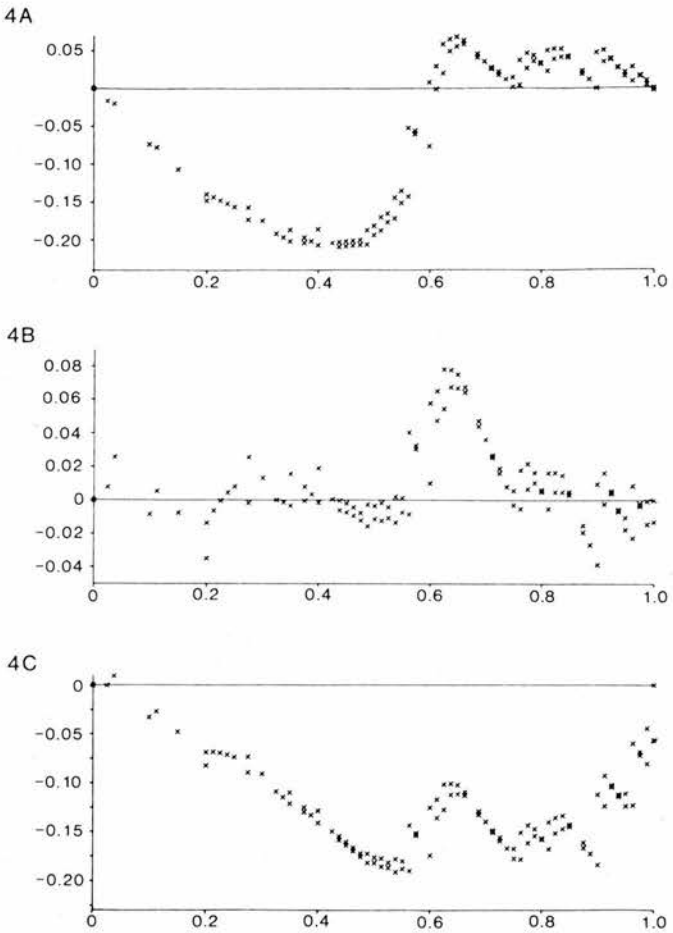


Fig. 4. A: slope-corrected $P-P$ plot of single-exponential distribution fitted to open-times in first-half of data. Ordinate, expected probability–observed probability; abscissa, observed probability. B: slope-corrected $P-P$ plot of double-exponential distribution fitted to open-times in first-half of data. Ordinate, expected probability–observed probability; abscissa, observed probability. C: slope-corrected $P-P$ plot of double-exponential distribution fitted to open-times in second-half of data but plotted against open-times in first-half. Ordinate, expected probability–observed probability; abscissa, observed probability.

Fig. 4B shows the slope-corrected $P-P$ plot for the best-fitting mixture of two exponential distributions fitted to the open-times in the first-half of the data. The deviations from the zero-line are substantially smaller than those in Fig. 4A, indicating a much better fit. The probability of the K–S statistic is 0.75 which indicates a satisfactory fit. Of course it cannot be thus concluded that a mixture of two exponentials is adequate. For this type of data there are strong reasons to believe that the distribution of open-times is a mixture of exponentials, so a specific likelihood ratio test of two exponentials against three exponentials is more powerful

than the portmanteau K–S test. However the improvement in fit of 3 exponentials over two is negligible in this case and so we are safe to conclude that a mixture of two exponential distributions is sufficient.

A mixture of two exponential distributions also gave a good fit to the open-times in the second-half of the data, but with different estimated parameter values. In the first-half of the data the means of the fitted exponentials (and standard errors) are 2.4 (0.7) and 34 (6), with proportions 0.47 (0.08) and 0.53. In the second-half of the data the means are 1.8 (0.7) and 50 (7), with proportions 0.31 (0.08) and 0.69. These sets of values are substantially different from one another as can be seen in Fig. 4C which is a slope-corrected P–P plot of the distribution estimated from the second half of the data plotted against the first-half of the data. There are more small open-times in the data than are predicted by the distribution. The K–S statistic has a probability value of 0.006. This confirms the evidence in the CUSUM plots that the ion-channel changes its behaviour in the middle of the recording period.

Discussion

The statistical analysis of patch-clamp data has been discussed by Colquhoun and Sigworth (1983), Horn et al. (1984) and Horn and Vandenberg (1984). For example Colquhoun and Sigworth (1983) illustrated the use of histograms and probability density functions, and the methods of the minimum χ^2 and maximum likelihood for fitting exponential distributions. Horn et al. (1984) used runs analysis to test for non-randomness between records. Horn and Lange (1984) used cumulative histograms and Pearson's χ^2 test for parallel samples to test for non-stationarity. Gration et al. (1981) tested for a specific form of randomness, that is for a Poisson process, although it is evident from their Fig. 1 that their data also exhibited local non-stationarity.

None of these authors however have illustrated the use of informal procedures such as CUSUM, Q–Q, or P–P, plots for patch-clamp data. The advantages of these techniques, as we have illustrated, is that they produce a relatively simple visual display of the structure of the data and allow subsequent confirmation after the fitting of exponentials. With these techniques it is possible to identify the position of any deviation from expected patterns; this can then provide a rational basis for editing and selecting data for further analysis. The use of the plots does not preclude the use of more formal statistical tests which are still required for confirmation.

References

Colquhoun, D. and Sigworth, F.J. (1983) Fitting and statistical analysis of single-channel records. In. B. Sakmann and E. Neher (Eds), Single Channel Recording, Plenum Press, New York.

Gration, K.A.F., Lambert, J.J., Ramsey, R. and Usherwood, P.N.R. (1981) Non-random openings and concentration-dependent lifetimes of glutamate-gated channels in muscle membrane, Nature (London), 291: 423–425.

Hajek, J. and Sidak, Z. (1967) Theory of Rank Tests, Academic Press, New York.
Horn, R. and Vandenberg, C.A. (1984) Statistical properties of single sodium channels, J. Gen. Physiol., 84: 505–544.
Horn, R., Vandenberg, C.A. and Lange, K. (1984) Statistical analysis of single sodium channels. Effects of N-bromoacetamide, Biophys. J., 45: 323–335.
Martin, R.J. (1985) γ-Aminobutyric acid- and piperazine-activated single-channel currents from *Ascaris suum* body muscle, Br. J. Pharmacol., 84: 445–461.
Pettitt, A.N. (1979) A non-parametric approach to the change-point problem, Appl. Statist., 28: 126–135.
Siegel, S. (1956) Nonparametric Statistics for the Behavioural Sciences, McGraw-Hill, Tokyo.
Wilk, M.B. and Gnanadesikan, R. (1968) Probability plotting methods for the analysis of data, Biometrika, 55: 1–17.
Woodward, R.H. and Goldsmith, P.L (1964) Cumulative Sum Techniques, I.C.I. Monograph No. 3, Oliver and Boyd, London.

19

GABA receptors in parasites of veterinary importance

K. A. F. Gration, I. D. Harrow,
Animal Health Biology Department, Pfizer Central Research, Sandwich, Kent, UK and
R. J. Martin,
Department of Veterinary Pharmacology, Royal (Dick) School of Veterinary Studies, Edinburgh, UK

1. INTRODUCTION

Veterinarians and farmers currently have a large arsenal of highly effective agents which can be used to control endo-(internal) and ecto-(external) parasite infections in domestic animals. Many of these agents act upon the central nervous systems and/or peripheral nerve–muscle systems of the parasites. Site of action studies on a range of anthelmintics, acaricides and broad-spectrum antiparasitic agents have identified cholinergic and γ-amino butyric acid (GABA) mediated neurotransmission as important target sites for antiparasitic chemotherapy, in addition to other sites, e.g. octopamine receptors.

At present, new antiparasitic agents are sought mainly by empirical screening and optimization of structure–activity relationships for any active leads discovered. Pharmacologists and medicinal chemists have, however, recognized the feasibility of rational drug design based on a knowledge of parasite physiology and biochemistry. Neurophysiological research, using known agents as probes, forms the basis of one approach to rational drug design founded on a better understanding of parasite nerve–muscle physio-

the effects of drugs in this preparation is complicated by the existence of several potential sites of action since the strip contains nerve cords as well as muscle cells. The dorsal and ventral nerve cords each contains excitatory and inhibitory motor axons, and the ventral nerve cord also contains interneurons (Stretton *et al.*, 1978). Synapses between motorneurons exist in both nerve cords, and in the ventral nerve cord the interneurons synapse with motorneurons and other interneurons. Therefore, in addition to neuromuscular synapses and muscle cells the preparation also contains several classes of neuronal synapse where drugs might act and lead to effects on muscle contraction. Because of the number of potential sites of action present in this preparation it must be accepted that it cannot be used to establish rigorously the site of action of a drug. However, it can be employed effectively for screening for potentially interesting neuro-active compounds and for establishing the rank order of potency within an active series of compounds. Limited mode of action studies are also possible.

The effects of GABA on the *Ascaris* muscle strip have been investigated. GABA application causes a decrease in muscle tension which is relatively small and difficult to quantify. Two methods can be employed to increase the sensitivity of the preparation to the inhibitory effects of GABA and GABA-mimetics. Both methods use acetylcholine (ACh) application to produce a standard contraction. Kass and co-workers (1982) have used prolonged doses (>1 min) of ACh against which inhibitory effects are measured. A second method uses a prepulse of GABA or GABA-mimetic applied prior to a short duration (10 sec) ACh dose. Both methods allow accurate determination of dose-inhibition relationships .

It is well known that GABA receptors in both invertebrates and vertebrates are associated with anion-selective ion channels and that, under normal physiological conditions, GABA-induced inhibition results from an influx of chloride ions into both muscle and nerve cells (Gershenfeld, 1973). Experiments with ascarid worms have shown that total replacement of Cl^- in the bathing saline with impermeant anions abolishes the inhibition caused by GABA and GABA-mimetics. The inhibition of ACh-induced contractions caused by ACh antagonists, however, is unaffected. This simple example of ion substitution, which can be used to identify the type of ion channel activated by a novel inhibitory agent, serves to demonstrate the potential usefulness of this type of preparation in preliminary mode of action studies.

2.2 Electrophysiological studies

To pursue the mode of action of an active agent further, it is necessary to employ more elaborate, and often time-consuming, electrophysiological techniques. These techniques offer the following advantages:

(1) Events related to the activation (agonism) and/or blockade (antagonism) of populations of receptor-ion channels can be measured directly using intracellular recording techniques.

(2) Drugs can be applied locally by iontophoresis to specific locations on individual muscle cells, or applied differentially in the bath to the dorsal and ventral halves of *Ascaris*.

(3) Currents generated by the activation of single receptor-ion channels can be recorded using the patch-clamp technique of Hamill *et al.* (1981).

(4) Using knowledge of the neuroanatomy of *Ascaris*, preparations can be produced in which synaptic inputs from single motorneurons can be studied.

2.2.1 Intracellular recording

Using intracellular recording techniques, spontaneous depolarizing potentials of 2–10 mV amplitude superimposed on a resting potential of −30 mV can be recorded from the bag region of *Ascaris* muscle cells (Jarman, 1959). ACh depolarizes these cells, while GABA hyperpolarizes them (Del Castillo *et al.*, 1964 a,b; Martin, 1980, 1982). The inhibitory receptors responsible for the hyperpolarizations were believed to be located exclusively at neuromuscular synapses in the syncytium (Del Castillo *et al.*, 1964a). However, after sectioning the arms of the muscle cells Brading and Caldwell (1971) showed that hyperpolarizations could still be recorded from the bag region in response to bath-applied GABA, suggesting that the bags also possess GABA receptors.

Iontophoretic drug application has been employed to study the properties of GABA-activated, receptor-ion channels on the bag membrane (Martin, 1980) and also to investigate the mode of action of the anthelmintic, piperazine (Martin, 1982). These studies have shown that activation of the GABA receptors evokes on outward current across the bag membrane. The reversal potential (approx. −61 mV) of the GABA-induced current is close to the value predicted by a Nernst Cl^- electrode (−64.8 mV) with an intracellular Cl^- concentration of 13.7 mM (Brading & Caldwell, 1971), suggesting that the outward current is generated by Cl^- ions entering the cell. This has been confirmed by ion substitution experiments which show that the current is abolished in Cl^--free saline (Gration & Harrow, unpublished). Investigation of the mode of action of piperazine has shown that, like GABA, this anthelmintic also evokes a Cl^--dependent outward current when applied to the muscle bag (Martin, 1982). Simultaneous application of GABA and piperazine from a double-barrelled iontophoretic pipette placed over the bag shows that GABA and piperazine occupy the same receptors. The dose–conductance relationships show that piperazine is 10–100 times less potent than GABA. No cholinergic antagonistic action of piperazine has been observed. The fact that piperazine and GABA share the same receptor site indicates that this anthelmintic acts as a GABA agonist in *Ascaris*. It is reasonable, therefore, to explain the piperazine-induced reversible paralysis of nematodes and their expulsion from the intestine during therapy (Desowitz, 1971) by its GABA-mimetic action.

2.2.2 Patch-clamp recording

The patch-clamp technique (Hamill *et al.*, 1981) has recently been used to measure currents flowing through single GABA-activated and piperazine-activated ion channels in *Ascaris* muscle (Martin, 1983, 1985). The technique has provided an explanation for the difference in potency between GABA and piperazine, which is unattainable using conventional intracellular recording techniques.

Single open channels, activated by GABA and piperazine, exhibit one mainstate conductance, plus two subconductance states in which the channels open to only 30% or 70% of the full level. The mainstate channel conductances for both agonists are similar (~21 pS), therefore conductance differences cannot explain the magnitude of the observed differences in potency. The difference in potency may be explained, however, by the fact that piperazine requires a higher concentration to achieve a similar opening rate to GABA. In addition, the effective mean open time for piperazine-activated channels is generally shorter than that for channels activated by GABA. Thus for example, 3.5 μM GABA in one typical experiment produced a mean opening rate of 3.9 channels per second with an effective mean open time of 33 ms and a probability of the channel being open of 0.14. On the other hand, another typical experiment using 500 μM piperazine produced a channel opening rate of 3.6 channels per second and an effective mean open time of 19 ms, giving a probability of 0.08 for the channel being open.

2.3 Synaptic pharmacology

In addition to the development of more incisive recording techniques, our understanding of the mode of action of anthelmintics and the neurophysiology of nematodes has been enhanced by the development of preparations in which the pharmacology of identified synapses can be studied. These preparations, which have been developed by Kass, Stretton and co-workers (Stretton *et al.*, 1978; Kass *et al.*, 1980, 1984) are based on a detailed knowledge of the neuroanatomy of *Ascaris*. They allow the effects of drugs on interneuron to motorneuron synapses within the ventral nerve cord to be examined independently of their effects on the neuromuscular synapses, or the muscle cells themselves. These preparations offer the opportunity for rigorous investigation of the site and mode of action of anthelmintics, as exemplified by the studies of Kass *et al.* (1980, 1984) on the avermectins. These authors have investigated the effects of avermectin $B1_a$ (AVM) on excitatory neuromuscular transmission, inhibitory neuromuscular transmission and transmission from interneurons to excitatory motorneurons. They found that a curare-sensitive mechanism is involved in the excitation of excitatory motorneurons via interneurons. This interneuron stimulation of excitatory motorneurons is blocked by AVM and the blockage is reversed by picrotoxin. The two GABA agonists, muscimol and piperazine, mimic the effects of AVM when applied to the ventral nerve cord of *Ascaris,* suggesting that the action of AVM is mediated by a picrotoxin-sensitive, GABA-ergic mechanism. Inhibitory neuromuscular transmission is also blocked by

AVM. Kass *et al.* (1980, 1984) have shown, however, that picrotoxin does not block the response of muscle to stimulation of the inhibitory motorneuron or to the application of GABA, nor does it reverse the AVM block of neuromuscular transmission. These observations suggest that the AVM-sensitive, picrotoxin-insensitive site at the inhibitory neuromuscular synapses differs from the AVM-sensitive, picrotoxin-reversible site in the ventral nerve cord.

The available evidence from neurophysiological investigations of the role of GABA in *Ascaris* suggests that it acts as a chemical messenger at neuronal and inhibitory neuromuscular synapses. The studies with AVM indicate that there are at least two distinct sites of action of AVM in *Ascaris* and, possibly, two pharmacologically different GABA–receptor-ion channel complexes. It is also worthy of note that the site of action of anthelmintics which effect GABA neurotransmission is not necessarily limited to the synapse, since it is clear that extra-synaptic GABA receptors may also be stimulated by piperazine during therapy (Martin, 1982).

3. GABA-MEDIATED NEUROTRANSMISSION IN CATTLE TICKS

Although a number of tick species are economically important parasites and are targets for chemical control, investigation of the pharmacology of cattle ticks is limited and there is little evidence either for or against the role of GABA as a neurotransmitter (Binnington & Obenchain, 1982). It is possible to speculate, however, that GABA should have a neurotransmitter role in these acarines by analogy with its function in other arthropods (Gershenfeld, 1973). Two approaches have been used to investigate this possibility.

3.1 Neuromuscular approach

When applied to the dorsal-ventral body muscle of the *Amblyomma hebraeum* GABA causes a dose-dependent and reversible increase in membrane conductance associated with membrane hyperpolarization (Gration, unpublished). The threshold concentration for GABA is 5 μM and the concentration required to give a half-maximal conductance increase is 40 μM. GABA-induced conductance changes are blocked by picrotoxin and the slope of the dose–conductance curves is reduced, indicating that this GABA antagonist acts non-competitively. GABA also reduces the amplitude of nerve-evoked, excitatory postsynaptic potentials recorded from the dorsal-ventral muscle fibres.

3.2 CNS approach

GABA also has inhibitory effects when applied to the central nervous system (synganglion) of *A. hebraeum*. At concentrations above 50 μM, GABA application causes a marked decrease in the frequency of action potentials recorded from pedal nerve IV. This decrease is readily reversed by washing with normal saline, and is blocked when the synganglion is bathed in Cl^--free saline.

Results obtained with both the neuromuscular and synganglion preparations indicate the presence of GABA receptors both on the muscle membrane and within the central nervous system. It seems likely from these preliminary results that GABA might function as a neurotransmitter at inhibitory synapses within ticks.

4. CONCLUSIONS

Neurophysiological research, conducted in both academic institutions and industry, has led to a better understanding of the mode of action and biological targets of antiparasitic agents. In particular, our understanding of the role of GABA in *Ascaris* has increased greatly over recent years, probably due to the impetus provided by the discovery of avermectins. Knowledge of tick pharmacology is still limited, however, and a greater research effort is required in this field. In the future, we hope that the combined efforts of scientists in academia and industry will provide sufficient understanding of the biological target sites in parasites to allow neuropharmacologists and medicinal chemists to predict the structures of entirely new agents for parasite chemotherapy.

REFERENCES

Ash, A. S. F., & Tucker, J. F. (1967) The bioassay of γ-aminobutyric acid using a muscle preparation form *Ascaris lumbricoides*. *J. Pharmac. Pharmacol.* **19**, 240–245.

Baldwin, E., & Moyle, V. (1947) An isolated nerve–muscle preparation from *Ascaris lumbricoides*. *J. Exp. Biol.* **23**, 277–291.

Binnington, K. C., & Obenchain, F. D. (1982) Structure and function of the circulatory, nervous and neuroendocrine systems of ticks. In: Obenchain, F. D., & Galwin, R. (eds.), *Physiology of Ticks*. Oxford, Pergamon Press pp. 351–398.

Brading, A. F., & Caldwell, P. C., (1971) The resting membrane potential of somatic muscle cells of *Ascaris lumbricoides*. *J. Physiol.* **217**, 605–624.

Burg, R. W., Miller, B. M., Baker, E. E., Birnbaum, J., Currie, S. A., Hartman, R., Kong, Y-L., Monaghan, R. L., Olson, G., Putter, I., Tunac, J. B., Wallick, H., Stapley, E. O., Oiwa, R., & Omura, S. (1979) Avermectins, new family of potent anthelmintic agents: Producing organism and fermentation. *Antimicrobial Agents and Chemotherapy* **15**, 361–367.

de Bell, J., Del Castillo, J., & Sanchez, V. (1963) Electrophysiology of the somatic muscle cells of *Ascaris lumbricoides*. *J. Cell. Comp. Physiol.* **62**, 159–177.

Del Castillo, J., De Mello, W. C., & Morales, T. (1964a) Mechanism of the paralysing action of piperazine on *Ascaris* muscle. *Br. J. Pharmac.* **22**, 463–477.

Del Castillo, J., De Mello, W. C., & Morales, T. (1964b) Inhibitory action of γ-aminobutyric acid (GABA) on *Ascaris* muscle. *Experientia* **20**, 145–146.

Desowitz, R. S. (1971) Antiparasitic chemotherapy. A. *Rev. Pharmac.* **11**, 351–368.

Egerton, J. R., Ostlind, D. A., Blair, L. S., Eary, C. H., Suhayda, D., Cifelli, S., Riek, R. F., & Campbell, W. C. (1979) Avermectins, new family of potent anthelmintic agents: Efficacy of the $B1_a$ component. *Antimicrobial Agents and Chemotherapy* **15**, 372–378.

Fritz, L. C., Wang, C. C., & Gorio, A. (1979) Avermectin $B1_a$ irreversibly blocks postsynaptic potentials at the lobster neuromuscular junction by reducing membrane resistance. *Proc. Natl. Acad. Sci., USA* **76**, 2062–2066.

Gershenfeld, H. M. (1973) Chemical transmission in invertebrate central nervous systems and neuromuscular junctions. *Physiol. Rev.* **53**, 1–112.

Hamill, O. P., Marty, A., Neher, E., Sakmann, B., & Sigworth, J. (1981) Improved patch-clamp techniques for high-resolution current recording from cells and cell-free membrane patches. *Pflugers Arch. Ges. Physiol.* **391**, 85–100.

Jarman, M. (1959) Electrical activity in the muscle cells of *Ascaris*. *Nature* **184**, 1244.

Kass, I. S., Wang, C. C., Walrond, J. P., & Stretton, A. O. W. (1980) Avermection $B1_a$, a paralysing anthelmintic that affects interneurones and inhibitory motoneurones in *Ascaris*. *Proc. Natl. Acad. Sci., USA* **77**, 6211—6215.

Kass, I. S., Larsen, D. A., Wang, C. C., & Stretton, A. O. W. (1982) *Ascaris suum:* Differential effects of avermectin $B1_a$ on the intact animal and neuromuscular strip preparations. *Exp. Parasitol.* **54**, 166–174.

Kass, I. S., Stretton, A. O. W., & Wang, C. C. (1984) The effects of avermectin and drugs related to acetylcholine and 4-aminobutyric acid on neurotransmission in *Ascaris suum*. *Molecular and Biochemical Parasitology* **13**, 213–225.

Martin, R. J. (1980) The effect of γ-aminobutyric acid on the input conductance and membrane potential of *Ascaris* muscle. *Br. J. Pharmac.* **71**, 99–106.

Martin, R. J. (1982) Electrophysiological effects of piperazine and diethylcarbamazine on *Ascaris suum* somatic muscle. *Br. J. Pharmac.* **77**, 255–265.

Martin, R. J. (1983) GABA single channel currents from *Ascaris* muscle. *J. Physiol.* **336**, 36–37P.

Martin, R. J. (1985) γ-aminobutyric acid and piperazine-activated single channel currents from *Ascaris suum* body muscle. *Br. J. Pharmac.* in press.

Mellin, T. N., Busch, R. D., & Wang, C. C. (1983) Postsynaptic inhibition of invertebrate neuromuscular transmission by avermectin $B1_a$. *Neuropharmacology* **22**, 89–96.

Ostlind, D. A., Cifelli, S., & Lang, R. (1979) Insecticidal activity of the anti-parasitic avermectin. *Vet. Record.* **105**, 168.

Stretton, A. O. W., Fishpool, R. M., Southgate,. E., Donmoyer, J. E., Walrond. J. P., Moses, J. E. R., & Kass, I. S. (1978) Structure and physiological activity of the motorneurones of the nematode *Ascaris*. *Proc. Natl. Acad. Sci., USA* **75**, 3493–3497.

Levamisole: mode of action

BEN G. HARRIS
Department of Biochemistry, Texas College of Osteopathic Medicine/North Texas State University, Fort Worth, TX 76107, U.S.A.

Levamisole is the L-isomer of tetramisole [2,3,5,6-tetrahydro-6-phenylimidazo-(2,1-*b*)thiazole hydrochloride]. Although the compound was developed initially as an anthelmintic, it has been used in many other areas such as immunoregulation (Brugmans, 1978), induction of interferon (Tyring & Lefkowitz, 1980), enhancement of prostaglandin activity (Capasso *et al.*, 1982), inhibition of alkaline phosphatase (Janssen, 1976), activation of suppressor T-cells (Rogers *et al.*, 1985), stimulation of chemotactic function of polymorphonuclear leucocytes (Stein *et al.*, 1985), to name just a few. In reviewing the vast literature on levamisole, it is evident that the precise mode of action of levamisole is not known. As an anthelmintic that is active primarily against nematodes, one of the actions of the drug may be as a cholinergic agonist (Van Nueten, 1972; Coles *et al.*, 1975; Lewis *et al.*, 1980; Donahue *et al.*, 1983; Harrow & Gration, 1985). Levamisole causes a spastic contraction of nematode muscle and Harrow & Gration (1985) found that levamisole acts as a potent agonist at acetylcholine receptors on muscle bag membranes of *Ascaris suum*. Lewis *et al.* (1980) have shown that levamisole-resistant strains of the nematode *Caenorhabditis elegans* lack normal cholinergic receptors. Thus, the paralysing action of levamisole might lie in this property of the compound. Levamisole also has other effects on parasitic worms. Van den Bossche & Janssen (1969) showed that levamisole inhibited the fumarate reductase of *A. suum* muscle but the levels required (1 mM) were probably too high to be of physiological significance. Wang & Saz (1974) showed that levamisole stimulated contraction of filariids, but this contraction was followed by a flaccid paralysis. Komuniecki & Saz (1982) and Nelson & Saz (1982) demonstrated that when adult *Litomosoides carinii* were incubated with levamisole, this resulted in elevated levels of glycogen, increased glucose incorporation into glycogen and decreased glycogen phosphorylase activity ratios. These results suggested that levamisole might have an influence on protein kinases or phosphatases. Donahue *et al.* (1983) conducted a study of levamisole on isolated, perfused muscle–cuticle sections of *A. suum*. This system had been previously shown to display a cyclic AMP-dependent glycogenolytic metabolism stimulated by 5-hydroxytryptamine as well as a cyclic AMP-independent, glycogen metabolism stimulated by the muscle contraction neurotransmitter, acetylcholine (Donahue *et al.*, 1981, 1982). Constant perfusion of levamisole elicited a muscle contraction followed by a period of flaccid paralysis. The higher the levamisole level, the shorter the time required to reach the flaccid paralysis stage. The paralysis phase was correlated with an activation of glycogen synthase and an inactivation of phosphorylase. Levamisole inhibited the elevation of cyclic AMP brought about by 5-hydroxytryptamine, thereby preventing an increase in the cyclic AMP-dependent protein kinase activity ratio. Levamisole did not inhibit the acetylcholine response of glycogen metabolism and this suggested that levamisole inhibited cyclic AMP-mediated, but not calcium-mediated, glycogenolysis. The results are consistent with a model in which levamisole inhibits the adenylate cyclase of the muscle membrane. However, the data do not indicate which proteins of the adenylate cyclase complex are inhibited, nor do they exclude other molecular events which may be inhibited or activated by levamisole.

Brugmans, J. (1978) *J. Rheumatol.* **5** (Suppl. 4), 115–121
Capasso, F., Mascolo, N. & Autore, G. (1982) *Prostaglandins* **23**, 427–432
Coles, C. G., East, J. M. & Jenkins, S. N. (1975) *Gen. Pharmacol.* **6**, 309–313
Donahue, M. J., Yacoub, N. J., Michnoff, C. A., Masaracchia, R. A. & Harris, B. G. (1981) *Biochem. Biophys. Res. Commun.* **101**, 112–117
Donahue, M. J., Yacoub, N. J. & Harris, B. G. (1982) *Am. J. Physiol.* **242**, R514–R521
Donahue, M. J., Masaracchia, R. A. & Harris, B. G. (1983) *Mol. Pharmacol.* **23**, 378–383
Harrow, I. D. & Gration, K. A. F. (1985) *Pestic. Sci.* **16**, 662–672
Janssen, P. A. J. (1976) *Prog. Drug Res.* **20**, 347–383
Komuniecki, P. R. & Saz, H. J. (1982) *J. Parasitol.* **68**, 221–227
Lewis, J. A., Wu, C.-H., Levine, J. H. & Berg, H. (1980) *Neuroscience* **5**, 967–989
Nelson, N. F. & Saz, H. J. (1982) *J. Parasitol.* **68**, 1162–1163
Rogers, C. N., Rogers, T. J. & Gilman, S. C. (1985) *J. Immunopharmacol.* **7**, 479–488
Stein, A. N., Diez, R. A., Sen, L. & Estevez, N. E. (1985) *Allergol. Immunopathol.* **13**, 127–134
Tyring, S. K. & Lefkowitz, S. S. (1980) *Experientia* **36**, 1323–1324
Van den Bossche, H. & Janssen, P. A. J. (1969) *Biochem. Pharmacol.* **18**, 35–42
Van Nueten, J. M. (1972) in *Comparative Biochemistry of Parasites* (Van den Bossche, H., ed.), pp. 101–115, Academic Press, New York
Wang, E. J. & Saz, H. J. (1974) *J. Parasitol.* **60**, 316–321

Received 28 July 1986

The γ-aminobutyric acid receptor of *Ascaris* as a target for anthelmintics

R. J. MARTIN
Department of Veterinary Preclinical Sciences, Royal (Dick) School of Veterinary Studies, Summerhall, Edinburgh University, Edinburgh EH9 1QT, U.K.

The electrophysiological effects of anthelmintics on nematodes can be studied in the parasite *Ascaris suum*. This pig parasite has large muscle cells which have allowed easy intracellular recording (e.g. Jaman, 1959). The muscle cells of *Ascaris* are composed of three parts called the spindle, the bag and the arm (Fig. 1*a*). The fibrillar spindle is contractile; it lies under the hypodermis and is arranged longitudinally. The nucleus of the cell is located in the bag region of the muscle. The bag is balloon-shaped, about 200 μm in diameter and fills the body cavity. The arm, a thin process, reaches transversely from the bag to one of the longitudinally running nerve cords. The arms come together to form a syncytium over the nerve cord and are electrically coupled in this region (De Bell *et al.*, 1963). The neuronal inputs to the muscle are via inhibitory or excitatory neuromuscular synapses found between the nerve cords and the syncytium. The anatomy and physiology of the motorneurons have been described by Stretton *et al.* (1978). Spontaneous depolarizing potentials of 2–10 mV amplitude superimposed on a

Abbreviation used: GABA, γ-aminobutyric acid.

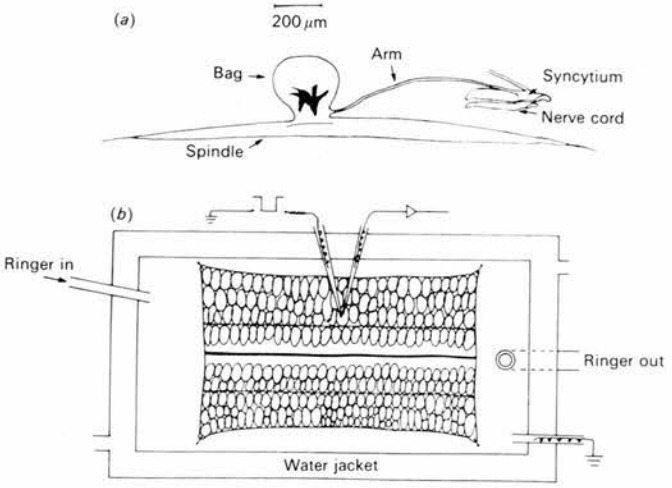


Fig. 1. *Ascaris muscle cell anatomy and experimental design*

(*a*) Diagram of an *Ascaris* muscle cell illustrating its anatomical features. (*b*) Experimental chamber and preparation. A section of *Ascaris* is pinned cuticle side down on to Sylgard in a chamber containing 1.5 ml of Ringer solution and perfused at a rate of 6.5 ml/min. The chamber is fitted with a water jacket to maintain the preparation at 22° C. Two potassium acetate-filled micropipettes are illustrated inserted into the bag region of the muscle cell. One pipette is used for current injection and the other is used for recording voltage responses. During the voltage-clamp experiments the same preparation is used.

resting potential of −35 mV are recorded in the muscle bag region. Acetylcholine depolarizes muscle cells (Del Castillo *et al.*, 1963), while piperazine and γ-aminobutyric acid (GABA) hyperpolarize them (Del Castillo *et al.*, 1964*a*,*b*).

It is the intention of this communication to describe properties of an extrasynaptic GABA receptor localized on the bag region of the muscle and effects of piperazine, diethylcarbamazine and dihydroavermectin B_{1a}.

Experimental approach

Samples of *Ascaris suum* are collected from the local slaughter house and maintained in a Locke solution at 37°C in a water bath. The *Ascaris* are used for experiments within 4 days. A 2 cm flap preparation is routinely used and is made from the anterior region of the worm by pinning it on to Sylgard in an experimental chamber. The preparation is usually maintained at 22–25°C to eliminate spike activity and to reduce muscle movement.

The preparation is usually bathed in a high Cl^- Ringer solution (Martin, 1980) to facilitate the recording of events mediated by the movement of Cl^- ions through the membrane. Normal *Ascaris* perienteric fluid, which bathes the muscle, contains a lower concentration of Cl^- ions and a higher concentration of organic acids.

Three electrophysiological techniques are used to examine the properties of the bag region of the muscle. The first approach is to place two microelectrodes into the bag to record membrane potential and the effect of injecting constant current pulses; this approach allows effects on membrane potential and membrane conductance to be examined during the bath application or iontophoretic application of various drugs. The second approach is to use a two-microelectrode voltage-clamp technique to examine the effect of iontophoretically applied drugs at different membrane potentials. The third approach is to use the patch-clamp technique on collagenase-treated preparations to examine drug effects on single-channel currents. These methods have been described in more detail (Martin, 1980, 1982, 1985).

Conductance and membrane potential recording

Bath-applied GABA in concentrations greater than 3 μM causes a reversible increase in input conductance which is associated with a hyperpolarizing potential. By applying various concentrations of GABA to the bath, dose–response curves are obtained. The conductance dose–response curve for GABA has an ED_{50} of 13 μM.

The GABA-induced conductance changes are abolished by perfusing the preparation with a low Cl^- Ringer solution. This is consistent with the GABA-induced conductance being mediated by Cl^- ions.

The bath application experiments with GABA show that large conductance changes can be observed in bags located well away from the nerve cord: it seems unlikely that these conductance changes can be explained by inhibitory receptors exclusively located at the syncytium; the resistance of the arm should limit the size of the conductance changes observable in the bag. In order to test for the presence of extrasynaptic GABA receptors, iontophoretic experiments can be carried out. By recording intracellularly from the bag region and applying the GABA to different locations on the muscle surface, it can be concluded that extrasynaptic GABA receptors are found on the bag as well at the syncytium.

In the high Cl^- Ringer solution, bath applications of piperazine also increase the input conductance of the bag and cause a hyperpolarization of the membrane. The conductance dose–response relationship contrasts with that of GABA in that piperazine is 100 times less potent. These conductance changes, like those produced by GABA, are also abolished by bathing the preparation in a low Cl^- Ringer solution. Thus both GABA and piperazine induce an increase in the Cl^- conductance of the membrane.

Picrotoxin in concentrations up to 500 μM slightly antagonizes but does not block the effect of GABA iontophoresis. This contrasts with the $GABA_a$ receptor of mammals.

Voltage-clamp experiments

The two-microelectrode voltage-clamp can be used to measure the GABA and piperazine reversal potentials. These experiments show the reversal potentials to be close to the predicted Nernst Cl^- potential (−63 mV). To test further the suggestion that piperazine and GABA are acting on the same receptor, both compounds can be applied simultaneously during voltage-clamp experiments. It is found that when piperazine occupies the GABA receptor, it reduces the amplitude of the GABA response.

Diethylcarbamazine is a piperazine derivative. In marked contrast to piperazine it does not act on the GABA receptor but produces a small decrease in membrane conductance associated with the depolarizing potential. This effect can be investigated under voltage-clamp and found to be associated with a block of voltage-sensitive K^+ channels by diethylcarbamazine.

Patch-clamp experiments

GABA in concentrations greater than 1 μM applied to an outside-out patch produces rectangular current pulses of varying duration but essentially constant amplitude (at a fixed potential). The amplitudes of the current steps at different transpatch potentials can be measured to obtain the conductance of the channel. The mean estimates of the channel conductance using GABA as an agonist is 22 pS. Rectangular current pulses with the same conductance are

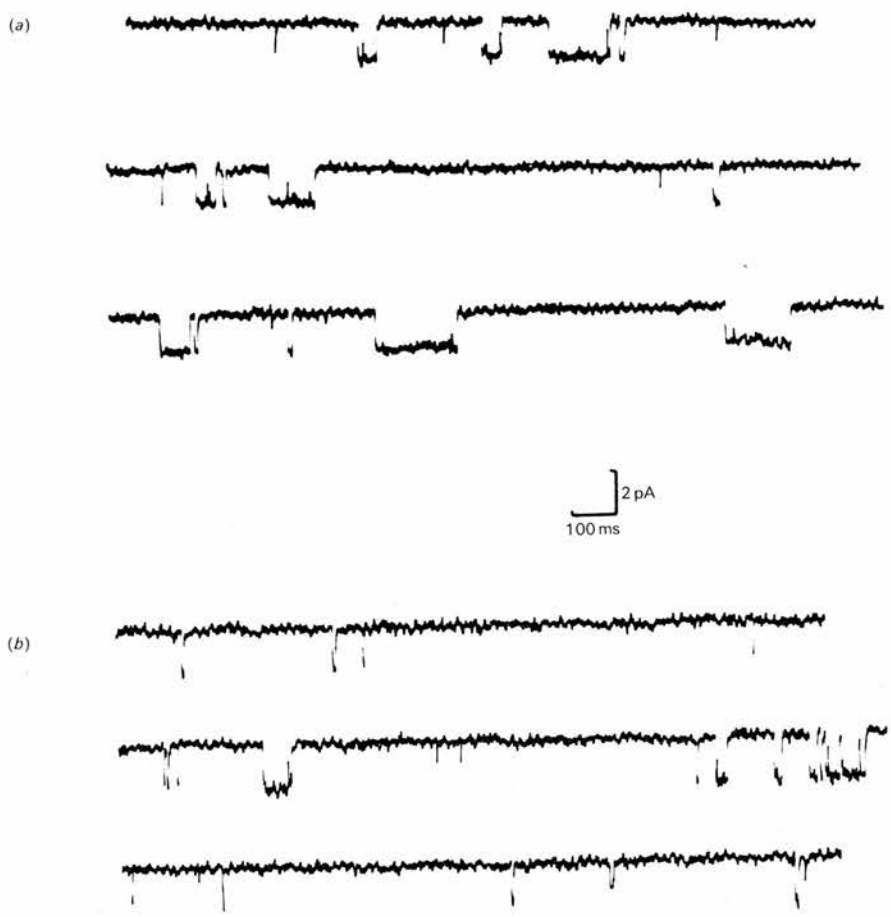


Fig. 2. *Continuous single-channel recordings using low agonist concentrations, cell-attached patches, a transpatch potential of −75 mV and Cl^- concentration equal on both sides of the membrane*

Brief and longer openings are seen (downwards, inwards curent). Some brief closings giving rise to bursts are seen: (*a*) three traces with 3 μM-GABA as agonist; (*b*) three traces with 500 μM-piperazine as agonist. Effective channel open times: GABA, 33 ms; piperazine, 18 ms.

also observed with piperazine in concentrations greater than 100 μM.

Fig. 2(*a*) shows a typical example of a cell-attached patch recording with 3 μM-GABA as the agonist; the transpatch potential is −75 mV. The effective mean open time in this experiment is 34 ms. When 500 μM-piperazine is used as the agonist instead of GABA, shorter mean open times are observed (Fig. 2*b*); here the effective mean channel open time is 18 ms.

Piperazine is some 100 times less potent than GABA in the *Ascaris* preparation; the main state channel conductances of both agonists are similar. The difference in potency between these two agonists is explained by the fact that piperazine requires a higher concentration to achieve a similar channel-opening rate; in addition, the effective mean open time for piperazine is shorter. Thus, for example, 3 μM-GABA in one typical experiment produces a mean opening rate of 3.9/s, with an effective mean channel open time of 33 ms and a probability of the channel being open of 0.14. On the other hand, in another typical experiment, using 500 μM-piperazine as the agonist, there is a mean channel opening rate of 3.6/s and an effective mean channel open time of 18 ms, giving a probability of 0.08 for the channel being open.

Piperazine has a heterocyclic ring structure and lacks a carboxyl group like that of GABA; adequate interaction with the amine moiety with a presumed anionic subsite of the receptor is enough to permit channel opening; the fact that the effective mean open time of GABA is generally longer than that of piperazine, suggests that some interaction between the carboxyl group of GABA and the receptor may be important for delaying channel closure in addition to facilitating channel opening.

The distributions of the GABA open times cannot be described by a single exponential, but are best described by a double exponential. For example, in the experiment illustrated in Fig. 2(*a*) with 3 μM-GABA as the agonist, the fast component has a mean value of 2.1 ms while the slow component has a mean value of 46 ms. For the piperazine experiment (Fig. 2*b*), the mean value of the fast component is 7.6 ms while the mean value of the slow component is 28 ms. After the double exponential has been fitted it is possible to estimate the relative number of fast and slow openings for both GABA and piperazine. In the experiments illustrated 36% of the GABA openings and 47% of the piperazine openings are of the fast type while the remainder are slow. As a consequence, the brief openings for GABA carry only 3% of the total current but for piperazine 19% of the

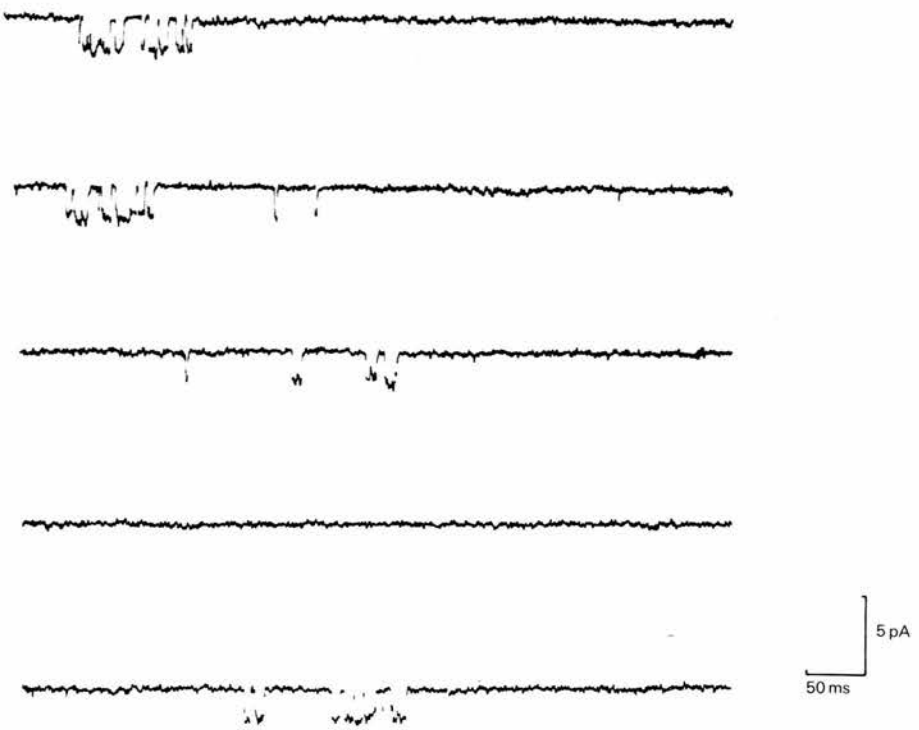


Fig. 3. *Single-channel recordings from the same cell-attached patch, with a transpatch potential −75 mV and Cl^- concentration equal on both sides of the membrane*

Brief openings are seen (downwards, inwards current). The channel amplitude is also irregular. The GABA concentration in the patch-pipette is 3 μM; the dihydroavermectin concentration is 0.1 μM. Effective mean channel open time 7.5 ms. Note that this is briefer than when dihydroavermectin is absent. The traces are not continuous.

current is carried by the brief openings. The fact that no simultaneous double openings are observed during these recordings suggests that there is only one channel present in the patch. This then implies that there are at least two open channel states rather than two separate channel populations.

The distributions of the closed times at low agonist concentrations of GABA or piperazine can also be examined. Since openings often occur in bursts which are due to the behaviour of brief (1–6 ms) closed periods occurring in sequence between brief or long openings, there is a fast component in the distribution of the exponentials which is required to describe channel closed times. The distributions of closed times at these low concentrations are best described by up to three exponentials. The second component in the distribution is due to the tendency of the burst to be separated by longer (5–150 ms) closed periods giving rise to clusterings of bursts. The third component is due to much longer closed periods which separate the clusters. These observations suggest that there are up to three closed states at these agonist concentrations.

The distribution of channel open and closed times is inconsistent with a simple two-step KM model (Katz & Miledi, 1972) which involves the binding of a single agonist molecule for channel opening. One suggestion is that the brief openings correspond to openings of the receptor channel occuped by only one agonist molecule and that the longer openings correspond to receptor-operated channels occupied by two agonist molecules. This has been suggested for the acetylcholine receptor and glutamate channel (Colquhoun & Sakmann, 1981; Cull-Candy & Parker, 1982). One attractive model, in which two agonist molecules can combine to two subunits of the receptor channel complex to produce opening, is the Monod–Wyman–Changeaux model (Colquhoun & Hawkes, 1977, 1981).

Effect of dihydroavermectin

The effects of 0.1–1 μM-dihydroavermectin B_{1a} dissolved in 1% dimethyl sulphoxide can be examined using the techniques of constant current injection or the patch-clamp technique. It is found that the bath application of concentrations of dihydroavermectin up to 1.2 μM has little effect on the resting membrane conductance or electrical activity of the preparation. It, therefore, does not act as a GABA agonist. Dihydroavermectin can also be tested as a GABA antagonist. It is found that concentrations greater than 0.1 μM and applied for longer than 2 min produce a long-lasting irreversible GABA antagonism. For example, in one preparation 50 μM-GABA produced a reversible increase in input conductance of 3.3 mS; after the application of 1.2 μM-dihydroavermectin for 10 min, the same concentration of GABA produced a conductance change of only 0.8 mS, which is less than 25% of the control. Washing the preparation fails to restore the GABA response.

To examine the antagonism at the single-channel level, cell-attached patch experiments are used in which 3 μM-GABA, together with concentrations of dihydroavermectin between 0.1 and 1 μM, is added to the patch pipette. Fig. 3 illustrates a typical recording from these experiments. The probability of opening is massively reduced and in Fig. 3 P_{open} is less than 0.05. This compares with a probability of the channel being open of 0.14 (Fig. 2*a*) when dihydroavermectin is absent.

Two other features of the antagonism are also noted. The

mean channel open time in the presence of dihydroavermectin is reduced to around 7.5 ms, which contrasts with 33 ms in the absence of dihydroavermectin. A further feature of the antagonism seen at single-channel level is a reduction in the mean channel current amplitude and an increase in the variance of the channel amplitude. For example, in the absence of dihydroavermectin, and using a driving force of -75 mV, a mean GABA channel current was measured to be 1.62 pA with a standard deviation of 0.36 pA; this gives a conductance of 21 pS. When 0.1 μM-dihydroavermectin is added to the patch pipette, in addition to the 3 μM-GABA, a mean channel current amplitude of 1.2 pA with a standard deviation of 0.56 is measured; this corresponds to a mean conductance of 16 pS. Thus, dihydroavermectin antagonized the actions of GABA by decreasing the probability of a channel being open, as well as reducing its mean conductance. Since dihydroavermectin takes several minutes to exert its effect and is highly lipid soluble, it seems that its mode of action is mediated via the membrane, perhaps by combining with a lipophilic site on the GABA receptor–ion channel complex, rather than by a combination with any hydrophilic site.

Discussion

It has been shown that piperazine acts as an agonist at the extrasynaptic GABA receptor on *Ascaris* muscle to increase the Cl^- conductance of the membrane. It is interesting that piperazine also acts in this way on crayfish muscle (Iravani, 1965) and on lobster muscle (Constanti & Nistri 1976), but not on rat sympathetic neurons (Connor *et al.*, 1981). Nistri & Constanti (1979) have suggested the existence of at least two separate types of GABA receptor in some invertebrates and some vertebrate preparations with piperazine as a selective agonist in invertebrates. When this is coupled with the fact that the GABA antagonist picrotoxin is a poor antagonist in the *Ascaris* preparation, unlike the $GABA_a$ receptor of mammals, it suggests the presence of a separate type of receptor in nematodes, i.e. the $GABA_n$ receptor (n: not antagonized by picrotoxin, n: for nematodes).

In conclusion then, this communication has illustrated the use of various electrophysiological techniques which have facilitated and advanced the study of anthelmintic mode of action. It is inevitable that these approaches will be used increasingly in the future to evaluate and assess the newer anthelmintics.

Colquhoun, D. & Hawkes, A. G. (1977) *Proc. R. Soc. London Ser. B* **199**, 231–262
Colquhoun, D. & Hawkes, A. G. (1981) *Philos. Trans. R. Soc. London Ser. B* **300**, 1–59
Colquhoun, D. & Sakmann, B. (1981) *Nature (London)* **294**, 464
Connor, J. D., Constanti, A., Duinn, I. M., Forward, A. & Nistri, A. (1981) *Br. J. Pharmacol.* **74**, 445–454
Constanti, A. & Nistri, A. (1976) *Br. J. Pharmacol.* **57**, 347–358
Cull-Candy, S. & Parker, I. (1982) *Nature (London)* **295**, 410–412
De Bell, J., Del Castillo, J. & Sanchez, V. (1963) *J. Cell. Comp. Physiol.* **62**, 159–177
Del Castillo, J., De Mellow, W. C. & Morales, T. (1963) *Arch. Int. Physiol.* **71**, 741–757
Del Castillo, J., De Mellow, W. C. & Morales, T. (1964*a*) *Br. J. Pharmacol.* **22**, 463–477
Del Castillo, J., De Mellow, W. C., & Morales, T. (1964*b*) *Experientia* **20**, 145–146
Iravani, J. (1965) *Naunyn-Schmieidebergs Arch. Exp. Pathol. Pharmakol.* **251**, 265–274
Jarman, M. (1959) *Nature (London)* **184**, 1244
Katz, B. & Miledi, R. (1972) *J. Physiol. (London)* **224**, 665–669
Martin, R. J. (1980) *Br. J. Pharmacol.* **71**, 99–106
Martin, R. J. (1982) *Br. J. Pharmacol.* **77**, 255–265
Martin, R. J. (1985) *Br. J. Pharmacol.* **84**, 445–461
Nistri, A. & Constanti, A. (1979) *Prog. Neurobiol.* **13**, 117–235
Stretton, A. O. W, Fishpool, R. M., Southgate, E. Denmoyer, J. E., Walrond, J. P., Moses, J. E. R. & Kass, I. S. (1978) *Proc. Natl. Acad. Sci. U.S.A.*, **75**, 3493–3497

Received 28 July 1986

Avermectins: action on target pest species

DENIS J. WRIGHT
Department of Pure and Applied Biology, Imperial College Silwood Park, Ascot, Berks. SL5 7PY, U.K.

The avermectins (AVM) are a novel group of biologically active compounds which possess a 16-membered lactone ring with a spiroacetal system (C-17 to C-25) and a dissacharide substituent at the C-13 position (see Fisher & Mrozik, 1984). First isolated in 1976 from the actinomycete, *Streptomyces avermitilis* (Burg *et al.*, 1979), the naturally occurring AVM can be separated into four major (A_{1a}, A_{2a}, B_{1a}, B_{2a}) and four minor (A_{1b}, A_{2b}, B_{1b}, B_{2b}) homologous components (Fig. 1) of which the B series are generally the more biologically active (Campbell *et al.*, 1983). Mixtures of homologous pairs containing at least 80% of the 'a' component and not more than 20% of the 'b' component are referred to as AVM A_1, AVM B_1 etc. A synthetic derivative of AVM B_1, 22,23-dihydroavermectin (DHAVM B_1), is available as a veterinary product for use against nematodes and arthropods (Campbell *et al.*, 1983), while AVM B_1 is currently being introduced for use against arthropod pests in horticulture and agriculture (Dybas & Green, 1984).

Structurally, AVM are similar to macrolide antibiotics but have not been shown to exhibit antimicrobial proper-

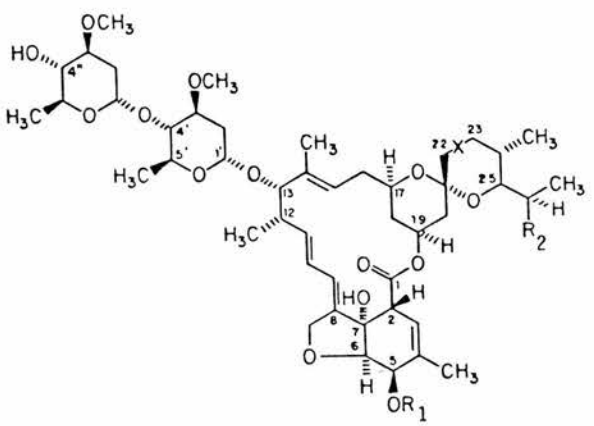


Fig. 1. *General structure of avermectins*

R_1 = CH_3 (component A), H (component B). R_2 = C_2H_5 (component a), CH_3 (component b). X = $-CH=CH-$ (component 1), $-CH_2-C(OH)H-$ (component 2).

Abbreviations used: AVM, avermectins; DHAVM, dihydroavermectin; GABA, γ-aminobutyric acid.

ties (Wang & Pong, 1982; Onishi & Miller, 1985). They are extremely toxic to nematodes, molluscs, various acarines and to a wide range of insects including members of the orders Diptera, Homoptera, Coleoptera and Lepidoptera, but are reportedly inactive against trematodes and cestodes (see Wright, 1986).

Biological activity against nematodes

The majority of studies have examined the inhibitory action of AVM on nematode movement, although work on the dog hookworm, *Dirofilaria immitis*, and the human filarial worm, *Onchocerca volvulus*, has suggested that AVM can inhibit the embryonic development of the microfilarial stage (Anantaphruti *et al.*, 1982; Campbell *et al.*, 1983).

Animal parasitic nematodes belonging to the family metastrongylidae appear to be particularly sensitive to AVM B_{1a}, complete paralysis of two such species occurring within 100 min of exposure to 3.6 aM, whereas at least 3.6 nM was required to produce the same response in other species (Sano *et al.*, 1981).

When AVM B_{1a} (1.5 μg) was injected into adults of *Ascaris suum*, the worms were found to be immobilized without showing either flaccid paralysis or hypercontraction and such worms were capable of movement when stimulated mechanically (Kass *et al.*, 1980). Several nematode species, including the plant parasite *Meloidogyne incognita* (J2 stage), show a marked triphasic response to > 1 nM-AVM B_{1a} or 1nM-AVM B_{2a}-23-one, comprising an initial loss of locomotor activity (1–10 min) during which the nematodes remain sensitive to touch, a recovery phase (10–30 min) and a final loss of activity when the nematodes are relatively insensitive to stimulation. Circumstantial evidence for the involvement of γ-aminobutyric acid (GABA) was provided by the observed ability of the GABA antagonist bicuculline to completely prevent the triphasic response to AVM (Wright *et al.*, 1984).

It is unlikely that AVM kill nematodes directly at therapeutic dosages and their effectiveness as anthelmintics appears to be due to their paralytic action (Sano *et al.*, 1981). The inhibitory effects of AVM B_1 and AVM B_{2a}-23-one on *M. incognita* have in fact been shown to be reversible (Wright *et al.*, 1983).

Biological activity against anthropods

In contrast to their action on nematodes, AVM kill insects and mites directly although rather less rapidly than many other neuroactive pesticides. However, it is uncertain whether the relative speed of kill with AVM is due to their mode of action, either because of the lack of hyperactive symptoms compared with other compounds, or to a relatively slow accumulation of AVM at critical target sites (Wright, 1986). The first symptoms of AVM poisoning, which are often observed within a few hours of application, such as paralysis of the hind legs of lepidopteran larvae (Putter *et al.*, 1981), may thus reflect an initial action at relatively exposed peripheral target sites.

In addition, like other groups of pesticides (Kumar & Chapman, 1982), AVM have been shown to have a number of sublethal effects on arthropods, impairing feeding and reproduction in various species (see Wright, 1986). In fact, the principal toxic action of DHAVM B_1 on many species of ticks appears to be on engorgement, moulting and reproduction (Campbell *et al.*, 1983).

The reduced reproductive potential of pesticide-treated arthropods may reflect secondary effects of poisoning, and whether AVM have a more specific action on reproduction is uncertain. There is evidence for AVM B_1 causing irreversible sterility in the imported fire ant, *Solenopsis invicta*, which is associated with cytological changes in the reproductive system of the queen, but this action could also be due to an indirect action via the neurosecretory system (Glancey *et al.*, 1982).

Action on chloride ion channels

Early electrophysiological studies suggested that AVM acted as a postsynaptic agonist of GABA, potentiating GABA chloride ion channel conductance in both arthropods and nematodes (Fritz *et al.*, 1979; Kass *et al.*, 1980). While work on mammalian brain membrane preparations has shown that AVM can: (1) stimulate presynaptic release of GABA, (2) potentiate GABA-receptor binding, (3) bind at specific high-affinity sites, and (4) potentiate binding of various benzodiazepines (Wang & Pong, 1982). It has been proposed that AVM B_{1a} influences benzodiazepine binding via the high-affinity AVM-binding site and that the latter is closely associated with the GABA–benzodiazepine–chloride ion channel complex (see Wright, 1986).

However, the effects of AVM on vertebrates cannot necessarily be related to their mode of action against the various groups of invertebrate pest species, particularly as pharmacological differences at receptor sites are apparent both between vertebrates and invertebrates (see Lummis & Sattelle, 1985; Abalis & Eldefrawi, 1986) as well as between different invertebrate preparations (see Wright, 1986).

In nematodes, no receptor–ligand binding studies have been reported and the existing electrophysiological evidence suggests that the principal action of AVM is at synapses believed to be mediated by GABA (Wright, 1986).

It has been shown in *A. suum* that 6 μM-AVM B_{1a} (1) blocks transmission between interneurons and excitatory motorneurons in the ventral nerve cord, reducing depolarization of muscle cells, and (2) blocks transmission between inhibitory motorneurons and muscle cells, thereby reducing hyperpolarization of the latter. Only the former action was found to be reversed by picrotoxin (Kass *et al.*, 1980). As the inhibitory motorneurons in nematodes receive their sole input from the axons of excitatory motorneurons, control of the latter is central to the regulation of locomotion (Johnson & Stretton, 1980) and the principal action of AVM would appear to be within the ventral nerve cord (Kass *et al.*, 1980, 1984).

However, it has recently been reported that 0.1 μM-DHAVM B_{1a} acts as a GABA antagonist at an extrasynaptic GABA receptor on the somatic muscle cells of *A. suum*, reducing chloride ion conductance (Martin, 1987). It would be of interest therefore to study the effects of 0.1 μM-DHAVM B_{1a} or 0.1 μM-AVM B_{1a} on neuronal transmission in *A. suum* at this concentration would appear to be more realistic in relation to the observed biological activity of AVM on nematodes (see Wright, 1986), and also considering the dose-dependent effects observed with such compounds on, for example, insect preparations (Table 1).

In insects, AVM have been shown to enhance binding of [^{3}H]GABA in nerve cord extracts of the cockroach, *Periplaneta americana*, within a rather narrow concentration range (Lummis & Sattelle, 1985; Table 1), while more recently Abalis & Eldefrawi (1986) have reported that very low concentrations of AVM B_{1a} (IC_{50} 10 pM) inhibited high-affinity binding of [^{3}H]muscimol to a putative GABA receptor in the brain of the honey bee, *Apis mellifera*. In addition, specific benzodiazepine sites are now believed to be present in the insect central nervous system (see Wright, 1986) although the effects of AVM on specific benzodiazepine binding in insects remain to be elucidated (T. N. Robinson & G. G. Lunt, personal communication).

However, there is also evidence for the involvement of non-GABAergic sites in the action of AVM. Scott & Duce (1985) examined chloride ion conductance in the extensor tibia muscle of the locust, *Schistocerca gregaria*, and found that in addition to dose-dependent effects of AVM on

SR95103 ACTS AS A GABA ANTAGONIST IN ASCARIS SUUM MUSCLE

By A.H. Duittoz & R.J. Martin. Department of Preclinical Veterinary Sciences, R.(D.)S.V.S., University of Edinburgh, Summerhall, Edinburgh EH9 1QH.

The distinctive properties of the GABA receptor in the parasite nematode Ascaris suum are of interest since they may be exploited therapeutically (Martin, 1987). It has been reported that the classical $GABA_a$ antagonists and the specific $GABA_b$ agonist Baclofen have no effect on GABA induced hyperpolarisations (Holden-Dye et al., 1988). We have examined effects of Picrotoxin, Bicuculline and the arylaminopyridazine derivatives; SR95531 and SR95103 (10^{-3}M), on cumulative GABA conductance dose-response relationships using techniques described previously (Martin, 1980). Only SR95103 displayed an antagonist effect (Fig. 1). Dose-response curves to GABA were shifted to the right in a parallel manner (10^{-4}M), (Fig. 2). A modified Schild analysis (Williams et al., 1988) suggested that SR95013 (tested at 10^{-4}, $3x10^{-4}$, 10^{-3}M) was a competitive antagonist and that two molecules of GABA but only one of SR95103 interacted with the receptor.

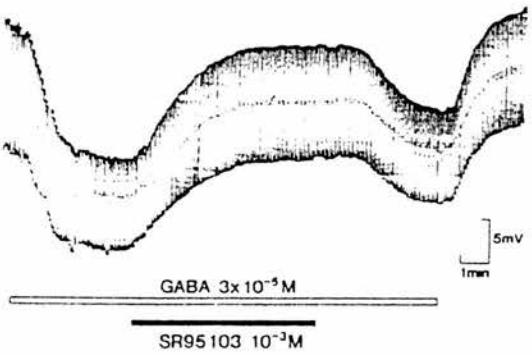


Fig. 1
Effect of GABA ($3x10^{-5}$M) and GABA ($3x10^{-5}$M) + SR95103 (10^{-3}M) on membrane input conductance. Glass microelectrodes: 10-20MΩ filled with K acetate 2M. Current pulse: 40nA, 2s, hyperpolarising. Ringer solution (mM): NaCl 134, KCl 3, $MgCl_2$ 15.7, Glucose 3, TRIS 5, adjusted to pH 7.6 with maleic acid. Resting membrane conductance: g=2.7μS; GABA ($3x10^{-5}$M) induced conductance change g=1.1μS; GABA ($3x10^{-5}$M) + SR95103 (10^{-3}M) g=0.3μS; GABA recovered its effect on conductance when SR95103 was washed.

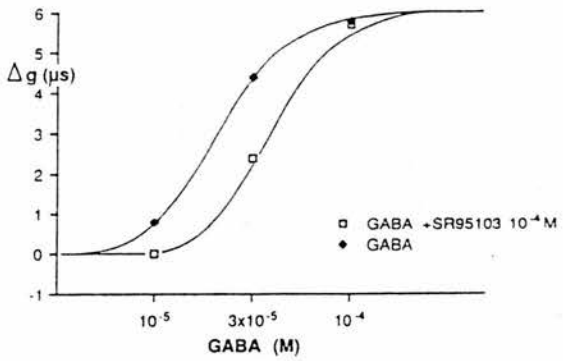


Fig. 2
Dose-response curves to GABA and GABA + SR95103 (10^{-4}M). Dose-response curves were fitted to the modified Hill equation by non linear regression.

HOLDEN-DYE, L., HEWITT, G.M., WANN, K.T., KROGSGAARD-LARSEN, P. & WALKER, R.J. (1988). Pestic. Sci. (in press).
MARTIN, R.J. (1980). Br. J. Pharmacol., 71, 99-106.
MARTIN, R.J. (1987). Bioch. Soc. Trans., 15, 61-65.
WILLIAMS, T.J., SMITH, D.A.S., BURTON, N.R. & STONE, T.W. (1988). Br. J. Pharmacol., 95, 805-810.

Comp. Biochem. Physiol. Vol. 98C, No. 2/3, pp. 417–422, 1991
Printed in Great Britain

0306-4492/91 $3.00 + 0.00
© 1991 Pergamon Press plc

EFFECTS OF THE ARYLAMINOPYRIDAZINE–GABA DERIVATIVES, SR95103 AND SR95531 ON THE *ASCARIS* MUSCLE GABA RECEPTOR: THE RELATIVE POTENCY OF THE ANTAGONISTS IN *ASCARIS* IS DIFFERENT TO THAT AT VERTEBRATE $GABA_a$ RECEPTORS

A. H. Duittoz and R. J. Martin

Department of Preclinical Veterinary Sciences, R.(D.)S.V.S., Summerhall, University of Edinburgh, Edinburgh, U.K. (Telephone: (031) 667-1011)

(*Received* 8 *June* 1990)

Abstract—1. GABA-induced changes in input conductance in the bag region of *Ascaris suum* muscle were monitored using a two-microelectrode current-clamp technique.

2. Effects of the arylaminopyridazine–GABA derivatives, SR95103 and SR95531 on GABA conductance responses were observed.

3. SR95103 was more potent than SR95531 as an antagonist; this potency order contrasts with vertebrate $GABA_a$ receptors.

4. The antagonism of SR95103 was associated with a parallel shift to the right in the GABA dose–response relationships.

5. A modified Schild plot was used to describe the action of SR95103: the data was consistent with 2 molecules of GABA but one molecule of antagonist interacting with the receptor.

6. The K_B for SR95103 was $64 \pm 13\ \mu M$ (mean $\pm$ SE, $N = 14$).

INTRODUCTION

A variety of anti-nematodal drugs, including piperazine and ivermectin may interact with parasite γ-aminobutyric acid (GABA) receptors, (Martin, 1987), so it is of interest to compare the pharmacology of parasite and host receptors in an attempt to identify and exploit differences for therapeutic purposes.

In mammals, GABA receptors have been divided into two main classes: $GABA_a$ receptors and $GABA_b$ receptors (Bowery *et al.*, 1983). Isoguvacine and piperidine-4-sulphonic acid (P4S) are selective $GABA_a$ agonists and bicuculline is a selective $GABA_a$ antagonist (Bowery *et al.*, 1983); baclofen is a specific $GABA_b$ agonist and phaclofen is a selective $GABA_b$ antagonist (Kerr *et al.*, 1987). The $GABA_a$ receptor is directly linked to a Cl channel; the $GABA_b$ receptor acts via a second messenger on a K or Ca conductance (Dunlap, 1981; Desarmenien *et al.*, 1982; Dutar and Nicoll, 1988). This classification is useful, although a simplification, since both classes appear to be heterogenous (Krogsgaard-Larsen, 1988; Levitan *et al.*, 1988; Pritchett *et al.*, 1989). Bicuculline and baclofen-insensitive GABA receptors have also been described (Ault and Nadler, 1983; Johnston and Allan, 1984) and tentatively named $GABA_c$ receptors (Johnston, 1986).

A nematode GABA receptor, amenable to electrophysiological study, is found on the extrasynaptic region of large muscle cells of *Ascaris suum* (Martin, 1980); this receptor is linked to a Cl channel (Martin, 1980, 1985). Previous pharmacological studies indicate that most $GABA_a$ agonists, except the sulphonic acid derivatives 3APS and P4S are active at the *Ascaris* receptor; but the $GABA_a$ antagonists picrotoxin, bicuculline, pitrazepin, securinine and TBPS are inactive (Holden-Dye *et al.*, 1988, 1989).

The actions of arylaminopyridazine derivatives have been investigated in the mammalian central nervous system, where they are potent and selective competitive antagonist of $GABA_a$ receptors (Chambon *et al.*, 1985); SR95531 is the most potent of the series. However, the action of this series of compounds remains to be fully explored in *Ascaris* and more generally in invertebrates. In these two papers we examine and describe the actions of SR95103 and SR95531 (Fig. 1) on the *Ascaris* GABA receptor: the first paper describes effects on GABA conductance dose–response relationships and shows that in *Ascaris*, SR95103 is more potent than SR95531; the second paper describes effects of SR95103 at the single-channel level. The action of these antagonists suggests that a knowledge of the pharmacology of arylaminopyridazine–GABA derivatives in *Ascaris* may be useful for the design of new anti-parasitic agents. A preliminary account of this work has appeared (Duittoz and Martin, 1989).

MATERIALS AND METHODS

Specimens of *Ascaris summ* were collected from the local slaughter house and maintained in Locke's solution at 37°C for up to 4 days. A 2 cm flap preparation (Martin, 1980) was mounted in the experimental chamber which had a volume of 2.5 ml. The preparation was bathed in a high-Cl, low-Ca solution containing (mM): NaCl 135; KCl 3.0; $MgCl_2$ 15.7; glucose 3.0; Tris 5.0; pH adjusted to 7.6 with maleic acid.

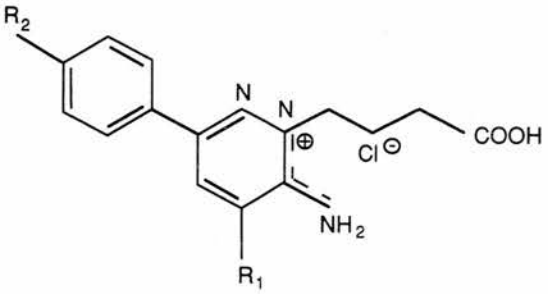


Fig. 1. Chemical structure of SR95103 and SR95531.

SR95103: $R_1 = -CH_3$; $R_2 = -H$.

SR95531: $R_1 = -H$; $R_2 = -OCH_3$.

Current-clamp technique

Two glass microelectrodes (Kacetate 2M filled) were introduced into the bag region of a muscle cell; one pipette (resistance 10–20 MΩ) was used to inject hyperpolarizing current pulses (40 nA, 2 sec, 0.2 Hz), the other pipette (resistance 20–30 MΩ) was used to record membrane potential. Signals were recorded with a laboratory made amplifier (Martin, 1982) in the current-clamp mode, and monitored on a Tectronix 2210 oscilloscope and a Lectromed two-channel chart-recorder.

Voltage-clamp technique

The voltage-sensitivity of the action of SR95103 was examined by applying GABA iontophoretically to the bag membrane with a third microelectrode; the two intracellular micropipettes, previously placed for current-clamp, were used for voltage-clamp under the control of an Axoclamp 2A (set in voltage-clamp mode). Details of this technique have been described previously (Martin, 1982). The holding-potential was 0 mV or −10 mV and 80 mV voltage-steps to −80 mV or −90 mV were made for 500 msec at 1 Hz. GABA was applied iontophoretically as a cation from a fine micropipette (20 MΩ) using a standard current charge of 150 nC to obtain each response. GABA 2 M, at pH 2.5 filled the iontophoretic pipette.

Data analysis

The input conductance of the bag was calculated directly from the amplitude of the plateau of the voltage-response to the injected current pulse; the I/V plot of the bag is linear during the injection of hyperpolarizing current and input conductance is unaltered by hyperpolarization over the range of membrane potentials observed during these experiments (Martin, 1980). The effect of GABA was then determined by measuring the change in input conductance. The bag region of the muscle cell was approximated to a sphere, consequently the input conductance was directly related to the change in membrane conductance. Dose–response relationships were described by the modified Hill equation (Nistri and Constanti, 1979):

$$\Delta G = \frac{\Delta G_{max}}{1 + (EC_{50}/x_a)^N},$$

where ΔG is the change in input conductance, ΔG_{max} is the maximum response, EC_{50} is the concentration of GABA producing 50% of the maximum response, x_a is the agonist concentration and N is the Hill coefficient. A non-linear regression programme (patternsearch, Colquhoun, 1971) was used to obtain the least-square estimates for ΔG_{max}, EC_{50}, and N. Dose–response curves were considered parallel if the Hill coefficient and ΔG_{max} for the control GABA dose–response curve and the response in the presence of antagonist were not significantly different.

Dose-ratios were measured for the effect of SR95103 on GABA dose–response curves and initially examined using a Schild plot (Arunlakshana and Schild, 1959). Since the slope of this plot was significantly less than unity, the dose-ratios were further examined using a modified Schild plot (Williams *et al.*, 1988) which has the advantage of taking account of the observed cooperativity seen at the GABA receptor. It is pointed out that the relationship, between receptor occupancy and fractional response, is in general not known and that physically plausible models for the interaction of agonist and antagonist do not predict simple or integral values for these plots. However it is considered that the plots provide a useful empirical approach for describing agonist and antagonist action.

Bath-application of drugs

Initially, GABA was bath-applied using a non-cumulative dose method with washing of the preparation between applications. GABA produced, as reported previously (Martin, 1980; Holden-Dye *et al.*, 1988), a dose-dependent hyperpolarization and an increase in input conductance. However, one limitation of this technique was that recovery of the resting input conductance was often incomplete after application of high concentrations of GABA; this may have been due to slight movement of the muscle flap preparation producing a decrease in the leaks resistance around the micropipettes.

It was found that recovery after application of high concentrations of GABA was more often complete if cumulative bath-application of GABA, without intermediate washing were used (Fig. 2). The method involved gentle

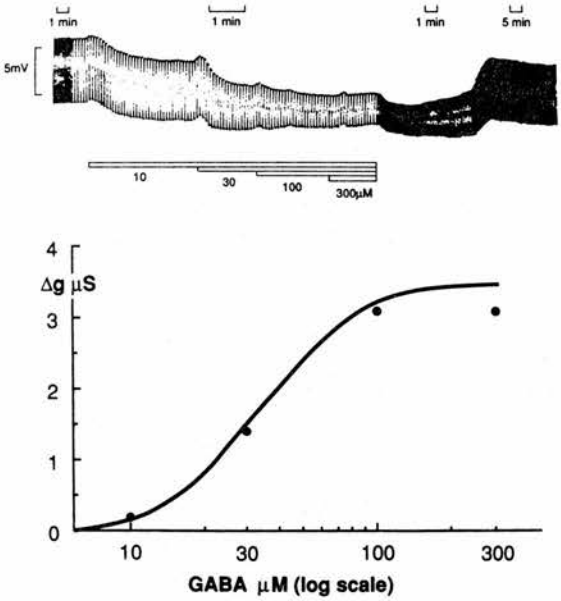


Fig. 2. GABA cumulative dose–response relationship. The upper trace illustrates the change in input conductance during cumulative application of GABA. The width of the trace represents the change in membrane potential during the injection of hyperpolarizing current pulses (see Methods). In this experiment, the resting input conductance was 3.0 μsec; in the presence of GABA 10 μM $\Delta G = 0.2$ μsec; in GABA 30 μM $\Delta G = 1.4$ μsec; in GABA 100 μM $\Delta G = 3.1$ μsec; in GABA 300 μM $\Delta G = 3.1$ μsec. The conductance returned to the resting level after washing. The chart speed was altered at the marked intervals during the experiment. The lower diagram shows the dose–response relationship. The experimental values are represented by filled circles (●); the solid line represents the fitted modified Hill equation ($\Delta G_{max} = 3.5$ μsec; $EC_{50} = 32.6$ μM; $N = 2.6$).

Table 1. Parameters (means ± SE) for the modified Hill equation used to describe cumulative and non-cumulative dose–response relationships (GABA)

	EC_{50} (μM)	ΔG_{max} (μsec)	N
Non-cumulative	24.9 ± 3.3	61 ± 0.1	2.6 ± 0.3
Cumulative	26.6 ± 2.3	4.8 ± 0.5*	1.9 ± 0.2

Note ΔG_{max} was smaller when cumulative doses were used. *Indicates $P \leqslant 0.05$

draining of the bath (vol 2.5 ml), and then flushing the bath with 5 ml of the next drug solution. This method of application has the advantage of a more certain drug concentration over the cell surface than the "local perfusion" technique using a micropipette. The bath was not perfused continuously because of the limited quantities of antagonist available.

When the dose–response relationships, obtained by non-cumulative and by cumulative application of GABA, were described by the modified Hill equation it was found that EC_{50}'s and Hill coefficients were not significantly different (Table 1). In contrast, ΔG_{max} was on average smaller when GABA was applied cumulatively. One possible explanation for the reduced maximum response seen with cumulative application is desensitisation. Despite this, ΔG_{max} was remarkably constant for the same cell, varying only between cells. Cumulative dose–response relationships were therefore used to examine the effect of SR95103 on EC_{50}, N and ΔG_{max}.

Statistical tests

Means and standard errors were calculated for EC_{50}, N and ΔG_{max} values for GABA alone and in the presence of different concentrations of antagonist. Statistical significance was assessed using a two-tailed independent t-test.

Drugs

GABA was obtained from Sigma; SR95531 [2-(3-carboxypropyl)-3amino-6-(p-methoxy)-phenylpyridazininium chloride] and SR95103 [2-(3-carboxypropyl)-3-amino-4-methyl-6-phenylpyridazinium chloride] (Fig. 1) were obtained as gifts from Sanofi (France).

RESULTS

The results reported here are based on an analysis of experiments conducted on 18 muscle cells from 13 preparations. Cells selected for recording and analysis had resting membrane potentials greater than −20 mV and resting input conductances between 1.9 and 4.0 μs (2.5 ± 0.1 μM, mean ± SE. $N = 18$). The recordings were also rejected if resting input conductances failed to return to at least 80% of the control after washing GABA from the preparation.

SR95531 and SR95103 as GABA antagonists

In mammalian preparations, SR95531 is the most potent arylaminopyridazine $GABA_a$ antagonist and will antagonise electrophysiological responses to GABA (Chambon *et al.*, 1985; Desarmenien *et al.*, 1987; Michaud *et al.*, 1986; Hamann *et al.*, 1988). In *Ascaris*, the application of 1 mM SR95531 had a small effect on conductance changes produced by 30 μM GABA (Fig. 3B).

SR95103 is less potent than SR95531 at the $GABA_a$ vertebrate receptor in rat brain membranes (Heaulme *et al.*, 1986a, b) and rat DRG cells (Chambon *et al.*, 1985). This contrasts with effects seen in *Ascaris* (Fig. 3A) where 1 mM SR95103, unlike SR95531, produces nearly complete antagonism. The antagonism reverses after washing.

The percentage antagonism of the response to 30 μM GABA produced by 1 mM concentrations of SR95103 and SR95531 was measured in a series of experiments; it was found that SR95103 reduced the response by 92.3 ± 3.2% (mean ± SE, $N = 5$) and that SR95531 reduced the response by 46.2 ± 6.7% (mean ± SE, $N = 5$). These observations illustrate the contrast between the pharmacology of a $GABA_a$ receptor and the *Ascaris* GABA receptor.

Dose-dependent nature of the SR95103 antagonism

The dose-dependent nature of the antagonism was tested by examining effects of 100, 300 and 1000 μM SR95103 on cumulative GABA dose–response curves. Figure 4 shows, from a single cell, the typical effects of 100 μM antagonist where there is a parallel shift to the right with no reduction in the maximum response. Table 2 shows pooled results with the mean and SE values for the parameters of the modified Hill equation used to describe the dose–response curves.

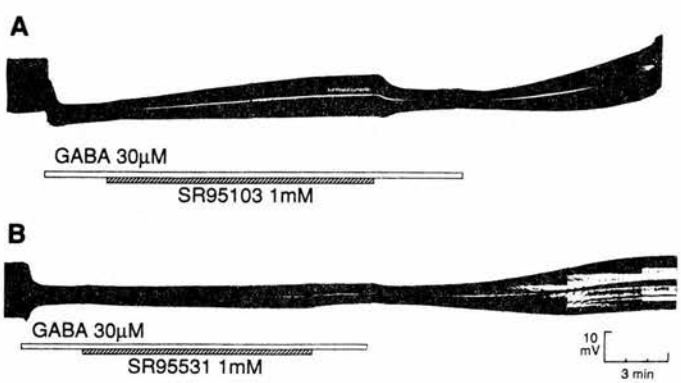


Fig. 3. SR95103 is a more potent GABA antagonist than SR95531. A: SR95103. The resting input conductance is 2.2 μsec. In the presence of GABA 30 μM $\Delta G = 4.4$. μsec. SR95103 1 mM antagonized 86% of the GABA response. The antagonism was completely reversed when the preparation was washed in 30 μM GABA. B: SR95531. SR95531 was tested in the same cell. The resting input conductance was 2.2. μsec. In the presence of 3 μM GABA $\Delta G = 44.4$. μsec. SR95531 1 mM antagonized only 36% of the GABA response. The antagonism was completely reversed when the preparation was washed in 30 μM GABA.

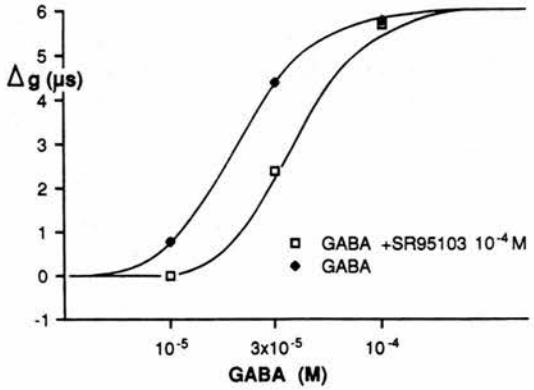


Fig. 4. Effect of SR95103 on the cumulative GABA dose–response relationship. [◆]: control GABA response and modified Hill fit; $\Delta G_{max} = 5.8\,\mu$sec; $EC_{50} = 24.4\,\mu$M; $N = 1.7$. [□]: GABA responses and modified Hill fit in the presence of SR95103 100 μM; $\Delta G_{max} = 5.8\,\mu$sec; $EC_{50} = 66.2\,\mu$M; $N = 1.5$. Ordinate: change in input conductance. Abscissa: GABA concentration.

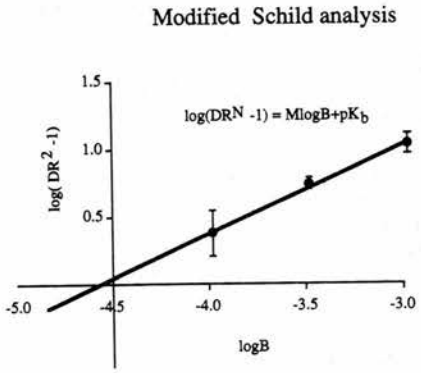


Fig. 5. Modified Schild plot. Agonist GABA. Antagonist SR95103. The plot of log $(DR^2 - 1)$ against log x_b appears linear with a slope of 0.62 ± 0.17 (mean $\pm$ SE, $N = 14$). The linear regression had an F value of 0.0041, indicating a better fit. The slope was not significantly less than 1.0 (t-test; $P = 0.05$).

It can be seen that SR95103 produces increases in the EC_{50}'s without a significant change in the Hill coefficient or ΔG_{max}.

Schild plots

Dose-ratios were determined from the change in EC_{50} values and a classical Schild plot obtained. This was characterized by an apparently linear relationship between log $(DR - 1)$ and log x_b and an intersect on the abscissa giving a pA_2 of 4.0. However this plot was characterized by a slope (0.45 ± 0.15 mean $\pm$ SE, $N = 14$) significantly ($P = 0.01$, t-test) less than 1.0. Thus the dose-ratios were smaller at higher antagonist concentrations, than predicted by the Schild equation.

One interpretation of this result is that SR95103 might not be acting on a single receptor in a competitive manner. However, the classical Schild analysis does not account for some cooperative models of agonist action involving two agonist binding sites, (see for example: Rang, 1971; Williams *et al.*, 1988). We therefore carried out a modified Schild analysis, where it was assumed that two agonist molecules were required to bind to activate the receptor and the slope of the plot is the number of antagonist molecules required to inhibit the receptor.

Figure 5 shows the modified Schild plot of log $(DR^2 - 1)$ against log x_b. The slope was 0.62 ± 0.17 (mean $\pm$ SE, $N = 14$) which is not significantly less than 1.0 ($P = 0.05$, t-test). These results, then, are consistent with a model which involves activation of the receptor by two agonists molecules but only one antagonist molecule is required. Although these results do not exclusively establish such a mode of action for SR95103 it does permit the estimation of an apparent dissociation constant. The arithmetic mean of the dissociation constant K_B as calculated from the modified Schild equation using $N = 2$ and $M = 1$, i.e.:

$$K_B = (DR^2 - 1)/x_b.$$

K_B was $64 \pm 13\,\mu$M (mean $\pm$ SE, $N = 14$).

Table 2. Parameters (mean $\pm$ SE) for the modified Hill equation used to describe cumulative GABA dose–response curves in the presence of SR95103

	EC_{50} (μM)	ΔG_{max} (μsec)	N
GABA alone ($N = 8$)	24.9 ± 3.3	6.1 ± 0.1	2.6 ± 0.3
GABA + 100 μM SR95103 ($N = 6$)	46.5 ± 4.2**	5.1 ± 0.6	2.3 ± 0.3
GABA + 300 μM SR95103 ($N = 3$)	81.2 ± 15.3**	5.5 ± 0.6	1.7 ± 0.7
GABA + 1000 μM SR95103 ($N = 4$)	119.1 ± 5.7**	4.5 ± 0.7	2.7 ± 0.6

**Indicates $P \leq 0.01$, t-test

Voltage-sensitivity of antagonism

The two-microelectode voltage-clamp technique with the iontophoretic application of GABA (Martin, 1982) was used to examine the voltage-sensitivity of the antagonism produced by bath application of 0.1–1 mM SR95103. A holding poltential of 0 or -10 mV was used and voltage steps to -80 mV or -90 mV were made for 500 msec at 1 Hz. A standard charge of 150 nC was used to eject the GABA as a cation from the iontophoretic pipette in the absence and then in the presence of the antagonist. The peak responses at the holding potential and at the step potential were measured from the envelope of the current trace. The voltage-sensitivity (V_s) of the antagonism was expressed as:

$$1 - \frac{\%\text{ antagonism at 0 or } -10\text{ mV},}{\%\text{ antagonism at } -80\text{ or } -90\text{ mV}}$$

If SR95103 were acting predominantly as an anion to produce a channel block, then it would be expected that the degree of channel block would decrease at more negative potentials. However the antagonism showed little evidence of voltage-sensitivity: $V_s = 0.05 \pm 0.17$ (mean $\pm$ SE, $N = 4$).

DISCUSSION

The main finding of this paper was that SR95103 but not SR95531 acts as a moderately potent GABA antagonist in *Ascaris* with an apparent K_B of 64 μM; the study also shows that the potency of the arylaminopyridazine GABA analogues can vary at the

Ascaris GABA receptor. In a previous study with SR95531 (Holden-Dye *et al.*, 1989), it was also found that SR95531 was not a potent antagonist in *Ascaris*. However, it was suggested that this class of compounds does not recognise the *Ascaris* Gaba receptor, although no other arylaminopyridazine GABA analogues were examined.

It has already been pointed out that $GABA_a$ receptors may be heterogenous (Levitan *et al.*, 1988; Pritchett *et al.*, 1989; for a review, see Krogsgaard-Larsen, 1988) but that it is still useful to compare the *Ascaris* receptor to a typical $GABA_a$ receptor. The greater relative potency of SR95103 compared to SR95531 in *Ascaris* contrasts with the relative potency at mammalian $GABA_a$ receptors; SR95531 displaces [^{3}H]GABA from rat brain membranes with a global $K_i = 0.15\,\mu M$ (Heaulme *et al.*, 1986a) and SR95103 has a K_i of $2.2\,\mu M$ (Chambon *et al.*, 1985); SR95103 has a pA_2 of 5 and SR95531 has a pA_2 of 7 in electrophysiological experiments on rat dorsal root ganglion cells (pA_2 values calculated from data presented by Chambon *et al.*, 1985; and Hamman *et al.*, 1988).

SR95531 is similar in structure to SR95103 (Fig. 1) but has a methoxy group on the 6-phenyl substituent of the pyridazine ring and no substituent on the 4-position; SR95103 has no substituent on the 6-phenyl ring but a methyl group in the 4-position on the pyridazine ring. This difference, and the greater relative potency of SR95103 on the *Ascaris* GABA receptor, indicates that its structural requirements for antagonists are different to a typical $GABA_a$ receptor. The lack of effect of bicuculline on *Ascaris* (Wann, 1987; Holden-Dye *et al.*, 1988), also supports this view. However, the agonist profile of $GABA_a$ and *Ascaris* receptors show a similar stereo-selectivity (Holden-Dye *et al.*, 1989) so that the structure–activity relationships of agonists are apparently correlated for the two receptor types.

Ariens *et al.* (1979) have argued that hydrophobic regions of a competitive antagonist molecule binding to "accessory" sites on the receptor are responsible for the molecule behaving as a competitive antagonist; and that the structure of the moiety binding to the agonist-recognition site is less critical than for the agonists. The mode of action and structure–activity relationships of arylaminopyridazine–GABA antagonists at the vertebrate $GABA_a$ receptor have also been explained in terms of Ariens' theory (Wermuth *et al.*, 1987). The fact that potencies of vertebrate $GABA_a$ agonists correlate with the potencies of agonists in *Ascaris*, but the potencies of antagonists do not, suggests that there are differences between the "accessory" sites of the $GABA_a$ receptor and the *Ascaris* GABA receptor. The differences in accessory binding sites revealed by the actions of the arylaminopyridazine–GABA antagonists, suggests that further exploration of the pharmacology of these compounds on the *Ascaris* GABA receptor may be useful for the design of new anthelmintic agents.

The examination of the antagonism shown by SR95103 was not described by a classical Schild plot with a slope of 1.0. However, this observation cannot be used to exclude a competitive mode of action, since even simple plausible models of agonist and antagonist action predict that the classical Schild plot will not have a slope of unity (Williams *et al.*, 1988). We used a modified Schild plot to describe the data, and obtained evidence which was consistent with two molecules of agonist but one molecule of antagonist interacting with the receptor. Intuitively, this is reasonable, if binding of two molecules of GABA to different sites is required to open the channel and binding of a single molecule of antagonist at either site would be sufficient to prevent opening.

In the subsequent paper the actions of SR95103 were further explored at the single-channel level.

Acknowledgements—This work was supported by the Wellcome Trust, SERC and the Harriet Thompson Trust.

REFERENCES

Alger B. E. and Nicoll R. A. (1982). Pharmacological evidence for two kinds of GABA receptors on rat hippocampal pyramidal cells studied *in vitro*. *J. Physiol., Lond.* **328,** 125–141.

Ariens E. J., Beld A. D., Miranda J. F. R. and Simonis A. M. (1979) The Pharmacon-Receptor-Effector concept. In *The Receptors* (Edited by O'Brien R. D.), Vol. 1, pp. 33–91. Plenum, New York.

Arunlakshana O. and Schild H. O. (1959) Some quantitative uses of drug antagonists. *Br. J. Pharmac. Chemother.* **14,** 48–58.

Ault B. and Nadler V. (1983) Differentiation of two bicuculline-insensitive actions of GABA in the rat hippocampal slice. *J. Physiol., Lond.* **345,** 70P.

Bowery N. G., Hill D. R. and Hudson A. L. (1983) Characteristics of $GABA_b$ receptor binding sites on whole rat brain synaptic membranes. *Br. J. Pharmac.* **78,** 191–206.

Chambon J. P., Feltz P., Heaulme M., Restle S., Schliechter R., Biziere K. and Wermuth C. G. (1985) Synthesis of SR95103 an arylaminopyridazine derivative of GABA. *Proc. natn Acad. U.S.A.* **82,** 1832–1836.

Colquhoun D. (1971) Non-linear curve fitting and the meaning of best estimate. In *Lectures on Biostatistics* pp. 257–272. Clarendon Press, Oxford.

Desarmenien M., Feltz P., Loeffler J. B. Occhipinti G. and Santangela F. (1982) Multiple GABA receptors on A_d and C primary afferent neurones in the adult rat. *Br. J. Pharmac.* **76,** 289P.

Desarmenien M., Desaulles E., Feltz P. and Hamann M. (1987) Electrophysiological study of SR42641, a novel aminopyridazine derivative of GABA; antagonist properties and receptor selectivity of $GABA_a$ vs. $GABA_b$ responses. *Br. J. Pharmac.* **90,** 287–298.

Duittoz A. H. and Martin R. J. (1989) SR95103 acts as a GABA antagonist in *Ascaris suum* muscle. *Br. J. Pharmac.* **97,** 490P.

Dunlap K. (1981) Two types of GABA receptor on embryonic sensory neurones. *Br. J. Pharmac.* **74,** 579–585.

Dutar P. and Nicoll R. A. (1988) A physiological role for $GABA_b$ receptors in the central nervous system. *Nature* **332,** 156–158.

Hamann M., Desarmenien M., Desaulles E., Bader M. F. and Feltz P. (1987) Quantitative evaluation of the properties of a pyridizanyl GABA derivative (SR95531), as a $GABA_a$ competitive antagonist. An electrophysiological approach. *Brain Res.* **442,** 287–296.

Heaulme M., Chambon J. P., Leyris R., Molimard J. C., Wermuth C. C. and Biziere K. (1986a) Biochemical characterization of three arylaminopiridazine GABA

derivatives with the $GABA_a$ receptor site. *Brain Res.* **384,** 224–231.

Heaulem M., Chambon J. P., Leyris R., Wermuth C. C. and Biziere K. (1986b) Specific binding of a phenylpyridazinium derivative endowed with $GABA_a$ receptor antagonist activity to rat brain. *Neuropharmacology* **25,** 1272–1283.

Holden-Dye L., Hewitt G. M., Wann K. T., Krogsgaard-Larsen P. and Walker R. J. (1988) Studies involving avermectin and the 4-aminobutyric acid (GABA) receptor of *Ascaris suum* muscle. *Pest. Sci.* **24,** 231–245.

Holden-Dye L., Krogsgaard-Larsen P., Nielsen L. and Walker R. J. (1989) GABA receptors on the somatic muscle cells of the parasitic nematode, *Ascaris suum*: stereoselectivity indicates similarity to a $GABA_a$-type agonist recognition site. *Br. J. Pharmac.* **98,** 841–850.

Johnston G. A. R. and Allan R. D. (1984) GABA agonists. *Neuropharmacology* **23,** 831–832.

Johnston G. A. R. (1986) Multiplicity of GABA receptors. In *Benzodiazepine/GABA Receptors and Chloride Channels: Structural and Functional Properties*, pp. 41–56. Alan R. Liss, New York.

Kerr D. I. B., Ong J., Prager R. H., Gythner B. D. and Curtis D. R. (1987) Phaclofen: a peripheral and central baclofen antagonist. *Brain Res.* **405,** 150–154.

Krogsgaard-Larsen P. (1988) GABA synaptic mechanisms: stereochemical and conformational requirements. *Medic. Res. Rev.* **8,** 27–56.

Levitan E. S., Schofield P. R., Burt D. R., Rhee L. M., Wisden W., Kohler M., Fujita N., Rodriguez H. F., Stephenson A., Darlison M. G., Barnard E. A. and Seeburg P. H. (1989) Structural and functional basis for $GABA_a$ receptor heterogeneity. *Nature* **335,** 76–79.

Martin R. J. (1980) The effect of γ-aminobutyric acid on the input conductance and membrane potential of *Ascaris* muscle. *Br. J. Pharmac.* **7,** 99–106.

Martin R. J. (1982) Electrophysiological effects of piperazine and diethylcarbamazine on *Ascaris suum* somatic muscle. *Br. J. Pharmac.* **77,** 255–265.

Martin R. J. (1985). γ-Aminobutyric acid- and piperazine-activated single-channel currents from *Ascaris suum* body muscle. *Br. J. Pharmac.* **84,** 445–461.

Martin R. J. (1987). The γ-aminobutyric acid receptor of *Ascaris* as a target for anthelmintics. *Biochem. Soc. Trans.* **15,** 61–65.

Michaud J. C., Mienville J. M. and Chambon J. P. (1986) Interaction of three arylaminopyridazine GABA derivatives with rat cortical GABA and Glycine receptors: an *in vivo* microiontophoretic study. *Neuropharmacology* **25,** 1197–1203.

Nistri A. and Constanti A. (1979) Pharmacological characterization of different types of GABA and glutamate receptors in vertebrates and invertebrates. *Prog. Neurobiol.* **13,** 117–235.

Pritchett D. B., Luddens H. and Seeburg P. H. (1989) Type I and Type II $GABA_a$-benzodiazepine receptors produced in transfected cells. *Science* **245,** 1389–1392.

Rang H. P. (1971) Drug receptors and their function. *Nature* **231,** 91–96.

Wann K. T. (1987) The electrophysiology of the somatic muscle cells of *Ascaris suum* and *Ascaridia gall. Parasitology* **94,** 555–566.

Wermuth C. G., Bourguignon J. J., Schleiver G., Gies J. P., Schoenfelder A., Melikian A., Bouchet M. T., Chantreux D., Molimard J. C., Heaulme M., Chambon J. P. and Biziere K. (1987) Synthesis– and structure–activity relationships of a series of aminopyridazine derivatives of GABA acting as selective $GABA_a$ antagonists. *J. Med. Chem.* **30,** 239–249.

Williams T. L., Smith D. A. S., Burton N. R. and Stone T. W. (1988) Amino acid pharmacology in neocortical slices: evidence of bimolecular actions from an extension of the Hill and Gaddum–Schild equations. *Br. J. Pharmac.* **95,** 805–810.

Comp. Biochem. Physiol. Vol. 98C, No. 2/3, pp. 423–432, 1991
Printed in Great Britain

0306-4492/91 $3.00 + 0.00
© 1991 Pergamon Press plc

EFFECTS OF SR95103 ON GABA-ACTIVATED SINGLE-CHANNEL CURRENTS FROM *ASCARIS SUUM* MUSCLE

A. H. DUITTOZ and R. J. MARTIN

Department of Preclinical Veterinary Sciences, R.(D).S.V.S. Summerhall, University of Edinburgh, Edinburgh, U.K. (Telephone: (031) 667-1011)

(*Received* 8 *June* 1990)

Abstract—1. An outside-out patch-clamp technique was used to examine the actions of SR95103 (30 μM to 2 mM) on GABA-activated single-channel currents recorded from the bag region of somatic muscle of *Ascaris suum*.

2. Effects of SR95103 on open-probability and the distributions of open-, closed- and burst-durations were examined quantitatively.

3. The mode of action of SR95103 is discussed; it is suggested that most of the antagonism is competitive and produced by a single molecule of SR95103 combining with the GABA receptor–channel complex; there is an additional, small non-competitive component, possibly a channel-blocking action.

INTRODUCTION

In the previous paper, we have described the action of SR95103 on the GABA receptor of *Ascaris* muscle under current-clamp. We have shown that SR95103 produces a parallel shift to the right in conductance dose–response curves, but that the classical Schild plot (Arunlakshana and Schild, 1959) had a slope less than 1. This observation, however, did not exclude competitive antagonism since it was possible to use a modified Schild plot (Williams *et al.*, 1988) to describe the observations, and which suggested that only one molecule of antagonist interacts with the receptor.

In order to investigate further the action of SR95103 on the *Ascaris* GABA receptor, a patch-clamp study was carried out to look at effects at the single-channel level. This paper describes the results of those experiments. It shows that most of the antagonism appears to be competitive but evidence for a small non-competitive component is seen at high antagonist concentrations.

MATERIALS AND METHODS

The preparation

Specimens of *Ascaris suum* were collected from the local abattoir and maintained in Locke solution (replaced daily) at 35°C in a water-bath. The parasites were used for experiments within four days. A 2 cm flap preparation was pinned down onto "Sylgard" in the experimental chamber and maintained at 22°C. Clean membranes were prepared with collagenase (350 I.U. ml^{-1}; Sigma Type 1A), applied for 20–30 min.

Solutions

The preparation was maintained in a solution containing (mM): NaCl; 35, Na acetate 105, KCl 2, $MgCl_2$ 2, HEPES 10, glucose 3, ascorbic acid 2, pH 7.2 with NaOH. Electrodes were filled with a solution containing (mM): CsCl 145, $MgCl_2$ 3, $CaCl_2$ 1, EGTA 11, HEPES 10, pH 7.2 with CsOH.

Recording technique

Standard patch-clamp techniques were used to obtain outside-out patches (Hamill *et al.*, 1981). Patch electrodes were made from micro-haematocrit capillary tubes (Garner glass 7052) and had a resistance of 1–5 MΩ. "Sylgard" was used to coat electrodes to improve the frequency responses (typically greater than 2 kHz). Currents were recorded with a List EPC-7 and a modified Sony Betamax video system for making records on tape. An agar-plug electrode was used to minimize junction potentials.

Data processing

Records on tape were played back into a CED 1401 interface, connected to a DCS 286 PC computer and under the control of PAT software (Dr J. Dempster, Strathclyde University). Records were filtered by an 8-pole Bessel filter, −3 dB at 1.0 kHz, and sampled at an interval of 100 μsec. The PAT software was used to obtain current amplitude histograms which were used to measure proportions of time $1, 2, 3, \ldots N$ channels were open. Records with less than 5% of all openings appearing as simultaneous openings were selected and used to measure channel open- and closed-times; the double openings were edited and not used for the analysis. The threshold for detection was set at 50% of the unit channel current. This method of detecting the transition between open- and closed-times is different to that described previously (Martin, 1985) where a double threshold system was used. The "effective mean open-times" described previously (Martin, 1985) approximate to mean "long" bursts in this study. The PAT software produced files of open and closed durations, which were transferred to a mainframe computer for further analysis.

Exponential curve-fitting

In these experiments, individual channel activations were interrupted by short closed-times. Bursts of openings were therefore defined as groups of openings separated by closed-times shorter than a specified time, T_{crit}. T_{crit} was chosen to make the proportion of long closings that were misclassified (as short) equal to the proportion of short intervals that were misclassified (as long). T_{crit} was therefore chosen by solving numerically the equation:

$$1 - \exp(-T_{crit}/T_s) = \exp(-T_{crit}/T_m)$$

(Colquhoun and Sakmann, 1985), where T_s and T_m are short and intermediate time constants in the distribution of all closed times. An interval of 1–2 msec was used so that only brief closings were classified as gaps in bursts. After T_{crit} has been determined, the files of open- and closed-times were rearranged to give files of burst durations.

The next stage in the analysis was the fitting of exponentials to the distributions of closed and burst durations. Only events greater than 0.5 msec (twice the dead time) were used to fit 1, 2, 3, or 4 exponentials to each data file to see which was the best fit. A maximum likelihood procedure (Martin, 1985) was used to estimate the parameters of the probability density function (p.d.f.) used to best describe the distributions:

$$\text{p.d.f.} = \sum_{i=1}^{K} a_i/T_i \exp(-t/T_i),$$

where a_i represents the area of the i^{th} component ($\Sigma a_i = 1$), T_i is the fitted time constant, t is time in msec and k is the number of exponentials fitted. A decrease of 3 log units with each additional component fitted was taken as a significant improvement in the fit.

Correction for missed events

After the exponentials had been fitted to the burst and closed-times, it was possible to correct for missing events, using the method described by Colquhoun and Sakmann, (1985). It was assumed that very short closings and openings will be missed in the usual analysis of open- and closed-times because of the limited resolution of the recording technique. The number of short events was estimated by extrapolation from the data which had been recorded.

Firstly, the total number of closed-times and burst-times was estimated from the observed number of events; this was done separately for the closed-times and burst-times. Secondly, the total time spent in gaps within bursts, i.e. gaps shorter than T_{crit}, including those which are undetected, was calculated. Thirdly, the corrected mean burst duration was calculated. Fourthly, the corrected total open-time was calculated. The corrected mean open-time estimated in this way is shorter than the mean open-time estimated in any other way because it allows for missed short events and reduces the mean value. The corrected mean length of an individual opening in a long burst was then calculated assuming that there were few gaps in the "short" bursts.

Stationarity

It was possible to examine open-times and closed-times in sequence and, to test for changes in their properties with time. Desensitization, for example, may produce after a delay, an increase in the mean closed-time and a reduction in the probability of the channel being open. CUSUM plots (see Glasbey and Martin, 1986) were used to examine for this and test for time dependent changes in channel durations (non-stationarity). An example of these plots is shown in Fig. 1; it can be seen that there is no evidence of change in channel properties throughout the record. This and similar observations on other patches, showed no evidence of changes in channel properties throughout the records.

Binomial distribution

If GABA channels in a patch have the same probability of being open and are independent, then the distribution of the proportion of time, P_r, that $0, 1, 2, \ldots N$, channels are open will be described by the binomial distribution:

$$P_r = N!/[r!(N-r)!] \times p^r(1-p)^{N-r},$$

where p is the probability that an individual channel is open and N is the number of channels present. The probability (p) of an individual channel being open was calculated from the areas under the amplitude histograms. If the proportion of total recording time spent with $1, 2, \ldots, N$ channels open was $T_1, T_2, \ldots T_n$ then:

$$p = (T_1 + 2T_2 \cdots + NT_n)/N.$$

The fraction of time which r channels and only r channels were open was calculated from the T values and plotted. The binomial distribution was then used with the value of p to predict the proportion of time with only $0, 1, 2, \ldots N$ channels open.

Percent antagonism

In order to compare the level of antagonism produced by different concentrations of SR95103 we defined the percentage of antagonism as:

$$\text{percent antagonism} = 100 \times (1 - p_{sr}/p_c),$$

where p_{sr} was the probability of an individual channel being open in the presence of SR95193 and p_c is the control probability in the absence of antagonist. The relationship between percent antagonism and SR95103 concentration was described by the modified Hill equation and a least-squares estimate of the parameters made as described in the preceeding paper.

t-Test

The mean and standard errors for these observations were calculated and examined with a two-tailed unpaired t-test, to determine if effects reached statistical significance.

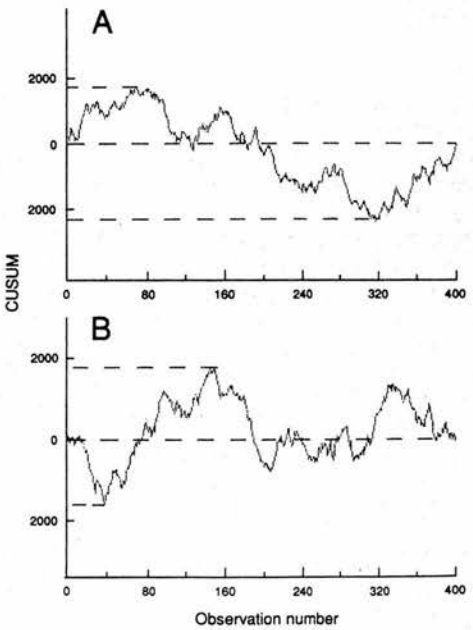


Fig. 1. CUSUM plot of closed and open times. The CUSUM (for closed times), $S_j = \Sigma (X_i - X_{mean})$ for $j = 1, \ldots, n$; where X_i is the rank order of the ith closed time, X_{mean} is the mean rank. A random fluctuation about zero is expected for channels which show stationary behaviour. The significance of the deviation may be tested (Glasbey and Martin, 1986) by determining D_a, the maximum values of $S_j/(1 + (a-1).j/n)$; where $a = 9.\ 1.$ and $1/9$ and then estimating the three p values for the maximum deviations:

$$p = 2 \exp \frac{-24aD_a^2}{n^2.(n+1)}.$$

This is also repeated for the open-times. A: closed times; ordinate, CUSUM; abscissa observation number. The p values were 0.17; 0.95; and 0.13; the closed times were considered to be in random order. B: open times; ordinate, CUSUM; abscissa, observation number. The p values were 0.12; 0.89; and 0.39; the open times were considered to be in random order.

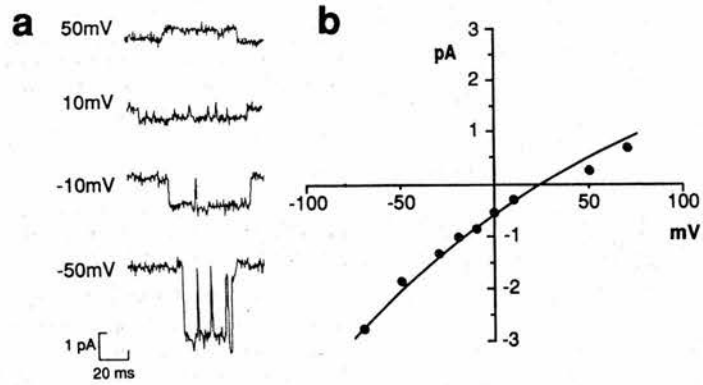


Fig. 2. Main-state GABA channel I/V relationship. a: channel openings to the main-state at four trans-patch potentials from +50 to −50 mV. b: plot of main-state channel currents at different potentials. The reversal potential was near +27 mV, the Nernst Cl potential. The solid line shows a plot of the I/V relationship predicted by the Goldman–Hodgkin–Katz constant field equation with a single channel permeability of 6.3×10^{-14} cm^3 sec^{-1}. Note the inward rectification.

RESULTS

The following report is based on an analysis of experiments on 11 outside-out patches prepared from separate parasites.

Single-channel I/V relationship

Non-symmetrical Cl concentrations across the patch (41 mM outside; 153 mM inside) were used throughout this series of experiments to increase the amplitude of the single-channel currents (at −50 mV) and to further test the identity of ions flowing through the channels. Figure 2 shows a representative I/V plot of the main (most frequent) conductance state seen in a particular patch. The plot shows inward rectification and a reversal potential of +27 mV; the rectification and a reversal potential close to this is predicted by the Goldman constant field equation (Hille, 1984) for a Cl ion-channel under these conditions. Figure 2 also shows (solid line) the I/V relationship predicted by the constant field equation for a Cl channel with a permeability of 6.3×10^{-14} cm^3 sec^{-1}.

The main-state conductance was analysed

GABA channels in *Ascaris* are characterised by the presence of more than one conductance state (Martin, 1985). The main-state at −50 mV had an amplitude of 1.7 pA, which corresponds to a chord-conductance of 22 pS, if a driving force of 77 mV is assumed. Two subconductance states which had amplitudes of 1.0 and 0.5 pA at −50 mV (conductances of 13 pS and 6.5 pS) were occasionally seen.

In the following analysis, the main-state conductance was used because it occurred most frequently; the channel current spent only a very small proportion of the open-time at the subconductance levels. The inclusion of subconductance states in the analysis was further minimized by threshold setting and editing records manually.

Channels have the same P_{open} and operate independently

The application of 3 μM GABA to outside-out patches produced the simultaneous opening of up to three channels. If GABA channels in a patch have the same probability of being open and behave independently, then the distribution of the proportion of time (P_r), that 0, 1, 2, ... N, channels are open will be described by the binomial distribution. Figure 3 shows predicted (arrows) and observed (bars) values of P_r from a typical patch record with three channels present and $p = 0.082$. It can be seen that observed and predicted values are close; the result is consistent with the channels behaving independently and having the same open probability. Similar results were obtained from all the patches.

As a consequence of these observations, the GABA channels were assumed to be homogenous; effects of SR95103 were not subsequently explained by a selective action on a group of GABA channels which have long open-times and a different open probability.

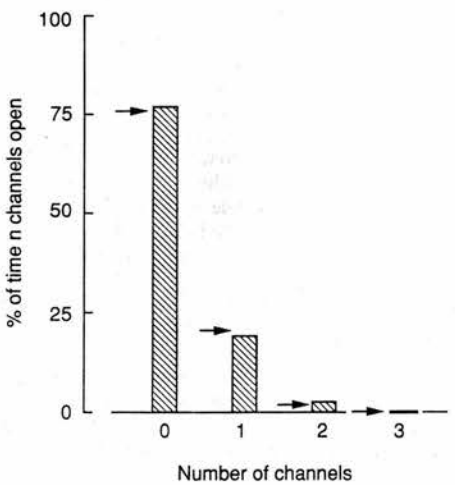


Fig. 3. Observed and binomial distribution of the proportion of time channels were, or predicted to be, open in a patch. The horizontal bars are the observed values of the % time spent with 0, 1, 2, and 3 channels open. The arrows indicate the values predicted by the binomial distribution with $N = 3$, the total number of channels present in the patch, and $p = 0.082$, the probability of channel opening.

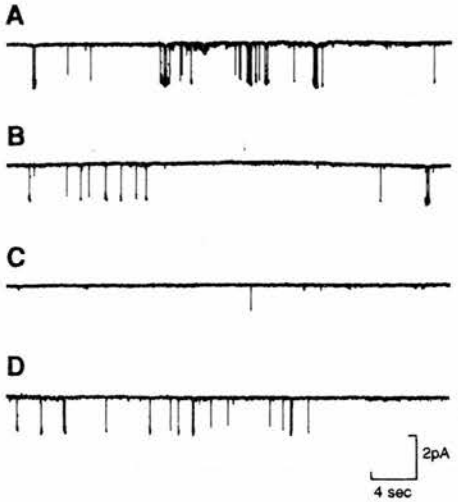


Fig. 4. Inhibitory effect of SR95103 on opening frequency of GABA channels. A: control; GABA 3 μM P_{open} 0.036. B: GABA 3 μM + SR95103 30 μM; P_{open} 0.007 C: GABA 3 μM; P_{open} 0.001 D: wash; GABA 3 μM alone. SR95103 reduces the opening frequency of the GABA channels.

SR95103 reduces GABA channel opening frequency but not amplitude

Figure 4 shows the inhibitory effect of SR95103 on opening frequency of GABA-activated channels at -50 mV. Figure 4A shows the effect of 3 μM GABA alone, where channel opening is seen, at this time scale, as clusters of inward current spikes. When 30 μM SR95103 was added, the frequency of opening reduced from 0.7 sec^{-1} to 0.35 sec^{-1} (Fig. 4B). The rate of channel opening was further reduced to less than 0.05 sec^{-1}, when SR95103 was increased to 100 μM (Fig. 4C). When the antagonist was washed from the preparation, the opening frequency returned to 0.5 sec^{-1} (Fig. 4D).

The lack of effect of SR95103 on the amplitude of GABA single-channel currents is illustrated in Fig. 5 which shows the current–amplitude histograms for the traces shown in Fig. 4. The current–amplitude histograms were fitted and described by Gaussian distributions. The control amplitude (Fig. 5A) was -1.74 ± 0.02 pA (mean $\pm$ SE); in the presence of 30 μM antagonist (Fig. 5B) it was -1.67 ± 0.04 pA (mean $\pm$ SE); in the presence of 100 μM antagonist (Fig. 5C) it was -1.72 ± 0.03 pA (mean $\pm$ SE). Similar results were obtained from all the other experiments; it was concluded that SR95103 does not affect single-channel conductance.

Modified Hill equation describes percent inhibition

The relative area under the open channel–current histogram allows estimation of the proportion (p) of time an individual channel is open in the patch (see above). In Fig. 5A for example, the control p was 0.036; in 5B SR95103 it was 0.025; in 5C it was 0.001. Figure 6 shows the dose–response relationship for the percent antagonism and the fitted modified Hill equation. With 3 μM GABA as the agonist, the Hill coefficient was 0.98, suggesting that only one molecule of SR95103 combines with the GABA receptor; the concentration producing half-saturation (IC_{50}) was 24 μM and the estimated percent inhibition at saturating concentrations of antagonist was 97%. The fact that the maximum antagonism is near 100% suggests that most, but perhaps not all, of the antagonism is produced by an action at a single binding site.

Effects of SR95103 on burst-distributions

Figure 7 illustrates representative channel currents at a high time-resolution and shows the effect of SR95103 on these currents: Fig. 7A shows examples of currents in the absence of antagonist; Fig. 7B shows bursts in the presence of 30 μM SR95103; Fig. 7C shows the shorter bursts seen in the presence of 100 μM SR95103; Fig. 7D shows the channel bursts after washing. The main apparent effect was a reduction in the mean burst length at the 100 μM concentration of antagonist. The effect reversed after SR95103 was washed off.

The effect of SR95103 on burst-times was explored by examining burst-time distributions. Figure 8 shows burst-time frequency histograms, from a representative experiment where the effect of 30 μM, then 100 μM SR95103, on the distribution of channel bursts produced by 3 μM GABA was examined. Inspection of these histograms shows that the effect of SR95103 is to produce an increase in the proportion of brief bursts. This effect was described

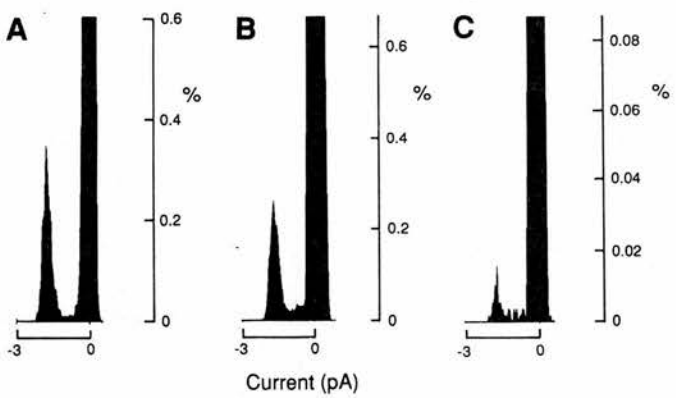


Fig. 5. GABA channel current–amplitude histograms and the lack of effect of SR95103. A: control GABA 3 μM; I = -1.74 ± 0.02 pA (mean $\pm$ SE). B: GABA 3 μM + SR95103 30 μM; I = -1.64 ± 0.04 pA (mean $\pm$ SE). C: GABA 3 μM + SR95103 100 μM; I = -1.72 ± 0.03 pA (mean $\pm$ SE).

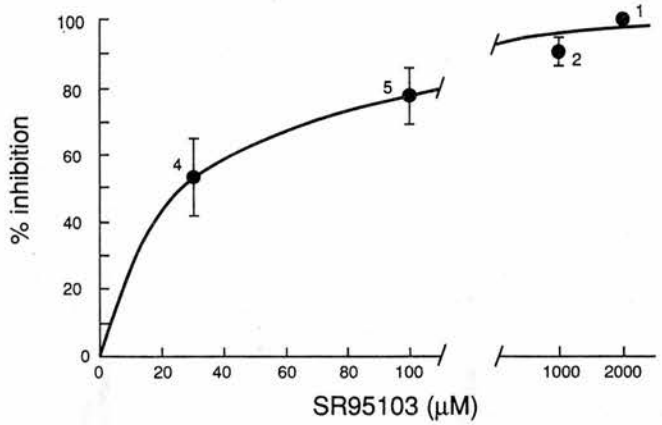


Fig. 6. Percent inhibition dose–response curve. Ordinate: percent inhibition (see methods) in the presence of 3 μM GABA. Abscissa: SR95103 concentration. The line fitted was a least-squares estimate of parameters for the modified Hill equation: Maximum percent inhibition, 97%; IC_{50}, 24 μM; N, 0.98.

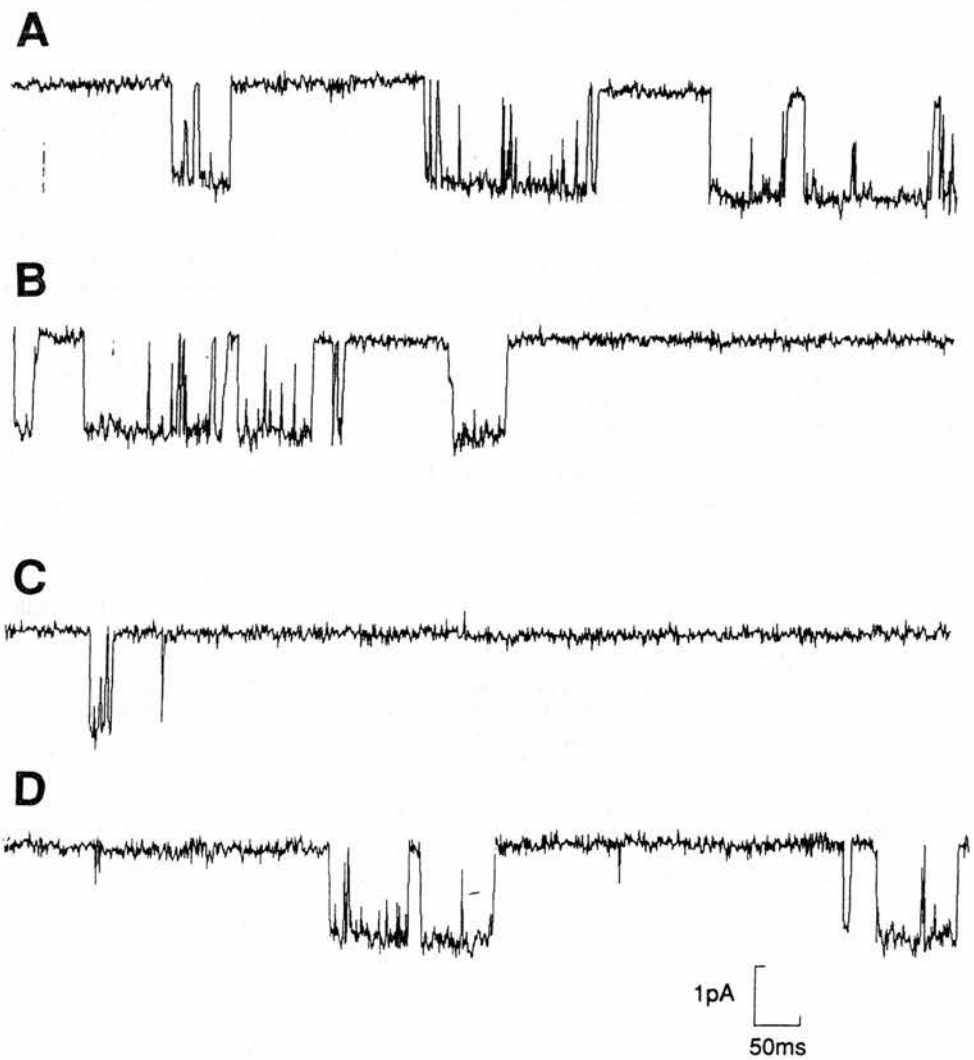


Fig. 7. Effect of SR95103 on channel currents seen at high time resolution. A: control; GABA 3 μM. B: GABA 3 μM + SR95103 30 μM. C: GABA 3 μM + SR95103 100 μM. D: wash; GABA 3 μM alone. Note the short bursts in C.

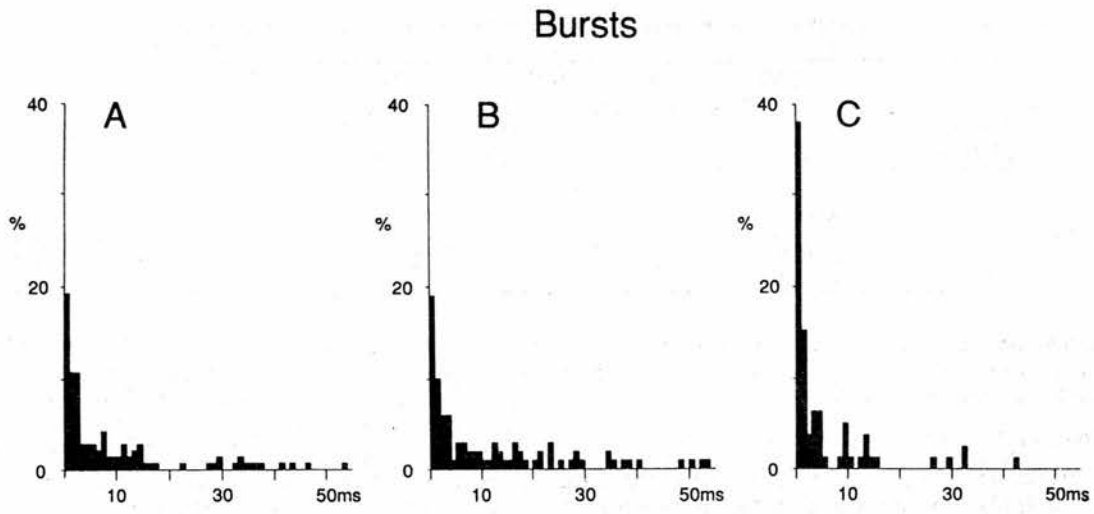


Fig. 8. Frequency histograms showing the effect of SR95103 on channel burst distributions. A: control GABA 3 μM; p.d.f. $a_1 = 0.56$, $t_1 = 3.1$ msec, $a_2 = 0.44$, $t_2 = 33.2$ msec; mean burst duration = 16.1 msec. B: GABA 3 μM + SR95103 30 μM; p.d.f. $a_1 = 0.30$, $T_1 = 1.6$ msec, $a_2 = 0.70$, $T_2 = 26.7$ msec; mean burst duration = 19.4 msec. C: GABA 3 μM + SR95103 100 μM; p.d.f. $a_1 = 0.82$, $T_1 = 1.6$ msec, $a_2 = 0.18$, $T_2 = 41.9$ msec; mean burst duration = 10.2 msec.

quantitatively by fitting exponential distributions. The control distribution (Fig. 8A) was best described by the sum of two exponentials, i.e.:

$$\text{p.d.f.}_{\text{burst}} = 0.57/3.1 \exp(-t/3.1) + 0.43/33 \exp(-t/33),$$

Where $\text{p.d.f.}_{\text{burst}}$ is the burst probability density function and t is time in msec. Thus 57% of the bursts were of the "short" type with a mean duration of 3.1 msec; the "long" type of burst had a mean duration of 33.2 msec. The short bursts appeared to be mostly single short openings, whereas the long bursts were mostly multiple openings. The effect of 30 μM SR95103 on this distribution was small (Fig. 8B), in contrast to the effect of 100 μM SR95103 (Fig. 8C). In 100 μM SR905103, the burst-distribution was best fitted by the equation:

$$\text{p.d.f.}_{\text{burst}} = 0.82/3.1 \exp(-t/3.1) + 0.18/41.9 \exp(-t/41.9).$$

The main effect then, was to increase the proportion of short bursts, in this experiment from 57 to 82%. Similar results were obtained in the other experiments using different patches, and are summarized in Table 1. The table shows that there is a statistically significant increase in the proportion of short bursts with 100 μM, but not 30 μM SR95103, and that there is no significant effect on the mean duration of the short or long bursts at either concentration. It is evident that the increase in short bursts with 100 μM SR95103 produces the reduction in the mean burst duration.

It has been shown (above), that a high concentration of SR95103 increases the proportion of short bursts; it was of interest to determine if an increase in agonist concentration could reverse this effect. In one patch 60 μM SR95103 was used to produce an increase in the proportion of short bursts from 25 to 83%; an increase in GABA concentration from 3 μM to 6 μM then partially reversed the effect of the

Table 1. Mean ± SE values of GABA channel properties measured in 3 μM GABA and, in addition, in the presence of SR95103 on at least four patches. *Significance at $p \leqslant 0.05$ when compared to control.

	Control GABA 3 μM	+SR95103 30 μM	+SR95103 100 μM
P open	0.052 ± 0.011	0.028 ± 0.008*	0.009 ± 0.004*
Channel conductance	22.4 ± 1.0 pS	22.6 ± 1.0 pS	23.3 ± 0.6 pS
Corrected mean open-time	8.4 ± 1.1 msec	9.9 ± 2.4 msec	4.5 ± 1.4 msec*
Mean burst duration	16.9 ± 2.5 msec	20.1 ± 3.9 msec	7.96 ± 3.63 msec
$\text{p.d.f.}_{\text{burst}}$			
a_1	0.418 ± 0.083	0.389 ± 0.090	7.96 ± 3.63*
T_1	2.3 ± 0.6 msec	1.6 ± 0.5 msec	1.3 ± 0.5 msec
a_2	0.581 ± 0.083	0.610 ± 0.090	0.255 ± 0.088*
T_2	26.6 ± 2.0 msec	27.4 ± 2.2 msec	22.0 ± 7.2 mesc
$\text{p.d.f.}_{\text{closed}}$			
a_1	0.459 ± 0.090	0.477 ± 0.122	0.440 ± 0.067
T_1	0.7 ± 0.2 msec	0.8 ± 0.3 msec	0.7 ± 0.3 msec
Alpha_2	103.5 ± 14.5 sec^{-1}	141.1 ± 71.2 sec^{-1}	246.6 ± 73.3 sec^{-1}*

Table 2. Effect of SR95103 on GABA channel burst distributions and the partial reversal by increasing GABA concentration

	Control GABA 3 μM	SR95103 30 μM +GABA 3 μM	SR95103 60 μM +GABA 3 μM	SR95103 60 μM +GABA 10 μM
Corrected Mean burst duration	23.8 msec	20.2 msec	2.3 msec	8.7 msec
p.d.f.$_{burst}$				
	a_1 0.246	0.241	0.829	0.591
	T_1 0.5 msec	0.7 msec	0.4 msec	1.0 msec
	a_2 0.754	0.759	0.171	0.409
	T_2 31.4 msec	26.4 msec	11.7 msec	19.8 msec

antagonist and decreased the proportion of short bursts from 83% to 60%. Further details of these results are shown in Table 2.

Effect of SR95103 on closed-time distributions

Inspection of Fig. 4 shows that the antagonism of SR95103 was associated with an increase in long closed-times. The effect of SR95103 on the closed-time distributions was examined by fitting exponentials to describe the p.d.f. Control GABA (3 μM) closed-time distributions were best described by three exponentials. In one representative patch the result was:

$$\text{p.d.f.}_{\text{closed}} = 0.29/0.7\exp(-t/0.7) + 0.16/6.0 \times \exp(-t/6.0) + 0.55/63\exp(-t/63),$$

where p.d.f.$_{closed}$ is the closed-time probability density function and t is time in msec. This result is comparable to that reported previously (Martin, 1985) and shows that there are at least three closed states giving rise to the "brief" (mean duration, 0.7 msec), "intermediate" (mean duration, 6.0 msec) and "long" (mean duration, 63 msec) types of closing. The effect of 30 and 100 μM SR95103 on the distribution of closed-times of this patch was to increase the apparent duration of intermediate and long closings. The closed-time distribution for the same patch with 30 μM SR95103 was best described by:

$$\text{p.d.f.}_{\text{closed}} = 0.20/1.7\exp(-t/1.7) + 0.36/15.4 \times \exp(-t/15.4) + 0.54/133\exp(-t/133).$$

The mean closed-time increased from 35.8 msec to 77.7 msec; the mean duration of the intermediate closings increased from 6.0 to 15.4 msec and the mean duration of the long closings increased from 63 to 133 msec.

At 100 μM SR95103, the mean closed-time increased to 99.6 msec; the mean intermediate closed-time increased to 21.8 msec and the mean long closed-times increased to 215 msec. The closed-time distribution was best described by:

$$\text{p.d.f.}_{\text{closed}} = 0.34/0.7\exp(-t/0.7) + 0.22/21.8 \times \exp(-t/21.8) + 0.44/215\exp(-t/215).$$

No increase in the number of components was required to describe the closed-distributions in this or other patches; therefore no increase in the number of closed states in the presence of the antagonist was detected. The effect of 30 μM and 100 μM SR95103 on closed-time distributions, from the other patches, was qualitatively similar, and was characterized by an increase in the duration of intermediate and/or long closings. However, there was a large variation in mean estimates for the intermediate closings and long closings, possibly due to the variation in the number of channels present in the patch. In contrast, SR95103 had no consistent effect on the duration of the brief closings; Table 1 shows mean values for the brief closings seen in the different patches.

Effect of SR95103 on corrected mean open-times

One difficulty in measuring open-times directly is that the unresolved brief closings lead to bursts appearing as long single openings (see Colquhoun and Hawkes, 1982). This artifact increases the observed open-times. However, it is possible to compensate for these unresolved closings by estimating the true number of closings by extrapolating from the closed-time distributions. The estimated total open-time is divided by the true number of closings to obtain the mean-open time (see Methods). The control mean opentime in 3 μM GABA for one typical patch was 11.9 msec; this was unchanged in 30 μM SR95103 and found to be 12.0 msec; however in 100 μM SR95103 it decreased to 5.8 msec. Table 1 shows the mean $\pm$ SE values obtained from the different patches and shows that there is a statistically significant decrease in the corrected mean open-time at the 100 μM antagonist concentration but not at 30 μM.

DISCUSSION

This patch-clamp study of SR95103 was carried out to further investigate the mode of antagonism. The percent inhibition dose–response curve was described by the modified Hill equation with a coefficient close to one. A lower antagonist concentration (30 μM), reduced the probability of the channel being open without significantly affecting the burst distribution, corrected mean open-time or channel conductance; only the mean duration of the two slower closed-time components was increased. A higher (100 μM) antagonist concentration, further decreased the probability of channel opening, but significantly increased the proportion of short bursts. In the subsequent discussion, it is suggested that SR95103 acts mostly as a simple competitive antagonist; but at higher concentrations there is an additional small non-competitive action, possibly channel block.

A possible kinetic scheme for the antagonism

A variety of patch-clamp studies in different preparations have been carried out on GABA-activated channels where the open-time distributions were described by two exponentials and the closed-time distributions described by three exponentials

(*Ascaris*: Martin, 1985; mouse spinal neurones; Jackson *et al.*, 1982; Sackmann *et al.*, 1983; Mathers, 1985; chick cerebral neurones; Weiss and Magleby, 1989; and bovine chromaffin cells; Bormann and Clapham, 1985). More recently, however, MacDonald *et al.* (1989) have described an additional open-time component, which suggests a greater complexity. Molecular biology studies on the GABA channel structure (Schofield *et al.*, 1987) have shown that the receptor–channel complex is formed by two alpha- and two beta-protein transmembrane subunits. The beta subunits were shown to bind GABA (Barnard *et al.*, 1986) so it was concluded that two agonist molecules combine with the receptor–channel complex to bring about opening. However, in contrast to GABA, the results of the current-clamp experiments presented in the previous paper, and the percent inhibition dose–response curve presented here, suggest that one molecule of SR95103 is responsible for most of the antagonism.

Figure 9 shows a minimal kinetic scheme which may explain these observations. It predicts (Colquhoun and Hawkes, 1977, 1982) in the absence of antagonist, three components to the closed-time distribution and two components to the open- and burst-time distribution. However, in the presence of the antagonist, an extra closed state should give rise to an extra component in the closed-time distribution.

Our experiments did not reveal an increase in the number of components in the closed-time distributions, but the long duration of many closed-times, seen in the presence of the antagonist, reduced the number of events available for analysis and the ability to separate components. There was also the further complication of different numbers of channels present in each patch. This complication gave rise to considerable variation in estimates of the mean duration of "intermediate" and "long" closed-times. Both of these factors would make the detection of any extra

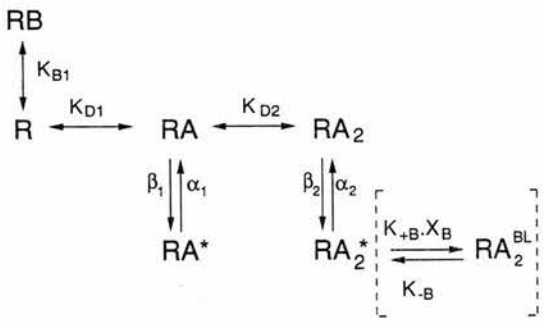


Fig. 9. Minimal kinetic scheme for agonist and antagonist action. The receptor–channel complex (R) has two sites to which the agonist (A), but one site to which the antagonist (B), combines. Open states (*) may occur only after isomerization of the single-bound or double-bound agonist receptor–channel complex. The dissociation constant for the first agonist molecule to combine (K_{D1}) is much larger than for the second agonist molecule (K_{D2}); the dose–response relationship would then be approximated by the modified Hill equation with $N = 2$. The channel closing rates are $alpha_1$ and $alpha_2$. $Alpha_1$ is larger than $alpha_2$ so that RA_2^* is the long open state. The channel opening rates are $beta_1$ and $beta_2$. The antagonist dissociation constant is K_{B1}. The putative blocked channel state (RA_2^{BL}) is also shown in brackets.

long closed-states in the presence of the antagonist difficult.

Low, but not high, concentrations of SR95103 appear to be competitive

Simple competitive antagonism predicts no change in the channel mean open-time or burst-distribution. In our experiments there was no significant effect of 30 μM SR95103 on corrected mean open-times or on the burst distribution, so it is argued that this concentration of antagonist behaves like a competitive antagonist. The effects of 100 μM, however, were not compatible with just simple competitive antagonism, because they were associated with reductions in corrected mean open-times and a significant increase in the proportion of short bursts.

Possible mode of action for SR95103

A variety of experimental preparations have been used to look at the action of arylaminopyridazine GABA derivatives on the vertebrate $GABA_a$ receptor. Binding studies (Chambon *et al.*, 1985; Heaulme *et al.*, 1986a, b) and electrophysiological studies (Chambon *et al.*, 1985; Michaud *et al.*, 1986; Desarmenien *et al.*, 1987) have indicated that the arylaminopyridazine derivatives of GABA can act as simple competitive antagonists.

SR95331 (a close derivative of SR95103) has been examined at the single-channel level, in bovine adrenal chromaffin cells (Hamann *et al.*, 1988); SR95331 reduced the open probability of GABA channels without affecting open and burst kinetics, an effect compatible with competitive antagonism. However, it was suggested that an additional channel-block might occur at higher concentrations, but the potent competitive action of the analogue did not allow further analysis.

A small inhibitory effect of SR95103 on the glycine receptors, as well as the GABA receptors, of rat cortical neurones has been described by Michaud *et al.* (1986), but not for other pyridazinyl GABA derivatives. The GABA- and glycine- activated channels both conduct Cl so that the pore of the channel might be a common site of action. These two reports raise the question of a channel-block mechanism in addition to competitive antagonism for SR95103.

Does SR95103 act as a channel-blocker?

A simple channel-block mechanism (see Colquhoun and Hawkes, 1983) predicts, at the current-clamp level, a reduction in the maximum response and a reduction in the slope of dose–response curves at higher antagonist concentrations; we did not observe such an effect with up to 1 mM SR95103 (previous paper). At the single channel level, the effect of channel-block on the burst duration depends on the duration of the blocked state. If the blocked state is brief (less than T_{crit}) then the burst duration and the number of gaps per burst would increase; we did not observe these effects. However, if the blocked state were longer than T_{crit}, then the observed mean long burst duration would get shorter and the mean open-time in the long bursts would decrease. Although the observed reduction in the mean duration of long bursts did not reach statistical significance (Table 1), there was a significant

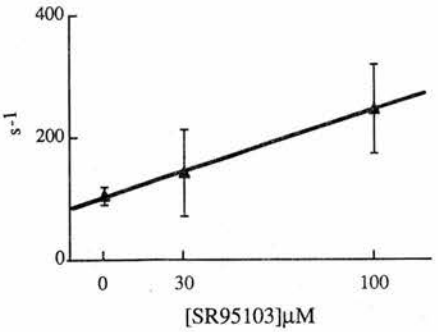


Fig. 10. Effect of SR95103 on mean open-times in long bursts. Ordinate: reciprocal of mean open times in long bursts. Abscissa: concentration of SR95103. The slope (obtained by least-squares regression) was $1.44\,M^{-6}\,sec^{-1}$ and could be interpreted as the channel blocking rate at -50 mV.

reduction in the corrected mean open-times in the long bursts.

We assumed that all brief closings occur in the long bursts and then calculated the mean duration of openings in the long bursts (see Methods). Figure 10 shows the observed linear relationship between the reciprocal of this duration and the concentration of SR95103. The reciprocal of this duration will be equal to the sum of the rate constants leading from the long open state (Fig. 9). The slope of the plot in Fig. 10, is then an estimate of the channel-blocking rate constant; it was $1.44\,M^{-6}\,sec^{-1}$.

Although SR95103 may act in part as a channel-blocker, this cannot play a big role in the antagonism of GABA conductance responses because high concentrations of SR95103 did not significantly depress the maximum response seen in current-clamp experiments. Thus, for example, if the mean blocked state lasted 10 msec and the blocking rate, k_{+BL} was $1.44\,M^{-6}\,sec^{-1}$ (see above) then with $3\,\mu M$ GABA and $100\,\mu M$ SR95103, we have estimated that the proportion of time the channel spends in the blocked state is only near 1%. The inclusion of a blocked state would produce a reduction of less than 2% in P_{open} when compared to a similar model without blocking. This estimate was based on an analysis of kinetic schemes with plausible rate constants. The illustration shows that such a channel-block would not be detectable at the current-clamp level.

CONCLUSION

It is concluded that SR95103 acts like a competitive antagonist at low concentrations, but at higher concentrations, there is an additional non-competitive element to the antagonism; this has some of the properties of channel-block.

Acknowledgements—This work was supported by the Wellcome Trust, SERC and the Harriet Thompson Trust.

REFERENCES

Arunlakshana O. and Schild H. O. (1959) Some quantitative uses of drug antagonists. *Br. J. Pharmac. Chemother.* **14,** 48–58.

Barnard E. A., Darlison M. G. and Seeburg P. (1987) Molecular biology of the $GABA_a$ receptor: the receptor channel superfamily. *TINS* **10,** 502–509.

Bormann J. and Clapham D. E. (1985) Gamma-aminobutyric acid receptor channels in adrenal chromaffin cells: a patch-clamp study. *Proc. natn Acad. Sci. U.S.A.* **82,** 2168–2172.

Chambon J. P., Feltz P., Heaulme M., Restle S., Schliechter R., Biziere K. and Wermuth C. G. (1985) Synthesis of SR95103 an arylaminopyridazine derivative of GABA. *Proc. natn Acad. U.S.A.* **82,** 1832–1836.

Colquhoun D. and Hawkes A. G. (1977) Relaxation and fluctuations of membrane currents that flow through drug-operated channels. *Proc. R. Soc. Ser. B.* **199,** 231–262.

Colquhoun D. and Hawkes A. G. (1982) On the stochastic properties of bursts of single ion channel openings. *Proc. R. Soc. Ser. B.* **211,** 205–235.

Colquhoun, D. and Hawkes, A. G. (1983). Stochastics of single ion-channels. In *Single-Channel Recordings* (Edited by Sackman B. and Neher E.), pp. 135–175. Plenum Press, New York.

Colquhoun D. and Sakmann B. (1985) Fast events in single channel currents activated by acetylcholine and its analogues at the frog muscle end-plate. *J. Physiol. Lond.* **369,** 501–577.

Desarmenien M., Desaulles E., Feltz P. and Hamann M. (1987) Electrophysiological study of SR42641 a novel aminopyridazine derivative of GABA, antagonist properties and receptor selectivity of $GABA_a$ vs $GABA_b$ responses. *Br. J. Pharmac.* **90,** 287–298.

Glasbey C. and Martin R. J. (1986) Exploratory and confirmatory plots of single-channel records. *J. Neurosci. Meth.* **16,** 239–294.

Hamill O. P., Marty A., Neher E., Sakmann B. and Sigworth F. J. (1981) Improved patch-clamp techniques for high-resolution current recording from cells and cell-free membrane patches. *Pflugers Archs ges. Physiol.* **391,** 85–100.

Hamann M., Desarmenien M., Desaulles E., Bader M. F. and Feltz P. (1987) Quantitative evaluation of the properties of a pyridizanyl GABA derivative (SR95531), as a $GABA_a$ competitive antagonist. An electrophysiological approach. *Brain Res.* **442,** 287–296.

Heaulme M., Chambon J. P., Leyris R., Molimard J. C., Wermuth C. C. and Biziere K. (1986a) Biochemical characterization of three arylaminopiridazine GABA derivatives with the $GABA_a$ receptor site. *Brain Res.* **384,** 224–231.

Heaulme M., Chambon J. P., Leyris R., Wermuth C. C. and Biziere K. (1986b) Specific binding of a phenylpyridazinium derivative endowed with $GABA_a$ receptor antagonist activity to rat brain. *Neuropharmacology* **25,** 1272–1283.

Hille B. (1984) *Ionic Channels of Excitable Membranes.* pp. 226–248. Sinauer, Sunderland, M.A.

Jackson M. B., Lecar H., Mathers D. A. and Barker J. L. (1982) Single-channel currents activated by gamma-aminobutyric acid, muscimol and (−) pentobarbital in cultured mouse spinal neurons. *J. Neurosci.* **2,** 889–894.

Macdonald R. L., Rogers C. J. and Twyman R. E. (1989) Kinetic properties of the $GABA_a$ receptor main conductance state of mouse spinal cord neurones in culture. *J. Physiol. Lond.* **410,** 479–499.

Martin R. J. (1985) γ-Aminobutyric acid- and piperazine-activated single channel currents from *Ascaris suum* body muscle. *Br. J. Pharmac.* **84,** 445–461.

Mathers D. A. (1985) Spontaneous and gamma-aminobutyric acid induced single channel currents in cultured murine spinal cord neurons. *Can. J. Physiol. Pharmac.* **63,** 1228–1233.

Michaud J. C., Mienville J. M. and Chambon J. P. (1986) Interaction of three arylaminopyridazine GABA derivatives with rat cortical GABA and glycine receptors: an *in vivo* microiontophoretic study. *Neuropharmacology* **25,** 1197–1203.

Sakmann B., Hamill O. P. and Bormann J. (1983) Patch-clamp measurements of elementary chloride currents activated by the putative inhibitory transmitters GABA and glycine in mammalian spinal neurons. *J. Neural Transmission Suppl.* **18,** 88–95.

Scholfield P. R., Darlison M. G., Fujita N., Burt D. R., Stephenson F. A., Rodriquez H., Rhee L. M., Ramachandron J., Reale V., Glencorse T. A., Seeburg P. H. and Barnard E. A. (1987) Sequence and functional expression of the $GABA_a$ receptor shows ligand gated receptor super family. *Nature* **328,** 221–227.

Weiss D. S. and Magleby K. L. (1989) Gating scheme for single gamma-aminobutyric acid activated chloride channels determined from stability plots, dwell-time distribution and adjacent interval deviations. *J. Neurosci.* **9,** 1314–1324.

Williams T. L., Smith D. A. S., Burton N. R. and Stone T. W. (1988) Amino acid pharmacology in neocortical slices: evidence of bimolecular actions from an extension off the Hill and Gaddum–Schild equations. *Br. J. Pharmac.* **95,** 805–810.

J. exp. Biol. **159**, 149–164 (1991)
Printed in Great Britain © *The Company of Biologists Limited 1991*

ANTAGONIST PROPERTIES OF ARYLAMINOPYRIDAZINE GABA DERIVATIVES AT THE *ASCARIS* MUSCLE GABA RECEPTOR

BY A. H. DUITTOZ AND R. J. MARTIN

Department of Preclinical Veterinary Sciences, R(D)SVS, University of Edinburgh, Summerhall, Edinburgh, EH9 1QH

Accepted 9 April 1991

Summary

1. In a previous study, it was shown that the potency order for two arylaminopyridazine derivatives, SR95531 and SR95103, was different in *Ascaris suum* when compared to vertebrate preparations. SR95531, the most potent analogue at the vertebrate $GABA_A$ receptor, was found to be very weak at antagonizing GABA responses in *Ascaris*, but SR95103, approximately 20 times less potent than SR95531 in vertebrate preparations, was more potent than SR95531 in *Ascaris*. These results suggested the existence of different accessory binding sites at the *Ascaris* GABA receptor.

2. To test this hypothesis, the effects of a series of arylaminopyridazine derivatives of GABA on the GABA response in *Ascaris suum* muscle were investigated using a two-microelectrode current-clamp technique.

3. The results showed that SR42627, a potent antagonist at the $GABA_A$ receptor, was one of the weakest analogues in *Ascaris* muscle. In contrast, SR95132, virtually inactive in vertebrate preparations, was equipotent to SR95103, the most potent analogue of the series in *Ascaris* muscle.

4. The three most potent analogues in *Ascaris*, SR95103, SR95132 and SR42666, displace GABA dose–response curves to the right without decreasing the maximal response. The modified Schild plots for these compounds are consistent with a competitive mechanism involving two molecules of GABA and only one molecule of antagonist interacting with the receptor. The estimated dissociation constants for SR95103, SR95132 and SR42666 are, respectively, 64, 65 and 105 $\mu mol\,l^{-1}$.

5. Structure–activity relationships for this series of compounds were examined in *Ascaris* and compared to those in vertebrates. Substitution on the pyridazine ring in the 4-position, while detrimental for the antagonist potency at the vertebrate $GABA_A$ receptor, appears to be a prerequisite for antagonistic activity on the *Ascaris* muscle GABA receptor. These results are interpreted in terms of the accessory binding site theory of Ariëns, and suggest the existence of different accessory binding sites on the *Ascaris* GABA receptor.

Key words: *Ascaris suum*, GABA, arylaminopyridazine GABA derivatives, antagonist.

Introduction

The GABA receptor has been described as a target for pesticide drugs (Eldefrawi and Eldefrawi, 1987) and anthelmintic drugs (Martin, 1982; Martin and Pennington, 1989). In the nematode parasite *Ascaris suum*, two well-known anthelmintics have been shown to interact with GABA receptors: piperazine (Del Castillo *et al.* 1963, 1964*a*; Martin, 1982, 1985) and ivermectin (Holden-Dye *et al.* 1988; Martin and Pennington, 1989). Pharmacological characterization of the *Ascaris* GABA receptor shows that, in terms of agonist properties, it is closely related to vertebrate $GABA_A$ receptors (Holden-Dye *et al.* 1989). This contrasts with the antagonist properties, since none of the classical $GABA_A$ antagonists are potent on *Ascaris*. Bicuculline, picrotoxin, securinine, pitrazepine, TBPS (tert-butylbicyclophosphothionate) and dieldrin are either weak or inactive GABA antagonists in *Ascaris* (Holden-Dye *et al.* 1988; Colqhoun *et al.* 1989). In agreement with these results, the arylaminopyridazine GABA derivative and potent $GABA_A$ antagonist SR95531 was shown to be very weak at antagonizing GABA responses in *Ascaris* (Holden-Dye *et al.* 1989; Duittoz and Martin, 1991*a*). However, its close analogue SR95103 was shown to antagonize GABA responses in a competitive manner with an apparent dissociation constant (K_B) of 64 μmol l^{-1} (Duittoz and Martin, 1991*a*,*b*). This contrasts with the vertebrate $GABA_A$ receptor, at which SR95531 is the most potent antagonist, being approximately 20 times more potent than SR95103 (Heaulme *et al.* 1986*b*). It was then suggested that arylaminopyridazine GABA derivatives would show structure–activity relationships in *Ascaris* different from those found at the vertebrate $GABA_A$ receptor (Duittoz and Martin, 1991*a*). In this study, other arylaminopyridazine derivatives were tested (Fig. 1); their relative potency in *Ascaris* muscle was compared to that in mammalian preparations, and the results are discussed in terms of accessory binding site theory (Ariëns *et al.* 1979).

Materials and methods

Ascaris suum were collected from the local abattoir and kept in Locke's solution at 37°C. They were used within 4 days. The muscle flap preparation, made as described by Martin (1980), was pinned down in an experimental chamber maintained at 22°C, and perfused with a high-chloride and low-calcium Ringer's solution containing (in mmol l^{-1}): NaCl, 135; KCl, 3; $MgCl_2$, 15.7; glucose, 3; Tris, 5; pH adjusted to 7.6 with maleic acid.

Two glass microelectrodes (10–30 MΩ), filled with 2 mol l^{-1} potassium acetate, were introduced into the bag region of a muscle cell; one was used to inject hyperpolarizing current pulses (40 nA, 2 s, 0.2 Hz), the other to record the membrane potential. The signals were recorded and amplified with an Axoclamp 2A, monitored on a Tektronix 2210 oscilloscope and played back on a Lectromed chart recorder. The input conductance of the bag was calculated from the voltage response to the injected current pulse; the I/V relationship is sufficiently linear during the injection of hyperpolarizing current to allow this (Martin, 1980).

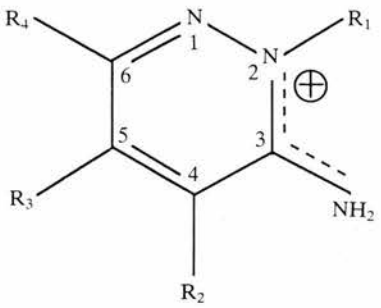


Fig. 1. Structure of arylaminopyridazine GABA derivatives.

	Substituents			
Name	R1	R2	R3	R4
SR95103	$-C_3H_6COOH$	$-CH_3$	$-H$	$-C_6H_5$
SR95531	$-C_3H_6COOH$	$-H$	$-H$	$-C_6H_4OCH_3$
SR42666	$-C_3H_6COOH$	$-CH_3$	$-H$	$-C_6H_4OCH_3$
SR95132	$-C_3H_6COOH$	$-C_6H_5$	$-H$	$-C_6H_5$
SR42640	$-C_3H_6COOH$	$-H$	$-CH_3$	$-C_6H_5$
SR42627	$-C_3H_6COOH$	$-CH_3$	$-H$	$-C_6H_4CH_3$
SR95133	$-C_3H_6COOH$	$-CH_3$	$-H$	$-C_{10}H_8$

The preparation was not perfused continuously because of the limited quantities of antagonist available. To detect any antagonist activity, 30 μmol l^{-1} GABA was applied first and, when the membrane conductance stabilized to its new value, the bath solution was replaced by 30 μmol l^{-1} GABA + 1 mmol l^{-1} antagonist. Antagonists found to be reasonably potent using this method were then tested at several concentrations on GABA dose–response curves. GABA dose–response curves were obtained by cumulative application of increasing GABA concentrations, without intermediate washing. The method involved gentle draining of the bath (2.5 ml) by suction, and then flushing the bath with 5 ml of the next GABA concentration. The antagonist was applied simultaneously with the first GABA concentration, and remained present at subsequent GABA concentrations. A control GABA dose–response curve without antagonist was always obtained from the same cell and dose ratios were calculated (see below).

Dose–response relationships were described by the modified Hill equation (Nistri and Constanti, 1979):

$$\Delta G = \frac{\Delta G_{max}}{1 + (EC_{50}/[X_A])^n},$$

where ΔG is the change in membrane input conductance, ΔG_{max} is the maximal response, EC_{50} is the GABA concentration producing 50 % of the maximal response, $[X_A]$ is the GABA concentration and n is the Hill coefficient. A nonlinear regression program (patternsearch, Colquhoun, 1971) was used to

estimate, ΔG_{max}, EC_{50} and n. The action of 1 mmol l^{-1} antagonist on the change in membrane input conductance induced by 30 μmol l^{-1} GABA was examined. The percentage of antagonism was then calculated:

$$\text{percentage of antagonism} = 100[1-(\Delta G_{ant}/\Delta G_c)],$$

where ΔG_c is the change in membrane input conductance produced by 30 μmol l^{-1} GABA and ΔG_{ant} is the change in membrane input conductance produced by 30 μmol l^{-1} + 1 mmol l^{-1} antagonist, measured after a 10 min application of the antagonist. The most potent compounds were then tested at concentrations of 100, 300 and 1000 μmol l^{-1} on GABA dose–response curves. Dose–response curves were considered parallel if the Hill coefficient and ΔG_{max} for the control GABA dose–response curve and the dose–response curves in the presence of the antagonist were not significantly different. Dose ratios were then determined from the ratios of the EC_{50} values measured and examined using the Schild analysis (Arunlakshana and Schild, 1959):

$$\log(DR - 1) = \log[X_B] + pK_B,$$

where DR is the dose ratio, $[X_B]$ is the antagonist concentration and pK_B is the negative logarithm of the dissociation constant of the antagonist–receptor complex. However, the classical Schild plot does not account for a stoichiometry greater than 1 between GABA and its receptor. Previous studies on the *Ascaris* muscle GABA receptor (Holden-Dye *et al.* 1988, 1989), and more generally on invertebrate GABA receptors and vertebrate $GABA_A$ receptors (see Nistri and Constanti, 1979, for a review; Schofield, 1989), have suggested that two molecules of GABA are likely to interact with the receptor. To account for positive cooperativity between GABA and its receptor we used a modified Schild analysis (Williams *et al.* 1988):

$$\log(DR^n - 1) = M\log[X_B] + pK_B,$$

where n is the Hill coefficient, M is the number of antagonist molecules interacting with the receptor, and the other symbols are explained above.

Means and standard errors (S.E.) were calculated. Statistical significance was assessed using a two-tailed independent t-test.

GABA was obtained from Sigma. SR95103, 2-(3-carboxypropyl)-3-amino-4-methyl-6-phenyl pyridazinium chloride; SR95531, 2-(3-carboxypropyl)-3-amino-6-*p*-methoxy phenyl pyridazinium chloride; SR42666, 2-(3-carboxypropyl)-3-amino-4-methyl-6-*p*-methoxy phenyl pyridazinium chloride; SR95133, 2-(3-carboxypropyl)-3-amino-4-methyl-6-α-napthyl pyridazinium chloride; SR95132, 2-(3-carboxypropyl)-3-amino-4-phenyl-6-phenyl pyridazinium chloride; SR42627, 2-(3-carboxypropyl)-3-amino-4-methyl-6-*p*-methyl phenyl pyridazinium chloride; and SR42640, 2-(3-carboxypropyl)-3-amino-5-methyl-6-phenyl pyridazinium chloride were gifts from Sanofi Recherche.

Results

The results reported here are based on the analysis of experiments recorded

from 32 cells from 19 preparations. Cells selected for recording and analysis had a resting membrane potential greater than −20 mV and a resting input conductance between 1.9 and 4.0 μS. Recordings were rejected if the resting input conductance failed to return to at least 80 % of the control value after the final wash.

Arylaminopyridazine derivatives do not affect the membrane conductance directly. SR95103, SR95531, SR42666, SR42640, SR42627, SR95133 and SR95132 were initially applied at 1 mmol l^{-1} in the absence of GABA. No change in membrane conductance was produced. The lack of activity of arylaminopyridazine derivatives on membrane conductance showed that they do not have agonist properties on GABA receptors, in spite of the GABA side chain in their structure.

Fig. 2 illustrates the effects produced by 1 mmol l^{-1} SR42640, SR42627, SR95133, SR42666 and SR95132 on the response to 30 μmol l^{-1} GABA; Table 1 summarizes the percentage of antagonism. SR42640 had the weakest effect and only antagonized 15 % of the response in Fig. 2A. Following the application of SR42640, the membrane hyperpolarized slightly (Fig. 2A); this is believed to be an artefact due to the application of the drug. SR42627 was not very potent, with only 29 % of the GABA response being antagonized in Fig. 2B. SR95133, the α-napthyl derivative, was more potent than SR95531 (Duittoz and Martin, 1991*a*). The potent antagonists were SR42666, the 4-phenyl derivative SR95132 and SR95103.

All these results are summarized and compared to results obtained in vertebrate preparations in Table 1. The results obtained in *Ascaris* and with vertebrates are difficult to compare quantitatively since they involve different techniques: an

Table 1. *Comparison of the potencies of some arylaminopyridazine GABA derivatives in vertebrate and in* Ascaris suum *muscle*

GABA derivative	Vertebrate K_B (μmol l^{-1})*	*Ascaris* muscle	
		Antagonism (%)†	K_B (μmol l^{-1})‡
SR95531	0.15	44.2±6.1 (*N*=5)	–
SR42666	0.31	76.6±6.6 (*N*=5)	104.8±19.7 (*N*=13)
SR42627	0.5	29, 13 (*N*=2)	–
SR95103	2.20	92.8±3.2 (*N*=5)	63.8±12.9 (*N*=14)
SR95133	2.60	58.0±8.0 (*N*=4)	–
SR42640	10.40	15, 5 (*N*=2)	–
SR95132	100.00	89.0±3.4 (*N*=5)	65.0±20.3 (*N*=9)

Values are mean±S.E.

*Measured by [^{3}H]GABA displacement from rat brain membranes; K_B, dissociation constant (Wermuth *et al.* 1987).

†Percentage antagonism of the response to 30 μmol l^{-1} GABA, produced by 1 mmol l^{-1} antagonist, in *Ascaris* muscle.

‡ K_B, dissociation constant, estimated from the modified Schild analysis, in *Ascaris*. It was not possible to measure quantitatively the antagonism of the low-potency analogues (SR42640, SR42627, SR95133 and SR95531) because the amount required exceeded that available for experimentation.

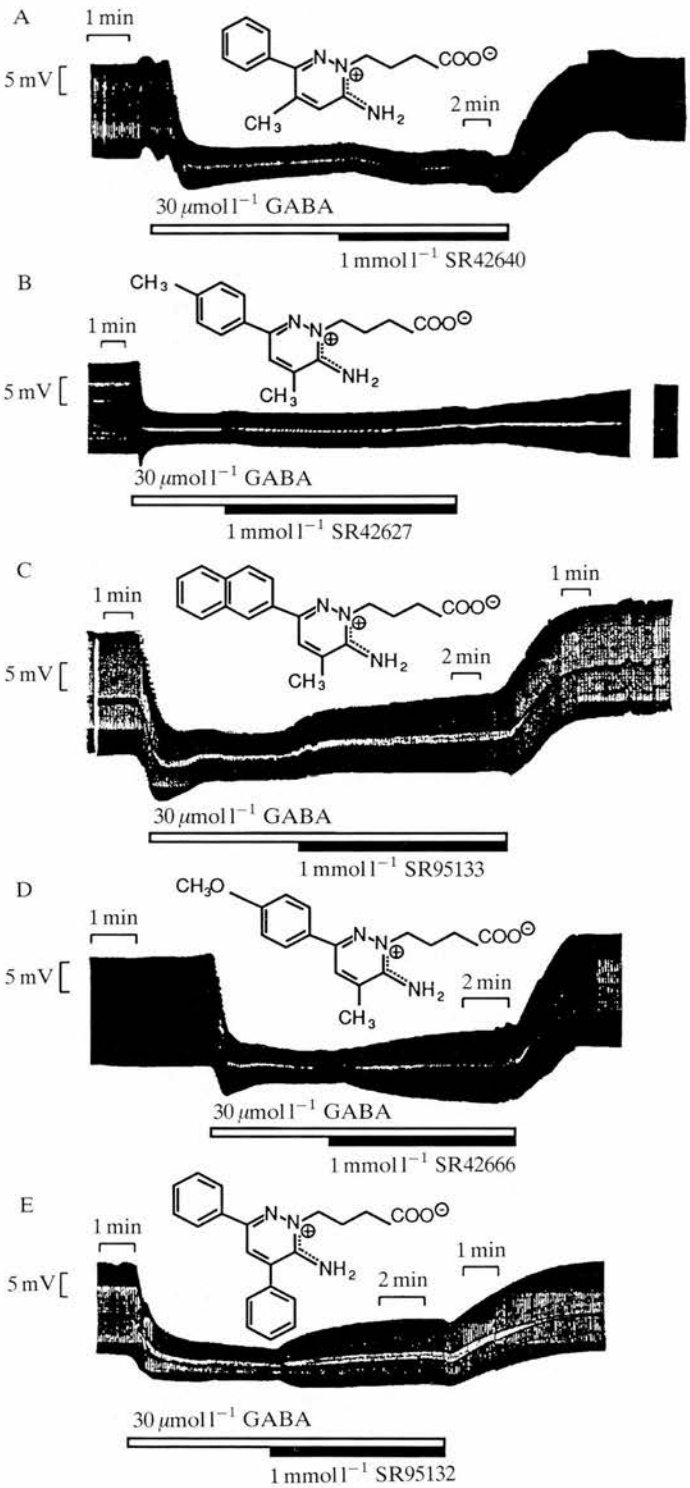

A
1 min
5 mV
2 min
30 μmol l⁻¹ GABA
1 mmol l⁻¹ SR42640
B
1 min
5 mV
30 μmol l⁻¹ GABA
1 mmol l⁻¹ SR42627
C
1 min
1 min
5 mV
2 min
30 μmol l⁻¹ GABA
1 mmol l⁻¹ SR95133
D
1 min
5 mV
2 min
30 μmol l⁻¹ GABA
1 mmol l⁻¹ SR42666
E
1 min
5 mV
1 min
2 min
30 μmol l⁻¹ GABA
1 mmol l⁻¹ SR95132

Fig. 2

Fig. 2. Effects of 1 mmol l^{-1} SR42640, SR42627, SR95133, SR42666 and SR95132 on the change in membrane input conductance produced by 30 μmol l^{-1} GABA. (A) Effect of 1 mmol l^{-1} SR42640: resting input conductance, G_0=2.2 μS; 30 μmol l^{-1} GABA, ΔG=4.6 μS; 1 mmol l^{-1} SR42640 + 30 μmol l^{-1} GABA, ΔG=3.9 μS; antagonism=15 %. (B) Effect of 1 mmol l^{-1} SR42627: resting input conductance, G_0=2.2 μS; 30 μmol l^{-1} GABA, ΔG=4.4 μS; 1 mmol l^{-1} SR42627 + 30 μmol l^{-1} GABA, ΔG=3.1 μS; antagonism=29 %. (C) Effect of 1 mmol l^{-1} SR95133: resting input conductance, G_0=2.0 μS; 30 μmol l^{-1} GABA, ΔG=3.8 μS; 1 mmol l^{-1} SR95133 + 30 μmol l^{-1} GABA, ΔG=1.4 μS; antagonism=63 %. (D) Effect of 1 mmol l^{-1} SR42666: resting input conductance, G_0=2.2 μS; 30 μmol l^{-1} GABA, ΔG=5.0 μS; 1 mmol l^{-1} SR42666 + 30 μmol l^{-1} GABA, ΔG=1.0 μS; antagonism=80 %. (E) Effect of 1 mmol l^{-1} SR95132: resting input conductance, G_0=2.0 μS; 30 μmol l^{-1} GABA, ΔG=3.7 μS; 1 mmol l^{-1} SR95132 + 30 μmol l^{-1} GABA, ΔG=0.7 μS; antagonism= 81 %.

electrophysiological approach in *Ascaris* and ligand-binding techniques in vertebrates. However, the potency order found in *Ascaris* can be compared to the potency order found in vertebrates. The two potent analogues in vertebrates, SR95531 and SR42627, are weak antagonists in *Ascaris*. In contrast SR95132, virtually inactive in vertebrates, is one of the most potent analogues in *Ascaris*.

In vertebrates, arylaminopyridazine derivatives act as competitive antagonists where they displace [^{3}H]GABA and [^{3}H]muscimol from their binding sites (Chambon *et al.* 1985; Heaulme *et al.* 1986*a*,*b*) and decrease [^{3}H]diazepam binding stimulated by GABA (Heaulme *et al.* 1986*a*). It has previously been shown that, in *Ascaris*, SR95103 produces a parallel shift, to the right, in GABA dose–response curves without a decrease in the maximum response (Duittoz and Martin, 1991*a*). The dose-dependency was best described by the modified Schild equation (Williams *et al.* 1988), suggesting that the mechanism was competitive and that only one molecule of SR95103 interacted with the GABA receptor (Duittoz and Martin, 1991*a*). The actions of SR95132 and SR42666 on GABA cumulative dose–response curves were examined at 100, 300 and 1000 μmol l^{-1}. SR95132 and SR42666 produced a parallel displacement to the right in GABA dose–response curves, without a reduction in the maximal response, suggesting a competitive mechanism. Fig. 3 illustrates the antagonism produced by SR95132. Note that in the presence of 3 μmol l^{-1} GABA the membrane was slightly depolarized without any detectable change in the membrane conductance (Fig. 3A); depolarization of the membrane was occasionally seen after application of low GABA concentrations (A. H. Duittoz and R. J. Martin, unpublished observations). Del Castillo *et al.* (1964*b*) also noticed that low GABA concentrations produced small, but statistically significant, depolarizations of the membrane. Dose ratios were calculated for each cell, as the ratio of EC_{50} values estimated for the GABA dose–response curves obtained in the absence and the presence of antagonist. Fig. 4A shows the dose–response curves for the traces shown in Fig. 3. The dose-dependent antagonism produced by SR42666 is illustrated in Fig. 5, and corresponding dose–response curves are illustrated in Fig. 6A. In Fig. 6A, ΔG_{max}

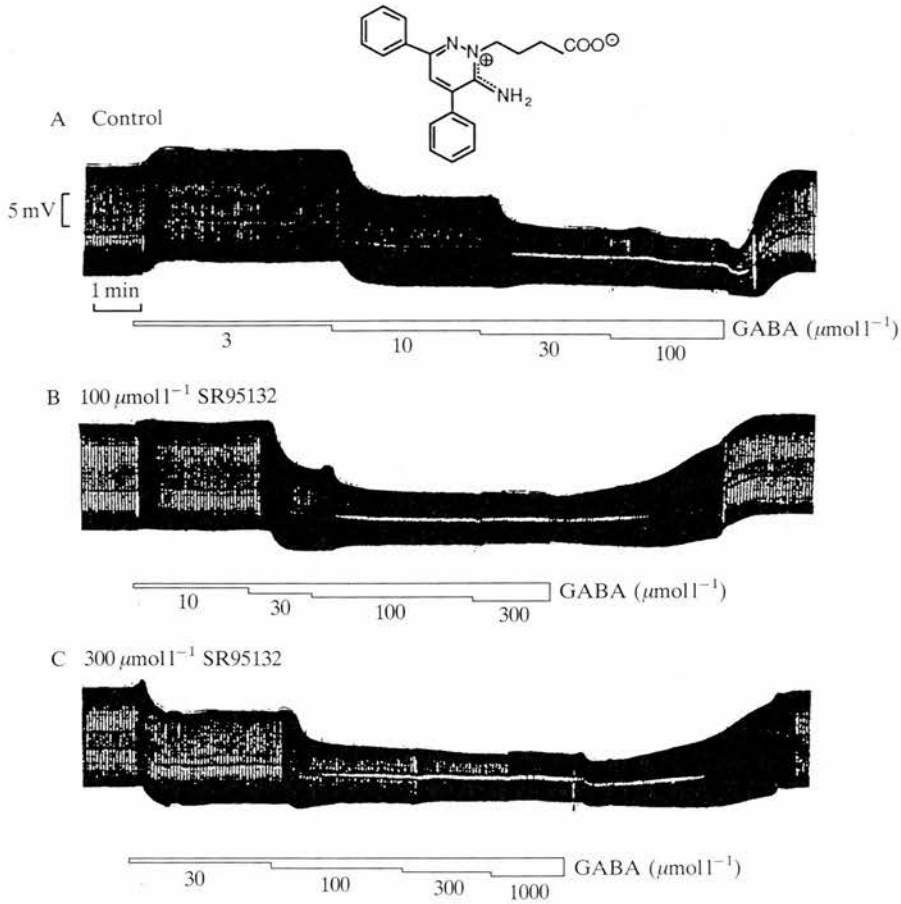


Fig. 3. Effects of 100 and 300 μmol l^{-1} SR95132 on the GABA dose–response relationship. (A) Control responses to cumulative application of GABA. Note the small depolarization observed with 3 μmol l^{-1} GABA where there was no detectable change in membrane input conductance. (B) The effect of 100 μmol l^{-1} SR95132. (C) The effect of 300 μmol l^{-1} SR95132. The corresponding dose–response curves are illustrated in Fig. 4. All three recordings were obtained from the same cell.

appears to be reduced in the presence of SR42666. This illustrates the difficulty in measuring high membrane conductance accurately. Errors made on ΔG measurements increase when the resistance decreases, so that the error in ΔG_{max} is large compared to the error in ΔG produced by lower concentrations of agonists. However, when results obtained from several cells are pooled, ΔG_{max} is not significantly affected by SR95103 (Duittoz and Martin, 1991*a*), SR42666 or SR95132.

The classical Schild plots for SR95132 (Fig. 4B) and SR42666 (Fig. 6B), log(DR−1) against log[X_B], were linear but with a slope different from 1: 0.73 for SR42666 (N=13) and 0.74 for SR95132 (N=9). However, the classical Schild plot

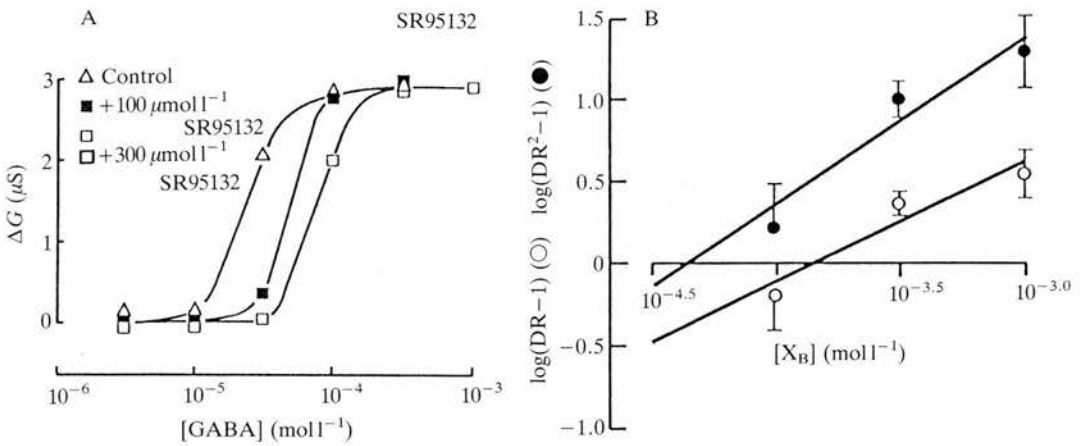


Fig. 4. Dose-dependency of the antagonism produced by SR95132. The lines correspond to the fitted modified Hill equation, whereas the points are the experimental data. (A) Dose–response curves for GABA. Control GABA dose–response curve (△); values estimated for the modified Hill equation are ΔG_{max}=2.8 μS, EC_{50}=19.8 μmol l^{-1}, n=2.6. Dose–response curve for GABA in the presence of 100 μmol l^{-1} SR95132 (■), values estimated for the modified Hill equation are: ΔG_{max}=2.8 μS, EC_{50}=37.6 μmol l^{-1} and n=3.2. Dose–response curve for GABA in the presence of 300 μmol l^{-1} SR95132 (□), values estimated for the modified Hill equation are: ΔG_{max}=2.8 μS, EC_{50}=77.2 μmol l^{-1} and n=3.5. (B) Schild and modified Schild plots; (○) Schild plot, log(DR−1)/log[X_B], where [X_B] is the concentration of antagonist. Correlation coefficient, r=0.71; slope=0.74±0.25, P=0.02 (F-test); $R^{\wedge 2}$=0.62. (●) Modified Schild plot, log(DR^2−1)/log[X_B]. Correlation coefficient r=0.75; slope=1.06±.32, P=0.01, (F-test); $R^{\wedge 2}$=0.66, suggesting a better fit than with the classical Schild plot. Values are mean±S.E., N=9.

does not account for a stoichiometry greater than 1 between GABA and its receptor. The modified Schild equation was therefore used (Williams *et al.* 1988), and log(DR^2−1) was plotted against log[X_B] (Figs 4B and 6B). This plot yielded a better fit for SR95132 ($R^{\wedge 2}$=0.66 against $R^{\wedge 2}$=0.62 for the Schild plot). The linear fit was not improved for SR42666 ($R^{\wedge 2}$=0.62), but, for both compounds, the slopes of the modified Schild plots were close to 1: 1.02 for SR42666 (N=13) and 1.06 for SR95132 (N=9). The interpretation of these linear regressions is limited, especially in terms of the goodness of fit, since only three concentrations of antagonist were used. A wider range of concentrations should be used for more reliable information. However, the use of higher concentrations of SR95132 and SR42666 was limited by the solubility of these compounds. Despite this, we believe that the use of the modified Schild analysis, rather than the classical one, is justified. The best argument is given by the strong evidence for bimolecular interaction between GABA and its receptor found in *Ascaris* (Holden-Dye *et al.* 1988) and more generally in vertebrate and invertebrate preparations (see Nistri and Constanti, 1979, for a review).

The results of the modified Schild analysis are apparently consistent with a

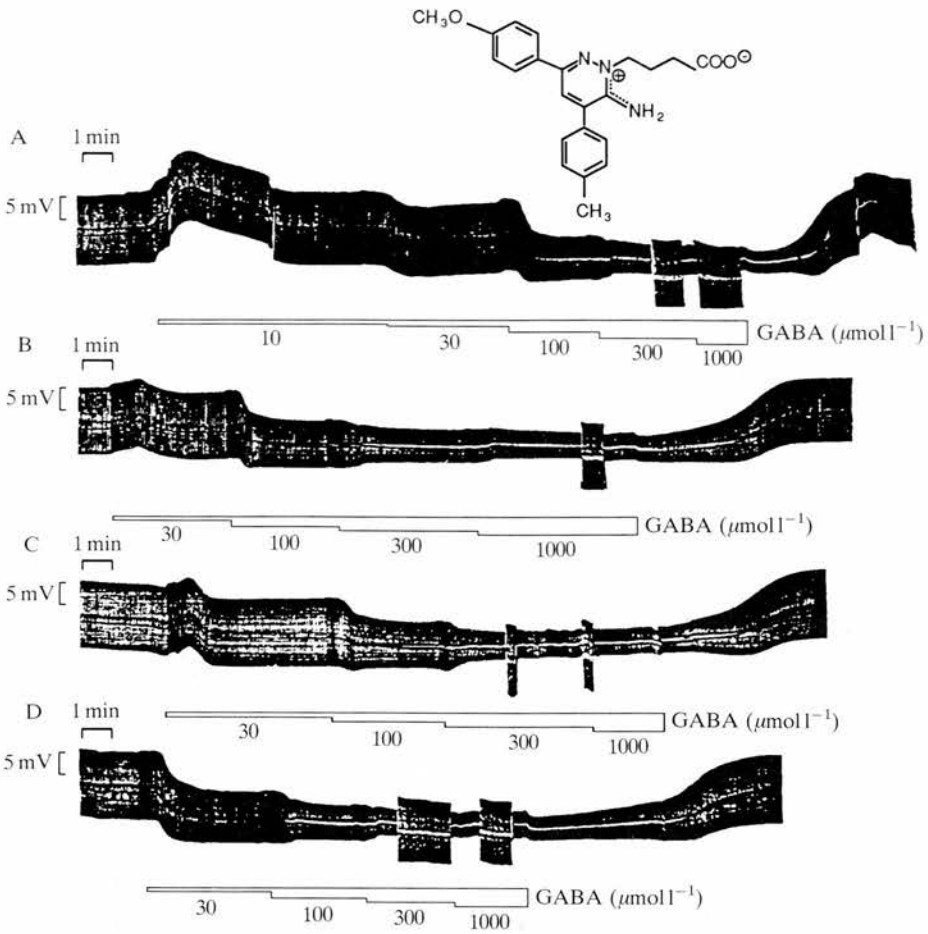


Fig. 5. Effects of 100, 300 and 1000 μmol l^{-1} SR42666 on the GABA dose–response relationship. (A) Control responses to cumulative application of GABA, G_0=2.2 μS. Note the transient depolarizing response in the presence of 10 μmol l^{-1} GABA and the temporary increase in gain from 5 mV to 2 mV per division during the application of 300 and 1000 μmol l^{-1} GABA. (B) In the presence of 100 μmol l^{-1} SR42666. Note the temporary increase in gain from 5 mV to 2 mV per division during the application of 1000 μmol l^{-1} GABA. (C) In the presence of 300 μmol l^{-1} SR42666. Note the temporary increase in gain from 5 mV to 2 mV per division during the application of 300 and 1000 μmol l^{-1} GABA. (D) In the presence of 1000 μmol l^{-1} SR42666. Note the gain changes in the presence of 300 and 1000 μmol l^{-1} GABA. The corresponding dose–response curves are illustrated in Fig. 6.

model that involves the activation of the receptor by two molecules of GABA but with only one molecule of SR42666 or SR95132 interacting with the receptor to block the effect. This is in agreement with previous results obtained with SR95103 (Duittoz and Martin, 1991*a*,*b*). Although these results do not establish such a mode of action, they provide a good quantitative description for the interaction

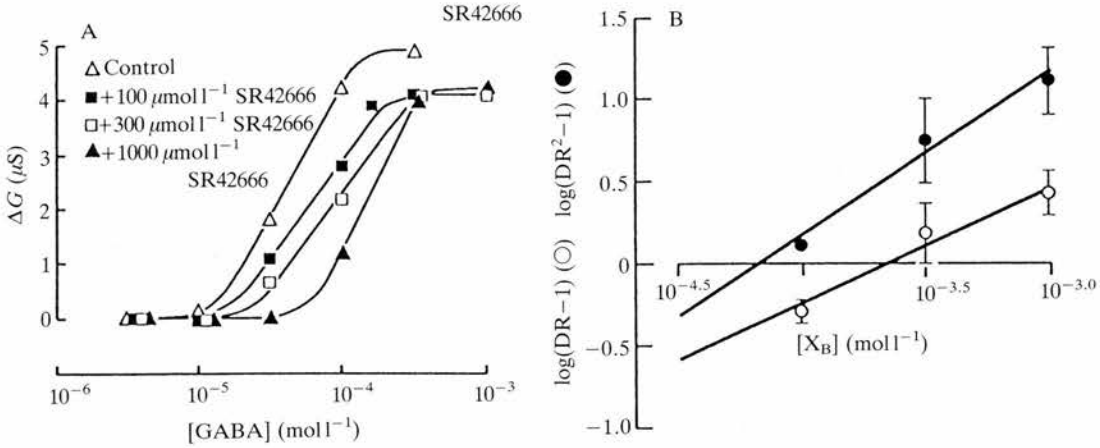


Fig. 6. Dose-dependency of the antagonism produced by SR42666. The lines correspond to the fitted modified Hill equation, whereas the points are the experimental data. (A) Dose–response curves for GABA. Control GABA dose–response curve (△); values estimated for the modified Hill equation are ΔG_{max}=4.9 μS, EC_{50}=39.9 μmol l^{-1}, n=2.1. GABA dose–response curve in the presence of 100 μmol l^{-1} SR42666 (■), values estimated for the modified Hill equation are ΔG_{max}=4.1 μS, EC_{50}=59.8 μmol l^{-1} and n=1.7. GABA dose–response curve in the presence of 300 μmol l^{-1} SR42666 (□), values estimated for the modified Hill equation are ΔG_{max}=4.3 μS, EC_{50}=89.7 μmol l^{-1} and n=1.8. GABA dose–response curve in the presence of 1000 μmol l^{-1} SR42666 (▲), values estimated for the modified Hill equation are ΔG_{max}=4.3 μS, EC_{50}=134.4 μmol l^{-1} and n=3.2. In this particular cell ΔG_{max} appears to be smaller in the presence of SR42666. However, in other cells, ΔG_{max} can be higher in the presence of SR42666 than for the control. This illustrates the difficulty in measuring high membrane conductance accurately. SR42666 and the other arylaminopyridazine GABA derivatives tested quantitatively did not affect ΔG_{max} or n significantly. (B) Schild and modified Schild plots; (○) Schild plot, log(DR−1)/log[X_B], where X_B is the concentration of antagonist. Correlation coefficient, r=0.78; slope=0.73±0.17, P=0.001 (F-test); R^2=0.62. (●) Modified Schild plot, log(DR^2−1)/log[X_B]. Correlation coefficient r=0.78; slope=1.02±.25, P=0.001, (F-test); R^2=0.62. Values are mean±S.E., N=13.

between antagonist and receptor, and allow the estimation of apparent dissociation constants. The dissociation constant, K_B, was estimated for the antagonists, assuming n=2 and M=1:

$$K_B = (DR^2 - 1)/K_B .$$

For SR42666, K_B=104.8±19.7 μmol l^{-1} (N=13); and for SR95132, K_B=65.0±20.3 μmol l^{-1} (N=9). SR95132 therefore appears equipotent to SR95103 (K_B=63.8±12.9 μmol l^{-1}, N=14, Duittoz and Martin, 1991*a*), whereas SR42666 is definitely less potent than SR95103 (t-test, $P \leqslant 0.05$). Since arylaminopyridazine GABA derivatives seem to act as competitive antagonist at the *Ascaris* GABA receptor, as they do at the vertebrate $GABA_A$ receptor, it is of interest to compare and discuss their respective structure–activity relationships.

Discussion

The measurement of the percentage of antagonism can be compared to a snapshot of the antagonist–receptor interaction, since only one concentration of antagonist and agonist are tested together. For that reason, it does not provide any information about the type of antagonism involved or any detailed quantitative information. However, within a family of compounds supposed to act in a similar manner, such as the arylaminopyridazine derivatives of GABA, the percentage of antagonism can be used to determine their potency sequence. The method is, nonetheless, a sensitive technique for detecting antagonism because the GABA concentration used, $30\,\mu mol\,l^{-1}$, is near to the EC_{50} for GABA and, therefore, in the middle of the linear part of the log dose–response curve.

When applied at $1\,mmol\,l^{-1}$ in the presence of $30\,\mu mol\,l^{-1}$ GABA, SR42627, SR42640, SR95133, SR95132, SR95103 and SR95531 present a potency order different from that observed at the vertebrate $GABA_A$ receptor (Wermuth *et al.* 1987). At the *Ascaris* GABA receptor the observed potency order is: SR95103≈SR95132>SR42666>SR95133>SR95531>SR42627>SR42640, whereas, at the mammalian $GABA_A$ receptor the potency order is: SR95531>SR42666>SR42627>SR95103>SR95133>SR42640>SR95132.

In *Ascaris*, the three most potent analogues, SR95103, SR95132 and SR42666, have been shown to displace GABA dose–response curves to the right without a decrease in the maximal response. The modified Schild analysis (Williams *et al.* 1988), which accounts for the positive cooperativity between GABA and its receptor, suggested a competitive mechanism in which only one molecule of the antagonist was required to block the effects produced by two molecules of GABA. In conclusion, on the basis of the results obtained with SR95103, SR95132 and SR42666, the mode of action of arylaminopyridazine derivatives of GABA in *Ascaris* is considered to be competitive. The difference in relative potencies of arylaminopyridazine GABA derivatives at the vertebrate and the *Ascaris* GABA receptors provides evidence for different structural requirements. The GABA-like moiety of the arylaminopyridazine derivatives, supposed to interact with the GABA recognition site on the GABA receptor, is the same for all the analogues tested here. The difference in relative potencies seen in *Ascaris* suggests that different parts of the molecule might be involved. The structure–activity relationships of pyridazine derivatives have been investigated in great details in the vertebrate nervous system (Wermuth *et al.* 1987) and discussed in terms of Ariëns' theory of accessory binding sites (Ariëns *et al.* 1979). In this theory, the substituents on the pyridazine ring play an important role in the binding of the antagonist to the receptor and in its potency.

In vertebrates, a very important role is played by the substituent in the 6-position (Wermuth *et al.* 1987). In the present study, all the analogues tested had a phenyl, substituted or not, in the 6-position on the pyridazine ring, except SR95133 (α-napthyl). The role played by the 6-substituent has been associated with the existence of additional binding interactions with the receptor, involving π electrons (Wermuth *et al.* 1987). The napthyl 6-substituent found in SR95133 also

presents π electrons for interaction with the receptor, and this may explain why SR95133 retains some antagonist properties.

The substituent effects on the 6-phenyl group can influence the potency. For example, substituents increasing the electron density ($-CH_3$, as in SR42627) on the aromatic system ($-OCH_3$, as in SR95531), increase the potency in mammalian preparations, in contrast to electron-withdrawing substituents (Wermuth *et al.* 1987). In vertebrates, the order of potency for the 6-phenyl substituents is $-OCH_3 > -CH_3 > -H$ (SR42666>SR42627>SR95103), and in *Ascaris* it is $-H > -OCH_3 > -CH_3$ (SR95103>SR42666>SR42627), suggesting an opposite effect. However, in *Ascaris*, the 6-phenyl substituent is not the limiting factor for the antagonist properties, the presence of a 4-substituent on the pyridazine ring is more important.

The role played by the 4-substituent in *Ascaris* is illustrated by the potent antagonists in *Ascaris*, SR95103, SR42666 and SR95132, which are all substituted on the 4-position of the pyridazine ring. This contrasts with the vertebrate preparations, where the substitution by a methyl or a phenyl group in the 4-position on the pyridazine ring was always detrimental to the antagonist potency (Wermuth *et al.* 1987). The order of potency for the 4-substituent is $-H > -CH_3 \gg -C_6H_5$ (SR95531>SR95103>SR95132). By comparison, in *Ascaris*, it is $-C_6H_5 \approx -CH_3 \gg -H$ (SR95132≈SR95103≫SR95531). To illustrate the importance of the 4-substituent in *Ascaris*, one can compare the potencies of SR42666 and SR95531: their chemical structure is identical except for the 4-methyl present in SR42666 but not in SR95531. SR42666 is more potent than SR95531 in *Ascaris*. This contrasts with mammalian preparations where SR95531 is more potent than SR42666. The presence of a 4-substituent appears to be a prerequisite for the antagonist potency of pyridazine GABA derivatives in *Ascaris*, whereas the opposite situation is found in vertebrates.

In vertebrates, computer graphic modelling of the pyridazinyl GABA derivatives and other known GABA antagonists was used to illustrate a plausible model for the interaction of competitive antagonists with the $GABA_A$ receptor (Wermuth and Rognan, 1987). The superimposition of various $GABA_A$ antagonists shows the existence of an anionic and a cationic system separated by a distance similar to that found in the GABA molecule (Wermuth and Rognan, 1987). The antagonist properties were explained by the presence of additional binding sites corresponding to the various aromatic or aliphatic rings of these compounds. Fig. 7 shows the superimposition of SR95531 and SR95132; the lack of activity of SR95132 on the vertebrate $GABA_A$ receptor was explained by the obstruction of the free access zone required for receptor recognition by the phenyl group in the 4-position (Wermuth and Rognan, 1987). Obviously this is not the case in *Ascaris*, where the presence of a substituent in the 4-position is apparently a requirement for the antagonistic activity.

The existence of different accessory binding sites responsible for antagonist properties in *Ascaris* would explain the weak activity of the classical competitive $GABA_A$ antagonists, such as bicuculline, pitrazepine, securinine (Holden-Dye

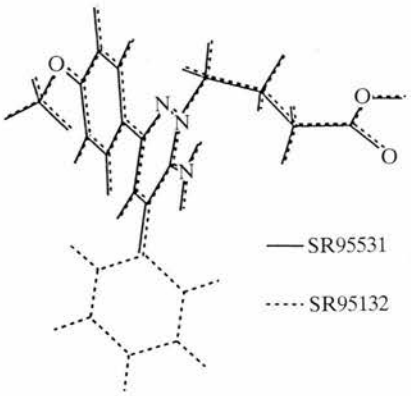


Fig. 7. Superimposition of SR95132 and SR95531. The superimposition of these two analogues shows that the 4-substituent is found in the proximity of the GABA recognition site. The inactivity of 4-substituted analogues at the vertebrate $GABA_A$ receptor was explained in terms of restriction of the free access zone required for interaction with the receptor. The volume occupied by the phenyl group of SR95132 is visualized. (Reproduced from Wermuth and Rognan, 1987, with permission.)

et al. 1988), tubocurarine and RU5135 (A. H. Duittoz and R. J. Martin, unpublished observations). The presence of alternative binding sites is not inconsistent with arylaminopyridazine derivatives acting as competitive antagonists, since the binding of the GABA-like moiety may be essential. In mammalian preparations, replacement of the GABA-like moiety by propionic, valeric or caproic acid analogues decreases the potency, although it does not lead to a complete loss of antagonistic activity (Wermuth *et al.* 1987). This suggests that the flexible side chain plays a role in the antagonist potency, but that a strict resemblance to GABA is not necessary. The existence of accessory binding sites on the GABA receptor is not the only possible explanation. For example, substituents on the pyridazine ring may influence the affinity of the antagonist for the GABA binding site, without binding to other parts of the receptor. In this case, the difference in relative potency seen between vertebrates and *Ascaris* would be explained by differences in the GABA binding site itself. However, agonist studies in *Ascaris* (Holden-Dye *et al.* 1989) have shown that the *Ascaris* muscle GABA receptor and the vertebrate $GABA_A$ receptor are correlated in terms of agonists properties, suggesting some structural similarities between the *Ascaris* and vertebrate GABA recognition sites. The hypothesis of different accessory binding sites on the *Ascaris* GABA receptor is, therefore, the most attractive one. Only a study of the molecular stucture of this receptor and its comparison to the structure of the vertebrate $GABA_A$ receptor would bring direct evidence for these putative sites.

These differences are obviously of great interest in the search for new anthelmintic drugs, and could lead to the synthesis of potent GABA antagonists to *Ascaris* GABA receptors, which are inactive in mammals and, therefore, without

toxicity or secondary effects in the host. Further characterization of the structure–activity relationships of pyridazine GABA derivatives may give rise to interesting developments in the future.

This work was supported by the Wellcome trust, the SERC and the Harriet Thompson scholarship. We thank Drs J. P. Chambon and M. Heaulme (Sanofi Recherche, France) for the gift of arylaminopyridazine GABA derivatives, and Dr C. Wermuth for helpful discussions.

References

Ariëns, E. J., Beld, A. D., Miranda, J. F. R. and Simonis, A. M. (1979). The pharmacon–receptor–effector concept. In *The Receptors*, vol. 1 (ed. H. Rang), pp. 33–91. New York: Plenum Press.

Arunlakshana, O. and Schild, O. (1959). Some quantitative uses of drug antagonists. *Br. J. Pharmac. Chemother.* **14**, 48–58.

Chambon, J. P., Feltz, P., Heaulme, M., Restle, S., Schliechter, R., Biziere, K. and Wermuth, C. G. (1985). Synthesis of SR95103, an arylaminopyridazine derivative of GABA. *Proc. natn. Acad. Sci. U.S.A.* **82**, 1832–1836.

Colquhoun, D. (1971). Non-linear curve fitting and the meaning of the best estimate. In *Lectures on Biostatistics* (ed. D. Colquhoun), pp. 257–272. Oxford: Clarendon Press.

Colquhoun, L., Holden-Dye, L. and Walker, R. J. (1989). 5-Nitro-2-(3-phenylpropylamino) benzoic acid (5-NPB) is a non-competitive antagonist at the *Ascaris* GABA receptor. *Br. J. Pharmac.* **97**, 369P.

Del Castillo, J., De Mello, W. C. and Morales, T. (1964*a*). Mechanism of the paralysing action of piperazine on *Ascaris* muscle. *Br. J. Pharmac.* **22**, 463–477.

Del Castillo, J., De Mello, W. C. and Morales, T. (1964*b*). Inhibitory action of γ-aminobutyric acid on *Ascaris* muscle. *Experientia* **20**, 141–143.

Del Castillo, J., Morales, T. and Sanchez, V. (1963). Action of piperazine on the neuromuscular system of *Ascaris*. *Nature* **200**, 706.

Duittoz, A. H. and Martin, R. J. (1991*a*). Effects of the arylaminopyridazine-GABA derivatives, SR95103 and SR95531, on the *Ascaris* muscle GABA receptor: the relative potency of the antagonists in *Ascaris* is different to that at vertebrate $GABA_A$ receptors. *Comp. Biochem. Physiol.* **98**, 417–422.

Duittoz, A. H. and Martin, R. J. (1991*b*). Effects of SR95103 on GABA-activated single-channel currents from *Ascaris suum* muscle. *Comp. Biochem. Physiol.* **98**, 423–432.

Eldefrawi, M. E. and Eldefrawi, A. T. (1987). Receptors for γ-aminobutyric acid and voltage dependent chloride channels as targets for drugs and toxicants. *FASEB J.* **1**, 262–271.

Heaulme, M., Chambon, J. P., Leyris, R., Molimard, J. C., Wermuth, C. G. and Biziere, K. (1986*a*). Characterization of three arylaminopyridazine GABA derivatives with the $GABA_A$ receptor site. *Brain Res.* **384**, 224–231.

Heaulme, M., Chambon, J. P., Leyris, R., Wermuth, C. G. and Biziere, K. (1986*b*). Specific binding of a phenylpyridazinium derivative endowed with $GABA_A$ receptor antagonist activity to rat brain. *Neuropharmac.* **25**, 1272–1283.

Holden-Dye, L., Hewitt, G. M., Wann, K. T., Krogsgaard-Larsen, P. and Walker, R. J. (1988). Studies involving Avermectin and the 4-aminobutyric acid (GABA) receptor in *Ascaris suum* muscle. *Pest. Sci.* **24**, 231–245.

Holden-Dye, L., Walker, R. J., Nielsen, L. and Krogsgaard-Larsen, P. (1989). Stereoselectivity of a bicuculline insensitive GABA receptor in *Ascaris suum* muscle. *Br. J. Pharmac.* **98**, 841–849.

Martin, R. J. (1980). The effects of γ-aminobutyric acid (GABA) on the input conductance and membrane potential of *Ascaris suum*. *Br. J. Pharmac.* **71**, 99–106.

Martin, R. J. (1982). Electrophysiological effects of piperazine and diethylcarbamazine on *Ascaris suum* somatic muscle. *Br. J. Pharmac.* **77**, 255–265.

MARTIN, R. J. (1985). γ-Aminobutyric acid and piperazine-activated single channel currents from *Ascaris* body muscle. *Br. J. Pharmac.* **84**, 445–461.

MARTIN, R. J. AND PENNINGTON, A. J. (1989). A patch-clamp study of effects of dihydroavermectin on *Ascaris* muscle. *Br. J. Pharmac.* **98**, 747–756.

NISTRI, A. AND CONSTANTI, A. (1979). Pharmacological characterization of different types of GABA and glutamate receptors in vertebrates and invertebrates. *Prog. Neurobiol.* **13**, 117–225.

SCHOFIELD, P. A. (1989). The $GABA_A$ receptor: molecular biology reveals a complex picture. *Trends pharmac. Sci.* **10**, 476–478.

TOSCANO-RICO, J. (1926). Sur la sensibilité de l'*Ascaris* à l'action de quelques drogues. *C.r. Séanc Soc. Biol.* **94**, 921–923.

WERMUTH, C. G., BOURGUIGNON, J. J., SCHLEWER, G., GIES, J. P., SCHOENFELDER, A., MELIKIAN, A., BOUCHET, M. J., CHANTREUX, D., MOLIMARD, J. C., HEAULME, M., CHAMBON, J. P. AND BIZIERE, K. (1987). Synthesis and structure activity relationships of a series of aminopyridazine derivatives of GABA acting as selective $GABA_A$ antagonists. *J. med. Chem.* **30**, 239–249.

WERMUTH, C. G. AND ROGNAN, D. (1987). Modélisation d'antagonistes des récepteurs $GABA_A$. *Actua. chim. Therap.* **14**, 215–229.

WILLIAMS, T. L., SMITH, D. A. S., BURTON, N. R. AND STONE, T. W. (1988). Amino-acid pharmacology in neocortical slices: evidence for bimolecular actions from an extension of the Hill and Gaddum–Schild equations. *Br. J. Pharmac.* **95**, 805–810.

The physiology and pharmacology of neuromuscular transmission in the nematode parasite, *Ascaris suum*

R. J. MARTIN, A. J. PENNINGTON, A. H. DUITTOZ, S. ROBERTSON *and* J. R. KUSEL*

*Department of Pre-clinical Veterinary Sciences, R.(D).S.V.S. University of Edinburgh, Edinburgh EH9 1QH and * Department of Biochemistry, University of Glasgow, Glasgow G12 8QQ*

SUMMARY

The organization of *Ascaris* motoneurones and nervous system is summarized. There is an anterior nerve ring and associated ganglia, main dorsal and ventral nerve cords which run longitudinally, and a small set of posterior ganglia. Cell bodies of motoneurones are found in the ventral nerve cord and occur in 5 repeating 'segments'; each contains 11 motoneurones. Seven morphological types of excitatory or inhibitory motoneurone are recognized.

Each *Ascaris* somatic muscle cell is composed of the contractile spindle; the bag region, containing the nucleus; the arm; and the syncytial region, the location of neuromuscular junctions. The resting membrane potential of muscle is approximately −30 mV and shows regular depolarizing, Ca-dependent 'spike potentials' superimposed on smaller Na^+- and Ca^{2+}-dependent 'slow waves' and even slower 'modulation waves'. The membrane shows high Cl^- permeability. Adjacent cells are electrically coupled so that electrical activity in the cells is synchronized. Acetylcholine (ACh) and γ-aminobutyric acid (GABA) affect the electrical activity. Bath-applied ACh increases membrane cation conductance, depolarizes the cells, alters the frequency and amplitude of spike potentials and produces contraction. Bath-applied GABA increases Cl^- conductance, decreases spike activity and causes hyperpolarization and muscle relaxation.

The extra-synaptic ACh receptors on the bag region of *Ascaris* muscle can be regarded as a separate subtype of nicotinic receptor. ACh and anthelmintic agonists (pyrantel, morantel, levamisole) produce a dose-dependent increase in cation conductance and membrane depolarization which is blocked by tubocurarine, mecamylamine but not by hexamethonium. The potency of GABA agonists, with the exception of sulphonic acid derivatives, correlates with the vertebrate $GABA_a$ receptor. The potency of antagonists does not. Thus, bicuculline, securinine, pitrazepine, SR95531 and RU5135 are potent vertebrate $GABA_a$ antagonists but have little effect on GABA receptors. The potency order of the arylaminopyridazine GABA antagonists: SR95103, SR95132, SR42666, SR95133, SR95531, SR42627 and SR42640 at the *Ascaris* GABA receptors contrasts with that at vertebrate $GABA_a$ receptors. It has been suggested that the receptor is referred to as a $GABA_n$ receptor.

Patch-clamp studies show that ACh activates a non-selective cation channel which has a main conductance of 40–50pS and apparent mean open time of 1·3 ms; a smaller channel of 20–30 pS with a similar open-time is also activated. Pyrantel and levamisole also produce openings with similar conductances and open-times. GABA activates a Cl^- channel with a main state conductance of 22 pS and an apparent mean open duration of 32 ms; conductance states of 10 and 15 pS are also seen. Piperazine similarly activates this channel but the mean open-time is shorter (14 ms). Ivermectin in high doses, is an antagonist which reduces the GABA channel conductance and P_{open}; it does, however, open 'small' Cl^- channels when applied to the outside surface of membrane. These channels have a conductance of 9–15 pS and very long open times (> 100 mS). 5-HT does not have a direct effect on membrane potential or conductance but acts on cAMP levels and glycogen metabolism. Dopamine, octopamine and AF1 may act as neurotransmitters or neuromodulators.

Key words: *Ascaris suum*, neuromuscular transmission, electrophysiology, pharmacology, anthelmintics.

INTRODUCTION

Estimates of global parasitism in the human population show that *Ascaris* may affect more than 1000 million people and give rise to considerable suffering in Third World countries as well as affecting the growth and performance of livestock (see for example, Horton, 1990). The treatment of nematode infections in man and animals with anthelmintic drugs plays a vital role in the control of these parasites.

The adult *Ascaris suum* is a common, large (up to 30 cm) nematode parasite found in the intestine of the pig. The frequent occurrence of this parasite means that it can be collected from local abattoirs on a weekly basis for study in the laboratory. The large size of the parasite, its muscle cells and some of its neurones have facilitated anatomical, biochemical, physiological and pharmacological studies, not possible on smaller nematodes. *A. suum* has been used frequently and successfully for examining the mode of action of a variety of anti-nematodal drugs.

A number of anthelmintics interfere selectively with neuromuscular transmission of the nematode parasite. The purpose of this paper is to review the physiology and pharmacology of neuromuscular transmission in the nematode parasite *A. suum*, and to provide a background useful for designing, testing and understanding the mode of action of anti-nematodal drugs.

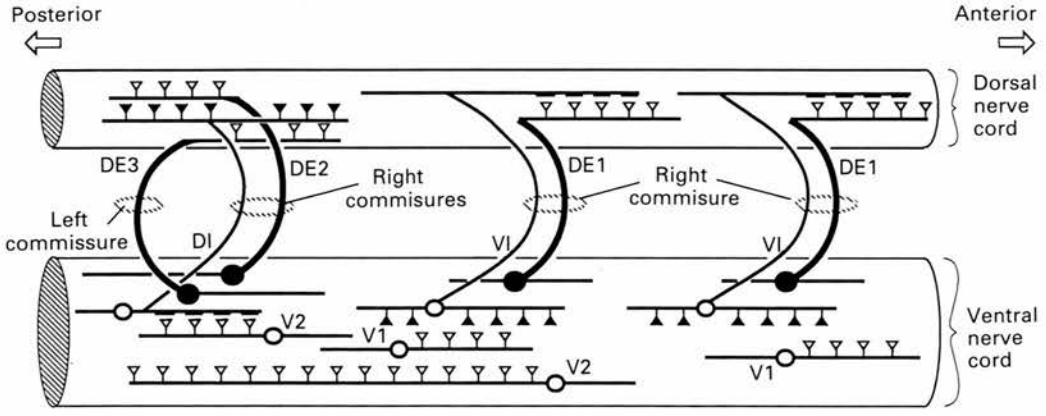


Fig. 1. Summary diagram of the anatomical organization of *Ascaris* motoneurones in one 'segment'. Eleven motoneurones are present in each 'segment'. There are 7 anatomical types, but only 2 physiological types (E, excitatory, cholinergic; I, inhibitory, GABAergic). DE1, dorsal excitor 1; DE2, dorsal excitator 2; DE3, dorsal excitator 3; DI, dorsal inhibitor; VI, ventral inhibitor; V1 and V2 ventral (excitatory) motoneurones. The cell bodies of all motoneurones are in the ventral cord. The commissures contain 1 or 2 axons and pass round the body wall.

LOCOMOTORY BEHAVIOUR

The body movements made by adult *Ascaris* allow the parasite to maintain its position in the pig intestine and alter the position of the head for feeding. Coordinated waves of contraction and relaxation, in the dorso-ventral plane only, can propagate anteriorly or posteriorly. The most common wave is of large amplitude, which propagates anteriorly and starts about half-way along the length of the animal near the vulva. This waveform gives rise to forward propulsion of the *Ascaris* when contained within a tube structure like the intestine (Johnson & Stretton, 1980). The more complex behaviour of the head is believed to be under the control of the cranial ganglia and sublateral nerve cords.

NERVOUS SYSTEM

Basic structure of Ascaris *nervous system*

Early studies of the nervous system of *Ascaris* (Hesse, 1892; Goldschmidt, 1908, 1909) showed that there are only a small number of neurones present (*ca.* 250) and that these are completely reproducible from animal to animal.

Goldschmidt (1908) described an anterior nerve ring, surrounding the pharynx with a series of associated ganglia. The ganglia associated with the circumferential nerve ring are the dorsal ganglion, the ventral ganglion, the two lateral ganglia, and the retrovesicular ganglion. The anatomy and electrophysiology of the retroversicular ganglia have been examined by Angstadt, Donmoyer & Stretton (1989); this ganglion containing 13 neurones, which are interneurones (including the neurones named AVF-, GAB-, RIF- and RIG-like) or motoneurones (DE2 and V2). The two main nerve cords arising from the nerve ring pass caudally to form the dorsal and ventral nerve cords; motoneurones are found scattered in the ventral nerve cord; and a second set of ganglia is found in the tail region (Goldschmidt, 1908, 1909). The nerve cords are connected by single or double transverse fires forming commissures (Hesse, 1892).

Stretton *et al.* (1978) described and classified the structure and physiology of motoneurones; they based their observations on tracing nerve fibres in serial sectors, and on intracellular recordings from muscle bags during electrical stimulation. The motor nervous system was divided into segments. Each segment usually has three right-hand commissures and one left-hand commissure (Fig. 1), and contains 11 motoneurones with 6 non-segmental interneurones crossing the segments. Each motoneurone cell body has two processes; one of the processes may have a single branch. The 11 motoneurones were separated into 7 types according to the distribution of their axon and dendrites: three types (DI, DE2 and DE3) are represented only once in each segment, while the remaining four types (DE1, VI, V1 and V2) occur twice in each segment (Fig. 1).

Excitatory and inhibitory potentials recorded in muscle after selective stimulation showed that DI and VI were inhibitory and that the remainder were, or were likely to be, excitatory (Stretton *et al.* 1978). Histochemical studies showed that choline acetyltransferase was present in DE1, DE2 and DE3 motoneurones, a finding consistent with the suggestion that acetylcholine is the excitatory neurotransmitter (Johnson & Stretton, 1985). GABA-immunoreactivity has been identified in the inhibitory motoneurones, DI and VI (Johnson & Stretton, 1987; Sithigorngul *et al.* 1989), a finding consistent with the suggestion that GABA is the inhibitory neurotransmitter.

The motoneurones of *Ascaris* are structurally

similar to motoneurones identified in *C. elegans* (White *et al.* 1976, 1986), suggesting that all nematodes may be organized in a similar way. Additional minor nerve cords in *Ascaris* have also been described (Johnson & Stretton, 1987). They include dorsal lateral, dorsal sublateral, ventral sublateral, and ventral lateral nerve cords which are all found adjacent to the lateral line.

Non-spiking motoneurones of Ascaris

Electrical stimulation of single motoneurons in dissected preparations did not produce all-or-none responses in muscle cells but responses which were graded with the intensity of the stimulus (Walrond *et al.* 1985); this implies that *Ascaris* motoneurons are non-spiking. Direct intracellular records from commissures confirmed the non-spiking nature of motoneurones; it showed that the neuronal membrane has a high resistance (61–251 $K\Omega$ cm^{-2}) and a long space constant (4–10 mm), suitable for passive conduction over long distances (Davis & Stretton, 1989*a*). Another property of the neuronal membrane is the presence of voltage-activated Ca^{2+} currents, which occur at the resting membrane potential; these currents may give rise to the tonic release of the neurotransmitter acetylcholine (Del Castillo, De Mello & Morales, 1963; Davis & Stretton, 1989*b*). The Ca^{2+} currents in *Ascaris* remain to be typed physiologically or pharmacologically and it is not known if they correspond to the vertebrate *T*, *L* or *N* type of Ca^{2+} channels.

Physiological interconnections of motoneurones

Walrond & Stretton (1985) showed, with the dissected preparation, that stimulation of the dorsal excitatory motoneurone, DE1, produced reciprocal inhibition in ventral muscle cells as a result of the projection onto the ventral inhibitory motoneurone, VI. They further showed that the motoneurones, DE2 and DE3 could also produce reciprocal inhibition as a result of projecting onto VIs in adjacent segments. Reciprocal inhibition in the ventral cord was suggested on anatomical grounds involving the putative excitatory motoneurones V1 and V2 and their projection onto the dorsal inhibitory motoneurone DI. In their paper, Walrond & Stretton (1985) demonstrated that stimulation of DE1, DE2 and DE3 produced, via a projection onto DI, inhibition in muscle fields adjacent to the dorsal excitatory field. The consequence of this synaptic organization, with reciprocal and adjacent inhibition, is that stimulation of a single excitatory motoneurone would produce an omega-shaped body waveform. This synaptic organization provides a basis for a model which can produce propagated waves of muscle contraction.

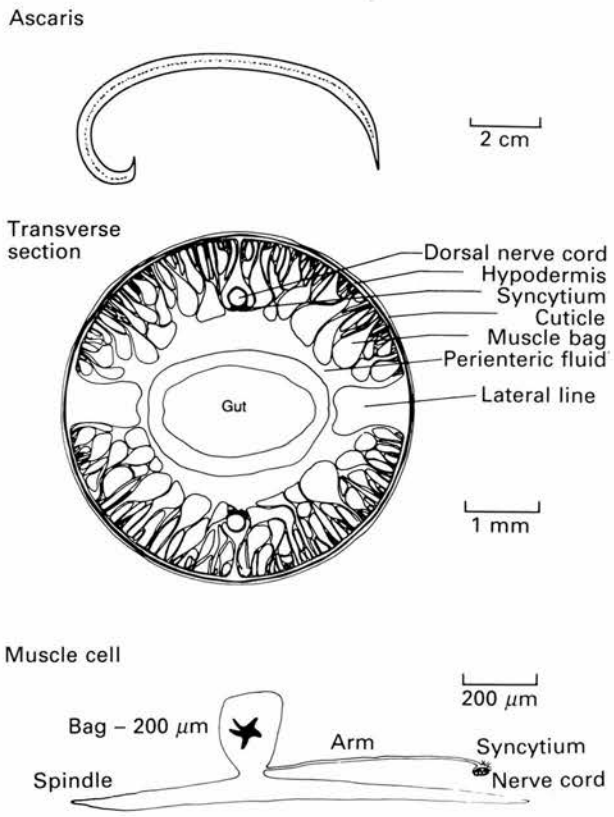


Fig. 2. *Ascaris*: transverse section through anterior region; muscle cell structure.

MUSCLE

Anatomy

Morphology of somatic muscle cells. The anatomy of *A. suum* body muscle was described as early as 1866 by Schneider (1866). It was then the subject of debate by several scientists (Goldschmidt, 1908, 1909; Cappe de Baillon, 1911) because of its unusual structure, with branches of the muscle passing to the nervous system, rather than branches of the nervous system reaching the muscles.

Fig. 2 shows in diagrammatic form the structure and location of *Ascaris* somatic muscle. There is the longitudinal contractile region, known as the spindle ('fuseau', Cappe de Baillon, 1911); it lies under the hypodermis and is composed of 'obliquely striated muscle' (Rosenbluth, 1965*a*, *b* 1967, 1969). Its striations form an acute angle, rather than the usual 90° of skeletal muscle, because of the different organization of thick and thin filaments. This organization allows the greater extensibility of smooth muscle and maintains the velocity of contraction of skeletal muscle. In *Ascaris*, fast twitch contraction is associated with Ca^{2+} fixation by actin, and is produced by acetylcholine; muscle relaxation is associated with a change in the phosphorylation state of light chain myosin (Martin & Donahue, 1987). The bag or belly ('panse', Cappe de Baillon, 1911) is a large 200 μm bag-shaped structure which

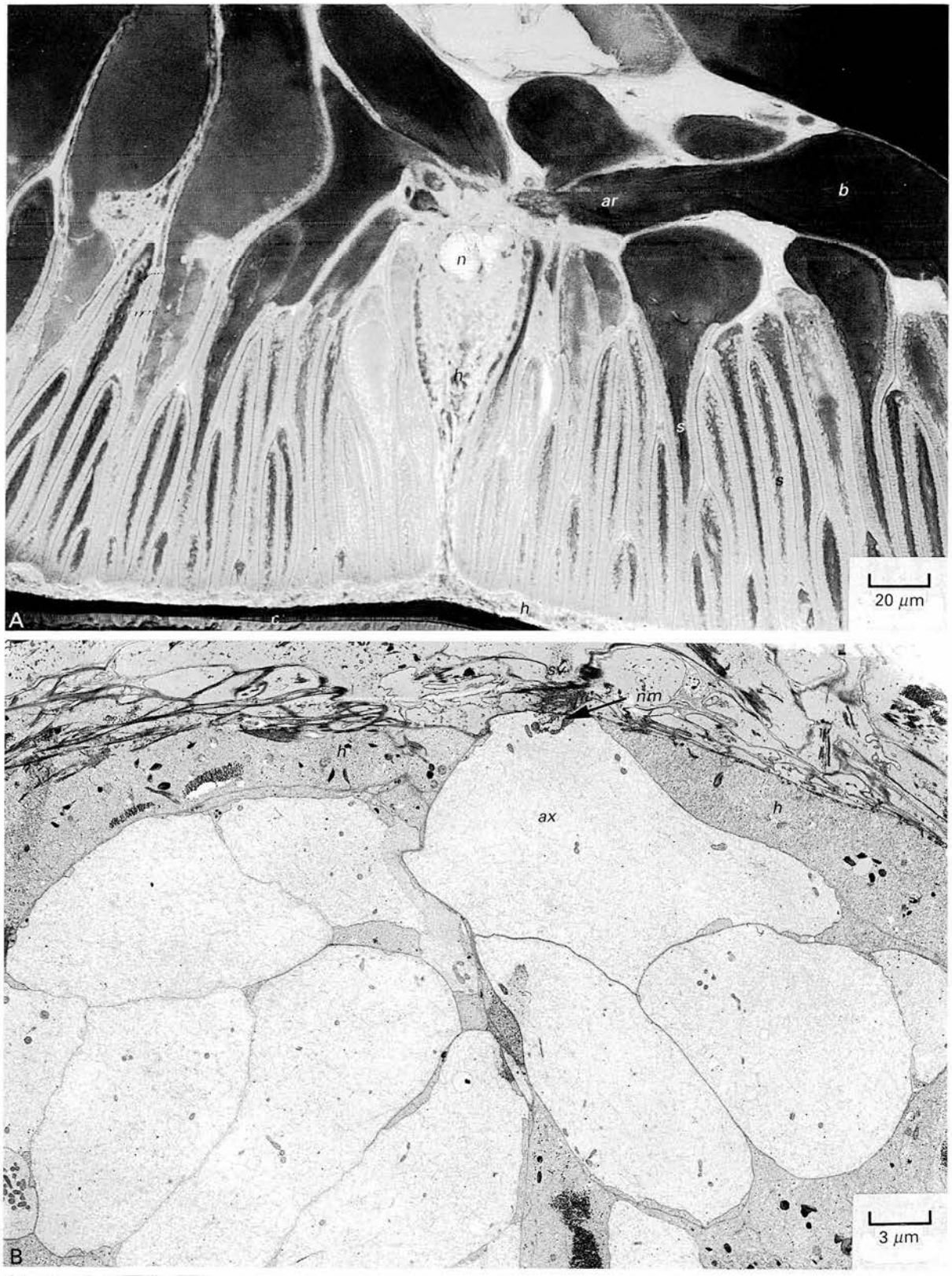


Fig. 3. (A) Photo-micrograph of nerve cord and muscle. *ar*; arm; *b*, bag; *s*, spindle; *h*, hypodermal chalice and hypodermis; *c*, outer and inner lamella of cuticle. (B) Transmission electron-micrograph of the dorsal nerve cord. *sy*, syncytium; *h*, hypodermis; *ax*, axon of motoneurone; *nm*, neuromuscular junction.

contains submembrane mitochondria, the nucleus and particulate glycogen (Rosenbluth, 1965*b*); it lies in the perienteric space (Fig. 2).

Each somatic muscle cell of *Ascaris* has on average 2·7 arms (Stretton, 1976). The arm is a thin process which arises from the base of the bag and passes to the syncytium which lies over the nerve cord (Fig. 2). When the arms reach the syncytium, they break

up into a number of fine processes or 'fingers'. Tight junctions are found between adjacent arms of the muscle cells at the syncytium (Rosenbluth, 1965b) and they are responsible for the electrical coupling seen between adjacent cells (De Bell, Del Castillo & Sanchez, 1963). Neuromuscular junctions (Fig. 3) are found between the syncytial region and a longitudinally-running axon of a motoneurone (Rosenbluth, 1965*b*). The neuromuscular junctions are formed by 2 μm extensions of the longitudinal axons which penetrate the hypodermal chalice and closely approach the syncytium. The synaptic region is associated with clear spherical 40 nm vesicles clustered under the pre-synaptic membrane; dense core vesicles, 80–100 nm in diameter; giant mitochondria; and membrane thickenings on the pre-synaptic and post-synaptic membrane (Rosenbluth, 1965*b*). Except in the head region, the dorsal muscle cells are only connected to the dorsal nerve cord, the ventral muscle cells are only connected to the ventral nerve cord; this arrangement is consistent with contraction which is only possible in the dorso-ventral plane.

Electrophysiology

Electrical activity of muscle cells. Jarman (1959) was the first to make intracellular recordings from *Ascaris* muscle cells. He described the presence of regular spontaneous depolarizing potentials superimposed on a resting potential of around -30 mV. The ionic basis of the low resting potential has been investigated by Del Castillo, De Mello & Morales (1964*a*) and Brading & Caldwell (1971). In both studies, extracellular K^+ had little effect on potential, in contrast to the effects of extracellular Cl^- and, to a lesser extent, Na^+. Ion flux experiments of Caldwell & Ellory (1968) showed that the permeability ratio for K^+, Na^+ and Cl^- was 1:4:7, respectively. These studies failed to provide a satisfactory explanation for the behaviour of the membrane potential. Brading & Caldwell (1971) suggested that an active electrogenic pump, possibly moving carboxylic acids, may explain why the original Goldman–Hodgkin–Katz equation was not sufficient for describing the behaviour of the membrane potential. Caldwell (1974) subsequently considered this problem in a review. The composition of peri-enteric fluid, which normally surrounds the muscle cells, is consistent with this hypothesis. Hobson *et al.* (1952*a*, *b*) found the peri-enteric fluid to contain low concentrations of Cl^- but high concentrations of volatile fatty acids. The volatile fatty acids (including 2-methyl butyrate and 2-methyl valerate) are produced from the anaerobic metabolism of glucose (Saz & Weil, 1962; Tsang & Saz, 1973).

The spontaneous depolarizing potentials described by Jarman (1959) were shown to be myogenic in origin and to arise at the syncytium (De Bell, 1965; De Bell *et al.* 1963). Three types of depolarizing potential have now been described (Fig. 4): (a) spikes of varying amplitude up to 30 mV and lasting 5–50 ms (De Bell *et al.* 1963; Weisblat & Russel, 1976); (b) slow waves up to 20 mV in amplitude and lasting 100–1000 ms (De Bell *et al.* 1963: Weisblat & Russel, 1976); and (c) a long lasting modulation wave around 5 mV, lasting 3–20 s and coinciding with contraction of the body wall (Weisblat & Russel, 1976).

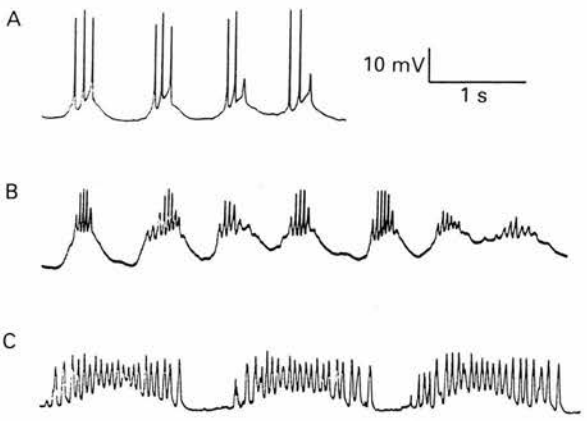


Fig. 4. Spontaneous electrical activity in a muscle cell at 37 °C. (A and B) Spikes and slow waves. (C) Modulation waves. Calibration bars 10 mV and 1 s in A and B; 10 mV and 12 s in C. Modified from Weisblat & Russel (1976).

Ion substitution experiments have shown that Ca^{2+} currents are responsible for the spikes and that both Na^+ and Ca^{2+} currents can produce the slow waves (Weisblat, Byerly & Russel, 1976). The Ca^{2+} spikes were not blocked by the Na^+ channel blocker, tetrodotoxin (Jarman & Ellory, 1969), and the Ca^{2+} channel blockers, verapamil and cinnarizine unexpectedly had no effect either; however, 'high concentrations' of ivermectin did block spiking (Wann, 1987). K^+ currents, activated by depolarization (Martin, 1982), may facilitate repolarization; these K^+ currents are blocked by 4-aminopyridine and the anthelmintic, diethylcarbamazine (Martin, 1982). The ionic basis of the modulation waves, inferred from the behaviour of 'square waves', suggests that Ca^{2+} currents are involved (Weisblat *et al.* 1976).

Jarman (1959) showed that the electrical activity seen in adjacent muscle cells was correlated. He found that anteriorly placed cells depolarized before cells behind them; he also found that cells nearest to a nerve cord depolarized before those placed laterally. De Bell *et al.* (1963) and Del Castillo *et al.* (1967, 1989) have used two intracellular micropipettes with current injection to record the electrical coupling which occurs between adjacent muscle cells. The coupling is consistent with the presence of tight junctions seen with the electron microscope (Rosenbluth, 1965*b*). Initial studies on the coupling

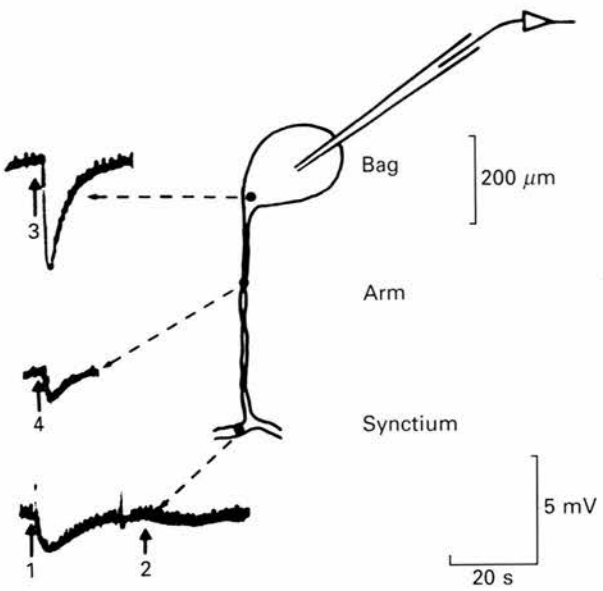


Fig. 5. Demonstration of synaptic and extrasynaptic GABA receptors by ionophoresis of GABA onto different regions of muscle cell. 0·4 nC, at the vertical arrow, was used to deliver GABA to the positions marked while the membrane potential was monitored in the bag. The effect at the syncytium was measured first (1). Then the ionophoresis pipette raised 50 μM (2) where a smaller response was seen. The largest response was seen at the bag (3) but a small response also occurred over the arm (4).

coefficients by Del Castillo *et al.* (1989) showed that the average coupling coefficient was 0·4 for cells oriented perpendicular to the long axis, but cells oriented parallel to the long axis showed no coupling. Physiological manipulation of this coupling remains to be demonstrated, although impairment of cell–cell coupling by bath-applied GABA has been demonstrated (De Mello & Maldonado, 1985).

Ascaris *muscle has acetylcholine and GABA receptors.* Initially, Baldwin & Moyle (1949) and later Norton & De Beer (1957) showed that both-applied acetylcholine produces contraction of muscle strips and, therefore, demonstrated the presence of acetylcholine receptors on muscle. Although at this time, piperazine was shown to produce reversible paralysis of *Ascaris in vitro* (Standen, 1955), it was not until Del Castillo *et al.* (1964*b*, *c*) demonstrated the hyperpolarizing effect of piperazine and GABA that inhibitory GABA receptors on muscle were recognized.

Bath-applied acetylcholine depolarizes and changes spike frequency and amplitude in muscle (Del Castillo *et al.* 1963); ionophoresis experiments have revealed that the receptors responsible for this are located synaptically at the synctial region (Del Castillo *et al.* 1963; Martin, 1982) and extrasynaptically on the bag region of the muscle (Martin, 1982). Bath-applied GABA produces hyperpolarization of muscle membrane (Del Castillo *et al.* 1964*a*; Martin, 1980) and ionophoresis experiments have shown that the GABA receptors responsible for this are at the syncytium and extrasynaptically over the surface of the rest of the cell including the bag region (Fig. 5) (Martin, 1980). The physiological function of the extrasynaptic acetylcholine and GABA receptors is not known, but they may be exploited in pharmacological experiments designed to look at receptor properties; they may also be activated by anthelmintics during therapy of the host animal.

Ionic basis of the electrical responses to acetylcholine and GABA. The ionic basis of electrical responses to acetylcholine and GABA have been investigated by applying transmitter ionophoretically to the bag region of the muscle cell and making current- or voltage-clamp records of the responses. Acetylcholine increases the non-selective cation conductance of the membrane with a reversal potential near O mV (Martin, 1982; Harrow & Gration, 1985). This is compatible with acetylcholine opening ion-channels permeable to both Na^+ and K^+. Ionophoresis of GABA onto the bag, on the other hand, produces a current which has a reversal potential near −65 mV and which is explained by the opening of ion-channels permeable to Cl^- ions (Martin, 1980).

Biochemistry

Biochemistry of acetylcholine. The presence of acetylcholine in *Ascaris* was first described by Mellanby in 1955. Choline acetyltransferase (CAT), the enzyme responsible for the synthesis of acetylcholine has been demonstrated in the commissural branches of the excitatory motoneurones as well as in the hypodermis (Johnson & Stretton 1980, 1985). The presence of CAT in the excitatory motoneurones is consistent with acetylcholine being the transmitter. The function of CAT in the hypodermis is not clear, but it has been suggested that the synthesis and release of acetylcholine from the hypodermis may cause tonic contraction by acting on extrasynaptic ACh muscle receptors (Johnson & Stretton, 1980). The hypodermal CAT has also been reported to be concentrated in two bands within 1 mm of the tip of the head, but the physiological function of this remains obscure (Johnson & Stretton, 1980).

Cholinesterase, the enzyme inactivating acetylcholine, was first reported in *Ascaris* by Bueding (1952). Lee (1962) described the distribution of this enzyme using histochemical techniques; in the head region, most of the activity was associated with the contractile region of the muscle in the extracellular matrix; enzyme activity was also observed in muscle arms near their endings on the nerve cords but not on the bag region; little or no staining was seen in the

Table 1. Potency of cholinergic agonists and antagonists in *Ascaris*
(Baldwin & Moyle (1957): lowest concentration producing contraction. Natoff (1969): range of agonist concentrations producing contraction; antagonist K_D. Rozhkova *et al.* (1980): EC_{50} muscle contraction; antagonist K_D. Harrow & Gration (1985): EC_{50} input conductance. Colquhoun *et al.* (1990): relative potency for agonists; IC_{50} for antagonists.)

	Contraction muscle strip			Electrophysiology input conductance	
	Baldwin & Moyle (1957) (μM)	Natoff (1969) (μM)	Rozhkova *et al.* (1980) (μM)	Harrow & Gration (1985) (μM)	Colquhoun *et al.* (1990)
Agonists					
Morantel	–	—	—	0·4	—
Pyrantel	—	—	—	0·4	—
Dimethylphenylpiperazinium	—	0·2–0·6	0·7	—	2
Pentyltrimethylammonium	—	—	1·1	—	—
Levamisole	—	—	—	20	—
Acetylcholine	1	6–55	6·1	110	1
Propionylcholine	—	2	—	—	—
Succinylcholine	—	—	3·1	—	—
Nicotine	1	2–38	3·5	—	0·3
Carbachol	—	5–55	4·1	—	0·5
Trimethylammonium	—	—	2·9	—	0·05
Muscarine	—	—	—	—	0·006
Furtrethonium	—	—	—	—	0·007
Arecoline	—	—	—	—	0·002
Suberyldicholine	—	—	4·7	—	—
Decamethonium	—	73–366	—	—	—
Antagonists					
N-methyllycaconitine	—	—	—	—	0·23
Bungarotoxin	—	—	—	—	1·4
Mecamylamine	—	0·25	—	—	0·33
Strychnine	100	—	—	—	1·29
Tubocuraine	100	2·34	0·5	—	3·1
Tetraethylammonium	—	—	6·0	—	—
Pancuronium	—	—	—	—	3·2
Atropine	—	80	80	—	6·7
Decamethonium	—	—	—	—	14
Hexamethonium	—	—	40	—	43

nervous tissue. No staining was seen caudal to the vulva, an observation consistent with propagation of contraction waves starting at the vulva and passing anteriorly. Johnson & Stretton (1980) have reported the presence of two types of cholinesterase, a 13 S and 5 S form, which are not distributed in the same way; the 5 S fragment may be regulated by muscle activity, but the 13 S fragment may not. Although cholinesterase is responsible for the breakdown of acetylcholine released from excitatory motoneurones, it is also secreted in the external environment by *Ascaris* and has been suggested to act as a 'biochemical holdfast' by blocking local peristalsis (Lee, 1970).

Neostigmine, a carbamate anti-cholinesterase in other preparations has an acetylcholine-potentiating effect in *Ascaris* (Del Castillo *et al.* 1963). Selective organophosphorous anti-cholinesterases, including metrifonate and haloxon (Martin, 1985*a*), are used as effective anthelmintics. The use of these compounds against nematodes shows cholinesterase to be an effective target site for anthelmintics.

Pharmacology

Pharmacology of the acetylcholine receptor. Initial experiments on the pharmacology of *Ascaris* acetylcholine receptors used contraction of muscle strips. Low concentrations of nicotine produced contraction (Toscano-Rico, 1926; Baldwin & Moyle, 1949; Natoff, 1969) like acetylcholine (Baldwin & Moyle, 1949; Natoff, 1969; Rozhkova, Malyutina & Shishov, 1980; Grzywacz, Szkudlinsks & Zandarowska, 1985; Onuaguluchi, 1989). The acetylcholine-induced contractions were blocked by tubocurarine but not by atropine (Baldwin & Moyle, 1949; Natoff, 1969; Rozhkova *et al.* 1980) so that the *Ascaris* acetylcholine receptor has some of the pharmacological properties of the vertebrate nicotinic receptor.

Natoff (1969) and Rozhkova *et al.* (1980) attempted to classify the receptor as either ganglionic or neuromuscular. These papers showed that the potent ganglionic nicotinic agonist, dimethylphenylpiperazinium (DMPP) is more potent than acetylcholine in *Ascaris*; the potent ganglionic nicotinic antagonist

Table 2. $GABA_a$ agonists potency in *Ascaris*
(Duittoz & Martin (1990): EC_{50} Input conductance dose–response curves described by the modified Hill equation with the estimated Hill coefficient between 2 and 4; the relative potency is given in parentheses; means ± S.E., $n = 3$–13; Holden-Dye *et al.* (1988, 1989): relative potency.)

Agonist*	EC_{50}, μM (rel. potency)†	Rel. potency‡
S-(+)-dihydromuscimol ± dihydromuscimol	8·3 ± 1·5 (3·704)	7·53
ZAPA	24·1 ± 4·6 (1·266)	1·46
GABA	30·7 ± 2·1 (1·000)	1
R-(−)-dihydromuscimol	—	0·85
TACA	65·7 ± 14·5 (0·467)	0·55
R-(−)-3-OH-GABA	—	0·25
IAA	76·1 ± 11·3 (0·403)	0·20
Muscimol	82·5 ± 20·4 (0·372)	0·55
Isoguvacine	124·2 ± 10·1 (0·247)	0·19
S-(+)-3-OH-GABA	—	0·13
GuAA	135·1 ± 18·0 (0·227)	0·16
Homo-beta-proline	233·6 ± 37·2 (0·131)	—
DAVA	366·5 ± 17·6 (0·084)	0·079
CACA	391·8 ± 83·2 (0·078)	0·031
Isonipecotic acid	409·2 ± 83·2 (0·075)	—
BGuPA	536·5 ± 49·7 (0·057)	0·085
THIP	N.A.	0·006
S-(−)-4-methyl-TACA	—	0·007

* GABA, gamma-amino butyric acid; DHM, dihydromuscimol; ZAPA, (Z)-3-[9(aminoiminomethyl)thiol]-2-propanoic acid; TACA, trans aminocrotonic acid; IAA, imidazole-4-acetic acid; IAA, imidazole-4-acetic acid; GuAA, guanido acetic acid; DAVA, delta-amino valeric acid; CAVA, *cis* aminocrotonic acid; BGuPA, beta-guanidino propionic acid. 3-Aminopropane sulphonic acid, piperadine-4-sulphonic acid, baclophen, glycine and alanine were without effect at concentrations below 1 mM (Holden-Dye *et al.* 1988, 1989; Martin & Duittoz unpublished). N.A.: not active at 1 mM.
† Duittoz & Martin (1990).
‡ Holden-Dye *et al.* (1988, 1989).

mecamylamine was the most potent acetylcholine antagonist in *Ascaris*, more potent than tubocurarine; in contrast, hexamethonium, a potent ganglionic antagonist in vertebrates, has a low potency in *Ascaris*. The *Ascaris* acetylcholine receptor cannot, therefore, be classified as either ganglionic or neuromuscular and can be regarded as a separate subtype of nicotinic receptor (i.e. the *Ascaris* ACh receptor).

Electrophysiological techniques have also been used to examine effects of cholinergic agonists and antagonists (Aubry *et al.* 1970; Aceves, Erliji & Martinez-Marnon, 1970; Martin, 1982; Harrow & Gration, 1985; Colquhoun, Holden-Dye & Walker, 1990); the potency of these compounds in *Ascaris* is summarized in Table 1. Levamisole and pyrantel are more potent agonists at the *Ascaris* ACh receptor than at vertebrate nicotinic receptors where they have only weak nicotinic actions (Aubry *et al.* 1970; Eyre, 1970). The selective action of these drugs allows them to be used as effective anthelmintics, killing the nematode parasite but not the host. The degree of selectivity will obviously affect the safety and efficacy of any nicotinic drug selected for therapeutic purposes.

It may be concluded that the *Ascaris* acetylcholine receptor is a subtype of nicotinic receptor and there are compounds which have a selective effect on the nematode acetylcholine receptor but not on the host receptors.

Pharmacology of the GABA receptor. The pharmacology of extrasynaptic GABA receptors has been studied using a two microelectrode recording technique to examine conductance dose–response relationships during the bath-application of GABA agonists and antagonists (Martin, 1980, 1982; Holden-Dye & Walker, 1988; Holden-Dye *et al.* 1988, 1989; Duittoz & Martin, 1989, 1990*a*) and at the single-channel level (Martin, 1985*a*, *b*; Martin & Pennington, 1990; Duittoz & Martin, 1990*b*).

Conductance dose–response relationships for a variety of bath-applied GABA agonists have been described by the modified Hill equation and the EG50s determined; these values are shown in Table 2 along with estimates of the relative potency of the agonists (Holden-Dye *et al.* 1989).

The agonist profile of the *Ascaris* receptor is similar, but not identical to that of the vertebrate $GABA_a$ receptor: (1) The stereoselectivity of the

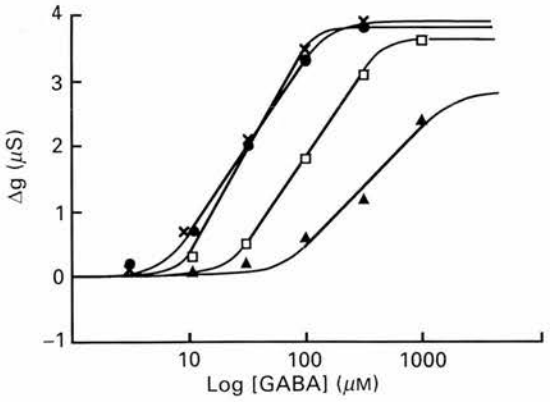


Fig. 6. Dose–response curves to GABA and GABA+RU5135 at 70 (●), 210 (□) and 700 (▲) μM. Ordinate: change in input conductance. Abscissa: GABA concentration (M), log scale. Dose–response curves were obtained from the same cell and the experimental values were fitted by the modified Hill equation. The solid line describes the fitted modified-Hill equation. GABA control (×): EC_{50}, 28·1 μM; Gmax, 3·8 μS; N, 2·1. GABA+RU5135 (70 μM): EC_{50}, 30·6 μM; Gmax, 4·0 μS; N, 1·3. GABA+RU5135 (210 μM): EC_{50}, 100·4 μM; Gmax, 3·7 μS; N, 1·5. GABA+RU5135 (700 μM): EC_{50}, 342·5 μM; Gmax, 2·9 μS; N, 1·2. RU5135 is 3-alpha-hydroxy-1,6,-imino-5-beta-17-aza-androstan-11-one produced by Roussel Uclaf (France).

Ascaris receptor and the vertebrate $GABA_a$ receptor for the enantiomers of dihydromuscimol, 3-OH-GABA, and 4-me-TACA is the same (Holden-Dye *et al.* 1989). (2) Most potent $GABA_a$ agonists are potent in *Ascaris*, so that the relative potency of $GABA_a$ agonists at vertebrate receptors is correlated with the relative potency of agonists at the *Ascaris* receptor ($r = 0{\cdot}74$, Holden-Dye *et al.* 1989). (3) The potency of the sulphonic acid GABA derivatives (3APS and P4S) as well as muscimol and isoguvacine (Table 2) is less than at the vertebrate $GABA_a$ receptor. (4) The anthelmintic piperazine acts as a selective GABA agonist in *Ascaris* (Martin, 1982).

There are, however, major pharmacological differences between the *Ascaris* GABA receptor and the vertebrate $GABA_a$ receptor. (1) Pentobarbitone and flurazepam do not potentiate GABA responses in *Ascaris*, as they do in the vertebrate (Holden-Dye *et al.* 1989). (2) The $GABA_a$ antagonists bicuculline, picrotoxin, securinine, pitrazepine, SR95531, dieldrin and TBPS are weak or inactive in *Ascaris* (Martin, 1980; Wann, 1987; Holden-Dye *et al.* 1988, 1989; Duttoz & Martin, 1990*a*). In addition, we have also tested one of the most potent $GABA_a$ antagonists, the steroid RU5135, and found that it too only acts as a weak non-competitive GABA antagonist in *Ascaris* (Fig. 6). The concentrations required to block the GABA response in *Ascaris* muscle (IC50 = 117 μM) were much higher than found at the $GABA_a$ receptor (IC50 = 5 nM; Simmonds & Turner, 1985). The insensitivity to all these drugs, therefore, distinguishes the *Ascaris* GABA receptor pharmacologically from the vertebrate $GABA_a$ receptors and confirms the earlier suggestion (Martin, 1987) that there is a separate type of receptor in nematodes, i.e. the $GABA_n$ receptor (n = not antagonized by picrotoxin; n = nematodes).

Arylaminopyridazine derivatives. We have investigated further the actions of arylamino-pyridazine-GABA derivatives (Fig. 7; Chambon *et al.* 1985; Wermuth *et al.* 1987) as antagonists at the *Ascaris* GABA receptor, using current-, voltage- and patch-clamp techniques with bath-application of the antagonists. Initially, the actions of SR95531 and SR95301 in *Ascaris* were examined (Duittoz & Martin, 1989, 1990). SR95301 was a more potent antagonist than SR95531 in *Ascaris*, this order of potency is the reverse at the vertebrate $GABA_a$ receptor (Duittoz & Martin, 1989). The antagonism of SR95103 was associated with a parallel shift to the right in the GABA dose–response relationships and the dose–ratio described by a modified Schild plot (Williams *et al.* 1988). The data were consistent with 2 molecules of GABA but one molecule of antagonist interacting with the receptor. The K_B for SR95103 was 64 μM and the antagonism showed little voltage-sensitivity. At the single-channel level, the actions of SR95103 were also consistent with competitive antagonism, with an additional small non-competitive component, possibly a channel-blocking action (Duittoz & Martin, 1990). Again, the antagonism seen in single-channel data was consistent with the GABA receptor combining with a single molecule of SR95103 but two molecules of GABA; this latter observation may be explained if the two GABA binding sites on the receptor are not identical, only one permitting the binding of SR95103.

Subsequently, in another series of experiments the actions of a series of arylaminopyridazine-GABA derivatives were tested and compared with the potency order seen in binding studies at the $GABA_a$ receptor (Table 3). Fig. 7 shows chemical structures of the analogues tested and the mean percentage reduction in the conductance response to 30 μM GABA produced by 1 mM antagonist. Compounds producing greater than 50% reduction all possessed a methyl or phenyl moiety on the 4-position of the pyridazine ring. SR95531 is the most potent vertebrate $GABA_a$ antagonist and SR95132 is the least potent. At the *Ascaris* GABA receptor, SR95103 and SR95132 are the most potent and SR95531 has a low potency. This difference is further evidence that the *Ascaris* receptor can be separated pharmacologically and suggests a rational basis for the design of new therapeutic agents.

Ariens *et al.* (1979) have argued that 'accessory' sites on receptors bind to hydrophobic regions of

Active compounds

Inactive or weak compounds

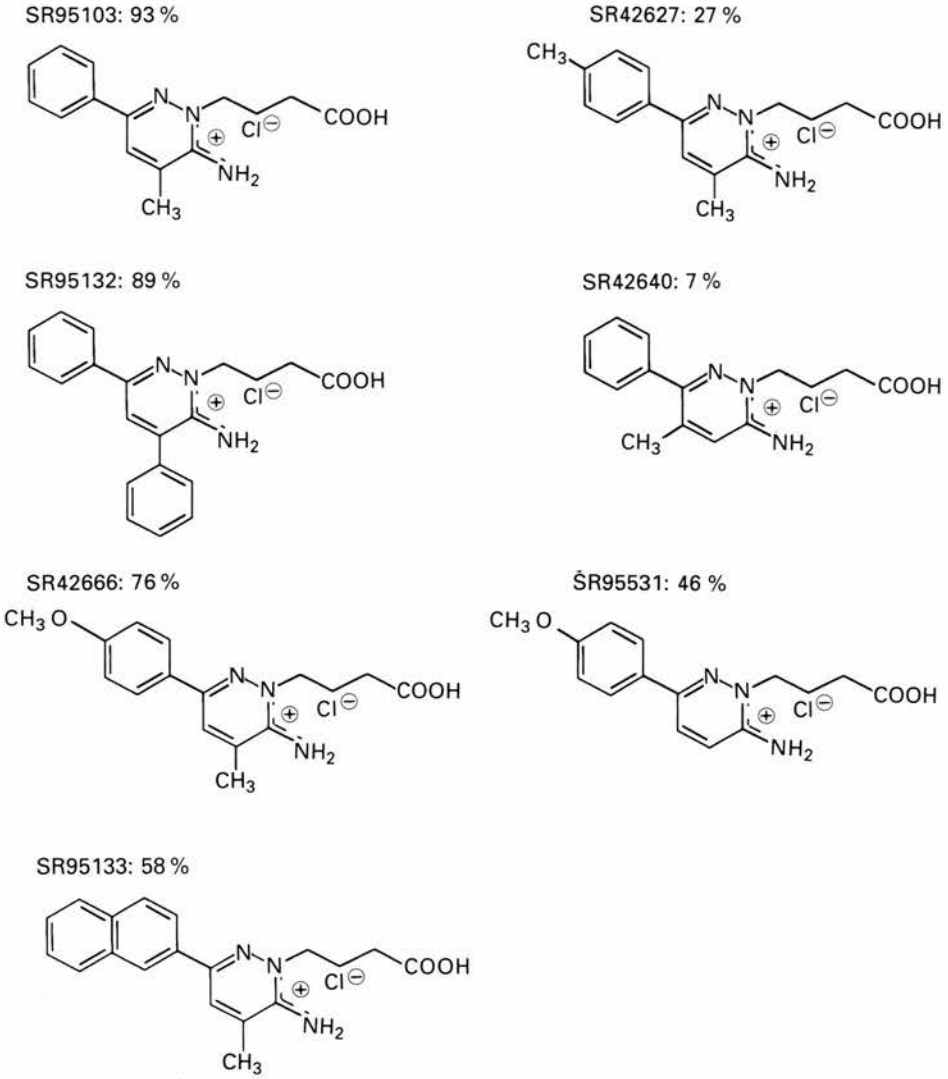


Fig. 7. Structure of arylaminopyridazine-GABA antagonists and the mean percentage inhibition produced by 1 mM antagonist of the conductance response produced by 30 μM GABA. Compounds producing greater than 50 % inhibition were considered active.

Table 3. Comparison of the potency of the arylaminopyridazine derivatives at the $GABA_a$ receptor by inhibiting [H^3]GABA binding and the percentage inhibition of the response to 30 μM GABA by 1 mM antagonist at the *Ascaris* receptor. (The two potency series do not equate, showing that the two receptor types are different.)

	$GABA_a$ binding: Ki (μM)	Inhibition in *Ascaris* (%)
SR95531	0·15	43
SR42666	0·31	76
SR42627	0·55	21
SR95103	2·20	93
SR95133	2·60	58
SR95640	10·40	7
SR95132	100·00	89

competitive antagonists and give rise to their antagonist nature; the structure of the hydrophobic regions is more important for the potency of competitive antagonists than the structure of the moiety binding to the agonist recognition site. The mode of action and structure activity relationships of arylaminopyridazine-GABA antagonists at the vertebrate $GABA_a$ receptor have been explained in terms of Ariens theory (Wermuth, 1987). The correlation between the agonist potencies at the $GABA_a$ and *Ascaris* receptors but not competitive antagonists suggests that 'accessory' sites on the vertebrate $GABA_a$ receptor and *Ascaris* receptor are different. Recognition and characterization of these accessory binding sites may allow the rational design of antagonists which have a selective action in *Ascaris*.

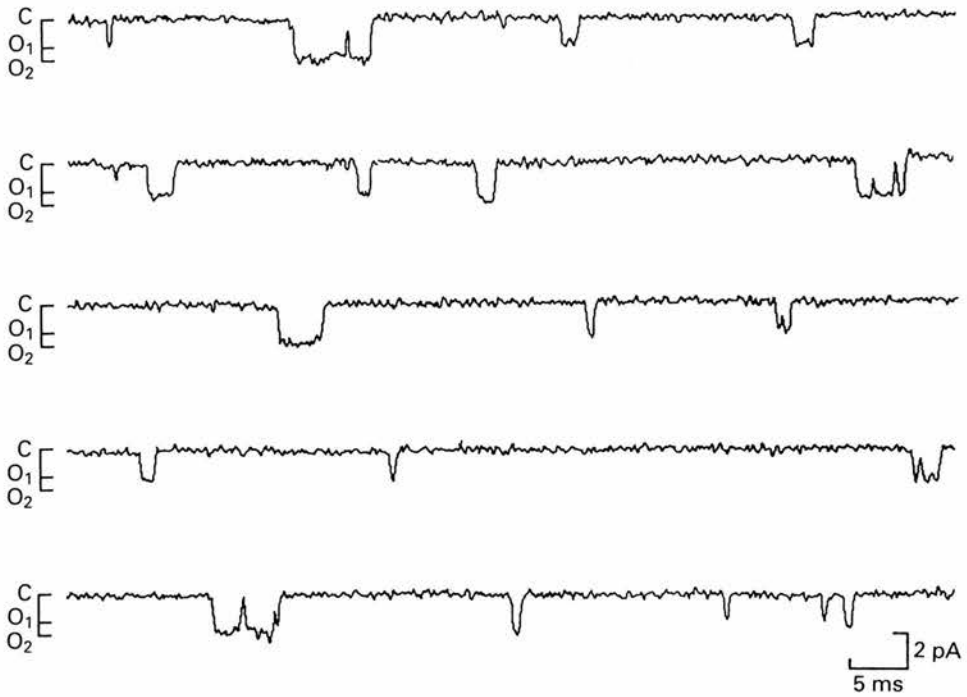


Fig. 8. Acetylcholine-activated channels in a cell-attached patch from a muscle vesicle. C, closed state; O_1, smaller conductance state; O_2, larger conductance state; Patch-potential, −50 mV. 10 μM ACh in the pipette. Pipette solution (mM): CsCl 140, $MgCl_2$ 2, EGTA 1, HEPES 10, pH 7·2 with CsOH. Bathing solution (mM): CsCl 35, Cs acetate 105, $MgCl_2$ 2, EGTA 1, HEPES 10, pH 7·2 with CsOH. Filter: −3 dB 2·5 kHz, 8-pole Bessel. The mean open time was 1·5 ms.

Biophysics

Muscle vesicle preparation. A muscle vesicle preparation suitable for biochemical, pharmacological and biophysical studies on the muscle membrane has been developed (Martin, Kusel & Pennington, 1990). These vesicles are prepared by incubating the flap preparation in collagenase (1 mg/ml for 10 min) and then washing in a saline solution without enzyme. Vesicles of 10–50 μM diameter then form as outgrowths of the original bag membrane over the next 1–2 h. The vesicles can be harvested using a Pasteur pipette and are suitable for patch-clamp studies. Their membranes contain high conductance Ca^{2+}-activated Cl^- channels (Thorn & Martin, 1987), GABA-activated channels, and acetylcholine-activated channels (Martin *et al.* 1990; Pennington & Martin, 1990). The vesicles are also suitable for fluorescence-recovery after photobleaching experiments (FRAP) designed to look at fluorescent-labelled probe movement in the membrane. Recent experiments with this approach have shown that ivermectin has no significant effect on the lateral diffusion coefficient ($8{\cdot}1 \times 10^{-9}$ cm^2 sec^{-1}) and that the membrane is not homogeneous, being composed of coalescent lipid 'domains' (Martin *et al.* 1990). The main advantage offered by the vesicle preparation is that it is not covered by any connective tissue so that it more readily permits anthelmintic mode of action studies involving fluorescent dye techniques and single-channel recording. For example, it was shown that ivermectin has no effect on muscle membrane fluidity or the proportion of mobile lipid (Martin *et al.* 1990).

ACh single-channel currents. Acetylcholine-activated single-channel currents (Fig. 8) have been recorded from cell-attached and isolated inside-out patches from muscle vesicles (Pennington & Martin, 1990). The channels activated by acetylcholine have at least two conductances: the larger was 40–50 pS and the smaller 25–35 pS; the I/V plots of both channels were linear and the average open-times were independent of patch potential. Kinetic analysis of the larger conductance channel showed that the distributions of open and burst durations were composed of two components (short and long) and analysis of the closed-time distributions showed that they were composed of at least three components (short, intermediate and long). These observations are interpreted to indicate that there are at least two open states and three closed states for the larger conductance channel. The average open-time was similar to that of the nicotinic channel at the frog neuromuscular junction and had a corrected mean open-time of 1·26 ms. High concentrations of acetylcholine (25–100 μM) produced a reduction in open probability and caused single-channel currents to occur in clusters with long closed-times (200 s)

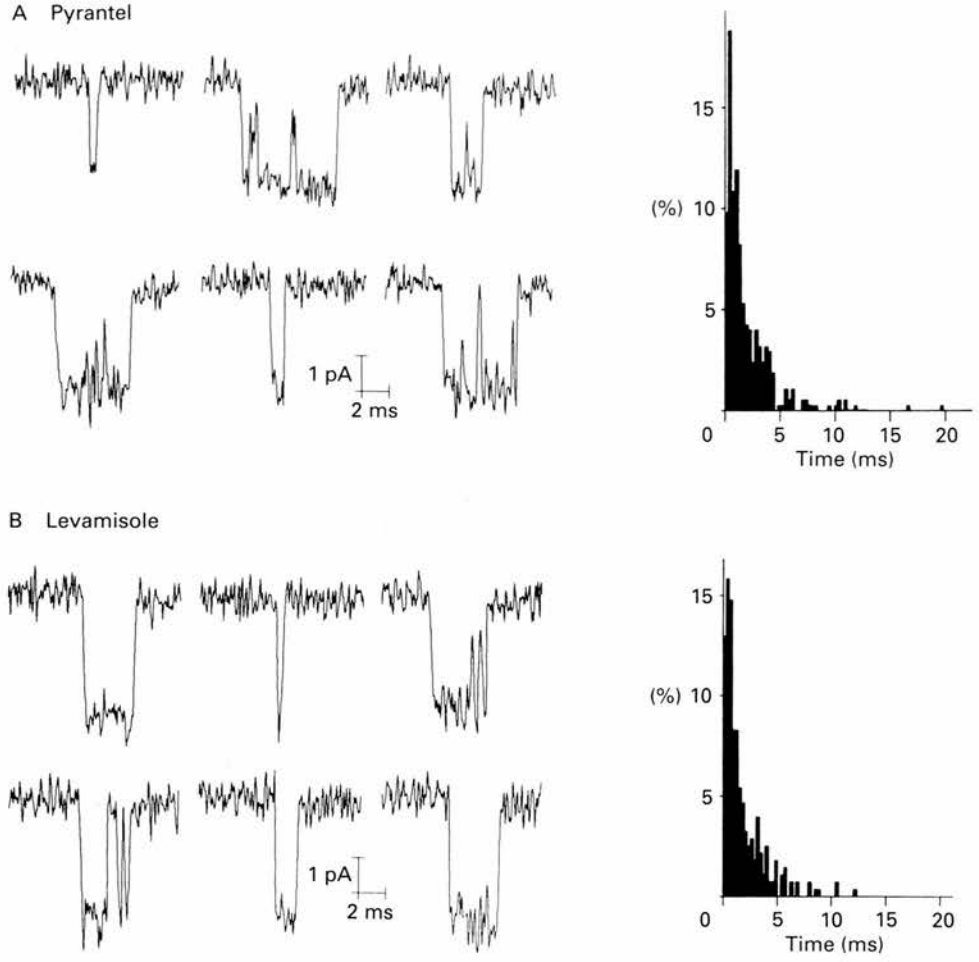


Fig. 9. Pyrantel (A)- and levamisole(B)-activated channels and their open-time histograms, from cell-attached patches from muscle vesicles. Openings are shown downwards. Patch-potential: −75 mV. 0·1 μM pyrantel or 10 μM levamisole in the pipette. Pipette solution (mM): CsCl 140, $MgCl_2$ 2, EGTA 1, HEPES 10, pH 7·2 with CsOH. Bathing solution (mM): CsCl 35, Cs acetate 105, $MgCl_2$ 2, EGTA 1, HEPES 10, pH 7·2 with CsOH. Filter: −3 dB 2·5 kHz, 8-pole Bessel. The mean open-times produced by pyrantel (1·09 ms) and levamisole (1·34 ms) were similar to those produced by acetylcholine. The open-time histograms are typical of channel open-times and show that the open-times vary and that their distribution is skewed with brief openings being more common.

between clusters; this behaviour has also been reported at the frog neuromuscular junction and described as desensitization. Earlier intracellular recordings and voltage-clamp experiments have shown that levamisole (Coles, East & Jenkins, 1975; Harrow & Gration, 1985), pyrantel (Aubry *et al.* 1970; Harrow & Gration, 1985) and morantel (Harrow & Gration, 1985) act as agonists at the extrasynaptic acetylcholine receptor on the bag. Recent experiments have now shown activation of acetylcholine receptors at the single-channel level by pyrantel and levamisole (Fig. 9). These experiments have also demonstrated that levamisole also acts at higher concentrations to produce a voltage-sensitive flickering channel block.

GABA single-channel currents. GABA- and piperazine-activated channels have been recorded using cell-attached and outside-out patches (Martin, 1985*a*, *b*). The channels opened by both agonists had a mainstate conductance of 22 pS but two subconductance states were also observed. The average duration of the effective openings (bursts) produced by GABA was in the region of 32 ms while the average duration of effective openings (bursts) produced by the anthelmintic piperazine was 14 mS (Fig. 10). High concentrations of GABA or piperazine produced desensitization, which was seen as a decrease in open probability due to the appearance of long closed-times. Piperazine is some 100 times less potent than GABA in *Ascaris* (Martin, 1982) and this difference in potency may be explained by the fact that piperazine requires a higher concentration to achieve a similar opening rate to GABA and, in addition, the average duration of openings produced by piperazine is shorter. The density of the extrasynaptic receptors was also estimated in these experiments (Martin, 1985*b*): only one channel was found in each area of membrane of about 2·4 μM^2.

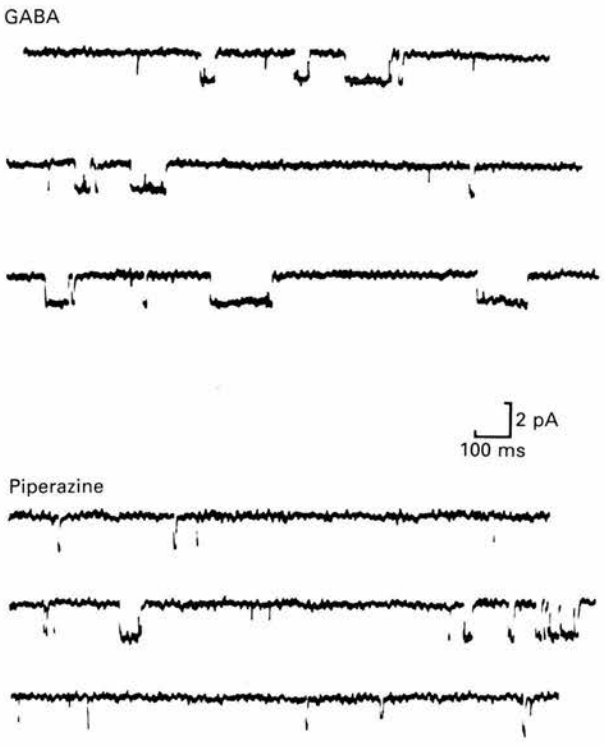


Fig. 10. GABA- and piperazine-activated channels. Cell-attached patches. Transpatch potential −75 mV. GABA: 3 μM GABA as agonist. Piperazine: 500 μM piperazine as agonist. Effective channel open times: GABA 33 ms; piperazine 18 ms. Channel conductance 22 pS for both agonists. Bathing solution (mM): NaCl 135, KCl, 3·0, $MgCl_2$ 15·7, glucose 3·0, and Tris adjusted to pH 7·6 with maleic acid. Pipette solution (mM): CsCl 140, $MgCl_2$ 15·7 and Tris adjusted to pH 7·6 with maleic acid.

Ivermectin

Effects of dihydroavermectin. Electrophysiological effects of the anti-parasitic agent dihydroavermectin on *Ascaris* muscle have been studied with intracellular micropipette recordings (Kass *et al.* 1980, 1982, 1984; Holden-Dye *et al.* 1988) and at the single-channel level with the patch-clamp technique (Martin & Pennington, 1989). In contrast to effects on other invertebrate preparations, dihydroavermectin does not act like GABA on *Ascaris* muscle (i.e. it does not produce a marked hyperpolarization with an increase in membrane conductance), even when high concentrations (20 μM–0·2 μM) are used. However, dihydroavermectin depresses GABA-activated channel currents by reducing mean conductances and probability of opening (Martin, 1987; Martin & Pennington, 1989). This GABA-blocking effect was also seen in current-clamp experiments (Holden-Dye *et al.* 1988).

Low concentrations of dihydroavermectin applied to the outside membrane by bath application to an outside-out muscle patch did produce opening of up to 13 channels (Martin & Pennington, 1989). The progressive opening of the channels over a period of 1–3 min produced a staircase effect. (Fig. 11). These channels conducted Cl^- ions and had conductances of 9–15 pS and long average open-times (greater than 100 ms). A long delay (greater than 15 s) between the application of dihydroavermectin and channel opening and its lipophilic nature suggest a site of action in the lipid phase of the membrane. The action of low concentrations of dihydroavermectin on inside-out patches was to produce, after a long delay (mean 2·5 min), noisy cation-selective channels which had conductances of 5–30 pS. It did not produce Cl^- channels. The study concluded that dihydroavermectin may act to open non-GABA-activated Cl^- channels by acting from the external membrane, but the speed of onset of the effect is slow. Thus, the mode of action of ivermectin appears to be to open a particular type of Cl^- channel, possibly only present in susceptible animals, rather than to act as a GABA agonist.

Electrophysiological effects of dihydroavermectin on *Ascaris* neurones have been determined using differential application of drugs to dorsal and ventral muscle flaps in split-chamber experiments (Kass *et al.* 1984). It was reported that 6 μM dihydroavermectin blocked the response of DE1 to indirect but not direct stimulation. These results suggest action of dihydroavermectin on interneurones in *Ascaris* nerve cords.

OTHER TRANSMITTERS

The action of 5-HT

In addition to the neurotransmitters, GABA and acetylcholine there is evidence that 5-HT (serotonin) may play a role in regulating muscle metabolism. 5-HT can be absorbed from the host or synthesized by *Ascaris* (Martin, Chaudhuri & Donahue, 1988); 5-HT receptors in muscle and intestine of *Ascaris* have been demonstrated using radiolabelled binding techniques (Chaudhuri & Donahue, 1989).

5-HT has no observable effect on muscle membrane potential (unpublished observations) but appears to regulate glycogen metabolism. In *Ascaris*, glycogen metabolism depends on glycogen synthetase for glycogen synthesis from glucose-6-phosphate, and glycogen phosphorylase for glycogen breakdown. 5-HT inactivates glycogen synthetase and activates glycogen phosphorylase by increasing the level of cAMP, resulting in breakdown of glycogen (Donahue *et al.* 1981).

The receptor binding studies of Chaudhuri & Donahue (1989) suggest that in *Ascaris* the muscle receptor is similar to the mammalian 5-HT_2 receptor. Ketanserin, a selective 5-HT_2 antagonist has a high affinity (K_D = 16·7 μM) for the muscle receptor but not the *Ascaris* intestinal receptor. The recognition of a 5-HT receptor in *Ascaris* muscle suggests another target site for the design of new anthelmintics.

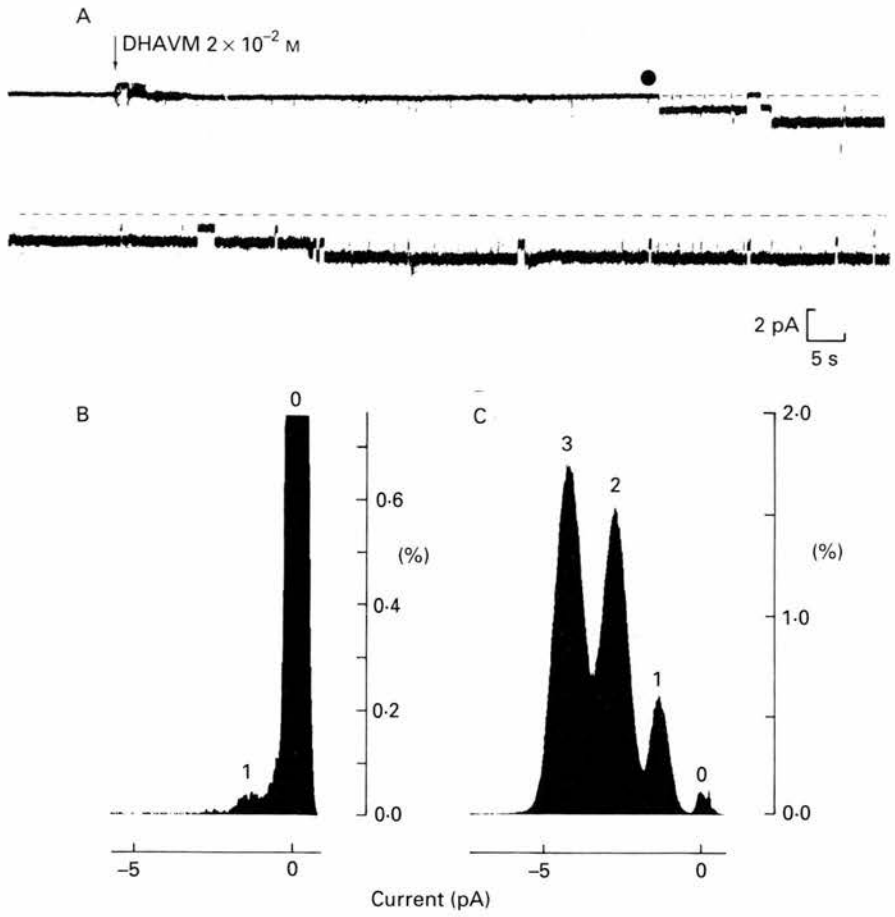


Fig. 11. (A) Staircase production of channels in outside-out patch (−75 mV) by 2 pM DHAVM. (B and C) Current amplitude histograms before (B) and after (C) activation of the channels at O; note the appearance of peaks 2 and 3 in C signifying the proportion of time 2 and 3 channels are open, in B only peak 1 is present signifying that occasionally one channel opened before activation. The conductance of the channels was 15 pS. Pipette solution (mM): CsCl 140, $CaCl_2$ 1, $MgCl_2$ 2, EGTA 11, HEPES 10, pH 7·2 with CsOH. Bathing solution (mM): NaCl 140, KCl 2, $CaCl_2$ 5, $MgCl_2$ 2, glucose 3 and HEPES 10, pH 7·2 with NaOH.

Other possible neurotransmitters

Other putative transmitters have been suggested to occur in nematodes but their presence in *Ascaris* remains to be confirmed. These transmitters include: dopamine (Sulston, Dew & Brenner, 1975); adrenaline and noradrenaline (Willett, 1980); octopamine (Hovitz *et al.* 1982). Immunoreactivity to FMRFamide-like peptides has been demonstrated in the pharyngeal nerves and the four major nerve cords of *Ascaris* (Davenport *et al.* 1988). One purified form has been sequenced and called AF1 (A for *Ascaris*, F for FMRFamide and 1 for the first purified) and has been shown to be biologically active and to reduce input resistance of inhibitory motoneurones (Cowden *et al.* 1989). Peptidergic transmission remains to be studied in greater detail; it seems likely that more peptides as transmitters may be recognized in future studies.

Second messengers

The involvement of second messengers in neurotransmission is at present not known. Donahue *et al.* (1982, 1983) have correlated changes in muscle activity produced by piperazine and levamisole with changes in glycogen metabolism. They have also proposed a role for cyclic AMP-mediated regulation. The involvement of other second messengers including Ca^{2+}, cyclic GMP and IP_3 has not yet been established in *Ascaris*.

CONCLUSION

The physiology and pharmacology of the neuromuscular transmission in *Ascaris* is an interesting subject area which may be studied for a variety of reasons. The nematode is a model parasite, readily collected from many abattoirs, and large enough for electrophysiological study Anthelmintic mode of action studies have identified sites of action for piperazine, dihydroavermectin, pyrantel and levami-

sole. The production of new anthelmintics may utilize this information in rational design.

We are pleased to acknowledge the financial support of the SERC, Wellcome Trust and Merck, Sharp and Dohme who have made this work possible.

REFERENCES

ACEVES, J., ERLIJI, D. & MARTINEZ-MARNON, R. (1970). The mechanism of the paralysing action of tetramisole on *Ascaris* somatic muscle. *British Journal of Pharmacology* **38**, 332–44.

ANGSTADT, J. D., DONMOYER, J. E. & STRETTON, A. O. W. (1989). Retrovesicular ganglion of the nematode *Ascaris*. *Journal of Comparative Neurology* **284**, 374–88.

ARIENS, E. J., BELD, A. D., MIRANDA, J. F. R. & SIMONIS, A. M. (1979). The Pharmacon-Receptor-Effector concept. In *The Receptors* vol. 1 (ed. O'Brien, R. D.), New York: Plenum.

AUBRY, M. L., COWELL, P., DAVEY, M. J. & SHEVDE, S. (1970). Aspects of the pharmacology of new anthelmintics: pyrantel. *British Journal of Pharmacology* **38**, 332–44.

BALDWIN, E. & MOYLE, V. (1949). A contribution to the physiology and pharmacology of *Ascaris lumbricoides* from the pig. *British Journal of Pharmacology* **4**, 145–52.

BRADING, A. F. & CALDWELL, P. C. (1971). The resting membrane potential of the somatic muscle cells of *Ascaris lumbricoides*. *Journal of Physiology* **217**, 605–24.

BUEDING, E. (1952). Acetylcholinesterase activity of *Schistosoma mansoni*. *British Journal of Pharmacology* **7**, 563–6.

CALDWELL, P. C. (1974). Possible mechanisms for linkage of membrane potentials to metabolism by electrogenic transport processes with special reference to *Ascaris* muscle. *Bioenergetics* **4**, 201–9.

CALDWELL, P. C. & ELLORY, J. C. (1968). Ion movement in the somatic muscle cells of *Ascaris lumbricoides*. *Journal of Physiology* **197**, 75–76P.

CAPPE DE BAILLON, P. (1911). Etude sur les fibres musculaires d'*Ascaris*. I. Fibres pariétales. *Cellule* **27**, 165–211.

CHAMBON, J. P., FELTZ, P., HEAULME, M., RESTLE, S., SCHLIECHTER, R., BIZIÈRE, K. & WERMUTH, C. G. (1985). Synthesis of SR95103 an arylaminopyridazine derivative of GABA. *Proceedings of the National Academy of Sciences USA* **82**, 1832–6.

CHAUDHURI, J. & DONAHUE, M. J. (1989). Serotonin receptors in the tissues of adult *Ascaris suum*. *Molecular and Biochemical Parasitology* **35**, 191–8.

COLES, G. C., EAST, J. M. & JENKINS, S. N. (1975). The mechanism of action of the anthelmintic levamisole. *General Pharmacology* **6**, 309–13.

COLQUHOUN, L., HOLDEN-DYE, L. & WALKER, R. J. (1989). 5-Nitro-2-(3-phenylpropylamino) benzoic acid, (5-NPB), is a non-competitive antagonist at the *Ascaris* GABA receptor. *British Journal of Pharmacology* **97**, 369P.

COLQUHOUN, L., HOLDEN-DYE, L. & WALKER, R. J. (1990). The pharmacology of cholinoceptors on the somatic muscle cells of the parasitic nematode *Ascaris suum*. *British Journal of Pharmacology* **99**, 253P.

COWDEN, C., STRETTON, A. O. W. & DAVIS, R. E. (1989). AF1, a sequenced bioactive neuropeptide isolated from the nematode *Ascaris suum*. *Neuron* **2**, 1465–73.

DAVENPORT, T. R. B., LEE, D. L. & ISAAC, R. E. (1988). Immunocytochemical demonstration of a neuropeptide in *Ascaris suum* (Nematoda) using antiserum to FMRF-amide. *Parasitology* **97**, 81–8.

DAVIS, R. E. & STRETTON, A. O. W. (1989*a*). Passive membrane properties of motoneurons and their role in long-distance signalling in the nematode *Ascaris*. *Journal of Neuroscience* **9**, 403–14.

DAVIS, R. E. & STRETTON, A. O. W. (1989*b*). Signalling properties of *Ascaris* motoneurons: graded active responses, graded synaptic transmission, and tonic transmitter release. *Journal of Neuroscience* **9**, 415–25.

DE BELL, J. T. (1965). A long look at neuromuscular junctions in nematodes. *Quarterly Review of Biology* **40**, (3) 233–51.

DE BELL, J. T., DEL CASTILLO, J. & SANCHEZ, V. (1963). Electrophysiology of the somatic muscle cells of *Ascaris lumbricoides*. *Journal of Cellular and Comparative Physiology* **62**, 159–77.

DE MELLO, W. C. & MALDONADO, H. (1985). Synaptic inhibition and cell communication; impairment of cell-to-cell coupling produced by gamma-aminobutyric acid (GABA) in the somatic musculature of *Ascaris lumbricoides*. *Cellular Biology International Report* **9**, 803–13.

DEL CASTILLO, J., DE MELLO, W. C. & MORALES, T. (1963). The physiological role of acetylcholine in the neuromuscular system of *Ascaris lumbricoides*. *Archives internationales de physiologie et de biochimie* **71**, 741–57.

DEL CASTILLO, J., DE MELLO, W. C. & MORALES, T. (1964a). Influence of some ions on the membrane potential of *Ascaris* muscle. *Journal of General Physiology* **48**, 129–40.

DEL CASTILLO, J., DE MELLO, W. C. & MORALES, T. (1964*b*). Inhibitory action of γ-aminobutyric acid (GABA) on *Ascaris* muscle. *Experientia* **20**, 141–3.

DEL CASTILLO, J., DE MELLO, W. C. & MORALES, T. (1964*c*). Mechanism of the paralysing action of piperazine on *Ascaris* muscle. *British Journal of Pharmacology* **22**, 463–77.

DEL CASTILLO, J., DE MELLO, W. C. & MORALES, T. (1967). The initiation of action potentials in the somatic musculature of *Ascaris lumbricoides*. *Journal of Experimental Biology* **46**, 263–79.

DEL CASTILLO, J., RIVERA, A., SOLORZANO, S. & SERRATO, J. (1989). Some aspects of the neuromuscular system of *Ascaris*. *Quarterly Journal of Experimental Physiology* **74**, 1071–89.

DONAHUE, M. J., MASARACCHIA, R. A. & HARRIS, B. G. (1983). The role of cyclic AMP-mediated regulation of glycogen metabolism in levamisole-perfused *Ascaris muscle*. *Molecular Pharmacology* **23**, 378–83.

DONAHUE, M. J., YACOUB, N. J. & HARRIS, B. J. (1982). Correlation of muscle activity with glycogen metabolism in muscle of *Ascaris suum*. *American Journal of Physiology* **242**, R514–R521.

DONAHUE, M. J., YACOUB, N. J., MICHINOFF, C. A., MASARACCHIA, R. A. & HARRIS, B. G. (1981). Serotonin

(5-hydroxytryptamine): a possible regulator of glycogenolysis in perfused muscle segmens of *Ascaris suum*. *Biophysics and Biochemical Research Communications* **101**, 112–17.

DUITTOZ, A. H. & MARTIN, R. J. (1989). SR95103 acts as a GABA antagonist in *Ascaris suum* muscle. *British Journal of Pharmacology* **97**, 490P.

DUITTOZ, A. H. & MARTIN, R. J. (1990*a*). Effects of the arylaminopyridazine-GABA derivatives, SR95103 and SR95531 on the *Ascaris* muscle GABA receptor: the relative potency of the antagonists in *Ascaris* is different to that at vertebrate $GABA_a$ receptors. *Journal of Comparative Biochemistry and Physiology* (In Press).

DUITTOZ, A. H. & MARTIN, R. J. (1990*b*). Effects of SR95103 on GABA-activated single-channel currents from *Ascaris suum* muscle. *Journal of Comparative Biochemistry and Physiology* (In Press).

EYRE, P. (1970). Some pharmacodynamic effects of the nematocides: methyridine, tetramisole and pyrantel. *Journal of Pharmacy and Pharmacology* **22**, 26–36.

GOLDSCHMIDT, R. (1908). Das Nervensystem von *Ascaris lumbricoides* und Megalocephala. Ein Versuch, in den Aufbau eines einfachen Nervensystems einzudringen, Zweiter Teil. *Zeitschrift für wissenschaftliche Zoologie* **90**, 73–136.

GOLDSCHMIDT, R. (1909). Das Nervensystem von *Ascaris lumbricoides* und Megalocephala. Ein Versuch, in den Aufbau eines einfachen Nervensystems einzudringen, Zweiter Teil. *Zeitchrift für wissenschaftliche Zoologie* **92**, 306–57.

GRZYWACZ, M., SZKUDLINSKS, J. & ZANDAROWSKA, E. (1985). Pharmacological receptors of *Ascaris lumbricoides suis L. Wiadomości Parazytologi* **31**, 153–61.

HARROW, I. D. & GRATION, K. A. F. (1985). Mode of action of the anthelmintics morantel, pyrantel and levamisole on the muscle cell membrane of the nematode *Ascaris suum*. *Pesticide Science* **16**, 662–72.

HESSE, R. (1892). Über das Nervensystem von *Ascaris lumbricoides* und *Ascaris megalocephala*. *Zeitschrift für wissenschaftliche Zoologie* **90**, 73–136.

HOBSON, A. D., STEPHENSON, W. & BEADLE, L. C. (1952*a*). Studies on the physiology of *Ascaris lumbricoides*. I. The relation of total osmotic pressure, conductivity and chloride content of the body fluid to that of the external environment. *Journal of Experimental Biology* **29**, 1–21.

HOBSON, A. D., STEPHENSON, W. & EDEN, A. (1952*b*). Studies on the physiology of *Ascaris lumbricoides*. II. The inorganic composition of the body fluid in relation to that of the environment. *Journal of Experimental Biology* **29**, 22–9.

HOLDEN-DYE, L., HEWITT, G. M., WANN, K. T., KROGSGAARD-LARSEN, P. & WALKER, R. J. (1988). Studies involving avermectin and the 4-aminobutyric acid (GABA) receptor of *Ascaris suum* muscle. *Pesticide Science* **24**, 231–45.

HOLDEN-DYE, L., KROGSGAARD-LARSEN, P., NEILSEN, L. & WALKER, R. J. (1989). GABA receptors on the somatic muscle cells of the parasitic nematode, *Ascaris suum*: stereoselectivity indicates similarity to a $GABA_a$-type agonist recognition site. *British Journal of Pharmacology* **98**, 841–50.

HOLDEN-DYE, L. & WALKER, R. J. (1988). ZAPA, (Z)-3-[(amino iminomethyl)thio]-2-propenoic acid hydrochloride, a potent agonist at GABA receptors on the *Ascaris* muscle cell. *British Journal of Pharmacology* **95**, 3–5.

HORTON, R. J. (1990). Benzimidazoles in a wormy world. *Parasitology Today* **6**, 106.

HORVITZ, R. H., CHALFIE, M., TRENT, C., SULSTON, J. E. & EVANS, P. D. (1982). Serotonin and octopamine in the nematode *Caenorhabditis elegans*. *Science* **206**, 1012–14.

JARMAN, M. (1959). Electrical activity in the muscle cells of *Ascaris lumbricoides*. *Nature, London* **184**, 1244.

JARMAN, M. & ELLORY, J. C. (1969). Effect of TTX on *Ascaris* somatic muscle. *Experientia* **25**, 507.

JOHNSON, C. D. & STRETTON, A. O. W. (1980). Neural control of locomotion in *Ascaris*: anatomy, electrophysiology and biochemistry. In *Nematodes as Biological Models*, vol. 1, pp. 159–195. New York: Academic Press.

JOHNSON, C. D. & STRETTON, A. O. W. (1985). Localization of choline acetyltransferase within identified motoneurons of the nematode *Ascaris*. *Journal of Neuroscience* **5**, 1984–92.

JOHNSON, C. D. & STRETTON, A. O. W. (1987). GABA-immunoreactivity in inhibitory motor neurons of the nematode *Ascaris*. *Journal of Neuroscience* **7**, 223–35.

KASS, I. S., LARSEN, D. A., WANG, C. C. & STRETTON, A. O. (1982). *Ascaris suum*: differential effects of avermectin B1a on the intact animal and neuromuscular strip preparations. *Experimental Parasitology* **54**, 166–74.

KASS, I. S., STRETTON, A. O. & WANG, A. O. (1984). The effects of avermectin and drugs related to acetylcholine and 4-aminobutyric acid on neuromuscular transmission in *Ascaris suum*. *Molecular and Biochemical Parasitology* **13**, 213–25.

KASS, I. S., WANG, C. C., WALDROND, J. P. & STRETTON, A. O. W. (1980). Avermectin B_{1a}, a paralysing anthelmintic that affects interneurones and inhibitory motorneurones in *Ascaris*. *Proceedings of the National Academy of Sciences, USA* **77**, 6211–15.

LEE, D. L. (1962). The distribution of esterase enzymes in *Ascaris lumbricoides*. *Parasitology* **52**, 241–60.

LEE, D. L. (1970). The fine structure of the excretory system in adult *Nippostrongylus brasiliensis* (Nematoda) and a suggested function for the excretory system of *Anisakis* larva (Nematoda: Anisakidae). *Journal of Parasitology* **59**, 289–98.

MARTIN, R. E., CHAUDURI, J. & DONAHUE, M. J. (1988). Seronotin (5-Hydroxytryptamine) turnover in adult female *Ascaris suum* tissue. *Comparative Biochemistry and Physiology* **91C**, 307–10.

MARTIN, R. E. & DONAHUE, M. J. (1987). Correlation of light chain phosphorylation and gamma aminobutyric acid receptors in *Ascaris suum* muscle. *Comparative Biochemistry and Physiology* **87**, 23–9.

MARTIN, R. J. (1980). The effect of γ-aminobutyric acid on the input conductance and membrane potential of *Ascaris* muscle. *British Journal of Pharmacology* **71**, 99–106.

MARTIN, R. J. (1982). Electrophysiological effects of piperazine and diethylcarbamazine on *Ascaris suum* somatic muscle. *British Journal of Pharmacology* **77**, 255–65.

MARTIN, R. J. (1985*a*) γ-aminobutyric acid- and piperazine-activated single channel currents from *Ascaris suum* body muscle. *British Journal of Pharmacology* **84**, 445–61.

MARTIN, R. J. (1985*b*) Chemotherapy of helminth infection: nematocides, fascioliacides. In *Introduction to Veterinary Pharmacology* (ed. Alexander, F. A.), pp. 355–373, London: Longman.

MARTIN, R. J. (1987). The γ-aminobutyric acid receptor of *Ascaris* as a target for anthelmintics. *Biochemical Society Transactions* **17**, 61–5.

MARTIN, R. J., KUSEL, J. R. & PENNINGTON, A. J. (1990). Surface properties of membrane vesicles prepared from muscle cells of *Ascaris suum*. *Journal of Parasitology* **76**, 340–8.

MARTIN, R. J. & PENNINGTON, A. J. (1989). A patch-clamp study of effects of dihydroavermectin on *Ascaris* muscle. *British Journal of Pharmacology* **98**, 747–56.

MELLANBY, H. (1955). The identification and estimation of acetylcholine in three parasitic nematodes (*Ascaris lumbricoides*, *Litomosoides carinii*, and the microfilariae of *Dirofilaria repens*). *Parasitology* **45**, 287–94.

NATOFF, I. L. (1969). The pharmacology of the cholinoceptor in muscle preparations of *Ascaris lumbricoides* var. *suum*. *British Journal of Pharmacology* **37**, 251–7.

NORTON, S. & DE BEER, E. J. (1957). Investigations on the action of piperazine on *Ascaris lumbricoides*. *American Journal of Tropical Medicine* **6**, 898–905.

ONUAGULUCHI, G. (1989). Some aspects of the pharmacology and physiology of the *Ascaris suum* muscle. *Archives of International Pharmacodynamics and Therapeutics* **298**, 264–75.

PENNINGTON, A. J. & MARTIN, R. J. (1990). A patch-clamp study of acetylcholine-activated ion channels in *Ascaris suum* muscle. *Journal of Experimental Biology* (In press).

ROSENBLUTH, J. (1965*a*). Ultrastructural organization of obliquely striated muscle fibres in *Ascaris lumbricoides*. *Journal of Cell Biology* **25**, 495–515.

ROSENBLUTH, J. (1965*b*). Ultrastructure of somatic muscle cells in *Ascaris lumbricoides*. II. Intermuscular junctions, neuromuscular junctions, and glycogen stores. *Journal of Cell Biology* **26**, 579–91.

ROSENBLUTH, J. (1967). Obliquely striated muscle. III. Contraction mechanism of *Ascaris* body muscle. *Journal of Cell Biology* **34**, 15–33.

ROSENBLUTH, J. (1969). Ultrastructure of dyads in muscle fibres of *Ascaris lumbricoides*. *Journal of Cell Biology* **42**, 817–25.

ROZHOVA, E. K., MALYUTINA, T. A. & SHISHOV, B. A. (1980). Pharmacological characteristics of cholinoreception in somatic muscle of the nematode *Ascaris suum*. *General Pharmacology* **11**, 141–6.

SAZ, H. J. & WEIL, A. (1962). A pathway of formation of α-methyl valerate by *Ascaris lumbricoides*. *Journal of Biological Chemistry* **237**, 2053–6.

SCHNEIDER, A. (1866). *Monographie der Nematoden*. Berlin.

SIMMONDS, M. A. & TURNER, J. P. (1985). Antagonism of inhibitory amino acids by the steroid derivative RU5135. *British Journal of Pharmacology* **84**, 631–6.

SITHIGORNGUL, P., COWDEN, C., GUASTELLA, J. & STRETTON, A. O. W. (1989). Generation of monoclonal antibodies against a nematode peptide extract: another approach for identifying unknown neuropeptides. *Journal of Comparative Neurology* **284**, 389–97.

STANDEN, O. D. (1955). Activity of piperazine, in vitro, against *Ascaris lumbricoides*. *British Medical Journal* **ii**, 20–2.

STRETTON, A. O. W. (1976). Anatomy and development of the somatic musculature of the nematode of *Ascaris*, *Journal of Experimental Biology* **64**, 773–88.

STRETTON, A. O. W., DAVIS, R. E., ANGSTADT, J. D., DONMOYER, J. E. & JOHNSON, C. D. (1985). Neural control of behaviour in *Ascaris*. *Trends in Neurosciences* **8**, 294–300.

STRETTON, A. O. W., FISHPOOL, R. M., SOUTHGATE, E., DONMOYER, J. E., WALROND, J. P., MOSES, J. E. R. & KASS, I. S. (1978). Structure and physiological activity of the motoneurons of the nematode *Ascaris*. *Proceedings of the National Academy of Sciences, USA* **75**, 3493–7.

SULSTON, J., DEW, M. & BRENNER, S. (1975). Dopamine neurons in the nematode *Caenorhabditis elegans*. *Journal of Comparative Neurology* **163**, 215–44.

THORN, P. & MARTIN, R. J. (1987). A high-conductance calcium-dependent chloride channel in *Ascaris suum* muscle. *Quarterly Journal of Experimental Physiology* **72**, 31–49.

TOSCANO RICO, J. (1926). Sur la sensibilité de l'Ascaris à l'action de quelques drogues. *Compte rendu des séances de la Société de Biologie, Paris* **94**, 921–3.

TSANG, V. C. & SAZ, H. J. (1973). Demonstration and function of 2-methyl-butyrate racemase in *Ascaris lumbricoides*. *Journal of Comparative Biochemistry and Physiology* **45B**, 617–23.

WALROND, J. P., KASS, I. S., STRETTON, A. O. W. & DONMOYER, J. (1985). Identification of excitatory and inhibitory motoneurons in the nematode by electrophysiological techniques. *Journal of Neuroscience* **5**, 1–8.

WALROND, J. P. & STRETTON, A. O. W. (1985). Reciprocal inhibition in the motor nervous system of the nematode *Ascaris*: direct control of ventral inhibitory motoneurons by dorsal excitatory motoneurons. *Journal of Neuroscience* **5**, 9–15.

WANN, K. T. (1987). The electrophysiology of the somatic muscle cells of *Ascaris suum* and *Ascaridia galli*. *Parasitology* **94**, 555–66.

WEISBLAT, D. A., BYERLY, L. & RUSSEL, R. L. (1976). Ionic mechanisms of electrical activity in the somatic muscle cell of the nematode *Ascaris lumbricoides*. *Journal of Comparative Physiology* **111**, 93–113.

WEISBLAT, D. A. & RUSSEL, R. L. (1976). Propagation of electrical activity in the nerve cord and muscle syncytium of the nematode *Ascaris lumbricoides*. *Journal of Comparative Physiology* **107**, 293–307.

WERMUTH, C. G., BOURGUIGNON, J. J., SCHLEIVER, G., GIES, J. P., SCHOENFELDER, A., MELIKIAN, A., BOUCHET, M. T., CHANTREAUX, D., MOLIMARD, J. C., HEAULME, M., CHAMBON, J. P. & BIZIÈRE, K. (1987). Synthesis and structure activity relationships of a series of arylaminopyridazine derivatives of GABA acting as selective $GABA_a$ antagonists. *Journal of Medicinal Chemistry* **30**, 239–49.

WHITE, J. G., SOUTHGATE, E., THOMSON, J. N. & BRENNER, S. (1976). The structure of the ventral cord of

Caenorhabditis elegans. Philosophical Transactions of the Royal Society, Series B. **275**, 298–327.

WHITE, J. G., SOUTHGATE, E., THOMSON, J. N. & BRENNER, S. (1986). The structure of the nervous system of *Caenorhabditis elegans. Philosophical Transactions of the Royal Society, B.* **314**, 1–340.

WILLETT, J. D. (1980). Control mechanisms in nematodes. In *Nematodes as Biological Models*, vol. I (ed. Zuckerman, B. M.), pp. 197–225. New York: Academic Press.

WILLIAMS, T. L., SMITH, D. A. S., BURTON, N. R. & STONE, T. W. (1988). Amino acid pharmacology in neonatal slices: evidence for bimolecular actions from an extension of the Hill and Gaddum-Schild equations. *British Journal of Pharmacology.* **95**, 805–10.

I 010 ELECTROPHYSIOLOGY OF *ASCARIS* MUSCLE, R.J. Martin, Department of Preclinical Veterinary Sciences, University of Edinburgh, Edinburgh EH9 1QH, U.K.

Each somatic muscle cell of *Ascaris suum* is divided into three regions: (i) The contractile spindle; (ii) The bag, an enlarged balloon-shaped structure which contains the nucleus and glycogen granules; (iii) The arm which is a process arising from the base of the bag and which joins the 'synctium', where it receives the synaptic input from the nerve cord.

The muscle resting potential is about -35mV and the membrane has been shown to have a high Cl permeability compared to Na and K. Superimposed on this potential are 3 types of depolarizing potential: (i) Ca spikes; (ii) Slow waves and (iii) Modulation waves. The depolarization of adjacent cells is correlated as a result of electrical coupling at the synctium; contraction is associated with the modulation waves. Ca currents and K currents responsible for the spikes can be seen under voltage-clamp. ACh depolarizes the muscle cells and opens non-selective cation channels located on the syncytial and bag membrane. The pharmacology of the ACh receptor is similar but not identical to the vertebrate ganglionic nicotinic receptor. GABA hyperpolarizes the muscle cells by opening Cl channels located at the syncytium and on the bag. The pharmacology of *Ascaris* GABA receptor differs from that of the vertebrate GABA receptors.

A muscle vesicle preparation has been developed which allows single-channel currents from the bag membrane to be recorded. ACh-activated channels show evidence of densensitization, two conductance levels (30-50pS and 15-25pS) and a mean open-time in the range 2-4ms.

The anthelmintics levamisole, pyrantel and morantel also activate the same channels. Their channel conductances are similar but they have shorter mean open-times. However these anthelmintics show differing degrees of open-channel block. GABA and piperazine open 20-40pS Cl channels which have mean open-times of 32 and 14ms respectively. Dihydroavermectin B1a does not activate GABA like channels, rather it acts as a non-competitive GABA antagonist. However it progressively opens 9-15pS Cl channels producing a 'staircase' effect. A Ca activated Cl channel is also found in the membrane and appears to underlie the resting membrane potential. It has a conductance of 200pS, is activated by Ca at the cytoplasmic membrane and is permeable to volatile fatty acids including alpha-methyl butyric acid. The volatile fatty acids are products of anaerobic breakdown of glycogen and their permeability suggests that this channel is involved in removal of anabolic wastes from the muscle cell.

These observations illustrate the value of the electrophysiological technique for investigating the physiology and pharmacology of nematode muscle and anthelmintic action (Martin et al, 1991).

Martin, R.J., Pennington, A.J., Duittoz, A.H., Robertson, S. and Kusel, J.R. (1991). The physiology and pharmacology of neuromuscular transmission in the nematode parasite *Ascaris suum*. Parasitology, 102, S41-S58.

I 011 PHYSIOLOGY OF SCHISTOSOME MUSCLE CELLS, Ralph A. Pax and Tim A. Day, Michigan State University, East Lansing, MI 48824.

Muscle fibers isolated from the platyhelminth Schistosoma mansoni have been studied with whole cell current- and volatge-clamp techniques. Fibers showed a marked time-dependent decrease in membrane resistance in response to depolarizing current injections. Voltage-clamp experiments revealed the presence of two distinct voltage-dependent outward currents. The most prominent current is a slowly activating, slowly and incompletely inactivating potassium current similar to delayed rectifier currents which have been described in a variety of cell types from a variety of organisms. Also present is a faster activating, quickly and completely inactivating potassium current that shares functional characteristics with "A"-currents. Three of the cell types studied possess a delayed rectifier current, but "A"-currents are present in only some of the fiber types. Though depolarization with high K$^+$ leads to contraction of the dispersed fibers, no voltage-dependent inward currents could be detected by whole cell voltage-clamp under any of our conditions.

Neurotransmitters and Neuropeptides in Helminths

I 012 NEUROPEPTIDES IN HELMINTHS, Chris Shaw[1] and David Halton[2], Comparative Neuroendocrinology Research Group, [1]School of Medicine, and [2]School of Biology and Biochemistry, The Queen's University of Belfast, Belfast BT7 1NN, Northern Ireland, U.K.

With respect to organization of the nervous system, helminths are the first group in evolutionary terms to display cephalization of neural elements and a bilaterally-symmetrical neuronal plan. Indeed, recent models of metazoan evolution propose that all phyla displaying these features arose from a common flatworm-type ancestor. In terms of neuronal number and structural complexity the helminth nervous system is considerably simpler than that of more highly-evolved organisms. For this reason the nervous system of helminths could be regarded as a useful model in unravelling the intricate functions of the vertebrate homolog. However, the neurochemistry of helminth nervous systems now appears to be of a similar order of complexity to that of more highly-evolved organisms with well developed cholinergic, aminergic and peptidergic components. The latter component has been the major thrust of neurochemical research in our laboratory. The concept that neuropeptides due to their relative chemical complexity are more recent acquisitions in evolutionary terms than small and chemically-simpler classical neurotransmitters is probably no longer tenable or generally accepted. The plethora of immunocytochemical investigations in many helminth species would suggest that their nervous systems possess an array of neuropeptides. Such studies have been carried out using antisera generated to regulatory peptides from both higher invertebrate and vertebrate sources and these antisera usually recognize epitopes within their respective peptide antigens which are either bioactive sites and/or highly-conserved sequences. Phe-Met-Arg-Phe amide (FMRF amide) was originally isolated from a bivalve mollusc and antisera generated to this peptide immunostain large numbers of neurons and fibres in representative species from all major invertebrate phyla including many helminths. Similar if not identical immunostaining patterns have been obtained using antisera generated to the C-terminal hexapeptide amides of the much larger (36 amino acid residues) vertebrate peptides pancreatic polypeptide (PP) and neuropeptide Y (NPY). This was attributed in the past to antiserum cross-reactivity, as both classes of peptides terminate in a chemically-similar dipeptide (Arg-Phe amide and Arg-Tyr amide, respectively). Preliminary gel permeation chromatographic analysis of helminth extracts identified immunoreactivity coeluting with vertebrate PP/NPY and not with the much smaller FMRF amide. Radioimmunoassay with both PP and NPY hexapeptide antisera indicate that the helminth peptide was structurally more similar in its C-terminus to vertebrate PP than to NPY, and cross-reactivity studies indicated that the PP antiserum did not cross-react with FMRF amide even when present in a million-fold molar excess over PP. The cestode, *Moniezia expansa*, contained high concentrations of this PP immunoreactive peptide (192 ng/g) and was available in sufficient quantity to facilitate isolation. This was achieved by sequential reverse-phase HPLC and the purified peptide was subjected to structural analysis using mass spectroscopy and automated Edman degradation. These established a molecular mass of 4599 Da and the sequence of 30 residues. The discrepancy in these masses indicated the presence of additional residues which were subsequently identified by sequencing of endoproteinase Glu-C fragments. This PP immunoreactive peptide, designated neuropeptide F (NPF) consisted of 39 amino acid residues terminating in an Arg-Pro-Arg-Phe amide. Analogous neuropeptides have been isolated from a turbellarian (*Artioposthia triangulata*) and a mollusc (*Helix aspersa*) and have been detected in extracts of a coelenterate (*Hydra vulgaris*), three trematodes (*Schistosoma mansoni, Diclidophora merlangi, Fasciola hepatica*), two annelids (*Lumbricus terrestris, Nereis virens*) and several insects including the coackroach, *Periplaneta* and the fleshfly, *Sarcophaga*. NPF is thus an abundant neuropeptide with a widespread distribution in invertebrate nervous systems. These data have been substantiated in immunocytochemical and radioimmunometric studies using antisera specific for the C-terminal region of the molecule which exhibit negligible cross-reactivity with vertebrate PP/NPY and invertebrate FMRF amide. These studies authenticate the distribution of NPF and have established that FMRF amide immunocytochemistry of invertebrate nervous systems is largely erroneous in that FMRF amide antisera immunostain NPF. In conclusion, NPF is the most abundant neuropeptide so far detected in helminth nervous systems and indeed occurs in abundance in representatives of all major invertebrate phyla investigated. This peptide may be a generalized neurotransmitter within invertebrates and probably represents the phylogenetic precursor of vertebrate PP/NPY.

J.-M. Sitamze[1], C.G. Wermuth[1] & R.J. Martin*. [1]Laboratoire de Chimie Organique, Faculte de Pharmacie, Universite Louis Pasteur, 74 Route du Rhin, B.P. 24 F67401, Strasbourg Cedex, France. [2]Department of Preclinical Veterinary Sciences, R.(D.)S.V.S., Summerhall, University of Edinburgh, Edinburgh, EH9 1QT.

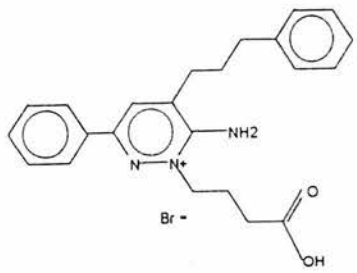


Figure1. NCS281-93 structure.

We have been examining the pharmacology of GABA antagonists in the nematode parasite *Ascaris suum* (Martin, 1993) with a view to finding a new approach for the development of anthelmintic compounds. A series of arylaminopyridazine-GABA derivatives were synthesised and their activity as GABA antagonists assessed electrophysiologically by measuring GABA-induced increases in chloride conductance in muscle cells (Duittoz and Martin, 1991). Within the series of compounds tested, NCS281-93 (Figure. 1), 2-(3-carboxy propyl)-3-amino-4-phenyl propyl: 6-phenyl pyridazinium bromide was found to be the most potent competitive GABA antagonist. The effect of different concentrations of NCS281-93 on GABA-chloride-conductance dose-response relationships was examined in muscle-flap preparations from seven adult female *Ascaris suum*. It was found that NCS281-93 produced a parallel shift to the right of the GABA dose-response curves. The data was analysed using a modified Schild equation (Duittoz and Martin, 1991) to describe the observations. The analysis allows for cooperativity of GABA and antagonist responses. The dissociation constant, K_B, was 4.7 $\pm$ 0.7μM (mean $\pm$ s.e.mean., N=11). The results demonstrate that potent antagonists of the nematode GABA receptor may be found in this series and offer a novel approach in the search for new anthelmintic agents.

Martin, R.J. (1993). Pharmacology and Therapeutics. 58, 13-50.
Duittoz. A.H. & Martin, R.J. (1991). J. Exp. Biol. 159, 149-164.

519P EFFECT OF INTERLEUKIN-4 ON INTERLEUKIN-1-INDUCED NEUTROPHIL MIGRATION AND ON ENDOTOXIN-INDUCED NITRIC OXIDE PRODUCTION IN MACROPHAGES AND NEUTROPHILS

Cs. Szabó, M. Perretti, C. Thiemermann, R. Flower & J. R. Vane, The William Harvey Research Institute, St. Bartholomew`s Hospital Medical College, Charterhouse Square, London, EC1M 6BQ, United Kingdom

Recent therapeutic strategies in experimental septic shock include the inhibition of polymorphonuclear granulocyte (PMN) infiltration or function and the inhibition of nitric oxide (NO) synthase (NOS) induction or activity. Identification of anti-inflammatory cytokines which inhibit both processes may be of importance for the therapy of circulatory shock and chronic inflammation. We have studied the effect of interleukin-4 (IL-4) on (i) PMN migration and (ii) induction of NOS in macrophages and PMNs.

PMN migration was studied in an air pouch model in male Swiss albino mice (Perretti and Flower, 1993). Dorsal s.c. air pouches

Reprinted from

European Journal of Pharmacology

European Journal of Pharmacology 276 (1995) 9–19

Novel arylaminopyridazine-GABA receptor antagonists examined electrophysiologically in *Ascaris suum*

Richard J. Martin [a,*], Jean-Marie Sitamze [b], Anne H. Duittoz [b], Camille G. Wermuth [b]

[a] *Department of Preclinical Veterinary Sciences R.(D.) S.V.S., Summerhall, University of Edinburgh, Edinburgh EH9-3QT, UK*
[b] *Departement de Pharmacochimie Moleculaire, L'Université Louis Pasteur, 67084 Strasbourg Cedex, France*

Received 20 October 1994; revised 14 December 1994; accepted 20 December 1994



ELSEVIER

European Journal of Pharmacology

The EUROPEAN JOURNAL OF PHARMACOLOGY publishes manuscripts on the mechanisms of action of chemical substances affecting biological systems.
Manuscripts submitted to the journal are only accepted on the understanding that: (1) they are subject to editorial review; (2) they have not been and will not be published in whole or in part in any other journal; (3) the recommendations from the declaration of Helsinki and the internationally accepted principles in the care and use of experimental animals have been adhered to.
In addition to full length papers, the journal publishes short communications and rapid communications. Acceptability of rapid communications will be decided by the editors of the journal, who will be advised by an external referee. Full length manuscripts and short communications are generally submitted to 2 referees who are chosen for their ability to evaluate the work. Authors may request that certain referees should not be chosen. Members of the editorial board will usually be called upon for advice when there is disagreement among the referees or between referees and authors, or when the editors believe that the manuscript has not received adequate consideration from the referees. In order to reduce mailing cost, manuscripts will not be returned. Only the decision of the editorial office, together with the advice of the referees will be sent to the author(s). Referees will be requested to keep the copy of the manuscript which they have received for evaluation, and to destroy it once they have been notified of the final decision concerning the manuscript. When authors submit a revised manuscript, they should reply to the comments of the referees, indicating which comments have been incorporated and the reasons for disregarding any suggestions considered unacceptable. Revised manuscripts should be returned in duplicate to the editors. A revised manuscript should be received by the editorial office not later than 5 weeks (in case of minor revision) or 10 weeks (in case of extensive revision) after the editorial decision was sent to the author(s); otherwise it will be processed as a new manuscript. Handwritten additions or corrections will not be accepted. Only complete retyping of the pages affected by revision is acceptable.
For further information please refer to the 'General instructions' at the end of this issue, and the 'Notice to authors' published in Vol. 272, No. 1, p. v.

Founded in 1967. Founding editors: David de Wied and Jacques van Rossum.

Editors: W.H. GISPEN, Utrecht (chairman) J. BRUINVELS, Utrecht F.P. NIJKAMP, Utrecht D.H.G. VERSTEEG, Utrecht

Honorary editor: D. DE WIED

Editorial board:

C. ADVENIER, Paris
J. ARNT, Valby
P.J. BARNES, London
L. BARTHÓ, Pécs
G. BIGGIO, Cagliari
J. BORRELL, Madrid
O.E. BRODDE, Halle
T.F. BURKS, Houston
E. COSTA, Orangeburg
L.X. CUBEDDU, Caracas
S. ELLIS, Washington
M. ENDOH, Yamagata
J.P.M. FINBERG, Haifa
J.A. GARCÍA-SÁINZ, Mexico
G.F. GEBHART, Iowa City
Y. IGNATOV, Leningrad
D.A. KHARKEVICH, Moscow
Z. KLEINROK, Lublin
R. KVETNANSKY, Bratislava
G. LAMBRECHT, Frankfurt/M
M. LAZDUNSKI, Valbonne
R. LEFEBVRE, Gent
X.Y. LI, Shanghai
W. LÖSCHER, Hannover
J.M. LUNDBERG, Stockholm
G.S. MARKS, Kingston
T. MASAKI, Kyoto
J. McCULLOCH, Glasgow
D.N. MIDDLEMISS, Harlow
H. MÖHLER, Zurich
E.E. MÜLLER, Milan
H.R. OLPE, Basel
J.A. RIBEIRO, Oeiras
M.R. ROSEN, New York
H.J. RUSKOAHO, Oulu
A. SARIA, Innsbruck
P.R. SAXENA, Rotterdam
R. SCHULZ, München
P.L. SHARMA, Chandigarh
P.F. SPANO, Brescia
J.C. STOCLET, Strasbourg
N.A. TERRAGNO, Buenos Aires
P.B.M.W.M. TIMMERMANS, Wilmington
T. TOMITA, Nagoya
D.J. TRIGGLE, Buffalo
B.J.R. WHITTLE, Beckenham
R.J. WINQUIST, Ridgefield

Consultants:

B. AHRÉN, Malmö; E. BEUBLER, Graz; G. BURNSTOCK, London; R. BUSSE, Frankfurt/M; A.G. CHAPMAN, London; S.J. COOPER, Durham; R. COUTURE, Montreal; J.M. CRAWLEY, Bethesda; S.E. DAHLÉN, Stockholm; W. DE JONG, Strasbourg; A. DEN HERTOG, Groningen; G. DI CHIARA, Cagliari; H.N. DOODS, Biberach; G.J. DUSTING, Parkville; S.H. FERREIRA, Ribeirao Preto; A.W. FORD-HUTCHINSON, Dorval; J.R. FOZARD, Basel; D. GANTEN, Berlin-Buch; J.F. GIUDICELLI, Le Kremlin-Bicêtre; A.R. GREEN, London; R.J. GRYGLEWSKI, Kraków; H. HAMON, Paris; A. HERMAN, Antwerpen; P. HOLZER, Graz; D. HOYER, Basel; J.P. HUIDOBRO-TORO, Santiago; L.J. IGNARRO, Los Angeles; S.D. IVERSEN, Oxford; H. KARAKI, Tokyo; S.J. KONTUREK, Kraków; G. KUNOS, Richmond; R. LAVERTY, Dunedin; B.E. LEONARD, Galway; B.R. LUCCHESI, Ann Arbor; C.A. MAGGI, Florence; I.G. MARSHALL, Glasgow; M.J. MILLAN, Croissy-sur-Seine (Paris); A.H. MULDER, Amsterdam; T. NABESHIMA, Nagoya; R.J. NAYLOR, Bradford; D.J. NUTT, Bristol; M. OTSUKA, Tokyo; J.M. PALACIOS, Barcelona; J.R. PARRATT, Glasgow; J.N. PENNEFATHER, Clayton; R. QUIRION, Verdun; M. RAITERI, Genova; U. RAVENS, Essen; D. REGOLI, Sherbrooke; B.P. ROQUES, Paris; H. SCHOEMAKER, Bagneux; K. SCHRÖR, Düsseldorf; E. SEIFEN, Little Rock; K.F. SEWING, Hannover; P. SKOLNICK, Bethesda; P. SNEDDON, Glasgow; S.H. SNYDER, Baltimore; N. SPERELAKIS, Cincinnati; K. STARKE, Freiburg; H.A.J. STRUYKER BOUDIER, Maastricht; R.K. TÜRKER, Ankara; P.A. VAN ZWIETEN, Amsterdam; B.B. VARGAFTIG, Paris; J.R. WALTERS, Bethesda; J. ZAAGSMA, Groningen

ELSEVIER

European Journal of Pharmacology 276 (1995) 9–19

ejp

Novel arylaminopyridazine-GABA receptor antagonists examined electrophysiologically in *Ascaris suum*

Richard J. Martin [a,*], Jean-Marie Sitamze [b], Anne H. Duittoz [b], Camille G. Wermuth [b]

[a] *Department of Preclinical Veterinary Sciences R.(D.) S.V.S., Summerhall, University of Edinburgh, Edinburgh EH9-3QT, UK*
[b] *Departement de Pharmacochimie Moleculaire, L'Université Louis Pasteur, 67084 Strasbourg Cedex, France*

Received 20 October 1994; revised 14 December 1994; accepted 20 December 1994

Abstract

The structure-activity relationships of 35 novel derivatives of 2-(carboxypropyl)-3-amino-4-methyl-6-phenyl pyridazine (SR 95103) were examined as γ-aminobutyric acid (GABA) antagonists in the flap preparation of the parasitic nematode, *Ascaris suum*, using a two-microelectrode current-clamp technique. All but one of the potent antagonists displaced GABA dose-response curves to the right without reduction in the maximum response. The dissociation constants of the more potent competitive antagonists were described using a model which assumed that two molecules of GABA were required to open the ion channel but that only one molecule of antagonist acted on each ion channel. By exploring the structure-activity relationship, the potency of the antagonist was increased from a K_B of 64 μM for SR 95103 to a K_B of 4.7 μM for NCS 281-93 (2-(3-carboxypropyl)-3-amino-4-phenylpropyl-6-phenyl pyridazine).

Keywords: Arylaminopyridazine; GABA (γ-aminobutyric acid) derivative; SR 95103; GABA receptor antagonist; (*Ascaris suum*)

1. Introduction

The γ-aminobutyric acid (GABA) receptor of nematode parasites has been identified as a site of action for anthelmintic drugs (Del Castillo et al., 1964a; Martin, 1987). The anthelmintic, piperazine, hyperpolarizes body muscle cells in the porcine nematode, *Ascaris suum*, by mimicking the action of the natural neuromuscular inhibitory transmitter GABA (Del Castillo et al., 1964a,b). Bath application of GABA or piperazine activates extrasynaptic GABA receptors on *Ascaris* muscle cells and produces an increase in membrane Cl^- conductance (Martin, 1980, 1982). The antibiotic anthelmintic, ivermectin, has also been shown to interact with GABA receptors on *Ascaris* muscle (Holden-Dye et al., 1988; Martin and Pennington, 1989) and to act as an antagonist. Thus pharmacological characterization of the *Ascaris* GABA receptor and its differences to vertebrate GABA receptors is of interest for the design of anthelmintic agents. For therapeutic reasons, it is also necessary to compare the *Ascaris* GABA receptor with vertebrate host $GABA_A$ receptors.

Pharmacological examination of the *Ascaris* GABA receptor has shown, to a first approximation, that the agonist profile is like that of a vertebrate $GABA_A$ receptor (Holden-Dye et al., 1989). In contrast, the antagonist profile is unlike that of a $GABA_A$ receptor. The $GABA_A$ antagonists bicuculline, picrotoxin, securinine, pitrazepine, *t*-butylbicyclophosphorothionate (TBPS), RU5135 and dieldrin are either weak or inactive in *Ascaris* (Martin, 1980; Holden-Dye et al., 1989; Martin et al., 1991). In vertebrates the arylaminopyridazine, SR 95331, is about 20 times more potent than SR 95103 as a $GABA_A$ antagonist (Heaulme et al., 1986) but SR 95531 has a lower potency than SR 95103 in *Ascaris* (Duittoz and Martin, 1991a). In *Ascaris* SR 95103 behaves as a competitive antagonist with a dissociation constant, K_B, of 64 μM (Duittoz and Martin, 1991b).

As a result of observations on SR 95103 and SR 95531 it was suggested that the structure-activity relationship of arylaminopyridazine GABA receptor antag-

* Corresponding author. Tel. 00-44-31-650-6094, fax 00-44-31-650-6576, e-mail R.J.Martin@ed.ac.uk.

0014-2999/95/$09.50 © 1995 Elsevier Science B.V. All rights reserved
SSDI 0014-2999(94)00778-0

onists would be different at the *Ascaris* GABA receptor and be unlike a vertebrate $GABA_A$ receptor (Duittoz and Martin, 1991a). In a study comparing a series of arylaminopyridazine derivatives, this hypothesis was confirmed and the results interpreted to indicate that accessory binding sites required for binding of an antagonist of vertebrate $GABA_A$ receptors were different to the accessory binding sites on *Ascaris* muscle GABA receptors (Duittoz and Martin, 1991b). The study also indicated that the action of novel arylaminopyridazine derivatives should be investigated with a view to examining further the structure-activity relationship of these compounds and to find a more potent antagonist to advance antiparasitic drug development.

This paper then describes results of experiments in which 35 novel arylaminopyridazine-GABA derivatives were synthesized and screened and the potency of the more potent analogues tested to determine their K_B. As a result of these experiments it was possible to identify NCS 281-93 as an antagonist that was an order more potent than SR 95103 at the *Ascaris* muscle receptor.

2. Materials and methods

2.1. Preparation and recording

Ascaris suum were collected from the local abattoir and kept in Locke's solution at 34°C. They were used within 4 days. A muscle flap preparation (Martin, 1980) was pinned, cuticle side down, in an experimental chamber and maintained at 22°C and bathed in a high-Cl^- and low-Ca^{2+} Ringer containing (mM): NaCl, 135; KCl, 3; $MgCl_2$, 15.7; glucose, 3; Tris, 5; pH 7.2 adjusted with maleic acid. For the experiments with the less soluble antagonists, 2% dimethyl sulphoxide (DMSO) was added to all the Ringer solutions to prevent precipitation of the antagonist. 2% DMSO had a small depressant effect on GABA-induced conductance changes so a fixed concentration was used in all solutions throughout the experiments with the less soluble antagonists. The DMSO had no direct effect on resting membrane conductances or potentials in *Ascaris*.

Two glass microelectrodes (10–40 MΩ) filled with 2 M K acetate were inserted into the bag region of the muscle cell: one was used for current injection (40 nA, 1 s, 0.25 Hz), the other was used for recording the voltage response. The signals were recorded and amplified with an Axoclamp 2A amplifier, monitored on a Tektronix 2210 oscilloscope and recorded on a Lecromed 216MX two-channel chart recorder. The input conductance of the bag was calculated from the voltage response to the hyperpolarizing current pulses:

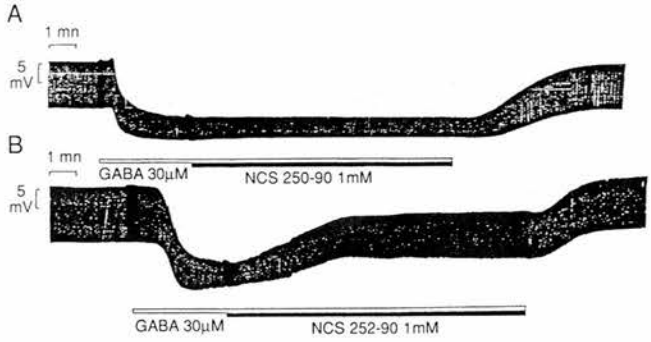


Fig. 1. Effect of 1 mM NCS 250-90 (A) and 1 mM NCS 252-90 (B) on the change in input conductance produced, ΔG_{con} (control) and ΔG_{ant} (with antagonist) by 30 μM GABA. A: NCS 250-90; resting membrane conductance, 3.3 μS; 30 μM GABA induced ΔG_{con}, 1.8 μS; 1 mM NCS 250-90 + 30 μM GABA, ΔG_{ant}, 1.8 μS; 0% antagonism. B: NCS 252-90; resting membrane conductance, 3.1 μS; 30 μM GABA induced ΔG_{con}, 1.4 μS; 1 mM NCS 252-90 + 30 μM GABA, ΔG_{ant}, 0.3 μS; 78.6% antagonism.

the I/V relationship is sufficiently linear during the injection of hyperpolarizing current to permit an accurate assessment of the input conductance.

The preparation was not perfused continuously because of the limited quantities of antagonist available. Initially to detect antagonist activity, 30 μM GABA was applied and when the membrane conductance stabilized to a new value, the bath solution was replaced with 30 μM GABA + 1 mM NCS compound (Fig. 1). In some experiments 30 μM GABA + 1 μM NCS compound or GABA + 0.1 mM NCS compound were also tested. Antagonists found to be more potent at 1 mM than SR 95103, i.e. to have a percent antagonism greater than 93% with this test, were tested at several concentrations against GABA dose-response curves (Fig. 2). GABA dose-response relationships were obtained by cumulative application of increasing GABA concentrations without washing between concentrations. The method used gentle draining of the bath (volume 6 ml) and then flushing the bath with 10 ml of the next GABA concentration. The antagonist was applied before the lowest GABA concentration and remained present when the higher concentrations of GABA were applied. A control GABA dose-response curve without the antagonist was always obtained first from the test cell to permit dose ratios to be calculated. The antagonists that readily dissolved in the aqueous phase and that did not require DMSO for solubility were easily washed off the preparation and repeated application of GABA yielded dose-response curves overlapping the controls; the more lipophilic antagonists requiring DMSO for solubility were only slowly washed from the preparation. Consequently antagonism was assessed by comparing control responses to GABA observed prior to antagonist application with the responses observed in the presence of antagonist.

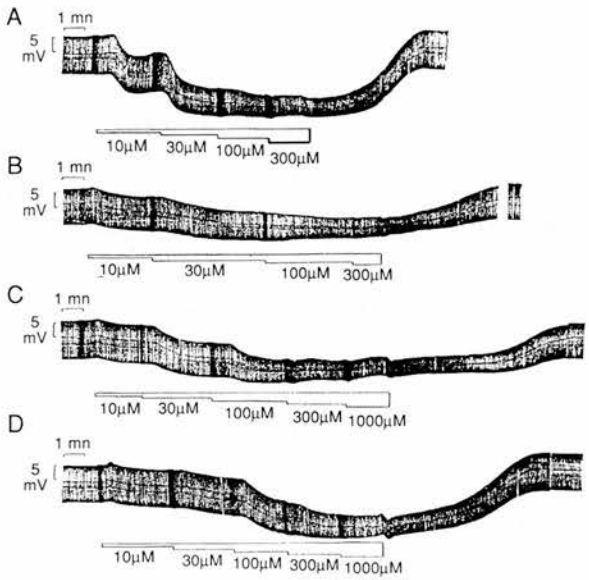


Fig. 2. Effect of 0.1, 0.3, 1 mM NCS 247-90 on GABA dose-response relationship. A: Control responses to cumulative application of GABA. B: In the presence of 0.1 mM NCS 247-90. C: In the presence of 0.3 mM NCS 247-90. D: In the presence of 1 mM NCS 247-90. The corresponding plot is shown in Fig. 3.

2.2. Analysis

The actions of 10 μM, 0.1 mM and/or 1 mM NCS compound on the change in input conductance produced by 30 μM GABA were used to calculate the percentage antagonism thus:

$$\text{percentage antagonism} = 100\left[1 - (\Delta G_{ant}/\Delta G_{con})\right],$$

where ΔG_{con} is the change in input conductance produced by the initial control application of 30 μM GABA and ΔG_{ant} is the change in input conductance produced by the application of 30 μM GABA + antagonist, allowing at least 10 min for the antagonist to reach its maximum effect.

Dose ratios determined from the plots of the GABA dose-response curves and the effects of NCS 281-93 were examined using the modified Schild plot (Williams et al., 1988):

$$\log(DR^{n_H} - 1) = M \times \log[X_B] + pK_B,$$

where the Hill coefficient, n_H, is 2 (Duittoz and Martin, 1991b) and M is the number of antagonist molecules interacting with the receptor, and pK_B is the negative logarithm of the dissociation constant of the antagonist receptor complex.

Dose-response relationships for NCS 281-93 were also fitted to the equation:

$$\Delta G = \Delta G_{max}/\left(1 + [ED_{50}/X_a]^{n_H} + [ED_{50}/X_a]^{n_H} \times [X_b/K_B]^m\right) \quad (1)$$

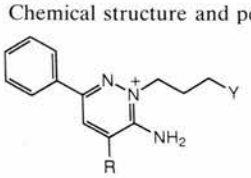
where ΔG is the change in input conductance; ΔG_{max} is the maximum change in input conductance; ED_{50} is the concentration of GABA producing 50% of the ΔG_{max} response; n_H is the Hill coefficient; X_b is the concentration of the NCS antagonist; K_B is the antagonist dissociation constant; M is the degree of cooperativity shown by the antagonist. A non-linear least squares estimate of the parameters of this equation was made using a program written in FORTRAN using the subroutine NAG E04CCF.

Means and standard errors (S.E.) were calculated. Statistical significance was assessed using a two-tailed independent t-test. All compounds cited as having a different potency in the Results section were tested with the t-test and had a significance level of $P < 0.05$.

2.3. Drugs

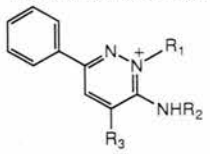
GABA was obtained from Sigma. The NCS compounds, Tables 1–6 and below, were synthesized and their purity confirmed by nuclear magnetic resonance (NMR) (Sitamze et al., 1992; Sitamze, 1993).

Table 1
Chemical structure and percent antagonism of derivatives with modification of the carboxyl function



Compound	Y	R	Benzocyclohepta(*e*-5,6)	% Antagonism (0.1 mM)		% Antagonism (1 mM)		K_B (μM)
SR 95103	COOH	CH_3	Absent	–		93 ± 3	($n = 5$)	64 ± 13 ($n = 13$)
NCS 248-90	SO_3H	H	Present	–		14 ± 5	($n = 6$)	–
NCS 249-90	SO_3H	CH_3	Absent	–		0, 0	($n = 2$)	–
NCS 250-90	SO_3H	CH_3CH_2	Absent	–		0, 0	($n = 2$)	–
NCS 256-91	COOH	H	Present	0, 16	($n = 2$)	57, 79	($n = 2$)	–
NCS 274-90	Tetrazolyl	$C_6H_5CH_2CH_2$	Absent	0, 10	($n = 2$)	44, 60	($n = 2$)	–
NCS 283-93	$OP(OH)_2$	CH_3	Absent	0 ± 0	($n = 3$)	0 ± 3	($n = 3$)	–

Table 2
Derivatives with modification of the GABA chain



Compound	R1	R2	R3	% Antagonism (0.1 mM)		% Antagonism (1 mM)		K_B (μM)
SR 95103	$(CH_2)_3COOH$	H	CH_3	–		93 ± 3	($n = 5$)	64 ± 13
NCS 194-83	$(CH_2)_4COOH$	H	CH_3	–		46 ± 9	($n = 4$)	–
NCS 259-91	No GABA side-chain	$C_6H_5CH_2CH_2$	CH_3	30 ± 18	($n = 3$)	69 ± 16	($n = 3$)	–
NCS 260-91	No GABA side-chain	$C_6H_5CH_2CH_2$	CH_3CH_2	0, 7	($n = 2$)	23, 29	($n = 2$)	–

2.3.1. Derivatives with modification of the carboxylic function (Table 1)

NCS 248-90, 2-(3-sulphonylpropyl)-3-amino-benzocyclohepta(*e*-5,6) pyridazinium bromide; NCS 249-90, 2-(3-sulphonylpropyl)-3-amino-4-methyl-6-phenyl pyridazine bromide; NCS 250-90, 2-(3-sulphonylpropyl)-3-amino-4-ethyl-6-phenyl pyridazinium bromide; NCS 256-91, 2-(3-carboxypropyl)-benzocyclohepta(*e*-5,6)-3-amino pyridazinium bromide; NCS 274-93, 2-(3-tetrazolylpropyl)-3-amino-4-phenylethyl-6-phenyl pyridazinium chloride; NCS 283-93, 2-(3-phosphonopropyl)-3-amino-4-methyl-6-phenyl pyridazinium bromide.

2.3.2. Derivatives with the length of the GABA chain modified (Table 2)

NCS 194-83, 2-(4-carboxybutyl)-3-amino-4-methyl-6-phenyl pyridazinium bromide; NCS 259-91, 3-phenylethylamine-4-methyl-6-phenyl pyridazinium tartrate; NCS 260-91, 3-phenylethylamine-4-ethyl-6-phenyl pyridazinium tartrate.

2.3.3. Acetoxyethyl derivatives (Table 3)

NCS 276-93, 2-(2′-acetoxyethyl)-3-amino-4-methyl-6-phenyl pyridazinium bromide; NCS 277-93, 2-(2′-acetoxyethyl)-3-amino-6-methoxyphenyl pyridazinium bromide; NCS 278-93, 1-(2′-acetoxyethyl)-2-amino-5-phenyl pyrazinium bromide; NCS 279-93, 2-(2′-acetoxyethyl)-3-amino-5-phenyl pyridazinium bromide.

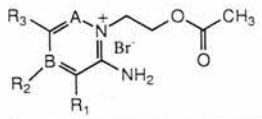
2.3.4. Derivatives with the amine function in position 3 modified (Table 4)

NCS 263-91, 2-(3-carboxypropyl)-3-phenylethylamino-4-ethyl-6-phenyl pyridazinium bromide; NCS 271-92, 2-(3-carboxypropyl)-4-phenylethyl-6-phenyl pyridazinium bromide; NCS 272-92, 2-(3-carboxypropyl)-4-biphenylethyl-6-phenyl pyridazinium bromide; NCS 273-92, 2-(3-carboxypropyl)-4-(2-ethylnaphthyl)-6-phenyl pyridazinium bromide; NCS 280-93, 2-(3-carboxypropyl)-3-(*N*′-acetyl-amino)-4-phenylethyl-6-phenyl pyridazinium bromide.

2.3.5. Derivatives with the substituants in position 4 modified (Table 5)

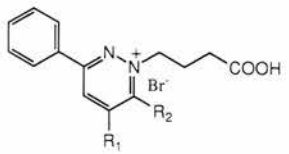
NCS 247-90, 2-(3-carboxypropyl)-3-amino-4-ethyl-6-phenyl pyridazinium bromide; NCS 252-90, 2-(3-carboxypropyl)-3-amino-4-isopropyl-6-phenyl pyridazinium bromide; NCS 251-90, 2-(3-carboxypropyl)-3-amino-4-benzyl-6-phenyl pyridazinium bromide; NCS 253-90, 2-(3-carboxypropyl)-3-amino-4-paramethoxybenzyl-6-phenyl pyridazine bromide; NCS 254-90, 2-(3-carboxypropyl)-3-amino-4-phenylethyl-6-phenyl pyridazinium bromide; NCS 258-91 2-(3-carboxypropyl)-3-amino-4-paramethylbenzyl-6-phenyl pyridazinium bro-

Table 3
Acetoxyethyl derivatives



Compound	R1	R2	R3	A	B	% Antagonism (1 mM)	
NCS 276-93	CH_3	H	C_6H_5	N	C	0, 10	($n = 2$)
NCS 277-93	$CH_3OC_6H_5$	H	H	N	C	0, 22	($n = 2$)
NCS 278-93	H	H	C_6H_5	C	N	37, 40	($n = 2$)
NCS 279-93	H	C_6H_5	H	N	C	50, 25	($n = 2$)

Table 4
Derivatives with the amine function in position 3 modified



Compound	R1	R2	% Antagonism (10 μM)		% Antagonism (0.1 mM)		% Antagonism (1 mM)		K_B (μM)	
SR 95103	CH_3	NH_2	–		–		93 ± 3	(n = 5)	64 ± 13	(n = 13)
NCS 263-91	CH_3CH_2	$NH(CH_2)_2C_6H_5$	–		24.3 ± 9	(n = 4)	68 ± 13	(n = 3)	–	
NCS 271-92	$C_6H_5CH_2CH_2$	H	0	(n = 1)	6, 0	(n = 2)	49, 38	(n = 2)	–	
NCS 272-92	Biphenyl$(CH_2)_2$	H	0	(n = 1)	12	(n = 1)	88 ± 12	(n = 3)	–	
NCS 273-92	Naphthyl$(CH_2)_2$	H	0, 0	(n = 2)	14, 21	(n = 2)	100, 100	(n = 2)	120, 140	(n = 2)
NCS 280-93	$C_6H_5CH_2CH_2$	$NHCOCH_3$	7, 0	(n = 2)	26, 31	(n = 2)	59, 100	(n = 2)	–	

mide; NCS 266-92, 2-(3-carboxypropyl)-3-amino-4-paramethoxyphenethyl-6-phenyl pyridazinium bromide; NCS 267-92, 2-(3-carboxypropyl)-3-amino-4-meta-methoxyphenethyl-6-phenyl pyridazinium bromide; NCS 268-92, 2-(3-carboxypropyl)-3-amino-4-[(4,3-methylenedioxy)]phenethyl-6-phenyl pyridazinium bromide; NCS 281-93, 2-(3-carboxypropyl)-3-amino-4-phenylpropyl-6-phenyl pyridazinium bromide; NCS 282-93, 2-(3-carboxypropyl)-3-amino-4-diphenylethyl-6-phenyl pyridazinium bromide.

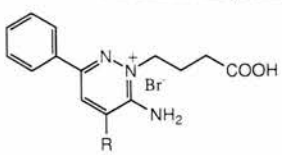
2.3.6. Derivatives with modification to the pyridazine ring (Table 6)

NCS 255-90, 3-(3-carboxypropyl)-2-amino-5-phenyl thiadiazolium; NCS 257-91, 1-(3-carboxypropyl)-2-amino 5-phenyl pyridazinium bromide; NCS 261-91, 3-phenethylamine-8-phenyl phthalazine; NCS 262-91, 3-(*n*-(2-aminoethylmorpholine))-8-phenyl phthalazine chlorhydrate; NCS 264-91, 2-(3-carboxypropyl)-3-*N*-(2-(aminoethylmorpholine))-8-phenyl phthalazinium bromide; and NCS 265-91, 2-(3-carboxypropyl)-3-phenethylamine-8-phenyl bromide.

3. Results

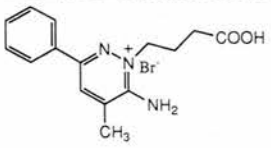
The results reported here are based on the analysis of experiments performed on 123 cells from more than 80 preparations. The results of similar tests on SR compounds (Duittoz and Martin, 1991b) are included for comparative purposes. Cells selected for recording and analysis had a resting membrane potential more

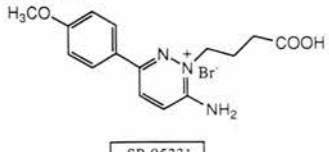
Table 5
Derivatives modified in position 4

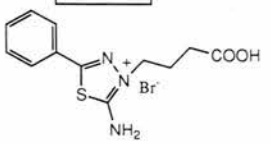


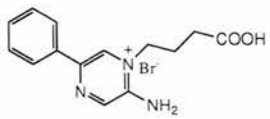
Compound	R	% Antagonism (10 μM)		% Antagonism (0.1 mM)		% Inhibition (1 mM)		K_B (μM)	
SR 95103	CH_3	–		–		93 ± 3	(n = 5)	64 ± 13	(n = 13)
SR 95132	C_6H_5	–		–		89 ± 3	(n = 5)	65 ± 20	(n = 9)
NCS 247-90	CH_3CH_2	–		–		95 ± 3	(n = 5)	55 ± 16	(n = 13)
NCS 251-90	$C_6H_5CH_2$	–		24, 48	(n = 2)	99 ± 1	(n = 3)	31 ± 14	(n = 3)
NCS 252-90	$(CH_3)_2CH$	–		–		81 ± 3	(n = 3)	–	
NCS 253-90	*p*-HO-$C_6H_5CH_2$	–		30,	(n = 1)	91 ± 5	(n = 3)	–	
NCS 254-90	$C_6H_5CH_2CH_2$	–		56 ± 4	(n = 4)	97, 100	(n = 2)	11 ± 3	(n = 4)
NCS 258-91	*p*-CH_3-$C_6H_4CH_2$	5, 11	(n = 2)	55, 42	(n = 2)	93, 86	(n = 2)	–	
NCS 266-92	*p*-MeO-$C_6H_4(CH_2)_2$	0	(n = 1)	15, 38	(n = 2)	88, 97	(n = 2)	–	
NCS 267-92	*m*-MeO-$C_6H_4(CH_2)_2$	0, 0	(n = 2)	18, 35	(n = 2)	73, 93	(n = 2)	–	
NCS 268-92	4,3-Methylenedioxy	0, 0	(n = 2)	0, 0	(n = 2)	74, 58	(n = 2)	–	
NCS 281-93	$C_6H_5CH_2CH_2CH_2$	24, 10	(n = 2)	57, 50	(n = 2)	94, 96	(n = 2)	4.7 ± 0.7	(n = 11)
NCS 282-93	$(C_6H_5)_2CHCH_2$	11, 27	(n = 2)	75, 42	(n = 2)	73, 100	(n = 2)	Non-competitive	

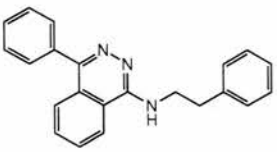
Table 6
Derivatives with a modified ring structure

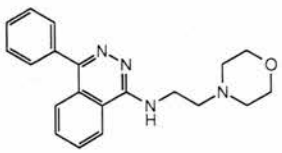

SR 95103

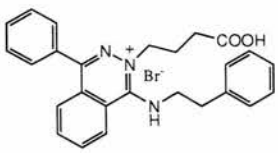

SR 95331

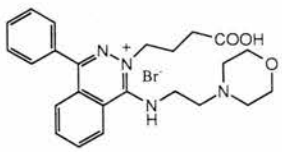

NCS 255-91


NCS 257-91


NCS 261-91


NCS 262-91


NCS 265-91


NCS 264-91

Compound	Ring modification	% Inhibition (0.1 mM)		% Inhibition (1 mM)	
SR 95103	None	–		93 ± 3	($n = 5$)
SR 95531	None	–		44 ± 6	($n = 6$)
NCS 255-90	Thiazolium			49 ± 9	($n = 4$)
NCS 257-91	Pyrazinium	0, 6	($n = 2$)	20, 65	($n = 2$)
NCS 261-91	Phthalazine	0, 0	($n = 2$)	14, 0	($n = 2$)
NCS 262-91	Phthalazine	0, 8	($n = 2$)	0, 25	($n = 2$)
NCS 264-91	Phthalazine	2.7 ± 3		8 ± 5	($n = 4$)
NCS 265-91	Phthalazine	43 ± 18	($n = 4$)	75 ± 24	($n = 3$)

negative than −20 mV and a resting input conductance between 2.0 and 3.5 μS. Recordings were rejected if the resting input conductance failed to return to less than 120% of the control after the final wash.

All of the antagonists were applied at a concentration up to 1 mM in the absence of GABA and found to have no effect on membrane potential or input conductance. The lack of effect of the compounds on input conductance showed that the compounds do not act as GABA agonists despite the presence of the GABA side-chain in the 2-[3-carboxypropyl] derivatives or as nicotinic agonists despite the acetylcholine side-chain in the 2-[2′-acetoxyethyl] derivatives.

Fig. 1A and B illustrates the first test for activity that was carried out on all of the antagonists: 30 μM GABA was applied initially and the conductance increase produced by the GABA allowed to come to a steady state; the antagonist was then applied at a concentration of 1 mM, on top of the GABA and again the input conductance permitted to come to a steady state. Fig. 1A shows the effect of a low potency compound, NCS 250-90: GABA increased the resting input conductance from 3.2 μS to 5.0 μS but this remained unchanged in the presence of the antagonist so that the percent antagonism was 0%. Fig. 1B shows the effect of a more potent antagonist, NCS 252-90: GABA increased the resting input conductance from 3.1 μS to 4.5 μS so that the input conductance change, ΔG, was 1.4 μS. In the presence of the antagonist, ΔG was 0.3 μS and the percent antagonism was 79%. The effects of 10 μM and 0.1 mM antagonist were also examined in a similar manner. Tables 1, 2, 3, 4, 5 and 6 summarize the percentage antagonisms observed and illustrate the structures of the compounds.

3.1. Derivatives with modification of the carboxylic function

Table 1 shows the list of compounds examined where the carboxylic group on the GABA chain has been replaced with sulphonic (NCS 248-90, NCS 249-90 and NCS 250-91), phosphonic (NCS 283-93) and tetrazole (NCS 274-93) groups. Comparison of the mean percentage antagonism for NCS 249-90 and NCS 250-90 with the mean percentage antagonism shown by SR 95103, and the percent antagonism shown by NCS 248-90 with the percent antagonism shown by NCS 256-91, demonstrates that the introduction of the sulphonic group significantly (all values at 1 mM $P < 0.01$) reduces potency and renders compounds inactive. The same is true when the phosphonic group of NCS 283-93 replaces the carboxylic group of SR 95103. Comparison of the antagonism shown by 0.1 mM concentrations of NCS 274-93 with that of NCS 254-90 (Table 5) shows that replacing a carboxylic group with a tetrazole group significantly ($P < 0.01$) reduces the potency of the antagonist.

3.2. Derivatives with the GABA side-chain modified

The significant ($P < 0.001$) reduction in the mean percent antagonism of 1 mM NCS 194-83 when compared to SR 95103 (Table 2) shows the effect of increasing the length of the acid side-chain from 4 to 5 atoms. Comparison of the structure and activity of NCS 260-91 (Table 2) with the structure and activity of NCS 263-91 (Table 4) shows that omission of the GABA side-chain leads to a significant ($P < 0.02$) reduction in activity. Similarly a comparison of the structure and activity of NCS 276-93 (Table 3) with that of SR 95103 (Table 1) shows that replacing the GABA side-chain with an acetylcholine side-chain leads to a large (significant $P < 0.01$) reduction in potency. None of the acetoxyethyl derivatives were potent. It appears then that a 4-carbon carboxylic side-chain on the 2-position of the pyridazine ring is important for the potency of the antagonist.

3.3. Derivatives with modification of the 3-amino moiety

Acylation of the 3-amino group leads to a reduction in activity: this is illustrated by comparing the percent antagonism produced by a 0.1 mM concentration of the acylated compound NCS 280-93 (Table 4) which is significantly ($P < 0.01$) less than the non-acylated analogue, NCS 254-90 (Table 5). Alkylation of the 3-amino group also leads to significant reduction ($P < 0.05$ at 1 mM) in activity and is seen by comparing NCS 263-91 (Table 4) with NCS 247-90 (Table 5). The requirement for the 3-amino group for activity is illustrated by comparing the poor activity of a derivative that lacks the amine moiety, NCS 271-92 (Table 4) with the derivative which possesses the amine group and a greater inhibitory potency, NCS 254-93 (Table 4); the significance level at 0.1 mM was $P < 0.01$. Thus it appears that a free amine group in position 3 is required for the potency of the antagonist.

3.4. Modification of groups in position 4

The effect of substitution in the 4-position of the pyridazine ring has already been pointed out (Duittoz and Martin, 1991b). Substitution in this position appears to be detrimental to antagonist potency at the vertebrate $GABA_A$ receptor but it is a prerequisite for antagonist potency at the *Ascaris* muscle GABA receptor. The series of compounds shown in Table 5 were designed to investigate further the structure-activity relationships of substituents in this position.

The high percentage antagonisms shown by the compounds: SR 95103, SR 95132, NCS 252-90, NCS 247-90, NCS 251-90, NCS 254-90, NCS 258-91, NCS 281-93, NCS 282-93 (Table 5) are consistent with the view that introduction of lipophilic groups in position 4 facilitates the potency of the antagonist. The effect of introduction of the methoxy group on the phenyl ring of the 4-position chain in NCS 266-92 and NCS 267-92 is to reduce the lipophilicity of the side-chain and to reduce the mean activity of the antagonists when compared to NCS 254-90 that lacks the methoxy group; the differences in potency, however, did not reach statistical significance. Comparison of NCS 268-92 (a 4,3-methylene dioxy derivative of NCS 251-90) did reveal a statistically significant reduction ($P < 0.05$ at 1 mM) following substitution of more lipophilic moieties.

3.5. Mode of action of more potent antagonists

It order to examine further the mode of action of the more potent antagonist, GABA dose-response curves were obtained in the absence and then in the presence of different concentrations of antagonist: Fig. 2 shows an example of an experiment carried out with the antagonist NCS 247-90. Representative dose-response curves are shown in Fig. 3 for NCS 273-92, NCS 247-90, NCS 251-90, and NCS 254-90, in Fig. 4 for NCS 282-93, and in Fig. 5 for NCS 281-93.

Although there may be a small shift to the right with NCS 282-93 (Fig. 4) it was clear that the antagonism shown by NCS 282-93 was non-competitive (two experiments) because of the reduction of the slope of the dose-response curves: the other antagonists produced a parallel shift to the right without an obvious reduction in the maximum response, suggesting a competitive mechanism.

Dose ratios were determined from these plots as the ratio of the concentrations producing nearly half the

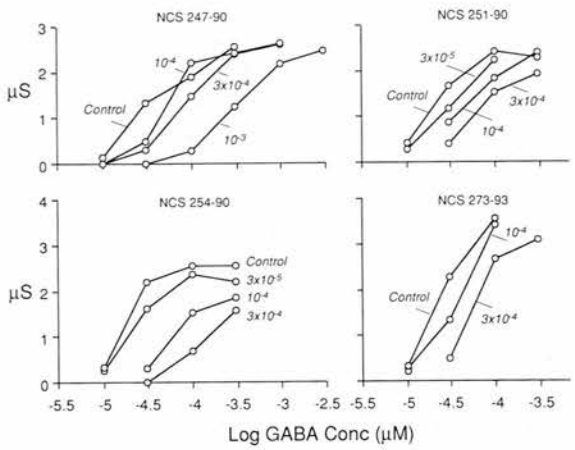


Fig. 3. Plots of GABA log-dose conductance-response relationships in single cells and the effect of antagonists: NCS 247-90, NCS 251-90, NCS 254-90 and NCS 273-90. Note that the shift to the right and the lack of depression in the maximum response suggest competitive antagonism.

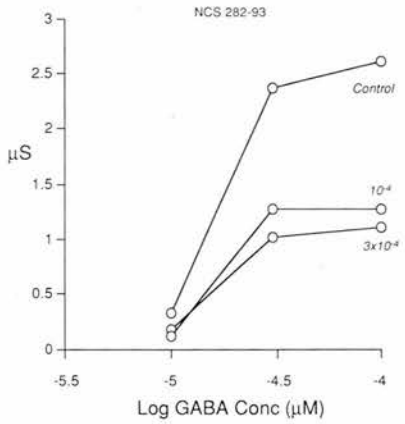


Fig. 4. Plot of GABA log-dose conductance-response relationship in a representative cell and the effect of the antagonist NCS 282-93. Note the small shift to the right but the reduction in the maximum response showing non-competitive antagonism.

maximum response observed. The dissociation constant, K_B, of the antagonists were then estimated for the antagonists with the equation:

$$K_B = (DR^2 - 1)/X_B,$$

where X_B is the antagonist concentration and DR is the dose ratio. The equation was used to take account of the cooperativity of the *Ascaris* GABA receptor which may be explained by two molecules of GABA being required to open the GABA channel but only one molecule of antagonist may interact with the receptor to prevent opening (Duittoz and Martin, 1991b).

The values of K_B determined are shown in Table 5. It can be seen that the potency of the antagonists increased from: SR 95103 with a K_B 64 μM (Duittoz and Martin, 1991b); to NCS 247-90 with a K_B of 55 μM; to NCS 251-90 with a K_B of 31 μM; to NCS 254-90 with a K_B of 11 μM; to NCS 281-93 with a K_B of 4.7 μM. Thus substituting the methyl group at position 4 in SR 95103 with a phenyl, phenylmethyl, phenylethyl, phenylpropyl leads to a progressive increase in the potency of the antagonist.

The effect of the most potent antagonist, NCS 281-93, on the GABA dose-response relationship was examined in three experiments by using a modified Schild plot, Fig. 4B, and by estimating the parameters of Eq. 1. The gradient of the modified Schild plot of Fig. 4B was 0.74. The non-linear least squares estimates for the constants of Eq. 1 were: n_H was 1.55; M was 0.95; G_{max} was 6.3 μS; the ED_{50} for GABA was 21 μM; and the K_B for NCS 281-83 was 8.6 μM. In two other

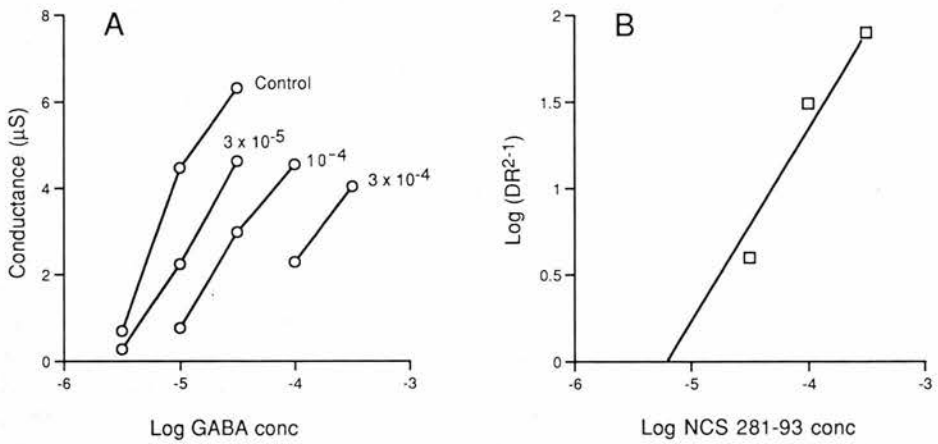


Fig. 5. A: Plot of the GABA log-dose-conductance response relationship in a representative cell and the effect of the antagonist NCS 281-93. Note the shift to the right and the absence of a reduced maximum response associated with the application of the antagonist. B: Modified Schild plot derived from the plot in (A); slope, 0.74; intercept on abscissa, 8 μM.

experiments similar results were obtained. These observations are consistent with the proposed mechanism whereby two molecules of GABA are required to produce opening but only one molecule of antagonist is required to produce blocking (Duittoz and Martin, 1991b). Similar values were estimated in single experiments for n_H and M with the antagonists: NCS 273-92, NCS 247-90, NCS 251-90, NCS 254-90 and NCS 282-93.

3.6. Modification of the pyridazine ring structure

Table 6 shows that NCS 255-90, a compound in which the pyridazine ring is replaced by a thiadiazolium ring, and NCS 257-91, a compound in which the pyridazine ring is replaced by a pyrazine ring, have approximately the same inhibitory potency as SR 95531, a pyridazine derivative not substituted in the 4-position. However NCS 255-90, NCS 257-91 and SR 95531 are all significantly ($P < 0.01$) less potent than SR 95103 (a pyridazine derivative with a 4-methyl substituent). These observations suggest that either the thiadiazolium or pyrazine ring could replace the pyridazine ring without a large change in potency. However, without substitution in a position equivalent to the 4-position on the pyridazine ring, there would be no increase in potency of the analogue.

Table 6 also shows the percent inhibition results obtained with the phthalazine derivatives: NCS 261-93, NCS 262-93, NCS 264-93, NCS 265-93. These compounds, except for NCS 265-93, are significantly ($P < 0.01$) less potent than SR 95103. Comparison of the structure activities of NCS 247-90, NCS 263-91 and NCS 265-91 suggests that the phthalazine ring does not reverse the loss in potency produced by acylation of the 3-amino moiety.

4. Discussion

We have measured the percent antagonism of the conductance response to 30 μM GABA as an initial measure of antagonist potency. Since this method used single concentrations of agonist and antagonist, it does not provide information about the type of antagonism involved. However, within a group of chemically related compounds such as the arylaminopyridazine derivatives, the percent antagonism can be used to indicate relative potencies. The method is a sensitive technique for detecting antagonism at the GABA receptor because the concentration of GABA selected, 30 μM, is near the EC_{50} for the GABA dose-response curve (Martin, 1980) and therefore in the linear section of the log dose-response curve. The method also permits a larger number of compounds to be screened for activity. The compounds that had a higher percent antagonism than the starting compound, SR 95103, were also examined by estimating their K_B values using a range of GABA as well as antagonist concentrations. The modified Schild analysis (Williams et al., 1988; Duittoz and Martin, 1991b) was used to determine K_B, since it allows for the cooperativety produced by two molecules of GABA being required for channel opening but only one molecule of antagonist being required to block the effect of GABA: this model has previously been shown to be appropriate for describing the action of the arylaminopyridazine derivatives at the *Ascaris* GABA receptor.

The estimated dissociation constant, K_B, or the mean antagonism obtained when applied at a concentration of 0.1 mM or 1 mM in the presence of 30 μM GABA gave the rank order of potency at the *Ascaris* muscle GABA receptor as: NCS 281-92 > NCS 254-90 > NCS 251-90 > NCS 247-90 > SR 95103 > NCS 258-91 > SR 95132 > NCS 272-92 ≈ NCS 282-93 > NCS 267-92 > NCS 252-90 > NCS 280-93 > SR 42666 ≈ NCS 273-92 > NCS 259-91 ≈ NCS 268-91 > SR 95133 > NCS 255-90 > NCS 194-83 ≈ SR 95531 ≈ NCS 271-93 ≈ NCS 257-91 > SR 42627 > NCS 260-90 > NCS 248-90 > SR 42640 ≈ NCS 264-90 ≈ NCS 261-91 ≈ NCS 283-90 > NCS 249-90 ≈ NCS 250-90. The potencies of the arylaminopyridazine derivatives obtained previously (Duittoz and Martin, 1991b) are also included to permit a fuller description of the antagonist profile. It is pointed out that because of the large number of compounds used in this list that the first of adjacent compounds is not necessarily significantly more potent than the second of the adjacent compounds but the list gives an indication of the relative potencies of the series of arylaminopyridazine derivatives tested. At a mammalian $GABA_A$ receptor the potency order of the compounds tested is: SR 95531 > SR 42666 > SR 42627 > SR 95103 > SR 95133 > SR 42640 > SR 95132 and it has already been pointed out that the different order in *Ascaris* (SR 95103 ≈ SR 95132 > SR 42666 > SR 95133 > SR 95531 > SR 42627 > SR 42640) distinguishes the receptors. This difference may be explained by differences in the accessory binding sites required by competitive antagonists rather than differences in the agonist binding site (Duittoz and Martin, 1991a,b).

4.1. Modification of the 2-position moiety

The structure-activity relationship showed that substitution of the carboxylic acid of the 2-(3-carboxypropyl) derivatives with sulphonic (NCS 249-90, NCS 250-90) or phosphonic acid (NCS 283-93) reduced potency. This effect appears comparable to the effect of substitution of the carboxylic group of GABA to produce 3-APS and P4S (Holden-Dye et al., 1989) which produces low potency agonists at the *Ascaris* GABA receptor. Lengthening the side chain of the 2-position

moiety (NCS 194-83, 5C like δ-aminovaleric acid) was also detrimental to the potency as it is for the agonist δ-aminovaleric acid. The observation that an intact GABA sequence is optimal for receptor recognition by the antagonist suggests that it is the 2-position moiety of the antagonist that binds to the *Ascaris* GABA agonist binding site. A distance of 5 A° between the acidic and basic function is likely to pertain since extended agonists (*trans*-aminocrotonic acid) are more potent than folded agonists (*cis*-crotonic acid), Holden-Dye et al., 1989). Complete removal of the 2-position moiety (NCS 259-91, NCS 260-91) did not lead to abolition of GABA receptor antagonist activity suggesting that the remaining molecule can still recognize part of the GABA receptor site. Similar conclusions have been obtained with other arylaminopyridazine GABA receptor antagonists for a mammalian $GABA_A$ receptor (Wermuth et al., 1987).

4.2. Modification of the 3-position

It has been concluded from agonist and antagonist structure-activity studies for a vertebrate $GABA_A$ receptor that: a GABA moiety bearing a positive charge is necessary for optimal receptor recognition by arylaminopyridazine derivatives and that additional binding sites by *N* substitution are only tolerated if they are part of a charge-delocalized amidinic or guanidinic system; replacement of the endo-exo amidinic system leads to total inactivation of the compound (Wermuth et al., 1987). This is supported by the fact that isosteric replacement of the 3-amino group by a neutral group leads to total inactivation. In *Ascaris*, by contrast, the compounds NCS 270-92, NCS 271-92, and NCS 273-92 which lack the 3-amino group still show antagonist activity at the GABA receptor, although they are reduced in potency compared to the 3-amino derivatives. The anthelmintic piperazine, which is a selective GABA agonist in *Ascaris* (Martin, 1982), also lacks an amidinic or guanidinic system delocalizing charge, again suggesting that delocalization is not an absolute requirement in *Ascaris*.

4.3. Substitution in the 4-position

In vertebrates, substitution in the 4-methyl group of SR 95103 with hydrogen (SR 95531), leads to an increase in potency but replacement with a phenyl group is detrimental to antagonist potency (Wermuth et al., 1987). By contrast, 4-position substitution appears to be a prerequisite for antagonist potency in *Ascaris* (Duittoz and Martin, 1991b). The difference between the vertebrate GABA receptor and the *Ascaris* receptor may be explained by obstruction of a free access zone between the anionic and cationic binding site (Wermuth and Rognan, 1987). The free access zone is required for receptor recognition in vertebrates but not *Ascaris* (Duittoz and Martin, 1991b). In the novel compounds studied in this paper, the introduction of more lipophilic groups increased the potency of the antagonist compound. Starting from a 4-methyl substitution (SR 95103), the potency of the antagonists increased from: a K_B of 64 μM, Duittoz and Martin (1991b); to NCS 247-90 with 4-phenyl substitution and a K_B of 55 μM; to NCS 251-90 with 4-phenylmethyl substitution and a K_B of 31 μM; to NCS 254-90 with 4-phenylethyl substitution and a K_B of 12 μM; to NCS 281-93 with a 4-phenylpropyl and K_B of 4 μM. Thus, substituting the methyl group at position 4 in SR 95103 leads to a progressive increase in the potency of the antagonists.

4.4. The GABA receptor as target site for anthelmintics

GABA receptors mediating an increase in the Cl^- conductance of neuronal membranes are found in vertebrates as well as in invertebrate muscle and nerve membranes (Nistri and Constanti, 1979) including nematode parasite membranes (Martin, 1980,1982). It has already been pointed out in the Introduction that the agonist profile of the *Ascaris* muscle GABA receptor and a vertebrate $GABA_A$ receptor are similar but that the antagonist profile is very different (Holden-Dye et al., 1989; Martin et al., 1991). These observations may be explained by vertebrate $GABA_A$ receptors and *Ascaris* muscle GABA receptors having similar agonist binding sites. The differences in the accessory binding sites required for antagonists may explain differences in the antagonist profiles (Ariëns et al., 1979; Wermuth et al., 1987; Duittoz and Martin, 1991b). It is therefore suggested that a selective GABA receptor antagonist for nematodes and *Ascaris* may be easier than an agonist to find.

Selective cholinergic agonist like levamisole, pyrantel and morantel are used as anthelmintics and appear to work by acting as agonists on nematode muscle acetylcholine receptors (Harrow and Gration, 1985; Martin et al., 1991). Stimulation of the acetylcholine receptors produces depolarization and spastic paralysis of the nematode leading to its expulsion. Unfortunately resistance to therapy with these compounds is increasing requiring higher concentrations of anthelmintic to be used (Sangster et al., 1991) or the change to a drug that has another mode of action. One way of increasing the effectiveness of a therapeutic regimen would be to add a selective GABA receptor antagonist along with the selective cholinergic agonist so that the two compounds could act in concert producing depolarization, contraction and spastic paralysis. Further study of the structure-activity relationships of arylaminopyridazines may permit the development of therapeutic approaches that can control nematode parasites resistant to other anthelmintic agents.

References

Ariëns, E.J., A.D. Beld, J.F.R. Miranda and A.M. Simonis, 1979, The pharmacon-receptor-effector concept, in: The Receptors, Vol. 1, ed. H. Rang (Plenum Press, New York) p. 33.

Del Castillo, J., W.C. De Mello and T. Morales, 1964a, Mechanism of the paralyzing action of piperazine on *Ascaris* muscle, Br. J. Pharmacol. 22, 463.

Del Castillo, J., W.C. De Mello and T. Morales, 1964b, Inhibitory action of γ-aminobutyric acid on *Ascaris* muscle, Experientia 20, 141.

Duittoz, A.H. and R.J. Martin, 1991a, Effects of the arylaminopyridazine-GABA derivatives SR95103 and SR95531, on the *Ascaris* muscle GABA receptor: the relative potency of the antagonists in *Ascaris* is different to that at vertebrate $GABA_A$ receptors, Comp Biochem. Physiol. 98, 417.

Duittoz, A.H. and R.J. Martin, 1991b, Antagonist properties of arylaminopyridazine GABA derivatives at the *Ascaris* muscle GABA receptor, J. Exp. Biol. 159, 149.

Harrow, I.D. and K.A.F. Gration, 1985, Mode of action of the anthelmintics morantel, pyrantel and levamisole on the muscle cell membrane of the nematode *Ascaris suum*, Pest. Sci. 16, 662.

Heaulme, M., J.P. Chambon, R. Leyris, C.M. Wermuth and K. Biziere, 1986, Specific binding of a phenylpyridazine derivative endowed with $GABA_A$ receptor antagonist activity to rat brain, Neuropharmacology 25, 1272.

Holden-Dye, L., G.W. Hewitt, K.T. Wann, P. Krogsgaard-Larsen and R.J. Walker, 1988, Studies involving avermectin and the 4-aminobutyric acid (GABA) receptor in *Ascaris suum* muscle, Pest. Sci. 24. 231.

Holden-Dye, L., R. Walker, L. Nielsen, P. Krogsaard-Larsen and R.J. Walker, 1989, Stereoselectivity of a bicuculline insensitive GABA receptor in *Ascaris suum* muscle, Br. J. Pharmacol. 98, 841.

Martin, R.J., 1980, The effects of γ-aminobutyric acid (GABA) on the input conductance and membrane potential of *Ascaris suum* muscle, Br. J. Pharmacol. 71, 99.

Martin, R.J., 1982, Electrophysiological effects of piperazine and diethylcarbamazine on *Ascaris suum*, Br. J. Pharmacol. 77, 255.

Martin, R.J., 1987, The γ-aminobutyric acid receptor of *Ascaris* as a target for anthelmintics, Biochem. Soc. Trans. 17, 61.

Martin, R.J. and A.J. Pennington, 1989, A patch-clamp study of effects of dihydroavermectin on *Ascaris* muscle, Br. J. Pharmacol. 98, 747.

Martin, R.J., A.J. Pennington, A.H. Duittoz, S.J. Robertson and J.R. Kusel, 1991, The physiology and pharmacology of neuromuscular transmission in the nematode parasite *Ascaris suum*, Parasitology 102, 541.

Nistri, A. and A. Constanti, 1979, Pharmacological characterization of different types of GABA and glutamate receptors in vertebrates and invertebrates, Prog. Neurobiol. 13, 117.

Sangster, N.C., C.W. Davis and G.H. Collins, 1991, Effects of cholinergic drugs on longitudinal contraction in levamisole-susceptible and -resistant *Haemonchus contortus*, Int. J. Parasitol. 21, 689.

Sitamze, J.M., 1993, Synthèse d'Antagonistes du GABA a Propriétés Ascaricides (Doctoral Thesis) (L'Université Louis Pasteur de Strasbourg, Strasbourg).

Sitamze, J.M., M. Schmitt and C.G. Wermuth, 1992, A general and convenient synthesis of 3-aminopyridazines, J. Org. Chem. 57, 3257.

Wermuth, C.G. and D. Rognan, 1987, Modelisation d'antagonistes des recepteurs $GABA_A$, Actua. Chim. Ther. 14, 215.

Wermuth, C.G., J. Bourguignon, G. Schlewer, J.P. Gies, A. Schoenfelder, A. Melikian, M.J. Bouchet, D. Chantreux, J.C. Molimard, M. Heaulme, J.P. Chambon and K. Biziere, 1987, Synthesis and structure activity relationships of a series of aminopyridazine derivatives of GABA acting as selective $GABA_A$ antagonists, J. Med. Chem. 30, 239.

Williams, T.L., D.A.S. Smith, N.R. Burton and T.W. Stone, 1988, Amino-acid pharmacology in neocortical slices: evidence for bimolecular actions from an extension of Hill and Gaddum-Schild equations, Br. J. Pharmacol. 95, 805.

Comp. Biochem. Physiol. Vol. 61C, pp. 37–40
Pergamon Press Ltd. 1978. Printed in Great Britain

0306-4492/78/0601-0037$02.00/0

2.1

GLYCINE AND GABA RECEPTORS ON LAMPREY BULBAR RETICULOSPINAL NEURONES

R. J. MARTIN

Department of Veterinary Pharmacology, University of Edinburgh, Royal (Dick) School of Veterinary Studies, Summerhall, Edinburgh EH9 1QH

(*Received* 31 *October* 1977)

Abstract—1. Intracellular recordings were made from the bulbar group of reticulospinal neurones of lamprey ammocoetes during the application of glycine and GABA to the bath.

2. Glycine and GABA produced a reversible dose–dependent hyperpolarization of the membrane potential. The hyperpolarizations were associated with an increase in the conductance of the cell membrane and an increase in the Cl permeability was implicated.

3. Strychnine antagonized the glycine potentials but not the GABA potentials. Picrotoxin antagonized the GABA potentials but not the glycine potentials. It was concluded that there are two types of inhibitory receptor on the lamprey bulbar reticulospinal neurones.

INTRODUCTION

The largest cells of the lamprey brain are reticulospinal cells which are found in different groups in the third and fourth ventricles (Rovainen, 1967). These neurones receive convergent sensory information from many afferent sources and they control motor activity (Rovainen, 1967; Wickelgren, 1977). The study of the neuropharmacology of these cells is of fundamental interest because these cells may belong to a reticulospinal system which has persisted in vertebrates throughout phylogeny (Shapovalov, 1975). γ-Amino butyric acid (GABA) has been applied iontophoretically to the reticulospinal neurones and has been found to have an inhibitory action. L-Glutamate on the other hand has been found to have an excitatory action (Wickelgren, 1977). This paper describes the effects of bath-applied glycine and GABA on the bulbar group of reticulospinal neurones in the lamprey ammocoete. It illustrates the fact that there are two separate inhibitory receptors on these neurones. It also indicates the sensitivity of these receptors.

METHODS

Experiments were conducted on twenty 10–15 cm lamprey ammocoetes (*Lampetra planeri* and *Lampetra fluviatilis*). They were anaesthetized in a solution of tricaine methane sulphonate (MS 222 Sandoz 10^{-4} g l^{-1}) and the rostral 2 cm head section removed to a saline bath for further dissection under the binocular microscope. The ventral body wall was divided along the midline and the tissues covering the ventral side of the notochord removed. The preparation was transferred to a perspex experimental chamber, opened out and mounted dorsal side uppermost onto Sylgard. The brain was exposed dorsally by an incision along the midline and illuminated from below. The choroid plexus which covered the third and fourth ventricles was then removed. The bulbar reticulospinal neurones were viewed with the aid of the dissecting microscope, adjacent to the medial longitudinal sulcus in the fourth ventricle. (see Rovainen, 1967).

The experimental chamber contained 5 ml of Ringer solution and usually had the following composition (mM): NaCl, 90; $NaHCO_3$, 20; KCl, 2.1; $CaCl_2$, 2.6; MgCl, 1.8; glucose, 4.0; bubbled with a jet of 95% O_2, 5% CO_2 which served both to stir the Ringer and buffer the pH at 7.1–7.2. The $MgCl_2$ was sometimes raised to 20 mM to suppress synaptic potentials. A Cl-free Ringer of the following composition (mM): Na_2SO_4, 45; sucrose, 45; $NaHCO_3$, 20; K_2SO_4, 1.05; $CaSO_4$, 2.6; Mg SO_4, 20; glucose, 4.0; was also used. The Ringer in the chamber could be completely changed by slow perfusion with fresh Ringer. The volume of the chamber was maintained with a constant head device. 0.25–0.5 ml of the drug solution in Ringer were added to the edge of the bath in concentrations, which, when diluted by the 5 ml of Ringer in the bath gave the final concentrations expressed in the results. The drugs used were glycine, GABA, strychnine and picrotoxin. The strychnine and picrotoxin solutions were made up immediately prior to their use.

Glass micropipettes, used for intracellular recordings were usually filled with 2 M K acetate. The micropipettes had d.c. resistances of 20–30 MΩ and were connected through an Ag–Ag Cl wire to a high-impedance preamplifier Current pulses were passed through the micropipettes using a bridge-balance circuit. The reference electrode in the bath was also an Ag–Ag Cl wire. The micropipettes were placed under visual control. Membrane potentials were monitored on a cathode ray oscilloscope and a pen recorder. A bipolar stimulating electrode was applied to the spinal cord in order to stimulate the bulbar reticulospinal cells antidromically to confirm the identity of the cells.

RESULTS

Bulbar reticulospinal neurones were identified in the middle of the fourth ventricle adjacent to the medial longitudinal sulcus. The resting membrane potential of 22 cells measured immediately after penetration had a value of 67 ± 5 mV (Mean ± S.D.). All cells showed the presence of spontaneous excitatory and inhibitory potentials in the normal Mg Ringer. Stimulation of the spinal cord resulted in antidromic action potentials which had overshoots of 20–30 mV. The resistances of the cells measured by current injection currents were 1–5 MΩ.

Glycine

The addition of glycine to the bath in concentrations greater than 10^{-5} M was followed by dose-dependent hyperpolarizations of the membrane potential Fig. 1(A). Three records from the same neurone illustrate the effects of adding glycine to the bath in increasing concentrations. The bath concentrations were 10^{-5} M, 10^{-4} M and 10^{-3} M. At high concentrations the hyperpolarizing responses declined after reaching an initial peak value even though the concentration of glycine in the bath was maintained. This indicated some desensitization of the responses to glycine. In Fig. 1(B), the peak amplitude of the glycine potentials was plotted against the log-concentration of glycine in the bath. The graph illustrates a dose-response relationship where the threshold of the bath-applied glycine was approx 10^{-5} M and the maximal effect attained at 5×10^{-4} M. The half-maximal effect, measured by interpolation was produced by approx 7.5×10^{-5} M. Glycine may have produced the hyperpolarization by direct action on the bulbar reticulospinal neurones or indirectly via inhibition of tonically active neurones with an excitatory input onto the bulbar neurones. In order to distinguish between these two possibilities the Mg concentration was raised to 20 mM to abolish chemically mediated synaptic transmission (Wickelgren, 1977). The procedure abolished the spontaneous synaptic potentials but failed to abolish the hyperpolarizing response to glycine. It was therefore established that glycine had a direct effect on bulbar reticulospinal neurones.

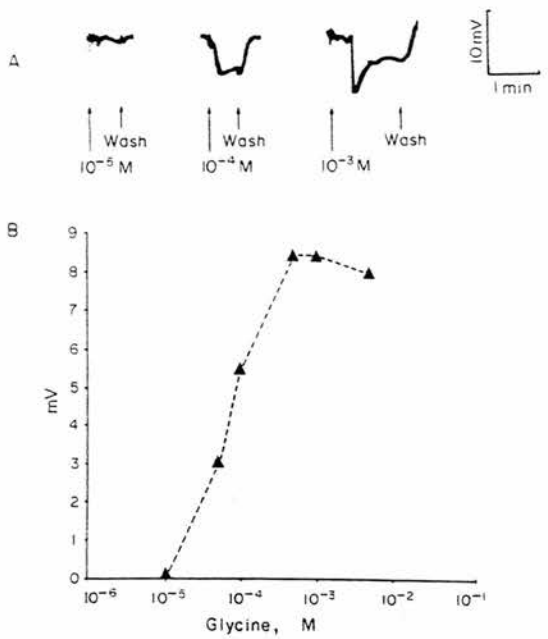


Fig. 1. (A)—The hyperpolarizing effect of 10^{-5}, 10^{-4} and 10^{-3} M glycine on the membrane potential of a bulbar reticulospinal neurone. Resting membrane potential −62 mV. K acetate-filled micropipettes used for recording. (B)—Dose-response relationship for the same neurone. Abscissa—$\log_{10}$ M concentration glycine. Ordinate—hyperpolarizing response (mV). Note the maximum hyperpolarization is 8.5 mV, suggesting this is the glycine equilibrium potential for this neurone.

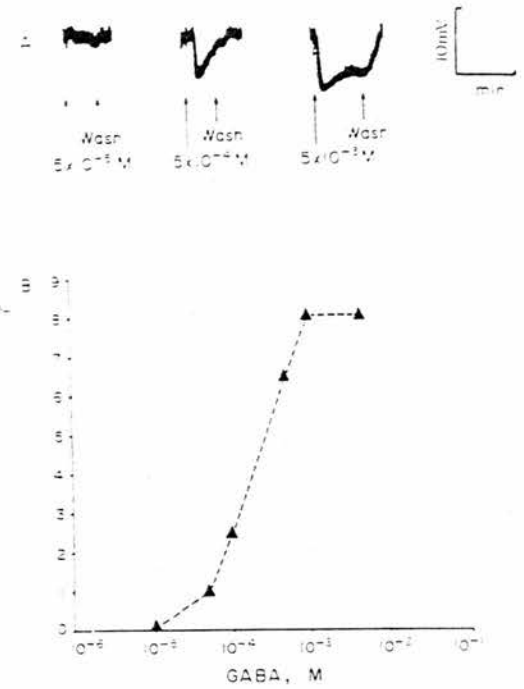


Fig. 2. (A)—The hyperpolarizing effect of 5×10^{-5}, 5×10^{-4} and 5×10^{-3} M GABA on the membrane potential of a bulbar reticulospinal neurone. Resting membrane potential −64 mV. K acetate-filled micropipettes used for recording. (B)—Dose-response relationship for the same neurone. Abscissa—$\log_{10}$ M concentration GABA. Ordinate—hyperpolarizing response (mV). Note the maximum hyperpolarization is 8.0 mV suggesting this is the GABA equilibrium potential for this neurone.

GABA

The response of bulbar reticulospinal neurones to the addition of GABA to the bath in concentrations greater than 10^{-5} M was similar to that of glycine. GABA produced dose-dependent hyperpolarizations, Fig. 2(A) and (B). Three records from the same neurone illustrate the effects of adding GABA to the bath in increasing concentrations. The bath concentrations were 5×10^{-5} M, 5×10^{-4} M and 5×10^{-3} M. At high concentrations the GABA responses declined in amplitude after reaching its initial peak value, even though the bath concentrations were maintained. In Fig. 2(B) the peak amplitude of the GABA potentials are plotted against the log-concentration of GABA in the bath. The graph illustrates a dose-response relationship where the threshold of the bath-applied GABA was approx 10^{-5} M and the maximal effect was obtained with 10^{-3} M. The half-maximal effect, measured by interpolation was produced by approx 1.8×10^{-4} M. The effect of GABA on the bulbar reticulospinal neurones also persisted in 20 mM Mg. This abolished the synaptic potentials without affecting the GABA potentials and established the direct effect of GABA on the bulbar reticulospinal neurones.

Two types of receptor

Since the effects of glycine and GABA on the bul

lar neurones are similar, they may have acted on the receptor population or on two similar, but not identical, receptor populations. In order to distinguish between these two possibilities the glycine-antagonist strychnine and the GABA-antagonist picrotoxin were used. Figure 3(A) illustrates the responses of bulbar reticulospinal neurones to the application of glycine and GABA in the absence of strychnine or picrotoxin. After the addition of strychnine (5×10^{-5} M) the bulbar cells only respond to GABA, Fig. 3(B) but not glycine. After the application of picrotoxin (5×10^{-4} M), it is seen that the bulbar neurones will respond to glycine but not GABA, Fig. 3(C). Thus strychnine will antagonize the glycine responses but not the GABA responses, while picrotoxin has the opposite effect. These observations illustrate the fact that there are two separate inhibitory receptors on the bulbar reticulospinal neurones.

Ionic mechanism of glycine and GABA potentials

Glycine and GABA produce inhibitory potentials in many preparations by increasing the Cl conduc-

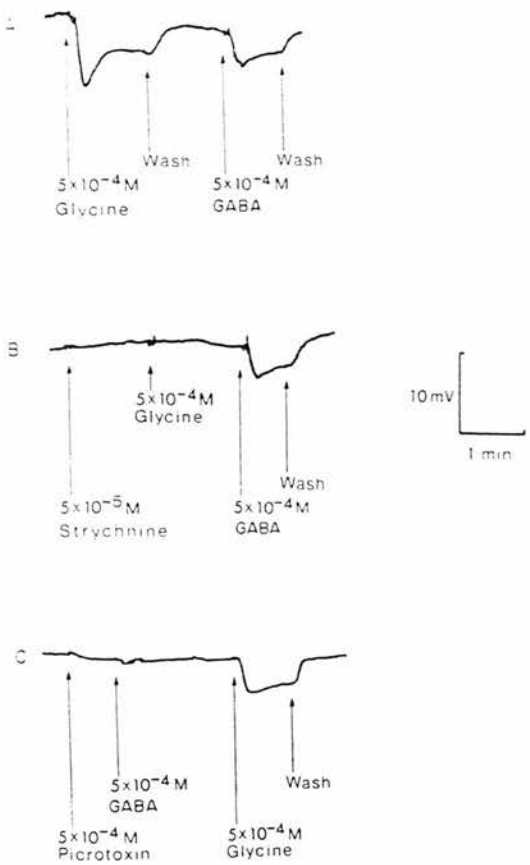


Fig. 3. Antagonism of the glycine and GABA potentials. (A)—The effect of 5×10^{-4} M glycine and 5×10^{-4} M GABA on the membrane potential of bulbar reticulospinal neurones. K acetate micropipettes used for intracellular recordings with the preparation bathed in the high-Mg Ringer. (B)—The effect of glycine and GABA in the presence of strychnine. Note that strychnine antagonizes the action of glycine but not GABA. (C)—The effect of glycine and GABA in the presence of picrotoxin. Note that picrotoxin antagonizes the action of GABA but not glycine.

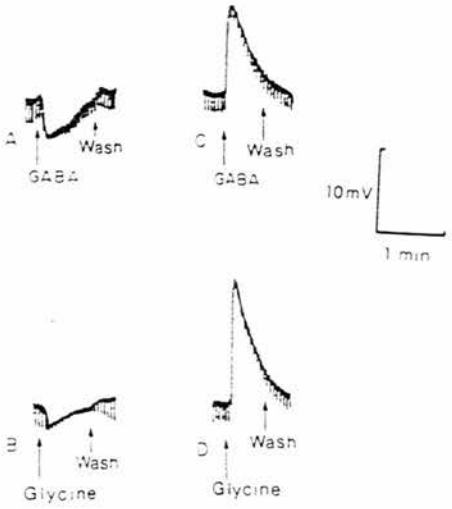


Fig. 4. Resistance changes during the GABA and glycine potentials. The resistances of bulbar neurones were monitored by injecting 2 nA hyperpolarizing current pulses during the application of 5×10^{-4} M GABA and glycine. The recordings (A) and (C) were made from one bulbar neurone, recordings (B) and (D) were from another bulbar neurone. K acetate-filled micropipettes were used. Recordings (A) and (B) were made in high-Mg normal-Cl Ringer. Recordings (C) and (D) were made shortly after bathing in Cl-free Ringer. (A)—GABA produced a hyperpolarization and a decrease in the resistance of the cell from 1.2 MΩ to 0.4 MΩ. (B)—Glycine produced a hyperpolarization and a decrease in the resistance of the cell from 1.2 MΩ to 0.2 MΩ. (C)—GABA produced a depolarization in the Cl-free Ringer. (D)—Glycine produced a depolarization in the Cl-free Ringer.

tance of the cell membranes. (Curtis & Johnston, 1974; Krnjević, 1976; Takeuchi, 1976). They also produced an increase in conductance in the lamprey reticulospinal neurones. This was demonstrated by monitoring the conductance of cells, by injecting current pulses through the recording micropipette and observing the resultant changes in membrane potential. Figures 4(A) and (B) illustrate records of the membrane potential during the injection of hyperpolarizing square wave pulses and the applications of 5×10^{-4} M glycine and GABA. The resistance of the cells fell during the application of glycine and GABA potentials. After washing the preparation the conductance returned towards resting levels.

In order to illustrate the involvement of Cl in the production of the glycine and GABA potentials, the preparation was bathed in Cl-free Ringer. This was expected to move the Cl equilibrium potential in a depolarizing direction and alter the polarity of the glycine and GABA potentials. Figures 4(C) and (D) illustrate depolarizing glycine and GABA potentials observed shortly after replacing the Ringer with Cl-free Ringer. Similar depolarizing glycine and GABA potentials were also produced when the intracellular Cl was increased by using 3 M KCl-filled recording micropipettes. These observations are consistent with the glycine and GABA potentials originating from an increase in Cl permeability.

DISCUSSION

Glycine and GABA produced hyperpolarizing potentials when applied in concentrations greater than 10^{-5} M. The sensitivity of the receptors on the bulbar reticulospinal neurones is similar to the glycine and GABA receptors on other preparations (Okamoto & Quastel, 1976). However it should be pointed out that the sensitivity of these receptors is relatively low and 10–100 times less than that of the ACH receptor on the frog neuromuscular junction (Fatt, 1950; Takeuchi, 1976). The results reported here suggest that glycine in addition to GABA may play a physiological role as an inhibitory transmitter at the synapse on the reticulospinal neurone. A further comparison of the behaviour of naturally occurring inhibitory potentials and the glycine and GABA potentials is necessary to test this hypothesis. E.M. studies of synapses on the reticulospinal neurones have only shown that there are two types of synaptic vesicle, possibly associated with an excitatory and an inhibitory input (Wickelgren, 1977). The possibility remains therefore, that only one of the two substances may be involved in inhibitory synaptic transmission even though there are two types of inhibitory receptor.

It is interesting that other vertebrate reticulospinal neurones possess similar glycine and GABA inhibitory receptors: the Mauthner cell (Diamond, Roper & Yasargel, 1973); Deiters' neurones (Brugencate & Engberg, 1971) and cat reticulospinal neurones (Tebēcis & Di Maria, 1972; Tebēcis & Ishikawa, 1973). It is perhaps not surprising that these possess similar glycine and GABA receptors since the reticulospinal neurones of higher vertebrates and reticulospinal neurones of lower vertebrates are believed to belong to a common system which is phylogenetically very old (Bowsher, 1973; Shapovalov, 1975). A further study of the receptors of this preparation may therefore yield results of predictive value in the study of higher vertebrates.

Acknowledgement—This work was made possible by the award of a grant from the Wellcome Trust.

REFERENCES

BOWSHER D. (1973) Brain behaviour and evolution. *Brain Behav. Evol.* **8**, 386–396.

BRUGENCATE G. TEN & ENGBERG I. (1971) Iontophoretic studies in Deiters' nucleus of the inhibitory actions of GABA and related amino acids and the interactions of strychnine and picrotoxin. *Brain Res.* **25**, 431–448.

CURTIS D. R. & JOHNSTON G. A. R. (1974) Amino acid transmitters in the mammalian central nervous system. *Ergebn. Physiol.* **69**, 97–188.

DIAMOND J., ROPER S. & YASARGIL G. M. (1973) The membrane effects and sensitivity to strychnine of neural inhibition of the Mauthner cell, its inhibition by glycine and GABA. *J. Physiol., Lond.* **232**, 87–111.

FATT P. (1950) The electromotive action of acetylcholine at the motor end-plate. *J. Physiol., Lond.* **111**, 408–422.

KRNJEVIĆ K. (1976) In *GABA in Nervous System Function* p. 269. Raven Press, New York.

OKAMATA K. & QUASTEL J. H. (1976) Effects of amino acids and convulsants on spontaneous action potentials in cerebellar cortex slices.

ROVAINEN C. M. (1967) Physiological and anatomical studies on large neurons of the central nervous system of the sea lamprey (*Petromyzon Marinus*). I. Muller and Mauthner cells. *J. Neurophysiol.* **30**, 1000–1023.

SHAPOVALOV A. I. (1975) Neuronal organization and synaptic mechanisms of supraspinal motor control in vertebrates. *Rev. Physiol. Biochem. Pharm.* **72**, 1–54.

TAKEUCHI A. (1976) In *GABA in Nervous System Function* p. 255. Raven Press, New York.

TEBĒCIS A. K. & DI MARIA A. (1972) Strychnine-sensitive inhibition in medullary reticular formation: evidence for glycine as an inhibitory transmitter. *Brain Res.* **48**, 373–383.

TEBĒCIS A. K. & ISHIKAWA T. (1973) Glycine and GABA as inhibitory transmitters in medullary reticular formation studies involving intra- and extra-cellular recordings. *Pflügers Arch. ges. Physiol.* **338**, 272–278.

WICKELGREN W. O. (1977) Physiological and anatomical characteristics of reticulospinal neurones in lamprey. *J. Physiol., Lond.* **270**, 89–114.

Brain Behav. Evol. *16:* 1–18 (1979)

A Study of the Morphology of the Large Reticulospinal Neurons of the Lamprey Ammocoete by Intracellular Injection of Procion Yellow

R. J. Martin

Department of Veterinary Pharmacology, Royal (Dick) School of Veterinary Studies, University of Edinburgh, Edinburgh

Key Words. Lamprey · Reticulospinal · Neurons · Morphology · Procion yellow

Abstract. 47 reticulospinal neurons of the lamprey brain-stem were stained by intracellular injection of Procion yellow, so that their morphology and dendroarchitecture could be determined. The vagal, bulbar, Mauthner, isthmic and mesencephalic groups could be distinguished by the shape and size of their somata and the distribution of their dendrites. However, they shared the following features: the somata of all these cells were relatively large (up to 80 μm largest diameter); the dendrites were extensively distributed in the brain-stem in an open-field arrangement; the initial segment expanded abruptly at the soma junction but tapered gradually to form a narrow axon, which joined the medial longitudinal fasciculus in the brain-stem.

Introduction

The large reticulospinal neurons of the lamprey are suitable for neuropharmacological studies [*Martin,* 1978]. A number of qualitative anatomical studies have established the positions of their cell bodies in the brain-stem [*Tretjakoff,* 1909; *Saito,* 1928; *Stefanelli,* 1933a, b, 1934; *Rovainen,* 1967; *Rovainen et al.,* 1973; *Nieuwenhuys,* 1972; *Wickelgren,* 1977], but only *Tretjakoff* [1909] has made a study of the dendrite structures using the Golgi technique. A detailed knowledge of the cell sizes and dendrite structure and distribution was therefore required for further studies of drug actions. Fortunately, the large size of the reticulospinal neurons allows them to be stained by intracellular injection of Procion yellow [*Stretton and Kravitz,* 1968]. This technique will reveal the structure of the soma and dendrites and has the advantage that it allows cells to be recognized electrophysiologically, prior to staining. This paper, therefore, describes the results of experiments in which the morphology of

the lamprey reticulospinal neurons was studied following the intracellular injection of Procion yellow.

Methods

Experiments were conducted on 10- to 15-cm lamprey ammocoetes *(Lampetra planeri* and *Lampetra fluviatilis).* They were anaesthetized in a solution of tricaine methane sulphonate (MS 222 Sandoz 10^{-4} g · ml^{-1}) and a rostral 2-cm head section was removed to a saline bath for further dissection under the binocular microscope. The ventral body wall was divided along the midline and the tissues covering the ventral side of the notochord removed. The preparation was transferred to a perspex experimental chamber, opened out and mounted, dorsal side uppermost, onto Sylgard. The brain was exposed dorsally by an incision along the midline and illuminated from below. The choroid plexus, which covered the third and fourth ventricles, was then removed. The isthmus, which divides the third and fourth ventricles, was divided dorsally and the brain-stem was gently opened out and flattened. The different groups of reticulospinal neurons in the third and fourth ventricles were then viewed with the aid of the dissecting microscope.

The experimental chamber contained 5 ml high-Mg Ringer solution and had the following composition (mmol): NaCl, 90; $NaHCO_3$, 20; KCl, 2.1; $CaCl_2$, 2.6; MgCl, 18; glucose, 4.0; bubbled with a jet of 95% O_2, 5% CO_2 which served both to oxygenate the Ringer solution and buffer the pH at 7.1–7.2. The high-Mg Ringer solution was used to suppress the synaptic potentials.

Glass micropipettes, used for intracellular recording and staining, were filled with 6% aqueous solution of Procion yellow (M-4R ICI). Their tips were broken so that they had an outside diameter of 1–2 μm. The micropipettes were connected through an Ag-AgCl wire to a high-impedance pre-amplifier. Current pulses were passed through the micropipettes using a bridge balance circuit. The micropipettes were placed under visual control, but the identity of the reticulospinal neurons was confirmed by antidromic stimulation of the spinal cord with a bipolar stimulating electrode. Dye was injected by means of a cathode current in 10-nA pulses lasting approximately 40 msec. Each pulse was separated by 10–20 msec. The physiological state of the reticulospinal cells was monitored by recording the antidromic spike intracellularly during current injection. Procion yellow injection continued for up to 20 min, and in this time the cell became orange when observed through the microscope.

The brain and spinal cords were fixed *in situ* in Heidenhain's Susa after the Procion had been allowed to diffuse throughout the cell for up to 12 h. They were removed after fixation, then dehydrated in alcohol, cleared in cedar-wood oil and mounted whole in DPX. The serial 20-μm sections were made by embedding the brain in Paraplast after clearing in cedar-wood oil. The stained cells were observed with a Leitz Ortholux fluorescent microscope using a B12 exciting filter and K510 and K530 absorbing filters. Large black and white prints were produced from which tracings and measurements were then made. The dimensions of the cell bodies were

taken as the lengths of the axes passing between dendrites and through the centre of the cell body [*Shadé,* 1964]. Only rostro-caudal and medio-lateral dimensions were obtained in whole-mounted preparations. The cell groupings were made according to the terminology of *Rovainen* [1967]. The extent of the distribution of the dendrites along rostral, caudal, medial, lateral and ventral planes was measured from the centre of the soma. Only well-stained cells were included in the analysis. Measurements of the brain-stem before and after histological processing showed that shrinkage was approximately 20%, but no correction was made for this shrinkage in the results expressed.

Results

Recognition of the Large Reticulospinal Neurons

The large reticulospinal cells were observed in the living preparation in the brain-stem with the aid of the dissecting microscope. As the micropipette was advanced towards the cell, an antidromic spike, following spinal cord stimulation, was recorded extracellularly. It was conducted at rates of 2–3 $msec^{-1}$. The successful penetration of a reticulospinal cell was associated with the appearance of a large DC potential (about 70 mV negative) and a large antidromic intracellular action potential. Synaptic potentials were not observed in preparations bathed in the high-Mg Ringer solution.

Number and Location of Reticulospinal Cells Stained

47 reticulospinal cells were successfully stained. These cells are divided, according to location, into vagal, bulbar, Mauthner, isthmic and mesencephalic groups (fig. 1) [*Rovainen,* 1967; *Rovainen et al.,* 1973].

Three to six bulbar cells were visible in the unstained preparations on either side of the sulcus medianus inferior in the middle of the fourth ventricle (fig. 1, B). Lateral to this group was the Mauthner cell (fig. 1, M^{th}), which was found on either side of the brain-stem. The vagal group (fig. 1, V) was seen as a caudal continuation of the bulbar group of reticulospinal cells. One isthmic cell (fig. 1, I) was visible on either side of the brain-stem and lay near to the isthmus midway between the edge of the fourth ventricle and the sulcus medianus inferior. There was one rostral medial mesencephalic and one caudal medial mesencephalic cell, while a lateral mesencephalic cell was situated more laterally in the third ventricle. (fig. 1, M). The visibility of these cells varied from preparation to preparation, so that it was not possible to assume that any of these cells which were not visible were missing.

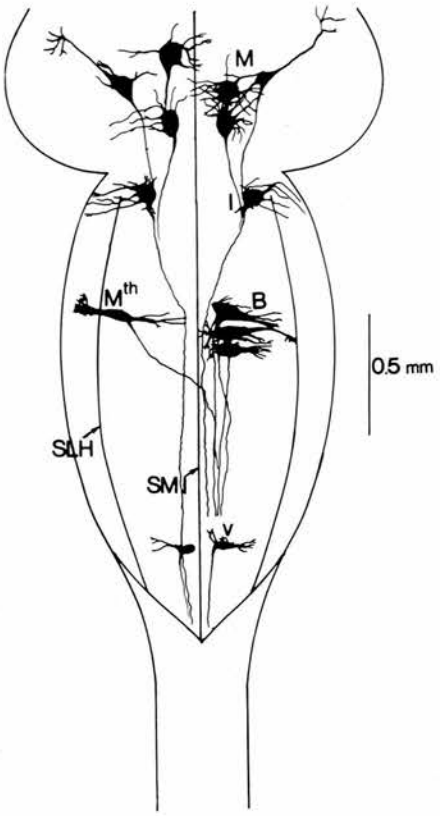


Fig. 1. Tracings of the large reticulospinal cells stained by intracellular injection of Procion yellow and observed in whole-mount preparations. The outline of the brain-stem, the positions of sulcus medianus inferior (SMI) and sulcus limitans of His (SLH), are marked with arrows. The brain-stem was divided dorsally at the isthmus and opened out by gentle lateral traction with the result that the third and fourth ventricles appear continuous. For reasons of clarity, only the left Mauthner cell (M^{th}) and right bulbar reticulospinal cells (B) are illustrated, but they occurred bilaterally. The left and right isthmic (I), mesencephalic (M) and vagal (V) groups are illustrated.

Somata Dimensions

Figures 1–7 illustrate the appearance of the cell bodies. Table I lists the mean and standard deviations of the dimensions of the somata. It can be seen that all the somata are large (usually bigger than 50 μm) and round or oval in outline. When viewed in whole-mount preparations, the

Table I. Dimensions of reticulospinal cells

Cell		Size of soma (mean ± SD), μm			Distribution of dendrites (mean ± SD), μm				
type	number	RC	ML	DV	rostral	caudal	medial	lateral	ventral
Vagal	1 SS 2 WM	23 ± 5	57 ± 5	35	43 ± 17	23 ± 5	53 ± 26	150 ± 36	140
Bulbar	5 SS 13 WM	44 ± 9	76 ± 10	43 ± 4	54 ± 50	69 ± 60	84 ± 41	191 ± 58	175 ± 25
Mauthner	3 WM	37 ± 2	67 ± 5	–	40 ± 14	23 ± 5	180 ± 33	127 ± 53	–
Isthmic	3 SS 5 WM	48 ± 12	68 ± 10	67 ± 5	52 ± 32	64 ± 41	43 ± 21	264 ± 68	187 ± 17
Mesencephalic									
Caudal	4 WM	73 ± 4	50 ± 4	–	117 ± 21	38 ± 12	30 ± 12	143 ± 26	–
Rostral	3 SS	52 ± 6	61 ± 8	52 ± 2	119 ± 45	80 ± 29	155 ± 80	175 ± 51	127 ± 17
Lateral	3 WM	33 ± 5	47 ± 2	–	197 ± 37	8 ± 12	100 ± 108	267 ± 24	–

For measurement technique, see Methods. SS = Serial section; WM = whole mount; RC = rostro-caudal; ML = medio-lateral; DV = dorso-ventral.

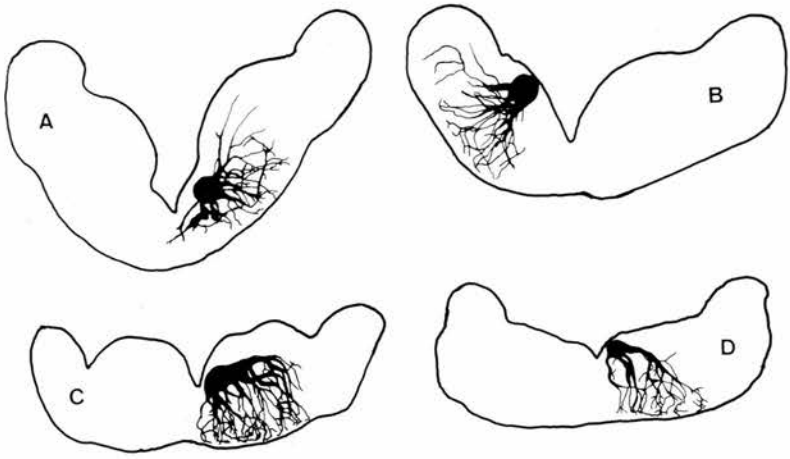


Fig. 2. Reconstructions of the large reticulospinal cells from transverse serial sections stained by intracellular injection of Procion yellow. Note the open-field arrangement of the dendrites with the soma of these cells located near the surface of the ventricle and their dendrites distributed ventrally in the outer zone of the brain-stem. A = Rostral medial mesencephalic cell; B = bulbar cell; C = isthmic cell; D = Vagal cell.

cell bodies of the Mauthner, bulbar and vagal reticular cells were oval in shape and orientated transversely (fig. 1–4, 7). However, cell bodies of the isthmic and medial mesencephalic cells were more rounded in appearance (fig. 1, 2, 5, 6). The isthmic cell and medial mesencephalic cells were the largest of the cells. The cell bodies of all these neurons were located just below the ventricular surface in the periventricular nuclei (fig. 2).

Dendrites

The dendrites appeared to be stained fairly uniformly, although the fluorescence was less intense in the distal portion of the dendrites than the proximal dendrites. This reduction in fluorescence appeared to be due to the reduction in the diameter of the distal dendrites, which occurred as a result of tapering. The tapering proximal dendrites often resembled cones attached to the somata at their bases (fig. 3–7).

The dendrites were long and covered large areas of the brain-stem, but were confined to the ipsilateral region of the brain-stem. The exception was the rostral medial mesencephalic cell (fig. 1, 6). This cell possessed dendrites which just crossed to the contralateral side. The den-

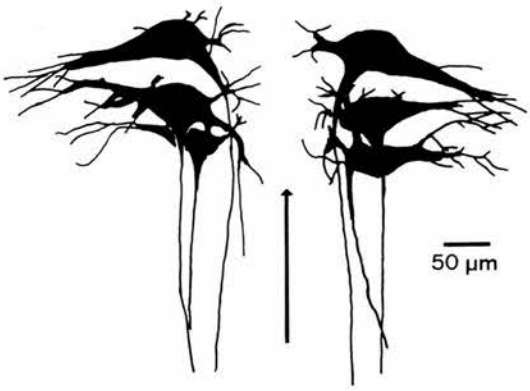
drites were distributed ventrally in the outer zone of the brain-stem, while dorsal dendrites were absent (fig. 2). They were formed in an open-field arrangement [*Lorente de No,* 1947]. The free intermingling of the dendrites with the passing axons in the ventral outer zone allows the cells to be described as 'hodophilic'.

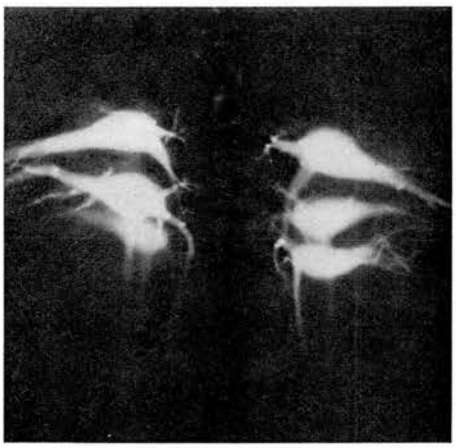
The dendrites were distributed beyond the limits of nuclei defined by cytoarchitectonic techniques [*Nieuwenhuys,* 1972]. They form 'noyaux ouverts' or open nuclei [*Mannen,* 1960]. For example, the bulbar reticular nucleus extends laterally as far as the sulcus intermedius ventralis [*Nieuwenhuys,* 1972]. However, the dendrites of the bulbar cells reached further laterally to the sulcus limitans of His (fig. 1, 2b, 7). The isthmic and mesencephalic reticular cells also possessed dendrites which passed beyond the limits of reticular nuclei previously defined by cytoarchitectonic techniques (fig. 1, 5, 6).

Overlapping of the dendrites was observed between the mesencephalic group of reticular cells (fig. 1, 6) and must have occurred between the medial dendrites of the Mauthner cell and the lateral dendrites of the bulbar cells (fig. 1). The transverse arrangement of the dendrites in the bulbar and vagal reticular cells limited the overlapping of dendritic fields within their groups (fig. 1, 3). Under the higher-power magnification of the microscope, the more distal dendrites showed a beaded and wavy pattern which was not present in the proximal dendrites. The distal dendrites were thread-like and hung like tendrils from the cell body (fig. 7). The distal dendrites, which reached the ventral surface of the brain, changed their direction and followed a horizontal course parallel to the ventral surface of the brain. They resembled plant roots which have become 'pot-bound' (fig. 7).

Initial Segments

The initial segments were distinguished from the proximal dendrites by the fact that they gave rise to a single caudally directed axons and, usually, they did not branch to give rise to fine dendrites. The initial segment tapered gradually to 2–3 μm at the axon hillock to form a narrow axon (fig. 1, 3–6). The initial segment and axon were stained, in some instances, for distances as far as the calamus scriptorius. The intensity of the fluorescence decreased gradually as the distance from the soma increased, so that the more distal portions of the axon became difficult to trace. It was possible to observe the narrow axons as they ran adjacent to the sulcus medianus inferior in the medial longitudinal fasciculus. No





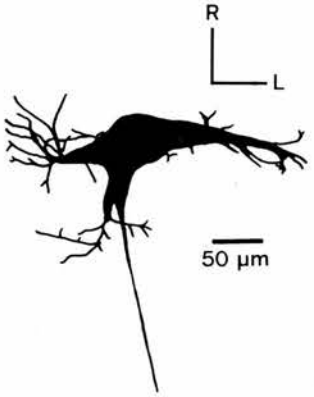
3a

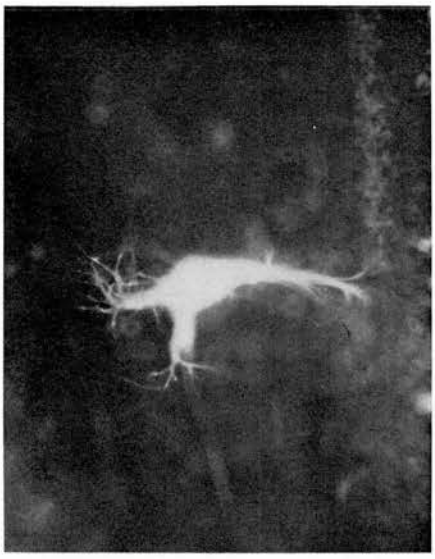
Fig. 3. A dorsal view of whole mounts of bulbar cells stained by intracellular injection of Procion yellow and their tracings. **a** Three left and three right bulbar reticulospinal cells in the same preparation; the vertical arrow points rostrally and marks the midline. **b** One right bulbar reticulospinal cell; R and L mark the rostral and lateral directions, respectively.

axon collaterals were observed. Some dendrites were observed which were attached to the initial segments (fig. 3b, 5, 6).

Bulbar Cells

Three to six bulbar cells were visible on either side of the sulcus medianus inferior. The cells had transverse oval somata (fig. 1, 3). The dimensions of the somata of the bulbar cells are listed in table I.





3b

Dendrites of bulbar cells tended to be arranged transversely with dendrites reaching laterally as far as the sulcus limitans of His and medially as far as the sulcus medianus inferior. Reconstructions from serial transverse sections of bulbar cells stained with Procion yellow illustrated the ventral distribution of the dendrites in the outer zone of the brain-stem where they intermingle with passing fibres (fig. 2b, 7). They seemed to form a curtain across the brain-stem where the cell body was located. Sometimes dendrites, which were distributed caudally to the cell body, were attached to the initial segment (fig. 3b). The most obvious fea-

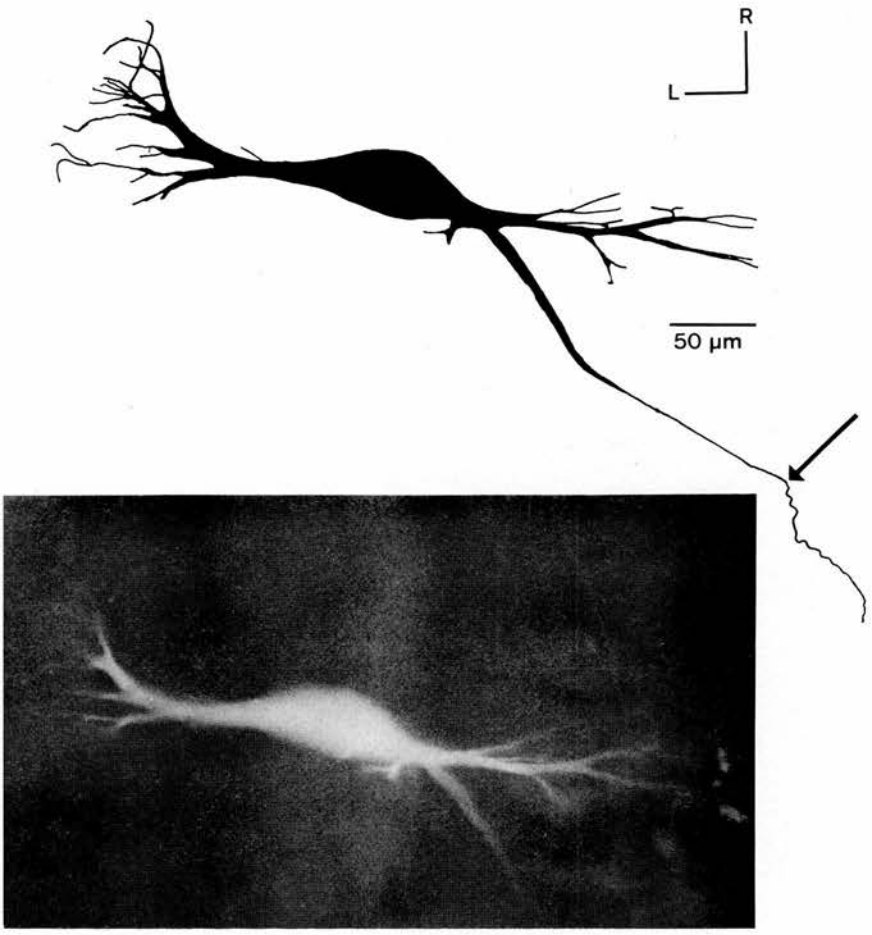


Fig. 4. A dorsal view of a whole-mount preparation of a left Mauthner cell stained by intracellular injection of Procion yellow and its ink tracings. R and L mark the rostral and lateral directions, respectively. The axon of the Mauthner cell crosses the midline caudally to the cell body at the position marked by the oblique arrow in the ink tracing.

ture of the bulbar cells was the large lateral proximal dendrite which gave the soma a characteristic oval shape (fig. 3, 7).

Vagal Cells

Three vagal reticulospinal cells were stained. Their cell bodies lay adjacent to the sulcus medianus inferior, caudal to the bulbar group of re-

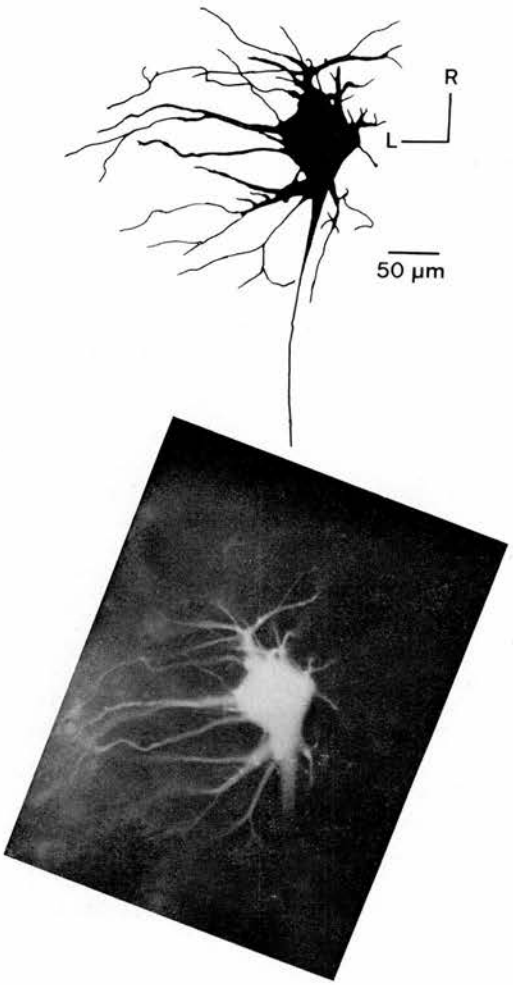


Fig. 5. Dorsal view of a whole-mount preparation of a left isthmic reticulospinal neuron stained by intracellular injection of Procion yellow and its ink tracing. R and L mark the rostral and lateral directions, respectively.

ticulospinal cells. They possessed the same morphological features as the bulbar reticulospinal cells, but they were smaller in size (fig. 1, 2d; table I).

Isthmic Cells

One isthmic cell was visible on either side of the brain and lay near the isthmus midway between the edge of the fourth ventricle and sulcus

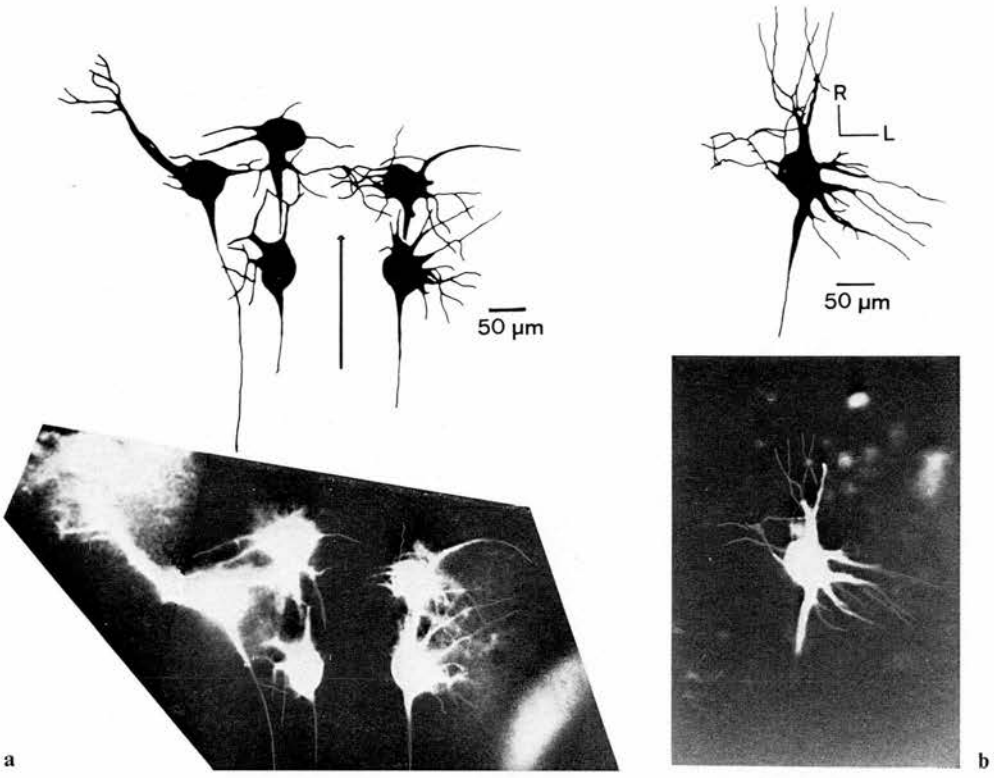


Fig. 6. Dorsal views of whole-mount dorsal preparations of mesencephalic reticulospinal cells stained by intracellular injection of Procion yellow and their ink tracings. **a** Three left and two right mesencephalic cells. Note the distinctive lateral mesencephalic cell with a characteristic dendrite, which extends rostrally and laterally, and note that the rostral medial mesencephalic cells have dendrites which cross the midline (the vertical arrow points rostrally and marks the position of the midline). **b** A left rostral mesencephalic cell. R and L mark the rostral and lateral directions, respectively.

medianus inferior (fig. 1). The somata of these cells were rounder than the bulbar and vagal cells. The dimensions of the cell are recorded in table I.

Long dendrites arose from the ventral surface of the soma and projected ventrally and laterally towards the edge of the fourth ventricle (fig. 1, 2, 5). The dendrites were particularly long (up to 350 μm lateral from the centre of the soma) and straight, although some branching was present. Medially directed dendrites were sparse. Sometimes a major den-

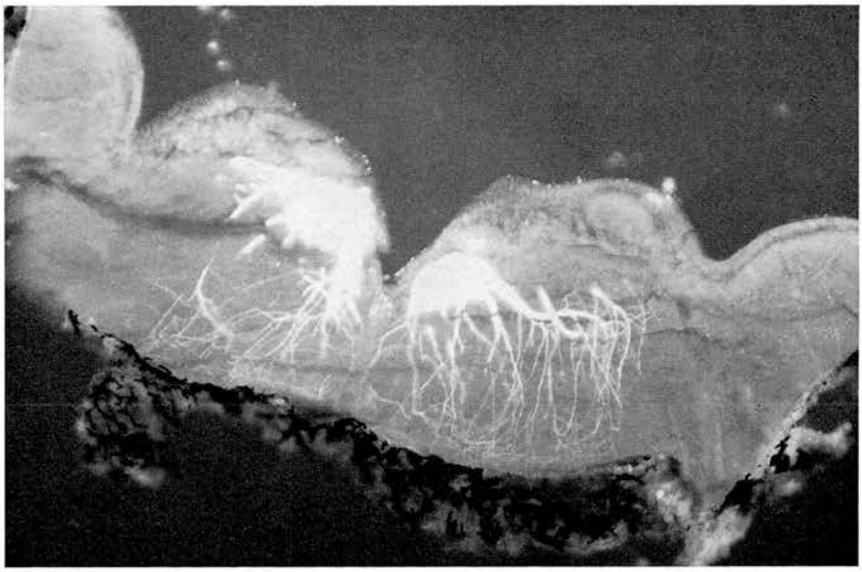


Fig. 7. A transverse section of two bulbar reticulospinal neurons stained by intracellular injection of Procion yellow. Note the open-field arrangement of the dendrites and the tendency of the distal dendrites to run parallel to the ventral surface of the brain-stem, so that they resemble plant roots which become 'pot-bound'. × 200.

drite was attached to the initial segment (fig. 5). The axon of the isthmic cell passed medially near the bulbar reticular cells to join the medial longitudinal fasciculus, but it did not cross the midline in the brain-stem.

Mesencephalic Cells

Two medial mesencephalic cells were visible in the third ventricle, on either side of the sulcus medianus inferior. The somata of these cells were round (fig. 1, 6). A lateral mesencephalic cell was also visible in the third ventricle (fig. 1, 6). The dimensions of the mesencephalic cells are listed in table I.

The dendrites of the rostral medial mesencephalic cell crossed to the contralateral side (fig. 1, 6). The caudal medial mesencephalic cell had dendrites which mainly projected rostrally and laterally (fig. 1, 6). The lateral mesencephalic cell had a characteristic morphology. It possessed a major dendrite which was distributed rostro-laterally towards the nucleus of the posterior commissure and divided into smaller branches near its

end (fig. 1, 6). Staining of more than one mesencephalic reticular cell illustrated some overlapping of the dendritic fields (fig. 1, 6).

Mauthner Cell

In addition to the reticular cells described previously, three Mauthner cells were injected with Procion yellow. They were visible, lateral to the bulbar reticulospinal cells (fig. 1). The somata were spindle-shaped and lay transversely across the brain-stem. The medially directed dendrites were relatively long and straight and overlapped the region occupied by the bulbar reticulospinal cells. A single lateral proximal dendrite gave rise to short distal dendrites which appeared tufted. The Mauthner cell of the lamprey ammocoete resembled the Mauthner cell described by *Bartelmez* [1915]. The initial segment was attached medially and directed obliquely across the brain-stem and formed an axon which crossed the sulcus medianus inferior, 200 μm caudal to the cell body (fig. 4). The dimensions of the Mauthner cell are listed in table I.

The Statistical Significance of Differences in Somata Size and Dendrite Distribution

It was possible that variations in the sizes of the somata and dendrite distributions of the reticulospinal neurons were due to random variation and that there were no significant differences between cell groups. F tests showed that there were significant differences in the somata sizes along the rostro-caudal ($p < 0.001$), medio-lateral ($p < 0.001$) and dorso-ventral ($p < 0.001$) axes. The cell bodies could not be considered to belong to a homogeneous population of reticular cells with random variations in somata size. F tests also showed that there were significant differences between reticular cell group dendrite distributions along the medial ($p < 0.001$), lateral ($p < 0.005$) and rostral ($p < 0.001$) planes. However, differences in distribution observed along the caudal planes and ventral planes (vagal, bulbar, isthmic and rostral medial mesencephalic cells) were not significant.

Discussion

Procion Yellow Staining of the Large Reticulospinal Neurons

After intracellular injection of Procion yellow, the dye diffused throughout the cell body and dendrites. Adequate amounts of dye had to

be injected and time allowed for diffusion without damage or deterioration of the cell in order to permit good staining of the dendrites. Experience showed that it was possible to confirm that sufficient dye had been injected into the cell when it became orange, as seen through the operating microscope in the living preparation. The condition of the cell was monitored throughout iontophoresis by recording the antidromic action potential. A deterioration in the condition of the cell was associated with a decrease in the amplitude of the antidromic spike. The time allowed for diffusion of the dye (up to 12 h) was considered sufficient because of the good filling of the dendrites which resulted. Thus the Procion yellow staining technique revealed the extensive distribution of the dendrites. The results contrast with the illustrations of *Tretjakoff* [1909], which suggest that the dendrites of the large reticular cells are less profuse.

The Narrow Axon in the Brain-Stem

The narrow axon in the brain-stem of the large reticulospinal cells is an interesting feature because it connects the cell body in the brain-stem to the giant axon in the spinal cord [*Bertolini*, 1964]. The giant axon of the spinal cord permits rapid conduction of an action potential, but the inclusion of the narrow axon in the brain-stem will increase the total conduction time between the soma and spinal cord. It is necessary to consider the reason for the inclusion of this feature in the design of the neuron. *Mellon and Kaars* [1974] have shown that such a narrow segment is necessary to prevent undue resistive and capacitance loads being placed on currents passing through the soma by a giant axon. Currents set up by a synapse on the cell body would leak along the length of a giant axon if it were attached directly to the soma. A significant current would not then cross a trigger zone at the axon hillock of the cell. Integration of the synaptic currents at the axon hillock would not then be possible because they would be shunted along the giant axon.

A Comparison of the Lamprey Reticulospinal Neurons and the Mammalian Reticular Neurons and the Evolution of Dendrite Patterns

Studies of the mammalian reticular formation [*Scheibel and Scheibel*, 1958; *Leontovich and Zhukova*, 1963; *Ramon-Moliner and Nauta*, 1966] have led to the hypothesis that it is composed of generalized neurons classified as 'isodendritic' and that these neurons represent stem neurons from which the other neurons with a more complex dendroarchitecture

have evolved [*Ramon-Moliner,* 1968]. *Ramon-Moliner and Nauta* [1966] have also suggested that neurons of primitive vertebrates like the lamprey are 'isodendritic'. There are, however, a number of differences as well as similarities between the mammalian and lamprey reticulospinal neurons which include dendroarchitecture, somata and axons.

Dendroarchitecture

Mammalian isodendritic neurons are characterized by a few long, rectilinear, sparsely branching dendrites which radiate from the cell body [*Ramon-Moliner and Nauta,* 1966]. Most dendrites of the lamprey reticulospinal neurons were long and distributed over wide areas of the brainstem, and they also showed sparse branching, except for the Mauthner cell. However, all the lamprey reticulospinal cells had dendrites arranged in an open field, and they were not distributed radially. The dendritic trees of lamprey reticulospinal neurons also appeared more profuse (fig. 7) than the dendritic trees of the mammalian isodendritic neurons. Mammalian reticular dendrites do not possess special features by which they can be recognized and therefore have a low 'topognostic' value [*Ramon-Moliner,* 1968]. This was also true of the bulbar and vagal groups of reticulospinal cells, but the Mauthner cell and lateral mesencephalic reticulospinal cells of the lamprey possessed distinctive dendrites of relatively high 'topognostic' value. On the other hand, the dendrites of the isthmic, bulbar and vagal group of lamprey reticulospinal cells tended to be distributed in a transverse plane, like mammalian reticular neurons [*Scheibel and Scheibel,* 1958]. Extensive intermingling of the dendrites with passing fibres characterizes mammalian isodendritic neurons [*Ramon-Moliner and Nauta,* 1966]. This also occurred in the large reticulospinal neurons of the lamprey as the dendrites were distributed in the outer fibre zone of the brain-stem.

Somata

The cell bodies of the lamprey reticulospinal neurons were round or oval when viewed dorso-ventrally. They differed from the mammalian isodendritic neurons which have polygonal shaped cell bodies.

Axons

Neither the Golgi staining [*Tretjakoff,* 1909] nor the Procion yellow staining (by intracellular injection) of the reticulospinal cells revealed the presence of any axon collaterals. This is in marked contrast to the mam-

malian reticular neurons which possessed many axons collaterals [*Scheibel and Scheibel,* 1958]. Some mammalian reticulospinal neurons possess axons which pass rostrally as well as an axon which descends the spinal cord [*Scheibel and Scheibel,* 1958]. None of the stained lamprey reticulospinal neurons possessed ascending axons.

Scheibel and Scheibel [1970] have already pointed out that the evolution of neurons with a complex dendroarchitecture from the basic stem isodendritic neurons, as hypothesized by *Ramon-Moliner* [1968], ignores the highly complex organization of neurons found in invertebrates, which are phylogenetically much older. They also point out the difficulty in fitting the evolution of dendrite patterns of cells like the cortical cells – cerebral, cerebellar or hippocampal in sequence. A further objection is now added. There are a number of features of the lamprey reticulospinal neurons which are unlike the stem 'isodendritic' neurons, and they occur in a primitive vertebrate like the lamprey ammocoete. An earlier view, which regards the isodendritic reticular neurons as primitive stem neurons [*Ramon-Moliner,* 1968], appears to represent an oversimplified explanation of the phylogenetic development of neurons with different dendrite patterns.

References

Bartelmez, G. W.: Mauthner's cell and nucleus motorius tegmenti. J. comp. Neurol. *25:* 87–128 (1915).

Bertolini, B.: Ultrastructure of the spinal cord of the lamprey. J. Ultrastruct. Res. 11: 1–24 (1964).

Leontovich, T. A. and Zhukova, G. P.: The specificity of the neuronal structure and topography of the reticular formation of the brain and spinal cord of carnivora. J. comp. Neurol. *121:* 347–380 (1963).

Lorente de No, R.: Action potentials of motoneurons of hypoglossus nucleus. J. cell. comp. Physiol. *29:* 207–288 (1947).

Mannen, H.: «Noyau fermé» et «noyau ouvert». Contribution à l'étude cytoarchitectonique du tronc cérébral envisagée du point de vue du mode d'arborisation dendritique. Archo ital. Biol. *98:* 330–350 (1960).

Martin, R. J.: Glycine and GABA receptors on lamprey bulbar reticulospinal neurons. Comp. Biochem. Physiol. (in press, 1978).

Mellon, DeF. and Kaars, C.: Role of regional cellular geometry in conduction of excitation along a sensory neuron. J. Neurophysiol. *37:* 1228–1238 (1974).

Nieuwenhuys, R.: Topographical analysis of the brain stem of the lamprey, *Lampetra fluviatilis.* J. comp. Neurol. *145:* 165–178 (1972).

Ramon-Moliner, E.: in Bourne, The structure and function of the nervous tissue, vol. 1 (Academic Press, New York 1968).

Ramon-Moliner, E. and Nauta, W. J. H.: The isodendritic core of the brain stem. J. comp. Neurol. *126:* 311–335 (1966).

Rovainen, C. M.: Physiological and anatomical studies on large neurons of the central nervous system of the sea lamprey *(Petromyzon marinus).* II. Muller and Mauthner cells. J. Neurophysiol. *30:* 1000–1023 (1967).

Rovainen, C. M.; Johnson, E. A.; Roach, E. A., and Mankovsky, J. A.: Projections of individual axons in lamprey spinal cord determined by tracings through serial sections. J. comp. Neurol. *149:* 193–201 (1973).

Saito, T.: Über die Müllerschen Zellen im Gehirn des japanischen Flussneunauges *(Etosphenus japonicus martens).* Folia anat. jap. *6:* 457–475 (1928).

Scheibel, M. E. and Scheibel, A. B.: in Jasper, Proctor, Knighton, Noshay and Costellow, Reticular formation of the brainstem (Brown, Boston 1958).

Scheibel, M. E. and Scheibel, A. B.: Of pattern and place in dendrites. Int. Rev. Neurobiol. *13:* 1–24 (1970).

Shadé, J. P.: On the volume and surface area of spinal neurons. Prog. Brain Res. 11: 261–271 (1964).

Stefanelli, A.: Numero, grandezza e forma di alcuni peculiari elementi nervosi dei Petromyzonti. Z. Zellforsch. mikrosk. Anat. *18:* 146–165 (1933a).

Stefanelli, A.: Le cellule e le fibre di Müller dei Petromyzonti. Archo ital. Anat. Embriol. *31:* 519–548 (1933b).

Stefanelli, A.: I centri tegmentali dell'encefalo dei Petromyzonti. Archo zool. ital. *20:* 117–202 (1934).

Stretton, A. O. W. and Kravitz, E. A.: Neuronal geometry. Determination with a technique of intracellular dye injection. Science *162:* 132–134 (1968).

Tretjakoff, D.: Das Nervensystem von Ammocoetes. II. Gehirn. Arch. mikr. Anat. *74:* 636 (1909).

Wickelgren, W. O.: Physiological and anatomical characteristics of reticulospinal neurons in lamprey. J. Physiol., Lond. *270:* 89–114 (1977).

R. J. Martin, Department of Veterinary Pharmacology,
Royal (Dick) School of Veterinary Studies, University of Edinburgh, Summerhall, Edinburgh (Scotland)

Comp. Biochem. Physiol., Vol. 63C, pp. 109 to 115
© Pergamon Press Ltd 1979. Printed in Great Britain
0306-4492/79/0330-0109$02.00/0

GLYCINE AND GABA INDUCED CONDUCTANCE CHANGES IN LAMPREY RETICULOSPINAL NEURONS AND THEIR ANTAGONISM BY STRYCHNINE, THEBAINE, BICUCULLINE AND PICROTOXIN

R. J. MARTIN
Dept. of Veterinary Pharmacology, Royal (Dick) School of Veterinary Studies, Summerhall, Edinburgh, Scotland

(*Received* 8 *November* 1978)

Abstract—1. Changes in input conductances in response to bath-applied glycine and GABA were measured in the soma of the bulbar group of reticulospinal neurons in lamprey adults and ammocoetes. Glass micropipettes filled with K acetate or K methyl sulphonate were used with a bridge balance circuit for injecting constant current pulses.

2. The responses showed that glycine was more potent than GABA but both agonists showed evidence of "cooperativity", with Hill coefficients significantly greater than one. (Glycine $nH = 1.77 \pm 0.14$ mean ± S.E; GABA $nH = 1.52 \pm 0.13$ mean ± S.E.). The coefficients of the Hill equation were obtained from a weighted least squares estimate.

3. Strychnine and thebaine antagonized the actions of glycine in a competitive manner but had little effect on the GABA responses. The K_I for strychnine was estimated to be $0.62 \pm 0.05\ \mu m$ (mean ± S.E.). The K_I for thebaine was estimated to be $5.6 \pm 0.3\ \mu m$ (mean ± S.E.).

4. Bicuculline antagonized the actions of GABA in a competitive manner but had little effect on the glycine responses. The K_I for bicuculline was estimated to be $2.6 \pm 0.2\ \mu m$ (mean ± S.E.). Picrotoxin antagonized the GABA responses in a non-competitive manner but had little effect on the glycine responses.

INTRODUCTION

Glycine and GABA appear to act as inhibitory transmitters by causing increased Cl conductances and hyperpolarizing potentials in neurons in the spinal cord and brainstem of vertebrates. Their actions have been extensively studied and reviewed (Krnjević, 1974; Curtis & Johnston, 1974; Roberts *et al.*, 1976; Johnston, 1978). There are however a number of difficulties in making quantitative studies of their actions on conductances. In particular, in vertebrates drug applications are often limited to iontophoretic techniques where concentrations are not readily controlled in the CNS. Nevertheless, the spinal cord and brainstem of the lamprey make particularly suitable vertebrate preparations, because they survive well in the isolated state and contain large visible cells ideal for intracellular recordings (Rovainen, 1967). Conductance changes in response to glycine and GABA have been observed in the spinal cord (Martin *et al.*, 1970; Homma & Rovainen, 1978) and brainstem (Wickelgren, 1977; Martin, 1978).

This paper describes the actions of bath-applied glycine and GABA on the input conductances of lamprey reticulospinal neurons. The antagonism of strychnine, thebaine bicuculline and picrotoxin is described and the relevant dissociation constants estimated.

METHODS

Experiments were conducted on 10–12 cm lamprey adults & ammocoetes (*Lampetra fluviatilis*). They were anaesthetized in a solution of tricaine methane sulphonate (MS 222 Sandoz 10^{-4} g ml^{-1}) and the rostral 2 cm head section removed to a saline bath for further dissection under the binocular microscope. The preparations were divided along the ventral midline and the tissue covering the ventral notochord removed. The preparation was then transferred to a perspex experimental chamber (Fig. 1), and mounted dorsal side uppermost onto Sylgard. The brain was exposed dorsally and illuminated from below. The choroid plexus which covered the third and fourth ventricles was then removed. The bulbar reticulospinal neurons were viewed with the aid of the dissecting microscope adjacent to the medial longitudinal sulcus in the fourth ventricle.

The experimental chamber contained 1 ml of oxygenated high-Mg Ringer to abolish synaptic potentials. It had the following composition, (mM): NaCl, 110; KCl, 2.1; $CaCl_2$, 2.6; $MgCl_2$, 20; glucose, 4; generally buffered with 5 mM Tris–maleate to pH 7.6, but a $NaHCO_3$–CO_2 buffer was

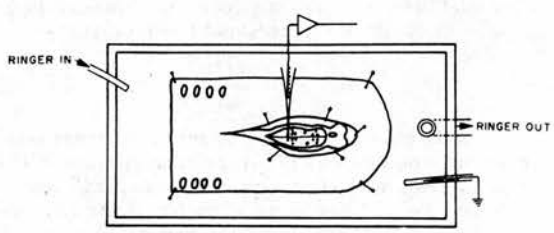


Fig. 1. A diagram of the experimental chamber and preparation. The flap preparation is pinned onto Sylgard and illuminated from below. The chamber contained 1 ml of Ringer and was perfused continuously at a rate of 10 ml min^{-1}.

also used. The high-Mg Ringer was used to block synaptic potentials rather than a low-Ca Ringer, which may sensitize the glycine and GABA receptors (Homma and Rovainen, 1978).

The drugs: glycine and GABA (B.D.H.); bicuculline, strychnine, and picrotoxin (Sigma); and thebaine (May and Baker) were administered dissolved in the Ringer at the concentrations described in the results. The bicuculline was made up and used within one half hour. In order to minimize the effect of glycine and GABA uptake mechanisms, cool Ringer (12°C) was perfused through the chamber and over the preparation at a constant rate of 10 ml/min^{-1}.

The glass micropipettes, used for intracellular recordings were filled with 2 M K methyl sulphonate or 2 M K acetate. The micropipettes had d.c. resistances of 10–20 MΩ and were connected through an Ag–AgCl wire to a high impedance preamplifier. Current pulses were passed through the micropipettes using a bridge balance circuit. The reference electrodes were connected to the bath via an agar-KCl bridge. Membrane potentials and resistance changes were monitored on a cathode ray oscilloscope and pen recorder.

The micropipettes were placed in the soma of the bulbar reticulospinal neurons under visual control and recordings selected from cells with stable resting potentials greater than 65 mV and input impedances greater than 4 MΩ. Input impedances varied between 4–20 MΩ. Input conductances were measured using constant current pulses up to 5 nA and 150 msec duration. Changes in input conductances due to the agonists were measured by subtracting resting input conductances from the conductances observed in the presence of the agonist solutions.

Analysis

The degree of cooperativity shown by the glycine and GABA dose-response relationships was described by estimating the coefficient (nH) of the Hill equation, 1 below.

$$\frac{\Delta G}{\Delta G_{max}} = \frac{A^{nH}}{A^{nH} + K} \quad (1)$$

G is the observed conductance change, ΔG_{max} is the maximum conductance change, A is the molar concentration of the amino acid (glycine or GABA), K is a constant and nH is the Hill coefficient. Equation 1 describes empirically the dose-response relationships reasonably well (Colquhoun, 1971), but the extent to which the Hill equation justifies physical models is discussed by Colquhoun (1973).

Equation 1 was fitted to the observations by weighted least squares regression, which is known to have advantages over linearizing transformations (Colquhoun, 1971). Minimization employed a routine Nelmead (Nelder & Mead, 1965) in the programme Minisquare 15 (author D. J. Finney). The observations were weighted by the reciprocal of the variance of ΔG observed at each amino acid concentration. Standard errors were calculated from the variance covariance matrix.

The inhibitory actions of strychnine, thebaine and bicuculline were described by the Schild (1949) equation,

$$x - 1 = \frac{[I]}{K_I} \quad (2)$$

where x is the equipotent dose-ratio and K_I is the apparent dissociation constant and $[I]$ is the concentration of the antagonist. This method used equal responses (null experiments) and avoided any assumptions about the relationship between the response and the fraction of receptors occupied. It seemed more appropriate to use the simpler analysis of Schild (1949) although it is recognized that null experiments yield results which are very nearly identical to predictions of various cooperative models (Colquhoun, 1973).

RESULTS

Conductance increases produced by glycine and GABA

The reticulospinal neurons recorded from had resting conductances of 0.05–0.25 μmho and showed no spontaneous synaptic potentials when bathed in the high-Mg Ringer. When the perfusing Ringer was changed to Ringer carrying glycine or GABA in concentrations greater than 10^{-5} M, conductance increases were observed in association with a small hyperpolarizing potential. An example is shown in Fig. 2, where the top trace shows the voltage responses to the current pulses shown in the lower trace. The application of glycine (3×10^{-5} M) produced a conductance change of 0.20 μmho, while the application of GABA (3×10^{-5} M) produced a conductance change of 0.09 μmho.

The conductance changes were dose-dependant and increased with an increase in agonist concentration. The effects of glycine and GABA were tested alternately in ascending concentrations on the same neurons of 16 preparations and the responses at each concentration of the agonist determined. Figure 3 illustrates the log dose-response relationships with the mean ± S.E. of the observations. It can be seen that glycine was more potent than GABA on a molar basis. The greater error in the observations observed at high conductances was due to the fact that small changes in resistance at high agonist concentrations corresponded to large conductance increases. The Hill coefficient of equation 1 was therefore estimated by weighting each observation by the reciprocal of the variance observed at each agonist concentration.

One feature of many dose-response relationships is a greater than linear relationship between response and agonist concentration at low doses (Colquhoun, 1973) and responses which are predicted by a form of the Hill equation with coefficients greater than 1. When dose-response relationships for glycine and GABA (not shown) were plotted on a linear scale they showed inflections near their origin. The Hill coefficients for glycine ($nH = 1.77 \pm 0.14$, mean ± S.E., $n = 82$) and GABA ($nH = 1.52 \pm 0.13$, mean ±

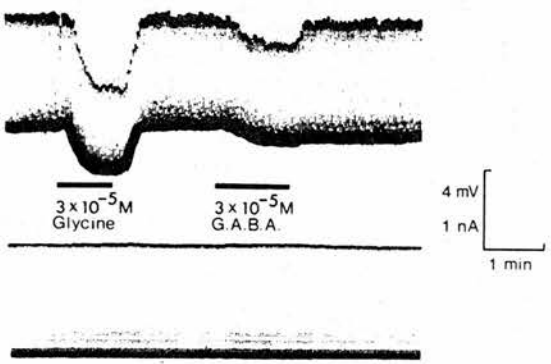


Fig. 2. The effect of glycine (3×10^{-5} M) and GABA (3×10^{-5} M) on input conductance. The glycine was applied during the period of the first horizontal bar and produced a reversible increase in conductance and a hyperpolarizing potential. GABA was also applied during the period of the second horizontal bar but produced a smaller increase in conductance and a smaller hyperpolarizing potential. The top trace represents the voltage responses to the constant depolarizing circuit pulses of the lower trace.

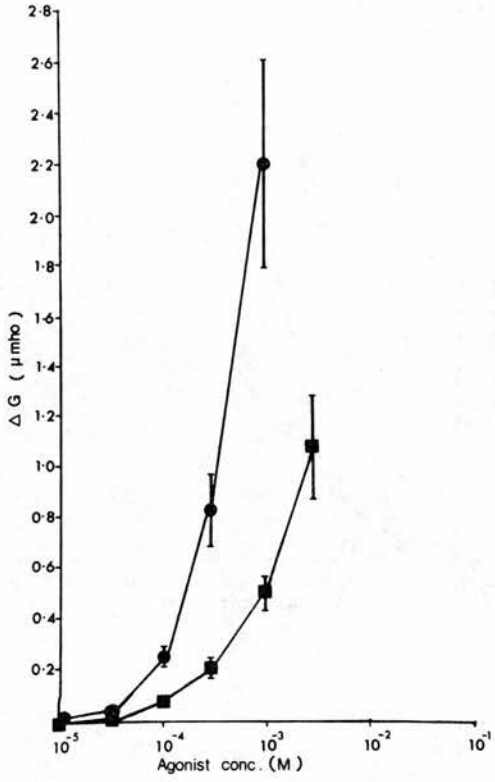


Fig. 3. The log dose-response relationships of glycine (●) and GABA (■). The points represent the mean of 14–16 observations. The vertical bars represent ± S.E. of the mean. Note that on a molar basis glycine is more potent than GABA.

S.E., $n = 79$) were obtained from the least square regressions. They both had Hill coefficients significantly (*t*-test, $P < 0.001$) greater than 1. Thus both glycine and GABA exhibited evidence of cooperativity.

The antagonism of strychnine, thebaine, bicuculline and picrotoxin

The actions of strychnine (5 preparations), thebaine (3 preparations), bicuculline (4 preparations) and picrotoxin (4 preparations) was studied by monitoring their effects on the log dose-response relationships of glycine and GABA. A typical example of the effects of strychnine (10^{-5} M) is shown in Fig. 4A, where it produced a large parallel shift to the right of the log dose-response curve for glycine but had little effect on the GABA responses. Strychnine produced similar effects in all 5 preparations. The effects of strychnine were also tested at different concentrations. It can be seen that the parallel displacement to the right is proportional to the strychnine concentration.

The effects of thebaine (10^{-5} M) were tested in 3 preparations, and in all cases thebaine produced a parallel shift to the right of the log dose-response curve for glycine but it had little effect on the GABA dose-response curve (Fig. 5B). The antagonism of strychnine (10^{-5} M) was seen to be greater than the antagonism of thebaine (10^{-5} M). The effects of thebaine were also tested at different concentrations (Fig. 5C). The results showed that the displacements of the glycine log-dose response curves were also proportional to the concentration of thebaine.

The effects of bicuculline (10^{-5} M) were tested in 4 preparations. In all 4 preparations, bicuculline produced a parallel displacement to the right of the log-dose response curve of GABA but had little effect on the glycine dose-response curve (Fig. 5C). The effects of bicuculline were also tested at different concentrations and as Fig. 5E shows, the displacement of the GABA log dose-response curve was proportional to the concentration of bicuculline.

The effects of picrotoxin (10^{-5} M) were tested in 4 preparations. In all 4 preparations, picrotoxin antagonized the GABA responses but had little or no effect on the glycine responses. However, picrotoxin did not produce a parallel shift to the right, but reduced the slope of the log dose-response curve. Higher concentrations of picrotoxin were also tested with similar results. Thus picrotoxin acted as a non competitive antagonist of GABA.

The above results suggested that strychnine, thebaine and bicuculline behaved like competitive antagonists. It was therefore possible to estimate the apparent dissociation constants, K_I of these antagonists for their receptors, by estimating equipotent doses before and after their application and using the Schild (1949) equation to calculate K_I. The K_I's were estimated by interpolation from the graphs shown in Figs 5, A, C and D. in the upper, middle and lower region of the dose-response curves. The mean ± S.E. of the estimated values and the number of the K_I's are shown in Table 1. Similar K_I's were obtained from the other preparations.

The competitive nature of the strychnine, thebaine and bicuculline antagonism was further tested by plotting $\log_{10}(x - 1)$ against $\log_{10}[I]$. The Schild (1949) equation predicts a linear relationship with unity slope for competitive antagonists. Such plots are shown in Fig 5B, D and E. After regression analysis, the graphs had slopes close to unity, i.e. 0.94 ± 0.06 (mean ± S.E.) for strychnine, 1.06 ± 0.04 (mean ± S.E.) for thebaine and 0.92 ± 0.05 (mean ± S.E.) for bicuculline. The intercepts on the abscissa of these graphs also gave estimates of the K_I values which can be seen to be similar to those shown in Table 1.

DISCUSSION

The effects of glycine and GABA on the input conductances of the reticulospinal cells were measured in the soma and compared in the same cells. From these results it is clear that on a molar basis glycine is more potent than GABA, producing greater conductance changes at lower doses. Homma & Rovainen (1978) have shown that glycine is also more potent than GABA when applied to lamprey spinal cord cells.

It is interesting that glycine is usually more potent than GABA in reducing the firing rate of cat reticular (Hösli & Tebēcis, 1970) and cat reticulospinal neuron (Tebēcis & Di Maria, 1972) since neurons like the lamprey reticulospinal neuron appear to persist in vertebrates throughout phylogeny (Shapovalov, 1975). In the cat medullary reticular formation, glycine has been proposed as an inhibitory transmitter (Tebēcis & Di Maria, 1972; Tebēcis & Ishikawa, 1973). Gly-

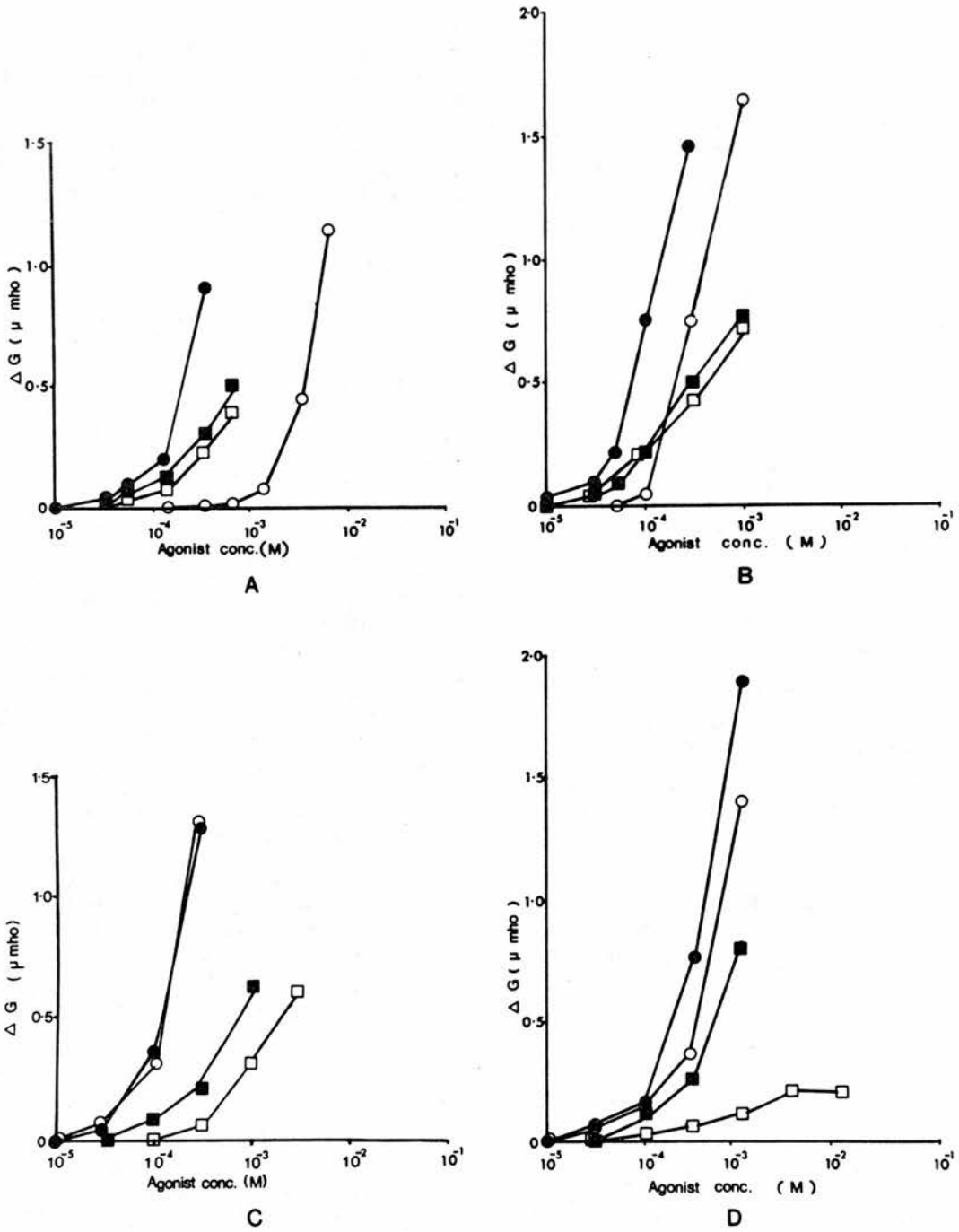


Fig. 4. The effect of antagonists on the log dose-response relationships. The antagonists were applied at concentrations of 10^{-5} M. The results are from single experiments but were similar in all the other preparations tested. The control glycine (●) and control GABA (■) relationships were determined first. Then the glycine + antagonist (○) & GABA + antagonist (□) relationships were determined. A. strychnine antagonism; B. thebaine antagonism; C. bicuculline antagonism; D. picrotoxin antagonism.

cine may also behave as an inhibitory transmitter in the lamprey medullary reticular formation.

Cooperativity

The dose-response curves were described by the Hill equation with coefficients for glycine and GABA significantly greater than 1. This means that there is a greater than linear relationship between the conductance increases and agonist concentrations at low doses. A variety of mechanisms could be responsible for such relationships. A likely possibility is the co-operative binding of the glycine and GABA receptors. so that binding of one molecule of glycine or GABA increases the binding of a second molecule. Young & Snyder (1974) have observed evidence for cooperative binding of glycine, which displaces labelled

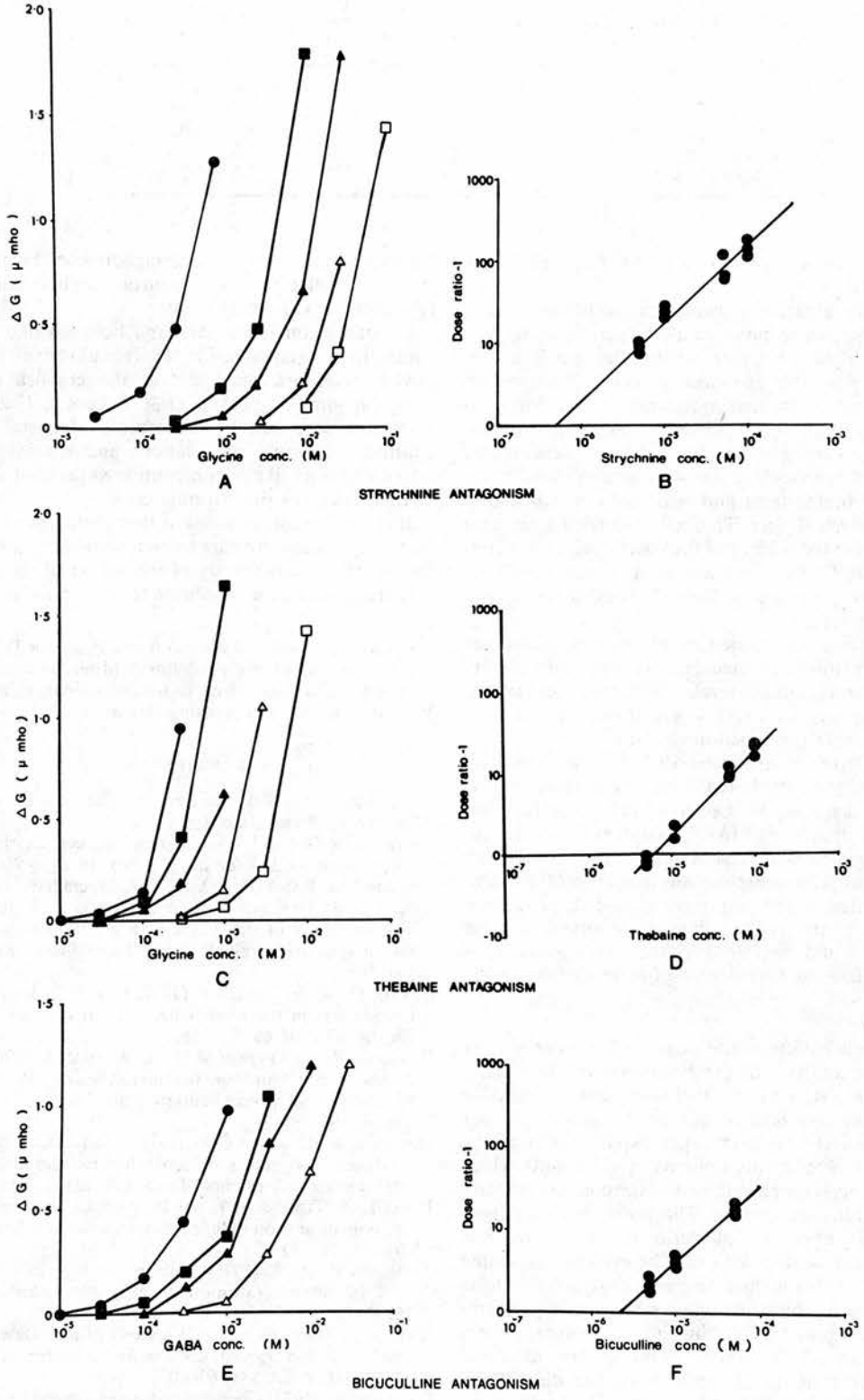


Fig. 5. The competitive nature of strychnine, thebaine and bicuculline antagonism. The left hand series of illustrations (A, C and E) show log dose-response relationships at different antagonist concentrations. The control dose-response relationships (●) were determined initially and relationships determined at antagonist concentrations of 5×10^{-6} M (■), 10^{-5} M (▲), 5×10^{-5} M (△) and 10^{-4} M (□). The right hand series (B, D and F) show plots made to test the validity of the Schild (1949) equation. The computed slopes (mean ± S.E.) were 0.94 ± 0.06 for strychnine, 1.06 ± 0.04 for thebaine and 0.92 ± 0.05 for bicuculline. Note that intercepts on the abscissa give K_I values similar to those expressed in Table 1.

Table 1. The estimates of K_I based on the Schild (1949) equation for strychnine, thebaine & bicuculline

	No. of observations	K_I (mean ± S.E. μM)
Strychnine + glycine	12	0.62 ± 0.05
Thebaine + glycine	11	5.6 ± 0.3
Bicuculline + GABA	9	2.6 ± 0.2

strychnine from synaptic membranes with a Hill coefficient of 1.7.

There are alternative explanations however. Sigmoid dose-response curves could be generated by heterogeneity of the receptors binding the agonists. Any high affinity site that produces no membrane response (including uptake mechanisms) would titrate low concentrations of glycine or GABA. This latter explanation seems unlikely in the present experiments because the preparation was very small (about 1 mm across the brain stem) and was perfused constantly with cool fresh Ringer. The cells recorded from also lay just under the surface of the fourth ventricle (Tretjakoff 1909). Other explanations of "cooperative" behaviour are discussed by Katz & Thesleff (1957) and Colquhoun (1973).

The physical consequences of the sigmoid dose-response relationship include a relative insensitivity to low "background" levels of transmitter and a greater response to larger levels of transmitter, perhaps increasing the signal/noise ratio.

Although the distribution of inhibitory synapses may be evenly distributed over the surface of the soma and dendrites (Wickelgren, 1977), the distribution of the glycine and GABA receptors on the reticulospinal neurons is at present unknown. It is therefore possible that these receptors are located on the extensive dendrites, which may have cable-like properties. The value of the Hill coefficients observed in these experiments and measured in the soma would thus underestimate the true degree of cooperativity.

The antagonists

The parallel shifts of the dose-response curves and subsequent analysis of the behaviour of dose-ratios shows that strychnine, thebaine and bicuculline behave like classical competitive antagonists for receptors on the lamprey reticulospinal neuron. The use of null experiments however, yield results which are generally compatible with various cooperative models (Colquhoun, 1973). The possibility that these compounds may be allosteric inhibitors remains therefore and is not ruled out. The evidence of Young & Snyder (1974) in fact suggests that strychnine is an allosteric inhibitor. Strychnine behaves like a competitive antagonist of glycine in the lamprey spinal cord (Homma & Rovainen, 1978), in the cat spinal cord (Curtis *et al.*, 1971) and in cerebellar slices (Okamoto & Quastel, 1976). However, Davidoff *et al.* (1969) concluded that the antagonism between strychnine and glycine based on an analysis of spiked discharges in cat spinal neurons was non competitive.

Bicuculline behaved like a competitive antagonist for the reticulospinal neuron GABA receptors, as it did in the lamprey spinal cord (Homma & Rovainen, 1978). However these observations contrast with the reported, non-competitive antagonism of bicuculline shown at the crayfish neuromuscular junctions (Takeuchi & Onodera, 1974).

Picrotoxin on the other hand behaved like a non competitive antagonist for the reticulospinal neuron GABA receptors, as it did at the crayfish neuromuscular junction (Takeucki & Takeuchi, 1969). Experiments described by Okamoto & Quastel (1976) contrast with these observations and suggested that picrotoxin acts like a competitive antagonist for the GABA receptors on Purkinje cells.

It can be said in conclusion that the lamprey brainstem preparation appears to be a suitable preparation for the quantitative study of the action of the inhibitory transmitters on vertebrate reticulospinal neurons.

Acknowledgements—I wish to thank Professor D. J. Finney for the use of his programme Minisquare 15, Miss E. Ryan for her excellent technical assistance, and the Wellcome Trust for supporting this work.

REFERENCES

COLQUHOUN D. (1971) *Lectures on Biostatistics.* Oxford University Press, Oxford.

COLQUHOUN D. (1973) The relation between classical and cooperative models for drug action. In *Drug Receptors* (Edited by RANG H. P.), p. 149. Macmillan, London.

CURTIS D. R., DUGGAN A. W. & JOHNSTON G. A. R. (1971) The specificity of strychnine as a glycine antagonist in the mammalian spinal cord. *Expl Brain Res.* **12**, 547–565.

CURTIS D. R. & JOHNSTON G. A. R. (1974) Amino acid transmitters in the mammalian central nervous system. *Ergebn. Physiol.* **69**, 97–188.

DAVIDOFF R. A., APRISON M. H. & WERMAN R. (1969) The effects of strychnine on the inhibition of interneurons by glycine and γ-aminobutyric acid. *Int. J. Neuropharmac.* **8**, 191–194.

HOMMA S. & ROVAINEN C. H. (1978) Conductance increases produced by glycine and γ-aminobutyric acid in lamprey interneurones. *J. Physiol., Lond.* **279**, 231–252.

HÖSLI L. & TEBÉCIS A. K. (1970) Actions of amino acids and convulsants on bulbar reticular neurones. *Expl Brain Res.* **11**, 111–127.

JOHNSTON G. A. R. (1978) Neuropharmacology of amino acid inhibitory transmitters. *Ann. Rev. Pharmac.* **18**, 269–290.

KATZ B. & THESLEFF S. (1957) A study of the "Desensitization" produced by acetylcholine at the motor end-plate. *J. Physiol., Lond.* **138**, 63–80.

KRNJEVIĆ K. (1974) Chemical nature of synaptic transmission in vertebrates. *Physiol. Rev.* **54**, 418–540.

MARTIN A. R., WICKELGREN W. O. & BERÀNEK R. (1970) Effects of iontophoretically applied drugs on spinal interneurones of the lamprey. *J. Physiol., Lond.* **207**, 653–665.

MARTIN R. J. (1978) Glycine and GABA receptors on lamprey bulbar reticulospinal neurones. *Comp. Biochem. Physiol.* **61C**, 37–40.

NELDER J. A. & MEAD R. (1965) A simplex method for function minimization. *Computer. J.* **7**, 308–313.

OKAMOTO K. & QUASTEL J. H. (1976) Effects of amino acids and convulsants on spontaneous action potentials in cerebellar cortex slices. *Br. J. Pharmac.* **57**, 3–15.

ROBERTS E., CHASE T. N. & TOWER D. B. (1976) *GABA in Nervous System Function.* Raven, New York.

ROVAINEN C. M. (1967) Physiological and anatomical studies on large neurons of the central nervous system of the sea lamprey (Petromyzon marinus). I. Muller and Mauthner cells. *J. Neurophysiol.* **30**, 1000–1023.

SCHILD H. O. (1949) pAx and competitive drug antagonism. *Br. J. Pharmac.* **4**, 277–280.

SHAPOVALOV A. I. (1975) Neuronal organization and synaptic mechanisms of supraspinal motor control in vertebrates. *Rev. Physiol. Biochem. Pharm.* **72**, 1–54.

TAKEUCHI A. & ONODERA K. (1972) Effect of bicuculline on the GABA receptor of the crayfish neuromuscular junction. *Nature, New Biol.* **236**, 55–56.

TAKEUCHI A. & TAKEUCHI N. (1969) A study of the action of picrotoxin on the inhibitory neuromuscular junction of the crayfish. *J. Physiol. Lond.* **205**, 377–391.

TEBÉCIS A. K. & DI MARIA A. (1972) Stychnine-sensitive inhibition in medullary reticular formation: evidence for glycine as an inhibitory transmitter. *Brain Res.* **40**, 373–383.

TEBÈCIS A. K. & ISHIKAWA T. (1973) Glycine and GABA as inhibitory transmitters in medullary reticular formation studies involving intra- and extra-cellular recordings. *Pflügers Arch. ges. Physiol.* **338**, 272–278.

TRETJAKOFF D. (1909) Das nervensystem von ammocoetes. II. *Gehirn. Arch. Mikr. Anat.* **74**, 636–779.

WICKELGREN W. O. (1977) Physiological and anatomical characteristics of reticulospinal neuron in lamprey. *J. Physiol., Lond.* **270**, 89–114.

YOUNG A. B. & SNYDER S. H. (1974) Strychnine binding in rat spinal cord membranes associated with the glycine receptor: cooperativity of glycine interactions. *Molec. Pharmac.* **10**, 790–809.

DISSIMILAR INFLUENCES OF SOME INJECTABLE ANAESTHETICS ON THE RESPONSES OF RETICULO-SPINAL NEURONES TO INHIBITORY TRANSMITTERS IN THE LAMPREY

K.D. CULLEN & R.J. MARTIN

Department of Veterinary Pharmacology, Royal (Dick) School of Veterinary Studies, Summerhall, Edinburgh EH9 1QH

1 Intracellular recordings were made from identified bulbar reticulo-spinal neurones in the medulla of lamprey ammocoetes. Responses to iontophoretically applied inhibitory transmitters were measured as changes in membrane potential and input resistance.

2 Dose-dependent alterations in the responses to γ-aminobutyric acid (GABA) and glycine during bath application of injectable anaesthetic drugs were measured; the compounds used were pentobarbitone, ketamine, metomidate and the steroid mixture alphaxalone/alphadolone (Saffan).

3 GABA responses were potentiated by pentobarbitone ($1-3 \times 10^{-4}$ M) and prolonged by ketamine (3.7×10^{-5} M); but depressed by high concentrations (10^{-3} M) of all drugs, as well as by anaesthetic concentrations of alphaxalone ($1-3 \times 10^{-5}$ M).

4 Glycine responses were depressed by alphaxalone ($1-3 \times 10^{-5}$ M) and by supra-anaesthetic concentrations of ketamine (3.7×10^{-4} M) and metomidate (1.8×10^{-3} M). No drug potentiated the glycine responses.

5 In the absence of an effect common to the 4 anaesthetics, it is concluded that neither potentiation nor inhibition of all GABA or glycine responses is an essential feature of anaesthesia. However, effects comparable to those described here may contribute to the overall clinical picture during anaesthesia of higher vertebrates. The findings do not support the notion that all anaesthetic agents act on biological membranes by a single mechanism.

Introduction

Anaesthesia is thought to result from a reversible drug-induced disruption of brain function. Since Sherrington (1906) drew attention to the susceptibility of reflex arcs, attention has focussed on the synapse as the site of action of anaesthetic drugs. It has become apparent that anaesthetics differ in their actions at individual synapses (Larrabee & Posternak, 1952) and that different central nervous pathways have unequal sensitivities (Mark & Steiner, 1958). Indeed some such differential action is required to explain the characteristic clinical states which follow administration of the various drugs (Vickers, Wood-Smith & Stweart, 1978).

In this study we have compared the abilities of four injectable anaesthetic drugs to interfere with the actions of the inhibitory transmitters γ-aminobutyric acid (GABA) and glycine. The drugs were applied to bulbar reticulospinal neurones in the medulla of the lamprey ammocoete, cells readily identifiable and known to possess distinct GABA and glycine receptors (Martin, 1978; Matthews & Wickelgren, 1979). Anatomical and pharmacological analogies have been drawn between these cells and cells in the central nervous systems of higher vertebrates (Shapovalov, 1975; Martin, 1979a).

The anaesthetics, chosen to represent four classes of compound used in clinical anaesthetic practice, were bath-applied to the preparation in concentrations similar to those likely to obtain in the brain during clinical anaesthesia (Richards, 1972; Minchin, 1981). Although anaesthetics could equally interfere with synaptic transmission by a presynaptic action, we have concentrated on postsynaptic mechanisms, applying the putative transmitters directly to the cells and taking steps to preclude transsynaptic effects.

Methods

The preparation

Ammocoetes 8–15 cm long of the species *Lampetra fluviatilis* and *Lampetra planeri* were anaesthetized with neutralized tricaine methane sulphonate (100 μg/l) and then transected caudal to the gills. The rostral portion was divided in the ventral midline and, after tissues covering the ventral notochord had been removed, was pinned out on Sylgard in the experimental chamber, dorsal surface uppermost. A simple

0007-1188/82/110493-12 $01.00

© The Macmillan Press Ltd 1982

dissection exposed the bulbar reticulo-spinal cells, clustered on either side of the midline near the centre of the 4th ventricle (Figure 1). The preparation was continuously perfused with a cooled Ringer solution at 6 ml/min, and the recorded temperature in the chamber (capacity, 1 ml) maintained at 8–10°C by the circulation of cooled fluid through an outer jacket.

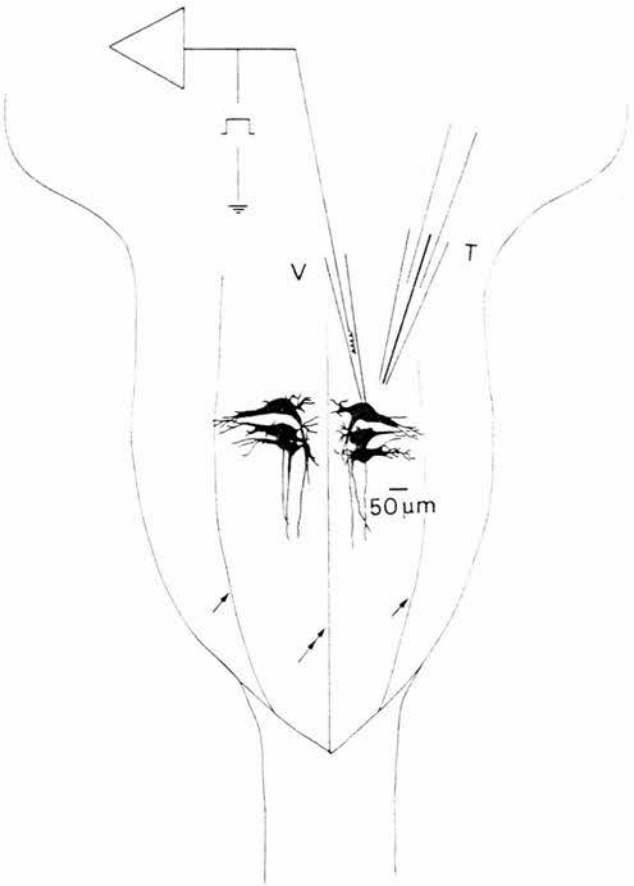


Figure 1 Diagram of the preparation showing the location of micropipettes. Bulbar reticulo-spinal cells lie in the floor of the 4th ventricle between the sulcus limitans of His (arrows) and the median longitudinal sulcus (double arrow) of the ammocoete larva. Positions of recording (V) and iontophoresis (T) electrodes are indicated.

Ringer solutions

The usual composition of the Ringer solution was (mM): NaCl 71, KCl 2.1, $CaCl_2$ 2.6, $MgCl_2$ 15, $NaHCO_3$ 20, NaH_2PO_4 0.18 and glucose 4.0. The pH was adjusted to 7.1–7.2 with HCl and the solution gassed with a mixture of CO_2 5% and 0_2 95%. The high concentration of magnesium was used to block the release of endogenous transmitter.

Recording system

Standard intracellular recording techniques were used, with direct visual control of cell penetration. The recording electrode was connected by an Ag/AgCl wire to a high impedance pre-amplifier which incorporated a bridge balance circuit enabling current pulses to be injected for the measurement of input impedance. When filled with 2 M potassium methyl sulphate the glass micropipettes used had d.c. resistances in the range 20–30 MΩ. An Ag/AgCl reference electrode was connected to the bath.

Membrane potentials were displayed on a cathode ray oscilloscope (Tektronix 5113 Dual Beam Storage Oscilloscope) and a permanent record made by a high speed pen recorder (Lectromed MX212). A thermistor probe connected to the pen recorder provided a continuous record of the temperature in the experimental chamber.

Iontophoresis

Three-barrelled assemblies were used for iontophoresis. The micropipettes were back-filled with GABA (0.5 M, pH 2.5), glycine (0.5 M, pH 5.0), or NaCl (0.5 M). GABA and glycine were ejected as cations. NaCl was incorporated as a control in some experiments; in others, application of current pulses of reversed polarity served instead. In all experiments an Ag/AgCl indifferent electrode was placed in the bath for the return of iontophoretic current. Retaining currents were not routinely employed, any leakage of drug was insufficient to cause detectable changes in the membrane potential or resistance of the cells.

The ejection cycle was controlled by a microiontophoresis programmer (Model 160, W-P Instruments Inc.) driven by a Digitimer. The transmitters were applied alternately by currents of the same strength, usually in the range 50 to 90 nA. Pulses lasting between 0.3 and 7.0 s were applied at intervals of 1 or 3 min. The pulse duration was determined for each transmitter individually and then kept constant for the duration of an experiment.

In experiments testing the influence of transmitter concentration on the anaesthetic effect only one transmitter was used. To vary the agonist dose a cycle of iontophoretic pulses of differing duration but the same amplitude was employed. The quantity of drug ejected by an iontophoretic pulse is affected by the immediately preceding pulse, but the use of a fixed pulse sequence ensured that this factor was unchanged during an experiment. Differences between the amounts of the agonist delivered by the test pulses were therefore constant although unknown, so measurements of the responses are comparable but only within an experiment.

The effects of anaesthetics on transmitter responses

Anaesthetics were dissolved in the perfusing Ringer solution and applied to the preparation. No application was continued after 25 min; this limit allowed the responses to recover before cell deterioration supervened. The sequence of iontophoretic pulses continued during the perfusion with anaesthetic. Changes in input resistance associated with the transmitter actions were monitored by the injection of constant hyperpolarizing current pulses (strength 0.5–1.0 nA, frequency 1 Hz) whose duration was long (30 ms) in relation to the time constant of the cell (< 10 ms). Because of the possibility that anaesthetic drugs may interact (Richards & White, 1981), only one was tested on any individual preparation. Most experiments were terminated within 10 h of dissection.

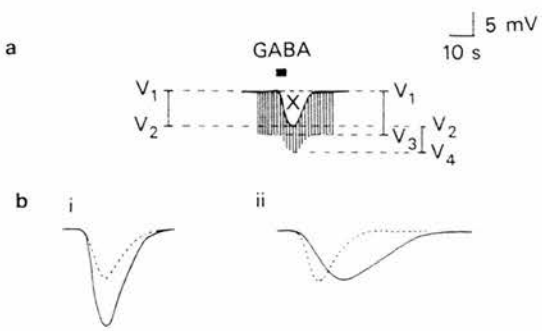


Figure 2 (a) Tracing of a typical response to an iontophoretic pulse of γ-aminobutyric acid (GABA). Vertical deflections (downward) from the resting membrane potential are in response to repeated injections of hyperpolarizing current pulses (1 nA, 30 ms). GABA was applied during the period indicated by the horizontal bar. Features measured: (1) peak change in membrane potential ($V_2 - V_1$), (2) membrane potential change in response to hyperpolarizing current pulses before ($V_3 - V_1$) and during ($V_4 - V_2$) action of GABA. The height of each vertical deflection is directly proportional to the input resistance. Because constant current pulses were used, the fractional change in input resistance at peak GABA effect is

$$\frac{(V_3 - V_1) - (V_4 - V_2)}{(V_3 - V_1)}.$$

(3) area (X) enclosed by the envelope of the membrane potential response. (b) Diagram to illustrate use of measurement of ratio area:peak. Control (- - -) and test (———) responses are superimposed. (i) Simple potentiation of membrane potential response. (ii) Alteration of response profile showing both delayed peak response and slowed recovery. In both (i) and (ii) the area of the response is increased from 9 mV.s (control) to 19 mV.s (test); but whereas in (i) the ratio remains 3.5 s, that in (ii) is increased from 3.5 s (control) to 7.2 s (test).

Drugs

The drugs used were GABA (Sigma), glycine (BDH), tricaine methane sulphonate (MS-222, Sandoz), pentobarbitone (May & Baker), ketamine (Vetalar, Parke-Davis), alphaxalone/alphadolone (Saffan, Glaxovet) and metomidate (Hypnodil, Janssen). The vehicle present in Saffan was kindly donated by Glaxovet. Although the product Saffan was used in the experiments, it will be referred to henceforth as alphaxalone because concentrations are expressed in terms of this constituent.

Analysis of results

The responses to GABA and glycine were essentially similar. Numerical values were obtained for the peak resistance changes as indicated in Figure 2a. A videoplan (Reichert-Jung) was used to measure the time integral of the membrane potential response (area 'X'). Figure 2b shows how the ratio of this area to the peak hyperpolarization distinguishes between an increase in area due solely to an altered peak amplitude and one effected by prolongation of the response. The ratio was calculated in experiments in which pentobarbitone or ketamine were tested, because these drugs altered the GABA response profile.

So that the results of different experiments could be compared, the changes in GABA and glycine responses measured during exposure to anaesthetics were expressed as percentages. Student's *t* test was applied to these standardized data to assess the statistical significance of the anaesthetic effects.

Results

Responses to γ-aminobutyric acid and glycine

Most cells had resting potentials in the range −60 to −65 mV and input resistances > 3 MΩ. The usual response to application of either GABA or glycine was a transient hyperpolarization accompanied by reduction in the input resistance to the cell. A small minority of cells (4 out of 92) showed depolarizing responses to both amino acids. High concentrations of either agonist elicited biphasic hyperpolarizing/depolarizing responses and were therefore avoided.

Effect of anaesthetics on the responses to γ-aminobutyric acid and glycine

Sixty-three ammocoetes were exposed to the anaesthetics: pentobarbitone (19 ammocoetes), ketamine (15), alphaxalone (19), metomidate (10); 10 ammocoetes were tested with the Saffan vehicle alone. No anaesthetic consistently altered the mem-

The effects of anaesthetics on transmitter responses

Anaesthetics were dissolved in the perfusing Ringer solution and applied to the preparation. No application was continued after 25 min; this limit allowed the responses to recover before cell deterioration supervened. The sequence of iontophoretic pulses continued during the perfusion with anaesthetic. Changes in input resistance associated with the transmitter actions were monitored by the injection of constant hyperpolarizing current pulses (strength 0.5–1.0 nA, frequency 1 Hz) whose duration was long (30 ms) in relation to the time constant of the cell (< 10 ms). Because of the possibility that anaesthetic drugs may interact (Richards & White, 1981), only one was tested on any individual preparation. Most experiments were terminated within 10 h of dissection.

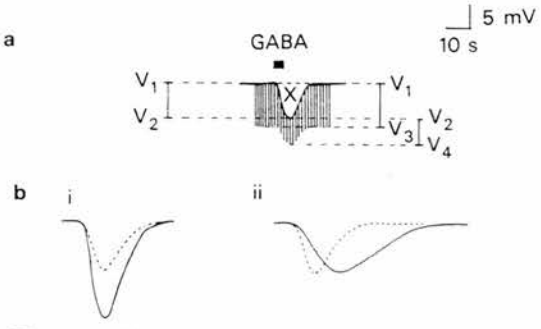


Figure 2 (a) Tracing of a typical response to an iontophoretic pulse of γ-aminobutyric acid (GABA). Vertical deflections (downward) from the resting membrane potential are in response to repeated injections of hyperpolarizing current pulses (1 nA, 30 ms). GABA was applied during the period indicated by the horizontal bar. Features measured: (1) peak change in membrane potential ($V_2 - V_1$), (2) membrane potential change in response to hyperpolarizing current pulses before ($V_3 - V_1$) and during ($V_4 - V_2$) action of GABA. The height of each vertical deflection is directly proportional to the input resistance. Because constant current pulses were used, the fractional change in input resistance at peak GABA effect is

$$\frac{(V_3 - V_1) - (V_4 - V_2)}{(V_3 - V_1)}.$$

(3) area (X) enclosed by the envelope of the membrane potential response. (b) Diagram to illustrate use of measurement of ratio area:peak. Control (---) and test (———) responses are superimposed. (i) Simple potentiation of membrane potential response. (ii) Alteration of response profile showing both delayed peak response and slowed recovery. In both (i) and (ii) the area of the response is increased from 9 mV.s (control) to 19 mV.s (test); but whereas in (i) the ratio remains 3.5 s, that in (ii) is increased from 3.5 s (control) to 7.2 s (test).

Drugs

The drugs used were GABA (Sigma), glycine (BDH), tricaine methane sulphonate (MS-222, Sandoz), pentobarbitone (May & Baker), ketamine (Vetalar, Parke-Davis), alphaxalone/alphadolone (Saffan, Glaxovet) and metomidate (Hypnodil, Janssen). The vehicle present in Saffan was kindly donated by Glaxovet. Although the product Saffan was used in the experiments, it will be referred to henceforth as alphaxalone because concentrations are expressed in terms of this constituent.

Analysis of results

The responses to GABA and glycine were essentially similar. Numerical values were obtained for the peak resistance changes as indicated in Figure 2a. A videoplan (Reichert-Jung) was used to measure the time integral of the membrane potential response (area 'X'). Figure 2b shows how the ratio of this area to the peak hyperpolarization distinguishes between an increase in area due solely to an altered peak amplitude and one effected by prolongation of the response. The ratio was calculated in experiments in which pentobarbitone or ketamine were tested, because these drugs altered the GABA response profile.

So that the results of different experiments could be compared, the changes in GABA and glycine responses measured during exposure to anaesthetics were expressed as percentages. Student's *t* test was applied to these standardized data to assess the statistical significance of the anaesthetic effects.

Results

Responses to γ-aminobutyric acid and glycine

Most cells had resting potentials in the range −60 to −65 mV and input resistances > 3 MΩ. The usual response to application of either GABA or glycine was a transient hyperpolarization accompanied by reduction in the input resistance to the cell. A small minority of cells (4 out of 92) showed depolarizing responses to both amino acids. High concentrations of either agonist elicited biphasic hyperpolarizing/depolarizing responses and were therefore avoided.

Effect of anaesthetics on the responses to γ-aminobutyric acid and glycine

Sixty-three ammocoetes were exposed to the anaesthetics: pentobarbitone (19 ammocoetes), ketamine (15), alphaxalone (19), metomidate (10); 10 ammocoetes were tested with the Saffan vehicle alone. No anaesthetic consistently altered the mem-

brane potential and only the highest concentrations of pentobarbitone and metomidate (10^{-3} M) affected the input resistance, causing a small reduction. The alterations in the GABA and glycine responses measured during exposure to the four anaesthetics are displayed in Table 1.

Most experiments were carried out at 8–10°C but the results were qualitatively similar at room temperature and at 2°C (not illustrated).

Pentobarbitone

The effects of pentobarbitone were complex and dose-dependent. Records from typical experiments are displayed in Figure 3. Low concentrations ($1-5 \times 10^{-4}$ M) potentiated the GABA responses in some cells, but only in 8 out of 19 tests did the potentiation exceed 10%. The remaining 11 tests showed little change. Potentiated responses were increased both in amplitude and duration (Table 1). In two preparations the concentration was raised to 10^{-3} M: this caused a reduction in amplitude of the GABA response.

No concentration of pentobarbitone significantly affected the glycine responses (Table 1, and see Figure 3).

Ketamine

Ketamine selectively potentiated the GABA re-

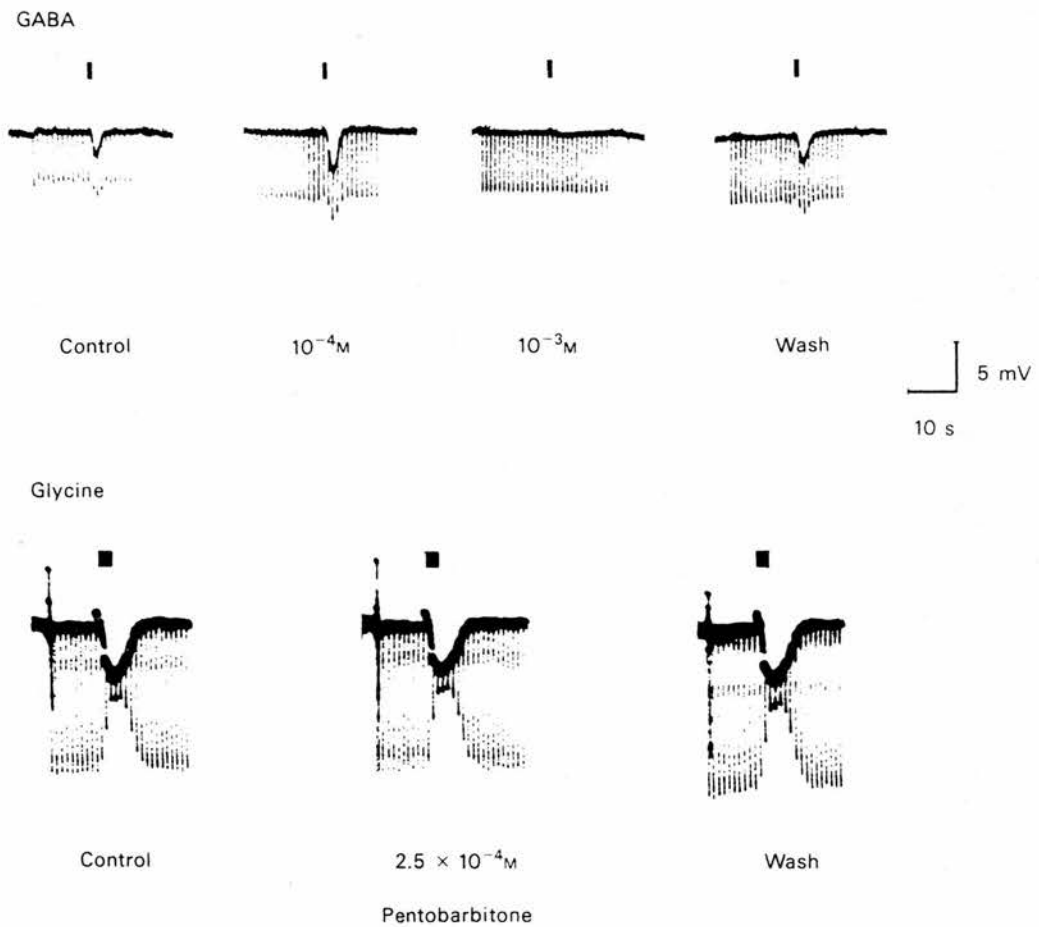


Figure 3 Effects of pentobarbitone on γ-aminobutyric acid (GABA) and glycine responses. Records from 2 cells showing: (upper traces), GABA potentiation by 10^{-4} M pentobarbitone and antagonism by 10^{-3} M pentobarbitone (no intervening wash); (lower traces) lack of effect of 2.5×10^{-4} M pentobarbitone on glycine responses. Durations of exposures to pentobarbitone: (upper trace) 13 min (10^{-4} M), 6 min (10^{-3} M); (lower trace) 14 min. Preparations washed for 8 min (upper trace), 14 min (lower trace). Iontophoretic pulses: GABA 0.5 s, 60 nA; glycine 3 s, 200 nA. Hyperpolarizing current pulses: 1 nA (upper traces), 0.7 nA (lower traces).

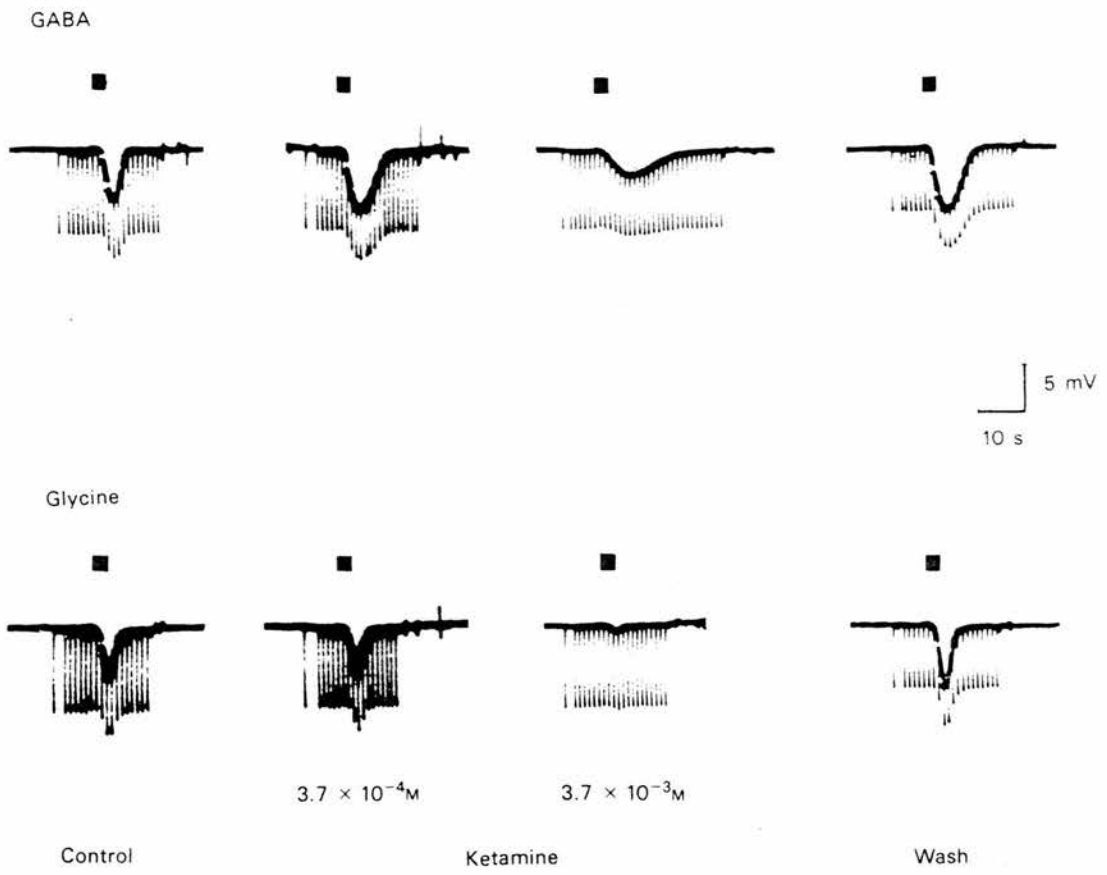


Figure 4 Effects of ketamine on γ-aminobutyric acid (GABA) and glycine responses. Records from 1 cell showing GABA potentiation by 3.7×10^{-4} M ketamine and complex effect of 3.7×10^{-3} M (no intervening wash). In this cell glycine responses were unaffected by 3.7×10^{-4} M ketamine but reversibly depressed by 3.7×10^{-3} M. Duration of exposure to ketamine: 8 min (3.7×10^{-4} M), 10 min (3.7×10^{-3} M). Preparation washed for 10 min (upper trace), 11 min (lower trace). Iontophoretic pulses: GABA and glycine 3 s, 60 nA. Hyperpolarizing current pulses: 1 nA.

sponses (Figure 4), an effect consistently detectable at 3.7×10^{-5} M and reaching statistical significance at 3.7×10^{-4} M Ketamine (Table 1). Unlike the potentiation by pentobarbitone, that due to ketamine was almost entirely attributable to prolongation of the response, as is shown by the respective area/peak ratios. Slowing of the onset and offset of the GABA response was most striking at high concentrations of ketamine (3.7×10^{-3} M).

In contrast, Table 1 records a dose-dependent antagonistic action of ketamine on glycine responses. This effect was statistically significant at 3.7×10^{-4} M when the response was measured as the peak change in resistance. Only two cells were tested with ketamine at 3.7×10^{-3} M but in both cases depression of the response was dramatic. No effect of ketamine on the response profile was detected for glycine (e.g. Figure 4).

Alphaxalone

The action of alphaxalone ($> 10^{-5}$ M) was consistently to depress responses to both GABA and glycine (Table 1, and see Figure 5). The commercial vehicle, which contains poly-oxyethylated castor oil, had an antagonistic action in some experiments (7 out of 10 tests using GABA and 3 out of 6 with glycine showed a reduction in response amplitude which exceeded 10%). This latter effect was small, and statistically significant only in the case of resistance measurements on GABA responses.

Metomidate

Metomidate, too, had a dramatic depressant action on both GABA and glycine responses (Figure 6), but only at high concentration (1.8×10^{-3} M). There was

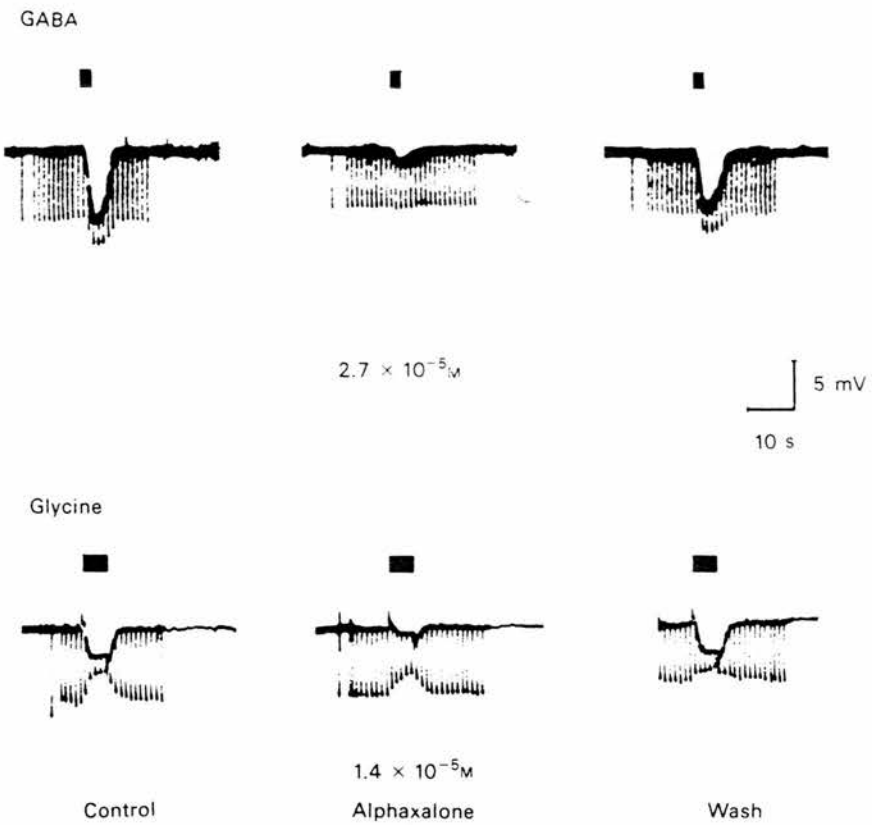


Figure 5 Effect of alphaxalone on γ-aminobutyric acid (GABA) and glycine responses. Records from 2 cells showing reversible depression of GABA (9 min exposure to 2.7×10^{-5} M alphaxalone) and of glycine responses (8 min exposure to 1.4×10^{-5} M). Preparations washed for 22 min (upper trace), 8 min (lower trace). Iontophoretic pulses: GABA 2 s, 30 nA; glycine 5 s, 500 nA. Hyperpolarizing current pulses: 1 nA in upper traces, 0.9 nA in lower traces.

no evidence of potentiation at any concentration (Table 1), nor of alteration in the response profile.

The effect of agonist dose on the modulating influence of anaesthetics

It was recognized that the agonist concentration at the receptors might affect the recorded influence of the anaesthetic drugs. Experiments were therefore performed in which different doses of a single transmitter were applied to a cell.

The same anaesthetic-transmitter combinations as previously described were tested in these experiments, each combination receiving 2–8 tests in between 2 and 4 preparations. Only the potentiation effects were consistently affected by transmitter dose, this being marked particularly with pentobarbitone, which only consistently potentiated GABA responses when short iontophoretic pulses were used. Measurements of peak change in input resistance obtained in one such experiment are shown in Figure 7. In this particular experiment 10^{-4} M pentobarbitone approximately doubled the response to a 0.5 s GABA pulse, whereas the response to a 2 s pulse was increased by only about a quarter. Higher concentrations of pentobarbitone caused a reversible loss of this effect.

Discussion

The lamprey as a model for the study of the effects of anaesthetics

The lamprey brainstem has several features that make it a suitable preparation in which to study the neuropharmacology of anaesthetic drugs. Intracellular recording from identified neurones is practicable and enables changes in input resistance and membrane potential to be measured. This is preferable to

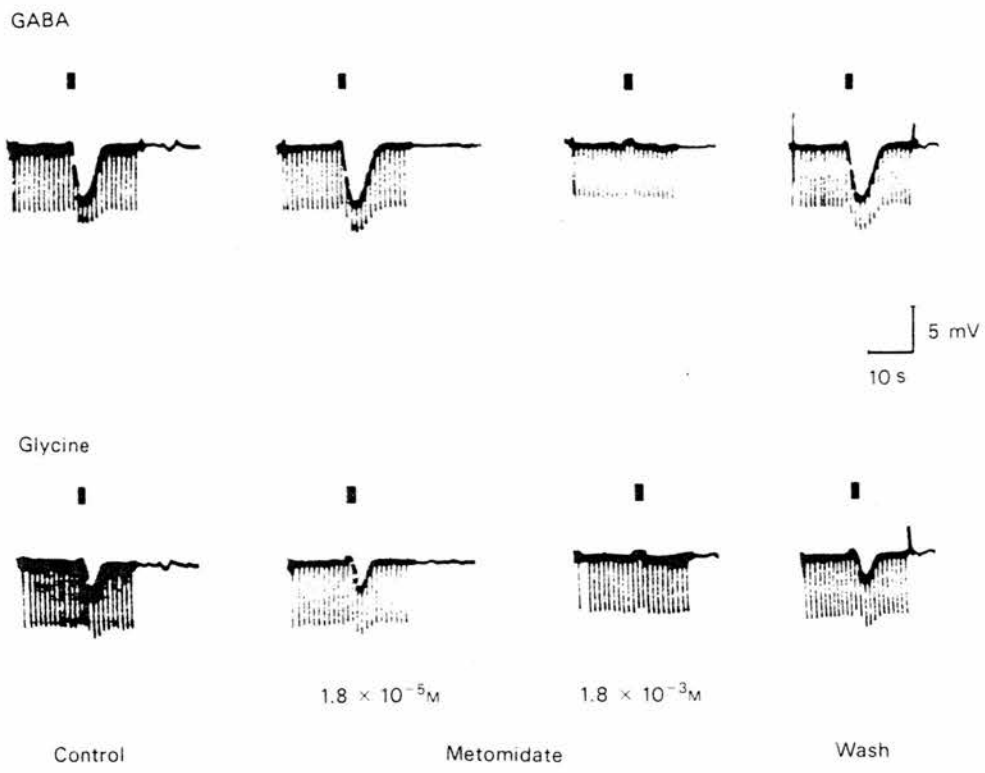


Figure 6 Effect of metomidate on γ-aminobutyric acid (GABA) and glycine responses. Records from 1 cell showing lack of effect of 1.8×10^{-5} M metomidate on GABA and glycine responses. Antagonism by 1.8×10^{-3} M metomidate is total in both cases. Duration of exposures to metomidate (no intervening wash): 10 min (1.8×10^{-5} M), 5 min (1.8×10^{-3} M). Preparation washed for 18 min (upper traces), 17 min (lower trace). Iontophoretic pulses: GABA and glycine 2 s, 300 nA. Hyperpolarizing current pulses: 1 nA.

the use of indirect measures of cell responses, such as changes in spike frequency. The bulbar reticulospinal cells lie close to the surface of the 4th ventricle, covered only by a single layer of ependymal cells; thus the diffusion path for drugs applied in the perfusing Ringer is short (Martin, 1979a, b). In the lamprey brain, blood vessels are confined to the periphery and so neither obscure nor impede access to the cells; visualization is also aided by the absence of myelin.

The neuro-biology of the lamprey has been studied in some detail (for review see Rovainen, 1979). Wickelgren (1977) described diverse sensory inputs to the bulbar neurones and reported that these cells constitute a major motor outflow to the somatic musculature. Any stimulation of the neurones by anaesthetics, effected either directly or via the removal of inhibitory influences, should therefore elicit movements. A similar result is predicted in higher vertebrates, where analogous cells are found (Shapovalov, 1975).

Anaesthetics differ in their postsynaptic effects

We set out to compare the abilities of four anaesthetic drugs to interfere with the responses of reticulospinal neurones to the inhibitory amino acid transmitters GABA and glycine. Many workers have stressed the GABA-potentiating properties of the barbiturates in a range of preparations (e.g. Barker & Ransom, 1978). In our study, as in that of Bowery & Dray (1978), the GABA-potentiating action of pentobarbitone was evident only in a proportion of cells, and showed marked dependence on the agonist dose, being detectable only if low amplitude or short iontophoretic currents were employed.

Ketamine also was found to potentiate GABA responses selectively, but the effect differed from that of pentobarbitone in that it was principally on the time course of the response; both the onset and offset of the GABA response were slowed by ketamine ($> 10^{-4}$ M). Other studies, e.g. Minchin (1981), suggest that this potentiation is not the re-

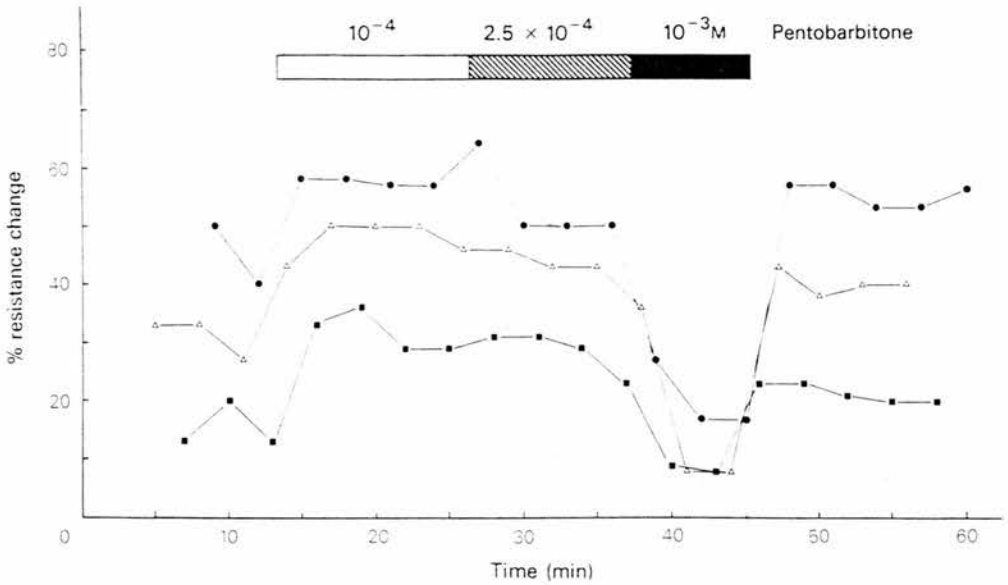


Figure 7 γ-Aminobutyric acid (GABA)-induced resistance changes measured in a single cell before, during and after application of increasing concentrations of pentobarbitone. Ordinate scale: GABA-induced resistance change (%); abscissa scale: time after pulse sequence started (min). GABA pulses (amplitude 60 nA) applied for 0.5 s (■), 1.0 s (△) and 2.0 s (●) in repeated sequence. Pentobarbitone 10^{-4} M approximately doubled the response to a 0.5 s GABA pulse whereas the response to a 2.0 s pulse increased by only about a quarter. Higher concentrations of pentobarbitone reversibly eliminated the potentiation.

sult of altered GABA uptake mechanisms. We are unaware of any other studies using ketamine that are directly comparable with ours.

In contrast, neither alphaxalone nor metomidate caused significant potentiation of GABA responses at any concentration tested; instead, both drugs produced parallel depressions of the responses to GABA and glycine. There are no previous reports of the effects of either anaesthetic on responses to the inhibitory transmitters; but etomidate, an imidazole derivative closely related to metomidate, has been studied: it is reported to be similar in action to pentobarbitone, selectively potentiating GABA responses at low doses (10^{-5} M) but having a depressant effect at high doses (10^{-3} M). As with the barbiturates, the potentiating action has been reported to show stereo-specificity (Hill & Taberner, 1975; Huang & Barker, 1980). We have not tested the optical isomers of metomidate separately, but those of etomidate have been shown to differ in their pharmacological actions (Hill & Taberner, 1975).

Although published information about the actions of alphaxalone/alphadolone on inhibitory mechanisms is lacking, Pennefather & Quastel (1980) described alterations in endplate currents recorded at the neuromuscular junction; and Smaje (1976) and Richards & Smaje (1976) reported depressed responses to acetylcholine and glutamate in the olfactory cortex.

Relevance to clinical anaesthesia

Although the reticulo-spinal cells are not concerned with consciousness, the effects we have described are likely to operate during anaesthesia and may be related to side effects produced by the drugs. Our results are hard to reconcile with a unitary biophysical hypothesis of anaesthetic action. Such a hypothesis predicts similarity of action of different anaesthetic compounds (Metcalfe, Hoult & Colley, 1974), however exerted, and this we have not observed. The concentrations at which the anaesthetics have been tested in this study include those likely to obtain in the brain during clinical anaesthesia (Table 3), and were themselves capable of inducing anaesthesia in lamprey ammocoetes (Table 2, and see appendix).

Our finding that neither GABA nor glycine responses were potentiated by alphaxalone and metomidate lends no support to the contention that inhibitory mechanisms are enhanced during anaesthesia. However, that idea derives largely from studies in which barbiturates or volatile anaesthetic agents have been used (e.g. Eccles, Schmidt & Willis,

Table 2 The effects of injectable anaesthetic drugs when bath-applied to intact lampreys

Drug	*Concentration* (M)	*Stage of anaesthesia reached after various time intervals*			
		2 min	5 min	10 min	30 min
Pentobarbitone	10^{-3}	—	—	I	I
Ketamine	3.7×10^{-5}	—	I	II–1	II–1
	3.7×10^{-4}	I	II–1	II–2	II–2
	3.7×10^{-3}	II–1	II–2	II–2	III/IV
Alphaxalone	2.7×10^{-6}	—	—	I	II–2
	2.7×10^{-5}	II–1	II–2	II–2	
	2.7×10^{-4}	II–2	III	III/IV	
Metomidate	1.8×10^{-5}	—	—	I–2	I–2
	1.8×10^{-4}	—	II–1	II–2	II–2
	1.8×10^{-3}	II–2	II–2	II–2	

Drugs dissolved in river water (unbuffered); times measured from moment of transfer of ammocoetes to anaesthetic solution. Classification of anaesthesia after McFarland (1959), tabulated stages are the averages for the group (3–8 ammocoetes).

1963), and those results are not contradicted by our experiments. There is no evidence that GABA and glycine receptors on the reticulo-spinal cells of the lamprey differ pharmacologically from those in higher vertebrates (Martin, 1979a; Nistri & Constanti, 1979).

Only with alphaxalone was depression of GABA and glycine responses seen at concentrations likely to be encountered during clinical anaesthesia in fish (Table 3) and higher vertebrates. Should a comparable depression of inhibitory mechanisms underlie the excitatory phenomena commonly observed during anaesthesia with alphaxalone/alphadolone in mammals, a logical preventive treatment would be premedication with a GABA-potentiating agent. It is interesting that there are clinical reports of a reduced incidence of tremors and purposeless movements when diazepam is used as a pre-medicant before anaesthesia with etomidate (Holdcroft, Morgan, Whitwam & Lumley, 1976) or alphaxalone/alphadolone (Vickers *et al.* 1978). The benzodiazepines as a group are known to potentiate the actions of GABA (Curtis, Lodge, Johnston & Brand, 1976).

This work was made possible by the generous support of the Wellcome Trust.

Appendix

Abilities of the drugs to anaesthetize lampreys (Table 2)

Experiments were carried out to ensure that the drugs used in the iontophoresis experiments were capable of inducing anaesthesia in intact lampreys. These experiments give an indication of the concentrations required but do not provide an accurate estimate of the concentration any anaesthetic reached in the brain. The behaviours of groups of 3 ammocoetes immersed in anaesthetic solutions were compared with that of an untreated group. Anaesthesia was assessed according to the criteria of McFarland

Table 3 Estimated brain concentrations of anaesthetics during clinical use in fish

Anaesthetic	*Dose*	*Brain Conc.* (M) (estimate)	*Effect on fish*	*Ref.*
Pentobarbitone	30 mg/kg i.p.	1.1×10^{-4}	Sedation	1
	48 mg/kg i.p.	1.8×10^{-4}	Apnoea	1
Alphaxalone	18 mg/kg i.p.	8.1×10^{-5}	Surgical anaesthesia	1
Ketamine	130 mg/kg i.m.	9.5×10^{-5}*	Surgical anaesthesia	1
Metomidate	7.5 mg/l (bath)	2.8×10^{-5}*	Surgical anaesthesia	2

*Upper limit. Ref. 1 = Oswald (1978), 2 = Stuart (1981).
Assumptions(Minchin, 1981): rapidly acting compounds (alphaxalone, metomidate) distributed in E.C.F. (= 30% body weight); slowly acting compounds (pentobarbitone, ketamine) distributed in total body water (= 66% body weight); protein binding 40% for alphaxalone and pentobarbitone.

(1959). The anaesthetics were dissolved in river water to the same concentrations as were employed in the iontophoresis experiments and each drug was tested on a minimum of 6 ammocoetes. Most of the experiments were conducted at room temperature (water temperature 15–17°C); but alphaxalone was also tested at 4°C, with similar results. It is recognized that both the rate of induction and the depth of anaesthesia in fishes are affected by temperature, the induction time commonly being shorter at higher temperature (discussed by McFarland, 1959).

Ketamine, alphaxalone and metomidate, when used at concentrations that affected the transmitter responses, induced similar behavioural states that were comparable to those McFarland (1959) reported in fish. A transient period of intense hyperactivity immediately after the introduction of high concentrations of metomidate or ketamine was attributed to the acid reaction of these solutions. A similar reaction of fish to the anaesthetic tricaine methane sulphonate has been described (e.g. Ohr, 1976). No such hyperactivity was noted following the introduction of pentobarbitone or alphaxalone.

The anaesthetic effect of alphaxalone ($> 10^{-5}$ M) stood out because of the rapidity of its onset coupled with the slow recovery; after the ammocoetes were removed from 2.7×10^{-4} M alphaxalone to fresh water it was an hour before there was slight movement in response to tail squeezing. During recovery there was a period when non-propulsive and rolling movements were observed, but frank convulsions were not elicited. In contrast, the lampreys were swimming within 30 min of their removal from 10^{-3} M metomidate. Recovery from high concentrations of ketamine was also slow, but was quiet in comparison to that of ammocoetes exposed to 3.7×10^{-5} M ketamine which was characterized by a period of apparent excitement.

The finding that bath application of even a high concentration of pentobarbitone induced only mild sedation, is consistent with reports that bath application of the barbiturates is an unsatisfactory method of anaesthetizing fis(see McFarland, 1959).

References

BARKER, J.L. & RANSOM, B.R. (1978). Pentobarbitone pharmacology of mammalian central neurones grown in tissue culture. *J. Physiol.*, **280,** 355–372.

BOWERY, N.G. & DRAY, A. (1978). Reversal of the action of amino acid antagonists by barbiturates and other hypnotic drugs. *Br. J. Pharmac.*, **63,** 197–215.

CURTIS, D.R., LODGE, D., JOHNSTON, G.A.R. & BRAND, S.J. (1976). Central actions of benzodiazepines. *Brain Res.* **118,** 344–347.

ECCLES, J.C., SCHMIDT, R. & WILLIS, W.D. (1963). Pharmacological studies on presynaptic inhibition. *J. Physiol.*, **168,** 500–530.

HILL, R.G. & TABERNER, P.V. (1975). Some neuropharmacological properties of the new non-barbiturate hypnotic etomidate. *Br. J. Pharmac.*, **54,** 241P.

HOLDCROFT, A., MORGAN, M., WHITWAM, J.G. & LUMLEY, J. (1976). Effect of dose and premedication on induction complications with etomidate. *Br. J. Anaesth.*, **48,** 199–205.

HUANG, L-Y.M. & BARKER, J.L. (1980). Pentobarbital: stereospecific actions of (+) and (−) isomers revealed on cultured mammalian neurones. *Science*, **207,** 195–197.

LARRABEE, M.G. & POSTERNAK, J.M. (1952). Selective action of anesthetics on synapses and axons in mammalian sympathetic ganglia. *J. Neurophysiol.*, **15,** 91–114.

McFARLAND, W.N. (1959). A study of the effects of anesthetics on the behaviour and physiology of fishes. *Publ. Inst. Mar. Sci., Univ. Texas*, **6,** 23–55.

MARK, R.F. & STEINER, J. (1958). Cortical projection of impulses in myelinated cutaneous afferent nerve fibres of the cat. *J. Physiol.*, **142,** 544–562.

MARTIN, R.J. (1978). Glycine and GABA receptors on lamprey bulbar reticulospinal neurones. *Comp. Biochem. Physiol.*, **61C,** 37–40.

MARTIN, R.J. (1979a). Glycine and GABA induced conductance changes in lamprey reticulospinal neurones and their antagonism by strychnine, thebaine, bicuculline and picrotoxin. *Comp. Biochem. Physiol.*, **63C,** 109–115.

MARTIN, R.J. (1979b). A study of the morphology of the large reticulospinal neurones of the lamprey ammocoete by intracellular injection of procion yellow. *Brain Behav. Evol.*, **16,** 1–18.

MATTHEWS, G. & WICKELGREN, W.O. (1979). Glycine, GABA and synaptic inhibition of reticulo-spinal neurones of lamprey. *J. Physiol.*, **293,** 393–415.

METCALFE, J.C., HOULT, J.R.S. & COLLEY, C.M. (1974). The molecular implications of a unitary hypothesis of anaesthetic action. In *Molecular Mechanisms in General Anaesthesia.* ed. Halsey, M.J., Miller, R.A. & Sutton, J.A. Edinburgh: Churchill Livingstone.

MINCHIN, M.C.W. (1981). The effect of anaesthetics on the uptake and release of γ-aminobutyric acid and D-aspartate in rat brain slices. *Br. J. Pharmac.*, **73,** 681–689.

NISTRI, A. & CONSTANTI, A. (1979). Pharmacological characterization of different types of GABA and glutamate receptors in vertebrates and invertebrates. *Prog. Neurobiol.*, **13,** 117–235.

OHR, E.A. (1976). Tricaine methanesulfonate – I. pH and its effects on anaesthetic potency. *Comp. Biochem. Physiol.*, **54C,** 13–17.

OSWALD, R.L. (1978). Injection anaesthesia for experimental studies in fish. *Comp. Biochem. Physiol.*, **60C,** 19–26.

PENNEFATHER, P. & QUASTEL, D.M.J. (1980). Actions of

anesthetics on the function of nicotinic acetylcholine receptors. *Prog. Anesthesiol.*, **2** (Molecular Mechanisms of Anesthesia), 45–57.

RICHARDS, C.D. (1972). On the mechanism of barbiturate anaesthesia. *J. Physiol.*, **227,** 749–767.

RICHARDS, C.D. & SMAJE, J.C. (1976). Anaesthetics depress the sensitivity of cortical neurones to L-glutamate. *Br. J. Pharmac.*, **58,** 347–357.

RICHARDS, C.D. & WHITE, A.E. (1981). Additive and non-additive effects of mixtures of short-acting intravenous anaesthetic agents and their significance for theories of anaesthesia. *Br. J. Pharmac.*, **74,** 161–170.

ROVAINEN, C.M. (1979). Neurobiology of lampreys. *Physiol. Rev.*, **59,** 1007–1077.

SHAPOVALOV, A.I. (1975). Neuronal organization and synaptic mechanisms of supra-spinal motor control in vertebrates. *Rev. Physiol. Biochem. Pharm.*, **72,** 1–54.

SHERRINGTON, C.S. (1906). *The Integrative Action of the Nervous System.* New Haven, Connecticut: Yale University Press.

SMAJE, J.C. (1976). General anaesthetics and the acetylcholine-sensitivity of cortical neurones. *Br. J. Pharmac.*, **58,** 359–366.

STUART, N.C. (1981). Anaesthesia in fishes. *J. small Anim. Pract.*, **22,** 377–383.

VICKERS, M.D.A., WOOD-SMITH, F.G. & STEWART, H.C. (1981). *Drugs in Anaesthetic Practice.* 5th Edition London: Butterworth.

WICKELGREN, W.O. (1977). Physiological and anatomical characteristics of reticulo-spinal neurones in lamprey. *J. Physiol.*, **270,** 89–114.

(Received April 27, 1982.
Revised June 9, 1982.)

Br. J. Pharmac. (1984), **82**, 659–666

Effects of injectable anaesthetics on responses to L-glutamate and on spontaneous synaptic activity in lamprey reticulo-spinal neurones

K.D. Cullen & R.J. Martin

Department of Veterinary Pharmacology, Royal (Dick) School of Veterinary Studies, Summerhall, Edinburgh, EH9 1QH

1 Intracellular recordings were made from reticulo-spinal cells in the medulla of lamprey ammocoetes; potential changes in response to iontophoretically applied L-glutamate were measured before, during and after the preparation was superfused with anaesthetic solutions.

2 Of the anaesthetics pentobarbitone, ketamine, alphaxalone/alphadolone (Saffan) and metomidate, only pentobarbitone ($> 10\,\mu$M) had a consistent dose-related depressant effect on glutamate responses.

3 Spontaneous excitatory postsynaptic potentials (e.p.s.ps) and inhibitory postsynaptic potentials (i.p.s.ps) were diminished in frequency by high concentrations (1 mM) of all anaesthetics. Anaesthetic concentrations of all drugs also reduced i.p.s.ps; for e.p.s.ps this was true of pentobarbitone ($100\,\mu$M) immediately, and of ketamine ($370\,\mu$M) and alphaxalone ($10-30\,\mu$M) after a transitory increase in activity.

4 Consideration of the results in the light of previous observations on inhibitory responses suggests a basis for some of the excitatory side effects of these compounds, assuming that the equivalent mammalian cells are similarly affected.

Introduction

The possibility and potential importance of interactions between anaesthetic drugs and neuronal responses to transmitters was recognized early in the study of CNS transmitters (e.g. Krnjević & Phillis, 1963). These early experiments frequently involved the iontophoretic application of transmitters to the spinal roots of anaesthetized animals; and it was common practice, when inhibitory transmitters were investigated, to employ an excitatory amino acid such as L-glutamate to activate neurones that were otherwise silent.

We have shown previously that the bulbar reticulospinal cells of the lamprey ammocoete respond to iontophoretic application of the inhibitory amino acids γ-aminobutyric acid (GABA) and glycine, and that these responses are differentially modified by bath applied anaesthetics (Cullen & Martin, 1982). We present here the results of complementary experiments in which responses to L-glutamate have been tested with the same four injectable anaesthetics. L-Glutamate has been shown to excite these cells, causing a small decrease in input resistance associated with a membrane depolarization and bursts of synaptic potentials (Wickelgren, 1977); and has been proposed as the probable natural excitatory transmitter (Matthews & Wickelgren, 1979). Application of glutamate in higher concentrations and the injection of depolarizing current pulses into the cells both elicit bursts of action potentials.

As in the previous publication, observations have in the main been confined to postsynaptic effects: raised magnesium concentrations have been used to suppress synaptic transmission and hence any indirect effects. However, examination of a cell's response to exogenous transmitters gives only a partial insight into the effects of anaesthetics on that cell's activity. Therefore, we have also investigated the effects of the anaesthetics on the spontaneous synaptic potentials that can be recorded from the reticulospinal cells in the presence of more physiological concentrations of magnesium. We have not examined the effects of the anaesthetics on the excitability of cells.

© The Macmillan Press Ltd 1984

Methods

The experiments were carried out using 12–15 mm ammocoetes of the species *Lampetra fluviatilis* and *Lampetra planeri*, and methods substantially the same as those described in detail previously (Cullen & Martin, 1982). These are briefly restated here.

An ammocoete was anaesthetized using 100 μM tricaine methane sulphonate (MS-222: Sandoz) and transected in the gill region. The rostral portion was transferred to the experimental chamber (liquid capacity 1 ml) where it was pinned to Sylgard and continuously perfused with cooled Ringer at a flow rate of 6 ml min^{-1}. This flow flushed tricaine methane sulphonate from the preparation before the experiment was started (1–2 h after anaesthetization). A coolant, circulated through an outer jacket, controlled the temperature in the chamber. Dissection of the brain stem exposed the bulbar reticulo-spinal cells in the floor of the 4th ventricle. These large cells are arranged symmetrically in 8 pairs on either side of the midline. Although most experiments were conducted at 10°C, the effect on spontaneous synaptic activity of temperature fluctuations within the range 2 to 18°C was also noted.

Solutions

For iontophoresis experiments a Ringer solution of the following composition was used (mM): NaCl 71, KCl 2.1, $CaCl_2$ 2.6, $MgCl_2$ 15, $NaHCO_3$ 20; NaH_2PO_4 0·18, glucose 4.0. The pH was adjusted to 7.1–7.2 with HCl and the solution aerated with a gas mixture of 5% CO_2 and 95% O_2 at a rate which did not alter the pH by more than 0.1. Observations of spontaneous synaptic potentials were made when the $[Mg^{2+}]$ of the perfusate was 1.8 mM.

Recording and iontophoresis

Standard electrophysiological techniques were employed. The resistance of the recording micropipettes, when filled with 2 M potassium methyl sulphate, was in the range 20–30 MΩ. After a cell had been penetrated, a continuous record of its membrane potential was made using a pen recorder (Lectromed: MX212). A bridge balance circuit incorporated in the high input impedance pre-amplifier allowed the injection of square hyperpolarizing current pulses through the recording electrode, and thus the measurement of the input resistance of cells. Spontaneous synaptic potential transients were recorded at high gain and with a slow paper speed. Because the membrane potential was sensitive to temperature changes, a continuous record was made also of the temperature in the bath. The shapes of individual transients were displayed on an oscilloscope screen (Tektronix 5113 Dual Beam Storage Oscilloscope).

Glutamate was applied by iontophoresis: ejected as an anion from a micropipette filled with 2 M glutamate at pH 8·7. Ejection was controlled by an iontophoresis programmer (Model 160: W–P Instruments Inc.) driven by a Digitimer (D100). Retaining currents were not routinely employed. Controls were provided by application of pulses of reversed polarity or by the incorporation of 0.5 M NaCl in one barrel of the electrode assembly. Two ejection procedures were used: (i) fixed test pulses repeated at intervals of 1 or 3 min, (ii) a repeated sequence of test pulses in order of increasing length – in case the anaesthetic effect was related to the dose of transmitter. The pulses used (70 to 400 nA) had durations between 1 s and 7 s. Since there was no direct measure of the drug concentration achieved at the cells' receptors, and since the pulse length bears a non-linear relation to the quantity of drug ejected from an electrode, the only valid comparisons are those between the responses of an individual cell to pulses of different length.

Anaesthetics were applied dissolved in the perfusing Ringer. No osmotic compensation was made because the anaesthetic concentration never exceeded 1 mM. When repeated anaesthetic applications were made to a preparation, at least twenty minutes was allowed as a recovery period between tests. More usually this period was between thirty and forty minutes; but when successive solutions were applied in order of increasing anaesthetic concentration there was sometimes no intervening wash.

In many cells the glutamate-evoked change in input resistance could not be measured accurately, so measurements were confined to the peak changes in membrane potential and in the area enclosed by the envelope of the response (see Figure 2 in Cullen & Martin, 1982). The results of different experiments were combined after the proportional change in glutamate response amplitude at the peak of the drug effect had been calculated. An unpaired t test was used to assess the statistical significance of anaesthetic effects.

Records of spontaneous synaptic activity are presented as segments of the chart records. Vertical transients represent membrane potential events. The lateral separation of spontaneous transients is indicative of their frequency; their length a measure of the amplitude of the potential displacements, within the limits imposed by the frequency response of the chart recorder. Possible distortions introduced by the recorder do not invalidate a qualitative assessment of changes in the level of synaptic activity. The duration of a typical small excitatory postsynaptic potential (e.p.s.p.) was in the range 30–40 ms; the frequency-response of the recorder was flat ±0.5dB at 100 Hz (manufacturer's specification).

Drugs

The drugs used were L-glutamate (BDH), tricaine methane sulphonate (MS-222, Sandoz), pentobarbitone (May & Baker), ketamine (Vetalar, Parke-Davis), alphaxalone/alphadolone (Saffan, Glaxovet) and metomidate (Hypnodil, Janssen). The vehicle present in Saffan was kindly donated by Glaxovet. Although the product Saffan was used in the experiments, it will be referred to henceforth as alphaxalone because concentrations are expressed in terms of this constituent.

Results

Responses of bulbar reticulo-spinal cells to glutamate

Most cells had resting membrane potentials in the range −60 to −70 mV. The response to glutamate, measured in a total of 45 cells, was always depolarizing, the magnitude and speed of onset/offset varying between cells. Small amplitude responses were seen in cells with high resting potentials as well as in those that were relatively depolarized. In 4 cells there was a fast low amplitude response which was not increased appreciably when the strength or duration of the iontophoretic pulses were increased; yet the depolarization was sustained and there was no sign of desensitization. These 4 cells showed a minimal change in input resistance. In other cells, input resistance decreases ranged from 65% to undetectable (< 15% in 28 cells; between 20% and 30% in 11 cells); their extent was not correlated with the change in membrane potential.

In the absence of anaesthetic effects, the glutamate response remained stable over periods of an hour or more. The different types of response were not distinguished when the effects of the anaesthetics were assessed.

Elevation of the $[Mg^{2+}]$ reduced the tendency for the glutamate-induced depolarization to be interrupted by synaptic potentials and intermittent firing of action potentials. However, in some experiments such potentials occurred even though there was no spontaneous activity between applications of glutamate. Response amplitudes were not measured in these experiments because the full extent of the depolarization was masked. There was no evidence that magnesium acted as an antagonist of the glutamate responses.

General effects of the anaesthetics

No anaesthetic consistently altered the membrane potential. Input resistance was only affected by the highest concentrations of pentobarbitone and metomidate (1 mM); which caused a small reduction (10–15%). Responses were measured in cells from a total of 33 ammocoetes. Numbers of ammocoetes exposed to the anaesthetics were: pentobarbitone 10, ketamine 7, alphaxalone 10, metomidate 4. In addition two ammocoetes were exposed only to the Saffan vehicle. Sample records are displayed in Figures 1 and 2, and the collected results for each drug are presented in Table 1.

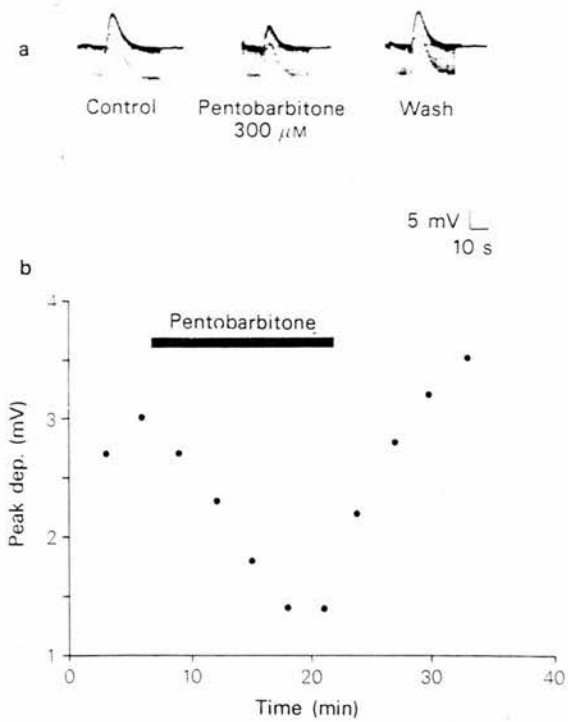


Figure 1 The effect of pentobarbitone on glutamate responses. (a) Pentobarbitone (300 μM) reduced both the depolarization and the change in input resistance produced by standard pulses of glutamate (exposure time: 3 min; wash time: 8 min; iontophoretic pulse: 600 nA, 2 s; hyperpolarizing pulses: 1 nA). (b) Serial measurements made during a different experiment when 300 μM pentobarbitone was applied for 18 min. The depolarizing responses to standard pulses of glutamate (200 nA) were depressed.

Pentobarbitone

A clear dose-related depression of the glutamate response was observed, and only in 3 out of 16 tests in which measurements were made did depression not exceed 10%. Figure 1 shows sample records from a cell exposed to 300 μM pentobarbitone, and serial measurements made during a different experiment.

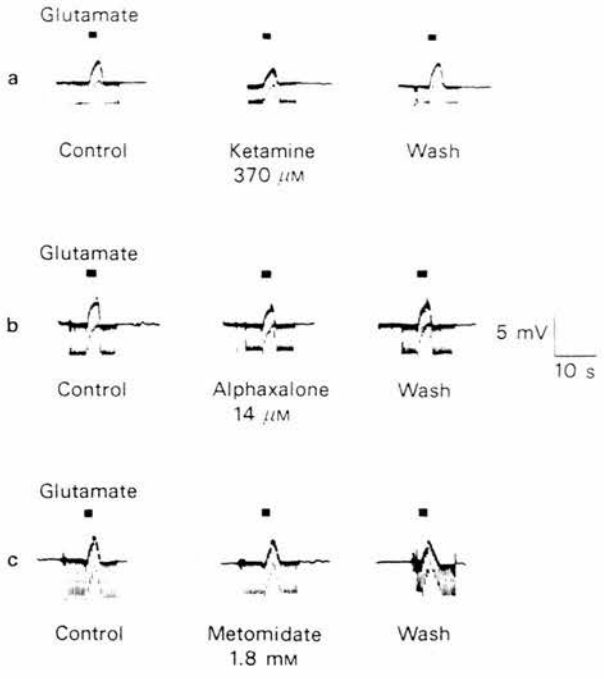


Figure 2 Effects of ketamine, alphaxalone and metomidate on glutamate responses. Ketamine (a) and alphaxalone (b) depressed the glutamate responses slightly but metomidate (c) had little effect. (a) Sample responses: control; after 8 min exposure to ketamine; after 10 min wash (iontophoretic pulse: 20 nA, 5 s; hyperpolarizing pulses: 1 nA). (b) Sample responses: control; after 11 min exposure to alphaxalone; after 27 min wash (iontophoretic pulses: 500 nA, 5 s; hyperpolarizing pulses: 0.9 nA). (c) Sample responses: control; after 7 min exposure to metomidate; after 16 min wash (iontophoretic pulses: 400 nA, 4 s; hyperpolarizing pulses: 1 nA).

The latter illustrate the reversible depression of glutamate responses during exposure to a relatively high concentration of pentobarbitone (300 μM).

Ketamine

Sample records from a single experiment are displayed in Figure 2a. The accumulated results (Table 1) suggest a dose-related depression detectable at 37 μM (the clinically relevant dose), but the effect did not reach statistical significance.

Alphaxalone

Alphaxalone 100–300 μM depressed the glutamate responses ($P<0.05$, using a 1 tailed test) but no other concentration had a statistically significant effect. However, more cells were depressed, and to a greater extent, in the presence of alphaxalone than when the commercial vehicle was presented alone. In the experiment illustrated in Figure 2b there was slight depression induced by 30 μM alphaxalone.

Table 1 The effects of anaesthetics on the responses to glutamate

Anaesthetic	*Peak glutamate response % change*
Pentobarbitone (μM)	
200–500	−39 ± 10(6)**
100	−17 ± 8(8)†
30	−17 ± 1(2)*††
Ketamine (μM)	
3,700	−50(1)
370	−12 ± 10(7)
37	−13 ± 13(6)
3.7	−4 ± 7(4)
Alphaxalone (μM)	
100–300	−20 ± 7(4)†
10–30	−4 ± 6(12)
1–3	−17 ± 10(7)
Saffan vehicle	−16 ± 9(4)
Metomidate (μM)	
1,800	−21 ± 13(3)
180	−18 ± 8(4)
18	+22 ± 17(3)

Each value represents the percentage change in response during application of an anaesthetic: mean ± s.e. mean. Numbers of observations in parentheses. Significant effects indicated (unpaired t tests): * $P<0.05$; ** $P<0.01$–2-tailed test; † $P<0.05$; †† P0.01–1-tailed test. The 1-tailed test assumes that none of the anaesthetics potentiates the effect of an excitatory transmitter. Saffan vehicle dilution equivalent to 10 to 100 μM.

Metomidate

Metomidate depressed glutamate responses only at supra-anaesthetic concentrations, and no concentration had a statistically significant effect. It is notable that in two out of three tests the depression by the highest concentration used (1.8 mM) did not exceed 15%. Records taken from an experiment in which the effects of metomidate were only slight are displayed in Figure 2c.

The effect of agonist dose on the anaesthetic effects

In no case did variation in the glutamate pulse length have any detectable effect on the influence of the anaesthetics (not illustrated).

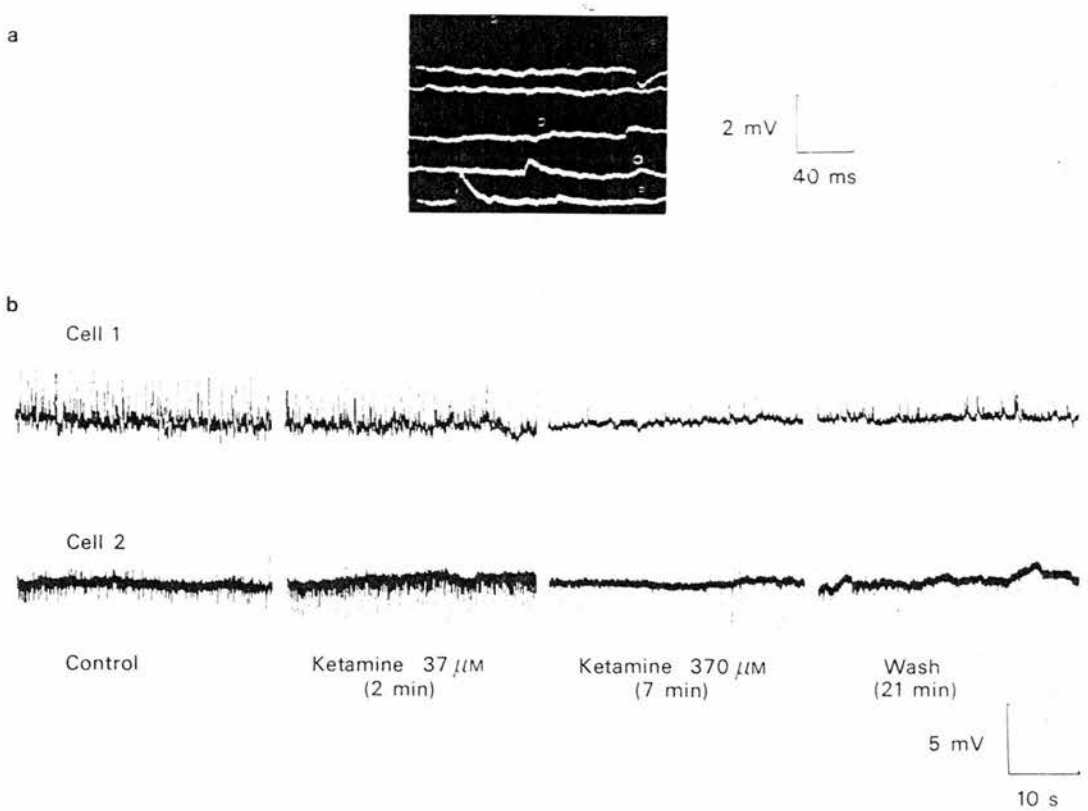


Figure 3 (a) Spontaneous membrane potential transients recorded in 'normal' Ringer (1.8 mM Mg^{2+}). Successive sweeps on oscilloscope stored and photographed. Upward transients (depolarizing) have been interpreted as e.p.s.ps; downward transients (hyperpolarizing) as i.p.s.ps. The larger amplitude transient in row 5 was produced by superimposition of e.p.s.ps. (b) The effects of ketamine on spontaneous synaptic activity. Sample records taken from two cells showing predominantly e.p.s.ps and i.p.s.ps respectively. Frequency of e.p.s.ps (cell1) and i.p.s.ps (cell2) initially increased by 37 μM ketamine. This increase was sustained for 3 min only and in cell 1 was barely detectable. A partially reversible loss of both e.p.s.ps and i.p.s.ps occurred during exposure to 370 μM ketamine (both samples taken after 7 min exposure). Records during wash period retouched.

Anaesthetic modulation of spontaneous synaptic activity

When intracellular recordings were made at high gain and the Ringer contained 1.8 mM Mg^{2+}, small brief perturbations of the membrane potential (amplitude 0.5–3.0 mV) could be distinguished. Such spontaneous potential changes occurred in both hyperpolarizing and depolarizing directions, and have been interpreted as inhibitory postsynaptic potentials (i.p.s.ps) and e.p.s.ps, respectively (see Gold & Martin, 1983). The rise and decay times varied with the amplitudes of the potentials, but small events commonly lasted 30–40 ms and had time constants close to 10 ms (rise) and 15 ms (decay). When displayed on an expanded time scale it was evident that some of the larger transients were composed of superimposed smaller events (Figure 3a). When the spontaneous activity was greatly increased, as during the application of glutamate, action potentials were elicited. In a few cells periodic depolarizations of 6–7 mV were each accompanied by a burst of action potentials. Other cells showed intermittent hyperactivity.

It was of interest to see whether the effects on transmitter responses would be reflected in anaesthetic effects on natural transmission. To this end 26 preparations were exposed to the anaesthetics: pentobarbitone 5, ketamine 13, alphaxalone 4 and metomidate 4 under conditions (1.8 mM Mg^{2+}) permitting the recording of spontaneous e.p.s.ps and i.p.s.ps from the reticulo-spinal cells.

The frequency of occurrence of spontaneous potentials showed strong temperature-dependence; individual events could not be resolved at 15°C, where-

Table 2 The effect of anaesthetics on spontaneous synaptic activity

	I.p.s.ps				*E.p.s.ps*			
	inc.	*dec.*	*n.c.*	*(dec.)*	*inc.*	*dec.*	*n.c.*	*(dec.)*
Pentobarbitone (μM)								
100	0	1	0	0	0	1	0	0
300–500	0	2	0	0	0	2	0	0
1,000	0	1	0	0	0	1	0	0
Ketamine (μM)								
0.37	1	0	0	0	1	0	0	0
3.7	0	0	1	0	1	0	0	0
37	1	2	4	0	3	1	3	0
370	0	6	0	0	0	6	0	0
Alphaxalone (μM)								
2.7	0	1	1	0	1	0	1	0
27	1	1	4	1	4	0	2	2
Metomidate (μM)								
18	0	2	5	0	1	0	3	2
180	1	2	1	0	1	2	1	0
1,800	1	2	0	1	1	3	0	1

Tabulated values are the numbers of tests in which an increased (inc.), decreased (dec.) or unchanged (n.c.) level of activity (frequency of potential transients) was observed. In a few cases there was a biphasic anaesthetic effect consisting of initial stimulation followed by suppression. These tests are recorded in the columns headed (dec.) in addition to that headed inc.

as at 4°C the transients were widely spaced in time (not illustrated). Elevation of the $[Mg^{2+}]$ in the Ringer to 15 mM abolished all these potentials. Sample traces are displayed in Figure 3 and the collected results from experiments at 10°C, when individual potential transients could usually be resolved, are shown in qualitative form in Table 2. The anaesthetic effects were time-dependent: there was no steady-state effect other than the quiescence seen during exposure to high concentrations of anaesthetics.

Apart from the depression caused by high concentrations of all anaesthetics, the principal finding was that i.p.s.ps were the more labile: they were reduced in frequency by all drugs at anaesthetic or supra-anaesthetic concentrations and this reduction was longer lasting than that of e.p.s.ps. When activity was enhanced it was predominantly excitatory; although when the increase was pronounced, as in the presence of 0.37 μM ketamine, it was impossible to resolve individual events and to ascribe a polarity to them.

E.p.s.ps were decreased in frequency by pentobarbitone (100 μM) immediately, and by alphaxalone (10–30 μM) and ketamine (370 μM) after a transitory increase. Sub-anaesthetic concentrations of ketamine (< 10 μM) stimulated activity in the one preparation tested. Below the high concentration (1 mM) at which all the drugs suppressed all spontaneous activity, metomidate had little effect.

Discussion

The most striking feature of these experiments was the lesser effect of anaesthetics on glutamate than on GABA and glycine responses (compare Cullen & Martin, 1982), despite the fact that small changes in membrane conductance would exert a more readily detectable effect on the glutamate response, whose reversal potential (about −35 mV: Matthews & Wickelgren, 1979) is far from the resting potential. This contrast, which was particularly dramatic with metomidate, indicates that the depressant effects of high concentrations of all the anaesthetics on the inhibitory responses cannot be the result of an entirely non-specific neuronal depression. None of the drugs caused potentiation of the glutamate responses, and only two had any consistent depressant effect.

Depression of glutamate responses by pentobarbitone is consistent with earlier findings that barbiturates depress responses to excitatory amino acids (e.g. Krnjević & Phillis, 1963; Crawford & Curtis, 1966; Johnson *et al.*, 1969; Richards & Smaje, 1976; Nicoll & Wojtowicz, 1980). A presynaptic effect may have contributed to the abolition of spontaneous potentials (Table 2) since pentobarbitone (100 μM) has not been shown to depress responses to GABA or glycine (Cullen & Martin, 1982). Pentobarbitone

had no effect likely to increase activity in the reticulo-spinal axons: all effects described would be expected to reduce motor responses to stimulation and so promote muscle relaxation.

The small, statistically insignificant inhibitory effect of ketamine on glutamate responses is consistent with the observation (Anis *et al.*, 1983) that ketamine selectively inhibits NMDA responses and has a lesser depressant effect on responses to glutamate, quisqualate and kainate. The pharmacology of the glutamate receptor present on lamprey reticulo-spinal cells has not been studied in detail but any NMDA receptors present should be inhibited by the 15 mM Mg^{2+} used (Evans & Watkins, 1978; Ault *et al.*, 1980).

Anaesthetic concentrations of ketamine depressed glycine responses more than those to glutamate, and i.p.s.ps were more susceptible to block than were e.p.s.ps. Both results predict a resultant disinhibition of these motor cells and so, potentially, exaggerated motor responses to stimulation. The increased frequency of spontaneous potentials seen during exposure to low concentrations of ketamine was not matched by an equivalent change in the cells' responses to exogenous amino acid transmitters.

The small depressant effect of alphaxalone, apparent only at high concentrations (100 μM), is consistent with the increased frequency of e.p.s.ps recorded from reticulo-spinal cells during exposure to low concentrations of alphaxalone, as is the depression of GABA and glycine responses shown previously. When the anaesthetic concentration was higher the presynaptic depressant effect implied by the abolition of e.p.s.ps and i.p.s.ps probably offset the disinhibition. However, the result contrasts with the 60–100% depression of glutamate-evoked firing by lower concentrations of alphaxalone (c. 10 μM) reported in the prepyriform cortex (Richards & Smaje, 1976). Alphaxalone's and metomidate's failure to depress glutamate responses markedly at low concentrations should reinforce the block of responses to inhibitory amino acids that we have described previously (Cullen & Martin, 1982).

It was a general finding that the i.p.s.ps were more susceptible to anaesthetic blockade. If i.p.s.ps are in part concerned with discriminative inhibition, as has been suggested by Andersen *et al.*, (1980), this may contribute to the reduction in the fine control of motor responses commonly found during induction and recovery from anaesthesia (e.g. Cullen & Martin, 1982); as also may the depression of the lamprey's reticulo-spinal cells, part of a pathway which has inhibitory as well as excitatory components (Buchanan, 1982; Buchanan & Cohen, 1982). Greater sensitivity of inhibitory than of excitatory mechanisms to anaesthetics has previously been described by Scholfield (1980) in the olfactory cortex; but Barker & Ransom (1978) in studies on cultured mouse neurones found the sensitivities of the GABA and glutamate responses to pentobarbitone to be about equal.

This work was made possible by the generous support of the Wellcome Trust.

References

ANDERSEN, P., DINGLEDINE, R., GJERSTAD, L., LANGMOEN, I.A. & LAURSEN, A.M. (1980). Two different responses of hippocampal pyramidal cells to application of GABA. *J. Physiol. (Lond.)*, **305,** 279–296.

ANIS, N.A., BERRY, S.C., BURTON, N.R. & LODGE, D. (1983). The dissociative anaesthetics, ketamine and phencyclidine, selectively reduce excitation of central mammalian neurones by N-methyl-aspartate. *Br. J. Pharmac.*, **79,** 565–575.

AULT, B., EVANS, R.H., FRANCIS, A.A., OAKES, D.J. & WATKINS, J.C. (1980). Selective depression of excitatory amino acid induced depolarisations by magnesium ions in isolated spinal cord preparations. *J. Physiol. (Lond.)*, **307,** 413–428.

BARKER, J.L. & RANSOM, B.R. (1978). Pentobarbitone pharmacology of mammalian central neurones grown in tissue culture. *J. Physiol. (Lond.)*, **280,** 355–372.

BUCHANAN, J.T. (1982). Identification of interneurons with contralateral, caudal axons in the lamprey spinal cord: synaptic interactions and morphology. *J. Neurophysiol.*, **47,** 961–975.

BUCHANAN, J.T. & COHEN, A.H. (1982). Activities of identified interneurons, motoneurons, and muscle fibres during fictive swimming in the lamprey and effects of reticulospinal and dorsal cell stimulation. *J. Neurophysiol.*, **47,** 948–960.

CRAWFORD, J.M. & CURTIS, D.R. (1966). Pharmacological studies on feline Betz cells. *J. Physiol. (Lond.)*, **186,** 121–138.

CULLEN, K.D. & MARTIN, R.J. (1982). Dissimilar influences of some injectable anaesthetics on the responses of reticulo-spinal neurones to inhibitory transmitters in the lamprey. *Br. J. Pharmac.*, **77,** 493–504.

EVANS, R.H. & WATKINS, J.C. (1978). Specific antagonism of excitant amino acids in the isolated spinal cord of the neonatal rat. *Eur. J. Pharmac.*, **50,** 123–129.

GOLD, M.R. & MARTIN, A.R. (1983). Characteristics of inhibitory post-synaptic currents in brain-stem neurones of the lamprey. *J. Physiol. (Lond.)*, **342,** 85–98.

JOHNSON, E.S., ROBERTS, M.H. & STRAUGHAN, D.W. (1969). The responses of cortical neurones to monoamines under differing anaesthetic conditions. *J. Physiol. (Lond.)*, **203,** 261–280.

KRNJEVIĆ, K. & PHILLIS, J.W. (1963). Iontophoretic studies of neurones in the mammalian cerebral cortex. *J. Physiol.*, **165,** 274–304.

MATTHEWS, G. & WICKELGREN, W.O. (1979). Glutamate and synaptic excitation of reticulospinal neurones of lamprey. *J. Physiol. (Lond.)*, **293,** 417–433.

NICOLL, R.A. & WOJTOWICZ, J.M. (1980). The effects of pentobarbital and related compounds on frog motoneurones. *Brain Res.*, **191,** 225–237.

RICHARDS, C.D. & SMAJE, J.C. (1976). Anaesthetics depress the sensitivity of cortical neurones to L-glutamate. *Br. J. Pharmac.*, **58,** 347–357.

SCHOLFIELD, C.N. (1980). Potentiation of inhibition by general anaesthetics in neurones of the olfactory cortex *in vitro*. *Pflügers Arch.*, **383,** 249–255.

WICKELGREN, W.O. (1977). Physiological and anatomical characteristics of reticulospinal neurones in lamprey. *J. Physiol. (Lond.)*, **270,** 89–114.

(*Received October 17, 1983. Revised February 2, 1984.*)

Zbl. Vet. Med. A, **25**, 181—188 (1978)
© 1978 Verlag Paul Parey, Berlin und Hamburg
ISSN 0300-8711/ASTM-Coden: ZVRAAX

Dept. of Veterinary Pharmacology,
Royal (Dick) School of Veterinary Studies,
University of Edinburgh, Edinburgh

α Agonist and Local anaesthetic properties of Xylazine

By

M. A. Aziz and R. J. Martin

With 6 figures

(Received for publication September 24, 1977)

Introduction

Xylazine (2-(2,6-Dimethylphenylamino)-4H-5,6 dihydro-1,3-thiazine), is used in veterinary practice as a sedative with analgesic and muscle relaxant properties. It has been reported to have central and peripheral autonomic effects, causing a brief rise in blood pressure followed by a prolonged hypotension with bradycardia and fall in cardiac output (Kroneberg, Oberdorf, Hoffmeister and Wirth, 1967; Clark and Hall, 1969). Kroneberg et al. (1967) considered that xylazine had a sympathomimetic action which caused a rise in blood pressure and a contracture of the nictitating membrane of cats. Later the α agonist activity of xylazine was found to be of a lower potency than noradrenaline (Autret, Schmitt, Fenard and Pétillot, 1970), and a central decrease of the sympathetic discharges induced by xylazine was suggested to be the predominant cause of the ensuing hypotension (Schmitt, Fournadjiev and Schmitt, 1970). It has also been suggested that xylazine causes a central increase in vagal tone and baroreceptor activity (Antonaccio, Robson and Kerwin, 1973). In addition to these effects xylazine inhibits the release of acetylcholine from the post-ganglionic fibres in the guinea pig ileum (Oberdorf, Hoffmeister and Kroneberg, 1967). The present work was carried out in an attempt to elucidate further the complex pharmacology of xylazine.

Methods

Frogs, rats, guinea pigs and rabbits were used. Anaesthesia for acute experiments was produced by urethane in 17 rats and 4 guinea pigs and by halothane in 4 rabbits. The trachea, jugular vein and common carotid artery were cannulated. Arterial blood pressure was recorded through a strain gauge on a Devices MX_4 pen recorder. The ECG's were traced on a Cambridge Transrite 4, Lead II.

The aortic strip was prepared according to Furchgott and Bhadrakom (1953), the rat anococcygeous muscle by the method of Gillespie (1972) and the guinea pig vas deferens by the method of Huchovíc (1961). The innervated vas deferens and an innervated rat colon preparation were stimulated with 1 V, 0.5 ms. square pulses at a rate of 30 Hz for five seconds every two minutes.

The rat uterus was prepared by the method of De Jalon, Bayo and De Jalon (1945). The guinea pig tracheal chain (Castillo and De Beer, 1947) was potentiated with carbachol (10^{-7} mol./l.) and the rat fundic strip (Vane, 1957) with serotonin (10^{-8} mol./l.). The rabbit jejunum and guinea pig ileum were prepared according to the method of Magnus (1904). The guinea pig isolated auricles were mounted at 30 °C in Kreb's solution (containing 2×10^{-3} mol./l. Ca Cl_2) and aerated with O_2.

The chick biventer cervices (Ginsborg and Warriner, 1960) and the rat phrenic nerve-diaphragm preparation (Bülbring, 1946) were stimulated with 3 V, 0.5 ms. square pulses at a rate of 0.2 Hz.

Tracings were recorded either on a Devices MX pen recorder or on a smoked drum. Data was statistically analysed using the Students' t test.

The frog sciatic nerve trunk was dissected and mounted in an experimental chamber. The chamber was provided with three separate compartments through which the nerve trunk was passed. The middle compartment contained the test solution and separated the other two compartments containing the recording and stimulating electrodes. The recording and stimulating compartments were filled with liquid paraffin to reduce the spread of current.

The conduction distance from the stimulating electrodes to the recording electrodes was 30 mm. The compartments were segregated by using soft paraffin wax around the nerve trunk. The nerve trunk was stimulated with 10 V, 0.1 ms. square pulses at 1 Hz. An oscilloscope and a high gain high input impedance preamplifier were used to record the compound action potential. Permanent records were made by direct photography of the oscilloscope.

Results

Effects of xylazine on blood pressure and heart rate

In rats, xylazine (0.02—0.08 mg./100 gm. i. v.) produced a dose-dependent brief hypertension, followed by a prolonged hypotension persisting more than 30 minutes (Fig. 1). The heart rate was significantly ($P < 0.001$) slowed from 424 ± 23 S. E. to 277 ± 15 S. E. (7 obs.) as calculated from the ECG tracings. Similar changes were observed in rabbits and guinea pigs. Following the i. v. administration of xylazine in rats, there was a depression in the

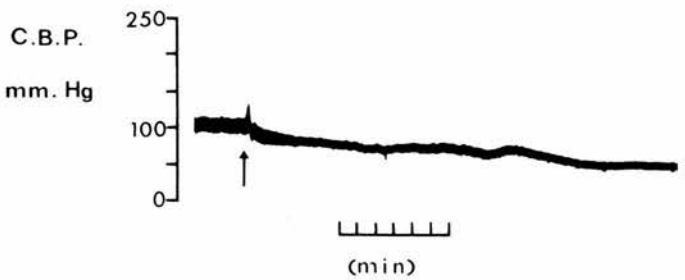


Fig. 1. The effect of xylazine (0.06 mg./100 gm. i. v.) on the rat blood pressure (C. B. P.). The arrow indicates the injection of xylazine. A brief period of hypertension is followed by a prolonged hypotension

amplitude of the P wave, QRS complex and T wave which lasted more than 30 minutes.

Phentolamine (50 μg./100 gm.) antagonised the hypertensive phase, while propranolol (50 μg./100 gm.) potentiated it and reduced the subsequent fall in blood pressure. These results suggested that xylazine might have both α and β agonist activities. An investigation of the effects of xylazine on isolated organs was performed to improve the understanding of its properties.

Sympathomimetic effects of xylazine

In order to detect any α agonist properties, xylazine was applied to the rabbit aortic strip, the rat anococcygeous muscle and the guinea pig vas deferens preparations. In doses of 10^{-6}—10^{-4} mol./l. xylazine contracted all the preparations while phentolamine, an α antogonist, reduced the responses. The administration of phentolamine converted the contractile response of the rabbit aortic strip to xylazine into a relaxation (Fig. 2 A and B). Xylazine, in addition to contracting the vas deferens, blocked the response to peripheral sympathetic stimulation (Fig. 2 C). This latter effect was presumably related to the local anaesthetic effect of xylazine. The parallel dose response curves of

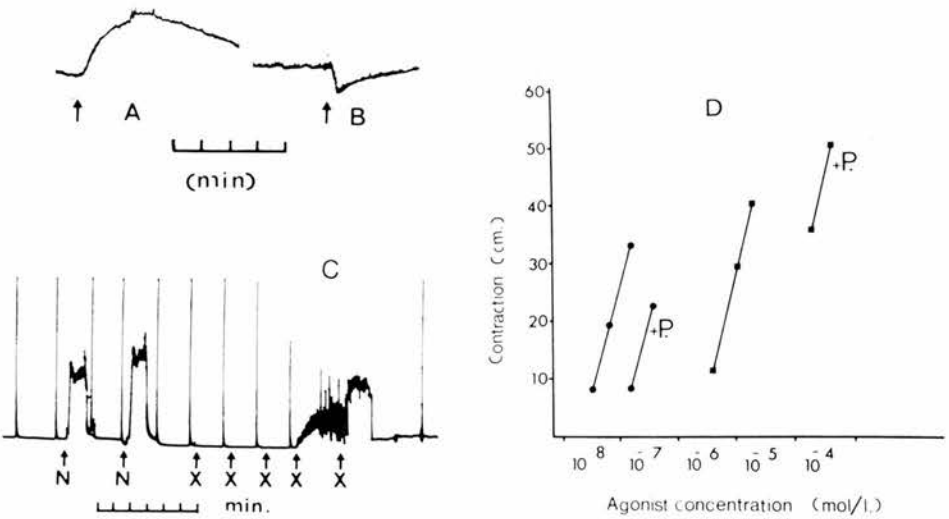


Fig. 2. A: Xylazine applied at a concentration of 10^{-4} mol./l. contracted the rabbit aortic strip. B: Xylazine applied at a concentration of 10^{-4} mol./l. relaxed the aortic strip in presence of phentolamine (10^{-7} mol./l.). C: The α agonistic and neurone inhibitory effects of xylazine (X) (increasing concentration 4×10^{-5} — 7×10^{-4} mol./l.) and the control response of noradrenaline (N) (4—8 $\times$ 10^{-6} mol./l.) on the guinea pig vas deferens stimulated with 1 v., 0.5 ms. square pulses at 30 Hz for 5 seconds every 2 minutes. D: The parallel log dose response curves of the rat anococcygeous muscle to noradrenaline (●) and xylazine (■), before and after the application of phentolamine (P) 10^{-7} mol./l.

the anococcygeous muscles to xylazine and noradrenaline and their antagonism by phentolamine (Fig. 2 D) illustrate the α agonist properties of xylazine.

The β effects of xylazine were tested on the rat uterus and guinea pig tracheal chain. Xylazine (10^{-4} mol./l.) decreased the contractions of the rat uterus to carbachol (10^{-6} mol./l.). It relaxed the guinea pig tracheal chain potentiated with carbachol (10^{-7} mol./l.). Similar responses were obtained with isoprenaline (10^{-9} mol./l.). These effects were partly reduced but not abolished with propranolol (10^{-6} mol./l.).

Antagonistic effects of xylazine

Xylazine (10^{-4} mol./l.) and atropine (10^{-8} mol./l.) inhibited the contractile responses of the rabbit jejunum and guinea pig ileum to acetylcholine (10^{-8} mol./l. — 10^{-7} mol./l.). In order to return the responses in presence of xylazine to the control level, the test dose of acetylcholine was increased to 10^{-6} mol./l. Xylazine partly antagonised the response of the guinea pig auricles to acetylcholine (Fig. 3, A and B). Higher concentrations of xylazine depressed the auricular contractions.

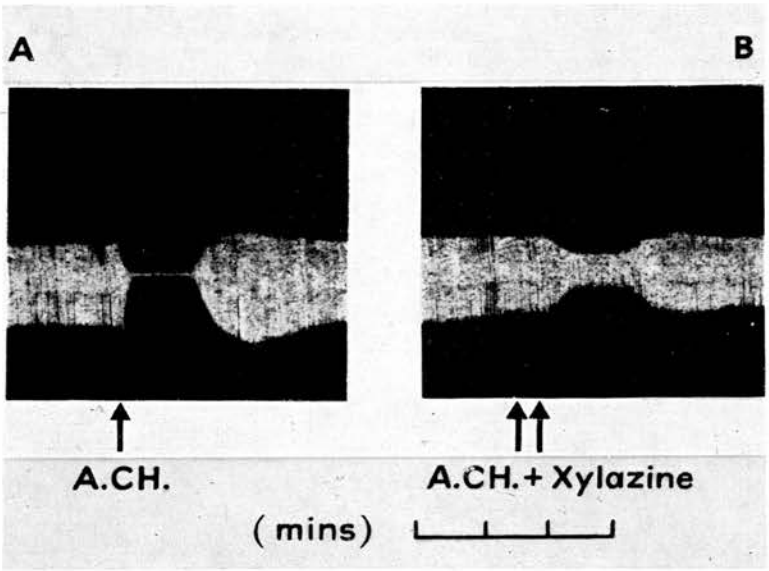


Fig. 3. A: The effect of acetylcholine (A. CH.) (10^{-6} mol./l.) on the amplitude of contraction of the isolated guinea pig auricles. B: The effect of acetylcholine (A. CH.) (10^{-6} mol./l.) in presence of xylazine (10^{-4} mol./l.) on the amplitude of contraction of the isolated guinea pig auricles

Antiserotonin and antihistamine effects of xylazine were observed. Xylazine (10^{-4} mol./l.) inhibited the maximum contraction responses of the rabbit jejunum, guinea pig ileum and rat fundic strip to 5-HT (10^{-8} mol./l. — 10^{-6} mol./l.), as well as the guinea pig ileum to histamine (10^{-7} mol./l.). Serotonin was increased to 10^{-5} mol./l. and histamine to 10^{-6} mol./l. to return the responses to the control level in presence of xylazine.

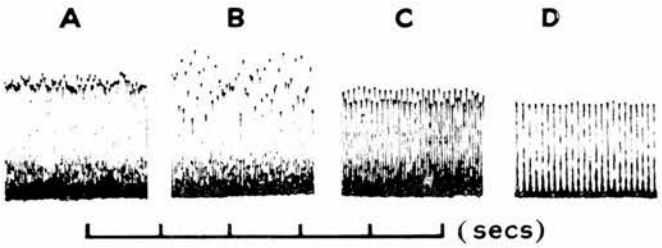


Fig. 4. The effects of xylazine (10^{-4} mol./l.) on the rate and amplitude of contractions of the isolated guinea pig auricles; A: control. B: one minute after the application of xylazine indicating arrhythmias. C: two minutes and D: three minutes after xylazine, showing the steady contractions with a decrease in the rate and amplitude

Effects of xylazine on isolated guinea pig auricles

Xylazine (10^{-4} mol./l.) significantly ($P < 0.001$) decreased the rate of contractions of the isolated auricles from 125 ± 3.9 S. E. to 83 ± 4.5 S. E. (6 obs). Arrhythmias were observed for about one minute. They were followed by steady contractions of the auricles at a lower rate and amplitude (Fig. 4). This myocardial depressant effect was not abolished by atropine (10^{-8} mol./l.), propranolol (10^{-7} mol./l.), phentolamine (10^{-7} mol./l.) or hexamethonium (10^{-5} mol./l.).

Neuromuscular blocking effects of xylazine

Xylazine (10^{-4} mol./l.) showed an effect on the chick biventer muscle, similar to d-tubocurarine (10^{-5} mol./l.). Although both acted synergistically on the neuromuscular junctions, the effect of xylazine was not antagonised with neostigmine. Similar results were obtained with xylazine on the rat phrenic nerve-diaphragm preparation (Fig. 5).

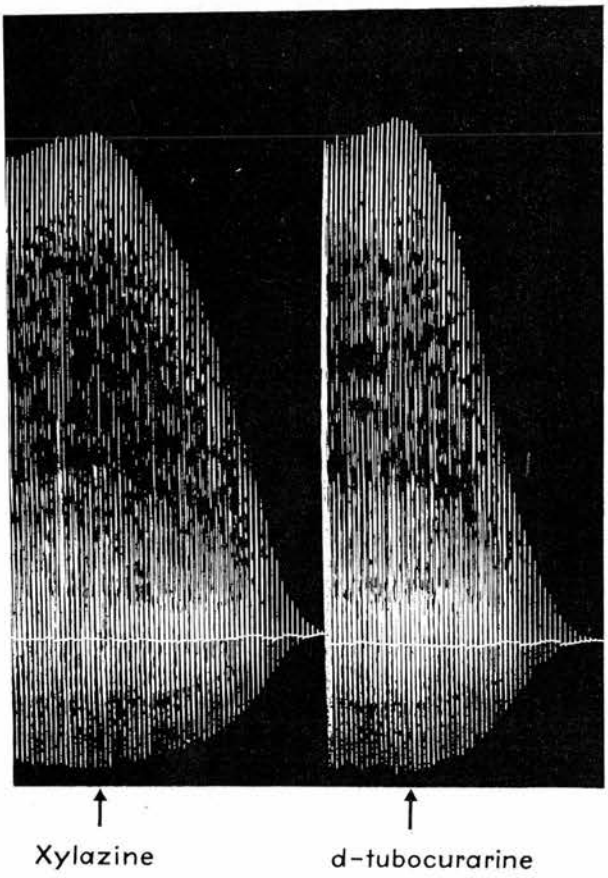


Fig. 5. The effects of xylazine (10^{-4} mol./l.) and d-tubocurarine (10^{-7} mol./l.) on the rat phrenic nerve-diaphragm. preparation stimulated with 3 V, 0.5 ms. square pulses at 0.2 Hz

Local anaesthetic effects of xylazine

Xylazine had a powerful and reversible local anaesthetic effect on the frog sciatic nerve trunk preparation. A complete blockage of the action potential was obtained with concentrations as low as 0.075 % (pH 7.4) (Fig. 6, A and B). Higher concentrations of xylazine produced a more rapid block and required a longer recovery time (Fig. 6, C). During the onset of the local anaesthetic effect, there was a reduction in the conduction velocity of

the compound action potential. Similar results were obtained with procaine hydrochloride 0.5 %.

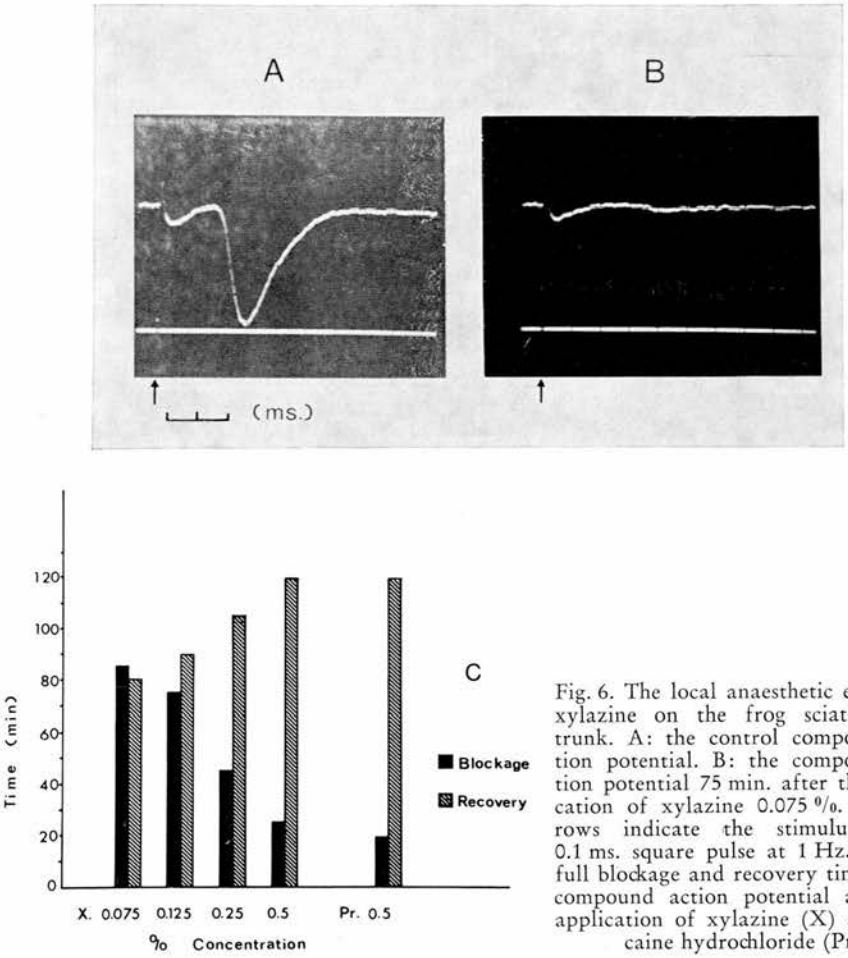


Fig. 6. The local anaesthetic effects of xylazine on the frog sciatic nerve trunk. A: the control compound action potential. B: the compound action potential 75 min. after the application of xylazine 0.075 %. The arrows indicate the stimulus, 10 V, 0.1 ms. square pulse at 1 Hz. C: The full blockage and recovery time of the compound action potential after the application of xylazine (X) and procaine hydrochloride (Pr.)

Discussion

The rise in blood pressure and the responses of the aortic strip, the anococcygeous muscle and the vas deferens, provided further evidence of the α agonist activity of xylazine. These results were consistent with observations reported by Kroneberg et al. (1967), Schmitt et al. (1970) and Autret et al. (1970), which also indicated the α agonist activity of xylazine.

The responses of the rat uterus and guinea pig tracheal chain to xylazine were reduced by propranolol, but the reduction was incomplete. The typical ionotropic β agonist effect on the guinea pig isolated auricles was not obtained. It is therefore doubtful whether xylazine had a β agonist activity.

The reduction in response to stimulation of the sympathetic nerves observed in the vas deferens and rat colon preparations produced by xylazine might indicate a specific inhibition of the adrenergic neurone function, as proposed by Kroneberg et al. (1967) and Schmitt et al. (1970). However, it seems more probable that this effect is explained by the local anaesthetic activity of xylazine.

Xylazine antagonised the effects of acetylcholine, serotonin and histamine on the rabbit jejunum, the guinea pig ileum and the rat fundic strip preparations. However, the neuromuscular blocking effect of xylazine was neither depolarizing nor competitive in nature. Xylazine antagonized the action of acetylcholine, but the effect was not abolished by neostigmine. The auricular depression caused by xylazine was not antagonised by atropine. All these effects may be explained by the local anaesthetic properties of xylazine.

The myocardial depression produced by xylazine probably caused the bradycardia and decreased cardiac output observed in horses (CLARK and HALL, 1969) and in sheep (unpublished observations). This myocardial depression can also explain the prolonged hypotension observed after xylazine administration.

It is concluded that xylazine has α agonistic and local anaesthetic activities. The myocardial depression resulting from the local anaesthetic activity is probably of clinical importance.

Summary

Xylazine given intravenously initially raised the blood pressure in rats, guinea pigs and rabbits. It contracted the aortic strip, the anococcygeous muscle and the vas deferens. These effects were antagonised with phentolamine. Xylazine depressed the rate and amplitude of contraction of the isolated auricles, and caused bradycardia in vivo. These effects were not antagonised with atropine. Xylazine inhibited neuromuscular transmission. This effect was neither depolarising nor competitive. Xylazine reversibly blocked the conduction in the frog sciatic nerve. It is concluded that xylazine has α agonist and local anaesthetic properties.

Acknowledgement

The authors wish to thank Professor F. ALEXANDER for his guidance and advice. Thanks are extended to Bayer U. K. for the generous gift of xylazine (Rompun®) used in this study.

Zusammenfassung

α-agonistische und lokalanästhetische Xylazinwirkungen

Intravenöse Applikation von Xylazin erhöhte initial den Blutdruck bei Ratten, Meerschweinchen und Kaninchen. Es führte zu einer Kontraktion von Aortenstreifen sowie des Musculus anococcygicus und des Vas deferens. Diese Effekte werden durch Phentolamin gehemmt. Xylazin reduzierte die Frequenz und Kontraktionen von isolierten Herzaurikeln und verursachte in vivo eine Bradykardie. Diese Effekte wurden durch Atropin nicht blockiert. Xylazin hemmte die neuromuskuläre Impulsübertragung. Dieser Effekt war weder depolarisierend noch kompetitiv. Xylazin führte zu einer reversiblen Blockade der Impulsleitung im N. ischiadicus des Frosches. Folgerung: Xylazin weist α-agonistische und lokalanaesthetische Eigenschaften auf.

Résumé

Actions α-agonistes et d'anesthésie locale de la xylazine

Une application intraveineuse de xylazine a augmenté initialement la pression sanguine chez des rats, des cobayes et des lapins. Elle a conduit à une contraction des stries de l'aorte, du Musculus anococcygicus et du Vas deferens. Ces effets furent inhibés par la phentolamine. La xylazine a réduit la

fréquence et les contractions d'oreillettes cardiaques isolées et a provoqué une bradycardie in vivo. Ces effets ne furent pas bloqués par l'atropine. La xylazine a inhibé la transmission de l'impulsion neuromusculaire. Cet effet ne fut ni dépolarisant ni compétitif. La xylazine provoqua un bloquage reversible de transmission d'impulsions dans le N ischiadicus chez la grenouille.

Conclusion: la xylazine présente des propriétés α agonistes et d'anesthésie locale.

Resumen

Acciones α-agónicas y anestésicas locales de la xilazina

La aplicación intravenosa de xilazina aumentaba inicialmente la tensión sanguínea en ratas, cobayas y conejos. Contraía las tiritas aórticas, el músculo anocoxígeo y el conducto deferente. Estos efectos eran inhibidos por la fentolamina. Xilazina reducía la frecuencia y amplitud de cantracciones de las aurículas aisladas y causaba bradicardia *in vivo*. Estos efectos no eran antagonizados por la atropina. Xilazina inhibía la transmisión neuromuscular. Este efecto no era ni despolarizante ni competitivo. Xilazina bloqueaba reversiblemente la conducción en el nervio ciático de la rana. Conclusión: Xilazina tiene propiedades α-agónicas y anestésicas locales.

References

1. Antonaccio, M. J., R. D. Robson, and L. Kerwin, 1973: Evidence for increased vagal tone and enhancement of baroreceptor reflex activity after xylazine in anaesthetized dogs. Europ. J. Pharmacol., *23*, 311—315.
2. Autret, A. M., H. Schmitt, S. Fenard, and N. Pétillot, 1970: Comparison of haemodynamic effects of a sympathomimetic drugs. Euro. J. Pharmacol., *13*, 208—217.
3. Bülbring, E., 1946: Observations on the isolated phrenic nervediaphragm preparation of the rat. Br. J. Pharmacol., *1*, 38—61.
4. Castillo, J. C., and E. J. de Beer, 1947: The tracheal chain. I. A preparation for the study of antispasmodics with particular reference to bronchodilator drugs. J. Pharmacol. Exp. Therap., *90*, 104—109.
5. Clark, K. W., and L. W. Hall, 1969: Xylazine — a new sedative for horses and cattle. Vet. Record., *85*, 512—517.
6. De Jalon, Bayo, and De Jalon, 1945: The rat uterus in preparation. Farmacoter. act., *3*, 313.
7. Furchgott, R. F., and S. Bhadrakom, 1953: Reactions of strips of rabbit aorta to epinephrine, isopropylaterenol, sodium nitrite and other drugs. J. Pharmacol. Exp. Therap., *108*, 129—143.
8. Gillespie, J. S., 1972: The rat anococcygeous muscle and its response to nerve stimulation and to some drugs. Br. J. Pharmacol., *45*, 404—416.
9. Ginsborg, B. L., and J. Warriner, 1960: The isolated chick biventer cervicis nerve-muscle preparation. Br. J. Pharmacol., *15*, 410—411.
10. Huchovíc, S., 1961: Responses of the isolated sympathetic nerve-ductus deferens preparation of the guinea pig. Br. J. Pharmacol., *16*, 188—194.
11. Kroneberg, G., A. Oberdorf, F. Hoffmeister und W. Wirth, 1967: Zur Pharmakologie von Bayer. 1470, eines Hemmstoffes adrenergischer und cholinergischer Neurone. Naunyn-Schmiedebergs Arch. Pharmak. exp. Path. *256*, 257—280.
12. Magnus, 1904: Pflügers Arch. ges. physiol., *102*, 123—151.
13. Oberdorf, A., F. Hoffmeister und G. Kroneberg, 1967: Zum Wirkungsmechanismus neuartiger vegetativ und zentralnervös wirksamer Pharmaka. Naunyn-Schmiedebergs Arch. Pharmak. exp. Path., *257*, 48—49.
14. Schmitt, H., G. Fournadjiev, G., and H. Schmitt, 1970: Central and peripheral effects of Bayer 1470 on the sympathetic system. Europ. J. Pharmacol., *10*, 230—238.
15. Vane, J. R., 1957: A sensitive method for the assay of 5-hydroxytryptamine. Br. J. Pharmacol., *12*, 344—349.

Address of authors: M. A. Aziz and R. J. Martin, Dept. of Veterinary Pharmacology, Royal (Dick) School of Veterinary Studies, Summerhall, Edinburgh University, Edinburgh.

seen with the mega-ohm technique, i.e. about 120 pS. Concentrations of glu between 10^{-4} M and 10^{-2} M have been investigated. At the higher glutamate concentrations, more than one channel was usually seen after Con A application, although, with time, some of these channels became inactive. Recordings were made from single patches over periods of up to 45 min. Kinetic analysis of these D-glutamate receptor channels is currently under way.

This work was supported by SERC Grant No. GR/D 67422.

References

1. Cull-Candy, S. G. & Usherwood, P. N. R. *Nature New Biol.*, **246** (1973) 62–4.
2. Kerry, C. J., Kits, K. S., Ramsey, R. L., Sansom, M. S. P. & Usherwood, P. N. R. *Biophys. J.*, **51** (1987) 137–44.
3. Kerry, C. J., Ramsey, R. L., Sansom, M. S. P., Usherwood, P. N. R. & Washio, H. *J. Exp. Biol.*, **127** (1987) 121–34.
4. Dudel, J., Franke, C., Hatt, H., Ramsey, R. L. & Usherwood, P. N. R. *Neurosci. Lett.* **88** (1988) 33–8.
5. Dudel, J., Franke, C., Hatt, H. & Usherwood, P. N. R. *Brain Res.*, in press.
6. Duce, J. A. & Usherwood, P. N. R. *J. Exp. Biol.*, **123** (1986) 307–23.
7. Evans, M. L. & Usherwood, P. N. R. *Brain Res.*, **358** (1985) 34–9.
8. Lea, T. J. & Usherwood, P. N. R. *Comp. Gen. Pharmacol.*, **4** (1973) 333–50.

Effect of Dihydroavermectin B_{1a} on Cl^- Single-channel Currents in *Ascaris* Muscle

R. J. Martin & A. J. Pennington

Department of Preclinical Veterinary Sciences, R(D)SVS, Summerhall, Edinburgh, UK

The effects of dihydroavermectin B_{1a} (DHAVM; 2×10^{-12}–2×10^{-7} M) on GABA-activated channels[1] and spontaneously active channels in *Ascaris* muscle membranes have been studied using outside-out patches and solutions favourable for recording Cl^- currents.

No evidence was found to suggest that DHAVM (2×10^{-7} M) can act as an ionophore; no channel currents were produced after application of DHAVM to the outside of patches which did not contain GABA-activated or spontaneously active channels; the patches remained quiet.

It was found that DHAVM (2×10^{-12} M) acts on a spontaneously active (*c.* 10 pS) channel to increase the probability of being open (P_{open}); patches which did not contain GABA-activated channels but which contained the channel showed an increase in P_{open} after DHAVM application (Fig. 1).

DHAVM (2×10^{-7} M) affected the properties of GABA-activated channels; after a delay it reduced P_{open} of GABA-activated channels and increased the variance of

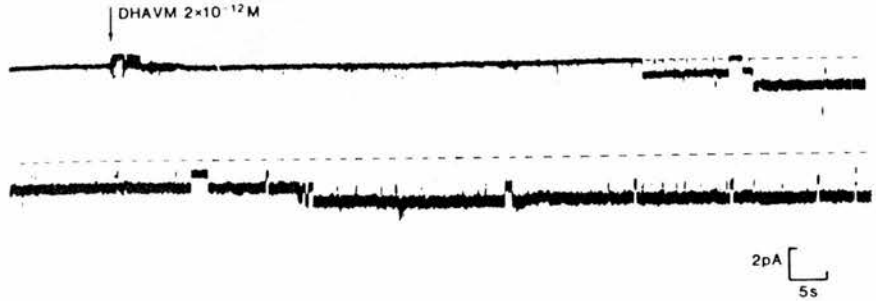


Fig. 1. DHAVM (2×10^{-12} M, dissolved in 1 g litre^{-1} aqueous DMSO) was added to the bath and thus to the outside of an outside-out patch. It dramatically increased P_{open} of spontaneously active channels which have an amplitude of 0·9 pA (10 pS). Patch potential: −75 mV. Pipette solution (mM): CsCl, 140; $MgCl_2$, 2; TRIS, 5; EGTA, 11; $CaCl_2$, 1; adjusted to pH 7·2. Bath solution (mM): Na acetate, 105; NaCl, 35; KCl, 2; $MgCl_2$, 2; TRIS, 5; glucose, 3; $CaCl_2$, 5. The dashed line represents the closed state. The lower trace continues the upper trace. Up to three channels are open at the end of the lower trace. The effect of DHAVM was not reversed on washing (not shown). Note the slow time scale and the increase in the noise limits as the channels open.

their channel currents; in some patches DHAVM produced an initial increase in P_{open} before the onset of antagonism.

A. J. Pennington is supported by the SERC. DHAVM was a gift from Pfizer Central Research (Dr K. Gration).

Reference

1. Martin, R. J. *Brit. J. Pharm.*, **84** (1985) 445–61.

Neurotransmitter, Neuromodulator and Ca^{2+} Channel Ligand Actions on Cultured Rat DRG Neurones are Regulated by a Pertussis Toxin-Sensitive G-Protein

Roderick H. Scott & Annette C. Dolphin

Department of Pharmacology, St George's Hospital Medical School, Cranmer Terrace, London SW17 0RE, UK

Activation of a wide variety of receptors for neurotransmitters and neuromodulators ($GABA_B$, noradrenaline (α_2), dopamine, substance P, adenosine (A_1) and opiate) results in inhibition of neuronal Ca^{2+} channel currents. Guanine nucleotide binding proteins (G-proteins) appear to couple these receptors with Ca^{2+} channels. The $GABA_B$ receptor agonist (−)-baclofen (2–100 μM), inhibited Ca^{2+} channel currents recorded from cultured dorsal root ganglion (DRG) neurones. This inhibitory action was prevented by pretreating the cells with pertussis toxin (2–5 h; 0·5 μg ml^{-1}).[1] These results suggest that a G_i- or G_o-type G-protein is involved in the response, as pertussis toxin selectively ADP-ribosylates α_i

[*From the Proceedings of the Physiological Society*, 4–5 *November* 1988
Journal of Physiology, **410**, 83*P*, 1989]

Ivermectin induces cation channels in isolated patches of *Ascaris* muscle

By R. J. Martin and A. J. Pennington. *Department of Preclinical Veterinary Sciences, R.(D.)S.V.S., Summerhall, University of Edinburgh*

We have used the patch-clamp technique to study effects of the anthelmintic ivermectin at the single-channel level using inside-out patches from muscle of the parasite *Ascaris suum* and low-Ca conditions to avoid Ca-activated Cl channels (Thorn & Martin, 1987). Ivermectin ($\geqslant$ 20 fM, bath-applied) induced long (seconds) channel bursts (Fig. 1*A*, *B*). The channels showed Cs permeability (Fig. 1*C*). Experiments in which the bath Cs was replaced by another cation produced changes in reversal potentials showing the permeability sequence as Cs > Rb > K > Na > Li > Ca.

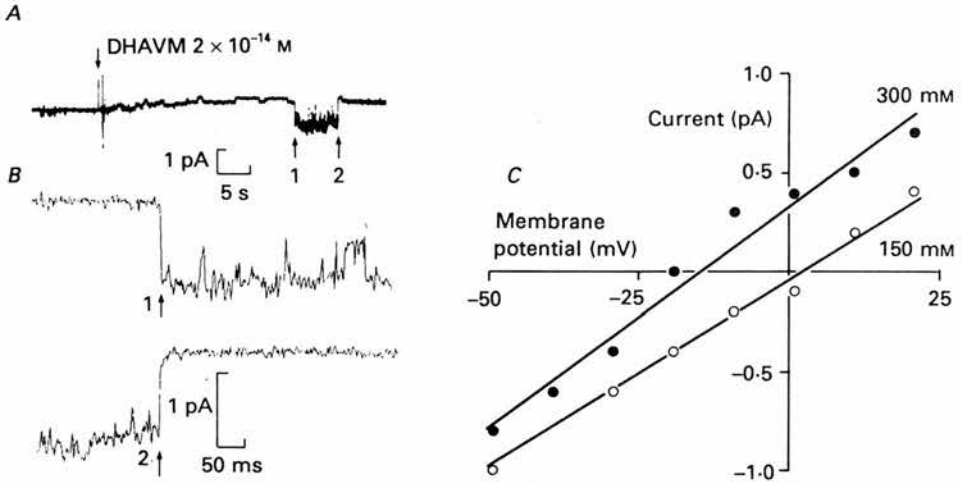


Fig. 1. Ivermectin-induced channels. Inside-out patch. Membrane potential: −50 mV. Pipette solution (mM): CsCl 150, HEPES 10, pH 7·2 with NaOH. Bathing solution (mM): CsCl 150, HEPES 10, EGTA 11, $CaCl_2$ 1, 0·1% DMSO, pH 7·2. 20–22 °C. Filter: −3 dB, 250 Hz, 8-pole Bessel. *A*, 2×10^{-14} M-DHAVM (ivermectin), added rapidly to the bath, produces a long (6·7 s) channel burst (vertical arrows 1 and 2) after a 28 s delay (similar bursts followed). *B*, opening (arrow 1) and closing (arrow 2) of the channel burst seen in *A* at a faster timescale. Note the open-channel noise. *C*, Effect of bath CsCl concentration on channel *I*/*V* plots. Results from the same experiment as *A* and *B*. ○, with 150 mM-CsCl. ●, with 300 mM-CsCl. Slope conductances 19·7 pS (○) and 22·3 pS (●). Shift in reversal potential: −16·5 mV. Permeability ratio: Cl/Cs = 0·03.

Supported by SERC.

REFERENCE

Thorn, P. & Martin, R. J. (1987). *Q. Jl exp. Physiol.* **72**, 31–49.

Br. J. Pharmacol. (1989), **98**, 747–756

A patch-clamp study of effects of dihydroavermectin on *Ascaris* muscle

R.J. Martin & A.J. Pennington

Department of Preclinical Veterinary Sciences, Summerhall, R.(D.)S.V.S, University of Edinburgh, Edinburgh

1 Effects of bath-application of the anti-parasitic agent 22,23 dihydroavermectin B_{1a} (DHAVM 20 fM to 0.2 μM) on outside-out and inside-out patches from collagenase-treated muscle membranes of *Ascaris suum* were examined.

2 DHAVM was tested as a γ-aminobutyric acid (GABA) agonist by application to outside-out patches. DHAVM failed to open characteristic GABA channels even when high concentrations (20 nM to 0.2 μM) were used. These high concentrations of DHAVM also failed to potentiate opening of channels activated by application of 3–4 μM GABA; instead they acted to depress GABA-activated channel currents by reducing mean conductances and P_{open}.

3 In outside-out patches, low concentrations of DHAVM (1 pM to 100 pM) produced opening of 0–13 channels, the number depending on the patch. The progressive opening of channels gave rise to a 'Staircase' effect. The conductance of these channels was 9–15 pS and open times were long (greater than 100 mS). Ion substitution experiments showed these channels to be permeable to Cl. The channels were not blocked by 20 μM picrotoxin. There was a long delay (greater than 15 s) between DHAVM application and channel opening; this delay and lipophilic nature of DHAVM suggested a site of action in the lipid phase of the membrane.

4 The effect of bath-application of low concentrations of DHAVM on inside-out patches was investigated under low-Ca conditions (to avoid Ca-activated Cl channels). DHAVM (20 fM to 1 nM) did not produce opening of Cl channels but produced opening after a long delay (mean 2.5 minutes) of noisy cation-selective channels which had conductances of 5–30 pS.

5 The actions of DHAVM are discussed.

Introduction

Avermectins, a family of highly lipid soluble macrocyclic lactones, derived from *Streptomyces avermitilis* (Burg *et al.*, 1979), have a biological activity against parasitic nematodes and insects but not against tape worms, flukes or their hosts (Egerton *et al.*, 1979; Campbell & Benz, 1984). The selective action and potency of avermectins means that these drugs can be used effectively in animals for treating a wide range of nematode infestations including intestinal nematodes like *Ascaris suum* (Campbell & Benz, 1984). In man an avermectin is used to control the nematode *Onchocerca volvulus* which causes river blindness.

The naturally occurring avermectins are separated into four major groups (A_{1a}; A_{2a}; B_{1a}; B_{2a}) and four minor groups (A_{1b}; A_{2b}; B_{1b}; B_{2b}). The B groupings are more active biologically. A synthetic B derivative (22-23 dihydroavermectin, known as ivermectin) has been developed for animal use.

One suggested mode of action for avermectins is that they are γ-aminobutyric acid (GABA) agonists or potentiators (Wang & Pong, 1982; Wright, 1986). This hypothesis has the advantage of explaining the immobilizing effect on nematode parasites and the reported lack of effect on parasites which do not possess GABA receptors; it can also explain the increase in membrane Cl conductance which has been associated with the action of avermectins (Fritz *et al.*, 1979; Duce & Scott, 1985; Lees & Beadle, 1986). However, this interpretation does not explain why avermectins can increase Cl conductances in preparations not sensitive to GABA (Duce & Scott, 1985; Lees & Beedle, 1986).

The effects of 22,23 dihydroavermectin B_{1a} (DHAVM) have been investigated on isolated patches of the bag region of muscle membrane from the nematode parasite of the pig, *Ascaris suum*. This part of the muscle is not innervated but has been

© The Macmillan Press Ltd 1989

shown to possess extrasynaptic GABA-activated Cl channels (Martin, 1980; 1985). It is shown that DHAVM is not a GABA agonist or potentiator but produces opening of channels permeable to Cl when applied to outside-out patches; DHAVM does not open Cl channels but produces non-selective cation channels when applied to inside-out patches under low-Ca conditions. Preliminary accounts of some of this work have appeared (Martin & Pennington 1988; 1989).

Methods

The methods have been described in detail previously (Martin, 1985) but are outlined below.

The preparation

Specimens of *Ascaris suum* were collected from the local abattoir and maintained in Locke solution (replaced daily) at 32°C in a water bath. The *Ascaris* were used for experiments within four days. The 2 cm flap preparations were pinned onto 'Sylgard' in an experimental chamber maintained at 22°C. Clean membranes were prepared by use of collagenase (Type 1A Sigma; 1 mg ml^{-1}) for 10 to 60 min, depending on the preparation.

Solutions

The preparations were maintained in a Ringer solution containing (mM): NaCl 140, KCl 2.0, $CaCl_2$ 5, $MgCl_2$ 2.0, glucose 3.0 and HEPES 10, pH 7.2 with NaOH. Electrodes for outside-out patches were filled with (mM): CsCl 140, $CaCl_2$ 1, $MgCl_2$ 2, EGTA 11, HEPES 10, pH 7.2 with CsOH. Electrodes for inside-out patches were filled with (mM): CsCl 150, $MgCl_2$ 5, HEPES 10, pH 7.2 with CsOH for low-Ca conditions. Once an isolated patch had been obtained the bath solution was changed as indicated in the results. Tris (5 mM) with maleic acid was used instead of HEPES for pH control of isolated patches in some experiments with no apparent effect on the observations.

Recording

Standard patch-clamp techniques were used to obtain outside-out or inside-out patches. Patch-electrodes were made from micro-haematocrit capillary tubes (Garner Glass 7052) and had a resistance of 1–3 mΩ: 'Sylgard' was used for coating the electrodes to improve frequency responses (typically greater than 2 kHz). Currents were recorded using a List EPC-7 and a modified Sony digital audio processor with a Sony Betamax video system for making records on tape. An agar-plug bath electrode was used to minimize changes in junction potentials as a result of solution changes. Despite this, small changes (3 mV) in junction potential still occurred as a result of changing Cl concentrations in the bath. Corrections were made for this effect when estimating reversal potentials.

Data processing

Records were analysed by playing back records on tape into a CED 1401 interface connected to DCS 286 PC computer and using the PAT software (Dr J. Dempster, Strathclyde University). Amplitude histograms produced by this software express the time spent at particular current levels as a percentage of the total signal time analysed. It does not equate simply with the relative frequency at which the various conductance states occur but does allow estimates of the proportion of time the channel passes particular levels of current. Attempts to fit these current amplitude histograms by multiple Gaussian functions to identify the probability of observing distinctive subconductance states were not generally successful because the subconductance states were not sufficiently separated. Cumulative distributions of open channel conductances were therefore constructed to illustrate the probability of observing conductance levels. Slope conductances from channel I/V plots were obtained by linear regression. Relative permeabilities of ions were calculated from reversal potentials (Hille, 1984).

Drugs

DHAVM was obtained as gifts from Pfizer Central Research and Merck, Sharp and Dhome. DHAVM was usually dissolved in dimethylsulphoxide (DMSO) to make a 1 μM stock which was maintained at −12 C°; it was diluted in Ringer, with 0.1% DMSO present as the carrier, to the concentrations described in the results. In some experiments ethanol was used as a carrier. The rest of the chemicals were purchased from Sigma.

Effect of the solvent

Most studies with avermectins have used DMSO (1% to 2%) as a carrier. Kass *et al.* (1984) reported that 1% DMSO had no effect on electrophysiological recordings. Duce & Scott (1985) found that in the leg muscle of locust DMSO (0.5 to 4%) increases input conductance and hyperpolarizes the membrane by increasing K but not Cl conductance. They also reported that at 2% DMSO, there was a reduction of GABA-induced Cl conductance changes. In this

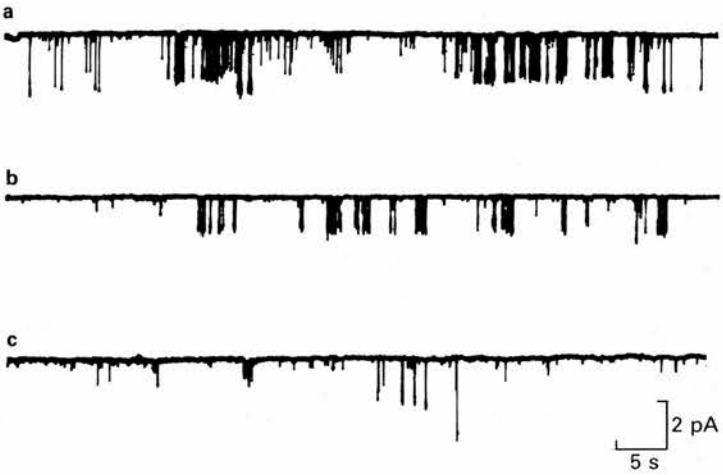


Figure 1 Effect of DHAVM (20 nM and 200 nM) on GABA-activated channels. (a) Control effect of 4 μM GABA; (b) in the presence of 4 μM GABA and 20 nM DHAVM; (c) in the presence of 4 μM GABA and 200 nM DHAVM. Outside-out patch, membrane potential: (a) and (b) -50 mV; (c) -75 mV. Pipette solution (mM):CsCl 140, $MgCl_2$ 2, $CaCl_2$ 1, EGTA 11, Tris 5, pH 7.2. Bath solution (mM):NaCl 140, KCl 2, $MgCl_2$ 2, Tris 5, glucose 3, $CaCl_2$ 5, pH 7.2.

study we used 0.1% DMSO; control experiments showed that it was without effect. As a further control 0.1% ethanol was also used as a carrier; no difference in the results was observed. Control applications of solutions containing carrier but no drug did not open channels in either outside-out or inside-out patches.

Results

The following experiments were carried out on 104 patch preparations from muscle cell bag regions. Effects of DHAVM (20 fM to 0.2 μM) were examined using 24 outside-out and 80 inside-out patches.

DHAVM is not a GABA agonist but acts as an antagonist

Wang & Pong (1982) have suggested that avermectins may act as GABA agonists or potentiators. It was possible to test this in *Ascaris* using the extra-synaptic GABA receptors present on the bag region of the somatic muscle. GABA agonists combine with extra-synaptic receptors on the outside membrane and open Cl channels which have conductances of 15 to 40 pS and mean open times of less than 35 ms; bursts and clusters of openings are also expected (Martin, 1985). DHAVM was therefore tested as a GABA agonist by applying it in the bath to outside-out patches. DHAVM in concentrations as high as 0.2 μM failed in all cases to open characteristic GABA channels.

DHAVM was also tested as a GABA potentiator. Outside-out patches were used and GABA channels activated initially by bath-application of 3 to 4 μM agonist; DHAVM (20 nM to 0.2 μM) was then added as well. The results of a typical experiment are shown at a low time resolution in Figure 1. The top trace shows GABA channels at -50 mV in the presence of agonist alone; the second trace shows GABA channels at -50 mV in the presence of 20 nM DHAVM; the bottom trace shows the GABA channels at -75 mV in the presence of 0.2 μM DHAVM. It can be seen that there was a dose-dependent reduction in the frequency of channel opening and that the amplitude of the channel currents was depressed in the presence of DHAVM; there was no potentiation.

The depressive effect of DHAVM on GABA channel currents at a higher time resolution is illustrated in Figure 2 for the same experiment as above. Figure 2a shows a typical GABA channel burst and current amplitude histogram in the presence of GABA alone (control): the current amplitude histogram had a peak at 1.8 pA:P_{open} was 0.2 with the channel conductance peak at 36 pS. Figure 2b shows the same in the presence of 20 nM DHAVM: P_{open} was 0.13 with the channel conductance peak at 28 pS. Figure 2c shows the same in the presence of 0.2 μM DHAVM:P_{open} was 0.11 with the channel conductance peaking near 20 pS.

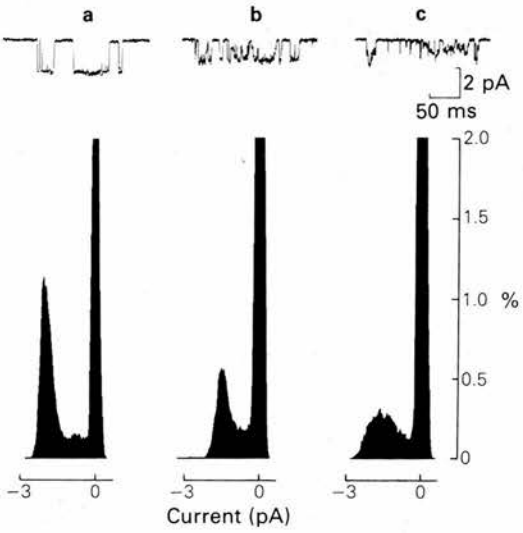


Figure 2 GABA-activated Cl channels and current amplitude histograms. (a) 4 μM GABA; −50 mV. (b) 4 μM GABA and 20 nM DHAVM; −50 mV. (c) 4 μM GABA and 200 nM DHAVM; −75 mV. From the same patch recording as Figure 1.

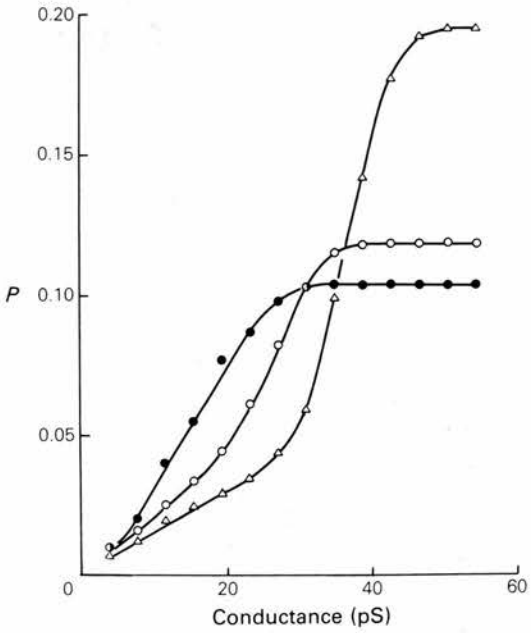


Figure 3 Effect of DHAVM on GABA-activated channel cumulative-conductance distributions; (△) 4 μM GABA, −50 mV; (○) 4 μM GABA and 20 nM DHAVM; −50 mV; (●) 4 μM GABA and 200 nM DHAVM, −75 mV. Distributions from the data shown in Figure 2. The ordinate scale is the probability of the channel being open (greater than 5 pS) and having a conductance less than or equal to that shown on the abscissa scale.

GABA channel currents are characterized by the presence of multiple conductance states (Bormann *et al.*, 1987); subconductance levels are also seen in *Ascaris* (Martin, 1985). It was possible that DHAVM may affect the relative proportion of time spent at different conductance levels. The effect of DHAVM on GABA channel conductance was examined by looking at cumulative distributions of channel conductances greater than 5 pS (i.e. open). Figure 3 illustrates these distributions which were obtained from the same experiments as those shown in Figures 1 and 2. These observations consistently showed that one effect of DHAVM is to depress the amplitude of the channel conductance and to reduce the proportion of time spent at higher conductance levels. The depressive effect of DHAVM on GABA channel currents shows that DHAVM acts as a blocker/antagonist on the *Ascaris* muscle GABA receptor.

Activation of channels in outside-out patches by DVAHM in the absence of GABA

In the experiments described in the previous section where DHAVM was added by itself to outside-out patches to test for a GABA agonist action, it was noticed that DHAVM produced open times and long burst durations with mean open times greater than 100 mS; some open times lasted for several seconds. The channels were readily distinguished from GABA-activated channels which had much shorter open times and showed shorter bursts and clusters of bursts.

Low concentrations (2 pM to 0.1 nM) of DHAVM were also tested and found to open 0–13 of these channels depending on the patch. The most dramatic response seen in four patches was the progressive opening of channels by DHAVM which gave rise to a 'Staircase' effect (Figure 4a and b). There was always a long delay between the addition of DHAVM to the bath and the onset of channel opening; this delay was much longer than required for GABA to open channels. Figure 4a shows the application of 2 pM DHAVM (vertical arrow) to an outside-out patch at −75 mV: 1.1 pA channels (conductance: 14.6 pS) were produced after a delay of 66 s (star); a second channel was activated after 80 s; a third channel was activated after 134 s. The mean open channel lifetime was measured as 164 ms. Figure 4b shows the opening of 13 channels after the addition of 20 nM DHAVM; the opening of channels starts after 32 s.

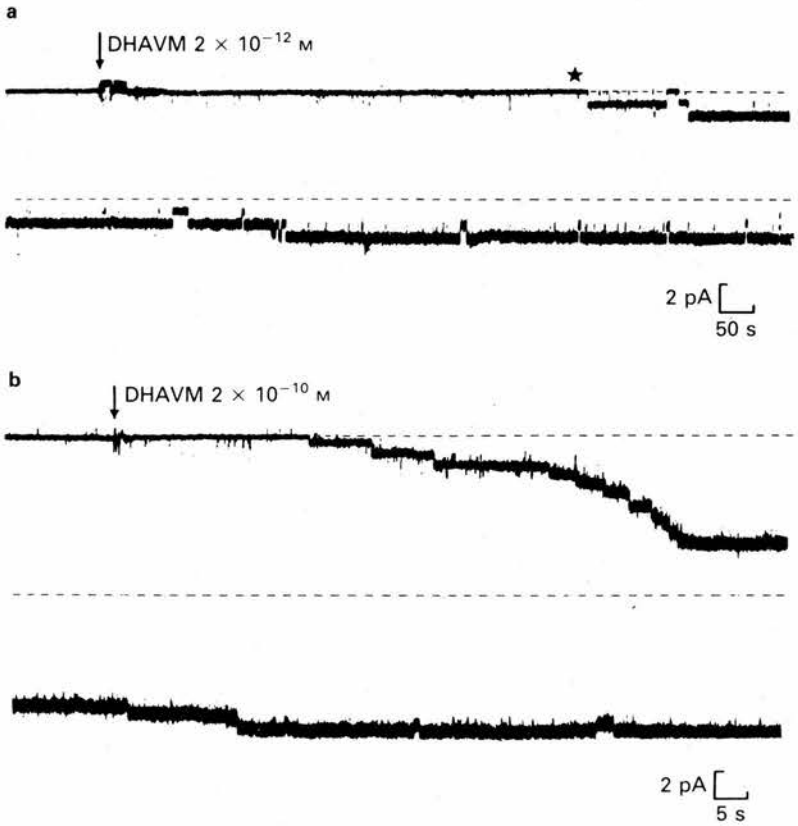


Figure 4 Staircase production of channels in outside-out patches by DHAVM. The dashed lines show the closed states. Pipette and bath solutions as for Figure 1. (a) −75 mV; 2 pM DHAVM after a delay of 66(*), 80 and 134 s produces opening of channels. The mean open time of 164 ms was measured during the period when only one channel was open. (b) −50 mV; 200 pM DHAVM produces 13 channels (from 32 to 86 s).

The permeability of the channels involved was investigated in three outside-out patches by examining the effect of Cl ion substitution. Figure 5 shows the I/V plot of DHAVM-activated channels obtained from the experiment shown in Figure 4b, first with 156 mM Cl and then with 51 mM Cl on the outside of the membrane. The channel conductance was reduced from 11.6 ± 0.3 pS (mean ± s.e.) to 9.1 ± 0.4 pS while the reversal potential shifted from near 0 mV to +23 mV. These potentials are close to the predicted values (of −1.7 and +26.7 mV respectively) of the Nernst equation for Cl and are consistent with the channel being permeable to Cl. Prolonged washing in DHAVM free Ringer containing 0.1% DMSO did not reverse channel opening; this was not unexpected since DHAVM is lipophilic. Picrotoxin (20 μM) applied after activation of the channels did not block the channel currents.

In order to estimate further the proportion of patches that contained Cl channels activated by DHAVM, a series of experiments on 14 isolated inside-out patches with 100 pM DHAVM present in the patch pipette was carried out. Low-Ca conditions were used with asymmetric Cl concentrations (reversal potential = −33.5 mV) to allow identification of Cl channels. Cl channels with conductances and open times similar to those described above were seen in 4 (29%) of the patches.

DHAVM activated channels when applied to inside-out patches

The effect of DHAVM (20 fM to 1 nM) on inside-out patches was tested in low-Ca conditions to avoid Ca-activated Cl channels (Thorn & Martin, 1987). Inside-out patches were formed with pipettes filled with 150 mM CsCl as the main constituent; Ca was not added. The patches were perfused with a bath Ringer which contained EGTA to buffer Ca to less than 10^{-8} M. Under these conditions it was found

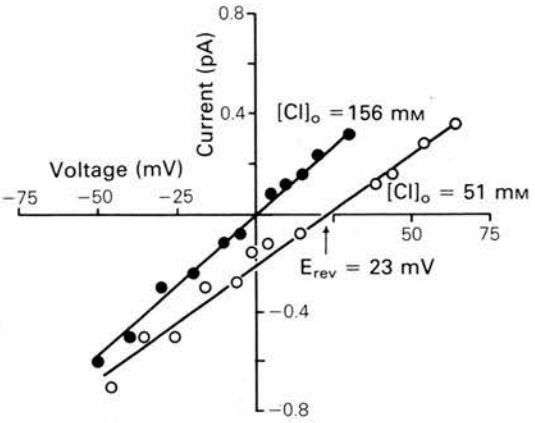


Figure 5 DHAVM-activated channel I/V plots from an outside-out patch in different Cl concentrations. Pipette solution (mM):CsCl 140, $MgCl_2$ 2, $CaCl_2$ 1, EGTA 11, Tris 5; pH 7.2 156 mM-Cl bath solution (mM):NaCl 140, KCl 2, $MgCl_2$ 2, Tris 5, glucose 3, $CaCl_2$ 5, pH 7.2. 51 mM-Cl bath solution (mM):NaCl 35, Na acetate 105, KCl 2, $MgCl_2$ 2, Tris 5, glucose 3, $CaCl_2$ 5, pH 7.2. The slope conductance in 156 mM. $[Cl]_0$ was 11.6 ± 0.3 pS (mean ± s.e.) with a reversal potential near 0-mV. In 51 mM-$[Cl]_0$ the slope conductance was reduced to 9.1 ± 0.4 pS (mean ± s.e.) and the reversal potential was +23 mV. Ringer-agar plug bath electrodes were used and corrections (3 mV) made for changes in junction potentials on solution change.

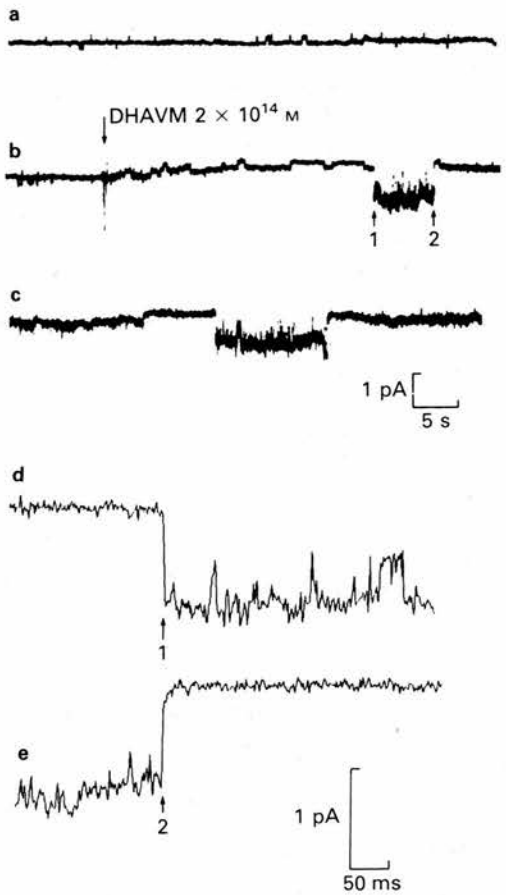


Figure 6 Production of channels in an inside-out patch by DHAVM, −50 mV. Pipette solution (mM):CsCl 150, HEPES 10, $MgCl_2$ 5, pH 7.2. Bath solution (mM):CsCl 150, HEPES 10, EGTA 11, $CaCl_2$ 1, 0.1% DMSO, pH 7.2. (a) Control recording, note the presence of spontaneous channels which have a low conductance; (b) 20 fM DHAVM added rapidly to the bath produces a long channel burst (6.7 s, vertical arrows 1 and 2) after a delay of 28 s, similar bursts follow; (c, d and e) show the burst of (b) at a higher time resolution.

that DHAVM (20 fM–1 nM) produced opening of 'noisy' channels in 52 of 66 patches, usually after a long delay (mean 2.5 min). The results of a typical experiment are shown in Figure 6: after the addition of 20 fM DVAVM there is a 28 s delay which is followed by a long 6.7 s channel burst. Subsequently similar noisy channel bursts followed. Figure 6d and e shows the channel burst of Figure 6b at a higher time resolution and illustrates further the noisy nature of the open channel.

Figure 7 shows current amplitude histograms of three DHAVM bursts obtained from the same experiment as Figure 6. The histograms consistently showed several peaks indicating the presence of multiple subconductance states. The range of subconductance states here was between 8 and 28 pS. The most common state had a conductance of 20 pS. The presence of multiple conductance states appeared to be the origin of the channel noise.

DHAVM-activated channels in inside-out patches are cation selective

The permeability of channels produced by DHAVM in inside-out patches was routinely examined by increasing the concentration of CsCl in the bath from 150 mM to 300 mM. Under these conditions it is predicted from the Nernst potential that a channel selective for Cs will have a reversal potential of −17.6 mV; a channel selective for Cl will have a reversal potential of +17.6 mV. The I/V plots in Figure 8 show that the effect on reversal potential was to produce a shift of −16.5 mV and to increase the conductance of the channel from 19.7 to 22.3 pS. The potential shift was close to that predicted by the Nernst equation for Cs. Similar results were obtained from all inside-out patches. It was con-

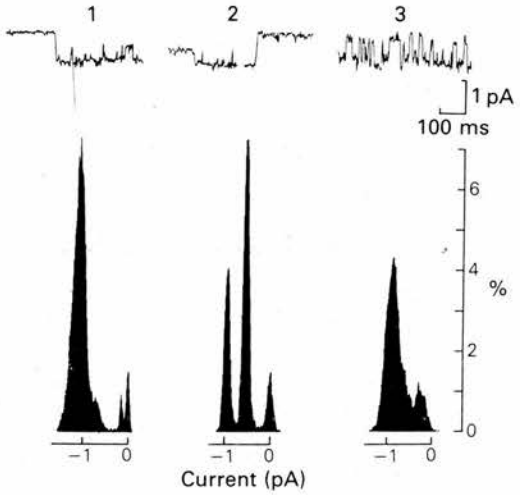


Figure 7 Three representative DHAVM channel bursts at high time resolution and current amplitude histograms from the same experiment as in Figure 6. Histograms are for a 7 s length of recording and show multiple subconductance states. The closed state is marked as zero current.

cluded that these channels were selective for Cs. The Cl/Cs permeability ratio was then calculated from the equation modified from Hille (1984):

$$E = RT/F \ln \frac{Cs_o + \alpha Cl_i}{Cs_i + \alpha Cl_o}$$

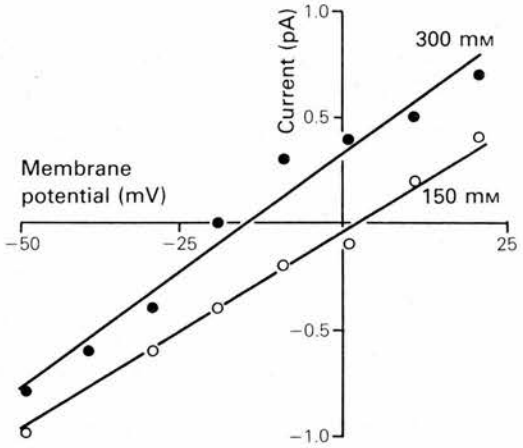


Figure 8 Effect of bath CsCl concentration on channel I/V plots. Results from the same experiment as Figure 6: (○) with 150 CsCl; (●) with 300 mM CsCl. Slope conductances 19.7 pS (○) and 22.3 pS (●). Shift in reversal potential −16.5 mV. Permeability ratio: Cl/Cs = 0.03.

where E = −16.5 mV; Cs_o is 150 mM, the concentration of Cs in the pipette; Cs_i is 300 mM, the concentration of Cs in the bathing Ringer; Cl_o is 150 mM, the concentration of Cl in the pipette; Cl_i is 300 mM, the concentration of Cl in the bathing Ringer; α is the Cl/Cs permeability ratio; R, T and F have their usual meaning. α is then estimated to be 0.03. Results obtained from other experiments were similar with α being less than 0.1: no evidence for activation of channels selectively permeable to Cl was ever seen under low-Ca conditions in inside-out patches. No 'Staircase' effect was seen in any of these inside-out patches.

Permeability sequence of the cation channel

In order to predict possible effects of the cation channel we looked at the permeability of the channel to different cations (in four preparations). The permeability sequence was found to be: Cs > Rb > K > Na > Li > Ca (Table 1) which is an Eisenman Type 1 series (Hille, 1984). This is compatible with a channel whose permeability is determined by dehydration energies of the permeant ions and which has a 'weak-field-strength' binding site controlling permeability; Cs is most easily dehydrated and therefore the most permeant. This channel is permeable to K, Na and Ca and can therefore be described as a 'non-selective cation channel'. The conductance sequence of the channel was not evaluated because of the presence and complication of subconductance states.

Discussion

We have shown that DHAVM depresses the opening of GABA channels and can produce the progressive opening of channels permeable to Cl with a conductance of 9–15 pS when applied to outside-out patches. DHAVM did not open Cl channels when applied to the inside of inside-out patches under low-Ca conditions. There was always a long delay between the onset of effect and application of the drug.

Depressive effects of DHAVM on GABA channel conductances

It has been reported previously that GABA channel current may exist in a number of subconductance states (Bormann *et al.*, 1987). GABA channel currents in *Ascaris* also show subconductance states (Martin, 1985). The separation of the subconductance states in this study was not usually sufficient to allow fitting of multiple Gaussian curves to

Table 1 Shifts in reversal potentials and relative permeability to cations shown by DHAVM-activated channels recorded in an inside-out patch in low-Ca conditions

	Cs^+	Rb^+	K^+	Na^+	Li^+	Ca^{2+}
Reversal potential (mV)	−14.3	−10.7	−5.6	+9.5	+10.7	−4.3
Relative permeability (P_x/P_{cs})	1.0	0.87	0.71	0.39	0.37	0.32

Pipette solution (mM):CsCl 150, HEPES 10, pH 7.2. Bath solution initially (mM):CsCl 150, HEPES 10, EGTA 11, $CaCl_2$ 1, 0.1% DMSO; pH 7.2. The 150 mM CsCl in the bath solution was then replaced by 300 mM CsCl and the shift in reversal measured as −14.3 mV. The other cations (X) using a 300 mM concentration of the Cl salt were then tested. The permeability relative to Cs was calculated from the equation:

$$E_{rev,Cs} - E_{rev,X} = RT/F \cdot \ln \frac{P_x[X]}{P_{Cs}[Cs]}$$

where E_{rev} was the observed reversal potential with the 300 mM concentration of the Cl salt present. The relative permeability of Ca was estimated from a modified form of this equation appropriate for divalent cations (Lewis, 1979). The main channel conductance varied between 22 pS and 10 pS in the different cation solutions but the conductance sequence was not evaluated because of the presence and complication of subconductance states.

the open channel current amplitude histograms. However the histograms showed that the depressive effect of DHAVM was associated with a reduction in the proportion of time the channels spend at the higher conductance levels. One explanation for this is that DHAVM decreased the relative frequency of higher conductance states. Alternatively DHAVM could produce states of very rapid opening and closing beyond the time resolution of the recording system; this could also appear to reduce the mean channel current.

Long delay before effect

The delay between effect and application observed here is interesting. It seems likely that DHAVM works in the lipid phase of the membrane because of its hydrophobic properties; the long delay may occur as DHAVM passes from the bathing solution into the membrane. The relationship between DHAVM concentration and the latency of channel opening was not obvious. Despite this we observed differences between outside-out and inside-out patches suggesting that DHAVM may not easily traverse the bilayer. It is unlikely that DHAVM acts in the aqueous phase. Similar long delays have been described for DHAVM in *Ascaris* (Kass *et al*; 1984) where effects on the nerve cord were examined and took 40 min to reach a maximum. In the locust preparation (Duce & Scott, 1985) DHAVM acted slowly on the non-GABA muscle bundle 33 with Cl conductances increasing over a period of at least 60 min.

Dose-dependent and reversible effects of DHAVM

We were not able to demonstrate clear-cut dose-response relationships for DHAVM. This was because of the practical problems of the finite life time of patch recording, the long delay and non-stationary nature of the response; DHAVM responses usually continued to increase with time in responsive patches. Reversibility was not seen after prolonged washing in DHAVM free Ringer containing 0.1% DMSO. However we did find in two patches that prolonged washing of the preparation with 4% DMSO in DHAVM-free Ringer produced a reduction in the number of channels open. We interpreted this observation as showing that the response may be reversed.

Effects of DHAVM on electrical properties of Ascaris suum

Effects of bath-application of avermectin on the electrical properties of *Ascaris* muscle flap preparations using intracellular recording electrodes have been reported by Holden-Dye *et al.* (1988). Avermectin was found to inhibit GABA-evoked increases in conductance and the associated membrane hyperpolarization with an apparent affinity constant in the mid-micromolar range. The depressant effect on GABA channel currents described here is consistent with these observations but was observed at concentrations 10 to 20 times lower. The difference in concentration may be related to the removal of connective tissue with collagenase for the preparation of 'clean' membranes for patch formation. It is unlikely that the mode of action of DHAVM as an antiparasitic agent involves only a GABA antagonistic effect on the muscle receptor as the action of DHAVM on the whole parasite would then be to produce muscle contraction rather than the observed paralysis (Wright 1986).

Another reported effect of 1 μM avermectin (Holden-Dye *et al.* 1988) was the block of sponta-

neous spiking activity after a delay of 25 min; this block appeared to be Cl-dependent since it did not occur in Cl-free Ringer. However no change in membrane potential or conductance was detected. The activation of low conductance Cl channels as reported here may underly this effect. The density of these Cl channels in this study appeared to be low since they were not present in large numbers in most patches; avermectin induced conductance changes may go undetected in the bag region of the muscle when using intracellular techniques. The very low concentrations of DHAVM required to activate these channels suggests these channels as a therapeutic site of action; this effect may explain the paralysing action of avermectins on nematodes. It is possible that when DHAVM acts on the whole worm that it also has an effect on the nervous system (Kass *et al.*, 1984) which could contain the same Cl channel as described here in the muscle.

Cation channel in inside-out patches

The therapeutic significance of the cation channels produced in inside-out patches is difficult to evaluate at this stage since it is not known if or how DHAVM moves across lipid bilayers. DHAVM may act via the inner membrane and bind with and open non-selective cation channels in the membrane. Alternatively DHAVM may act via the inner membrane as a pore-former to produce the channel itself.

Activation of the cation channel in intact cell preparations could produce depolarization and spiking since the relative permeability of Na/K is equal to 0.49. Although no depolarizing effect has been reported in *Ascaris*, Lees & Beadle (1985) have reported that application of DHAVM produces an excitatory effect in addition to an increase in Cl conductance in some cultured insect neurones.

Movement of Ca through the DHAVM cation channel could produce secondary changes as a result of an increase in cytoplasmic Ca. The secondary effects could include activation of Ca-activated Cl channels in *Ascaris* (Thorn & Martin, 1987) or the release of transmitter. Ca-dependent effects of DHAVM reported in other preparations include: a Ca-dependent potentiation of the frog endplate potential and miniature endplate potential frequency (Fritz *et al.*, 1979); release of GABA, dopamine, noradrenaline and acetylcholine from rat brain synaptosomes (Wang & Pong, 1982); and a potentiation of GABA-mediated transmission in rats (Williams & Yarborough, 1979). Some of these results might be explained by DHAVM producing non-selective cation channels. The relationship between the effect of DHAVM on non-selective cation channels and paralysis of the nematode parasites is uncertain.

Conclusion

This study has shown in a nematode parasite preparation that DHAVM is not a GABA agonist or potentiator and that its mode of action may involve the opening of non-GABA-activated Cl channels and non-selective cation channels. The speed of onset of effects is slow.

This work was supported by SERC and Merck, Sharp and Dhome. We thank Dr M. Turner and Dr J.M. Schaeffer for advice and useful discussion.

References

BORMANN, J., HAMILL, O.P. & SAKMANN, B. (1987). Mechanism of anion permeation through channels gated by glycine and γ-aminobutyric acid in mouse cultured spinal neurones. *J. Physiol.*, **385**, 243–286.

BURG, R.W., MILLER, B.M., BAKER, E.E., BIRNBAUM, J., CURRIE, J.A., HARTMAN, R., KONG, Y-L., MONAGHAN, R.L., OLSEN, G., PUTTER, I., TUNAC, J.P., WALLICK, H., STAPLEY, E.O., OIWA, R. & OMURA, S. (1979). Avermectins, new family of potent anthelmintic agents: producing organism and fermentation. *Antimicrob. Agents Chemother.*, **15**, 361–367.

CAMPBELL, W.C. & BENZ, G.W. (1984). Ivermectin: a review of efficacy and safety. *J. Vet. Pharmacol. Ther.*, **7**, 1–16.

DUCE, I.R. & SCOTT, R.H. (1985). Actions of Dihydroavermectin B_{1a} on insect muscle. *Br. J. Pharmacol.*, **85**, 395–401.

EGERTON, J.R., OSTLIND, D.A., BLAIR, L.S., EARY, C.H., SUHAYDA, D., CIFELLI, S., REIK, R.F. & CAMPBELL, W.C. (1979). Avermectins, new family of potent anthelmintic agents: efficacy of the B_{1a} component. *Antimicrob. Agents Chemother.*, **15**, 372–378.

FRITZ, L.C., WANG, C.C. & GORIO, A. (1979). Avermectin B_{1a} irreversibly blocks postsynaptic potentials at the lobser neuromuscular junction by reducing muscle membrane resistance. *Proc. Natl Acad. Sci. U.S.A.*, **76**, 2062–2066.

HILLE, B. (1984). *Ionic Channels of Excitable Membranes.* Sinauer. Sunderland, Massachusetts.

HOLDEN-DYE, L., HEWITT, G.M., WANN, K.T., KROGSGAARD-LARSEN, P. & WALKER, R.J. (1988). Studies involving Avermectin and the 4-aminobutyric acid (GABA) Receptor of *Ascaris suum* muscle. *Pestic. Sci.*, **24**, 231–245.

KASS, I.S., STRETTON, A.O.W. & WANG C.C. (1984). The effects of avermectin and drugs related to acetylcholine and 4-aminobutyric acid on neurotransmission in *Ascaris suum. Molec. Biochem. Parasit.*, **13**, 213–225.

LEES, G. & BEADLE, D.J. (1986). Dihydroavermectin B_1: actions on cultured neurones from insect central nervous system. *Brain Res.*, **366**, 369–372.

LEWIS, C.A. (1979). Ion-concentration dependence of the reversal potential and the single channel conductance of

ion channels at the frog neuromuscular junction. *J. Physiol.*, **286**, 417–445.

MARTIN, R.J. (1980). The effect of γ-aminobutyric acid on the input conductance and membrane potential of *Ascaris* muscle. *Br. J. Pharmacol.*, **71**, 99–106.

MARTIN, R.J. (1985). γ-aminobutyric acid- and piperazine-activated single-channel currents from *Ascaris suum* body muscle. *Br. J. Pharmacol.*, **84**, 445–461.

MARTIN, R.J. & PENNINGTON, A.J. (1988). Effect of dihydroavermectin B_{1a} on Cl single-channel currents in *Ascaris*. *Pestic. Sci.*, **24**, 90–91.

MARTIN, R.J. & PENNINGTON, A.J. (1989). Ivermectin induces cation channels in isolated patches of *Ascaris* muscle. *J. Physiol.*, **410**, 83P.

THORN, P. & MARTIN, R.J. (1987). A high-conductance calcium-dependent chloride channel in *Ascaris suum*. *Q. J. Exp. Physiol.*, **72**, 31–49.

WANG, C.C. & PONG, S.S. (1982). Actions of avermectin B_{1a} on GABA nerves. In *Membranes and Genetic Disease*. ed. Shepard, J.R., Anderson, V.E. & Eatong, J.W., pp. 373–395. New York: Liss.

WRIGHT, D.J. (1986). Biological activity and mode of action of avermectins. In *Neuropharmacology and Pesticide Action*. ed. Ford, M.G., Lunt, G.G., Reay, R.C. & Usherwood, P.N.R. Chichester: Ellis Horwood.

WILLIAMS, M. & YARBOROUGH, F. (1979). Enhancement of *in vitro* binding and some of the pharmacological properties of diazepam by a novel anthelmintic agent, avermectin B_{1a}. *Eur. J. Pharmacol.*, **56**, 273–276.

Received January 18, 1989
Revised May 9, 1989
Accepted June 13, 1989)

J. Parasitol., 76(3), 1990, p. 340–348
© American Society of Parasitologists 1990

SURFACE PROPERTIES OF MEMBRANE VESICLES PREPARED FROM MUSCLE CELLS OF *ASCARIS SUUM*

R. J. Martin, J. R. Kusel*, and A. J. Pennington

Department of Preclinical Veterinary Sciences, Summerhall, R.(D.)S.V.S. University of Edinburgh, Edinburgh, United Kingdom

ABSTRACT: To facilitate biochemical, pharmacological, and biophysical studies on the membrane of the body muscle of *Ascaris suum*, a method for preparing intact vesicles was developed. Vesicles were prepared by incubating a muscle flap preparation with 1 mg/ml collagenase in a saline solution and then washing in saline without enzyme. The vesicles then formed gradually over the next hour as outgrowths of the original surface membrane from the bag region of the muscle. The vesicles were harvested readily by suction using a Pasteur pipette. The structure of the vesicles was examined with the transmission electron microscope. The whole-cell patch-clamp technique showed that the vesicles had a high input resistance and that the membrane was complete. The vesicle membrane was shown to contain Ca-activated Cl channels and gamma-aminobutyric acid-activated Cl channels. The vesicles also were shown to be suitable for fluorescence recovery after photobleaching studies designed to examine lateral and vertical movement of a lipid probe (5-N [octadecanoyl]-aminofluorescein) in the membrane. This probe had a mean lateral diffusion coefficient (D_L) of 8.1 × 10^{-9} cm^2/sec, but only a proportion (68.4%) of the probe was mobile. The latter observation illustrated the nonuniform nature of the membrane. Ivermectin (10^{-7} M) had no effect on D_L or percent recovery. Trypan blue quenching experiments showed that the lipid probe remained in the outer monolayer of the membrane. These observations illustrate the experimental value of the vesicles; they are potentially useful in discerning anthelmintic mode of action and in drug screening.

Many antiparasitic drugs act by altering the properties of target cell membranes. They may act by gating ion channels and thereby altering the electrical resistance of the membrane; piperazine acts in this way on *Ascaris* muscle to open Cl channels (Martin, 1982). Alternatively, they may act on phospholipids forming the membrane bilayer and alter fluidity of the membrane; praziquantel may act in this way and disrupt the organization of target cell membranes by altering phase characteristics (Harder et al., 1988).

Examination of these drug-induced changes is carried out most precisely on exposed membranes that are not covered by overlying layers. The patch-clamp technique can be used to examine the behavior of single ion channels (Hamill et al., 1981), whereas the fluorescence recovery after photobleaching (FRAP) technique can be used to examine the mobility of the phospholipid bilayer (Axelrod et al., 1976; Koppel et al., 1976).

This paper describes the preparation of muscle membrane vesicles from the nematode *Ascaris suum*; we show that patch-clamp and FRAP can be applied to these vesicles.

Received 28 July 1989; revised 20 November 1989; accepted 8 January 1990.

* Department of Biochemistry, University of Glasgow, Glasgow, United Kingdom.

MATERIALS AND METHODS

Preparation of vesicles

Specimens of *A. suum* were collected from the local abattoir at weekly intervals and maintained at 37 C in Locke's solution until required. Muscle flap preparations were produced and mounted cuticle side down in an experimental chamber (Martin, 1980). The preparation was maintained at 37 C in the experimental solution and observed with a dissecting microscope. The experimental solution contained (mM): 105 Na acetate; 35 NaCl; 2 KCl; 2 $MgCl_2$; 2 ascorbic acid; 3 glucose; 10 N-2-hydroxyethylpiperazine-N′-2-ethanesulfonic acid (HEPES), pH 7.2; 1 mg/ml collagenase (Sigma type IA). After 20 min the preparation was washed with a solution with the same composition except that the collagenase had been omitted. The vesicles then formed as outgrowths of the bag region of the muscle over the next 20–30 min. They were harvested by gentle suction using a Pasteur pipette.

Electron microscopy

Vesicles were fixed shortly after collection in 3% glutaraldehyde in 0.1 M Na cacodylate buffer for 1–2 hr, washed in 0.1 M Na cacodylate buffer, postfixed in 1% osmium tetroxide in 0.1 M Na cacodylate buffer, washed in buffer, dehydrated in graded acetone, left in acetone/Araldite overnight, and then embedded in Araldite. Thin sections (60 nm) were stained with saturated uranyl acetate in 50% ethanol and with Reynolds' lead citrate. Sections were viewed with a Philips 400 transmission electron microscope.

Patch-clamp recordings

Cell-attached and whole-cell recordings were obtained from the vesicle using conventional techniques (Hamill et al., 1981). The vesicles were mounted in an experimental chamber at room temperature (18–22 C)

and viewed using phase-contrast microscopy. The extracellular solution was as described above, but in the cell-attached patch experiments 5 mM $CaCl_2$ was added to activate high-conductance Cl channels (Thorn and Martin, 1987). Patch electrodes for cell-attached patches and for the whole-cell clamp were filled with (mM): 140 CsCl; 10 HEPES; 11 ethyleneglycol-bis(beta-aminoethyl ether) N,N,N′,N′-tetraacetic acid; 1 $CaCl_2$; pH 7.2 with CsOH. Currents were recorded using a List EPC 7 amplifier. It was possible also to make isolated inside-out and outside-out patches from the vesicles, but these were not used in this study.

FRAP technique

The vesicles were labeled with 5-N (octadecanoyl)-aminofluorescein ([^{18}C]Fl) by incubating the flap preparation during the collagenase treatment (20 min) in experimental solution to which was added 10 μg of the probe in 5 μl ethanol for every ml of experimental solution. The preparation was then washed thoroughly to remove the collagenase and excess [^{18}C]Fl. The vesicles then were harvested as before and mounted on a glass slide in a shallow pool confined by a square of silicone grease and covered with a glass coverslip.

Measurements of 2-dimensional lateral diffusion of the lipid fluorescent probe were made using the FRAP technique (Axelrod et al., 1976; Foley et al., 1986) and a laser–microscope combination (Garland, 1981). A low-powered water-cooled argon laser (Lexel model 85; 100 mW all lines maximum power) and a 40× objective were used throughout. The $1/e^2$ radius of the focused laser spot was 1–1.2 μM at the sample. The recovery times (D_L values) and percent recovery were calculated by a nonlinear least squares fit to equation 12 of Axelrod et al. (1976). Experimental data were collected using a Hewlett-Packard Model 85 microcomputer connected to the fluorescence measuring electronics.

Ivermectin (10^{-7} M) carried in 0.1% ethanol in the extracellular bathing Ringer's solution was prepared by diluting Ivomec (MSD AGVET, Hoddesdon). It was used to examine its effect on D_L and percent recovery by comparing control values from vesicles in the absence of ivermectin (but with 0.1% alcohol) and then after 10–60 min following addition of the drug to the vesicles.

The depth of the insertion of the fluorescent probe in the membrane was determined by measuring Foster resonance energy transfer quenching by the nonpermeant molecule trypan blue used at a concentration of 0.25% (Foley et al., 1986). Thus, if trypan blue quenched all the fluorescence from the probe, the probe was present only in the outer phospholipid monolayer with little translocation of the probe taking place between the inner and outer monolayers.

RESULTS

Preparation of the vesicles

Figure 1A shows the dorsal and ventral halves of an *A. suum* flap preparation pinned out into an experimental chamber and treated with collagenase. The mass of circular bodies that can be seen are the bag region of the somatic muscle cells. The contractile spindle region of the muscle cell lies under the bags and is not visible. A photomicrograph of the edge of the preparation (Fig. 1B) shows the formation of vesicles as outgrowths of the bag. The vesicles also form on the bags from the rest of the preparation but are not so easily seen as those formed at the edge. The number and size of the vesicles that were present increased with time.

Figure 1C shows a vesicle that has been harvested and viewed using phase-contrast microscopy. The vesicles were spherical and ranged in diameter from 5.1 μm to 116.2 μm (mean of 55 vesicles, 31.8 μm; median, 35.5 μm; SD, 19.4 μm).

Electron microscopy

Vesicles were formed as outgrowths of the muscle cell bag region; it is therefore expected that their structure reflects that of the parent bag. Rosenbluth (1965) examined the ultrastructure of *Ascaris lumbricoides* muscle bags and described them as large homogenous sacs packed with a central mass of discrete glycogen granules. These glycogen granules are extremely dense in lead-stained sections but are not membrane bound. The glycogen granules extend nearly to the plasma membrane. In the cortical region under the plasma membrane there is a row of mitochondria that contain few cristae. The plasma membrane is illustrated by Rosenbluth (1965) as being convoluted and covered by an extracellular matrix and another membrane. The structure of the vesicles as seen with transmission electron microscopy is illustrated in Figure 2.

It can be seen that the plasma membrane of a typical vesicle is smooth (Fig. 2), with no overlying extracellular matrix or other membrane. In the center of the vesicles there was a large granular electron-dense mass similar in structure to that produced by the glycogen found in the normal bags (Fig. 2A). The cortex of the vesicle was homogenous and contained only a few mitochondria or other organelles (Fig. 2B).

An interesting feature of most vesicles was the presence of a stalk that presumably represented the original region of contact between the bag and vesicle during formation. The cortical region of the vesicle was narrower in this region so that the mass of glycogen approached the plasma membrane at the location of the stalk. The plasma membrane appeared continuous at the stalk, as elsewhere, suggesting that the electrical resis-

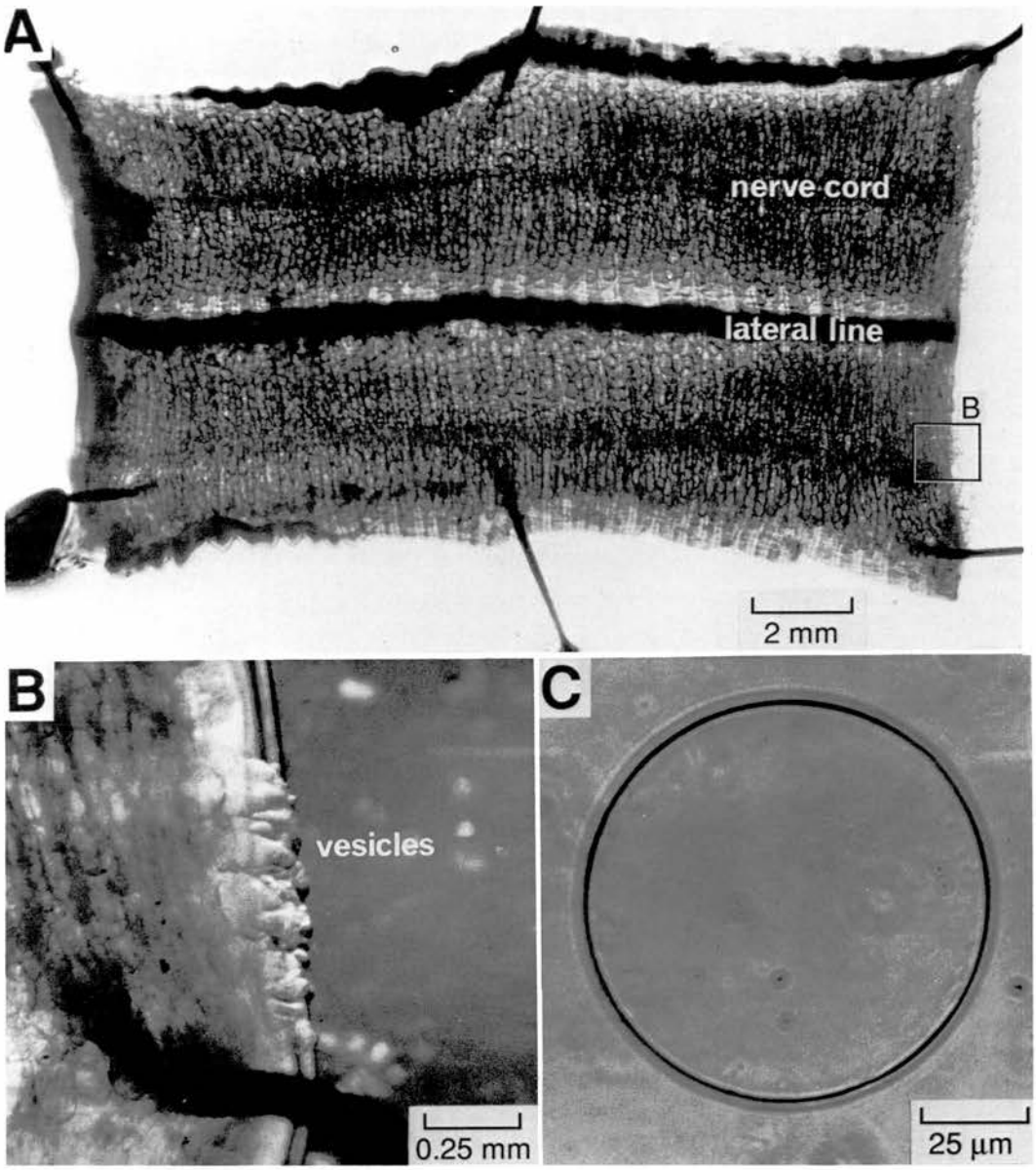


FIGURE 1. Preparation of vesicles from the flap preparation. **A.** *Ascaris* flap preparation made from an anterior section of *Ascaris suum*. The dorsal and ventral body wall are pinned out onto Sylgard after cutting the parasite along 1 lateral line and eviscerating the preparation. **B.** The formation of vesicles. These develop after collagenase treatment (1 mg/ml) as outgrowths of the muscle cell bag and are seen more easily at the edge of the preparation. **C.** A single large vesicle after harvesting and viewed using phase-contrast microscopy.

tance between the inside and outside of the vesicle would be found to be high.

Electrical properties of vesicles

The integrity of the vesicle cell membrane was assessed by making recordings from the whole vesicle using the whole-cell voltage-clamp technique. Whole-cell voltage-clamp records were made (at 18–22 C) from the vesicle in the conventional manner. Estimates of the membrane potential from the 0 current level showed that in freshly harvested vesicles the membrane potential was around −15 mV. The membrane potential of vesicles prepared for more than 2 hr

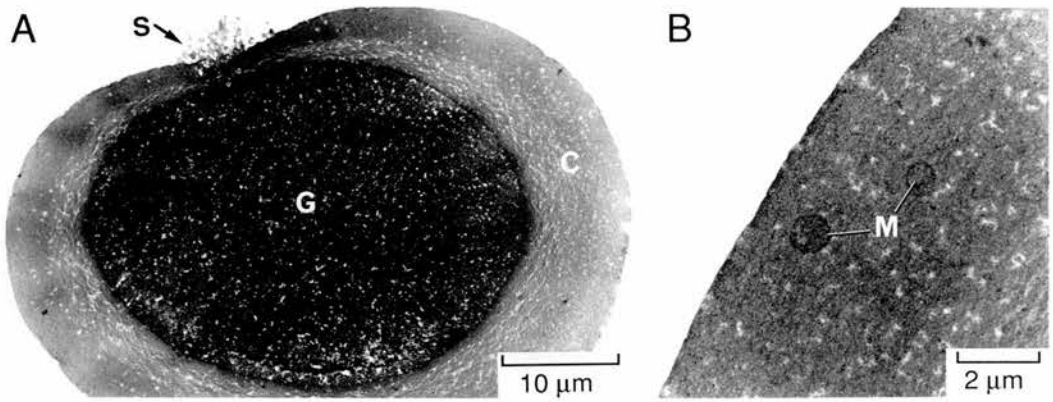


FIGURE 2. Transmission electron micrographs of vesicles. **A.** Section through the middle of a vesicle showing the central glycogen core (G), the surrounding cortex (C), and the stalk (S) that marks the former attachment site of the vesicle to the bag. **B.** Smooth surface membrane of a vesicle showing no overlying matrix. Mitochondria (M).

was near 0 mV. All estimates of membrane potential gave values less than −35 mV, the typical membrane potential of *A. suum* muscle (Martin, 1980). The low resting potential of vesicles is like that seen in collagenase-treated flap preparations; it may be explained by suppression (at 18–22 C) of an active transport mechanism that normally maintains the membrane potential (Martin, 1985). Subsequently, in this paper it is assumed that the membrane potential of the vesicle approximates to 0 mV.

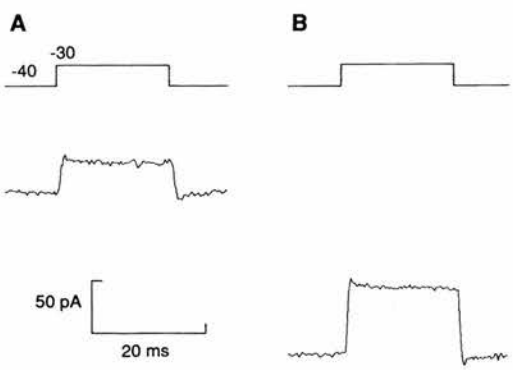


FIGURE 3. Whole-cell voltage clamp records from a vesicle showing the high-input resistance and effect of 10 μM GABA. **A.** The vesicle was held at a potential of −40 mV and stepped to −30 mV for 20 msec; the lower trace shows the current response, and the top trace shows the membrane potential. A voltage step of 10 mV associated with a current pulse of 33 pA shows that the input resistance of the vesicle was 3.0 GΩ. **B.** Ten μM GABA produces an inward current of 152 pA at −40 mV that is shown by the downward movement of the current trace. The current pulse associated with the voltage pulse increased in size to 75 pA, showing that GABA had reduced the input resistance of the vesicle to 1.3 GΩ.

Figure 3A shows a whole-cell clamp current record of a vesicle held at −40 mV and stepped to −30 mV for 20 msec. The current response, corrected for capacitance of the pipette and vesicle, allows a direct measure of the input resistance of the vesicle. Because a current of 33 pA was required to depolarize the cell by 10 mV, it allows an estimate of 3.0 GΩ as the input resistance of the vesicle. This is what would be expected if the membrane had sealed, forming a vesicle in which the inside is electrically isolated from the outside.

Gamma-aminobutyric acid (GABA)-activated currents using the whole-cell clamp

The effect of application of 10 μM GABA, an inhibitory transmitter in *A. suum* that increases Cl conductance of the bag membrane by gating channels (Martin, 1980, 1982), is shown in Figure 3B. It can be seen that GABA caused an inward (downward) current to flow at −40 mV and an increase in membrane conductance, shown as an increase in the size of the current pulse associated with the depolarizing step. The direction of the steady GABA-induced current is inward because the negatively charged Cl ions leave the vesicle under the influence of the potential and concentration gradient. The calculated Nernst Cl potential under these recording conditions was +27 mV; it is assumed that the contents of the patch pipette equilibrate with the intracellular

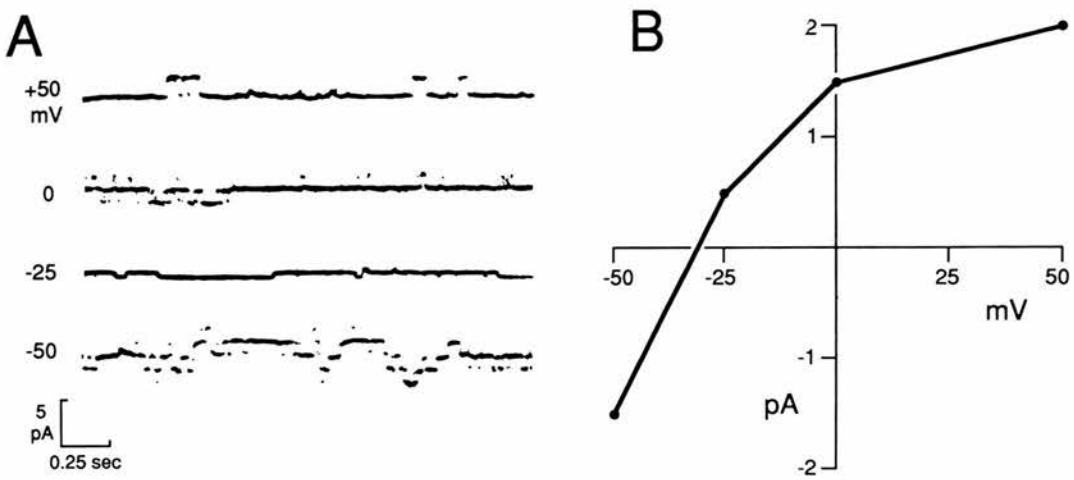


FIGURE 4. Cell-attached patch records showing Ca-activated Cl channels. **A.** Single-channel records at different trans-patch potentials. The resting membrane potential of the vesicle was assumed to be 0 mV, so that the trans-patch potential was determined by the pipette potential but had the opposite polarity (i.e., a pipette potential of −50 mV produced a trans-patch potential of +50 mV). **B.** I/V relationship of the channel currents. Ordinate, amplitude of the single-channel current; abscissa, trans-patch potential. The channel currents reduce in amplitude and reverse as the trans-patch potential approaches a reversal potential of −27 mV. The channels show characteristic rectification and have maximum slope conductances of 80 pS.

contents of the vesicle and increase the Cl concentration above the extracellular concentration of the bath.

Ca-activated Cl channels in cell-attached patches

In *A. suum* muscle membrane high conductance Cl channels are found that are activated by micromolar concentrations of Ca on the cytosolic side of the membrane (Thorn and Martin, 1987). These channels may also be activated after a delay if Ca is present in millimolar concentrations in the bath; it is presumed that Ca crosses the membrane and increases the cytosolic concentration. Figure 4 shows cell-attached patch recordings from a vesicle with 5 mM Ca present in the bath; it shows at different trans-patch potentials the large Ca-activated Cl channels that often were seen in vesicle patches with 5 mM Ca in the bath. The channel currents reversed their polarity near a trans-patch potential of −27 mV. The polarity of the reversal potential contrasts with that in the above section because the patch pipette containing the higher Cl is on the outside membrane, not inside as before. The slope of the channel I/V plot (Fig. 4B) at its steepest point was 80 pS; the plot showed characteristic rectification with less current being carried when the patch was depolarized. In addition, the probability of the channel opening decreased as the patch was depolarized. The behavior of these channels in the vesicle was comparable to that seen in the intact bag.

Lateral diffusion of membrane lipids seen by FRAP experiments

Figure 5 illustrates data from a typical FRAP experiment. It illustrates the fluorescence intensity of a membrane spot before and after photobleaching. The computer-generated least squares fit for the best value for D_L also is shown. The fluorescence was monitored continuously from a 1.2-μm-radius area illuminated by the laser focused on the vesicle membrane under study. The steady level of fluorescence was monitored and then the spot was bleached by increasing the power of the laser by 10^4 for 0.1 sec at time 0. The high intensity laser pulse bleaches approximately half the fluorescent molecules in the membrane on which the laser is focused. After bleaching, the spot gradually recovers its fluorescence as unbleached molecules in the surrounding membrane move into the bleached area. D_L was then calculated from the kinetics of the recovery (Axelrod et al., 1976). In an idealized bilayer, D_L for [^{18}C]Fl is expected to be 10^{-8} cm^2/sec, whereas the recovery is expected to be 100% (Cherry, 1979).

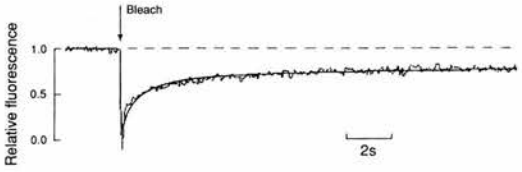


FIGURE 5. Fluorescence recovery after photobleaching (FRAP) curve for [^{18}C]Fl in the vesicle. The observed fluorescence intensity has been plotted after normalization to a prebleach intensity of 1.0 arbitrary units on the ordinate. The bleach pulse was applied at the vertical arrow. The smooth curve is the nonlinear least squares fit to the data. D_L, 7 × 10^{-9} cm²/sec; percent recovery, 68%.

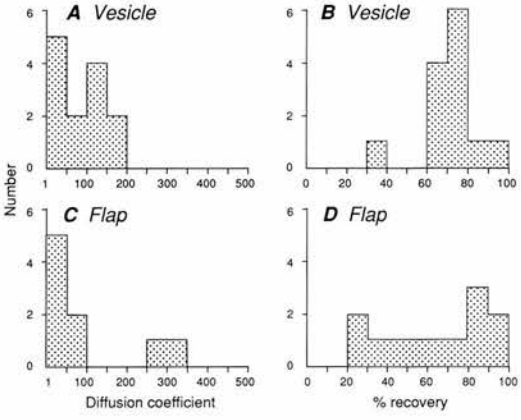


FIGURE 6. Histograms of the estimated D_L and percent recovery values in vesicles and a flap preparation. **A.** D_L values from 13 vesicles: mean ± SD, 8.1 ± 5.6 × 10^{-9} cm²/sec. **B.** Percent recovery values from the same 13 vesicles: mean ± SD, 68 ± 8%. **C.** D_L values from 10 bag cells from flap preparation (no collagenase): mean ± SD, 8.7 ± 11 × 10^{-9} cm²/sec. **D.** Percent recovery values from the same 10 bag cells: mean ± SD, 81 ± 5%.

Figure 6A, B shows representative histograms of the estimates of D_L and percent recovery from vesicles from a single flap preparation. Vesicles from other preparations showed similar properties. The mean D_L value was 8.1 × 10^{-9} cm²/sec, but there was considerable variation between vesicles with the observed range between 2.0 and 20.6 × 10^{-9} cm²/sec. In this series of experiments single observations were made on each vesicle; the large variation between vesicles suggests that the vesicles are not a homogenous population and that the properties of individual vesicles vary. This was confirmed in a further series of experiments using paired observations on each vesicle; it was found that the variability between vesicles was greater than within vesicles.

The percent recovery was estimated using a computer to fit the theoretical curve and to estimate the percent recovery at infinite time. The mean recovery was 68.4% (range 60–94%) so that 31.6% of the fluorescence on average was unable to diffuse laterally (this is the immobile fraction in the 1-μM spot over the time scale of the experiment). The less than 100% recovery shows that the membrane of individual vesicles is not homogenous.

It was of interest to determine if the process of vesicle formation increased the diffusion coefficient (perhaps by breaking down cytoskeletal structures of the cell). FRAP studies were therefore carried out on the muscle bag region using an intact flap preparation. The probe [^{18}C]Fl was applied for 20 min to the preparation (without collagenase), which was washed thoroughly in buffer before the FRAP study. Figure 6C, D shows histograms of the D_L values and the percent recovery estimates. These results show the large variation in values obtained from both preparations; there was no significant difference between values from the bag region of the muscle in the intact flap preparation and the vesicle.

Effect of ivermectin on lateral diffusion and percent recovery

Ivermectin is a wide-spectrum anthelmintic with an action against *A. suum* and can open Cl channels in *A. suum* muscle membrane (Martin and Pennington, 1989). It was of interest to determine if part of this effect was related to an action on membrane fluidity; an alteration in membrane fluidity may affect physically the opening or closing of proteins that form the transmembrane ion channels. Experiments were therefore carried out to determine if ivermectin had an action on lateral diffusion or percent recovery.

Ivermectin (10^{-7} M) was found to have no significant effect on either lateral diffusion or percent recovery. For example, in 1 representative group of 5 vesicles, the control D_L was 15.9 ± 4.7 × 10^{-9} cm²/sec (mean ± SD) and the control percent recovery was 76.5 ± 5.9 (mean ± SD). In these same vesicles after addition of ivermectin, D_L was 16.2 ± 5.0 × 10^{-9} cm²/sec (mean ± SD) and the percent recovery was 73.9 ± 2.1 (mean ± SD). The control solutions contained 0.1% ethanol as did the ivermectin solutions. Ivermectin produced no significant effect on D_L or percent recovery in other vesicles examined.

Vertical distribution of lipid probe from trypan blue quenching

The lipid probe incorporated in the vesicle membrane could be located in the outer phospholipid monolayer or be distributed equally between the monolayers as a result of movement of phospholipids or their markers moving between the 2 layers. To explore the vertical distribution of the lipid probe, we used trypan blue as a nonpermeant quencher of fluorescein on the outer membrane. The absorption spectrum of trypan blue overlaps that of the lipid probe (Foley et al., 1986) used here: the energy transfer efficiency from the emission spectrum of [^{18}C]Fl to the absorption spectrum of trypan blue is 50% at a distance of 4 nm; it decreases rapidly at greater distances and is negligible at distances comparable to the thickness of the membrane (9 nm). Only those probes that have fluorescent lipids on the external membrane could be quenched by trypan blue; it is only when the fluorescent head group is located in the outer polar region that quenching is seen. This interpretation is valid only if trypan blue does not enter the vesicle: observation showed that trypan blue only entered a few (probably damaged) vesicles; these were excluded from the study.

Figure 7 is a histogram of the fluorescence levels observed in vesicles in the absence and then the presence of 0.25% trypan blue. The vesicles for this experiment were collected from the same flap. Eleven vesicles were used to measure the control relative fluorescence, and a separate 11 vesicles from the same flap preparation were used to estimate the level of quenching by trypan blue. The histogram shows that trypan blue quenches almost completely; it reduced the relative fluorescence from a mean of 603 units to 52 units. This corresponds to a reduction to 9% of the control. Because 50% quenching would indicate that [^{18}C]Fl was distributed equally in the membrane, we conclude that the lipid probe is almost completely located in the outer membrane of the vesicle and does not gain access to the inner membrane over the time scale (1 hr) of the experiment.

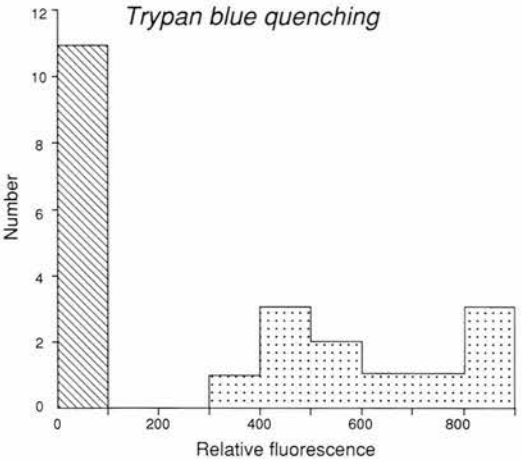


FIGURE 7. Histogram of the effect of trypan blue on relative fluorescence of [^{18}C]Fl in the membrane. The shaded area represents the fluorescence (mean ± SD, 52 ± 20 units) in the presence of trypan blue. The stippled area represents the control fluorescence (mean ± SD, 603 ± 183 units). Eleven unpaired vesicles from the same flap preparation were used, and values were corrected for autofluorescence, background and dark current. Trypan blue reduced the fluorescence to 9% of the control.

DISCUSSION

Formation of the vesicles

We have described in this paper a method of preparing isolated vesicles from the muscle of a parasitic nematode. The electrically isolated vesicles form under collagenase treatment as outgrowths of the bag membrane, but the mechanism of vesicle formation is not certain. Collagenase may act by producing small punctures in the extracellular matrix covering the bag membrane; the bag membrane then appears to blow out through the punctures under the influence of a high intracellular pressure. This explanation for vesicle formation is consistent with the gradual increase in vesicle size with time and the presence of the stalk that acts like the neck of a balloon.

FRAP observations

The results of the trypan blue study presented here show that over the time scale of the experiment (1 hr), the [^{18}C]Fl did not flip-flop into the inner monolayer of the vesicle membrane. Thus, all lateral diffusion data are relevant to the outer monolayer.

The lipid probe [^{18}C]Fl had a mean lateral diffusion coefficient of 8.1×10^{-9} cm^2/sec, but this varied greatly between the muscle vesicles. In artificial bilayers and some eucaryotic cell membranes, the D_L value for this probe is about 10×10^{-9} cm^2/sec. The schistosome surface membrane (Foley et al., 1986) yields a value for lipid diffusion similar to that seen in *A. suum* vesicles.

The percent recovery of [^{18}C]Fl shows that ap-

proximately 70% is inserted in regions of the membrane in which it can diffuse. The recovery curve never proceeds to completion because the probe cannot diffuse laterally into approximately 30% of the membrane; such regions have been called domains and represent regions of immobile lipid (Wolf et al., 1981). This immobile lipid may have a special lipid composition or may be in contact with the cytoskeleton. The percent recovery seen in artificial membranes is near 100% and contrasts with that seen in real membranes. It is evident that the vesicle membrane is not homogenous and that variation occurs within as well as between vesicles.

Effect of vesicle formation on lateral diffusion

The formation of vesicles from the bag muscle might have led to the alteration of diffusion: vesicle formation with the disruption of cytoskeletal networks has been reported (Tank et al., 1982) to increase protein lateral diffusion but not lipid diffusion in mammalian muscle vesicles; in *Schistosoma mansoni,* vesicle formation from the surface membrane resulted in an increase in the lateral diffusion of 1 lipid probe but not the [^{18}C]Fl probe as used here (Foley et al., 1986). However, in our study there was no change in the mean value of the estimates for lateral diffusion obtained from untreated flaps or vesicle preparations of *A. suum*; this result may be explained if cytoskeletal networks do not affect lipid lateral diffusion in this preparation.

FRAP studies in other nematodes

FRAP studies have been carried out only on the external epicuticle surface of other nematodes (Kennedy, Foley, Knox et al., 1987; Kennedy, Foley, Kuo et al., 1987); no study has been made of any nematode cellular membrane previously. The surface of parasitic nematodes in most species is highly restricted with percent recoveries of less than 20% and D_L values of 6.5 $\times$ 10^{-10} cm^2/sec being observed. This is consistent with the putative acellular glycocalyx structure of the epicuticle that guards against the external environment. The muscle cell membrane as observed here is more mobile and less restricted than the epicuticle.

Predicted movements of lipid-soluble anthelmintics in the membrane

Theoretical predictions (Saffman and Dellbruck, 1975) suggest that the size of the diffusing molecule has little effect on the speed of lateral movement in the membrane. This means that other lipid-soluble molecules could move at a rate similar to [^{18}C]Fl in the membrane. From this it is possible to estimate the rate of movement of lipid-soluble anthelmintics (e.g., ivermectin) in the membrane. In 2 dimensions (i.e., in the membrane) the displacement due to diffusion is given by: $x = (4D_Lt)^{1/2}$, where x is the average displacement of a single molecule after time t, and D_L is the lateral diffusion rate. If D_L is taken as 8×10^{-9} cm^2/sec, then in 1 sec an anthelmintic molecule dissolved in the membrane would move on average 1.8 μm, and in 100 sec it would move 18 μm. It seems possible that the slow onset of action of ivermectin in isolated tissues (Duce and Scott, 1985) and *A. suum* muscle membrane (Martin and Pennington, 1989) may arise from the slow movement of the drug. However, the prediction is valid only if the lipid probe used here to measure lateral diffusion diffuses in the same domains and at the same rate as ivermectin; this remains to be tested.

The trypan blue quenching experiments showed that there was little movement of the probe between the outer monolayer and the inner monolayer of the membrane. If lipid-soluble anthelmintics behave in the same way, it is expected that their effects will be related to the membrane surface to which they are applied. It has been reported that ivermectin only activates Cl channels when applied to the outer monolayer of a patch membrane but has no such effect when applied to the inner monolayer of the membrane (Zufall et al., 1989).

Potential usefulness of the vesicles

We have described here a technique for making isolated muscle membrane vesicles from the parasite *A. suum* and have shown that the membranes of these vesicles may be examined with patch-clamp or FRAP techniques. Anthelmintics that produce electrophysiological or membrane mobility changes in muscle could be studied using these vesicles to elucidate their mode of action. The vesicles may prove useful in the future for drug screening.

ACKNOWLEDGMENTS

We are pleased to acknowledge Merck, Sharpe and Dohme (U.S.A.), SERC (U.K.), and the Wellcome Trust (U.K.) for their grants to R.J.M. and J.R.K.; their generous support allowed this study to be carried out.

LITERATURE CITED

AXELROD, D., D. E. KOPPEL, J. SCHLESSINGER, J. ELSON, AND W. W. WEBB. 1976. Mobility measurement by analysis of fluorescence photobleaching recovery kinetics. Biophysics Journal **16:** 1055–1069.

CHERRY, R. J. 1979. Rotational and lateral diffusion of membrane proteins. Biochimica et Biophysica Acta **559:** 289–327.

DUCE, I. R., AND R. H. SCOTT. 1985. Actions of dihydroavermectin B_{1a} on insect muscle. British Journal of Pharmacology **85:** 395–401.

FOLEY, M., A. N. MACGREGOR, J. R. KUSEL, P. B. GARLAND, T. DOWNIE, AND I. MOORE. 1986. The lateral diffusion of lipid probes in the surface of *Schistosoma mansoni*. Journal of Cell Biology **103:** 807–818.

GARLAND, P. B. 1981. Fluorescence photobleaching recovery: Control of laser intensities with an acousto-optic modulator. Biophysics Journal **33:** 481–482.

HAMILL, O. P., A. MARTY, E. NEHER, B. SAKMANN, AND F. J. SIGWORTH. 1981. Improved patch-clamp techniques for high-resolution current recording from cells and cell-free membrane patches. Pflugers Archiv geshern Physiologie **391:** 85–100.

HARDER, A., J. GOOSENS, AND P. ANDREWS. 1988. Influence of praziquantel and Ca^{2+} on the bilayer–isotropic–hexagonal transition of model membranes. Molecular and Biochemical Parasitology **29:** 55–60.

KENNEDY, M. W., M. FOLEY, K. KNOX, W. HARNETT, M. J. WORMS, J. R. KUSEL, J. BIRMINGHAM, AND P. B. GARLAND. 1987. Are the biophysical properties of the surface lipid of filariae different from other parasitic nematodes? *In* Molecular paradigms for eradicating helminth parasites, A. J. MacInnis (ed.). Alan R. Liss, Inc., New York, p. 289–300.

———, ———, Y.-M. KUO, J. R. KUSEL, AND P. B. GARLAND. 1987. Biophysical properties of the surface lipid of parasitic nematodes. Molecular and Biochemical Parasitology **22:** 233–240.

KOPPEL, D. E., D. AXELROD, J. SCHLESSINGER, E. L. ELSON, AND W. W. WEBB. 1976. Dynamics of fluorescent marker concentration as a probe of mobility. Biophysics Journal **16:** 1315–1329.

MARTIN, R. J. 1980. The effect of γ-aminobutyric acid on the input conductance and membrane potential of *Ascaris* muscle. British Journal of Pharmacology **71:** 99–106.

———. 1982. Electrophysiological effects of piperazine and diethylcarbamazine on *Ascaris suum* somatic muscle. British Journal of Pharmacology **77:** 255–265.

———. 1985. γ-aminobutyric acid- and piperazine-activated single channel currents from *Ascaris suum* body muscle. British Journal of Pharmacology **84:** 445–461.

———, AND A. J. PENNINGTON. 1989. A patch-clamp study of effects of dihydroavermectin on *Ascaris* muscle. British Journal of Pharmacology **98:** 747–756.

ROSENBLUTH, J. 1965. Ultrastructure of *Ascaris lumbricoides* 2. Intermuscular junctions, neuromuscular junctions and glycogen stores. Journal of Cell Biology **26:** 579–591.

SAFFMAN, P. G., AND M. DELLBRUCK. 1975. Brownian motion in biological membranes. Proceedings of the National Academy of Sciences USA **72:** 3111–3113.

TANK, D. W., E.-S. WU, AND W. W. WEBB. 1982. Enhanced molecular diffusability in muscle membrane blebs: Release of lateral constraints. Journal of Cell Biology **92:** 207–212.

THORN, P., AND R. J. MARTIN. 1987. A high-conductance calcium-dependent chloride channel in *Ascaris suum* muscle. Quarterly Journal of Experimental Physiology **72:** 31–49.

WOLF, D. E., W. KINSEY, W. LENNARZ, AND M. EDIDIN. 1981. Changes in the organization of sea urchin egg plasma membrane upon fertilization indications from lateral diffusion rates of lipid soluble fluorescent dyes. Developmental Biology **18:** 133–138.

ZUFALL, F., C. FRANKE, AND H. HATT. 1989. The insecticide avermectin B_{1a} activates a chloride channel in crayfish muscle membrane. Journal of Experimental Biology **142:** 191–205.

Parasitol Res (1992) 78:341–348

Parasitology Research

© Springer-Verlag 1992

Distribution of a fluorescent ivermectin probe, bodipy ivermectin, in tissues of the nematode parasite *Ascaris suum*

R.J. Martin [1], J.R. Kusel [2], S.J. Robertson [1], A. Minta [3], and R.P. Haugland [3]

[1] Department of Preclinical Veterinary Sciences, R.(D.) S.V.S. Summerhall, University of Edinburgh, Edinburgh EH9 1QH, UK
[2] Department of Biochemistry, University of Glasgow, Glasgow, UK
[3] Molecular Probes, Eugene, OR, USA

Accepted January 15, 1991

Abstract. A fluorescent derivative of the anthelmintic ivermectin (4″-5,7-dimethyl bodipy proprionylivermectin, referred to hereafter as bodipy ivermectin) was synthesized for an investigation of the distribution of avermectins. Injected into adult *Ascaris suum* at doses greater than 0.1 µg per worm, it produced a dose-dependent immobilization. Fluorescent microscopy of frozen sections revealed the distribution of the probe in the whole nematode. Staining of collagenase-isolated muscle cells was studied using bath application of bodipy ivermectin. The trypan-blue quenching technique showed that the ivermectin probe was located in the outer monolayer of the muscle membrane. The cytoplasm was not stained. The interpretation of these observations is discussed in view of the known lipophilic nature of avermectins. Staining of the muscle membrane and nerve cord is consistent with the view that avermectins act at these sites. The significance of the hypodermal and lateral line staining is also discussed.

Avermectins are a family of highly lipophilic macrocyclic lactones derived from *Streptomyces avermitilis* (Burg et al. 1979). They show biological activity against parasitic nematodes and insects but not against tapeworms, flukes, or the parasite hosts (for a review see Cambell and Benz 1984). The mode of action of avermectins has been the subject of a number of studies (Fritz et al. 1979; Mellin et al. 1983; Duce and Scott 1985; Martin and Pennington 1989), which show that avermectins depress motor activity by increasing muscle-membrane Cl permeability. In a patch-clamp study on *Ascaris* muscle membrane (Martin and Pennington 1989), 22,23-dihydroavermectin B1a produced the opening of non-γ-aminobutyric acid-activated 9-15pS Cl channels following its application at low (100 pM) concentrations to the outside surface of membrane patches. In addition to their action on muscle membranes in *Ascaris*, it has also been suggested that avermectins have an inhibitory action in the nerve cord (Kass et al. 1984).

For the further investigation of the mode of action of avermectins, a fluorescent derivative of dihydroavermectin B1a (bodipy ivermectin) was prepared and its distribution in tissues of adult *Ascaris* was observed. This report describes these experiments, which showed that the fluorescent probe is active and accumulates in muscle membranes and within the nerve cord; the latter two observations are consistent with an action of avermectins in muscle and nerve-cord membranes.

Materials and methods

Collection and maintainance of Ascaris suum

Specimens of *A. suum* were collected from the local abattoir at weekly intervals and were maintained at 37° C in Locke's solution until required. The Locke's solution was changed daily.

Injection technique

The injection solution contained 105 mM Na acetate, 35 mM NaCl, 2 mM KCl, 2 mM $MgCl_2$, 3 mM glucose, 10 mM HEPES, and 2% Tween-80 (pH 7.2). In all, 100 µl of the solution (containing 1 µg bodipy ivermectin) was injected using a fine 25-gauge needle. The injection site was the peri-enteric space of adult *A. suum* at 5 cm from the anterior end. The 2% Tween-80 was used as an inert carrier for the extremely lipophilic bodipy ivermectin; dimethylsulfoxide (DMSO) was not used since it acts as a "sorption promoter" and can increase the membrane penetration of large molecules; this effect could have distorted the distribution of bodipy ivermectin. The parasites were then maintained in Locke's solution at 37° C and their motility was assessed after 24 h. Control injections had no effect.

Histology

Cylindrical sections were taken at 1-cm intervals from the injection site and then mounted onto cork blocks attached to metal chucks using water frozen with dichlorodifluoromethane freezer spray.

Reprint requests to: R.J. Martin

Transverse sections measuring 30 μm in thickness were cut with a Bright OFT/AS cryostat and mounted on glass slides using phosphate buffer and glass coverslips. The sections were viewed on a Leitz Ortholux fluorescent microscope using a fluorescein isothiocyanate (FITC) filter. Photographs were taken with TRI X 400 ASA black and white film.

Preparation of muscle vescicles, isolated muscle cells, and cuticle and hypodermal flap

Muscle vesicles were prepared from the flap preparation using the brief collagenase treatment technique previously described by Martin et al. (1990) and were maintained at 37° C in experimental solution, which had the same composition as the injection solution except that the Tween-80 had been omitted. The vesicles were divided into groups, one of which was preincubated with 100 ng dihydroavermectin B1a/ml for 1 h. This was followed by the addition of 1- to 100-ng/ml concentrations of bodipy ivermectin to both groups of vesicles and incubation for a further 45 min. The two groups of vesicles were washed in experimental solution. All of these solutions contained a final concentration of 0.1% ethanol as a carrier. The vesicles were mounted on glass slides in wells formed by silicone grease and were covered with glass coverslips for quantitation of the fluorescence.

The method used to prepare isolated muscle cells has been described elsewhere (Johnson and Stretton 1985). Cotton thread was used to tie off anterior regions of the *Ascaris*; the sections had the appearance of a short chain sausages. The sections were injected with experimental solution containing 4 mg collagenase/ml (Sigma Type I). These injected parasites were incubated for 2 h at 37° C in Locke's solution. At the end of this period, 2-cm cylindrical sections were taken, cut along one lateral line, and pinned out onto Sylgard. Gentle perfusion of the flap preparation with experimental solution produced separation of the muscle cells from the remaining flap. The isolated muscle cells were collected in a Pasteur pipette, placed in 3.5-cm petri dishes, and bathed in bodipy ivermectin at 1 μg/ml for 1 h. The flap preparation, now devoid of muscle cells, was bathed in bodipy ivermectin at 1 μg/ml for 1 h. The flap preparation and the isolated muscle cells were washed in experimental solution, mounted on glass slides in wells formed by silicone grease, and covered with glass coverslips.

Quantitation of the level of fluorescence

The level of fluorescence was quantitated using a laser-microscope combination (Garland 1981) consisting of a low-power water-cooled argon laser (Lexel model 85) and a 40× objective. The $1/e^2$ radius of the focused spot was 1–1.2 μm on the membrane. A Hewlett-Packard Model 85 microcomputer connected to the fluorescence-measuring devices was used to determine mean levels of fluorescence; this approach proved to be satisfactory for small numbers of vesicles.

Trypan-blue quenching

The depth of insertion of the bodipy ivermectin into the muscle membrane was determined by measuring the Foster resonance energy-transfer quenching by the nonpermeant molecule trypan blue used at a concentration of 0.25% (Foley et al. 1986). The technique predicts that if trypan blue quenches all of the fluorescence from bodipy ivermectin, the probe is present only in the outer phospholipid monolayer, with little translocation occurring between the inner and the outer monolayer.

Preparation of bodipy ivermectin

The fluorescent ivermectin derivative (Fig. 1) was prepared with the aim of attemting to follow the disposition of an avermectin in *A. suum*. Structure-activity studies (for a review see Fisher and Mrozik 1984) have shown that the active site of the avermectins lies within the area of the macrocyclic lactone ring and spiroacetal subunit; the oleandrosyl disaccharide substituent is not essential for biological activity since the aglycone is active. Substitution at the 4″-position does not abolish the biological activity (Schaeffer et al. 1989). A fluorescent bodipy ivermectin derivative was therefore prepared from 22,23-dihydroavermectin B1a.

The fluorescent derivative of ivermectin was synthesized using a modification of the method for preparing the luminol derivative of avermectin (Schaeffer et al. 1989). The key intermediate is a 4″-*O*-22,23-dihydroavermectin B1a monoester of succinic acid (Mrozik et al. 1982). The succinic acid was activated as its succinimidyl ester by treatment with dicyclohexylcarbodiimide and *N*-hydroxysuccinide in dimethylformamide solution as described by Schaeffer et al. (1989) and then condensed directly with *N*-[(4,4-difluoro-4-boro-3a,4a-diaza-*s*-indacene)proprionyl]ethylenediamene (bodipy ethylenediamene). Following precipitation with water, the fluorescent product was purified by preparative silica-gel thin-layer chromatography (TLC) using 10% chloroform in methanol for elution. The new yellow fluorescent band was scraped from the TLC sheet, dissolved in ethyl acetate, and evaporated to a solid. The product was shown by TLC to be pure and free of both other ivermectin derivatives and other fluorescent dyes. Its concentration was estimated based on the assumption that its extinction coefficient would be the same as that of the free bodipy dye (about 80,000 cm^{-1} M^{-1} at 503 nm).

Stability of bodipy ivermectin

To ensure that our fluorescent studies using bodipy ivermectin were measuring the intact molecule rather than a degradation product,

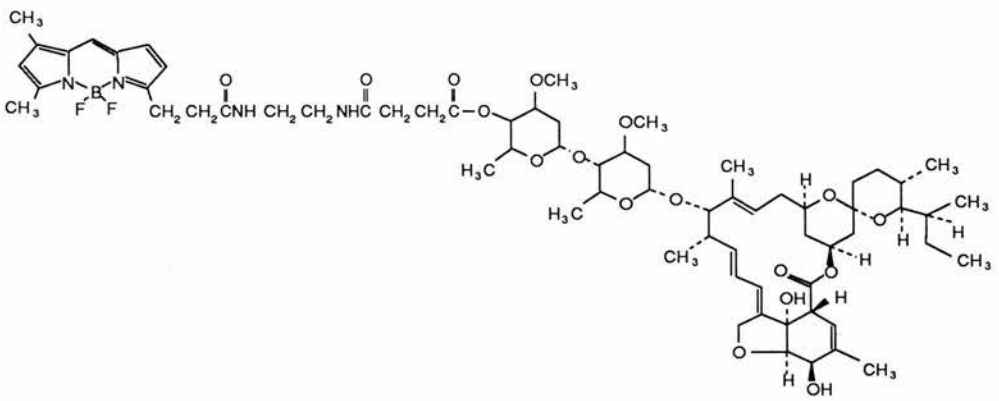


Fig. 1. Chemical structure of bodipy ivermectin

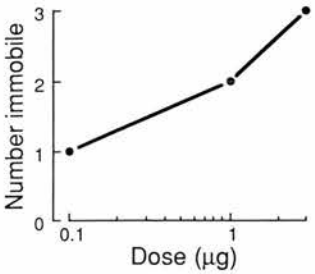


Fig. 2. Immobilization dose-response curve for adult *Ascaris* injected with bodipy ivermectin. Three worms were injected at each dose and immobilization was measured at 24 h after injection. Control injections had no effect

the bodipy ivermectin was incubated with *Ascaris* tissue as follows: 1 μg bodipy ivermectin was incubated in 1.0 ml (containing 0.1% ethanol) experimental solution with (a) a standard flap preparation (Martin 1980) and (b) a standard vesicle preparation (1000 vesicles). After incubation for 1 h at 37° C, the bodipy ivermectin in the mixtures was extracted into chloroform:methanol (2:1, v/v). The chloroform:methanol extract was dried down to 100 μl with oxygen-free nitrogen, and 10-μl portions were applied to Whatman silica-gel-backed plates for TLC.

TLC was carried out using silica-gel-backed plates placed in chromatography tanks containing diethyl ether. In the presence of this developing solvent, bodipy ivermectin shows an R_f value of 0.8 as detected by illumination with UV light. Chromatography of stock bodipy ivermectin solution and of extracts of bodipy ivermectin incubated with *Ascaris* muscle vesicles and with the flap preparation revealed co-migration of the fluorescent molecules with stock bodipy ivermectin. No other fluorescent molecules could be detected at other positions of migration on the plate.

Bodipy ivermectin retains biological activity

Kass et al. (1982) have shown that the direct injection of dihydroavermectin B1a into *Ascaris* produces a paralysis that is neither flaccid nor rigid. A similar paralysis was produced following the injection of bodipy ivermectin. Figure 2 shows that the paralysis produced by the injection of bodipy ivermectin in amounts greater than 0.1 μg per worm was dose-dependent. Control injections produced no effect. Although the relative potency of bodipy ivermectin was not assessed in this study, it seemed to be similar to that previously described for dihydroavermectin Ba1 (Kass et al. 1982).

Electron microscopy

Shortly after their collection, isolated muscle cells were fixed with 3% gluteraldehyde in 0.1 M Na cacodylate buffer for 1–2 h, washed in 0.1 M Na cacodylate buffer, postfixed with 1% osmium tetroxide in 0.1 M Na cycodylate buffer, washed in buffer, dehydrated overnight in graded acetone/Araldite, and embedded overnight in Araldite. Thin sections (60 nm) were stained with saturated uranyl acetate in 50% ethanol and with Reynold's lead citrate. Sections were viewed with a Philips 400 transmission electron microscope.

Results

Fluorescent microscopy of frozen sections

The level of fluorescence seen in the sections was greatest in the region of the injection site. It decreased gradually and was not detectable at distances of greater than 4 cm. The distribution of the fluorescence due to bodipy ivermectin is therefore described for frozen sections taken at 1.5–2 cm from the injection site. The level of autofluorescence was observed by examining sections taken from regions located at greater than 5 cm from the injection site and from control-injected *Ascaris*. Autofluorescence was always detected in the medullary region of muscle spindles, in the intestinal cells, and in the outer cuticle layer; thus fluorescence seen in these regions was not considered to represent a positive result.

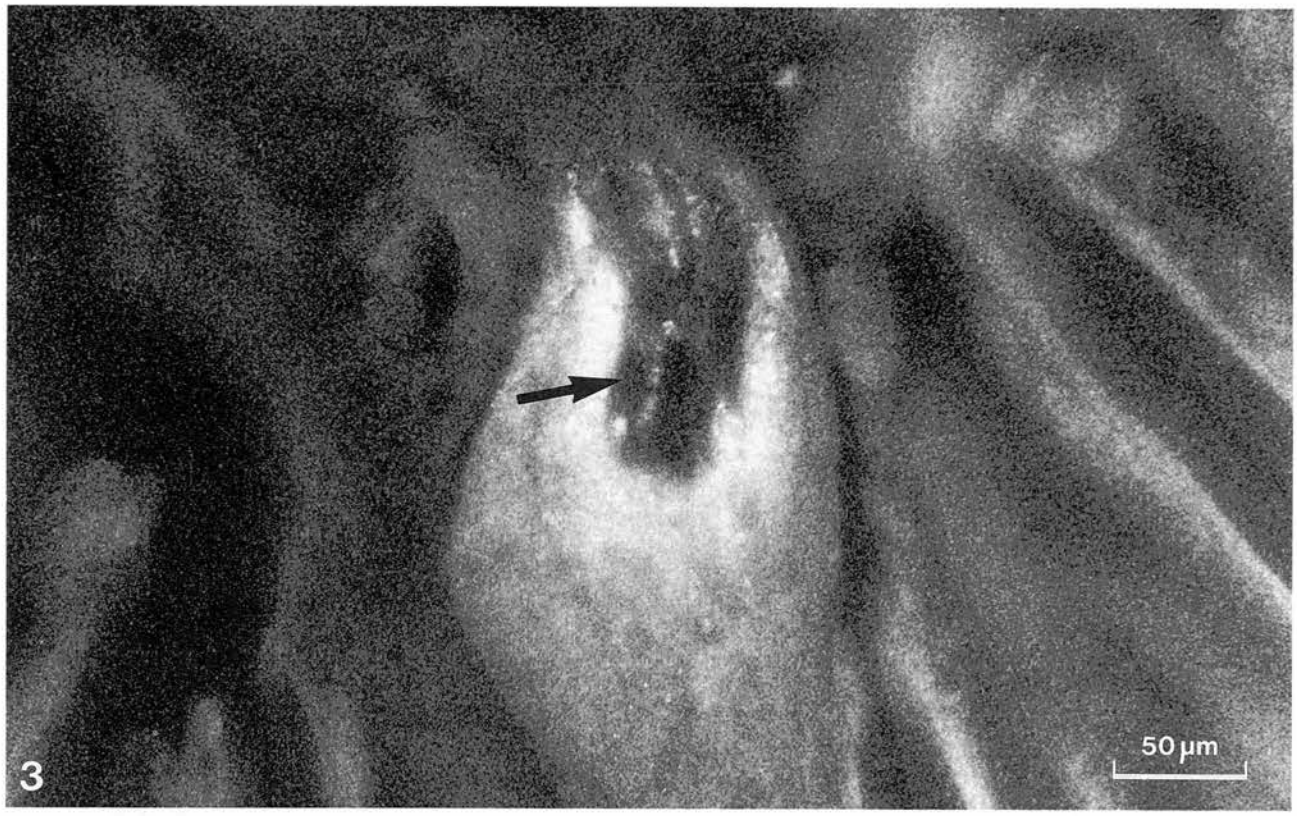
Figure 3 shows a transverse section through the nerve cord and the hypodermal chalice. The neuronal membranes of the nerve cord and/or septa were stained but the cytoplasm of the nerve processes was not, the latter manifesting in cross section as dark centers surrounded by a circle of fluorescence (arrow in Fig. 3). The level of fluorescence in the area immediately surrounding the nerve cord was consistently high and greater than that in other regions of the hypodermal chalice, suggesting that there was a process by which concentration occurred. Figure 3 also shows that fluorescence was not found within the syncytium, the muscle region overlying the nerve cord.

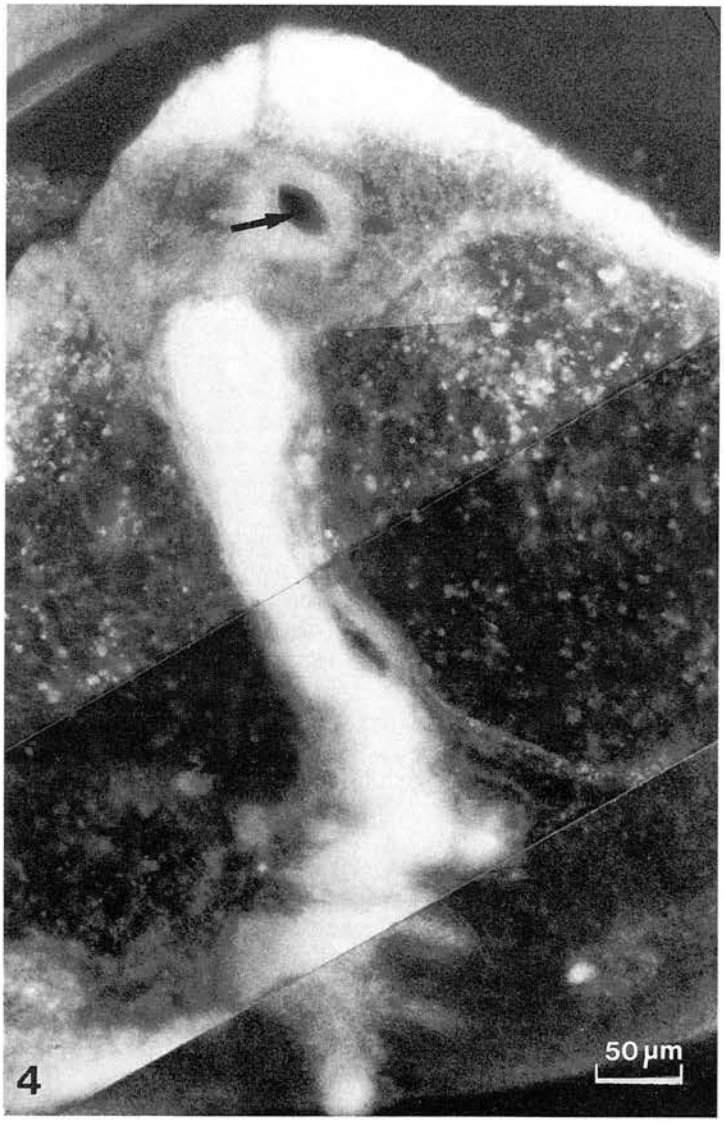
Figure 4 shows a section through the lateral line. It can be seen that the bodipy ivermectin concentrated in the area directly in contact with the peri-enteric fluid in the outer region of the lateral line. However, it was not concentrated within the excretory canal. It was also seen in bands in the deeper layers of the lateral line. These bands sometimes formed channels and may be produced by the uptake of bodipy ivermectin by phagocytic elements in the lateral line (Borradaile and Potts 1958). The hypodermal layers were also found to take up bodipy ivermectin (Fig. 5). The appearance of the staining was usually beaded and continuous around the worm.

A low level of fluorescence in the muscle-cell bag region was regularly detected in the transverse sections, but this level was much lower than that seen in the hypodermal chalice, the lateral line, or the hypodermis. Figure 6 summarizes in diagrammatic form the distribution of bodipy ivermectin in frozen sections.

Staining of neuronal tissue in the cuticle and hypodermal flap preparation

The identity of motor neuron connections in *A. suum* has been determined using serial sections (Stretton et al. 1978). These studies have shown that cell bodies of motor neurons lie within the ventral nerve cord and are connected to the dorsal nerve cord by regularly repeating commissures. Two easily identified commissural axons arise from the motor neurons DE1 and VI (Fig. 7). DE1 is excitatory, with acetylcholine being the neurotransmitter; VI is inhibitory, with γ-aminobutyric acid serving as the neurotransmitter (Martin 1980). The uptake of bodipy ivermectin by these axons was examined visually and quantified by focusing the laser with a 40× objective and measuring the fluorescence observed in the adjacent hypodermal layer as well as over the axons. Under the microscope, both commissural axons failed to show evidence of staining, appearing as two dark parallel lines within the fluorescent hypodermis. Quantitation of the







Figs. 3–5

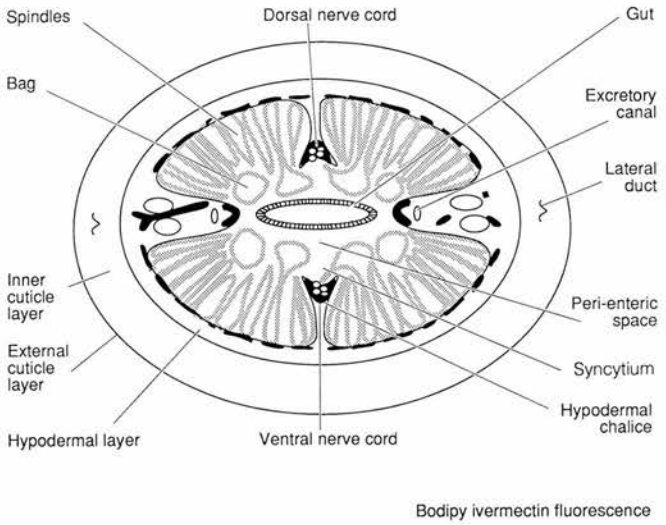


Fig. 6. Diagram of the distribution of bodipy ivermectin in frozen transverse sections. Note that the two lateral lines are formed by the invaginating tissues that surround the excretory canals. The fluorescence was greatest in the hypodermal chalice, in the hypodermal layers, and in regions indicated in the lateral line

Table 1. Levels of relative fluorescence seen in the cuticle and hypodermal flap preparation

	Control	Bodipy-treated
Hypodermal chalice	128.5 ±16.06 units ($n=5$)	224.02±8.5 (units ($n=10$)
Hypodermis	93.36± 5.4 units ($n=5$)	235.58±9.1 units ($n=9$)
DE1	–	151.7 ± 8.1 units ($n=10$)

Data represent mean values±SE

fluorescence levels confirmed this view; the results are summarized in Table 1. The level of fluorescence measured both axons was less than that found in the surrounding hypodermal tissue. The reduction in fluorescence following ivermectin treatment was greatest for the larger commissural axon DE1 and lower for the smaller commissural axon VI. The control level of fluorescence seen in the axons was the same as that found in the control hypodermis.

Fig. 3. FITC fluorescence shown in a transverse section through a nerve cord and hypodermal chalice of *Ascaris* following the injection of 1 µg bodipy ivermectin. The *arrow* indicates the nerve cord in the chalice. Note the fluorescence surrounding and within the nerve cord. The dark, unstained regions within the cord correspond to the cytoplasm of the axons or dendrites of the neurons; the fluorescent circles surrounding these dark regions represent the membrane of the nerve cells or the septa dividing the nerve cord. The section was taken at 1.5 cm anterior to the injection site

Fig. 4. FITC fluorescence shown by the lateral line in a transverse section of *Ascaris* following the injection of 1 µg bodipy ivermectin. The *arrow* indicates the excretory canal. The section was taken at 1 cm from the injection site

Fig. 5. FITC fluorescence shown by the hypodermal region following the injection of 1 µg bodipy ivermectin. The section was taken at 1 cm from the injection site

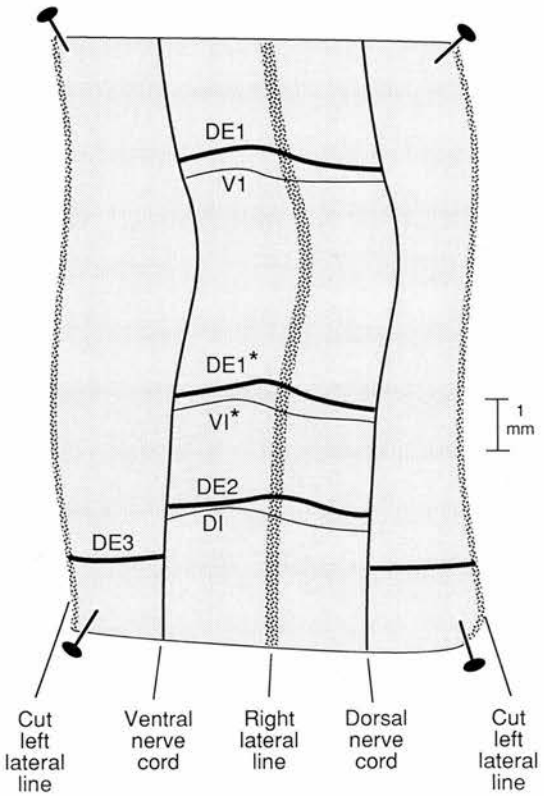


Fig. 7. Diagram of the location of the commissural axons DE1 and VI, the lateral lines, and the hypodermal chalice in the hypodermis and cuticle preparation

Table 1 also shows the mean levels of fluorescence in the hypodermal chalice of control and bodipy-ivermectin-treated preparations. The increase in fluorescence shown by the hypodermal chalice following treatment (95.5 units) was lower than that exhibited by the hypodermis (142 units).

Fluorescence in isolated muscle cells

Isolated muscle cells were bathed in 1 µg bodipy ivermectin/ml for 1 h before being washed. Figure 8A shows an unstained collagenase-isolated muscle cell and its constituent parts, which comprise the contractile spindle region; the bag region, which contains the nucleus; the arm; and the fingers. The level of fluorescence was usually higher in the spindle region, although this was not invariably the case. The most striking feature of the staining was the small-beading pattern seen just under the membrane of the bag and arm regions Fig. 8B–D).

The bodipy ivermectin incorporated into the muscle membrane could have been either localized in the outer phospholipid monolayer of the membrane or equally distributed between the inner and outer monolayers as a result of diffusion through the membrane. To explore the vertical distribution of bodipy ivermectin, we used trypan blue as a nonpermeant quencher of bodipy on the outer membrane followed by quantitation using the argon laser. The absorption spectrum of trypan blue overlaps with that of the probe used in the present study.

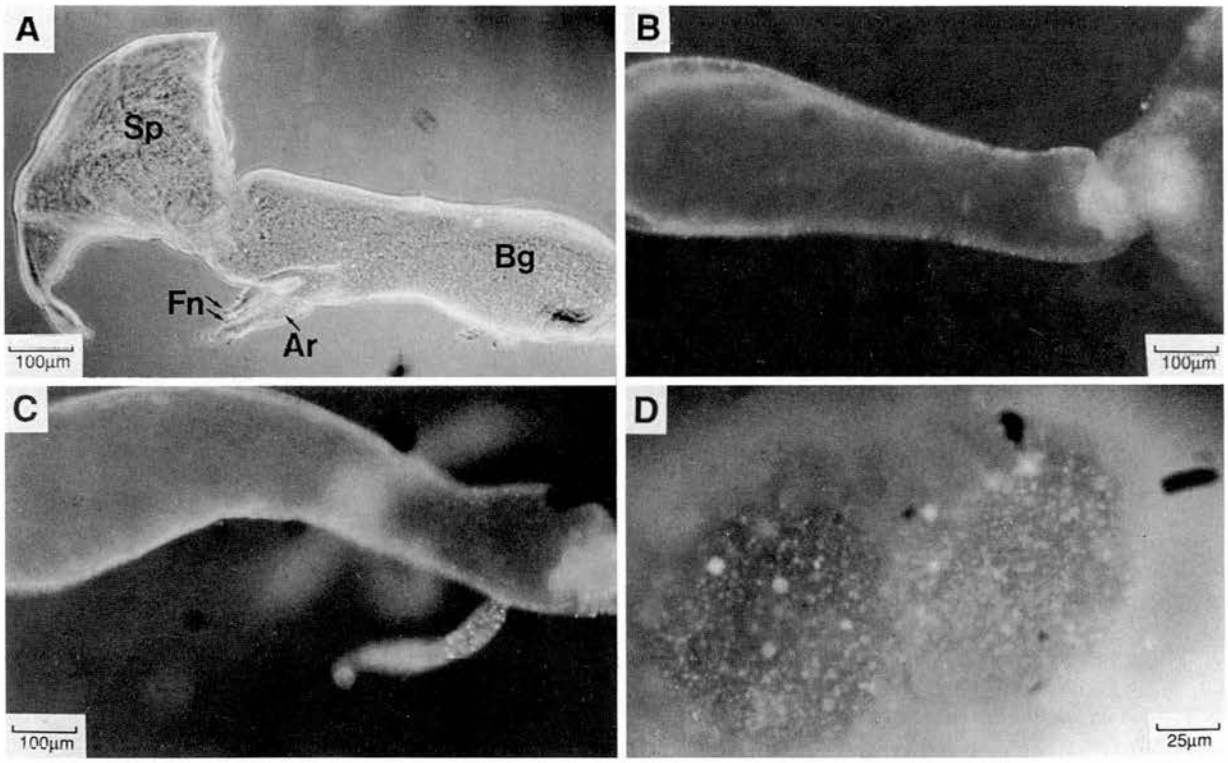


Fig. 8A–D. Collagenase-isolated muscle cells. **A** Phase-contrast micrograph of an unstained muscle cell. *Bg*, Bag region; *Sp*, spindle region; *Ar*, arm; *Fn* fingers. **B** FITC photomicrograph showing the fluorescent beading under the surface of the bag membrane in cells incubated in bodipy ivermectin. **C** FITC photomicrograph showing the fluorescence of the bag membrane and beading in the arm region. **D** FITC high-power photomicrograph showing the fluorescence and beading of the bag membrane

It is expected (Foley et al. 1986) that the efficiency of energy transfer from the emission spectrum of bodipy ivermectin to the absorption spectrum of trypan blue is 50% at a distance of 4 nm; it decreases rapidly at greater distances and is negligible at distances comparable with the thickness of the membrane (9 nm). Bodipy ivermectin inserted with its fluorescent head groups in the external monolayer might be expected to the totally quenched by the trypan blue. If the bodipy ivermectin were equally distributed between the two monolayers, 50% quenching would be observed. The above interpretation is valid only if trypan blue does not enter the muscle cells. Our observations showed that only a few muscle cells, probably damaged, took up the trypan blue; these were excluded from the study.

Table 2 shows the fluorescence levels observed in the different regions of the muscle cells in the absence and presence of 0.25% trypan blue. The muscles were obtained from the same preparation. Five muscle cells were used to measure the control level of fluorescence, and another five were used to measure the experimental fluorescence and the level of quenching by trypan blue. The table shows that trypan blue almost completely quenched the fluorescence in the spindle region, reducing the relative fluorescence from a mean of 84 units to a mean of 1.1 units; this corresponds to a reduction to 1.3% of the control value. In the bag region, the mean level of fluorescence was reduced from 63.5 to 16.8 units, corresponding to a reduction to 25% of the control value. It was concluded from these observations that the bodipy ivermectin was located only in the outer monolayer of the membrane of the spindle, but this was not entirely the case in the bag region. The likely explanation for the failure of trypan blue to quench all of the bag fluorescence seemed to involve the submembrane beading. This was confirmed simply by direct visual examination, which revealed that in the presence of trypan blue, the only fluorescence remaining in the bag was the fluorescent submembrane beading.

Table 2. Fluorescence levels observed in isolated muscle cells

	Control	Trypan blue
Spindle	84.1 ±13.6 units ($n=5$)	1.1 ±0.48 units ($n=5$)
Arm	88.67±14.0 units ($n=5$)	6.18±3.5 units ($n=4$)
Bag	63.48± 9.15 units ($n=5$)	16.75±6.57 units ($n=4$)

Data represent mean values±SE

Submembrane beading may be attributable to lipophilic pinocytotic vesicles

Transmission electron microscopy of sections through the bag membrane (Fig. 9) revealed the presence of submembrane vacuoles in the bag region of the muscle cell. These vacuoles measured 1–4 μm in diameter and their

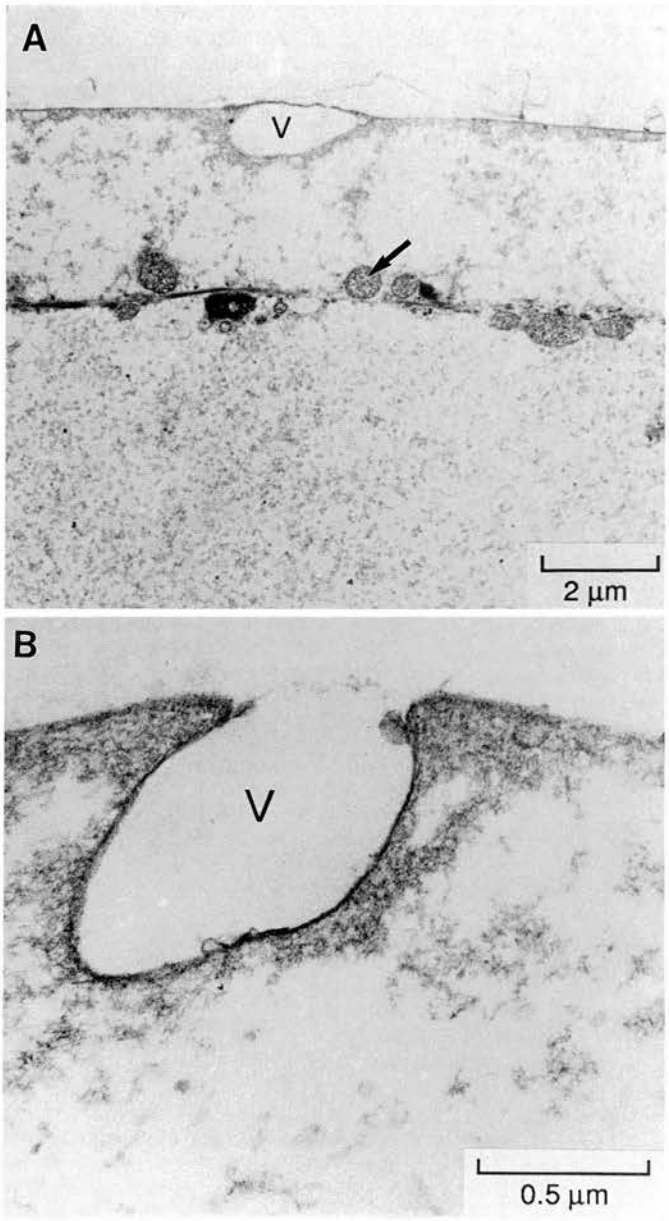


Fig. 9A, B. Transmission electron micrographs showing the submembrane vesicels (*V*). The *arrow* shows the mitochondrial layer separating the submembrane region from the glycogen granules that fill the bag region of the muscle cell

appearance was similar to that previously described for "pinocytotic vesicles" in other cells (Novikoff and Holtzman 1970). Such vesicles may allow the entry into cells of molecules in bulk, including bodipy ivermectin.

Discussion

Bodipy distribution and the lipophilic nature of avermectins

In the work reported herein, we do not consider that the distribution of bodipy ivermectin simply reflects the distribution of putative receptor sites for avermectins. In view of the well-known, extremely lipophilic nature of avermectins, it is likely that some of the staining resulting from treatment with bodipy ivermectin (summarized in Fig. 3) was nonspecific due to the distribution of a lipophilic compound in hydrophobic regions of the tissues. Nevertheless, the present observations do enable an assessment of the tissue distribution of avermectins in the parasitic nematode *Ascaris suum*. The fluorescence seen in all of the tissues was attributable to bodipy ivermectin and not to any metabolite, as TLC of extracts of labeled tissues (see Materials and methods) revealed that bodipy ivermectin was the only fluorescent constituent.

Staining of muscle membranes and the nerve cord

The bodipy ivermectin staining of muscle membranes and the concentration of the ivermectin probe seen in the nerve cord in this study are consistent with the view that muscle and nerve-cord membranes may be sites of action for avermectins. The trypan-blue studies on the distribution of bodipy ivermectin in the muscle cell showed that the probe was restricted to the outer monolayer of the membrane and that it did not cross to the inner monolayer, as might be expected if distribution were controlled only by lipophilicity. The observation that the probe remained in the outer monolayer of the membrane suggests that binding to putative avermectin receptors also takes place in the outer monolayer; such a restricted movement may explain why only the application of dihydroavermectin to the outer membrane results in the opening of Cl channels in membrane patches (Martin and Pennington 1989). Concentration of unquenchable fluorescence in submembrane vesicles may represent a mechanism of uptake of bodipy ivermectin into the muscle cell.

Uptake by the hypodermis

The detection of bodipy ivermectin in the hypodermal region is an interesting observation, since this region is not directly involved in motor activity. Hypodermal cells appear to have a number of functions, including the transport of drugs and nutrients (Ho et al. 1990), the transport of Cl ions (Hobson et al. 1952), phagocytosis, and a major depot function since they contain many storage granules and lipid droplets (White 1988). Since bodipy ivermectin, like other avermectins, is very lipophilic, it is likely to concentrate in the lipid-rich region of the hypodermal layer. One possible effect at this site, provided that action is exerted on hypodermal-cell Cl channels, would be to upset the hypodermal transport of Cl ions (Hobson et al. 1952). Such an action might represent another site of action for the avermectins.

Ivermectin appears to be absorbed through the cuticle of *A. suum*, with the diffusion coefficient being $5.46\ cm^2\ s^{-1} \times 10^6$, but the rate-controlling impediment is a 5- to 10-µm-thick lipid barrier of the hypocuticle (Ho et al. 1990). This layer appears to correspond to

the location of the bodipy ivermectin seen in the frozen sections (Fig. 5). If this layer were to behave only as a passive sink for lipophilic compounds, it would buffer the concentration, thereby restricting the concentration of avermectins at other active sites in the parasite. Thus, the staining of this region appears to be of therapeutic significance.

Possible drug clearance by the lateral line

The structure and function of the lateral line of *A. suum* has been examined by Kummel et al. (1969) and Wright and Newall (1976). The observations of these authors lead to the conclusion that it has an excretory function like that of the Malpighian tubules of insects and that "urine" production by the lateral canal is strictly an active secretory process. When injected into the peri-enteric region, a number of substances, including carmine and indigo, are taken up by the tissues of the lateral line; Borrodaile and Potts (1958) have suggested that the highly vacuolated cells of the lateral line are phagocytic. These phagocytic elements may correspond to the coelomocytes of *Caenorhabditis elegans* (White 1988). The uptake of bodipy ivermectin from the peri-enteric fluid by the lateral line may be part of an excretory process. Although little is known about the excretion of drugs by nematodes, it is clear that an efficient excretory system would detoxify the parasite and make it less susceptible to the theapeutic action of drugs. A better understanding of the mechanisms and control of drug excretion in nematodes may contribute to the future chemical control of resistant parasites.

Acknowledgements. We would like to thank Merck, Sharp and Dohme (USA) for financial support and for the gift of 22,23 dihydroavermectin B1a.

References

Borradaile LA, Potts FA (1958) The invertebrata: a manual for the use of students, 3rd edn. (Revised by Kerkut GA) Cambridge University Press, Cambridge

Burg RW, Miller BM, Baker EE, Birnbaun J, Currie JA, Hartman R, Kong Y-L, Monaghan RL, Olson G, Putter I, Tunac JP, Wallick H, Stapley EO, Oiwa R, Omura S (1979) Avermectins, new family of potent anthelmintic agents: producing organism and fermentation. Antimicrob Agents Chemother 15:361–367

Cambell WC, Benz GW (1984) Ivermectin: a review of efficacy and safety. J Vet Pharmacol Ther 7:1–16

Duce IR, Scott RH (1985) Actions of dihydroavermectin B1a on insect muscle. Br J Pharmacol 85:395–401

Fisher MH, Mrozik H (1984) The avermectin family of macrolide-like antibiotics. In: S Omura (ed) Macrolide antibiotics. Academic Press, New York, pp 553–606

Foley M, MacGregor AN, Kusel JR, Garland PB, Downie T, Moore I (1986) The lateral diffusion of lipid probes in the surface of *Schistosoma mansoni*. J Cell Biol 103:807–818

Fritz LC, Wang CC, Gorio A (1979) Avermectin Bia irreversibly blocks postsynaptic potentials at the lobster neuromuscular junction by reducing muscle membrane resistance. Proc Natl Acad Sci USA 76:2062–2066

Garland PB (1981) Fluorescence photobleaching recovery: control of laser intensities with an acoustico-optic modulator. Biophys J 33:481–482

Ho NFH, Geary TG, Raub TJ, Barsuhn CL, Thompson DP (1990) Biophysical transport properties of the cuticle of *Ascaris suum*. Mol Biochem Parasitol 41:153–165

Hobson AD, Stephenson W, Beadle LC (1952) Studies on the physiology of *Ascaris lumbricoides*: I. The relation of the total osmotic pressure, conductivity and chloride content of the body fluid to that of the external environment. J Exp Biol 29:1–21

Johnson CD, Stretton AOW (1985) Localization of choline acetyltransferase within identified motoneurons of the nematode *Ascaris*. J Neurosci 5:1984–1992

Kass IS, Larsen DA, Wang CC, Stretton AOW (1982) *Ascaris suum*: differential effects of avermectin B1a on the intact animal and neuromuscular strip preparations. Exp Parasitol 54:166–174

Kass IS, Stretton AOW, Wang CC (1984) The effect of avermectin and drugs related to acetylcholine and 4-aminobutyric acid on neurotransmission in *Ascaris suum*. Mol Biochem Parasitol 13:213–225

Kummel G, Dankwarth L, Braun-Schubert G, Gertz K-H (1969) Zur Struktur und Funktion des Exkretionssystems von *Ascaris lumbricoides* L. Z Vergl Physiol 64:118–134

Martin RJ (1980) The effect of γ-aminobutyric acid on the input conductance and membrane potential of *Ascaris* muscle. Br J Pharmac 71:99–106

Martin RJ, Pennington AJ (1989) A patch-clamp study of effects of dihydroavermectin on *Ascaris* muscle. Br J Pharmacol 98:747–756

Martin RJ, Kusel JR, Pennington AJ (1990) Surface properties of membrane vesicles prepared from muscle cells of *Ascaris suum*. J Parasitol 76:340–348

Mellin TN, Busch RD, Wang CC (1983) Postsynaptic inhibition of invertebrate neuromuscular transmission by avermectin B1a. Neuropharmacology 22:89–96

Mrozik H, Eskola P, Fisher MH, Egerton JR, Cifelli S, Ostlund DA (1982) Avermectin acyl derivatives with anthelmintic activity. J Med Chem 25:658–663

Novikoff AB, Holtzman E (1970) Cells and organelles. Holt, Rinehart and Winston, New York

Schaeffer JM, Stiffey JH, Mrozik H (1989) A chemiluminescent assay for measuring avermectin binding sites. Anal Biochem 177:291–295

Stretton AOW, Fishpool RM, Southgate E, Donmoyer JE, Walrond JP, Moses JER, Kass IS (1978) Structure and physiological activity of the motoneurons of the neamtode *Ascaris*. Proc Natl Acad Sci USA 75:3493–3497

White J (1988) In: Wood WB (ed) The nematode *Caenorhabditis elegans*. Cold Spring Harbor Laboratory, Cold Spring Harbor, New York, pp 81–122

Wright DJ, Newall DR (1976) In: Croll NA (ed) The organization of nematodes. Academic Press, New York, pp 163–210

On the distribution of a fluorescent ivermectin probe (4″ 5,7 dimethyl-bodipy proprionylivermectin) in *Ascaris* membranes

R. J. MARTIN[1] *and* J. R. KUSEL[2]

[1] *Department of Pre-clinical Veterinary Sciences, R.(D.) S.V.S. Summerhall, University of Edinburgh, Edinburgh EH9 1QH*
[2] *Department of Biochemistry, University of Glasgow, Glasgow*

(*Received 28 September 1991; revised 29 October 1991; accepted 29 October 1991*)

SUMMARY

The distribution of the fluorescent ivermectin derivative (4″ 5,7 dimethyl bodipy proprionylivermectin, referred to here as bodipy ivermectin) was studied in muscle vesicle membranes from the parasite *Ascaris suum*. Incubation in bodipy ivermectin, at concentrations greater than 1 ng/ml, produced a dose-dependent fluorescence in the vesicles. The level of fluorescence was not depressed (but increased) by prior incubation with 1 μM unlabelled ivermectin. This observation suggested that most of the bodipy ivermectin was free in the lipid phase of the membrane and not associated with a receptor. The trypan blue quenching technique showed that the bodipy ivermectin did not cross the membrane bilayer but remained in the outer monolayer. Lateral mobility of the probe in the membrane was studied using the fluorescence recovery after photobleaching (FRAP) technique. The lateral diffusion coefficient (D_L) was $14{\cdot}0 \times 10^{-10}$ cm^2/s which was nearly three times faster than the lipid probe octadecanoyl-aminofluorescein in membranes from the same preparations; only 46% of the probe was mobile, showing that within a 1·2 μm radius the distribution of the bodipy ivermectin in the membrane was not homogeneous. These observations are used to suggest that: the site of action of ivermectin is located in the outer monolayer of the membrane (possibly on the Cl^- channel); and that the speed of onset of action in isolated membrane preparations may be limited by diffusion in the membrane.

Key words: *Ascaris suum*, 4″ 5,7 dimethyl bodipy proprionylivermectin, bodipy ivermectin, membrane distribution.

INTRODUCTION

Avermectins are a family of highly lipophilic macrocyclic lactones, derived from *Streptomyces avermitilis* (Burg *et al.* 1979). They have a biological activity against parasitic nematodes and insects but not against tapeworms, flukes or their hosts (for a review see Cambell & Benz, 1984). The selective action and potency of avermectins means that these drugs can be used in man and animals to treat a wide range of nematode infestations, including the intestinal nematodes like *Ascaris suum*.

The mode of action of avermectins has been the subject of a number of studies in sensitive preparations (e.g. Fritz, Wang & Gorio, 1979; Mellin, Busch & Wang, 1983; Duce & Scott, 1985; Martin & Pennington, 1989), in which avermectins were shown to increase membrane Cl^α permeability.

In a patch-clamp study on *Ascaris* muscle membrane (Martin & Pennington, 1989) 22,23 dihydroavermectin B1a produced opening of non-GABA-activated 9–15 pS Cl^α channels, when applied in low (100 pM) concentrations to the outside surface of membrane patches, but not when applied to the inner surface of membrane patches. This observation is not predicted if dihydroavermectin is lipophilic and free to move through the membrane. In addition it was found that there was a long delay (tens of seconds) between application of the dihydroavermectin and opening of the Cl^α channels; the delay may have been due to diffusion of dihydroavermectin in the membrane to the site of action.

In order to investigate the distribution and movement of avermectins in membranes, a biologically active fluorescent derivative of dihydroavermectin B1a (4″ 5,7 dimethyl bodipy proprionylivermectin, Fig. 1) was prepared. This paper describes its distribution in *Ascaris* muscle vesicle membranes when followed by laser optics (Martin, Kusel & Pennington, 1990). The experiments (i) show that the probe does not cross the outer lipid monolayer of the membrane and (ii) estimate the lateral diffusion rate of the probe in the outer monolayer of the membrane.

MATERIALS AND METHODS

Preparation of vesicles

The preparation of the vesicles has been described in detail previously (Martin *et al.* 1990) but the method is outlined below. Specimens of *Ascaris suum* were collected from the local abattoir at weekly intervals and maintained at 37 °C in Locke's solution until

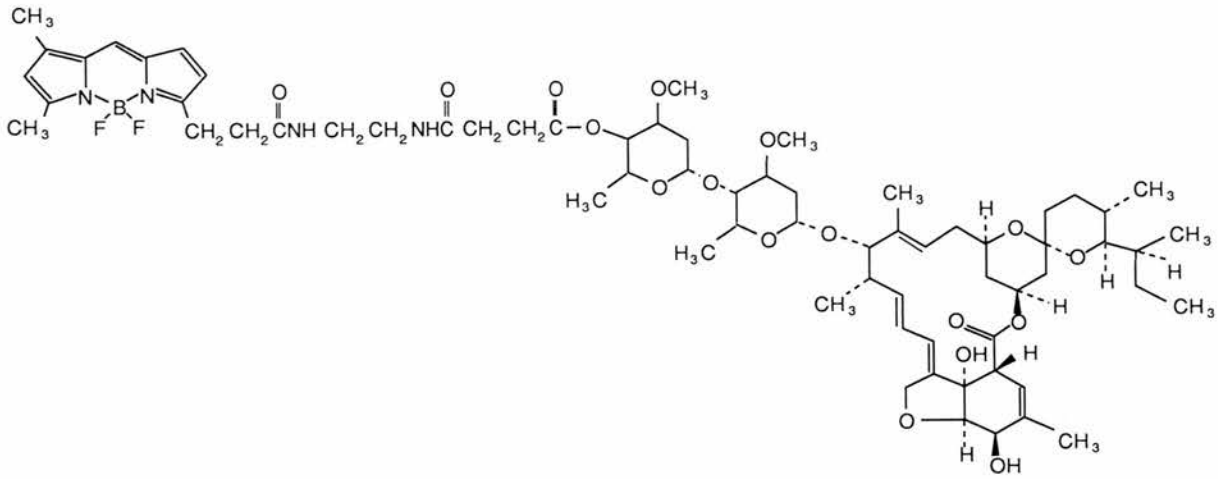


Fig. 1. Chemical structure of bodipy ivermectin. The fluorescent moiety (5,7 dimethyl bodipy) was inserted onto the 4″ position of 22,23 dihydroavermectin to retain biological activity.

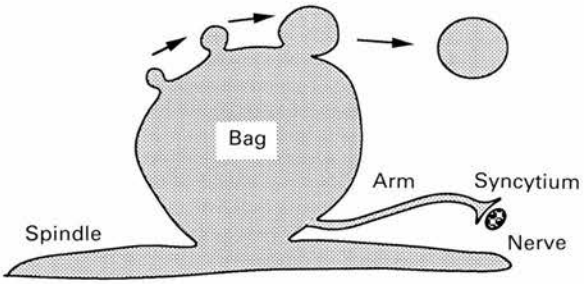


Fig. 2. Diagram of muscle cell from *Ascaris* and the formation of a vesicle.

required. Muscle flap preparations were produced and mounted cuticle side down in an experimental chamber (Martin, 1980). The preparation was maintained in an experimental solution containing (mM): 105 Na acetate; 35 NaCl; 2 KCl; 2 $MgCl_2$; 3 glucose; 10 HEPES, pH 7·2 and 1 mg/ml collagenase (Sigma type 1A). After 20 min the preparation was washed in a solution of the same composition but with the collagenase omitted. The vesicles then formed as outgrowths of the bag region of the muscle over the next 20–30 min (Fig. 2). They were then harvested with a Pasteur pipette.

FRAP technique

At least 1000 vesicles were placed in each plastic universal bottle (cut down in size for convenience) and maintained in 2 ml of experimental solution at 37 °C. The vesicles were labelled by adding bodipy ivermectin (dissolved in ethanol) to the vesicles and then incubating for 30 min. Differing concentrations (1 ng–1 μg/ml) of bodipy ivermectin were used but during the labelling the concentration of ethanol was maintained at 0·1 %. The vesicles were then washed and mounted on a glass slide in a shallow pool confined by a square of silicone grease and covered with a glass cover-slip.

Measurements of 2-dimensional lateral diffusion of the fluorescent probe were made using the FRAP technique (Axelrod *et al.* 1976; Foley *et al.* 1986) and a laser-powered microscope combination (Garland, 1981). The laser was a low-powered water-cooled argon laser (Lexel model 85; 100 mW all lines maximum power) which was used with a 40× objective. The $1/e^2$ radius of the laser spot focused on the membrane was 1–1·2 μm. The recovery-time (D_L) values and percentage recovery were calculated using a non-linear least-squares fit to equation 12 of Axelrod *et al.* (1976). Experimental data were collected using a Hewlett–Packard Model 85 microcomputer connected to the fluorescence measuring electronics.

22,23 dihydroavermectin B1a (1 μg/ml) carried in 0·1 % ethanol in the experimental solution was used to examine the effects on uptake of bodipy ivermectin. It was added to the vesicles and incubated with them for 30 min prior to adding the bodipy ivermectin.

The depth of insertion of the bodipy ivermectin into the membrane was determined by measuring Foster resonance energy transfer quenching by the non-permeant molecule trypan blue used at a concentration of 0·25 % (Foley *et al.* 1986). The technique predicts that if trypan blue quenched all the fluorescence from bodipy ivermectin, the probe is present only in the outer phospholipid bilayer with little translocation occurring between the inner and outer monolayer.

Quantitation of the level of fluorescence in the vesicles

The level of fluorescence was usually quantitated using the laser described above; the approach proved satisfactory for small numbers of vesicles. For larger numbers of vesicles, the level of fluorescence was measured using flow cytometry on a FACScan

(Becton Dickinson) with Facscan Research software for analysis.

Fluorescent probes

Bodipy ivermectin (4″ 5,7 dimethyl bodipy proprionylivermectin, Fig. 1) was synthesized by Dr A. Minta and Dr H. Haughland of Molecular Probes Inc., Eugene, Oregon, USA using a method described for preparing the luminol derivative (Schaeffer, Stiffy & Mrozik, 1989). The biological activity of the bodipy ivermectin probe was confirmed following injection into adult *A. suum*. In amounts greater than 0·1 μg/worm, it produced a dose-dependent immobilization; although the relative potency of the bodipy ivermectin was not assessed in this study, it is pointed out that its potency is of a similar order to that described for dihydroavermectin (Kass *et al.* 1982). The stability was checked by incubating the compound with a standard vesicle preparation for 1 h, extraction in chloroform: methanol and thin-layer chromatography. Chromatography of stock bodipy ivermectin and extracts of bodipy ivermectin incubated with the vesicles yielded co-migration of the fluorescent molecules with stock bodipy ivermectin. No other fluorescent molecules could be detected at other migration positions on the plate. 5-*N*(octadecanoyl) aminofluorescein (Molecular Probes Inc.) was used as a lipid probe (Foley *et al.* 1986).

RESULTS

FACScan measures fluorescence in many vesicles

The level of fluorescence produced in muscle vesicles incubated in bodipy ivermectin was clearly dose dependent. The fluorescence produced by bodipy ivermectin in samples of 1000 vesicles, at the different concentrations of bodipy ivermectin, was measured using flow cytometric analysis on a FACScan to determine and count the fluorescence in each vesicle. Fig. 3A shows an example of the distribution of fluorescence in 1000 vesicles which was produced following incubation of 100 ng/ml bodipy ivermectin. As the concentration of bodipy ivermectin increased, the mean level of fluorescence shown by the vesicles increased but the shape of the fluorescence distribution was similar. Fig. 3B shows the relationship between the mean level of fluorescence and the concentration of bodipy ivermectin at concentrations of 1–300 ng/ml. Control vesicles showed that in the absence of bodipy ivermectin, there was a low level of autofluorescence of less than 30 units (not shown). At a dose of 1 ng/ml, the mean level of fluorescence was 58 units and this increased at 300 ng/ml, to a mean level of 148 units, without showing signs of saturation. Similar results were obtained from two other experiments carried out on different preparations.

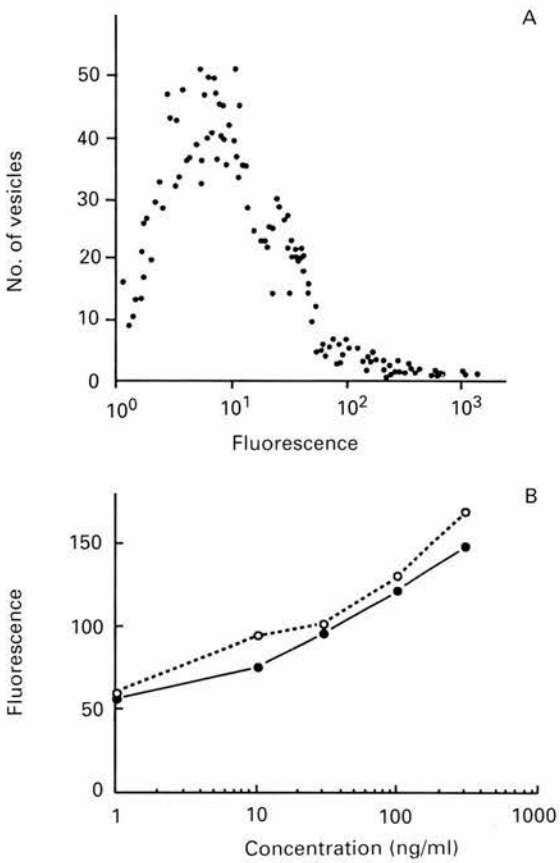


Fig. 3. (A) An example of a FACScan fluorescence histogram of vesicles incubated in 100 ng/ml bodipy ivermectin; 1000 vesicles were counted. The mean fluorescence level on the relative scale was 115 units. (B) Fluorescence–concentration relationship. (—●—) Control; (---○---) relationship in the presence of 1 μg/ml unlabelled dihydroavermectin. Note that the unlabelled ivermectin did not depress the level of fluorescence, implying that most of the fluorescent probe is in the lipid phase of the membrane.

Ivermectin binding sites in nematodes have been reported to have a high affinity (K_D = 0·29 nM) but low capacity (Schaeffer & Haines, 1989; Schaeffer *et al.* 1989); also the avermectins are very lipophilic and poorly soluble in the aqueous phase. It seemed likely, therefore, that, at the concentrations used in our experiments, most of the bodipy ivermectin would be in the lipid phase of the membrane, not associated with a protein receptor. This is consistent with the lack of saturation observed in Fig. 3A. As a further test of this interpretation vesicles were pre-incubated with 1 μM 22,23 dihydroavermectin B1a (unlabelled ivermectin) in an attempt to show an inhibition of the uptake of the fluorescent probe by the vesicles. The results of this experiment are shown in Fig. 3B which shows that there was no reduction in fluorescence when compared to the control but rather there was an increase. The increase in fluorescence was a consistent observation but its origin remains obscure and is the subject of further investigation. However, as a result of all these

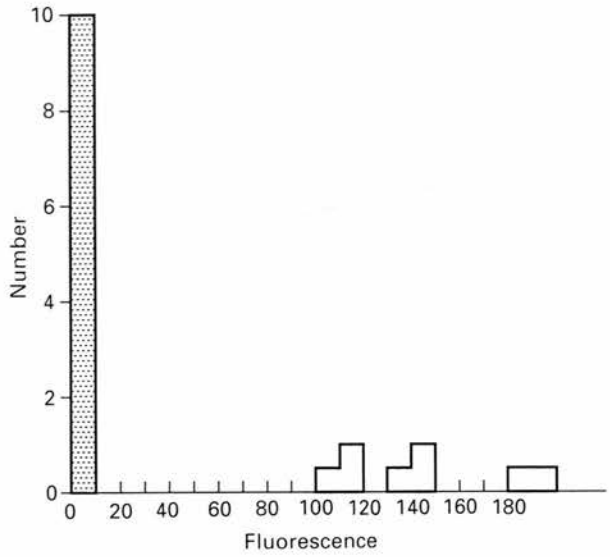


Fig. 4. Histogram of fluorescence levels in control (□) and trypan blue-quenched (▨) vesicles. Note that nearly all the fluorescence disappeared showing that the bodipy ivermectin was located in the outer monolayer of the membrane.

observations, it was concluded that most of the bodipy ivermectin was in the lipid phase of the membrane.

Trypan blue quenching shows that bodipy ivermectin remains in the outer monolayer

The bodipy ivermectin incorporated into the vesicle membrane could have been located in the outer phospholipid monolayer, or be equally distributed between the two monolayers as a result of diffusion through the membrane. In order to explore the vertical distribution of bodipy ivermectin, we used trypan blue as a non-permeant quencher of bodipy on the outer membrane and quantitation using the argon laser. The absorption spectrum of trypan blue overlaps with that of the probe used here. It is expected (Foley *et al.* 1986) that the energy transfer efficiency from the emission spectrum of bodipy ivermectin to the absorption spectrum of trypan blue is 50 % at a distance of 4 nm; it decreases rapidly at greater distances and is negligible at distances comparable to the thickness of the membrane (9 nm). Only bodipy ivermectin in the external bilayer could be quenched by the trypan blue; it is only when the fluorescent head group is located on the outer polar region that quenching is seen. If the bodipy ivermectin were equally distributed between the two monolayers, it was expected that 50 % quenching would be observed. The above interpretation is only valid if trypan blue does not enter the vesicles: observations showed that only a few, probably damaged, took up the trypan blue; these were excluded from the study.

Fig. 4 is a histogram of the fluorescence levels observed in vesicles in the absence and presence of 0·25 % trypan blue. The vesicles were from the same preparation. Ten vesicles were used to measure the control level of fluorescence, and a separate 9 were used to measure the fluorescence and the level of quenching by trypan blue. The histogram shows that the trypan blue quenches almost completely; it reduced the relative fluorescence from a mean of 136 units to a mean of 0·06 units. This corresponds to a reduction to 0·04 % of the control. We concluded that the bodipy ivermectin was completely located in the outer membrane of the vesicle and did not gain access to the inner membrane over the time-scale (163 min) of the experiment.

Mobility of bodipy ivermectin

The lateral diffusion coefficient of bodipy ivermectin was determined using the FRAP technique on the stained vesicles. Fig. 5A illustrates the results of a typical experiment where the fluorescence intensity of a membrane spot before and after bleaching was followed. The least-squares fit and the value of D_L is also shown. The fluorescence was monitored from an area of 1·2 μm radius illuminated by the laser focused on the vesicle membrane under study. The steady level of fluorescence from the spot was monitored and the spot bleached by increasing the power of the laser by 10000 for 50 ms at time 0. After bleaching, the spot gradually recovered its fluorescence as unbleached molecules of bodipy ivermectin moved into the bleached area. D_L was then calculated from the kinetics of the recovery (Axelrod *et al.* 1976). In Fig. 5A, D_L for bodipy ivermectin was $10{\cdot}6 \times 10^{-10}$ cm^2/s. Fig. 5B shows the histogram of estimates of D_L: the mean $\pm$ S.E. was $14 \pm 4 \times 10^{-10}$ cm^2/s ($n = 10$).

The percentage recovery was estimated using a computer to estimate the percentage recovery at infinite time; for the experiment illustrated in Fig. 5A the bodipy trace showed a 74·9 % recovery. Again, this value varied between vesicles and had a mean $\pm$ S.E. of $46{\cdot}0 \pm 3{\cdot}2$ %, ($n = 10$). Thus, on average, 54 % of the bodipy ivermectin was unable to diffuse laterally in the 1·2 μm radius membrane spot over the time scale of the experiment. Less than 100 % recovery implies that the bodipy ivermectin is not distributed in an homogeneous manner in the membrane and that there are at least 2 compartments.

Comparison with octadecanoyl-aminofluorescein

5-*N* (octadecanoyl)-aminofluorescein C_{18}Fl is an 18 carbon lipid probe which has been used to estimate lateral diffusion rates in a variety of membranes (e.g. Foley *et al.* 1986). It was of interest to compare the lateral mobility of bodipy ivermectin with this probe. In order to minimize variability between preparations and to allow comparison with bodipy ivermectin, vesicles from the same flap preparation

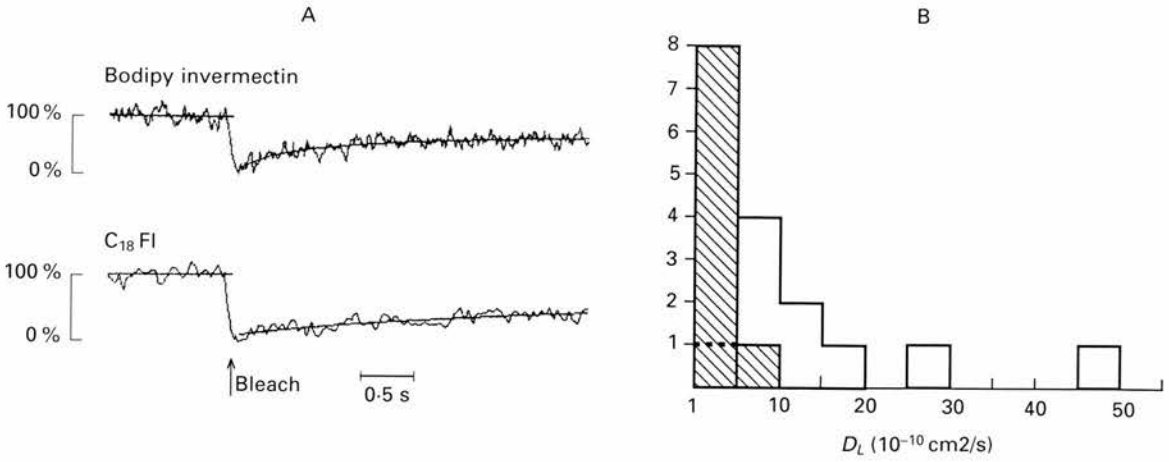


Fig. 5. (A) Fluorescence recovery after photobleaching (FRAP) curve for bodipy ivermectin and 5-*N*(octadecanoyl)-aminofluorescein (C_{18}Fl) in two separate vesicles. The observed fluorescence has been plotted after normalization to a pre-bleach intensity of 1·0 arbitrary units on the ordinate. The smooth curve is the non-linear least-squares fit to the data. The best fit for bodipy ivermectin gave a D_L value of $10{\cdot}6 \times 10^{-10}$ cm^2/s and recovery of 74·9 %. The best fit for C_{18}Fl gave a D_L value of $2{\cdot}0 \times 10^{-10}$ cm^2/s and recovery of 74·4 %. (B) Histogram of D_L values obtained for bodipy ivermectin (□) and C_{18}Fl (▨) from vesicles derived from the same preparation.

were used for the C_{18}Fl experiments as had been used for the bodipy ivermectin experiments. Fig. 5A shows a representative FRAP curve which had a D_L value of $2{\cdot}0 \times 10^{-10}$ cm^2/s and recovery of 74·4 %. Note that bodipy ivermectin has a faster diffusion rate than the lipid probe but that the percentage recovery was similar. The histogram of the D_L values is shown in Fig. 5B. The mean ± S.E. D_L for C_{18}Fl was $3{\cdot}6 \pm 0{\cdot}7 \times 10^{-10}$ cm^2/s ($n = 9$) and a mean ± S.E. percentage recovery was 43·4 ± 5 % ($n = 9$).

Comparison of the mean D_L value shows that diffusion for bodipy ivermectin was at least three times faster than for C_{18}Fl when vesicles from the same preparation were compared. The D_L values were significantly different (Student's t-test, $P < 0{\cdot}01$). However, the mean percentage recovery values (46·0 for bodipy ivermectin; 43·4 for C_{18}Fl) were not distinguishable, implying that the two probes distribute into domains, which occupy a similar area.

One possible explanation for the faster diffusion of bodipy ivermectin was that this probe may have increased the 'mobility' of the membrane. It was possible to test for, and exclude this as an explanation, by incubating vesicles in the less fluorescent bodipy ivermectin and staining with the much more fluorescent C_{18}Fl probe. Since the level of fluorescence from the C_{18}Fl probe was over five times that produced by bodipy ivermectin, FRAP experiments would indicate the D_L and percentage recovery values for C_{18}Fl rather than bodipy ivermectin. Under these conditions, again using vesicles from the same preparation as shown in Fig. 5, it was found that C_{18}Fl had a D_L value of $3{\cdot}9 \pm 0{\cdot}9 \times 10^{-10}$/s and percentage recovery of 54 ± 7 (means ± S.E., $n = 7$). Thus it was concluded that, on average, bodipy ivermectin has a faster lateral diffusion rate than C_{18}Fl.

DISCUSSION

Is bodipy ivermectin a suitable probe?

The fluorescent bodipy ivermectin derivative was prepared with the aim of being able to follow its distribution in membrane using FRAP, in order to throw more light on the action of the therapeutic agent ivermectin. Structure-activity studies (Fisher & Mrozik, 1989) have shown that the active site of the ivermectin molecule lies within the area of the macrocyclic lactone ring and spiroacetal subunit; the oleandrosyl disaccharide substituent is not essential for biological activity since the aglycone retains biological activity. Substitution on the 4″ position does not abolish biological activity (Fisher & Mrozik, 1989) and has allowed the preparation of a luminol ivermectin derivative which retains biological activity against *C. elegans* (Schaeffer *et al.* 1989). This luminol derivative has to be visualized by adding horse-radish peroxidase and hydrogen peroxide and is not suitable for FRAP studies. A fluorescent bodipy moiety was therefore substituted at the 4″ position to permit direct visualization of an ivermectin derivative which was predicted to retain biological activity. This was checked and confirmed by injecting the probe into *Ascaris*. It appears then that the bodipy ivermectin derivative is a suitable probe for following the parent compound.

The site of action for avermectins may be within the outer bilayer

Bath application of 22,23 dihydroavermectin B1a only produces opening of non-GABA-activated Cl^- channels after tens of seconds when applied to the outside surface of isolated patches of *Ascaris* muscle membrane, but not when applied to the inside

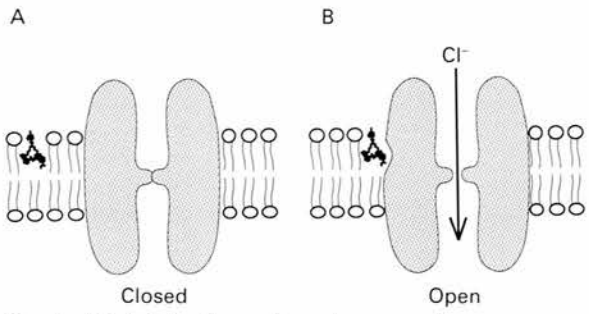


Fig. 6. Model for the action of avermectins.
(A) Avermectin molecules in the outer monolayer of the cell membrane can diffuse laterally but not vertically.
(B) The avermectin molecule combines with a Cl^- channel at a site confined to the outer monolayer to bring about opening of the channel.

surface (Martin & Pennington, 1989). Despite the lipophilic nature of 22,23 dihydroavermectin B1a the non-symmetrical action may be explained if movement of the molecule between the two phospholipid layers of the membrane is restricted like phospholipids. This view is supported by the behaviour of bodipy ivermectin which was shown not to cross from the outer to the inner monolayer. In this respect dihydroavermectin would behave like many phospholipids which do not 'flip-flop' across the membrane bilayer (Housley & Stanley, 1982). The fact that the bodipy ivermectin does not cross to the inner membrane monolayer and does not 'flip-flop' is inconsistent with any suggestion that ivermectin acts as an ionophore to carry ions across the membrane.

Fig. 6 shows a putative site of action for the avermectins on the Cl^α channel located in the outer membrane bilayer, and consistent with the observations above. It is suggested that the macrocyclic lactone/spiroacetal group reacts with a site on the Cl^α channel and that the oleandosyl dissaccharide remains in or near the aqueous phase. This scheme predicts that the speed of onset of drug action may be slow following bath application to isolated tissues and will be influenced by diffusion in the outer monolayer. It also predicts that overlying tissues and membranes may prevent access to active sites. Dimethyl sulphoxide is often used to solubilize avermectins and in a sufficient concentration will act as a 'sorption promotor' facilitating the movement of large molecules across membranes by increasing membrane fluidity. The effect of overlying membranes and slow onset may then be reduced by high concentrations of dimethyl sulphoxide.

Another prediction of this model is that the concentration of avermectins in the outer membrane monolayer will be influenced by their solubility in the membrane. Thus it may be that animals which show a particular sensitivity to avermectins have Cl^α channels in membranes in which avermectins are more soluble.

Partition of the probe within the outer monolayer

In this study it was shown that, on average, 46% of the bodipy ivermectin was inserted into regions of the membrane in which it can diffuse and that the mobile fraction had a lateral diffusion coefficient (D_L) of $14 \times 10^{\alpha 10}$ cm^2/s. The recovery curve never proceeds to completion because the probe cannot diffuse laterally into approximately 54% of the membrane; such regions have been called domains and represent regions of immobile lipid (Wolf *et al.* 1981). These domains must occur within and be smaller than the laser spot (1·2 μm radius) used in this experiment. The distribution of the ivermectin probe in the membrane was not homogeneous.

A high concentration of unlabelled ivermectin failed to reduce the level of fluorescence seen in the vesicle membrane suggesting that most of the bodipy ivermectin was unbound in the lipid phase of the membrane.

The lateral mobility of the ivermectin probe

The mean lateral diffusion rate of bodipy ivermectin was found to be $14 \times 10^{\alpha 10}$ cm^2/s but this varied considerably between vesicles. From the D_L value it was possible to calculate the mean rate of lateral movement in the membrane. In 2 dimensions (i.e. in the membrane) the displacement of a single molecule after time t, is given by:

$$x = \sqrt{(4D_L t)},$$

where x is the average displacement (cm) of a single molecule after time t (seconds), and (D_L) is the lateral diffusion rate constant. Then, in 1 s the ivermectin probe dissolved in the membrane would move, on average, a distance of 0·75 μm and in 100 s it would move 7·5 μm. This slow movement may largely explain the long delay observed in isolated outside-out patches of membrane following bath-application of ivermectin and the opening of Cl^α channels. Theoretical predictions (Saffman & Dellbruck, 1975) suggest that the size of molecules has little effect on the speed of lateral movement in the membrane. However, it was noted that bodipy ivermectin had a lateral diffusion rate that was nearly three times faster than a lipid probe. The reason for this is not known, but one explanation could be that the ivermectin partitions into a 'cholesterol poor' domain of the membrane which is more highly disordered; in this respect the probe resembles protein aggregates in the membrane (Housley & Stanley, 1982). The lipid probe was likely to partition into regions where cholesterol is likely to be present as well.

We are pleased to acknowledge Merck, Sharp and Dohme (USA) for financial support.

REFERENCES

AXELROD, D. D., KOPPEL, E., SCHLESSINGER, J., ELSON, J. & WEBB, W. W. (1976). Mobility measurement and analysis of fluorescence photobleaching recovery kinetics. *Biophysics Journal* **16**, 1055–69.

BURG, R. W., MILLER, B. M., BAKER, E. E., BIRNBAUM, J., CURRIE, J. A., HARTMAN, R., KONG, Y.-L., MONAGHAN, R. L., OLSEN, G., PUTTER, I., TUNAC, J. P., WALLICK, H., STAPLEY, E. O., OIWA, A. R. & OMURA, S. (1979). Avermectins, new family of potent anthelmintic agents: producing organism and fermentation. *Antimicrobial Agents for Chemotherapy* **15**, 361–7.

CAMBELL, W. C. & BENZ, G. W. (1984). Ivermectin: a review of efficacy and safety. *Journal of Veterinary Pharmacology and Therapeutics* **7**, 1–16.

DUCE, I. R. & SCOTT, R. H. (1985). Actions of dihydroavermectin B1a on insect muscle. *British Journal of Pharmacology* **85**, 395–401.

FISHER, M. H. & MROZIK, H. (1984). The avermectin family of macrolide-like antibiotics. In *Macrolide Antibiotics* (ed. Omura, S.), pp. 553–606. New York: Academic Press.

FOLEY, M., MACGREGOR, A. N., KUSEL, J. R., GARLAND, P. B., DOWNIE, T. & MOORE, I. (1986). The lateral diffusion of lipid probes in the surfaces of *Schistosoma mansoni*. *Journal of Cell Biology* **103**, 807–18.

FRITZ, L. C., WANG, C. C. & GORIO, A. (1979). Avermectin B1a irreversibly blocks postsynaptic potentials at the lobster neuromuscular junction by reducing muscle membrane resistance. *Proceedings of the National Academy of Sciences, USA* **76**, 2062–6.

GARLAND, P. B. (1981). Fluorescence photobleaching recovery: control of laser intensities with an acoustico-optic modulator. *Biophysics Journal* **33**, 481–2.

HOUSLEY, M. D. & STANLEY, K. K. (1982). *Dynamics of Biological Membranes*. Chichester: John Wiley and Sons.

KASS, I. S., LARSEN, D. A., WANG, C. C. & STRETTON, A. O. W. (1982). *Ascaris suum*: differential effects of avermectin B1a on the intact animal and neuromuscular strip preparations. *Experimental Parasitology* **54**, 166–74.

MARTIN, R. J. (1980). The effect of γ-aminobutyric acid on the input conductance and membrane potential of *Ascaris* muscle. *British Journal of Pharmacology* **71**, 99–106.

MARTIN, R. J., KUSEL, J. R. & PENNINGTON, A. J. (1990). Surface properties of membrane vesicles prepared from muscle cells of *Ascaris suum*. *Journal of Parasitology* **76**, 340–8.

MARTIN, R. J. & PENNINGTON, A. J. (1989). A patch-clamp study of effects of dihydroavermectin on *Ascaris* muscle. *British Journal of Pharmacology* **98**, 747–56.

MELLIN, T. N., BUSCH, R. D. & WANG, C. C. (1983). Postsynaptic inhibition of invertebrate neuromuscular transmission by avermectin B1a. *Neuropharmacology* **22**, 89–96.

SAFFMAN, P. G. & DELLBRUCK, M. (1975). Brownian motion in biological membranes. *Proceedings of the National Academy of Sciences, USA* **72**, 3111–13.

SCHAEFFER, J. M. & HAINES, H. W. (1989). Avermectin binding in *Caenorhabditis elegans*: a two-state model for the avermectin binding site. *Biochemical Pharmacology* **38**, 2329–39.

SCHAEFFER, J. M., STIFFY, J. H. & MROZIK, H. (1989). A chemiluminescent assay for measuring avermectin binding sites. *Analytical Biochemistry* **177**, 291–5.

WOLF, D. E., KINSEY, W., LENNARZ, W. & EDIDIN, M. (1981). Changes in the organization of sea urchin egg plasma membrane upon fertilization: indications from lateral diffusion rates of lipid soluble fluorescent dyes. *Developmental Biology* **18**, 133–8.

Asia Pacific Journal of Pharmacology 1992; 7: 231–244

Review Article

ELECTROPHYSIOLOGICAL EFFECTS OF ANTHELMINTICS IN THE PARASITIC NEMATODE *ASCARIS SUUM*

RJ Martin

Department of Preclinical Veterinary Sciences. R.(D.) S.V.S., Summerhall, University of Edinburgh, Edinburgh, EH9 1QT, Scotland, U.K.

(Received 13 May 1991, Accepted 22 April 1992)

I. Introduction 231

II. The Organization of the Neuromuscular System of *Ascaris*
A. The Neuronal Organization 232
B. Anatomy of the Somatic Muscle Cells 233

III. Experimental Methods
A. Collection and Maintenance of *Ascaris* 233
B. Intracellular Recordings from Muscle Flap Preparations 233
C. Two-microelectrode Current-clamp Technique 234
D. Two-microelectrode Voltage-clamp Technique 234
E. Patch-clamp Technique for Recording Single-ion channels 235

IV. Electrophysiological Effects of Anthelmintics in *Ascaris*
A. Electrophysiological Effects of Piperazine 236
B. Pharmacology of the *Ascaris* GABA Receptor 237
C. *Ascaris* Muscle has Acetylcholine Receptors 238
D. The Ionic Basis of the Acetylcholine Response 238
E. Electrophysiological Effects of Levamisole Pyrantel and Morantel 238
F. Single-channel Currents Activated by Acetylcholine, Levamisole, Pyrantel and Morantel 239
G. Electrophysiological Effects of Ivermectin 240
H. Avermectins may also have an Action in the Nervous System of *Ascaris* 242

V. Conclusion 242

Key words: *Ascaris suum*, Nematode, Anthelmintics, Electrophysiology, Levamisole, Pyrantel, Morantel, Ivermectin.

Introduction

Intestinal nematode parasites cause serious and frequent disease in man and animals. Estimates suggest that more than 1000 million people in the Third World are infected by the large intestinal nematode parasite, *Ascaris lumbricoides*; these people suffer poor growth and malnutrition as a result. The growth and performance of livestock in both affluent and poorer countries is also affected by intestinal nematode parasites.

The control of intestinal nematodes in man and animals involves hygiene and management to prevent infection as well as the use of anthelmintics to cure established infection.

A number of anthelmintics like piperazine and levamisole act by interfering with the normal action of membrane ion-channels in parasites and therefore have pronounced electrophysiological effects. These electrophysiological effects have been recorded from a nematode parasite of the pig, *Ascaris suum*.

Correspondence: RJ Martin

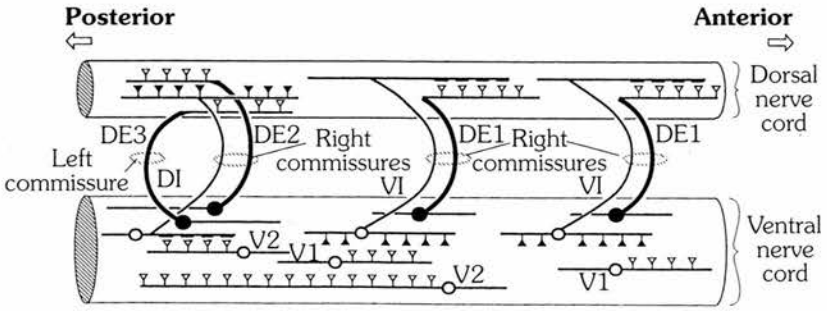


Fig. 1. Diagram of anatomy of motor neurone organization of one 'segment' of *Ascaris* Eleven motor neurones are present in each segment. There are 7 anatomical types, but only two physiological types (E: excitatory, cholinergic. I: inhibitory, GABAergic). DE1: dorsal excitator 1. DE2: dorsal excitator 2. DE3: dorsal excitator 3. DI: dorsal inhibitor. VI: ventral inhibitor. V1 and V2 ventral (excitatory) motor neurones. The cell bodies of all motor neurones are in the ventral cord. The commissures are axons which pass around the body wall.

Adult *Ascaris suum* are common, large, (up to 30cm) worm-like parasites found in the intestine of many pigs. The frequent occurrence of the parasites means that they can be collected from most abattoirs on a weekly basis for laboratory study. The large size of this parasite and its muscle cells have facilitated anatomical, biochemical, physiological and pharmacological studies, more difficult on smaller nematodes.

The purpose of this paper is to: (i) review the organization of the neuromuscular system of *Ascaris*; (ii) review the experimental methods available for recording electrophysiological effects of anthelmintics in *Ascaris*; (iii) review the electrophysiological effects of anthelmintics and the pharmacology of the receptors on which they act. It is also hoped that the account will provide a useful background for understanding the action of these drugs which act in this way.

II. THE ORGANIZATION OF THE NEUROMUSCULAR SYSTEM OF *ASCARIS*

A. The neuronal organization

Since the early studies of Goldschmidt (1 & 2) it has been known that there is only a small number of neurones present (circa 250) in *Ascaris*. The neurones are found in the same position and have the same structure in each animal. Indecently the same organization and neuronal structure appears to occur throughout nematodes (3 & 4).

There are two main nerve cords which arise from a crainial pharyngeal nerve ring; they form the dorsal and ventral nerve cord (Fig. 1). The motor neurones are found scattered in the ventral nerve cord and connect to the dorsal nerve cord via commissures which contain single or double fibres.

Stretton *et al.*, (5) have described and classified the anatomy and physiology of motor neurones. The motor nervous system is divided into segments; each segment usually has three paired right-hand commissures, one left-hand commissure and contains 11 motor neurones with 6 non-segmental interneurones crossing the segments. Each motor neurone cell body has two processes; one of the processess may have a single branch. The 11 motor neurones are separated into 7 anatomical types according to the distribution of their axon and dendrites: three types (DI, DE2 and DE3) are only found once in each segment, but the remaining four types (DE1, VI, V1 and DE3) are represented twice in each segment.

Intracellular recordings from muscle showed that stimulation of DI and VI produced inhibitory hyperpolarizing potentials and that the other motor neuronal types were or were likely to be excitatory (5). Histological studies showed that choline acetyltransferase was present in DE1, DE2 and DE3 motor neurones, a finding consistent with the suggestion that acetylcholine is an excitatory transmitter in *Ascaris* (6). GABA-immunoreactivity has been identified in the inhibitory motor neurones, DI and VI (7:8), a finding consistent with the suggestion that GABA is the

inhibitory transmitter. In addition to the transmitters acetylcholine and GABA, it is likely that peptides as co-transmitters are also present in motor neurones of *Ascaris* (9). The most abundant peptides are immunogenically similar to FMRFamide (9). Two of these have been isolated from *Ascaris* and characterized. The first is named AF1 (*Ascaris F*MRFamide-like peptide *1*); the second is named AF2 (9).

B. Anatomy of the somatic muscle cells

The structure of *Ascaris* muscle cells was described as early as 1866 by Schneider (10) but was the subject of debate by several scientists (1; 2; 11) because of its peculiar structure, with branches of the muscle passing to the nervous system rather than processes of the nervous system passing to the muscle cells.

Fig. 2 shows in diagrammatic form the location and structure of *Ascaris* somatic muscle cells. Each cell is composed of three regions: there is the contractile spindle region which lies under the hypodermis and is composed of obliquely striated muscle (12; 13 14); there is the bag region which is a large 200µM bag-shaped structure, located in the perienteric space, which contains the nucleus and particulate glycogen; there is the arm which is a thin process arising from the base of the bag and passing to the syncytium where it breaks up into a number of fine processes or fingers that are electrically coupled to the fingers of adjacent cells. Neuromuscular junctions are formed between the longitudinal axons and the syncytium by 2µM extensions of the longitudinal axons which penetrate the hypodermal chalice and approach the syncytium. Synaptic vesicles are of two types: 40nM clear vesicles, clustered near the presynaptic membrance and dense-core vesicles, 80-100nm in diameter. Except in the head, only dorsal muscle cells are connected to the dorsal nerve cord; the ventral muscle cells are likewise only connected to the ventral nerve cord. This arrangement is consistent with contraction which is only possible in the dorso-ventral plane.

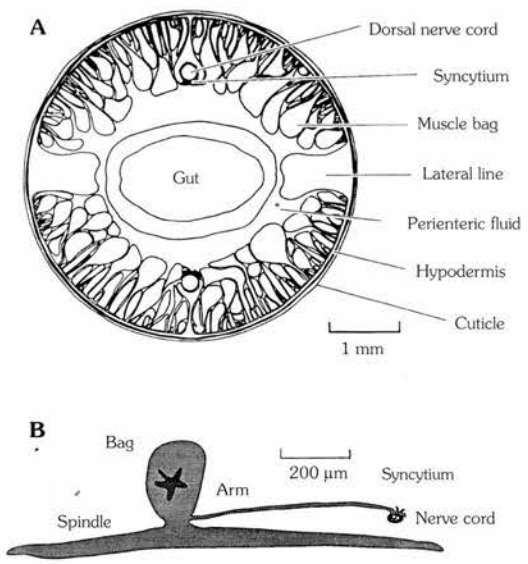


Fig. 2. Top: Diagram of a transverse section through the body wall of *Ascaris* in the anterior region. Bottom: diagram of muscle cell structure.

III. EXPERIMENTAL METHODS

A. Collection and maintenance of *Ascaris*

Specimens of *Ascaris suum* may be obtained most easily from abattoirs where the pig intestines are emptied for the preparation of sausage skins. The worms should be placed in a flask containing Locke's solution at 37°C immediately after removal. The parasites are then returned to the laboratory and maintained at 37°C in a water bath containing Locke's solution which is replaced daily. Under these conditions the parasites survive for over one week but it is probably best to use them within four days.

B. Intracellular recordings from muscle flap preparations

Jarman (15) was the first to make intracellular recordings from muscle cells of *Ascaris*. He described the use of the flap preparation (Fig. 3) and intracellular micropipettes for recording.

Muscle flaps are usually made from 2cm cylindrical sections of the worm which have been taken from a region 6cm behind the head. These sections are then cut along one of the lateral lines and the intestine of the parasite removed. The preparation is pinned, cuticle side down onto

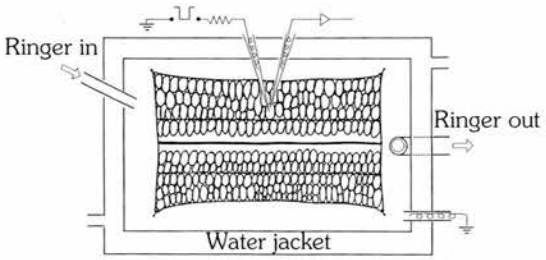


Fig. 3. Diagram of a flap preparation as viewed down a dissecting microscope and mounted on Sylgard in an experimental chamber. The chamber is fitted with a water jacket to maintain the temperature of the preparation. Two microelectrodes are shown inserted into the bag region of a muscle cell. One may be used for current injection, the other is used for recording voltage responses.

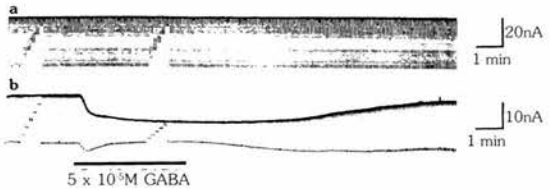


Fig. 4. The effect of 50μM GABA on membrane potential and input conductance. The top trace shows the injection of hyperpolarizing current pulses. The lower trace shows membrane potentials and the responses to injected current. The resting conductance increased from 2.1μS to 4.9μS. Although GABA produces hyperpolarization in most preparations, in some preparations it was small despite the production of a large conductance change; this is explained by variations in intracellular CI concentration and consequent effects on E_{CI}.

Sylgard in an experimental chamber surrounded by a water jacket which maintains the temperature of the preparation. The preparation can be perfused at a constant rate if bath-application of various drugs is required. Micropipettes can be placed under visual control with a dissecting microscope and micromanipulators.

Jarman (15) observed in muscle cells the presence of regular depolarizing potentials superimposed on a resting potential of around -35mV. The reason for the low resting potential has been investigated by Del Castillo *et al.* (16) and Brading and Caldwell (17). These studies have failed to explain the membrane potential in terms of the simple Goldman-Hogkin-Katz equations; but it was suggested by Brading and Caldwell (17) that an active electrogenic pump, possibly one responsible for moving carboxylic acids may be involved in maintaining the potential.

C. Two-microelectrode current-clamp technique

Muscle cells of *Ascaris* are large enough to permit two micropipettes to be placed in the bag region of the muscle cell. One may be used for current injections and the other may used to record the voltage response (Fig. 3) This approach allows membrane potential and conductance responses to drugs to be observed (18). Conductance changes in response to drugs applications are determined from ohmic responses to hyperpolarizing current pulse. Fig. 4 illustrates the effect of 30μM GABA on the membrane potential and input conductance: the top trace shows hyperpolarizing current pulses of 250ms duration (downward deflection); the bottom trace of Fig. 4 shows the hyperpolarizing voltage responses; the input conductance increased from a resting value of 2.1μS to 4.9μS. Conductance dose-response relationships may be determined using this approach and have been used to examine effects of the anthelmintic piperazine (19) and levamisole, morantel and pyrantel (20).

D. Two-microelectrode voltage-clamp

Since two microelectrodes can be placed simultaneously in the muscle bag for current-clamp, it only requires a change of amplifier to be able to carry out voltage-clamp of the bag. An example of a suitable amplifier is an Axoclamp 2A. Although the shape muscle cell of *Ascaris* suggests that the space-clamp may not be complete at distant regions from the bag, insertion of a third microelectrode into the bag region showed that the voltage-clamp was good in the bag. The advantage of voltage-clamp is that agonist induced currents can be observed at different membrane potentials to determine reversal potentials. For example piperazine when allied by ionophoresis to the bag produces a current that has a reversal potential near -65mV (19). Since the Nernst potential for CI in these experiments was also -65mV, it was concluded that piperazine opens channels permeable to CI ions.

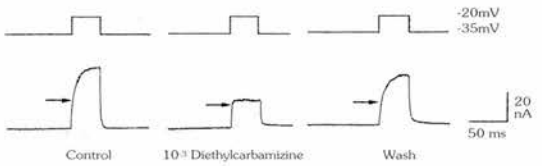


Fig. 5. The blocking action of 1mM diethylcarbamazine on the voltage-activated outward K current. Top trace: membrane potential. Lower trace: current.

In addition to being able to examine agonist channel current reversal potentials, the voltage-clamp technique allows voltage-activated currents to be observed and the effect of anthelmintics on these currents to be observed. Diethycarbamazine has a blocking action on voltage-activated K currents in *Ascaris*, Fig. 5. The blocking of these currents may explain the increased contractility produced when diethylcarbamazine is applied to *Ascaris* muscle strips.

E. Patch-clamp technique for recording single-ion channels

Single-channel currents, produced as ion-channels open and close, may be recorded from *Ascaris* muscle by applying the patch-clamp techniques of Hamill *et al.* (21). Patch-clamp recordings have been made from *Ascaris* whole muscle cells in situ (22) and from *Ascaris* isolated muscle vesicles (23).

To record from muscle cells in situ, it is necessary to treat flap preparations with collagenase (1mg ml^{-1}) for 1 hour to remove superficial connective tissue and the extracellular matrix which normally covers bag membranes. This permits patch-pipettes to 'seal' onto the membrane on suction.

Patch-pipettes are made using a two stage pulling process (21) to produce micropipettes with an outside tip diameter of 1µm. The patch-pipettes are then 'fire-polished' by bringing them close to a hot wire while they are viewed down a microscope. The function of the fire polishing is to 'melt' away any sharp edges so that when the pipette is pressed against the muscle membrane, there is no penetration of the cell. The fire polished pipette is then placed in a suction holder and connected to the head stage of the patch-clamp amplifier.

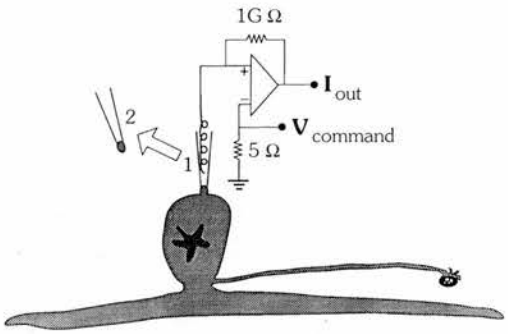


Fig. 6. Cell-attached (1) and outside-out (2) patch recording from the bag region of *Ascaris* muscle cells. The patch pipette is shown connected to an I/V converter which acts to record the channel currents collected from the patch membrane.

Micromanipulators then allow the patch-pipette to be placed onto the bag membrane, Fig. 6. Gentle suction (5cm water) which reduces the pressure in the patch-pepitte draws the muscle membrane into the tip of the pipette and is associated with a large increase in the resistance of the pipette. The resistance usually increases

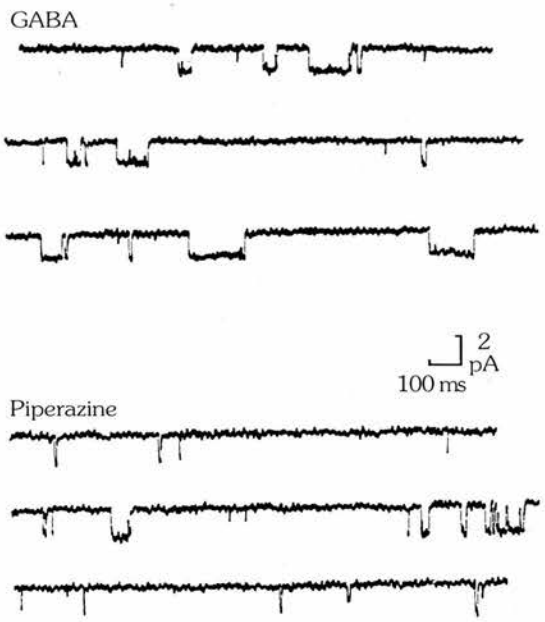


Fig. 7. Single-channel currents. Openings downwards. Top traces: channels currents activated by 3µM GABA; -75mV; effective mean open-time 32ms. Lower traces: channel currents activated by 500µm piperazine; -75mV; effective mean open-time 14ms.

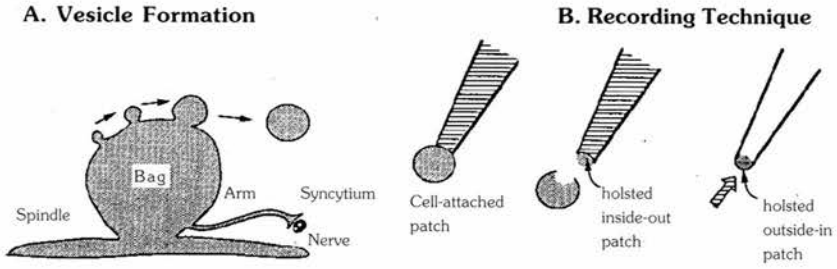


Fig. 8. Diagram of vesicle formation from the bag region of the muscle and the different types of patch used for recording.

to > 1 Giga ohm and is usually referred to as a Giga-seal. The advantage of this type of seal is that it reduces the background noise in the current record and allows 'single-channel' currents of 1pA to be resolved, Fig. 7.

More recently we have developed a muscle vesicle preparation, Fig. 8, for *Ascaris* (23) which can be viewed under phase contrast and which is easier to use experimentally. Vesicles are prepared from the bag preparation using the same collagenase solution as described before, but the collagenase is only applied to the preparation for ten minutes before washing it off. If the flap preparation is then placed in an incubator at 37°C for at least 1 hour, vesicles gradually form from the bag region and 'bud off' allowing them to be collected from the bottom of the bath using a Pasteur pipette. These vesicles are particularly suitable for patch-clamp recording.

IV. ELECTROPHYSIOLOGICAL EFFECTS OF ANTHELMINTICS IN *ASCARIS*

A. Electrophysiological effects of piperazine

Piperazine, Fig. 9 has a heterocyclic ring structure. It produces reversible paralysis of *Ascaris suum* in vitro (24) and was suggested to act like an acetylcholine agonist (25). However, Del Castillo *et al.* (26) recorded the intracellular membrane potential from *Ascaris* muscle during the bath-application of piperazine and found that piperazine produced a Cl dependent hyperpolarization that mimicked the stimulation of nerve cord. They therefore proposed that piperazine mimicked the action of a naturally occurring inhibitory transmitter of *Ascaris*. Subsequently Del Castillo *et al.* (27) showed that GABA has a similar effect to piperazine but was 100 times more potent.

The receptors responsible for the effects of piperazine were originally reported to be located only at the synaptic (syncytial) region of the muscle cell since responses to ionophoretic application were reported to only occur at this site (26).

The two-microelectrode current-clamp and voltage-clamp techniques were used by Martin (18; 19) to study GABA and piperazine conductance changes in the bag region of muscle cells. It was found from ionophoresis experiments that piperazine and GABA produced a dose-dependent increase in Cl conductance in the bag region by acting on extrasynaptic receptors of the bag. Piperazine was some 10-100 times less potent than GABA in producing conductance changes. Thus there are synaptic receptors located at the syncytium which are affected by piperazine as well as extrasynaptic receptors on the muscle surface of the bag. Simultaneous application of piperazine and GABA from two separate ionophoretic pipettes during

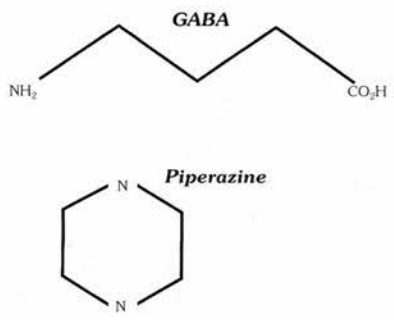


Fig. 9. Chemical structure of GABA and piperazine.

voltage-clamp experiments confirmed that piperazine and GABA, in fact, activate the same receptor.

GABA and piperazine activated single-channel currents have been recorded from collagenase treated whole muscle cells in situ in flap preparation (22). It was found that GABA (in concentrations greater than 1μM) or piperazine (in concentration greater than 200μM) applied to the extracellular surface of membrane patch brought about opening of rectangular shaped current pules of varying duration but essentially constant amplitude, Fig. 7. The I/V plots showed that both agonists opened channels which had conductances in the region of 22pS; although occasionally two subconductance states were sometimes seen.

At low concentrations of GABA the effective mean open-time was in the region of 32ms: in contrast the effective mean open-time produced by low concentrations of piperazine was in the region of 14ms. The explanation for the difference in the potency of the two agonists was explained by the fact that piperazine required a much higher concentration to produce channel opening and the fact that piperazine activated channels were open for a shorter time.

The observation that piperazine is a GABA receptor agonist, but does not posses a carboxyl group unlike GABA, is interesting and suggests that the *Ascaris* GABA receptor may not require the carboxyl group for channel opening. In turns out that piperazine is most effective on intestinal parasites in a high CO_2 environment: the carbon dioxide may therefore combine with one of the nitrogen atoms of piperazine and substitute for the carboxyl group. Thus piperazine is a more effective GABA agonist in a high CO_2 environment.

B. Pharmacology of the *Ascaris* GABA receptor

Since piperazine has been shown to act on *Ascaris* muscle GABA receptors, it is possible that the pharmacology of the receptors and any difference between it and the host GABA receptors could be exploited for therapeutic purposes. The pharmacology of *Ascaris* muscle GABA receptors has been studied using the two microelectrode current-clamp techniques to determine conductance dose-response relations during the bath-application of GABA agonists and antagonists (18; 19; 28; 29; 30; 31; 32). The effects piperazine and SR95103 and at the single-channel level have also been observed (22; 23).

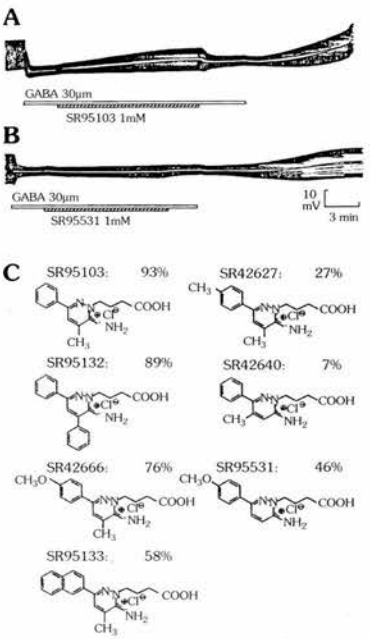


Fig. 10. A: Effects of SR95103 on the GABA conductance response. B: Effect of SR95531 on the GABA conductance response. C: Chemical structure of arylaminopyridazine-GABA antagonists and the mean percentage inhibition produced by 1mM antagonist of conductance increases produced by 30μM GABA.

The *Ascaris* GABA receptor agonist profile is similar, although not identical to vertebrate $GABA_a$ receptors. One difference is that the potency of sulphonic acid GABA derivatives (3APS & P4S) is less than at vertebrate $GABA_a$ receptors and piperazine is a selective agonist. The major pharmacological difference between vertebrate $GABA_a$ receptors and the *Ascaris* GABA receptor is that the $GABA_a$ antagonists bicuculline, securinine, pitrazepine and SR95531 are weak or inactive in *Ascaris*.

A series of experiments with the arylaminopyridazine GABA antagonists, Fig. 10 was therefore carried out to further explore the pharmacology of the GABA antagonists in *Ascaris* (32). It was found that SR95103 and SR95132 are the most potent and that SR95531 has a low potency. The potency order of this series of arylaminopyridazines contrasted with that seen

at the vertebrate $GABA_a$ receptor and was further evidence that the GABA receptor of *Ascaris* can be separated pharmacologically. It was concluded that this difference might be exploited for future therapeutic purposes.

C. *Ascaris* muscle has acetylcholine receptors

In addition to GABA receptors it has now been shown that *Ascaris* muscle has acetylcholine receptors. Bladwin & Moyle (34) and then later Norton and De Beer (25) showed that bath-applied acetylcholine produces contraction of muscle strips and therefore demonstrated the presence of acetylcholine receptors on muscle. Intracellular recordings of muscle membrane potential by Del Castillo *et al.* (35) showed that acetylcholine produces depolarization and changes in spike frequency and amplitude. Although Del Castillo *et al.* (35) suggested that the acetylcholine receptors were only located at the synaptic (syncytial) region, it was later found that the receptors were also distributed extrasynaptically over the muscle surface and could be found on the bag region as well (19).

D. The ionic basis of the acetylcholine response

Ascaris acetylcholine receptors on muscle activate non-selective cation channels like those activated by nicotinic agonist in vertebrates. This was shown by examining the current response to ionophoretically applied acetylcholine to the bag region under voltage-clamp (19). It was found that acetylcholine increases the non-selective cation conductance of the membrance with a reversal potential near 0mV. This is compatible with acetylcholine opening a channel permeable to both Na and K.

E. Electrophysiological effects of levamisole, pyrantel and morantel

The non-selective cation channels opened by acetylcholine are also activated by a range of nicotinic agonists (36) as well as the anthelmintics levamisole, pyrantel and morantel. The chemical structures of pyrantel, morantel and levamisole are shown is Fig. 11. Levamisole is an imidothiazole and is chemically distinct from pyrantel and morantel which are tetrahydropyrimidines. It might be predicted therefore, that some pharmacological properties of pyrantel and morantel may be distinguished from levamisole.

Aubry *et al.*, (37) reported aspects of the pharmacology pyrantel and some of its analogues in a variety of vertebrate and helminth preparations. They showed that intracellular recording from muscle cells of *Ascaris* during that bath-application of pyrantel mimicked the action of acetylcholine: both agonists produced depolarization, increase in spike discharge frequency and contracture. The effects of acetylcholine and pyrantel on contraction of *Ascaris* muscle strips were blocked by the nicotinic antagonist tubocurarine. Pyrantel was more potent than acetylcholine and its actions were persistent and not reversed by repeated washing. Piperazine was also reported to antagonize the actions of pyrantel: an effect which can now be interpreted as physiological antagonism with piperazine acting on GABA receptors not acetylcholine receptors.

Aceves *et al.*, (38) reported in the same volume of the British Journal of Pharmacology as Aubry *et al.* (37) that the effects of tetramisole (a d, l racemic mixture, of which levamisole is the laevo isomer) was to produce depolarization and an increase in spike frequency.

However the effects on muscle contraction were reported not to be antagonised by high doses of tubocurarine (in contrast to pyrantel); this observation suggested that levamisole might have acted on different receptors compared to pyrantel. This suggestion has not been substantiated subsequently.

The two microelectrode current-clamp and two microelectrode voltage-clamp techniques were used by Harrow and Gration (20) to examine the mode of action of morantel, pyrantel and levamisole

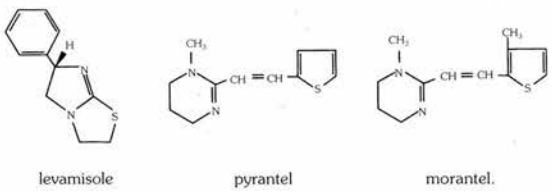


Fig. 11. Chemical structure of levamisole, pyrantel, morantel.

when applied by to the bag region of *Ascaris* muscle. Microperfusion of acetylcholine and the anthelmintics increased input conductance and depolarized the membrane potential of muscle bags. Currents following ionophoretic application of fixed doses of acetylcholine and the anthelmintics were observed at different potentials under voltage-clamp. The reversal potentials of all the agonists was near 0mV as had been reported earlier for acetylcholine (19). This is explained by the anthelmintics opening an ion-channel which is permeable to both Na and K. Simultaneous ionophoretic application experiments of acetylcholine and pyrantel showed that both agonists acted on the same receptor. The relative potencies of acetylcholine and the anthelmintics was determined from the current clamp experiments where changes in input conductance were measured and found to be: morantel = pyrantel > levamisole > acetylcholine. Thus pyrantel and morantel were more potent than levamisole.

Interestingly the current-voltage relationships described by Harrow and Gration (20) for acetylcholine, levamisole, morantel and pyrantel were non-linear, with the current failing to increase sufficiently on hyperpolarization. If the probability of the ion channels being open were to remain constant as the membrane potential is increased, it would be expected that the I/V plots would be linear; thus if the conditions of the voltage-clamp were satisfactory, the non-linear I/V plot implies that, the proportion of time the channels are open, decreases with hyperpolarization. In addition to this observation, dose-response relationships for morantel and pyrantel declined after reaching a maximum as agonist concentration was increased; they were described as being 'bell shaped' but desensitization was not observed.

These phenomena may be explained by open channel-block by the agonist (39). The anthelmintics levamisole, pyrantel and morantel are organic cations and in addition to acting as an agonist opening channels, may enter open ion-channels under the influence of the voltage-field; they are too big to pass through the channel like Na or K and would therefore produce a voltage-sensitive open channel-block (e.g. 39 & 40). Channel-block may explain the 'bell shaped' dose-response relationships of Harrow and Gration (20) with low concentrations of the anthelmintics acting as an agonist opening the ion-channel and higher concentrations producing ion-channel block.

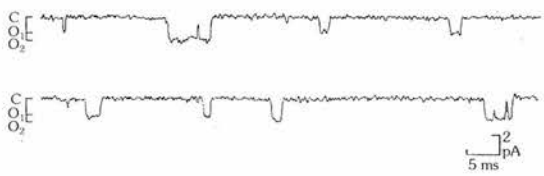


Fig. 12. Acetylcholine-activated channels in a cell attached patch from a muscle vesicle. C: closed state. O_1 smaller conductance. O_2: larger conductance. -50mV. Mean open time: 1.5ms.

The non-linear I/V plots under voltage-clamp may also be explained by open channel-block since the anthelmintics are large cations and present on the outer membrane and will be drawn increasingly into the channel as the membrane is hyperpolarized. Although these results appear to be explained by the anthelmintics acting as agonist and open channel-blockers, other explanations including voltage-sensitive desensitization and poor space-clamping have been suggested by Harrow and Gration (20).

F. Single-channel currents activated by acetylcholine, levamisole, pyrantel and morantel

Properties of single-channel currents activated by acetylcholine, Fig. 12, have been recorded from cell-attached and isolated-inside out patches from *Ascaris* muscle vesicles (41). The channels are non-selective cation channels and have at least two conductances, 40-50pS and 25-35pS. The I/V plots of both channels are linear and channel open-times are essentially indepedent of patch-potential. Kinetic analysis of the larger conductance openings shows that they have two open-states, brief ones lasting on average 1.2ms and longer ones lasting 4.9ms. In addition it was observed that the openings occurred in bursts which were seen as a sequence of openings separated by brief closings and that high concentrations of acetylcholine produced sequences of openings (Clusters) which were separated by long (200 seconds) closed periods characteristic of desensitization. The kinetics

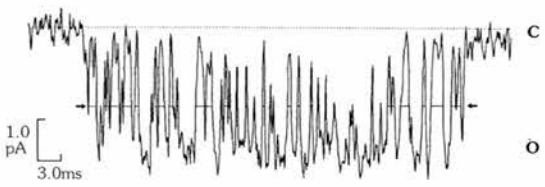


Fig. 13. Levamisole (30μM) activated channels from an isolated inside-out patch. -75mV. Note the long burst of the 'flickering' or rapid sequence of opening and closings characteristic of open channel-block. C: closed state. O: open state.

of the smaller conductance channel have not been studied in detail but are not obviously different to that of the larger conductance channels.

Levamisole-activated channel currents have also been recorded from the vesicle preparation (42). The ion-channels were also shown to be cation-selective and to have similar kinetic properties to acetylcholine-activated channels when levamisole was applied at low concentrations. At higher concentrations of levamisole a 'flickering' channel-block was observed, Fig. 13 during hyperpolarization. The characteristic voltage-sensitive flickering seen with levamisole and with other open channel-blockers (40) shows that the anthelmintics may also act as open channel-blockers in addition to acting as an agonist.

It was also found that high concentrations of levamisole could activate channels when applied to the cytoplasmic membrane via the bath while recording from channels with an inside-out patch. This observation can be explained by the pKa of levamisole which is 8.0 and the pH of the bath which was 7.2; under these conditions 15% of the levamisole is in an unionized form and can diffuse from the bath through the membrane of the patch to reach the extracellular receptor facing the pipette solution. The high proportion of unionized levamisole means that this anthelmintics can readily cross lipid barriers including the nematode cuticle to reach the active site which appears to be on the muscle surface of the parasite. The anthelmintics pyrantel and morantel have yet to be studied fully at the single-channel level but preliminary observations, show that they too open cation-selective channels with a similar conductance.

G. Electrophysiological effects of ivermectin

Avermectins are a family of highly lipid soluble macrocyclic lactones derived from *Streptomyces avermitilis*. The anthelmintic action of these compounds is now well recognised and has been reviewed by Cambell and Benz (43). The mode of action of these compounds is still the subject of active study but in a number of preparations avermectins increase the Cl conductance of muscle or nerve preparations of susceptible species. Electrophysiological effects of 22, 23 dihydroavermectin B1a (DHAVM) in *Ascaris* has been reported by Kass *et al.* (44; 45; 46) Martin (47); Martin and Pennington (48); Holden-dye and Walker (49); and Rheinhallt *et al.* (50). Application of micromolar concentrations of DHAVM to *Ascaris* muscle under current-clamp normally produces little effect, either hyperpolarization or by showing a conductance increase, when the preparation is bathed in normal solutions (44; 47; 49).

One suggested mode of action for avermectins is that they are GABA agonists or potentiators and that this may explain the increase in membrane Cl conductance seen in a number of preparations (51; 52). Since the *Ascaris* muscle bags contain GABA receptors it would be expected that such an action would produce hyperpolarization and an increase in conductance comparable to that observed with piperazine (19). Since this was not observed it makes such an action unlikely in *Ascaris*.

The effect of avermectins on *Ascaris* GABA channels has been studied with the current-clamp and patch-clamp technique (48; 49). GABA dose-response relationships) obtained with the current clamp-technique are depressed by avermectins in a non-competitive manner; the potency of a variety of avermectins seen in this study were reported to correlate with their antinematodal potency. It was therefore argued that the GABA antagonistic action in *Ascaris* muscle might represent a sight of action.

The effect of avermectins on GABA single-channel currents was studied by Martin and Pennington (48) using outside-out patches. Fig. 14 shows the effect on these

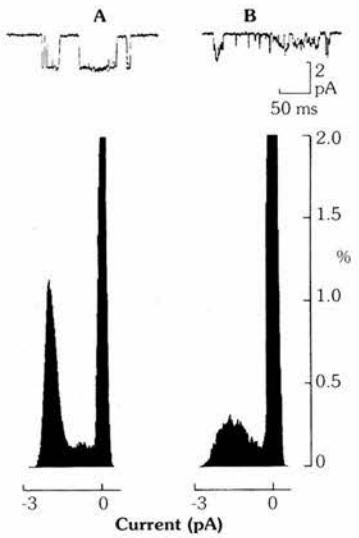


Fig. 14. 4μM GABA-activated channels and current amplitude histograms in the presence and absence of 200nM dihydroavermectin B1a. Outside-out patch recording. Note that dihydroavermectin reduces the mean channel current.

currents: it can be seen that DHAVM produces a dose-dependent reduction in the channel conductance and that there is also a dose-dependent reduction in the frequency of channel openings. This effect would appear as non-competitive antagonism if the effect were examined with the current-clamp technique.

Low concentrations (< 0.1nM) of DHAVM were also added to outside-out patches (48) and produced after a delay greater than 15 seconds the 'Staircase' effect: this was characterized by the progressive opening of Cl channels with an open-time greater than 100ms and conductances of 9-15pS, Fig. 15. Interestingly these channel currents were not produced when avermectin was added to the cytoplasmic membrane when inside-out patches were used. This observation was taken as indicating that DHAVM does not cross the patch membrane bilayer during the lifetime of the experiment, despite DHAVM being very lipophillic.

The membrane distribution of avermectins was further tested with a fluorescent ivermectin derivative, bodipy ivermectin, using the trypan blue quenching and FRAP (fluorescence recovery after photobleaching) techniques (53; 54). The experiments showed that the ivermectin probe did not migrate or 'flip-flop' across the membrane during the period of the experiment and that the lateral diffusion rate was of the ivermectin probe was 14×10^{-10}cm2 sec^{-1}. The slow lateral diffusion rate was suggested to explain the delay between DHAVM application and the opening of channels in outside-out patches. As a result of these observations a model for the mode of action for the avermectins was produced, Fig. 16. It is suggested that avermectins act on a Cl channel present in tissues of susceptible species in the lipid phase of the outer monolayer of the membrane.

Recently experiments in which Cl was replaced by NO_3 and recording the mean membrane potential from the bag regions of many muscles (50) have reported that high concentrations of avermectin produce a mean 3mV hyperpolarization over a period of 1 hour. These results are consistent with the patch-clamp observa-



Fig. 15. Staircase production of channels in an outside-out patch by dihydroavermectin. The dashed lines show the closed states. -75mV. Note the small size of the channels and their long open-times.

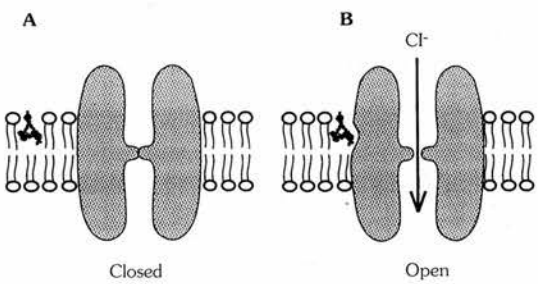


Fig. 16. Suggested mode of action for ivermectin. Ivermectin remains in the outer bilayer of the membrane and combines with a C1 channel only present in a susceptible species to produce opening.

tions which demonstrated opening of Cl channels by DHAVM and suggest the reason that the hyperpolarizing action of avermectins in *Ascaris* was missed was that there is a small response and a very slow onset.

H. Avermectins may also have an action in the Nervous system of *Ascaris*

A slit-chamber technique described by Kass *et al.* (46) has allowed the differential application of avermectin to the dorsal and ventral halves of *Ascaris*. In the experiments the two nerve cords remain connected by the commissures of only two motor neurones: these are the ventral inhibitory motor neurone VI and the dorsal excitatory neurone DE1. The responses to electrical stimulation of nerve cords or motor neurones were recorded by intracellular microelectrodes placed in the bags. It was found that avermectins blocked the response of DE1 to indirect stimulation via the nerve cord but not to direct stimulation: this observation was interpreted as suggesting that avermectins block transmission between interneurones in the spinal cord and the excitatory motor neurones. In addition the hyperpolarizing response in muscle to direct stimulation of VI was blocked by avermectin, an observation consistent antagonism of muscle GABA receptors described above.

These later observations suggest that avermectins may have more than one site of action and that one site may be within the nervous system.

Conclusion

This review has described the *Ascaris* preparation and its use for studying the electrophysiological effects of anthelmintics. It has helped our understanding of the mode of action of a number of compounds. It seems likely that its use will continue as our understanding and requirement for anthelmintics increases in the future.

References

1. Goldschmidt R. Das Nervensystem von *Ascaris lumbricoides* und *Megalocephala*. I Zeitschift fur wissenschaftliche Zoologie 1908; 90: 73-136.
2. Goldschmidt R. Das Nervensystem von *Ascaris lumbricoides* und *Megalocephala*. II Zeitschift fur wissenschaftliche Zoologie 1909; 92: 306-357.
3. White JG, Southgate E, Thomson JN, Brenner S. The structure of the ventral cord of *Caenorhabditis elegans*. Philosophical Transactions of the Royal Society, Series B. 1976; 275; 298-327.
4. White JG, Southgate E, Thomson JN, Brenner S. The structure of the nervous system of *Caenor-habditis elegans*. Philosophical Transactions of the Royal Society, Series B. 1986; 314: 1-34.
5. Stretton AOW, Fishpool RM, Southgate E, Donmoyer JE, Waldrond JP, Moses JER, & Kass IS. Structure and physiological activity of the motoneurons of the nematode *Ascaris*. Proceedings of the National academy of Sciences, USA 1978; 75: 3493-7.
6. Johnson CD, Stretton AOW. Localization of choline acetyltransferase within identified motoneurons of the nematode *Ascaris*. Journal of Neuroscience 1985; 5: 1984-92.
7. Johnson CD. Stretton AOW. GABA-immunoreactivity in inhibitory motor neurons of the nematode *Ascaris*. Journal of Neuroscience 1987; 7: 223-35.
8. Sithigorngul P, Cowden C, Guastella J, Stretton AOW. Generation of monoclonal antibodies against a nematode peptide extract: another approach for identifying unknown neuropeptides. Journal of Comparative Neurology 1989; 284: 389-97.
9. Stretton AOW, Cowden C, Sithigorngul, Davis RE. Neuropeptides in the nematodes *Ascaris suum* 1991; Parasitology; 102: s107-s116.
10. Schneider A. Monographie der Nematode. Berlin. 1866.
11. Cappe De Baillon P. Etude sur les fibres musculaires d'*Ascaris*. I. Fibres parietales. Cellule 1911; 27: 165-211.
12. Rosenbluth J. Ultrastructural organization of obliquely striated muscle fibres in *Ascaris lumbricoides*. Journal of Cell Biology 1965; 25: 495-515.
13. Rosenbluth J. Ultrastructure of somatic muscle cells in *Ascaris* lumbricoides. II. Intermuscular junctions, neuromuscular junctions, and glycogen stores. Journal of Cell Biology 1965; 26: 579-91.
14. Rosenbluth J. Obliquely striated muscle III. Contraction mechanism of *Ascaris* body muscle. Journal of Cell Biology 1967; 34: 15-33.
15. Jarman M. Electrical activity in the muscle cells of *Ascaris* lumbricoides. Nature 1959; 184: 1244.
16. Del Castillo J, De Mello WC, Morales T. Influance of some ions on the membrane potential of *Ascaris* muscle. Journal of General Physiology 1964; 48: 129-40.
17. Brading AF, Caldwell PC. The resting membrane potential of the somatic muscle cells of *Ascaris lumbricoides*. Journal of Physiology 1971; 217: 605-624.
18. Martin RJ. The effect of γ-aminobutyric acid on the input conductance and membrane potential of *Ascaris* muscle. British Journal of Pharmacology. 1980; 71: 99-106.

19. Martin RJ. Electrophysiological effects of piperazine and diethylcarbamazine on *Ascaris suum* somatic muscle. British Journal of Pharmacology. 1982; 77: 255-65.
20. Harrow ID, Gration KAF. Mode of action of the anthelmintics morantel, pyrantel and levamisole on the muscle cell membrane of the nematode *Ascaris suum*. Pesticide Science 1985; 16: 662-72.
21. Hamill OP, Marty A, Neher E, Sakmann B, Sigworth FJ. Improved patch-clamp techniques for high resolution current recording from cells and cell free membrane patches. Pflugers Archives geshurn Physiologie 1981; 391: 85-100.
22. Martin RJ. Y-aminobutyric acid- and piperazine activated single-channel currents from *Ascaris suum* body muscle. British Journal of Pharmacology 1985; 84: 445-61.
23. Martin RJ, Kusel JR, Pennington AJ. Surface properties of membrane vesicle prepared from muscle cells of *Ascaris suum* 1990. Journal of Parasitology 76: 340-8.
24. Stranden OD. Activity of piperazine in vitro against *Ascaris lumbricoides* British Medical Journal 1955; II: 20-2.
25. Norton S, De Beer EJ. Investigations on the action of piperazine on *Ascaris lumbricoides*. American Journal of Tropical Medicine 1957; 6: 898-905.
26. Del Castillo J, De Mello WC, Morales T. Mechanism of the paralysing action of piperazine on *Ascaris* muscle. British Journal of Pharmacology 1964; 22: 463-77.
27. Del Castillo J, De Mello WC, Morales T. Inhibitory action of y-aminobutyric acid (GABA) on *Ascaris* muscle. Experientia 1964; 20: 141-3.
28. Holden-dye L, Walker RJ. ZAPA, (Z)-3-[(amino ininomethyl) thio]-2-propenoic acid hydrochloride, a potent agonist at GABA receptors the *Ascaris* muscle cell. British Journal of Pharmacology 1988; 95: 3-5.
29. Holden-dye L, Hewitt GM, Wann KT, Krogsgaard-Larsen P, and Walker RJ. Studies involving avermectin and the y-aminobutyric acid (GABA) receptors on the somatic muscle cells of the parasitic nematode, *Ascaris suum* Pesticide Science 1988; 24: 231-45.
30. Holden-dye L, Krogsgaard-larsen P, Nielsen L, Walker RJ. GABA receptors on the somatic muscle cells of the parasitic nematode, *Ascaris suum*: stereoselectivity indicates similarity to a $GABA_a$-type agonist recognition site. British Journal of Pharmacology 1989; 98: 841-50.
31. Duittoz AH, Martin RJ. Effects of the arylaminopyridazine-GABA derivatives, SR95103 and SR95531 on the *Ascaris* muscle GABA receptor: the relative potency of the antagonists in *Ascaris* is different to that at vertebrate $GABA_a$ receptors. Comparative Biochemistry and Physiology 1991; 98C: 417-22.
32. Duittoz AH, Martin RJ. Antagonist properties of arylaminopyridazine GABA derivatives at the *Ascaris* muscle GABA receptor. Journal of Experimental Biology 1991; 159: 149-64.
33. Duittoz AH, Martin RJ. Effects of SR95103 on GABA-activated single-channel currents from *Ascaris* muscle. Comparative Biochemistry and Physiology. 1991; 98C: 423-32.
34. Baldwin E, Moyle V. A contribution to the physiology and pharmacology of *Ascaris lumbricoides* from the pig. Journal of Physiology 1949; 4: 145-52.
35. Del Castillo J, De Mello WC, Morales T. The physiological role of acetylcholine in the neuromuscular system of *Ascaris lumbricoides*. Archives Internationals de physiologie et de biochemie 71: 741-57.
36. Colquhoun L, Holden-dye L, Walker RJ. The pharmacology of cholinoceptors on the somatic muscle cells of the parasitic nematode *Ascaris suum*. Journal of Experimental Biology 1991; 158; 509-30.
37. Aubry ML, Cowell P, Davy ML, Shevde S. Aspects of the pharmacology of a new anthelmintic: pyrantel. British Journal of Pharmacology 1970; 38: 332-44.
38. Aceves J, Erliji D, Martinez-Marnon R. The mechanism of the paralysing action of tetramisole on *Ascaris* somatic muscle. British Journal of Pharmacology 1970; 38: 602-7.
39. Colquhoun D, Sakmann B. Fast events in single channel currents activated by acetylcholine and its analogues at the frog muscle end-plate. Journal of Physiology 1985; 369: 501-57.
40. Neher E, Steinbach JH. Local anaesthetics transiently block currents through single acetylcholine receptor channels. Journal of Physiology 1978; 277: 153-76.
41. Pennington AJ, Martin RJ. A patch-clamp study of acetylcholine activated ion channels in *Ascaris suum* muscle. Journal of Experimental Biology 1990; 154: 201-21.
42. Robertson SJ, Martin RJ. Levamisole-activated single-channel currents in isolated muscle vesicles from *Ascaris suum* British Journal of Pharmacology 1991; 102: 147P.
43. Cambell WC Benz GW Ivermectin: a review of efficacy and safety. Journal of Veterinary Pharmacology and Therapeutics. 1984; 7: 1-16.
44. Kass IS, Larsen DA, Wang CC Stretton AOW. Ascaris suum. differential effects of avermectin B1a on the intact animal and neuromuscular strip preparations. Experimental Parasitology 1982; 54: 166-74.
45. Kass IS, Stretton AOW, Wang AO. The effects of avermectin and drugs related to acetylcholine and 4-aminobutyric acid on neuromuscular transmission in *Ascaris suum* Molecular and Biochemical Parasitology 1984; 13: 213-25.
46. Kass IS, Wang CC Walrond JP Stretton AOW. Avermectin B1a, a paralysing anthelmintic that effects interneurones and inhibitory motorneurones in *Ascaris*. Proceedings of the national Academy of Sciences USA 1980; 77: 6211-15.
47. Martin RJ. The Y-aminobutyric acid receptor of *Ascaris* as a target for anthelmintics. Biochemical Society Transactions 1987; 17: 61-5.
48. Martin RJ, Pennington AJ. A patch-clamp study of effects of dihydroavermectin on *Ascaris* muscle. British Journal of Pharmacology 1989; 98: 747-56.
49. Holden-dye L, Walker RJ. Avermectin and avermectin derivatives are antagonists at the

4-aminobutyric acid (GABA) receptors on the somatic muscle cells of *Ascaris*; is this the site of anthelmintic action? Parasitology 1990; 101: 265-71.

50. Rheinhallt P, Holden-dye L, Walker RJ. Ivermectin increases the anion conductance of the resting membrane potential of *Ascaris suum* muscle bag cells. British Journal of Pharmacology. 1991; 104: 439P.
51. Wang CC, Pong SS. Actions of avermectin B1a on GABA nerves. In: Membranes and Genetic Disease. Ed. Sherard JR, Anderson VE, Eatong JW. 1982. New York: Liss 373-395.
52. Wright DJ. Biological activity and mode of action of avermectins. In: Neuropharmacology and Pesticide Action. Ed: Ford MG, Lunt GG, Reay RC, Usherwood PNR, 1986. Chichester: Ellis Horwood.
53. Martin RJ, Kusel JR, Robertson SJ, Minta A, Haughland RP. Distribution of a Fluorescent Ivermectin Probe, Bodipy Ivermectin, in Tissues of the Nematode Parasite Ascaris suum 1992. Parasitology Research; 78: 341-48.
54. Martin RJ, Kusel JR. On the distribution of a fluorescent ivermectin probe (4" 5, 7 dimethylbodipy proprionylivermectin) in *Ascaris* membranes. Parasitology. 1991; 104: 549-55.

An electrophysiological preparation of *Ascaris suum* pharyngeal muscle reveals a glutamate-gated chloride channel sensitive to the avermectin analogue, milbemycin D

R. J. MARTIN

Department of Preclinical Veterinary Sciences, R.(D.) S.V.S., Summerhall, University of Edinburgh, Edinburgh EH9 1QT

(*Received 1 June 1995; revised 6 July 1995; accepted 6 July 1995*)

SUMMARY

An electrophysiological preparation of *Ascaris suum* pharyngeal muscle suitable for recording changes of input conductance using a 2-microelectrode current clamp and pharmacological study is described. The preparation is shown to contain a glutamate-gated Cl (ion sensitive) channel sensitive to the avermectin analogue, milbemycin D. The application of glutamate produces a dose-dependent increase in Cl conductance and the effect of glutamate is potentiated by milbemycin D. Milbemycin D also produced a dose-dependent increase in input conductance.

Key words: glutamate, avermectin, milbemycin, chloride channel, anthelmintic, *Ascaris suum*.

INTRODUCTION

The avermectins and milbemycins are a group of structurally related, macrocyclic-lactone antibiotic anthelmintics used to control nematode parasites in man and animals (Campbell & Benz, 1984). They are broad spectrum and used to control onchocerciasis (river blindness) in humans and gastrointestinal, cardiac and respiratory nematode parasites of domestic animals. There is evidence to suggest that the mode of action of these compounds is to selectively paralyse the parasite by increasing muscle Cl permeability but the identity of the channel targeted by the avermectins and milbemycins has been controversial (see Arena (1994) for a recent review). Cloning of a GluCl-α ion-channel subunit and a GluCl-β ion-channel subunit from the model soil nematode *Caenorhabditis elegans* and co-expression of the subunits in *Xenopus* oocytes has led to the identification of a glutamate-gated chloride channel that has been shown to be sensitive to the avermectin compounds: 22,23-dihydroavermectin B_{1a}, and milbemycin D (Cully *et al.* 1994). The effect of these avermectin compounds, at low concentrations, was to potentiate the action of glutamate, and at higher concentrations, these compounds opened the glutamate-gated channel directly. The selective therapeutic action of avermectins and milbemycins might be explained by effects on glutamate-gated Cl ion-channels that are present in parasitic nematodes but that are not present in host animals.

Molecular experiments using the *lacZ* marker suggest that the GluCl-β subunit of the glutamate channel is expressed in the pharynx of *C. elegans* pM4 muscle (Laughton, Wolstenholme & Lunt, 1995). The muscle is required for pharyngeal pumping/feeding and is known to receive an inhibitory motor neurone, M3, that is not likely to be GABAergic (Avery *et al.* 1994) but glutamatergic (Avery, 1993). The location of the avermectin-sensitive glutamate-gated chloride channel, however, remains to be identified in parasitic nematodes as does its pharmacology. This paper describes a nematode parasite preparation suitable for electrophysiological and pharmacological study from the pig intestinal parasite, *Ascaris suum*. Experiments show that the pharyngeal muscle of this parasite possesses glutamate receptors that gate chloride channels and that are sensitive to the avermectin analogue, milbemycin D.

MATERIALS AND METHODS

The preparation

Ascaris suum were collected from the local abattoir and maintained in Locke's solution at 35 °C that was replaced daily. The pharyngeal muscle of *A. suum* was dissected out (Fig. 1) and mounted on Sylgard in an experimental chamber containing 6 ml of a well-stirred bathing solution maintained at 37 °C.

Solutions

The preparation was bathed, except where stated, in a low-Ca high-Cl solution containing (mM): NaCl,

 Copyright © 1996 Cambridge University Press

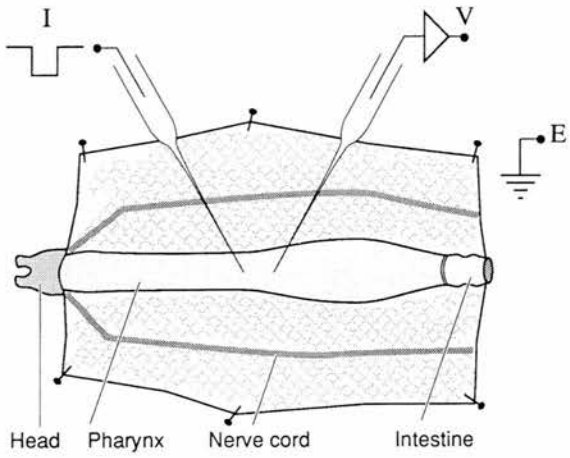


Fig. 1. *Ascaris suum* pharyngeal preparation and 2-microelectrode current clamp technique for measuring input conductance. The position of the current injection micropipette (I), voltage recording pipette (V) and bath earth (E) are shown.

132; KCl, 2·4; $MgCl_2$, 10; glucose, 11; HEPES, 5; 2% dimethyl sulphoxide (Me_2SO); pH 7·4, adjusted with NaOH. The low-Ca was used to abolish spontaneous action potentials and inhibitory potentials; the high-Cl was used to enhance conductance responses to glutamate. A zero-Cl solution was also used in which all the Cl was replaced by acetate.

Recording

Two glass micropipettes, filled with 2 M K acetate, were inserted into the pharyngeal muscle, in the mid-region, with the aid of a dissecting microscope and trans-illumination. The voltage recording micropipette had a resistance of 20–25 MΩ and the current injection electrode, a modified patch-pipette, had a resistance of 5 MΩ. Constant current clamp rectangular pulses of 1·5 μA lasting 1 s were injected at a rate of 0·2 Hz with an Axoclamp 2A fitted with a HS 2 (H = × 10) headstage to pass the hyperpolarizing current pulses. The time-constant of the membrane potential response was about 100 ms and the 1 s pulse duration was designed to permit the membrane potential to come to equilibrium. The current–voltage relationship of the pharyngeal muscle was examined and found to be linear in the ranges used. Current injection and voltage responses were monitored on an oscilloscope and voltage responses recorded on an Electromed 2-channel pen recorder. Large currents were injected into the pharyngeal muscle so the voltage responses recorded inside the pharynx during current injection were corrected for the effect of the series resistance of the bathing solution by subtracting the potential response (typically 3 mV) recorded just outside the pharynx during current injection. An agar bridge was used as a bath earth.

Pen records (Figs 2, 4, and 5) display the membrane potential as the upper thick line and a downward movement of the upper thick line indicates hyperpolarization. The regular downward spikes are the membrane potential responses to hyperpolarizing current pulses. The gaps between the upper and lower parts of the trace are due to rapid movement of the pen producing a skipping effect. The width of the trace reflects the input conductance of the muscle cell and a reduction in the width of the trace indicates an increase in input conductance.

Drugs

Concentrated stock solutions of L-glutamate (Sigma) and milbemycin D (Ciba Geigy) were added in volumes not more than 300 μl to the well-stirred bath. The stock solutions were made up in the standard bathing solution with 2% Me_2SO. 2% Me_2SO had no detectable effect on glutamate responses. Mixing was complete within 1 min (dye test). The preparation was washed by draining of the bath and replacement of the bathing solution 3 times. Milbemycin D was chosen as a representative of the avermectin compounds that have been shown to have a potent potentiating effect on glutamate-gated Cl channels (see Culley *et al.* (1994), table 1).

Analysis

Concentration–effect relationships were obtained by applying the drugs cumulatively. Responses were measured as the change in input conductance produced by the drugs after 4 min application. Glutamate dose–response relationships were described by the modified Hill equation:

$$\Delta G = \Delta G_{max}/[1+(ED_{50}/X_a)^{nH}],$$

where ΔG is the difference between the resting input conductance, observed in the absence of glutamate, and the input conductance observed after addition of the glutamate at a concentration of X_a; ΔG_{max} is the maximum predicted conductance change; ED_{50} is the concentration of glutamate producing the half maximum response; and nH is the Hill coefficient. A simplex routine (NAG E04CCF) was used in the FORTRAN non-linear least squares fitting program.

RESULTS

Initial experiments were carried out in a more physiologically appropriate bathing solution (APF solution: Byerly & Masuda, 1979) that had high-Ca (6 mM) and reduced-Cl (110 mM) concentrations designed to mimic the peri-enteric fluid that normally surrounds the pharyngeal muscle. Spontaneous hyperpolarizing potentials and pharyngeal action potentials were observed in this solution similar to those already described by Del Castillo &

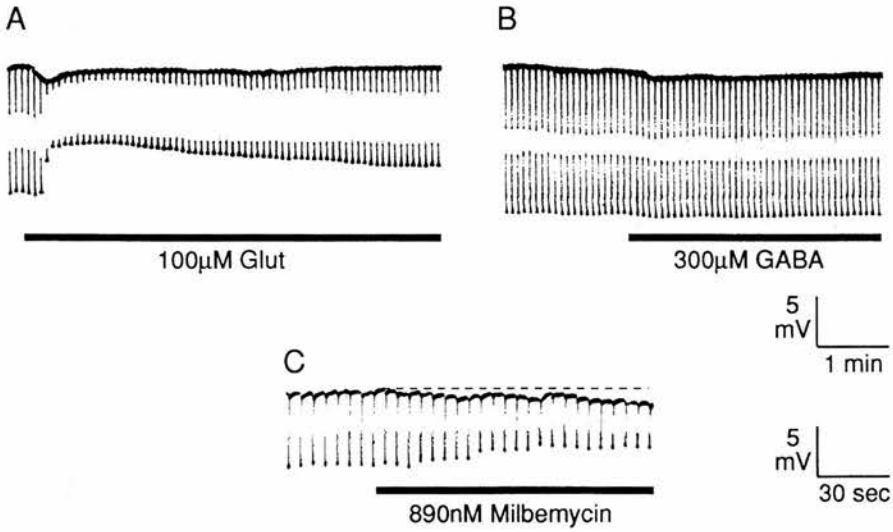


Fig. 2. (A) Effect of application of 100 μM L-glutamate on membrane potential and input conductance. Glutamate (applied during horizontal bar) produced a transient small hyperpolarization of 1 mV associated with an input conductance change from 157 μS to a peak of 429 μS (ΔG: 272 μS) desensitizing to 231 μS (ΔG: 74 μS) after 4 min. (B) After washing the preparation the input conductance of the pharynx returned towards control levels (142 μS) and the effect of 300 μM GABA was tested without effect (applied during the horizontal bar). The lack of effect of GABA was not due to desensitization because subsequent application of 100 μM L-glutamate increased the input conductance again (not shown). (C) Effect of 890 nM milbemycin D (different preparation from (A) and (B)) on the membrane potential and input conductance. Milbemycin slowly produced an increase in input conductance that was not reversed on washing (not shown).

Morales (1967). Although it was possible to see hyperpolarizing and conductance effects of glutamate under these conditions, the effects of glutamate and milbemycin D on the input conductance of the pharyngeal muscle were more pronounced and conditions more stable when the preparation was bathed in the low-Ca, high-Cl solution. The following description is based on the results of successful experiments from 10 pharyngeal preparations bathed in the low-Ca, high-Cl solution. The recordings were made from preparations with stable membrane potentials of -27 to -40 mV and resting input conductances not greater than 400 μS. Recordings were rejected if either of the microelectrodes came out during recording, if the input conductance declined progressively in the absence of any drug, or if in the absence of milbemycin D, the input conductance failed to return within $\pm 20\%$ of the control after washing L-glutamate.

Effect of glutamate

Fig. 2A shows typical effects of the application of 100 μM glutamate on pharyngeal input conductance and membrane potential: glutamate produced a transient small hyperpolarization of 1 mV associated with an input conductance change from 157 μS to a peak of 429 μS (ΔG: 272 μS) desensitizing to 231 μS (ΔG: 74 μS) after 4 min. Fig. 2B shows the same preparation after washing, where the resting input conductance returned to 142 μS and the application of 300 μM GABA has no detectable effect on the input conductance. The lack of effect of GABA could not be explained by desensitization of the receptor by glutamate because subsequent application of glutamate produced a conductance response. GABA consistently (5 preparations) produced little or no effect on input conductance at concentrations less than 300 μM. The effect of glutamate, in all preparations, was to produce a desensitizing and reversible increase in input conductance associated with a small change in membrane potential; the membrane potential was usually hyperpolarizing but in some preparations a small depolarizing potential was observed.

The glutamate-induced increase in conductance was dose dependent (Fig. 3). It was sigmoidal when plotted on an arithmetical ordinate, suggesting the existence of cooperativity and that more than one agonist molecule was required to open the ion-channel involved in producing the conductance response. When the dose–response curve of Fig. 3 was fitted by the modified Hill equation, nH was 2·75, again demonstrating the presence of positive cooperativity; the ED_{50} was 78 μM; ΔG_{max} was 305 μS. Similar numerical values were obtained in other dose–response relationships: nH was $2{\cdot}07 \pm 0{\cdot}26$; ED_{50} was 60 ± 11 μM; ΔG_{max} was 299 ± 132 μS (means $\pm$ S.E., $n = 4$).

Cl mediates the glutamate conductance increase

Bathing the pharyngeal preparations in zero-Cl solutions for about 30 min reversibly abolished the

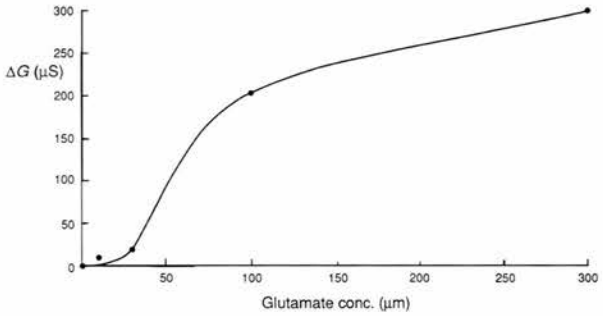


Fig. 3. Glutamate dose–response relationship plotted with an arithmetic scale ordinate. The sigmoidal relationship implies the presence of cooperativity and the involvement of more than 1 molecule of glutamate being required to open the channel. The points were from a single experiment and the line was fitted to the modified Hill equation with nH as 2·75, ED_{50} as 78 μM, ΔG_{max} as 305 μS.

glutamate conductance responses and demonstrated that the glutamate effect was mediated by a Cl channel. The approach of the method is to bath the preparation in zero-Cl for a long time to leach any intracellular or extracellular Cl from the preparation. The Cl is leached from the preparation after 20–30 min and then the application of glutamate does not produce any conductance change because there is no Cl ion (intracellular or extracellular) to carry current and produce a response. For example, Fig. 4A shows a preparation bathed in high-Cl solution where the resting input conductance was 158 μS and application of 100 μM glutamate produced a hyperpolarization of 7 mV and the conductance change, ΔG, was 342 μS. When the preparation was bathed in zero-Cl for 33 min (Fig. 4B), the resting input conductance of the pharynx decreased to 120 μS, and 100 μM glutamate produced little potential change and no detectable conductance change. When the preparation was returned to the high-Cl solution for 32 min (Fig. 4C) the resting input conductance increased to 176 μS and 100 μM glutamate produced a hyperpolarization of 2·5 mV and a ΔG of 196 μS. Similar effects were observed in 3 preparations examined in this way: in all 3 preparations, the zero-Cl solution abolished the glutamate-induced conductance response and indicated that it was a Cl ion-channel opened by glutamate. It is pointed out that the effect of zero-Cl on the glutamate-induced conductance was time dependent until all the intracellular Cl was removed: the glutamate-induced conductance changes decreased progressively as Cl was leached from the preparation. Interestingly, the zero-Cl also increased the resting input conductance of the pharynx indicating a resting Cl permeability of the pharyngeal muscle.

The effect of glutamate on membrane potential in the high-Cl solution was described earlier as usually a hyperpolarizing response but sometimes a depolarizing response was observed. The variation in the potential response can be explained by small variations in intracellular Cl concentration giving rise to variations in the glutamate reversal potential around the resting membrane potential.

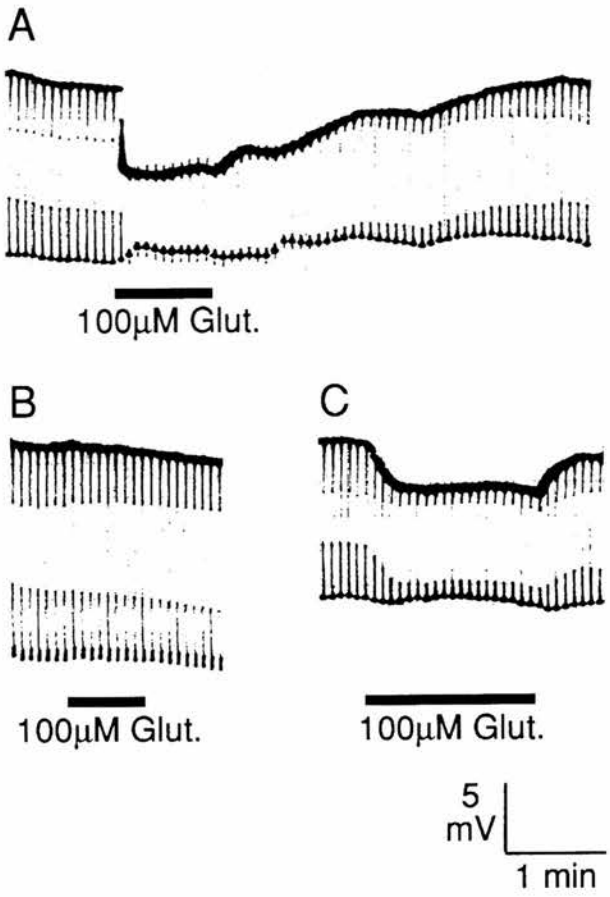


Fig. 4. Effect of low-Cl on the glutamate responses. (A) High-Cl solution; resting input conductance 158 μS, membrane potential −35 mV, 100 μM glutamate produced a hyperpolarization of 7 mV and ΔG was 342 μS. (B) Zero-Cl for 33 min, resting input conductance of pharynx decreased to 120 μS membrane potential decreased to −31 mV; 100 μM glutamate produced little membrane potential change and no detectable ΔG. (C) The preparation was returned to a high-Cl solution for 32 min, the resting conductance increased to 176 μS, the membrane potential was −27 mV; 100 μM glutamate produced a hyperpolarization of 2·5 mV and a ΔG of 196 μS. It is pointed out that the amplitude of the conductance response in (C) is smaller than in (A), an effect which may be explained by desensitization following applications of glutamate.

Effect of milbemycin D

The effect of milbemycin D on the *C. elegans* avermectin-sensitive glutamate receptor expressed in *Xenopus* oocytes is to produce a potentiation of glutamate effects and to produce a slow irreversible increase in conductance of the membrane (Cully *et*

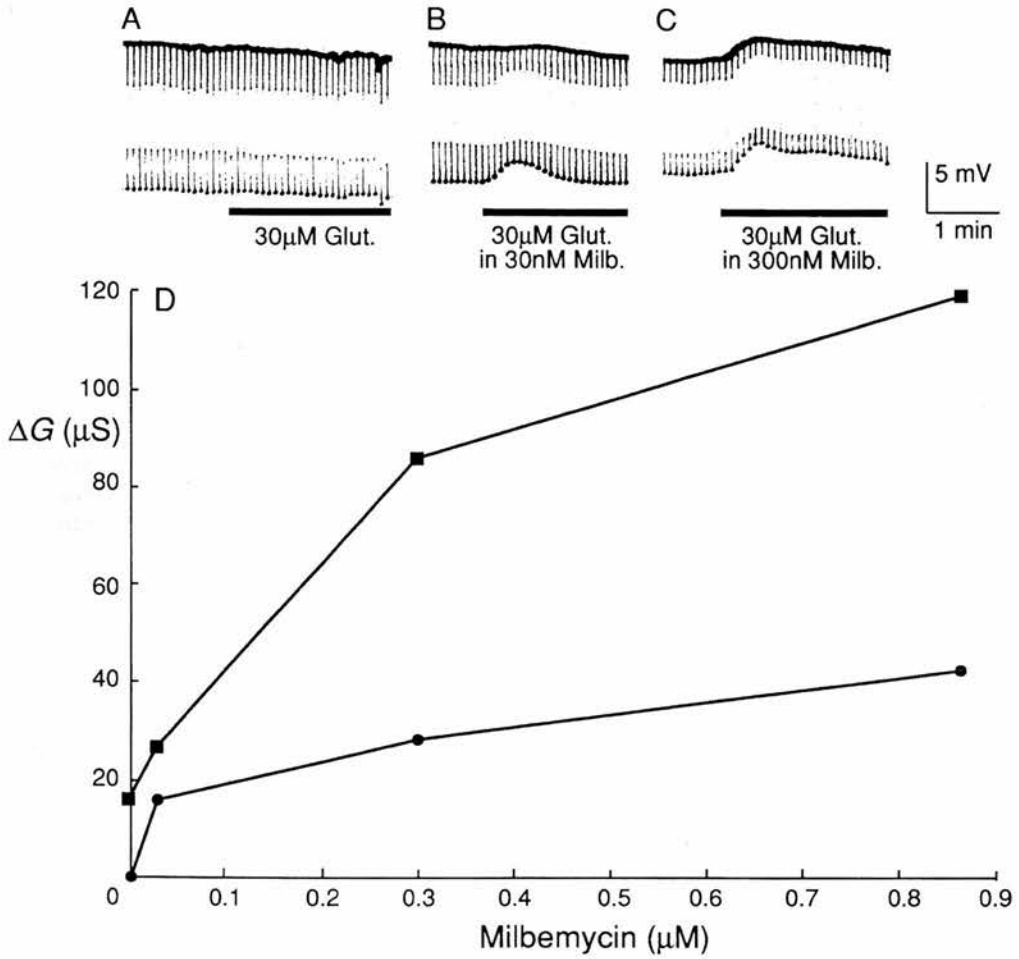


Fig. 5. Glutamate potentiation effects of milbemycin D. (A) Control 30 μM glutamate response, peak ΔG, is small, 16 μS. (B) In the presence of 30 nM milbemycin D the peak ΔG produced by 30 μM glutamate increased to 27 μS. (C) Milbemycin D (300 nM) increased the peak ΔG to 86 μS. In this particular preparation the glutamate response was a small depolarizing potential, indicating that the Cl-reversal potential was slightly depolarized relative to the membrane potential. (D) (■) Plot of peak ΔG produced by 30 μM glutamate against milbemycin concentration; (●) plot of resting input conductance of the pharynx against milbemycin concentration. Results from the same experiment as (A), (B) and (C).

al. 1994). The effects of milbemycin D on the input conductance of the *A. suum* pharyngeal preparation is shown in Figs 2C, 5A, B and C.

In Fig. 2C, 890 nM milbemycin D slowly increased the resting conductance of the membrane from 353 to 857 μS and gave rise to a 2 mV hyperpolarization. Although milbemycin D mimicked the effect of glutamate on membrane potential and conductance, its effect was not reversed on repeated washing (not shown) as expected for a lipophilic compound. A similar failure to reverse avermectin effects with washing has been observed with the expressed receptor (Cully *et al.* 1994).

A potentiating effect of milbemycin D on the effects of glutamate is shown in Fig 5A, B and C: 30 nM milbemycin D increased the peak ΔG produced by 30 μM glutamate from 16 μS (Fig. 4A) to 27 μS (Fig. 5B) and in Fig. 5C it is shown that 300 nM milbemycin D further increased the peak ΔG to 86 μS. In this particular preparation the glutamate potential response was a small depolarizing potential, indicating that the Cl-reversal potential was slightly depolarized relative to the membrane potential. The effect of milbemycin D concentration on the input conductance and the peak ΔG produced by 30 μM glutamate is plotted for this experiment in Fig. 5D: the figure emphasizes that the potentiation of glutamate was dose dependent as was the effect of milbemycin on input conductance. The potentiation of the glutamate response by milbemycin D indicates that milbemycin and glutamate are interacting somehow with the same channel and that the glutamate-gated Cl channel described here is analogous to the *C. elegans* channel, expressed in *Xenopus* oocytes.

DISCUSSION

This paper describes an electrophysiological preparation that possesses a glutamate-gated chloride channel in a parasitic nematode, *A. suum*, a target species for the avermectins and milbemycins. The

fact that milbemycin D produced a dose-dependent potentiation of the glutamate response shows that this group of anthelmintics can affect this channel as has been described for *C. elegans* (Cully *et al.* 1994). Glutamate-gated chloride channels have only been described in invertebrates and are found in crustacean and insect muscle and insect neurones (Lea & Usherwood, 1973; Lingle & Marder, 1981; Horseman *et al.* 1988; Wafford & Sattelle, 1989). This observation may explain the selective effects of the avermectins and milbemycins on invertebrates. The data for the existence of a glutamate-gated chloride channel in nematodes have previously been based on expression of cRNA derived from the soil nematode *C. elegans* (Arena, 1994).

The avermectins and milbemycins may have more than one site of action in nematodes, including antagonistic effects on GABA receptors of somatic muscles (Martin & Pennington, 1989; Holden-Dye & Walker, 1990). However, the extremely high sensitivity of the pharyngeal muscle to the paralysing effect of the avermectins observed in the parasitic sheep nematode, *Haemonchus contortus* (Geary *et al.* 1993), suggests that the pharyngeal muscle, required for feeding by the nematode parasite, is an important target site. The effects of glutamate reported in this study were observed in the absence of added Ca and in the presence of relatively high Mg. These conditions were chosen to abolish the spontaneous post-synaptic potentials and to allow stable resting membrane potentials to be recorded. The effect of bath-applied L-glutamate under these conditions implies that the glutamate receptors, responsible for the conductance increase, are located post-synaptically and/or extrasynaptically on the *A. suum* pharyngeal muscle membrane. The molecular experiments with *C. elegans* using the *lacZ* marker also indicate a post-synaptic or extra-synaptic location for the glutamate channel on the muscle of the pharynx (Laughton *et al.* 1995).

The electrophysiological preparation of the *A. suum* pharynx for studying a glutamate-gated chloride channel sensitive to the macrocyclic lactone anthelmintics will allow quantitative and qualitative pharmacological characterization of the receptor-operated ion-channel to be carried out in a parasitic nematode; it will allow comparison of the properties of the expressed receptor from *C. elegans* and the properties of a native receptor of a parasitic nematode. It will allow a comparison of the potency of the various avermectins and milbemycins used for parasite control and in addition permit the effects of other novel therapeutic agents acting on this site to be examined.

This work was made possible by the generous support of the Wellcome Trust.

REFERENCES

ARENA, J. P. (1994). Expression of *Caenorhabditis elegans* messenger-RNA in xenopus oocytes: a model system to study the mechanism of action of avermectins. *Parasitology Today* **10**, 35–7.

AVERY, L. (1993). Motor-neuron m3 controls pharyngeal muscle-relaxation timing in *Caenorhabditis elegans*. *Journal of Experimental Biology* **175**, 283–97.

AVERY, L., DAVIS, M. W., DENK, W., DENT, J. & HESS, G. (1994). M3 is an inhibitory glutamatergic pharyngeal motoneuron. *Worm Breeder's Gazette* **13**, 72.

BYERLY, L. & MASUDA, M. O. (1979). Voltage-clamp analysis of the potassium current that produces a negative-going action potential in *Ascaris* muscle. *Journal of Physiology* **288**, 263–84.

CAMPBELL, W. C. & BENZ, G. W. (1984). Ivermectin: a review of efficacy and safety. *Journal of Veterinary Pharmacology and Therapeutics* **7**, 1–16.

CULLY, D. F., VASSILATIS, D. K., LIU, K. K., PARESS, P. S., VANDERPLOEG, L. H. T. & SCHAEFFER, J. M. (1994). Cloning of an avermectin-sensitive glutamate-gated chloride channel from *Caenorhabditis elegans*. *Nature, London* **371**, 707–11.

DEL CASTILLO, J. & MORALES, T. (1967). The electrical and mechanical activity of the esophageal cell of *Ascaris lumbricoides*. *Journal of Generative Physiology* **50**, 603–30.

GEARY, T. G., SIMS, S. M., THOMAS, E. M., VANOVER, L., DAVIS, J. P., WINTERROWD, C. A. & KLEIN, R. (1993). *Haemonchus contortus* – ivermectin-induced paralysis of the pharynx. *Experimental Parasitology* **77**, 88–96.

HOLDEN-DYE, L. & WALKER, R. J. (1990). Avermectin and avermectin derivatives are antagonists at the 4-aminobutyric acid (GABA) receptors on the somatic muscle cells of *Ascaris*: is this the site of anthelmintic action? *Parasitology* **101**, 265–71.

HORSEMAN, B. G., SEYMOUR, C., BERMUDEZ, I. & BEADLE, D. J. (1988). The effects of L-glutamate on cultured insect neurons. *Neuroscience Letters* **85**, 65–70.

LAUGHTON, D. L., WOLSTENHOLME, A. J. & LUNT, G. (1995). The beta subunit of the avermectin sensitive glutamate receptor is expressed in the pm4 pharyngeal muscle cells. *Worm Breeder's Gazette* **14**, 48.

LEA, T. J. & USHERWOOD, P. N. R. (1973). The site of action of ibotenic acid and the identification of two populations of glutamate receptors on insect muscle-fibres. *Comparative and General Pharmacology* **4**, 333–50.

LINGLE, C. & MARDER, E. (1981). A glutamate-activated chloride conductance on a crustacean muscle. *Brain Research* **212**, 481–8.

MARTIN, R. J. & PENNINGTON, A. J. (1989). A patch-clamp study of effects of dihydroavermectin on *Ascaris* muscle. *British Journal of Pharmacology* **98**, 747–56.

WAFFORD, K. A. & SATTELLE, D. B. (1989). L-glutamate receptors on the cell body membrane of an identified insect motor neuron. *Journal of Experimental Biology* **144**, 449–62.

REFERENCES

wden, C., Sithigorngul, P., Brackley, P., Guastella, J. & Stretton, A.O.W. (1993). *J. Comp. Neurol.* **333**, 455–468.
aule, A.G., Shaw, C. Bowman, J.W., Halton, D.W., Thompson, D.P., Thim, L., Kubiak, T.M., Martin, R.A. & Geary, T.G. (1995). *Peptides* **16**, 87–93.
rri, H.R., Holden-Dye, L. & Walker, R.J. (1991). *Exp. Physiol.* **76**, 597–606.

-Glutamate and L-aspartate increase input onductance of *Ascaris suum* pharyngeal muscle

A. Murray and R.J. Martin

epartment of Preclinical Veterinary Sciences, R(D)SVS, ummerhall, University of Edinburgh, Edinburgh H9 1QT

Ascaris suum is a large intestinal nematode parasite of igs and sometimes humans. Avermectins are a group of ntibiotic anthelmintics used to treat infections of such ematodes in domestic animals and man. Cully *et al.* (1994) ave cloned and expressed a glutamate-gated Cl^- channel om *C. elegans*, sensitive to the avermectins. The presence f a glutamate-gated Cl^- channel, sensitive to an avermectin, as also been demonstrated in pharyngeal muscle of *Ascaris uum* (Martin, 1996).

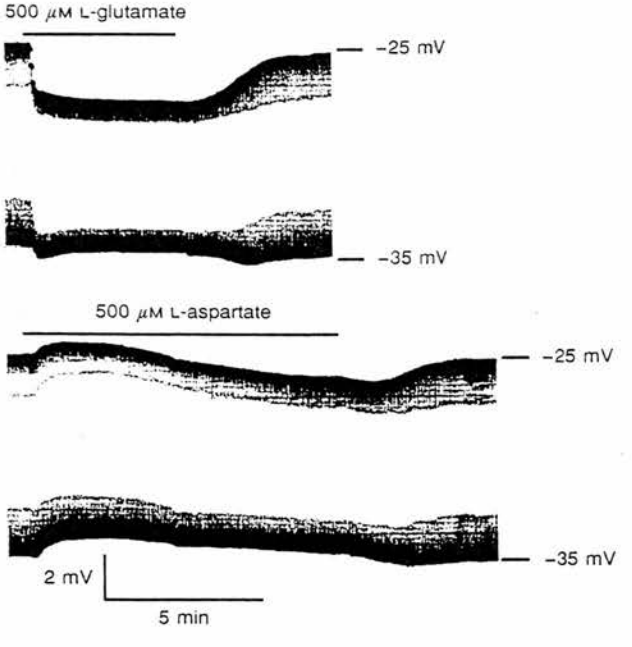


Fig. 1. Effect of 500 μM L-glutamate and 500 μM L-aspartate on input conductance of an *Ascaris* pharyngeal preparation. Methods: Martin (1996). The traces are potential records in response to hyperpolarizing current pulses (1·5 μA, 1 s, 0·5 Hz (not shown)).

We have now examined the effects of L-glutamate ($n = 4$) nd L-aspartate ($n = 4$) on input conductance of *Ascaris* haryngeal muscle using a two-microelectrode current-lamp technique. Bath-applied L-glutamate produced a reversible hyperpolarization and increase in conductance; L-aspartate produced an initial depolarization followed by a hyperpolarization and increase in conductance (Fig. 1). The conductance dose–response relationships were sigmoid with G_{max} of 134 and 56·1 μS, ED_{50} of 318 and 973 μM and n_H of 1·1 and 2·0 for glutamate and aspartate, respectively.

Our results show that receptors present in the *Ascaris* pharyngeal muscle are different from the expressed receptors of Cully *et al.* (1994), which are insensitive to L-aspartate.

Iain Murray holds an MRC studentship.

REFERENCES

Cully, D.F., Vassilatis, D.K., Liu, K.K., Paress, P.S., Van der Ploeg, L.H.T., Schaeffer, J.M. & Arena, J.P. (1994). *Nature* **371**, 707–711.
Martin, R.J. (1996). *Parasitology* **112**, 247–252.

Single-channel recordings from tegument-derived vesicles of *Schistosoma mansoni*

A.P. Robertson, R.J. Martin and J.R. Kusel*

*Department of Preclinical Veterinary Sciences, R(D)SVS, University of Edinburgh, Edinburgh EH9 1QH and *Department of Biochemistry, University of Glasgow, Hillhead, Glasgow*

Schistosomiasis is a widespread tropical disease of man caused by the trematode *Schistosoma mansoni*. The disease is usually treated with praziquantel, a highly effective drug with few side effects. The exact mechanism by which praziquantel kills the parasite has yet to be determined (for review, see Redman *et al.* 1996). Praziquantel causes an influx of calcium across the parasite tegument, suggesting that the drug may act on a specific ion channel within the tegument. We have developed a method for forming membrane vesicles from the schistosome tegument that allows the application of the patch-clamp technique.

Treatment of *S. mansoni* in low pH media (Gibco BHK-21 adjusted to pH 3·75 with 5 M HCl) for 15–30 min resulted in the formation of membrane vesicles from the tegument. In order to check the origin and structure of the vesicles, parasites were pre-treated with 4-aminofluoroscein to label the outer tegumental membrane and examined using fluorescence microscopy. The results showed that some of the vesicles originated from the outer tegumental membrane. Scanning electron microscopy revealed that the vesicles possessed a smooth surface suitable for applying the patch-clamp technique. Transmission electron microscopy demonstrated that some vesicles possessed the double bilayer found in the outer tegument of the adult schistosome.

Our patch-clamp recordings showed the presence of a large conductance (290 pS), non-selective cation channel with similarities to those channels previously described by Day *et*

73 Russell, M.W. and Wu, H. (1991) **Distribution, persistence, and recall of serum and salivary antibody responses to peroral immunization with protein antigen I/II of *Streptococcal mutans* coupled to the cholera toxin B subunit.** *Infect. Immun.* 59, 4061–4070
74 Lee, A. and Chen, M. (1994) **Successful immunization against gastric infection with *Helicobacter* species: use of a cholera toxin B-subunit-whole-cell vaccine.** *Infect. Immun.* 62, 3594–3597
75 Lycke, N., Tsuji, T. and Holmgren, J. (1992) **The adjuvant effect of *Vibrio cholera* and *Escherichia coli* heat-labile enterotoxins is linked to their ADP-ribosyltransferase activity.** *Eur. J. Immunol.* 22, 2277–2281
76 Sun, J., Holmgren, J. and Czerkinsky, C. (1994) **Cholera toxin B subunit: an efficient transmucosal carrier-delivery system for induction of peripheral immunological tolerance.** *Proc. Natl Acad. Sci. USA* 91, 10795–10799
77 Sixma, T.K. *et al.* (1991) **Crystal structure of a cholera toxin-related heat-labile enterotoxin from *E. coli*.** *Nature* 351, 371–377

Praziquantel:
An Urgent and Exciting Challenge

C.A. Redman, A. Robertson, P.G. Fallon, J. Modha, J.R. Kusel, M.J. Doenhoff and R.J. Martin

The anthelmintic drug praziquantel has proved useful in the treatment of schistosomiasis. The precise mechanism by which praziquantel kills the parasites has yet to be elucidated. Here, John Kusel and colleagues review the current theories on praziquantel action and suggest future avenues for research, which becomes urgent in the light of some reports of drug resistance.

Schistosomiasis is widespread in tropical areas and continues to spread rapidly, as recent outbreaks in Senegal have shown[1]. No vaccine exists for human populations, although vaccine candidates have been proposed[2]. Treatment of the disease worldwide relies very heavily on praziquantel (PZQ), a highly effective drug with few side effects[3]. The effectiveness of this drug against schistosomes, and against other helminths, is well documented[3,4], but the precise mechanisms by which the drug affects the parasite have yet to be elucidated[5]. Recent reports from Senegal suggest that this drug is not always very effective and that resistant strains may have developed[6]. An excellent article on PZQ has just been published[7].

PZQ-sensitive sites

PZQ acts within the tegument and muscle cells of the schistosome. The structure of the tegument is shown in Fig. 1; the surface membrane is represented as a highly complex double bilayer, the lipids and proteins of which may be organized into domains of differing properties and composition[8,9]. Variation has been observed in the distribution and the extent of the damage to the surface of adult parasites with respect to species, sex and individuals[10,11]. Differences between juvenile and adult[12–15] and male and female worms of *S. mansoni* have been observed[11,16]. These differences in susceptibility suggest membrane composition may be an important factor in PZQ-induced damage. Differences in membrane properties and phospholipid composition have been reported for different ages/sexes of *S. mansoni*[14,17,18]. However, other explanations, such as possible differences in distribution of PZQ-sensitive sites, must be considered.

PZQ induces a Ca^{2+} influx across the tegument, thought to be vital in the drug's effect, causing an immediate muscular contraction[19]. Bathing parasites in Ca^{2+}-free medium blocks this PZQ-induced contraction[20–23]. The effect of such treatment is not immediate, however, requiring more than ten minutes to take effect. This is explained by the draining of sequestered Ca^{2+} from pools in the worm. Evidence suggests that the tegument of the worm contains PZQ-sensitive sites. This is from work carried out on normal worms and worms which have had their tegument removed[24]. PZQ-induced contraction was found to be biphasic in normal parasites when incubated in high-Mg^{2+} medium, while only the larger, second contraction was observed in detegumented worms. The presence of these PZQ-sensitive sites in the surface would explain why the tegument is so susceptible to damage by PZQ. However, the tegument is electrically coupled to muscle cells, so that a rise in intrategumental Ca^{2+} might lead to increased Ca^{2+} in the sarcoplasmic reticulum which could lead to contraction[25]. The electrical coupling between the tegument and the muscle cells would explain why any physical or chemical change in the schistosome environment, affecting the tegument, will produce changes in the muscle cells. This means that external agents, such as PZQ, may produce muscle contraction by interacting with tegument rather than muscle cells directly.

The anatomical basis for the coupling between the tegument and muscle cells could be junctional complexes between the tegument and muscle cells[26] (Fig. 1)[27]. These PZQ-sensitive sites may also occur in muscle cells. This conclusion is based on observations on detegumented schistosomes that still contract in response to PZQ application, as well as initial observations on dissociated muscle fibres which contract when exposed to low concentrations of PZQ[24].

The relationship between PZQ and Ca^{2+} influx would suggest that sites of action are Ca^{2+}-permeable

Christopher Redman, Jayant Modha and **John Kusel** are at the Davidson Building, Division of Biochemistry and Molecular Biology, Institute of Biological and Life Sciences, The University of Glasgow, Glasgow, UK G12 8QQ. Padraig Fallon and Michael Doenhoff are at the School of Biological Sciences, University of Wales, Bangor, UK LL57 2UW. Alan Robertson and Richard Martin are at the Department of Physiology, Royal (Dick) Veterinary School, Edinburgh University, Summerhall, Edinburgh, UK EH9 1QH.
Tel: +44 141 330 4621. Fax: +44 141 330 4620, e-mail: gbca66@udcf.gla.ac.uk

© 1996, Elsevier Science Ltd 0169-4758/96/$15.00

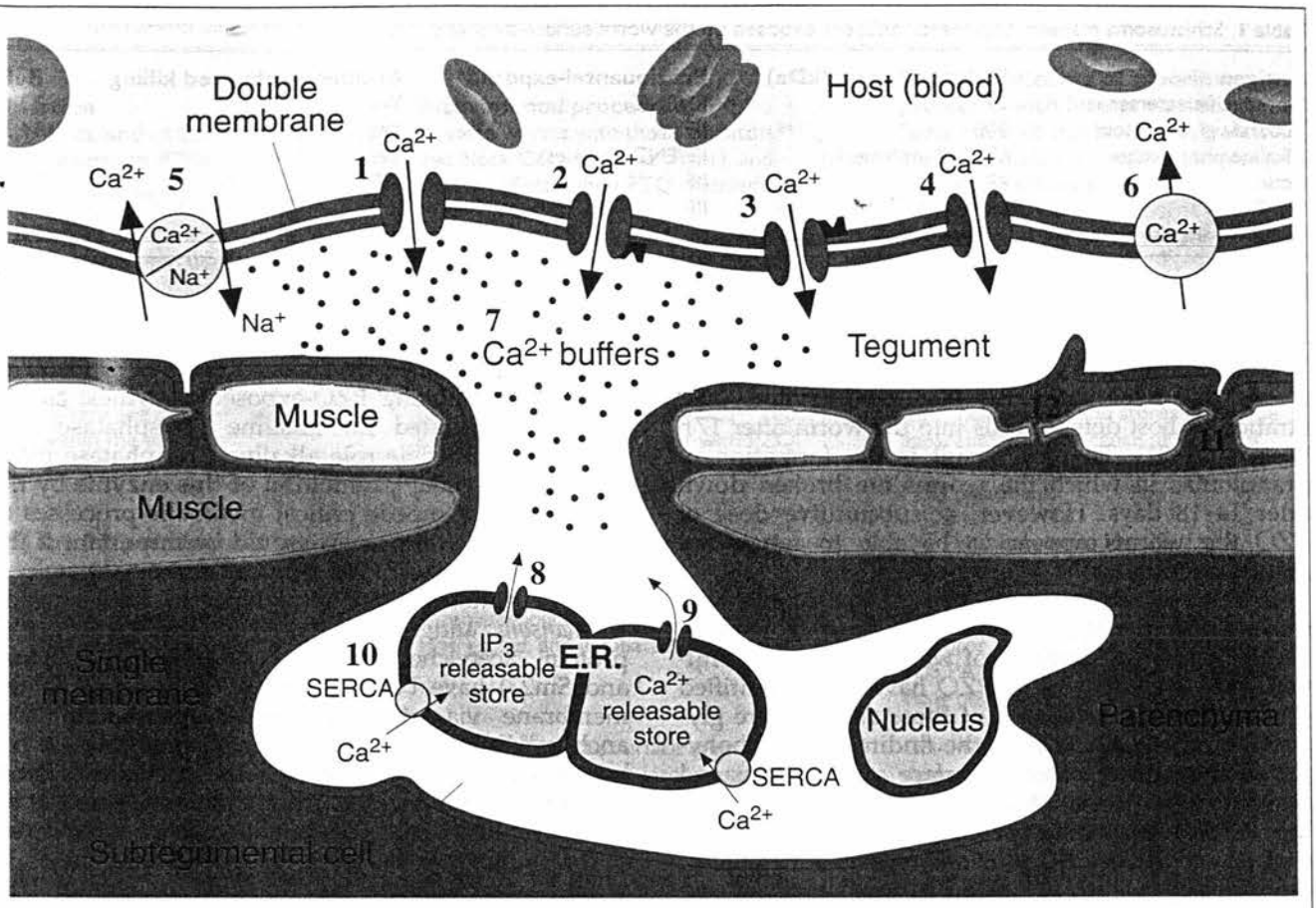


Fig. 1. Diagram representing the *Schistosoma* tegument, underlying muscle layers and parenchyma, and showing the three electrical compartments recognized by an advancing micropipette. (1)–(10) are common cellular factors/components responsible for modulating intracellular [Ca^{2+}]: (1) second messenger-gated Ca^{2+} channel; (2) calcium release activated Ca^{2+} channel; (3) agonist-gated Ca^{2+} channel; (4) voltage-gated Ca^{2+} channel. PZQ increasing the P_{open} of (1)–(4) could account for the observed influx of Ca^{2+} across the tegument. (5) Na^+/Ca^{2+} exchange pump; (6) Ca^{2+} pump, inhibition of either (5) or (6) by PZQ could lead to an increase in intrategumental [Ca^{2+}]; (7) reduction in buffering capacity induced by PZQ would lead to an increase in the free [Ca^{2+}]. PZQ can also induce effects when the parasite is bathed in Ca^{2+}-free media, suggesting the drug also interacts with intracellular calcium stores (found in rough endoplasmic reticulum); (8) and (9) are release channels for Ca^{2+} stores, sensitive to inositol triphosphate and Ca^{2+}, respectively. PZQ may cause either of these types of channel to open and release calcium from these stores. (10) SERCA (sarco endoplasmic reticulum calcium) pumps responsible for filling the intracellular calcium stores. Inhibition of SERCA pumps by PZQ is a possibility. Factors (1) to (10) will be present in the muscle cells of the parasite, thus accounting for the action of the drug on tegumented worms. However, there are pathways of low electrical resistance between tegument and muscle cell (11), and from muscle cell to muscle cell (12), which may be conduits for PZQ action. (1)–(6) could also face onto extracellular spaces. Factors (1)–(6) are shown spanning the double membrane of the *Schistosoma* outer tegument as their specific location in this structure has not been determined. (Diagram modified from Ref. 27.)

ion channels in the membranes of the tegument and muscle cells[24] (Fig. 1). Ca^{2+}-influx may be blocked by Mg^{2+} or La^{3+}, but not Ni^{2+}, Co^{2+} or the Ca^{2+} channel blocker D-600 (Refs 21,22). These channels must be pharmacologically distinct from the host Ca^{2+} channels, otherwise PZQ would be toxic to the host and not therapeutically effective. High Mg^{2+}/Ca^{2+} medium decreases PZQ-induced vacuolation[28], suggesting that either Mg^{2+} affects on Ca^{2+} influx, perhaps by inhibiting Ca^{2+} ion channels, or it inhibits vacuolation. However, these putative ion channels have yet to be observed physiologically. The biphasic PZQ tetanic contraction of the parasite may be due to two or more populations of Ca^{2+} ion channels, perhaps of different types (Fig. 1).

The electrical properties of dissociated muscle cells have also been studied using whole-cell voltage clamp[5]. Three types of muscle cell, and two types of voltage-activated outward K^+ currents were identified. All three types of cell possessed the delayed rectifier-like K^+ current, but only two of the muscle cell types possessed the rapidly inactivating 'A' K^+ current. These dissociated muscle cells contract by bathing in high external K^+, which suggests the presence of voltage-activated Ca^{2+} currents. They also contract in response to PZQ. Interestingly, no voltage-activated inward currents were detected despite the evidence of voltage-activated Ca^{2+} currents present in these cells. The failure to detect any voltage-activated currents may relate to the whole cell voltage-clamp technique used, which involves breaking into the cell and presumably dialysing the contents of the cell: Ca^{2+} currents easily run down in small cells and require all voltage-activated outward currents to be blocked before they can be seen. A detailed investigation of the voltage-activated inward currents and the influence of PZQ using different methods to isolate the muscle cells seems a rational next step.

Table 1. Schistosoma mansoni tegumental antigens exposed on the worm surface by praziquantel

Antigen	Molecular mass (kDa)	Praziquantel-exposed[a]	Antibody-enhanced killing	Refs
Nonspecific esterase	27	IIF/ENZ	Yes	33
Tubercle glycoprotein	200	IIF	Yes	34,35
Alkaline phosphatase	67–260 (polymeric)	IIF/ENZ (females)	Yes	34,36
Actin	43	IIF	NT[b]	37
Sm23	23	IIF	NT	38
Acetylcholinesterase	(polymeric)	IIF	NT	39

[a]Exposure demonstrated by indirect immunofluorescence (IIF) or by quantitative enzyme assays (ENZ). [b]NT, not yet tested.

Antigen exposure

In animal models, curative doses of PZQ result in the exposure of antigens[29] and binding and penetration of host defence cells into the worm after 17 h (Refs 19,30,31). The end result is the formation of granulomas in which the worms are broken down after 14–18 days. However, at subcurative dose of PZQ the worms appear to be able to repair the tegumental lesions[19].

It has been shown that the host immune system plays an important role in PZQ-induced parasite death, *in vivo*[32]. A number of worm tegumental antigens that are exposed by PZQ have been identified (Table 1)[33–39]. The majority of these antigens are glycoproteins, consistent with the finding that carbohydrates are exposed on the surface of PZQ-damaged worms[38,40]. However, it may be that, once exposed, these molecules are shed from the surface[40]. The synergistic activity of PZQ plus antibody is attributed to the antibody binding to specific exposed epitopes and thereby immunologically enhancing worm death[32,33]. Perhaps these specific antibodies allow an immune-based action to take place against PZQ-induced epitopes before the worm is able to repair the areas of damage. The specific antibodies are able to induce increased macrophage binding to the worm surface within two hours, *in vitro* (C. Graham, unpublished). Alternatively the antibody-mediated enhancement of mortality of drug-treated worms may be a result of antibodies inhibiting PZQ-exposed enzymes, as has been demonstrated for alkaline phosphatase[36]. In view of the possible role alkaline phosphatase plays in nutrient uptake[41], inhibition of this enzyme by the antibody may impede critical metabolic processes of the worm. Such processes would be important if the worm were to repair PZQ-induced damage.

It is of interest that the majority of PZQ-exposed *S. mansoni* antigens (the 200 kDa tubercle glycoprotein, acetylcholinesterase, alkaline phosphatase and Sm23) have been shown to be attached to the membrane via glycosylphosphatidylinositol (GPI) anchors[38,42,43], perhaps on the inner membrane, as has been suggested for the acetylcholine receptor[39]. These proteins can be released from the worm surface by bacterial phosphatidylinositol-specific phospholipase C (PIPLC)[42–44]. It has been proposed that the GPI-anchor may facilitate the selective release of that protein by a phospholipase[45]. A GPI-specific phospholipase D (GPIPLD) activity has been detected in *S. mansoni*, either endogenous or adsorbed onto the surface from the host plasma[46]. It might be envisaged that GPIPLD in the membrane could cause release of the GPI-linked antigens, exposed by PZQ[45] (Fig. 2). An increase in alkaline phosphatase activity on the

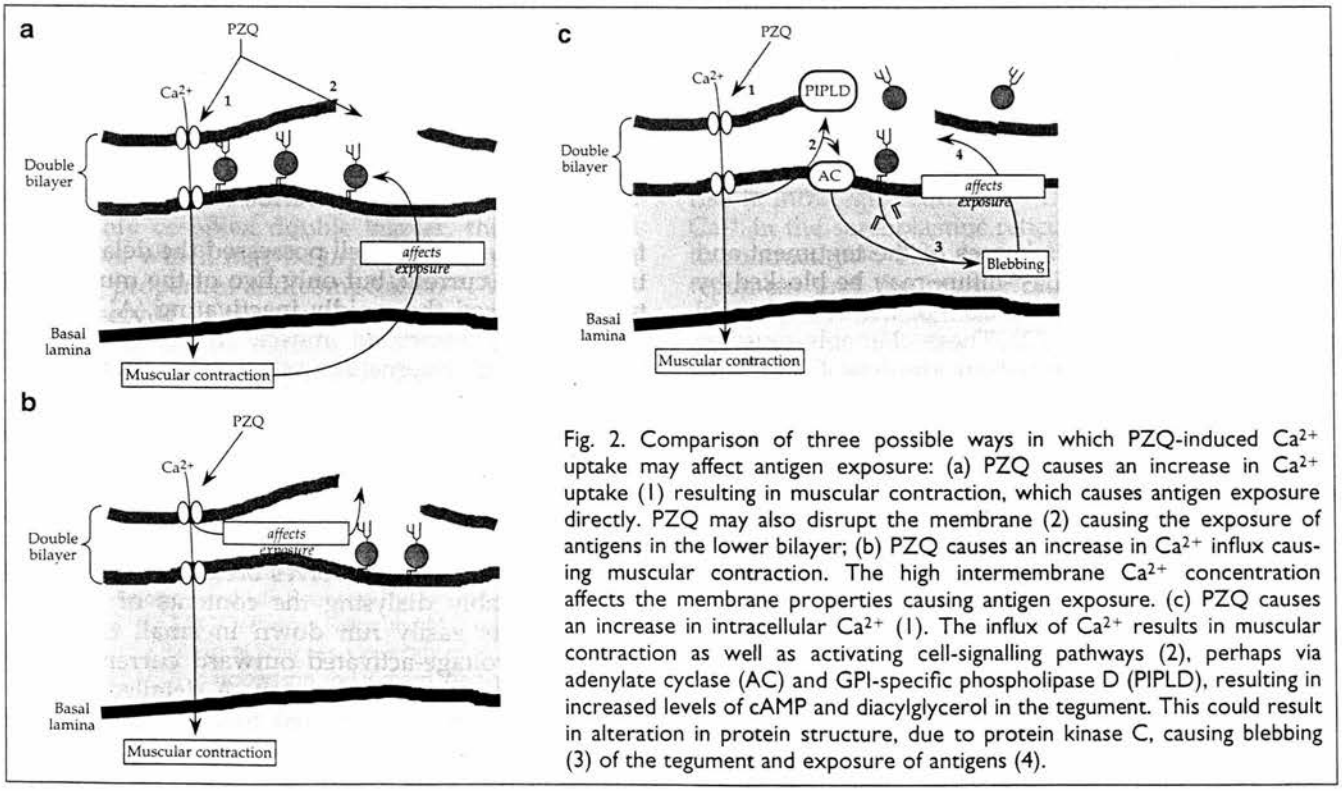


Fig. 2. Comparison of three possible ways in which PZQ-induced Ca^{2+} uptake may affect antigen exposure: (a) PZQ causes an increase in Ca^{2+} uptake (1) resulting in muscular contraction, which causes antigen exposure directly. PZQ may also disrupt the membrane (2) causing the exposure of antigens in the lower bilayer; (b) PZQ causes an increase in Ca^{2+} influx causing muscular contraction. The high intermembrane Ca^{2+} concentration affects the membrane properties causing antigen exposure. (c) PZQ causes an increase in intracellular Ca^{2+} (1). The influx of Ca^{2+} results in muscular contraction as well as activating cell-signalling pathways (2), perhaps via adenylate cyclase (AC) and GPI-specific phospholipase D (PIPLD), resulting in increased levels of cAMP and diacylglycerol in the tegument. This could result in alteration in protein structure, due to protein kinase C, causing blebbing (3) of the tegument and exposure of antigens (4).

Table 2. Summary of experiments[a] that may elucidate crucial questions

Question	Experimental procedure	Possible outcome of experiment; problems with interpretation
(1) What kind of Ca^{2+} channel is sensitive to PZQ?	Incubate worms with those inhibitors[54,55] that block Ca^{2+} channels (Fig. 1), and observe effects when PZQ is added.	Some channels may be very different from mammalian channels; inhibitors may not be effective.
(2) Does Ca^{2+} (in absence of PZQ) induce antigen exposure?	Load worms with 'caged' Ca^{2+} (Refs 56,57), and photoactivate[b]; measure antigen exposure.	If Ca^{2+} release increases antigen exposure, Fig. 2a is invalid.
(3) Does PZQ induce antigen exposure via Ca^{2+}?	Load worms with 'caged' Ca^{2+} chelator (diazo-2) and treat with PZQ after photoactivation; measure antigen exposure.	Ca^{2+} sequestration should prevent antigen exposure, if Figs 2b and 2c are valid.
(4) Where are the Ca^{2+} stores within the parasite?	Load worms with fluorescent Ca^{2+} reporting compound (fluo-3) and treat with PZQ.	Ca^{2+}-rich vesicles and stores should be apparent by fluorescence or confocal microscopy; these may deplete with PZQ treatment.
(5) Are PZQ-sensitive Ca^{2+} channels located in the surface membrane?	Patch-clamp studies on isolated membrane vesicles[58].	Ca^{2+} channels, once identified, may respond to PZQ in isolated membranes.
(6) Can radioactive derivative of PZQ be used to crosslink PZQ-sensitive site?	Photoactivable PZQ derivative might be synthesized, and incubated with the worm.	Photoactivation and crosslinking to receptor might identify binding protein on SDS PAGE (see Ref. 59 for an example using chloroquine).
(7) Can antigens that synergize with the immune system be located in the membrane fraction?	Fractionate isolated surface membrane into detergent-soluble and -insoluble fractions; look for distribution of relevant antigens (Table 1).	GPI-linked proteins often found in detergent-insoluble membrane domain. Photobleaching studies might confirm 'immobile' character in living worms.
(8) Do antigens synergizing with the immune system become released from the parasite after PZQ treatment?	After PZQ treatment *in vitro*, measure release of GPI-anchored antigens from the surface of the medium.	Those synergizing may not be released; release may be seen only with non-synergizing antigens.
(9) What is the nature of the surface membrane repair after PZQ treatment?	Measure uptake of exogenous lipid, and parasite synthesis of lipid and protein by membrane after PZQ damage.	Compare with other kinds of damage (eg. by basic protein) and especially PZQ-resistant forms. Rates of HSP70 synthesis increase.
(10) What is the nature of the variability to PZQ action over the worm's surface?	Fluorescent PZQ could be used to observe distribution of PZQ binding sites. Fluorescent PZQ might be synthesized.	Antibodies to PZQ-sensitive sites would be valuable if Question 6 was answered with identification of a protein.
(11) Can PZQ induce Ca^{2+} influx in the absence of Ca^{2+} channels[60]?	Prepare membrane vesicles which, by patch clamp, have no Ca^{2+} channels. Observe effects of PZQ.	PZQ may alter membrane lipid properties to allow Ca^{2+} influx.

[a] In all experiments suggested, both PZQ-sensitive and -resistant strains of *Schistosoma mansoni* should be compared.
[b] 'Caged' compounds and fluorescent derivatives can be obtained or custom synthesized by Molecular Probes, Eugene, Oregon, USA.

surface of the parasite after PZQ exposure[38] suggests that this enzyme may not be released into the plasma, by either endogenous or exogenous phospholipases. Synergism between PZQ and the immune system may be seen with antibodies against those antigens which remain in the membrane after PZQ treatment. The antibody isotype will also be important in recruiting secondary effector mechanisms.

Drug resistance

Progress in the understanding of the mode of action of a drug may be made by comparative studies on drug-resistant and -susceptible isolates. By comparison with microbial infection, however, suitable definition of drug resistance may be more difficult to formulate for parasitic infections, and for schistosomiasis in particular, because of the variation in susceptibility of different maturation stages and sexes of the parasite to the drugs in question. For example, post-larval but immature schistosomes not previously exposed to schistosomicidal drugs have a 'natural resistance' or 'tolerance' to doses that will kill older worms[12], and PZQ in particular is more effective against female than against male worms under certain circumstances[19,36].

In contrast to such inherent resistance that depends on geographic origin, maturational state or sex, 'true resistance' to a schistosomicidal drug has been defined as a genetically transmitted loss of sensitivity in a parasitic population that was previously sensitive to that drug[45]. By this definition, a recently described, selectively bred laboratory isolate of *S. mansoni*[47] that was insusceptible to doses of PZQ that killed unselected isolates would appear to be expressing 'true

resistance'. Comparison of the properties of this resistant isolate, and of isolates from Senegal which are also putatively insusceptible to PZQ may help in elucidating the mode of action of this drug and the nature of the resistance. There are several possible explanations for resistance in human populations and in selectively bred isolates. It may be that drug insusceptibility is due to a delay in maturation of the parasite, resulting in prolongation of the immature state which is 'naturally resistant' or 'tolerant' to the drug. The mutation or absence of a PZQ-receptor protein[5], and the modulation of the expression, exposure or immunogenicity of the specific proteins which render the normal parasites susceptible to immunologically inflicted damage are other possibilities. Insusceptibility in Senegal may be due to the absence of antibodies against those surface antigens that have been shown to synergize with the immune system after PZQ treatment (Table 1).

Membrane fluidity and metabolism

When we consider the effects of PZQ on the double bilayered surface membrane, it is possible to envisage very rapid (occurring in the first few minutes) and longer-term (over several hours) effects. A very rapid decrease in membrane fluidity was observed when octadecanoylamino-fluorescein (AF18) was used as a probe in photobleaching experiments[18]. The fluidity of another fluorescent probe, PKH2 (Sigma) increased after PZQ treatment. This may indicate that AF18 and PKH2 enter different domains. Domains in the surface membrane have been observed by several workers[8,9,48]. It may be possible that PZQ preferentially inserts into particular domains, as opposed to general insertion. In mammalian cells, certain domains have been found to be rich in cholesterol, sphingomyelin and GPI-linked proteins[48,49]. The GPI-linked antigens that are exposed after PZQ treatment in *S. mansoni* may occur in such domains. It has been observed that the action of GPIPLD, such as that found on the surface of *S. mansoni*[46], may be affected by the physical state of the bilayer in which the substrates are located[50]. Alternatively the antigens, such as alkaline phosphatase[32], may be orientated in the membrane such that the anchor is protected from the GPIPLD activity. It is important to find out whether or not these GPI-anchored antigens are released from the membrane *in vivo*.

If antigens were released by a phospholipase, *in vivo*, then a rise in intracellular diacylglycerol may occur[46] (Fig. 2). Phorbol esters, which activate protein kinase C, were shown to cause vacuolation of the worm surface[50]. This vacuolation was believed to involve the signal transduction pathway, perhaps via diacylglycerol[51]. It may be that the PZQ-induced Ca^{2+} influx causes the activation of protein kinase C, by activation of a phospholipase, as in other systems[52,53]. The phosphorylation of proteins by protein kinase C could destabilize the tegument, causing the vacuolation and antigen exposure[51] (Fig. 2c).

Several, longer-term effects of PZQ have been observed. *In vitro* studies analysing the binding of fluorescent lectins to PZQ-damaged regions of the parasite surface show carbohydrate moieties to have high rates of lateral diffusion, suggesting possible shedding of these antigens[18]. As discussed above, this may involve phospholipase activity. PZQ also stimulates heat shock protein 70 (HSP70) synthesis and secretion over a 24 h period (N. Wardy, PhD Thesis, University of Glasgow, 1994). HSP70 is likely to be important in membrane repair, but its secretion may stimulate the immune response of the host, and play a role in the immune dependence of chemotherapy. Lipid uptake is also decreased by PZQ, as measured by AF18 insertion. This effect over a period of days might result in a diminished ability of the worm to repair regions of PZQ-induced damage.

Future perspectives

Figure 2 suggests some possible consequences of an increase in tegumental Ca^{2+} ion concentration. (1) The increase in Ca^{2+} causes muscular contraction, while tegumental damage and antigen exposure is a separate consequence of PZQ binding to the surface membrane; (2) an increase in Ca^{2+} causes both contraction and antigen exposure; (3) a signalling pathway is triggered by an increase in Ca^{2+}, involving activation of adenylate cyclase (Type I) or phospholipase D, leading to cytoskeletal changes and antigen exposure. Experiments can be designed to investigate these possibilities. Comparison of susceptible and resistant parasites could reveal more about the mechanism of PZQ activity. The use of the *R* (−) (active) and *S* (+) (inactive) stereoisomers of PZQ in experiments would reveal whether or not the effects observed are relevant to the activity of PZQ.

Table 2 gives a brief summary of some experiments[54–60] that may answer some crucial questions. Questions 1, 5, 6 and 10 are directed to the identification of the PZQ site; Questions 2 and 3 to the role of Ca^{2+} in antigen exposure; Question 4 to the location of Ca^{2+} stores; and Questions 7–9 to the location and properties of synergizing antigens in the surface membrane. It is possible that PZQ can perturb the surface membrane[60] as a primary event[7] and that Ca^{2+} influx is a consequence of this perturbation. Question 11 is directed to this. Answers to these questions should (1) determine whether or not there is a PZQ site, (2) define the role of Ca^{2+} in inducing antigen exposure, and (3) help to determine the physiological basis for resistance. If there is a PZQ-specific binding protein, its gene can be identified as has been done with the ivermectin binding protein in *C. elegans*[61]. A recent paper reports the binding of PZQ with *S. japonicum* glutathione-*S*-transferase[62].

Acknowledgements

We would like to thank the Wellcome Trust and the BBSRC for support. We would also like to thank Donato Cioli for advice and for enabling us to read his article on PZQ (Ref. 7) prior to publication, Alison Agnew and Marcela Camacho for allowing us to read Ref. 39 prior to publication, and Achim Harder for advice and critical discussion.

References

1 Stelma, F.F. *et al.* (1993) **Epidemiology of *Schistosoma mansoni* infections in a recently exposed community in northern Senegal.** *Am. J. Trop. Med. Hyg.* 49, 701–706

2 Grezel, D. *et al.* (1993) **Protective immunity induced in rat schistosomaiasis by single dose of the SM28GST recombinant antigen: effector mechanisms involving IgE and IgA antibodies.** *Eur. J. Immunol.* 23, 454–460

3 Andrews, P. *et al.* (1983) **Praziquantel.** *Med. Res. Rev.* 3, 147–200

4 Harnett, W. (1988) **The anthelmintic action of praziquantel.** *Parasitology Today* 4, 144–146

5 Day, T.A., Bennett, J.L. and Pax, R.A. (1992) **Praziquantel: the enigmatic antiparasitic.** *Parasitology Today* 8, 342–344

6 Fallon, P.G., Sturrock, R.F. *et al.* (1995) **Diminished susceptibility to Praziquantel in a Senegal isolate of *Schistosoma mansoni*.** *Am. J. Trop. Med. Hyg.* 53, 61–62

7 Cioli, D. *et al.* **Antischistosomal drugs, past, present...and future?** *Pharmacol. Ther.* (in press)

8 Kusel, J.R. and Gordon, J.F. (1989) **Biophysical properties of the schistosome surface and their relevance to its properties under immune and drug attack.** *Parasitol. Immunol.* 11, 431–451

9 Caulfield, J.P. *et al.* (1991) **Low density lipoproteins bound to *Schistosoma mansoni* do not alter the lateral diffusion or shedding of lipids in the outer surface membrane.** *J. Cell Sci.* 99, 167–173

0 Becker, B. *et al.* (1980) **Light and electron microscopic studies on the effect of praziquantel on *Schistosoma mansoni*, *Dicrocoelium dendriticum* and *Fasciola hepatica* (Trematoda) *in vitro*.** *Z. Parasitenkunde* 63, 113–128

1 Shaw, J.R. and Erasmus, D.A. (1983) ***Schistosoma mansoni*: the effects of a subcurative dose of praziquantel on the ultrastructure of worms *in vivo*.** *Z. Parasitenkunde* 69, 73–90

2 Sabah, A.A. *et al.* (1986) ***Schistosoma mansoni*: chemotherapy of infections of different ages.** *Exp. Parasitol.* 61, 294–303

3 Flisser, A. *et al.* (1990) ***Schistosoma mansoni*: enhanced efficacy of praziquantel treatment in immune mice.** *Parasitol. Immunol.* 11, 319–328

4 Rumjanek, F.D. (1987) in *Biochemistry and Physiology in the Biology of Schistosomes, from Genes to Latrines* (Rollinson, D. and Simpson, A.J., eds), pp 163–183, Academic Press

5 Xiao, S-H. *et al.* (1984) **Praziquantel induced vesicle formation in the tegument of male *Schistosoma mansoni* is calcium dependent.** *J. Parasitol.* 70, 177–179

6 Modha, J. *et al.* (1990) **Immune dependence of schistosomicidal chemotherapy: an ultrastructural study of *Schistosoma mansoni* adult worms exposed to praziquantel and immune serum *in vivo*.** *Parasitol. Immunol.* 12, 321–324

7 Vial, H.J. (1985) **Renewel of the membrane complex of *Schistosoma mansoni* is closely associated with lipid metabolism.** *Mol. Biochem. Parasitol.* 17, 203–218

8 Lima, S. *et al.* (1994) **Effects of culture and praziquantel on membrane fluidity parameters of adult *Schistosoma mansoni*.** *Parasitology* 109, 57–65

9 Mehlhorn, H. *et al.* (1981) ***In vivo* and *in vitro* experiments on the effect of praziquantel on *Schistosoma mansoni*: a light and electron microscopic study.** *Arzneimittel Forschung* 31, 544–554

0 Pax, R.A. *et al.* (1984) ***Schistosoma mansoni*: differences in acetylcholine, dopamine and serotonin control of circular and longitudinal parasite muscles.** *Exp. Parasitol.* 58, 314–324

1 Fetterer, R.H. *et al.* (1980) ***Schistosoma mansoni*: characterization of the electrical potential from the tegument of adult males.** *Exp. Parasitol.* 49, 353–365

2 Wolde-Mussie, E. *et al.* (1982) ***Schistosoma mansoni*: calcium efflux and the effects of calcium-free media on the responses of the adult male musculature to praziquantel and other agants inducing contraction.** *Exp. Parasitol.* 53. 270–278

3 Pax, R.A. *et al.* (1979) **Effects of fluoxetine and imipramine on male *Schistosoma mansoni*.** *Comp. Biochem. Physiol.* 64, 123–126

4 Blair, K.L. *et al.* (1994) ***Schistosoma mansoni*: myogenic characteristics of phorbol ester induced muscle contraction.** *Exp. Parasitol.* 78, 302–316

5 Thompson, D.P. *et al.* (1982) **Microelectrode studies of the tegument and subtegumental compartments of the male *Schistosoma mansoni*: an analysis of electrophysiological properties.** *Parasitology* 85, 163–178

6 Silk, M.A. and Spence, I.M. (1969) **Ultrastructural studies of the blood fluke *Schistosoma mansoni*. III. The nervous tissue and sensory structures.** *S. A. J. Med. Sci.* 34, 11–20

7 Kostyuk, P. and Verkhratsky, A. (1994) **Calcium store in neurons and glia.** *Neurosci.* 63, 381–404

8 Bricker, C.S. *et al.* (1983) **The relationship between tegumental disruption and muscle contraction in *Schistosoma mansoni* exposed to various compounds.** *Z. Parasitenkunde* 69, 61–71

9 Harnett, W. and Kusel, J.R. (1986) **Increased exposure of parasite antigens at the surface of adult male *Schistosoma mansoni* exposed to praziquantel *in vitro*.** *Parasitology* 93, 401–405

0 Brindley, P.J. and Sher, A. (1987) **The chemotherapeutic effect of praziquantel against *Schistosoma mansoni* is dependent on host antibody response.** *J. Immunol.* 136, 215–220

1 Doenhoff, M. *et al.* (1987) **Evidence for an immune-dependent action of praziquantel on *Schistosoma mansoni* in mice.** *Trans. R. Soc. Trop. Med. Hyg.* 81, 947–951

32 Fallon, P.G. *et al.* (1992) **Immune-dependent chemotherapy of schistosomiasis.** *Parasitology* 105, S41–S48

33 Doenhoff, M. *et al.* (1988) **Anti-schistosome chemotherapy enhanced by antibodies specific for a parasite esterase.** *Immunology* 65, 507–510

34 Brindley, P.J. *et al.* (1989) **Role of the host antibody in the chemotherapeutic action of praziquantel against *Schistosoma mansoni*: identification of target antigens.** *Mol. Biochem. Parasitol.* 34, 99–108

35 Tanaka, T. *et al.* (1993) ***Schistosoma*: a 200 kDa chemotherapeutic target antigen is differentially localized in African vs Oriental species.** *Exp. Parasitol.* 76, 293–301

36 Fallon, P.G. *et al.* (1994) **Quantification of praziquantel-induced damage on the surface of adult *Schistosoma mansoni* worms: estimation of esterase and alkaline phosphatase activity.** *Parasitol. Res.* 80, 623–625

37 Linder, E. and Thors, C. (1992) ***Schistosoma mansoni*: praziquantel-induced tegumental lesion exposes actin of surface spines and allows binding of actin depolarizing factor gelsolin.** *Parasitology* 105, 71–79

38 Koster, B. and Strand, M. (1994) ***Schistosoma mansoni*, immunolocalization of 2 different fucose-containing carbohydrate epitopes.** *Parasitology* 108, 433–446

39 Camacho, M. *et al.* (1995) **Nicotinic acetylcholine receptors on the surface of the blood fluke *Schistosoma mansoni*.** *Mol. Biochem. Parasitol.* 71, 127–134

40 Lima, S. *et al.* (1994) **Altered behaviour of carbohydrate-bound molecules and lipids in areas of the tegument of adult *Schistosoma mansoni* worms damaged by praziquantel.** *Parasitology* 109, 469–477

41 McLaren, D. (1980) in *Schistosoma mansoni: the Parasite Surface in Relation to Host Immunity* (Brown, K.N., ed.), pp 1–27, Research Studies Press

42 Espinoza, B. *et al.* (1991) **Acetylcholinesterase from *Schistosoma mansoni*: immunological characterization.** *Immunol. Lett.* 28, 167–174

43 Sauma, S. and Strand, M. (1990) **Identification and characterisation of glycosylphosphatidylinositol-linked *Schistosoma mansoni* adult worm immunogens.** *Mol. Biochem. Parasitol.* 38, 199–210

44 Espinoza, B. *et al.* (1991) **Phosphatidylinositol-specific phospholipase C induces biosynthesis of acetylcholinesterase via diacylglycerol in *Schistosoma mansoni*.** *Eur. J. Biochem.* 195, 863–870

45 Cioli, D. *et al.* (1993) **Drug resistance in schistosomes.** *Parasitology Today* 9, 162–166

46 Hawn, T.R. and Strand, M. (1993) **Detection and partial characterization of glycophosphatidylinositol-specific phospholipase activities from *Fasciola hepatica* and *Schistosoma mansoni*.** *Mol. Biochem. Parasitol.* 59, 73–82

47 Fallon, P.G. and Doenhoff, M.J. (1994) **Drug-resistant schistosomiasis: resistance to praziquantel and oxamniqine induced in *Schistosoma mansoni* in mice is drug specific.** *Am. J. Trop. Med. Hyg.* 51, 83–88

48 Mayor, S. *et al.* (1994) **Sequestration of glycosylphosphatidylinositol-anchored proteins in caveolae triggered by crosslinking.** *Science* 264, 1948–1951

49 Ferguson, M.A.J. (1994) **What can GPI do for you?** *Parasitology Today* 10, 48–52

50 Low, M.G. and Huang, K.S. (1991) **Factors affecting the ability of glycosylphosphatidylinositol-specific phospholipase D to degrade membrane anchors of cell surface proteins.** *Biochem. J.* 279, 483–493

51 Wiest, P.M. *et al.* (1992) ***Schistosoma mansoni*: characterization of phosphoinositide response.** *Exp. Parasitol.* 74, 38–45

52 Sugiya, H. and Furuyama, S. (1990) **Sphingosine increases inositol triphosphate in rat parotid acinar-cells by a mechanism that is independent of protein kinase C but dependent on extracellular calcium.** *Cell Calcium* 11, 469–475

53 Berridge, M.J. and Irvine, R.F. (1984) **Inositol triphosphate, a novel second messenger in cellular signalling transduction.** *Nature* 312, 315

54 Hosey, M.M. and Lazdunski, M. (1988) **Calcium channels: molecular pharmacology, structure and regulation.** *J. Membr. Biol.* 104, 81–105

55 Somlyo, A.P. and Somlyo, A.V. (1994) **Signal transduction and regulation in smooth muscle.** *Nature* 372, 231–236

56 McCray, J.A. and Trentham, D.R. (1989) **Properties and uses of photoreactive compounds.** *Annu. Rev. Biophys. Biophys. Chem.* 18, 239–270

57 Sands, W. and Kusel, J.R. (1992) **Changes in the lateral diffusion**

of fluorescent lipid analogues in the surface membrane of adult male *Schistosoma mansoni*. *Mol. Biochem. Parasitol.* 53, 233–240
58 Dixon, D.M. and Martin, R.J. (1993) **Patch clamp and chloride channels in *Ascaris suum*.** *Parasitology Today* 9, 341–344
59 Foley, M. *et al.* (1994) **Photoaffinity labelling of chloroquine-binding proteins in *Plasmodium falciparum*.** *J. Biol. Chem.* 269, 6955–6961
60 Harder, A. *et al.* (1988) **Influence of praziquantel and Ca^{2+} on the bilayer-isotropic-hexagonal transition of model membranes.** *Mol. Biochem. Parasitol.* 29, 55–60
61 Cully, D.F. *et al.* (1994) **Cloning of an avermectin-sensitive glutamate-gated chloride channel from *Caenorhabditis elegans*.** *Nature* 371, 707–711
62 McTigue, M.A. *et al.* (1995) **Crystal structure of a schistosomal drug and vaccine target: glutathione-S-transferase from *Schistosoma japonica* and its complex with the leading antischistosomal drug Praziquantel.** *J. Mol. Biol.* 246, 21–27

Plasmodium vivax: Merozoites, Invasion of Reticulocytes and Considerations for Malaria Vaccine Development

M.R. Galinski and J.W. Barnwell

Several Plasmodium vivax *merozoite proteins have been characterized over the past few years, including two that bind specifically to reticulocytes. Here, Mary Galinski and John Barnwell examine* P. vivax *merozoites and constituent molecules that are involved in host cell selection and invasion, and that also are viewed as malaria vaccine candidates. They also discuss how knowledge of the reticulocyte-binding proteins furthers the development of a conceptual framework for malaria merozoite invasion at the molecular level, not only for* P. vivax, *but for all species of the parasite.*

Plasmodium vivax and *P. falciparum* are the two most prevalent species of human malaria, together afflicting a few hundred million people annually[1]. Although the percentage of these cases caused by *P. vivax* versus *P. falciparum* is uncertain, it can be conservatively estimated that as many as 35 million cases of vivax malaria occur each year. Moreover, chloroquine-resistant strains have recently been observed[2–4], and relapse parasitemias due to primaquine-resistant liver-stage hypnozoites have become widespread and are being noted more and more frequently[5,6]. Vivax malaria is undoubtedly a major public health problem for many countries, with associated socioeconomic ramifications. Now, and probably increasingly so in the future, there is a need for alternative prophylactic and therapeutic tools for control and management of these infections.

Despite the fact that *P. vivax* is a major pathogen, basic research on molecular and cellular biological aspects of this parasite has been limited, with only a few laboratories focusing research programs on this species. One prominent reason for this lack of attention is that *P. vivax* cannot be cultured continuously *in vitro*. This contrasts with the availability of a *P. falciparum* culture system[7] that has greatly facilitated investigations of this species in many laboratories worldwide.

Mary R. Galinski and John W. Barnwell are at New York University Medical Center, Department of Medical and Molecular Parasitology, 341 East 25th Street, NY 10010, USA.
Tel: +1 212 263 6793/6956, Fax: +1 212 263 7475, e-mail: Mary.Galinski@ccmail.med.nyu.edu

An outstanding trait of *P. vivax* that has enabled it, to a large degree, to evade scientific scrutiny is that its primary host red blood cell is the reticulocyte, which normally accounts for only about 1% of the human red blood cell population. Reticulocytes are not easily obtained routinely on a daily basis in sufficient quantities to maintain laboratory cultures. This fact also hampers any systematic investigation of optimum culture conditions for *P. vivax*, which appears to be another important factor affecting the maintenance of this parasite *in vitro*. Although it is not known why *P. vivax* is restricted to this young red blood cell population, the discovery of proteins that bind specifically to reticulocytes[8] provides the beginning of an explanation for how *P. vivax* targets this host cell.

This review features the *P. vivax* reticulocyte-binding proteins[8] and also outlines work that has been accomplished in recent years to characterize *P. vivax* merozoites. We, and others, have circumvented the fact that there is no culture system for *P. vivax* by: (1) obtaining limited amounts of this parasite, as required, from Saimiri monkey adapted infections; and (2) by making use of the closely related simian malarias *P. cynomolgi* and *P. knowlesi*[9], which serve as biological model systems, and are also used to generate homologous DNA and antibody reagents/probes that crossreact with *P. vivax*. In addition, although there is no long-term culture system for *P. vivax*, short term culture with significant reinvasion is possible, thus permitting *in vitro* investigations on merozoite invasion[10,11]. This body of *P. vivax* investigations has not only broadened our knowledge of *P. vivax* merozoite proteins, but also has provided valuable insights about functionally analogous proteins in *P. falciparum*.

Plasmodium vivax: the parasite

The distinct phylogenetic paths of *P. vivax* and *P. falciparum* probably evolved tens of millions of years ago[12]. This period of time has allowed for considerable biological differences to develop between these predominant species of malaria[13,14]. Most notably: (1) *P. vivax* can remain dormant in the liver as hypnozoites[15], which can initiate a blood-stage infection even months after an initial sporozoite infection; (2) it

© 1996, Elsevier Science Ltd 0169-4758/96/$15.00

REFERENCES

Cowden, C., Sithigorngul, P., Brackley, P., Guastella, J. & Stretton, A.O.W. (1993). *J. Comp. Neurol.* **333**, 455–468.

Maule, A.G., Shaw, C. Bowman, J.W., Halton, D.W., Thompson, D.P., Thim, L., Kubiak, T.M., Martin, R.A. & Geary, T.G. (1995). *Peptides* **16**, 87–93.

Parri, H.R., Holden-Dye, L. & Walker, R.J. (1991). *Exp. Physiol.* **76**, 597–606.

L-Glutamate and L-aspartate increase input conductance of *Ascaris suum* pharyngeal muscle

I.A. Murray and R.J. Martin

Department of Preclinical Veterinary Sciences, R(D)SVS, Summerhall, University of Edinburgh, Edinburgh EH9 1QT

Ascaris suum is a large intestinal nematode parasite of pigs and sometimes humans. Avermectins are a group of antibiotic anthelmintics used to treat infections of such nematodes in domestic animals and man. Cully *et al.* (1994) have cloned and expressed a glutamate-gated Cl^- channel from *C. elegans*, sensitive to the avermectins. The presence of a glutamate-gated Cl^- channel, sensitive to an avermectin, has also been demonstrated in pharyngeal muscle of *Ascaris suum* (Martin, 1996).

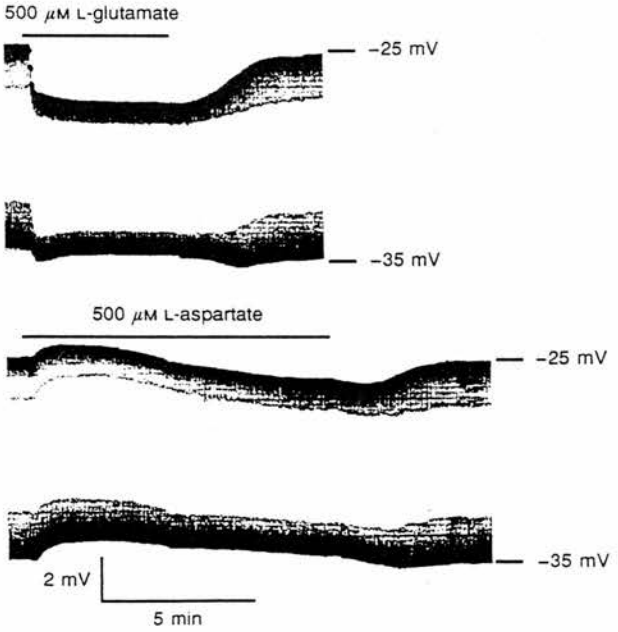


Fig. 1. Effect of 500 μM L-glutamate and 500 μM L-aspartate on input conductance of an *Ascaris* pharyngeal preparation. Methods: Martin (1996). The traces are potential records in response to hyperpolarizing current pulses (1·5 μA, 1 s, 0·5 Hz (not shown)).

We have now examined the effects of L-glutamate ($n = 4$) and L-aspartate ($n = 4$) on input conductance of *Ascaris* pharyngeal muscle using a two-microelectrode current-clamp technique. Bath-applied L-glutamate produced a reversible hyperpolarization and increase in conductan L-aspartate produced an initial depolarization followed by hyperpolarization and increase in conductance (Fig. 1). T conductance dose–response relationships were sigmoid wi G_{max} of 134 and 56·1 μS, ED_{50} of 318 and 973 μM and n_H 1·1 and 2·0 for glutamate and aspartate, respectively.

Our results show that receptors present in the *Asca* pharyngeal muscle are different from the expres receptors of Cully *et al.* (1994), which are insensitive L-aspartate.

Iain Murray holds an MRC studentship.

REFERENCES

Cully, D.F., Vassilatis, D.K., Liu, K.K., Paress, P Van der Ploeg, L.H.T., Schaeffer, J.M. & Arena, J.P. (19 *Nature* **371**, 707–711.

Martin, R.J. (1996). *Parasitology* **112**, 247–252.

Single-channel recordings from tegument-deriv vesicles of *Schistosoma mansoni*

A.P. Robertson, R.J. Martin and J.R. Kusel*

*Department of Preclinical Veterinary Sciences, R(D)S University of Edinburgh, Edinburgh EH9 1QH a *Department of Biochemistry, University of Glasg Hillhead, Glasgow*

Schistosomiasis is a widespread tropical disease of m caused by the trematode *Schistosoma mansoni*. The dise is usually treated with praziquantel, a highly effective d with few side effects. The exact mechanism by wh praziquantel kills the parasite has yet to be determined (review, see Redman *et al.* 1996). Praziquantel causes influx of calcium across the parasite tegument, suggest that the drug may act on a specific ion channel within tegument. We have developed a method for form membrane vesicles from the schistosome tegument t allows the application of the patch-clamp technique.

Treatment of *S. mansoni* in low pH media (Gi BHK-21 adjusted to pH 3·75 with 5 M HCl) for 15–30 r resulted in the formation of membrane vesicles from tegument. In order to check the origin and structure of vesicles, parasites were pre-treated with 4-aminofluoros to label the outer tegumental membrane and examined u fluorescence microscopy. The results showed that some of vesicles originated from the outer tegumental membr Scanning electron microscopy revealed that the ves possessed a smooth surface suitable for applying the pa clamp technique. Transmission electron microsc demonstrated that some vesicles possessed the double bil found in the outer tegument of the adult schistosome.

Our patch-clamp recordings showed the presence large conductance (290 pS), non-selective cation channel similarities to those channels previously described by Da

[illegible] (110 pS) potassium-selective channel (Fig. 1) and a smaller conductance (20 pS) sodium-selective channel.

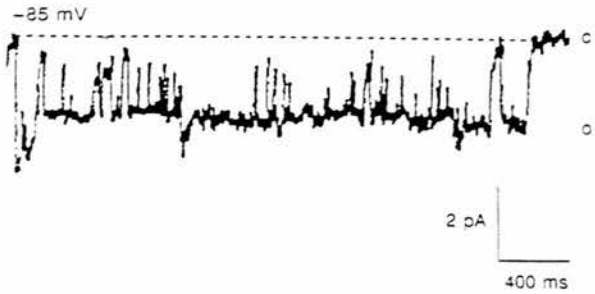


Fig. 1. Examples of single-channel openings from an isolated inside-out patch, at −85 mV. The patch shows a K^+-selective channel; reversal potential was −70 mV (predicted Nernst E_K was −85 mV).

We hope that further study of the ion channels present in the schistosome tegumental membrane will lead to a description of which ion channel may be responsible for the calcium entry induced by praziquantel treatment.

This work was supported by a BBSRC studentship and the Wellcome Trust.

REFERENCES

Day, T.A., Bennet, J.L. & Pax, R.A. (1992). *Exp. Parasitol.* **74**, 348–356.

Redman, C.A., Robertson, A.P., Fallon, P.G., Modha, J., Kusel, J.R., Doenhoff, M.J. & Martin, R.J. (1996). *Parasitol. Today* **12**, 14–20.

Effect of aluminium lactate on electrical activity in an identified neuron of *Lymnaea stagnalis, in vitro*

M.M. Campbell, C.R. McCrohan, K.N. White and J.J. Powell*

*School of Biological Sciences, University of Manchester, Manchester M13 9PT and *Rayne Institute, St Thomas' Hospital, London SE1 7EH*

Aluminium is ubiquitous in the environment and neurotoxic. Bioavailability of aluminium is influenced by pH and the ligand to which it is bound. The neurotoxicity of aluminium lactate, a water-soluble compound at neutral pH, was examined in an identified molluscan neuron, cell RPD1 of *Lymnaea stagnalis*. Intracellular recordings were made in the isolated central nervous system maintained in Mops-buffered saline at pH 7·4. Aluminium lactate and sodium lactate (control) were applied extracellularly to give final concentrations of 100 and 300 μM, respectively.

Cell RPD1 was usually silent under control conditions. A response to aluminium lactate ($n = 6$) occurred after a delay of 10–70 s. The cell was depolarized by up to 20 mV. Inhibitory and excitatory synaptic inputs increased in frequency and amplitude, indicating activation of presynaptic neurons. Activity was induced in RPD1, usua[lly] in the form of bursts of action potentials occurring a[t] maximum frequency of 10–44 per minute and contain[ing] between two and nine spikes. Spike amplitude and durat[ion] within bursts were 72·5 ± 0·5 mV (mean ± S.E.M.) a[nd] 4·9 ± 0·2 ms, respectively, compared with 79·8 ± 1·0 [mV] and 4·2 ± 0·3 ms in control. Spike afterhyperpolarizat[ion] was reduced between spikes in bursts. In half of t[he] preparations, significant spike broadening subsequent[ly] occurred after 4–10 min; some action potentials ha[d] durations of up to 3 s.

Application of sodium lactate produced no response [in] four out of six preparations. However, in two preparations small depolarization was seen, lasting 15–90 s and leadin[g] to a train of spikes. This might be attributable to a short-lasting decrease in intracellular pH induced by lactate (De Hemptinne *et al.* 1983). No changes in spike shape were observed.

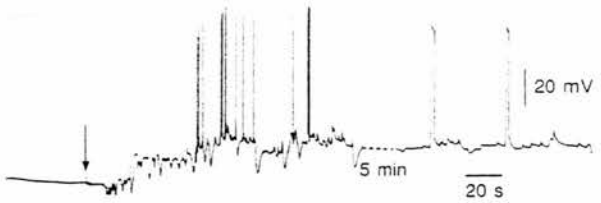


Fig. 1. Effect of aluminium lactate superfusion (100 μM; arrow) on electrical activity of RPD1 neuron.

Aluminium lactate is clearly bioavailable at neutral pH producing repeatable effects on electrical activity. The changes in spike shape are consistent with a reduction in K^+ conductance, although other actions cannot be ruled out.

REFERENCE

De Hemptinne, A., Marrannes, R. & Vanheel, B. (1983). *Am. J. Physiol.* **245**, C178–183.

Voltage-activated ionic currents from isolated squid giant axon Schwann cells

Euan R. Brown*, Isao Inoue† and Izuo Tsutsui‡

**The Marine Biological Association Laboratory, Plymouth*
†*Institute for Enzyme Research, Tokushima University, Tokushima, Japan and* ‡*N.I.P.S., Okazaki, Japan*

The squid giant axon and associated Schwann cells are an excellent *in situ* system to study neuron–glial interaction (Abbott *et al.* 1995). However, it has not been possible to obtain detailed information about Schwann cell membrane properties. We have developed a method for isolating giant axon Schwann cells and subjecting them to whole-cell voltage clamp.

Squid (*Loligo forbesi*) were decapitated and giant axons cleaned of small fibres in Ca^{2+}-free artificial seawater (ASW

Pestic. Sci. 1996, **48**, 343–349

Anthelmintic Actions of the Cyclic Depsipeptide PF1022A and its Electrophysiological Effects on Muscle Cells of *Ascaris suum*†

Richard J. Martin,[a]* Achim Harder,[b] Michael Londershausen[b] & Peter Jeschke[b]

[a] Department of Preclinical Veterinary Sciences, R.(D.)S.V.S., Summerhall, University of Edinburgh, Edinburgh EH9 1QH, UK
[b] Business Group Animal Health, Institute of Parasitology, Bayer 51368 Leverkusen, Germany

(Received 27 February 1996; revised version received 20 May 1996; accepted 9 August 1996)

Abstract: The cyclic depsipeptide PF1022A, given orally to mice, showed very good anthelmintic activity against *Heligmosomoides polygyrus* and *Heterakis spumosa* at 50 mg kg^{-1}. *In vitro*, PF1022A was very active against *Trichinella spiralis* and had good activity against *Nippostrongylus brasiliensis* at 1 $\mu g\ ml^{-1}$. An 18-membered enniatin analogue, JES 1798, showed good activity only against *N. brasiliensis* at 10 $\mu g\ ml^{-1}$. The optical antipode of PF1022A had poor activity even at 100 $\mu g\ ml^{-1}$. The effects of PF1022A on the membrane potential and input conductance of somatic muscle of *Ascaris suum* were examined using a two-microelectrode current-clamp technique. PF1022A did not antagonize the effects of the selective nicotinic agonist levamisole. PF1022A and an analogue, JES 1798, but not the PF1022A antipode, produced a small time-dependent increase in input conductance associated with no potential change. The increase in input conductance did not occur in the Cl^--free bathing solution, suggesting that the increase in input conductance was mediated by Cl^- ions. The addition of high concentrations of Ca^{2+} to the preparation after the addition of PF1022A did not lead to production of Ca^{2+}-activated Cl^- channels, suggesting that its mode of action was not that of a Ca^{2+} ionophore. The mechanism by which the cyclic depsipeptide might increase the Cl^- conductance is discussed.

Key words: cyclic depsipeptide, PF1022A, electrophysiology, anthelmintic, *Ascaris suum*, mode of action, *Heligmosomoides polygyrus*, *Heterakis spumosa*, mouse

1 INTRODUCTION

The 24-membered cyclic depsipeptide PF1022A is a fermentation product of a strain of *Myclia sterilia* that was isolated from microflora on the leaf of the plant *Camellia japonica*, collected from the Ibaragi Prefecture in Japan. The potent antinematodal property of this agent against *Toxocara canis*[1] and *Toxocara cati*,[1] intestinal nematodes of dogs and cats, and against *Ascaridia galli*,[2] an intestinal nematode of chickens, was reported in 1990 and 1992.[1,2] Recently the chemical synthesis of this and the radiolabelled compound have been reported.[3,4]

PF1022A appears to exert its anthelmintic effect on neuromuscular transmission of nematodes rather than by affecting energy metabolism. This is suggested by experiments with PF1022A on the motility of *Angiostrongylus cantonsis*;[5] low concentrations (10^{-13}–10^{-6} g ml^{-1}; 0·1 pM–1 μM) of PF1022A depress the motility of the preparation within 100 min and 50 μM picrotoxin and 30 μM bicuculline and 20 mM Ca^{2+} antagonize the action of PF1022A. These experiments suggest that PF1022A is neuropharmacologically active and that part of the effect of PF1022A may be explained by an antagonism of acetylcholine receptors and/or a GABAergic effect.

* To whom correspondence should be addressed.
† One of a collection of papers on various aspects of pest control research contributed by staff of Bayer AG and collated by Dr M. Londershausen and Dr A. Turberg.

Pestic. Sci. 0031-613X/96/$09.00 © 1996 SCI. Printed in Great Britain

Other novel related cyclic depsipeptides, like JES 1798, a derivative of the naturally occurring enniatins like enniatin A, B, C and beauvercin, which are 18-membered cyclic depsipeptides,[6] have been synthesized.[7]

In this paper experiments on the anthelmintic and electrophysiological effects of PF1022A and JES 1798 are reported, the aim of which was to test further their anthelmintic activities and to determine if PF1022A behaved like a nicotinic antagonist or a GABA agonist.

2 METHODS

2.1 In-vitro experiments

The larvae of the nematode *Trichinella spiralis* were isolated from skeletal muscles and diaphragms of SPF/CFWI mice and stored in sodium chloride solution (9 g litre^{-1}), supplemented with Canesten (20 μg ml^{-1}). Twenty larvae per estimation were incubated in a solution (2 ml) containing: Batcho Capstone, 20; yeast extract 10; glucose 5; KH_2PO_4, 0·8; K_2HPO_4, 0·8 g litre^{-1}; pH 7·2 supplemented with sisomycin (10 μg ml^{-1}) and canesten (1 μg ml^{-1}). The test compound (10 mg) was dissolved in dimethylsulfoxide (DMSO; 0·5 ml) and added to the incubation medium to give final concentrations of 100, 10, 1, 0·1 and 0·01 μg ml^{-1}. The experiment was stopped after 5 days of incubation at 19°C. Activity was assessed on a scale 0–3 where 3 = full activity (all larvae dead); 2 = good activity (<100% but >50% of the larvae dead); 1 = weak activity (>50% of larvae still alive) and 0 = no activity (number of living larvae equals that in the control).[8]

Adult nematodes of *Nippostrongylus brasiliensis* were isolated from the small intestine of female Wistar rats, stored in sodium chloride (9 g litre^{-1}), supplemented with Sisomycin (20 μg ml^{-1}) and Canesten (2 μg ml^{-1}). The incubation of each group of male or female worms was performed in 1·0 ml medium, which was collected for the estimation of the level of activity of the acetylcholinesterase secreted by *N. brasiliensis*. Details of the incubation and determination are as described by Rapson, *et al.*[9] The level of activity of the test compound was assessed on a scale 0–3 where 3 = full activity (95%–100% enzyme inhibition); 2 = good activity (75%–95% inhibition); 1 = weak activity (50–75% inhibition); 0 = negligible activity (<50% inhibition).

2.2 In-vivo experiments

For all experiments, male mice of the strain SPF/CFWI, 16–18 g body weight on receipt, were used. Five animals were housed per macrolon cage and given water and 'Sniff' rat feed, (13-cm feed pellets), *ad libitum*. Mice were given a mixed infection of the tapeworm *Hymenolepis nana* and the nematodes *Heligmosomoides polygyrus*, *Heterakis spumosa* and *Trichinella spiralis*. The infective material from *H. nana* was collected from mouse faeces 14–21 days after infection. Third-stage larvae of *H. polygyrus* were collected from mouse faeces 21 days after infection. *Heterakis* eggs were obtained from female worms isolated from mouse colon 35–42 days after infection and after incubation at 27°C for three weeks. *T. spiralis* larvae were obtained from pepsin-treated skeletal muscles and diaphragm from Wistar rats 20 days after infection.

The mixed infection was produced by an initial oral infection of 90 embryonated *H. spumosa* eggs on day 1; on day 7, 100 *T. spiralis* larvae were given orally; on day 34, 60–70 *H. polygyrus* larvae were given orally; on day 36, 100 eggs of *H. nana* were given orally. Treatment with the test compounds began on day 46 and ended on day 49. On day 57 the mice were killed with carbon dioxide and dissected. *H. nana* were isolated from the small intestine and the number of tapeworms estimated microscopically with a magnification of ×16. *H. spumosa* were isolated from caecum and colon and counted macroscopically. *H. polygyrus* were examined in the duodenum after removal and pressing in a compressor; parasites were counted microscopically with a magnification of × 40. For examination of *T. spiralis* larvae, a 1-cm^2 piece of abdominal muscle was dissected and pressed between two plastic sheets, using a hand press, and the parasites in the pressed muscle examined microscopically (×40). The level of anthelmintic activity against the three species of nematode was graded using the following criteria: 3 = cure (no parasites detectable); 2 = active (<20% of parasites remaining); 1 = trace effect (<50% but >20% of parasites remaining); 0 = ineffective (>50% of parasites remaining). The activity against *H. nana* was graded on a scale 0–3, where 3 = cure (no parasites detectable); 2 = effective (some parasites expelled, tapeworm strobila excreted); 1 = trace effect (tapeworm strobila excreted or macerated) and 0 = ineffective (all parasites remaining).

Test compounds were dissolved or suspended in 'Cremophor' EL (0·2 ml emulsifier g^{-1} test compound) and 0·5 ml of this solution (or suspension) was administered to each mouse daily for four consecutive days. For each test compound, one mouse received the highest dose of 250 mg kg^{-1}. If anthelmintic activity was detected at this dose, lower doses of 100, 50, 25 and 10 mg kg^{-1} were tested down to the level where no anthelmintic activity was detectable.

2.3 Preparation of *Ascaris suum* muscle for electrophysiology

Details of the preparation have been described fully elsewhere[10,11] but they are outlined below. *Ascaris suum* were collected from the local abattoir and maintained in Locke's solution at 35°C and the solution replaced daily. A body flap preparation of *A. suum* was

made from a region about 3 cm from the head and mounted on Sylard in an experimental chamber containing 6 ml of a well-stirred bathing solution maintained at 37°C. The experiments reported here are based on observations on 16 preparations of *A. suum*, each compound (and experiment) was tested on at least two separate preparations.

2.4 Electrophysiological experiments

The preparation was bathed, except where stated, in a low-Ca^{2+} high-Cl^- solution containing sodium chloride, 132; potassium chloride, 2·4; magnesium chloride, 10; glucose, 11; HEPES, 5 mM and DMSO, 10 ml litre^{-1}; pH 7·4, adjusted with sodium hydroxide. The low-Ca^{2+} solution was used to abolish spontaneous depolarizing potentials and high-Cl^- solution was used to enhance Cl^- conductance responses. In some cases a zero-Cl^- solution was used in which all the Cl^- ions were replaced by acetate.

For recording, two glass micropipettes filled with potassium acetate (2 M), were inserted into the bag region of the muscle with the aid of a dissecting microscope and illumination from below. The micropipettes had a resistance of 20–25 MΩ. Constant current-clamp pulses of 40 nA for 1 s were injected at a rate of 0·2 Hz with an Axoclamp 2A to produce hyperpolarizing pulses. The current–voltage relationship of the muscle was examined and found to be linear in the hyperpolarizing ranges used. Current injection and voltage responses were monitored on an oscilloscope and voltage responses recorded on an Electromed two-channel pen recorder. The figures illustrating the electrophysiological responses were prepared directly from the original pen recordings: the width of a trace (envelope of the trace) is inversely proportional to the input conductance. An agar bridge was used as a bath earth. Concentrated stock solutions of the drugs PF1022A, JES 1798 or PF1022A antipode were added in volumes $\lesssim 300$ µl to the well-stirred bath. The stock solutions were made up in the standard bathing solution with DMSO (10 ml litre^{-1}). At this concentration DMSO had no detectable effect on GABA responses. Mixing was complete within 1 min (dye test). The relative molecular masses of PF1022A, PF1022A antipode and JES 1798 are 948, 948 and 556, respectively. The preparation was washed by draining the bath and replacing the bathing solution three times. The significance of effects of PF1022A and PF1022A antipode on input conductance change was compared using values at 10 and 20 min and a two-way analysis of variance with replications.

3 RESULTS AND DISCUSSION

PF1022A had full anthelmintic activity *in vitro* against *T. spiralis* and *N. brasiliensis* at 1 µg ml^{-1} (1·05 µM) (Table 1). Previously we have reported that PF1022A, at similar low concentrations,[3] has full anthelmintic activity *in vitro* against *Heterakis spumosa*, a lumen-dwelling nematode of the mouse. In contrast, the PF1022A optical antipode exerted only a slight anthelmintic activity against *N. brasiliensis* at the high concentration of 100 µg ml^{-1}, whereas the enniatin derivative JES 1798 had good anthelmintic activity *in vitro* at 10-fold higher concentrations against *N. brasiliensis* compared to PF1022A (Table 1).

PF1022A also showed full anthelmintic activity *in vivo* at the oral dose-rate of 50 mg kg^{-1} against *H. polygyrus* as well as against *H. spumosa* in the mouse (Table 2). There was no detectable effect against the cestode *H. nana* or *T. spiralis* larvae in the muscle. We have already reported the activity of JES 1798 *in vivo* against the sheep nematodes *Haemonchus contortus* and *Trichostrongylus colubriformis* at an oral dose-rate of 1–5 mg kg^{-1}, when administered intravenously or orally.[7]

To test the mode of action of PF1022A using electrophysiological methods we chose the nematode *Ascaris suum*. This pig nematode parasite has the advantage of being large enough to allow intracellular recording micropipettes to be used and has been studied extensively using electrophysiological methods. The aim in

TABLE 1
Anthelmintic Activity of PF1022A, PF1022A Antipode and JES 1798 *in vitro* against *Trichinella spiralis* Larvae and *Nippostrongylus brasiliensis* Adults[a]

	Trichinella spiralis			Nippostrongylus brasiliensis		
Concentration (µg ml^{-1})	*PF1022A*	*PF1022 antipode*	*JES1798*	*PF1022A*	*PF1022 antipode*	*JES1798*
100	3	1	0	3	1	2
10	3	0	0	3	0	0
1	3	0	0	2	0	nd
0·1	2	0	0	0	0	nd

[a] 0 = no activity; 1 = slight activity; 2 = good activity; 3 = full activity. For quantitation of the effect of the test compound see Section 2.1. Each compound was tested in two different experiments ($n = 2$) at each concentration. 1 µg ml^{-1} is equivalent to 1·05 µM PF1022A, 1·05 µM PF1022 antipode or 1·89 µM JES1798.

TABLE 2
Anthelmintic Activity of PF1022A against Different Helminths of the Mouse[a]

Doseage (*mg kg*$^{-1}$)	*Hymenolepis nana*	*Heligmosomoides polygyrus*	*Heterakis spumosa*	*Trichinella spiralis larvae*
100	0	3	3	0
50	0	3	3	0
25	0	2	0	0
10	0	1	0	0
5	0	0	0	0

[a] 0 = no activity; 1 = slight activity; 2 = good activity; 3 = full activity. For quantitation of the effect of the test compound see Section 2.1. Each dose level was tested in two different experiments ($n = 2$) with three mice being used at each dose level.

these experiments was to determine if the anthelmintic effects of the cyclic depsipeptides could be explained by either a nicotinic antagonist action or a GABA agonist action as proposed[5] or both.

Levamisole is a selective nicotinic agonist in *A. suum* and will depolarize the muscle and increase the input conductance.[12] Figure 1 shows that adding 30 μM levamisole to the bath produced a 15-mV depolarization and increased the input conductance of the muscle cell from 2·53 μS to 4·35 μS. Addition of PF1022A to the bath at 10^{-6} g ml^{-1} (1·05 μM) had little effect: after 10 min the input conductance increased slightly to 4·25 μS and there was little effect on membrane potential. The same effect was reproduced in another preparation of *A. suum*. Since the effect of levamisole was not reversed by PF1022A ($n = 2$), it was concluded that PF1022A is not a nicotinic antagonist in *A. suum*.

Piperazine is a regularly used anthelmintic that acts as a GABA agonist in nematodes.[11] Bath-applied piperazine produces a marked dose-dependent increase in Cl^- conductance of the muscle membrane as well as a large hyperpolarizing potential in cells of *A. suum*.[11] We tested the effect of PF1022A as a GABA agonist using the same methods.

Figure 2A illustrates the effect of PF1022A (10^{-6} g ml^{-1}; 1·05 μM) on input conductance in high-Cl^- bath solution and on membrane potential. It can be seen that there is a slow, time-dependent increase in input conductance of the membrane from a resting value of 1·74 μS to 2·00 μS over a period of 30 min. The membrane potential shows no detectable change during this period. The effect of PF1022A was not reversed by washing (not shown). The small time-dependent effect on input conductance was reproducible (Table 3) but it did not occur in the absence of Cl^- in the bath (Fig. 2B), showing that Cl^- ions are involved in mediating the response. Also no conductance effect was observed with the biologically inactive isomer, PF1022A antipode, (Fig. 2C). The change in conductance produced by PF1022A at 10 min and 20 min was significantly greater than that produced by PF1022A antipode ($P < 0{\cdot}001$, F test).

The slow time-dependent effects of PF1022A on conductance and the absence of an effect by the PF1022A antipode suggests that the effect may be related to the anthelmintic action of these drugs. However, it is difficult to explain the small and time-dependent increases in Cl^- conductance produced by the cyclic depsipeptides as a simple GABA agonist effect. First, except for piperazine, the structures of GABA agonists that are active in *A. suum*[13,14] possess a carboxyl group separated from a charged ammonium group by a distance of

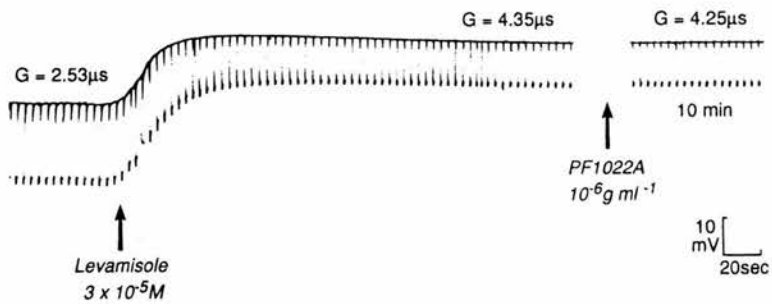


Fig. 1. PF1022A (10^{-6} g ml^{-1}: 1·05 μM) does not antagonise the nicotinic effect of levamisole. Levamisole (30 μM) produces a 15 mV depolarization and an increase in input conductance from 2·53 μS to 4·35 μS but these effects are not antagonized by PF1022A (10^{-6} g ml^{-1}; 1·05 μM). The rapid movement of the pen recorder at the onset and offset of the current injection pulse produces pen skipping but the envelope of the trace (width) is directly related to the input resistance (= 1/input conductance) of the preparation.

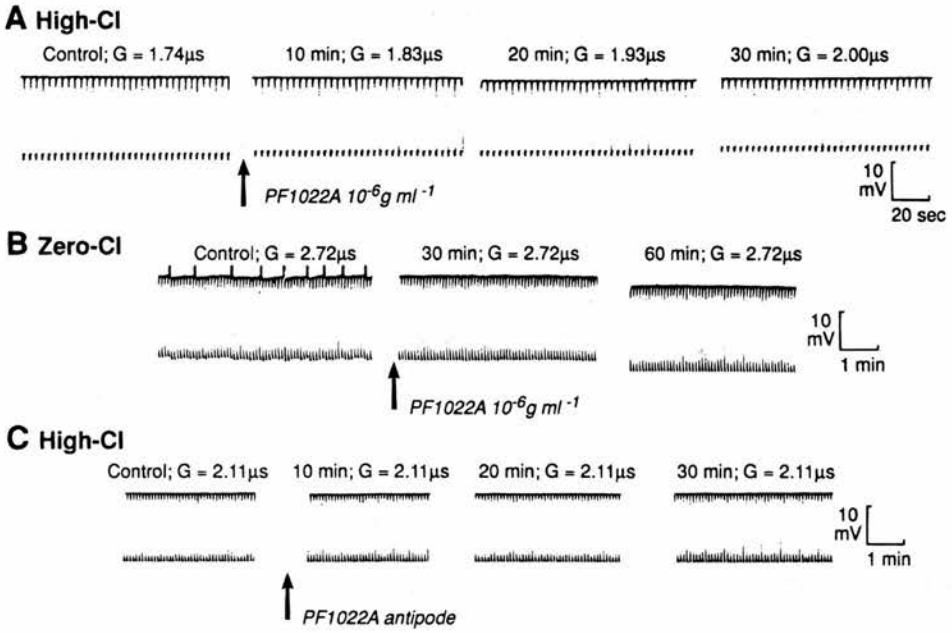


Fig. 2. Effect of PF1022A and PF1022A antipode on the input conductance of the *Ascaris* muscle membrane. Constant current clamp pulses of 40 nA for 1 s were injected at a rate of 0·2 Hz with an Axoclamp 2A to produce hyperpolarizing pulses. A: In high $-Cl^-$ bath solution PF1022A (10^{-6} g ml^{-1}; 1·05 μM) produces a small increase (0·26 μS) in input conductance over a period of 30 min. B: In zero $-Cl^-$ bath solution PF1022A (10^{-6} g ml^{-1}; 1·05 μM) produces no change in input conductance over 60 min. C: In high $-Cl^-$ bath solution PF1022 antipode (10^{-6} g ml^{-1}; 1·05 μM) produces no change in input conductance.

5 Å and, second, GABA agonists produce a marked hyperpolarization and larger increase in Cl^--conductance of the muscle membrane.[10,11] PF1022A does not induce any obvious hyperpolarization.

As a further test of the electrophysiological effects of cyclic depsipeptides, JES 1798, another active anthelmintic analogue of PF1022A, was tested. At 10^{-6} g ml^{-1} (1·89 μM) it also produced a small and slow increase in input conductance of the membrane (Fig. 3). Enniatins like enniatin A, B or C, as well as beauvercin, are known to induce cation fluxes across membranes[7] and might produce a secondary increase in

TABLE 3

Effect of PF1022A, PF1022A Antipode and JES1798 on the Input Conductance of *Ascaris* Muscle and Membrane Potential

	10 min ΔG (μS)	*20 min* ΔG (μS)	*30 min* ΔG (μS)	*10 min* *mV change*
PF1022A (10^{-6} g ml^{-1})				
exp. 1	0·09	0·19	0·26	0
exp. 2	0·18	0·29	0·36	0
exp. 3	0·17	0·17	nd[b]	0
PF1022A antipode (10^{-6} g ml^{-1})				
exp. 1	0·04	0·06	nd	0
exp. 2	−0.05	−0.05	nd	0
exp. 3	0	0	0	0
JES1798 (10^{-6} g ml^{-1})				
exp. 1	0·12	0·26	nd	0
exp. 2	nd	nd	nd	0

[a] The input conductance change following addition of the compounds was determined at 10, 20 and 30 min. The change in membrane potential was determined after 10 min. Each experiment was conducted on a separate preparation made from a fresh *Ascaris*. Two-way analysis of variance with replication showed that the effects of PF1022A on ΔG were significantly ($P < 0·001$, F test) greater than PF1022A antipode.

[b] nd: not determined.

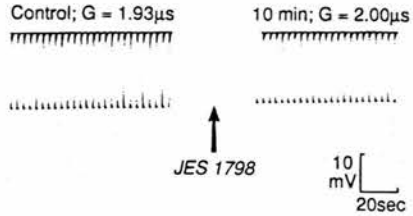


Fig. 3. Effect of enniatin JES 1798 on input conductance of *Ascaris* muscle. In high $-Cl^-$ bath solution JES1798 (10^{-6} g ml^{-1}; 1·89 μM) produces a conductance change, 0·07 μS, after 10 min.

Cl^- conductance, as discussed later. From our observations it can be concluded that cyclic depsipeptides are not potent GABA agonists because (1) they did not produce a marked hyperpolarization and (2) they did not produce a large increase in input conductance.

Ascaris muscles contain Cl^- channels that are activated by an increase in intracellular Ca^{2+} concentrations.[15] The cyclic depsipeptides have a macrocyclic lactone ring structure, so it is possible that they act as an ionophore, carrying cations,[7] including Ca^{2+}, across the cell membrane, leading to the observed increase in membrane conductance. Although experiments were carried out in the absence of added Ca^{2+} ions in the bath, we decided to check for the possibility of PF1022A facilitating the entry of Ca^{2+} ions into the muscle cell leading to activation of the Ca^{2+}-dependent Cl^- channels. Our experiments, however, indicated that the addition of Ca^{2+} ions (2–6 mM) to the bath solution did not enhance the effect of PF1022A on input conductance (not shown). This observation suggests that PF1022A does not produce its effect on input conductance by acting as a Ca^{2+} ionophore.

A number of possible explanations for the mode of action of the active cyclic depsipeptides remain:

1. The cyclic depsipeptides may combine with one of the subunits of the GABA receptor-channel, but not at the GABA binding site, and predispose the channel towards opening; it could then potentiate the action of GABA. We have not looked for GABA potentiation in these experiments. One disadvantage of this explanation is that it predicts toxic effects on the host animal as well as on the parasite; the host animal also has peripheral GABA receptors as well as the parasite.
2. Another explanation is that the cyclic depsipeptides are selectively metabolized by the nematode parasites to a GABA agonist. The anthelmintic action is explained by the local production of a GABA agonist in the parasite but not in the host.
3. The cyclic depsipeptides lead to partial activation of Cl^- channels that are present only in the parasite: the Ca^{2+}-activated Cl^- channels.[15] Such an effect could be produced directly on the channel or by secondary effects, as the cyclic depsipeptides insert into membranes and act as an ionophore leading to changes in intracellular Na^+ or pH. We found no evidence in this study that PF1022A acts as a Ca^{2+} ionophore. The Ca^{2+}-activated channel is, however, also sensitive to intracellular pH changes as well intracellular Ca^{2+} changes.
4. The cyclic depsipeptides have a macrocyclic lactone structure; their effects on muscle tone may be antagonized by pictrotoxin[5] and cyclic depsipeptides have selective toxic effects on nematode parasites. All these observations may be explained if the depsipeptides act in a similar way to the avermectins, also macrocyclic lactones, and lead to opening of glutamate-gated Cl^- channels that are present only in invertebrate species.[16] Recently this receptor has been localized on the *A. suum* pharyngeal muscle, and testing the effects of the macrocyclic lactones on this receptor by electrophysiological means is now possible.[17] These possibilities remain to be tested in future experiments.

REFERENCES

1. Fukashe, T., Koike, T., Chinone, S., Akihama, S., Iagake, H., Takagi, M., Shimizu, T., Yaguchi, T., Sasaki, T. & Okada, T., Anthelmintic effects of PF1022, a new cyclic depsipeptide, on intestinal parasitic nematodes in dogs and cats. *Proc. 110th Meeting Jap. Soc. Vet. Sci.*, 1990, p. 122.
2. Takagi, M., Sasaki, T., Yagushi, T., Kodama, Y., Okada, T., Miyadoh, S. & Koyama, M., On a new cyclic depsipeptide, PF1022A with anthelmintic effects. *Nippon Nogeikagaku Kaishi*, **65** (1991) 326.
3. Pleiss, U., Harder, A., Turberg, A., Londershausen, M., Iinuma, N., Mencke, N., Jeschke, P. & Bonse, G., Synthesis of (^{3}H-menthyl) PF1022A. *J. Radiolab. Comp.*, **38** (1995) 61–9.
4. Scherkenbeck, J., Plant, A., Harder, A. & Mencke, N., A highly efficient synthesis of the anthelmintic cyclooctadepsipeptide PF1022A. *Tetrahedron*, **51** (1995) 8459–70.
5. Terada, M., Neuropharmacological mechanism of action of PF1022A, an antinematode anthelmintic with a new structure of cyclic depsipeptide, on *Angiostrongylus cantonensis* and isolated frog rectus. *Jap. J. Parasitol.*, **41** (1992) 1–16.
6. Berdy, J., Aszalos, A., Bostian, M. & McNitt, K. L., Depsipeptide antibiotics. *CRC Handbook of Antibiotic Compounds*, Vol. IV, Part 2 (19) 171–6.
7. Jeschke, P., Scherkenbeck, J., Plant, A., Harder, A. & Mencke, N., Enniatins and enniatin derivatives used to control endoparasites. Patent WO 93/25543 (1993).
8. Jenkins, D. C. & Carrington, T. S., *In-vitro* screening test for compounds active against the parenteral stages of *Trichinella spiralis*. *Tropenmed. Parasitol.*, **32** (1981) 31–4.
9. Rapson, E. B., Jenkins, D. C. & Chilwan, A. S., Improved detection of anthelmintic activity in an *in-vitro* screen utilizing adult *Nippostrongylus brasiliensis*. *Z. Parasitenkd.*, **73** (1987) 190–1.
10. Martin, R. J., The effect of γ-aminobutyric acid on the input conductance and membrane potential of *Ascaris* muscle. *Brit. J. Pharmacol.*, **71** (1980) 99–106.
11. Martin, R. J., Electrophysiological effects of piperazine and diethylcarbamazine on *Ascaris suum* somatic muscle. *Brit. J. Pharmacol.*, **77** (1982) 255–65.

12. Harrow, I. D. & Gration, K. A. F., Mode of action of the anthelmintics morantel, pyrantel and levamisole in the muscle cell membrane of the nematode *Ascaris suum*. *Pestic. Sci.*, **16** (1985) 662–72.
13. Holden-Dye, L., Krogsgaard-Larsen, P., Neilsen, L. & Walker, R. J., GABA receptors on the somatic muscle cells of the parasitic nematode, *Ascaris suum:* stereoselectivity indicates similarity to a GABA-type agonist recognition site. *Brit. J. Pharmacol.*, **98** (1989) 841–50.
14. Martin, R. J., Sitamze, J. M. Duittoz, A. H. & Wermuth, C. G., Novel arylaminopyridazine-GAB A receptor antagonists examined electrophysiologically in *Ascaris suum*. *Eur. J. Pharmacol.*, **276** (1995) 9–19.
15. Thorn, P. & Martin, R. J., A high-conductance calcium-dependent chloride channel in *Ascaris suum* muscle. *Quart. J. Exp. Physiol.*, **73** (1987) 31–49.
16. Cully, D. F., Vassilatis, D. K., Liu, K. K., Paress, P. S., Vanderploeg, L. H. T. & Schaeffer, J. M., Cloning of an avermectin-sensitive glutamate-gated chloride channel from *Caenorhabditis elegans*. *Nature* (*London*), **371** (1994) 707–11.
17. Martin, R. J., An electrophysiological preparation of the pharyngeal muscle of *Ascaris suum* reveals a glutamate-gated chloride channel sensitive to the avermectin analogue, milbemycin D. *Parasitol.*, **112** (1995) 247–52.

[*From the Proceedings of the Physiological Society*, 22–23 *September* 1989
Journal of Physiology, **420**, 91*P*, 1990]

Acetylcholine-activated single channel currents from isolated *Ascaris suum* muscle

By R. J. Martin and A. J. Pennington. *Department of Preclinical Veterinary Sciences, R(D)SVS, Summerhall, University of Edinburgh, Edinburgh EH9 1QH*

The site of action of a group of antiparasitic drugs (including pyrantel) is an acetylcholine receptor on the muscle of *Ascaris suum* (Harrow & Gration, 1985). We have used the patch-clamp technique to further investigate the action of acetylcholine on this tissue, at the single-channel level, using muscle vesicles from *Ascaris suum*. Our preliminary results show that acetylcholine activates a cation selective channel, which has a main state conductance of 40–50 pS (Fig. 1). The distribution of open times was described by a single exponential, with mean open times between 1 and 4 ms. Smaller conductance (25–35 pS) channel currents were also activated by acetylcholine, their properties require further investigation.

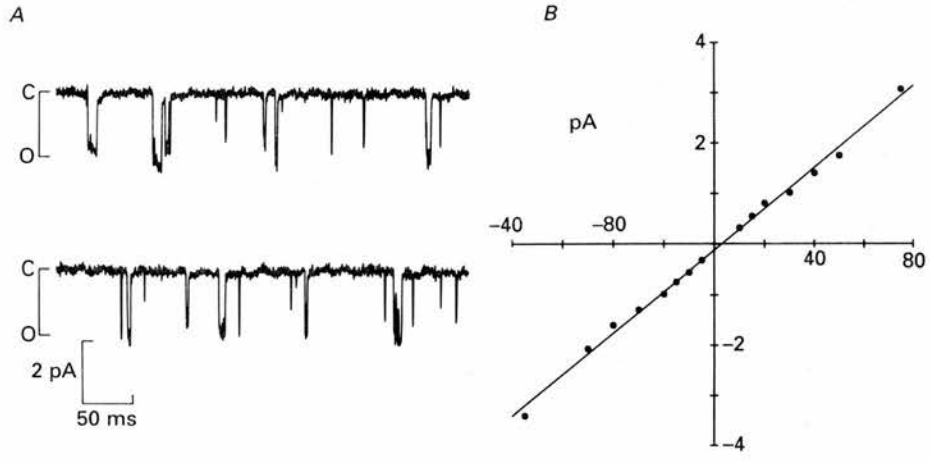


Fig. 1. *A*, Acetylcholine-activated channels. Cell-attached patch from a muscle vesicle (vesicles were formed by collagenase treatment of a muscle flap preparation of *Ascaris suum*). C, closed state; O, open state. Estimated patch potential: −50 mV, 10 μM-acetylcholine in pipette solution. Pipette solution (mM): CsCl, 140; $MgCl_2$, 2; EGTA, 1; HEPES, 10; pH 7·2 with CsOH. Bathing solution (mM): CsCl, 35; Csacetate, 105; $MgCl_2$, 2; EGTA, 1; HEPES, 10; pH 7·2 with CsOH. Filter: −3 dB 1 KHz, 8-pole Bessel. Main state = −2·07 pA, mean open time = 2·17 ms. B, I/V plot from the same experiment as *A*, slope conductance = 41 pS, reversal pd = 2·9 mV.

Supported by SERC.

REFERENCE

Harrow, I. D. & Gration, K. A. F. (1985). *Pesticide Sci.* **16**, 662–672.

J. exp. Biol. **154**, 201–221 (1990)
Printed in Great Britain © *The Company of Biologists Limited 1990*

A PATCH-CLAMP STUDY OF ACETYLCHOLINE-ACTIVATED ION CHANNELS IN *ASCARIS SUUM* MUSCLE

BY A. J. PENNINGTON AND R. J. MARTIN

Department of Preclinical Veterinary Sciences, Summerhall, Royal (Dick) School of Veterinary Studies, University of Edinburgh, Edinburgh

Accepted 14 June 1990

Summary

Acetylcholine-activated single-channel currents were recorded from cell-attached and inside-out patches of isolated muscle vesicles from *Ascaris suum*. Acetylcholine (1–10 μmol l^{-1}) activated cation-selective channels of two amplitudes: 40–50 pS and 25–35 pS. Both channels had linear I/V relationships and mean open durations independent of voltage. The larger conductance was analysed in detail to determine its open-, closed- and burst-time kinetics; the open and burst durations were composed of two components (short and long), while closed durations had at least three components (short, intermediate and long). The data were then corrected to allow for missing short events in order to estimate various parameters including corrected mean open time (1.26+0.11 ms, mean±S.E.). Values were also derived for the efficacy (β/α=4.9) and affinity [$1/K_D=147\times10^3$ (mol l^{-1})$^{-1}$] of acetylcholine at this receptor. Larger concentrations of acetylcholine (25–100 μmol l^{-1}) were shown to produce desensitization and caused single-channel currents to occur in clusters with long closed times (mean 171 s) between clusters. It was concluded that the extrasynaptic muscle of *Ascaris suum* contains two types of acetylcholine-activated ion channel and these are possible sites of action of various anthelmintic drugs. This paper is the first to describe acetylcholine-activated single-channel currents in invertebrate muscle.

Introduction

Ascaris suum is a parasitic nematode which lives in the intestine of the pig and is a target species for a variety of anthelmintic drugs, including pyrantel and levamisole, which are thought to be acetylcholine agonists. Acetylcholine has long been known to have effects on the muscle cells of *Ascaris suum* (Del Castillo *et al.* 1963); application of acetylcholine to whole worms or muscle-flaps will cause the muscle to contract. It is now believed that acetylcholine is the excitatory neuromuscular transmitter in nematodes (Willett, 1980; Johnson and Stretton, 1985; Gration *et al.* 1986). It has also been shown that there are extrasynaptic acetylcholine receptors on the bag region of *Ascaris suum* muscle, which respond to ionophoretically applied acetylcholine (Martin, 1982). Acetylcholine acts on

Key words: acetylcholine channel, patch-clamp, *Ascaris suum*, muscle.

these receptors to increase input conductance and to produce depolarization. The effect of acetylcholine on *Ascaris* muscle is blocked by tubocurarine but not by atropine, hence these muscle receptors may be classified pharmacologically as nicotinic (Natoff, 1969; Rozhkova *et al.* 1980; Martin, 1982).

The pharmacology of the nicotinic receptors on *Ascaris* muscle differs from that of any type of vertebrate nicotinic receptor. Mecamylamine is a very potent blocker of *Ascaris* nicotinic receptors; this normally blocks the nicotinic receptors of autonomic ganglia in vertebrates, but not skeletal muscle receptors (Natoff, 1969; Rozhkova *et al.* 1980). These differences are exploited therapeutically by various nicotinic anthelmintic compounds which act selectively on the acetylcholine receptor of this parasite (Aubry *et al.* 1970; Coles *et al.* 1975; Harrow and Gration, 1985).

Acetylcholine acts on nicotinic receptors and has been shown to activate cation-selective single-channel currents in vertebrate preparations (for a review, see Schuetze and Role, 1987) and in certain insect neurones (Sattelle, 1986; Beadle *et al.* 1989). The aim of the present study was to record acetylcholine-activated single-channel currents from nematode muscle. This was done using isolated muscle vesicles formed from the bag region of the muscle cells of *Ascaris suum*. Recordings obtained were analysed: (a) to characterise this ion channel, (b) to compare it with other nicotinic channels, and (c) as a basis for future study of anthelmintic compounds on this channel. A preliminary account of some of this work has appeared (Martin and Pennington, 1990).

Materials and methods

In general the methods of Hamill *et al.* (1981) were followed. The application of these methods to *Ascaris* has been described previously (Martin, 1985), as has the development of the method for the use of isolated muscle vesicles (Martin *et al.* 1990).

The vesicle preparation

Ascaris suum were collected from the local abattoir and maintained in Locke solution (replaced daily) at 32°C in a water bath. The *Ascaris* were used for experiments within 4 days. Muscle-flap preparations were treated with collagenase (Sigma type 1A) $1\,mg\,ml^{-1}$ for 10–20 min at 37°C to produce isolated muscle vesicles. The vesicles were harvested using a Pasteur pipette and maintained at 37°C until they were transferred to the experimental chamber for patch recording. They were always used within a few hours of formation. Recordings were made at room temperature (15–22°C). The experimental chamber was mounted on the stage of a Reichert–Jung Biostar inverted microscope, and vesicles were viewed at ×200 magnification.

Solutions

Muscle-flap preparations and vesicles were maintained in a solution containing (in $mmol\,l^{-1}$): NaCl, 35; sodium acetate, 105; KCl, 2; $MgCl_2$, 2; Hepes, 10;

glucose, 3; ascorbic acid, 2; and EGTA, 1; pH adjusted to 7.2 with NaOH. Collagenase was applied to the muscle flap in this solution but without the EGTA. In the experimental chamber vesicles were bathed in the following solution (in $mmol\,l^{-1}$): CsCl, 35; caesium acetate, 105; $MgCl_2$, 2; Hepes, 10; and EGTA, 1; pH adjusted to 7.2 with CsOH. Electrodes for cell-attached or inside-out patches were filled with (in $mmol\,l^{-1}$): CsCl, 140; $MgCl_2$, 2; Hepes, 10; and EGTA, 1; pH adjusted to 7.2 with CsOH. In experiments to study the ion-selectivity of the channel, the bath solution was diluted 50:50 with distilled water giving a solution with $70\,mmol\,l^{-1}$ Cs^+ and $19.5\,mmol\,l^{-1}$ Cl^-. Most of the recordings were made with Cs^+ as the main cation to block the K^+ channels known to occur in this membrane. All solutions used during recordings were Ca^{2+}-free, to avoid recording from Ca^{2+}-activated Cl^- channels (Thorn and Martin, 1987).

Recording

Recordings were made from cell-attached or inside-out patches. Patch electrodes, made from micro-haematocrit capillary tubes (Garner Glass 7052), had a resistance of 1–3 MΩ and were coated with Sylgard to improve frequency responses. Currents were recorded using a List EPC-7 and a Racal Thermionic Store Four FM tape recorder.

Data processing

Records were analysed using a CED 1401 interface and DCS 286 PC computer, with software from Dr J. Dempster, Strathclyde University. Filtering was by an eight-pole Bessel filter, 3 dB, 2.5 kHZ, sampling time 40 μs and minimum detectable interval of 0.16 ms. Threshold for channel opening was set at 70 % to exclude the smaller-amplitude channel when a patch contained both amplitudes.

Exponential curve fitting

In our experiments individual channel activations were interrupted by short closed periods (the Nachschlag phenomenon, Colquhoun and Sakmann, 1985), so bursts of openings, as well as single openings, can be considered. Bursts are defined as groups of openings separated by gaps that are all shorter than a specified length, T_{crit}. The mean length of the gaps between bursts was several 100-fold greater than the mean length of gaps within bursts, so the choice of T_{crit} was not critical and a value of 1 ms was chosen from examination of the data.

The next stage of the analysis was exponential fitting of the open, closed and burst durations by the method of maximum likelihood (Colquhoun and Sigworth, 1983; Martin, 1985), to a probability density function (p.d.f.) of the form:

$$\text{p.d.f.} = \sum_{i=1}^{K} \frac{a_i e^{(-t/T_i)}}{T_i}, \qquad (1)$$

where a_i represents the area of the ith component ($\Sigma a_i = 1$), T_i is the fitted time constant, t represents time and K equals the number of exponential terms fitted. A burst distribution, for example, may be fitted by two exponentials; in general it is

not correct to identify the components with particular physical events or to use 'short bursts' or 'long bursts' as though there were two quite separate types of phenomena. Nevertheless, such terms are generally used (Colquhoun and Sakmann, 1985) as a way of discussing the mathematical components that have been identified; in some cases the components do have an approximate physical significance (Colquhoun and Hawkes, 1982).

Correction for missing events

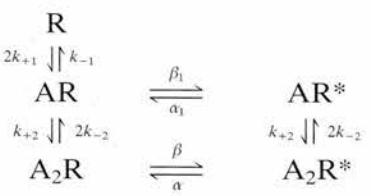
Once exponential components had been fitted to the burst and closed durations, it was possible to correct the data for missing events, using the method of Colquhoun and Sakmann (1985). The assumptions are that very short closings and very short openings will be missed in a standard analysis of open and closed durations, because of limitations of the resolution of the recording technique, and that, using the kinetic information about the data that have been recorded, it is possible to extrapolate back to calculate the number of short events that are likely to have been missed.

The first stage in this correction process is to estimate the total number of events from the observed number of events; this is done separately for gaps and for bursts. N_{bursts} is the estimated total number of bursts and N_{gaps} is the estimated total number of gaps. The next stage in the correction process is to calculate the total time spent in gaps within bursts, (m_{TS}), the corrected number of short gaps per long burst (N_{o}) and the corrected mean burst length (MB). Then the corrected mean open time in long bursts (E) and the corrected total open time ($CTOT$) are calculated, allowing for the missed short gaps.

The corrected open probability (COP) equals $CTOT$ divided by t_{max}; this makes the assumption that in each sample analysed there was only one of the main state conductance channels opening. This is believed to be correct, as double openings were only observed very occasionally and such samples were not analysed; however, if the number of large channels per patch is greater than 1, the values given for open probability are overestimates. Corrected mean open time is $CTOT/N_{\text{gaps}}$. The corrected mean open time is shorter than the mean open time calculated in any other way, because allowing for missed short events reduces the mean value.

Rate constants

This analysis can be extended if we adopt the same model of acetylcholine interacting with its receptor as Colquhoun and Sakmann (1985):



where R denotes the closed receptor-channel molecule, R* the open state and A the agonist (two molecules of agonist are believed to bind to each receptor). Oscillations between the two open states are believed to be very slow and this pathway could be omitted. Oscillations between A_2R^* and A_2R would cause short gaps within bursts and AR* possibly represents brief openings. This allows us to calculate a value for the rate constant for channel closing (α), the rate constant for channel opening (β) and the dissociation rate constant (k_{-2}) (Colquhoun and Sakmann, 1985). Then a value can be obtained for efficacy (this equals β/α), and a value proportional to the potency may be obtained from $(\beta/\alpha)^{1/2}/k_{-2}$.

If we then assume $k_{-1}=k_{-2}$ and $K_1=K_2$ (so $k_{+1}=k_{+2}$), and that the association rate constant $k_{+2}=1.0\times10^8\,m^{-1}\,s^{-1}$, as do Colquhoun and Sakmann (1985), because anything greater than $10^8\,m^{-1}\,s^{-1}$ is physically implausible (Gutfreund, 1972) and a value for k_{+2} of less than $7\times10^7\,m^{-1}\,s^{-1}$ is very unlikely (Colquhoun and Ogden, 1988), then, from our own values of k_{-2}, we can derive a value for the equilibrium constant ($K_D=k_{-2}/k_{+2}$) and for affinity ($=1/K_D$).

Stationarity

Five samples of data were tested for stationarity using the QSUM method, which has been described in detail previously (Glasbey and Martin, 1986). The data tested were shown to be stationary and were subsequently used for the detailed analysis of open-, closed- and burst-time kinetics. The maximum length of these samples was 40 s.

The results were also studied for any changes occurring with time by analysing sequential samples from the same recording using the full analysis described above. This showed no significant change in the open-, closed- or burst-time kinetics for up to 15 min, with 1, 3 or 10 $\mu mol\,l^{-1}$ acetylcholine. Open probability also did not change with time, so no observable desensitization was occurring at these concentrations over the time course of an experiment. This does not exclude the possibility of some very fast desensitization occurring in the 5–10 s between patch formation and the commencement of recording.

Results

Single-channel currents

The results reported for 1–10 $\mu mol\,l^{-1}$ acetylcholine were obtained from 57 patches (see Table 1); the recordings were from cell-attached or inside-out patches of membrane, with acetylcholine present in the pipette from the beginning of the recording. In addition to these, a few ($N=3$) recordings were made from outside-out patches, where application of acetylcholine to the bath solution was seen to activate channels in otherwise quiet patches.

Acetylcholine activates two conductances

Acetylcholine (1–10 $\mu mol\,l^{-1}$) present on the outside surface of the muscle membrane of *Ascaris suum* activated single-channel currents with a main state

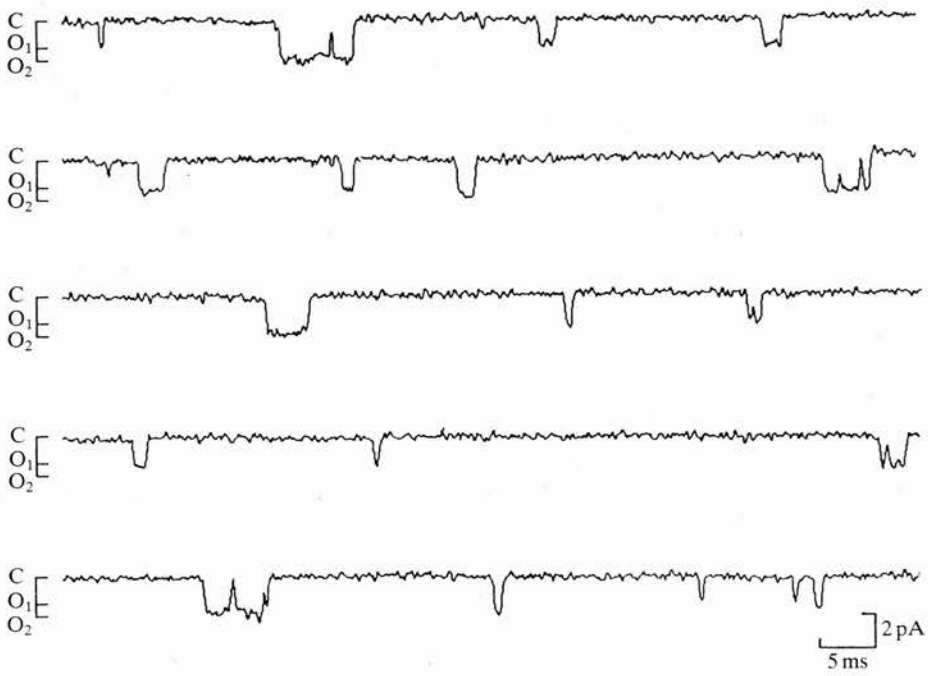


Fig. 1. Acetylcholine-activated channels. A cell-attached patch from a muscle vesicle. C, closed state; O_1, smaller conductance channel (34 pS); O_2, larger conductance channel (48 pS). Estimated patch potential: −50 mV, 10 μmol l^{-1} acetylcholine in pipette solution.

conductance of 40–50 pS and a smaller conductance of 25–35 pS (Fig. 1 and Table 1). These channels had very short mean open times in the range of a few milliseconds (Fig. 1) and both types of channel had a linear I/V relationship (Fig. 2).

The currents activated by acetylcholine were of two amplitudes (Fig. 3). The amplitude histogram has been fitted by two Gaussian curves, showing that there are two types of event in this patch with conductances of 42 and 24 pS (means of the Gaussian curves). Some of our recordings (N=3) showed just the smaller conductance state, and some patches (N=5) showed just the larger conductance, but most patches (N=13) contained both types of conductance. When both conductance states were present in a patch we never observed transitions from one amplitude to the other (which would have been expected if the smaller conductance was a sub-conductance state of the larger one). We only saw transitions from the closed state to one or other of the conductance states, which argues strongly for there being two types of ion channel in the *Ascaris suum* muscle membrane, both activated by acetylcholine.

Table 1. *Experimental details and channel conductances*

[Acetylcholine] (μmol l^{-1})	Total no. of patches	Inside-out patches	Cell-attached patches	Channels observed		Main-state conductance (pS) (mean±S.E.)
				Number	%	
1	24	5	19	5	21 %	46.4±2.87
3	19	4	15	12	63 %	52.1±1.63
10	14	1	13	4	29 %	44.6±5.00
All	57	10	47	21	37 %	48.1±1.94

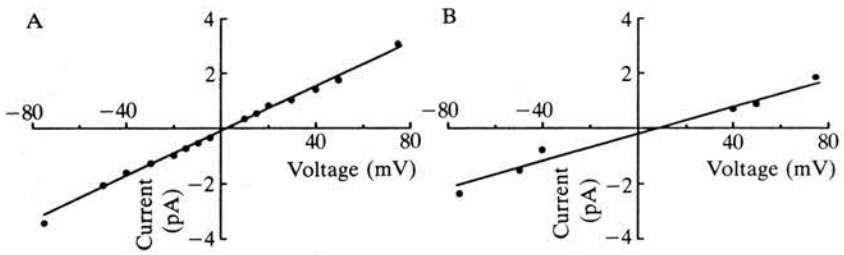


Fig. 2. I/V plots for acetylcholine-activated channels in a cell-attached patch with 10 μmol l^{-1} acetylcholine in the pipette. A and B are from the same patch. (A) Larger channel: slope conductance 41 pS; reversal potential 2.9 mV; correlation=0.998, N=15. (B) Smaller channel: slope conductance 25 pS; reversal potential 7.9 mV; correlation=0.989, N=6.

Voltage-sensitivity of open times

To examine the voltage-sensitivity of channel open times, apparent mean open times (obtained directly from the PAT software, without correction for missed short events) were examined at different patch potentials. The apparent mean open durations of the large-conductance channel were measured in this way in five experiments, for between nine and 16 different potentials in each experiment. The mean open time was found to be insensitive to voltage (e.g. for six of 14 potentials for one cell-attached patch with 10 μmol l^{-1} acetylcholine: −75 mV, 2.38 ms; −50 mV, 2.44 ms; −40 mV, 2.25 ms; +40 mV, 2.13 ms; +50 mV, 2.27 ms; +75 mV, 2.01 ms. In each experiment all the values were tested for a correlation between potential and open time and none was found). In agreement with this, samples of data from the same experiment but at different patch potentials (±50 mV, ±75 mV) showed no differences in open-, closed- or burst-time kinetics with changes in potential.

Acetylcholine-activated channels are cation selective

Both types of channel activated by acetylcholine in these experiments were cation selective. In eight experiments with solutions containing symmetrical cation

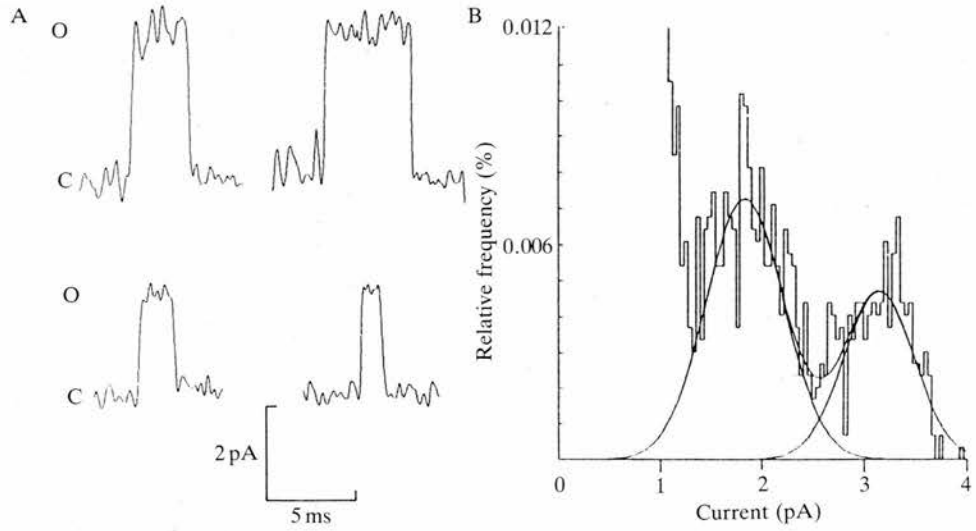


Fig. 3. (A) Individual single-channel openings of two different conductances recorded from a cell-attached patch with 10 μmol l^{-1} acetylcholine in the pipette. Patch potential: +75 mV. Top traces show the larger channel: 3.14 pA (42 pS), lower traces show the smaller channel: 1.83 pA (24 pS). (B) Amplitude histogram showing the distribution of these two channel amplitudes. The histogram has two distinct peaks fitted by two Gaussian curves; the means of the curves are 3.14 pA and 1.83 pA and these correspond to the single-channel events shown in A. (% is the relative frequency of each amplitude.)

concentrations but asymmetrical anion concentrations the reversal potential was found to be near zero and to be consistent with a cation-selective channel (Fig. 2). In four experiments with isolated inside-out patches, this was further tested by changing the cation and anion concentrations in the bathing solutions. Observed shifts in reversal potential were consistent with those predicted by the Nernst equation for a cation conductance (Fig. 4). In the experiment illustrated, the reversal potential shifted from 5 to 21 mV for a change in $[Cs^+]$ from 140 to 70 mmol l^{-1}; the predicted values for a cation channel in these solutions would be 0 and 18 mV, respectively. In these experiments an anion conductance would have shifted the reversal potential in the opposite direction to that observed. For the experiment illustrated (Fig. 4) the predicted reversal potentials for an anion channel were −33 and −51 mV, respectively.

In most experiments the conducting cation was caesium, but acetylcholine channel currents were also observed in two experiments (with outside-out patches) when Cs^+ was replaced by Na^+, indicating that the channels were also permeable to Na^+. The channel was less permeable to Na^+ than to Cs^+, as the conductance of the channel was less when it was conducting Na^+ than when it was conducting Cs^+.

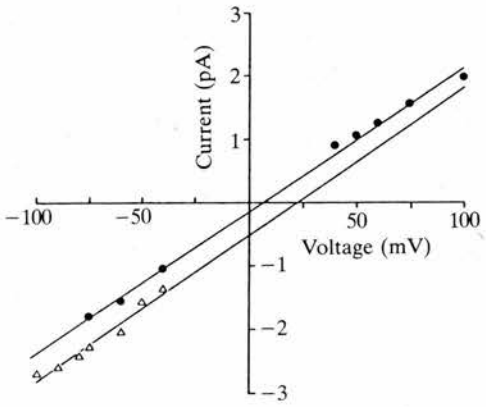


Fig. 4. I/V plot for acetylcholine-activated cation channels in an inside-out patch with 3 μmol l^{-1} acetylcholine in the pipette. Initial solutions (●) were as in Materials and methods: predicted reversal potentials, Cl^- −33 mV, Cs^+ 0 mV. △, bath solutions changed to 70 mmol l^{-1} Cs^+ and 19.5 mmol l^{-1} Cl^-; predicted reversal potentials, Cl^- −51 mV, Cs^+ 18 mV. The actual reversal potentials were, 5 mV (●) and 21 mV (△) which is consistent with this being a cation channel. Lines were fitted by linear regression as in Fig. 2.

Exponential curve fitting

Only the larger channel conductance was analysed in detail to determine its open-, closed- and burst-time kinetics (as described in Materials and methods). Data files used for this analysis were from 12 experiments, from cell-attached and inside-out patches exposed to 1, 3 or 10 μmol l^{-1} acetylcholine. The files contained apparent open and closed times (obtained directly from the PAT software, without correction for missed short events). The number of events analysed varied between 198 and 2000, but was generally greater than 350. Bursts were made up of either single openings or multiple openings separated by short gaps (<1 ms); a typical burst with multiple openings is illustrated in Fig. 5.

The open times and burst times were best fitted by two exponentials and the closed times by three exponentials (Fig. 6). The results obtained are given in Table 2, which presents the kinetic details for 1, 3 and 10 μmol l^{-1} acetylcholine. The results were pooled as there were no significant changes with concentration.

Open-time distribution

The open times were best fitted by two exponentials (Table 2). The two components will be referred to as short openings and long openings. T_1 for short openings had a mean value of 1.18 ms, which is very short but comparable to values obtained for other acetylcholine-activated channels. T_2 for long openings had a mean value of 4.89 ms, again consistent with results for other acetylcholine-activated channels (Numa, 1986; Schuetze and Role, 1987). The short component

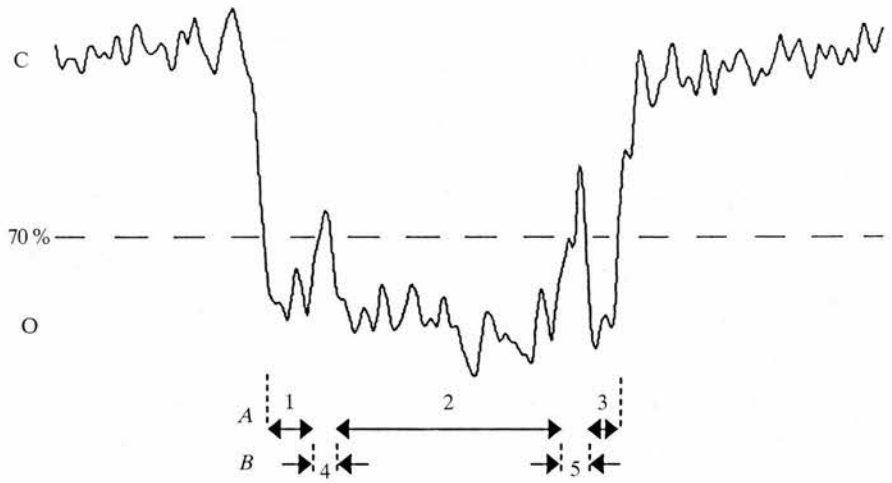


Fig. 5. Typical burst. C: closed state, O: open state (2.42pA). The 70 % line shows 70 % of unit current (1.68 pA) level. The trace was from a cell-attached patch, with 1 μmol l^{-1} acetylcholine at −50 mV. *A*, open durations within the burst: 1=1.44 ms, 2=6.08 ms, 3=0.84 ms. *B*, short gaps in the burst, 4=0.24 ms, 5=0.20 ms.

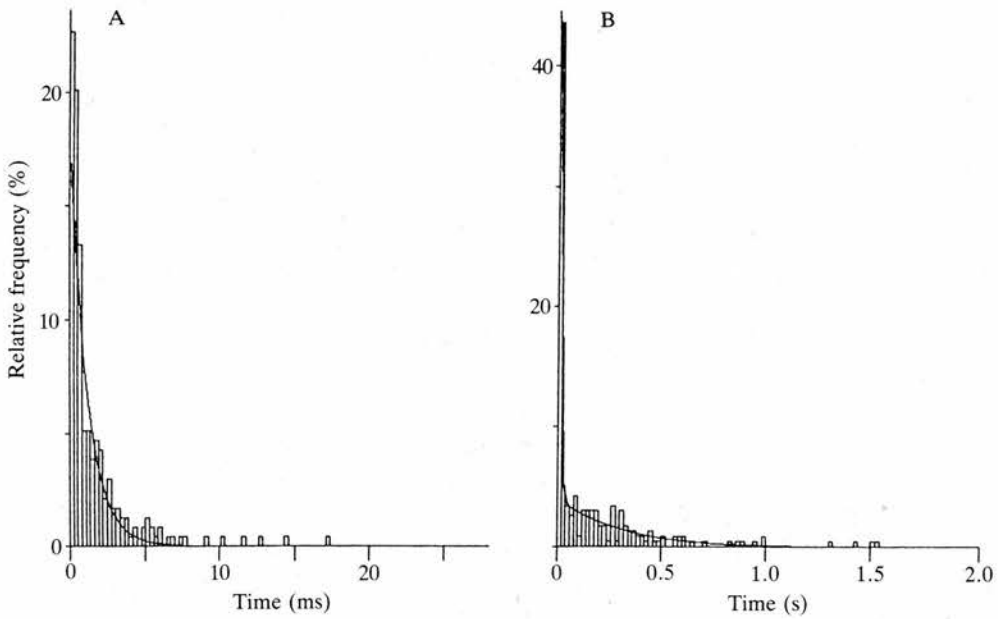


Fig. 6. (A) Open-time histogram. (B) Closed-time histogram. Results from a cell-attached patch, with 1 μmol l^{-1} acetylcholine at −50 mV. (% is the relative frequency of the open and closed durations.)

Table 2. *Open-, burst- and closed-time kinetics*

[Acetylcholine] (μmol l^{-1})	N	T_1 (ms)	T_2 (ms)	T_3 (ms)	A_1	A_2
Open times						
1–10	12	1.18±0.08	4.89±0.60	–	0.80±0.05	–
25	2	0.48±0.18	1.38±0.09	–	0.61±0.21	–
Burst times						
1–10	12	1.17±0.21	7.62±2.71	–	0.66±0.07	–
25	2	0.28±0.02	1.44±0.30	–	0.20±0.01	–
Closed times						
1–10	12	0.20±0.03	196.6±85.8	549.7±165.4	0.48±0.07	0.31±0.07
25	2	0.17±0.02	300.8±129.8	1142.0±930.9	0.34±0.03	0.61±0.03

T_1, T_2 and T_3 are the time constants and A_1 and A_2 the areas of the components of the p.d.f.
For openings and bursts, two exponentials were fitted and $A_2=1-A_1$.
For closings, three exponentials were fitted and $A_3=1-(A_1+A_2)$.
Values are means±1 S.E.M.; N is the number of experiments.

comprised 80% of the openings and the long component 20%, hence the proportion of charge carried by the two types of opening was approximately 1:1.

The number of open states of the channel must be at least the number of exponential components that are needed to fit the open-time distribution (Colquhoun and Hawkes, 1982), suggesting that the *Ascaris* acetylcholine-activated channel has at least two open states.

Burst-time distribution

The burst times were also best fitted by two exponentials (Table 2). The two components will be referred to as short bursts and long bursts. T_1 for short bursts (mean 1.17 ms) is nearly the same as T_1 for short openings (mean 1.18 ms), showing that these shorter bursts were made up of single openings, although T_2 for long bursts (mean 7.62 ms) is longer than T_2 for long openings (mean 4.89 ms), as these bursts are multiple openings.

Short bursts account for 66% of events and long bursts for 34%. Thus, long bursts are most important for carrying current with only one-quarter of the current carried by short bursts.

Closed-time distribution

The closed times were best fitted by three exponentials (Table 2). The three components will be referred to as short, intermediate and long gaps. This result shows that the channel has at least three closed states. The short gaps were very consistent, with a T_1 of 0.20±0.03 ms (mean±S.E., $N=12$). The time constants for intermediate and long gaps showed greater variability and, when comparing the results of individual experiments, the values of T_2 and T_3 did not always seem to refer to the same components. For example, in one experiment with 10 μmol l^{-1} acetylcholine T_2 was 30.9 ms and T_3 was 102.6 ms, while in another experiment

with 10 μmol l^{-1} acetylcholine T_2 was 291.4 ms and T_3 was 666.9 ms. This suggests there may be more closed states occurring, but only three are detectable in any one experiment.

We were not successful in our attempts to fit more than three exponentials to the closed times in this analysis; there may be some long infrequent closed states contributing a very small percentage to the total area. It might be necessary to fit the closed times with up to six exponentials to describe fully the close time distribution, since it has been reported in other preparations that desensitizing concentrations of acetylcholine are best fitted by six exponentials: the usual three exponentials, two for putative desensitized closed states and a sixth exponential for channel block (Sakmann *et al.* 1980; Colquhoun and Sakmann, 1983; Sine and Steinbach, 1984; Ogden and Colquhoun, 1985). In our experiments it is unclear whether any desensitization has occurred with 1–10 μmol l^{-1} acetylcholine, so we proceed on the assumption of three closed states. If there is any desensitization at these concentrations it occurs quickly in the few seconds before recording begins.

T_1 for short gaps was 0.2 ms, and this represented the very short closings which occur within bursts. T_2 for intermediate gaps had a mean value of 196.6 ms, and T_3 for long gaps had a mean value of 549.7 ms. The mean values for areas (Table 2) indicate that 48 % of gaps were short, 31 % were intermediate and 21 % were long. Hence, the proportions of time occupied by short, intermediate and long gaps were in the ratio 1:635:1202. Thus, short gaps contribute very little to the total closed time, although there were a relatively large number of them.

All the kinetic details quoted have been for the larger-conductance channel. So far we have only recorded from one patch in which the smaller-conductance channel occurred alone and frequently enough for detailed analysis. The results of this analysis showed no significant difference from the parameters quoted in Table 2, but further experimentation and analysis are necessary before any conclusions can be made about the kinetics of the smaller channel.

Correction for missing events

The next stage in the analysis was to correct the data for missing events using parameters obtained from fitting multiple exponentials. Some of the corrected values which best describe the channel characteristics are given in Table 3. The analysis calculated numbers of long and short bursts, numbers of long, intermediate and short gaps and values for the total time spent in gaps within bursts and for corrected total open time, which were subsequently used to generate the other corrected values given in Table 3.

The corrected mean open time at 1–10 μmol l^{-1} acetylcholine was very consistent in all 12 experiments analysed, with a value of 1.26±0.11 ms (mean±S.E.). The uncorrected values, obtained from the PAT program, of approximately 2 ms were larger because they contained undetected short gaps. The results showed that the corrected mean open time did not change with the concentration of acetylcholine (Table 3).

The corrected open probability had a mean value of 0.029±0.013 (Table 3), but

Table 3. *Channel characteristics corrected for missing short events*

[Acetylcholine] (μmol l^{-1})	N	Corrected mean open time (ms)	Corrected open probability	Corrected mean burst length (ms)	Corrected short gaps/ long burst	Corrected mean open time in long bursts (ms)
1	3	1.25±0.13	0.017±0.009	2.83±0.48	2.04±0.54	1.33±0.06
3	5	1.28±0.22	0.030±0.027	3.98±2.08	6.60±2.54	1.10±0.26
10	4	1.26±0.23	0.037±0.022	3.05±0.74	3.57±0.83	1.09±0.17
1–10	12	1.26±0.11	0.029±0.013	3.38±0.86	4.45±1.18	1.15±0.12
25	2	0.86±0.14	0.0052±0.0037	1.25±0.23	0.73±0.10	0.71±0.30

Each of these characteristics is defined in Materials and methods.
Values are means±1 S.E.M.; N is the number of experiments.

was concentration-dependent, with the open probability increasing with increasing concentration from 1 to 10 μmol l^{-1} acetylcholine. The mean corrected open probability for 1 μmol l^{-1} acetylcholine was 1.7 %, for 3 μmol l^{-1} it was 3 % (a 71 % increase over 1 μmol l^{-1}), and for 10 μmol l^{-1} it was 3.7 % (a 117 % increase over 1 μmol l^{-1}). The corrected mean burst length (3.38±0.86 ms, mean±S.E., N=12) and corrected short gaps per long burst (4.45±1.18, mean±S.E., N=12) were more variable than the corrected mean open time. The results suggest that the bursts were longest at 3 μmol l^{-1} acetylcholine and that bursts activated by this concentration have the largest number of short gaps per long burst.

The corrected mean open time in long bursts (1.15±0.12 ms, mean±S.E., N=12) was a consistent parameter and was not concentration-dependent (Table 3). The corrected values for this parameter are shorter than the uncorrected values, again because the correction allows for unresolved short gaps.

The range of parameters in Table 3 characterises the behaviour of this ligand-activated cation channel when activated by acetylcholine; future results obtained by activating this channel with other agonists may be compared with these parameters.

Desensitization at higher agonist concentrations

Experiments at 25 μmol l^{-1} acetylcholine (N=5) produced a different pattern of channel opening to that observed at lower concentrations; single-channel currents occurred in clusters with long closed times (mean 171 s) between each cluster (Fig. 7). The effect became more pronounced at 50 or 100 μmol l^{-1} acetylcholine (N=8), where no channel openings were observed.

At 25 μmol l^{-1} acetylcholine, two of the experiments on cell-attached patches were analysed in detail; the channel kinetics was studied in the first cluster of openings to occur in each recording. The open times and burst times were best fitted by two exponentials and the closed times by three exponentials, as with lower concentrations (1–10 μmol l^{-1}) of acetylcholine (Table 2). The data from

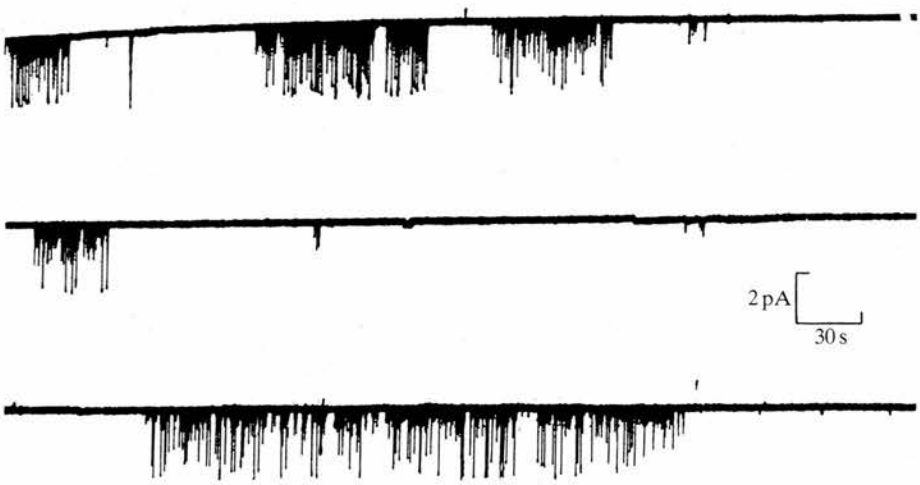


Fig. 7. Desensitisation at higher agonist concentrations in a cell-attached patch with 25 μmol l^{-1} acetylcholine in pipette. Patch potential −50 mV. Traces are continuous and show the very long closed periods that occur at this concentration between groups of openings. The duration of clusters of openings was 60.7±30.2 s (mean±S.E., N=10) in one experiment and 59.6±15.0 s (mean±S.E., N=10) in the other. The durations of the very long closings between these clusters were 221.6±49.3 s and 120.2±46.3 s (mean±S.E., N=10) for the two experiments.

these two experiments were corrected for missing events (Table 3). Examination of these results showed that there were three components to this desensitization.

Very long closed states

Clusters were separated by very long closed times (mean 170 s) (see Fig. 7). These represent a desensitized state or states that did not occur at lower agonist concentrations. Such long closed times have been described before and fitted with two exponential components (Sakmann *et al.* 1980; Colquhoun and Sakmann, 1983; Colquhoun and Ogden, 1988). It has also been reported that acetylcholine desensitization occurs as a biphasic process, with both fast and slow processes. The very long closed times are considered to correspond to slow desensitization processes (Cachelin and Colquhoun, 1989). It is also possible that a rapid type of desensitization occurred during patch formation and before the commencement of recording; this would not have been detected by the present experiments (Brett *et al.* 1986).

Open probability decreases with time

When several samples (N=4) were analysed from successive clusters of openings in the same experiment, it was found that some of the kinetic parameters changed with time. The open probability was found to be lower within each subsequent group of openings, as there was an increase in T_2 for closings from 430.6 ms to 829.8 ms in 22 min (these closed times had only been fitted with two

exponentials). Despite this, the open- and burst-time kinetics and the corrected mean open time were unchanged even after 25 min. Hence, the reduction in open probability that occurred over 20–30 min might represent the appearance of an additional, long closed state occurring within clusters (rather than the observed ones increasing in length). This would represent another component of desensitization.

Mean open times are reduced

The results show that mean open times and burst times were shorter at 25 μmol l^{-1} than at lower acetylcholine concentrations: at 25 μmol l^{-1} T_1 and T_2 for openings and for bursts are reduced and the corrected mean open time is reduced to 0.86 ms compared with 1.26 ms for 1, 3 or 10 μmol l^{-1} acetylcholine. Closed times at 25 μmol l^{-1} acetylcholine are longer than for lower concentrations. The reduced corrected mean open time suggests that channel block may be occurring. However, if channel block is occurring at 25 μmol l^{-1} acetylcholine in the *Ascaris* muscle it is of a type different from the 'classical' fast channel block observed with acetylcholine at the frog end-plate (Ogden and Colquhoun, 1985). At the frog end-plate, fast flickering shut of the channel causes an increase in the number of short gaps per long burst and a reduced channel amplitude. Our experiments showed a reduction in the number of short gaps per long burst and no change in channel amplitude, suggesting a slowly acting type of channel block (Hille, 1984).

Discussion

Conductance of acetylcholine-activated channels

Acetylcholine-activated single-channel currents have been recorded with conductances in the range 20–60 pS from vertebrate muscle (see reviews by Schuetze and Role, 1987; Numa, 1986), from vertebrate nervous tissue (Cull-Candy and Mathie, 1986; Derkach *et al.* 1987; Mathie *et al.* 1987) and from invertebrate neurones (Sattelle, 1986; Sattelle *et al.* 1986; Beadle *et al.* 1989) in the cockroach and (Wu *et al.* 1983) in *Drosophila*. Our report is the first to describe these channels in invertebrate muscle.

In most preparations, the conductance of the acetylcholine-activated channel is greater with Cs^+ than with Na^+ as the conducting cation (the sequence is usually $K^+ > Cs^+ > Na^+ > Li^+$, Sakmann *et al.* 1985), but the conductance may be reduced in the presence of 1 mmol l^{-1} Ca^{2+} or Mg^{2+} (Mishina *et al.* 1986). Our conductances were measured with Cs^+ as the conducting cation, in the absence of Ca^{2+}, but with 2 mmol l^{-1} Mg^{2+} present. The effects of Ca^{2+} and Mg^{2+} on our channel were not investigated, but the conductance of the acetylcholine-activated channel might be greater in the absence of Mg^{2+}.

Our channels were of two amplitudes: 40–50 pS and 25–35 pS. One possible explanation for obtaining these ranges of conductance (rather than the channels having exactly the same conductance in each patch) is that our recordings were made at room temperature, which varied from 15 to 22 °C. It has been shown that

the conductance of acetylcholine channels may increase with temperature, from 40 pS at 13 °C to 55–60 pS at 20–25 °C and 70–75 pS at 37 °C (Mulrine and Ogden, 1989).

Ascaris muscle is like that of many other species, e.g. rat, mouse, human, *Xenopus* and calf (Schuetze and Role, 1987), in having channels of two different conductances, both activated by acetylcholine. The two types of channel in vertebrate muscle are described in three ways: as 'embryonic' and 'adult' channels; as 'fast' and 'slow' channels; or as 'junctional' and 'extrajunctional' channels (Schuetze and Role, 1987). The only one of these descriptions that might fit the two channels in the *Ascaris* is that of 'fast' and 'slow', but so far we have insufficient data on the mean open times of the smaller channel so we refer to them simply as the larger- and smaller-conductance channels.

In bovine muscle, the two types of channel conductance recorded have been shown to be due to two separate ion channels with differences in protein structure (Mishina *et al.* 1986). No information is available about the protein structure of the channels in *Ascaris suum*, but our results strongly suggest that there will be two types of channel with differences in the protein structures. In the rest of the discussion we will consider the larger channel only.

Voltage-sensitivity

Another feature of vertebrate acetylcholine-activated channels is that single-channel I/V plots are almost always linear (as ours was) while the whole-cell currents may show very marked rectification (Sakmann *et al.* 1985). This is believed to be due to the mean open time of such channels being voltage dependent. Preparations in which the whole-cell current is linear have a mean open time independent of voltage (Sakmann *et al.* 1985).

Some of the features of the *Ascaris* channel are compared with those of other preparations in Table 4. Our open time durations were not voltage-sensitive nor did the amplitude of the channel currents show rectification. In this respect the *Ascaris* channel resembles the channel from *Torpedo* and is unlike the many mammalian muscle channels (e.g. Sakmann *et al.* 1985) or the channels of the frog or *Xenopus* (Colquhoun and Sakmann, 1985; Brehm *et al.* 1984). The mean open times can be calculated in various ways, but comparable values for *Ascaris* and *Torpedo* using the time constant T_2 having fitted two exponentials to the open times, show that the *Ascaris* channel has much longer open times (T_2=4.9 ms) than the *Torpedo* channel (T_2=0.6 ms), and is much closer to the channel in the frog end-plate (T_2=4.2 ms) in this respect.

A great deal of work has been done on the protein structure of nicotinic acetylcholine receptors, especially from *Torpedo* electroplax and calf muscle (Numa, 1986). This has included the production of hybrids such as the one described in Table 4 formed from the α-subunit of calf and the β, γ and δ subunits of *Torpedo*. This particular hybrid is of interest because its properties are closer to those of the *Ascaris* channel than to those of either the calf or the *Torpedo* channel from which it was formed.

Table 4. *Acetylcholine-activated channels in various preparations*

Preparation	Conductance (pS)	Mean open time (ms)	Corrected mean open time (ms)	Voltage-dependence of open times	Reference
Ascaris suum	48	4.9	1.26	No	Present paper
Torpedo	42	0.6	–	No	Sakmann *et al.* (1985)
Calf muscle	40	7.6	–	Yes	
Hybrid	42	3.2	–	No	
Frog muscle (end-plate)	44	4.2	1.40	Yes	Colquhoun and Sakmann (1985)
Xenopus muscle	64	<1	–	Yes	Brehm *et al.* (1984)

Mean open time (ms) is the time constant for the longer of two exponentials fitted to the open times.

Corrected mean open times (ms) is as defined in Materials and methods.

Each study used a range of acetylcholine concentrations.

The hybrid listed contained the α-subunit of calf and the β, γ and δ subunits of *Torpedo*.

Rate constants

Our data were corrected for missing short events and the results obtained are summarised in Table 3. The analysis was extended, using the model of Colquhoun and Sakmann (1985) of acetylcholine interacting with its receptor, outlined in Materials and methods. The rate constants for channel closing (α) and channel opening (β) and the dissociation rate constant (k_{-2}) can be calculated from our corrected data (Table 5).

The highest mean values for α and β and the lowest mean value for k_{-2} were obtained at 3 μmol l^{-1} acetylcholine. The results were tested using *t*-tests, but a combination of small sample sizes and relatively large variation in the results for each concentration meant that the differences were not statistically significant.

Table 5. *Estimates of rate constants and efficacy*

[Acetylcholine] (μmol l^{-1})	N	α (s^{-1})	β (s^{-1})	k_{-2} (s^{-1})	β/α
1	3	753±36	3649±884	1044±298	4.85
3	5	1082±190	5957±1761	504±60	5.51
10	4	998±160	3988±631	635±138	4.00
1–10	12	972±97	4724±803	682±103	4.86
25	2	1705±715	2539±91	1771±305	1.49

Derivation of rate constants is described in detail in Materials and methods.

β/α=efficacy.

Values are means±1 S.E.M.; N is the number of experiments.

This is what would be expected, as α, β and k_{-2} would not normally vary with low agonist concentrations (i.e. concentrations too low to cause significant desensitization or channel block (Sakmann *et al.* 1980; Colquhoun and Sakmann, 1985; Colquhoun and Ogden, 1988).

The combined values for 1, 3 and 10 μmol l^{-1} acetylcholine were compared with those of Colquhoun and Sakmann (1985) for 0.1 μmol l^{-1} acetylcholine. Their value of α for acetylcholine is 714 s^{-1}, ours is 972 s^{-1}; their value for β is 30 600 s^{-1}, ours is 4724 s^{-1}; their value for k_{-2} is 8150 s^{-1} and ours is 682 s^{-1}, showing very similar values for α, but our values of β and k_{-2} are approximately 10-fold less than theirs. Thus, the behaviour of acetylcholine at the receptor on *Ascaris* extrasynaptic muscle differs significantly from that reported for the frog muscle end-plate. This is not surprising, as responses to acetylcholine at an end-plate would be much faster than for extrasynaptic muscle (this is reflected in the rate constant for channel opening (β) which was 10 times faster at the frog end-plate than in our system).

The results at 25 μmol l^{-1} acetylcholine (Table 5) were tested, using *t*-tests, with the results obtained for 1, 3 and 10 μmol l^{-1} acetylcholine combined. This showed that α was significantly higher ($P=0.02$) at 25 μmol l^{-1} than at 1, 3 and 10 μmol l^{-1} and hence that the rate of channel closing increased with increasing agonist concentration, while β was not significantly different at 25 μmol l^{-1} compared with 1–10 μmol l^{-1}, indicating that the rate of channel opening remained unchanged. These results are consistent with the occurrence of channel block at 25 μmol l^{-1} acetylcholine. It has been predicted that, with desensitization, α should be independent of agonist concentration while β should increase with increasing agonist concentration but, with channel block, α should increase with increasing agonist concentration while β should be independent of agonist concentration (Sakmann *et al.* 1980). Our results also show that the dissociation rate constant, k_{-2}, was significantly higher ($P=0.001$) at 25 μmol l^{-1} than at 1–10 μmol l^{-1}. This, together with the increased rate of channel closing (α), is responsible for the reduction observed in corrected mean open time 25 μmol l^{-1} compared with 1–10 μmol l^{-1}.

Efficacy, affinity and potency

The final step in the analysis of our data was to estimate values for efficacy, affinity and potency of acetylcholine at the *Ascaris* receptor and compare these estimates with the values obtained by Colquhoun and Sakmann (1985) for the frog end-plate receptor.

Values for efficacy (β/α) are given in Table 5. The values for 1, 3 and 10 μmol l^{-1} acetylcholine are very similar and were combined, giving a mean value of 4.9; this compares to Colquhoun and Sakmann's (1985) value of 43 for 0.1 μmol l^{-1} acetylcholine and shows that acetylcholine has a much lower (1/10) efficacy at the *Ascaris* receptor than at the frog receptor. The efficacy at 25 μmol l^{-1} on our receptor was 1.49, which is lower than for the other concentrations and reflects the higher value of α for 25 μmol l^{-1} acetylcholine.

We estimated values for the equilibrium constant (K_D) and the affinity ($1/K_D$). For 1, 3 and 10 μmol l^{-1} acetylcholine, K_D was 6.8 μmol l^{-1} [affinity= 147×10^3 (mol l^{-1})$^{-1}$] compared to Colquhoun and Sakmann's values of K_D=80 μmol l^{-1} [affinity=12.5×10^3 (mol l^{-1})$^{-1}$]. Hence, affinity is 10 times higher at the *Ascaris* receptor than at the frog receptor. The values at 25 μmol l^{-1} acetylcholine for our receptor were: K_D=17.7 μmol l^{-1} [affinity= 56×10^3 (mol l^{-1})$^{-1}$]. The affinity at 25 μmol l^{-1} acetylcholine is lower than at the other concentrations, which reflects the finding that the dissociation rate constant k_{-2} was higher at 25 μmol l^{-1} than at the lower concentrations.

Potencies were estimated relative to the potency of acetylcholine at the frog end-plate (Colquhoun and Sakmann, 1985). This gave a potency at 1, 3 and 10 μmol l^{-1} acetylcholine of 4.04, suggesting that acetylcholine is four times as potent on *Ascaris* muscle as at the frog end-plate. The potency at 25 μmol l^{-1} acetylcholine on *Ascaris* muscle was 0.86, reflecting the much lower efficacy and the higher value of k_{-2} at 25 μmol l^{-1} acetylcholine compared with the other concentrations.

Desensitization

Nothing is known about the physical nature of desensitized states of the acetylcholine receptor, but desensitization can be effected by calcium (Chemeris *et al.* 1982; Oswald, 1983) and phosphorylation of the receptor may accelerate desensitization (Huganir *et al.* 1986). The role these play in the normal mechanism of desensitization is unclear. Three different reaction schemes have been fitted to observations of desensitization by Cachelin and Colquhoun (1989) and all three require two distinct desensitized conformations of the receptor. Desensitization probably results from the receptor-channel molecule adopting long-lived shut conformations in which the agonist binding sites are occupied, with the onset of desensitization being slower at lower agonist concentrations (Cachelin and Colquhoun, 1989).

The occurrence of desensitization at the *Ascaris* acetylcholine receptor is of particular interest, because it may be relevant therapeutically. It may be that giving too high a dose of certain anthelmintics is less effective than using a lower dose. Various nicotinic anthelmintics, such as pyrantel and levamisole, have a selective action on acetylcholine receptors in nematodes, but not on those of the vertebrate host (Aubry *et al.* 1970; Coles *et al.* 1975; Harrow and Gration, 1985).

Harrow and Gration (1985), using intracellular current-clamp on muscle cells of *Ascaris suum*, showed that high doses of morantel and pyrantel (>100 μmol l^{-1}) produced smaller responses than lower concentrations, while no such effect was reported for levamisole or acetylcholine (up to 10 mmol l^{-1}). The lack of desensitization with acetylcholine at concentrations up to 10 mmol l^{-1} is in sharp contrast to our finding that the response was completely abolished at a concentration of 50 μmol l^{-1}. Another report on the actions of pyrantel and levamisole (Coles *et al.* 1975) contradicts the results of Harrow and Gration (1985) and it

would be very interesting to study them at a range of concentrations at the single-channel level.

This research was supported by the SERC and the Wellcome Trust.

References

AUBRY, M. L., COWELL, P., DAVEY, M. J. AND SHEVDE, S. (1970). Aspects of the pharmacology of a new anthelmintic: pyrantel. *Br. J. Pharmac.* **38**, 332–344.

BEADLE, D. J., HORSEMAN, G., PICHON, Y., AMAR, M. AND SHIMAHARA, T. (1989). Acetylcholine-activated ion channels in embryonic cockroach neurons growing in culture. *J. exp. Biol.* **142**, 337–355.

BREHM, P., KULLBERG, R. AND MOODY-CORBETT, F. (1984). Properties of non-junctional acetylcholine receptor channels on innervated muscle of *Xenopus laevis*. *J. Physiol., Lond.* **350**, 631–648.

BRETT, R. S., DILGER, J. P., ADAMS, P. R. AND LANCASTER, B. (1986). A method for the rapid exchange of solutions bathing excised membrane patches. *Biophy. J.* **50**, 987–992.

CACHELIN, A. B. AND COLQUHOUN, D. (1989). Desensitization of the acetylcholine receptor of frog end-plates measured in a vaseline-gap voltage clamp. *J. Physiol., Lond.* **415**, 159–188.

CHEMERIS, N. K., KAZACHENKO, V. N., KISLOV, A. N. AND KURCHIKOV, A. L. (1982). Inhibition of acetylcholine responses by intracellular calcium in *Lymnea stagnalis* neurones. *J. Physiol., Lond.* **323**, 1–19.

COLES, G. C., EAST, J. M. AND JENKINS, S. N. (1975). The mechanism of action of the anthelmintic levamisole. *Gen. Pharmac.* **6**, 309–313.

COLQUHOUN, D. AND HAWKES, A. G. (1982). On the stochastic properties of bursts of single ion channel openings and of clusters of bursts. *Phil. Trans. R. Soc. Ser.* B **300**, 1–59.

COLQUHOUN, D. AND OGDEN, D. C. (1988). Activation of ion channels in the frog end-plate by high concentrations of acetylcholine. *J. Physiol., Lond.* **395**, 131–159.

COLQUHOUN, D. AND SAKMANN, B. (1983). Bursts of openings in transmitter-activated ion channels. In *Single Channel Recording* (ed. B. Sakmann and E. Neher), pp. 345–364. New York: Plenum Press.

COLQUHOUN, D. AND SAKMANN, B. (1985). Fast events in single-channel currents activated by acetylcholine and its analogues at the frog muscle end-plate. *J. Physiol., Lond.* **369**, 501–557.

COLQUHOUN, D. AND SIGWORTH, F. J. (1983). Fitting and statistical analysis of single channel records. In *Single Channel Recording* (ed. B. Sakmann and E. Neher), pp. 191–264. New York: Plenum Press.

CULL-CANDY, S. G. AND MATHIE, A. (1986). Ion channels activated by acetylcholine and γ-aminobutyric acid in freshly dissociated sympathetic neurons of the rat. *Neurosci. Lett.* **66**, 275–280.

DEL CASTILLO, J., DE MELLO, W. C. AND MORALES, T. (1963). The physiological role of acetylcholine in the neuromuscular system of *Ascaris lumbricoides*. *Archs int. Physiol.* **71**, 741–757.

DERKACH, V. A., SELYANKO, A. A. AND SKOK, V. I. (1983). Acetylcholine-induced current fluctuations and fast excitatory post-synaptic currents in rabbit sympathetic neurones. *J. Physiol., Lond.* **336**, 511–526.

GLASBY, C. A. AND MARTIN, R. J. (1986). Exploratory and confirmatory plots of single-channel records. *J. Neurosci. Methods* **16**, 239–249.

GRATION, K. A. F., HARROW, I. D. AND MARTIN, R. J. (1986). GABA receptors in parasites of veterinary importance. In *Neuropharmacology and Pesticide Action* (ed. M. G. Ford, G. G. Lunt, R. C. Reay and P. N. R. Usherwood), pp. 414–422. Chichester, England: Ellis Horwood.

GUTFREUND, H. (1972). *Enzymes: Physical Principles*. London: Wiley.

HAMILL, O. P., MARTY, A., NEHER, E., SAKMANN, B. AND SIGWORTH, F. J. (1981). Improved patch-clamp techniques for high-resolution current recording from cells and cell-free membrane patches. *Pflügers Arch. ges. Physiol.* **391**, 85–100.

HARROW, I. D. AND GRATION, K. A. F. (1985). Mode of action of the anthelmintics morantel,

pyrantel and levamisole on muscle cell membrane of the nematode *Ascaris suum*. *Pestic. Sci.* **16**, 662–672.

HILLE, B. (ed.) (1984). Mechanisms of block. In *Ionic Channels of Excitable Membranes*, pp. 272–302. Sunderland, Sinauer Associates Inc.

HUGANIR, R. L., DELCOUR, A. H., GREENGARD, P. AND HESS, G. P. (1986). Phosphorylation of the nicotinic acetycholine receptor regulates its rate of desensitization. *Nature* **321**, 774–776.

JOHNSON, C. D. AND STRETTON, A. O. W. (1985). Localization of choline acetyltransferase within identified motoneurons of the nematode *Ascaris*. *J. Neurosci.* **5**, 1984–1992.

MARTIN, R. J. (1982). Electrophysiological effects of piperazine and diethylcarbamazine on *Ascaris suum* somatic muscle. *Br. J. Pharmac.* **77**, 255–265.

MARTIN, R. J. (1985). Gamma-aminobutyric acid- and piperazine-activated single-channel currents from *Ascaris suum* body muscle. *Br. J. Pharmac.* **84**, 445–461.

MARTIN, R. J., KUSEL, J. R. AND PENNINGTON, A. J. (1990). Surface properties of membrane vesicles prepared from muscle cells of *Ascaris suum*. *J. Parasitol.* **76**, 340–348.

MARTIN, R. J. AND PENNINGTON, A. J. (1990). Acetylcholine-activated single channel currents from isolated *Ascaris suum* muscle. *J. Physiol., Lond.* **420**, 91P.

MATHIE, A., CULL-CANDY, S. G. AND COLQUHOUN, D. (1987). Single-channel and whole-cell currents evoked by acetylcholine in dissociated sympathetic neurons of the rat. *Proc. R. Soc.* B **232**, 239–248.

MISHINA, M., TAKAI, T., IMOTO, K., NODA, M., TAKAHASHI, T., NUMA, S., METHFESSEL, C. AND SAKMANN, B. (1986). Molecular distinction between foetal and adult forms of muscle acetylcholine receptor. *Nature* **321**, 406–411.

MULRINE, N. AND OGDEN, D. C. (1989). Activation of ion channels at the rat end-plate *in vitro* by acetylcholine at low and physiological temperatures. *J. Physiol., Lond.* **415**, 35P.

NATOFF, I. L. (1969). The pharmacology of the cholinoceptor in muscle preparations of *Ascaris lumbricoides var. suum*. *Br. J. Pharmac.* **37**, 251–257.

NUMA, S. (1986). Molecular basis for the function of ionic channels. *Biochem. Soc. Symp.* **52**, 119–143.

OGDEN, D. C. AND COLQUHOUN, D. (1985). Ion channel block by acetylcholine, carbachol and suberyldicholine at the frog neuromuscular junction. *Proc. R. Soc.* B **225**, 329–355.

OSWALD, R. E. (1983). The effects of calcium on the binding of phencyclidine to acetylcholine receptor-rich membrane fragments from *Torpedo californica* electroplaque. *J. Neurochem.* **41**, 1077–1084.

ROZHKOVA, E. K., MALYUTINA, T. A. AND SHISHOV, B. A. (1980). Pharmacological characteristics of cholinoreception in somatic muscle of the nematode *Ascaris suum*. *Gen. Pharmac.* **11**, 141–146.

SAKMANN, B., METHFESSEL, C., MISHINA, M., TAKAHASHI, T., TAKAI, T., KURASAKI, M., FUKUDA, K. AND NUMA, S. (1985). Role of acetylcholine receptor sub-units in gating of the channel. *Nature* **318**, 538–543.

SAKMANN, B., PATLAK, J. AND NEHER, E. (1980). Single acetylcholine-activated channels show burst kinetics in presence of desensitizing concentrations of agonist. *Nature* **286**, 71–73.

SATTELLE, D. B. (1986). Insect acetylcholine receptors, biochemical and physiological approaches. In *Neuropharmacology and Pesticide Action* (ed. M. G. Ford, G. G. Lunt, R. C. Reay and P. N. R. Usherwood), pp. 445–497. Chichester, England: Ellis Horwood.

SATTELLE, D. B., SUN, Y. A. AND WU, C. F. (1986). Neuronal acetylcholine receptor: patch clamp recording of single channel properties from dissociated insect neurones. *IRCS Med. Sci.* **14**, 65–66.

SCHUETZE, S. M. AND ROLE, L. W. (1987). Developmental regulation of nicotinic acetylcholine receptors. *A. Rev. Neurosci.* **10**, 403–457.

SINE, S. M. AND STEINBACH, J. H. (1984). Agonists block currents through acetylcholine receptor channels. *Biophys. J.* **46**, 277–283.

THORN, P. AND MARTIN, R. J. (1987). A high-conductance calcium-dependent chloride channel in *Ascaris suum* muscle. *Q. Jl exp. Physiol.* **72**, 31–49.

WILLETT, J. D. (1980). Control mechanisms in nematodes. In *Nematodes as Biological Models*, vol. 1 (ed. B. M. Zuckerman), pp. 197–225. New York: Academic Press.

WU, C. F., SUZUKI, N. AND POO, M. M. (1983). Dissociated neurons from normal and mutant *Drosophila* larval central nervous system in cell culture. *J. Neurosci.* **3**, 1888–1899.

Br. J. Pharmacol. (1993), **108**, 170–178 © Macmillan Press Ltd, 1993

Levamisole-activated single-channel currents from muscle of the nematode parasite *Ascaris suum*

S.J. Robertson & R.J. Martin

Dept of Preclinical Veterinary Sciences, Royal (Dick) School of Veterinary Studies, Summerhall, University of Edinburgh, Edinburgh, EH9 1QH

1 The patch-clamp technique was used to examine levamisole-activated channels in muscle vesicles from *Ascaris suum*. Cell-attached and isolated inside-out patches were used.

2 Levamisole (1–90 μM), applied to the extracellular surface, activated channels which had apparent mean open-times in the range 0.80–2.85 ms and linear I/V relationships with conductances in the range 19–46 pS. Ion-replacement experiments showed the channels to be cation selective.

3 The kinetics of the channels were analysed. Generally open- and closed-time distributions were best fitted by two, and three expotentials respectively, indicating the presence of at least two open states and at least three closed states. The distributions of burst-times were best-fitted by two exponentials.

4 Channel open- and burst-times were voltage-sensitive: at low levamisole concentrations (1–10 μM), they increased with hyperpolarization. At higher concentrations of levamisole (30 μM and 90 μM) flickering channel-block was observed at hyperpolarized potentials. Using a simple channel-block model, values for the blocking dissociation constant, K_B were determined as 123 μM at − 50 mV, 46 μM at − 75 mV and 9.4 μM at − 100 mV.

5 At the higher concentration of levamisole (30 μM and 90 μM) long closed-times separating 'clusters' of bursts were observed, at both hyperpolarized and depolarized membrane potentials and this was interpreted as desensitization.

Keywords: Levamisole; *Ascaris*; nicotinic-channels

Introduction

Nematode parasites inflict much suffering on human and animal hosts. Approximately one in five of the world's human population is infected with intestinal nematodes (Standen, 1975), while infestation in domestic animals is a major source of economic loss. Antihelminthic drugs, such as levamisole, are used to control these infestations.

Studies on the mode of action of levamisole indicate it is a selective agonist at acetylcholine receptors present on the muscle cells of parasitic nematodes. One such nematode is *Ascaris suum*. Levamisole and acetylcholine treatment of *Ascaris suum* results in depolarization and spastic paralysis of the muscle (Aceves *et al.*, 1970; Van Neuten, 1972; Coles *et al.*, 1975; Martin, 1982; Harrow & Gration, 1985; Colquhoun *et al.*, 1991).

The acetylcholine receptors of *Ascaris* muscle have been classified as nicotinic, as nicotinic agonists produce contractions antagonised by tubocurarine, whereas muscarinic agonists and antagonists have little effect on this preparation (Natoff, 1969; Rozkova *et al.*, 1980; Martin, 1982, Colquhoun *et al.*, 1991). The pharmacology of the acetycholine receptors on *Ascaris* muscle is most like that of the nicotinic ganglionic receptors of vertebrates, most notably mecamylamine is a potent antagonist at both receptor sites (Natoff, 1969; Rozkova *et al.*, 1980).

The aim of the present study was to investigate the action of levamisole at the single-channel level in *Ascaris* by use of the extrasynaptic acetylcholine receptors present in isolated muscle vesicles (Martin *et al.*, 1990; Pennington & Martin, 1990). Our results show that levamisole opens cation selective channels, but in addition, produces open channel-block and desensitization.

[1] Author for correspondence.

Methods

Single-channel recordings of levamisole-activated currents were made from *Ascaris* muscle vesicles. In general the data were analysed by the same methods as used in previous studies with acetylcholine (Pennington & Martin, 1990).

The vesicle preparation

Ascaris suum were collected from the local abattoir, maintained in Locke solution (replaced daily) at 32°C and used within 4 days. To prepare the vesicles, a 2 cm section from the anterior region of the worm was taken, cut along one of the lateral lines and pinned out to form a muscle-flap preparation. This muscle flap was treated with collagenase solution for about 10 min at 37°C, (composition as follows): mM NaCl 35, Na acetate 105, KCl 2, $MgCl_2$ 2, HEPES 10, glucose 3, ascorbic acid 2 and collagenase (1 mg ml^{-1}) pH adjusted to 7.2 with NaOH. The preparation was then kept in a maintenance solution at 37°C (composition as follows): mM NaCl 35, Na acetate 105, KCl 2, $MgCl_2$ 2, HEPES 10, glucose 3, ascorbic acid 2 and EGTA 1; pH adjusted to 7.2 with NaOH. The vesicles formed over the next hour, as outgrowths from the bag region of the muscle cells. The vesicles were used within 5 h.

Electrical recordings

The vesicles were transferred to the experimental chamber where recordings were made at room temperature (15–22°C). The experimental chamber was mounted on the stage of a Reichert-Jung Biostar inverted microscope and viewed at × 200 magnification. Vesicles were bathed in the experimental chamber in the following solution (composition mM): CsCl 35, Cs acetate 105, $MgCl_2$ 2, HEPES 10 and EGTA 1; pH adjusted to 7.2 with CsOH.

Recordings were made from either isolated inside-out pat-

ches or cell-attached patches. Patch-electrodes were made from micro-haematocrit capillary glass (Garner Glass 7052) with a resistance of 1–3 MΩ. The pipettes were coated with-Sylgard to improve frequency responses. Electrodes were filled with pipette solution (composition, mM) CsCl 140, $MgCl_2$ 2, HEPES 10 and EGTA 1; pH 7.2 with CsOH. To examine the effects of levamisole, different concentrations of levamisole were placed in the pipette solution. All of the recordings were made with Cs^+ as the main cation to avoid contamination of patch recordings with K^+ channels known to be present in the membrane. The solutions were also Ca^{2+}-free to avoid contamination of patch recordings with Ca^{2+}-activated Cl^- channels known to occur in this membrane (Thorn & Martin, 1987).

In experiments to determine ion-selectivity of the channel, the ionic composition of the bath solution was altered by diluting 50:50 with distilled H_2O. Inside-out patches were used for these experiments to ensure changes in ionic concentration at the cytoplasmic membrane surface.

Currents were recorded with a List EPC-7 and a modified Sony digital audio processor with a Betamax video recorder.

Data processing

Records were analysed with a CED 1401 interface and a DCS286 PC Computer, with PAT software kindly supplied by John Dempster, Strathclyde University. The records were filtered by an eight-pole Bessel filter, 3 dB, 1.5 kHz; the sampling time was 70 μs and the minimum detectable interval was 0.3 ms. The threshold for channel opening was set at 70% of the single channel amplitude determined from channel amplitude histograms so as to include only full openings. In some experiments a 50% threshold was also used to examine the effect on open times. Little practical difference was observed. It is pointed out that corrected P_{open} values were determined (Colquhoun & Sakmann, 1985) for levamisole concentrations between 2 and 10 μM and found to be not significantly different from apparent P_{open} values obtained from the Dempster software. Subsequently in this manuscript only apparent P_{open} values are quoted.

In these experiments, individual channel activations were interrupted with short close periods (the 'Nachschlag' phenomenon, Colquhoun & Sakmann, 1985), so bursts of openings as well as single openings were considered. Bursts were defined as groups of openings separated by gaps that are shorter than a specified length, T_{crit}. T_{crit} was determined by numerically solving the following equation:

$$1 - e^{-T_{crit}/T1} = e^{-T_{crit}/T2}$$

where T1 represents the brief closed state T1, and T2 represents the slightly longer closed state T2. The equation finds a value for T_{crit} which balances the proportion of gaps within a burst misclassified (as gaps between bursts) and gaps between a burst misclassified (as gaps within a burst) (Colquhuon & Sakmann, 1985). In general a value of 1 ms was used in these experiments. This particular value was not so important since gaps between bursts were several hundred fold larger than gaps within bursts.

Exponential curve fitting

Exponential curves were fitted to the open-, closed-, and burst-time by the method of maximum likelihood (Colquhoun & Sigworth, 1983; Martin, 1985) to a probability density function (p.d.f) of the form:

$$\text{p.d.f.} = \sum_{i=1}^{k} \frac{A_i e(^{-t}/T_i)}{T_i}$$

where A_i = the area of the ith component; T_i = the fitted time constant; t = time and K = number of exponentials fitted.

After exponential curve fitting, the data were corrected for missing events (Colquhoun & Sakmann, 1985; Pennington & Martin, 1990). This was carried out to compensate for brief events missed due to limited resolution of the recording apparatus.

The flickering channel-block seen at high levamisole concentrations was analysed by the simple channel-block scheme described by Adams (1976) and Colquhoun & Sakmann (1985):

$$C \underset{\alpha}{\overset{\beta}{\rightleftharpoons}} O \underset{k_{-B}}{\overset{k_{+B}.X_B}{\rightleftharpoons}} B$$

where C denotes the closed state; O denotes the open state; B denotes the blocked state; X_B is the drug concentration; k_{+B} is the blocking rate constant; k_{-B} is the unblocking rate constant; α is channel closing-rate and β is the channel opening-rate. The model predicts that:

$$\text{mean open-time} = 1/(\alpha + k_{+B}.X_B),$$

$$\text{mean block-time} = 1/k_{-B},$$

$$\text{channel-block dissociation constant, } K_B = k_{-B}/k_{+B}$$

The slope of the reciprocal plot of mean durations of long openings (T2), against levamisole concentration was used to determine values for k_{+B}.

The mean block durations were determined by selecting the distinctive blocked times seen during flickering bursts greater than 0.3 ms (our limit of resolution). The method of maximum likelihood was then used to fit a single exponential to obtain a value for the mean block duration. It is pointed out that there was inevitably some overlap between the blocked time and the 'Nachschlag' closings, however this error is minimal as the interruptions due to channel block far exceed the number of interruptions due to the 'Nachschlag' closings.

Drugs

Levamisole ((−)-(5)-2,3,5,6-tetrahydro-6-phenylimadaz[2,1-b]thiazole]) was obtained as levamisole hydrochloride from Sigma chemical company, Fancy Road, Poole, Dorset, BH17 7NH. Collagenase, Sigma type 1A, was also obtained from Sigma chemical company.

Statistical analysis

The method of least squares was used to obtain the best fits for the exponential equations used to described the voltage-sensitivity of the rate constants k_{+B} and k_{-B} and the dissociation constant K_B, a Spearman correlation coefficient (r) was used to test the quality of the fits. Values are given as mean ± s.e.mean. Levels of significance were obtained by use of Student's t tests, a significance level of 0.05 was used.

Results

With levamisole in concentrations between 1–90 μM, in the patch-pipette, channel currents in 43% of 143 cell-attached and isolated inside-out patches were recorded. These channels had apparent mean open-times in the millisecond range and amplitudes of around 2.5 pA at −75 mV. Detailed analysis of channel data from a single patch recorded from both the cell-attached and the isolated inside-out configuration showed no significant differences in channel kinetics. In 20 experiments with levamisole omitted from the

patch pipette solution no such channel openings were observed. It was therefore concluded that levamisole activated these currents.

Channel conductance and current/voltage relationships

The pipette and bath-solutions had symmetrical cation concentrations but non-symmetrical anion concentrations (pipette main-ions: Cs^+ 140 mM, Cl^- 144 mM: bath main-ions: Cs^+ 140 mM, Cl^- 39 mM). Under these conditions with isolated inside-out patches, the predicted Nernst reversal potential for a cation selective channel is 0 mV, and for an anion channel is − 33 mV. In 26 out of 31 experiments the I/V plots of levamisole-activated channels were linear with reversal near 0 mV (Figure 1) indicating that these channels were cation-selective and could conduct Cs^+. The slopes had an average conductance of 32.9 ± 1.23 pS (mean ± s.e., $n = 26$) and ranged between 19–46 pS.

As a further test of the permeability of the channel the bath-solution was diluted 50:50 with distilled water. The predicted effect of this is to produce a shift in the Nernst reversal potential from 0 mV to + 18 mV for a cation selective channel and from − 33 mV to − 51 mV for an anion selective channel. In the experiment illustrated in Figure 1, the reversal potential shifted from 0 mV to + 13 mV.

Calculation of the relative permeability of Cs^+ and Cl^- with the Goldman constant field equation (Hille, 1984), revealed that Cs^+ was ten times more permeable than Cl^-. Similar results were obtained in three other experiments.

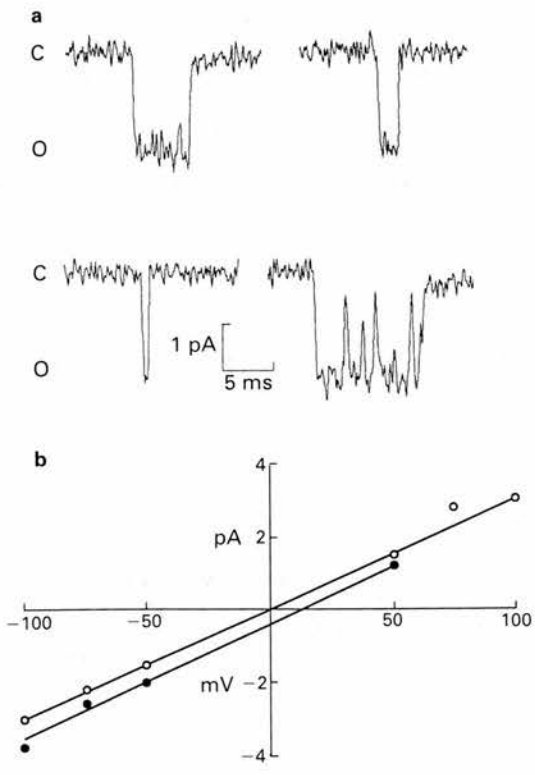


Figure 1 (a) Individual channel openings recorded from an isolated inside-out patch, at a membrane potential of − 75 mV and with levamisole 3 μM. The conductance of these channel currents was 26 pS. C: denotes the closed state. O: denotes the open state. (b) I/V plot of channel currents activated by 3 μM levamisole in an isolated inside-out patch. The initial plot (○) has a conductance of 31 pS and a 0 mV reversal potential. Dilution of the bath solution (●) produced a shift in the reversal potential to + 13 mV. The predicted Nernst potentials during the initial I/V plot were: for Cs^+, 0 mV; for Cl^- − 33 mV. The predicted Nernst potentials for the I/V plot obtained with the diluted solution were: for Cs^+, 18 mV; for Cl^-, − 51 mV.

Exponential curve-fitting

Channel data from 31 patches were analysed at various membrane potentials, ranging from + 150 mV to − 150 mV. The data were best-fitted by the sum of exponentials (see Methods). Files contained between 200 and 10,000 apparent open-, burst- and closed-times.

With 2–10 μM levamisole in the pipette the open- and burst-time distributions were best-fitted by two exponentials, while closed-time distributions were best-fitted by three exponentials (Table 1,2,3). Since the number of open-, burst- and closed- states must at least equal the number of exponential components fitted (Colquhoun & Hawkes, 1982), levamisole-activated channels in *Ascaris* have at least two open-states, at least two burst-states and at least three closed-states. Higher concentrations of levamisole (30 μM and 90 μM) produced substantial changes in the distribution of both the open- and closed-times, these changes are considered in the sections on channel-block and desensitisation.

Voltage-sensitivity of open- and burst-time durations

At lower concentrations of levamisole (2–10 μM) the corrected mean open-times (Figure 2) and corrected mean burst-times exhibited a degree of voltage-sensitivity, decreasing with depolarization. For example the value at − 75 mV for the corrected mean open-time was 1.47 ± 0.11 ms (mean ± s.e., $n = 10$), this value was significantly greater ($P < 0.03$) than the value for the corrected mean open-time at + 75 mV of 1.10 ± 0.25 ms ($n = 4$). The corrected mean burst duration at − 75 mV was 2.50 ± 0.28 ms ($n = 16$), this compared to a value of 1.50 ± 0.25 ms ($n = 4$) at + 75 mV where the corrected mean burst durations were also significantly reduced ($P < 0.05$).

Probability of channel opening

The probability of the channel being open (P_{open}) was concentration-dependent at depolarized potentials where P_{open} increased with concentration. However at hyperpolarized potentials concentration had no significant effect on P_{open}. Figure 3 illustrates the effect of concentration on P_{open} at ± 75 mV. Similar results were observed at ± 100 mV. It is suggested subsequently that the explanation for the failure of P_{open} to increase at − 75 mV and − 100 mV is due to the blocked state of the channel, which occurs with high concentrations of levamisole at hyperpolarized potentials, directly closing without re-entering the open-state.

At low agonist concentrations the membrane potential had little affect on P_{open}. For example, in one experiment with 3 μM levamisole, P_{open} was 0.0061 at + 75 mV compared to 0.0078 at − 75 mV; similar results were obtained in 8 other experiments with 2–10 μM levamisole. This lack of effect of membrane potential on P_{open} contrasts with the effect of membrane potential on open-times; the lack of effect on P_{open} is explained by the compensating increase in the rate of channel opening at depolarized potentials. For example in one experiment with 3 μM levamisole, the channel opening rate at − 75 mV was 8.6 channel openings per second compared to 13.6 channel openings per second at + 75 mV.

Evidence of channel block

At higher concentrations of levamisole (30 μM and 90 μM), there was a recognisable change in the kinetics of channel opening (Figure 4). At hyperpolarized potentials, channel openings were briefer than at lower concentrations and appeared as sequences of openings separated by brief closings characteristic of a 'flickering' channel-block (see, Neher & Steinbach, 1978). This behaviour may be explained by levamisole acting to produce a voltage-sensitive open channel-block, in addition to its action as an agonist. The cationic charge and large size of levamisole is consistent with

Table 1 Open-time kinetics for levamisole-activated channels

Levamisole conc. (μM)		*Open-times* (ms) A1	A2	T1	T2
Membrane potential − 75 mV					
2–10	(n = 17)	0.66 ± 0.06	0.34 ± 0.06	0.88 ± 0.10	2.30 ± 0.24
30	(n = 9)	0.78 ± 0.09	0.22 ± 0.09	0.37 ± 0.09	0.69 ± 0.08
90	(n = 12)		1.00		0.57 ± 0.06
Membrane potential − 100 mV					
2–10	(n = 13)	0.59 ± 0.08	0.41 ± 0.08	0.86 ± 0.12	2.54 ± 0.36
90	(n = 5)		1.0		0.39 ± 0.05
Membrane potential + 75 mV					
3–10	(n = 4)	0.62 ± 0.10	0.38 ± 0.10	0.71 ± 0.10	1.60 ± 0.14
30	(n = 5)	0.66 ± 0.07	0.34 ± 0.07	0.48 ± 0.07	1.22 ± 0.29
90	(n = 8)	0.66 ± 0.08	0.34 ± 0.08	0.64 ± 0.10	2.02 ± 0.28
Membrane potential + 100 mV					
3–10	(n = 4)	0.79 ± 0.12	0.21 ± 0.12	0.71 ± 0.08	2.35 ± 0.50
30	(n = 4)	0.81 ± 0.04	0.19 ± 0.04	0.50 ± 0.10	2.03 ± 0.47
90	(n = 4)	0.67 ± 0.06	0.33 ± 0.06	0.65 ± 0.07	1.88 ± 0.24

T1 and T2 are the time constants representing the two open states. The proportion of brief openings (T1) and long openings (T2) are represented by the areas of A1 and A2. Values are mean ± s.e..

Table 2 Closed time kinetics for levamisole-activated channels

Levamisole conc. (μM)		*Closed times* (ms) A1	A2	A3	A4	T1	T2	T3	T4
Membrane potential − 75 mV									
2–10	(n = 18)	0.46 ± 0.04	0.26 ± 0.05	0.28 ± 0.05		0.35 ± 0.04	237 ± 41	821 ± 127	
30	(n = 9)	0.46 ± 0.06	0.20 ± 0.04	0.28 ± 0.04	0.06 ± 0.02	0.76 ± 0.16	24 ± 10	228 ± 80	1586 ± 446
90	(n = 11)	0.55 ± 0.04	0.17 ± 0.02	0.22 ± 0.03	0.06 ± 0.02	0.63 ± 0.08	12 ± 3	251 ± 107	2528 ± 714
Membrane potential − 100 mV									
2–10	(n = 14)	0.38 ± 0.05	0.26 ± 0.04	0.34 ± 0.08		0.37 ± 0.04	224 ± 52	1081 ± 139	
90	(n = 6)	0.51 ± 0.07	0.25 ± 0.03	0.18 ± 0.06	0.07 ± 0.02	1.57 ± 0.32	20 ± 12	223 ± 131	3684 ± 2579
Membrane potential + 75 mV									
3–10	(n = 5)	0.22 ± 0.05	0.56 ± 0.09	0.21 ± 0.09		0.24 ± 0.04	132 ± 38	595 ± 115	
30	(n = 5)	0.21 ± 0.09	0.09 ± 0.05	0.57 ± 0.08	0.12 ± 0.03	0.38 ± 0.23	8 ± 4	137 ± 73	675 ± 261
90	(n = 8)	0.22 ± 0.38	0.38 ± 0.05	0.34 ± 0.06	0.05 ± 0.02	0.56 ± 0.15	32 ± 11	127 ± 30	961 ± 380
Membrane potential + 100 mV									
2–10	(n = 4)	0.31 ± 0.04	0.52 ± 0.08	0.15 ± 0.05		023 ± 0.06	146 ± 22	672 ± 189	
30	(n = 4)	0.10 ± 0.02	0.42 ± 0.26	0.34 ± 0.14	0.13 ± 0.10	0.44 ± 0.01	51 ± 38	172 ± 74	526 ± 247
90	(n = 5)	0.10 ± 0.03	0.40 ± 0.07	0.46 ± 0.65	0.04 ± 0.02	0.38 ± 0.08	16 ± 4	87 ± 36	427 ± 128

Closed states are represented by three exponentials at 2–10 μM levamisole. Brief closings (T1), intermediate closings (T2) and long closings (T3), their relative proportions are represented by the areas A1, A2 and A3. At 30–90 μM there are four closed states represented by the time constants T1, T2, T3 and T4. Their relative proportions are represented by the areas A1, A2 and A3 and A4. All values are the mean ± s.e., n is the number of experiments.

Table 3 Burst-time kinetics for levamisole-activated channels

Levamisole conc. (μM)		*Burst-times* (ms) A1	A2	T1	T2
Membrane potential − 75 mV					
2–10	(n = 19)	0.49 ± 0.07	0.51 ± 0.07	1.24 ± 0.19	3.07 ± 0.35
30	(n = 8)	0.61 ± 0.09	0.39 ± 0.09	0.59 ± 0.15	2.06 ± 0.42
90	(n = 9)	0.59 ± 0.07	0.41 ± 0.07	0.74 ± 0.19	2.23 ± 0.32
Membrane potential − 100 mV					
2–10	(n = 12)	0.56 ± 0.07	0.44 ± 0.07	1.29 ± 0.22	3.78 ± 0.50
90	(n = 4)	0.44 ± 0.08	0.56 ± 0.08	0.30 ± 0.15	2.93 ± 0.96
Membrane potential + 75 mV					
3–10	(n = 5)	0.46 ± 0.08	0.54 ± 0.08	0.69 ± 0.03	1.89 ± 0.29
30	(n = 5)	0.77 ± 0.08	0.23 ± 0.08	0.66 ± 0.19	2.33 ± 0.79
90	(n = 7)	0.73 ± 0.05	0.27 ± 0.05	0.93 ± 0.23	2.73 ± 0.64
Membrane potential + 100 mV					
2–10	(n = 5)	0.71 ± 0.06	0.29 ± 0.06	1.06 ± 0.21	2.54 ± 0.48
30	(n = 3)	0.82 ± 0.08	0.18 ± 0.08	0.69 ± 0.21	4.01 ± 1.52
90	(n = 5)	0.69 ± 0.06	0.31 ± 0.06	0.80 ± 0.22	2.33 ± 0.52

T1 and T2 are the time constants representing the two burst states. The proportion of brief bursts (T1) and the long bursts (T2) are represented by the areas A1 and A2. Values are mean ± s.e..

the direction of the voltage-sensitivity of the block. In order to describe the effect further, a simple channel-block model (Adams 1976; Colquhoun & Sakmann, 1985) was used.

The presence of open channel-block reduced the duration of the open-states at hyperpolarized potentials. Table 1 shows that this reduction in open-times at 30 μM levamisole was associated with a reduction of both the brief and longer components of the open-time distribution. At − 75 mV with 90 μM levamisole where the open-durations were also reduced, only one open-state could be detected. The loss of one component at this concentration is most likely due to the brief openings reducing to a level below the limit of resolution of the recording apparatus, as a result of channel-block. At 90 μM the corrected mean open-time at − 75 mV was 0.63 ± 0.06 ms (mean ± s.e., $n = 11$), a value significantly lower than that at + 75 mV which was 1.30 ± 0.26 ms (mean ± s.e., $n = 8$), ($P < 0.02$). Thus mean open-times showed a reversed direction of voltage-sensitivity at the higher levamisole concentrations. At + 75 mV where no channel-block was observed, there was no significant reduction in the mean duration of the two open-time components compared to values at lower concentrations (2–10 μM).

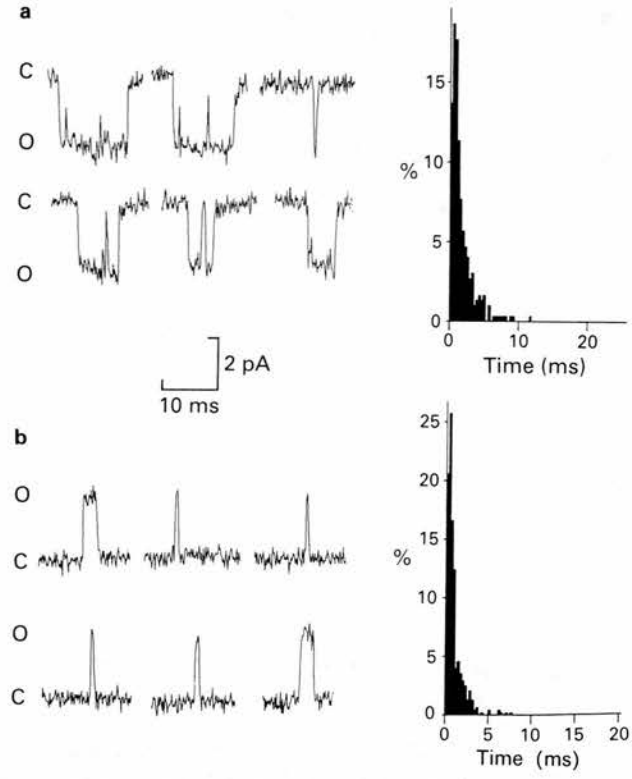


Figure 2 Levamisole (3 μM)-activated channels from a cell-attached patch illustrating the voltage-sensitivity of open-time durations. C: denotes the closed state. O: denotes the open state. (a) Individual channels recorded at − 75 mV and histogram of open-times at this potential. The open-times were fitted by two exponentials (not shown) with time constants of 0.92 ms and 2.14 ms. The corrected mean open-time was 1.59 ms. (b) Individual channels recorded at + 75 mV and histogram of open-times at this potential. The open-times were fitted by two exponentials (not shown) with time constants of 0.53 ms and 1.45 ms. The corrected mean open-time was 0.91 ms.

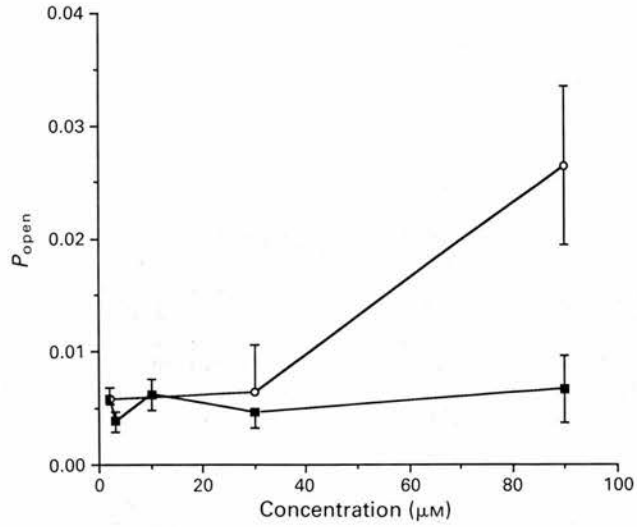


Figure 3 Graph showing P_{open} versus levamisole concentration; (■) − 75 mV membrane potential; (○) + 75 mV membrane potential. All values are mean (with vertical bars showing s.e.). $n = 4$ to $n = 9$.

Estimation of blocked-times

Mean block durations at membrane potentials of − 35 to − 100 mV for both 30 μM and 90 μM are shown in Table 4. Comparison of values at both 30 μM and 90 μM showed concentration did not affect mean block-times. The lack of effect of concentration on blocked-times is consistent with predictions of the simple channel-block model. Values obtained for mean block durations at both 30 μM and 90 μM were subsequently combined and their reciprocals used to estimate k_{-B} values (Figure 5).

Estimation of k_{+B}

The forward blocking-rate constants k_{+B} were determined from plots of the reciprocals of the mean duration of long open-times (T2) against drug concentration (Figure 6). Long open-times were used in preference to the brief open-times because they are more accurately determined, the short open durations are close to the limit of resolution of the setup and at 90 μM value for T1 appears to fall below the limit of resolution of the recording apparatus. In calculating k_{+B}, results obtained with 90 μM levamisole were not included. These points deviated from the straight line obtained with results at lower concentrations (2–30 μM). This may be due to the fact that at higher concentrations the mechanism of block may be more complex than the simple channel-block mechanism. However it is more likely that at the the higher concentration (90 μM) some of the open-time durations are lower than the limit of resolution of the recording apparatus, making the open-time duration an overestimation at this concentration. This interpretation is further supported by the fact that at 90 μM with hyperpolarized potentials open-times distributions could only be fitted by a single exponential.

Values for the forward blocking-rate constant, k_{+B} at − 50 mV, was $2.06 \times 10^7\ M^{-1}\ s^{-1}$; at − 75 mV it was $3.82 \times 10^7\ M^{-1}\ s^{-1}$; and at − 100 mV it was $6.58 \times 10^7\ M^{-1}\ s^{-1}$. As predicted by the simple channel block model, k_{+B} increased with membrane hyperpolarization. The voltage sensitivity of k_{+B} was described by the equation: $k_{+B} = k_{+BO} \cdot \exp^{(E/Vk)}$. Where k_{+B} is the forward blocking rate constant at the membrane potential E, k_{+BO} is the value for k_{+B} at 0 mV and Vk is a constant. The value for k_{+BO} was $0.83 \times 10^7\ M^{-1}\ s^{-1}$ and Vk was − 35.5 mV. The correlation coefficient (r) was 0.97. Therefore k_{+B} showed an e-fold change every 36 mV. It was also possible to estimate the closing rate constants (α_2) for the long openings. This was the intercept of the plot of 1/T2 versus concentration. At − 50 mV the value for α_2 was $447\ s^{-1}$, at − 75mV it was $396\ s^{-1}$; and at − 100 mV it was $143\ s^{-1}$. As can be observed the closing rate decreases with membrane hyperpolarization, this supports earlier observations where open durations were longer at hyperpolarized potentials.

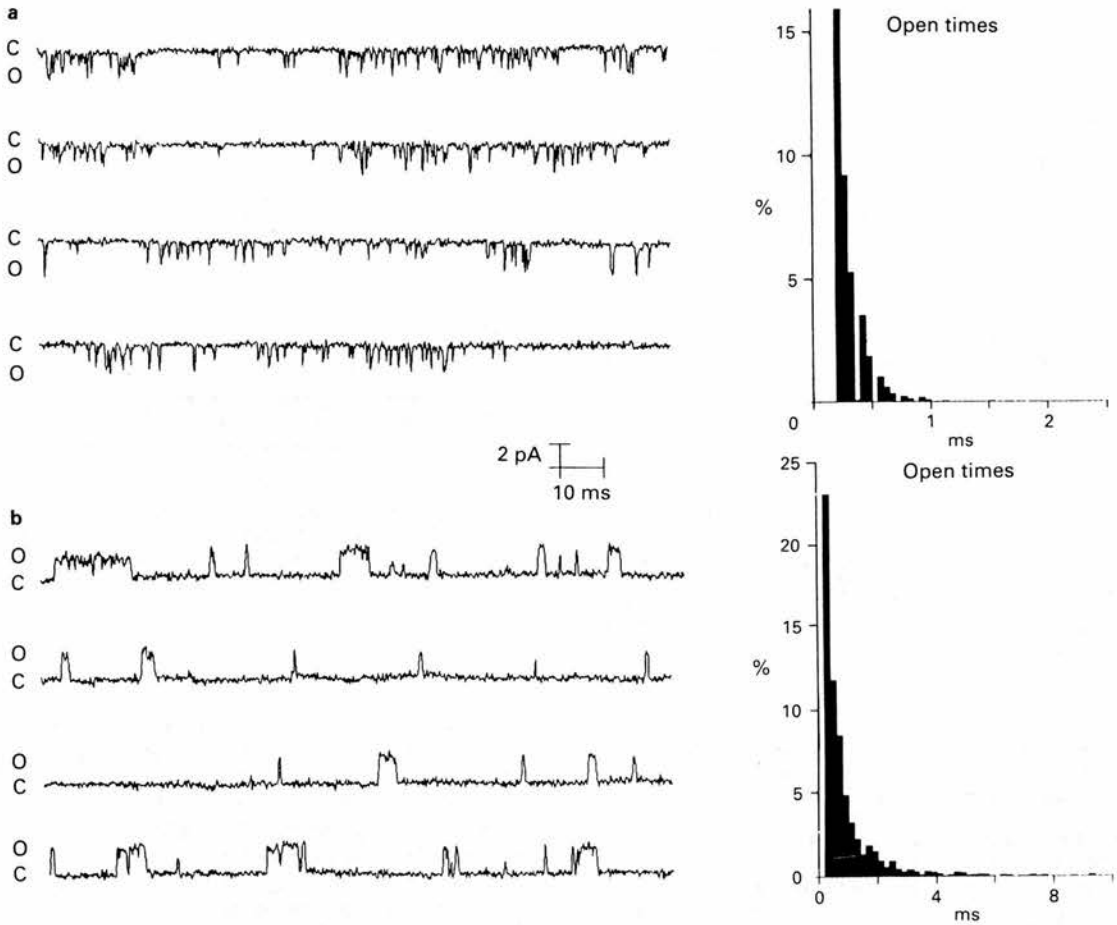


Figure 4 Levamisole-(30 μM) activated channels and open-time histograms from an isolated inside-out patch. (a) Membrane potential − 75 mV; (b) membrane potential + 75 mV. The open-times in this patch were fitted with two exponentials (not shown). (a) TI = 0.14 ms T2 = 0.69 ms; (b) T1 = 0.41 ms T2 = 1.91 ms. Note the presence of flickering open channel-block in (a).

Table 4 The effect of membrane potential on mean block time

	Mean block time (ms) *Membrane potential*			
Levamisole conc. (μM)	*− 35 mV*	*− 50 mV*	*− 75 mV*	*− 100 mV*
30		0.38 ± 0.05 ($n = 5$)	0.87 ± 0.18 ($n = 9$)	2.07 ± 0.34 ($n = 4$)
90	0.27 ± 0.05 ($n = 4$)	0.50 ± 0.07 ($n = 6$)	0.71 ± 0.09 ($n = 11$)	1.55 ± 0.18 ($n = 6$)
30 + 90	0.27 ± 0.05 ($n = 4$)	0.44 ± 0.05 ($n = 11$)	0.78 ± 0.10 ($n = 20$)	1.76 ± 0.18 ($n = 10$)

Values are mean ± s.e.

Determination of K_B

The values for k_{+B} and k_{-B} determined above were used to calculate the channel-block dissociation constant, K_B. At − 50 mV, K_B was $2.55 \times 10^3\ s^{-1}/2.06 \times 10^7\ M^{-1}\ s^{-1}$ or 123 μM; at − 75 mV, K_B was $1.75 \times 10^3\ s^{-1}/3.82 \times 10^7\ M^{-1}\ s^{-1}$ or 46 μM; and at − 100 mV, K_B was $0.62 \times 10^3\ s^{-1}/6.58 \times 10^7\ M^{-1}\ s^{-1}$ or 9.4 μM. The semi-log plot of K_B versus membrane potential is shown in Figure 7, this shows an e-fold change in K_B every 19.4 mV.

Burst durations

As stated earlier, the burst durations exhibit a degree of voltage-sensitivity. The bursts consisted of two components; the brief bursts (mean T1) and the longer bursts (mean T2). Values for T1 and T2, with their respective proportions A1 and A2 are listed in Table 3. The simple channel-block model predicts that the mean burst-length should increase with concentration. In order to examine this prediction the corrected mean burst lengths were determined at different levamisole concentrations. For example at − 75 mV with 2–10 μM levamisole the corrected mean burst length was 2.50 ± 0.28 ms ($n = 16$); with 30 μM levamisole it was 1.14 ± 0.32 ms ($n = 6$); and with 90 μM levamisole it was 1.40 ± 0.21 ($n = 9$). Thus there was no significant increase in the corrected mean burst duration. Similar results were obtained at − 100 mV. It was concluded that the mean burst durations did not increase with increasing levamisole concentration, a result not predicted by the simple channel-block model.

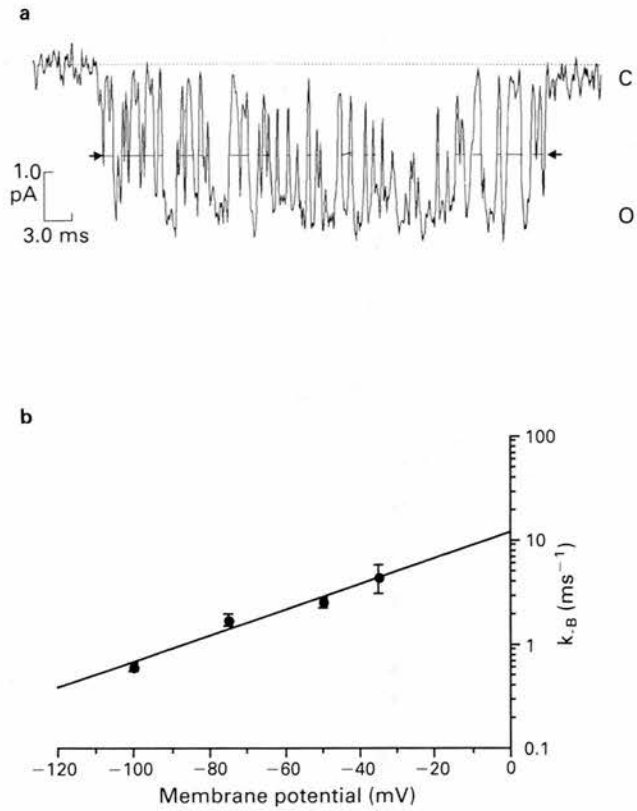


Figure 5 (a) Illustration of channel activity with 30 μM levamisole; isolated inside-out patch, − 75 mV. Fast flickering channel-block can be clearly observed. C: denotes the closed state. O: denotes the open state. The mean blocked-times were calculated from the measurements of blocked durations (indicated by the line between the arrows). In this experiment the mean blocked-time was 0.43 ms. (b) Semi-log plot of K_{-B} against membrane potential, all values are mean ± s.e.. The voltage sensitivity of K_{-B} was described by the equation: $K_{-b} = K_{-BO}.\exp^{(E/Vk)}$. Where K_{-B} is the unblocking rate constant at the membrane potential E, K_{-BO} is the value for K_{-B} at O m V and Vk is a constant. The value for K_{-BO} was 11.99 ms^{-1} and Vk was 35.02 mV.

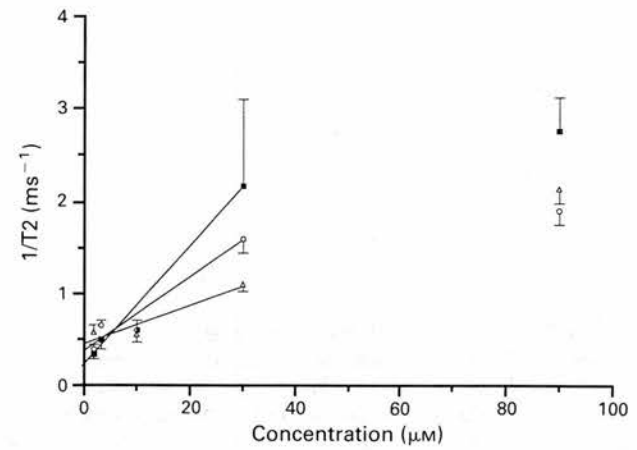


Figure 6 Reciprocal plot of open-time constant T2 against concentration, at − 50 mV (△), − 75 mV (○) and − 100 mV (■). The intercept represents the closing rate constant (α_2) and the slope represents the forward blocking rate (K_{+B}). Each point is the mean ± s.e. (vertical bars). Lines were fitted to 2–30 μM by least square regression without including the results at 90 μM. Values for K_{+B} were determined as − 50 mV, 2.06×10^7 M^{-1} s^{-1}; − 75 mV, 3.82×10^7 M^{-1} s^{-1}; and − 100 mV, 6.58×10^7 M^{-1} s^{-1}. The closing rate constant α_2 was also determined: − 50 mV, 447s^{-1}; − 75 mV, 396 s^{-1}; and − 100 mV, 143 s^{-1} from the intercept on the ordinate scale.

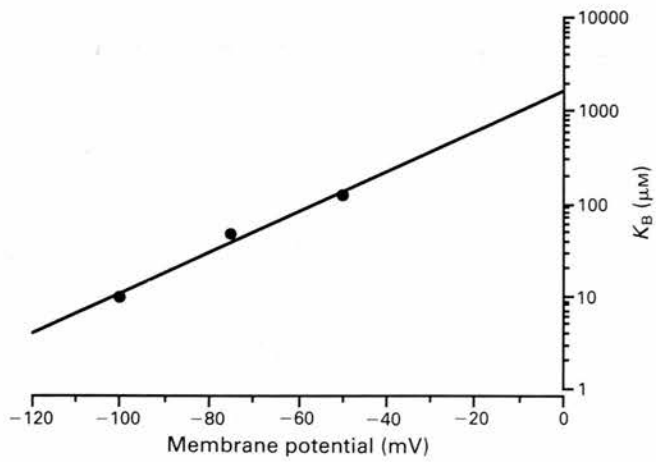


Figure 7 Semi-log plot of K_B versus membrane potential. The voltage-sensitivity of K_B was described by the equation: $K_B = K_{BO}.\exp^{(E/Vk)}$. Where K_B is the dissociation rate constant at the membrane potential E, K_{BO} is the value for K_B at 0 mV and Vk is a constant. The value for K_{BO} was 1780 μM and Vk was 19.4 mV.

Desensitization

At higher concentrations of levamisole (30 μM and 90 μM) long closed-times were seen in some patches between clusters of channel opening (Figure 8). These closed-times lasted many seconds and were observed at both depolarized and hyperpolarized potentials. The details of the closed-time components observed at higher concentrations are summarized in Table 2. These very long closed periods appear to correspond to a slow desensitization process (Cachelin & Colquhoun, 1989) and are similar to the very long closed-times observed with high concentrations of acetycholine in *Ascaris* (Pennington & Martin, 1990). In addition to the long closed durations, shorter closed times (between 10 and 50 ms) were detected at high levamisole concentrations. These might also be part of a desensitized state as they occur at both depolarized and hyperpolarized potentials but only with high concentrations.

Discussion

The simple block model

The simple channel-block model was used in this paper in order to describe quantitatively some of the effects observed

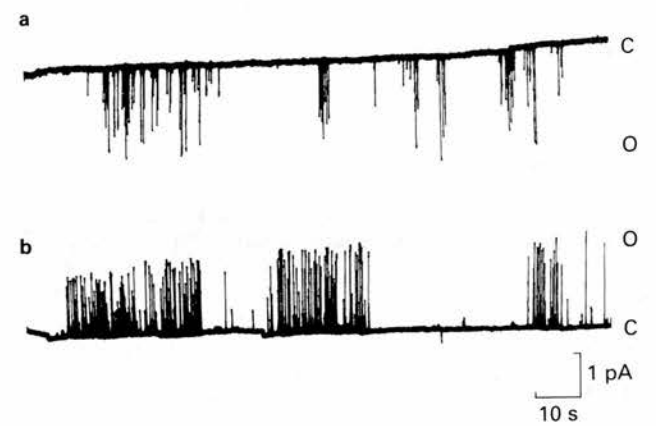


Figure 8 Channel current showing long (seconds) closed-times between clusters of openings. C: denotes closed state, O: denotes open state; 90 μM levamisole, cell attached patches. (a) − 75 mV; (b) + 75 mV. The long closed periods were interpreted as desensitization.

with levamisole. The predictions of this model, for a charged blocker, include the expectations that: the corrected mean open-times decrease with increasing levamisole concentration; burst durations increase with increasing drug concentration; the forward blocking rate constant (k_{+B}), the unblocking rate (k_{-B}), and the dissociation constant K_B all vary with membrane potential (k_{+B} and k_{-B} should have equal but opposite voltage-dependences); and the mean block duration and therefore k_{-B} are independent of drug concentration. The data presented in this report are consistent with the above predictions except that burst durations did not increase with concentration. This implies that the model used is a useful approximation but not a completely sufficient model.

We did not observe the predicted increase in the average duration of bursts, although there were frequent examples of long flickering bursts (see Figure 5). One possible explanation for the absence of increased mean burst durations could be that the channel might enter a closed state directly from the blocked state without reopening, i.e. the channel closes trapping levamisole or the blocked channel enters into a desensitised state. Limitations of the simple channel-block model are discussed further by Neher (1983).

One further difficulty in using the simple channel-block model is the presence of two open-states (O1 and O2). In our analysis it seems probable at 90 μM that the brief open-state (O1) fell below the limit of resolution of the recording set up. Thus the values for k_{-B} would be appropriate for the open-state O2 at 90 μM. Since the values for k_{-B} were not significantly different from the values for k_{-B} at 30 μM where the open-state O1 could still be resolved, it implies that the presence of O1 did not affect our estimation of k_{-B} for the open-state O2. Since the values for k_{+B} were determined from the values of the open-state O2 (see methods), our determination of K_B is likely to be an estimate of the dissociation constant for the block of the open-state O2.

Comparison with acetylcholine-activated channels in Ascaris

At the single-channel level both acetylcholine (Pennington & Martin, 1990) and levamisole activate channels in the same concentration range: acetylcholine 1–100 μM; levamisole 1–90 μM. The I/V relationship with both levamisole and acetylcholine are linear, both agonists showed evidence of desensitization with long closed periods appearing at higher concentrations.

Although acetylcholine and levamisole appear to activate the same channels there are some differences in the behaviour of the single-channel currents. Acetylcholine activates channels with two distinguishable conductance levels (25–35 pS and 40–50 pS) (Pennington & Martin, 1990); in contrast single-channel currents activated by levamisole had a range of detectable conductance levels between 19–46 pS with a mean of 32.9 ± 1.23 pS ($n = 26$).

The open-, closed-, and burst-time durations for levamisole or acetylcholine activated channels in this preparation show that both compounds produced two open-states and two burst-states and at least three closed-states. However the mean duration of the apparent open-times and burst-times for levamisole were shorter than for acetylcholine. The mean duration of apparent brief and long openings produced by acetylcholine (1–10 μM) was 1.18 ms and 4.89 ms, which compares with 0.80 ms and 2.30 ms for 2–10 μM levamisole under similar conditions. The mean brief and long burst durations for 1–10 μM acetylcholine were 1.17 ms and 7.62 ms compared to 1.24 ms and 3.70 ms for 2–10 μM levamisole.

A further difference between the effects of acetylcholine and levamisole is related to channel-block. Pennington & Martin (1990) did not find significant evidence for channel-block with acetylcholine on this preparation, although they did observe a reduction in the mean open-time at higher concentrations (25 μM) which might be interpreted as signs of block. Our results clearly show that levamisole blocks the channel at hyperpolarized potentials.

Comparison with previous voltage-clamp experiments in Ascaris

Harrow & Gration (1985) examined the effects, in *Ascaris*, of both acetylcholine and levamisole using two-microelectrode current-clamp and voltage-clamp. They found that the I/V relationship obtained from two-microelectrode voltage-clamp experiments obtained by applying levamisole by microperfusion or iontophoresis to *Ascaris* muscle had both linear (0 to −30 mV) and non-linear sections (> −30 mV). They suggested that the non linearity was due to a voltage-sensitive channel-block and/or desensitization. In our experiments we observed some desensitization at higher concentrations of levamisole, but this appeared at both depolarized and hyperpolarized membrane potentials, not just at membrane potentials greater than −30 mV. Channel-block was clearly observed in our experiments, the degree of block increased on membrane hyperpolarization. This is consistent with the voltage-sensitivity of the non linearity observed by Harrow & Gration (1985) and suggests that their observation reflects channel-block but not desensitization.

Harrow & Gration (1985) have shown that levamisole is an agonist at all concentrations (1 μM–10 mM) producing a sigmoid dose-response curve obtained under current-clamp conditions with a membrane potential of −30 mV. Our results clearly show that channel-block occurs at −35 mV and at this potential K_B was calculated at 285 μM. It is interesting to note that Harrow & Gration (1985) did not observe a reduction in the maximum conductance response with high concentrations (10 mM). This observation of Harrow & Gration (1985) is consistent with our observations at hyperpolarized potentials which showed that P_{open} failed to decrease at higher concentrations, despite the presence of channel block.

Possible therapeutic significance

Receptor desensitization produced by levamisole may have significant effects therapeutically; some *Ascaris* parasites continuously treated with higher doses of levamisole recover from the levamisole-induced paralysis (Aceves *et al.*, 1970; Coles *et al.*, 1974; 1975). This recovery may be due to desensitization since like desensitization, recovery occurs only at higher doses. Consequently it is suggested that lower doses which do not produce desensitization, potentially have a greater therapeutic effect. Also the fact that P_{open} in these experiments did not increase at hyperpolarized potentials when 2–90 μM levamisole was used suggests that high concentrations would not be therapeutically advantageous.

Therefore in conclusion, these experiments confirm that levamisole acts at the acetylcholine receptor on *Ascaris suum* muscle, both opening and blocking the channel.

We are grateful for the financial support of Merck Sharp & Dohme.

References

ACEVES, J., ERLI, J.D. & MARTINEZ-MARANON, R. (1970). The mechanism of the paralysing action of tetramisole on *Ascaris suum* muscle. *Br. J. Pharmacol.*, **38,** 602–607.

ADAMS, P.R. (1976). Drug blockade of open end-plate channels. *J. Physiol.*, **260,** 531–552.

CACHELIN, A.B. & COLQUHOUN, D. (1989). Desensitisation of the acetylcholine receptor of frog end-plates measured in a vaseline-gap voltage clamp. *J. Physiol.*, **415,** 159–188.

COLES, G.C., EAST, J.M. & JENKINS, S.N. (1974). The mode of action of four anthelmintics. *Experientia*, **30,** 1265–1266.

COLES, G.C., EAST, J.M. & JENKINS, S.N. (1975). The mechanism of action of the anthelmintic levamisole. *Gen. Pharmacol.*, **6,** 309–313.

COLQUHOUN, D. & HAWKES, A.G. (1982). On the stochastic properties of bursts of single ion channel openings and clusters of bursts. *Phil. Trans. R. Soc.*, **B300,** 1–59.

COLQUHOUN, D. & SAKMANN, B. (1985). Fast events in single channel currents activated by acetylcholine and its analogues at the frog muscle end-plate. *J. Physiol.*, **369,** 501–557.

COLQUHOUN, D. & SIGWORTH, F.W. (1983). Fitting and statistical analysis of single-channel records. In *Single Channel Recordings.* ed. Sackman, B. & Neher, E. pp. 191–264. New York: Plenum Press.

COLQUHOUN, L., HOLDEN-DYE, L. & WALKER, R.J. (1991). The pharmacology of cholinoceptors on the somatic muscle cells of the parasitic nematode *Ascaris suum. J. Exp. Biol.*, **158,** 509–530.

HARROW, I.D. & GRATION, K.A.F. (1985). Mode of action of the anthelmintic Morantel, pyrantel and levamisole on the muscle cell membrane of the nematode *Ascaris suum. Pesticide Sci.*, **16,** 662–672.

HILLE, B. (1984). In *Ionic Channels of Excitable Membranes*, p. 233. Sunderland: Sinauer Associates Inc.

MARTIN, R.J. (1982). Electrophysiological effects of piperazine and diethylcarbamazine on *Ascaris suum* muscle. *Br. J. Pharmacol.*, **77,** 255–265.

MARTIN, R.J. (1985). γ-Aminobutyric acid and piperazine activated single channel currents from *Ascaris suum* body muscle. *Br. J. Pharmacol.*, **84,** 445–461.

MARTIN, R.J., KUSEL, J.R. & PENNINGTON, A.J. (1990). Surface properties of membrane vesicles prepared from muscle cells of *Ascaris suum. J. Parasit.*, **76,** 340–348.

NATOFF, I.L. (1969). The pharmacology of the cholinoceptor in muscle preparation of *Ascaris lumbricoides* var. *suum. Br. J. Pharmacol.*, **37,** 251–257.

NEHER, E. (1983). The charge carried by single-channel currents of rat cultured muscle cells in the presence of local anaesthetics. *J. Physiol.*, **339,** 663–678.

NEHER, E. & STEINBACH, J.H. (1978). Local anaesthetics transiently block currents through single acetylcholine receptor channels. *J. Physiol.*, **277,** 153–176.

PENNINGTON, A.J. & MARTIN R.J. (1990). A patch clamp study of acetylcholine activated ion channels in *Ascaris suum* muscle. *J. Exp. Biol.*, **154,** 201–221.

ROZKOVA, E.K., MALYUTINA, T.A. & SHISHOV, B.A.(1980). Pharmacological characteristics of cholinoreceptors in somatic muscles of the nematode *Ascaris suum. Gen. Pharmacol.*, **11,** 141–146.

STANDEN, D.D. (1975). Chemotherapy of intestinal helminthiasis. *Prog. Drug Res.*, **19,** 158–165.

THORN, P. & MARTIN, R.J. (1987). A high conductance Ca-dependent CI- channel in *Ascaris suum* muscle. *Q. J. Exp. Physiol.*, **72,** 31–49.

VAN NEUTEN, J.M. (1972). Pharmacological aspects of tetramisole. In *Comparative Biochemistry of Parasites.* ed. Van Den Bossche, H. pp. 101–115. New York: Academic press.

(Received May 18, 1992
Revised August 24, 1992
Accepted September 8, 1992)

Sci. 1993, 37, 293–299

ıe Activation of Nicotinic Acetylcholine eceptors in the Nematode Parasite *Ascaris um* by the Application of Levamisole to the ytoplasmic Surface of Muscle Membrane

ın J. Robertson* & Richard J. Martin

of Preclinical Veterinary Sciences, Royal (Dick) School of Veterinary Studies, Summerhall, ersity of Edinburgh, Edinburgh EH9 1QH, UK

sed manuscript received 21 January 1993; accepted 4 February 1993)

Abstract: The patch-clamp technique was used to examine activation by levamisole of nicotinic acetylcholine receptors in muscle vesicle preparations from *Ascaris suum*. Previous experiments have shown that levamisole, when applied at concentrations greater than 30 μM to the extracellular surface of the membrane, activated channels which showed characteristics of a voltage-sensitive open channel-block and desensitisation. In this study initial experiments were performed where channels were activated with levamisole (2 μM) applied in the patch-pipette. Isolated inside-out patches were used. In addition, levamisole (30–926 μM) was added to the cytoplasmic membrane surface via the bath solution. In eight out of nine experiments, addition of levamisole to the bath solution resulted in an increase in channel activity, a voltage-sensitive open channel-block and desensitisation. The open channel-block occurred at hyperpolarised potentials, an observation consistent with levamisole (a cationic substance) blocking the channel from the extracellular surface. Thus it was concluded that levamisole crossed from the cytoplasmic side of the membrane, via the lipid phase, to the extracellular surface of the patch. In the presence of high cytoplasmic concentrations of levamisole, open channel-block was not observed at depolarised potentials, suggesting channel asymmetry.

1 INTRODUCTION

ıtode parasites inflict much suffering on human and ıl hosts. Anthelmintic drugs, such as levamisole, are o control these infestations. Studies on the mode of ı of levamisole indicate that it is a selective agonist otinic acetylcholine receptors present on the muscle of the parasitic nematode *Ascaris suum*.[1–3] This ı of levamisole results in depolarisation of muscle inducing spastic paralysis of the nematode.[1–6] ysis of levamisole-activated single-channel currents *caris suum* on application of levamisole to the extracellular surface of the patch has shown: (i) the channels are cation selective with linear I/V plots; (ii) the channel conductance is approximately 35 pS; (iii) generally there are two open states and three closed states; and (iv) at high concentrations (> 30 μM) desensitisation and open channel-block occur. Desensitisation occurs at both depolarised and hyperpolarised potentials whereas channel-block is only observed at hyperpolarised potentials.[7]

Changeux *et al.*[8] have reviewed the structure of nicotinic receptors from a variety of vertebrate preparations. They report common properties of acetylcholine-gated channels among the species. In general the receptor is thought to be a 290 kD glycoprotein composed of five subunits with a stoichiometry $\alpha_2\beta\gamma\delta$. Several charged rings have been located within the channel-pore. If the *Ascaris* nicotinic channel has a similar structure to that

ent address: Dept of Physiology and Pharmacology, rsity of Strathclyde, 204 George Street, Glasgow W, UK.

Sci. 0031-613X/93/$06.00 © 1993 SCI. Printed in Great Britain

reported by Changeux *et al.*[8], it is possible that open channel-block occurs when levamisole enters the channel from the extracellular solution and binds to one of these charged rings. It was therefore of interest to determine if levamisole could also give rise to open channel-block by entering from the cytoplasmic solution.

2 METHODS

Recordings of single-channel currents resulting from the activation of nicotinic channels by levamisole were made from *Ascaris suum* muscle vesicles. In general the methods used are similar to those used in previous investigations with acetylcholine and levamisole.[7,9]

2.1 The vesicle preparation

Ascaris suum were collected from the local abattoir, maintained in Locke's solution (replaced daily) at 32 °C and used within four days. To prepare the vesicles, a 2-cm section from the anterior region of the worm was taken, cut along one of the lateral lines and pinned out on sylgard to form a muscle-flap preparation. The muscle flap was treated for 10 min at 37°C with a solution of the following composition: sodium chloride, 35; sodium acetate, 105; potassium chloride, 2; magnesium chloride, 2; 2-[4-(2-hydroxyethyl)piperazin-1-yl]-ethanesulfonic acid (HEPES), 10; glucose, 3; ascorbic acid, 2 mM; collagenase 1 mg ml^{-1}; pH adjusted to 7·2 with sodium hydroxide. The preparation was then maintained at 37°C in a collagenase-free solution of the same composition as above, but with the collagenase replaced by ethylenedioxybis(ethylenenitrilo)tetra (acetic acid) (EGTA), 1 mM. Over the next hour vesicles formed as outgrowths from the bag region of muscle cells. Vesicles were used within 5 h.

2.2 Recordings

The vesicles were transferred to the experimental chamber which was coated with polylysine to aid adherence and bathed at room temperature (15–22°C) in a solution of the following composition: cesium chloride, 35; cesium acetate, 105; magnesium chloride, 2; HEPES, 10; EGTA, 1 mM; pH adjusted to 7·2 with cesium hydroxide. The experimental chamber was mounted on the stage of a Reichert-Jung Biostar inverted microscope and viewed at × 200 magnification.

Single-channel currents from isolated inside-out patches were made and recorded using a List EPC-7 and a modified Sony digital audio processor (PCM 701ES) with a Sony Betamax video recorder (SL-HF100E). Patch-electrodes were made from micro-haematocrit capillary glass (Garner Glass 7052) and had resistance of 1–3 MΩ. The pipettes were coated with sylgard to improve frequency responses and filled with a solution of the following composition: cesium chloride, 140; magnesium chloride, 2; HEPES, 10; EGTA, 1 mM; levamisole, 2 μM; pH 7·2 with cesium hydroxide. Note that Cs^+ was the main cation in both the bath and pipette solutions to remove possible interference from K channels, known to occur in this preparation. The solutions were also calcium-free to remove the possible interference from Ca^{2+}-activated Cl^- channels also known to be present in this preparation.[10]

To determine the effect of intracellular application levamisole (30–926 μM) was also added to the bath solution therefore giving access to the cytoplasmic side of the inside-out patch.

2.3 Data processing

Records were analysed using a CED 1401 interface and a DCS286 PC Computer, with software kindly supplied by John Dempster, Strathclyde University. The records were filtered by an eight-pole Bessel filter, 3 dB, either at a frequency of 1·5 kHz with a sampling time of 70 μs or at a frequency of 1 kHz with a sampling time of 100 μs. This set-up gives a minimum resolvable interval of 0·30 ms. A 70% threshold for channel opening was set from channel amplitude histograms, therefore excluding all but full openings.

2.4 Exponential curve fitting

Exponential curves were fitted to the open and closed times by the method of maximum likelihood[11,12] to a probability density function (p.d.f.) of the form:

$$\text{p.d.f.} = \sum_{i=1}^{K} \frac{A_i e(-t/T_i)}{T_i}$$

where A_i = the area of the ith component; T_i = the fitted time constant; t = time and K = number of exponentials fitted.

2.5 Determination of the pKa of levamisole

A plot of the dependence of the pH on the addition of OH^- to a solution of levamisole yields a titration curve. The inflection point of this curve is the pKa.[13] In these experiments the pKa of levamisole was determined by titrating a solution of levamisole (10 mM; pH ~ 2·0 with hydrochloric acid) with sodium hydroxide (1 M). The pKa was then determined from the resulting graph.

2.6 Drugs

Levamisole, [(−)-(*S*)-2,3,5,6-tetrahydro-6-phenylimidazo[2,1-*b*]thiazole] was obtained as levamisole hydrochloride from Sigma Chemical Co., Fancy Road, Poole.

TABLE 1
Open-Time Kinetics for Levamisole-Activated Channels

Levamisole concentration (μM)		*Open-time kinetics*[a]			
Pipette	*Bath*	*A1*	*A2*	*T1*	*T2*
Membrane potential −75 mV					
2–10	0 ($n = 17$)[b]	0·66 (±0·06)	0·34 (±0·06)	0·88 (±0·10)	2·30 (±0·24)
2	0 ($n = 3$)	0·49 (±0·18)	0·51 (±0·18)	0·42 (±0·18)	2·98 (±0·34)
2	30	0·85	0·15	1·21	2·66
2	90	0·24	0·76	0·94	1·97
2	120		1		1·32
2	120		1		1·18
2	142		1		1·99
2	926		1		0·16
Membrane potential +75 mV					
3–10	0 ($n = 4$)[b]	0·65 (±0·10)	0·38 (±0·10)	0·71 (±0·10)	1·60 (±0·14)
2	0	0·56	0·44	0·55	2·37
2	0	0·59	0·41	0·59	2·40
2	30	0·42	0·58	0·48	3·37
2	60	0·91	0·08	0·82	3·63
2	71	0·52	0·48	0·35	1·87
2	90	0·51	0·49	0·89	2·99
2	807	0·62	0·58	0·65	1·74
2	807	0·80	0·20	1·23	1·90

Open kinetics: $T1$ and $T2$ are the time constants which represent mean durations of the open states; their areas are represented ..., $A1$ and $A2$ respectively; $A1 + A2 = 1$.
Data from Ref. 7.

Dorset BH17 7NH, UK. Collagenase, Sigma type 1A, was also obtained from Sigma Chemical Co.

2.7 Statistics

The degree of significance of r was tested using Student's two-tailed t-tests.

3 RESULTS

Application of levamisole (2 μM) to the extracellular surface of the patch resulted in channel activation. Kinetic analyses of these channels (Table 1) confirmed results found from previous investigations.[7] At both depolarised and hyperpolarised membrane potentials, the distributions of open times were best described by two exponentials and the distributions of closed states were best described by three exponentials. Since the number of open and closed states must at least equal the number of exponential components fitted,[14] it follows that these channels have at least two open states and three closed states.

3.1 Application of levamisole to the cytoplasmic surface of the membrane results in an increase in channel activity

Levamisole (2 μM) was applied in the pipette to induce nicotinic channel activation as described above. In eight out of nine experiments, addition of levamisole (30–926 μM) to the cytoplasmic surface of the patch via the bath solution resulted in an increase in channel activation. Figure 1 illustrates an experiment from an isolated inside-out patch: initially 2 μM levamisole was present in the extracellular solution. The addition of 71 μM levamisole to the cytoplasmic face of the patch is marked with an arrow. In this particular experiment the probability of a channel being open (P_{open}) increased from 0·0038 to 0·0225 on addition of levamisole to the bath solution. Control experiments showed that washing the cytoplasmic side of patch membranes with bath solution alone did not lead to an increase in channel activation ($n = 3$).

Cytoplasmic addition of levamisole increased P_{open} in a concentration-dependent manner at both depolarised and hyperpolarised membrane potentials (Table 2). There was a positive correlation between P_{open} and concentration, at both depolarised (correlation co-

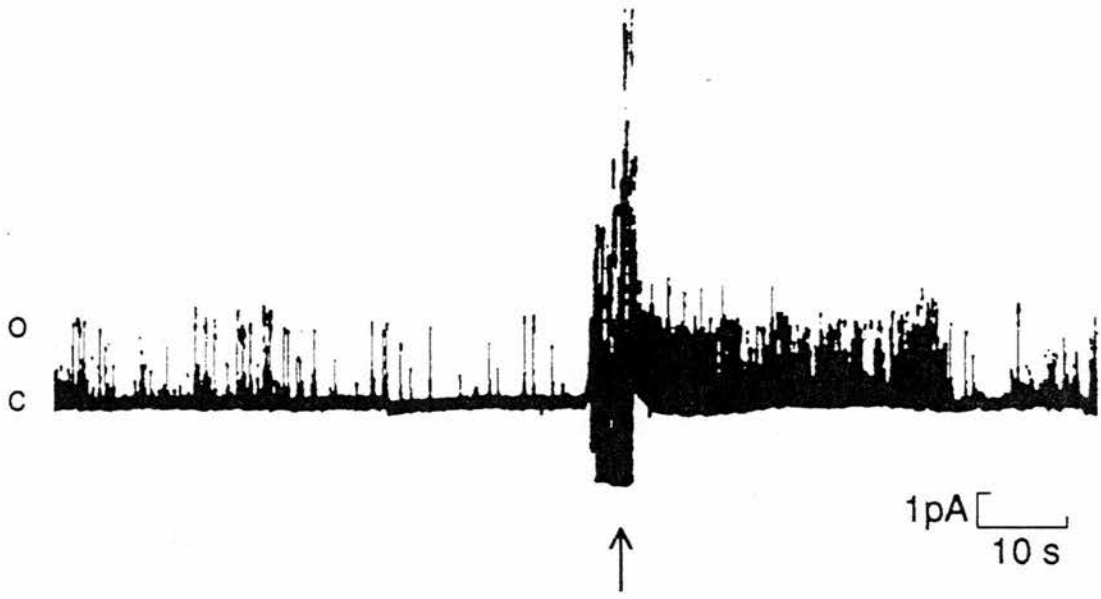


Fig. 1. Channel records from an isolated inside-out patch, +75 mV. Levamisole (2 μM) was present in the pipette to activate the nicotinic channels; the addition of 71·4 μM levamisole to the bath is shown by the arrow. In this experiment P_{open} increased from 0·0038 to 0·0225.

TABLE 2
Increase in P_{open} after the Addition of Levamisole to the Extracellular Solution[a]

Levamisole conc. (μM)	*Increase in* P_{open} (%)	
	Membrane potential	
	−75 mV	+75 mV
30	68	100
71·4	—	558
90	123	480
120	690	1200
120	287	250
142	−49	−40
807	1733	2967
926	1614	4614

[a] At both potentials these data can be fitted to a straight line using the method of least squares. At −75 mV the correlation coefficient (r) was 0·94 ($P < 0·005$) for a straight-line relationship. At +75 mV the correlation coefficient (r) was 0·96 ($P < 0·001$) for a straight-line relationship.

efficient (r): 0·96; $P < 0·001$) and hyperpolarised potentials (correlation coefficient (r): 0·94; $P < 0·005$).

3.2 Current–voltage relationships before and after bath application of levamisole

The increase in channel activity may be explained in one of two ways. Levamisole added to the cytoplasmic surface of the membrane may activate another type of channel or, in some way, cause an increase in opening of the nicotinic channels. Current–voltage relationships were therefore determined to see if the channels before and after cytoplasmic application of levamisole had the same conductance (Fig. 2). This experiment illustrated that there was no detectable change in the current-voltage relationship after the addition of levamisole to the bath and hence the experiment suggested that the increase in channel activity when levamisole was added to the bath was due to an increased opening of the nicotinic acetylcholine channels already activated by levamisole in the pipette.

3.3 High cytoplasmic concentrations of levamisole lead to desensitisation and open channel-block

3.3.1 Desensitisation

The addition of levamisole (30–926 μM) to the bath solution produced long closed periods between clusters of channel openings (Fig. 3). These closed-time durations lasted many seconds and were observed at both depolarised and hyperpolarised potentials. This desensitised condition was observed as an additional long closed state ($T4$) resulting in the distribution of closed times being best described by four exponentials. In one experiment, the addition of 807 μM levamisole to the bath solution (at +75 mV) resulted in the distribution of closed times being best described by four exponentials represented by the mean durations $T1$ (1·03 ms); $T2$ (9 ms); $T3$ (102 ms) and $T4$ (1077 ms). These very long closed durations (represented by $T4$) appear to correspond to a slow desensitisation process[13] and are similar to the very long closed times observed with high concentrations of acetylcholine and levamisole applied to the extracellular surface of membrane patches from *Ascaris*.[7,10] Similar

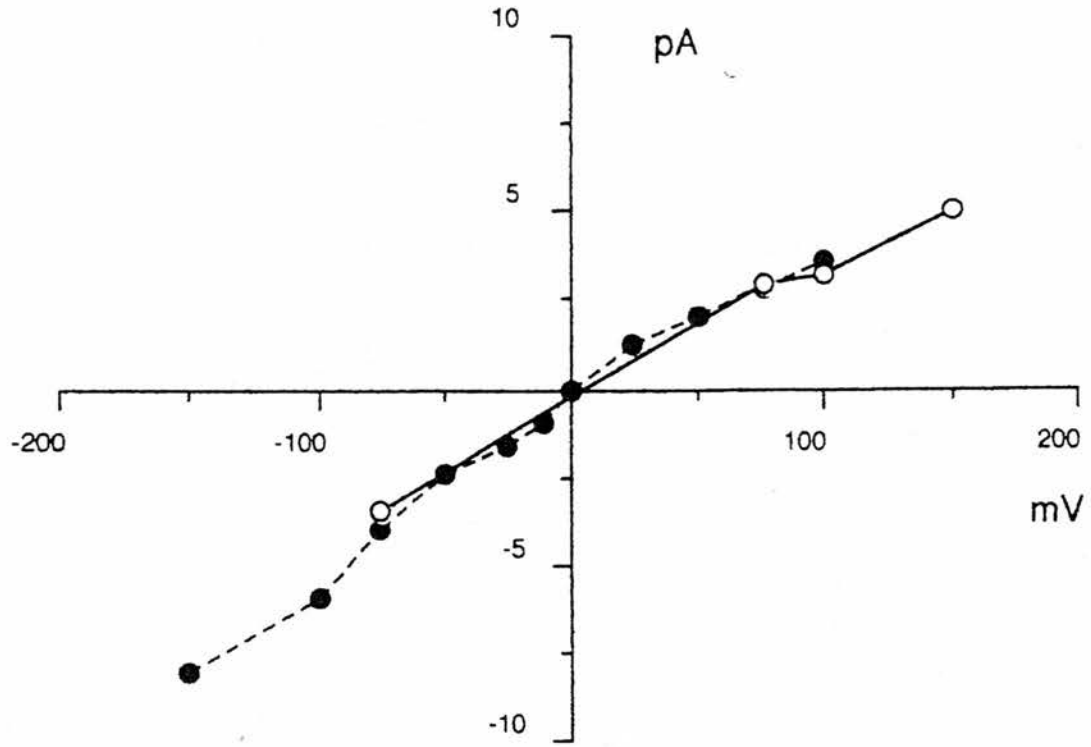


Fig. 2. (●) Current–voltage relationship for an experiment with 2 μM levamisole in the pipette compared to (○) current–voltage relationship after the addition of 142 μM levamisole to the bath solution.



Fig. 3. Channel records from an isolated inside-out patch with 2 μM levamisole in the pipette solution and 807 μM levamisole in the bath solution, +75 mV. The long closed periods are thought to represent the desensitised state of the receptor.

values were recorded in five other experiments at both depolarised and hyperpolarised membrane potentials.

3.3.2 *Channel-block*

Figure 4 illustrates channel openings at both depolarised and hyperpolarised potentials, following bath application of 926 μM levamisole. In this experiment, the mean open time at +75 mV was 1·35 ms, compared to the mean open time at −75 mV which was 0·16 ms.

Channel openings at +75 mV showed no evidence of alteration in mean open times with the addition of high concentrations of levamisole to the bath (Table 1). This result has also been observed with high extracellular levamisole concentrations.[7]

At hyperpolarised potentials, increasing cytoplasmic levamisole concentrations resulted in a marked reduction in the mean open times when compared to control values with just 2 μM levamisole in the pipette. Openings appeared in sequences separated by brief closings, characteristic of a 'flickering' open channel-block.[7,15] This behaviour only occurred during hyperpolarisation; the same phenomenon has been observed with high concentrations of extracellularly-applied levamisole (30–90 μM). This suggests that in both cases the block originates from the cationic agent, levamisole, acting from the same side of the channel (Fig. 4).

As stated earlier, the distribution of open times with 2 μM levamisole in the pipette, was best described by two exponentials; however on addition of increasing concentrations of levamisole to the bath solution, the distribution of open times at −75 mV was best described by a single exponential (Table 1). The loss of one exponential component has been reported in previous experi-

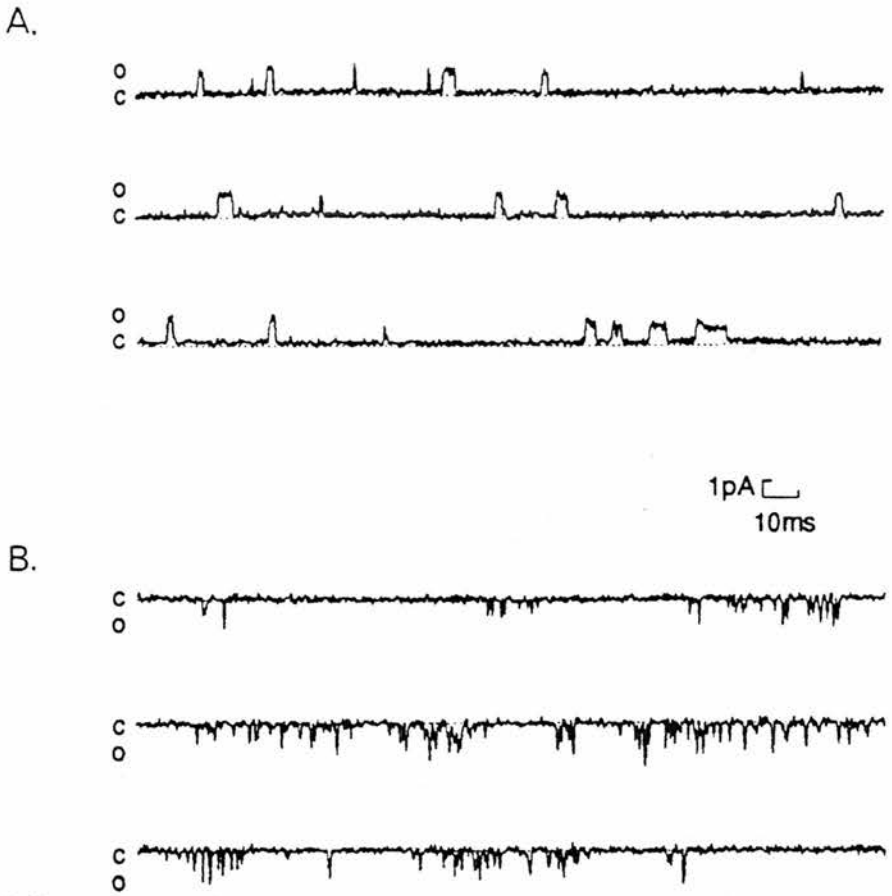


Fig. 4. Channel records from an isolated inside-out patch with 2 μM levamisole in the pipette and 926 μM levamisole in the bath solution. A. membrane potential +75 mV, mean open time 1·35 ms. B. membrane potential −75 mV, mean open time 0·19 ms

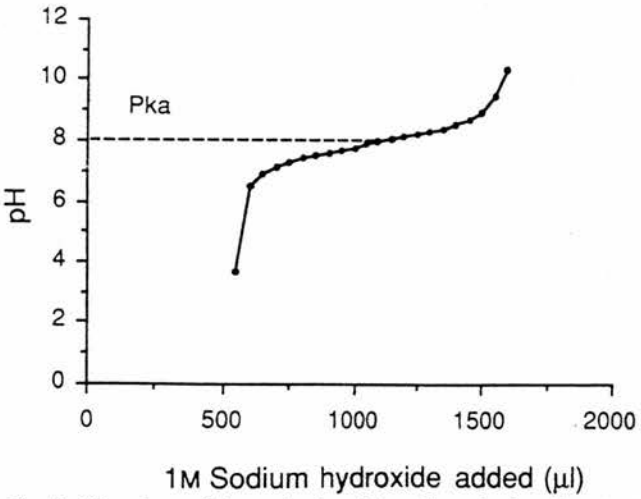


Fig. 5. Titration of levamisole with sodium hydroxide (1 M). The pKa of levamisole is 8·0.

ments with high extracellular concentrations of levamisole (90 μM).[7]

3.4 Does levamisole pass through the membrane?

One explanation for the increase in channel activity and alteration of channel kinetics with high concentrations of levamisole present in the bath solution is that levamisole in the uncharged form crosses the membrane, via the lipid phase, increasing the extracellular concentration of levamisole in the pipette. To determine the amount of un-ionised levamisole present in bath solutions, the pKa of levamisole was estimated from a simple titration of levamisole with sodium hydroxide (1 M) (Fig. 5). The pKa was calculated as 8·0; similar results were obtained in two other experiments. Using the Henderson Hasselbalch equation,[16] the ratio of the concentration of un-ionised to ionised levamisole was 0·158 at pH 7·2. Therefore approximately 16% of the levamisole is in the un-ionised form which may be able to diffuse across the membrane, down a concentration gradient and increase the extracellular concentration.

4 DISCUSSION

As previously reported, levamisole application (2 μM) to the extracellular face of the membrane patch activates single-channel currents with at least two open states and three closed states. The mean duration were comparable to those obtained in previous experiments.[7]

Application of high concentrations of levamisole (> 30 μM) to the bath solution altered channel kinetics an increase in P_{open}, open channel-block and desensi-

...ion were observed. Channel behaviour was similar ...hat observed in previous experiments with high ...acellular levamisole concentrations.[7]

...ith high concentrations of levamisole in the bath ...ion, no evidence of channel-block occurring at ...olarised membrane potentials was observed. This is ...ted by the fact that increasing the concentration of ...misole in the cytoplasmic solution at hyperpolarised ...mbrane potentials did not alter the open-time con...ts. If levamisole could enter the channel pore from ...cytoplasmic solution one would expect to observe ...nnel-block at depolarised potentials due to the ...onic nature of this drug. This finding suggests that ...*Ascaris* nicotinic channel has an asymmetric ...ture.

...hannel open times showed a marked reduction at ...5 mV as the concentration of bath-applied levamisole ...eased. With concentrations above 120 μM, the distri...ons of openings were best described by a single ...nential. It appears that open channel-block reduces ...mean open times $T1$ and $T2$; high concentrations ...120 μM) reduce $T1$ to such a level that it falls below ...limit of resolution of the recording system and can ...longer be detected. Such an effect has previously been ...orted with respect to open channel-block observed ...h 90 μM levamisole applied to the extracellular surface ...the pipette.[7] It is thus concluded that the reduction in ...n durations appears to be the result of a voltage-...sitive open channel-block, consistent with a cationic ...cking agent approaching the channel from the ...acellular side of the membrane.

...he detection of an additional closed state, repre...ting desensitisation, was observed with application of ...misole both to the cytoplasmic surface and to the ...acellular surface of the membrane. As desensitisation ...urs with high agonist concentrations the question ...efore became: did levamisole act on a receptor at a ...oplasmic site or did it diffuse across the membrane, ...easing the concentration in the extracellular sol...n? As already shown, 16% of levamisole at pH 7·2 ...in the un-ionised form, which is able to diffuse across ...membrane. The membrane-crossing property of ...misole is consistent with the observations that ...lication of levamisole to the bath solution: (i) did not ...r channel conductance; (ii) increased channel ac...y; (iii) induced a desensitised state and; (iv) produced ...oltage-sensitive open channel-block on hyper...arisation. It is pointed out that high extracellular concentrations of levamisole also produced these same effects and that levamisole has previously been reported to cross membranes in *Ascaris suum*.[17,18] The ability to cross lipid barriers like membrane or cuticle has an obvious therapeutic significance for the treatment of parasitic infestations.

ACKNOWLEDGEMENT

We would like to thank Merck Sharp & Dohme for financial support.

REFERENCES

1. Aceves, J., Erli, J. D. & Martinez-Maranon, R., *Brit. J. Pharmacol.*, **38** (1970) 602–7.
2. Van Neuten, J. M., In *Comparative Biochemistry of Parasites*. ed. H. Vanden Bossche. Academic Press, New York, 1972, pp. 101–15.
3. Coles, G. C., East, J. M. & Jenkins, S. N., *Gen. Pharmacol.*, **6** (1975) 309–13.
4. Martin, R. J., *Brit. J. Pharmacol.*, **77** (1982) 255–65.
5. Harrow, I. D. & Gration, K. A. F., *Pestic. Sci.*, **16** (1985) 662–72.
6. Colquhoun, L., Holden-Dye, L. & Walker, R. J., *J. Exp. Biol.*, **158** (1991) 509–30.
7. Robertson, S. J. & Martin, R. J., *Brit. J. Pharmacol.*, **108** (1993) 170–8.
8. Galzi, J.-L., Revah, R., Bessis, A. & Changeux, J.-P., *Annu. Rev. Pharmacol.*, **31** (1991) 37–72.
9. Pennington, A. J. & Martin, R. J., *J. Exp. Biol.*, **154** (1990) 201–21.
10. Thorn, P. & Martin, R. J., *Quart. J. Exp. Physiol.*, **72** (1987) 31–49.
11. Colquhoun, D. & Sigworth, F. W., In *Single Channel Recordings*, ed. B. Sackman & E. Neher. Plenum Press, New York, 1983, pp. 191–264.
12. Martin, R. J., *Brit J. Pharmacol.*, **84** (1985) 445–61.
13. Cachelin, A. B. & Colquhoun, D., *J. Physiol.*, **415** (1989) 159–88.
14. Colquhoun, D. & Hawkes, A. G., *Phil. Trans. Roy. Soc. London Ser. B*, **300** (1982) 1–59
15. Neher, E. & Steinbach, J. H., *J. Physiol.*, **277** (1978) 153–76.
16. In *Biochemistry*, ed. L. Stryer. Freeman & Co., New York, 1988, 3rd edn, pp. 41–42.
17. Verheyen, A., Borgers, M., Vanparijs, O. & Thienpont, D., In *Biochemistry of Parasites and Host Parasite Relationships*, ed. H. Vanden Bossche. Elsevier, Amsterdam, 1976, pp. 605–18.
18. Vanden Bossche, H. & Janssen, P. A. J., *Life Sci.*, **6** (1967) 1781–92.

Reprinted from

European Journal of Pharmacology

European Journal of Pharmacology 271 (1994) 273–282

The action of pyrantel as an agonist and an open channel blocker at acetylcholine receptors in isolated *Ascaris suum* muscle vesicles

Susan J. Robertson [a,*], Anne J. Pennington [b], A. Mark Evans [a], Richard J. Martin [a]

[a] *University of Edinburgh, Department of Preclinical Veterinary Sciences, Royal Dick School of Veterinary Sciences, Summerhall, Edinburgh, EH9 1QH, UK*

[b] *University of Edinburgh, Department of Pharmacology, 1 George Square, Edinburgh, EH8 9JZ, UK*

Received 28 June 1994; revised MS received 29 August 1994; accepted 16 September 1994



ELSEVIER

European Journal of Pharmacology

The EUROPEAN JOURNAL OF PHARMACOLOGY publishes manuscripts on the mechanisms of action of chemical substances affecting biological systems.

Manuscripts submitted to the journal are only accepted on the understanding that: (1) they are subject to editorial review; (2) they have not been and will not be published in whole or in part in any other journal; (3) the recommendations from the declaration of Helsinki and the internationally accepted principles in the care and use of experimental animals have been adhered to.

In addition to full length papers, the journal publishes short communications and rapid communications. Acceptability of rapid communications will be decided by the editors of the journal, who will be advised by an external referee. Full length manuscripts and short communications are generally submitted to 2 referees who are chosen for their ability to evaluate the work. Authors may request that certain referees should not be chosen. Members of the editorial board will usually be called upon for advice when there is disagreement among the referees or between referees and authors, or when the editors believe that the manuscript has not received adequate consideration from the referees. In order to reduce mailing cost, manuscripts will not be returned. Only the decision of the editorial office, together with the advice of the referees will be sent to the author(s). Referees will be requested to keep the copy of the manuscript which they have received for evaluation, and to destroy it once they have been notified of the final decision concerning the manuscript. When authors submit a revised manuscript, they should reply to the comments of the referees, indicating which comments have been incorporated and the reasons for disregarding any suggestions considered unacceptable. Revised manuscripts should be returned in duplicate to the editors. A revised manuscript should be received by the editorial office not later than 5 weeks (in case of minor revision) or 10 weeks (in case of extensive revision) after the editorial decision was sent to the author(s); otherwise it will be processed as a new manuscript. Handwritten additions or corrections will not be accepted. Only complete retyping of the pages affected by revision is acceptable.

For further information please refer to the 'General instructions' at the end of this issue, and the 'Notice to authors' published in Vol. 251, No. 1, p. v.

Editors

D. DE WIED, Utrecht (chairman) J. BRUINVELS, Utrecht F.P. NIJKAMP, Utrecht D.H.G. VERSTEEG, Utrecht

Editorial board

J. ARNT, Valby
P.J. BARNES, London
J. BOCKAERT, Montpellier
J. BORRELL, Madrid
T.F. BURKS, Houston
E. COSTA, Orangeburg
G. DI CHIARA, Cagliari
F.J. EHLERT, Irvine
J.P.M. FINBERG, Haifa
J.A. GARCÍA-SÁINZ, Mexico
H. GLOSSMANN, Innsbruck
A.R. GREEN, London
A. HERMAN, Antwerpen
J.P. HUIDOBRO-TORO, Santiago
Y. IGNATOV, Leningrad
J.L. IMBS, Strasbourg
D.A. KHARKEVICH, Moscow
S.J. KONTUREK, Kraków
G. KUNOS, Richmond
R. KVETNANSKY, Bratislava
G. LAMBRECHT, Frankfurt/M
M. LE MOAL, Bordeaux
X.Y. LI, Shanghai
J.M. LUNDBERG, Stockholm
G.S. MARKS, Kingston
H. MATTHIES, Magdeburg
D.N. MIDDLEMISS, Harlow
H. MÖHLER, Zurich
H.R. OLPE, Basel
M. OTSUKA, Tokyo
G. PEPEU, Florence
U. RAVENS, Essen
J.A. RIBEIRO, Oeiras
M.R. ROSEN, New York
H.J. RUSKOAHO, Oulu
P.R. SAXENA, Rotterdam
P.L. SHARMA, Chandigarh
P.F. SPANO, Brescia
N.A. TERRAGNO, Buenos Aires
H. TESCHEMACHER, Lahn-Giessen
P.B.M.W.M. TIMMERMANS, Wilmington
T. TOMITA, Nagoya
D.J. TRIGGLE, Buffalo
E.S. VIZI, Budapest
R.J. WINQUIST, Ridgefield

Consultants

B. AHRÉN, Malmö; E. BEUBLER, Graz; M.G. BOGAERT, Gent; G. BURNSTOCK, London; R. BUSSE, Frankfurt/Main; R. CASTEELS, Leuven; N. CHAND, Cranbury; A.G. CHAPMAN, London; S.E. DAHLÉN, Stockholm; W. DE JONG, Strasbourg; A. DEN HERTOG, Groningen; H.N. DOODS, Biberach; S.H. FERREIRA, Ribeirao Preto; A.W. FORD-HUTCHINSON, Dorval; J.R. FOZARD, Basel; D. GANTEN, Berlin-Buch; J.F. GIUDICELLI, Le Kremlin-Bicêtre; R.J. GRYGLEWSKI, Kraków; H. HAMON, Paris; P. HOLZER, Graz; D. HOYER, Basel; L.J. IGNARRO, Los Angeles; L.L. IVERSEN, Harlow; S.D. IVERSEN, Oxford; G.A.R. JOHNSTON, Sydney; H. KARAKI, Tokyo; J.D. KOHLI, Lucknow; G.L. KOVÁCS, Szombathely; R. LAVERTY, Dunedin; B.E. LEONARD, Galway; J. LEYSEN, Beerse; W. LÖSCHER, Hannover; B.R. LUCCHESI, Ann Arbor; C.A. MAGGI, Florence; I.G. MARSHALL, Glasgow; J. McCULLOCH, Glasgow; M.J. MILLAN, Croissy-sur-Seine (Paris); A.H. MULDER, Amsterdam; T. NABESHIMA, Nagoya; R.J. NAYLOR, Bradford; D.J. NUTT, Bristol; J.M. PALACIOS, Barcelona; J.R. PARRATT, Glasgow; J.N. PENNEFATHER, Clayton; R. QUIRION, Verdun; M. RAITERI, Genova; M.J. RAND, Heathcote; D. REGOLI, Sherbrooke; B.P. ROQUES, Paris; J. SCHEEL-KRÜGER, Glostrup; H. SCHOEMAKER, Bagneux; K. SCHRÖR, Düsseldorf; P. SEEMAN, Toronto; E. SEIFEN, Little Rock; K.F. SEWING, Hannover; P. SKOLNICK, Bethesda; P. SNEDDON, Glasgow; S.H. SNYDER, Baltimore; N. SPERELAKIS, Cincinnati; K. STARKE, Freiburg; H.A.J. STRUYKER BOUDIER, Maastricht; H. TAKAGI, Kyoto; R.K. TÜRKER, Ankara; P.A. VAN ZWIETEN, Amsterdam; B.B. VARGAFTIG, Paris; J.R. WALTERS, Bethesda; J. ZAAGSMA, Groningen

ELSEVIER

European Journal of Pharmacology 271 (1994) 273–282

ejp

The action of pyrantel as an agonist and an open channel blocker at acetylcholine receptors in isolated *Ascaris suum* muscle vesicles

Susan J. Robertson [a,*], Anne J. Pennington [b], A. Mark Evans [a], Richard J. Martin [a]

[a] *University of Edinburgh, Department of Preclinical Veterinary Sciences, Royal Dick School of Veterinary Sciences, Summerhall, Edinburgh, EH9 1QH, UK*

[b] *University of Edinburgh, Department of Pharmacology, 1 George Square, Edinburgh, EH8 9JZ, UK*

Received 28 June 1994; revised MS received 29 August 1994; accepted 16 September 1994

Abstract

The anthelmintic pyrantel is believed to act as an agonist at acetylcholine receptors on somatic muscle from the parasite *Ascaris suum*. This study aimed to confirm this mode of action of pyrantel. Single-channel recordings from muscle vesicles formed from the extrasynaptic region of the bag of somatic muscle cells of *Ascaris suum* were made using the patch-clamp technique. Pyrantel (0.03–100 μM) activated cation-selective channels with at least 2 conductance levels: main conductance 41 ± 2.04 pS (mean $\pm$S.E., $n = 28$), smaller conductance 22.4 ± 0.34 pS (mean $\pm$S.E., $n = 8$). The current/voltage plots showed a linear relationship. Detailed kinetic analysis revealed that activation of the receptor by pyrantel resulted in at least 2 distinct open and burst states and at least 3 distinct closed states. The mean open time of the channel, with 0.1 μM pyrantel, was 1.53 ± 0.22 ms (mean $\pm$S.E., $n = 7$) at -75 mV. We have previously shown that acetylcholine activated channels with similar properties to the pyrantel-activated channels (Pennington, A.J. and R.J. Martin, 1990, J. Exp. Biol. 154, 201) confirming that pyrantel is an acetylcholine agonist. With high concentrations (100 μM) of pyrantel a sequence of rapid openings and closings of the channel was observed, indicating the presence of an open channel block. Previous experiments have shown that the anthelmintic levamisole, which also acts as an acetylcholine agonist on this preparation, induced channel block at hyperpolarised potentials with high concentrations (Robertson, S.J. and R.J. Martin, 1993, Br. J. Pharmacol. 108, 170). A comparison is made of the actions of the 3 agonists pyrantel, levamisole and acetylcholine at the nicotinic receptor in *Ascaris* muscle, and implications for the therapeutic use of the compounds are discussed.

Keywords: Pyrantel; Acetylcholine; Ion channel; *Ascaris*, muscle; Anthelmintic; Parasitic nematode

1. Introduction

Anthelmintic drugs are widely used, worldwide, due to the common occurrance of infestation with intestinal nematodes in both humans and domestic animals. A greater understanding of the detailed mode of action of these drugs would aid in the most efficient use of the currently available compounds and the development of more effective drugs. One such anthelmintic, pyrantel, is thought to act as an acetylcholine agonist in the parasitic nematode *Ascaris suum* (Aubry et al., 1970; Van Neuten, 1972; Coles et al., 1975; Harrow and Gration, 1985). This parasite is found in the intestine of the pig and can result in severe economic loss if heavy infestation occurs. A close relative of *Ascaris suum* is the parasite *Ascaris lumbricoides* which inhabits the human gut. Thus studies on *Ascaris suum* are also informative for the control of human nematode parasites. *Ascaris suum* makes a suitable model for the investigation of the mode of action of anthelmintic compounds as it has large muscle cells which facilitate electrophysiological techniques.

The bag region of *Ascaris* somatic muscle cells is known to contain extrasynaptic receptors for acetylcholine (Brading and Caldwell, 1971; Martin, 1982). These acetylcholine receptors are blocked by *d*-tubo-

* Corresponding author. Present address: University of Strathclyde, Department of Physiology and Pharmacology, 204 George Street, Glasgow, G1 1XW, UK. Tel. 041-552-4400 ext. 2012, fax 041-552-2562.

0014-2999/94/$07.00 © 1994 Elsevier Science B.V. All rights reserved
SSDI 0014-2999(94)00570-2

curarine but not by atropine, and hence are classified as nicotinic (Natoff, 1969; Rozhkova et al., 1980; Martin, 1982; Colquhoun et al., 1991). Classification on the basis of potency of vertebrate ganglionic agonists suggests that the *Ascaris* nicotinic receptor may be similar to the vertebrate ganglionic receptor. However, the antagonist profile of this receptor makes the classification more difficult. Mecamylamine, a ganglionic antagonist, and benzoquinonium, a neuromuscular junction blocker, are the 2 most potent antagonists. The ganglionic blocker hexamethonium, in contrast, has only a weak antagonistic activity and the neuromuscular junction blockers, decamethonium, *d*-tubocurarine and pancurium were not potent (Natoff, 1969; Rozhkova et al., 1980; Colquhoun et al., 1991; Walker et al., 1991). The detailed pharmacological profile of this receptor differs from that of vertebrate nicotinic receptors, hence it is possible that anthelmintic compounds such as pyrantel and levamisole exploit therapeutic differences by acting selectively on the acetylcholine receptors of the parasite and not on those of the host.

Earlier studies on *Ascaris suum* have reported drug-induced contraction of *Ascaris suum* muscle, when acetylcholine, pyrantel or levamisole was applied to whole worms or to a flap preparation (Del Castillo et al., 1963; Aubry et al., 1970; Aceves et al., 1970; Van Neuten, 1972; Coles et al., 1975; Harrow and Gration, 1985). All 3 compounds caused depolarization and increased spike discharge frequency during intracellular recordings from the muscle cells. Studies using intracellular current-clamp and voltage-clamp techniques have shown that pyrantel increases the input conductance and depolarises the muscle cells of *Ascaris suum*, an action consistent with that of acetylcholine and levamisole (Harrow and Gration, 1985).

Our previous studies using the patch-clamp techniques (Pennington and Martin, 1990; Robertson and Martin, 1993) confirmed the presence of levamisole- and acetylcholine-activated cation-selective channels in the somatic muscle of *Ascaris suum*. We now present a detailed study of the action of pyrantel on these channels from the somatic muscle cells of *Ascaris suum*. Our data indicate that pyrantel is an agonist at the acetylcholine receptors and at higher concentrations produces open channel block. The properties of the 3 agonists: acetylcholine, pyrantel and levamisole are compared. Preliminary reports of these data have been published (Robertson et al., 1991, 1992).

2. Materials and methods

Experiments with pyrantel were performed in the same way as previous experiments with acetylcholine (Pennington and Martin, 1990) and levamisole (Robertson and Martin, 1993) so that the results would be directly comparable. The methods have been described previously (Martin, 1985; Martin et al., 1989) but are outlined below.

2.1. Electrophysiological recording

Ascaris suum from the local abattoir was kept in Locke's solution at 32°C, and used within 4 days. Muscle vesicles were prepared from a muscle-flap preparation, which was treated with collagenase solution for 10 min at 37°C (in mM): NaCl 35, Na acetate 105, KCl 2, $MgCl_2$ 2, Hepes 10, glucose 3, ascorbic acid 2, and collagenase 1 mg/ml (pH 7.2 with NaOH); and then kept in a maintenance solution at 37°C (in mM): NaCl 35, Na acetate 105, KCl 2, $MgCl_2$ 2, Hepes 10, glucose 3, ascorbic acid 2, and EGTA 1 (pH 7.2 with NaOH). The vesicles formed over the next hour and were used within 5 h. Vesicles were placed in a bathing solution containing (in mM): CsCl 35, Cs acetate 105, $MgCl_2$ 2, Hepes 10, and EGTA 1 (pH 7.2 with CsOH). Recordings were made from isolated inside-out patches or cell-attached patches at room temperature (15–22°C), using a List EPC-7 and a modified Sony digital audio processor with a Betamax video recorder. Patch electrodes were made from Garner glass 7052, coated with Sylgard, and fire polished. They had a resistance of 1–3 MΩ when filled with a solution containing (in mM): CsCl 140, $MgCl_2$ 2, Hepes 10 and EGTA 1 (pH 7.2 with CsOH) to which pyrantel (0.03–100 μM) was added. Ion selectivity of the channel was determined in inside-out patches by diluting bath solution 50:50 with distilled H_2O.

2.2. Data analysis

Records were analysed using a CED 1401 interface, a PC computer, and PAT software kindly supplied by Dr. John Dempster, Strathclyde University. Records were filtered by an eight-pole Bessel filter, −3 dB, 1.5 kHz; the sampling time was 70 μs and the minimum detectable interval was 0.30 ms. The threshold for channel opening was set, from channel amplitude histograms to include only full openings, usually at 70% of the channel amplitude. In some experiments a 50% threshold was also used to examine the effect on open times, but little practical difference was observed. Individual channel activations were interrupted with short closed periods, so bursts of openings as well as single openings were considered. Bursts were defined as groups of openings separated by gaps that are shorter than a specified length (τ_{crit}), which was determined by the method of Colquhoun and Sakmann (1985). In general a value of 1 ms was used in these experiments; this particular value was not very important since gaps between bursts were several hundred-fold larger than gaps within bursts. However, at hyperpolarised poten-

tials when channel block was observed τ_{crit} values of up to 5.3 ms were sometimes used.

2.3. Exponential curve fitting

Exponential curves were fitted to the open, closed, and burst times by the method of maximum likelihood (Colquhoun and Sigworth, 1983; Martin, 1985). After exponential components were fitted to the apparent burst and closed durations, it was possible to correct the data for missing events, using the method of Colquhoun and Sigworth (1983) and Colquhoun and Sakmann (1985).

2.4. The simple sequential channel-block model

The simple sequential channel-block scheme described by Adams (1976) and Colquhoun and Sakmann (1985) was used to describe the open channel block observed with pyrantel. This allowed comparison with experiments performed with levamisole-activated channels (Robertson and Martin, 1993) in the same preparation:

$$C \underset{\alpha}{\overset{\beta'}{\rightleftharpoons}} O \underset{k_{-B}}{\overset{k_{+B} \cdot X_B}{\rightleftharpoons}} B$$

where C denotes the closed state; O denotes the open state; B denotes the blocked state; X_B is the drug concentration; k_{+B} is the blocking rate constant; k_{-B} is the unblocking rate constant; α is channel closing rate and β' is the channel opening rate. The model predicts that: mean open-time $= 1/(\alpha + k_{+B} \cdot X_B)$; mean block-time $= 1/k_{-B}$; channel-block dissociation constant, $K_B = k_{-B}/k_{+B}$. The slope of the reciprocal plot of mean durations of long openings (τ_2) against pyrantel concentration was used to determine values for k_{+B}. The mean block durations were determined by selecting the distinctive blocked times seen during flickering bursts greater than 0.3 ms (the limit of resolution of the set-up). The method of maximum likelihood was then used to fit a single exponential to obtain a value for the mean block duration.

2.5. Drugs

Pyrantel ((*E*)-1,4,5,6-tetrahydro-1-methyl-2-[2-(2-thienyl)vinyl] pyrimidine) was obtained as pyrantel tartrate, kindly supplied by Pfizer (Sandwich, Kent, UK). Collagenase, Sigma type 1A, was supplied by Sigma Chemical Company.

2.6. Statistical analysis

The method of least squares was used to obtain the best fits for the exponential equations used to describe

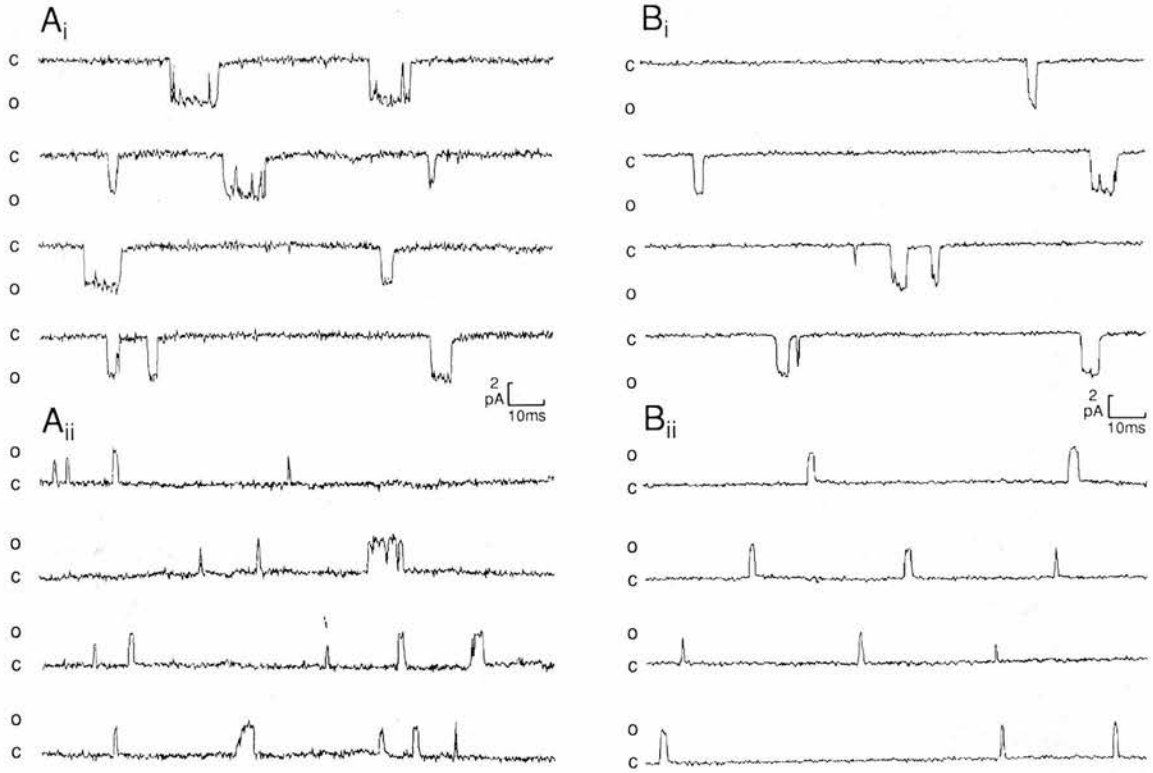


Fig. 1. (A) Pyrantel-activated channels from a cell-attached patch illustrating the voltage sensitivity of open-time duration, 0.1 μM. (i) Individual channels recorded at −75 mV. The corrected mean open time was 1.63 ms. (ii) Individual channels recorded at +75 mV. The corrected mean open time was 0.97 ms. (B) Acetylcholine-activated channels from a cell-attached patch, 3μM. (i) Individual channels recorded at −75 mV. The corrected mean open time was 1.55 ms. (ii) Individual channels recorded at +75 mV. The corrected mean open time was 1.1 ms. C: denotes the closed state. O: denotes the open state.

the voltage sensitivity of the rate constants k_{+B} and k_{-B} and the dissociation constant K_B; a Spearman correlation coefficient (r) was used to test the quality of the fits. Levels of significance were tested using Student's t-tests, using a significance level of 0.05.

3. Results

3.1. Single-channel currents

The results reported here for 0.03–100 μM pyrantel were obtained from a series of 297 patches, with pyrantel present in the pipette from the beginning of the recording; 42% of patches studied contained pyrantel-activated ion channels. The channels had short mean open times in the range of a few milliseconds, and looked similar to channels activated previously by acetylcholine (Pennington and Martin, 1990). Single-channel currents activated either by pyrantel or by acetylcholine are illustrated in Fig. 1. In 20 control experiments with no pyrantel or acetylcholine in the patch pipette no such channel openings were observed.

3.2. Current-voltage relationships and channel conductance

Using isolated inside-out patches, with solutions containing symmetrical cation concentrations but non-symmetrical anion concentrations, the reversal potentials for the pyrantel-activated channels were near zero (2.77 ± 0.89 mV, mean $\pm$ S.E., $n = 28$) and the current-voltage plots were linear ($n = 28$). Under these conditions the predicted reversal potential for a cationic

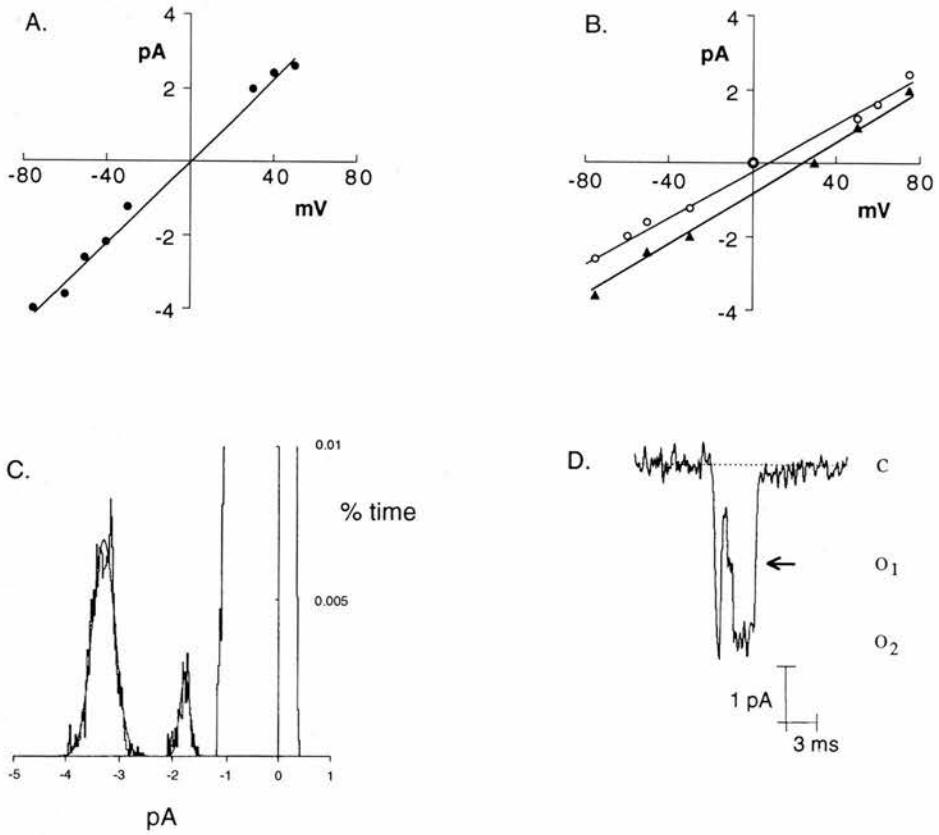


Fig. 2. (A and B) I/V plots for cation channels activated by 1 μM pyrantel. (A) Cell-attached patch, slope conductance = 54 pS, reversal potential = -1.5 mV, correlation = 0.969, $n = 8$. (B) Inside-out patch, initial (○): slope conductance = 31 pS, correlation = 0.994, $n = 8$ (140 mM Cs^+, 39 mM Cl^-); with diluted bath solution (70 mM Cs^+, 9.5 mM Cl^-, ▲): slope conductance = 36 pS, correlation = 0.997, $n = 6$. Predicted reversal potentials with the original bath solution (○) were Cl^- : -33 mV and Cs^+ : 0 mV and with the diluted bath solution (▲) were Cl^- : -51 mV and Cs^+ : 18 mV. The actual reversal potentials were 5.03 mV and 23 mV consistent with a cation conductance. (C and D) For a cell-attached patch, at -75 mV, with 0.03 μM pyrantel. (C) An all-points histogram showing distribution of channel amplitude. The amplitude histogram has 2 open conductance levels fitted by 2 gaussian curves: mean 3.3 ± 0.30 pA (44 pS) and 1.8 ± 0.52 pA (24 pS) (means $\pm$S.D.). (D) Illustration of a single-channel opening. C: denotes the closed state. O_2 denotes a main conductance of 3.19 pA (42 pS) and O_1 a lower conductance which appears as a shoulder on the main conductance of 1.84 pA (24 pS); this smaller conductance appears to be a subconductance state.

conductance is 0 mV and an anionic conductance is −33 mV, hence the results indicate that pyrantel activates a cation-selective channel (Fig. 2). This was further tested by altering the cation and anion concentrations by diluting the bath solution 50:50 with distilled water: the observed shifts in reversal potential were found to be consistent with those predicted by the Nernst equation for a cation conductance.

Pyrantel (0.03–100 μM) activated channels with 2 distinguishable conductance levels: 41 ± 2.04 pS (mean ± S.E., $n = 28$) and 22.4 ± 0.34 pS (mean ± S.E., $n = 8$). Occasionally even smaller conductance levels were also observed. Channel openings were sometimes observed to step from one conductance level to another (Fig. 2). This may represent the transition from the main conductance level to a smaller subconductance level. However, the presence of 2 channels with different conductances cannot be excluded.

3.3. Exponential curve fitting

The data files used for the subsequent analysis were obtained from experiments with a sufficiently high channel frequency; the number of events analysed varied from 200 to 1500. Only the larger conductance channel was analysed. These experiments were performed on cell-attached or inside-out patches, with 0.1–100 μM pyrantel present in the patch pipette. In general the open and burst times were best-fitted by the sum of 2 exponentials and the closed times by the sum of 3 exponentials (Figs. 3 and 4). Assuming that the channel can exist in several more-or-less discrete states and that the rate constants for transitions between states are constant (as do Colquhoun and Sakmann, 1985), then the number of open states of the channel must at least equal the number of exponential components needed to fit the open-time distribution (Colquhoun and Hawkes, 1982). This indicates the presence of at least 2 open and 2 burst states and at least 3 closed states. Higher concentrations of pyrantel (100 μM) resulted in significant changes in channel kinetics: the loss of one open state at hyperpolarised potentials and the presence of an additional closed state at both depolarised and hyperpolarised potentials. This will be considered subsequently under the sections 3.8 'Channel block' and 3.10 'Desensitisation'.

3.4. Open-time distributions show a degree of voltage sensitivity

Open-time kinetics were analysed for a range of pyrantel concentrations (0.1–100 μM) and a variety of potentials (±50, ±75, ±100 mV). At low concentrations (0.1–10 μM) the open-time durations can best be described by the sum of 2-exponential components as

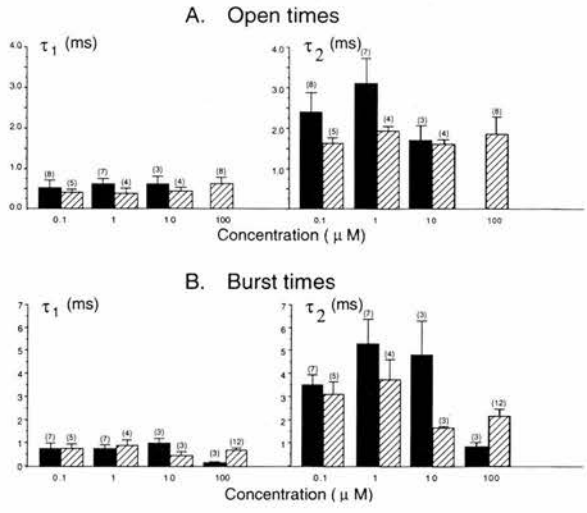


Fig. 3. Histograms of the time constants (τ_1 and τ_2) obtained by fitting 2-exponential components to: (A) open times and (B) burst times, at −75 mV (■) and at +75 mV (□). Data are means ± S.E., with n numbers in brackets. At most concentrations of pyrantel the open and burst time durations were best described by the sum of 2-exponential components with time constants τ_1 and τ_2. With high concentrations (100 μM) some of the data was best described by 1-exponential component. The bars for 100 μM represent values when 2-exponential components best described the data, when 1-exponential was the best representation for the data the values for τ (ms) for the open times were 0.30 ± 0.02 ($n = 11$) at −75 mV and 0.61 ± 0.17 ($n = 6$) at +75 mV, and for the burst times were 0.43 ± 0.02 ($n = 8$) at −75 mV and 0.90 ($n = 2$) at +75 mV.

is illustrated for ±75 mV in Fig. 3. Data at −75 mV with 0.1 μM pyrantel show 2-exponential components with means 0.52 ms and 2.40 ms. Channel open times showed a degree of voltage sensitivity; in general the corrected mean open times (CMOT) were longer at hyperpolarised potentials than at depolarised potentials (Fig. 3), and the open times tended to be longer the more strongly hyperpolarised the membrane was and become shorter as the membrane was more strongly depolarised. For example for 0.1 μM pyrantel the CMOT at −100 mV, −75 mV, −50 mV and +75 mV were 1.71 ± 0.39 ms (4), 1.53 ± 0.22 ms (7), 1.23 ± 0.16 ms (5) and 0.78 ± 0.13 ms (5) respectively, while for 1 μM pyrantel the CMOT at −75 mV, +75 mV and +100 mV were 2.47 ± 0.45 (5), 1.28 ± 0.17 (4) and 1.08 ± 0.29 (3) respectively (values are means ± S.E., followed by n number). The values for +75 mV are significantly shorter ($P < 0.01$) than at −75 mV, and the values at ±75 mV for the whole range of concentrations used are given in Table 1. With higher concentrations of pyrantel (100 μM) the opening durations dramatically reduced at hyperpolarised potentials (Fig. 3) resulting in the open durations being best described by 1-exponential component. This was thought to be due to open channel block (see below).

3.5. Burst-time distributions exhibit a degree of voltage sensitivity

Burst-time kinetics were analysed for a range of pyrantel concentrations (0.1–100 μM) and a variety of potentials ($\pm$50, $\pm$75, $\pm$100 mV). Bursts were described as a sequence of openings separated by closing shorter than a specified length τ_{crit} (see Materials and methods). At low concentrations (0.1–10 μM) the burst durations can best be described by the sum of 2-exponential components as is illustrated for $\pm$75 mV in Fig. 3. Data for 0.1 μM pyrantel at $-$75 mV show 2-exponential components with mean durations 0.75 ms and 3.49 ms. With low concentrations the burst-time durations also showed a degree of voltage sensitivity (Table 1); for example for 0.1 μM pyrantel the corrected mean burst duration (CMBD) at $-$100 mV, $-$75 mV, $-$50 mV and +75 mV were 2.51 $\pm$ 0.36 ms (3), 2.28 $\pm$ 0.42 ms (6), 1.58 $\pm$ 0.30 ms (5) and 1.12 $\pm$ 0.21 ms (5) respectively, while for 1 μM pyrantel the CMBD at $-$75 mV, +75 mV and +100 mV were 3.25 $\pm$ 0.91 (4), 1.91 $\pm$ 0.49 (4) and 1.46 $\pm$ 0.20 (3) respectively (values are means $\pm$S.E., followed by n number). The values for +75 mV are significantly shorter ($P < 0.02$) than at $-$75 mV.

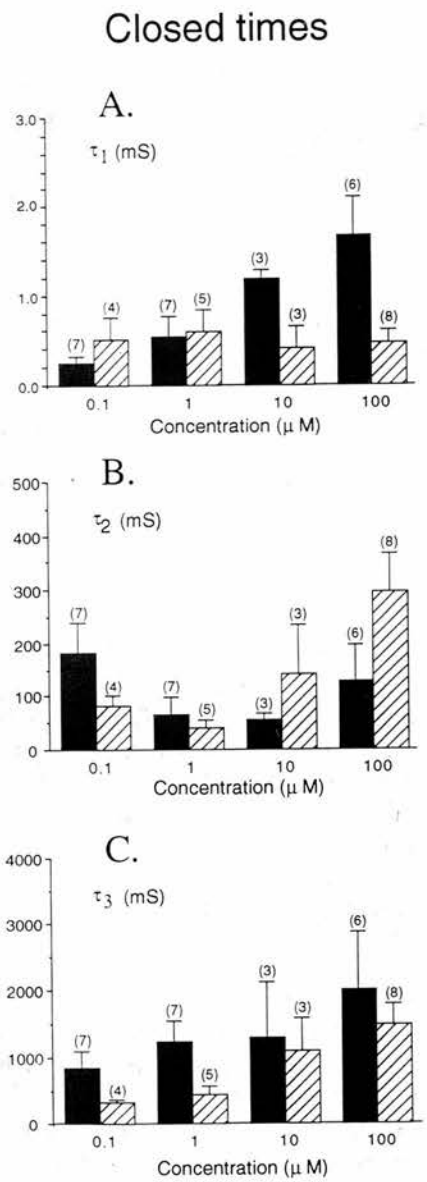


Fig. 4. Histograms of the time constants (τ_1, τ_2 and τ_3) obtained by fitting 3-exponential components to the closed times, at $-$75 mV (■) and at +75 mV (□). Data are means $\pm$S.E., with n numbers in brackets. τ_1, τ_2 and τ_3 are illustrated in parts (A), (B) and (C) respectively. At most concentrations the closed time durations were best described by the sum of 3-exponentials; however, with 100 μM the closed times were occasionally best described by 4-exponential components; this additional component τ_4, is not shown in the figure.

Table 1
Values for CMOT and CMBD for pyrantel at membrane potential $\pm$75 mV

Pyrantel concentration	Corrected mean open times (ms)	
	$-$75 mV	+75 mV
0.1 μM	1.53 $\pm$ 0.22 (n = 7)	0.78 $\pm$ 0.13 (n = 5)
1 μM	2.47 $\pm$ 0.45 (n = 5)	1.28 $\pm$ 0.17 (n = 4)
10 μM	1.49 $\pm$ 0.18 (n = 4)	0.88 $\pm$ 0.04 (n = 4)
100 μM	0.40 $\pm$ 0.03 (n = 10)	1.10 $\pm$ 0.14 (n = 11)
Pyrantel concentration	Corrected mean burst durations (ms)	
	$-$75 mV	+75 mV
0.1 μM	2.28 $\pm$ 0.42 (n = 6)	1.12 $\pm$ 0.21 (n = 5)
1 μM	3.25 $\pm$ 0.91 (n = 4)	1.91 $\pm$ 0.49 (n = 4)
10 μM	1.73 $\pm$ 0.22 (n = 5)	1.10 $\pm$ 0.04 (n = 4)
100 μM	0.80 $\pm$ 0.18 (n = 10)	1.47 $\pm$ 0.27 (n = 11)

Corrected values for mean open time (CMOT) and for mean burst duration (CMBD).

At higher concentrations of pyrantel, values for burst durations reduced at hyperpolarised potentials but not at depolarised potentials, compared to the values obtained for lower concentrations of pyrantel. For example with 100 μM pyrantel at $-$75 mV, the CMBD was 0.80 $\pm$ 0.18 ms (mean $\pm$ S.E., n = 10), which is significantly shorter ($P < 0.001$) than values with 0.1 μM pyrantel (2.28 ms). This resulted in some of the burst distributions at higher concentrations being described by a single-exponential component (Fig. 3), as was the case for some open-time distributions.

3.6. Closed-time distribution

Closed-time kinetics were analysed for a range of pyrantel concentrations (0.1–100 μM) and a variety of potentials ($\pm$50, $\pm$75, $\pm$100 mV). The closed durations can best be described by the sum of 3-exponential components, indicating the presence of at least 3 closed states as is illustrated for $\pm$75 mV in Fig. 4. Data for 0.1 μM pyrantel at $-$75 mV show that the closed-time

Table 2
Values for P_{open} for pyrantel-activated channels at membrane potentials of ±75 mV

Concentration	P_{open}	
	−75 mV	+75 mV
0.03 μM	0.0065 ± 0.0020 (4)	--
0.1 μM	0.0077 ± 0.0020 (6)	0.0061 ± 0.0021 (6)
1 μM	0.0055 ± 0.0024 (7)	0.0037 ± 0.0013 (5)
10 μM	0.0033 ± 0.0013 (5)	0.0023 ± 0.0009 (5)
100 μM	0.0011 ± 0.0005 (10)	0.0036 ± 0.0008 (14)

durations were best described by the sum of 3-exponentials with means 0.25 ms, 182 ms, and 840 ms. As the concentration of pyrantel was increased (100 μM) an additional closed state was observed, thought to be due to the phenomenon of desensitisation; this additional component is not illustrated in Fig. 4.

3.7. P_{open}

Values for P_{open} were determined for concentrations of pyrantel between 0.03 and 100 μM. At the lower concentrations (0.1–10 μM) there was no significant difference between values for P_{open} at depolarised and hyperpolarised potentials (Table 2). A concentration-dependent effect on P_{open} was observed at hyperpolarised potentials but not depolarised potentials. The value for P_{open} at −75 mV with 100 μM pyrantel in the pipette solution (0.0011 ± 0.0005; mean ± S.E., $n = 10$) was significantly lower than values for P_{open} with lower concentrations ($P < 0.03$).

3.8. Channel block

With higher concentrations of pyrantel (100 μM) there was an obvious change in the open-time kinetics of the channel at hyperpolarised potentials, channel openings were briefer and occasionally appeared as a sequence of rapid openings separated by brief closing reminiscent of a flickering channel block (Fig. 5). Thus it appeared that in addition to its action as an agonist, pyrantel may enter the channel pore to effect an open channel block. The voltage-sensitive nature of this block is consistent with the cationic charge of pyrantel. In order to describe this effect further, a simple sequential channel-block model (Adams, 1976; Colquhoun and Sakmann, 1985) was used.

The simple channel-block model predicts a decrease in open times with increasing concentration of blocker; Table 1 shows that in these experiments there was a significant reduction in the CMOT at hyperpolarised potentials with increasing concentrations of pyrantel. For example at −75 mV with 0.1 μM pyrantel, the open-time duration was best fitted by the sum of 2-exponential components with time constants 0.52 ms and 2.40 ms and the CMOT was 1.53 ms. At −75 mV with 100 μM pyrantel, the open-time durations were best described by 1-exponential component with time constant 0.30 ms and the CMOT at this concentration was 0.40 ms. This represents a significant reduction in CMOT with concentrations of pyrantel of 0.1 μM and 100 μM, $P < 0.001$. The reduction in CMOT was due to a reduction in duration of both the brief (τ_1) and longer (τ_2) openings (Fig. 3). It appeared that the reduction in brief openings led to the values of τ_1 falling below the limit of resolution of the recordings. Thus with 100 μM pyrantel, only 1-exponential component was resolved in the open-time distributions. The long open times (τ_2) were used in preference to the brief open times, since they were better resolved. An estimate of the forward channel blocking rate, k_{+B}, was determined from the reciprocal plot of the open-time constant, τ_2, against concentration (see Materials and methods); the slope of this plot represents k_{+B} and the intercept α. Values were determined at both −50 mV and −75 mV. At −50 mV, α was 840 s^{-1} and k_{+B} was 2.18×10^7 M^{-1} s^{-1}, a line was fitted to the data by the method of least squares and had a correlation coefficient of 0.913; at −75 mV α decreased to 380 s^{-1} and k_{+B} increased to 3.09×10^7

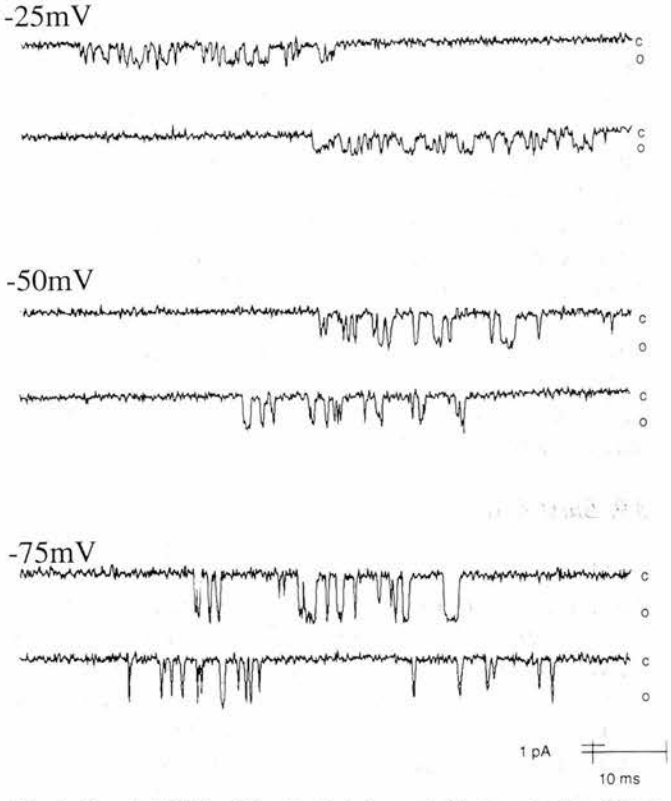


Fig. 5. Pyrantel (100 μM) activated channels C: denotes the closed state. O: denotes the open state. Channel openings at membrane potentials −25 mV, −50 mV, −75 mV. Note the difference in scale from Fig. 1.

M^{-1} s^{-1}. This represents an e-fold change in k_{+B} every 72 mV.

Estimates of the unblocking rate constant k_{-B} were determined from the reciprocal of the mean block durations observed with 100 μM pyrantel. The mean block durations were 1.43 ± 0.24 ms (mean ± S.E., n = 11) at −75 mV and 1.23 ± 0.01 ms (mean ± S.E., n = 3) at −50 mV. Thus there appeared to be an increase in the mean block time with increasing hyperpolarisation but the results did not reach statistical significance. However, in one good experiment the voltage sensitivity was quite evident. The mean block duration was 0.76 ms at −25 mV, 1.14 ms at −50 mV and 1.48 ms at −75 mV. The voltage sensitivity of k_{-B} was described for this experiment by the equation: $k_{-B} = k_{-B0} \cdot \exp(E/V\text{k})$, where k_{-B} is the unblocking rate constant at membrane potential E, k_{-B0} is the value for the unblocking rate constant at 0 mV and Vk is a constant. The value for k_{-B0} was 1.80 ms^{-1} and Vk was 67.5 mV suggesting an e-fold change in k_{-B} every 67 mV.

It was possible from the values determined for k_{-B} and k_{+B} to calculate the dissociation rate constant for open channel block ($K_B = k_{-B}/k_{+B}$). At −50 mV, K_B was 37 μM (0.81×10^3 $s^{-1}/2.18 \times 10^7$ M^{-1} s^{-1}) and at −75 mV, K_B was 20 μM (0.61×10^3 $s^{-1}/3.09 \times 10^7$ M^{-1} s^{-1}); this represents an e-fold change every 40 mV. In accordance with the channel-block model for a cationic channel blocker, K_B decreased with membrane hyperpolarisation.

The open durations at depolarised potentials with 100 μM pyrantel could only be fitted by a single-exponential component in some experiments (Fig. 4). The loss of 1 open-time component and the observation (not shown) of channels occasionally 'flickering' between the open and closed state suggest open channel block at depolarised potentials. Channel block by an ion against the voltage gradient has previously been reported for the blockade of GABA channels with penicillin (Twyman et al., 1992), but experiments with higher concentrations of pyrantel would be needed to study this phenomenon in more detail.

3.9. Burst durations

The simple channel-block model predicts that the corrected mean burst duration should increase linearly with concentration of blocker at hyperpolarised but not depolarised potentials. The corrected mean burst duration did not vary significantly at +75 mV; however, in contrast to the expectations of the simple channel-block model the corrected mean burst duration did not increase but decreased at −75 mV (Table 1). For example, the value obtained for the corrected mean burst duration at 100 μM, 0.80 ± 0.18 ms (mean ± S.E., n = 10) was significantly lower ($P < 0.001$) than the value of 2.28 ± 0.42 ms (mean ± S.E., n = 6) obtained with 0.1 μM pyrantel. Possible explanations for the reduction in corrected mean burst duration are considered in the Discussion.

3.10. Desensitisation

With 100 μM pyrantel the closed-time distributions were best described by 4-exponential components in 5 out of 11 experiments at −75 mV and in 5 out of 13 experiments at +75 mV. Data obtained for the mean of 5 experiments at −75 mV were τ_1: 0.89 ± 0.42 ms, τ_2: 79 ± 38 ms, τ_3: 645 ± 163, and τ_4: 5705 ± 2257. Similar values were obtained at +75 mV. The additional component, τ_4, was thought to represent a desensitised state of the receptor (Cachelin and Colquhoun, 1989). Desensitised states of this receptor have been observed with high concentrations of acetylcholine (Pennington and Martin, 1990) and levamisole (Robertson and Martin, 1993) where they produce an additional long non-voltage-sensitive component in the closed-time distributions.

4. Discussion

In this study we have shown that the tetrahydropyrimidine, pyrantel, activates ion channels in *Ascaris* muscle with very similar properties to those activated by the natural excitatory transmitter acetylcholine (Fig. 1 and Pennington and Martin, 1990)

4.1. General comparison of currents activated by acetylcholine, pyrantel and levamisole from Ascaris suum

The actions of pyrantel, levamisole and acetylcholine on *Ascaris* muscle cells had previously been studied using both current-clamp and voltage-clamp techniques (Harrow and Gration, 1985) but had not before been studied at the single-channel level. Harrow and Gration concluded from their studies that these compounds activate the same cation channel because acetylcholine and the anthelmintics activated currents with similar reversal potentials. They further supported this conclusion by showing that acetylcholine and pyrantel compete for the same membrane receptor. The acetylcholine receptor on *Ascaris* muscle has been classified as nicotinic by a number of groups, most recently by Colquhoun et al. (1991) and Walker et al. (1991). The main evidence for this classification is that nicotinic agonists produce contractions of the muscle which are antagonised by various nicotinic antagonists, such as *d*-tubocurarine, whereas muscarinic agonists have little effect on this preparation. Therefore by adding our single-channel data on acetylcholine (Pennington and Martin, 1990), levamisole (Robertson and

Table 3
Comparison of single-channel properties for acetylcholine-, pyrantel- and levamisole-activated channels from *Ascaris suum* muscles

Compound	Concentration	No. of states	Conductance levels	CMOT (−75 mV)	P_{open} (−75 mV)
Acetylcholine	1 −10 μM	O 2 C 3 B 2	25 −35 pS ($n = 21$) 40 −50 pS ($n = 21$)	1.26 ± 0.11 ms ($n = 12$)	0.029 ± 0.013 ($n = 12$)
Pyrantel	0.1–10 μM	O 2 C 3 B 2	22 ± 0.34 pS ($n = 8$) 41 ± 2.04 pS ($n = 28$)	1.73 ± 0.20 ms ($n = 17$)	0.0057 ± 0.0010 ($n = 22$)
Levamisole	1 −10 μM	O 2 C 3 B 2	32.9 ± 1.23 pS ($n = 26$)	1.47 ± 0.11 ms ($n = 12$)	0.0052 ± 0.006 ($n = 20$)

O = open, C = closed, B = burst; voltage sensitivity applies to open and burst times.

Martin, 1993) and pyrantel (in this paper) to the previously published information about these compounds (Harrow and Gration, 1985; Colquhoun et al., 1991; Walker et al., 1991), we are led to the conclusion that the anthelmintics, pyrantel and levamisole, act at the nicotinic acetylcholine receptor on the somatic muscle of *Ascaris suum*.

A detailed comparison of the actions of pyrantel, levamisole and acetylcholine at the single-channel level is made in Table 3. Each compound activates channels with at least 2 open states, 2 burst states and 3 closed states. Channel mean open times are in the millisecond range with values of approximately 1.5 ms. As expected with different agonists acting on the same receptor, some minor differences in channel properties were noted between the 3 agonists (Table 3). For example, a flickering channel block was observed with high concentrations of pyrantel (100 μM) and levamisole (100 μM) (Robertson and Martin, 1993) but not with acetylcholine (Pennington and Martin, 1990). Harrow and Gration noted from their voltage-clamp experiments that pyrantel and levamisole produced current/voltage relationships which had linear (−30 to +10 mV) and non-linear components (−80 to −30 mV). They suggested the non-linear components could be due to either an agonist induced channel block or voltage-sensitive desensitisation. Our results with pyrantel and levamisole show that the non-linear component is probably due to agonist induced channel block as the desensitisation observed with these compounds was not voltage sensitive.

4.2. Channel block

In order to qualitatively describe the agonist-induced channel block by pyrantel and to compare these results with those obtained with levamisole (Table 4) (Robertson and Martin, 1993), the simple channel-block model was used. Both pyrantel and levamisole blocked the channel at hyperpolarised potentials in a voltage-sensitive manner with the dissociation rate constant for block (K_B) showing an e-fold change every 20 mV for levamisole compared to every 40 mV for pyrantel. The difference in voltage sensitivity suggests that levamisole and pyrantel block the channel by binding to different sites within the channel pore. Comparison of the dissociation constants for block reveals that pyrantel has a lower value for K_B than levamisole, therefore pyrantel has a stronger blocking action.

The predictions of the simple channel-block model for a charged blocking agent include the expectations that: the corrected mean open time decreases with increasing concentration; burst durations increase with increasing drug concentration; the forward blocking rate constant (k_{+B}), the unblocking rate (k_{-B}), and the dissociation constant K_B all vary with membrane potential. The data presented in this report are consistent with the above predictions except one: the burst

Table 4
Comparison of agonist-induced block on nicotinic acetylcholine receptors by pyrantel and levamisole

Rate constant	Pyrantel	Levamisole
K_B voltage sensitivity	e-fold every 40 mV	e-fold every 20 mV
−50 mV	37 μM	123 μM
−75 mV	20 μM	46 μM
k_{+B} voltage sensitivity	e-fold change every 72 mV	e-fold change every 36 mV
−50 mV	2.18 ± 10^7 M^{-1} s^{-1}	2.06 ± 10^7 M^{-1} s^{-1}
−75 mV	3.09 ± 10^7 M^{-1} s^{-1}	3.82 ± 10^7 M^{-1} s^{-1}
k_{-B} voltage sensitivity	e-fold change every 67 mV	e-fold change every 35 mV
−50 mV	0.81×10^3 s^{-1}	2.06×10^3 s^{-1}
−75 mV	0.61×10^3 s^{-1}	1.75×10^3 s^{-1}

durations did not increase with concentration. This implies that the model used is a useful approximation for a general comparison but not a completely sufficient model. At hyperpolarised potentials the burst durations decreased rather than increased with high pyrantel concentrations. The presence of another exit route from the blocked state to another closed-state without the blocked channel re-opening could explain this observation ($C \rightleftharpoons O \rightleftharpoons B \rightleftharpoons CB$). This putative closed-state (CB) might arise if the blocked state directly entered a desensitised state or if the blocked channel pore closed and trapped the pyrantel molecule. This extended blocking model is further discussed by Murrell et al. (1991). Further limitations of the simple channel-block model are discussed by Adams (1977), Neher and Steinbach (1978) and Neher (1983).

To conclude, pyrantel acts as an agonist and an open channel blocker of the acetylcholine receptor on the somatic muscle of *Ascaris suum*. The results presented in this paper suggest very high doses of pyrantel should be avoided due to the occurrence of desensitisation and agonist-induced open channel block which may render high therapeutic doses less effective treatment for nematode infection than lower doses.

Acknowledgments

We would like to thank Merck Sharp and Dohme (USA), the Wellcome Trust and the S.E.R.C. for financial support.

References

Aceves, J., J.D. Erli and R. Martinez-Maranon, 1970, The mechanism of the paralysing action of tetramisole on *Ascaris suum* muscle, Br. J. Pharmacol. 38, 602.

Adams, P.R., 1976, Drug blockade of open end-plate channels, J. Physiol. 260, 531.

Adams, P.R., 1977, Voltage jump analysis of procaine action at frog end-plate, J. Physiol. 268, 291.

Aubry, M.L., P. Cowell, M.J. Davey and S. Shevde, 1970, Aspects of the pharmacology of a new anthelmintic: pyrantel, Br. J. Pharmacol. 38, 332.

Brading, A.F. and P.C. Caldwell, 1971, The resting membrane potential of the somatic muscle cells of *Ascaris lumbricoides*, J. Physiol. 217, 605.

Cachelin, A.B. and D. Colquhoun, 1989, Desensitization of the acetylcholine receptor of frog end-plates measured in a vaseline-gap voltage clamp, J. Physiol. 415, 159.

Coles, G.C., J.M. East and S.N. Jenkins, 1975, The mechanism of action of the anthelmintic levamisole, Gen. Pharmacol. 6, 309.

Colquhoun, D. and A.G. Hawkes, 1982, On the stochastic properties of bursts of single ion channel openings and of clusters of bursts, Phil. Trans. R. Soc. Lond. B 300, 1.

Colquhoun, D. and B. Sakmann, 1985, Fast events in single-channel currents activated by acetylcholine and its analogues at the frog muscle end-plate, J. Physiol. 369, 501.

Colquhoun, D. and F.J. Sigworth, 1983, Fitting and statistical analysis of single channel records, in: Single Channel Recording, eds. B. Sakmann and E. Neher (Plenum Press, New York) p. 191.

Colquhoun, L., L. Holden-Dye and R.J. Walker, 1991, The pharmacology of cholinoceptors on the somatic muscle cells of the parasitic nematode *Ascaris suum*, J. Exp. Biol. 158, 509.

Del Castillo, J., W.C. De Mello and T. Morales, 1963, The physiological role of acetylcholine in the neuromuscular system of *Ascaris lumbricoides*, Arch. Int. Physiol. 71, 741.

Harrow, I.D. and K.A.F. Gration, 1985, Mode of action of the anthelmintics morantel, pyrantel and levamisole on muscle cell membrane of the nematode *Ascaris suum*, Pesticide Sci. 16, 662.

Martin, R.J., 1982, Electrophysiological effects of piperazine and diethylcarbamazine on *Ascaris suum* somatic muscle, Br. J. Pharmacol. 77, 255.

Martin, R.J., 1982, γ-Aminobutyric acid- and piperazine-activated single-channel currents from *Ascaris suum* body muscle, Br. J. Pharmacol. 84, 445.

Martin, R.J. (1985) Gamma-aminobutyric acid and piperazine-activated single channel currents from *Ascaris suum* body muscle muscle, Br. J. Pharmacol. 84, 445.

Martin, R.J., J.R. Kusel and A.J. Pennington, 1989, Surface properties of membrane vesicles prepared from muscle cells of *Ascaris suum*, J. Parasitol. 76, 340.

Murrell, R.D., M.S. Braun and D.A. Haydon, 1991, Actions of *n*-alcohols on nicotinic acetylcholine receptor channels in cultured rat myotubes, J. Physiol. 437, 431.

Natoff, I.L., 1969, The pharmacology of the cholinoceptor in muscle preparations of *Ascaris lumbricoides var. suum*, Br. J. Pharmacol. 37, 251.

Neher, E., 1983, The charge carried by single-channel currents of rat cultured muscle cells in the presence of local anaesthetics, J. Physiol. 339, 663.

Neher, E. and J.H. Steinbach, 1978, Local anaesthetics transiently block currents through single acetylcholine receptor channels, J. Physiol. 277, 153.

Pennington, A.J. and R.J. Martin, 1990, A patch-clamp study of acetylcholine-activated ion channels in *Ascaris suum* muscle, J. Exp. Biol. 154, 201.

Robertson, S.J. and R.J. Martin, 1993, Levamisole-activated single-channel currents in isolated muscle vesicles from *Ascaris suum*, Br. J. Pharmacol. 108, 170.

Robertson, S.J., A.J. Pennington, A.M. Evans and R.J. Martin, 1991, Pyrantel- and levamisole-activated single channel currents in isolated muscle vesicles from *Ascaris suum*, Pesticide Sci. 32, 511.

Robertson, S.J., A.J. Pennington, A.M. Evans and R.J. Martin, 1992, Pyrantel-activated single-channel currents in the nematode parasite *Ascaris suum*, Br. J. Pharmacol. 107, 154P.

Rozhkova, E.K., T.A. Malyutina and B.A. Shishov, 1980, Pharmacological characteristics of cholinoreception in somatic muscle of the nematode *Ascaris suum*, Gen. Pharmacol. 11, 141.

Twyman, R.E., R.M. Green and R.L. MacDonald, 1992, Kinetics of open channel-block by penicillin of $GABA_A$ receptor channels from the mouse spinal chord neurons in culture, J. Physiol. 445, 97.

Van Neuten, J.M., 1972, Pharmacological aspects of tetramisole, in: Comparative Biochemistry of Parasites, ed. H. Van Den Bossche (Academic Press, New York) p. 101.

Walker, R.J., L.M. Colquhoun, H.R. Parri, R.G. Williams and L. Holden-Dye, 1991, Pharmacology of the *Ascaris* nervous system, in: Molecular Basis of Drug and Pesticide Action, ed. I.R. Duce (Elsevier Applied Science, London, New York).

Oxantel-activated single channel currents in the muscle membrane of *Ascaris suum*

V. M. E. DALE *and* R. J. MARTIN

Department of Preclinical Veterinary Sciences, R. (D.) S. V. S. Summerhall, University of Edinburgh, Edinburgh EH9 1QH

(*Received 8 July 1994; revised 6 October 1994; accepted 7 October 1994*)

SUMMARY

The patch clamp technique was used to investigate the action of the anthelmintic drug, oxantel, on nicotinic acetylcholine receptor (nAChR) currents recorded from vesicles of the somatic muscle cells of the nematode parasite *Ascaris suum*. The amplitudes of the currents were analysed at different membrane potentials to determine the single channel conductance. Also the open and closed durations were measured to determine the kinetic properties of the activated channel. Oxantel activated single nAChR currents throughout a concentration range 10–100 μM, these currents were not observed with oxantel-free pipette solutions. The mean open time of the activated channels at a membrane potential of −75 mV and a concentration of 10 μM was 1·34 ms. At higher concentrations the open times were shorter and voltage sensitive, decreasing in duration on hyperpolarization, thus suggesting open channel block. The kinetics were analysed using a simple channel block model. The forward block rate, $K+B$, increased with increasing oxantel concentration but showed little increase as the membrane was hyperpolarized. $K+B$ was $2{\cdot}41 \times 10^7$ $M^{-1}s^{-1}$ at −50 mV and $2{\cdot}64 \times 10^7$ $M^{-1}s^{-1}$ at −100 mV. The unblocking rate constant, $K-B$, did exhibit voltage sensitivity being 443·6 s^{-1} at −50 mV and 86·8 s^{-1} at −100 mV. Thus the blocking dissociation constant KB ($= K-B/K+B$) was 18·5 μM at −50 mV and 3·3 μM at −100 mV. The simple channel block scheme was found to be insufficient to explain fully the observations made; reasons for this are discussed.

Key words: oxantel, *Ascaris suum*, acetylcholine, channel block.

INTRODUCTION

Oxantel is an *m*-oxyphenol analogue of the anthelmintic drug pyrantel, it is similar in structure to the anthelmintics pyrantel and morantel, all three drugs are organic cations. Oxantel was developed from pyrantel for its activity against whipworms, (*Trichuris* spp.). Despite pyrantel being a highly effective broad-spectrum nematocide it has no effect against the latter. Oxantel, however, has a very potent activity against whipworms and is therefore an important therapeutic agent in the control of whipworm infestation in dogs, pigs (McFarland & Howes, 1972) and man (Lim, 1978). Unlike pyrantel and morantel, oxantel has little *in vivo* activity against the nematode parasite of the pig, *Ascaris suum*, despite its close structural relationship to these drugs. The chemical structure of oxantel and pyrantel is shown in Fig. 1.

As shown, oxantel has a benzene ring which means that it is a more lipophilic compound than pyrantel. The lipophilic nature of oxantel may explain its lack of a therapeutic effect *in vivo* against *Ascaris suum*.

Ascaris is a parasitic nematode found in the small intestine of the pig. It is a large worm, hence ideal for use in electrophysiological experiments. For example, the patch clamp technique (Hamill *et al.* 1981) can be used to examine the behaviour of single ion channels in *Ascaris* musculature using a muscle vesicle preparation (Martin & Pennington, 1990).

Martin & Pennington (1990) used the patch clamp technique to describe acetylcholine-activated single channel currents in membrane vesicles formed from the extrasynaptic bag region of the muscle cells of *A. suum*. The effect of acetylcholine (ACh) on the muscle is blocked by tubocurarine but not by atropine, hence these ACh receptors can be classified as nicotonic (Colquhoun, Holden-Dye & Walker, 1991). However, the pharmacology of these nicotinic Ach receptors differs from that of vertebrate nicotinic receptors sufficiently for selective use of various nicotinic anthelmintic drugs (Harrow & Gration, 1985).

Harrow & Gration (1985) used intracellular current clamp and voltage clamp techniques to illustrate that the nicotinic anthelmintics, levamisole, pyrantel and morantel act as potent agonists at ACh receptors on the muscle bag membrane of *A. suum* opening cation selective channels. Nonlinear I/V relationships were described for levamisole, morantel and pyrantel under voltage clamp the current failing to increase on hyperpolarization of the membrane. The nonlinear I/V plot can be explained if all three anthelmintics are actually acting to block the open channels at higher concentrations.

Subsequent patch clamp studies (Robertson & Martin, 1992) with levamisole have allowed the mode of action of this agonist to be investigated at the single channel level. It was found that whilst levamisole acts as an agonist of the *Ascaris* nAChR at

 Copyright © 1995 Cambridge University Press

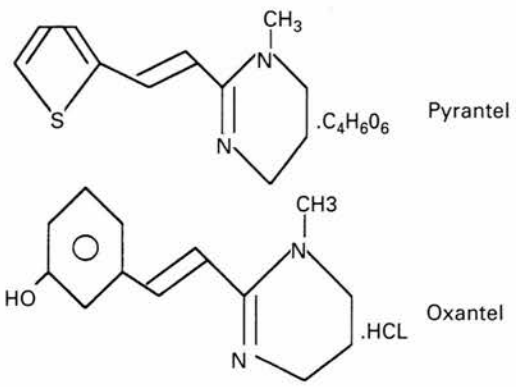


Fig. 1. Chemical structure of oxantel and pyrantel.

low concentrations, at higher concentrations it produces a flickering channel block at negative membrane potentials. The simple channel block scheme (Adams, 1976; Colquhoun & Sakmann, 1985) was used to describe these findings.

It is therefore reasonable to expect an agonist action of oxantel on the nAChR of *Ascaris* muscle. The aim of this study is to investigate at single channel level the action of oxantel on the nAChR of *A. suum* using the patch clamp technique, and the effect of oxantel concentration and membrane polarization on the kinetics of any channel activations.

MATERIALS AND METHODS

Preparation of the isolated muscle vesicles

Ascaris suum were collected weekly from the local abattoir. They were kept for up to 4 days at 32 °C in a water bath in Locke solution which was replaced daily. Muscle vesicles were prepared daily. A 1 cm portion of the cranial end of the worm was cut off, this segment was then cut longitudinally along the lateral line and the gut stripped away. The resulting muscle flap was pinned out in a small dish. The flap was then treated with collagenase (Sigma type 1A) for 10–20 min at 37 °C. This treatment resulted in individual vesicles budding off the bag region of the somatic muscle cells. These vesicles were then maintained at 37 °C until they were harvested with a Pasteur pipette and transferred to an experimental chamber for patch recording. The vesicles were used within 5 h of formation. Recordings were made at room temperature. The experimental chamber was mounted on the stage of a Nikon inverted microscope and viewed at × 200 magnification.

Solutions

An extracellular solution was used for maintaining the vesicles and muscle flap preparations. This solution contained (in mmol/l): NaCl, 35; sodium acetate , 105; KCl, 2; $MgCl_2$, 2; Hepes, 10; glucose, 3; ascorbic acid, 2; and EGTA, 1; pH adjusted to 7·2 with NaOH. The collagenase was applied to the flap preparation in extracellular solution modified by omitting the EGTA.

In the experimental chamber the vesicles were bathed in a solution containing (mmol/l): CsCl, 35; caesium acetate, 105; $MgCl_2$, 2; Hepes, 10; and EGTA, 1; pH adjusted to 7·2 with CsOH.

The membrane of the muscle vesicles is known to contain potassium ion channels, it also contains calcium-activated chloride channels (Thorn & Martin, 1987). Thus all the solutions used were calcium free, and contained caesium as the main cation to block the potassium ion channels.

The pamoate salt of oxantel (Sigma) was used. This was insoluble in water and was therefore dissolved in dimethyl sulphoxide (Me_2SO) before further dilution in pipette solution, the maximum concentration of Me_2SO in the pipette solution was 1 %. A 1 % concentration of Me_2SO was also present in the control pipettes containing no oxantel. The pipette solution contained (mmol/l): CsCl, 140; $MgCl_2$, 2; Hepes, 10; and EGTA, 1; pH adjusted to 7·2 with CsOH.

Recording channel currents

Patch electrodes were made from micro-haematocrit capillary tubes (Garner glass) these were coated with Sylgard to improve the frequency response. The pipettes were lowered, using micromanipulators, onto the surface of the vesicles. The application of a small degree of suction resulted in the formation of a high resistance 'Giga seal'. Channel currents were recorded with a lest EPC-7 and a modified Sony digital audio processor onto a Betamax video cassette recorder number SA500. All recordings were made from cell-attached patches. The resistance of the pipettes ranged from 3 to 10 MΩ.

Data analysis

The patch clamp recordings were analysed with a CED 1401 interface and an IBM 386 computer, with PAT software supplied by John Dempster of Strathclyde University. Kinetic analysis of the open and closed times was carried out. A threshold for channel opening was set at 70 % of the single channel amplitude determined from channel amplitude histograms so as to include only full openings. The subconductance channels had an amplitude below the 70 % threshold and were therefore edited out and excluded from further analysis. The data were filtered by an eight-pole Bessel filter, 3 dB at 1·5 KHz. The sample interval was set at 70 μs.

The PAT software was used to detect the channel open–closed transitions and produce a list of open and closed durations. This list was then edited to eliminate interference from openings to apparent subconductance levels or from any excessive noise.

Thus all subconductance openings were defined as closure. The PAT program was also used to plot frequency histograms of the channel amplitudes, and of the channel open and closed durations.

The list of open and closed times was transferred to the university mainframe computer for further analysis. The mainframe computer was used to fit exponentials to the open times, closed times, and to carry out the burst analysis. The method of maximum likelihood was used to fit the exponential curves (Colquhoun & Sigworth, 1983; Martin, 1985) to a probability density function of the form:

$$p.d.f. = \sum_{i=1}^{k} \frac{ai \exp(-t/T)}{Ti},$$

where ai represents the area of the ith component, Ti is the fitted time-constant, t represents the time, and k is the number of exponentials fitted. After fitting the exponential curves the data were corrected for missing events (Colquhoun & Sakmann, 1985). The analysis compensated for brief events missed due to the limited resolution of the recording apparatus and permitted the evaluation of mean open and mean closed times.

The probability of channel opening was calculated as the total open time divided by the sum of the total open time and the total closed time, the corrected figures for mean open and closed times were used.

In these experiments the individual channel activations were interrupted by very brief (1 ms) closed periods (the 'Nachschlag' phenomenon, Colquhoun & Sakmann, 1985), thus bursts of openings as well as single channel openings were considered in the analysis. A burst was defined as a single opening or group of openings separated by gaps shorter than a specified length Tcrit, a burst is considered to represent a single activation of the acetylcholine channel.

Simple channel block model

The simple channel block model (Adams, 1976; Colquhoun & Sakmann, 1985) was used to analyse the data:

$$C \underset{\beta}{\overset{\alpha}{\rightleftharpoons}} O \underset{K+B.Xb}{\overset{K\text{-}B}{\rightleftharpoons}} B,$$

C denotes the closed state of the channel, O the open state, B the blocked state, $K+B$ is the blocking rate constant, K–B the unblocking rate constant, α is the channel closing rate and β the channel opening rate, Xb is the concentration of the agonist drug. This model predicts that:

mean open time $= 1/\alpha + K + B.Xb$,
mean block time $= 1/K - B$,

channel block dissociation constant, $KB = K - B/K + B$. Two methods were used to calculate the blocking rate of this reaction: (i) the blockage frequency plot and (ii) a plot of the reciprocal of the mean open time (Ogden & Colquhoun, 1985). The blockage frequency plot is a plot of the number of blockages per unit open time against agonist concentration. The gradients of the slopes of these 2 graphs were used as an estimate of $K+B$.

RESULTS

Single channel recordings were obtained using 3 concentrations of oxantel in the patch pipette, 10, 30 and 100 μM. The potential difference across the cell membrane was varied between -100 mV and $+100$ mV and the resultant currents recorded for detailed analysis.

Figures 2 and 3 illustrate representative currents recorded from the membrane patches at a concentration of 30 μM oxantel, at (A) $+75$ mV and (B) -75 mV. At least 4 separate recordings were made at each potential for each concentration of oxantel. The number of events in each recording ranged from 200 to 2500 depending on the degree of channel activity in the patch. If oxantel was omitted from the patch pipettes no currents were observed. Thus it was concluded that it was the oxantel that activated the currents.

Channel conductance

The pipette and bath solutions had a symmetrical cation concentration but a non-symmetrical anion concentration. The predicted Nernst reversal potential for a cation selective channel was 0 mV, and for an anion selective channel was -33 mV. The actual reversal potential of the channels was determined by drawing a line of best fit through the I/V plots obtained for each experiment. Fig. 4 is an I/V plot when oxantel was present at a concentration of 30 μM. In each case the reversal potential was close to 0 mV, hence confirming the channels to be cation selective, conducting caesium ions. The latter result was expected from previous studies investigating the nature of the *Ascaris* acetylcholine channel (Martin & Pennington, 1990; Robertson & Martin, 1992). The average slope conductance of the channel (mean $\pm$ S.E.) was $33{\cdot}7 \pm 2{\cdot}2$ pS.

Apparent subconductance levels appeared sporadically throughout the patches, these were filtered out before the detailed kinetic analysis and were therefore not analysed further. Transitions from the subconductance to the main conductance state were not observed, which would be expected if the smaller conductance was a subconductance state of the larger one. Oxantel may therefore be opening 2 discrete types of ion channel in *Ascaris* muscle. Pennington & Martin (1990) also noted two conductance states in *Ascaris* muscle activated by acetylcholine, again these appeared to be due to the presence of 2 types of ion channel.

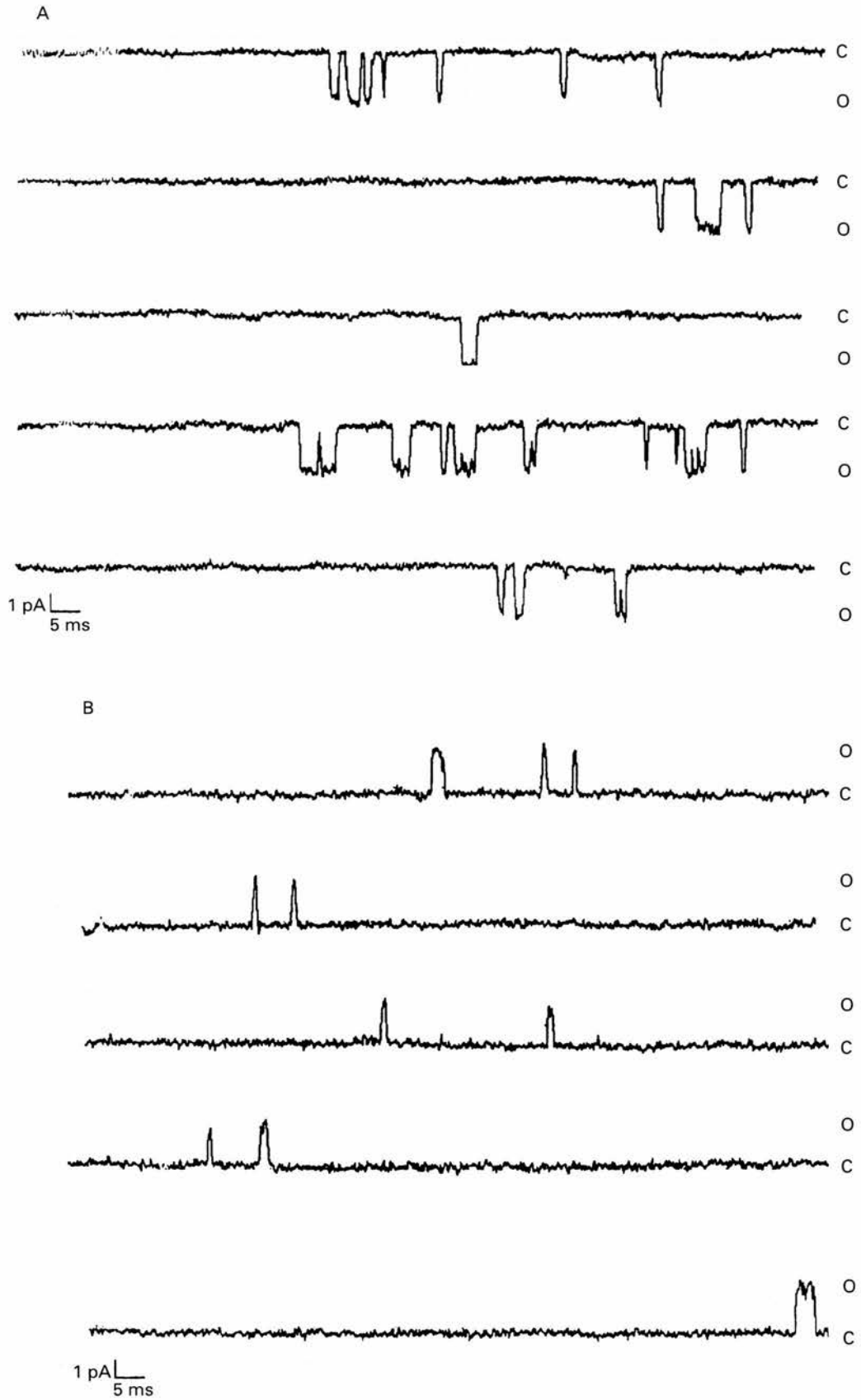


Fig. 2. A series of channel openings recorded from a membrane patch at +75 mV (A) and −75 mV (B), at an oxantel concentration of 30 μM. C denotes the closed state and O denotes the open state.

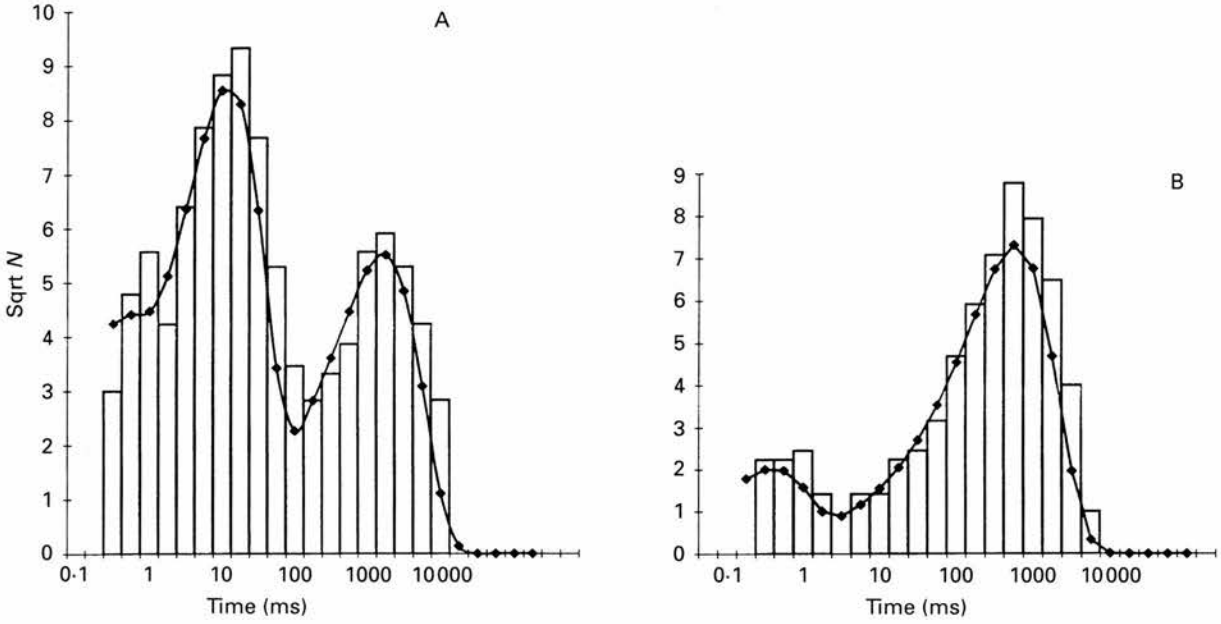


Fig. 3. Semilog plot of the frequency distribution of the closed times at an oxantel concentration of 30 μM, at +75 mV (A) and −75 mV (B); the lines of best fit illustrate the number of exponentials fitted to the distributions.

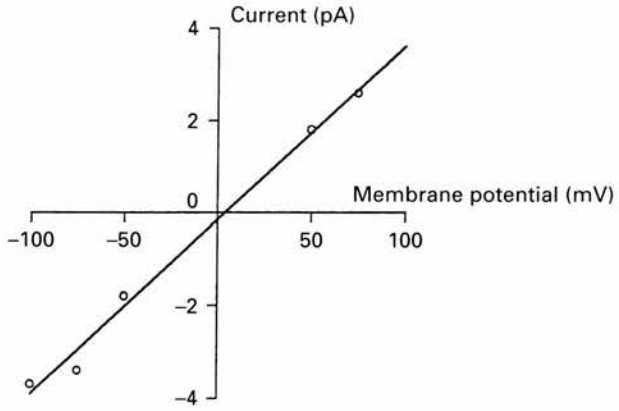


Fig. 4. An I/V plot of the currents activated by 30 μM oxantel with the line of best fit shown. The slope conductance of the channels was 33·7 ± 2·2 pS.

Exponential curve fitting

The number of exponentials used to fit the open, closed and burst distributions varied with both the concentration of the drug and the polarization of the patch membrane. If a channel can exist in several discrete states, then the number of open, closed and burst states must be at least equal to the number of exponential components that are needed to fit the distribution of the open, closed and burst states (Colquhoun & Hawkes, 1982).

10 μM concentration of oxantel in the pipette

At a concentration of 10 μM oxantel two exponentials were fitted to the open time distribution at both positive and negative membrane potentials, these values are shown in Table 1. These 2 exponentials represent at least 2 discrete open states of the channel. At both positive and negative membrane potentials the open times could be separated into openings that had a brief mean open time, and openings that had a long mean duration, these values are shown in Table 1. The open times showed no voltage sensitivity.

Table 2 illustrates the closed time distributions at each concentration of oxantel at +75 mV and −75 mV. At positive potentials 2 exponentials were fitted to the closed time distribution. These 2 exponentials represent 2 types of shut state of the channel, a very brief gap and a much longer gap. At a lower agonist concentration such as 10 μM, these brief closures between openings are consistent with a mechanism in which the channel opens and closes several times during a single receptor occupancy rather than being the result of channel block by the agonist (Colquhoun & Sakmann, 1981). The long closures represent periods of receptor inactivity. At negative potentials again 2 exponentials were fitted to the closed time distribution representing a very brief gap and a long gap. However, occasionally a third exponential was detected as a gap of intermediate length. The mean ± S.E. of this gap at all the negative membrane potentials was 5·14 ± 0·91 ms and the relative frequency was 0·27 ± 0·03 (mean ± S.E.). The fact that this intermediate gap was only evident at negative potentials suggests that it may represent open channel block because the oxantel molecules are cationic and would therefore tend to be drawn into, thus blocking, the open channel at negative membrane potentials.

Two exponentials were fitted to the distribution of bursts at both positive and negative potentials (see Table 3). These two exponentials represented a brief time component and a longer time component. The

Table 1. Open time kinetics for oxantel-activated single channel currents

($T1$ and $T2$ are the time-constants representing the two open states. The proportion of brief openings ($T1$) and long openings ($T2$) are represented by the areas of $A1$ and $A2$. Values are mean ± S.E.)

Oxantel concentration (μM)	Open times (ms)			
	$T1$	$T2$	$A1$	$A2$
Membrane potential +75 mV				
10 ($n = 4$)	0·74 ± 0·05	4·4 ± 1·4	0·8 ± 0·07	0·21 ± 0·1
30 ($n = 3$)	0·7 ± 0·06	1·7 ± 0·4	0·69 ± 0·05	0·3 ± 0·1
100 ($n = 4$)	0·6 ± 0·03	1·9 ± 0·2	0·7 ± 0·05	0·2 ± 0·1
Membrane potential −75 mV				
10 ($n = 4$)	0·89 ± 0·22	2·6 ± 0·6	0·7 ± 0·1	0·3 ± 0·1
30 ($n = 3$)	—	1·1 ± 0·1	—	1
100 ($n = 4$)	—	0·3 ± 0·03	—	1

Table 2. Closed time kinetics of oxantel-activated single channel currents

(The closed times are represented by up to three exponentials. Brief closings ($T1$), intermediate closings ($T2$) and long closings ($T3$), their relative proportions are represented by the areas $A1$, $A2$ and $A3$. All values are the mean ± S.E.)

Oxantel concentration (μM)	Closed times (ms)					
	$T1$	$T2$	$T3$	$A1$	$A2$	$A3$
Membrane potential +75 mV						
10 ($n = 4$)	0·575 ± 0·3	—	1098 ± 425	0·23 ± 0·07	0·77 ± 0·07	—
30 ($n = 3$)	0·36 ± 0·03	—	661 ± 179	0·07 ± 0·03	0·91 ± 0·02	—
100 ($n = 6$)	2·5 ± 1·5	—	596 ± 250	0·16 ± 0·04	0·84 ± 0·04	—
Membrane potential −75 mV						
10 ($n = 4$)	0·35 ± 0·04	5·35 ± 0·66	1556 ± 424	0·14 ± 0·02	0·32 ± 0·02	0·54 ± 0·03
30 ($n = 4$)	—	4·4 ± 0·07	1716 ± 749	—	0·6 ± 0·06	0·4 ± 0·06
100 ($n = 6$)	—	8·6 ± 0·4	772 ± 299	—	0·66 ± 0·03	0·34 ± 0·03

Table 3. Burst time kinetics of oxantel-activated single channel currents

($T1$ and $T2$ are the time-constants representing the short and long bursts of channel openings, respectively; $A1$ and $A2$ are the areas of these two time-constants. The mean open time of the channel openings is also shown for comparison with the $T1$ time-constant.)

Oxantel concentration (μM)	Burst times (ms)				Mean open time (ms)
	$T1$	$T2$	$A1$	$A2$	
Membrane potential +75 mV					
10 ($n = 4$)	0·8 ± 0·1	5·7 ± 1·5	0·8 ± 0·06	0·22 ± 0·06	1·34
30 ($n = 3$)	0·93 ± 0·13	20·2 ± 3·7	0·9	0·1	0·96
100 ($n = 5$)	0·95 ± 0·11	31·7 ± 6·9	0·87 ± 0·03	0·13 ± 0·03	0·94
Membrane potential −75 mV					
10 ($n = 5$)	1 ± 0·3	16·3 ± 1·3	0·68 ± 0·1	0·4 ± 0·1	1·34
30 ($n = 4$)	1·2 ± 0·2	21·02 ± 4·5	0·4 ± 0·04	0·6 ± 0·04	1·06
100 ($n = 4$)	0·4 ± 0·04	38 ± 6·6	0·36 ± 0·06	0·64 ± 0·04	0·35

bursts of openings were well characterized at positive potentials. A burst consisted of a series of channel openings separated by very brief gaps, the individual bursts being separated by the longer gaps. Each burst is interpreted as the openings of a single ion channel as the result of a single receptor occupancy by the drug oxantel. At positive potentials the choice of TCrit was not essential because the gaps between the bursts were several hundred-fold greater than gaps within the bursts, a TCrit = 1 ms was therefore

used. The occurrence of the intermediate gap at negative potentials led to the appearance of clusters of bursts. A cluster consisted of a series of bursts of openings, each burst separated by the gap of an intermediate length, the individual clusters being separated by the long duration gaps. If it is assumed that the intermediate gap is the result of channel block then a cluster still represents a series of channel openings resulting from a single receptor occupancy. At negative potentials a TCrit = 50 ms was used such that the intermediate gap was included within the definition of a burst.

30 μM concentration of oxantel in the pipette

At a concentration of 30 μM oxantel two exponentials were fitted to the open time distribution at positive membrane potentials, again these represented the very brief open time and the longer open time, (see Table 1). At negative potentials, however, only one exponential was fitted to the open time distribution. It is likely that the loss of one open time exponential at the negative potentials was due to the brief openings reducing in magnitude to a level below the limit of resolution of the recording equipment, therefore only the longer openings were apparent.

At positive and negative potentials two exponentials were fitted to the closed time distributions (see Table 2). At positive potentials these represented a short gap and a much longer gap. At negative potentials they represented a gap of intermediate length and a very long gap. The mean $\pm$ S.E. of the intermediate gap at all the negative potentials was $5{\cdot}75 \pm 1{\cdot}04$ ms and the area was $0{\cdot}57 \pm 0{\cdot}03$. However, the recordings showed that the very brief closures of the channel were still occurring but presumably these were too brief to be resolved during the kinetic analysis. The duration of the intermediate gap and its area had both increased as the concentration of oxantel increased, this is consistent with the theory that the gap represents open channel block. Also as the membrane was hyperpolarized the area of the intermediate gap increased from 0·53 at -50 mV to 0·62 at -100 mV, again this voltage sensitivity of the proportion of gaps of intermediate length suggests that they are representative of open channel block. Fig. 3 illustrates the frequency distribution of the closed times at a concentration of 30 μM at (A) $+75$ mV and (B) -75 mV, the lines of best fit illustrate the number of exponentials fitted to each distribution.

The distribution of bursts was very similar to that at a concentration of 10 μM (see Table 3), with the appearance of clusters of bursts at negative potentials due to the occurrence of the intermediate gap at these potentials. Again 2 exponentials were fitted to the burst distribution and the TCrit values used were the same as those used at a concentration of 10 μM oxantel.

100 μM concentration of oxantel in the pipette

At a concentration of 100 μM oxantel the open time distribution (see Table 1) was fitted by two exponentials at positive potentials representing a short component, and a longer component. At negative potentials only 1 exponential was fitted to the open time distribution similar to the findings at 30 μM. Also the burst distribution was best fitted by two exponentials similar to the findings at lower concentrations of agonist, with clusters of bursts appearing at negative potentials (see Table 3). The closed time distribution was best fitted by two exponentials at both negative and positive potentials (see Table 2). At positive potentials these two exponentials represented a very brief gap and a very long gap, similar to the results found at lower concentrations of agonist. At negative potentials the 2 exponentials represented an intermediate gap with a mean of $8{\cdot}15 \pm 1$ ms and a mean area of $0{\cdot}66 \pm 0{\cdot}04$, and a long gap. However, similar to the findings at 30 μM concentration, the recordings clearly showed that there were very brief closings occurring at negative potentials, presumably these being too brief to be resolved during the kinetic analysis. There was a small increase in the duration of the intermediate gap length with increasing hyperpolarization, from 0·62 at -50 mV to 0·68 at -100 mV. Again the increase in the duration of the intermediate gap and its area with increased drug concentration and the increase in its area with hyperpolarization are consistent with it representing open channel block by the agonist molecules.

Probability of channel opening

The probability of the channel being open (Popen) was dependent on oxantel concentration at both negative and positive membrane potentials. For example at $+75$ mV Popen was (mean $\pm$ S.E.) $2{\cdot}5 \times 10^{-3}$ ($\pm 1{\cdot}3 \times 10^{-3}$) at 10 μM and $3{\cdot}4 \times 10^{-3}$ ($\pm 1 \times 10^{-3}$) at 100 μM, at -75 mV Popen was $1{\cdot}4 \times 10^{-3}$ ($\pm 0{\cdot}3 \times 10^{-3}$) at 10 μM and $2{\cdot}9 \times 10^{-3}$ ($\pm 0{\cdot}9 \times 10^{-3}$) at 100 μM. Popen was clearly greater at positive than negative potentials and increased with oxantel concentration.

Evidence of channel block

At each concentration of oxantel used the kinetics of channel opening changed when the membrane potential was negative. The change became more obvious at the higher drug concentrations. At negative membrane potentials, the channel openings appeared as clusters of bursts of openings due to the presence of the intermediate gap, which was not present at positive potentials. This observation can be explained by the hypothesis that oxantel is acting to produce a voltage sensitive open channel block in

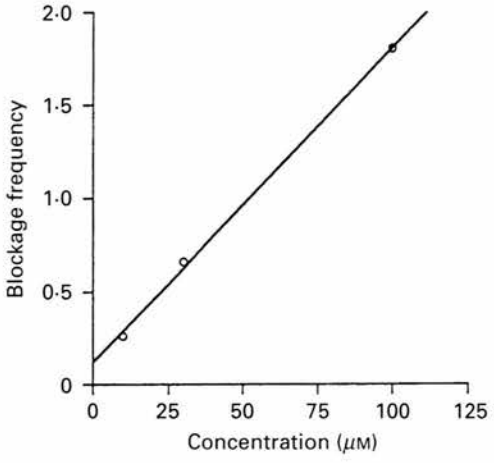


Fig. 5. The blockage frequency plot at a membrane potential of −75 mV. The gradient of the line of best fit is used to estimate the forward blocking rate constant, $K+B$.

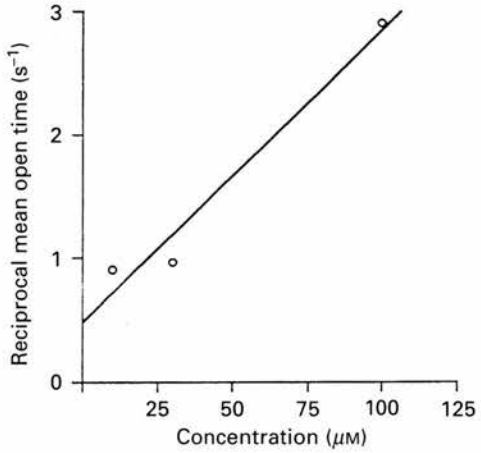


Fig. 6. A plot of the reciprocal of the mean open time of the channels at a membrane potential of −75 mV. The gradient of the line of best fit is an estimation of the forward blocking rate constant $K+B$.

Table 4. Estimates of the forward blocking rate, $K+B$

Membrane potential (mV)	$K+B$ estimate from the blockage frequency plots, ($M^{-1}s^{-1}$)	$K+B$ estimate from the reciprocal of the mean open time plot ($M^{-1}s^{-1}$)
−50	$1{\cdot}09 \times 10^7$	$2{\cdot}41 \times 10^7$
−75	$1{\cdot}76 \times 10^7$	$2{\cdot}37 \times 10^7$
−100	$1{\cdot}714 \times 10^7$	$2{\cdot}64 \times 10^7$

addition to its action as an agonist. The gap of an intermediate length that appeared at negative potentials was assumed to be representative of the open channel block. The proportion of these intermediate gaps increased with hyperpolarization of the membrane and also with increasing concentration of the drug. These findings both support the hypothesis of open channel block (Ogden & Colquhoun, 1985). The voltage sensitivity of the block (i.e. the channel block only being evident at negative potentials), is consistent with the large size and the cationic charge of the oxantel molecules.

Table 5. $K-B$ variation with concentration of oxantel at a membrane potential of −75 mV

Concentration of oxantel (μM)	$K-B$ (s^{-1})
10	177
30	202
100	116

Further evidence that open channel block was occurring was that at negative potentials only one exponential was fitted to the open time distribution, as opposed to 2 exponentials at positive potentials (see Table 1). This was due to the briefer open time component, $T1$, reducing to a level below the limit of resolution of the recording equipment at negative potentials. The duration of $T2$ is much briefer at negative potentials than at positive potentials. This result was expected as open channel block at negative potentials would markedly reduce the time that current could flow through an open channel. The voltage sensitivity of the probability of channel opening, with Popen being greater at positive potentials, is also consistent with the hypothesis that open channel block is occurring.

Blockage frequency plot and plot of the reciprocal of the mean open time

A blockage frequency plot and a plot of the reciprocal of the mean open time was drawn for each of the negative membrane potentials used, i.e. −50 mV, −75 mV and −100 mV. Fig. 5 illustrates the blockage frequency plot at −75 mV and Fig. 6 illustrates the plot of the reciprocal of the mean open time at −75 mV. Table 4 gives the forward blocking rate constant, $K+B$, values as estimated from the blockage frequency plots and the plots of the reciprocal of the mean open time for each negative membrane potential. If the simple open channel block model is sufficient to explain the observations then the slopes of the blockage frequency plots will be the same as those from the plots of the reciprocal of the mean open time and will equal $K+B$. However, if the simple channel block scheme does not apply then the slopes of the blockage frequency plot will be less than $K+B$ (Ogden & Colquhoun, 1985). The $K+B$ estimate from the blockage frequency plot at a membrane potential of −100 mV was $1{\cdot}71 \times 10^7$ $M^{-1}s^{-1}$, which was significantly lower

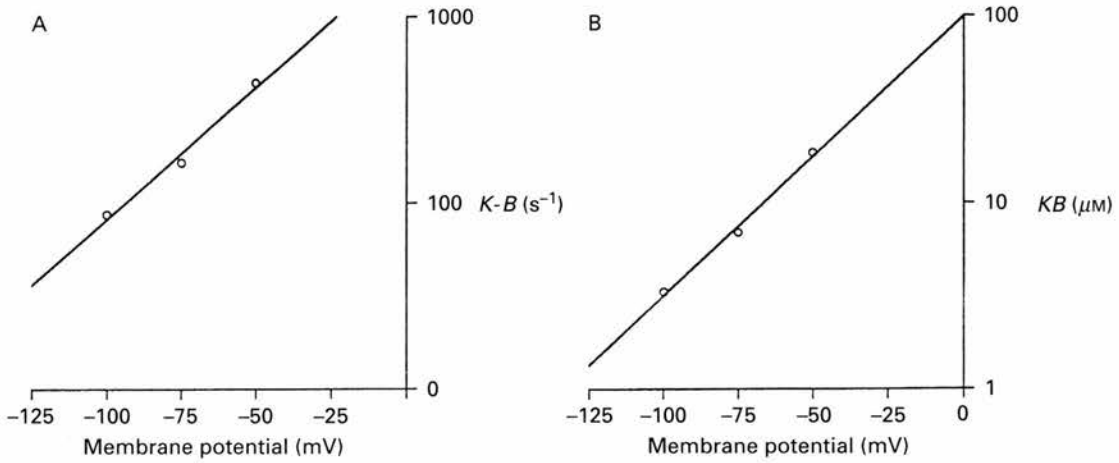


Fig. 7. (A) Semi-log plot of $K-B$ against membrane potential. (B) Semi-log plot of KB against membrane potential.

Table 6. A comparison of the KB values for oxantel and levamisole

(The KB values for levamisole are taken from Robertson & Martin (1992).)

Membrane potential (mV)	KB value for oxantel (μM)	KB value for levamisole (μM)
−50	18·5	123
−75	6·9	46
−100	3·3	9·4

(ANOVA $P = 0{\cdot}01$) than the estimate of $K+B$ from the plot of the reciprocal of the mean open time which, at a membrane potential of −100 mV was $2{\cdot}64 \times 10^7$ M^{-1}s^{-1}. Therefore the simple channel block model cannot be used to explain fully the channel block that occurred in this study. $K+B$ increased with increasing concentration of oxantel as predicted by the simple channel block scheme. However, for a cation such as oxantel it would be expected that $K+B$ would increase with membrane hyperpolarization, this was not the case.

Estimation of the unblocking rate constant $K-B$

The simple channel block scheme predicts that the unblocking rate constant, $K-B$, can be estimated as the reciprocal of the mean blocked time. The values for $K-B$ were 443·6 s^{-1} at −50 mV, 164·8 s^{-1} at −75 mV and 86·8 s^{-1} at −100 mV. Table 5 shows the $K-B$ values at a membrane potential of −75 mV at each concentration of oxantel. Clearly $K-B$ showed no dependence on drug concentration; this is predicted from the simple channel block scheme. $K-B$ did, however, show a clear voltage sensitivity, as the membrane was hyperpolarized further the unblocking rate-constant decreased. This would be expected for a cation such as oxantel because, as the inside of the cell becomes increasingly negative, the positively charged oxantel molecules will have a greater electrostatic force retaining them in the open channel pores. The voltage sensitivity of $K-B$ was described by the equation:

$$K-B = K-B0 \exp(E/vK),$$

where $K-B$ is the unblocking rate constant at a membrane potential E, $K-B0$ is the value for $K-B$ at a membrane potential 0 mV and vK is a constant. Fig. 7A is a semi-log plot of $K-B$ against membrane potential. $K-B0$ was 2137·5 s^{-1}, vK was 30·8. Therefore $K-B$ shows an e-fold change every 30·8 mV.

Determination of the channel block dissociation constant, KB

The channel block dissociation constant, KB, is equal to the ratio $K-B/K+B$. The $K+B$ estimate from the reciprocal mean open time plot was used as a more accurate estimate of the variable. The values for KB are shown in Table 6, where they are compared with the KB values for levamisole. The voltage sensitivity of KB was described by the equation:

$$KB = KB0 \exp(E/vK),$$

where KB is the blocking dissociation constant at the membrane potential E, $KB0$ is the value for KB at 0 mV and vK is a constant. Fig. 7B is a semi-log plot of KB against membrane potential. The value for $KB0$ was 99·5 μM, vK was 29·1. Therefore KB shows an e-fold change every 29·1 mV. KB decreased with hyperpolarization, this is a reflection of the voltage sensitivity of the $K-B$ values.

Burst-time distributions

Two exponentials were fitted to the burst times at all concentrations of oxantel and at both positive and negative potentials. The time-constant $T1$ describes the short bursts and the time-constant $T2$ describes the long bursts of openings. $T1$ and $T2$ at +75 mV and −75 mV for each concentration of oxantel are

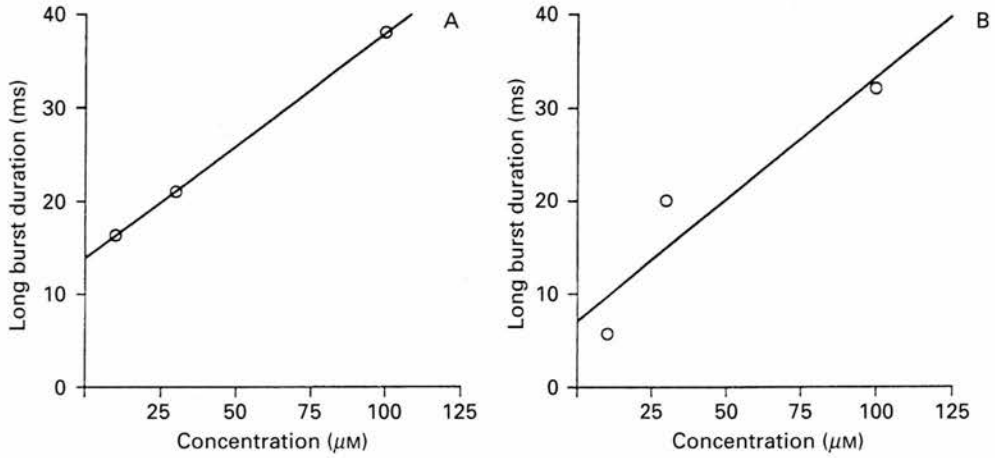


Fig. 8. (A) Long burst duration versus concentration of oxantel at −75 mV; (B) long burst duration versus concentration of oxantel at +75 mV.

shown in Table 3. $T1$ exhibited no concentration dependence at either negative or positive potentials and it approximated to the mean open time (as shown). The area of the $T1$ component was greater at positive potentials, a result which was expected as at these potentials the channel openings occurred mainly in short bursts with only very brief within burst gaps, see Table 2. $T2$ represented long bursts, the area of $T2$ was significantly greater at negative potentials, again a result which was expected as at negative potentials most bursts consisted of long clusters of openings which contained the intermediate gap assumed to represent open channel block.

Fig. 8A is a plot of T2 against oxantel concentration at −75 mV, Fig. 8B is a plot of $T2$ against oxantel concentration at +75 mV. At both positive and negative potentials the duration of $T2$ increased with increasing concentration of oxantel. The simple channel block scheme predicts a linear increase in burst length with increasing concentration of oxantel; Fig. 8A illustrates that to be the case at negative membrane potentials.

Long closed periods

Table 2 illustrates the kinetics of the closed time distributions at +75 mV and −75 mV at each concentration of oxantel used. At negative potentials the duration of the longest gaps were greater than at positive potentials. Also at both negative and positive potentials the duration of the longest gap decreased as the concentration of oxantel increased. This decrease may be due to the probability of channel opening increasing as the concentration increases.

DISCUSSION

The aim of this study was to investigate the effect of the anthelmintic drug, oxantel, on the nicotinic acetylcholine receptor located on the bag region of the somatic muscle cells of the parasitic nematode *Ascaris suum*. The patch clamp technique was used which allowed a very detailed study of the single ion channel kinetics. The results indicated conclusively that oxantel is an agonist of the nACh receptor because inclusion of oxantel in the patch pipettes activated single channel currents. The currents activated by oxantel showed similarities to the single channel currents activated in *Ascaris* by acetylcholine. Acetylcholine activates channels in the concentration range 1–100 μM (Pennington & Martin, 1990), so did oxantel. Acetylcholine activates channels with two distinguishable conductance levels, 25–35 pS and 40–50 pS (Pennington & Martin, 1990). Evidence of the presence of 2 conductance states was also seen with oxantel. Both acetylcholine and oxantel activated cation selective channels.

In addition the data indicate that the oxantel is, at higher concentrations, also acting to block the open ion channels. Ogden & Colquhoun (1985) investigated the possible blocking action of acetylcholine receptor agonists acting on the frog neuromuscular junction. Robertson & Martin (1992) found that levamisole blocked the open acetylcholine activated ion channels when at high concentrations whilst acting as a receptor agonist at low concentrations.

Predictions of the simple channel block scheme

The results presented in this paper were related to the predictions of the simple channel block model outlined earlier. This model makes the following predictions for a charged blocking molecule – (1) that the corrected mean open times will decrease as the concentration of oxantel is increased, (2) that $K+B$, $K-B$ and therefore KB will all exhibit voltage sensitivity because of the electrostatic forces on the blocking molecule, (3) that the block duration and therefore $K-B$ are independent of drug con-

centration, and (4) that the $K+B$ estimates from the plot of the reciprocal of the mean open time and the blockage frequency plot will be equal.

Deviations of the results from these predictions

The data presented in this paper are not consistent with all the above predictions, hence implying that the simple channel block model is an approximation and oversimplified in this case.

$K+B$ did not exhibit the expected voltage sensitivity. However, this lack of voltage sensitivity of $K+B$ does not rule out the possibility of a voltage-sensitive step in the block process. If the diffusional barrier, which is voltage insensitive, is the rate limiting step for the blocking reaction then any sequentially located voltage-sensitive barrier will have no effect (Kuo & Hess, 1993). The strong voltage sensitivity of $K-B$ suggests that the blocking molecule does indeed lie within the membrane field. The $K+B$ estimate from the blockage frequency plot was significantly less than the estimate from the plot of the reciprocal of the mean open time plot. This finding suggests that the channel may be able to shut around and trap the agonist molecule, thus leading to a long-lived shut blocked state of the channel, and/or there may be a direct route from the blocked state or states to the resting state which would allow recovery from block without re-opening of the channel.

Why does oxantel have no therapeutic effect against Ascaris?

This is a pertinent question as oxantel clearly is an agonist of *Ascaris* nAChR channels *in vitro*, yet *in vivo* has no effect on the worm but is highly effective against *Trichuris* infestations (Lim, 1978).

The difference in efficacy of the drug between nematode species may reflect variations in the precise nature of the nAChR. The nAChR is a pentemer formed by 4 different types of protein subunit, ($\alpha, \beta, \gamma, \delta$) with an $\alpha 2\beta\gamma\delta$ stoichiometry (Lindstrom, Merlie & Yogeeswaran, 1979). The subunits are arranged in a barrel stave arrangement with an aqueous pore of at least 6·5 Å diameter connecting the extra- and intracellular aqueous phases which constitutes the ion channel. The precise amino acid sequences of the subunits varies between species, which may effect the functional properties of the receptor.

The occurrence of ion channel block at relatively low concentrations of the agonist is probably a significant factor in the lack of therapeutic effect of oxantel against *Ascaris* (Adams *et al.* 1980). No data are available at the present time regarding the KB values for the anthelmintic pyrantel. However, the KB values for oxantel are significantly lower than those for levamisole as shown in Table 6. The blocking of the acetylcholine channels by oxantel is effectively counteracting its action as an agonist of the receptor. It may be that the nAChR in *Trichuris* differs such that ion channel block does not occur so readily.

Does desensitization account for the long closed periods?

Desensitization describes the phenomenon of long periods of channel inactivity seen between channel activation. Nothing is known about the physical nature of desensitized states. Desensitization is probably the result of the receptor–channel complex adopting a long-lived shut conformation in which the agonist binding sites are occupied. The onset of desensitization is slower at lower agonist concentrations (Cachelin & Colquhoun, 1989). Voltage sensitive desensitization is not a feature of single channel currents produced by acetylcholine in *Ascaris* (Pennington & Martin, 1990). The results presented here show, however, that the duration of the longest shut periods is voltage sensitive, being longer when the membrane was negative, thus these long gaps may not represent desensitization. The direction of the voltage sensitivity of these long gaps suggests that there may be a block component contributing to the long gaps at negative potentials, for example a long-lived shut blocked state.

Comparison of results with previous patch clamp studies investigating the properties of anthelmintics on the nAChR of Ascaris suum

Robertson & Martin (1992) found that for levamisole $K+B$ was strongly voltage sensitive increasing with hyperpolarization. The lack of voltage sensitivity of $K+B$ in these experiments may be due to differences in the nature of the blocking molecule. As illustrated earlier the oxantel molecule has a benzene ring which will increase the lipophilic nature of the molecule. This may influence the mechanics of the open channel block which takes place and may, in part, explain why in this study the open channel block was evident at a relatively low concentration of the agonist drug, i.e. at 10 μM concentration. The latter observation may explain why oxantel has no therapeutic effect against *A. suum* worms *in vivo*, despite being a close analogue of the very effective drug pyrantel.

We are pleased to acknowledge the financial support of the Horserace Betting Levy Board who have made this work possible.

REFERENCES

ADAMS, P. R. (1976). Drug blockade of open end-plate channels. *Journal of Physiology* **260**, 531–52.

ADAMS, D. J., DWYER, T. M. & HILLE, B. (1980). The

permeability of endplate channels to monovalent and divalent metal cations. *Journal of General Physiology* **75**, 493–510.

CACHELIN, A. B. & COLQUHOUN, D. (1989). Desensitization of the acetylcholine receptor of frog end plates measured in a vaseline gap voltage clamp. *Journal of Physiology* **415**, 159–88.

COLQUHOUN, D. & HAWKES, A. G. (1982). On the stochastic properties of bursts of single ion channel openings and clusters of bursts. *Philosophical Transactions of the Royal Society* B **300**, 1–59.

COLQUHOUN, D., HOLDEN-DYE, L. & WALKER, R. J. (1991). The pharmacology of cholinoceptors on the somatic muscle of the parasitic nematode *Ascaris suum*. *Journal of Experimental Biology* **158**, 509–30.

COLQUHOUN, D. & SAKMANN, B. (1981). Fluctuations in the microsecond time range of current through single acetylcholine receptor ion channels. *Nature, London* **294**, 464–6.

COLQUHOUN, D. & SAKMANN, B. (1985). Fast events in single channel currents activated by acetylcholine and its analogues at the frog muscle end-plate. *Journal of Physiology* **369**, 501–57.

COLQUHOUN, D. & SIGWORTH, F. W. (1983). Fitting and single channel analysis of single channel records. In *Single Channel Recordings* (ed. Sakmann, B. & Nehere, E.), pp. 191–264. New York: Plenum Press.

HAMILL, O. P., MARTY, A., NEHER, E., SAKMANN, B. & SIGWORTH, F. J. (1981). Improved patch clamp techniques for high resolution recording from cells and cell-free membrane patches. *Pflügers Archives European Journal of Physiology* **391**, 85–100.

HARROW, I. D. & GRATION, K. A. F. (1985). Mode of action of the anthelmintics morantel, pyrantel and levamisole on the muscle cell membrane of the nematode *Ascaris suum*. *Pesticide Science* **16**, 662–72.

KUO, C. & HESS, P. (1993). Ion permeation through the L-type calcium channel in rat phaeochromocytoma cells: two sets of ion binding sites in the pore. *Journal of Physiology* **466**, 629–55.

LIM, J. K. (1978). Anthelmintic effect of oxantel and oxantel–pyrantel in intestinal nematode infections. *Drugs* **15** (Suppl 1), 99–103.

LINDSTROM, J., MERLIE, J. & YOGEESWARAN, G. (1979). Biochemical properties of acetylcholine receptor subunits from *Torpedo californica*. *Biochemistry* **18**, 4465–70.

MARTIN, R. J. (1985). γ-aminobutyric acid and piperazine activated single channel currents from *Ascaris suum* body muscle. *British Journal of Pharmacology* **84**, 445–61.

MARTIN, R. J. & PENNINGTON, A. J. (1990). A patch clamp study of acetylcholine activated ion channels in *Ascaris suum* muscle. *Journal of Experimental Biology* **154**, 201–21.

MCFARLAND, J. W. & HOWES, H. L. (1972). Novel anthelmintic agents. 6. Pyrantel analogs with activity against whipworm. *Journal of Medicinal Chemistry* **15**, 365–8.

OGDEN, D. C. & COLQUHOUN, D. (1985). Ion channel block by acetylcholine, carbachol and suberyldicholine at the frog neuromuscular junction. *Proceedings of the Royal Society of London*, B **225**, 329–55.

PENNINGTON, A. J. & MARTIN, R. J. (1990). A patch clamp study of acetylcholine-activated ion channels in *Ascaris suum* muscle. *Journal of Experimental Biology* **154**, 201–21.

ROBERTSON, S. J. & MARTIN, R. J. (1992). Levamisole-activated single channel currents from muscle of the nematode parasite *Ascaris suum*. *British Journal of Pharmacology* **108**, 170–8.

THORN, P. & MARTIN, R. J. (1987). A high conductance Ca-dependant chloride channel in *Ascaris suum* muscle. *British Journal of Pharmacology* **72**, 31–49.

Pharmac. Ther. Vol. 58, pp. 13–50, 1993
Printed in Great Britain. All rights reserved

0163-7258/93 $24.00
© 1993 Pergamon Press Ltd

Associate Editor: P. KÖHLER

NEUROMUSCULAR TRANSMISSION IN NEMATODE PARASITES AND ANTINEMATODAL DRUG ACTION

R. J. MARTIN

Department of Preclinical Veterinary Sciences, R.(D.)S.V.S., Summerhall, University of Edinburgh, Edinburgh EH9 1QT, U.K.

Abstract—Some anthelmintic drugs interfere selectively with nematode neuromuscular transmission. These drugs include: the nicotinic agonists, e.g. levamisole, the gamma-amino butyric acid agonist piperazine, and the avermectins which open Cl^- channels. The physiology and pharmacology of neuromuscular transmission in nematodes is reviewed and the actions of antinematodal drugs which interfere with the transmission described. The results of experiments on the large porcine-intestinal nematode parasite, *Ascaris suum*, form the basis of the account presented but experiments on other nematodes suggest that these observations may be generalized. Results of some experiments on the small free living nematode *Caenorhabditis elegans* are also included.

CONTENTS

1. Introduction 14
2. Motor Behaviour 14
3. Neuronal Organization 15
   3.1. Anatomy of the nematode nervous system 15
   3.2. Properties of single nerve cells 16
   3.3. Motorneurone nerve cell interconnections 17
4. Anatomy of Somatic Muscle Cells 17
5. The Pharyngeal Muscle 18
6. Electrophysiology of Somatic Muscle 20
   6.1. Membrane potential 20
   6.2. Depolarizing potentials 20
7. Acetylcholine 22
   7.1. Effects of acetylcholine on *Ascaris* muscle 22
   7.2. Ionic basis of the electrical responses to acetylcholine 23
   7.3. Acetylcholine single-channel currents 23
   7.4. Acetylcholine receptors on motorneurones 25
   7.5. Biochemistry of acetylcholine 25
   7.6. Cholinesterase antagonists as anthelmintics 26
   7.8. Pharmacology of the acetylcholine receptors 26
8. Nicotinic Anthelmintics 27
   8.1. Chemical structure 27
   8.2. Effects on intracellular potential 28
   8.3. Effect on input conductance and membrane currents 29
   8.4. Single-channel currents activated by nicotinic anthelmintics 30
9. GABA 31
   9.1. Effects of GABA on *Ascaris* muscle 31
   9.2. Pharmacology of the *Ascaris* GABA receptor 32
   9.3. GABA binding sites in *C. elegans* 34
   9.4. GABA and piperazine single-channel currents 34
10. Macrocyclic Lactones 35
   10.1. Effects of dihydroavermectin B1a on conductance and membrane potential 35
   10.2. Effects of dihydroavermectin at the single-channel level 36
   10.3. Actions of avermectins on the nervous system of *Ascaris* 37

10.4. Binding studies of avermectins in the nematode *C. elegans* 37
10.5. *C. elegans* RNA in *Xenopus* oocytes induces Cl^- avermectin-sensitive currents 38
10.6. Distribution of bodipy ivermectin in tissues of *Ascaris* 39
11. Other Transmitters 41
11.1. Serotonin effects and pharmacology 41
11.2. Peptides 42
11.3. Glutamate 44
11.4. Other possible neurotransmitters 44
11.5. Second messengers 44
12. Conclusion 45
Acknowledgments 45
References 45

1. INTRODUCTION

Parasitic nematode infestations affect both man and animals, giving rise to considerable suffering, poor growth and performance. A number of anthelmintics used to treat these infestations interfere selectively with nematode neuromuscular transmission. Levamisole, for example, opens acetylcholine gated cation-channels in nematode somatic muscle to produce depolarization and spastic paralysis but does not affect channels of the host. The gamma-amino butyric acid (GABA) agonist piperazine, and the avermectins open different types of membrane Cl^- channels in nematodes to produce paralysis. All these drugs selectively paralyze nematode parasites of man and animals; the parasites then are no longer capable of the movement required for maintaining position and are swept away effecting a cure. A knowledge of the organization of nematode neuromuscular transmission is desirable for understanding anthelmintic modes of action. The purpose of this paper then, is to review the physiology and pharmacology of neuromuscular transmission in nematode parasites and to describe actions of antinematodal drugs which interfere with transmission.

The nematode parasite model most frequently studied is *Ascaris suum*. It is a common, large (up to 30 cm in length) nematode found in the small intestine of the pig. The frequent occurrence of the parasite means that it can be collected from local abattoirs on a weekly basis for study in the laboratory. The large size of the parasite, its somatic muscle cells and some of its neurones, have helped anatomical, biochemical, physiological and pharmacological studies, which are more difficult on smaller nematodes. Consequently, *A. suum* has been used frequently and successfully for examining the mode of action of antinematodal drugs. The results of these experiments on *Ascaris* therefore form the basis of the account presented here. A number of significant experiments have also been carried out on other smaller nematodes suggesting that these observations may be applicable to all nematodes. Binding studies using biochemical techniques have utilized the small free living nematode *Caenorhabditis elegans*, which is easily grown in the laboratory. Observations on other nematodes are therefore included where appropriate.

2. MOTOR BEHAVIOUR

Most, but not all, nematode parasites have to maintain their position in the host animal and this is achieved by sinusoidal body movements. Body movements made by the adult *A. suum* allow it to maintain its position in the intestine. It is capable of a coordinated wave of contraction and relaxation that is propagated anteriorly or posteriorly (Jarman, 1970; Crofton, 1971). The most common is a large amplitude wave, which starts about half-way along the animal and which propagates anteriorly. This wave gives rise to forward propulsion of *A. suum* when it is contained in a narrow tube like the intestine. The sinusoidal waves of nematodes are only possible in the dorsoventral plane because the somatic muscle is divided into dorsal and ventral halves innervated by their respective major nerve cord. The more complex behaviour of the head required for feeding is under the control of the cranial ganglia and sublateral nerve cords.

In contrast to the active motile nematode parasites like *A. suum*, there are 'inhibited' larval stages of trichostrongylid nematodes or the adults of the filarial worm *Onchocerca volvulus*, the nematode

are via commissures, which are single or paired (Fig. 1). The pattern of the commissures repeats itself down the length of the body with each repeat consisting of three paired right-hand commissures and one left-hand commissure. Each repeat then defines a segment. Each segment contains 11 motorneurones and six large non-segmental interneurones crossing the segments. Each motorneurone cell body has two processes and one of these may branch. The 11 motorneurones of each segment have been separated into seven anatomical types according to the distribution of their axon and dendrites: four types (VI, V1, V2, and DE1) are represented twice; three types (DI, D2, D3) are represented only once in each segment. The dendrites of DE1, DE2 and DE3 and V1 and V2 receive their input from interneurones via *en passant* synapses. In contrast, the motorneurones DI and VI receive their input from axons of the other motorneurones, that is from DE1, DE2, DE3 in the dorsal nerve cord and from V1 and V2 in the ventral nerve cord.

Selective electrical stimulation of the motorneurones DI and VI and intracellar recordings from somatic muscle cells (Stretton *et al.*, 1978), revealed inhibitory synaptic potentials in muscle and showed that DI and VI were inhibitory. Selective stimulation of the remaining types of motorneurone in the segments showed that DE1, DE2, DE3, V1 and V2 were, or were likely to be, excitatory motorneurones.

The enzyme involved in the biosynthesis of acetylcholine, choline acetyltransferase (CAT), was localized histochemically in DE1, DE2, DE3, V1 and V2 (Johnson and Stretton, 1985), a finding which is consistent with the suggestion that acetylcholine is an excitatory neurotransmitter of these motorneurones. Histochemical techniques were also used to demonstate GABA-immunoreactivity in the inhibitory motorneurones, DI and VI (Johnson and Stretton, 1987; Sithigorngul *et al.*, 1989; Guastella *et al.*, 1991a,b; Guastella and Stretton, 1991). This finding is consistent with the suggestion that GABA is the inhibitory transmitter of DI and VI.

Neurones that are anatomicaly analogous to those of *A. suum* are found in *C. elegans* the small free living nematode which is the commonly used, for genetic experiments (White *et al.*, 1976, 1986; Lewis *et al.*, 1980). The numbers, arrangement and morphology of the neurones are nearly identical to those found in *A. suum* (Stretton *et al.*, 1978, 1985). Since these two nematode species are well separated on an evolutionary time scale, it suggests that the basic neuronal organization of nematodes is the same.

3.2. PROPERTIES OF SINGLE NERVE CELLS

Intracellular recordings made from the commissures of the motorneurones DE1, DE2, DE3, DI, and VI have shown that these cells have low resting membrane potentials, -30 to -40 mV, like muscle cells (Davis and Stretton, 1989a). Current injection into the commissures did not produce all-or-none spikes and was associated with synaptic responses in muscle cells which were graded (Davis and Stretton, 1989b). It was concluded from these studies that the motorneurones were non-spiking and released transmitter tonically; it was also shown that hyperpolarization of the axons reduces release of transmitter while depolarization increases it. The presence of Ca^{2+} currents activated by depolarization of the neurones may, in addition, facilitate the tonic release of transmitter. The long space-constants of these neurones, 4–10 mm, was due to the high membrane resistance which was in the range 61–251 kohms cm^{-2}. The relatively short distance that these motorneurones have to conduct and their long space-constants allows them to be non-spiking. In contrast, the much longer interneurones found in the ventral nerve cord may spike in order to conduct the length of the adult (30 cm). Properties of the *Ascaris* motor nervous system have also been studied using extracellular recording techniques (Davis and Stretton, 1992).

The ability of quiescent ventral inhibitory motorneurones in *A. suum* to generate slow depolarizing potentials in response to continuous current injection was investigated by Angstadt and Stretton (1989). They found that repetitive 20 mV depolarizing slow potentials with a period of about 700 msec were produced and that these depolarizing potentials were blocked by Ca^{2+}-channel blockers, suggesting the involvement of Ca^{2+} currents. The rhythmic potentials in VI gives rise to rhythmic inhibitory potentials in ventral muscle cells and may contribute to locomotory behaviour.

responsible for river blindness. These helminths do not require coordinated motor activity to maintain their position; their neuromuscular system is not well developed and the parasite is not so vulnerable to drugs affecting locomotion.

3. NEURONAL ORGANIZATION

3.1. Anatomy of The Nematode Nervous System

The studies of Hesse (1892), and Goldschmidt (1908, 1909), showed that there are only about 250 neurones present in *Ascaris* and that the position and structure is completely reproducible from animal to animal.

In the head region, Goldschmidt (1908), described a nerve ring surrounding the pharynx and a series of associated ganglia. The ganglia which together contain 162 neuronal nuclei consist of a dorsal ganglia, a ventral ganglia, two lateral ganglia and the retrovesicular ganglion. The anatomy and electrophysiology of the retrovesicular ganglion has been described in further detail by Angstadt *et al.* (1989). Two major nerve cords arise from the nerve ring dorsally and ventrally, and pass caudally along as the major dorsal nerve cord and the major ventral nerve cord. The cell bodies of nearly all motor neurones are found scattered in the ventral nerve cord and total 75 in number.

In addition to the major nerve cords, there are also pairs of minor lateral and sublateral nerve cords (Johnson and Stretton, 1987). In the anterior region of the nematode there is: the left and right dorsal sub-lateral cords and the left and right ventral sub-lateral cords as well as the left and right dorsal lateral cords. These minor nerve cords in the anterior region are involved in the more complicated movements of the head required for feeding. In the tail region the four minor nerve cords are: the left and right dorsal and ventral lateral nerve cords. These nerve cords are involved with the more complicated tail movements associated with copulation.

Stretton *et al.* (1978) described and classified the anatomy and physiology of the motorneurones of *A. suum*: they based their observations on tracing nerve fibres in serial sections and on intracellular recordings from muscle cells during electrical stimulation experiments. Since the cell bodies of motorneurones are located in the ventral cord, the connections to the dorsal nerve cord

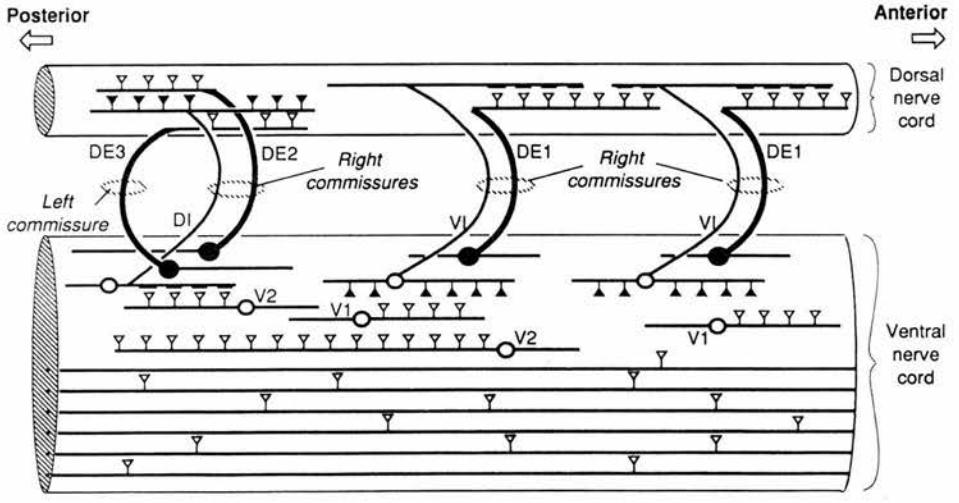


FIG. 1. Summary diagram of anatomical organization of *Ascaris suum* dorsal and ventral nerve cords in one 'segment'. Eleven motorneurones are present in each 'segment'. Six large interneurones run the length of the ventral cord. There are seven anatomical types of motorneurone, but only two physiological types (E = excitatory, cholinergic; I = inhibitory, GABAergic). DE1, dorsal excitator 1. DE2, dorsal excitator 2. DE3, dorsal excitator 3. DI, dorsal inhibitor. VI, ventral inhibitor. V1 and V2 ventral (excitatory) motoneurones. The cell bodies of all motorneurones are in the ventral cord. The commissures are axons of motorneurones which pass round the body; they are paired or single axons.

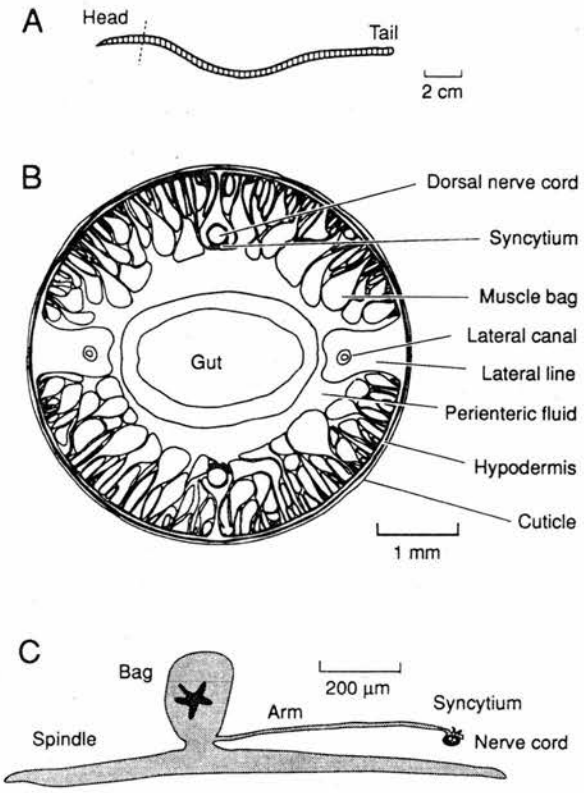


FIG. 2. (A) Diagram of *A. suum* showing the location of the transverse section of B. (B) Diagram of a transverse section through body. (C) Diagram of the structure of a somatic muscle cell.

as 'fingers'. Tight junctions form between adjacent fingers in the syncytium (Rosenbluth, 1965b) which are responsible for the electrical coupling seen between adjacent cells (De Bell *et al.*, 1963).

Neuromuscular junctions are formed by 2 μm extensions of the longitudinal axons which penetrate the hypodermal chalice and closely associate with the syncytium (Fig. 3). The synaptic region is associated with: clear spherical 40 nm vesicles clustered under the presynaptic membrane around tubules, dense core vesicles (80–100 nm in diameter), giant mitochondria and membrane thickenings on the presynaptic and postsynaptic membrane (Rosenbluth, 1965b). Except in the head region, the dorsal muscle cells are only connected to the dorsal nerve cord, while the ventral muscle is only connected to the ventral nerve cord. Contraction is therefore only possible in the dorso-ventral plane.

5. THE PHARYNGEAL MUSCLE

In addition to the organization of somatic muscle, pharyngeal muscle is also considered since future anthelmintics might be designed which affect feeding via an action on this muscle; it also has an interesting physiology.

Pharyngeal muscle of *A. suum* forces food into its intestine. It developes from about 30 cells which fuse to become one functional tube shaped cell (Goldschmidt, 1904; Del Castillo and Morales, 1967a), which is 1 cm long and 1 mm in diameter. The triradiate lumen is closed when the muscle is relaxed. Its contractile fibres are radially oriented (Mapes, 1966; Reger, 1966), so that when these fibres contract during depolarization the outer diameter of the cell expands and the lumen opens because the sarcoplasm is incompressible. When the lumen opens, food is sucked into the pharynx through a one-way valve near the mouth. Then as the pharyngeal muscle cell repolarizes the contractile fibres relax and elastic components that were stretched rapidly close the

3.3. Motorneurone Nerve Cell Interconnections

Over 2000 synapses from serial sections of *A. suum* nerve cords have been examined by light or electron microscopy by Stretton *et al.* (1978, 1985). Each motorneurone has distinctive regions where it receives an input from the large interneurones. In addition to these sites there are synaptic contacts between the motorneurones themselves. This implies that motorneurones also possess acetylcholine and GABA receptors in the same way that the somatic muscle does. The majority of synaptic contacts between motorneurones fall into three types: excitatory axons projecting onto opposite inhibitory dendrites (ventral excitator onto dorsal inhibitor or dorsal excitator onto ventral inhibitor) and reciprocal synapses between excitatory and inhibitory axons in each nerve cord (ventral excitator projecting onto ventral inhibitor and dorsal excitator projecting onto dorsal inhibitor). Walrond *et al.* (1985) and Walrond and Stretton (1985) reported that in addition to responses in muscle cells known to be directly innervated by a particular dorsal excitatory motorneurone, some excitatory and some inhibitory responses are produced in muscles which are not directly innervated. The excitatory field in the muscle cell produced by stimulation of excitatory motorneurones was sandwiched between a cranial and a caudal inhibitory zone. The excitatory field was further divided into two: one was produced by direct synaptic input from the motorneurone and the other was produced by a slowly propagating wave in the syncytium which began in the region of the direct synaptic input.

Walrond and Stretton (1985) subsequently showed, with the dissected preparation, that stimulation of the dorsal excitatory motorneurone, DE1, produced reciprocal inhibition in ventral muscle cells as a result of the projection onto the ventral inhibitory motorneurone, VI. They also showed that the motorneurones DE2 and DE3 could produce reciprocal inhibition as a result of projecting onto VIs in adjacent segments. Reciprocal inhibition in the ventral cord was suggested on anatomical grounds involving the putative excitatory motorneurones V1 and V2 and their projection onto the dorsal inhibitory motorneurone DI. The report of Walrond and Stretton (1985) demonstated that stimulation of DE1, DE2 and DE3 produced, via a projection onto the DI, inhibition in muscle fields adjacent to the dorsal excitatory field. The consequence of this synaptic organization, with reciprocal and adjacent inhibition, is that stimulation of a single excitatory motorneurone would produce an omega-shaped body waveform. This synaptic organization provides a basis for propagated waves of muscle contraction.

4. ANATOMY OF SOMATIC MUSCLE CELLS

The anatomy of somatic muscle cells of *A. suum* was described by Schneider as early as 1866. Because the muscle cells have an unusual structure, with processes of the muscle going to the nervous system, rather than processes of the nervous system going to the muscle, it was the subject of considerable debate by scientists of the day (Schneider, 1866; Goldschmidt, 1908; Cappe de Baillon, 1911). Figure 2 shows, in diagrammatic form, a transverse section through the anterior region of *A. suum* and the structure of somatic muscle cells together with their connection to the nervous system.

The contractile region, known as the spindle ('fuseau', Cappe de Baillon, 1911) lies under the hypodermis and is composed of 'obliquely striated muscle' (Rosenbluth, 1965a,b, 1967, 1969). The actin and myosin filaments are arranged in an acute angle, in contrast to the 90° angle of vertebrate skeletal muscle. This organization allows the greater extensibility of smooth muscle but still allows the velocity of contraction to be maintained. The fast contraction of *Ascaris* muscle, associated with Ca^{2+} fixation by actin, is produced by acetylcholine: relaxation produced by GABA is associated with a change in the phosphorylation state of light chain myosin (Martin and Donahue, 1987).

The bag or belly ('panse', Cappe de Baillon, 1911) is a large 200 μm bag-shaped structure which contains the nucleus and particulate glycogen (Rosenbluth, 1965a,b). It lies in the peri-enteric space and its turgidity probably provides the pressure against the collagen layers of the cuticle which allows the nematode to be sufficiently rigid to contract and move (Harris and Crofton, 1957).

Each somatic muscle cell of *A. suum* has an average of 2.7 arms (Stretton, 1976). The arms are thin processes which pass from the base of the belly towards the syncytium, which lies over the nerve cord. As the arms reach the syncytium, they break up into a number of finer processes known

lumen forcing the food in the lumen into the intestine of the *Ascaris* through a second one-way valve.

Del Castillo and Morales (1967a,b), and Byerly and Masuda (1979), have examined the electrophysiology of the pharyngeal muscle using current-clamp and voltage-clamp techniques. It has a resting membrane potential of -35 mV and a positive-going action potential that reaches $+30$ to $+50$ mV which is associated with opening of the lumen. The potential remains depolarized from 150 msec to several seconds with the open lumen; then the potential is suddenly returned to negative values by a unique negative-going action potential carried by a K^+ current to allow rapid closing of the lumen. The K^+ current is different from all other K^+ currents since it is analagous to the classical Na^+ current of nerve and muscle except for inversion of its voltage-dependencies.

Byerly and Masuda (1979) also describe two distinct postsynaptic potentials resulting from the action of the pharyngeal nervous system. There was a depolarizing postsynaptic potential with a reversal potential of -10 mV which frequently triggered the positive-going action potential. In addition there was a hyperpolarizing postsynaptic potential with a reversal potential of -40 mV which could trigger the negative-going spike when the membrane was depolarized. The pharmacology of the receptors involved has not been further explored but might offer future target sites for anthelmintics.

6. ELECTROPHYSIOLOGY OF SOMATIC MUSCLE

6.1. MEMBRANE POTENTIAL

Jarman (1959) made intracellular recordings from *A. suum* muscle cells fairly soon after the development of the intracellular recording technique. He described the presence of regular spontaneous spike-like depolarizing potentials which were superimposed on an unusually low resting potential of around -30 mV. Similar membrane potentials were also observed in the poultry nematode, *Ascaridia galli* (Wann, 1987), and sheep nematode, *Haemonchus contortus* (Atchison *et al.*, 1992). The ionic basis of the resting potential in *A. suum* was subsequently investigated by Del Castillo *et al.* (1964a) and Brading and Caldwell (1971). Both studies reported that extracellular K^+ had little effect on the potential in contrast to the effects of extracellular Cl^- and to a lesser extent extracellular Na^+ Radiolabelled ion-flux experiments of Caldwell and Ellory (1968), have revealed that the permeability ratio for K^+, Na^+ and Cl^- was 1:4:7 again illustrating the importance of Cl^- and to a lesser extent Na^+. Consequently, Brading and Caldwell (1971) noted that the original Goldman–Hodgkin–Katz equation was not able to describe the behaviour of the membrane potential and suggested that an active electrogenic pump, possibly moving carboxylic acids, might explain the behaviour of the membrane potential. Caldwell subsequently considered this problem in a theoretical paper (Caldwell, 1974).

The composition of peri-enteric fluid, which normally surrounds the muscle cells, is consistent with movement of carboxylic acids across the muscle cell membrane. Hobson *et al.* (1952a,b) found that the peri-enteric fluid contains low concentrations of Cl^- but high concentrations of carboxylic acid. The carboxylic acids (acetate, propionate, succinate, 2-methylbutyrate and 2-methylvalerate) are produced inside muscle cells from the anaerobic metabolism of glucose (Saz and Weil, 1962; Tsang and Saz, 1973). Recently, we have initiated an investigation of the permeability properties of a high conductance Ca^{2+}-dependent Cl^- channel (Fig. 4) in the muscle membrane of *A. suum* (Thorn and Martin, 1987; Dixon *et al.*, 1992) and found that it is permeable to these carboxylic acids (M. A. Volkanov, R. J. Martin and D. M. Dixon, unpublished observations). Thus a Ca^{2+}-activated Cl^- channel permeable to the products of anaerobic fermentation appears to have a major influence on the membrane potential of muscle.

6.2. DEPOLARIZING POTENTIALS

The spontaneous depolarizing potentials, described in muscle by Jarman (1959), were shown to be myogenic in origin and appear to arise at the syncytium (De Bell *et al.*, 1963; De Bell, 1965). Three types of depolarizing potential have now been recognized (Fig. 5). They consist of: (i) spikes of varying amplitude up to 30 mV and lasting 5–50 msec (De Bell *et al.*, 1963; Weisblat and Russel,

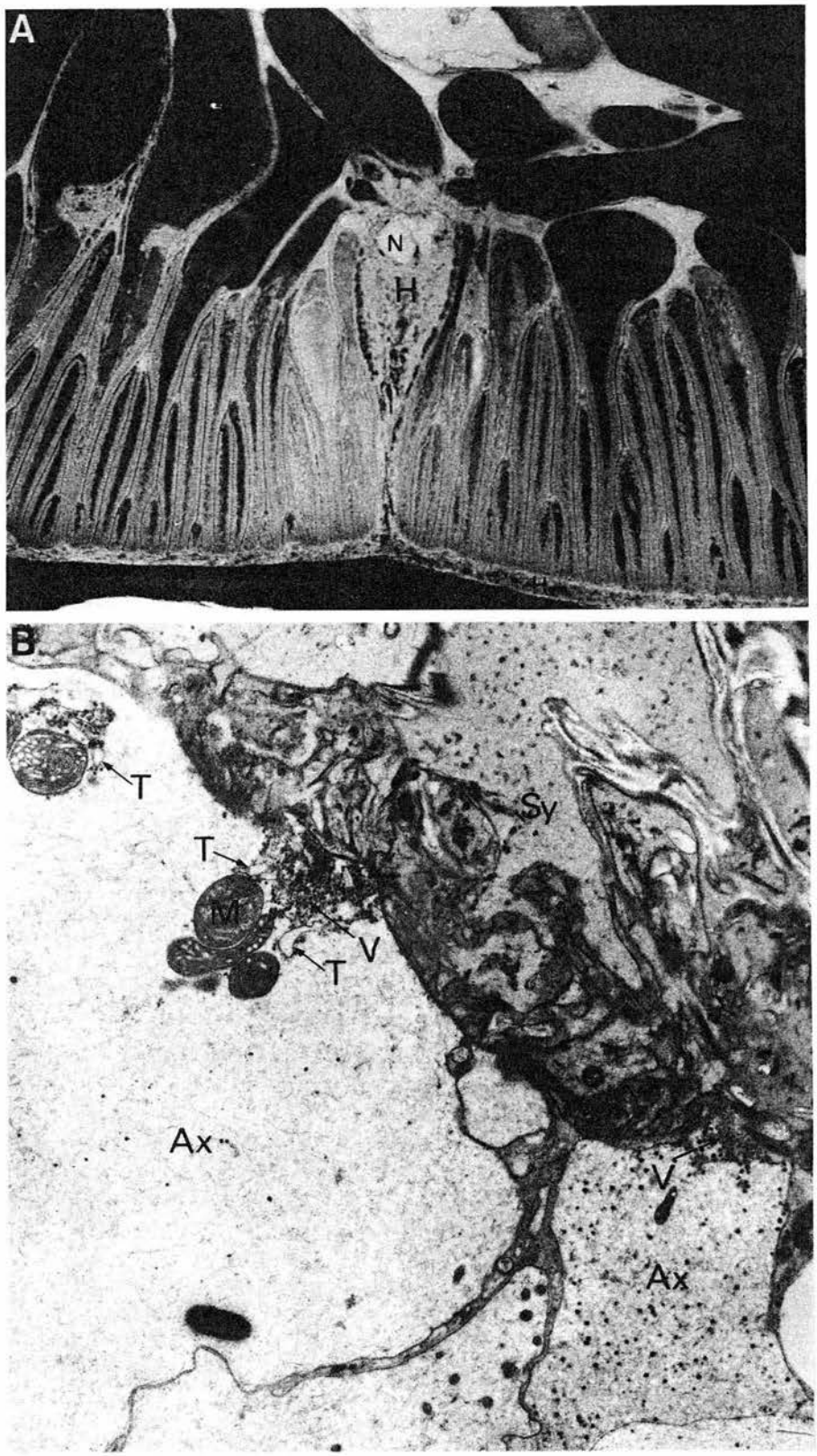


FIG. 3. (A) Photomicrograph of a transverse section through the body wall. × 70. Ar, arm; H, hypodermis; B, bag; S, spindle; N, nerve cord; B, electronmicrograph of neuromuscular synapses; T, tubules; SY, syncytium; M, mitochondia; V, synaptic vesicl; AX, axon. Note the presence of the electron dense vesicles as well as the clear vesicles. × 70,000.

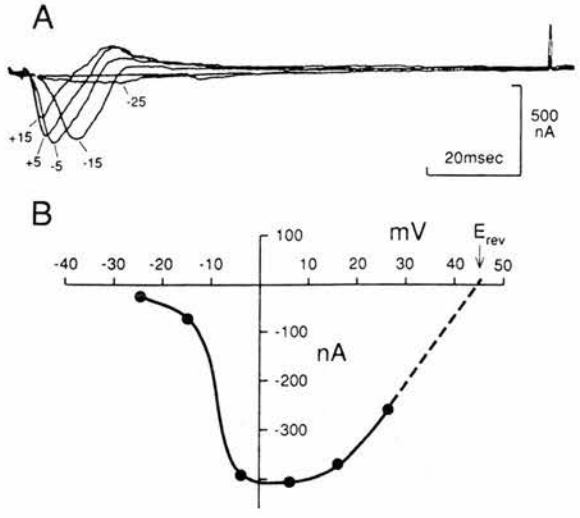


FIG. 6. (A) Inward Ca^{2+} currents produced by depolarizing voltage-clamp steps of the bag membrane from a holding potential of -35 mV to the potentials shown on the current trace. (B) Current–voltage plot of the peak Ca^{2+} current against step potential.

Del Castillo *et al.* (1989), showed that the average coupling coefficient was 0.4 for cells oriented perpendicular to the long axis, but cells oriented parallel to the long axis showed no coupling. Physiological manipulation of this coupling remains to be demonstrated, although impairment of cell–cell coupling by bath-applied GABA has been demonstrated (De Hello and Maldonado, 1985). Thus GABA and GABA receptor agonists may reduce coordinated activity.

Ion-substitution experiments have been used to examine effects on the spike potentials and slow waves (Weisblat *et al.*, 1976). It was found that Ca^{2+} was required to support the spike potentials and that Na^+ and Ca^{2+} was required for the slow waves. Interestingly, the Ca^{2+} spikes are not blocked by the Na^+ channel blocker tetrodotoxin (Jarman and Ellory, 1969), or by the Ca^{2+} channel blockers verapamil or cinnarizine but required 'high concentrations' of ivermectin to produce block (Wann, 1987). The currents responsible for the spike potentials have been recorded under a two-microelectrode voltage-clamp (Martin *et al.*, 1992b). These Ca^{2+} currents producing spike depolarization (Fig. 6) appear to inactivate rapidly. The two K^+ currents which facilitate repolarization consist of a low threshold rapidly inactivating current, an I_a-like current and a higher threshold noninactivating current, an I_k-like current (Fig. 7). K^+ currents are reduced by 4-aminopyridine and the anthelmintic diethylcarbazine (Martin, 1982). The ionic basis of the slow waves and modulation waves has not yet been investigated under voltage-clamp but the behaviour of 'square waves' suggests that Ca^{2+} currents are involved (Weisblat *et al.*, 1976).

7. ACETYLCHOLINE

7.1. EFFECTS OF ACETYLCHOLINE ON *ASCARIS* MUSCLE

Initially, Baldwin and Moyle (1949), and then Norton and De Beer (1957), bath-applied acetylcholine and showed that it produces contraction of muscle strips and as a result demonstrated the presence of acetylcholine receptors on muscle. Bath-applied acetylcholine was found to produce depolarization and change spike frequency and amplitude in muscle (Del Castillo *et al.*, 1963). Ionophoresis experiments revealed that the receptors responsible for this are located synaptically at the syncytial region (Del Castillo *et al.*, 1963), and extrasynaptically on the bag region of the muscle (Martin, 1982).

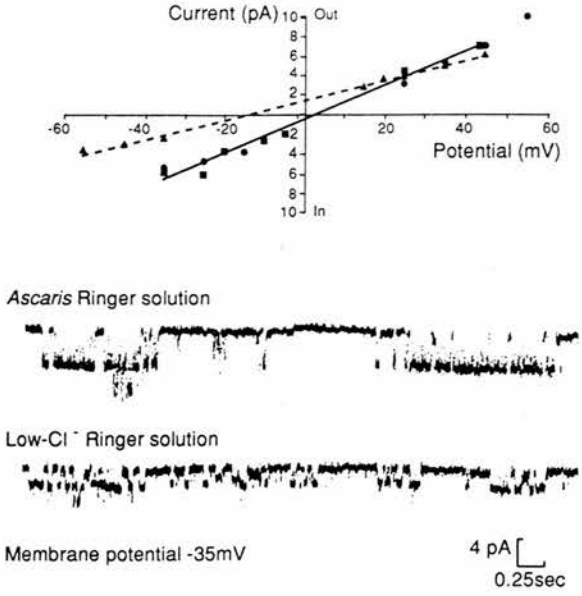


FIG. 4. Ca^{2+}-dependent Cl^- channels. Ca^{2+}-dependent Cl^- channels active in the presence of 2mM Ca^{2+} applied to the inside membrane of an inside-out patch. The recording at -35 mV shows these channels in a high Cl^- Ringer (*Ascaris* Ringer) and a low Cl^- Ringer in the bath. The I/V plot shows the relationship between current amplitude and patch potential in symmetrical Cl^- (■ and ●) and when the Cl^- concentration was reduced at the cytoplasmic surface of the membrane (A). Note that the reduced Cl^- causes a hyperpolarizing shift in the zero current potential and a reduction in the slope conductance of the membrane and shows that that the channel conducts Cl^-.

1976); (ii) slow waves up to 20 mV in amplitude and lasting 100–1000 msec (De Bell *et al.*, 1963; Weisblat and Russel, 1976); and (iii) a long lasting modulation wave, around 5 mV, lasting 3–20 sec and coinciding with contraction of the body wall (Weisblat and Russel, 1976).

The electrical activity seen in adjacent muscle cells is correlated (Jarman, 1959): anteriorly placed cells depolarize before cells behind them; cells nearest to a nerve cord depolarize before those placed laterally. The coupling allows adjacent muscle cells to synchronize depolarization and contraction. De Bell *et al.* (1963) and Del Castillo *et al.* (1967, 1989) have used simultaneous recording and current injection from two intracellular micropipettes to record the electrical coupling which occurs between adjacent muscle cells. The coupling is consistent with the presence of tight junctions seen with the electron microscope (Rosenbluth, 1965b). Initial studies on the coupling coefficients by

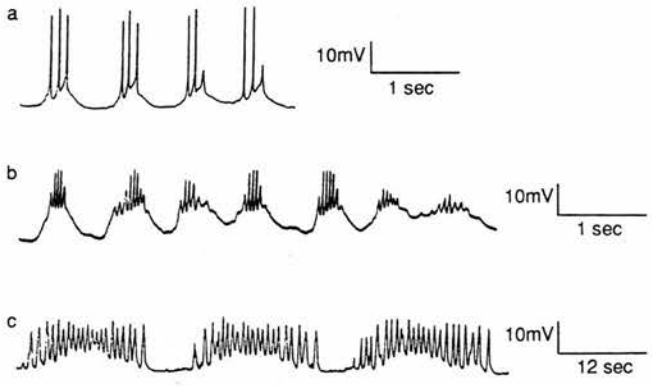


FIG. 5. Spontaneous electrical activity in a muscle cell at 37°C. (A and B) Spikes and slow waves. (C) Modulation waves. Calibration bars 10 mV and 1 sec in A and B; 10 mV and 12 sec in C. Modified from Weisblat and Russell (1976).

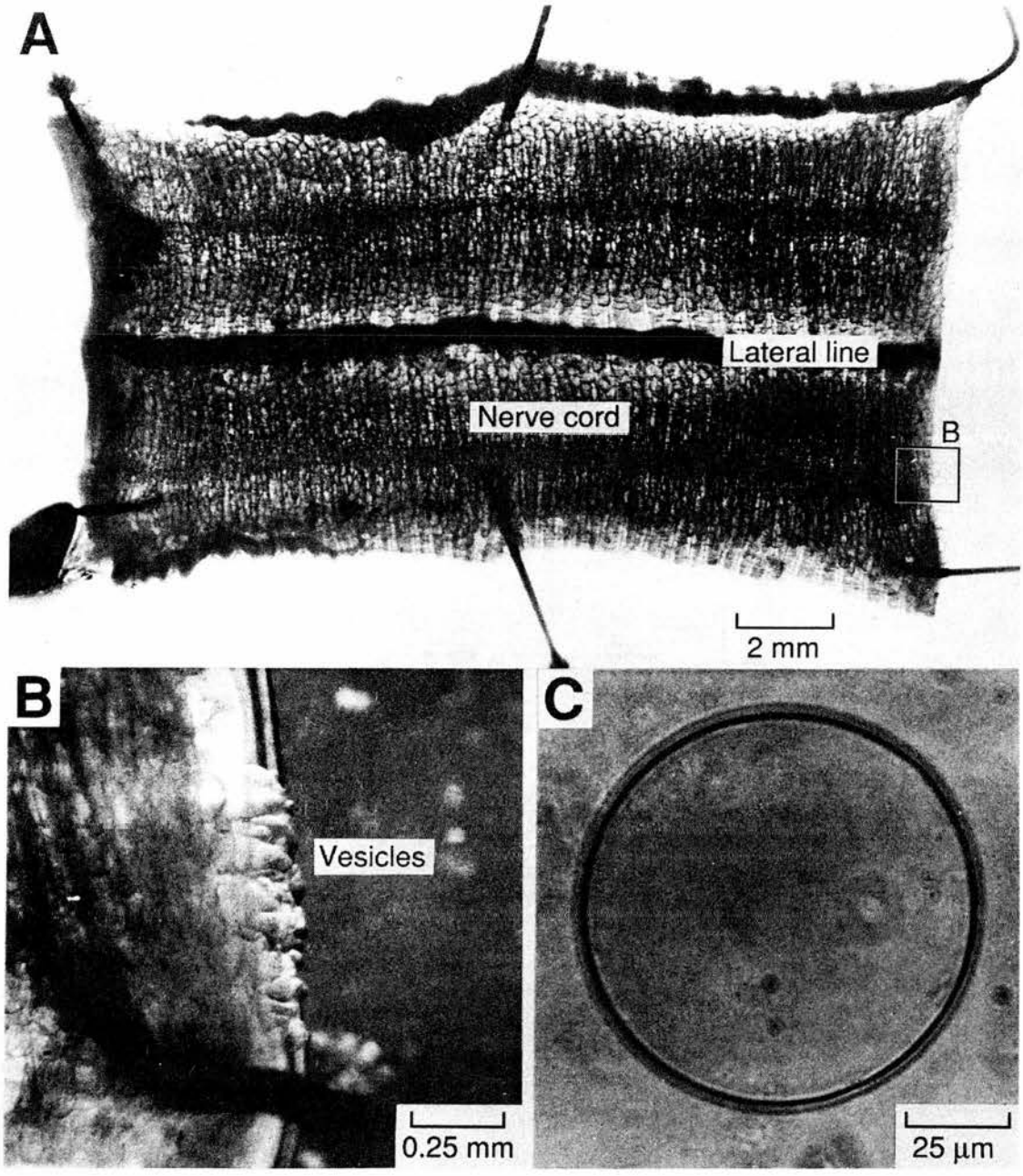


FIG. 8. (A) Photograph of the flap preparation. (B) Enlargement of the edge of the flap showing the formation of vesicles following 10 min in 1 mg ml^{-1} collagenase and incubation for 1 hr at 37°C. (C) A phase contrast photomicrograph of a muscle vesicle.

with a Pasteur pipette. The main advantage offered by the vesicle preparations is that they can be viewed under phase contrast, and that they are not covered by any connective tissue so that they permit 'Giga-seal' formation required for recording single-channel currents (Fig. 9). As shown in Fig. 10, acetylcholine-activated single-channel currents have been recorded from cell-attached and isolated inside-out patches using this preparation (Pennington and Martin, 1990). The channels activated by acetylcholine have at least two conductances: the larger was 40–50 pS and the smaller 25–35 pS; the I/V plot of both channels were linear; and the average open-times were independent of patch potential. Kinetic analysis of the larger conductance channel showed that the distributions of open- and burst-durations were composed of two components (short and long) and analysis of the closed-time distributions showed that they were composed of at least three components (short,

7.2. Ionic Basis of The Electrical Responses To Acetylcholine

The ionic basis of electrical responses to acetylcholine has been investigated by applying transmitter ionophoretically to the bag region of the muscle cell and making current- or voltage-clamp records of the responses. It has been shown that acetylcholine increases the non-selective cation conductance of the membrane and that the reversal potential associated with the response is near 0 mV (Martin, 1982; Harrow and Gration, 1985): the response is compatible with acetylcholine opening ion-channels permeable to both Na^+ and K^+.

7.3. *Acetylcholine Single-channel Currents*

A muscle vesicle preparation suitable for making single-channel recordings from *A. suum* muscle membrane has been developed (Fig. 8) (Martin *et al.*, 1990). The technique involves treating a flap preparation with collagenase for a brief period of 10 min, followed by incubation in collagenase-free solution; the vesicles then form by 'budding off' from the bag region and may be collected

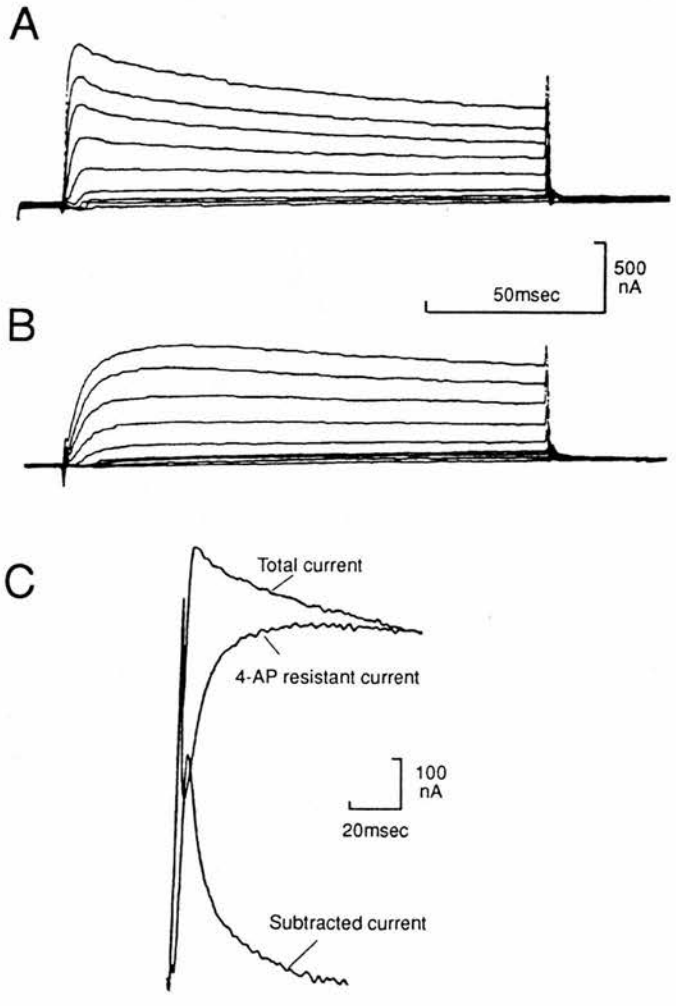


FIG. 7. The two types of bag membrane K^+ current under voltage-clamp. (A) Total outward K current produced under voltage-clamp by deplarizing steps from -40 mV; the depolarizing voltage steps were increased by 10 mV on each step and produced the series of superimposed currents. (B) The experiment was repeated on the same cell in the presence of 4 mM 4-aminopyridine which has been described as a selective blocker of a rapidly inactivating K^+ current known as I_a. Note the loss of the rapidly activating current. (C) Subtraction of the two currents seen in (A) and (B) following the maximum deplarizing step reveals the I_a current.

extracellular matrix; enzyme activity was also observed in muscle arms near their endings on the nerve cords but not on the bag region; little or no staining was seen in the nervous tissue. No staining was seen caudal to the vulva, an observation consistent with propagation of contraction waves starting at the vulva and passing anteriorly. Johnson and Stretton (1980) have reported the presence of two types of cholinesterase, a 13 S and 5 S form, which are not distributed in the same way. The 5 S fragment has a K_m for acetylcholine of 25 μM and is inhibited by the detergent sodium deoxycholate. The 13 S form has a K_m for acetylcholine of 100 μM and are reversibly inhibited by low concentrations of the detergent Triton X-100. These two forms of acetylcholinesterase are also found in *C. elegans*, where they are products of separate genes (Johnson and Stretton, 1980). The distribution of the 5 S form is greatest anterior to the vulva region while the 13 S form predominates posterior to the vulva. Since the most active region is the muscle anterior to the vulva, it is suggested that the 5 S form is involved in motor activity. Although cholinesterase is responsible for the breakdown of acetylcholine released from excitatory motorneurones, it is also secreted in the external environment by *A. suum* and has been suggested to act as a 'biochemical holdfast' by blocking local peristalsis (Lee, 1970).

CAT the enzyme responsible for the synthesis of acetylcholine, has been demonstrated in the commissural branches of the excitatory motorneurones as well as in the hypodermis (Johnson and Stretton, 1980, 1985). The presence of CAT in the excitatory motorneurons is consistent with acetylcholine being the transmitter. The function of CAT in the hypodermis is not clear, but it has been suggested that the synthesis and release of acetylcholine from the hypodermis may cause tonic contraction by an action on extrasynaptic acetylcholine muscle receptors (Johnson and Stretton, 1980). The hypodermal CAT is concentrated in two bands within 1 mm of the tip of the head. The most anterior band in the hypodermis is in a region without somatic muscle and is in direct contact with the pseudocoelom. Thus release of acetylcholine from the anterior band of CAT could provide a source of acetylcholine in the body cavity; the extrasynaptic acetylcholine receptors found on the muscle may then be affected tonically by this scource of acetylcholine (Johnson and Stretton, 1980).

7.6. CHOLINESTERASE ANTAGONISTS AS ANTHELMINTICS

Anticholinesterases have been shown to potentiate the electrophysiological effects of acetylcholine in *Ascaris* by Del Castillo *et al.* (1963), who used the carbamate neostigmine. A large number of organophosphorous anticholinesterases have been tested in *A. suum* by Knowles and Casida (1966) who found that many of these compounds were toxic to the parasite and were inhibitors of *A. suum* acetylcholinesterase. The organophosphates which were not active against *Ascaris* were not active against their acetylcholinesterase.

A number of organophosphorous anticholinesterases, originally introduced as insecticides, are now used for their anthelmintic properties. They include: metriphonate (trichlorfon), dichlorvos, napthalophos, crufomate and haloxon (Martin, 1985a; Roberson 1988). The use of these compounds against nematodes shows that the cholinesterases of nematodes are different from the mammalian hosts and that they are an effective target site for anthelmintics. The role of these drugs is generally restricted to the treatment of specific roundworm infestations since the organophosphorous anthelmintics are do not have a very broad spectrum. They have an advantage over most other anthelmintics (except ivermectin) in also controlling arthropod parasites.

The acetylcholinesterases of nematode parasites differ between species: acetylcholinesterase of *H. contortus* forms an irreversible complex with haloxon; acetylcholinesterase from *A. suum* is also bound by haloxon but the complex is reversible allowing the esterase to recover within 24 hr; the esterase–holoxon complex of *Bunostomum* is unstable and lasts for as little as 30 mins (Roberson, 1988). The failure of haloxon against *Bunostomum* is attributable to the rapid recovery of its esterase from the drug. Similar short periods of inhibition in a number of other nematodes can explain the narrow spectrum of the organophosphorous anthelmintics.

7.7. PHARMACOLOGY OF THE ACETYLCHOLINE RECEPTOR

Initial experiments on the pharmacology of *A. suum* acetylcholine receptors used contraction of muscle strips. Low concentrations of nicotine produced contraction (Toscano-Rico, 1926; Baldwin

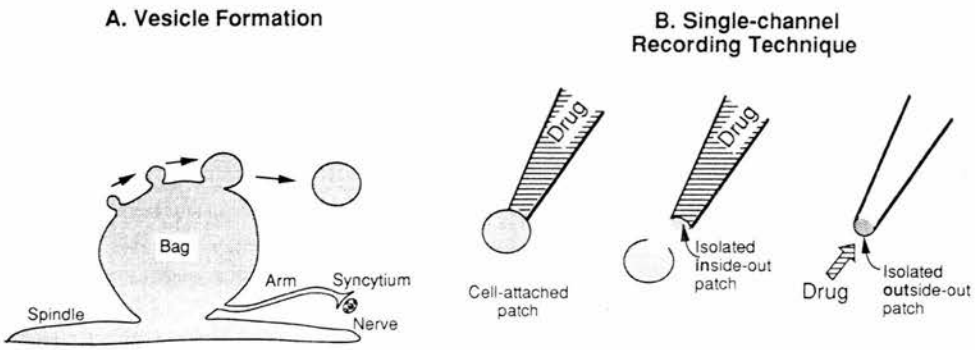


FIG. 9. (A) Diagram of the formation of muscle vesicles from the bag. (B) Diagram of the three types of patch used to make single-channel recordings of drug activated channels.

intermediate and long). These observations are interpreted as indicating that the larger conductance has at least two open-states and three closed-states. The average open-time was similar to that of the nicotinic channel at the frog neuromuscular junction and had a corrected mean open-time of 1.26 msec. High concentrations of acetylcholine (25–100 μM) produced a reduction in open probability and caused single-channel currents to occur in clusters with long closed-times (200 sec) between clusters; this behaviour has also been reported for the frog neuromuscular junction and described as desensitization.

7.4. Acetylcholine Receptors on Motorneurones

The presence of acetylcholine receptors on motorneurones has been pointed out by Stretton (1992) who commented that they were also involved in the contraction responses of muscle strip preparation following bath-applied acetylcholine agonists. The neuronal acetylcholine receptors were detected by recording intracellularly from the commissural axons of motorneurones. It was also suggested that the pharmacology of these receptors may differ from the muscle receptors.

7.5. Biochemistry of Acetylcholine

The presence of acetylcholine in *A. suum* was described originally by Mellanby in 1955. He observed that acetylcholine was found in *Ascaris* head and body walls, and that the head contained 10 times more acetylcholine than the body wall (0.39 mg g^{-1} vs 0.025 mg g^{-1}).

Cholinesterase, the enzyme inactivating acetylcholine, was first reported in *A. suum* by Bueding (1952). Lee (1962) described the distribution of this enzyme using histochemical techniques: in the head region, most of the activity was associated with the contractile region of the muscle in the

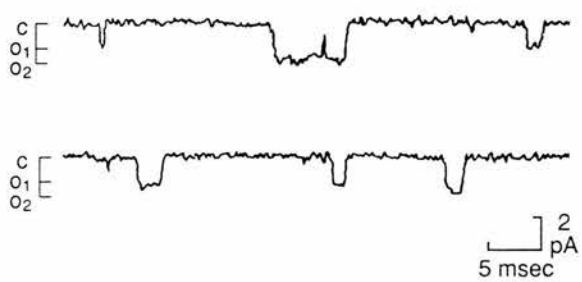


FIG. 10. Acetylcholine-activated channels in a cell-attached patch from a muscle vesicle. C: closed state. 01: smaller conductance state. 02: larger conductance state. Patch-potential: − 50 mV. The pipette contained 10 μM ACh. Pipette solution (mM): CsCl, 140; $MgCl_2$, 2; EGTA, 1; HEPES, 10; pH 7.2 with CsOH. Bathing solution (mM): CsCl, 35; Cs acetate, 105; $MgCl_2$,2; EGTA, 1; HEPES, 10; pH 7.2 with CsOH. Filter: -3 dB 2.5 KHz, 8-pole Bessel. The mean open time was 1.5 msec.

TABLE 1. *Potency of Cholinergic Agonists and Antagonists in* A. suum

	Contraction muscle strip			Electrophysiology input conductance	
	μM	μM	μM	μM	
Agonists					
Morantel				0.4	
Pyrantel				0.4	
Metahydroxphenyl-propyltrimthylammonium					9
Dimethylphenylpiperazinium		0.2–0.6	0.7		2
Pentyltrimethylammonium			1.1		
Levamisole				20	
Acetylcholine	1	6–55	6.1	110	1
Propionylcholine		2			
Succinylcholine			3.1		
Nicotine	1	2–38	3.5		0.3
Carbachol		5–55	4.1		0.5
Trimethylammonium			2.9		0.05
Muscarone					0.006
Furtrethonium					0.007
Arecoline					0.002
Suberyldicholine			4.7		
Decamethonium		73–366			
McN-A-343					no effect
Bethanacol					no effect
Methacoline					no effect
Oxtremorine					no effect
NMTHT					no effect
Pilocarpine					weak
Muscarine					hyperpolarization
Antagonists					
N-methyllycaconitine					0.23
Benzoquinonium					0.29
Chlorisondamine					1.74
Bungarotoaxin					1.4*
Mecamylamine		0.25			
Strychnine	100				1.29
Tubocurarine	100	2.34	0.5		3.1
Tetraphenyphosphonium					1.9
Quinacrine					2.1
Tetraethylammonium			6.0		
Pancuronium					3.2
Trimethaphan					4.27
Atropine		80	80		6.7
Decamethonium					14.0
Hexamethonium			40		43
Dihydro-beta-erythroidine					100

Baldwin and Moyle (1949): lowest concentration producing contraction. Natoff (1969): range of agonist concentrations producing contraction; antagonist K_D. Rozhkova *et al.* (1980): EC_{50} muscle contraction; antagonist K_D. Harrow and Gration (1985): EC_{50} input conductance. Colquhoun *et al.* (1990, 1991): Walker *et al.* (1992): relative potency for agonists; IC_{50} for antagonists.

8.2. EFFECTS ON INTRACELLULAR POTENTIAL

Aceves *et al.* (1970) used intracellular recording techniques on *A. suum* muscle to observe effects of bath-applied tetramisole (a D,L racemic mixture of which levamisole is the laevo-isomer). Tetramisole produced depolarization, an increase in spike frequency and contraction. The effects were reported not to be antagonized by high doses of tubocurarine. This observation suggested that levamisole might have acted on different receptors compared to acetylcholine but the observation has not yet been substantiated.

Aubry *et al.* (1970) described in the same journal and volume as Aceves *et al.* (1970) the

and Moyle, 1949; Natoff 1969), like acetylcholine (Baldwin and Moyle, 1949; Natoff, 1969; Rozhkova *et al.*, 1980; Grzywacz *et al.*, 1985; Onuaguluchi, 1989). The acetylcholine-induced contractions were blocked by tubocurarine but not by atropine (Baldwin and Moyle, 1949; Natoff, 1969; Rozhkova *et al.*, 1980), so that the *A. suum* acetylcholine receptors have some of the pharmacological properties of vertebrate nicotinic receptors. Experiments on 'cut worm' preparations of the smaller nematode *C. elegans* following mutation led to a similar conclusion but also suggested the presence of two types of acetylcholine receptor, one of which was resistant to levamisole (Lewis *et al.*, 1980). Nicotinic-like receptors have also been observed in the sheep intestinal nematode H. contortus (Atchison *et al.*, 1992), and the filarial nematode *Dipetalonema vitiae* (Christ *et al.*, 1990).

Natoff (1969) and Rozhova *et al.* (1980) attempted to classify the receptors as either ganglionic or neuromuscular. These papers reported that: (i) the potent ganglionic nicotinic agonist dimethylphenylpiperazinium was more potent than acetylcholine in *Ascaris*; (ii) the potent ganglionic nicotinic antagonist mecamylamine is the most potent acetylcholine antagonist in *Ascaris*, more potent than tubocurarine; (iii) in contrast, hexamethonium, a potent ganglionic antagonist in vertebrates, had a low potency in *Ascaris*. The *Ascaris* acetylcholine receptors cannot, therefore, be classified as either ganglionic or neuromuscular and can be regarded as a separate sub-type of nicotinic receptors (e.g. the $ACh_{Ascaris}$ receptors).

Electrophysiological techniques have also been used to examine effects of cholinergic agonists and antagonists on muscle (Aubry *et al.*, 1970; Aceves *et al.*, 1970; Martin, 1982; Harrow and Gration, 1985; Colquhoun *et al.*, 1989, 1990, 1991; Walker *et al.*, 1992). The potency of these compounds in *Ascaris* is summarized in Table 1. Levamisole and pyrantel are more potent agonists at the *Ascaris* muscle acetylcholine receptor than at vertebrate nicotinic receptors, where they have only weak nicotinic actions (Aubry *et al.*, 1970; Eyre, 1970). The selective action of these drugs allows them to be used as effective anthelmintics, killing the nematode parasite but not the host. The degree of selectivity will obviously affect the safety and efficacy of any nicotinic drug selected for therapeutic purposes.

In an extensive study of the pharmacology of muscle cholinoceptors in *Ascaris*, using membrane potential and input conductance responses (Colquhoun *et al.*, 1991), it was found that pilocarpine and muscarine caused a slight hyperpolarization (up to 3 mV) rather than a depolarization. These observations raise the possibility that in addition to the nicotinic-like receptors, muscle cells may possess muscarinic-like receptors for acetylcholine. Arevalo and Saz (1991) have observed that acetylcholine increases the levels of phosphorylcholine, 1,2-diacylglycerides and phosphatidic acid, and with the demonstration of the presence of phospholipase C activity in *A. suum* muscle were able to suggest that phospholipid hydrolysis may be associated with the acetylcholine responses of muscle via second messenger pathways. Protein kinase C activity was also detected by Arevalo and Saz (1991), and its activity found to depend on Ca^{2+}, 1,2-diacylglyceride and phospholipid. The existence of a second type of muscle acetylcholine receptor might explain why some nematodes may recover following nicotinic anthelmintic treatment (Aceves *et al.*, 1970; Coles *et al.*, 1974, 1975), and why nicotinic receptors are not essential for the survival of different genetic forms of the nematode *C. elegans* (Lewis *et al.*, 1980, 1986, 1992). The pharmacology of neuronal acetylcholine receptors remains as a topic for further study (Stretton, 1992).

8. NICOTINIC ANTHELMINTICS

8.1. Chemical Structure

The anthelmintics which appear to act as agonists at nicotinic acetylcholine receptors of nematodes include (Fig. 11): the imidazothiazoles (levamisole and butamisole), the tetrahydropyrimidines (pyrantel, morantel and oxantel), the quaternary ammonium salts (bephenium and thenium) and the pyridines (methyridine) (Broome and Greenhal, 1961; Van Den Bossche, 1985; Harrow and Gration, 1985; Roberson, 1988). The electrophysiological effects of levamisole, pyrantel and morantel have been studied in greatest detail and are described below.

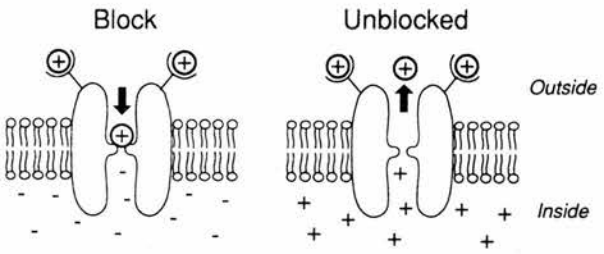


FIG. 12. Diagram of open-channel block produced by cationic agonists during hyperpolarization of the membrane and the relief of block on depolarization. The diagram suggests that open-channel block will increase with hyperpolarization.

pyrantel > levamisole = acetylcholine. Thus morantel and pyrantel are more potent than levamisole at this receptor site.

In addition to these observations, Harrow and Gration (1985) also described non-linear current–voltage relationships for levamisole, morantel and pyrantel under voltage-clamp: the current failed to increase sufficiently on hyperpolarization. Conductance dose–response relationships for morantel and pyrantel declined after reaching a maximum as the concentration of the drug increased; they were described as being 'bell-shaped'. One explanation for these phenomena is that of open channel-block (Colquhoun and Sakmann, 1985) by the anthelmintics. Levamisole, pyrantel and morantel are organic cations and in addition to acting as an agonist opening channels, will enter open ion-channels driven by the voltage-field. Since these anthelmintics are too big to pass through the channel, they will produce a voltage sensitive open-channel block (Fig. 12). The 'bell-shaped' dose–response relationships of pyrantel and morantel may be explained by low concentrations acting mostly as an agonist and high concentrations producing open channel-block.

8.4. SINGLE-CHANNEL CURRENTS ACTIVATED BY NICOTINIC ANTHELMINTICS

Levamisole-activated channel currents have also been recorded from the vesicle preparation (Fig. 13; Robertson and Martin, 1992). The ion-channels were also shown to be cation selective and to have similar kinetic properties to acetylcholine-activated channels at low levamisole concentrations. The channels had apparent mean open-times in the range 0.8–2.85 msec and had linear I/V relationships with conductances in the range 20–45 pS. At higher levamisole concentrations a 'flickering' open channel-block was observed (Fig. 14). The characteristic voltage-sensitive flickering seen with levamisole and other open channel-blockers (Neher and Steinbach, 1978), clearly demonstrates that anthelmintics may also act as open-channel blockers in addition to acting as an agonist. The dissociation constant for the channel block at -50 mV was 123 μM. In addition, levamisole, at higher concentrations (30 and 90 μM) also produced long closed-times separating 'clusters' of openings which were interpreted as desensitization.

Thus at the single-channel level both acetylcholine and levamisole activate channels in the same concentration range (acetylcholine, 1–100 μM; levamisole, 1–90 μM). Both of the agonists showed evidence of desensitization with long closed periods appearing at higher concentrations. Receptor desensitization produced by levamisole may be important therapeutically: some namatodes continuously treated with higher doses of levamisole recover from the levamisole induced paralysis (Aceves *et al.*, 1970; Coles *et al.*, 1974, 1975; Lewis *et al.*, 1980). This recovery may be due to desensitization since, like desensitization, recovery occurs only at higher doses. It, therefore, seems that lower doses which do not produce desensitization, potentially have a greater therapeutic effect.

Single-channel currents activated by pyrantel have also been observed (Robertson *et al.*, 1992). These channel currents have the same amplitude as the levamisole-activated currents when recorded under the same conditions (Fig. 14). The currents are activated by lower concentrations of pyrantel (0.03 μM), than levamisole, although they are shorter in duration with apparent mean open-times in the range 0.5–1 msec. Open channel-block is also observed for pyrantel but the degree of block is much greater than that obtained with levamisole (the channel-block dissociation constant for pyrantel is 20 μM at -50 mV). The therapeutic significance of the greater channel-block produced

pharmacological properties of pyrantel and some of its analogues, in a variety of vertebrate and helminth preparations. They also used intracellular recording techniques from muscle cells of *Ascaris* and showed that bath-application of pyrantel and acetylcholine produced depolarization, an increase in spike frequency and contracture. Pyrantel was more potent than acetylcholine and its actions were not reversed on washing. The effects of acetycholine and pyrantel on *Ascaris* muscle strips were blocked by tubocurarine, suggesting that they were nicotinic. In addition piperazine was also reported to antagonize the actions of pyrantel: an effect which is now explained as 'physiological' antagonism rather than pharmacological antagonism with piperazine acting on GABA receptors not acetylcholine receptors. A depolarizing effect of levamisole, pyrantel and morantel in *H. contortus* has also been described (Atchison *et al.*, 1992).

8.3. Effect on Input Conductance and Membrane Currents

The two-microelectrode current-clamp and two-microelectrode voltage-clamp techniques (Martin, 1982; Harrow and Gration, 1985) have been used to examine the effects of acetylcholine, levamisole, pyrantel and morantel applied to the bag region of *A. suum* muscle. These four agonists increase the input conductance and depolarize the membrane. The results of voltage-clamp experiments following ionophoretic application of fixed doses of the anthelmintics (Harrow and Gration, 1985) showed that the currents produced had reversal potentials near 0 mV, as had been reported for acetylcholine (Martin, 1982). The reversal potential of 0 mV is explained by the anthelmintics opening an ion-channel which is permeable to both Na^+ and K^+ ions. Simultaneous ionophoretic application of acetylcholine and pyrantel showed that both agonists acted on the same receptor. The relative potencies of the anthelmintics and acetylcholine was: morantel =

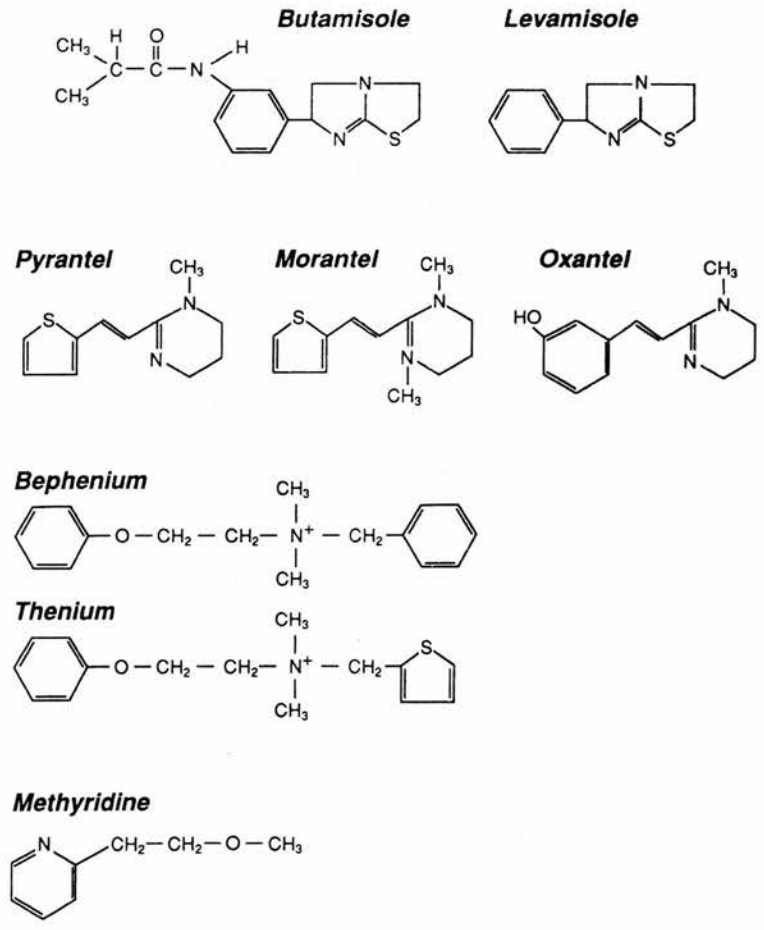


Fig. 11. Chemical structure of nicotinic anthelmintics.

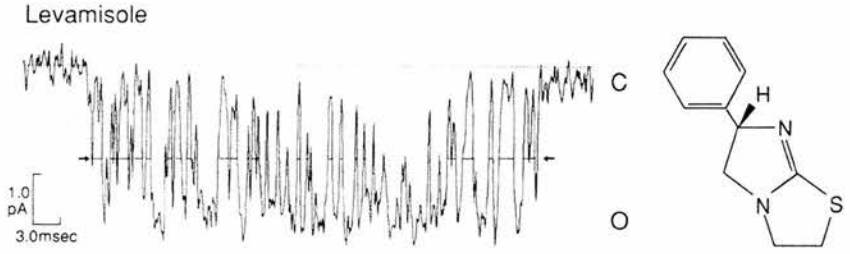


FIG. 14. Flickering open channel-block by levamisole from cell-attached patches from muscle vesicles. Openings (O) are shown downwards. Closings (C) Patch-potential: −75 mV. The pipette contained 30 μM pyrantel. Pipette solution (mM): CsCl, 140; $MgCl_2$, 2; EGTA, 1; HEPES, 10; pH 7.2 with CsOH. Bathing solution (mM): CsCl, 35; Cs acetate, 105; $MgCl_2$, 2; EGTA, 1; HEPES, 10; pH 7.2 with CsOH. Filter: −3dB 2.5KHz, 8-pole Bessel.

hyperpolarizing effect of bath-applied piperazine and GABA that inhibitory GABA receptors on muscle were recognized. Ionophoresis experiments have now shown that the GABA receptors responsible for this are located at the syncytium (Del Castillo *et al.*, 1964c) and extrasynaptically over the surface of the rest of the cell including the bag region (Martin, 1980) (Fig. 15). Ionophoresis of GABA onto the bag, when examined under voltage-clamp, produces a current which has a reversal potential near −65 mV and which is explained by the opening of ion-channels permeable to Cl^- (Martin, 1980). The physiological function of the extrasynaptic GABA receptors is not known, but they may be exploited in pharmacological experiments designed to look at receptor properties; they may also be activated by anthelmintics during therapy of the host animal.

9.2. PHARMACOLOGY OF THE *ASCARIS* GABA RECEPTOR

The pharmacology of extrasynaptic GABA receptors has been studied using a two-microelectrode recording technique to examine conductance dose–response relationships during the bath-application of GABA agonists and antagonists (Martin, 1980, 1982; Holden-Dye and Walker, 1988; Holden-Dye *et al.*, 1988, 1989; Duittoz and Martin, 1989, 1990a) and at the single-channel level (Martin, 1985b; Martin and Pennington, 1989; Duittoz and Martin, 1990b).

Conductance dose–response relationships for a variety of bath-applied GABA agonists have

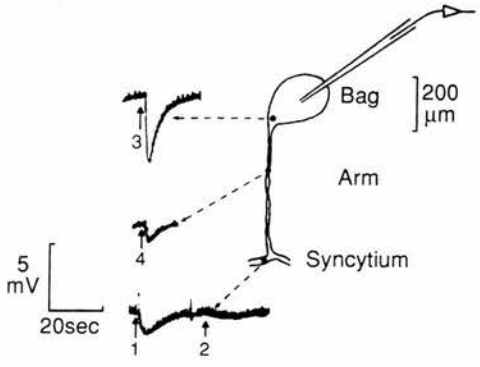


FIG. 15. Demonstration of synaptic and extrasynaptic GABA receptors by ionophoresis of GABA onto different regions of muscle cell and the recording of intracellular membrane potential from the bag. GABA was delivered with 0.4 nC at the vertical arrow while the membrane potential was monitored in the bag. The effect at the syncytium was measured first (1). Then the ionophoresis pipette raised 50 μM (2) where a smaller response was seen. The largest response was seen at the bag (3) but a small response also occurred over the arm (4).

by pyrantel remains to be evaluated. Morantel has also been shown to produce open-channel block (Evans and Martin, 1992).

The effects of nicotinic anthelmintics on neuronal acetylcholine receptors of *A. suum* or other nematodes remains to be examined.

9. GABA

9.1. Effects of GABA on *Ascaris* Muscle

Initially the anthelmintic, piperazine, was shown to produce reversible paralysis of *A. suum in vitro* (Standen, 1955), but it was not until Del Castillo *et al.* (1964b,c) demonstrated the

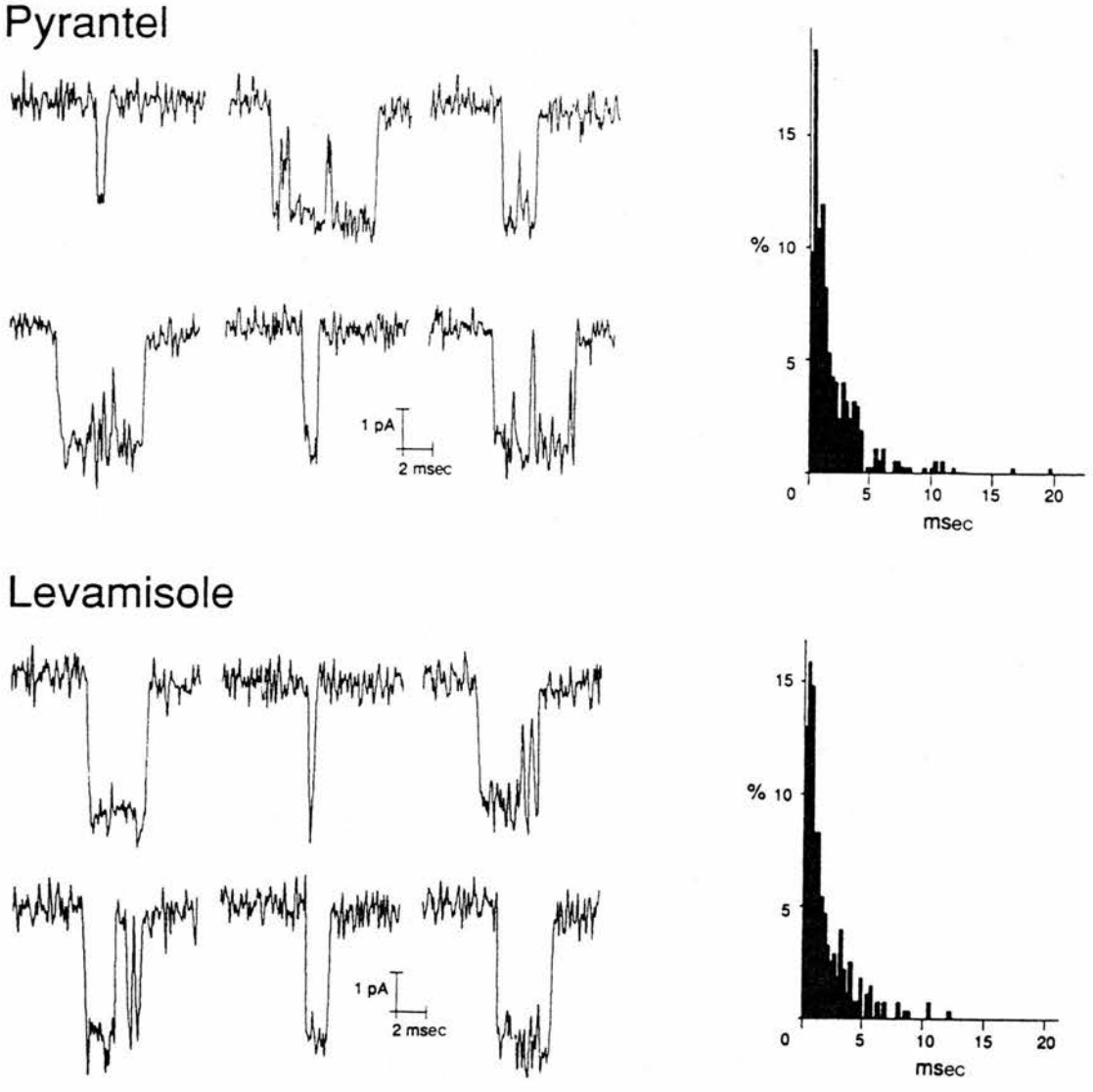


Fig. 13. Pyrantel- and levamisole-activated channels and their open-time histogranis, from cell-attached patches of muscle vesicles. Openings are shown downwards. Patch-potential: −75 mV. The pipette contained 0.1 μM pyrantel or 10μM levamisole. Pipette solution (mM): CsCl 140, $MgCl_2$ 2, EGTA 1, HEPES 10, pH 7.2 with CsOH. Bathing solution (mM): CsCl, 35; Cs acetate, 105; $MgCl_2$, 2; EGTA, 1; HEPES, 10; pH 7.2 with CsOH. Filter: −3 dB 2.5 KHz, 8-pole Bessel. The mean open-times produced by pyrantel (1.09 msec) and levamisole (1.34 msec) were similar to those produced by acetylcholine. The open-time histograms are typical of channel open-times and show that the open-times vary and that their distribution is skewed with brief openings being more common.

TABLE 3. *Potency of Arylaminopyridazine Derivarives at* Ascaris *GABA Receptors and Vertebrate $GABA_a$ Receptors*

	$GABA_a$ binding K_i (μM)	% Inhibition in *Ascaris*
SR95531	0.15	43
SR42666	0.31	76
SR42627	0.55	21
SR95103	2.20	93
SR95133	2.60	58
SR95640	10.40	7
SR95132	100.00	89

Comparison of the potency of the arylaminopyridazine derivatives at the $GABA_a$ receptor by inhibiting [H^3]GABA binding and the percent inhibition of the response to 30 μM GABA BY 1 mM antagonist at the *Ascaris* receptor show that the two potency series do not equate and that the two receptor types are different.

separate type of receptor in nematodes, i.e. the $GABA_n$ receptor (n: not antagonized by picrotoxin; n for nematodes). Ariens *et al.* (1979) have argued that 'accessory' sites on receptors, bind to hydrophobic regions of competitive antagonists and give rise to their antagonist nature; the structure of the hydrophobic regions are more important for the potency of competitive antagonists than the stucture of the moiety binding to the agonist recognition site. The mode of action and structure–activity relationships of arylaminopyridazine–GABA antagonists at the vertebrate $GABA_a$ receptor has been explained in terms of Ariens theory (Wermuth *et al.*, 1987). The correlation between the agonist potencies at the GABA and *Ascaris* receptors, but not competitive antagonists, suggests that 'accessory' sites on the vertebrate $GABA_a$ receptor and *Ascaris* receptor are different.

9.3. GABA BINDING SITES IN *C. ELEGANS*

The presence of GABA, using GABA immunoreactivity, was initially demonstrated in several motorneurones of the ventral nerve cord of the free living nematode *C. elegans* (McIntyre *et al.*, 1986). As a result of this obervation Schaeffer and Bergstrom (1988) measured and detected the presence of: (i) GABA, (ii) GABA binding sites, (iii) the GABA synthesizing enzyme glutamate decarboxylase and (iv) the GABA degrading enzyme GABA transaminase in *C. elegans*. It was found that muscimol but no other GABA agonists or antagonists competed for the binding site. The compounds tested were: isoguvacine, imidazole acetic acid, bicuculline, picrotoxin, nipecotic acid, 3-aminopropane sulphonic acid, baclofen, aminooxyacetic acid, diazepam, and ivermectin at concentrations up to 100 μM. Interestingly a GABA binding inhibition factor with a molecular weight of 11 kDa in the venom of the spider *Calilena agelenldae* was also reported. GABA binding sites in *A. suum* remain to be described.

9.4. GABA AND PIPERAZINE SINGLE-CHANNEL CURRENTS

GABA- and piperazine-activated channels have been recorded using cell-attached and outside-out patches (Martin, 1985b). The channels opened by both agonists had a mainstate conductance of 22 pS but two subconductance states were also observed. The average duration of the effective openings (bursts) produced by GABA was in the region of 32 msec while the average duration of effective openings (bursts) produced by the anthelmintic piperazine was 14 msec (Fig. 16). High concentrations of GABA or piperazine produced desensitization, which was seen as a decrease in open probability due to the appearance of long closed-times. Piperazine is some 100 times less potent than GABA in *A. suum* (Martin, 1982) and this difference in potency may be explained by the fact that piperazine requires a higher concentration to achieve a similar opening rate to GABA, and in addition, the average duration of openings produced by piperazine are shorter. The density of the extrasynaptic receptors was also estimated in these experiments (Martin, 1985b): only one channel was found in each area of membrane of about 2.4 μm^2.

TABLE 2. *$GABA_a$ Agonist Potency in* A. suum

Agonist	EC_{50}: μM* (relative potency)	Relative potency†
S-(+)-dihydromuscimol		7.53
± dihydromuscimol	8.3 ± 1.5 (3.704)	
ZAPA	24.1 ± 4.6 (1.266)	1.46
GABA	30.7 ± 2.1 (1.000)	1
R-(−)-dihydromuscimol		0.85
TACA	65.7 ± 14.5 (0.467)	0.55
R-(−)-3-OH-GABA		0.25
IAA	76.1 ± 11.3 (0.403)	0.20
Muscimol	82.5 ± 20.4 (0.372)	0.55
Isoguvacine	124.2 ± 10.1 (0.247)	0.19
S-(+)-3-OH-GABA		0.13
GuAA	135.1 ± 18.0 (0.227)	0.16
Homo-beta-proline	233.6 ± 37.2 (0.131)	
DAVA	366.5 ± 17.6 (0.084)	0.079
CACA	391.8 ± 83.2 (0.078)	0.031
Isonipecotic acid	409.2 ± 83.2 (0.075)	
BGuPA	536.5 ± 49.7 (0.057)	0.085
THIP	N.A.	0.006
S-(−)-4-methyl-TACA		0.007

Martin *et al.* (1991): EC_{50} input conductance dose–response curves described by the modified Hill equation with the estimated Hill coefficient between 2–4: the relative potency is given in brackets; means ± SE $n = 3$–13.

†Holden-Dye *et al.* (1988, 1989): relative potency.

GABA, gamma-amino butyric acid; DHM, dihydromuscimol; ZAPA, (*Z*)-3-[9aminoiminomethylthiol]-2-propenoic acid; TACA, *trans*-aminocrotonic acid; IAA, imidazole-4-acetic acid; IAA, imidazole-4-acetic acid; GuAA, guanido acetic acid; DAVA, delta-amino valeric acid; CACA, *cis*-aminocrotonic acid; BGuPA, beta-guanidino proprionic acid. 3-aminopropane sulphonic acid, piperadine-4-sulphonic acid, baclophen, glycine, alanine were without effect at concentrations below 1 mM (Holden-Dye *et al.*, 1988, 1989; R. J. Martin and A. H. Duittoz, unpublished). N.A., not active at 1 mM.

been described by the modified Hill equation and the EC_{50}s determined; these values are shown in Table 2 along with estimates of the relative potency of the agonists (Holden-Dye *et al.*, 1989).

The agonist profile of the *Ascaris* receptor is similar, but not identical to that of the vertebrate $GABA_a$ receptor:

(1) the stereoselectivity of the *Ascaris* receptor and the vertebrate $GABA_a$ receptor for the enantiomers of dihydromuscimol, 3-OH-GABA, and 4-me-TACA is the same (Holden-Dye *et al.*, 1989).

(2) the most potent $GABA_a$ agonists are potent in *Ascaris*, so that the relative potency of $GABA_a$ agonists at vertebrate receptors is correlated with the relative potency of agonists at the *Ascaris* receptor ($r = 0.74$; Holden-Dye *et al.*, 1989).

There are, however, major pharmacological differences between the *Ascaris* GABA receptor and the vertebrate $GABA_a$ receptor:

(1) the potency of the sulphonic acid GABA derivatives (3APS and P4S) as well as muscimol and isoguvacine (Table 2) is less than at the vertebrate $GABA_a$ receptor;

(2) the anthelmintic piperazine acts as a selective GABA agonist in *Ascaris* (Martin, 1982);

(3) pentobarbitone and flurazepam do not potentiate GABA responses in *Ascaris*, as they do in the vertebrate (Holden-Dye *et al.*, 1989);

(4) the $GABA_a$ antagonists bicuculline, picrotoxin, securinine, pitrazepine, RU5135, dieldrin and TBPS are weak or inactive in *Ascaris* (Martin, 1980; Wann, 1987; Holden-Dye *et al.*, 1988, 1989; Martin *et al.*, 1991);

(5) the potency of a series of arylaminopyridazine–GABA derivatives which act as competitive vertebrate $GABA_a$ antagonists as well as competitive antagonists of the *Ascaris* GABA receptor do not equate (Table 3) (Duittoz and Martin, 1990a,b, 1991).

These differences therefore distinguish the *Ascaris* GABA receptor pharmacologically from vertebrate $GABA_a$ receptors and confirm the earlier suggestion (Martin, 1987) that there is a

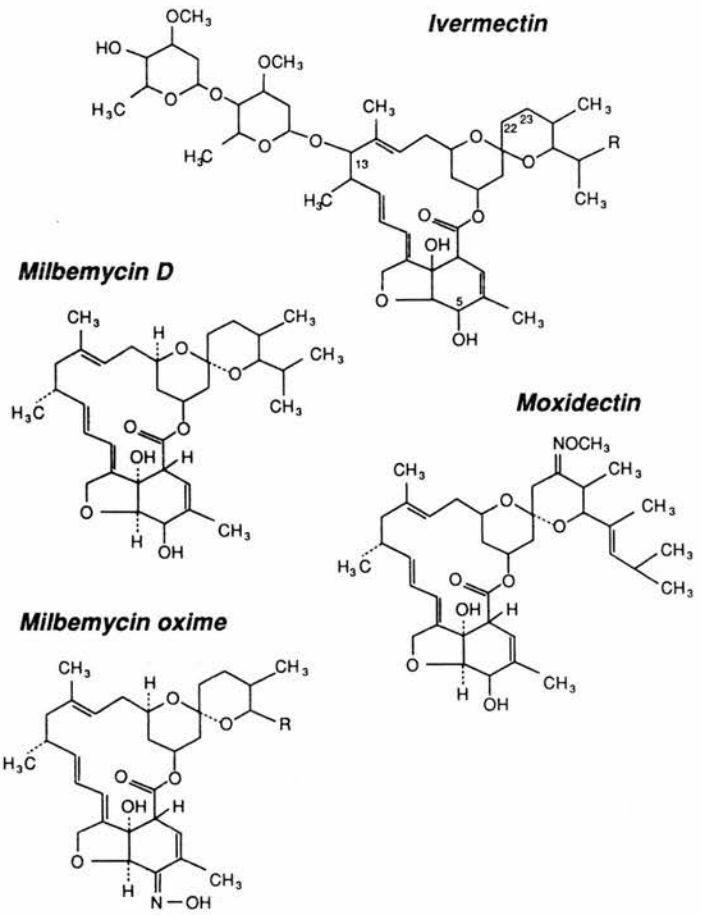


FIG. 17. Chemical structure of ivermectin and milbemycins. Ivermectin is 80% 22,23 dihydroavermectin B1a (R is sec butyl) and 20% 22,23-dihydroavermectin B1b (R is iso propyl).

of avermectins seen in this study were reported to correlate with their antinematodal potency. It was therefore argued that the GABA antagonistic action in *Ascaris* muscle might represent a sight of action although the concentrations used in these experiments were high.

10.2. EFFECTS OF DIHYDROAVERMECTIN AT THE SINGLE-CHANNEL LEVEL

The effect of dihydroavermectin on GABA single-channel currents was studied by Martin and Pennington (1989) using outside-out patches. Figure 18 shows the effect of dihydroavermectin on these currents: dihydroavermectin produces a dose-dependent reduction in the single-channel conductance and frequency of GABA channel opening. This effect would be seen as non-competitive antagonism of GABA responses if the effect were examined with the current-clamp technique.

In addition to effects on GABA channels it was found that dihydroavermectin opened other low conductance Cl^- channels in the membrane (Martin and Pennington, 1989). Low concentrations of dihydroavermectin applied to the outside membrane by bath-application to an outside-out muscle patch produced opening of up to 13 channels (Martin and Pennington, 1989). The progressive opening of the channels over a period of 1–3 min was described as a 'staircase' effect (Fig. 19). The channels conducted Cl^- ions, had conductances of 9–15 pS and long average open-times (greater than 100 msec). The long delay (greater than 15 sec) between application of dihydroavermectin and channel opening, and the lipophilic nature of the avermectins, suggests a site of action in the lipid phase of the membrane. The study concluded that dihydroavermectin acts to open the non-GABA-activated Cl^- channels by acting from the external membrane, but the

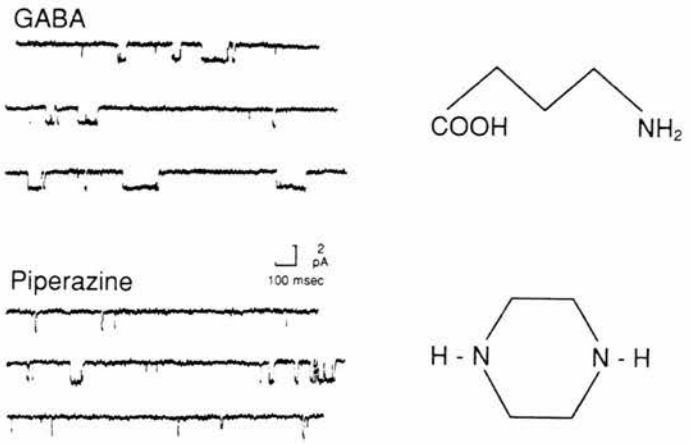


FIG. 16. GABA and piperazine activated channel currents. Cell-attached patches. Transpatch potential −75mV. GABA: 3 μM GABA as agonist. Piperazine: 500 μM piperazine as agonist. Effective channel open times: GABA 33 msec; Piperazine 18 msec. Channel conductance 22 pS for both agonists. Bathing solution (mM): NaCl, 135; KCl, 3.0; $MgCl_2$, 15.7; glucose, 3.0; Tris, 5 adjusted to pH 7.6 with maleic acid. Pipette solution (mM): CsCl, 140; $MgCl_2$, 15.7; Tris, 5 adjusted to pH 7.6 with maleic acid.

10. MACROCYCLIC LACTONES

The avermectins (and related milbemycins) are a group of very hydrophobic macrocyclic lactones which have broad spectrum anthelmintic (Campbell and Benz, 1984) and insecticidal properties and are derived from *streptomyces* micro-organisms. The group (Fig. 17) includes: ivermectin, a mixture of 80% 22,23 dihydroavermectin B1a and 20% 22,23 dihydroavermectin B1b derived from *Streptomyces avermitllis;* milbemycin D derived from *S. hygroscopocus*; moxidectin derived from *S. aureolacrimosus noncyanogenus*; and milbemycin oxime derived from *S. hyroscopicus* as a mixture of 80% milbemycin A4 and 20% milbemycin A3. The avermectins have been examined experimentally in great detail.

In a number of preparations avermectins produce a reduction in motor activity so that the parasites are excluded from the host. This immobilization may be explained by a reduced excitability of muscle or nerve produced by an increase in membrane Cl^- conductances. These studies are reviewed.

10.1. EFFECTS OF DIHYDROAVERMECTIN B1A ON CONDUCTANCE AND MEMBRANE POTENTIAL

Electrophysiological effects of the antiparasitic agent 22,23 dihydroavermectin B1a on *A. suum* muscle have been studied with intracellular micropipette recording techniques (Kass *et al.*, 1980, 1982, 1984; Wann, 1987; Holden-Dye *et al.*, 1988; Holden-Dye and Walker, 1990; Rheinhallt *et al.*, 1991). In contrast to effects on other invertebrate preparations, application of dihydroavermectin does not mimic the effects of GABA on *A. suum* muscle: it does not produce a marked hyperpolarization with an increase in membrane conductance when the preparation is in normal concentrations of Cl^- (Kass *et al.*, 1982, 1984; Holden-Dye *et al.*, 1988). However an irreversible inhibitory effect on spiking in *A. suum* muscle cells has been observed after bath-application of avermectin (Wann, 1987).

One suggested mode of action for the avermectins was that they were GABA agonists or potentiators and that this may explain the increase in membrane Cl^- conductance seen in a number of preparations (Wright, 1986). Since the *Ascaris* muscle bags contain GABA receptors it would be expected that such an action would produce hyperpolarization and an increase in conductance comparable to that observed with piperazine (Martin 1982). Since this effect is not observed, it makes such an action unlikely in *Ascaris*.

GABA dose–response relationships obtained with the current-clamp technique are depressed by avermectins in a non-competitive manner (Holden-Dye and Walker, 1990). The potency of a variety

TABLE 4. *Inhibition of [^{3}H]IVM binding to* C. elegans *Membranes by Analogues of Avermectin*

Compound	IVM-luminol K_i (nM)	[^{3}H]IVM
IVM	0.21	0.26
AVM B2a	0.24	0.19
AVM Bla 4″-*O*-phosphate	0.27	0.30
22,23-Dihydro-AVM Bla aglycone	2.1	0.7
AVM Bl monosaccharide	2.7	1.1
2,3,8,9,10,11,22,23-octahydro-AVM Bla	>1000	>1000

Data modified from Schaeffer *et al.* (1989c).

respectively. The inactive analogue 2,3,8,9,10,22,23-octahydroavermectin B1a had a K_i less than 1 μM in the assay. Similar results were obtained with tritiated ivermectin when it was used for the assay. The amount of specific receptor present in the nematode appeared to be low despite the fact that it had a high affinity and was reported to be 3.45–3.80 pmol mg^{-1}.

The binding properties of the ivermectin receptor in *C. elegans* have also been studied using cochlioquinone A, a yellow pigment originally isolated from a strain of *Cochliobolus miyabeanus*, a mould of rice (Schaeffer *et al.*, 1990). In this study it was reported that cochlioquinone A had a nematocidal action against *C. elegans* and interacted directly (competitively) with the ivermectin binding site with an apparent K_i of 30 μM. Cochlioquinone A was much less effective against ivermectin-resistant mutants. Although there is no obvious stuctural similarity between cochlioquinone A and the avermectins the competitive antagonism seen in the binding study and the lack of effect on ivermectin-resistant mutants supported the view that cochlioquinone A and ivermectin act on the same binding site.

It has also been possible to photoaffinity label the avermectin binding sites in *C. elegans* with an azido-avermectin analogue (Roher *et al.*, 1992). The azido-avermectin derivative was shown to be biologically active and had a K_d of 0.14 nM and on photoactivation linked to three polypeptides of 53, 47 and 8 kDa. The detection of three polypeptides bound after photoactivation suggests the presence of more than one receptor. However, the three proteins may have arisen from degradation of a single protein during isolation; or may be derived from the subunits of a single heterotrimeric protein during isolation; or may have arisen from tissue specific proteins.

10.5. *C. ELEGANS* RNA IN *XENOPUS* OOCYTES INDUCES Cl^- AVERMECTIN-SENSITIVE CURRENTS

The small size of *C. elegans* has so far precluded electrophysiological study. As an alternative, it has been possible to inject *Xenopus laevis* oocytes with poly $(A)^+$ RNA, in order to express receptor operated membrane ion-channels derived from the nematode (Arena *et al.*, 1991, 1992). The injected oocytes responded to exposure with avermectin by increasing the Cl^- current across the membrane but control injected oocytes showed no response to avermectin. Ivermectin produced an increase in current which was essentially irreversible and which was slow in onset with peak responses occurring after 49 sec. A water soluble ivermectin derivative was also used, Ivermectin-PO_4, which was also slow in onset and not reversible on washing: it had an ED_{50} of 90 nM and a Hill coefficient of 1.1. Octahydroavermectin, a biologically inactive analogue had no effect on the oocytes injected with the poly$(A)^+$ RNA. The effect of GABA was also tested on these injected oocytes and found to be without effect: the lack of effect of GABA is consistent with the view that avermectins activate a Cl^- channel present in target species and which is not a GABA receptor activated channel. The molecular size of the RNA was determined to be 1.0–2.5 kb by electrophoresis on a denaturing agarose gel.

Interestingly, glutamate and ibotenate also activated the same Cl^- current but GABA did not; the glutamate agonists quisqualate, kainate and *N*-methyl-D-aspartate were also inactive (Arena *et al.*, 1992). These observations suggest that the GABA-activated Cl^- channel is not a site of action in nematodes but that one target site for the avermectins in nematodes is a glutamate activated Cl^- channel, possibly similar to the 'H' receptors in arthropods (Cull-Candy, 1976; Scott

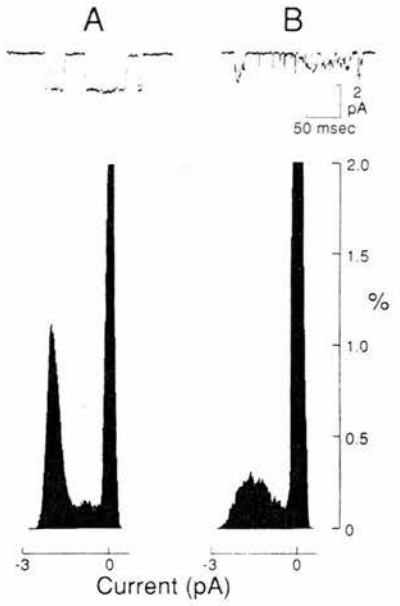


FIG. 18. Effect of dihydroavermection B1a on GABA single-channel currents recorded from an outside-out patch. A: Control GABA channel openings produced by 4 μM GABA (above); current amplitude histogram (below). B: GABA channel currents (above) and current amplitude histogram (below) from the same preparation but following the addition of 200 nM dihydroavermectin. Note that dihydroavermectin reduces the mean channel current and increases the variance of the open channel current.

speed of onset of the effect is slow. Thus the mode of action of ivermectin in *A. suum* appears to involve the opening of a particular type of Cl^- channel, possibly only present in susceptible animals, rather than to act to open GABA channels.

10.3. Actions of Avermectins on The Nervous System of *Ascaris*

The split chamber technique described by Kass *et al.* (1984) has permitted the selective application of avermectin to the dorsal and ventral halves of *Ascaris*. These experiments permit the dorsal and ventral nerve cord to remain connected by the commissures of only two motor neurones: these are VI (ventral inhibitory motor neurone) and DE1 (dorsal excitatory neurone). Intracellular potentials in the bag were recorded in response to electrical stimulation of nerve cords. It was found that avermectin blocked the response of DE1 to indirect stimulation but not direct stimulation: the observations were interpreted as suggesting that avermectins block transmission between interneurones in the spinal cord and the excitatory motor neurones. It was also found by these authors that the hyperpolarizing response of muscle following direct stimulation of VI was blocked by avermectin, an observation consistent with the antagonism of muscle GABA receptors described above. These observations together with the observations referred to above, suggest that avermectins have more than one site of action and that these include ion-channels in muscle membrane and in neuronal membranes.

10.4. Binding Studies of Avermectins in The Nematode *C. elegans*

C. elegans are very small free-living nematodes that are very sensitive to the avermectins. Specific high affinity avermectin binding sites have been identified and characterized using tritiated 22,23 dihydroavermectin and a luminol 22,23 dihydroavermectin derivative in this nematode (Schaeffer and Haines, 1989; Schaeffer *et al.*, 1989c). It was found that the ability of various avermectin analogues to displace the luminol ivermectin derivative was correlated with the potency of the avermectin analogues as anthelmintics (Table 4). For example ivermectin, avermectin B2a, and avermectin B1a 4′-*O*-phosphate were potent inhibitors with K_I values of 0.2, 0.24, and 0.29 nM,

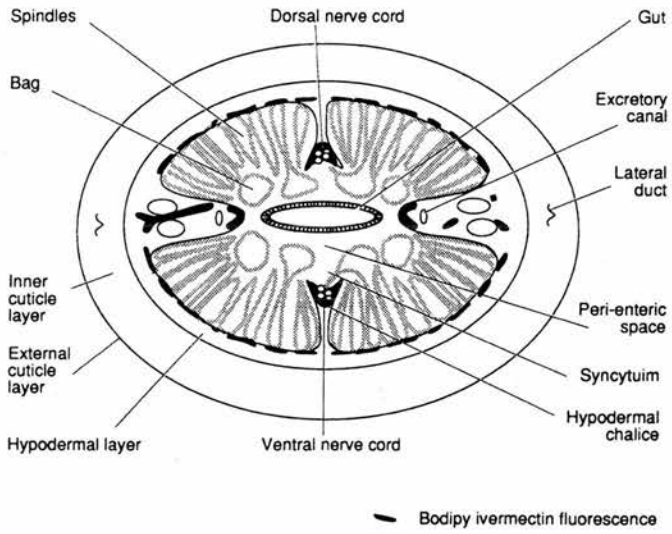


FIG. 21. Sites of accumulation of bodipy ivermectin seen in frozen transverse sections of *A. suum* following injection at a more distal site into the perienteric space. Note that the probe concentrates around the nerve cords, in the hypodermal layer and in the lateral canal.

(Martin *et al.*, 1992a). Fluorescent microscopy of frozen sections has revealed the distribution of the probe in the whole nematode. The probe accumulates in muscle membranes and within the nerve cord (Fig. 21); these two sites are consistent with an action of avermectins on muscle and nerve membrane. Additional sites of accumulation are: (i) the lateral line, a site which may be associated with drug clearance and (ii) the hypodermal region, a site which is involved in a number of transport functions including Cl^- ions (Hobson *et al.*, 1952a,b), drugs and nutrients (Ho *et al.*, 1990). Ho *et al.* (1990) have measured the diffusion coefficient of ivermectin through the cuticle of *A. suum* an important route of entry into nematodes, and found it to be 5.46 $cm^2\ sec^{-1} \times 10^6$ but the rate-controlling impediment is a 5–10 μm thick lipid barrier of the hypocuticle. This layer appears to correspond to the location of the accumulation site of bodipy ivermectin seen in the frozen sections. If this layer were to behave as a passive sink for lipophillic compounds, it would buffer their concentration, thereby restricting the concentration of avermectins at other active sites in the parasite.

Bodipy ivermectin distribution has also been studied in muscle vesicle membranes from *A. suum* (Martin and Kusel, 1992). The vesicles are suitable for fluorescence recovery after photobleaching experiments (FRAP) designed to look at fluorescent-labelled probe movement in the membrane (Fig. 22). FRAP experiments have shown that ivermectin has no significant effect on the lateral diffusion coefficient of the membrane (fluidity) at concentrations less than 1μM and that the lateral diffusion coefficient for bodipy ivermectin was $14 \times 10^{-10}\ cm^2\ sec^{-1}$. Although the lateral diffusion rate for bodipy ivermectin was nearly three times faster than the lipid probe octadecanoyl-aminofluorescein, it was estimated that, on average, a molecule of bodipy ivermectin would take 100 sec to move a distance of 7.5 μm in these membranes. The FRAP experiments also showed that only 46% of the probe was mobile, showing that within a 1.2 μm radius the distribution of the bodipy ivermectin in the membrane was not homogenous and that the membrane is not homogenous being composed of coalescent lipid 'domains' (Fig. 22A) (Martin *et al.*, 1990; Martin and Kusel, 1992).

The trypan blue quenching technique has allowed the verticle distribution of bodipy ivermectin to be determined (Fig. 22); it showed that the bodipy ivermectin did not cross the membrane bilayer of these membranes but remained in the outer bilayer. The FRAP and trypan blue observations were used to suggest that (i) the site of action of ivermectin is located in the outer monolayer of the membrane, possibly on the Cl^- channel (Fig. 23) and (ii) the speed of onset of action in the isolated membrane preparations may be limited by diffusion in the membrane.

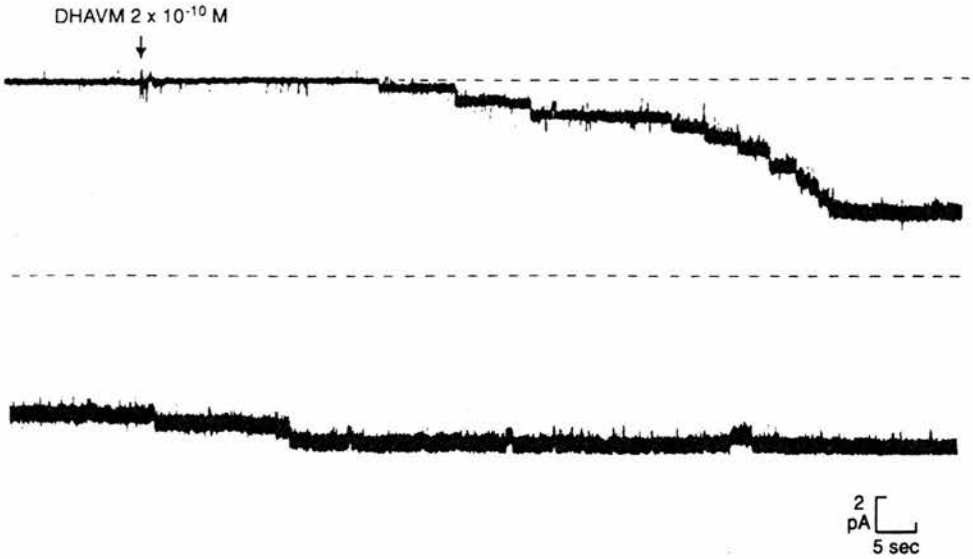


FIG. 19. Staircase production of Cl^- channels in an outside-out patch (− 75 mV) by 200 pM DHAVM. The dashed line indicates the closed level of current. The conductance of the channels was 15 pS.

and Duce, 1985). The status of glutamate as a transmitter in nematodes is uncertain since no localization of glutamate in neurones has been made. It remains an area for future work.

10.6. Distribution of Bodipy Ivermectin in Tissues of *Ascaris*

A fluorescent derivative of ivermectin (4′-5,7 dimethyl bodipy proprionylivermectin; Fig. 20) has been prepared and injected into adult *Ascaris* where it produces dose-dependent immobilization

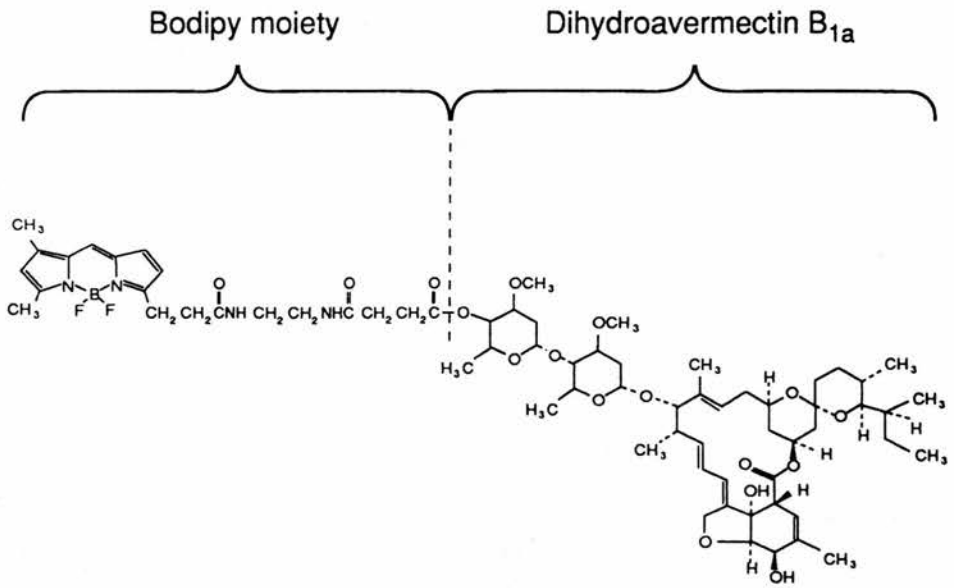


FIG. 20. Chemical structure of bodipy ivermectin.

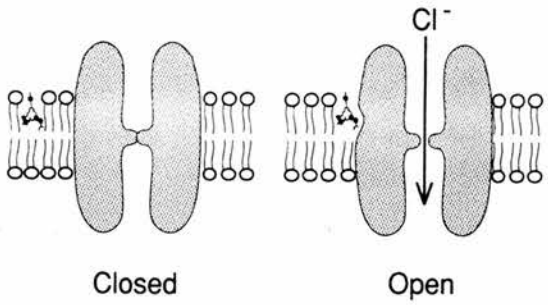


FIG. 23. Suggested mode of action for dihydroavermectin. Dihydroavermectin remains in the outer monolayer of the membrane and combines with the target Cl^- channel to produce opening.

glycogen breakdown. 5-HT inactivates glycogen synthetase and activates glycogen phosphorylase by increasing the level of cyclic AMP, resulting in breakdown of glycogen (Donahue *et al.*, 1981).

The receptor binding studies of Chaudhuri and Donahue (1989) suggest that in *A. suum* the muscle receptor is similar to the mammalian 5-HT_2 receptor: ketanserin, a selective 5-HT_2 antagonist, has a high affinity (K_D = 16.7 nM) for the muscle receptor but not the *A. suum* intestinal receptor. Williams and Donahue (1992) have reported further pharmacological evidence that the 5-HT receptor may be unique to nematodes. The recognition of a distinctive 5-HT receptor suggests another target site for the design of new anthelmintics.

11.2. PEPTIDES

FMRFamide-like peptides have been found in the pharyngeal nerves and the four major nerve cords of *A. suum* using immunocytochemical staining (Davenport *et al.*, 1988). Use of the wholemount preparation of the head region of *A. suum* (Johnson and Stretton, 1987) which contains nearly 180 neurones, the wholemount of the tail region (Sithigorngul *et al.*, 1990) which contains about 38 neurones and the hypodermal-cuticle flap which contains the motorneurones, has permitted a survey of the immunohistochemistry of nearly all the neurones in *A. suum*. A variety of antisera known to recognize one of 42 known peptides from either vertebrates or invertebrates have been screened and the location of some of these peptides in *A. suum* neurones has been possible (Table 5) (Sithigorngul *et al.*, 1990). Twelve different staining patterns have been recognized by these experiments suggesting that there are at least 12 putative families of peptide present.

The most specific staining seen by Sithigorngul *et al.* (1990) was with anti-LHRH which occurred in just one pair of neurones. Anti-FMRFamide however recognized the largest subset of neurones and stained over half of the neurones in *A. suum*. A series of fractionations on an acid–methanol extract of around 5000 *A. suum* heads were made and assayed with radio-immunoassay (Cowden *et al.*, 1989). After final fractionation (there were at least 10 peaks on the first HPLC step) the peptide that showed immunoreactivity was Lys–Asn–Glu–Phe–Ile–Arg–Phe (KNEFIRF). Amidation of this peptide was confirmed by fast atom bombardment mass-spectroscopy. The peptide was sequenced and called AF1 (A for *Ascaris*, F for FMRFamide, and 1 for the first purified). It has been shown to be biologically active and to reduce input resistance of inhibitory motoneurones (Cowden *et al.*, 1989).

The second peptide from *Ascaris* isolated, AF2, (Cowden and Stretton, 1990) has the amino acid sequence Lys–His–Glu–Tyr–Leu–Arg–Phe (KHEYLRFamide). In addition evidence for the existence of at least three other FMRFamide-like sequences was reported by Stretton *et al.* (1991). In addition to these peptides in *Ascaris* Smart *et al.* (1992a) described the primary structure of a novel peptide TE-6 and the chromatographic and immunological characterization of neuropeptide Y-like and pancreatic polypeptide-like peptides (Smart *et al.*, 1992b).

Once the sequence of the peptides is known it is possible to synthesize the peptides in reasonable amounts and to assay them for biological activity. Injection of 0.1 ml of 10^{-6} M AF1 or AF2 into the anterior region of *Ascaris* blocks locomotory movement in the injection site (Stretton *et al.*,

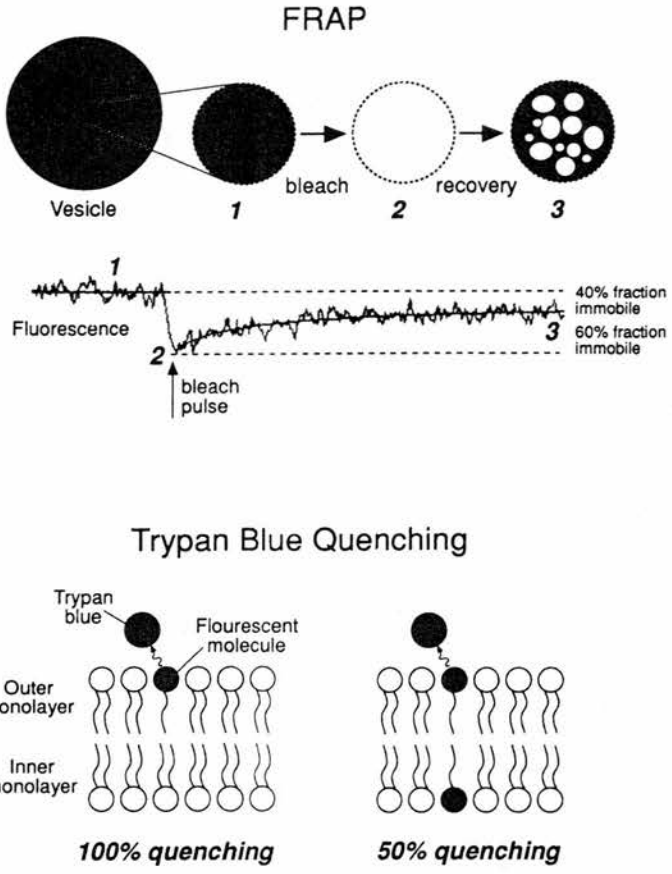


FIG. 22. FRAP and Trypan blue techniques. The FRAP technique used was to stain muscle vescicles with bodipy ivermectin and then to focus an argon laser onto a 1.2 μm spot on the surface of the vesicle. The fluorescence was then monitored with time and the level of fluorescence displayed. The intensity of the laser was momentarily increased to produce bleaching of the 1.2 μm spot and the the level of fluorescence followed. During recovery the unbleached probe in the area surrounding the spot moved in. The lateral diffusion rate was determined from the recovery curve. Since the recovery does not reach 100% of the starting level, immobile domains within the spot are shown to be present. The Trypan Blue Quencing technique relies on Foster energy transfer from the probe to the non-permeant quencher which is only possible if the probe is located in the outer membrane. One hundred percent quenching indicates that the probe is only located in the outer cell membrane.

11. OTHER TRANSMITTERS

11.1. Serotonin Effects and Pharmacology

In addition to the neurotransmitters GABA and acetylcholine, there is evidence that serotonin (5-HT) may play a role in regulating muscle metabolism. 5-HT can be absorbed from the host or synthesized by *Ascaris* (Chaudhuri *et al.*, 1988; Martin *et al.*, 1988); 5-HT receptors in muscle and intestine of *Ascaris* have been demonstrated using radiolabelled binding techniques (Chaudhuri and Donahue, 1989). 5-HT has also been shown to be present in two neurones, which may be neurosecretory, in the pharynx as well as cells of the posterior ventral nerve cord in males (Stretton and Johnson, 1985). The ultrastructural distribution of 5-HT in *Ascaris* has been described using X-ray spectrometry (Martin and Donahue, 1989). 5-HT has also been shown to play an important part in egg-laying in *C. elegans* (Desai *et al.*, 1983).

5-HT has no observable effect on *A. suum* somatic muscle membrane potential (unpublished observations) but appears to regulate glycogen metabolism. It does, however, produce effects on movement of the head (Stretton, 1992). In *Ascaris*, glycogen metabolism depends on glycogen synthetase for glycogen synthesis from glucose-6-phosphate, and glycogen phosphorylase for

intracellular micropipettes were placed in the commissural axons of motor neurones to measure input conductance changes showed that AF1 produced large increases in input conductance in both dorsal and ventral inhibitory motor neurones. No effect was observed on one of the excitatory neurones (DE1). *Ascaris* motorneurones are non-spiking neurones which rely on their high membrane resistance to propagate electrical signals over long distances (Davis and Stretton, 1989a). An increase in input conductance reduces the space constant and removes the neuronal locomotory circuit.

FMRFamide-like immunoreactivity has also been reported in *C. elegans* (Li and Chalfie, 1986), *Goodeyus ulmi* (Leach *et al.*, 1937) and *Panagrellus redivivus* (Geary *et al.*, 1992) which are free living nematodes. In *C. elegans* FRMFamide-like immunoreactivity is only found in 25 neurones (Li, 1990) in contrast to *Ascaris* where over half, 180, are immunoreactive. Li (1990) has cloned and sequenced a gene that encodes eight potential neuropeptides sequences; seven share the C-terminal sequence PNFLRFamide including SADPNFLRFamide, SDPNFLRFamide, SQPNFLRFamide, AADPNFLRFamide, PNFLRFamide and TNFMRYamide. Geary *et al.* (1992) have described the primary structure of two FMRFamide-like peptides from *Panagrellus redivivus*: PF-1 is SDPNLFLRFamide, the other is SADPNFLRFamide. None of these peptides is very like AF1 or AF2. Thus it is possible that many more FRMFamide like peptides may be isolated from nematodes. Peptidergic transmission remains to be studied in greater detail; it seems likely that more peptides as transmitters may be recognized in future studies. The successful discovery of non-peptidyl ligands for some vertebrate receptors encourages the view that FMRFamide receptors may be useful target sites for the development of future anthelmintics.

11.3. GLUTAMATE

Shinozaki and Konishi (1970) first pointed out that a number of anthelmintics including kainate have a chemical structure similar to the excitatory amino acid glutamate. They also demonstrated the excitatory effect kainate can have on vertebrate neurones. Schaeffer *et al.* (1989a,b) have identified glutamate binding sites in *C. elegans* and shown that argiopine differentiates between vertebrate and invertebrate binding sites. Stretton (1992) has commented on the depolarizing action of glutamate and kainate on DE2 motorneurones of *A. suum*. Arena *et al.* (1992) have described a Cl^- channel gated by glutamate produced in *Xenopus* following injection of RNA derived from *C. elegans*. These observations together suggest that glutamate may behave as a neurotransmitter acting on particular neurones in nematodes. The action of kainate as a glutamate receptor agonist and its historical use as an anthelmintic, as well as effects of avermectins, together suggest a therapeutic significance for glutamate receptors in nematodes. However more work is required to evaluate their distribution and pharmacology.

11.4. OTHER POSSIBLE NEUROTRANSMITTERS

Other putative transmitters have been suggested to occur in nematodes but their presence in *Ascaris* remains to be confirmed. These transmitters include: dopamine which is present in eight sensory neurones in the female *Ascaris suum* (Sulston *et al.*, 1975), adrenaline and noradrenaline (Willett, 1980) and octopamine (Hovitz *et al.*, 1982).

11.5. SECOND MESSENGERS

Little information concerning the involvement of second messengers in neuromuscular transmission in nematodes is available. Donahue *et al.* (1982, 1983) have correlated changes in muscle activity, produced by piperazine and levamisole, with changes in glycogen metabolism. They have also proposed a role for cyclic AMP-mediated regulation. The involvement of other second messengers, including Ca^{2+}, cyclic GMP and IP_3, has been established in *Ascaris* (Arevalo and Saz, 1991).

1991). The effects on muscle strip contraction were multiple: they included muscle contraction, muscle relaxation, contraction and rhythmic activity (Cowden *et al.*, 1989; Cowden and Stretton, 1990).

Intracellular records of membrane potential made from the commissural axons of motorneurones showed that effects of AF1 were to abolish slow oscillatory potentials at concentrations as low as 10^{-9} M (Cowden *et al.*, 1989); these effects reversed on washing. Experiments in which two

TABLE 5. *Peptide-like Immunoreactivity Detected in* A. suum *Neurones*

Peptide antiserum	Neurone subset stained
Mammalian peptides	
ACTH	no
Bombesin	no
Calcitonin	no
CCK8	yes
CGRP	yes
CRF	yes
β-endorphin	no
FSH	no
Gastrin	yes
GIP	no
Glucagon	no
Growth hormone	no
GRF	no
Insulin	no
Leu-enceplalin	yes
LH	no
LHRH	yes
Met-encephalin	yes
Motilin	no
MSH	yes
Neurophysin	no
Neurotensin	no
NPY-1	yes
NPY-2	no
Oxytocin	yes
Prolactin	no
Somatostatin	no
Substance P	?
TSH	no
Vasopressin	?
VIP-1	yes
VIP-2	yes
Molluscan peptides	
BCP	?
ELH	no
FMRFamide	yes
L11	yes
SCPb	yes
Peptide A	no
Peptide 9	no
Peptide 16A	no
Peptide 12b	yes
Arthropod peptides	
LAKH	?
Proctolin	no
RPCH	no

Data modified from Sithigorngul *et al.* (1990) and Stretton (1992).

COLES, G. C., EAST, J. M. and JENKINS, S. N. (1974) The mode of action of four anthelmintics. *Experientia* **30:** 1265–1266.

COLES, G. C., EAST, J. M. and JENKINS, S. N. (1975) The mechanism of action of the anthelmintic levamisole. *Gen. Pharmac.* **6:** 309–313.

COLQUHOUN, D. and SAKMANN, B. (1985) Fast events in single-channel currents activated by acetylcholine and its analogues at the frog muscle end-plate. *J. Physiol. (Lond.)* **369:** 501–557.

COLQUHOUN, L. HOLDEN-DYE, L. and WALKER, R. J. (1989) 5-*N*-2-(3-phenylpropylamino) benzoic acid, (5-NPB), is a non-competitive antagonist at the *Ascaris* GABA receptor. *Br. J. Pharmac.* **97:** 369.

COLQUHOUN, L., HOLDEN-DYE, L. and WALKER, R. J. (1990) The pharmacology of cholinoceptors on the somatic muscle cells of the parasitic nematode *Ascaris suum*. *Br. J. Pharmac.* **99:** 253.

COLQUHOUN, L., HOLDEN-DYE, L. and WALKER, R. J. (1991) The pharmacology of cholinoceptors on the somatic muscle cells of the parasitic nematode *Ascaris suum*. *J. exp. Biol.* **158:** 509–530.

COWDEN, C. and STRETTON, A. O. W. (1990) AF2, a nematode neuropeptide. *Soc. Neurosci. Abstr.* **16:** 305.

COWDEN, C., STRETTON, A. O. W. and DAVIS, R. E. (1989) AF1, a sequenced bioactive neuropeptide isolated from the nematode *Ascaris suum*. *Neuron* **2:** 1465–1473.

CROFTON, N. D. (1971) Form, function and behavior. In: *Plant Parasitic Nematodes*, Vol. 1, pp. 83–113, ZUKERMAN, B., MAI, W. and ROHDE, R. (eds) Academic Press, New York.

CULL-CANDY, S. G. (1976) Two types of extrajunctional L-glutamate receptors in locust muscle fibres. *J. Physiol. (Lond.)* **225:** 449–464.

DAVENPORT, T. R. B., LEE, D. L. and ISAAC, R. E. (1988) Immunocytochemical demonstration of a neuropeptide in *Ascaris suum* (Nematoda) using anti serum to FMRF-amide. *Parasitology* **97:** 81–88.

DAVIS, R. E. and STRETTON, A. O. W. (1989a) Passive membrane properties of motoneurons and their role in long-distance signalling in the nematode Ascaris. *J. Neurosci.* **9:** 403–414.

DAVIS, R. E. and STRETTON, A. O. W. (1989b) Signalling properties of *Ascaris* motoneurons: graded active responses, graded synaptic transmission, and tonic transmitter release. *J. Neurosci.* **9:** 415–425.

DAVIS, R. E. and STRETTON, A. O. W. (1992) Extracellular recordings from the motor nervous system of the nematode, *Ascaris suum*. *J. comp. Physiol.* **171:** 17–28.

DE BELL, J. T. (1965) A long look at neuromuscular junctions in nematodes. *Quart. Rev. Biol.* **40:** 233–251.

DE BELL, J. T., DEL CASTILLO, J. and SANCHEZ, Y. (1963) Electrophysiology of the somatic muscle cells of *Ascaris lumbricoides*. *J. Cell comp. Physiol.* **62:** 159–177.

DEL CASTILLO, J. and MORALES, T. (1967a) The electrical and mechanical activity of the esophageal cell of *Ascaris lumbricoides*. *J. gen. Physiol.* **50**: 603–630.

DEL CASTILLO, J. and MORALES, T. (1967b) Extracellular action potentials recorded from the interior of the giant esophageal cell of *Ascaris*. *J. gen. Physiol.* **50:** 631–645.

DEL CASTILLO, J., DE MELLO, W. C. and MORALES, T. (1963) The physiological role of acetylcholine in the neuromuscular system of *Ascaris lumbricoides*. *Arch. Int. Physiol. Biochem.* **71:** 741–757.

DEL CASTILLO, J., DE MELLO, W. C. and MORALES, T. (1964a) Influence of some ions on the membrane potential of *Ascaris* muscle. *J. gen. Physiol.* **48:** 129–140.

DEL CASTILLO, J., DE MELLO, W. C. and MORALES, T. (1964b) Inhibitory action of γ-aminobutyric acid (GABA) on *Ascaris* muscle. *Experientia* **20:** 141–143.

DEL CASTILLO, J., DE MELLO, W. C. and MORALES, T. (1964c) Mechanism of the paralysing action of piperazine on *Ascaris* muscle. *Br. J. Pharmac.* **22:** 463–477.

DEL CASTILLO, J., DE MELLO, W. C. and MORALES, T. (1967) The initiation of action potentials in the somatic musculature of *Ascaris lumbricoides*. *J. exp. Biol.* **46:** 263–279.

DEL CASTILLO, J., RIVERA, A., SOLORZANO, S. and SERRATO, J. (1989) Some aspects of the neuromuscular system of *Ascaris*. *Quart. J. exp. Physiol.* **74:** 1071–1089.

DE MELLO, W. C. and MALDONADO, H. (1985) Synaptic inhibition and cell communication; impairment of cell-to-cell coupling produced by gamma-aminobutyric acid (GABA) in the somatic musculature of *Ascaris lumbricoides*. *Cell. Biol. Int. Rep.* **9:** 803–813.

DESAI, C., GARRIGA, G., MCINTYRE, S. L. and HORVITZ, H. R. (1983) A genetic pathway for the development of the *Caenorhabditis elegans* HSM motor neurons. *Nature*. **336:** 293–294.

DIXON, D. M., VOLKANOV, M. and MARTIN, R. J. (1993) A patch–clamp study of the ionic selectivity of the large conductance Ca–activated chloride channel in muscle vesicles prepared from *Ascaris suum*. *J. Memb. Biol.* **131:** 143–149.

DONAHUE, M. J., YACOUB, N. J. MICHINOFF, C. A., MASARACCHIA, R. A. and HARRIS, B. G. (1981) Serotonin (5-hydroxytryptamine): a possible regulator of glycogenolysis in perfused muscle segments of *Ascaris suum*. *Biochem. biophys. Res. Commun.* **101:** 112–117.

DONAHUE, M. J., YACOUB, N. J. and HARRIS, B. J. (1982) Correlation of muscle activity with glycogen metabolism in muscle of *Ascaris suum*. *Am. J. Physiol.* **242:** R514–R521.

DONAHUE, M. J., MASARACCHIA, R. A. and HARRIS, B. G. (1983) The role of cyclic AMP-mediated regulation of glycogen metabolism in levamisole-perfused *Ascaris* muscle. *Molec. Pharmac.* **23:** 378–383.

DUITTOZ, A. H. and MARTIN, R. J. (1989) SR95103 acts as a GABA antagonist in *Ascaris suum* muscle. *Br. J. Pharmac.* **97:** 490P.

DUITTOZ, A. H. and MARTIN, R. J. (1990a) Effects of the arylaminopyridazine-GABA derivatives, SR95103 and SR95531 on the *Ascaris* muscle GABA receptor: the relative potency of the antagonists in *Ascaris*, is different to that at vertebrate $GABA_a$ receptors. *J. comp. Biochem. Physiol.* **98C:** 417–422.

12. CONCLUSION

The physiology and pharmacology of the neuromuscular transmission of nematodes is based mostly on observations on *A. suum* and *C. elegans*. *Ascaris* is a pig parasite, readily collected from many abattoirs, and large enough for electrophysiological study. *C. elegans* is a small free living nematode which may be grown in the laboratory and which is suitable for genetic studies. Anthelmintic mode of action studies have identified sites of action for the nicotinic anthelmintics like levamisole, the GABA agonist piperazine, and the avermectins. The production of new anthelmintics may utilize this information in rational design.

Acknowledgments—I wish to express my debt and gratitude to past and present members of the Edinburgh laboratory who have contributed to the ideas and experiments presented here. Peter Thorn, Anne Pennington, Anne Duittoz, Susan Robertson, Mark Evans, Diane Dixon, John Kusel and Momchil Volkanov are gratefully acknowledged. I am also pleased to acknowledge the financial support of the SERC, Wellcome Trust, Merck (U.S.A.), Pfizer Central Research U.K. and the British Council, who have made this work possible.

REFERENCES

ACEVES, J., ERLIJI, D. and MARTINEZ-MARNON, R. (1970) The mechanism of the paralysing action of tetramisole on *Ascaris* somatic muscle. *Br. J. Pharmac.* **38:** 332–344.

ANGSTADT, J. D. and STRETTON, A. O. W. (1989) Slow active potentials in ventral inhibitory motor neurons of the nematode *Ascaris*. *J. comp. Physiol.* **166:** 165–177.

ANGSTADT, J. D., DONMOYER, J. E. and STRETTON, A. O. W. (1989) Retrovesicular ganglion of the nematode *Ascaris*. *J. comp. Neurol.* **284:** 374–388.

ARENA, J. P., LIU, K. K., PARESS, P. S. and CULLY, D. F. (1991) Avermectin-sensitive chloride currents induced by *Caenorhabditis elegans* RNA in *Xenopus* oocytes. *Molec. Pharmac.* **40:** 368–374.

ARENA, J. P., LIU, K. K., PARESS, P. S., SCHAEFFER, J. M. and CULLY, D. F. (1992) Expression of a glutamate-activated chloride current in *Xenopus* oocytes injected with *Caenorhabditis elegans* RNA: evidence for modulation by elegans avermectin. *Molec. Brain Res.* **15:** 339–348.

AREVALO, J. and SAZ, N. J. (1991) Phospholipids and protein kinase C in acetylcholine-dependent signal transduction in *Ascaris suum*. *Molec. Biochem. Parasitol.* **48:** 151–161.

ARIENS, E. J., BELD, A. D., MIRANDA, J. F. R. and SIMONIS, A. M. (1979) The pharmacon receptor–effector concept. In: *The Receptors*, Vol. 1, pp. 33–91, O'BRIEN, R. D. (ed.) Plenum, New York.

ATCHISON, W. D., GEARY, T. D., MANNING, B., VANDEWAA, E. A. and THOMPSON, D. P. (1992) Comparative neuromuscular blocking actions of levamisole and pyrantel-type anthelmintics on rat gastrointestinal and nematode somatic muscle. *Toxic. Appl. Pharmac.* **112:** 133–143.

AUBRY, M., COWELL, P., DAVEY, M. J. and SHEVDE, S. (1970) Aspects of the pharmacology of new anthelmintics: pyrantel. *Br. J. Pharmac.* **38:** 332–344.

BALDWIN, E. and MOYLE, Y. (1949) A contribution to the physiology and pharmacology of *Ascaris lumbricoides* from the pig. *Br. J. Pharmac.* **4:** 145–152.

BRADING, A. F. and CALDWELL, P. C. (1971) The resting membrane potential of the somatic muscle cells of *Ascaris lumbricoides*. *J. Physiol. (Lond.)* **217:** 605–624.

BROOME, A. W. J. and GREENHAL, G. H. (1961) A new anthelmintic with unusual properties. *Nature* **189:** 59–60.

BUEDING, E. (1952) Acetylcholinesterase activity of *Schistosoma mansoni*. *Br. J. Pharmac.* **7:** 563–566.

BYERLY, L. and MASUDA, M. O. (1979) Voltage-clamp analysis of the potassium current that produces a negative-going action potential in *Ascaris* muscle. *J. Physiol. (Lond.)* **288:** 263–284.

CALDWELL, P. C. (1974) Possible mechanisms for linkage of membrane potentials to metabolism by electrogenic transport processes with special reference to *Ascaris* muscle. *Bioenergetics* **4:** 201–209.

CALDWELL, P. C. and ELLORY, J. C. (1968) Ion movement in the somatic muscle cells of *Ascaris lumbricoides*. *J. Physiol. (Lond.)* **197:** 75–76.

CAMPBELL, A. M. and BENZ, G. W. (1984) Ivermectin; a review of efficacy and safety. *J. Vet. Pharmac. Ther.* **7:** 1–16.

CAPPE DE BAILLON, P. (1911) Etude sur les fibres musculaires d'*Ascaris*. I. Fibres parietales. *Cellule* **27:** 165–211.

CHAUDHURI, J. and DONAHUE, M. J. (1989) Serotonin receptors in the tissues of adult *Ascaris suum*. *Molec. Biochem. Parasitol.* **35:** 191–198.

CHAUDHURI, J., MARTIN, R. E. and DONAHUE, M. J. (1988) Evidence for the absorption and synthesis of 5-hydroxytryptamine in perfused muscle and intestinal tissue and whole worms of adult *Ascaris suum*. *Parasitology* **96:** 157–170.

CHRIST, D., GOEBAL, M. and SAZ, N. J. (1990) Actions of acetylcholine and GABA on spontaneous contractions of the filariid, *Dipetalonema viteae*. *Br. J. Pharmac.* **101:** 971–977.

KNOWLES, C. O. and CASIDA, J. E. (1966) Mode of action of organophosphates and anthelmintics. Cholinesterase inhibition in *Ascaris lumbricoides*. *J. Agric. Food Chem.* **14:** 566.

LEACH, I., TRUDGILL, D. I. and GAHAN, P. B. (1987) Immunocytochemical localization of neurosecretary amines and peptides in the free-living nematode *Goodeyus ulmi*. *Histochemistry* **19:** 471–475.

LEE, D. L. (1962) The distribution of esterase enzymes in *Ascaris lumbricoides*. *Parasitology* **52:** 241–260.

LEE, D. L. (1970) The fine structure of the excretory system in adult *Nippostrongylus brasiliensis* (Nematoda) and a suggested function for the excretory system of *Anlsakis* larva (Nematoda: Anisakidae). *Parasitology* **59:** 289–298.

LEWIS, J. A., WU, C.-H., LEVINE, J. H. and BERG, H. (1980) Levamisole-resistant mutants of the nematode *Caenorhabditis elegans* appear to lack pharmacological acetylcholine receptors. *Neuroscience* **5:** 967–989.

LEWIS, J. A., FLEMING, J. T., MCLAFFERTY, S., MURPHY, H. and WU, C. (1986) The levamisole receptor, a cholinergic receptor of the nematode *Carnorhabditis elegans*. *Soc. Neurosci. Abstr.* **12:** 246.

LEWIS, J. A., FLEMING, J. T. and BIRD, D. (1992) Cloning nematode acetycholine receptor genes. In: *Neurotox '91*, pp. 155–164, DUCE, I. R. (ed.) Elsevier Applied Science, London and New York.

LI, C. (1990) FMRFamide-like immunoreactivity in *C. elegans Soc. Neurosci. Abstr.* **16:** 305.

LI, C. and CHALFIE, M. (1986) FMRFamide-like immunoreactivity in *C. elegans*: *Soc. Neurosci. Abstr.* **12:** 246.

MAPES, C. J. (1966) The fine structure of fibrillar components and plasma membrane contacts in esophageal myoepithelium of *Ascaris lumbricoides* (var. *suum*). *J. Ultrastruct. Res.* **14:** 602–617.

MARTIN, R. J. (1980) The effect of γ-aminobutyric acid on the input conductance and membrane potential of *Ascaris* muscle. *Br. J. Pharmac.* **71:** 99–106.

MARTIN, R. J. (1982) Electrophysiological effects of piperazine and diethylcarbamazine on *Ascaris suum* somatic muscle. *Br. J. Pharmac.* **77:** 255–265.

MARTIN, R. J. (1985a) Chemotherapy of helminth infections: nematocides, fascioliacides In: *Introduction to Veterinary Pharmacology*, pp. 357–354, ALEXANDER, F. A. (ed.) Longman, London and New York.

MARTIN, R. J. (1985b) γ-Aminobutyric acid- and piperazine-activated single channel currents from *Ascaris suum* body muscle. *Br J. Pharmac.* **84:** 445–461.

MARTIN, R. J. (1987) The γ-aminobutyric acid receptor of *Ascaris* as a target for anthelmintics. *Biochem. Soc. Trans.* **17:** 61–65.

MARTIN, R. E. and DONAHUE, M. J. (1987) Correlation of light chain phosphorylation and gamma aminobutyric acid receptors in *Ascaris suum* muscle. *Comp. Biochem. Physiol.* **87:** 23–29.

MARTIN, R. E. and DONAHUE, M. J. (1989) Tissue and ultrastuctural localization of 5-hydroxytryptamine (serotonin) in tissues of *Ascaris suum* with energy dispersive X-ray spectrometry of immunoreactive structure. *Int. J. Parasitol.* **19:** 585–596.

MARTIN, R. J. and KUSEL, J. R. (1992) On the distribution of a fluorescent ivermectin probe (4',5,7-dimethylbodipy proprionyliverinectin) in *Ascaris* membranes. *Parasitology* **104:** 549–554.

MARTIN, R. J. and PENNINGTON, A. J. (1989) A patch-clamp study of effects of dihydroavermectin on *Ascaris* muscle. *Br. J. Pharmac.* **98:** 747–756.

MARTIN, R. E., CHAUDHURI, J. and DONAHUE, M. J. (1988) Serotonin (5-Hydroxytryptamine) turnover in adult female *Ascaris suum* tissue. *Comp. Biochem. Physiol. C.* **91:** 307–310.

MARTIN, R. J., KUSEL, J. R. and PENNINGTON A. J. (1990) Surface properties of membrane vesicles prepared from muscle cells of *Ascaris suum*. *J. Parasitol.* **76:** 340–348.

MARTIN, R. J., PENNINGTON, A. J., DUITTOZ, A. H., ROBERTSON, S. J. and KUSEL, J. R. (1991) The physiology and pharmacology of neuromuscular transmission in the nematode parasite *Ascaris suum*. *Parasitology* **102:** 541–558.

MARTIN, R. J., KUSEL, J. R., ROBERTSON, S. J., MINTA, A. and HAUGHLAND, R. P. (1992a) Distribution of a fluorescent ivermectin probe, bodipy ivermectin, in tissues of the nematode parasite *Ascaris suum*. *Parasitol. Res.* **78:** 341–348.

MARTIN, R. J., THORN, P., GRATION, K. A. F. and HARROW, I. A. (1992b) On the voltage-activated Ca^{2+} and K^+ currents of the muscle cells of *Ascaris* suum. *J. exp. Biol.* **173:** 75–90.

MCINTYRE, S. L., HORVITZ, H. R. and WHITE, J. G. (1986) *Worm Breeders Gazette* **9:** 55–56.

MELLANBY, H. (1955) The identification and estimation of acetylcholine in three parasitic nematodes (*Ascaris lumbricoides*, *Litomosoides carinii*, and the microfilariae of *Dirofilaria repens*). *Parasitology* **45:** 287–294.

NATOFF, I. L. (1969) The pharmacology of the cholinoceptor in muscle preparations of *Ascaris lumbricoides* var *suum*. *Br. J. Pharmac.* **37:** 251–257.

NEHER, E. and STEINBACH, J. H. (1978) Local anaesthetics transiently block currents through single acetylcholine recptor channels. *J. Physiol.* (*Lond*). **277:** 153–176.

NORTON, S. and DE BEER, E. J. (1957) Investigations on the action of piperazine on *Ascaris lumbricoides*. *Am. J. Trop. Med.* **6:** 898–905.

ONUAGULUCHI, G. (1989) Some aspects of the pharmacology and physiology of the *Ascaris suum* muscle. *Arch. Int. Pharmacodyn. Ther.* **298:** 264–275.

PENNINGTON, A. J. and MARTIN, R. J. (1990) A patch-clamp study of acetylcholine activated ion channels in *Ascaris suum* muscle. *J. exp. Biol.* **154:** 201–221.

REGER, J. F. (1966) The fine structure of fibrillar components and plasma membrane contacts in esophageal myoepithelium of *Ascaris lumbricoides* (var. *suum*). *J. Ultrastruct. Res.* **154:** 602–617.

RHEINHALLT, P., HOLDEN-DYE, L. and WALKER, R. J. (1991) Ivermectin increases the anion conductance of the resting membrane potential of *Ascaris suum* muscle bag cell. *Br. J. Pharmac.* **104:** 439.

DUITTOZ, A. H. and MARTIN, R. J. (1990b) Effects of SR95103 on GABA-activated single-channel currents from *Ascaris suum* muscle. *J. comp. Biochem. Physiol* **98C:** 423–432.

DUITTOZ, A. A. and MARTIN, R. J. (1991) Antagonist properties of arylaminopyridazine GABA derivatives at the *Ascaris* muscle GABA receptor. *J. exp. Biol.* **159:** 149–164.

EVANS, A. M. and MARTIN, R. J. (1992) Morantel: an agonist and a slowly dissociating blocker of nicotinic acetylcholine channels from *Ascaris suum*. *Br. J. Pharmac.* **107:** 21.

EYRE, P. (1970) Some pharmacodynamic effects of the nematocides methyridine tetramisole and pyrantel. *J. Pharm. Pharmac.* **22:** 26–36.

GEARY, T. G., PRICE, D. A., BOWMAN, J. W. WINTERROWD, C. A., MACKENZIE, C. D., GARRISON, R. D., WILLIAMS, J. F. and FRIEDMAN, A. R. (1992). 2 FMRFamide-like peptides from *Panagrellus redivivus*. *Peptides* **13:** 209–214.

GOLDSCHMIDT, R. (1904) Der Chromidialapparat Lebhaft Funktionierender Gewebszellen. *Zool. J.* **21:** 41–140.

GOLDSCHMIDT, R. (1908) Das Nervensystem von *Ascaris lumbricoides* und megalocephala. Ein Yersuch, in den Aufbau eines einfachen Nervensystems einzudringen, Zweiter Teil. *Z. Wissen. Zool.* **90:** 73–136.

GOLDSCHMIDT, R. (1909) Das Nervensystem von *Ascaris lumbricoides* und megalocephala. Ein Yersuch, in den Aufbau eines einfachen Nervensystems einzudrringen, Zweiter Teil. *Z. Wissen. Zool.* **92:** 306–357.

GRZYWACZ, M., SZKUDLINSKS, J. and ZANDAROWSKA, E. (1985) Pharmacological receptors of *Ascaris lumbricoides suis L. Wiad. Parazytol.* **31:** 153–161.

GUASTELLA, J. and STRETTON, A. O. W. (1991) Distribution of 3H-GABA uptake sites in the nematode *Ascaris*. *J. comp. Neurol.* **307:** 598–608.

GUASTELLA, J., JOHNSON, C. D. and STRETTON, A. O. W. (1991) GABA-immunoreactive neurons in the nematode *Ascaris*. *J. comp. Neurol.* **307:** 584–597.

HARRIS, J. E. and CROFTON, N. D. (1957) Structure and function in the nematodes. Internal pressure and cuticular structure in *Ascaris*. *J. exp. Biol.* **34:** 116–30.

HARROW, I. D. and GRATION, K. A. F. (1985) Mode of action of the anthelmintics morantel, pyrantel and levamisole on the muscle cell membrane of the nematode *Ascaris suum*. *Pest. Sci.* **16:** 662–672.

HESSE, R. (1892) Uber das Nervensystem von *Ascaris lumbricoides* und *Ascaris megalocephala* 1. *Z. Wiss. Zool.* **90:** 73–136.

HO, N. F. H., GEARY, T. G., RAUB, T. J., BARSUHN, C. L. and THOMPSON, D. P. (1990) Biophysical transportation studies of the cuticle of *Ascaris suum*. *Molec. Biochein. Parasitol.* **41:** 153–165.

HOBSON, A. D. STEPHENSON, W. and BEADLE, L. C. (1952a) Studies on the physiology of *Ascaris* lumbricoides I. The relation of total osmotic pressure, conductivity and chloride content of the body fluid to that of the external environment. *J. exp. Biol.* **29:** 1–21.

HOBSON, A. D., STEPHENSON, W. and EDEN, A. (1952b) Studies on the physiology of *Ascaris lumbricoides* II. The inorganic composition of the body fluid in relation to that of the environment. *J. exp. Biol.* **29:** 22–29.

HOLDEN-DYE, L. and WALKER, R. J. (1988) ZAPA, (*Z*)-3-[(amino iminomethyl)thio]-2-propenoic acid hydrochloride, a potent agonist at GABA receptors on the *Ascaris* muscle cell. *Br. J. Pharmac.* **95:** 3–5.

HOLDEN-DYE, L. and WALKER, R. J. (1990) Avermectin and avermectin derivatives are antagonists at the 4-aminobutyric acid (GABA) receptors on the somatic muscle cells of *Ascaris*: Is this the site of anthelmintic action. *Parasitology* **101:** 265–271.

HOLDEN-DYE, L., HEWITT, G. M., WANN, K. T., KROGSGAARD-LARSEN, P. and WALKER, R. J. (1988) Studies involving avermectin and the 4-aminobutyric acid (GABA) receptor of *Ascaris suum* muscle. *Pest. Sci.* **24:** 231–245.

HOLDEN-DYE, L., KROGSGAARD-LARSEN, P. NEILSEN, L. and WALKER, R. J. (1989) GABA receptors on the somatic muscle cells of the parasitic nematode, *Ascaris suum*: stereoselectivity indicates similarity to a $GABA_a$-type agonist recognition site. *Br. J. Pharmac.* **98:** 841–850.

HORVITZ, R. H., CHALFIE, M., TRENT, C., SULSTON, J. E. and EVANS, P. D. (1982) Serotonin and octopamine in the nematode *Caenorhabditis elegans*. *Science* **206:** 1012–1014.

JARMAN, M. (1959) Electrical activity in the muscle cells of *Ascaris lumbricoides*. *Nature* **184:** 1244.

JARMAN, M. (1970) A muscle-domain hypothesis for *Ascaris* postural waves. *Parasitology* **61:** 475–489.

JARMAN, M. and ELLORY, J. C. (1969) Effect of TTX on *Ascaris* somatic muscle. *Experientia* **25:** 507.

JOHNSON, C. D. and STRETTON, A. O. W. (1980) Neural control of locomotion in *Ascaris*: anatomy, electrophysiology, and biochemistry. In: *Nematodes as Biological Models*, Vol. 1, pp. 159–195, Academic Press, New York.

JOHNSON, C. D. and STRETTON, A. O. W. (1985) Localization of choline acetyltransferase within identified motoneurons of the nematode *Ascaris*. *J. Neurosci.* **5:** 1984–1992.

JOHNSON, C. D. and STRETTON, A. O. W. (1987) GABA-immunoreactivity in inhibitory motor neurons of the nematode *Ascaris*. *J. Neurosci.* **7:** 223–235.

KASS, I. S., WANG, C. C., WALDROND, J. P. and STRETTON, A. O. W. (1980) Avermectin B_{1a}, a paralysing anthelmintic that affects interneurones and inhibitory motorneurones in *Ascaris*. *Proc. natn. Acad. Sci. U.S.A.* **77:** 6211–6215.

KASS, I. S., LARSEN, D. A., WANG, C. C. and STRETTON, A. D. (1982) *Ascaris suum*: differential effects of avermectin Bla on the intact animal and neuromuscular strip preparations. *Exp. Parasitol.* **54:** 166–174.

KASS, I. S., STRETTON, A. O. and WANG, A. O. (1984) The effects of averinecti and drugs related to acetylcholine and 4-aminobutyric acid on neuromuscular transmission in *Ascaris suum*. *Molec. Biochem. Parasitol.* **13:** 213–225.

ROBERSON, E. L. (1988) Antinematodal drugs. In: *Veterinary Pharmacology and Therapeutics*, pp. 882–927, BOOTH, N. E. and MCDONALD, L. E. (eds), Iowa State University Press, Ames.

ROBERTSON, S. J. and MARTIN, R. J. (1992) Levamisole-activated single-channel currents from muscle membranes of *Ascaris suum*. *Br. J. Pharmac.* **108,** 170–178.

ROBERTSON, S. J., PENNINGTON, A. J., EVANS, A. J. and MARTIN, R. J. (1992) Pyrantel activated single channel currents in the nematode parasite *Ascaris suum*. *Br. J. Pharmac.* **107:** 154.

ROHER, S. P., MEINKE, P. T., HAYES, E. C., MROZIK, H. and SCHAEFFER, J. M. (1992) Photoaffinity labelling of avermectin binding sites from *Caenorhabditis elegans* and *Drosophilia melanogaster*. *Proc. natn. Acad. Sci. U.S.A.* **89:** 4168–4172.

ROSENBLUTH, J. (1965a) Ultrastructural organization of obliquely striated muscle fibres in *Ascaris lumbricoides*. *J. Cell Biol.* **25:** 495–515.

ROSENBLUTH, J. (1965b) Ultrastructure of somatic muscle cells in *Ascaris lumbricoides*. II. Intermuscular junctions, neuromuscular junctions, and glycogen stores. *J. Cell Biol.* **26:** 579–591.

ROSENBLUTH, J. (1967) Obliquely striated muscle. III. Contraction mechanism of *Ascaris* body muscle. *J. Cell Biol.* **34:** 15–33.

ROSENBLUTH, J. (1969) Ultrastucture of dyads in muscle fibres of *Ascaris lumbricoides*. *J. Cell Biol.* **42:** 817–825.

ROZHOVA, E. K. MALYUTINA, T. A. and SHISHOV, B. A. (1980) Pharmacological characteristics of cholinoreception in somatic muscle of the nematode *Ascaris suum*. *Gen. Pharmac.* **11:** 141–146.

SAZ, N. J. and WEIL, A. (1962) A pathway of formation of alpha-methyl valerate by *Ascaris lumbricoides*. *J. biol. Chem.* **237:** 2053–2056.

SCHAEFFER, J. M. and BERGSTROM, A. R. (1988) Identification of gamma-aminobutyric acid and its binding sites in *Caenorhabditis elegans*. *Life Sci.* **43:** 1701–1706.

SCHAEFFER, J. M. and HAINES, H. W. (1989) Avermectin binding in *Caenorhabditis elegans*: a two-state model for the avermectin binding site. *Biochem. Pharmac.* **38:** 2339–2349.

SCHAEFFER, J. M., BERGSTROM, A. R. and TURNER, M. J. (1989a) MK-801 is a potent nematocidal agent: characterization of MK-801 binding sites in *Caenorhabditis elegans*. *Biochem. J.* **260:** 923–926.

SCHAEFFER, J. M., RUIZ-SANCHEZ, J., SHIH, T. L. and MROZIK, H. (1989b) Argiopine differentiates between vertebrates and invertebrate glutamate binding sites. *Pest. Biochem. Physiol.* **35:** 26–32.

SCHAEFFER, J. M., STIFFEY, J. H. and MROZIK, H. (1989c) A chemiluminescent assay for measuring avermectin binding sites. *Anal. Biochem.* **177:** 291–295.

SCHAEFFER, J. M., FRAZIER, E. G., BERGSTROM, A. R., WILLIAMSON, J. M., LIESCH, J. M., and GOETZ, M. A. (1990) Cochlioquinone A, a nematocidal agent which competes for specific [^{3}H]ivermectin binding sites. *J. Antibiot.* **XLIII:** 1179–1182.

SCHNEIDER, A. (1866) *Monograpgie der Nematoden*. Berlin.

SCOTT, R. H. and DUCE, I. R. (1985) Effects of 22,23 dihydroavermectin on locust (*Schistocerca gregaria*) muscles may involve several sites of action. *Pest. Sci.* **16:** 599–604.

SHINOZAKI, H. and KONISHI, S. (1970) Actions of several anthelmintics and insecticides on rat cortical neurons. *Brain Res.* **24:** 368–371.

SITHIGORNGUL, P., COWDEN, C., GUASTELLA, J. and STRETTON, A. O. W. (1989) Generation of monoclonal antibodies against a nematode peptide extract: another approach for identifying unknown neuropeptides. *J. comp. Neurol.* **284:** 389–397.

SITHIGORNGUL, P., STRETTON, A. O. and COWDEN, C. (1990) Neuropeptide diversity in *Ascaris*: an immunocytological study. *J. comp. Neurol.* **294:** 362–376.

SMART, D., SHAW, C., CURRY, W. J., JOHNSTON, C. F., THIM, L., HALTON, D. W. and BUCHANAN, K. D. (1992a) the primary structure of TE-6: a novel neuropeptide from *Ascaris suum*. *Biochem. biophys. Res. Commun.* **187:** 1323–1329.

SMART, D., SHAW, C., JOHNSTON, C. F., THIM, L., HALTON, D. W., FAIRWEATHER, I. and BUCHANAN, K. D. (1992b) Chromatographic and immunological characterization of neuropeptide Y-like and pancreatic polypeptide-like peptides from the nematode *Ascaris suum*. *Comp. Biochem. Physiol. C.* **102:** 477–481.

STANDEN, O. D. (1955) Activity of piperazine *in vitro*, against *Ascaris lumbricoides*. *Br. Med. J.* **II:** 20–22.

STRETTON, A. O. W. (1976) Anatomy and development of the somatic musculature of the nematode of *Ascaris*. *J. exp. Biol.* **64:** 773–788.

STRETTON, A. O. W. (1992) Chemical intracellular signalling mechanisms in the nervous system of the nematode *Ascaris suum*: potential sites of action of new generations of anthelmintic drugs. In: *Neurotox '91*, pp. 123–138, DUCE, I. R. (ed.) Elsevier Applied Science, London and New York.

STRETTON, A. O. W. and JOHNSON, C. D. (1985) GABA and 5HT immunoreactive neurons in *Ascaris*. *Soc. Neurosci Abstr.* **11:** 626.

STRETTON, A. O. W., FISHPOOL, R. M., SOUTHGATE, E., DONMOYER, J. E., WALROND, J. P., MOSES, J. E. R. and KASS, I. S. (1978) Structure and physiological activity of the motoneurons of the nematode *Ascaris*. *Proc. natn. Acad. Sci. U.S.A.* **75:** 3493–3497.

STRETTON, A. O. W., DAVIS, R. E., ANGSTADT, J. D., DONMOYER, J. E. and JOHNSON, C. D. (1985) Neural control of behaviour in *Ascaris*. *Trends Neurosci.* **8:** 294–300.

STRETTON, A. O. W., COWDEN, C., SITHIGGORNGUL, P. and DAVIS, R. E. (1991) Neuropeptides in the nematode *Ascaris suum*. *Parasitology*. **102:** 5107–5116.

SULSTON, J., DEW, M. and BRENNER, S. (1975) Dopamine neurons in the nematode *Caenorhabditis elegans*. *J. comp. Neurol.* **163:** 215–244.

THORN, P. and MARTIN, R. J. (1987) A high-conductance calcium-dependent chloride channel in *Ascaris suum* muscle. *Quart. J. exp. Physiol.* **72:** 31–49.

TOSCANO RICO, J. (1926) Sur la sensilitie de l'*Ascaris* a l'action de quelques drogues. *Comp. Rend. Soc. Biol. Paris.* **94:** 921–923.

TSANG, V. C. and SAZ, N. J. (1973) Demonstration and function of 2-methyl-butyrate racemase in *Ascaris lumbricoides*. *J. comp. Biochem Physiol.* **45B:** 617–623.

VAN DEN BOSSCHE, H. (1985) Pharmacology of anthelmintics. Chemotherapy of gastrointestinal helminths. *Handbook exp. Parasitol.* **77:** 125–181.

WALKER, R. J., COLQUHOUN, L. M., PARRI, H. R. WILLIAMS. R. G. and HOLDEN-DYE, L. (1992) Pharmacology of the *Ascaris* nervous system. In: *Neurtox* '91, pp. 105–121, DUCE, I. R. (ed.) Elsevier Applied Science London and New York.

WALROND, J. P. and STRETTON, A. O. W. (1985) Reciprocal inhibition in the motor nervous system of the nematode *Ascaris*: direct control of ventral inhibitory motoneurons by dorsal excitatory motoneurons. *J. Neurosci.* **5:** 9–15.

WALROND, J. P., KASS, I. S., STRETTON, A. O. W. and DONMOYER, J. (1985) Identification of excitatory and inhibitory motoneurons in the nematode by electrophysiological techniques. *J. Neurosci.* **5:** 1–8.

WANN, K. T. (1987) The electrophysiology of the somatic muscle cells of *Ascaris suum* and *Ascaridia galli*. *Parasitology* **94:** 555–566.

WEISBLAT, D. A. and RUSSEL, R. L. (1976) Propagation of electrical activity in the nerve cord and muscle syncytium of the nematode *Ascaris lumbricoides*. *J. comp. Physiol.* **107:** 293–307.

WEISBLAT, D. A., BYERLY, L. and RUSSEL, R. L. (1976) Ionic mechanisms of electrical activity in the somatic muscle cell of the nematode *Ascaris lumbricoides*. *J. comp. Physiol.* **111:** 93–113.

WERMUTH, C. G., BOURGUIGNON, J. J., SCHLEIVER, G., GIES, J. P., SCHOENFELDER, A., MELIKIAN, A., BOUCHET, M. T., CHANTREAUX, D., MOLIMARD, J. C., HEAULME, M., CHAMBON, J. P. and BIZIERE, K. (1987) Synthesis and structure–activity relationships of a series of arylaminopyridazine derivatives of GABA acting as selective $GABA_a$ antagonists. *J. Med. Chem.* **30:** 239–249.

WHITE, J. G., SOUTHGATE, E., THOMSON, J. N. and BRENNER, S. (1976) The structure of the ventral cord of *Caenorhabditis elegans*. *Phil. Trans. R. Soc. Lond. B.* **275:** 298–327.

WHITE, J. G., SOUTHGATE, E., THOMSON, J. N. and BRENNER, S. (1986) The structure of the nervous system of *Caenorhabditis elegans*. *Phil. Trans. R. Soc. Lond. B.* **314:** 1–340.

WILLETT, J. D. (1980) Control mechanisms in nematodes. In: *Nematodes as Biological Models*, Vol. I, pp. 197–225, ZUCKERMAN, B. M. (ed.) Academic Press. New York.

WILLIAMS, J. A. and DONAHUE, M. J. (1992) Identication of a novel 5-HTN (Nematoda) receptor from *Ascaris suum*. *Comp. Biochem. Physiol.* **101:** 469–474.

WRIGHT, D. J. (1986) Biological activity and mode of action of avermectins. In: *Neurobiology and Pesticide Action*, pp. 174–202, FORD, M. G., LUNDT, G. G., REAY, R. C. and USHERWOOD, P. N. R. (eds) Ellis Horwood, Chichester.

CHANNELS FROM *ASCARIS SUUM*?

A.M. Evans & R.J. Martin, Department of Preclinical Veterinary Sciences, University of Edinburgh, Summerhall, Edinburgh EH9 1QH

The anthelmintic morantel has been shown to activate nicotinic-acetylcholine receptors in muscle cells of the parasitic nematode Ascaris suum (Harrow & Gration, 1985). Using muscle membrane vesicles from Ascaris we have now studied the activation by morantel of these receptors at the single-channel level (for methods refer to Pennington & Martin, 1990). Standard patch-clamp techniques were employed. Morantel (0.006-600μM) was applied via the pipette solution. Single-channel currents were observed throughout this concentration range, although qualitatively the probability of opening (Popen) at 0.006μM was very low relative to the maximum observed at 6μM. The conductance of morantel-activated single-channel currents was estimated from the slope of I/V plots obtained from excised inside-out patches exposed to symmetrical [Cs^+] and non-symmetrical [Cl^-]. The I/V relationship was linear and exhibited a reversal potential close to 0mV, as would be expected for a channel permeable to cations rather than anions. Two conductance states were observed, the larger being approximately 40pS and the smaller approximately 25pS. Increasing the concentration of morantel had no effect on the open-channel conductance. Analysis of the kinetics of the main conductance state was carried out using vesicle-attached patches to avoid run-down. In the presence of 6 and 10μM morantel the single-channel open-times were best fitted by up to 2 exponentials (suggesting at least 2 open-channel states) and the closed-times by up to 4 exponentials (suggesting at least 4 closed states). The mean open-times (approximately 1ms) exhibited a modest increase on membrane hyperpolarisation, while the mean closed-times exhibited no clear voltage-dependence. This was in stark contrast to our findings with 60-600μM morantel in the pipette solution. Here the mean open-times decreased and the mean closed-times increased with membrane hyperpolarisation. There was also a dramatic reduction in the frequency of opening on hyperpolarisation. These effects increased with increasing morantel concentration, giving rise to both a concentration-dependent and voltage-dependent reduction in Popen. For example, in the presence of 60 and 100μM morantel the Popen (mean$\pm$s.e.m.) fell from 0.004$\pm$0.0001 (n=3) and 0.004$\pm$0.0007 (n=4) respectively at +75mV, to 0.001$\pm$0.0005 (n=3) and 0.0002$\pm$0.00008 (n=4) respectively at -75mV. We can explain these results by suggesting that while morantel is an agonist of the nicotinic acetylcholine channels, it also acts as a slowly dissociating cation open-channel-blocker. Interestingly what appeared to be fast flickering open-channel block was also observed with morantel (100 and 600μM), but only at depolarised potentials.

Harrow, I.D. & Gration, K.A.F. (1985). Pesticide Sci., 16, 662-672.
Pennington, A.J. & Martin, R.J. (1990). J. Exp. Biol., 154, 210-221.

22P (18-36) NEUROPEPTIDE Y IS A POTENT RAT MAST CELL DEGRANULATOR

D. Haworth*, J-A. Culbert and D. S. Thomson (introduced by B. Cox), ICI Pharmaceuticals, Alderley Park, Macclesfield, Cheshire, SK10 4TG.

Neuropeptide Y (NPY) is a potent pressor molecule while the C-terminal analogue (18-36) NPY is predominantly depressor (Boublik et al, 1989). High doses of NPY have been shown to reduce blood pressure following the initial pressor response and it has been suggested that this is due to histamine release from mast cells (Grundemar et al, 1990). We have compared the effects of (18-36) NPY with an NPY analogue which has pressor activity, (13-36) NPY (Potter et al, 1989), and investigated the contribution of mast cell amine release to the depressor effect of (18-36) NPY.

Mast cell degranulation was estimated in vitro by measurement of [^{14}C]-5HT release from rat peritoneal mast cells (Stechschulte & Austen, 1974). Effects on blood pressure were measured in pentobarbitone anaesthetised, syrosingopinised (5mgkg^{-1}day^{-1} s.c. for 2 days), bilaterally vagotomised AP rats, weighing appproximately 300g. (18-36) NPY was a potent mast cell degranulator in vitro (EC_{50}, 41nM) and was 24-fold more potent than (13-36) NPY (EC_{50} 970nM). In vivo, (18-36) NPY caused a transient pressor followed by a prolonged depressor response. Cummulative dosing (2.4 to 72nmol) produced a maximal pressor response of 32$\pm$5mmHg (mean$\pm$s.e.m., n=4) and depressor response of 42$\pm$2mmHg. In contrast, (13-36) NPY (2.0 to 60nmol) caused only a pressor response (32$\pm$4mmHg maximum).

Treatment with a combination of tiotidine (5mgkg^{-1} i.v.), mepyramine (0.5mgkg^{-1}) and methysergide (5mgkg^{-1}) reduced but did not abolish the depressor response to (18-36) NPY. Only if rats were additionally pretreated with Dextran T70 (Macrodex, 1ml) to degranulate mast cells and plasma volume was restored by a further Macrodex injection did (18-36) NPY fail to lower blood pressure. Following this treatment, the cummulative dose of (18-36) NPY required to increase systolic pressure by 25mmHg decreased 4-fold, from 48.8$\pm$9.8 to 11.0$\pm$2.9nmol, when compared with controls ($p<0.01$). There was no significant change in the pressor response to (13-36) NPY in rats treated with dextran, tiotidine, mepyramine and methysergide.

These results indicate that (18-36) NPY is a potent rat mast cell degranulator, releasing both histamine and 5HT which mediate the depressor response. The genuine pressor effect of (18-36) NPY is therefore masked because of these mast cell products. The possibility of NPY and its analogues causing mast cell degranulation should be considered when interpreting effects on blood pressure.

Boublik, J., Scott, N., Taulane, J., Goodman, M., Brown, M. & Rivier, J. (1989) Int. J. Peptide Protein Res. 33, 11-15. Grundemar, L., Wahlstedt, C., Shen, G. H., Zukowska-Grojec, Z. & Hakanson, R. (1990) Eur. J. Pharmacol. 179, 83-87. Potter, E. K., Mitchell, L., McCloskey, M. J. D., Tseng ,A., Goodman, A., Shine, J. & McCloskey, D. I. (1989) Regulatory Peptides 25, 167-177. Stechschulte, D. J. & Austen, K. F. (1974) J. Immunol. 112, 970-978.

*Journal of Physiology (1993), **459**, 394P*

At positive potentials the cationic agonist morantel blocks nicotinic-acetylcholine channels in muscle membrane vesicles isolated from *Ascaris suum*

A.M. Evans and R.J. Martin

Department of Preclinical Veterinary Sciences, R(D)SVS, Summerhall, University of Edinburgh, Edinburgh EH9 1QH

We have investigated the activation by the anti-helminthic drug morantel of nicotinic-acetylcholine (nACh) channels in muscle-membrane vesicles from *Ascaris suum*. Standard patch-clamp techniques were employed to study the single-channel kinetics in the vesicle-attached configuration (for methods see Pennington & Martin, 1990). When added to the pipette solution in high concentrations (60–600 μM) morantel, in addition to opening nACh channels, produced a fast flickering block at positive potentials (Fig. 1); at negative potentials a more complex form of channel block was observed (Evans & Martin, 1993). When the membrane potential was changed from +100 to +50 mV, the mean open-time decreased and the mean duration of the short gaps increased, as would be expected if a cation such as morantel was acting as a channel blocker. A concentration-dependent increase in the frequency of the short gaps was also observed, together with a concomitant decrease in the mean open time. The data were analysed assuming simple open-channel block. At each positive potential studied (+100, +75 and +50 mV) forward blocking rate constants (k_{+B}) were estimated from the slope of the reciprocal of mean open time against morantel concentration; the unblocking rate constants (k_{-B}) were estimated from the reciprocal of mean duration of the short gaps, which was independent of concentration. From plots of ln k_{+B} and ln k_{-B} against potential we obtained values of 2.3×10^7 M^{-1} s^{-1} and 765 s^{-1} for k_{+B} and k_{-B} at 0 mV (K_D = 33 μM). Our data predict an e-fold decrease in the K_D for a 22 mV step towards 0 mV, from a positive potential.

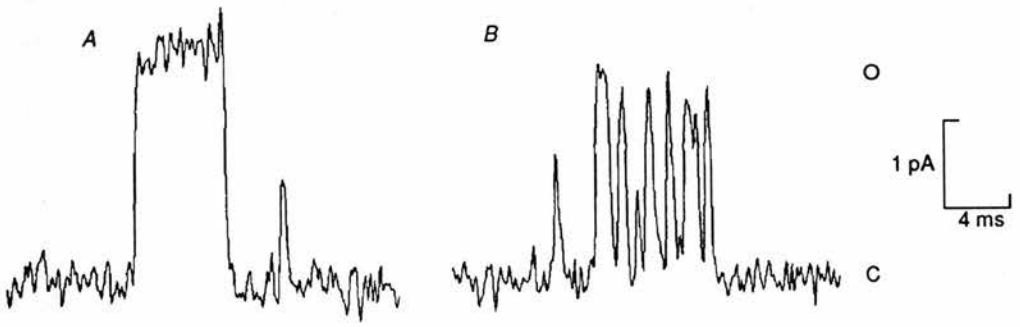


Fig. 1. Morantel-activated single-channel currents. The pipette solution contained 6 μM (*A*) and 600 μM (*B*) morantel. Membrane potential +75 mV. Note the flickering block in *B*. C, closed; O, open.

Supported by the Wellcome Trust.

REFERENCES

Evans, A.M. & Martin, R.J. (1993). *J. Physiol.* **459**, 489*P*.
Pennington, A.J. & Martin, R.J. (1990). *J. Exp. Biol.* **154**, 201–221.

Journal of Physiology (1993), 467, 254P

On the block by morantel of nicotinic acetylcholine channels isolated from *Ascaris suum*: rate constants for multi-ion block estimated by maximum likelihood

A.M. Evans and R.J. Martin

Department of Preclinical Veterinary Science, R. (D.) S. V. S., Summerhall, University of Edinburgh, Edinburgh EH9 1QH

We have previously reported the complex nature of the block by morantel of nicotinic acetylcholine (nACh) channels in membrane vesicles isolated from the somatic muscle cells of *Ascaris suum* (Evans & Martin, 1992*a*, *b*). Single-channel records were obtained using the patch-clamp technique. Morantel, an agonist and channel blocker at these nACh receptors, was added to the pipette solution and channel activity was studied using vesicle-attached patches. At high concentrations of morantel (10–600 μM), two blocked states were observed at negative membrane potentials: a brief block (4–20 ms), the duration of which was concentration independent; and a long block (up to 7 s), the duration of which was concentration dependent. In addition, the concentration–block relationship had a Hill coefficient of 1.6, suggesting the involvement of at least two blocking molecules of morantel in the channel. We proposed a simple sequential block scheme (Fig. 1) involving two molecules of morantel entering the open channel, to explain these observations. We have now estimated the values of the rate constants for this model by maximum likelihood to the entire sequence of open- and closed-times observed at −75 mV with 100 μM morantel using the approach of Horne & Lange (1983). β' was $3.6 \pm 0.9\ s^{-1}$; α was $1430 \pm 180\ s^{-1}$; k_{-B} was $16.0 \pm 1.48 \times 10^6\ M^{-1}\ s^{-1}$; k_{-B} was $29.4 \pm 6.7\ s^{-1}$; γ was $100 \pm 35\ s^{-1}$; δ was $114 \pm 60\ s^{-1}$; $k_{-B'}$ was $26.5 \pm 3.9 \times 10^6\ M^{-1}\ s^{-1}$; $k_{-B'}$ was $63 \pm 14\ s^{-1}$ (mean ± S.E.M., $n = 6$). These parameters were also found to predict the observed effects of morantel concentration on the degree of block and probability of opening.

$$C \underset{\alpha}{\overset{\beta'}{\rightleftharpoons}} O \underset{k_{-B}}{\overset{k_{+B} \cdot x_a}{\rightleftharpoons}} MB_1 \underset{\delta}{\overset{\gamma}{\rightleftharpoons}} MB_2 \underset{k_{-B'}}{\overset{k_{+B'} \cdot x_a}{\rightleftharpoons}} MB_1MB_2$$

Fig. 1. Sequential block model describing multi-ion channel block by morantel. C, closed; O, open; MB_1, block site 1 occupied; MB_2, block site 2 occupied; MB_1MB_2, both block sites occupied; $k_{+B'}$, $k_{-B'}$, β', α, γ, δ, k'_{-B} and $k'_{-B'}$ are rate constants; x_a, morantel concentration.

Supported by the Wellcome Trust.

REFERENCES

Evans, A.M. & Martin, R.J. (1992*a*). *J. Physiol.* **459**, 394*P*.
Evans, A.M. & Martin, R.J. (1992*b*). *J. Physiol.* **459**, 489*P*.
Horne, R. & Lange, K. (1983). *Biophys. J.* **43**, 207–223.

Morantel may bind to more than one site within nicotinic-acetylcholine channels from *Ascaris suum*

A.M. Evans and R.J. Martin

Department of Preclinical Veterinary Sciences, R(D)SVS, Summerhall, University of Edinburgh, Edinburgh EH9 1QH

Using the patch-clamp technique, we have established that morantel opens and then blocks nicotinic-acetylcholine (nACh) channels in muscle membrane vesicles from *Ascaris suum* (for methods see Pennington & Martin, 1990). Morantel was added to the pipette solution and the single-channel kinetics studied in the vesicle-attached configuration. In common with the observations made at positive membrane potentials (Evans & Martin, 1993) the mean open time declined with increasing morantel concentration (0.6–600 μM). At negative potentials, however, the voltage sensitivity was lost. Furthermore a concentration- and voltage-dependent increase in mean closed time was observed at negative but not positive membrane potentials. The effects on open and closed times resulted in a voltage- and concentration-dependent fall in the probability of opening (P_o). The marked voltage sensitivity suggests that these effects were not allied to receptor desensitization but due to open-channel block by the cationic agonist morantel. However, when the degree of block (1–[P_o at –75 mV/P_o at +75 mV]) was plotted against morantel concentration, the curve was well fitted by a Hill equation with a coefficient greater than 1, suggesting positive co-operativity. We have also identified a short- and a long-lived block state, both of which increased in duration as the membrane potential was made more negative. One was independent of concentration and had a value of 4–20 ms at –75 mV; the second showed a marked concentration dependence and increased from 0.89 ± 0.19 s at 60 μM to 5 ± 2 s at 100 μM (mean ± S.E.M., $n = 4$, at –75 mV). One explanation for these observations is that of multi-ion channel block. Figure 1 shows a sequential model which describes two binding sites for morantel within the nACh channel and may explain, at least in part, our findings.

$$C \longleftrightarrow O \underset{k_{-B}}{\overset{k_{+B}.x_a}{\rightleftharpoons}} MB_1 \underset{\delta}{\overset{\gamma}{\rightleftharpoons}} MB_2 \underset{k_{-B'}}{\overset{k_{+B'}.x_a}{\rightleftharpoons}} MB_1MB_2$$

Fig. 1. A model describing multi-ion channel-block by morantel. C, closed; O, open; MB_1, block-site 1 occupied; MB_2, block-site 2 occupied; MB_1MB_2, both block sites occupied; k_{+B}, k_{-B}, γ, δ, $k_{+B'}$ and $k_{-B'}$ are rate constants; x_a, morantel concentration.

Supported by the Wellcome Trust.

REFERENCES

Evans, A.M. & Martin, R.J. (1993). *J. Physiol.* **459**, 394*P*.
Pennington, A.J. & Martin, R.J. (1990). *J. Exp. Biol.* **154**, 201–221.

On the block by morantel of nicotinic acetylcholine channels isolated from *Ascaris suum*: positive co-operativity between at least two blocking molecules

A.M. Evans and R.J. Martin

Department of Preclinical Veterinary Sciences, R(D)SVS, Summerhall, University of Edinburgh, Edinburgh EH9 1QH

We have recently reported the agonist action and complex channel block produced by morantel at nicotinic acetylcholine channels in membrane vesicles isolated from muscle cells of *Ascaris suum* (Evans & Martin, 1993*a*, *b*). In order to examine the mechanism of block further, we have assumed that: in the absence of any channel block there would be no significant increase in the probability of channel opening (P_o) with morantel concentration (0.6–600 μM) since we approach saturation of agonist binding sites; in the absence of any block the ratio P_o –75 mV/P_o +75 mV would be constant and independent of morantel concentration; no significant reduction in P_o results from the block at +75 mV.

The relationship between degree of block, [1 – (P_o –75 mV/P_o +75 mV)], and morantel concentration was best fitted by a Hill equation with a coefficient of 1.6, suggesting positive co-operativity between at least two molecules of morantel. The simple sequential model in Fig. 1*A* predicts the relationship between degree of block and morantel concentration would be described by the expression in Fig. 1*B*. Using estimates of rate constants (Fig. 1*A*) from experimental data we have found that this is so.

A

$$C \underset{\alpha}{\overset{\beta'}{\rightleftharpoons}} O \underset{k_{-B}}{\overset{k_{+B} \cdot x_a}{\rightleftharpoons}} MB_1 \underset{\delta}{\overset{\gamma}{\rightleftharpoons}} MB_2 \underset{k_{-B'}}{\overset{k_{+B'} \cdot x_a}{\rightleftharpoons}} MB_1MB_2$$

B

$$1 - \frac{R}{1 + \frac{\beta'}{\alpha + \beta'}\left(\frac{x_a}{K_B} + \frac{x_a \cdot \gamma}{K_B \cdot \delta} + \frac{x_a^2 \cdot \gamma}{K_B \cdot K_{B'} \cdot \delta}\right)}$$

Fig. 1. *A*, simple sequential model describing channel block by two morantel molecules. C, closed; O, open; MB_1, block site 1 occupied; MB_2, block site 2 occupied; MB_1MB_2, both block sites occupied. β', α, k_{+B}, k_{-B}, γ, δ, $k_{+B'}$ and $k_{-B'}$ are rate constants; x_a, morantel concentration. *B*, relationship between degree of block and morantel concentration; R is ratio P_o –75mV/P_o +75 mV in absence of block (2.9 at 0.6 μM) and ($\beta'/\alpha + \beta'$) is P_o at –75 mV in the absence of block (0.004 at 0.6 μM); $K_B = k_{-B}/k_{+B}$ and $K_{B'} = k_{-B'}/k_{+B'}$. k_{+B} and $k_{+B'}$ were given the value 2.2×10^7 M^{-1} s^{-1} (estimated from slope of 1/mean open time against morantel concentration at –75 mV). k_{-B} and $k_{-B'}$ were 202 s^{-1} (taken from the reciprocal duration of short gaps observed at –75 mV with 100 μM morantel). Best fit to experimental data obtained when ratio γ/δ was 61.

Supported by the Wellcome Trust.

REFERENCES

Journal of Physiology (1993) 467. 254P

On the block by morantel of nicotinic acetylcholine channels isolated from *Ascaris suum*: rate constants for multi-ion block estimated by maximum likelihood

A.M. Evans and R.J. Martin

Department of Preclinical Veterinary Science, R. (D.) S. V. S., Summerhall, University of Edinburgh, Edinburgh EH9 1QH

We have previously reported the complex nature of the block by morantel of nicotinic acetylcholine (nACh) channels in membrane vesicles isolated from the somatic muscle cells of *Ascaris suum* (Evans & Martin, 1992*a*, *b*). Single-channel records were obtained using the patch-clamp technique. Morantel, an agonist and channel blocker at these nACh receptors, was added to the pipette solution and channel activity was studied using vesicle-attached patches. At high concentrations of morantel (10–600 μM), two blocked states were observed at negative membrane potentials: a brief block (4–20 ms), the duration of which was concentration independent; and a long block (up to 7 s), the duration of which was concentration dependent. In addition, the concentration–block relationship had a Hill coefficient of 1.6, suggesting the involvement of at least two blocking molecules of morantel in the channel. We proposed a simple sequential block scheme (Fig. 1) involving two molecules of morantel entering the open channel, to explain these observations. We have now estimated the values of the rate constants for this model by maximum likelihood to the entire sequence of open- and closed-times observed at −75 mV with 100 μM morantel using the approach of Horne & Lange (1983). β' was $3.6 \pm 0.9\ s^{-1}$; α was $1430 \pm 180\ s^{-1}$; k_{-B} was $16.0 \pm 1.48 \times 10^6\ M^{-1}\ s^{-1}$; k_{-B} was $29.4 \pm 6.7\ s^{-1}$; γ was $100 \pm 35\ s^{-1}$; δ was $114 \pm 60\ s^{-1}$; $k_{-B'}$ was $26.5 \pm 3.9 \times 10^6\ M^{-1}\ s^{-1}$; $k_{-B'}$ was $63 \pm 14\ s^{-1}$ (mean ± S.E.M., $n = 6$). These parameters were also found to predict the observed effects of morantel concentration on the degree of block and probability of opening.

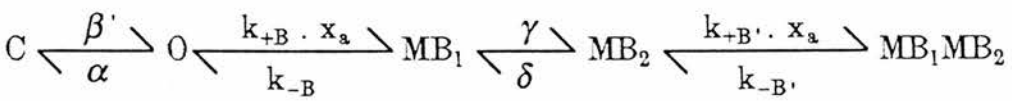


Fig. 1. Sequential block model describing multi-ion channel block by morantel. C, closed; O, open; MB_1, block site 1 occupied; MB_2, block site 2 occupied; MB_1MB_2, both block sites occupied; $k_{+B'}$, $k_{-B'}$, β', α, γ, δ, k'_{-B} and $k'_{-B'}$ are rate constants; x_a, morantel concentration.

Supported by the Wellcome Trust.

REFERENCES

Evans, A.M. & Martin, R.J. (1992*a*). *J. Physiol.* **459**, 394*P*.
Evans, A.M. & Martin, R.J. (1992*b*). *J. Physiol.* **459**, 489*P*.
Horne, R. & Lange, K. (1983). *Biophys. J.* **43**, 207–223.

British Journal of Pharmacology (1996) 118, 1127–1140 © 1996 Stockton Press All rights reserved 0007–1188/96 $12.00

Activation and cooperative multi-ion block of single nicotinic-acetylcholine channel currents of *Ascaris* muscle by the tetrahydropyrimidine anthelmintic, morantel

*A.M. Evans & [1]R.J. Martin

Department of Preclinical Veterinary Sciences, R.(D).S.V.S, University of Edinburgh, Summerhall, Edinburgh EH9 1QH

1 We have investigated activation and block, by the tetrahydropyrimidine anthelmintic, morantel, of nicotinic-acetylcholine receptor (AChR) currents in membrane vesicles isolated from somatic muscle cells of the nematode parasite *Ascaris suum*. Standard single-channel recording techniques were employed. Morantel in the pipette (6 nM to 600 μM), activated single nicotinic AChR currents.

2 Kinetic properties of the main-conductance state of morantel-activated currents were investigated in detail throughout the concentration range, 0.6 μM to 600 μM. Open-time distributions were best fitted by a single exponential. Mean open-times were slightly voltage-dependent, increasing from 0.9 ms at +75 mV to 1.74 ms at −75 mV in the presence of 0.6 μM morantel. At low concentrations, closed-time distributions were best fitted by the sum of two or three exponential components.

3 As the concentration of morantel was increased (100–600 μM), fast-flickering open channel-block was observed at positive potentials, even though morantel, a cation, was only present at the extracellular surface of the membrane. The block rate was dependent on morantel concentration and both block rate and duration of block increased as the potential became less positive. A simple channel-block mechanism did not explain properties of this block.

4 At negative potentials, as the morantel concentration increased, a complex block was observed. With increases in morantel concentration two additional gap components appeared in closed-time distributions: one was short with a duration (~13 ms) independent of morantel concentration; the other was long with a duration that increased with morantel concentration (up to many minutes). In combination, these two components produced a marked reduction in probability of channel opening (*Po*) with increasing morantel concentration. The relationship between the degrees of block and morantel concentration had a Hill coefficient of 1.6, suggesting the involvement of at least two blocking molecules. The data were analysed by use of a simple sequential double block kinetic model.

Keywords: *Ascaris*; morantel; nicotinic-channels

Introduction

The somatic muscle cells which line the body wall of the nematode parasite *Ascaris suum* have been shown to contract in response to acetylcholine (Baldwin & Moyle, 1949; Natoff, 1969). The contraction is associated with a depolarization of the muscle cells (Del Castillo *et al.*, 1963), which is mediated by a ligand-gated, non-selective cation channel (Martin, 1982; Harrow & Gration, 1985; Pennington & Martin, 1990). This channel therefore serves the same function as those in muscle and nerve in vertebrates, and has been classified as nicotinic (Toscano Rico, 1926; Baldwin & Moyle, 1949; Natoff, 1969; Rozhova *et al.*, 1980). However, the nicotinic-acetylcholine receptor (AChR) found in the somatic muscle cells of *Ascaris* is clearly a distinct subtype for which there are a number of selective agonists, including the imidazothiazoles like levamisole and the tetrahydropyrimidines like morantel, (for a review see Martin *et al.*, 1991). The selective agonists, levamisole and morantel, are frequently used for therapeutic purposes as anthelmintics to control nematode parasite infestations of both animals and man.

In an electrophysiological study of the effects of nicotinic AChR agonists on the somatic muscle cells of *Ascaris*, Harrow and Gration (1985) obtained bell-shaped concentration-conductance curves for the tetrahydropyrimidine morantel, while sigmoidal curves were obtained with acetylcholine and the imidazothiazole levamisole. They also observed that morantel but not levamisole produced a markedly non-linear current/voltage (I/V) plot under voltage-clamp. No conclusive explanation for the self-antagonism or non-linear I/V plots exhibited by morantel was obtained. Because of the therapeutic importance of morantel as an anthelmintic, additional investigation is required to provide an understanding of its actions.

In a recent study Robertson and Martin (1993a) found that the anthelmintic levamisole both activated and blocked single nicotinic AChR currents isolated from the somatic muscle cells of *Ascaris*, even though this compound exhibits no clear self-antagonism with respect to the macroscopic nicotinic AChR currents (Harrow & Gration, 1985). This may be explained by the fact that levamisole produced fast-flickering open channel-block, which was marked only at holding potentials more negative than the normal resting potential of the cell. A more extreme form of channel-block or additional effects may underline the self-antagonism observed with morantel.

In this investigation, we have examined the effects of morantel at single nicotinic AChRs found on somatic muscle of the parasitic nematode *Ascaris suum*. Morantel was found to activate as well as block single nicotinic AChR currents. The degree of block produced by morantel was marked. With positive holding potentials a fast-flickering open channel-block was observed; at negative potentials a complex block, showing positive 'cooperativity' and a marked concentration-dependent reduction in the probability of channel opening was observed. The block was described by using a simple sequential double block model. Preliminary accounts have been published in abstract form (Evans & Martin, 1992a,b; 1993a,b).

[1] Author for correspondence.
*Present address: Department of Pharmacology, Mansfield Road, Oxford OX1 3QT.

Methods

The preparation and some of the analytical methods have been described previously (Robertson & Martin, 1993a). Briefly, muscle membrane vesicles were prepared by collagenase treatment from the somatic muscle cells of the nematode parasite, *Ascaris suum*. These muscle vesicles were mounted in a bath under phase contrast and single channel currents recorded using cell-attached or isolated inside out patches (Hamill *et al.*, 1981). Morantel (6 nM – 600 μM), the anthelmintic agonist under study, was added to the patch-pipette solution.

Solutions

The bath solution used was (concentration in mM): CsCl 35, CsAcetate 105, $MgCl_2$ 2, EGTA 1, HEPES 10, pH adjusted to 7.2 with CsOH. All experiments were performed at room temperature (18 – 22°C). The pipette solution contained (concentration in mM): CsCl 140, $MgCl_2$ 2, HEPES 10, pH adjusted to 7.2 with CsOH.

The concentration of the sole conducting cation (Cs^+) was symmetrical with respect to the bath and pipette solutions, while the concentration of the main anion (Cl^-) was non-symmetrical. Thus the morantel-activated single-channel currents, carried by the non-selective cation channel of the nicotinic-acetylcholine receptor (nAChR), could be identified by their reversal potential (0 mV).

Data analysis

Open- and closed-times To enable analysis of the kinetics of the single-channel currents activated by morantel, tapes of experimental records were replayed through an 8 pole Bessel filter (−3dB, 1.5 kHz), digitized every 70 μs (CED 1401 lab. interface) and stored in a data file on the hard disc of an IBM 386 (PS/2, model 70) via the PAT V6.1 single-channel analysis program (J. Dempster, Department of Physiology and Pharmacology, Strathclyde University). The system rise time and dead time were 0.22 ms and 0.14 ms, respectively. For the present study data were accepted for analysis when the activity of only a single channel was apparent, i.e. when no multiple openings were observed in the entire experimental record (> 5 min). The initial stages of the analysis were performed by use of the PAT V6.1 software. Single-channel current amplitude distributions were determined by constructing point amplitude histograms from a running average of the digitized record according to the methods of Patlak (1988). The open channel amplitude distributions were fitted by the sum of one or more Gaussian components by use of the Dempster software.

Transitions between open- and closed-states were determined by setting a threshold at approximately 75% of the current amplitude of the main-conductance state. In order to eliminate interference from openings to an apparent subconductance state, each event was then observed and edited appropriately, i.e. those closures which did not clearly enter the subconductance state and did not approach 50% of the main conductance state amplitude were designated open. As transitions to the subconductance state were very rare (see results), it was assumed that the gating kinetics of the main conductance state were independent of the subconductance openings. Thus for the purposes of this study all openings to the subconductance state, and all transitions to this state from the main conductance state were defined as closed. Edited files of open- and closed-times were compiled and stored on floppy disc. These data files were then transferred to the Edinburgh University VAX-11/780 main frame computer system for further analysis. A minimum resolvable interval, $t_{min} = 0.42$ ms, (for data filtered at 1.5 kHz) and maximum resolvable interval t_{max}, equal to the duration of the recording, was then imposed on the data and a conditional probability function of the form:

$$\text{p.d.f.} = \frac{\sum_{i=1}^{k} \frac{a_i}{\tau_i} . e^{-t\tau_i}}{\sum_{i=1}^{k} a_i (e^{-t\,\min\tau_i} - e^{-t\,\max\tau_i})} \quad (1)$$

fitted to the open- and closed-times by the method of maximum likelihood (Colquhoun & Sigworth, 1983, p. 245) with the help of the NAG minimizing subroutine, E04CCF. In the p.d.f., a_i represents the area of the i^{th} component ($\sum a_i = 1$), τ_i is the time constant or mean value of the i^{th} component, t represents time and k equals the number of exponential terms fitted. In general the sample length was 70 s. However, for experiments where the probability of opening was low due to channel-block (concentrations $\geqslant 100$ μM morantel, at negative holding potentials), the sample time had to be extended up to 4 min in order to record enough events for analysis. The apparent mean open- and closed-times were estimated by the summing of the relative area of each exponential component multiplied by the time constant of that component.

Bursts were defined as single openings or groups of openings separated by the shortest gap component or closures that occur (Colquhoun & Sigworth, 1983; Colquhoun & Sakmann, 1985). Thus for the purposes of burst analysis a critical time (t_{crit}) was determined numerically (Robertson & Martin 1993a) for each data set. All closed-times with a duration less than t_{crit} were defined as those being within a burst of openings, while all closures with a duration greater than t_{crit} were defined as those with separate bursts.

Blockage duration and frequency at positive potentials The duration of the block, that produced a fast-flickering channel-block at positive potentials, was similar to the short 'within-activation' closures so an accurate measure of their duration and frequency was only made when the frequency of block was high relative to the frequency of the 'within-activation' closures. Thus the duration of block was taken as the short time constant (τ_l) from the closed-time distribution at concentrations greater or equal to 100 μM, the concentration at which the mean open-time of the morantel-activated currents began to decline.

Blockage frequency Plots of blockage frequencies were constructed for high concentrations of morantel at positive potentials from estimates of the total corrected number of blockages in the records and the total corrected open-times. The technique of Colquhoun and Sigworth (1983, p.246) for estimating the corrected number of events with a particular probability density function and value of t_{crit} was used: the number of blockages was taken as the corrected total number of short closings (time constant τ_l) assumed to be blockages under these conditions (see results). The technique of Colquhoun and Sakmann (1985, p.505) for estimating the corrected total open-time was used: this method corrects for missed events; it calculates the total time spent in gaps within bursts (m_{TS}), including those undetected; it calculates the total time occupied by bursts ($N_b m_b$) and determines the corrected total open-time from the difference ($N_b m_b - m_{TS}$). The corrected number of blockages (short closing) per corrected open time was then obtained.

Drugs

Morantel was a gift from Pfizer, Sandwich, U.K.

Least squares estimation

Non-linear least squares estimates were obtained with programs written in FORTRAN and run on the Edinburgh VAX-11/780 mainframe. The NAG subroutine E04CCF which minimizes functions specified by the user and utilizes the simplex method was employed.

Results

When added to the pipette solution, morantel activated single non-selective cation channel currents in membrane patches of vesicles isolated from the somatic muscle cells of *Ascaris suum*; no such events were observed in the absence of an agonist of the nAChRs ($n=84$). The conductance and kinetics of activation of these currents are similar to those described for acetylcholine- and levamisole-activated single-channel currents (Pennington & Martin, 1990; Robertson & Martin, 1993a). The concentration-dependence of activation of these nicotinic-acetylcholine receptor currents (nAChR) has been studied in relation to other agonists (Robertson & Martin, 1993a) and will not form part of this investigation, which will focus on the properties of the channel-block produced by morantel.

Morantel-activated currents have multiple conductance states

Single-channel conductance values showed substantial variation when individual current amplitudes were compared and it became clear that at least two open channel conductance states were activated by morantel (6 nM–600 μM). Figure 1a shows examples of the two current amplitudes commonly observed under a holding potential of −50 mV. These two states were clearly resolved within the amplitude histogram shown in Figure 1b. In addition to the main state peak at −2.5 pA, a secondary peak was detected at −2.0 pA; each was fitted well by a single Gaussian distribution. Although rare, transitions between the two conductance states were observed (Figure 1c). However, in general the open channel noise was virtually indistinguishable from that of the closed channel noise, and openings to each conductance state appeared to be discrete and independent events.

Both main- and sub-conductance states exhibit inward rectification

Figure 2a shows examples of single-channel openings to the main conductance state, as recorded from an excised inside-out patch in the presence of 6 μM morantel and a range of holding potentials (+75 mV to −75 mV). The individual current amplitudes were clearly greater at negative holding potentials, the unitary conductance increasing from (mean ± s.e.mean; $n=6$ patches) 32.41 ± 1.09 pS at +75 mV to 40.4 ± 1.1 pS at −75 mV. Figure 2b shows the I/V plot of main state openings from the same patch as in (a); in common with the unitary conductance the mean slope conductance increased from 30 pS at positive potentials to 40 pS at negative potentials. The I/V plot for the sub-conductance openings also exhibited inward rectification (Figure 2c); the unitary conductance increased from 26 ± 0.9 pS at +75 mV to 30 ± 1 pS at −75 mV ($n=6$).

Single-channel kinetics

Only the kinetics of the main conductance state of morantel-activated openings were studied (see methods). All the data were obtained from vesicle-attached patches to reduce problems associated with rundown. The resting membrane potential of the vesicle is 0 mV as a result of the displacement of the intravesicular content by the bath solution (Martin *et al.*, 1990) and the single-channel I/V relationships of vesicle-attached patches were indistinguishable from those obtained using excised inside-out patches.

Open-times

In general the apparent open-times were best fitted with a single exponential, suggesting the presence of a single open-state for morantel-activated single-channel currents (Table 1). In the presence of low concentrations of morantel (6 nM and 6 μM) the apparent mean open-time was greater at negative holding potentials. For example, with 0.6 μM morantel the mean open-time increased from 0.9 ms at a holding potential of +75 mV to 1.73 ms at −75 mV. These findings suggest that the shutting rate constant, α, is slightly slower at negative than at positive holding potentials. The voltage-sensitivity corresponds to an e-fold increase in the closing rate for every +156 mV change in potential.

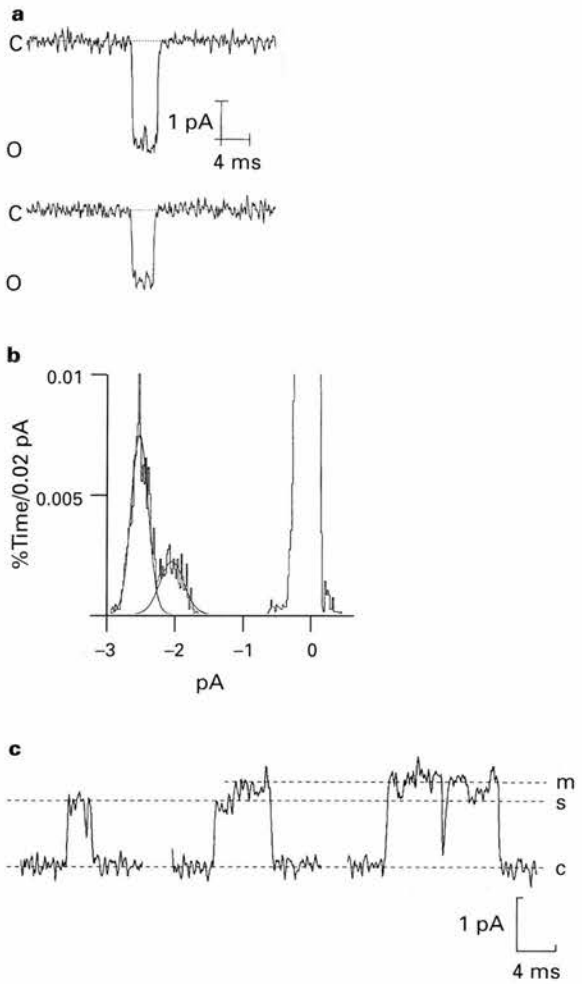


Figure 1 Morantel-activated single-channel currents have at least two conductance states. (a) Examples of the two current amplitudes observed within records of single-channel currents activated by morantel (6 μM) under a holding potential of −50 mV; c, closed-state; o, open-state. In this and all subsequent figures, records of single-channel currents were filtered at 1.5 kHz (-3dB). (b) Patlak amplitude histogram showing the zero current level and the two peaks of the open channel currents. The open channel current was fitted with a double Gaussian giving mean open channel current amplitudes (± s.d.) of 2.0 ± 0.18 pA and 2.5 ± 0.13 pA. The records in (a) and (b) were taken from the same excised inside-out patch under a holding potential of −50 mV. (c) Examples of transitions between the main (m) and sub-conductance (s) states of single-channel currents activated by 6 μM morantel in an excised inside-out patch at a potential of +50 mV. c: closed-state.

Closed-times

Morantel-activated single-channel currents exhibited more complex closed-time distributions. In the absence of channel-block, the closed-time distributions were best fitted by two or three exponential components at both positive and negative holding potentials (Table 2). For example with 6 μM morantel the time constants fitted to the closed-time distribution at +75 mV were 0.13 ms (τ_1), 97 ms (τ_2) and 781 ms (τ_3), reflecting the presence of short, intermediate and long gaps. The short gaps had a duration which was independent of morantel concentration, and were assumed to represent brief closures during single activations of the channel as has been described in previous studies with other agonists (Robertson & Martin,

1993a) and for nicotinic AChRs in muscle and nerve of vertebrates (Colquhoun & Sakmann, 1985). These will be termed 'within-activation' closures. Three time constants were not always resolved because the intermediate component probably represents infrequent events which are too few to allow accurate or consistent identification.

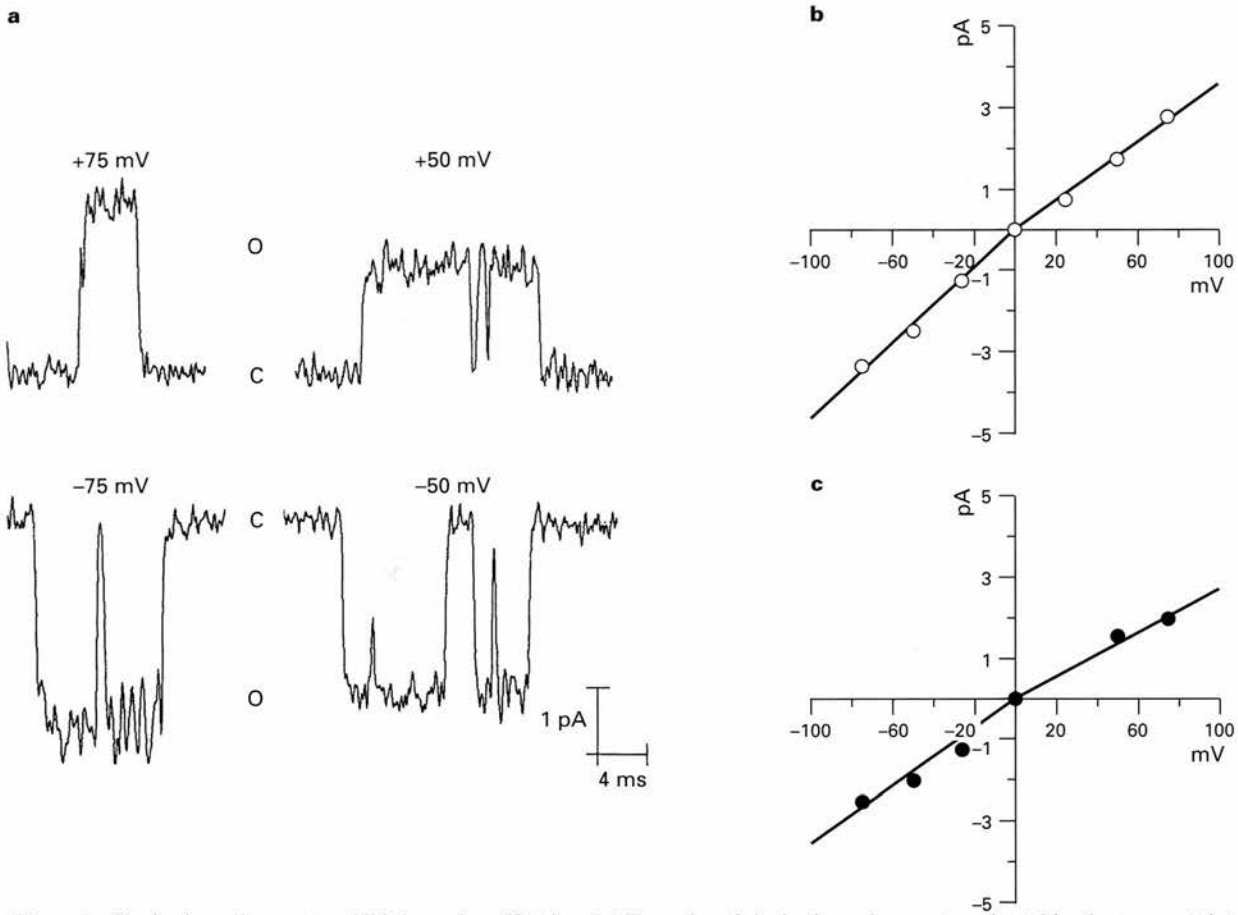


Figure 2 Single channel currents exhibit inward rectification. (a) Examples of single-channel currents activated by 6 μM morantel at four holding potentials (+75 mV, +50 mV, −50 mV and −75 mV), each represents an opening to the main-conductance state. Note the greater amplitude of the currents elicited at negative holding potentials. (b) Current-voltage relationship obtained from the same patch as the records in (a). The data at positive and negative potentials were fitted separately. The cord conductance increased from (mean ± s.e.mean) 30 ± 1.1 pS at positive potentials to 40 ± 1.1 pS at negative potentials, suggesting inward rectification. (c) Current-voltage relationship for openings (not shown) to the sub-conductance state taken from the same patch as (a and b). The unitary conductance was 24 pS at +75 mV and 39 pS at −75 mV. Channels were activated by 6 μM morantel.

Table 1 Open-time kinetics: probability density functions observed at +75 mV and at −75 mV with vesicle attached patches and concentrations of morantel between 0.006 μM and 600 μM

Vm (mV)	*Conc.* (μM)	n	*A1*	*A2*	τ_1 (ms)	τ_2 (ms)
75	0.006	2	1.00	0.00	0.80	
75	0.6	2	1.00	0.00	0.90	
75	6	3	1.00	0.00	0.72 ± 0.07	
75	6	1	0.53	0.47	0.46	1.26
75	10	6	1.00	0.00	0.87 ± 0.10	
75	30	3	1.00	0.00	0.88 ± 0.19	
75	60	3	1.00	0.00	0.81 ± 0.12	
75	100	4	1.00	0.00	0.64 ± 0.13	
75	300	5	1.00	0.00	0.27 ± 0.02	
75	600	6	1.00	0.00	0.25 ± 0.07	
−75	0.006	2	1.00	0.00	1.07	
−75	0.6	2	1.00	0.00	1.73	
−75	6	4	1.00	0.00	1.57 ± 0.24	
−75	10	6	1.00	0.00	1.16 ± 0.11	
−75	30	3	1.00	0.00	0.67 ± 0.15	
−75	60	3	1.00	0.00	0.46 ± 0.05	
−75	100	4	1.00	0.00	0.36 ± 0.04	

Data shown are means ± s.e.mean. In general a single exponential component was distinguished. No single channel events were recorded at 600 μM and too few for analysis at 300 μM morantel at −75mV.

The long time constant was consistently observed and represented a large proportion of the closed-times. Although not studied in detail the duration of the long component was clearly greater with low concentrations (6 nM, $n=2$, Table 2). Taken together with studies relating to mammalian nAChR (Colquhoun & Sackmann, 1985) it is likely that this long component represents the long closures separating individual channel activations and will therefore be termed 'between-activation' closures. As no marked increase in the probability of channel opening (see below), nor decrease in the duration of these long closures was observed between 0.6 μM and 100 μM (Table 2), we were probably close to or beyond the point of saturation of the agonist binding site(s) with 0.6 μM morantel as predicted from the activation by morantel of the macroscopic currents in the somatic muscle cells (Harrow & Gration, 1985). These long 'between-activation' closures may therefore represent an inactive and/or desensitized state of the agonist-receptor complex.

In summary then, at low concentrations the single-channel currents activated by morantel were best described assuming a single open state and two closed states.

Burst-times

At low concentrations (up to 10 μM), at positive and negative potentials, the burst distributions of morantel-activated channels were usually best fitted by one component (Table 3); and the mean burst-time was only slightly greater than the mean open-time of the channels (see Tables 1 and 3). This appeared to be due to the low frequency and brief duration of the 'within-activation' closures (<1 ms; see closed-time kinetics).

At higher morantel concentrations (30 μM – 100 μM), again at positive and negative potentials an additional second longer burst component (Table 3) was separated out and was associated with the appearance of channel-block that is later de-

Table 2 Closed-time kinetics: probability density functions observed at +75 mV and at −75 mV with vesicle attached patches and concentrations of morantel between 0.006 μM and 600 μM

Vm (mV)	*Conc* (μM)	n	*A1*	*A2*	*A3*	*A4*	τ_1 (ms)	τ_2 (ms)	τ_3 (ms)	τ_4 (ms)
75	0.006	2	0.47	0.00	0.53	0.00	0.14		2251	
75	0.6	2	0.07	0.00	0.93	0.00	0.26		949	
75	6	4	0.25±0.18	0.08±0.05	0.67±0.13	0.00	0.13±0.03	97±10	781±575	
75	10	6	0.25±0.18	0.38±0.25	0.37±0.18	0.00	0.44±0.04	148±98	818±294	
75	30	1	0.32	0.68	0.00	0.00	0.19	111		
75	30	2	0.48	0.17	0.35	0.00	0.11	186	836	
75	60	3	0.33±0.04	0.67±0.04	0.00	0.00	0.35±0.01	214.5±47.47		
75	100	4	0.42±0.07	0.25±0.13	0.33±0.16	0.00	0.29±0.04	269±224	835±460	
75	300	5	0.51±0.05	0.10±0.02	0.39±0.03	0.00	0.38±0.02	43.78±15.43	1141±348	
75	600	6	0.55±0.07	0.12±0.04	0.33±0.08	0.00	0.57±0.07	63±0.07	1186±360	
−75	0.006	2	0.22	0.00	0.78	0.00	0.37		2139	
−75	0.6	2	0.44	0.00	0.56	0.00	0.17		1153	
−75	6	4	0.30±0.10	0.21±0.12	0.33±0.02	0.16±0.05	0.49±0.24	12.50±5.00	203±43	940±373
−75	10	6	0.20±0.08	0.33±0.07	0.47±0.07	0.00	0.79±0.39	180±53	978±82	
−75	30	2	0.19	0.00	0.81	0.00	2.39		799	
−75	30	1	0.14	0.23	0.63		1.86	19.12	303	
−75	60	3	0.10±0.02	0.32±0.08	0.58±0.02	0.00	1.96±1.20	72±28	858±193	
−75	100	4	0.00	0.18±0.05	0.40±0.06	0.42±0.07		13.30±5.00	301±133	3376±842

Data shown are means±s.e.mean. Up to four exponential components were distinguished. At −75mV, no single-channel events were recorded at 600 μM and too few were available for analysis at 300 μM morantel.

Table 3 Burst-time kinetics: probability density functions observed at +75 mV and at −75 mV with vesicle attached patches and concentrations of morantel between 0.006 μM and 600 μM

Vm (mV)	*Conc.* (μM)	n	*A1*	*A2*	τ_1 (ms)	τ_2 (ms)
75	0.006	2	1.00	0.00	0.81	
75	0.6	2	1.00	0.00	0.92	
75	6	2	1.00	0.00	0.97	
75	6	2	0.00	0.00	0.46	1.26
75	10	6	0.51	0.49	0.53	1.38
75	30	3	0.00	1.00		1.36±0.26
75	60	3	0.58±0.2	0.42±0.23	0.76±0.24	3.5±1.8
75	100	4	0.52±0.1	0.48±0.16	0.69±0.32	2.66±0.62
75	300	5	0.00	1.00		1.14±0.21
75	600	6	0.00	1.00		1.09±1.15
−75	0.006	2	1.00	0.00	1.9	
−75	0.6	2	1.00	0.00	2.01	
−75	6	4	1.00	0.00	2.41±0.36	
−75	10	6	1.00	0.00	1.73±0.21	
−75	30	1	1.00	0.00	1.39	
−75	30	2	0.71	0.29	0.58	5.74
−75	60	3	0.83±0.0	0.19±0.01	0.46±0.01	2.78±1.34
−75	100	4	0.83±0.0	0.17±0.02	0.43±0.06	12.39±5.84

Data shown are means±s.e.mean. Up to two exponential components were required to describe the burst distributions. At −75 mV, no single-channel events were recorded at 600 μM and too few events were observed for analysis at 300 μM morantel.

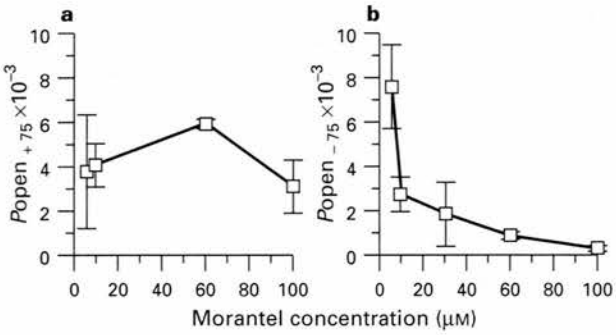


Figure 3 A concentration-dependent decline in *Po* is observed at negative but not positive holding potentials. Plots of the probability of channel opening against morantel concentration at (a) +75 mV and (b) −75 mV. Each point represents the mean of at least three observations from patches where the activity of only a single channel was evident. The vertical bars represent the s.e.mean of each set of data.

scribed in detail. The brief burst-time constant, τ_1, then described 'short bursts' that had similar durations to mean open-times. The longer burst-time constant, τ_2, described 'long bursts' that were due to sequences of openings separated by short 'within-activation' closures and/or short block periods.

Increasing morantel concentration decreases Po *at negative but not positive potentials*

At positive potentials the probability of channel opening (*Po*) appeared constant and independent of morantel concentration between 6 μM ($3.83 \pm 2.6 \times 10^{-3}$; mean ± s.e.mean, $n=4$) and 100 μM (3.19 ± 10^{-3}; $n=4$), suggesting that we were at or approaching saturation of the nicotinic AChR agonist binding site(s) as predicted from the studies of the macroscopic currents activated by morantel (Harrow & Gration, 1985). This point is illustrated in Figure 3a, which shows a plot of *Po* against morantel concentration at a holding potential of +75 mV. Between 100 μM and 600 μM morantel, however, a small concentration-dependent reduction in *Po* was observed (not shown) associated with the onset of a fast-flickering open channel-block.

At negative holding potentials a marked concentration-dependent reduction in *Po* was observed between 6 μM and 100 μM morantel. This is illustrated in Figure 3b which shows a plot of *Po* against morantel concentration, obtained with a holding potential of −75 mV; *Po* declined from $7.68 \pm 1.89 \times 10^{-3}$ ($n=4$) at 6 μM to $0.31 \pm 0.12 \times 10^{-3}$ ($n=4$) at 100 μM. The decline in *Po* resulted from the complex form of open channel-block that is considered subsequently.

A flickering channel-block occurs at positive potentials

A fast-flickering open channel-block was observed at positive holding potentials as the concentration of morantel was increased over the range 100 μM to 600 μM. Figure 4a shows the fast-flickering channel-block with channel openings recorded in the presence of 600 μM morantel over a range of positive holding potentials (+125 mV to +50 mV). It can be seen that the duration and frequency of the block events increases as the holding potential was made less positive, an effect consistent with the cationic nature of morantel. This channel-block led to a concentration-dependent reduction in the mean open-time

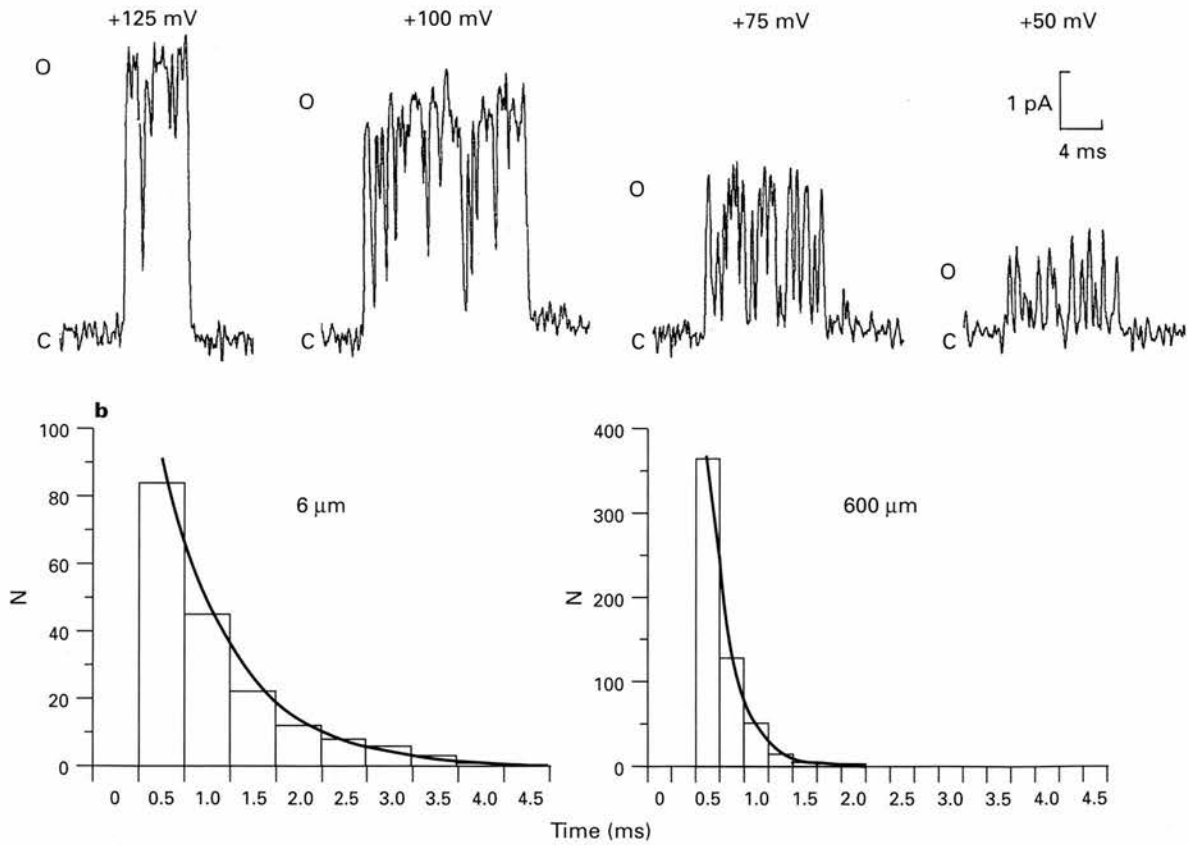


Figure 4 With high concentration of morantel fast flickering open channel-block is observed at positive potentials. (a) Fast flickering block of single-channel currents activated by 600 μM morantel at +125 mV, +100 mV, +75 mV and +50 mV; vesicle-attached patch configuration. Note the increase in the frequency and duration of the block as the holding potential is made less positive (+125 mV to +50 mV). Records were obtained in the vesicle-attached patch configuration. c, closed; o, open. (b) Open-time distributions. Single exponential fits to open-time histograms obtained in the presence of 6 and 600 μM morantel and a pipette potential of +75 mV; the time constants fitted were 0.8 ms and 0.25 ms respectively. N is the number of channel openings.

from 0.72 ± 0.07 ms (mean $\pm$ s.e.) with 6 μM morantel to 0.25 ± 0.7 ms with 600 μM morantel, Figure 4b and Table 1.

Fast-flickering channel-block has been explained by a simple open channel-block mechanism (Adams, 1976; Neher & Steinbach, 1978) in which a single large-blocking-ion moves repeatedly into and out of the open ion-channel. In the following sections we describe properties of the channel-block at positive potentials and show that it has properties inconsistent with the simple channel-block mechanism.

The channel-blocking rate, k_{+B}, at positive potentials Figure 5a illustrates plots of reciprocal mean open-time against morantel concentration for holding potentials of +100 mV, +75 mV and +50 mV. It is likely that the gradients of such plots are a valid method of estimating the channel-blocking rate, k_{+B}, for a variety of complicated processes governing channel-block (Ogden & Colquhoun, 1985). For each plot the line was fitted by the method of least squares; the slope ($\pm$s.e.mean) gave values for k_{+B} of $3.3 \pm 0.9 \times 10^6$ M^{-1} s^{-1}, $6.1 \pm 1.4 \times 10^6$ M^{-1} s^{-1} and $9.8 \pm 0.7 \times 10^6$ M^{-1} s^{-1} at +100 mV, +75 mV and +50 mV, respectively. Clearly then k_{+B} increased as the holding potential was made less positive.

k_{+B} is also a factor determining the slope of blockage frequency plots, but the slopes of these plots are proportionately less than k_{+B} if simple channel-block does not occur and if the blocked state can enter other closed or blocked states without directly reopening (Ogden & Colquhoun, 1985). Figure 5b shows plots of the number of block durations per unit open-time against morantel concentration, the slopes of which had values of 2.3×10^6 M^{-1}s^{-1} at +75 mV and 5.8×10^6 M^{-1}s^{-1} at +50 mV. These slopes are similar but less than the previously estimated k_{+B} values suggesting that the blocked state is able to enter another closed or blocked state without always having to reopen.

Voltage-sensitivity of k_{+B} at positive potentials Figure 6a describes the voltage-sensitivity of k_{+B} (obtained from plots of 1/mean open-time) against the positive holding potential with a line fitted by the method of least squares to the observations. The slope of the line, V_K, predicts an e-fold decrease in k_{+B} for every +46 mV change in membrane potential and the intercept predicts that k_{+B} at 0 mV has a value of 2.94×10^7 M^{-1}s^{-1}.

The voltage-dependence of ion channel-blocking rates has been explained by a Woodhull model (Neher & Steinbach 1978; Hille 1992) and the relative position of the block site within the channel determined from the voltage-sensitivity. δ, the relative or apparent electrical distance from the extracellular surface of the pore is $2(F/RT)/k_{+B}$, where F, R and T have their usual meaning and for our purposes F/RT is 25 mV at 20°C. From our data we obtain a relative electrical distance (δ) of 1.1, greater than the width of the channel: this value cannot be explained by a single block site within the channel. One explanation, considered later, for the large and apparently impossible δ may be that of multi-ion channel-block (Hille, 1992).

The block duration at positive potentials and its voltage-sensitivity

The channel unblocking rate, k_{-B}, would be equal to the reciprocal of the mean block duration if the fast-flickering block were governed by a simple open channel-block mechanism

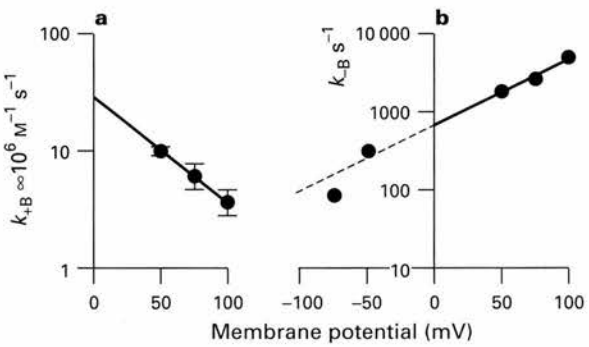


Figure 6 The forward blocking and unblocking rate constants are voltage-sensitive. (a) k_{+B} versus membrane potential; (b) k_{-B} versus membrane potential. The lines were fitted by least squares. From the intercept of each line on the abscissa scale values of 2.94×10^7 M^{-1}s^{-1} and 765 s^{-1} were obtained for k_{+B} and k_{-B}, respectively, at 0 mV. The slopes predict an e-fold decrease in k_{+B} for every +46 mV change in potential and an e-fold increase in k_{-B} for +44 mV change in holding potential. The vertical bars represent s.e.mean of each set of data.

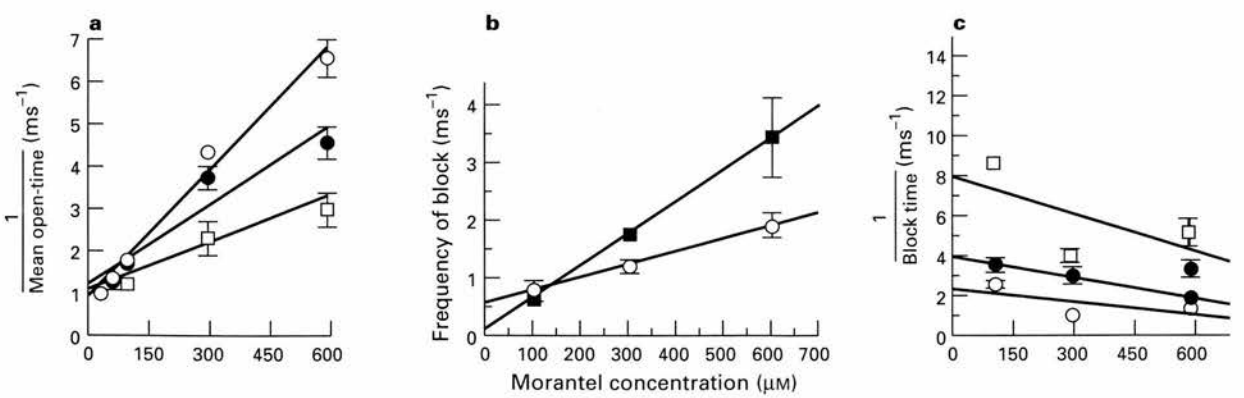


Figure 5 Estimation of the forward blocking and unblocking rate constants. (a) Plot of the reciprocal mean open-time against morantel concentration for holding potentials of +100 mV (□) +75 mV (○) and +50 mV (●). Lines were fitted to the points by least squares. The slope of the lines predicted values ($\pm$s.e.mean) for the forward blocking rate constant, k_{+B}, at $3.37 \pm 0.88 \times 10^6$ M^{-1}s^{-1} (+100 mV), $6.14 \pm 1.36 \times 10^6$ M^{-1}s^{-1} (+75 mV) and $9.84 \pm 0.74 \times 10^6$ M^{-1}s^{-1} (+50 mV). Intercepts with the abscissa scale predicted values of 104.1 s^{-1} (+100 mV), 1185 s^{-1} (+75 mV) and 891 s^{-1} (+50 mV) for the channel closing rate constant α. (b) Plot of the frequency of block against morantel concentration under holding potentials of +75 mV (○) and +50 mV (■). Estimates of the frequency of block were obtained by dividing the total open-time by the estimated total number of short gaps. Each point represents the mean of at least three observations. The slope of the plot was 6×10^6 M^{-1}s^{-1} at +50 mV and 3×10^6 M^{-1}s^{-1} at +75 mV. (c) The reciprocal of the duration of the short block against morantel concentration for patch potentials of +100 mV (□) +75 mV (○) and +50 mV (●). The correlation between reciprocal block time and morantel concentration was not significant. The points represent the mean of at least three observations. In all sections the vertical bars represent s.e.mean of each set of data.

(Adams, 1976; Neher & Steinbach, 1978) or, in more complex schemes, as we suspect here, be equal to the sum of all exit rates from the blocked state. The reciprocal of the mean block duration then provides an upper estimate for k_{-B}.

Figure 5c shows a plot of the reciprocal of the block duration against morantel concentration for a holding potential of +100 mV, +75 mV and +50 mV. There was no significant correlation between morantel concentration and the mean block durations at any of the holding potentials studied. As might be expected for the cation morantel, the block duration decreased as the holding potential was made more positive, giving upper limits for k_{-B} at +100 mV (100–600 μM), +75 mV (100–600 μM) and +50 mV (100 μM–600 μM) in the region of (mean ± s.e.mean) 5165 ± 746 s^{-1}, 2781 ± 254 s^{-1} and 1878 ± 226 s^{-1}, respectively.

Figure 6b shows a semi-log plot of the upper estimates for k_{-B} against potential and the line fitted to the points observed at positive potentials by the method of least squares. We find the intercept with the abscissa at 0 mV to be 767 s^{-1}, while the slope, V_k, shows an e-fold decrease every −44 mV change in membrane potential, which is numerically close to but opposite in polarity to the voltage-sensitivity of the blocking rate, k_{+B}. Although the interpretation of the voltage-sensitivity of these estimated blocking rates for k_{+B}, depends on the blocking mechanism involved we can again say that observations do not support a simple channel-block mechanism because the predicted relative electrical distance of the site of block would be 1.1 and greater than the width of the channel.

The flickering-block at positive potentials then shows a number of features not consistent with the simple block. In addition, Table 3 shows at positive potentials, that the mean duration (t_2) of the 'long bursts', did not increase linearly with concentration in the range 30 μM–100 μM in a manner predicted by the simple open channel-block mechanism. Further inconsistencies were seen at negative potentials.

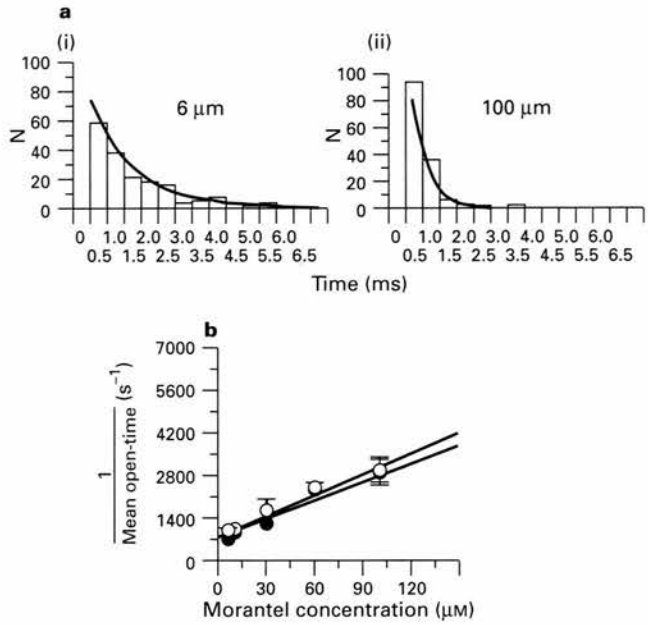


Figure 7 Concentration-dependent reduction in mean open-time at negative holding potentials. (a) Single exponential fits to open-time distributions obtained in the presence of (i) 6 and (ii) 100 μM morantel and a pipette potential of −75 mV; the time constants fitted were 1.28 ms (6 μM) and 0.43 ms (100 μM). N is the number of channel openings. (b) Plots of the reciprocal of mean open-time against morantel concentration for holding potentials of −50 mV (●) and −75 mV (○). The lines were fitted by least squares. The slope had a value of $2.27 \pm 0.3 \times 10\,M^{-1}s^{-1}$ at −50 mV and $1.9 \pm 0.3 \times 10^7\,M^{-1}s^{-1}$ at −75 mV. The intercept of the lines was 773 s^{-1} at −50 mV and 745 s^{-1} at −75 mV.

Channel-block and open- and closed-times at negative potentials

We have commented earlier on the marked concentration-dependent reduction in *Po* observed with negative holding potentials. The mechanism underlying this decline in *Po* involved effects on open-times and on closed-times.

Effect on open-times At negative potentials a concentration-dependent reduction in mean open-time occurred between 6 μM and 100 μM morantel (Table 1). Figure 7a shows examples of the open-time distributions obtained at 6 μM and 100 μM. The time constants fitted declined from 1.57 ms with 6 μM to 0.36 ms with 100 μM morantel (Table 1). The slope of the relationship between the reciprocal of the mean open-time and morantel concentration was linear and is a measure of the channel blocking rate, k_{+B}. Figure 7b shows such plots for holding potentials of −50 mV and −75 mV, each line was fitted by the method of least squares. The slope for the two potentials was nearly the same: $2.3 \times 10^7\,M^{-1}s^{-1}$ at −50 mV and $1.9 \times 10^7\,M^{-1}s^{-1}$ at −75 mV.

The values of k_{+B} at −50 mV and −75 mV are almost identical to that of k_{+B0} estimated from the analysis of the flickering channel-block observed at positive potentials: $2 \times 10^7\,M^{-1}s^{-1}$ (Figure 6a). This may be explained if a potential barrier acts as the rate limiting step for k_{+B} at positive potentials but a voltage-insensitive diffusion-barrier becomes the rate-limiting step for k_{+B} at negative membrane potentials. However, the reduction in mean open-time does not explain the marked concentration- and potential-dependent decline in *Po* measured under negative holding potentials, particularly when we consider the loss of voltage-sensitivity of k_{+B} at negative potentials.

Effect on closed-times At negative holding potentials a concentration- and voltage-dependent increase in mean closed-time was observed. At −75 mV the mean closed-time increased from (mean ± s.e.mean) 224 ± 42 at 6 μM to 1908 ± 506 at 100 μM and the changes in the closed-time distributions resulted in the appearance of two distinctive voltage-sensitive gap components: a 'short block' and a 'long block'.

Short block One of these gap components was short (mean duration ~13 ms) and is referred to here as the short block. The short block had a duration that appeared independent of morantel concentration. It was first noticed at low frequencies with 6 μM morantel at −75 mV when the best fit to the closed-time distribution increased from three to four exponential components; under these conditions the short block had a duration of 12.5 ms ($t2$; Table 2). Between 6 μM and 100 μM, the short block was not resolved due to aggregation with 'within-activation' channel closures. However, in the presence of 100 μM morantel the channel openings occurred singly or in doublets (Figure 8b) separated by gaps with a mean duration of 13.3 ms (Table 2, $t1$, 100 μM −75 mV). Under these conditions the short block represented the majority of the short gaps observed; few if any brief 'within-activation' closures were observed.

Although the duration of the short block was not concentration-dependent, it was voltage-dependent (Figure 9d, Table 2) and was related to the block periods measured at positive holding potentials. When the line fitted to the relationship between the reciprocal of the block time (k_{-B}) and holding potential at positive potentials was extrapolated to −50 mV and −75 mV, it accurately predicted the duration of the short gaps observed at both negative potentials when 100 μM morantel was present (Figure 6c) suggesting that its origin was the same.

Long block The other gap component was long (seconds), increased in duration with concentration, and is referred to here as the long block. The concentration-dependent nature of the long block is illustrated in Figure 8c which compares ty-

pical single channel records obtained at +75 mV and −75 mV in the presence of 10, 100 and 600 μM morantel. The long block observed at −75 mV with 100 μM morantel increased in duration still further when the concentration was raised to 600 μM, such that open events were not observed in records as long as 10 min. These long block gaps were absent at positive potentials and their appearance showed no time-dependence: they were observed at negative potentials immediately after patch formation and disappeared when the holding potential was made positive (+50, +75 or +100 mV).

Figure 9a shows representative closed-time distributions obtained in the presence of 0.6 μM morantel at +75 mV and −75 mV: there is no real difference in the duration of the long time constants fitted at the two potentials. Figures 9b, c and d show representative closed-time distributions obtained with 30, 60 and 100 μM morantel at +75 mV and −75 mV: at −75 mV a concentration- and voltage-dependent increase in the longest gap component is observed; the mean duration of the longest time constant fitted to the closed-time distribution at −75 mV with 30 μM morantel concentration was 303 ms, with 60 μM it was 990 ms, and with 100 μM it was 4016 ms. Figure 9d shows that a clear separation was obtained at 100 μM morantel between the long block and the 'between-activation' closures: 'between-activation' closures were identified by the fact that their mean duration remained virtually the same at +75 mV (813 ms) and −75 mV (517 ms). It is pointed out, however, that the simple averages of closed-time constants (Table 2) observed in different preparations only indicate the presence of the concentration- and voltage-dependent long block when concentrations at 60 μM or greater are used and the longest gap component at +75 mV is compared with the longest gap component at −75 mV. Variability between patch recordings associated with the heterogeneous population of channels and animals (see Martin *et al.*, 1991) may have lead to aggregation of the long block with 'between-activation' closures at lower concentrations.

Degree of block shows cooperativity

The degree of block may be defined as Po_{-75}/Po_{+75} providing the following assumptions are valid: (1) In the absence of channel-block there is no significant increase in *Po* with morantel concentration over the range 0.6–100 μM. This seems valid from the relationship between *Po* and concentration measured under a holding potential of +75 mV (Figure 3a).

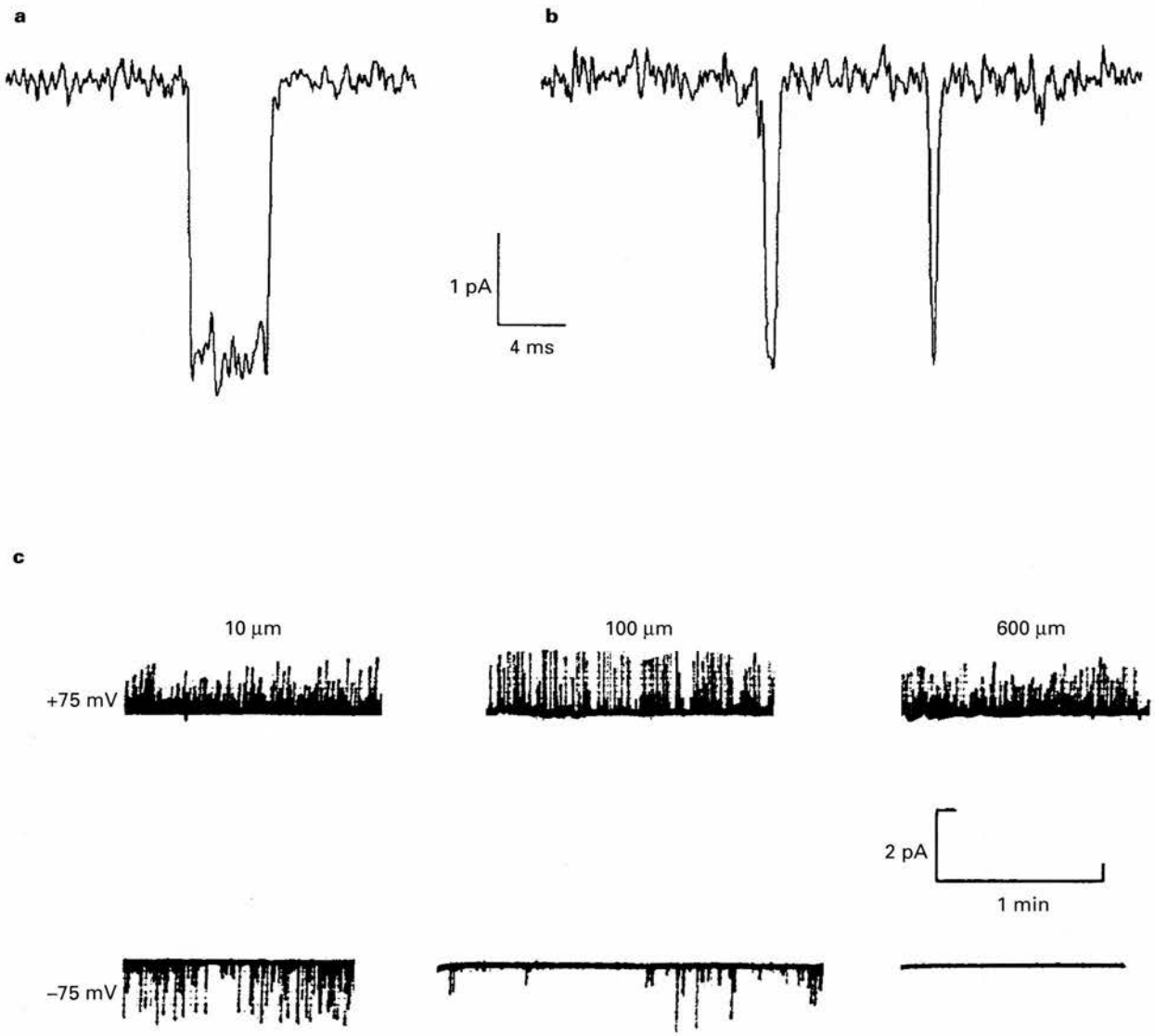


Figure 8 The short block and concentration-dependent long block gaps at negative holding potentials. (a) Typical opening produced by 6 μM morantel; note the single uninterrupted opening lasting 4 ms, −75 mV. (b) A 'doublet' of brief openings separated by the short block observed in the presence of 100 μM morantel, −75 mV. (c) Concentration- and voltage-dependence of the additional long block gap observed in the presence of morantel is illustrated at lower time resolution; current records were activated by 10 μM, 100 μM and 600 μM morantel recorded at +75 mV and −75 mV. Recordings were made in the vesicle-attached patch configuration, first at −75 mV and then at +75 mV.

(2) Between 0.6 μM and 100 μM, the reduction in Po resulting from channel-block at +75 mV is small relative to the reduction in Po observed at negative holding potentials, and may be ignored. (3) In the absence of channel-block the ratio Po_{-75}/Po_{+75} would be constant and independent of morantel concentration. Figure 10a shows a plot of Po_{-75}/Po_{+75} against

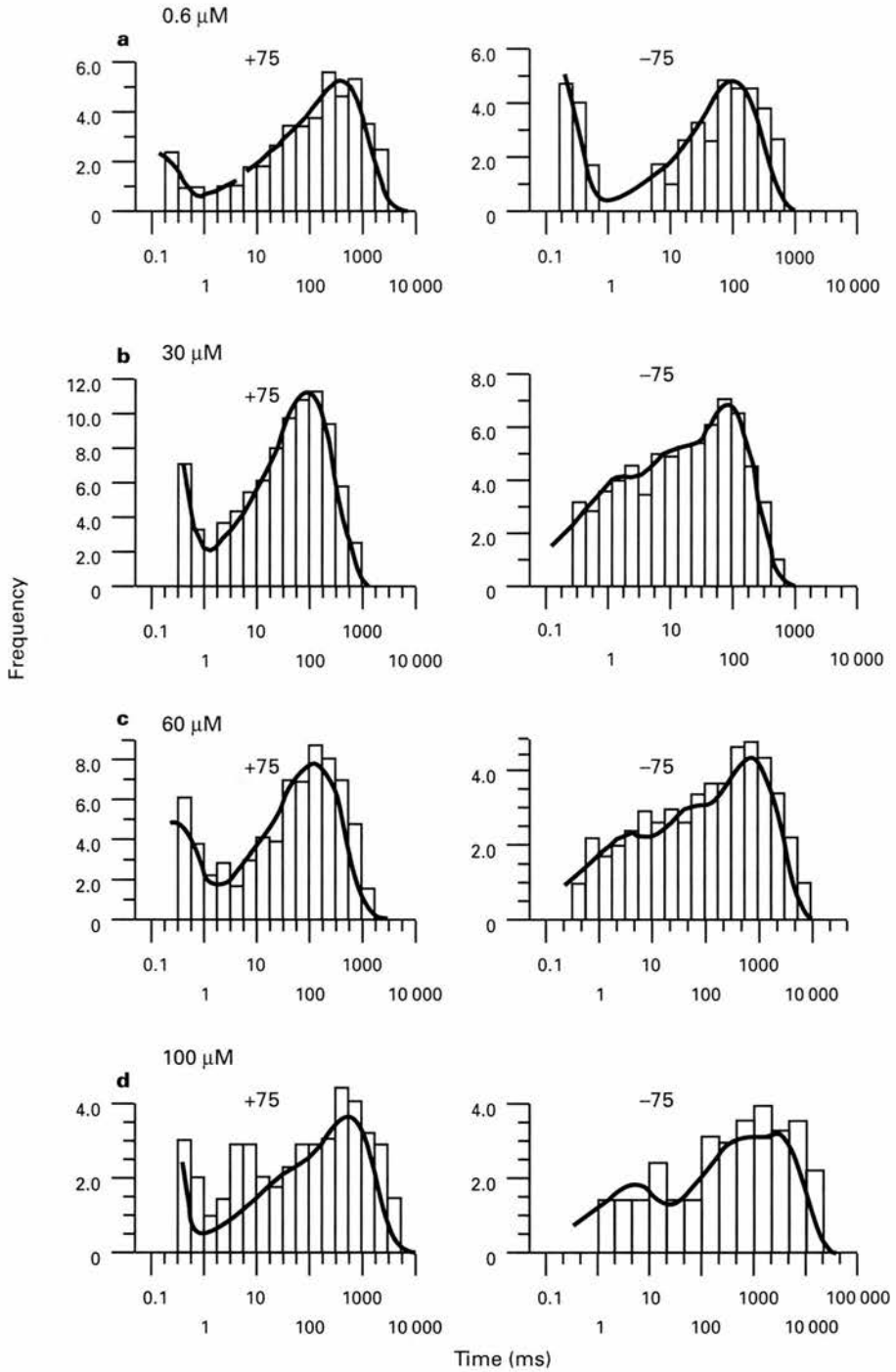


Figure 9 Concentration- and voltage-dependence of the longest gap component in the closed-time distributions. Distributions of closed-times obtained in the presence of different concentrations of morantel at +75 mV and −75 mV are shown on a log scale (abscissa scales 4 bins per log unit except for (d) −75 where 3 bins per log unit was used) against the square root of frequencies (ordinate scales) and maximum likelihood fits to each individual closed time (see methods pdfs) shown by continuous lines. In (a–d) distributions at −75 mV (right panels) were obtained immediately after patch formation and then distributions at +75 mV (left panels) were obtained subsequently from the same patch. (a) +75: Distributions obtained with 0.6 μM morantel, +75 mV, three exponentials fitted, $\tau_1 = 0.12$ ms (area 0.16), $\tau_2 = 38.5$ ms (area 0.08) and $\tau_3 = 510$ ms (area 0.76). (a) −75: The duration of the longest time constant fitted was similar when the holding potential was −75 mV; two exponentials fitted, $\tau_1 = 0.17$ ms (area 0.50) and $\tau_2 = 570$ ms (area 0.50). (b) +75: Distributions obtained with 30 μM morantel, +75 mV, two exponentials fitted, $\tau_1 = 0.19$ ms (area 0.32) and $\tau_2 = 111$ ms (area 0.68). (b) −75: At −75 mV the duration of the longest time constant was greater, $\tau_1 = 1.9$ ms (area 0.14), $\tau_2 = 19$ ms (area 0.20) and $\tau_3 = 303$ ms (area 0.66). (c) +75: Distributions obtained with 60 μM morantel, +75 mV, two exponentials fitted, $\tau_1 = 0.27$ ms (area 0.26) and $\tau_2 = 187$ ms (area 0.74). (c) −75: At −75 mV the duration of the longest time constant is much longer; $\tau_1 = 3.9$ ms (area 0.13), $\tau_2 = 55$ ms (area 0.21) and $\tau_3 = 990$ ms (area 0.66). (d) +75: 100 μM morantel, +75 mV, three exponentials fitted, $\tau_1 = 0.13$ ms (area 0.73), $\tau_2 = 50$ ms (area 0.045) and $\tau_3 = 813$ ms (area 0.225). (d) −75: At −75 mV the longest time constant (long block gaps) exceeded those observed with 30 μM or 60 μM morantel, $\tau_1 = 7$ ms (area 0.16), $\tau_2 = 517$ ms (area 0.30) and $\tau_3 = 4016$ ms (area 0.54).

morantel concentration. The relationship was fitted by non-linear least squares regression to the Hill equation:

$$R = \frac{R_{max}}{1 + (\frac{x_a}{IC_{50}})^{n_H}}$$

where R represents the degree of block at concentrations x_a, IC_{50} the concentration at which 50% block was observed and n_H the Hill coefficient. R_{max} is the ratio Po_{-75}/Po_{+75} in the absence of block. The best fit was obtained with an R_{max} of 2.9, IC_{50} of 10 μM and n_H of 1.6. A value for n_H greater than 1 suggests the involvement of at least two blocking molecules.

The use of the ratio Po_{-75}/Po_{+75} has the advantage of being able to normalize the data and so reducing inter-patch variability. We also fitted the Hill equation to the plot of Po_{-75} against morantel concentrations >than 0.6 μM (Figure 10b) and found that it had a similar n_H value (1.7), suggesting that our ratio analysis is not compromised.

Sequential double block model

In order to describe the positive cooperativity shown by the block quantitatively, we have used a minimal model describing a two-ion open channel-block (Evans & Martin, 1992b; Evans & Martin, 1993a,b). The simple channel-block model was extended to incorporate a second binding site for morantel within the channel pore:

$$\underset{\beta'}{\overset{\alpha}{\rightleftharpoons}} \quad O \quad \underset{k_{-B'}}{\overset{k_{+B'}.x_a}{\rightleftharpoons}} \quad MB1 \quad \underset{\delta}{\overset{\gamma}{\rightleftharpoons}} \quad MB2 \quad \underset{k_{-B'}}{\overset{k_{+B'}.x_a}{\rightleftharpoons}} \quad MB1MB2$$

where $\overline{C}$ is the distinguishable closed state and O is open, MB1 represents the occupation of a block site near the mouth of the pore, MB2 represents the occupation of a second block site deeper within the pore, and MB1MB2 represents a double occupation. $\beta'\alpha$, k_{+B}, k_{-B}, γ, δ, $k_{+B'}$ are rate constants and x_a represents the morantel concentration.

The model requires that: the occupation of the site MB1 by a molecule of morantel allows access, by that molecule alone, to site MB2; it allows MB1 to be occupied while MB2 is occupied; but does not allow a molecule bound to MB2 to leave the channel pore while MB1 is occupied. Thus as the concentration of morantel is increased the frequency of occupation of MB1 and thus MB2 increases; furthermore, the frequency of double occupation and thus the duration of time the molecule bound to site MB2 is held within the pore also increases. Hence the model may explain the occurrence of the additional long gaps with a duration dependent on morantel concentration.

The model is simplified with only one closed-state opening: we excluded the brief 'within-activation' closed-state from the model as it does not influence greatly the *Po*-morantel-concentration relationship. Also, we have ignored the concentration-dependence of the opening rate constant β' as we appeared to be at or beyond the point of receptor saturation with the lowest concentrations studied.

The relationship between the degree of block and morantel concentration predicted by this model may be determined from the principles of microscopic reversibility. The model describing the double-ion block of the channel pore predicts that if there is little or no block at +75 mV and we let

$R = (1 + \frac{\alpha_{+75}}{\beta'_{+75}})/(1 + \frac{\alpha_{-75}}{\beta'_{-75}})$ then :

$$\frac{P_{o-75}}{P_{o+75}} = \frac{R}{1 + \frac{\beta'}{\alpha+\beta'}(\frac{x_a}{K_B} + \frac{x_a}{K_B}\cdot\frac{\gamma}{\delta} + \frac{\gamma}{\delta}\cdot\frac{x_a^2}{K_B.K'_B})} \qquad (2)$$

Where $\beta'/(\alpha+\beta')$ are the values at −75 mV; K_B is k_{-B}/k_{+B} at −75 mV; K'_B is k'_{-B}/k'_{+B} at −75 mV and γ/δ are also at −75 mV.

Estimation of some of the parameters of equation 2 We can already provide estimates for a number of the parameters described in equation 2 from our experimental records. R was taken as 2.71, the ratio Po_{-75}/Po_{+75} in the presence of 0.6 μM morantel when little or no block was observed at −75 mV. This is nearly the same as R_{max} estimated from the fit to the Hill equation (Figure 10a). $\beta'/(\alpha+\beta')$ was taken as *Po* in the presence of 0.6 μM morantel at a holding potential of −75 mV, when little or no block was observed: this was 0.004.

For the proposed sequential double block scheme, a plot of the reciprocal of mean open-time against morantel concentration would have an intercept of $1/\alpha$ and a slope of k_{+B}. As we showed earlier this plot gave a value for k_{+B} of 1.9×10^7 $M^{-1}s^{-1}$ at −75 mV (Figure 7b). If, as we suspect, MB1 represents the same binding site as that conferring block at positive potentials, then k_{+B} loses its voltage-sensitivity at negative holding potentials.

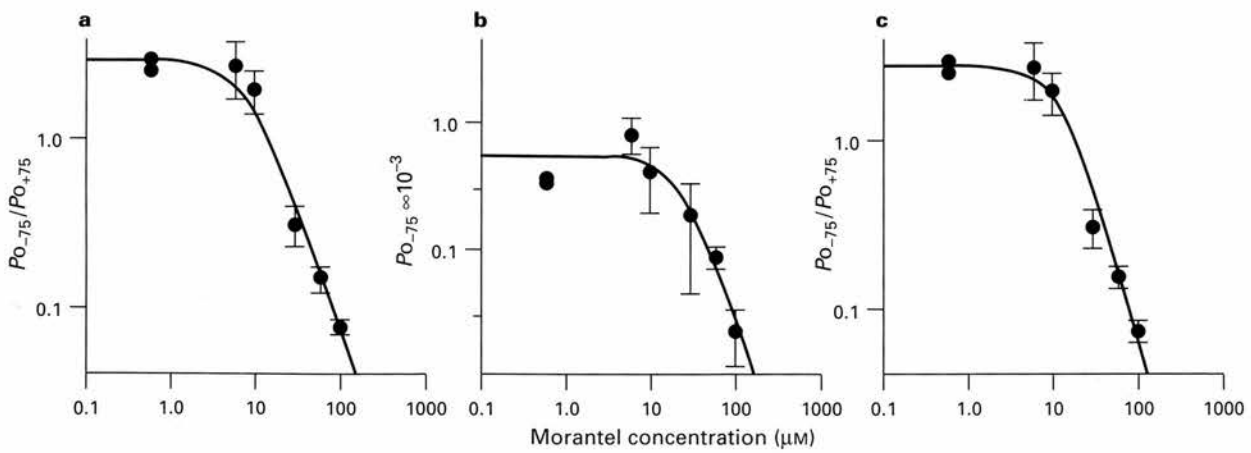


Figure 10 The relationship between *Po* and morantel concentration suggests positive cooperativity between at least two blocking molecules. (a), (b) and (c) show log-log plots of the degree of block against morantel concentration. The vertical bars represent s.e.mean for each set of data which comprise at least three observations. (a) Po_{-75}/Po_{+75} is plotted against morantel concentration, with the line representing the least squares fit to the Hill equation which gave values of 10 μM for the IC_{50} and 1.6 for n_H. This suggests positive cooperativity between at least two blocking molecules. (b) The Hill plot of Po_{-75} against morantel concentrations greater than 0.6 μM (12 μM for the IC_{50} and 1.7 for n_H). (c) The same data as in (a) fitted by least squares to equation 2, the limiting slope was close to 1.6, as for (a) and (b).

The sequential model also predicts that at a given holding potential, the sum of the rate constants, k_{-B} and γ, may be derived from the reciprocal of the mean duration of the short block periods (τ_1 or 13.3 ms; Table 2) in the presence of 100 μM morantel and a holding potential of −75 mV. At this point the degree of block is high and we may assume that the majority of the short gaps represent the short block periods and few if any short 'within-activation closures' occur.

Estimation of remaining parameters of equation 2 by non-linear regression

The values of the parameters mentioned above (k_{+B},$k_{-B}+\gamma$, R and $\beta'/(\alpha+\beta')$) were fixed and the remaining parameters of equation 2 determined from non-linear least squares fits to the relationship between Po_{-75}/Po_{+75} and morantel concentration. We found that it was possible to make estimates of the three parameters: K_B, K'_B and γ/δ, if the estimates for K'_B were constrained in the analysis to be equal or greater than K_B. This is reasonable since prior entry of one molecule of morantel into the channel and binding at MB2 might slow the entry rate (k'_{+B}) of a second molecule by repulsion as well as increasing its exit rate (k'_{-B}). Fixing these parameters then allowed estimation of the following rate constants: k_{+B}, 2×10^7 $M^{-1}s^{-1}$; k_{-B}, 22.01 s^{-1}, γ, 54 s^{-1}; δ, 54 s^{-1}. K_B and K'_B were found to have the same value, 1.1 μM, suggesting that the dissociation constant at the first block site does not increase when the second block site MB2 is occupied. Figure 10c shows the line of best fit obtained for equation 2, with the parameters above, and that the limiting slope of the plot was near at 1.6. The plot shows that equation 2, and thus the sequential model, describes our experimental observations. In contrast, the simple channel-block scheme (Adams, 1976; Neher & Steinbach, 1978) and a simple sequential model, where the blocked state enters a single desensitized state, failed to describe our experimental data.

Morantel does not block nicotinic AChR currents when applied to the cytoplasmic surface of the patch

When single nitotinic AChRs were activated in excised inside-out patches by addition of 0.6 μM morantel to the pipette solution, a concentration with which no channel-block was observed, bath application of 1 mM morantel to the cytoplasmic surface of the patch altered neither the single-channel conductance, mean open-time nor *Po* (not shown). These findings are similar to the effects observed at the *Ascaris* nicotinic AChR with levamisole (Robertson & Martin, 1993b).

Discussion

Conductance properties

The nicotinic-acetylcholine receptors (AChR) from the somatic muscle cells of *Ascaris* displayed at least two conductance states when activated by morantel as has been observed for acetylcholine- and levamisole-activated single-channel currents (Pennington & Martin, 1990; Robertson & Martin, 1993a). Both main- and sub-conductance states exhibited inward rectification. The main-conductance increased from a mean of 32 pS at +75 mV to 40 pS at −75 mV. Although the inward rectification has not been obtained in the *Ascaris* preparation previously, such rectification has been seen in studies of rat sympathetic ganglionic nicotinic AChRs (Mathie *et al.*, 1990) and Torpedo nicotinic AChRs (Imoto *et al.*, 1988). As for these nicotinic AChRs our results in *Ascaris* may be explained by an asymmetrical organization of the pore of the *Ascaris* channel, which is suggested by the fact that the block produced by morantel and another agonist levamisole (Robertson & Martin, 1993b) only occurred when the drug was present at the extracellular but not cytoplasmic surface of the patches. With a symmetrical pore one would expect to observe block after application to extracellular and intracellular surfaces.

Single channel kinetics

In the absence of channel-block, both open- and burst-time distributions were usually described by a single exponential, revealing the presence of one open-state. The mean open-times were only modestly voltage-sensitive and increased from 0.7 ms at +75 mV to 1.4 ms at −75 mV, due to a reduction in the channel closing rate constant α; this corresponds to an e-fold reduction for every 213 mV. Although such a voltage-sensitive reduction in the closing rate constant is also a feature of vertebrate nicotinic AChR channels, they are more sensitive with an e-fold reduction every 78 mV for skeletal muscle receptors (for example see Colquhoun & Ogden, 1988), and an e-fold reduction for every 156 mV for the ganglionic receptors (for example see Mathie *et al.*, 1990).

The closed-time distributions were more complex and were described by the sum of two or three exponential components, revealing at least two closed states. In general these closed events could be classified as short 'within-activation' and long 'between-activation' closures. Neither component exhibited any appreciable voltage-dependence.

Channel-block at positive potentials

At positive holding potentials a fast flickering open channel-block was observed in the presence of high concentrations (>60 μM) of morantel. The voltage-sensitivity of the blocking rate, k_{+B} predicted an e-fold increase for every 44 mV negative shift in holding potential and a value for the relative electrical distance for a single morantel block site of 1.1. This is inconsistent with a single block site within the channel pore for a monovalent cation, such as morantel. Further inconsistencies with the predictions of simple bimolecular channel-block included the slopes of frequency block plots and the finding that the burst length appeared independent of morantel concentration.

Channel-block at negative holding potentials

A more complex form of open channel-block was clearly present at negative holding potentials and comprised two identifiable block durations: one whose duration was short (~13 ms) and independent of morantel concentration and another whose duration was long and increased in a concentration-dependent manner (up to minutes). These two components conspired to produce a marked reduction in the probability of channel opening with increasing morantel concentration. This relationship could not be described assuming simple channel-block; when the data were fitted to the Hill equation, the best fit was obtained with a Hill coefficient of 1.6, suggesting positive cooperativity between at least two blocking molecules. The suggestion that there is more than one block site in the ion pore for large organic molecules is not novel (Adelman & French, 1978; Davies *et al.*, 1989; Gingrich *et al.*, 1993; Maconochie & Steinbach, 1995) and cooperative multi-ion block of channels by simple ions is well recognized (for discussion see Hille, 1992). In the present investigation we used a minimal sequential double block model that describes such a cooperative interaction (Results). The model requires that the occupation of a binding site, MB1, near the mouth of the channel pore precedes binding to the second site, MB2, deeper within the pore. It allows MB1 and MB2 to be occupied simultaneously but does not allow a molecule at MB2 to leave the channel when MB1 is occupied. Thus as the concentration of morantel increases the occupation of MB1 increases so that there is a concentration-dependent increase in the duration of the occupation of the MB2 site.

The nicotinic AChR appears to have multiple binding sites for channel-blocking molecules: quinacrine azide, a derivative of a channel-blocker photoaffinity labels an M1 region believed

to form part of the 25–30 A° funnel entrance of the open channel (Dipaola *et al.*, 1990); $TPMP^+$ photoaffinity labels an MII region of the pore that appears to be the QX 222 blocking site (Hucho *et al.*, 1986). If we consider the large size of the extracellular antrum of the vertebrate nicotinic AChR pore (Zhorov *et al.*, 1991), the existence of more than one binding site for a blocking molecule is quite plausible. It is tempting to suggest that a site equivalent to the outer 20' region in the MII region of the pore (Lester, 1992) may represent the MB1 site and the QX 222 binding site (the 10' hydrophobic ring and 6' anionic ring on the inner MII region of the pore, Galzi *et al.*, 1991; Lester, 1992), may represent the MB2 block site.

Values of rate constants estimated from the sequence of open- and closed-times also supports the sequential double block model

Horn and Lange (1983) have described a technique for the estimation of rate constants for any kinetic scheme, by fitting the parameters of the hypothesized Q matrix of the model to the entire sequence of open and closed dwell times by maximum likelihood. We also tested this approach to estimate directly the rate of constants of our block model from records showing only one active channel. The techniques of Colquhoun and Hawkes (1977, 1981) were used to make these estimates and programs written in FORTRAN using conditional probability density functions, of the form described in equation 1. It has been pointed out by Fredkin and Rice (1992), that this sort of approach may be successful for complicated schemes but sometimes fails for simple models. Apparently reliable estimation rate constants is particularly difficult when the closed-states are not well separated, because there is an inherent ambiguity in the closed-state kinetics due to aggregation. We chose the 100 μM concentration results at −75 mV, because this was the concentration where we consistently separated both the short, and long, block durations from the normal channel closures.

Table 4 shows the mean and s.e.mean values obtained for the rate constants of the model at −75 mV. The striking feature of these results is the similarity to those results obtained from the *Po* least squares estimates. For example the maximum likelihood estimates gave values of 1.5 μM for K_B, 24 s^{-1} for k_B, 57 s^{-1} for γ, 51 s^{-1} for δ and 1.6 μM for $K_{B'}$: these values compare with 1.1 μM for K_B and $K_{B'}$, 21 s^{-1} for k_{-B} and 54 s^{-1} for γ and δ obtained from the least squares estimation. The similar estimates for the dissociation constants, K_B and K'_B, obtained by both methods, lends support for the use of our simple sequential double block model. We also checked the predictions of the model and found that the estimated rate constants predicted the concentration-dependence of *Po*, the Hill coefficient, as well as the probability density functions of the open and closed-times for 100 μM morantel (data not shown).

Other processes used to explain deviations from the predictions of simple open channel-block

One alternative explanation of our findings is that of desensitization. It is likely that desensitization in general is a phenomena associated with high agonist concentrations and results from long-lived shut states which have the agonist binding sites occupied. At vertebrate nicotinic AChR the channel openings during desensitization are seen as clusters separated by long closed-times which may have mean durations as long as 34 s (Sakmann *et al.*, 1980; Colquhoun & Ogden, 1988). Such long-lived desensitized states could explain our observations if they occurred only at negative potentials and were concentration-dependent in duration. However, when observed in vertebrate and *Ascaris* preparations, these long desensitized/closed-times are essentially not voltage-sensitive (Colquhoun & Ogden, 1988; Robertson & Martin, 1993a). Moreover when present, voltage-sensitive desensitization appears to be Ca^{2+}-dependent and supported by depolarization of the cell membrane (Manthey, 1966, 1970; Mildei, 1980). The Ca^{2+} concentration of our solutions was deliberately low to minimize any Ca^{2+}-dependent changes in single-channel activity. In addition, the long concentration- and voltage-dependent gaps in single-channel records obtained with morantel as the agonist did not increase in frequency with the passage of time as they are expected to do if they were explained by desensitization.

Table 4 Rate constants estimated by maximum likelihood for the sequential multi-ion channel-block model from the sequence of open- and closed- times with 100 μM morantel and at −75 mV

β'	α	k_{+B}	k_{-B}	γ	δ	k'_{+B}	k'_{-B}
3.14 ±0.70	1144 ±160	16.1 ±2.3	23.7 ±4.0	56.7 ±20.1	51.3 ±13.2	29.1 ±7.3	47.6 ±16.0

Data shown are means ± s.e.mean, $n=4$. Note that $K_B = k_{-B}/k_{+B} = 1.47$ μM; $K'_B = k'_{-B}/k'_{+B} = 1.64$ μM; $\gamma/\delta = 1.1$. Units are s^{-1} except for k_{+B} and k'_{+B} which are $\mu M^{-1}s^{-1}$.

We also estimated, from our data, rate constants for a sequential model (C↔O↔B↔D) in which the blocked channel (B) could enter a desensitized state (D) and found that the mean duration of the desensitized state would have to be voltage-dependent and concentration-dependent to explain our data. If desensitization were the explanation for the long block periods at negative potentials, then the duration of the desensitized state would be expected to have the same mean duration (it did not) throughout the concentration range, 10–100 μM morantel, where the *Po* plot (Figure 3a) indicates receptor saturation. For these reasons we believe that the voltage-sensitive and concentration-dependent long gaps seen at negative potentials in this study cannot be explained by desensitization.

One further alternative explanation of our findings could lie in the presence of a closed-trapped-blocked state (Gurney & Rang, 1984). Ogden & Colquhoun (1988) have discussed in some detail the implications of such mechanisms, which could result in a concentration-dependent reduction in mean burst length but which still predict a linear relationship between the reciprocal mean open-times and the concentration of the blocking molecule. However the presence of concentration-dependent and voltage-sensitive long-block durations are not readily explained by models encompassing a closed-trapped-blocked state, which would predict a concentration-independent gap duration.

Conclusion

We have observed that morantel both opens and blocks the nitotinic AChR in the somatic muscle cells of *Ascaris*. The mechanism of block appears complex showing cooperativity and may be explained by the presence of two block sites within the channel pore. The marked voltage-sensitivity and bell-shaped concentration-dependence of macroscopic currents produced by morantel (Harrow & Gration, 1985) may be explained by the behaviour of the channel currents seen in this study.

This work was sponsored by the Wellcome Trust. We would like to thank Dr D.C. Ogden and Dr M.B. Cannell for reading the manuscript and for a helpful discussion of our findings.

References

ADAMS, P.R. (1976). Drug blockade of open end-plate channels. *J. Physiol.*, **260,** 531–552.

ADELMAN, W.J. & FRENCH, R.J. (1978). Blocking of squid axon potassium channel by external caesium ions. *J. Physiol.*, **276,** 13–25.

BALDWIN, E. & MOYLE, V. (1949). A contribution to the physiology and pharmacology of *Ascaris lumbricoides* from the pig. *Br. J. Pharmacol.*, **4,** 145–152.

COLQUHOUN, D. & HAWKES, A.G. (1977). Relaxation and fluctuations of membrane currents that flow through drug-operated channels. *Proc. R. Soc. (Lond.)*, **B199,** 231–262.

COLQUHOUN, D. & HAWKES, A.G. (1981). On the stochastic properties of single ion channels. *Proc. R. Soc. (Lond.)*, **B211,** 205–235.

COLQUHOUN, D & OGDEN, D.C. (1988). Activation of ion channels in the frog end-plate by high concentrations of acetylcholine. *J. Physiol.*, **395,** 131–159.

COLQUHOUN, D. & SAKMANN, B. (1985). Fast events in single-channel currents activated by acetylcholine and its analogues at the frog muscle end-plate. *J. Physiol.*, **369,** 501–557.

COLQUHOUN, D. & SIGWORTH, F.J. (1983). Fitting and statistical analysis of single-channel records. In *Single-channel Recording*, ed. Sakmann, B. & Neher, E., pp. 191–263. New York: Plenum Press.

DAVIES, N.W., SPRUCE, A.E., STANDEN, N.B. & STANFIELD, P.R. (1989). Multiple blocking mechanisms of ATP-sensitive potassium channels of frog skeletal muscle by tetra-ethylammonium ions. *J. Physiol.*, **413,** 31–48.

DEL CASTILLO, J., DE MELLO, W.C. & MORALES, T. (1963). The physiological role of acetylcholine in the neuromuscular system of *Ascaris lumbricoides*. *Arch. Internat. Physiol. Biochimie*, **71,** 741–757.

DIPAOLA, M., KAO, P.N. & KARLIN, A. (1990). Mapping the -subunit site photolabelled by the non-competitive inhibitor (3H)quinacrine azide in the active state of the nicotinic acetylcholine receptor. *J. Biol. Chem.*, **265,** 11017–11029.

EVANS, A.M. & MARTIN, R.J. (1992a). The cationic agonist blocks nicotinic acetylcholine channels from *Ascaris suum* at positive potentials. *J. Physiol.*, **459,** 394P.

EVANS, A.M. & MARTIN, R.J. (1992b). Morantel may bind to more than one site within nicotinic acetylcholine channels from *Ascaris suum*. *J. Physiol.*, **459,** 489P.

EVANS, A.M. & MARTIN, R.J. (1993a). On the block by morantel of nicotinic acetylcholine channels isolated from *Ascaris suum*: positive cooperativity between at least two blocking molecules. *J. Physiol.*, **467,** 171P.

EVANS, A.M. & MARTIN, R.J. (1993b). On the block by morantel of nicotinic acetylcholine receptors isolated from *Ascaris suum*: rate constants for multi-ion block estimated by maximum likelihood. *J. Physiol.*, **467,** 254P.

FREDKIN, D.R. & RICE, J.A. (1992). Maximum likelihood estimation and identification directly from single-channel recordings. *Proc. R. Soc. (Lond.)*, **B294,** 125–132.

GALZI, J., REVAH, F., BESSIS, A. & CHANGEUX, J. (1991). Functional architecture of the nicotinic acetylcholine receptor: from electric organ to brain. *Ann. Rev. Pharmacol.*, **31,** 37–72.

GINGRICH, B.J., BEARDSLEY, D. & YUE, D.T. (1993). Ultra-deep blockade of Na^+ channels by a quaternary ammonium ion: catalysis by a transition-intermediate state? *J. Physiol.*, **471,** 319–341.

GURNEY, A.M. & RANG H.P. (1984). The channel-blocking action of methonium compounds on rat submandibular ganglion cells. *Br. J. Pharmacol.*, **82,** 623–642.

HAMILL, O.P., MARTY, A., NEHER, E., SAKMANN, B. & SIGWORTH, F.J. (1981). Improved patch-clamp techniques for high-resolution current recording from cells and cell-free membrane patches. *Pflügers Archiv.*, **391,** 85–100.

HARROW, I.D. & GRATION, K.A.F. (1985). Mode of action of the anthelmintics morantel, pyrantel and levamisole on the muscle cell membrane of the nematode *Ascaris suum*. *Pest Sci.*, **16,** 662–672.

HORN, D. & LANGE, K. (1983). Estimating kinetic constants from single channel data. *Biophysics J.*, **43,** 207–223.

HILLE, B. (1992). *Ionic Channels of Excitable Membranes*. Second Edition. pp. 390–422. Sunderland, Massachusetts: Sinauer Associates Inc.

HUCHO, F., OBERTHUR, W. & LOTTSPEICH, F. (1986). The ion channel of the nicotinic acetylcholine receptor is formed by the homologous helices MII of the receptor subunits. *FEBS Letts.*, **205,** 137–142.

IMOTO, K., BUSCH, C., SAKMANN, B., MISHINA, M., KONNO, T., NAKAI, J., BUJO, H., MORI, Y., FUKUDA, K. & NUMA, S. (1988). Rings of negatively charged amino acids determine the acetylcholine receptor channel conductance. *Nature*, **335,** 645–648.

LESTER, H.A. (1992). The permeation pathway of neuromuscular-gated ion channels. *Ann. Rev. Biophys. Biomol. Struct.*, **21,** 267–293.

MACONOCHIE, D.J. & STEINBACH, J.H. (1995). Block by acetylcholine of mouse muscle nicotinic receptors, stabley expressed in fibroblasts. *J. Gen. Physiol.*, **106,** 113–147.

MANTHEY, A.A. (1966). The effect of calcium on desensitisation of membrane receptors at the neuromuscular junction. *J. Gen. Physiol.*, **49,** 963–976.

MANTHEY, A.A. (1970). Further studies on the effect of calcium on the time course of action of carbamyl choline at the neuromuscular junction. *J. Gen. Physiol.*, **56,** 407–419.

MARTIN, R.J. (1982). Electrophysiological effects of piperazine and diethylcarbamazine on *Ascaris suum* somatic muscle. *Br. J. Pharmacol.*, **77,** 255–265.

MARTIN, R.J., KUSEL, J.R. & PENNINGTON, A.J. (1990). Surface properties of membrane vesicles prepared from muscle cells of *Ascaris suum*. *J. Parasitol.*, **76,** 340–348.

MARTIN, R.J., PENNINGTON, A.J., DUITTOZ, A.H., ROBERTSON, S. & KUSEL, J.R. (1991). The physiology and pharmacology of neuromuscular transmission in the nematode parasite *Ascaris suum*. *Parasitology*, **102,** S41–S58.

MATHIE, A., COLQUHOUN, D. & CULL-CANDY, S.G. (1990). Rectification of currents activated by nicotinic acetylcholine receptors in rat sympathetic ganglion neurones. *J. Physiol.*, **427,** 625–655.

MILEDI, R. (1980). Intracellular calcium and desensitisation of acetylcholine receptors. *Proc. R. Soc. (Lond.)*, **209,** 447–452.

NATOFF, I.L. (1969). The pharmacology of cholinoceptors in muscle preparations of *Ascaris lumbricoides* var. *suum*. *Br. J. Pharmacol.*, **37,** 251–257.

NEHER, E. & STEINBACH, J.H. (1978). Local anaesthetics transiently block currents through single acetylcholine receptor channels. *J. Physiol.*, **277,** 153–176.

OGDEN, D.C. & COLQUHOUN, D. (1985). Ion channel-block by acetylcholine, carbachol and suberyldicholine at the frog neuromuscular junction. *Proc. R. Soc. (Lond.)*, **B225,** 329–355.

PATLAK, J.B. (1988). Sodium channel sub-conductance levels measured with a new variance-mean analysis. *J. Gen. Physiol.*, **92,** 412–430.

PENNINGTON, A.J. & MARTIN, R.J. (1990). A patch-clamp study of acetylcholine-activated ion channels in *Ascaris suum* muscle. *J. Exp. Biol.*, **154,** 201–221.

ROBERTSON, S.J. & MARTIN, R.J. (1993a). Levamisole-activated single-channel currents from muscle of the nematode parasite *Ascaris suum*. *Br. J. Pharmacol.*, **108,** 170–178.

ROBERTSON, S.J. & MARTIN, R.J. (1993b). The application of levamisole, either to the extracellular or cytoplasmic surface, activates nicotinic single channels in membranes of the nematode parasite *Ascaris suum*. *Pest. Sci.*, **37,** 293–299.

ROZHOVA, E.K., MALYUTINA, T.A. & SHISHOVA, B.A. (1980). Pharmacological characteristics of cholinoreception in somatic muscle of the nematode *Ascaris suum*. *Gen. Pharmacol.*, **11,** 141–146.

SAKMANN, B.J., PATLAK, J. & NEHER, E. (1980). Single acetylcholine-activated channels show burst-kinetics in the presence of desensitizing concentrations of agonist. *Nature*, **286,** 71–73.

TOSCANO RICO, J. (1926). Sur la sensibilite de l'Ascaris a l'action de quelques drogues. *Compte Rendu Seances Soc. Biol.*, **94,** 921–923.

ZHOROV, B.S., BROVTSYNA, N.B., GMIRO, V.E., LUKOMSKAYA, N.Y., SERDYUK, S.E., POTARYEVA, N.N., MAGAZANIK, L.G., KURENNITY, D.E. & SKOK, V.I. (1991). Dimensions of the ion channel in neuronal nicotinic acetylcholine receptor as estimated from analysis of the conformation-activity relationships of open channel-blocking drugs. *J. Memb. Biol.*, **121,** 119–132.

(Received October 10, 1995
Revised March 7, 1996
Accepted March 11, 1996)

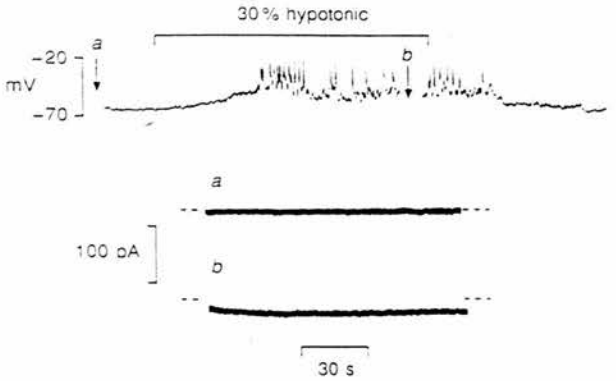


Fig. 1. Effects of a hypotonic bath solution on electrical activity (upper trace) in a single isolated rat β-cell. At points *a* and *b*, the amplifier was switched to voltage clamp to record whole cell current (lower traces) at −70 mV. The dotted lines represent zero current.

It is suggested that activation of the volume-sensitive conductance generates an inward current, leading to depolarization, enhanced electrical activity and insulin release.

REFERENCE

Best, L., Sheader, E.A. & Brown, P.D. (1996). *Pflügers Arch.* **431**, 363–370.

Arachidonic acid alters membrane mechanical properties of sarcolemmal vesicles from rabbit skeletal muscle

J.A. Nichol and O.F. Hutter

Institute of Physiology, University of Glasgow, Glasgow G12 8QQ

The behaviour of diverse ion channels is modified by short-term exposure to arachidonic acid (AA) at 1–100 μM (Meves, 1994). Hydrophobic interaction of AA with the channel proteins (Ordway *et al.* 1991) and/or modulation of channel protein function through perturbation of the lipid bilayer may be responsible. Hitherto the case for the latter mechanism has rested on fluorescence depolarization measurements that point to a decreased order of membrane lipid acyl chains by AA (Anel *et al.* 1993). Here we report that the mechanical properties of a cell membrane are equally sensitive to AA.

Membrane tensile strength, T^*, and the modulus of area elasticity, K, of sarcolemmal vesicles were measured by pipette aspiration (Nichol & Hutter, 1996). The observed reduction in T^* and decrease in K (Table 1) indicate that intercalation of the hairpin-shaped AA molecule disturbs the packing of the normal lipid components of the bilayer, so as to decrease membrane cohesion. Changes in the conformation of membrane channel proteins that require matching deformation in the lipid bilayer will thereby be facilitated.

Table 1. Effects of arachidonic acid on membrane strength and elasticity

AA (μM)	n	T^* (mN m^{-1}) (median)	K (mN m^{-1}) (mean ± S.E.M.)
0	85	14·8	531 ± 6
2	42	13·3	398 ± 14
4	74	11·0	306 ± 36
8	17	5·9	159 ± 13

Lysolipids affect membrane mechanical properties in a similar manner to AA (Nichol & Hutter, 1993), and they also modulate ion channels (Burnashev *et al.* 1989). However, at present, insufficient data are available to test whether similar changes in membrane mechanical properties produced by different chemical agents produce comparable changes in channel function, or not. At all events the present results emphasize that measurements of membrane mechanical properties constitute a simple, precise way of quantifying membrane perturbation equal in sensitivity to spectroscopic methods.

REFERENCES

Anel, A.A., Richieri, G.V. & Kleinfeld, A.M. (1993). *Biochemistry* **32**, 530–536.

Burnashev, N.A., Undrovenas, L.A., Fleidervish, I.A. & Rosenshtraukh, L.V. (1989). *Pflügers Arch.* **415**, 124–126.

Meves, H. (1994). *Prog. Neurobiol.* **43**, 175–186.

Nichol, J.A. & Hutter, O.F. (1993). *J. Physiol.* **407**, 333*P*.

Nichol, J.A. & Hutter, O.F. (1996). *J. Physiol.* **493**, 187–198.

Ordway, R.W., Singer, J.J. & Walsh, J.V. (1991). *Trends Neurosci.* **14**, 96–100.

Levamisole-activated single-channel currents from isolated muscle vesicles of *Oesophagostomum dentatum*

A.P. Robertson*, H. Bjorn†, N.C. Sangster‡ and R.J. Martin*

**Department of Preclinical Veterinary Sciences, University of Edinburgh, Edinburgh EH9 1QH, †Department of Pharmacology and Pathology, Royal Veterinary and Agricultural University, Federiksberg C, Denmark and ‡Department of Veterinary Pathology, University of Sydney, NSW 2006, Australia*

Levamisole, a drug used to treat many nematode parasite infections, acts as a selective agonist at nematode nAChRs and activates channel currents in the large nematode *Ascaris suum* (Robertson & Martin, 1993). Its continued use has produced field resistance to levamisole in a number of parasitic nematodes, including the small nodular-worm of pigs, *Oesophagostomum dentatum* (Bjorn *et al.* 1991). To examine single-channel properties of *O. dentatum* nAChRs we have used a muscle vesicle preparation. Levamisole-sensitive adult *O. dentatum* were recovered from the

intestine of experimentally infected pigs, slaughtered humanely 28 days post-infection. Muscle-flap preparations were made using a micro-scalpel and fine pins, and muscle vesicles prepared for cell-attached patch recordings of levamisole-activated currents (for method, see Robertson & Martin, 1993).

Our results from eight patches showed that levamisole activates a cation-selective channel (Fig. 1) with conductances of 28–46 pS and mean open times at −75 mV between 1·3 and 3·2 ms in levamisole-sensitive *O. dentatum*.

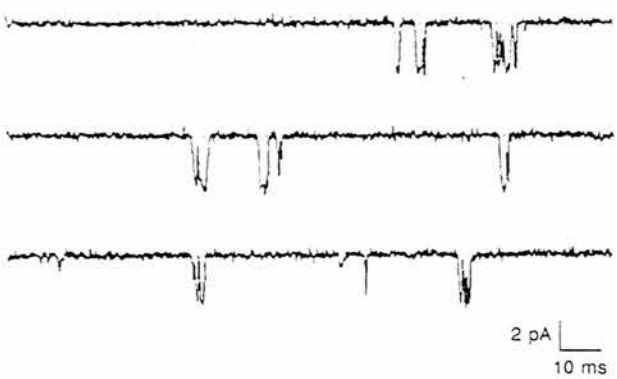


Fig. 1. Levamisole-activated channels. Vesicle-attached patch. Openings downwards. Patch-potential −75 mV, 10 μM levamisole in pipette. Main state −3·07 pA. Filter, −3 dB, 1·5 kHz, 8-pole Bessel.

Supported by the Wellcome Trust.

REFERENCES

Bjorn, H., Roepstorff, A., Waller, P.J. & Nansen, P. (1991). *Vet. Parasitol.* **37**, 21–30.

Robertson, S.J. & Martin, R.J. (1993). *Br. J. Pharmac.* **108**, 170–178.

A comparison of whole-cell currents in isolated mucosal and connective tissue rat mast cells

P.B. Hill, R.J. Martin and H.R.P. Miller

Departments of Preclinical Veterinary Sciences and Veterinary Clinical Studies, R(D)SVS, University of Edinburgh, Edinburgh EH9 1QH

Subpopulations of mast cells with distinct biochemical and functional characteristics have been identified in rodents and man. Based on their anatomical locations, these cells are designated mucosal mast cells or connective tissue mast cells and differ in terms of protease content, proteoglycan content, and response to secretagogues. Previous studies have shown that this heterogeneity also extends to their electrophysiological properties: mucosal-type mast cells possessed only a K^+-selective inwardly rectifying current (McCloskey & Qian, 1994), whereas connective tissue mast cells did not appear to have whole-cell currents unless stimulated with secretagogues or second messengers (Matthews *et al.* 1989). We recorded whole-cell currents in fifty-six rat bone marrow-derived mast cells (mucosal phenotype) and fifty-four rat peritoneal mast cells (connective tissue phenotype) using the amphotericin B perforated patch technique. Voltage steps were applied from −140 to +100 mV from a holding potential of −40 mV. The pipette solution contained (mM): 137 KCH_3SO_4 or KCl, 2·7 NaCl, 1 $CaCl_2$, 3 $MgCl_2$ and 10 Hepes; pH 7·3. The extracellular solution contained (mM): 137 NaCl, 2·7 KCl, 2 $CaCl_2$, 5 $MgCl_2$, 10 Hepes and 5·6 glucose; pH 7·3. Bath temperature was varied between room temperature (16–20 °C) and 37 °C with a Peltier device.

As previously reported, only the mucosal-type mast cells exhibited an inwardly rectifying K^+ current. However, in contrast to previous studies, we found that an outwardly rectifying chloride current could be demonstrated in both cell types. Important features of the current were: (1) activation at potentials more positive than −30 mV; (2) reduction in current amplitude and chloride conductance when the extracellular Cl^- concentration was reduced to 16·7 mM by substituting Na^+-isethionate for NaCl; (3) reversible blockade by the chloride channel blocker DIDS (20 μM); (4) dependence on temperature – the current could be elicited in a significant proportion of cells by increasing the bath temperature to > 25 °C; (5) dependence on a cytoplasmic component – the current was rarely observed when currents were recorded using the conventional whole-cell voltage clamp technique; (6) the current was more commonly observed and was greater in magnitude when peritoneal mast cells were incubated overnight in the presence of 10 ng ml^{-1} stem cell factor, an important survival factor for connective tissue mast cells; (7) the current could also be activated by a 33% decrease in extracellular osmolality.

The results show that an outwardly rectifying chloride conductance can be observed in both mucosal and connective tissue-type mast cells without stimulating the cells with secretagogues or intracellular second messengers. This current could help to maintain a negative membrane potential when mast cells degranulate, and may play a role in volume regulation.

Supported by the Wellcome Trust.

REFERENCES

McCloskey, M.A. & Qian, Y.X. (1994). *J. Biol. Chem.* **269**, 14813–14819.

Matthews, G., Neher, E. & Penner, R. (1989). *J. Physiol.* **418**, 131–144.

Copyright © 1997 Elsevier Science B.V. . All rights reserved.
Wed Jan 8 17:12:49 1997: EJP: 55779:

Heterogeneous levamisole receptors: a single-channel study of nicotinic acetylcholine receptors from *Oesophagostomum dentatum*

Richard J. Martin,[a,*] Alan P. Robertson,[a] Henrik Bjorn [b] & Nicholas C. Sangster [c]

[a] *Department of Preclinical Veterinary Sciences, R.(D.)S.V.S., Summerhall, University of Edinburgh, Edinburgh, EH9 1QH, UK*
[b] *Department of Pharmacology and Pathology, Royal Veterinary and Agricultural University, Frederiksberg C, Denmark*
[c] *Department of Veterinary Pathology, University of Sydney, Sydney, NSW 2006, Australia*

Received 3 October 1996; revised 13 December 1996; accepted 20 December 1996

A muscle vesicle preparation from *Oesophagostomum dentatum*, a 5 mm parasitic nematode, was developed for single-channel recording. Properties of nicotinic acetylcholine receptors activated by the anthelmintic levamisole (10 μM) were investigated using cell-attached and isolated inside-out patches. The current-voltage relationships of the single-channel currents were linear with conductances in the range 24.6–57.7 pS (mean 39.5 pS). The distributions of open times were fitted with a single exponential and mean open times were in the range 0.98–4.43 ms (2.2 ms). The distributions of conductances and open times of the channels showed that the receptors could not be described as a single homogeneous population. There were two main channel subtypes: one subtype, designated *G35*, had a mean conductance of 35.2 pS and open time of 1.6 ms; another subtype, designated *G45*, had a mean conductance of 44.6 pS and open time of 2.7 ms. A channel with a conductance near 25 pS, designated *G25*, and a channel with a conductance near 55 pS, designated *G55*, were also observed. The designations were based on the mean conductances, *G*, of the channel subtypes. A model for the heterogeneous population of nicotinic acetylcholine channels predicting four subtypes of receptor separated by their conductance is discussed and related to the development of levamisole resistance. © 1997 Elsevier Science B.V. All rights reserved.

Keywords: Levamisole; Nicotinic acetylcholine receptor; Heterogeneity; (*Oesphagostomum dentatum*); Patch clamp

1. Introduction

Levamisole is an anthelmintic drug used for the control and treatment of many parasitic nematode infections. The electrophysiological effects of levamisole on nematodes are often studied in the pig intestinal nematode, *Ascaris suum*, because of its availability, large size and close relationship to the human *ascariasis* parasite. Levamisole acts as a selective nicotinic agonist, producing spastic paralysis of parasitic nematodes but not of the host (Aceves et al., 1970); it produces depolarization of somatic muscle cells by increasing the input conductance of muscle to cations (Harrow and Gration, 1985). Patch-clamp experiments on *Ascaris suum* muscle have demonstrated that levamisole gates nicotinic acetylcholine receptor ion channels that conduct monovalent cations non-selectively with single-channel conductances in the range 19–46 pS and mean open times in the range 0.8–2.9 ms (Robertson and Martin, 1993).

Resistance to levamisole therapy is now spread widely and a serious problem limiting the treatment of different parasites (Prichard, 1994). Genetic experiments on the model soil nematode *Caenorhabditis elegans* have identified 11 genes involved in producing levamisole resistance and three of these genes, *unc-38*, *unc-29*, *lev-1*, encode subunits of a nicotinic acetylcholine receptor (Lewis et al., 1980; Fleming et al., 1996). The small size of *C. elegans* has so far limited electrophysiological studies and resistant strains of *Ascaris* are not available. To overcome these problems we have selected the nodular worm of the pig, *Oesphagostomum dentatum* (Fig. 1), for further study. *O. dentatum* is a 5 mm

* Corresponding author. Tel.: (44-131) 650 6094/5; fax: (44-131) 650 6576; e-mail: R.J.Martin@ed.ac.uk

PII: S0014-2999(96)00996-X

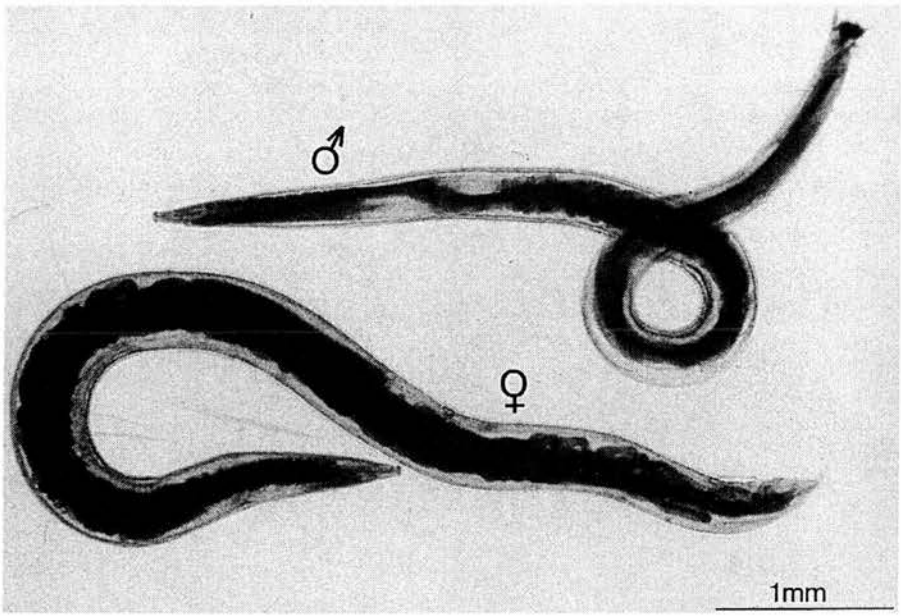


Fig. 1. Photomicrograph of an unstained female (top) and male (bottom) *O. dentatum* after recovery from the intestine of a pig. The female is about 5 mm in length.

intestinal nematode parasite of pigs causing nodular lesions. It may be maintained by cryopreservation of L_3 larvae and experimental infection; anthelmintic-resistant strains of *O. dentatum* are available (Bjorn, 1994).

In this paper we describe a method for recording levamisole-activated single-channel currents from membrane vesicles prepared from somatic muscle of *O. dentatum*. We describe some of the properties of the channel currents, revealing heterogeneity of the receptor-operated ion channels, and we discuss a model for this heterogeneity.

2. Materials and methods

2.1. *Preparation of adult O. dentatum*

At the Royal Veterinary and Agricultural School, Frederiksberg, Copenhagen, 10 000 L_3 larvae were administered by stomach tube to 25 kg Landrace X pigs. Infection was confirmed by faecal egg counts on day 21 after infection. Pigs were slaughtered in the conventional manner by electrical stunning and bleeding out. The adult worms were collected from the large intestine and cleaned using the agar migration technique (Slotved et al., 1996) and then placed in a stainless steel thermos flask, at 37°C, containing a maintenance solution (composition mM): NaCl, 150; KCl, 2.7; $CaCl_2$, 2; $MgCl_2$ $6H_2O$, 0.3; PIPES, 10; NaOH, 13; glucose, 11; $NaHCO_3$, 12 and penicillin, 0.06 g l^{-1}; streptomycin, 0.1 g l^{-1}. The adults were shipped overnight by TNT International to arrive the next day in Edinburgh.

At Edinburgh the adult *O. dentatum* were removed from the thermos flask and placed in Petri dishes containing maintenance solution in an incubator at 20°C. The maintenance solution was changed daily. Under these conditions adult *O. dentatum* survived for 7–14 days.

2.2. *Preparation of muscle vesicles*

The adult female *O. dentatum* is about 5 mm long, larger than the male (Fig. 1) and is slightly easier to dissect. For some reason unknown to us the females usually survived longer than the males after collection, so we only used the female for preparation of muscle vesicles.

A single female worm was pinned, with small insect mounting pins, through the head and tail in a 2.5 cm Petri dish with Sylgard resin lining the base. The preparation was bathed in solution-1, a low-Ca^{2+} maintenance solution containing (mM): NaCl, 35; Na acetate, 105; KCl, 2; $MgCl_2$, 2; HEPES 10; glucose, 3; EGTA, 1; ascorbic acid, 0.5; adjusted to pH 7.2 with NaOH. Solution-1 is based on *Ascaris* solutions (Martin, 1980) and contains reduced Cl^-.

Under the dissecting microscope a microscalpel, made from a broken razor fitted to a pencil-like holder, was used to cut through the cuticle and body wall on one side into the peritoneal cavity and along the length of the nematode.

EJP: 55779 Copyright © 1997 Elsevier Science B.V. . All rights reserved.

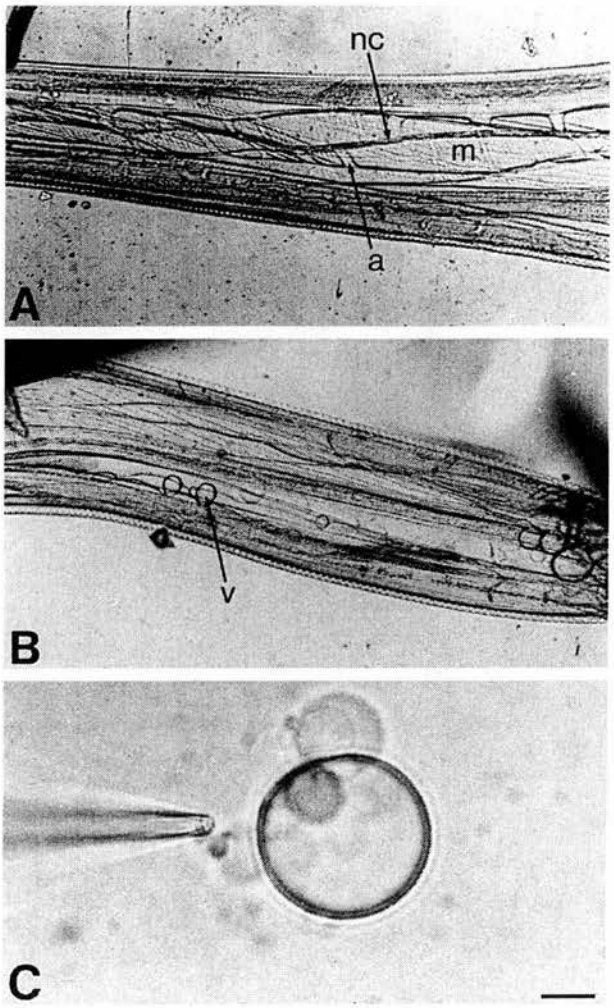


Fig. 2. Photomicrographs of the preparation of muscle vesicles. A: Flap preparation of *O. dentatum* produced by cutting the worm through the cuticle with a microscalpel and pinning it open cuticle side down onto a plate of Sylgard in a small Petri dish. M, muscle cell; a, muscle arm; nc, nerve cord. Magnification×20. B: Collagenase treatment and incubation results in the appearance of vesicles (V) which bleb off the muscle cell. Magnification×20. C: Vesicle viewed under phase contrast together with a patch pipette that was approaching the vesicle for recording. Scale bar 10 μm.

The preparation was opened out and pinned flat with more small insect mounting pins (Fig. 2A). The preparation was washed and placed in solution-2, containing (mM): NaCl, 35; Na acetate, 105; KCl, 2; $MgCl_2$, 2; HEPES 10; glucose, 3; ascorbic acid, 0.5; collagenase (1 mg ml^{-1}) adjusted to pH 7.2 with NaOH and maintained at 37°C. The preparation was maintained in solution-2 at 37°C for 10 min and then washed in solution-1 and again maintained at 37°C. Vesicles (10–50 μm in size) formed over the next hour as outgrowths from the muscle (Fig. 2B). The vesicles were used within the next 5 h.

2.3. *Patch-clamp recordings*

Individual vesicles were harvested with the aid of a micropipette with a tip of 100 μm fitted to a microsyringe driver and manipulator. The vesicles were harvested from the flap preparation and transferred to the experimental chamber where recordings were made at room temperature (15–22°C). The experimental chamber was mounted on the stage of a Nikon TMS-PH3 inverted microscope and viewed at ×300 under phase contrast for the patch clamp experiments (Fig. 2C).

The vesicles were bathed in a high-Cs solution-3, designed to reduce K currents: it contained (mM): CsCl, 35; Cs acetate, 105; $MgCl_2$, 2; dithiothreitol, 0.1; HEPES, 10 and EGTA, 1; pH adjusted to 7.2 with CsOH. Our initial patch recordings were made from preparations that were obtained using solutions without adding dithiothreitol to solution-3 (the bath solution). We found, however, that the patches were often very fragile and broke down easily

EJP: 55779 Copyright © 1997 Elsevier Science B.V. . All rights reserved.

when potentials exceeding ±50 mV were applied across the patch. We reasoned that the muscle membranes may be oxidized because they were exposed to a higher than normal pO_2 unlike their natural environment in the large intestine. To reduce oxidation, we incorporated 100 μM dithiothreitol in solution-3. We were aware of the possibility of high concentrations of dithiothreitol inactivating nicotinic channels (Kao and Karlin, 1996) so we tried decreasing concentrations of dithiothreitol to determine the lowest concentration that would permit recording of nicotinic channels from stable membranes. As a consequence of adding 100 μM dithiothreitol concentrations to solution-3 we were able to make records of channel activity from patches which were able to resist potentials in excess of ±100 mV.

Recordings were made using cell-attached patch recordings or isolated inside-out patch recordings. Patch electrodes were made from Garner (7052) capillary glass with a resistance of 1 MΩ. The pipettes were coated on the outside to near their tips with Sylgard to improve the frequency responses. Patch pipettes were filled with solution-4 which was (mM): CsCl, 140; $MgCl_2$, 2; HEPES 10; EGTA, 1; levamisole 0.01; pH 7.2 with CsOH. Solutions-3 and -4 were Ca^{2+}-free to reduce the contamination of patch recordings with Ca^{2+}-activated channels.

2.4. *Data processing*

Currents were recorded with an Axopatch 200 B and modified Sony digital audioprocessor onto DAT tape. Channel records were analyzed with an Axon Instruments Digidata 1200 A interface, an RM Pentium computer with Pclamp V6.0 software using Fetchan and pSTAT programs. The records were digitally filtered at 1.5 kHz by the software; the sampling time was 25 μs; and the minimum detectable interval was 0.3 ms. The threshold for channel opening was set at 50% of the single-channel amplitude and durations and channel states measured with Fetchan programs with a minimum resolvable interval of 100 μs. pSTAT was used to describe the distributions of the open, closed, and burst times. Exponential curves were fitted to the durations using the non-linear simplex maximum likelihood procedure. Gaussian curves were fitted using non-linear simplex least squares to the distribution of channel current amplitudes to determine the mean channel amplitude at particular potentials. Bursts of openings were defined with a critical gap length set at 3 ms.

The data are expressed as means±S.E.M. Mean open times, mean conductances of the channel subtypes were compared using a Student's *t*-test (one tail).

2.5. *Chemicals*

Levamisole hydrochloride, dithiothreitol and collagenase type IA were purchased from Sigma Chemical Company.

3. Results

3.1. *Levamisole-activated channels*

We selected low-Ca^{2+} and high-Cs^- solutions for recording to avoid contamination by Ca^{2+}-activated channels or by Na^+ or by K^+ channels. In addition we used symmetrical Cs^+ but non-symmetrical Cl^- concentrations in the bath and pipette to give, in isolated patches, a reversal potential of −33 mV for a Cl^--selective channel and a 0 mV reversal potential for a non-selective cation channel. Under the recording conditions selected we could observe two kinds of channel in cell-attached and isolated inside-out patches.

The first type, observed occasionally, had a reversal potential near 0 mV in isolated patches, a small (5–10 pS) conductance, and was voltage-sensitive opening more frequently when the patch was depolarized for several seconds. These channel currents were not interpreted as nicotinic channels because they could be recorded in the absence of levamisole in the pipette. They were classified as non-selective cation channels because they had reversal potentials near 0 mV. This channel may underlie a slow non-selective cation current like that recognised in *Ascaris* (Martin and Valkanov, 1996). This kind of channel current was edited out of the current records when necessary.

Fig. 3A and B illustrates representative recordings at +50 mV and −50 mV of the other kind of channel current we saw in the patches. This channel was recognised as the nicotinic acetylcholine receptor because: (1) it was not present if levamisole was not present in the patch pipette; (2) the channel showed little voltage sensitivity, opening at positive and negative membrane potentials; (3) the channel had conductances that ranged between 24–58 pS; (4) the channel had brief openings in the millisecond range. This kind of channel is similar to the nicotinic channel currents of *Ascaris* (Robertson and Martin, 1993). Fig. 3A shows examples of these channel currents recorded from a cell-attached patch recorded with a pipette potential of +50 mV. It can be seen that the currents are brief (millisecond) outward current pulses that have an amplitude of 2.3 pA and they occur in bursts with very brief (~ 0.3 ms) closings separating the openings of a burst.

EJP: 55779 Copyright © 1997 Elsevier Science B.V. . All rights reserved.

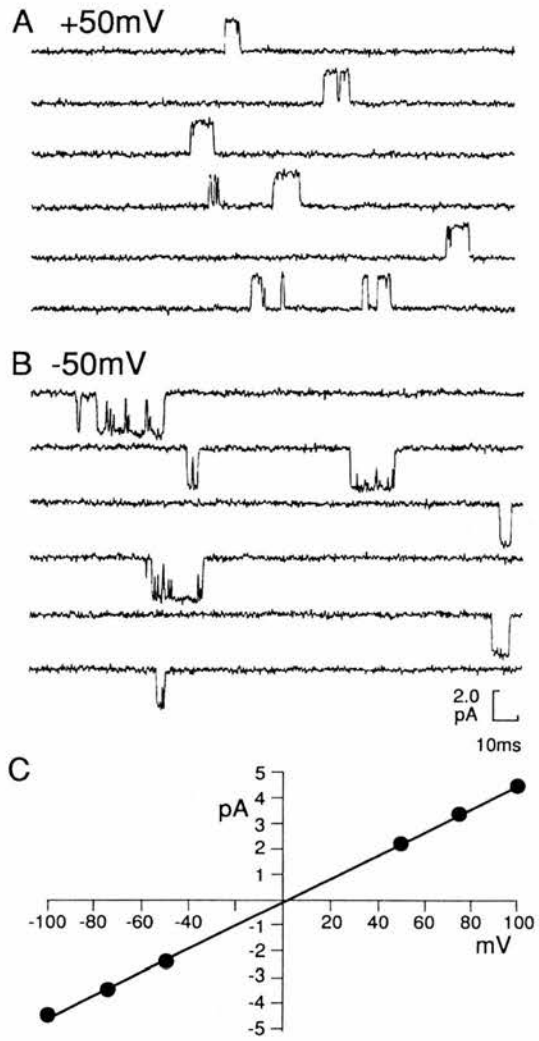


Fig. 3. Nicotinic acetylcholine receptor channel currents at pipette potential, A: +50 mV and B: −50 mV in a cell-attached patch. C: Current-voltage relationship and least squares fit giving a conductance of 45.1±0.5 pS with a reversal potential close to 0 mV.

Fig. 3B shows that at −50 mV, the channel currents are inward with an amplitude of −2.5 pA. Nicotinic acetylcholine receptor channel currents like these were seen in 24 of 91 cell-attached patch recordings made.

3.2. *Channel current-voltage relationships*

The channel currents like those shown in Fig. 3A and B were recorded at different pipette potentials, allowing the current-voltage relationship (Fig. 3C) to be determined. The slope (least squares fit) of the current-voltage plot in Fig. 3C gave a conductance of 45.1±0.5 pS with a reversal potential close to 0 mV. The mean slope conductance measured from 16 patches ranged between 24.6–57.7 pS, and had a mean of 39.5±2.0 pS.

Current-voltage plots from these channels were also recorded from isolated inside-out patches: the plots also had linear current-voltage relationships with all reversal potentials close to 0 mV. Because the predicted Nernst reversal potential for a cation-selective channel was 0 mV (symmetrical Cs^+ across the isolated patch), and for a Cl^- channel it was −33 mV, we concluded that: (1) the channels we were recording from were permeable to Cs^+ and they were non-selective cation channels; (2) the membrane potential of the vesicles was close to zero. We were able to conclude that the membrane potential of the muscle vesicles was close to zero because the reversal potentials of channels recorded from the isolated inside-out patches were the same as that of the cell-attached patches. The membrane potentials of muscle vesicles prepared from *Ascaris* are also close to zero (Martin et al., 1990). Although the reason why the membrane potential of the vesicles collapses is not known, we concluded that the membrane potential of *O. dentatum* vesicles, like those of

EJP: 55779 Copyright © 1997 Elsevier Science B.V. . All rights reserved.

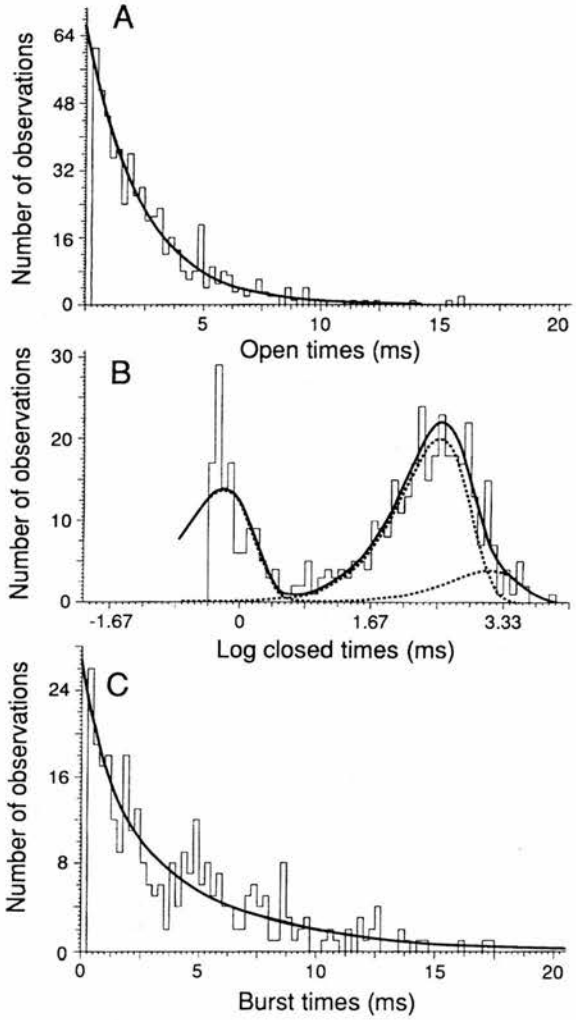


Fig. 4. Open-, closed- and burst-time distributions at −50 mV from the same experiment illustrated in Fig. 3. A: Histogram and single exponential fit to open-time distribution. The mean open time was 2.3 ms. B: Closed-time histogram plotted on a $\log_{10}$-time scale with the line fitting the three-exponential fit (solid line) and the separate components (dotted line). The three time constants of the closed-time distributions were: a fast component, t_1, 0.62 ms which had an area of 0.366; an intermediate component, t_2, of 336 ms that had an area of 0.5; and a long component, t_3, of 1455 ms that had an area of 0.103. C: Burst-time distribution. Bursts were defined as a sequence of openings separated by a closing less than 3 ms in duration. Two exponentials were fitted to the burst distribution. The t_1 of the brief component was 1.1 ms and its area was 0.15; t_2 was 4.9 ms with an area of 0.85. The mean burst duration was 4.3 ms.

Ascaris, are equal but opposite in sign to the pipette potential applied to cell-attached patches.

3.3. *Open-time distributions*

Fig. 4A shows the distribution of open times observed in a cell-attached patch at a membrane potential of −75 mV. A single exponential was fitted to the distribution giving a mean open time of 2.3 ms. The mean open time recorded at −50 to −100 mV from patches ranged between 0.98–4.43 ms, and had a mean of 2.2±0.2 ms, n= 15.

3.4. *Closed-time distributions*

The closed-time distributions were best fitted using three exponentials. Fig. 4B shows the closed-time distribution for the same experiment as in Fig. 3 and Fig. 4A displayed and plotted on a log-time scale. The three time constants of the closed distributions were: a fast component, t_1, 0.62 ms which produced the bursts and had an area of 0.366; an intermediate component, t_2, of 336 ms that had an area of 0.5; and a long component, t_3, of 1455 ms that separated the

EJP: 55779 Copyright © 1997 Elsevier Science B.V. . All rights reserved.

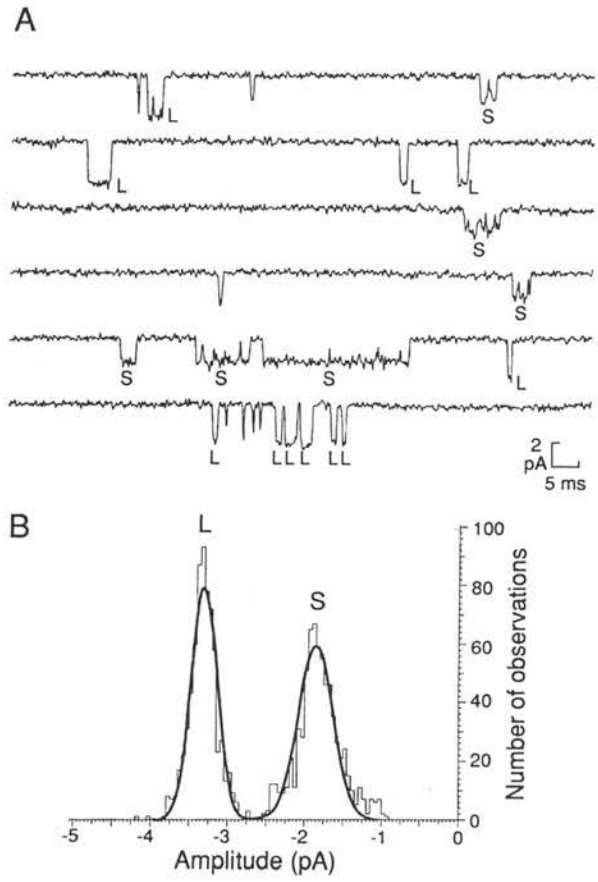


Fig. 5. A: Cell-attached patch recording at −75 mV showing a small (S) and larger (L) nicotinic acetylcholine receptor channel present. B: Amplitude histogram of open-channel amplitudes. Smaller conductance channel: mean current= −1.8±0.2 pA (24.8 pS) labelled S (panel A). Larger conductance channel: mean current= −3.3±0.2 pA (43.8 pS) labelled L (panel A). Histograms of the amplitudes of the open-channel currents were fitted with Gaussian distributions. 49% of the events were to the smaller amplitude, 51% were to the larger amplitude.

clusters of channel openings and which had an area 0.103. Of nine channels analysed, at potentials ranging between −50 and −100 mV, the mean duration of the t_1 was 0.68±0.11 ms with an area of 0.43±0.06 ms; the mean duration of t_2 was 23±11 ms with an area of 0.13±0.03; the mean duration of t_3 was 873±150 ms with an area of 0.44±0.06.

3.5. *Burst distributions*

Fig. 4C illustrates the burst distribution of the currents recorded from the same experiment as in Fig. 3 and Fig. 4A and B. The burst distribution was fitted with a single exponential with a time constant of 4.3 ms. The mean burst duration (−50 mV and −100 mV) recorded from eight patches was 4.57±0.98 ms, n= 8.

3.6. *The channel currents show differences in their conductances and mean open times revealing heterogeneity*

Some channel recordings suggested the presence of more than one nicotinic channel: Fig. 5A shows a cell-attached recording at −75 mV where two separate channels were observed: there is a small amplitude (1.8 pA= 24.8 pS labelled S, Fig. 5A) and a large amplitude (3.3 pA= 43.8 pS labelled L, Fig. 5B). Histograms of the amplitudes of the open-channel currents from this experiment are fitted with two Gaussian distributions (Fig. 5B), further emphasizing the presence of two different channel types. The fact that direct transitions from one open level to another were very rare in this experiment suggests that the different conductance levels that we observed was not produced by a single type of nicotinic acetylcholine receptor but rather two channels with similar but different properties. As a further test of the different properties of these two channels, we carried out a separate kinetic analysis on the two channel currents. We were able to separate these currents during analysis by editing because of the large difference in their amplitudes.

EJP: 55779 Copyright © 1997 Elsevier Science B.V. . All rights reserved.

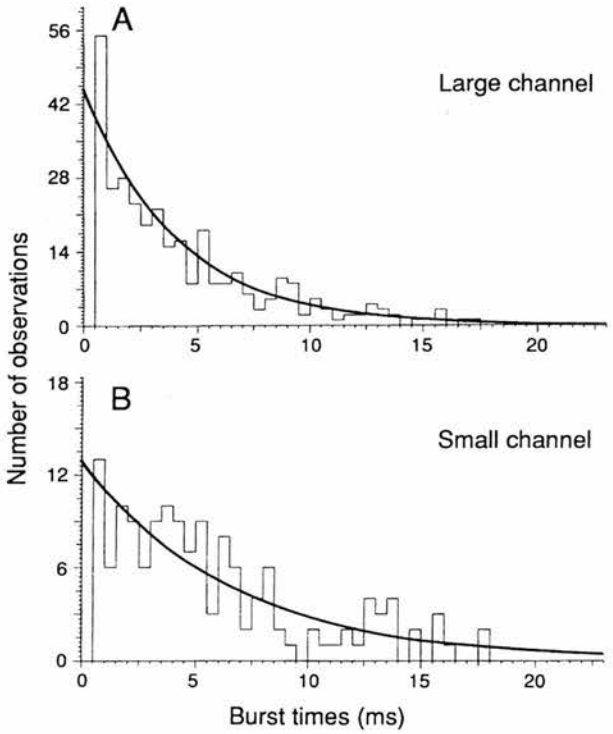


Fig. 6. Burst-time histograms of the smaller and larger channel shown in Fig. 5. The mean burst duration of the L channel was 4.07 ms (panel A), clearly smaller than the S channel value which was 6.53 ms (panel B).

As a result of the kinetic analysis we found that the mean open time of the S channel was 2.27 ms and similar to the L channel, 2.33 ms. However, the mean burst duration of the S channel was 6.53 ms (Fig. 6A) and clearly longer than the L channel which was 4.07 ms (Fig. 6B). The longer burst duration of the S channel compared to the L channel is suggested in the sample of channel currents shown in Fig. 5A.

There were also differences in the closed-time kinetics. The S channel closed-time distribution was $t_1 = 0.68$ ms (area 0.546), $t_2 = 3.95$ ms (area 0.076), $t_3 = 1124$ ms (area 0.378). The L channel distribution was $t_1 = 0.65$ ms (area 0.371), $t_2 = 8.48$ ms (area 0.150), $t_3 = 545$ ms (area 0.479).

Fig. 7A is a histogram of all the channel conductances: it shows values which ranged between 24.6–57.7 pS; the presence of two main peaks at 35 pS and 45 pS; separated observations at 24.6 pS and 57.7 pS.

Fig. 7B is a frequency histogram showing the observed mean open times with ranges between 1.0–4.5 ms. It too shows the presence of two main peaks at 1.75 ms and 2.5 ms and again two separated observations. Fig. 7 implies that there are at least two main different types of nicotinic acetylcholine receptor present, each type characterized by a particular conductance and open time.

We separated out the channels with mean open times 1.25–2.00 ms and conductances 28.40–40.25 pS (designated the *G35* subtype because the mean conductance, *G*, was 35 pS), and the channels with mean open times 2.25–3.25 ms and conductances 43.80–45.60 pS (designated the *G45* subtype because the mean conductance was 45 pS) to determine their mean conductances and open times. The *G35* subtype had a mean conductance of 35.2±1.8 pS and mean open time of 1.6±0.1 ms, $n = 6$. The *G45* subtype had a mean conductance of 44.6±0.35 pS and mean open time of 2.7±0.2 ms, $n = 6$. Open times and conductances of *G35* and *G45* were significantly different (conductances, $P = 0.002$; mean open times, $P = 0.0002$). The presence of channels with properties outside the range of the properties of *G35* and *G45* (Fig. 7) suggests the presence of additional subtype groups. The 24.6 pS channel had a conductance that appeared less than the *G35* group but had a mean open time of 2.3 ms; the 57.7 pS channel had a conductance that apeared to be greater than the *G45* group and had a mean open time of 0.98 ms. Table 1 summarizes the properties of the subtypes of channel.

4. Discussion

The nicotinic acetylcholine receptors of nematode muscle have a pharmacological profile resembling mammalian neuronal nicotinic acetylcholine receptors (Colquhoun et al., 1991). For example dimethylphenylpiperazinium is an

EJP: 55779 Copyright © 1997 Elsevier Science B.V. . All rights reserved.

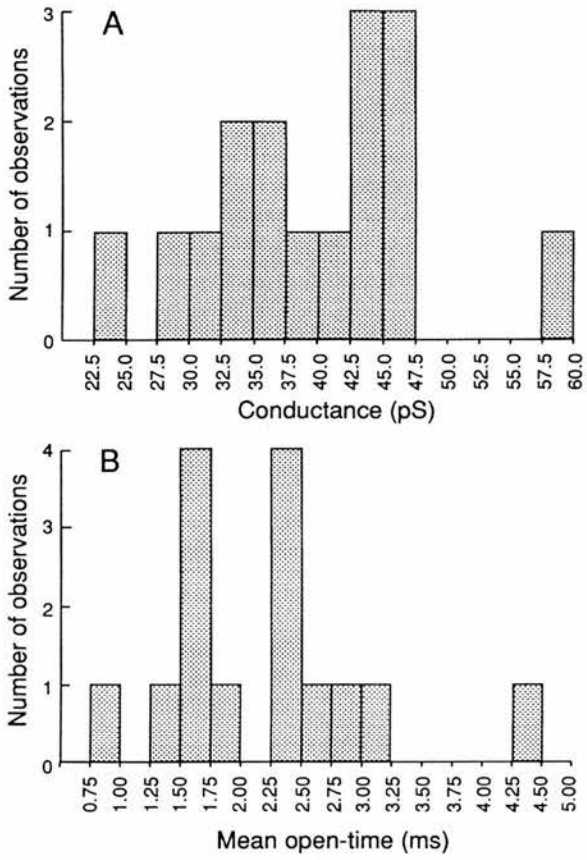


Fig. 7. A: Frequency histogram of the channel conductances from different patches. Bin width 2.5 pS. Note the presence of two main peaks and two outliers. B: Frequency histogram of the mean open times. Note the presence of two main peaks and two outliers. The total number of observations is one less in panel B than in panel A because of the limited frequency of channel openings observed at −50 or −75 mV in one recording.

Table 1. Summary of mean±S.E.M. values of the proposed levamisole receptor subtypes

Channel type	Conductance (pS)	Mean open time (ms)
G25	24.6	2.27
G35	35.2±1.8	1.6±0.1
G45	44.6±0.35	2.7±0.2
G55	57.7	0.98

agonist and mecamylamine is an antagonist at both receptors. Initially, in this discussion we refer to the heterogeneous nature of neuronal nicotinic acetylcholine receptors, and then argue that the nicotinic receptors of nematodes may be similar. The presence of heterogeneous nicotinic acetylcholine receptors in nematodes may provide a mechanism for the development of anthelmintic resistance.

4.1. *Structure of vertebrate neuronal nicotinic receptors*

The structure of the *Torpedo* electric organ nicotinic acetylcholine receptor is a pentamer of homologous subunits known as α, β, γ, δ with a stoichiometry of 2:1:1:1 (Changeau et al., 1996); the subunits are arranged like barrel staves around a central cation-selective ion channel. Although the stoichiometric structures of most mammalian neuronal nicotinic acetylcholine receptors are not known, they are often assumed to be a similar pentameric structure arising from the co-expression of 2α and 3β subunits (Lindstrom et al., 1987) but multiple stoichiometries (5α, 4α:1β, 3α:2β, 2α:3β, 1α:4β) or different arrangements around the ion-channel pore (e.g. ααββδ vs. αβαββ) are possibilities (McGehee and Role, 1995). Families of genes for neuronal α and β subunits exist: currently seven α subunits and three β subunits are recognised (McGehee and Role, 1995). The different α and β subunits are denoted by different subscript numbers (α_1, α_2, α_3; β_2, β_3, β_4). If the stoichiometry and subunit combination of a neuronal nicotinic acetylcholine receptor were

EJP: 55779 Copyright © 1997 Elsevier Science B.V. . All rights reserved.

known it might be specified as $2\alpha_3 3\beta_2$. However, the stoichiometry is not known and expressed receptors are referred to without reference to the stoichiometry of the subunit combination ($\alpha_3\beta_2$).

4.2. *The pharmacology of the neuronal nicotinic acetylcholine receptors varies with subunit composition*

Although the pharmacological profile of neuronal nicotinic acetylcholine receptors can vary with the molecular structure of the α subunit, it is also influenced by the β subunit structure. Expressed $\alpha_3\beta_2$ and $\alpha_3\beta_4$ have different macroscopic dose-response relationships, with $\alpha_3\beta_2$ showing a lower agonist dissociation constant and a more shallow dose-response curve (smaller Hill coefficient) than $\alpha_3\beta_4$ receptors: dimethylphenylpiperazinium is about 10× more potent as an agonist on the $\alpha_3\beta_2$ receptors than the $\alpha_3\beta_4$ receptors (Covernton et al., 1996). Agonist binding sites are thought to be formed at specific subunit interfaces with the α subunit and adjacent unit (Karlin and Akabas, 1995) so that pharmacological differences can occur as the β subunit composition changes.

4.3. *Biophysical properties of neuronal nicotinic acetylcholine receptors show heterogeneity*

Single-channel studies on neuronal nicotinic acetylcholine receptors in sympathetic neurones (Mathie et al., 1991), habenula neurones (Connolly et al., 1995) or on $\alpha_3\beta_2$ or $\alpha_3\beta_4$ expressed in *Xenopus* oocytes (Papke et al., 1996; Papke and Heineman, 1996) have shown that their channels have conductances and kinetics which vary dramatically from patch to patch. For example, the sympathetic nicotinic acetylcholine receptors have conductances constant in individual patches, but they vary from 26 to 48 pS between patches (Mathie et al., 1991). The expressed $\alpha_3\beta_2$ nicotinic acetylcholine receptors produce channels with conductances between 4–18 pS and were grouped into two main conductances (Papke et al., 1996). When an increased proportion of the cRNA for the β_2 was injected into the oocyte there was an increase in the proportion of patches where small conductance channels were observed, suggesting that the stoichiometry of α_3 to β_2 subunits could vary (Papke et al., 1996). The $\alpha_3\beta_4$ receptors had conductances that ranged between 11–24 pS and could be grouped into three main conductances which showed kinetic differences (Papke and Heineman, 1996).

Thus heterogeneity of the receptors produced by a variation in structure, arrangement or stoichiometry of the subunits making up the pentameric channel can lead to a variation in the pharmacological and biophysical properties of nicotinic acetylcholine receptors (McGehee and Role, 1995). The diversity of the neuronal nicotinic channels appears to arise from the differential or developmentally regulated expression of related genes (McGehee and Role, 1995).

4.4. *Heterogeneity of O. dentatum nicotinic acetylcholine receptors*

In this study of the muscle nicotinic acetylcholine receptors we have seen that the single channels can have conductances and mean open times that show significant variation between patches. The variation in conductance is far wider than expected from experimental errors or open-channel noise and is greater than that produced by vertebrate muscle nicotinic acetylcholine receptors (Garner et al., 1984). Such variation has been correlated with heterogeneity of the structure and pharmacology of vertebrate neuronal nicotinic acetylcholine receptors. In this study we were able to distinguish two main groups, *G35* and *G45*, of levamisole-activated channels on the basis of the conductance and mean open time of the channels. We also found evidence of additional nicotinic acetylcholine receptor subtypes (*G25* and *G55*). Heterogenous nicotinic acetylcholine receptor channel currents from *Ascaris suum*, with conductances ranging between 19–50 pS and distinguishable peaks at 24 pS and 42 pS, have been observed (Pennington and Martin, 1990; Robertson et al., 1994) but discrimination of the subtypes was less clear, perhaps because of variations in the source of the *Ascaris* that were derived from field infections.

4.5. *Nicotinic acetylcholine receptor subunit genes in nematodes predict heterogeneity of levamisole receptors*

Three genes encoding nicotinic acetylcholine receptor subunits in the model soil nematode, *C. elegans*, associated with levamisole resistance are *unc-38*, *unc-29* and *lev-1* (Lewis et al., 1980; Fleming et al., 1996). *Unc-38* encodes an α subunit while the *unc-29* and *lev-1* encode β subunits. Pairwise expression of *unc-38* and *unc-29* or *unc-38* and *lev-1* or co-expression of all three subunits in *Xenopus* oocytes results in levamisole-induced currents but *unc-38* expressed alone does not produce levamisole-activated currents. These observations suggest that the levamisole receptor cannot be comprised of a homo-oligomer of *unc-38* subunits and that channels are formed from a heterologous subunit combination.

Fig. 8 illustrates the eight possible arrangements of *unc-38*, *unc-29*, and *lev-1* with two *unc-38* subunits fixed in position but with eight possible variations in the position of the β subunits. If a functional channel could be produced with 1–5 *unc-38* subunits then there would be 3^4 (81) different receptor configurations. These receptors might be differentiated by their biophysical or pharmacological properties with the conductances being determined by the subunits making

EJP: 55779 Copyright © 1997 Elsevier Science B.V. . All rights reserved.

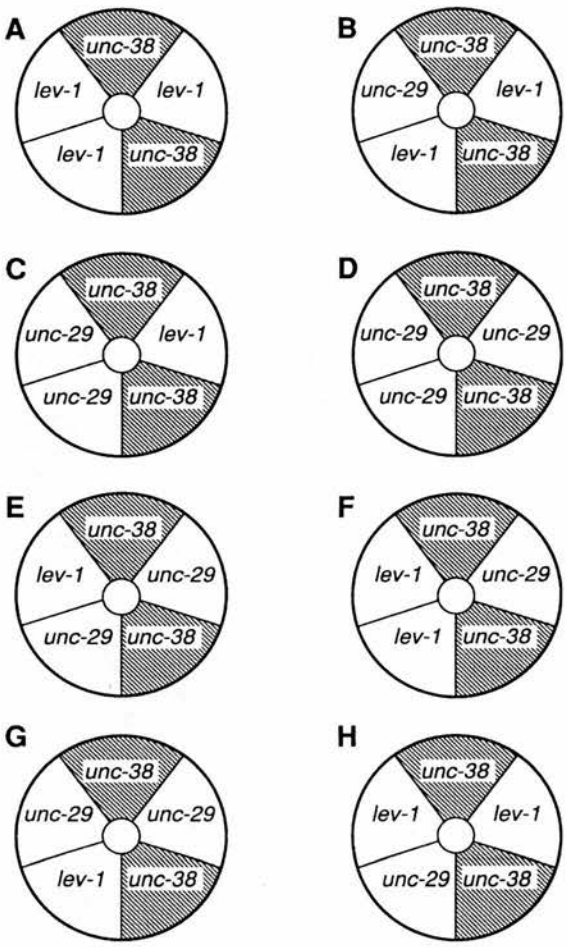


Fig. 8. Diagram of some possible subunit arrangements of *unc-38*, *unc-29* and *lev-1* subunits forming the nematode nicotinic acetylcholine receptor channel sensitive to levamisole. The *unc-38* is equivalent to the α subunit of vertebrate nicotinic channels. The *unc-29* and *lev-1* subunits are equivalent to vertebrate β subunits. The diagram shows that there are up to eight different combinations possible if two *unc-38* subunits are non-adjacent. If the conductance of the channel were determined only by the number of *unc-29* or *lev-1* subunits present in this scheme (assuming interactions between adjacent subunits do not affect overall channel conductance) then four distinct channel types would be distinguished on a basis of channel conductance (C has the same stoichiometry as E and G but the subunits are rearranged. B has the same stoichiometry as F and H but the subunits are rearranged. The diagram also illustrates that if the binding of the agonist molecule is at the interface of the *unc-38* subunit and an adjacent molecule then the binding of the agonist (including levamisole) will depend on subunit composition.

up the channel pore and the agonist binding sites being determined by the interfaces between the *unc-38* subunit and adjacent units. Fig. 8, for example, shows four different stoichiometric combinations (but with different arrangements) of the subunits and predicts the existance of four nicotinic acetylcholine receptor subtypes distinguished by evenly spaced conductance intervals (e.g. *G25*, *G35*, *G45*, and *G55*) as we have observed here. However, it is pointed out that this model may be oversimplified, ignoring interactions between adjacent subunits that affect the overall conductance of the channel.

4.6. *Development of anthelmintic resistance*

The properties of vertebrate neuronal receptors show us that potency of different agonists at nicotinic acetylcholine receptors varies with the subunit structure of the channel (e.g. Covernton et al., 1996). It is reasonable to imagine that the sensitivity of a strain of nematode parasites to a nicotinic anthelmintic like levamisole may also depend upon the pattern of subunit expression of the muscle nicotinic receptors. An increase in expression of one subunit combination may increase the required therapeutic dose of levamisole. The expression of different subunits in nematodes may arise from the continued presence of levamisole in the environment in the same way as the density of particular subunit

EJP: 55779 Copyright © 1997 Elsevier Science B.V. . All rights reserved.

stoichiometry increases in the human brain after chronic exposure to nicotine (Peng et al., 1994) if the nematode species can survive; or it may increase as a results of selection pressure as a result of clonal expansion.

Acknowledgements

We are pleased to acknowledge the financial support of the Wellcome Trust. Ref. 043509/z/95/z/JRS/SH.

References

Aceves, J., Erliji, D., Martinez-Marnon, R., 1970. The mechanism of the paralysing action of tetramisole on *Ascaris* somatic muscle. Br. J. Pharmacol. 38, 602–607.

Bjorn, H., 1994. Workshop summary: Anthelmintic resistance. Vet. Parasitol. 54, 321–325.

Changeau, J.-P., Devillers-Thiery, A., Chemouilli, P., 1996. Acetylcholine receptor: an allosteric protein. Science 225, 1335–1345.

Colquhoun, L., Holden-Dye, L., Walker, R.J., 1991. The pharmacology of cholinoceptors on the somatic muscle-cells of the parasitic nematode *Ascaris-suum*. J. Exp. Biol. 158, 509–530.

Connolly, J.G., Gibb, A.J., Colquhoun, D., 1995. Heterogeneity of neuronal nicotinic acetycholine receptors in thin slices of rat medial habenula. J. Physiol. (London) 484, 87–105.

Covernton, P.J.O., Kojima, H., Sivilotti, L.G., Gibb, A.J., Colquhoun, D., 1996. Comparison of neuronal nicotinic receptors in rat sympathetic neurones with subunit pairs expressed in *Xenopus* oocytes. J. Physiol. (London) 481, 27–34.

Fleming, J.T., Baylis, H.A., Satelle, D.B., Lewis, J.A., 1996. Molecular cloning and in vitro expression of *C. elegans* and parasitic nematode ionotropic receptors. Parasitology (in press).

Garner, P., Ogden, D.C., Colquhoun, D., 1984. Conductances of single ion channels opened by nicotinic agonists are indistinguishable. Nature 309, 160–162.

Harrow, I.D., Gration, K.A.F., 1985. Mode of action of the anthelmintics morantel, pyrantel and levamisole on muscle-cell membrane of the nematode *Ascaris suum*. Pest. Sci. 16, 662–672.

Kao, C.Y., Karlin, A., 1996. Acetylcholine receptor binding site contains a disulfide cross link between adjacent half-cystinyl residues. J. Biol. Chem. 261, 8085–8088.

Karlin, A., Akabas, M., 1995. Towards a structural basis for the function of nicotinic acetylcholine-receptors and their cousins. Neuron 15, 1231–1244.

Lewis, J.A., Wu, C.-H., Levine, J.H., Berg, H., 1980. Levamisole-resitant mutants of the nematode *Caenorhabditis elegans* appear to lack pharmacological acetycholine receptors. Neuroscience 5, 967–989.

Lindstrom, J., Schoefpfer, R., Whiting, P., 1987. Molecular studies of the neuronal nicotinic acetylcholine receptor family. Pflüg. Arch. 1, 281–337.

Martin, R.J., 1980. The effect of γ-aminobutyric acid on the input conductance and membrane potential of *Ascaris* muscle. Br. J. Pharmacol. 71, 99–106.

Martin, R.J., Valkanov, M.A., 1996. Effects of acetylcholine on a slow voltage-activated non-selective cation-current mediated by non-nicotinic receptors on isolated *Ascaris* musle bags. J. Exp. Physiol. 81, 909–925.

Martin, R.J., Kusel, J.R., Pennington, A.J., 1990. Surface properties of membrane-vesicles prepared from muscle cells of *Ascaris suum*. J. Parasitol. 76, 340–348.

Mathie, A., Cull-Candy, S.G., Colquhoun, D., 1991. Conductance and kinetic properties of single nicotinic acetylcholine receptor channels in rat sympathetic neurones. J. Physiol. (London). 439, 717–750.

McGehee, D.S., Role, L.W., 1995. Physiological diversity of nictotinic acetylcholine receptors expressed by vertebrate neurons. Annu. Rev. Physiol. 57, 521–546.

Papke, R.L., Boulter, J., Patrick, J., Heinmann, S., 1996. Single channel currents of rat neuronal nicotinic acetylcholine receptors expressed in *Xenopus laevis* oocytes. Neuron 3, 589–596.

Papke, R.L., Heineman, F., 1996. The role of the β_4-subunit in determining the kinetic properties of rat neuronal nicotinic acetycholine α_4-receptors. J. Physiol. (London). 440, 95–112.

Peng, X., Anand, R., Whiting, P., Lindstrom, J., 1994. Nicotine-induced increase in neuronal nicotinic receptors results for a decrease in rate of receptor turnover. Mol. Pharmacol. 46, 532–530.

Pennington, A.J., Martin, R.J., 1990. A patch-clamp study of acetylcholine-activated ion channels in *Ascaris suum* muscle. J. Exp. Biol. 154, 210–221.

Prichard, R.K., 1994. Anthelmintic resistance. Vet. Parasitol. 54, 259–268.

EJP: 55779 Copyright © 1997 Elsevier Science B.V. . All rights reserved.

Robertson, S.J., Martin, R.J., 1993. Levamisole-activated single-channel currents from muscle of the nematode parasite *Ascaris suum*. Br. J. Pharmacol. 108, 170–178.

Robertson, S.J., Pennington, A.J., Evans, A.M., Martin, R.J., 1994. The action of pyrantel as an agonist and an open channel blocker at acetylcholine receptors in isolated *Ascaris suum* muscle vesicles. Eur. J. Pharmacol. 271, 273–282.

Slotved, H.C., Barnes, E.H., Bjorn, H., Christensen, C.M., Eriksen, L., Roepstorff, A., Nansen, P., 1996. Recovery of *Oesophagostomum dentatum* from pigs by isolation of parasites migrating from large intestinal contents embedded in agar-gel. Vet. Parasitol. 63, 237–245.

EJP: 55779 Copyright © 1997 Elsevier Science B.V. . All rights reserved.

[*From the Proceedings of the Physiological Society*, 12–13 *April* 1984
Journal of Physiology, **354**, 46*P*]

A high conductance anion channel in somatic muscle cells of *Ascaris suum*

BY R. J. MARTIN and P. THORN. *Department of Veterinary Pharmacology, Royal (Dick) School of Veterinary Studies, University of Edinburgh EH9 1QH*

Ascaris muscle cells have been shown to have a high permeability to Cl^- (Del Castillo, De Mello & Morales, 1964). We used the patch clamp technique with giga-seal recordings (Hamill, Marty, Neher, Sakmann & Sigworth, 1981) to observe unitary currents in collagenase-treated preparations. We recorded from the membrane in the

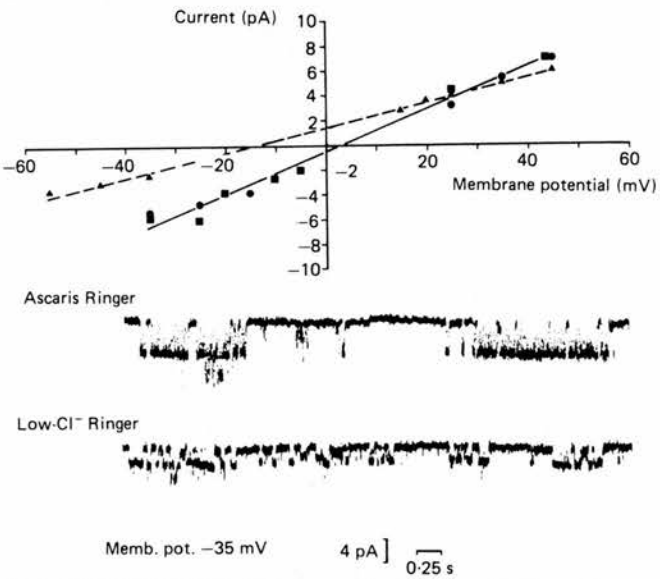


Fig. 1 shows the I/V relationship and examples of inward channel currents (opening downwards) with up to two channels present in an inside-out patch with different Cl^- concentrations on the intracellular side of the patch and 140 mM-Tris Cl^- in the pipette. Membrane potentials were corrected for a measured pipette potential of +4·7 mV. Control *Ascaris* Ringer: □ and continuous line ((mM) 135 NaCl, 3 KCl, 15·7 $MgCl_2$, 3 $CaCl_2$, 5 Tris, 3 glucose, pH 7·6). Low-Cl^- *Ascaris* Ringer: △ and dotted line (substitution of 85 mM-NaCl with 85 mM-Na acetate). Return to *Ascaris* Ringer: ●. Lines calculated by linear regression. 30 °C.

cell body region of somatic muscle cells. A spontaneous high conductance (130–230 pS) channel was seen in most of the cell-attached and isolated inside-out patches. The channel conductance and reversal potential were unaffected by substitution of the cations with Tris. Lowering the Cl^- concentration on the intracellular side of the patch had a reversible effect on the I/V relationship and reversal potential (Fig. 1). These experiments are consistent with this channel being permeable to Cl^-.

P.T. holds a S.E.R.C.–C.A.S.E. studentship with Pfizer Central Research.

REFERENCES

DEL CASTILLO, J., DE MELLO, W. C. & MORALES, T. (1964). *J. gen. Physiol.* **48**, 129–140.
HAMILL, O. P., MARTY, A., NEHER, E., SAKMANN, B. & SIGWORTH, F. J. (1981). *Pflügers Arch.* **391**, 85–100.

Quarterly Journal of Experimental Physiology

If your library does not subscribe to this Journal, please ask them to do so.

Quarterly Journal of Experimental Physiology (1987) **72**, 31–49
Printed in Great Britain

A HIGH-CONDUCTANCE CALCIUM-DEPENDENT CHLORIDE CHANNEL IN *ASCARIS SUUM* MUSCLE

P. THORN AND R. J. MARTIN

Department of Preclinical Veterinary Sciences, R.(D.)S.V.S., Summerhall, University of Edinburgh EH9 1QH

(RECEIVED FOR PUBLICATION 3 JUNE 1986)

SUMMARY

The properties of a high-conductance Ca-dependent Cl channel in the body muscle membrane of the nematode parasite *Ascaris suum* were examined with the patch-clamp technique. In *Ascaris* Ringer solution the current–voltage relationships of the channel appeared linear during hyperpolarization with a slope conductance of 200 pS (in symmetrical 175 mM-Cl): during depolarization the slope conductance reduced. Cation and anion replacement experiments showed this channel to be permeable to Cl ions. In artificial perienteric fluid (in symmetrical 78 mM-Cl) the channel conductance was found to be 114 pS. Subconductance states were seen when the patch was depolarized. The channel conductance showed saturation with increasing Cl concentrations. The channel was voltage sensitive: the probability of the channel being open and the mean open time of the channel reduced when the patch was depolarized. Mean channel open times between 2·4 and 215 ms were observed. Frequency histograms of the distributions of open and closed times were fitted with two and three exponentials respectively; this suggests complex channel kinetics with multiple open and closed states. Ca applied to the intracellular surface of the patch increased in a dose-dependent manner the number and probability of the channels being open. These channels were seen in about 20% of all patches and occasionally up to 15 channels were seen in a single patch. The distributions of the probabilities of seeing N channels open in multichannel patch records were not always well fitted by the binomial distribution: it is suggested that adjacent channels could have different probabilities of being open. The possible functions of this channel are discussed.

INTRODUCTION

Ascaris suum is a worm-like nematode parasite found in the small intestine of pigs. The *Ascaris* body cavity contains a perienteric fluid (Fig. 1*A*) which has a Cl concentration of 52 mM (Hobson, Stephenson & Eden, 1952). Hobson, Stephenson & Beadle (1952) have shown that the Cl concentration of the perienteric fluid is maintained at a lower concentration than that of the environment. They demonstrated that Cl is transported across the body wall to the outside and that the active site of this transport is a feature of the muscle or hypodermis. One possible pathway for the movement of Cl is through the bag regions of the muscle cells.

Electrophysiological studies on the bags have shown a high membrane permeability to Cl compared with K (Del Castillo, De Mellow & Morales, 1964; Brading & Caldwell, 1971). Subsequent studies have indicated an influence of Ca on its membrane permeability (Weisblat, Byerly & Russel, 1976). During patch-clamp studies on the extrasynaptic γ-aminobutyric acid (GABA) receptor (Martin, 1985) a large-conductance ion channel was frequently observed which was abolished by perfusing the preparation with a low-Ca Ringer solution. This paper describes the results of a patch-clamp study which has characterized the channel as Ca dependent, voltage sensitive and permeable to Cl. A preliminary account of some of this work has already been published (Martin & Thorn, 1984).

METHODS

Details of the preparation and methods have been described previously (Martin, 1980, 1985). They are outlined below.

The preparation

Specimens of *Ascaris suum* obtained from the local slaughter-house were maintained in Locke solution (replaced daily) at 32 °C in a water-bath. The *Ascaris* were about 20 cm in length and used within 4 d. A 2 cm flap preparation, made from a section taken 5 cm from the head was pinned into the experimental chamber. The temperature (25–30 °C) of the preparation and chamber was maintained by a water-jacket and monitored by a thermocouple device. The preparation was continuously perfused only during experiments involving the application of different experimental solutions.

Enzyme treatment

Clean muscle membranes were prepared with collagenase (1 mg in 1 ml) applied to the preparation for a period of 0·5–1·5 h. It was then washed liberally to remove the debris before recording. The enzyme treatment lowers the resting potential and causes an increase in intracellular Cl to near extracellular levels (Martin, 1985).

Ringer solutions

Several different types of bathing Ringer solution were used (Table 1). *Ascaris* Ringer solution was used for most experiments since it readily permitted giga-seal formation and its high Cl concentration facilitated the examination of Cl currents by increasing their amplitudes. An artificial perienteric fluid (APF) with HEPES buffer was also used because its ionic concentrations (particularly the lower Cl) approximates to normal extracellular ionic concentrations in the whole parasite (Hobson *et al.* 1952) and allowed a check on the properties of the anion channel. The NaCl solutions used in the determination of the Cl concentration–channel conductance relationship contained 5 mM-HEPES and 1 mM-$CaCl_2$, adjusted to pH 7·6 with NaOH.

Patch-electrode solution

Except where stated the patch electrode was filled with the same (but filtered) solution as the bathing Ringer solution. During studies on the channel permeability it was filled with either *Ascaris* Ringer solution, one-fifth *Ascaris* Ringer solution, or Tris Ringer solution (Table 1). These allowed an examination of the effect of anion and cation replacement.

Fabrication of patch electrodes

The patch pipettes were made from glass microhaematocrit tubing (Hawksley Cat. No. 1604, external diameter 1·4 mm) and pulled on a vertical micro-electrode puller (SRI Cat. No. 2001); the tip diameters were approximately 0·5 μm and filled electrodes had resistances of 2–4 MΩ.

Recording

A cell-attached patch was formed when a patch electrode was pushed gently against the bag membrane (see Fig. 1*A* and *B*) and suction applied to the pipette. The seal resistance, in favourable preparations, then gradually increased to greater than 1 GΩ. Isolated inside-out patches were easily formed by gently lifting the patch of the bag membrane. In some patches, immediately after isolation, the channel currents were very small in amplitude (conductance < 20 pS) and opened with slow rise times; in these cases exposure to air (Hamill, Marty, Neher, Sakmann & Sigworth, 1981) produced channel openings of full conductance and rapid rise times.

Two types of high-gain current–voltage (*I–V*) converters were used to monitor the currents. Initially a laboratory-made amplifier based on a Teledyne Philbrick op-amp with a 1 GΩ feed-back resistor and 3 dB cut off of 1 kHz was used. Subsequently a List EP-7 was used and the signals actively filtered using a Kemo VBF/4 at 1 kHz (3 dB). Both systems gave similar results.

The signal was recorded on a Racal Thermionic Store Four FM tape recorder (slowest frequency response used 1250 Hz, 1 dB) and monitored on an oscilloscope (Tektronix 5103N) and a chart recorder (Lectromed type MX 216).

Table 1. *Solutions: electrolyte concentrations (mM)*

	NaCl	NaAc	KCl	$CaCl_2$	$MgCl_2$	Glucose	Tris	HEPES
Ascaris Ringer solution	135	—	3·0	3·0	15·7	3·0	5·0	—
Tris Ringer solution	—	—	—	3·0	15·2	3·0	140	—
One-fifth *Ascaris* Ringer solution	27	—	0·6	0·5	3·14	0·6	1·0	—
Low-Cl *Ascaris* Ringer solution	50	85	3·0	3·0	15·7	3·0	5·0	—
APF	23	110	24	6·0	5·0	11	—	5·0
Low-Ca APF	23	110	24	—	11	11	—	5·0
NaCl Ringer solutions	50–500	—	—	1	—	—	—	5·0

The Ringer solutions containing 5 mM-Tris were corrected to pH 7·6 with Maleic acid; Tris Ringer solution containing 140 mM-Tris was corrected to pH 7·6 with HCl; the Ringer solution containing HEPES were corrected to pH 7·6 with NaOH. Low-Ca APF contained a total Ca of 3·7 μM as measured by flame photometry; this gave an estimated free-Ca of 1·5 μM. A zero-Ca APF Ringer solution was prepared by adding 0·5 mM-EGTA to the low-Ca APF

Junction potentials

In order to minimize the effect of junction potentials an agar-bridge bath electrode was used. The electrode for the pipette was prepared using an Ag wire fused with AgCl. Zero current potentials were routinely measured for each pipette before forming a seal; these initial electrode potentials were offset.

Data analysis

Single-channel current amplitudes were measured by hand from chart recordings at different patch potentials. Often the *I–V* relationships showed non-linearity on depolarization; therefore slope conductances were estimated by regressions of the linear portion of the *I–V* relationship mostly obtained during hyperpolarization of the patch.

Records showing only a single-channel opening were analysed with the aid of a Cromemco microcomputer programmed to sample and digitize every 200 μs. Channel openings were registered when the current level was greater than 75% of the full channel amplitude. Closings were registered when the current level fell below 25% of the full amplitude. Channel records containing subconductance levels were excluded. Effective mean open and closed times are quoted without correction for unresolved short intervals. The channel records were checked for stationarity using Q-sums and the K–S statistic (Glasbey & Martin, 1986). The distributions of the open and closed times greater than 0·5 or 1 ms were fitted by the sum of a number (1, 2, 3 and 4 of exponentials) using a maximum-likelihood procedure (Martin, 1985). It was taken that a reduction of 3 log units following the addition of each extra exponential component indicated a significant improvement in fit.

Multichannel records were analysed using a BBC microcomputer and Unilab interface sampling at 100 kHz to give probability density histograms of current amplitude. This allowed estimates of the proportion of the time spent with 0, 1, 2...n channels open to be made.

Drugs

Collagenase (C-1030 Sigma) and the Ca ionophore A23187 (Calbiochem) were used. The A23187 was applied in a concentration of 10 μg ml^{-1} in the perfusing Ringer solution. It was made up from a stock 0·5 mg ml^{-1} solution in methanol.

RESULTS

The following experiments were carried out on the muscle cells from more than 200 preparations. Most experiments were completed within 4 h following enzyme treatment; this was because the membrane gradually became too fragile and easily broke after giga-seal formation. More than 200 successful giga-seal recordings were made during this study.

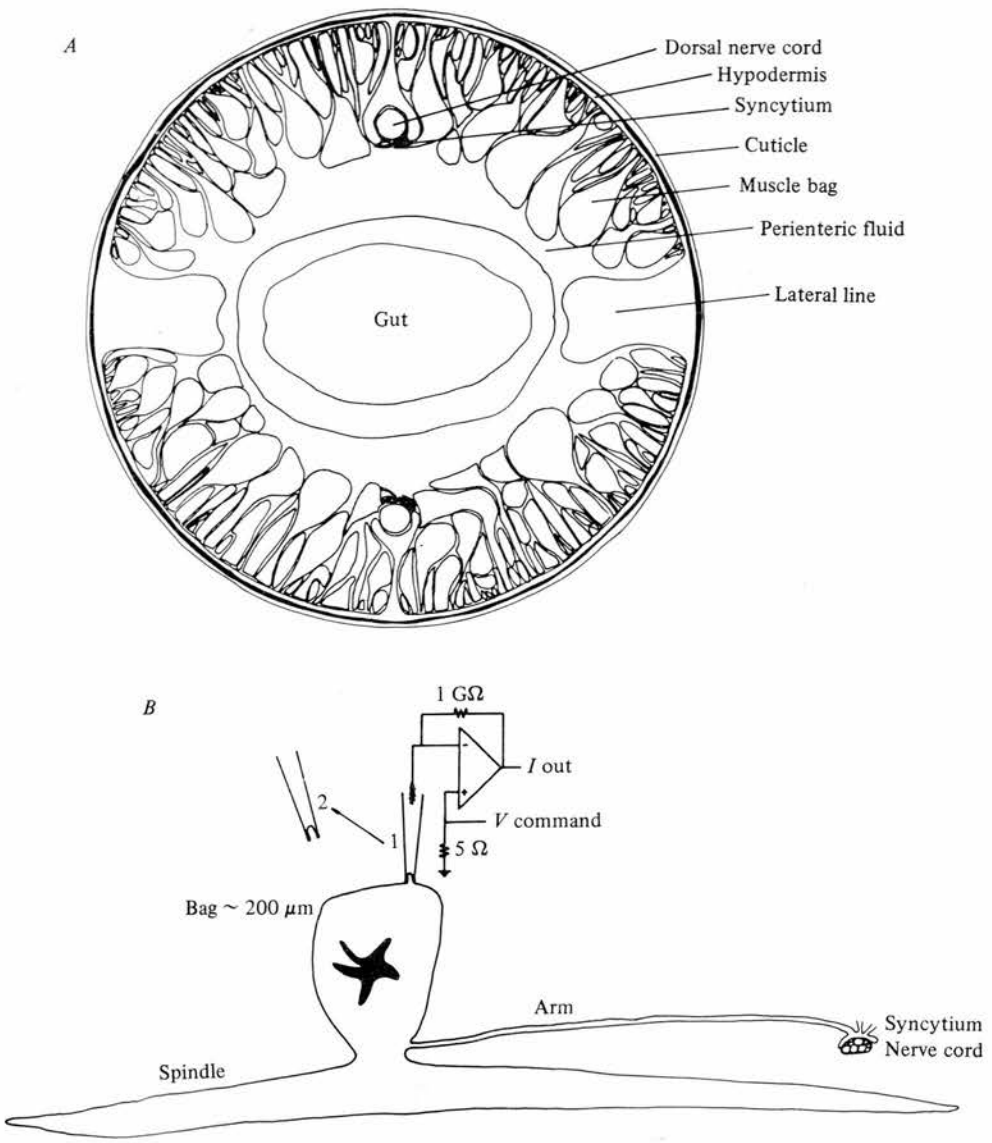


Fig. 1. *A*, diagram of a cross-section through the anterior region of *Ascaris suum*. The nerve cords are held in an extension of the hypodermis which form a cup-like structure. All the muscle cell bodies (bags) project into the body cavity which is filled with perienteric fluid. In the centre is the gut. *B*, diagram of a single muscle cell and recording technique. The cell is divided into three main regions: the cell body or bag region overlies the contractile muscle spindle; an arm extends from the bag to a nerve cord. The muscle is electrically coupled to adjacent muscle cells and also receives chemical synaptic contact with the nerve cords at the syncytium. The bag membrane was the main recording site in these experiments. We used both cell-attached patches (1) and isolated inside-out patches (2).

Initial observations on channel behaviour

Many cell-attached or isolated inside-out recordings using *Ascaris* Ringer solution resulted in current records like those seen in Fig. 2*A*. These show the activity of a large-conductance channel with a reversal potential near 0 mV. On average one in five

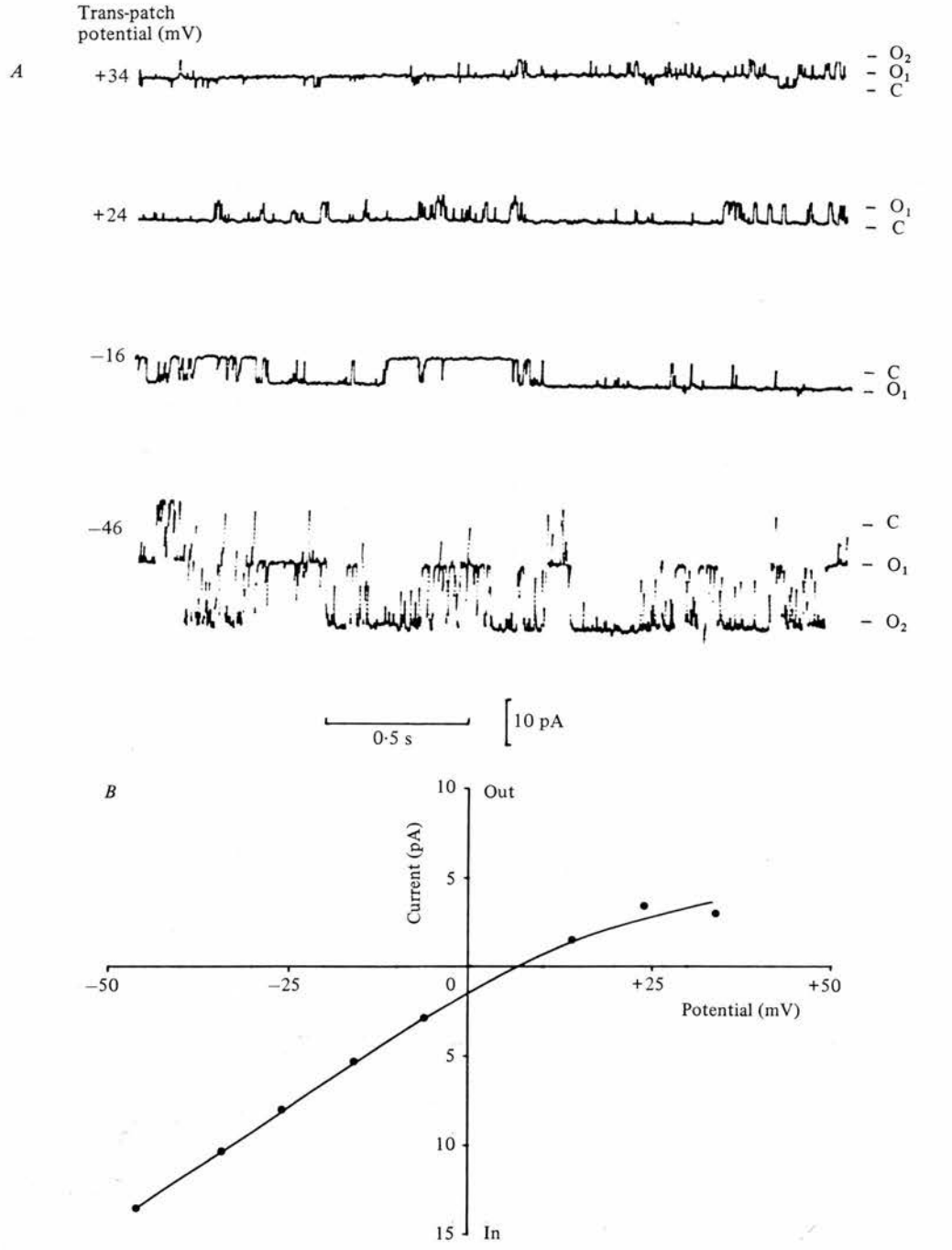


Fig. 2. *A*, current records obtained at different trans-patch potentials for the high-conductance channel. The records were obtained from an isolated inside-out patch held at the four different potentials indicated. The patch was bathed on both sides of the membrane with *Ascaris* Ringer solution, 30 °C. The currents are inward for the two negative or hyperpolarized holding potentials and outward for the two positive or depolarized holding potentials. Up to two channels are seen. The current levels with no channels open are indicated by C. The current levels with one channel opening are indicated by O_1, two channels open are indicated by O_2. *B*, a plot of the single-channel current amplitude against the trans-patch potential from the same experiment. The relationship is linear during hyperpolarization although there are deviations at depolarized potentials. The linear portion of the line gives a conductance of 220 pS.

patches showed the presence of this channel: however, this average varied dramatically from preparation to preparation. In some preparations patches from different cells all showed channel openings while in other preparations no patches showed channel activity: the reason for this is not known.

With trans-patch potentials held between +50 and −50 mV, smaller-conductance channels were only rarely observed and were excluded in the analysis. The effect of isolating the patch on channel opening also varied with preparations: in some preparations there was an immediate increase in channel opening with up to fifteen channels being observed in the patch; some cell-attached patches, which had a great deal of channel activity, showed little increase in activity on isolation. This variation in behaviour was subsequently explained by variations in intracellular Ca and the Ca-dependent nature of the large-conductance channel. Perfusion of the intracellular side of the isolated patches, often within a period of minutes, lead to a reduction in the number of active channels in the patch. This loss was due to the mechanical disturbance by the perfusion rather than any change in the ionic constituents of the perfusing Ringer solution: this problem of the loss of activity made the effects of changing Ca and Cl concentrations difficult to study.

Channel conductance

Fig. 2*A* and *B* shows typical current records and the channel *I–V* relationship. In this experiment the patch was an isolated inside-out patch with *Ascaris* Ringer solution on both sides of the membrane. The *I–V* relationship was linear during hyperpolarization but on depolarization the slope conductance often reduced considerably. This rectification was seen in over half the channel records and is not predicted on the basis of the constant field equation for a channel bathed in symmetrical solutions. In twenty experiments at 30 °C this channel had a slope conductance during hyperpolarization of 200 ± 7 pS (mean ± S.E.M.) when measured using isolated patches and symmetrical *Ascaris* Ringer solution.

Channel permeability

Initially in order to look at the channel permeability, patch recordings were made using one-fifth *Ascaris* Ringer solution in the patch electrode: with *Ascaris* Ringer solution in the bath, shifts in the channel reversal potential would indicate whether the channel was permeable to anions or cations. In all these experiments the reversal potential moved up to a maximum of 40 mV in the depolarizing direction; this is predicted by the Nernst equation for an anion channel. Further studies were conducted where the cations were placed in the patch electrode with the large impermeant ion Tris: these experiments showed no effect on conductance or the reversal potential of the channel *I–V* plot, again indicating an anion channel. Fig. 3 shows the effect of cation replacement on the *I–V* relationship using an isolated patch. The filled circles show the points obtained with Tris Cl in the patch pipette and *Ascaris* Ringer solution in the bathing solution.

In seven such experiments the mean slope conductance was 204 ± 16 pS (mean ± S.E.M.) and the reversal potential was always near 0 mV. Also shown in Fig. 3 is the lack of effect on the channel currents of replacing cations on both sides of the membrane with Tris.

The effect of anion replacement was also examined using cell-attached and isolated patches. The bag membrane of *Ascaris* is permeable to Cl; after collagenase treatment the intracellular Cl concentration approaches that of the bathing Ringer solution (Martin, 1985). It was therefore possible to reduce the intracellular Cl concentration after cell-attached patches had been formed by reducing the Cl in the bathing Ringer solution. In all such experiments bathing the preparation in low-Cl *Ascaris* Ringer solution reduced the

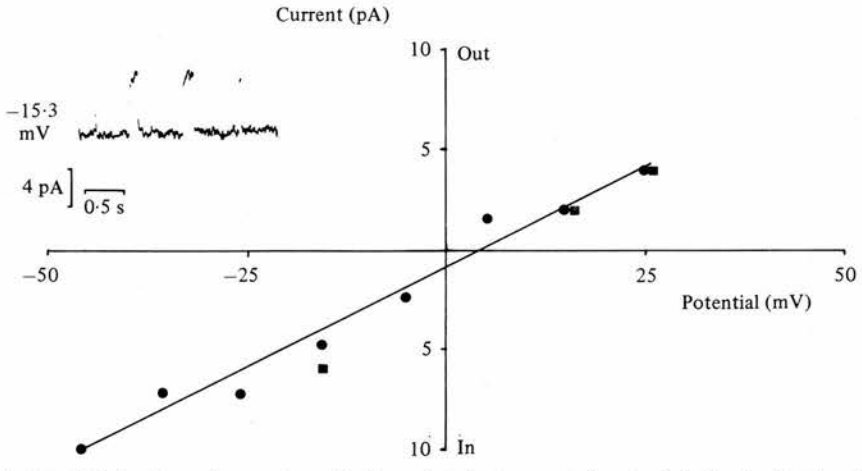


Fig. 3. A plot of single-channel current amplitude against the trans-patch potential of an isolated patch with Tris Cl in the pipette. The points (●) were obtained with Tris Cl on the extracellular side of membrane patch and *Ascaris* Ringer solution on the intracellular side. The points (■) were obtained from the same experiment with Tris on both the intracellular side and the extracellular side of the membrane patch. In the top left-hand corner is an example of the current records obtained at −15 mV with Tris Cl on both sides of the patch.

slope of the conductance and shifted the reversal potential in the hyperpolarizing direction. Similar experiments with isolated patches were more difficult to do since changing the bathing Ringer solution on the intracellular side of the patch was often associated with loss of channel activity; however, Fig. 4 shows one such successful experiment. It can be seen from the *I–V* plot that when the patch is bathed with symmetrical 175 mM-Cl there is a slope conductance of 200 pS, and a 0 mV reversal potential. When the Cl on the intracellular side of the patch was reduced to 90 mM there was a reduction in the slope conductance to 100 pS and an 18 mV hyperpolarizing shift in the reversal potential. An 18 mV shift was predicted by the Nernst equation for a Cl channel.

It was concluded from these observations that this large-conductance channel has a high permeability to Cl with no discernible permeability to cations. The conductance of this channel was therefore tested in APF Ringer solution which approximates more closely to the normal extracellular milieu and has a lower Cl concentration. The channel conductance in this medium was found to be 114 ± 5 pS (mean $\pm$, S.E.M., $n = 5$).

Channel conductance–Cl-concentration relationship

It is clear from the preceding section that the channel conductance varies with Cl concentration. The constant field equation predicts a linear relationship between channel conductance and Cl concentration with equal concentrations on both sides of the membrane (eqn. (1)).

$$g = F^2/RT.P.\mathrm{Cl}, \tag{1}$$

where g is the channel conductance, Cl is the concentration on both sides of the patch and P is the channel permeability. R, T and F have their usual meaning.

Fig. 5 illustrates the effects of Cl concentration on channel conductance: isolated inside-out patches bathed in symmetrical NaCl Ringer solution (Table 1) at 30 °C were used, conductances were measured as before. The relationship showed saturation at high Cl concentrations; such saturation has been reported previously e.g. Sakmann & Trube

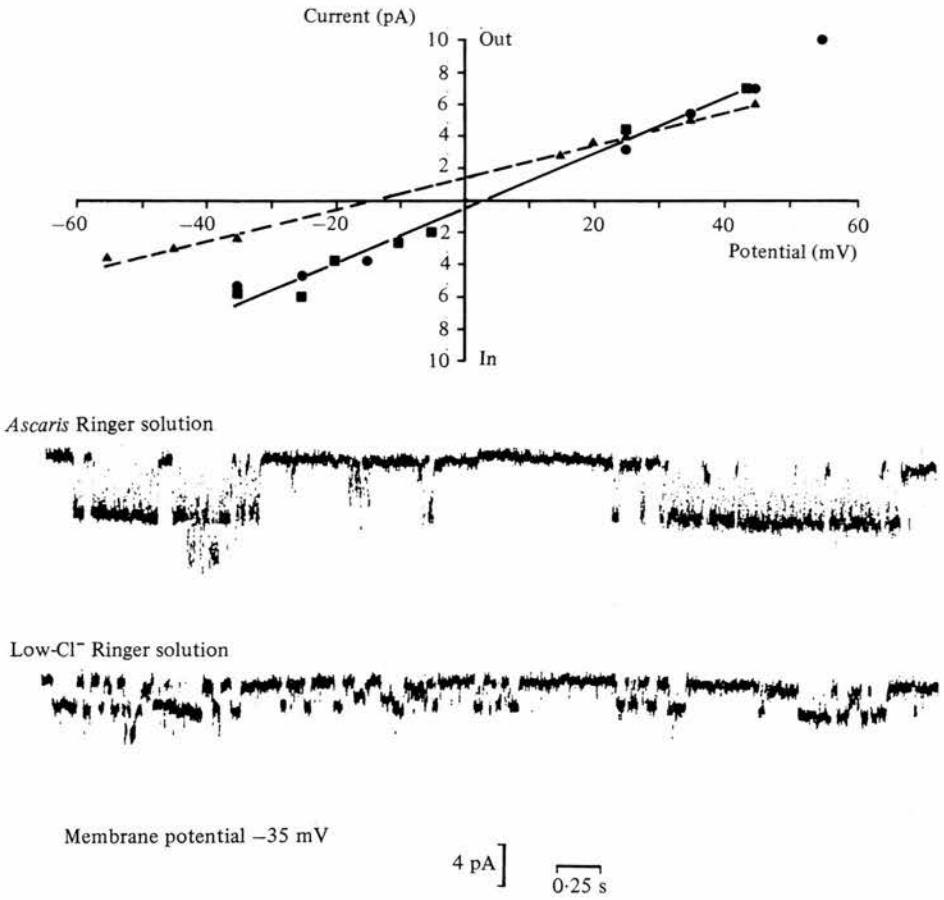


Fig. 4. The *I–V* relationship and representative examples of inward currents (openings downwards) with up to two channels present in an inside-out patch with different Cl concentrations on the intracellular side of the patch and Tris Cl in the pipette. Control *Ascaris* Ringer solution: ■ and continuous line. Low-Cl *Ascaris* Ringer solution: ▲ and dashed line. Return to *Ascaris* Ringer solution: ●, lines calculated by linear regression. 30 °C.

(1984). The line drawn in Fig. 5 has been fitted to the points using non-linear regression and the Michaelis–Menten equation:

$$g = G_{\max} \cdot \mathrm{Cl}/(K_m + \mathrm{Cl}), \tag{2}$$

where g is the conductance, $G_{\max}$ is the conductance at saturating Cl and K_m is the Cl concentration producing half saturation. $G_{\max}$ was 422 pS and K_m was 188 mM; non-linear regression was used. The equation is based on the following reaction scheme (eqn. (3)), where R stands for a binding site of the channel, Cl_o and Cl_i are extracellular and intracellular Cl concentrations respectively,

$$\mathrm{Cl}_o + R \leftrightharpoons \mathrm{Cl}R \cdot \cdots \cdot \mathrm{Cl}R \leftrightharpoons R + \mathrm{Cl}_i.$$

Subconductance states

Fig. 6*A* is an example of channel currents showing a subconductance state 75% of the main state; it was from an isolated patch with symmetrical *Ascaris* Ringer solution and a trans-patch potential of +30 mV. This interpretation was made on the grounds that the

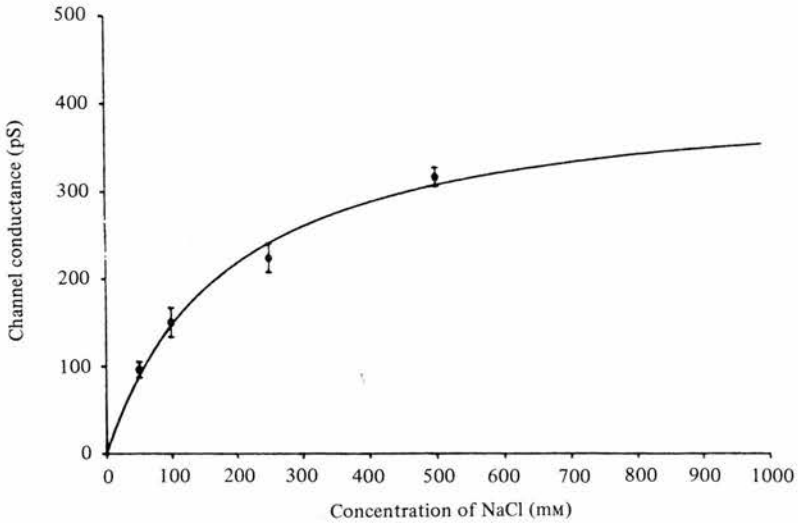


Fig. 5. The Cl concentration–channel conductance relationship. The points plotted are the mean ± S.E.M. of the conductances from observations on the *I–V* relationship of at least four isolated patches bathed in symmetrical NaCl Ringer solution (Table 1) and at 30 °C. The line was fitted to the equation $g = G_{max} \cdot Cl/(K_m + Cl)$ by non-linear regression where $G_{max} = 422$ pS and $K_m = 188$ mM.

records show 'instantaneous' steps to the subconductance level and to the full conductance level from the closed level, as well as 'instantaneous' steps between the subconductance and full conductance levels. During depolarization several subconductance levels were seen. No systematic study of the levels of subconductance and their relationship with membrane potential was made. No subconductance states were observed during hyperpolarization. Similar observations were obtained using APF Ringer solution and cell-attached patches.

Fig. 6*B* shows the *I–V* plot for a cell-attached patch recording made with *Ascaris* Ringer solution; the continuous line shows the relationship with the full main-state conductance of the channel and the dashed line shows the relationship of the most frequently observed subconductance state.

Voltage sensitivity

Fig. 7*A*, *B* and *C* illustrates the voltage-sensitive behaviour of this channel at different patch potentials. This experiment was on a cell-attached patch where the cell resting potential is unknown. The quoted potentials will therefore be offset by the resting potential. Previous work suggests that the resting potential in these conditions was below −15 mV (Martin, 1985). This cell-attached patch recording using *Ascaris* Ringer solution shows a feature of all recordings, that is, a decrease in channel opening as the patch is depolarized; the number of channels opening simultaneously declines on depolarization from three to one. Fig. 7*B* shows the relationship between the probability of the channel being open and the applied patch potential. Here it was assumed that the probability of opening was the same for each channel in the patch. Fig. 7*C* shows the relationship between mean open time and the patch potential in the same patch as before. In ten similar experiments it was found that the probability of opening measured at patch potentials between −55 and +70 mV decreased, on average, 6% for every 10 mV depolarization. The mean channel open time, which varied between 2·4 and 215 ms, decreased on average by 6 ms for every 10 mV (mean of six observations).

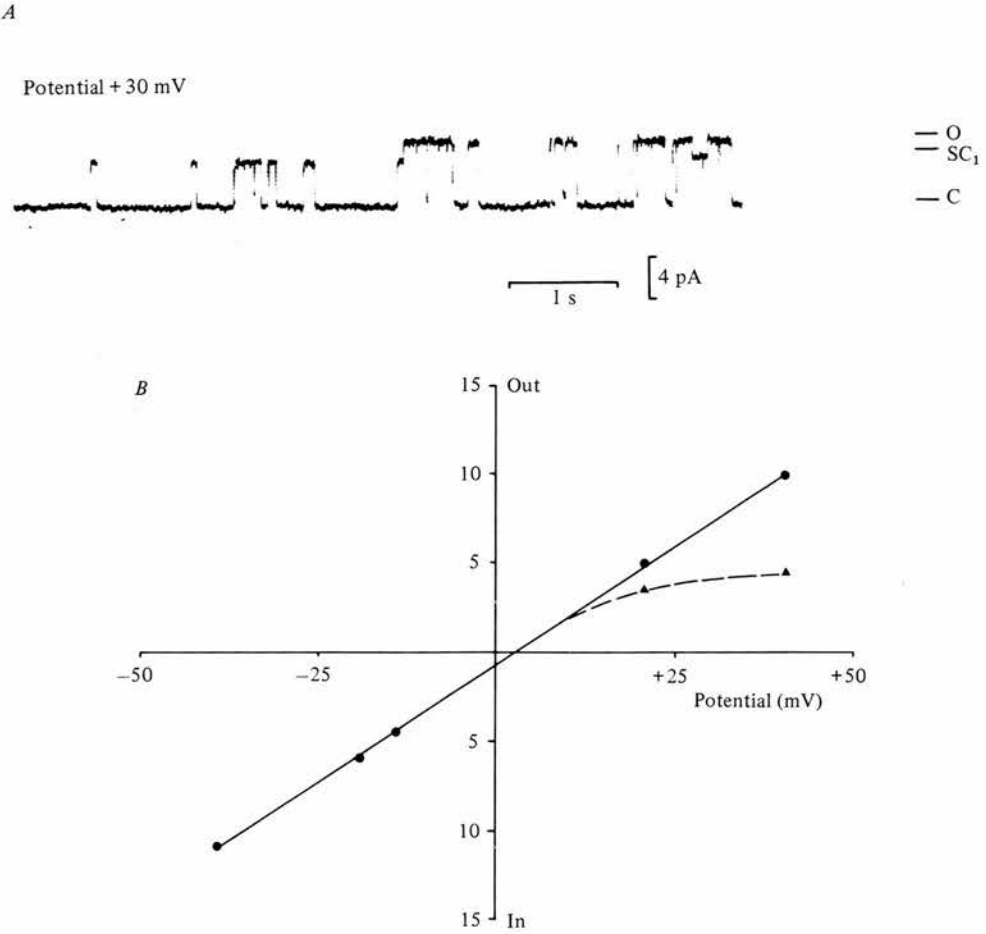


FIG. 6. *A*, channel current records showing subconductance states; isolated inside-out patch; patch potential +30 mV; symmetrical *Ascaris* Ringer solution; main open state, O; closed state, C; subconductance state, SC_1. *B*, a plot of single-channel current amplitudes against trans-patch potential for a cell-attached patch. This graph shows the full conductance of the channel (●) and also the subconductance state of the channel (▲). Subconductance states were only seen at depolarized trans-patch potentials. *Ascaris* Ringer solution was used for the pipette and bathing Ringer solution.

The mean open time for multichannel patches was calculated by the summation of the times spent above each channel level, divided by the total number of observed openings. Similar observation were made using APF Ringer solution.

Distribution of open and closed times suggest complex channel kinetics

Fig. 8 shows open and closed time frequency histograms at −40 and −10 mV from an isolated patch in symmetrical *Ascaris* Ringer solution. The records were obtained from a patch showing only a single-channel opening; at −40 mV the channel was in its main-state conductance. The open distribution (Fig. 8*A* and eqn. (4)) at −40 mV was best described by two exponentials which had a minor component (19% of the total openings) due to openings with a mean open time of 2·7 ms and a major component (81% of the total openings) due to long openings with a mean open time of 61 ms. The closed distribution

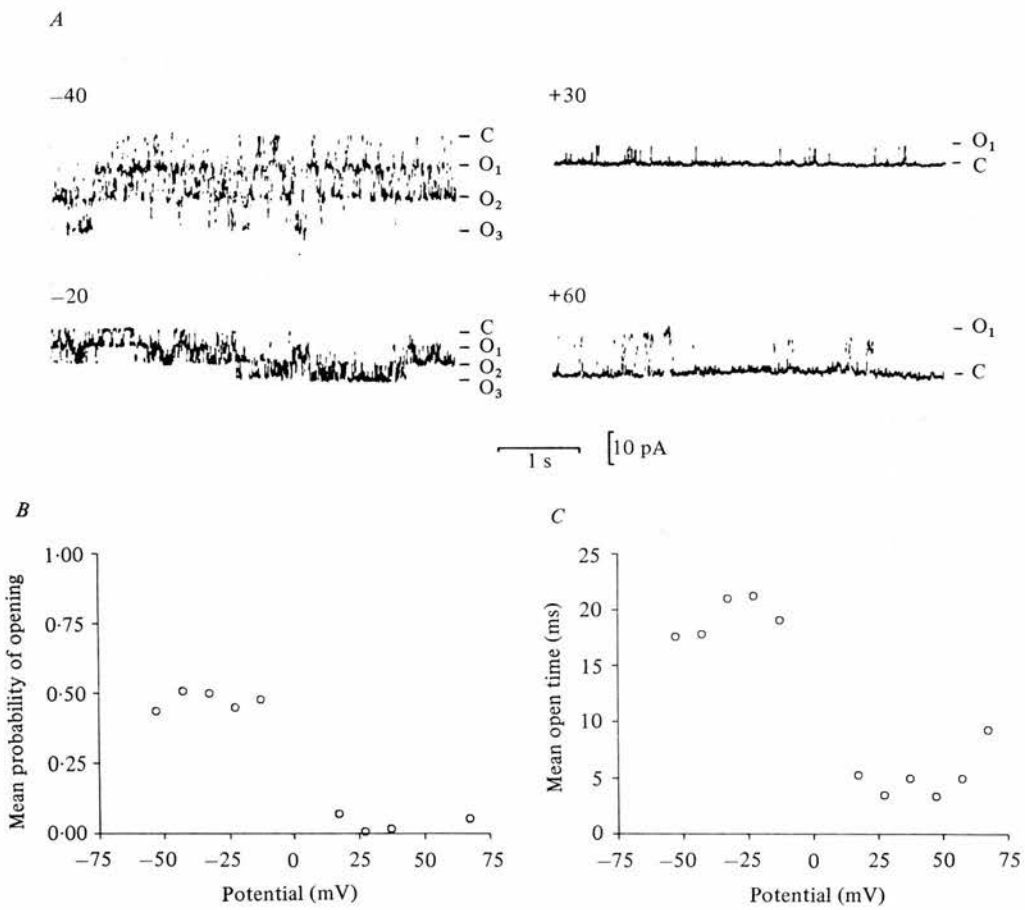


Fig. 7. *A*, examples of current records taken from the same cell-attached patch held at different applied potentials. The current levels indicating zero, one, two and three channels open are shown by C, O_1, O_2 and O_3 respectively. There seem to be up to three channels opening at the hyperpolarized potentials. This is reduced to only one channel open at any given time when the patch is depolarized. The voltage sensitivity is due to marked reduction in the probability of opening and the mean open time. *B*, a graph of the probability of the channel opening against the patch potential derived from the same cell-attached-patch experiment as the channel records in *A*. The dramatic reduction in the probability of the channel opening seen as the patches depolarized was typical of the activity of this high-conductance anion channel. *C*, a graph of the mean open time of the channel against the patch potential derived from the same cell-attached-patch experiment as in *A*. The reduction in the mean open time when the patch was depolarized again was typical of the activity of this high-conductance anion channel.

at −40 mV (Fig. 8 *B* and eqn. (5)) was best described by three exponentials: there was a brief type separating openings into bursts (61% of the total closings, mean closed time 1·1 ms); there was a smaller component separating bursts into clusters (18% of the total closings, mean closed time 10 ms); the third component separating clusters (21% of the total closings) had a mean closed time of 110 ms. These observations suggest the presence of at least two open states and three closed states at −40 mV.

$$P_{\text{open}-40} = 0{\cdot}19/2{\cdot}7 \exp(-t/2{\cdot}7) + 0{\cdot}81/61 \exp(-t/61) \text{ and} \quad (4)$$

$$P_{\text{closed}-40} = 0{\cdot}61/1{\cdot}1 \exp(-t/1{\cdot}1) + 0{\cdot}18/10 \exp(-t/10) + 0{\cdot}21/110 \exp(-t/110), \quad (5)$$

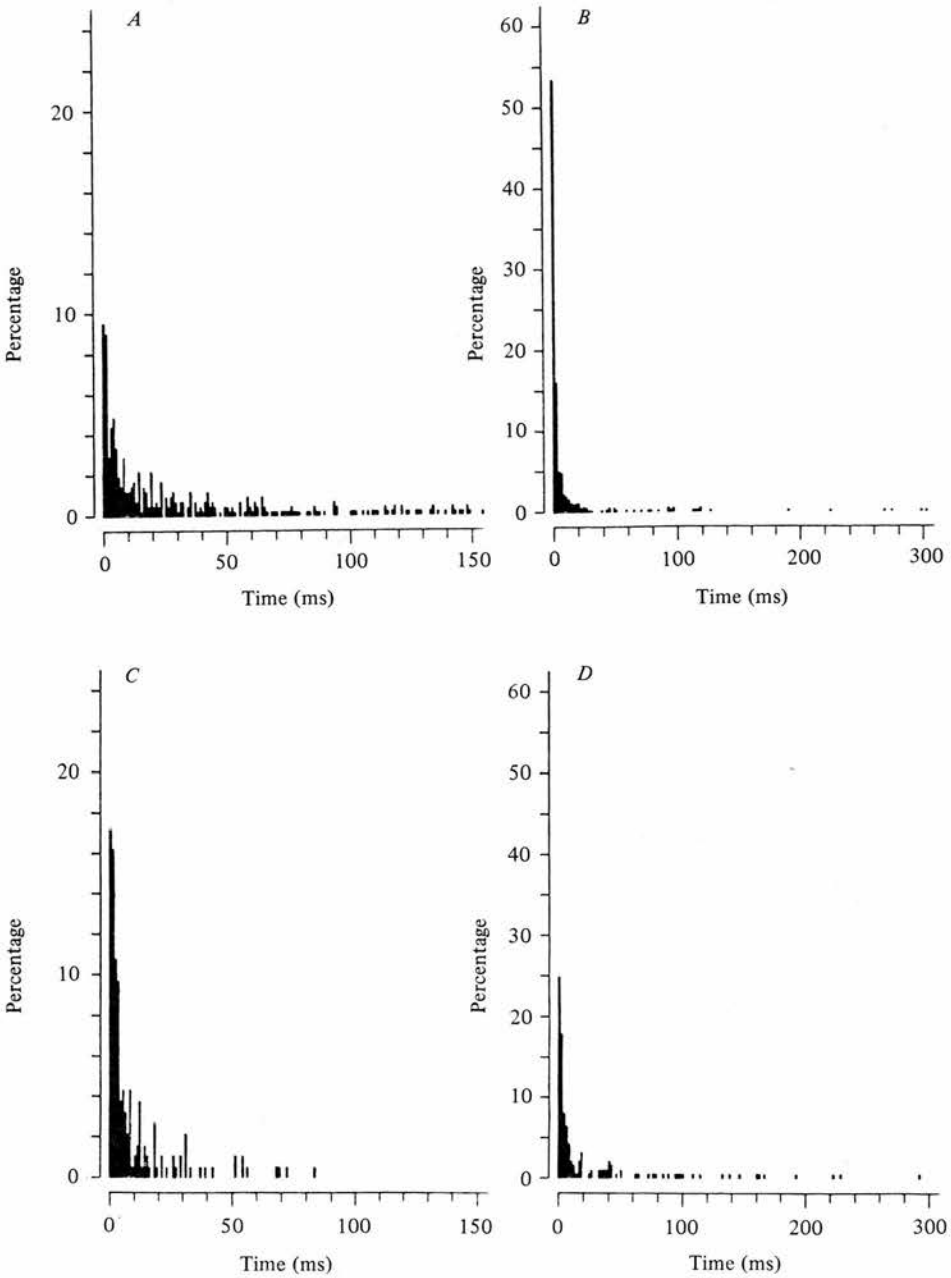


Fig. 8. Four open and closed time histograms. Graphs *A* and *B* are the open and closed times respectively, both taken at a trans-patch potential −40 mV. Graphs *C* and *D* are the open times respectively, both taken at a trans-patch potential of −10 mV. An isolated patch with symmetrical *Ascaris* Ringer solution was used. Only single-channel openings were seen. The probability density functions of the open and closed times are described in the text. Bin widths: open times, 1 ms; closed times, 2 ms. $n = 409$ in *A* and *B*; 185 in *C* and *D*. Mean times: 51 ms (*A*); 14 ms (*B*); 11 ms (*C*); 79 ms (*D*).

where $P_{\text{open}-40}$ and $P_{\text{closed}-40}$ are the probability density functions of open and closed states at -40 mV and t is the time in milliseconds.

Two components in the open time distributions and three components in the closed time distributions were distinguished at potentials between -40 and -10 mV; however, the proportion of time the channel was open decreased on depolarization. Eqns. (6) and (7) describe the distribution of the open and closed times at -10 mV.

$$P_{\text{open}-10} = 0{\cdot}58/1{\cdot}9 \exp(-t/1{\cdot}9) + 0{\cdot}62/16 \exp(-t/16) \text{ and} \quad (6)$$

$$P_{\text{closed}-10} = 0{\cdot}66/3{\cdot}5 \exp(-t/3{\cdot}5) + 0{\cdot}25/44 \exp(-t/44) + 0{\cdot}19/242 \exp(-t/242), \quad (7)$$

where $P_{\text{open}-10}$ and $P_{\text{closed}-10}$ are the probability density functions of open and closed states at -10 mV.

At depolarized potentials the number of components recognized in the open time distribution varied between one and two; the number of components in the closed distribution varied between two and three: this variation was in part due to reduced resolution because of the very brief open times and the appearance of subconductance states. It is clear from these observations that the channel shows complex kinetics with the distributions of open and closed times suggesting multiple states.

Effect of intracellular Ca

Fig. 9 shows the typical effect of Ca application to the intracellular side of an isolated patch. In this experiment the bath was perfused with symmetrical zero-Ca APF Ringer solution. It can be seen that when Ca was applied briefly (2 s) using diffusion from a second micropipette placed nearby and containing 0·5 M calcium acetate, there is a dramatic increase in the number of channels open. The channels then closed down as the Ca concentration declined.

Fig. 10 *A* and *B* shows similar experiments on two separate isolated patches in symmetrical zero-Ca APF which were designed to compare the effects of intracellular application of $CaCl_2$ and calcium acetate. It can be seen that calcium acetate only stimulates channel openings but that $CaCl_2$ increases the amplitude of channel current as well. This latter effect can be explained by an increase in Cl on the intracellular side of the patch producing an increase in channel conductance. The *I–V* plot of the Ca-activated channel in APF and *Ascaris* Ringer solution showed that it had the same high conductance as the channel previously described. These results taken together indicate the presence of a Ca-dependent Cl channel in the membrane.

Dose-dependent effect of Ca

Fig. 11 shows examples of current records using a cell-attached patch from a preparation previously treated with the Ca ionophore A23187. Different intracellular free-Ca concentrations were achieved by perfusing the preparations with different Ca concentrations in the bath (applied randomly). It can be seen that the number of channels opening and the probability of being open increases with the free-Ca concentration. The dose producing 50% of the maximum response (ED_{50}) in this preparation was 200 μM. Similar results were obtained from three other preparations. Although this approach illustrates the Ca-dependent nature of the channel, uncertainties about the concentration of Ca inside the cell prevent an accurate estimation of the ED_{50}. In an attempt to overcome the equilibration problem associated with cell-attached patches isolated patches were used, but this was more difficult since channel activity was frequently lost as a result of the mechanical disturbance associated with perfusion.

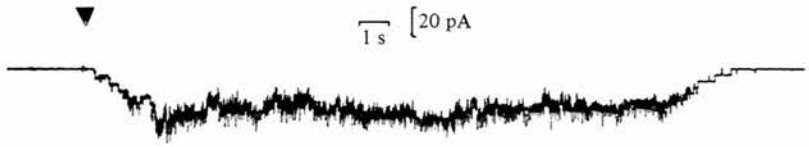


Fig. 9. Channel records showing the effect of Ca applied to the intracellular surface of an isolated patch. A broken pipette (containing 0·5 mM calcium acetate) was used to apply Ca by diffusion to the intracellular side of the membrane patch for a period of about 2 s. The start of the application indicated by (▼). The trans-patch potential was maintained throughout the experiment at −35 mV: the bathing Ringer solution was Ca-free APF; the patch pipette contained the same Ringer solution.

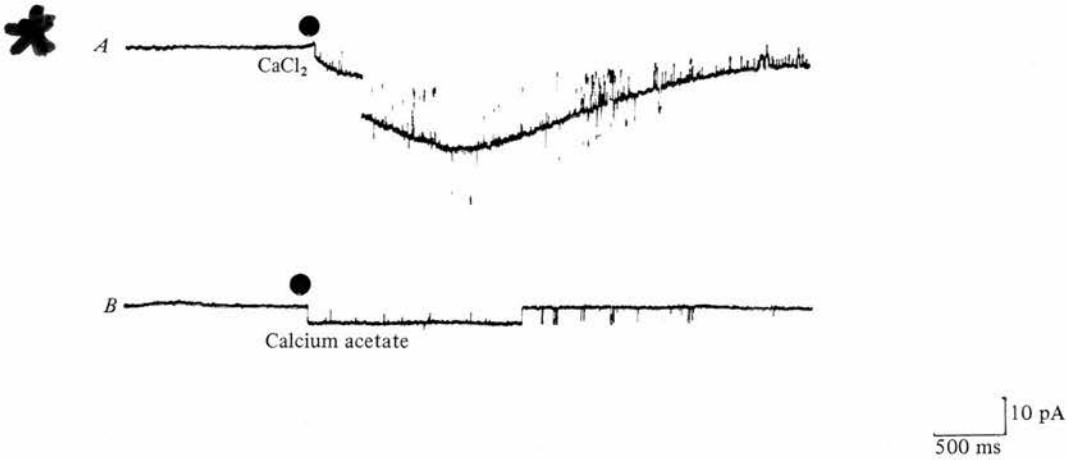


Fig. 10. Current records taken from isolated patches showing the differential effect of application of $CaCl_2$ and calcium acetate to the intracellular surface of an isolated patch. Patch potentials −40 mV. *A*, current records showing the effect of application of $CaCl_2$; after application (●) there is a transient increase in the probability of opening and also an increase in the channel amplitude. *B*, current records showing an increase in the probability of opening after the application of calcium acetate (●) but no increase in the amplitude of the single-channel current. This difference is explained by an increase in the Cl concentration at the intracellular surface of the membrane.

Binomial distribution

Fig. 12 shows the observed times (bars) 0, 1, 2 and 3 channels were open in a multichannel isolated-patch recording (using *Ascaris* Ringer solution) at four different patch potentials. If the channels were operating independently with the same probability of opening, the time spent with 0, 1, 2...n channels open would be described by the binomial distribution (eqn. (10)).

$$P_r = \frac{n}{r\,(n-r)}\,P^r(1-P)^{n-r}, \tag{10}$$

where n is the number of channels in the patch, r is the number of channels open and P is the probability that any given channel is open. P was estimated from the total proportion of open time spent at each channel level divided by n. Fig. 12 also shows the prediction of the binomial distribution. It can be seen that when the patch was hyperpolarized two channels were open more frequently than predicted; less time was spent with one and three channels open than predicted. At more depolarized patch potentials the deviations from the binomial distribution were less. The probability of each channel opening was found to

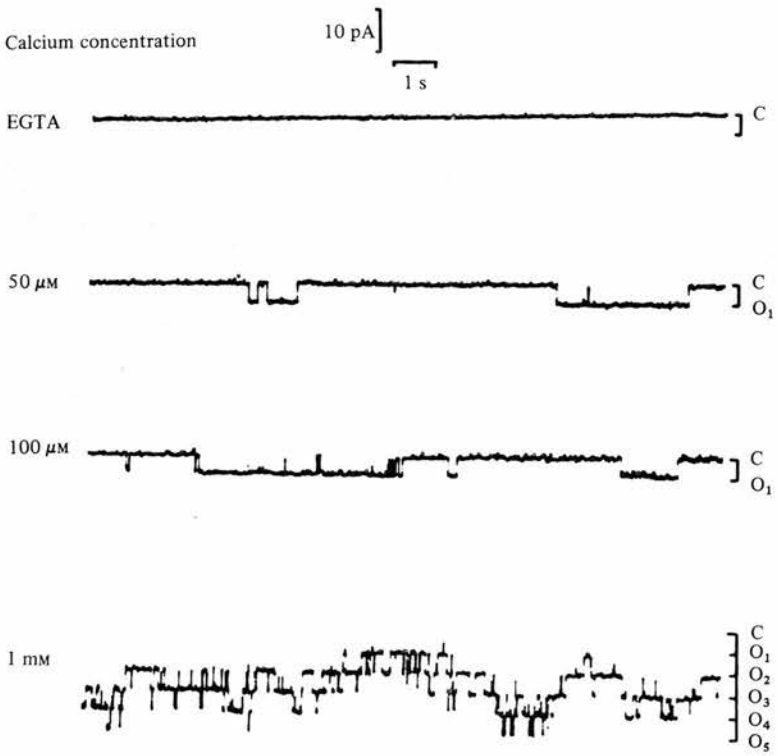


Fig. 11. Current records from a cell-attached patch all held at a trans-patch potential of −40 mV. The preparation was made permeable to Ca using the ionophore A23187. The preparation was bathed in different free-Ca concentrations applied in random order, by constant perfusion for at least 300 s. Up to five channels are open in this patch. The current level indicates the different number of channels open C, O_1, O_2, O_3, O_4 and O_5. EGTA contains zero-Ca.

decrease considerably on depolarization. Similar results were obtained from twelve experiments analysed in the same way. There is more than one explanation for these observations centred on the fact that the assumptions of the binomial distribution are not adequate during hyperpolarization but that they become an adequate approximation during depolarization. They are discussed later.

DISCUSSION

Voltage sensitivity

The Ca-dependent Cl channels of the *Ascaris* preparation increased their probability of being open as the membrane potential was hyperpolarized. This particular pattern of behaviour is similar to the Cl conductance of *Aplysia* neurones reported by Chesnoy-Marchais (1983) and the Cl channel of the mollusc, *Lymnaea stagnalis*, studied by Geletyuk & Kazachenko (1985). The voltage dependence of the molluscan Cl channel was shown to be dependent on the extracellular K ion concentration, this contrasts with apparently normal channel behaviour of the *Ascaris* Cl channel in the absence of K and Na ions. The Ca-dependent Cl conductance found in *Xenopus* oocytes was activated by depolarization (Miledi, 1982). High-conductance voltage-sensitive anion channels have been found in

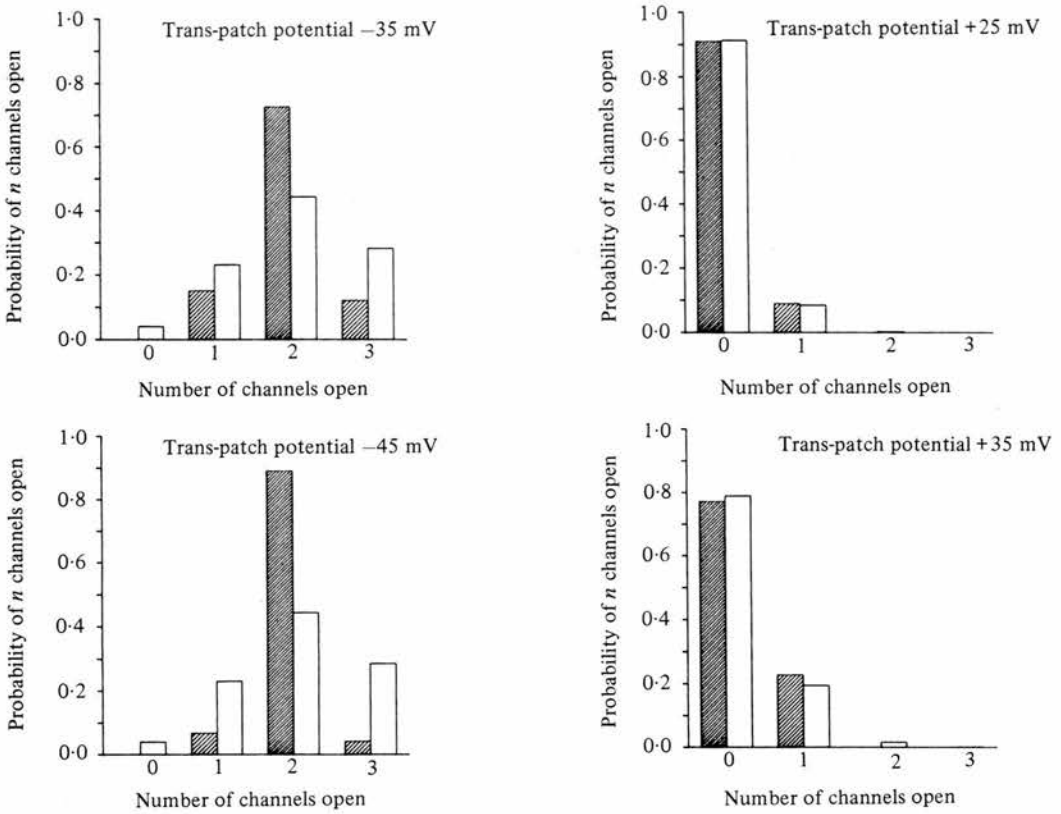


Fig. 12. Plots of the probability of zero, one, two and three channels opening. There are four graphs taken from the same isolated-patch experiment, each at the indicated trans-patch potential. The open bars show the probability of zero, one, two and three channels open predicted by the binomial distribution calculated from the observed mean probability of opening. The shaded bars show the observed probability of seeing zero, one, two and three channels open. The values are not in close agreement over all potentials.

many other preparations. These include: rat muscle (Blatz & Magleby, 1983), rabbit bladder epithelial tissue (Hanrahan, Alles & Lewis, 1985) and Schwann cells (Gray, Bevan & Ritchie 1984). All are characterized as having a voltage 'window'. In the Schwann cell the Cl channel is active only within a limited range of potentials, i.e. between -10 and -40 mV. Outside this range the channel probability of being open decreases. In epithelial tissue a high-conductance Cl channel is described as being spontaneously active between ± 20 mV. In rat muscle the channel is active at around a trans-patch potential of 0 mV rapidly and reversibly closing at potentials away from 0 mV. These observations taken together indicate the wide and varying voltage sensitivity for Cl channels.

Other modulating factors

Isolated patches from the *Ascaris* preparation often lost their activity during mild mechanical disturbance of the patch such as perfusion, even in the presence of Ca. Gray *et al.* (1984) have described a Cl channel in the Schwann cell and Kolb, Brown & Murer (1985) describe a Cl channel in MDCK secretory epithelial cells; both types of channels show an increase in the probability of opening when the patch is isolated. This behaviour on isolation is opposite to that which is observed for this *Ascaris* channel. The suggested

modulating factor or factors in *Ascaris* may be responsible for some variations seen in the Ca sensitivity of individual preparations. However, this is not the only explanation; for example the Ca sensitivity of channels may change during development (Blair & Dionne, 1985).

Subconductance

Reduced current steps at depolarized potentials were a property of the Cl-channel *I–V* relationships. The non-linearity was thought to be due to the reduced probability of the channel being open in the main state and the occurrence of subconductance levels at depolarized potentials. We also considered the possibility that the non-linearity represented the activity of other channels which were observed only when the high-conductance Cl channel was turned off during depolarization. We have not observed in this preparation smaller-conductance channels in the absence of the large Cl channel which are voltage sensitive and also close down on depolarization. We therefore believe that the non-linearity seen in the *I–V* plots is due only to the appearance of subconductance states during depolarization. We have not seen subconductance during hyperpolarization.

Binomial distribution and channel opening

In this study of the Ca-dependent Cl channel of *Ascaris* we found that the behaviour of multichannel records could not be well described by the binomial distribution. This observation contrasts with some other reports from multichannel records e.g. Barratt, Magleby & Pallotta (1983); where the distributions of the time spent with different numbers of channels open in the patch were well described by the binomial distributions. However, other studies on channel activity described by Miller (1982), have shown distributions different to that predicted by the binomial. In the *Torpedo* electroplax preparation, Miller (1982) suggested that two channels are coupled together and that their openings are linked.

One explanation for our observations on multichannel records not fitting with the binomial could be due to the relatively short (200 s) sample times we have used compared with the slow channel kinetics: since there are likely to be at least two open main states it could have been that the sample favoured the long opening state of one channel but the brief opening state of another. Thus it would appear that two channels observed have a different probability of being open. Another possible explanation for the behaviour of the channels is a connexion between the channels opening such that when one channel opens this makes the opening of another adjacent channel less likely. In fact our observations are consistent with both types of behaviour. However, we believe that the simpler explanation is that the channels do indeed have differing probabilities of opening. This difference in the probability of opening may decline on depolarization so that the binomial distribution better describes the number of channels open.

Function of the Ca-dependent Cl channel

The resting membrane potential of the *Ascaris* has been the subject of a number of studies (e.g. Del Castillo *et al.* 1964; Brading & Caldwell, 1971). One of the conclusions of their work was the fact that membrane potential is not greatly influenced by K but that Cl has a marked effect. Cl has also been shown to have a greater permeability than Na or K (Caldwell & Ellory, 1968). The large conductance of the Ca-activated Cl channels described in this paper, the frequency with which they were observed and the fact that they can be fully activated at -35 mV suggests that they can contribute to the resting Cl permeability of the membrane. This is particularly likely if the intracellular Ca concentration is high.

The movement of Cl ions against an ionic gradient observed by Hobson *et al.* (1952) indicates the presence of a Cl pump. This may be situated either in the hypodermis or the somatic muscle. If the pump were situated in the somatic muscle cells the membrane potential would be critically dependent on the activity of this pump given the high permeability of the membrane to Cl (Cauldwell & Ellory, 1968). In mammalian skeletal muscle for example the combination of high permeability to Cl and a Cl pump have been used to account for the resting potential which may not be adequately described by the passive distribution of ions (Dulhunty, 1978).

The bag membrane of *Ascaris* normally shows regular depolarizing and spike potentials involving the influx of Ca (Jarman, 1959; Weisblat *et al.* 1976). A rise in the intracellular Ca concentration associated with the spike could lead to the activation of Ca-dependent Cl channels. Other Ca-activated Cl conductances have been reported in mouse spinal neurones (Owen, Segal & Barker, 1983), *Xenopus* oocyte (Miledi, 1982) and molluscan neurones (Geletyuk & Kazachenko, 1985); all have been suggested to produce a repolarization after an action potential. A Ca-activated Cl conductance in rat dorsal root ganglia cells observed by Mayer (1985) has been proposed to give rise to depolarizing long-lasting after-potentials. In the *Ascaris* Cl channel the voltage sensitivity is not compatible with a function of repolarization after a Ca spike.

Ca-dependent Cl channels have also been described in glandular secretory tissue where their existence is important for salt secretion e.g. Marty, Tan & Trautmann (1984) and Findlay & Petersen (1985). In the lacrimal-gland preparation (Marty *et al.* 1984) the unit conductance of the Ca-dependent Cl channel is 1–2 pS which is two orders of magnitude smaller than channels reported here. None the less, it is possible that this channel found in *Ascaris* is also involved in movement of Cl across the body wall.

We would like to thank the technical staff of the department, and also the staff at the abattoir for supply of *Ascaris* throughout this project. P. Thorn is a S.E.R.C. C.A.S.E. student with Pfizer Central Research; we are pleased to acknowledge the advice of Dr R. A. F. Gration.

REFERENCES

Barrett, J. N., Magleby, K. L. & Pallotta, B. S. (1982). Properties of single calcium-activated potassium channels in cultured rat muscle. *Journal of Physiology* **331**, 211–230.

Blair, L. C. S. & Dionne, V. E. (1985). Developmental acquisition of Ca sensitivity by K channels in spinal neurons. *Nature* **315**, 329–330.

Blatz, A. L. & Magleby, K. L. (1983). Single voltage-dependent chloride selective channels of large conductance in cultured rat muscle. *Biophysics Journal* **43**, 237–241.

Brading, A. F. & Caldwell, P. C. (1971). The resting membrane potential of somatic muscle cells of *Ascaris lumbricoides*. *Journal of Physiology* **217**, 605–624.

Caldwell, P. C. & Ellory, J. C. (1968). Ion movements in somatic muscle cells of *Ascaris lumbricoides*. *Journal of Physiology* **197**, 75–76*P*.

Chesnoy-Marchais, D. (1983). Characterization of a chloride conductance activated by hyperpolarization in *Aplysia* neurones. *Journal of Physiology* **342**, 277–308.

Del Castillo, J., De Mellow, W. C. & Morales, T. (1964). Influence of some ions on the membrane potential of *Ascaris* muscle. *Journal of General Physiology* **48**, 129–140.

Dulhunty, A. F. (1978). The dependence of membrane potential on extracellular chloride concentration in mammalian skeletal muscle fibres. *Journal of Physiology* **276**, 67–82.

Findlay, I. & Petersen, O. H. (1985). Acetylcholine stimulates a Ca^{2+} dependent Cl^- conductance in mouse lacrimal acinar cells. *Pflügers Archives* **403**, 328–330.

Geletyuk, V. I. & Kazachenko, V. N. (1985). Single Cl^- channels in molluscan neurones: multiplicity of conductance states. *Journal of Membrane Biology* **86**, 9–15.

Glasbey, C. A. & Martin, R. J. (1986). Exploratory and confirmatory plots of single channel records. *Journal of Neuroscience Methods* **16**, 239–249.

GRAY, P. T. A., BEVAN, S. & RITCHIE, J. M. (1984). High conductance anion-selective channels in rat cultivated Schwann cells. *Proceedings of the Royal Society* B **221**, 395–409.

HAMILL, O. P., MARTY, E., NEHER, B., SAKMANN, B. & SIGWORTH, F. J. (1981). Improved patch-clamp techniques for high-resolution current recording from the cells and cell-free membrane patches. *Pflügers Archiv* **391**, 85–100.

HANRAHAN, J. W., ALLES, W. P. & LEWIS, S. A. (1985). Single anion-selective channels in basolateral membrane of a mammalian tight epithelium. *Proceedings of the National Academy of Sciences of the U.S.A.* **82**, 7791–7795.

HOBSON, A. D., STEPHENSON, W. & BEADLE, L. C. (1952). Studies on the physiology of *Ascaris lumbricoides*. 1. The relation of the total osmotic pressure, conductivity and chloride content of the body fluid to that of the external environment. *Journal of Experimental Biology* **29**, 1–21.

HOBSON, A. D., STEPHENSON, W. & EDEN, A. (1952). Studies on the physiology of *Ascaris lumbricoides*. 2. The inorganic composition of the body fluid in relation to that of the external environment. *Journal of Experimental Biology* **29**, 22-29.

JARMAN, M. (1959). Electrical activity in the muscle cells *Ascaris* muscle. *Nature* **184**, 1244.

KOLB, H. A., BROWN, C. D. A. & MURER, H. (1985). Indentification of a voltage-dependent anion channel in the apical membrane of a Cl^--secretory epithelium (MDCK). *Pflügers Archiv* **403**, 262–265.

MARTIN, R. J. (1980). The effect of γ-aminobutyric acid on the input conductance and membrane potential of *Ascaris* muscle. *British Journal of Pharmacology* **71**, 99–106.

MARTIN, R. J. (1985). γ-aminobutyric acid- and piperazine-activated single-channel currents from *Ascaris suum* body muscle. *British Journal of Pharmacology* **84**, 445–461.

MARTIN, R. J. & THORN, P. (1984). A high conductance anion channel in somatic muscle cells of *Ascaris suum*. *Journal of Physiology* **354**, 46*P*.

MARTY, A., TAN, Y. P. & TRAUTMANN, A. (1984). Three types of calcium-dependent channel in rat lacrimal glands. *Journal of Physiology* **357**, 293-325.

MAYER, M. L. (1985). A calcium-activated chloride current generates the after-depolarization of rat sensory neurones in culture. *Journal of Physiology* **364**, 217–239.

MILEDI, R. (1982). A calcium-dependent transient outward current in *Xenopus laevis* oocytes. *proceedings of the Royal Society* B **215**, 491-497.

MILLER, C. (1982). Open-state substructure of single chloride channels from *Torpedo* electroplax. *Philosophical Transactions of the Royal Society B* **299**, 401–411.

OWEN, D. G., SEGAL, M. & BARKER, J. L. (1983). A Ca-dependent Cl conductance in cultured mouse spinal neurones. *Nature* **311**, 567–570.

SAKMANN, B. & TRUBE, G. (1984). Conductance properties of single inwardly rectifying potassium channels in ventricular cells from guinea-pig heart. *Journal of Physiology* **347**, 641–657.

WEISBLAT, D. A., BYERLY, L., & RUSSEL, R. L. (1976). Ionic mechanisms of electrical activity in somatic muscle of the nematode *Ascaris lumbricoides*. *Journal of Comparative Physiology* **111**, 93–113.

Journal of Neuroscience Methods, 24 (1988) 283–287
Elsevier

NSM 00835

The distribution of numbers of open channels in multi-channel patches

C.A. Glasbey [1] and R.J. Martin [2]

[1] *Scottish Agricultural Statistics Service, University of Edinburgh, Edinburgh (U.K.) and* [2] *Department of Preclinical Veterinary Services, Royal (Dick) School of Veterinary Studies, Summerhall, University of Edinburgh, Edinburgh (U.K.)*

(Received 19 August 1987)
(Revised 8 February 1988)
(Accepted 15 February 1988)

Key words: Binomial distribution; Correlated-binomial model; Generalized binomial distribution of Poisson; Interaction of channels

Assumptions inherent in use of the binomial distribution are relaxed in order to identify alternative distributions with different variances, for fitting to the frequency distributions of numbers of open channels in multi-channel patches. The variance is less than that for the binomial distribution with the same expectation when either there is a negative interaction between channels or channels have different probabilities of being open. When the variance is greater, this may be because of positive interaction between channels or non-stationary behaviour. Use of the distributions and lack-of-fit statistics is illustrated.

Introduction

A record from a multi-channel patch can show how many channels are open at a given time, but not which ones they are nor the number which are closed. By averaging over time, a distribution is obtained of the frequencies with which different numbers of channels are open. When the binomial distribution fits well to this, it provides a simple explanation and summary of important features of channel behaviour. This paper addresses the problem of what to do when the binomial fit is poor.

Assumptions inherent in the use of the binomial distribution are identified. By relaxing each of these in turn, generalized binomial distributions are found. A similar approach in a different area of application is followed by Edwards (1960). Properties and methods of fitting are considered. The distributions are illustrated using a set of observed frequency counts of numbers of open channels in a multi-channel patch at different transpatch potentials. The binomial does not describe the frequency distributions of the number of channels open (Thorn and Martin, 1987).

Methods

In the following account the data are treated as idealised in that the frequency of response of the recording system does not affect them.

If there are n channels under a patch, and each has a probability p of being open, independent of the state of all other channels, then the probability of i channels being open at a particular time is

$$P_i = \frac{n!}{i!(n-i)!} p^i (1-p)^{n-i} \quad \text{for } i = 0, 1, \ldots, n$$

where $n!$ denotes n factorial, that is $n \times (n-1)$

Correspondence: C.A. Glasbey, Scottish Agricultural Statistics Service, University of Edinburgh, The King's Buildings, Mayfield Road, Edinburgh EH9 3JZ, U.K.

0165-0270/88/$03.50 © 1988 Elsevier Science Publishers B.V. (Biomedical Division)

$\times \ldots \times 2 \times 1$. This is the binomial distribution; see for example, Johnson and Kotz (1969, pp. 50–86). The number of open channels has an expected (mean) value of np and a variance of $np(1-p)$, which is always of smaller magnitude than the expected value. Given observed frequencies $x_0, x_1, \ldots, x_m$, summing to 1, of 0, 1, ..., m channels being open in a particular experiment, parameters n and p can be estimated by maximizing the scaled log-likelihood

$$\sum_{i=0}^{m} x_i \log_e P_i$$

using a numerical optimization routine. However, if p is small and n is large, then the binomial distribution approaches the Poisson distribution and n becomes indeterminate (Sachs et al., 1982). More simply, if n is assumed to be known, then the estimator of p is simply

$$\frac{1}{n} \sum_{i=0}^{m} i x_i$$

Three important assumptions which underly the use of the binomial distribution are: (a) all channels have the same probability p of being open, (b) channels behave independently of one another, and (c) the value of p remains constant over the course of the experiment. We will consider the effect of relaxing each assumption in turn.

Consider a population of channels under the patch, which all have the same conductance, but where each channel has different kinetics: this might arise, for example, if the channels could exist in different long-lasting states of phosphorylation (Spruce et al., 1987). If the jth channel has probability q_j of being open, then the probability of i channels being open is the coefficient of t^i in the probability generating function

$$[(1-q_1)+q_1 t] \times [(1-q_2)+q_2 t] \times \ldots \times [(1-q_n)+q_n t]$$

For example, if n equals 3, then this expression equals

$$\begin{aligned}&[(1-q_1)(1-q_2)(1-q_3)]t^0 \\ &+ [q_1(1-q_2)(1-q_3) + (1-q_1)q_2(1-q_3) \\ &+ (1-q_1)(1-q_2)q_3]t^1 + [q_1 q_2(1-q_3) \\ &+ q_1(1-q_2)q_3 + (1-q_1)q_2 q_3]t^2 + [q_1 q_2 q_3]t^3\end{aligned}$$

and the probability of no open channels is the coefficient of t^0, that is $[(1-q_1)(1-q_2)(1-q_3)]$, one open channels has a probability given by the coefficient of t^1, that is

$$\begin{aligned}&[q_1(1-q_2)(1-q_3) + (1-q_1)q_2(1-q_3) \\ &+ (1-q_1)(1-q_2)q_3]\end{aligned}$$

and similarly for coefficients of t^2 and t^3. This is called the generalized binomial distribution of Poisson. (See for example, Johnson and Kotz, 1969, p. 80.) The number of open channels has an expected value of $n\bar{q}$, where $\bar{q}$ is the average q-value, that is

$$\bar{q} = \frac{1}{n} \sum_{j=1}^{n} q_j$$

and a variance of

$$n\bar{q}(1-\bar{q}) - \sum_{j=1}^{n} (q_j - \bar{q})^2$$

Therefore the variance of the generalized binomial distribution of Poisson is less than that of the binomial distribution with the same mean value, unless all the q-values are equal, in which case the distributions are identical. Samuels (1965) proved that, whatever the q-values, the distribution has the same form as the binomial, that is it is unimodal and has a characteristic bell shape except at the boundary constraints of 0 and n. Values of q can be estimated from data by numerically maximizing the scaled log-likelihood, as for the binomial distribution.

A channel may interact with one or several of its neighbours as proposed in the "lattice model" of Changeux et al. (1967). The dimer model is the simplest and can be based, for example, on the nicotinic receptor of the electric organ which can be found in a dimeric form joined by disulphide bonds between adjacent δ subunits (Reynold and Karlin, 1978). From a statistical perspective, Kupper and Haseman (1978) and Altham (1978) considered a generalization of the binomial distribution which allows the binary variables, channels in our case, to interact with one another. The simplest generalization is where there are only pair-wise interactions, which are all equal. For example, if a channel has a probability p of being

open, but there is a correlation of c between pairs of channels, then the probability of two channels both being open is $p^2 + cp(1-p)$, rather than p^2 as in the binomial distribution when channels behave independently. The probability of neither channel being open is $(1-p)^2 + cp(1-p)$, and the probability of one open and one closed channel is $2p(1-p) - 2cp(1-p)$. This has been termed the additive generalization of the binomial distribution by Altham (1978), and for n channels leads to

$$P_i = \frac{n!}{i!(n-i)!} p^i (1-p)^{n-i} \times \left[1 + \frac{c}{2p(1-p)} \left\{(i-np)^2 + i(2p-1) - np^2\right\}\right]$$

Values of c need to be restricted to ensure that P_i does not take negative values. The number of open channels has an expected value of np, as for the binomial distribution, but a variance of

$$np(1-p)\{1 + (n-1)c\}$$

When c equals zero the distribution reduces to the binomial. For c greater than zero the distribution has greater variance than the binomial, and for c less than zero it has smaller variance than the binomial. Again, values for p and c, and n if required, can be estimated by maximizing the scaled log-likelihood, as for the binomial distribution.

Altham (1978) also considered a multiplicative generalization of the binomial distribution which allows for more extreme interactions but is more difficult to interpret and has the undesirable property that if a subset only of a group of interacting channels is under the patch, then this will not have the same form of distribution. Kupper and Haseman (1978) set their choice of additive pairwise interactions within the framework of a more general model which allows for interactions between triplets, quadruplets, etc. of binary variables over and above that resulting from pairs interacting.

The third generalization of the binomial distribution is that which arises from allowing p to vary. Mathematically, the simplest assumption is that p follows a beta distribution, which is a continuous distribution between 0 and 1 with two parameters, and leads to a beta-binomial distribution (Johnson and Kotz, 1969, pp. 78–79). However, this does not necessarily make any physical sense. In the case of ion channels, any drift over time in the probability p of a channel being open will manifest itself as non-stationarity in the time record. The effect will always be to inflate the variance of the frequency distribution over that for a binomial distribution with the same expectation.

In summary, relaxing assumption (a) will decrease the variance, (c) will increase it and (b) may do either.

Illustration of lack-of-fit statistic

Idealised frequencies (portions of time) with which channels are open in a patch may be estimated from current-density histograms (Thorn and Martin, 1987). An example at 4 hyperpolarised potentials from an inside-out patch in which 0, 1, 2 and 3 high conductance Cl channels were open is shown in Table I. Binomial, correlated binomial and generalized binomial distributions were fitted, in each case by maximizing the scaled log-likelihood with n set to 3, the maximum number of channels which were ever open. Table I summarizes the results, giving estimated parameter values and fitted frequencies for the data.

In the Table is also given a lack-of-fit statistic

$$1000 \times \left\{ \sum_{i=0}^{m} x_i (\log_e x_i - \log_e P_i) \right\}$$

which takes the value of zero when the fit is perfect, that is $P_i = x_i$ for all i, and is otherwise positive. The statistic is the scaled difference between the maximized value of the log-likelihood for a particular distribution and the maximum possible. If the data consisted of independent counts then a formal likelihood-ratio test of significance could be performed using this statistic. However, this is not the case, but it does not

TABLE I

PARAMETER ESTIMATES, OBSERVED AND ESTIMATED FREQUENCIES OF OPEN CHANNELS AND LACK-OF-FIT STATISTICS FOR 3 DISTRIBUTIONS FITTED TO DATA AT EIGHT TRANSPATCH POTENTIALS WITH n SET TO 3

B denotes the binomial distribution, aB the additive generalization of the binomial distribution and gBP the generalized binomial distribution of Poisson

Transpatch potential (mV)	Distribution	% probability channel open	% correlation	% frequencies of (0, 1, 2, 3) channels open (observed values bracketted)	lack-of-fit statistic
−46				(11, 38, 40, 11)	
	B	51		12, 37, 38, 13	3
	aB	51	−5	10, 39, 40, 11	0
	gBP	30, 55, 67		11, 38, 40, 11	0
−36				(0, 16, 51, 33)	
	B	72		2, 17, 43, 38	32
	aB	72	−13	0, 15, 52, 32	0
	gBP	46, 70, 100		0, 16, 51, 33	0
−26				(0, 34, 64, 1)	
	B	55		8, 33, 41, 17	256
	aB	55	−30	0, 45, 52, 3	35
	gBP	2, 66, 99		0, 34, 64, 1	0
−16				(7, 36, 57, 0)	
	B	50		13, 38, 37, 12	182
	aB	50	−28	4, 53, 43, 0	63
	gBP	0, 75, 75		6, 38, 56, 0	1

invalidate the use of the statistic to measure lack of fit.

The observed distributions have smaller variances than the binomial distributions with the same means. Poisson's generalization achieves a near perfect fit in all four cases. The correlated generalization also fits well at potentials of −36 mV and −46 mV, by assuming a negative association between channels, but cannot achieve a sufficiently severe reduction in variance at the two other potentials of −16 mV and −26 mV.

Discussion

We have suggested a treatment for data provided that they are not limited by the frequency response of the recording system. This is more likely to occur when the channel currents are large and have long dwell times but not when currents are small and/or brief.

The frequency distribution of multi-channel patches has been assumed to be described by the binomial distribution (e.g. Barrett et al., 1982). More recently several accounts have appeared where the binomial fails to predict the frequency distribution (Benham and Bolton, 1983; Spruce et al., 1987, Thorn and Martin, 1987).

The lack of fit of the binomial distribution to an observed frequency distribution of open channels under a multi-channel patch may be due to channels having different probabilities of opening, channels interacting or channels changing behaviour over time. If the latter possibility can be eliminated by examining time records, then the choice is between the other two.

In cases where the observed variance is less than that for the binomial distribution there are two contending explanations. The results may be explained either by channels interacting negatively or by channels having different probabilities of opening. In the data set used here the generalised

binomial distribution fits more closely but uses more parameters to do so.

If the variance is greater than that for a binomial distribution with the same expectation, then this can only be explained by positive interaction between channels, i.e. when one channel opens the probability of others opening increases, and conversely with closures.

It may be possible to use other features of channel records, such as transition probabilities, to distinguish between competing theories. Records may even show evidence of channel interaction without the frequency distribution being affected (Yeramian et al., 1986).

Acknowledgements

We thank Peter Thorn for permission to use the data and Bernard Ginsborg for his interest in our work. C.A. Glasbey and R.J. Martin acknowledge financial support, respectively, from the Agricultural and Food Research Council and the Science and Engineering Research Council.

References

Altham, P.M.E. (1978) Two generalizations of the binomial distribution, Appl. Statist., 27: 162–167.

Barrett, J.N., Magleby, K.L. and Pallotta, B.S. (1982) Properties of single calcium-activated potassium channels in cultured rat muscle, J. Physiol. (Lond.), 331: 211–230.

Benham, C.D. and Bolton, T.B. (1983) Patch-clamp studies of slow potential-sensitive potassium channels in longitudinal smooth muscle cells of rabbit jejunum, J. Physiol (Lond.), 340: 469–486.

Changeux, J.P., Thiery, J., Tung, Y. and Kittel, C. (1967) On the cooperativity of biological membranes, Proc. Natl. Acad. Sci. U.S.A., 57: 335–341.

Edwards, A.W.F. (1960) The meaning of binomial distribution, Nature (Lond.) 186: 1074.

Johnson, N.L. and Kotz, S. (1969) Distributions in Statistics, Volume 1: Discrete Distributions, Wiley, New York.

Kupper, L.L. and Haseman, J.K. (1978) The use of a correlated binomial model for the analysis of certain toxicological experiments, Biometrics, 34: 69–76.

Reynold, J.A. and Karlin, A. (1978) Molecular weight in detergent solution of acetylcholine receptor from *Torpedo californica*, Biochemistry, 17: 2035–2038.

Sachs, F., Neil, J. and Beukakati, N. (1982) The automated analysis of data from single ionic channels, Pflügers Arch, 395: 331–340.

Samuels, S.M. (1965) On the number of successes in independent trials, Ann. Math. Statist., 36: 1272–1278.

Spruce, A.E., Standen, N.B. and Stanfield, P.R. (1987) Studies of the unitary properties of adenosine-5′-triphosphate-regulated potassium channels of frog skeletal muscle, J. Physiol. (Lond.), 382: 213–236.

Thorn, P. and Martin, R.J. (1987) A high conductance calcium-dependent chloride channel in *Ascaris suum* muscle, Q. J. Exp. Physiol., 72: 31–49.

Yeramian, E., Trautmann, A. and Claverie, P. (1986) Acetylcholine receptors are not functionally independent, Biophys. J., 50: 253–263.

J. Membrane Biol. 131, 143–149 (1993)

The Journal of
Membrane Biology
© Springer-Verlag New York Inc. 1993

A Patch-Clamp Study of the Ionic Selectivity of the Large Conductance, Ca-Activated Chloride Channel in Muscle Vesicles Prepared from *Ascaris suum*

D.M. Dixon, M. Valkanov†, and R.J. Martin

Department of Pre-Clinical Veterinary Sciences, R.(D).S.V.S., University of Edinburgh, Edinburgh EH9 1QH, and †Central Laboratory of Biophysics, Bulgarian Academy of Sciences, Sofia, Bulgaria

Summary. Plasma membrane vesicles prepared from the bag region of the somatic muscle cell of the parasite *Ascaris suum* contain a large conductance, voltage-sensitive, calcium-activated chloride channel. The ability of this channel to conduct a variety of anions has been investigated using the patch-clamp technique on isolated inside-out patches of muscle membrane. Symmetrical Cl solutions (140 mM) produced single-channel I/V plots with reversal potentials of 0 mV, substitution of bath Cl by 140 mM NO_3, Br and I caused depolarizing shifts in the reversal potentials. Replacement of the internal Cl by F (140 mM) caused a large hyperpolarizing shift in the reversal potential. The channel displayed a permeability sequence of $I > Br = NO_3 > Cl > F$ which differed from the corresponding conductance sequence $Cl > NO_3 = Br = I > F$. The ionic environment within the channel pore has been investigated using Reuter and Stevens (1980) plots to describe the selectivity and "fluidity" of the channel pore. In addition, the approach of Wright and Diamond (1977) was employed to estimate the number of cationic binding sites within the channel pore. The channel is relatively fluid but the number of cationic binding sites varies inversely with the ionic radius of the anion from 2.15 for F to 0.89 for the large planar anion NO_3.

Key Words *Ascaris suum* · chloride channels · calcium · anion channel · ionic permeability

Introduction

Ascaris suum is a large intestinal nematode parasite of the pig which has been developed as a preparation suitable for electrophysiological study (Jarman, 1959; Martin, 1980). The somatic muscle cells of *Ascaris* (Rosenbluth, 1965*a*,*b*; 1967) are divided into three regions: (i) a large balloon-shaped structure containing the nucleus known as the bag, (ii) a contractile spindle region, (iii) a thin process known as the arm that passes from the bag to a nerve cord.

Studies investigating the ionic basis of the resting membrane potential recorded from the bag region of the muscle cell (Del Castillo, DeMellow & Morales, 1964; Brading & Caldwell, 1971) found that the low resting membrane potential, −30 mV, was little affected by extracellular potassium but extracellular chloride had large effects, demonstrating a relatively high chloride permeability. Ion flux experiments (Caldwell & Ellory, 1968) recorded permeability ratios for K, Na and Cl of 1 : 4 : 7, respectively.

Subsequently, single-channel studies on the muscle bag region have shown that there are at least three types of chloride channel present in the membrane. There is a 22 pS GABA-activated channel (Martin, 1985), a 9–15 pS channel which may be activated by the anthelmintic dihydroavermectin (Martin & Pennington, 1989) and a 200 pS high conductance Ca-activated chloride channel (Thorn & Martin, 1987). In this paper we have investigated further the nature of the anion permeability of the high conductance Ca-activated chloride channel with a view to gaining further insight into its function.

Materials and Methods

Preparation of Muscle Vesicles

A. suum were obtained from the local slaughter house and maintained at 37°C in Locke's solution. The Locke's solution was changed daily and the worms were discarded after 4–5 days. A 2 cm section of worm, taken 5 cm below the head region, was cut along one lateral line, the gut removed and the resulting flap pinned out, cuticle side down, onto the base of a Sylgard coated petri dish. The preparation was washed with extracellular solution (concentration in mM): NaCl, 35; Na Acetate, 105; KCl, 2; $MgCl_2$, 2; HEPES, 10; glucose, 3; ascorbic acid, 2; EGTA, 1; pH 7.2 with NaOH. The flap was then incubated for 10 min in enzyme solution (collagenase, 1 mg/ml in EGTA-free extracellular solution). Following enzyme treatment the preparation was thoroughly washed and incubated in extracellular solution at 37°C. Approximately 1

hr after collagenase treatment vesicles could be seen "budding" off the bag region of the muscle cell. These muscle vesicles were easily harvested with a Pasteur pipette and placed into the recording chamber.

Recording Setup

Microelectrodes were pulled from micro-hematocrit capillary glass (Garner Glass 7052) of resistance 1–3 MΩ and coated with Sylgard to improve frequency responses. Single-channel recordings were made from inside-out patches of muscle membrane with seal resistances >1GΩ. The currents were monitored using a List EPC7 current-voltage converter. The signal was filtered by an 8-pole Bessel filter (3 dB, 1 kHz), recorded on computer diskette using an IBM PC2/70 and monitored on an oscilloscope (Tektronix 5113 dual beam). Experiments were carried out using CED Patch Clamp Software in conjunction with a CED 1401 intelligent interface. Using this system, a precise pattern of pulsed stimulation was applied to the patch and recorded directly to disk for analysis. The two protocols used to stimulate channel activity are illustrated below. Voltage sensitivity of the channel openings was illustrated using stimulation protocol 1 while continuous *I/V* plots were obtained using stimulation protocol 2 (*see* Fig. 1). Samples were taken at a rate of 7.5 kHz and currents were averaged over 10 points (i.e., over 1.3 ms) to further reduce noise during estimation of reversal potentials.

Experimental Procedure

Experiments were performed at room temperature (15–22°C). The experimental chamber was mounted on the stage of a Reichert-Jung Biostar inverted microscope and viewed at 200× magnification.

Ion substitution experiments were carried out using a series of fine capillary perfusion tubes supplying various solutions to the recording chamber. Gravity fluid supply provided a steady linear flow of test solutions into which the patch electrode was moved allowing up to five different solutions to be tested on each patch. The pipette solution remained constant throughout all experiments: (in mM) chloride, 140; Mg Acetate, 2; Ca Acetate, 1; HEPES, 10; pH 7.2 with CsOH. The bath solution was: (in mM) test anion, 140; Mg Acetate, 2; Ca Acetate, 1; HEPES, 10; pH 7.2 with CsOH, test anions being either Cl, I, F, Br, or NO_3. Initial recordings for each patch were made between bath and pipette before perfusion was initiated to ascertain whether the mechanical disturbance of the patch by the liquid flow had any effect on channel activity. In addition, each anion was tested both as the bath anion and as a perfused anion to ensure the perfusion procedure had no effect on the ability of the channel to conduct each particular anion. In approximately 10% of patches channel activity would cease when perfusion commenced. This phenomenon was independent of the anion species being perfused; these experiments were discarded, all other recordings were unaffected by the perfusion treatment.

The chamber was grounded using an agar bridge/AgCl electrode. Junction potentials were measured and were negligible <0.2 mV and were subsequently ignored in all calculations.

Analysis

Continuous *I/V* plots were recorded directly onto an IBM PC2/70 for analysis using CED patch-clamp software. Leakage currents were subtracted from *I/V* relationships and both slope conductance and reversal potentials were determined directly from each sweep using cursors provided by the software.

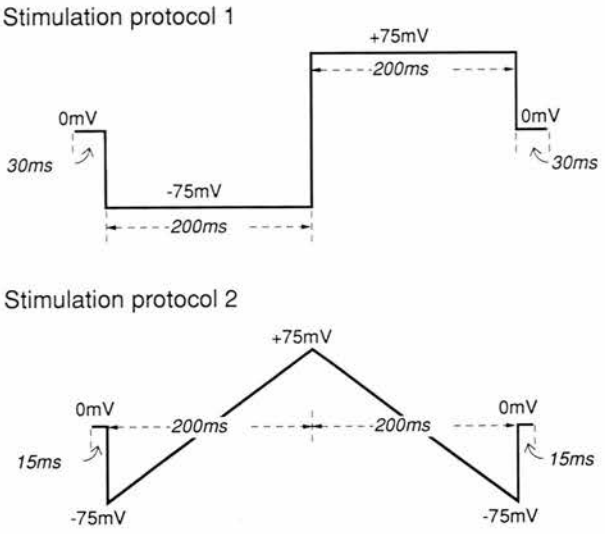


Fig. 1. Diagrammatic representation of the parameters used to stimulate channel activity.

Determination of Permeability Ratios

In ion substitution experiments the Goldman-Hodgkin-Katz equation (Goldman, 1943; Hodgkin & Katz, 1949) was used to calculate the relative permeability P_A/P_{Cl} of anions A^- with respect to Cl^-.

$$Erev = \frac{RT}{F} \ln \frac{[[Cl_i] + P_A/P_{Cl}[A_i]]}{[[Cl_o] + P_A/P_{Cl}[A_o]]} \quad (1)$$

Subscripts *i* and *o* denote internal and external ion species respectively and R, T and F have their usual meanings.

Data Analysis

Results are expressed as mean ± SEM. Significance was tested using unpaired *t*-test. The following *P* values apply to the notation used in the permeability and conductance sequences given in the results section.

=: no significance difference
>: $P < 0.05$
≥: $0.1 < P < 0.05$

Results

All experiments were carried out on vesicles harvested not more than 4 hr before, after which time the quality of the preparation began to decline. Using stimulation protocol 1 (Fig. 1), large amplitude (−14 pA) currents were recorded at the hyperpolarized

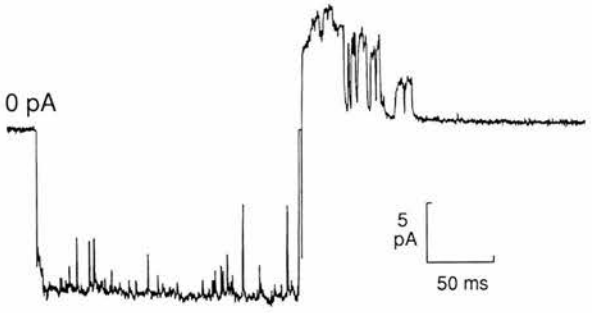


Fig. 2. Voltage dependence of Ca-activated chloride currents obtained from an isolated inside-out patch in symmetrical chloride (140 mM) solution using stimulation protocol 1.

potential of −75 mV (Fig. 2) in symmetrical chloride (140 mM) solution. Upon step depolarization to +75 mV both the current amplitude and the frequency of opening decreased (Fig. 2). In addition substates were seen in many preparations at depolarized potentials (*see* Thorn & Martin, 1987). Consequently, channel conductance was calculated from the linear (hyperpolarized potentials) of the *I/V* relationship.

The calcium-dependent chloride channel in *Ascaris* is selectively permeable to chloride (Thorn & Martin, 1987). All permeability studies in this series of experiments were carried out using the cesium salts of the anions under test. The possible permeability of cesium was assessed using an external (pipette) solution containing 70 mM CsCl, 2 mM $MgCl_2$, 1 mM $CaCl_2$, 10 mM HEPES and an internal (bath) solution containing 140 mM CsCl, 2 mM $MgCl_2$, 1 mM $CaCl_2$, 10 mM HEPES. Assuming the channel only conducts chloride, the reversal potential predicted using the Goldman-Hodgkin-Katz equation [Eq. (1)] is 16.45 mV. The actual reversal potential, measured in two experiments under the ionic conditions described above, was 16.72 mV and 14.5 mV, indicating the cesium permeability of the channel is negligible.

The effect on the conductance and reversal potential of the calcium-activated chloride channel, upon replacing intracellular chloride with the other halides and the anion nitrate, is illustrated in Fig. 3. Symmetrical chloride solution (140 mM) (Fig. 3*A*) affords an *I/V* graph that passes through the origin giving a reversal potential of 0.03 ± 0.47 mV and a slope conductance of 144.3 ± 1.4 pS (Table). Substitution of the bath chloride with Br^-, I^- or NO_3^- (140 mM) causes a depolarizing shift in the *I/V* plot for each ion, thereby producing a positive reversal potential of 3.35 ± 0.66; 8.28 ± 2.06 and 2.87 ± 0.37 mV, respectively (Table). The slope conductance upon substitution of the bath chloride with Br^-, I^- or NO_3^- (140 mM) reduced to 118.8 ± 1.1, 112.6

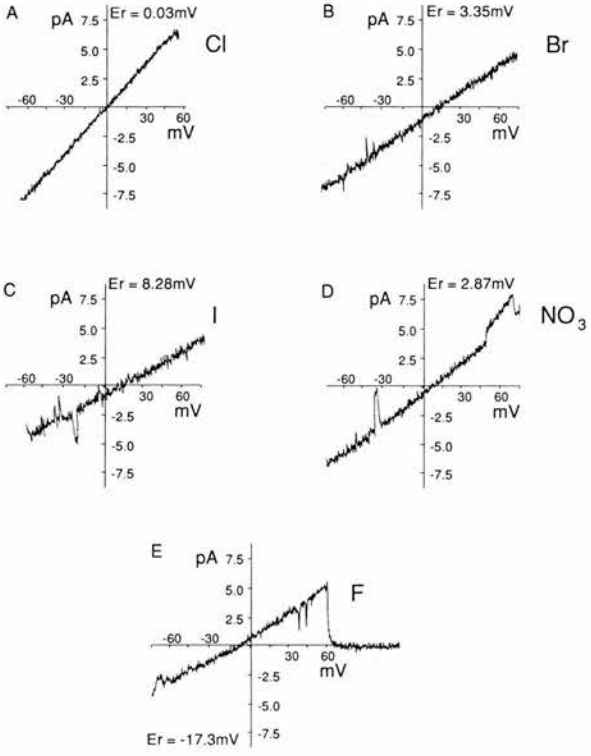


Fig. 3. *I/V* plots from isolated inside-out patches. Pipette solution contains 140 mM chloride the bath solution is varied: (*A*) chloride; (*B*) bromide; (*C*) iodide; (*D*) nitrate and (*E*) fluoride, each at a concentration of 140 mM.

± 1.8 and 128.1 ± 1.1 pS, respectively. However, application of F^- to the inside of the patch results in a hyperpolarizing shift in the *I/V* relationship, affording a negative reversal potential of −17.3 ± 1.99 mV and a reduced conductance of 78.2 ± 1.2 pS. The *I/V* relationships illustrated in Fig. 3 are the result of a single sweep from −75 to +75 mV as produced by stimulation protocol 2. Both Fig. 3*A* and *B* show a single-channel opening for the whole duration of the sweep. The channel can be observed closing during depolarization in Fig. 3*E* and briefly closing and opening again during hyperpolarization in Fig. 3*D*. Also in Fig. 3*D*, in the depolarization quadrant of the *I/V* plot, a second channel opens, thereby producing a portion of the record with a steeper gradient, i.e., larger conductance. This second channel can be seen somewhat briefly in Fig. 3*C* during hyperpolarization.

The reversal potentials were used to calculate the permeability ratios P_A/P_{Cl} of anions A^- relative to Cl^- [Eq. (1), Table]. Figure 4 shows a plot of selectivity isotherms taken from Wright and Diamond (1977), the permeability ratio P_A/P_{Cl} of an anion relative to chloride is plotted on the ordinate with the permeability of I^- relative to Cl^- plotted

Table. Data obtained from isolated inside-out patches

Internal ion (140 mM)	Reversal potential (mV)	P_A/P_{Cl}	Conductance (pS)	nq	Number of patches
Chloride	+0.03 ± 0.47	1.05 ± 0.02	144.3 ± 1.4	1.43	5 (46)
Iodide	+8.28 ± 2.06	1.34 ± 0.11	112.6 ± 1.8	1.65	3 (17)
Bromide	+3.35 ± 0.66	1.16 ± 0.03	118.8 ± 1.1	1.78	3 (17)
Fluoride	−17.3 ± 1.99	0.52 ± 0.04	78.2 ± 1.2	2.15	3 (18)
Nitrate	+2.87 ± 0.37	1.12 ± 0.02	128.1 ± 1.1	0.89	5 (10)

External (pipette) solution contained 140 mM chloride. P_A/P_{Cl} represents the permeability ratio of anion A^- to Cl^-. Numbers in parentheses refer to the total number of I/V plots constructed for each anion. nq is number of cationic binding sites within channel pore.

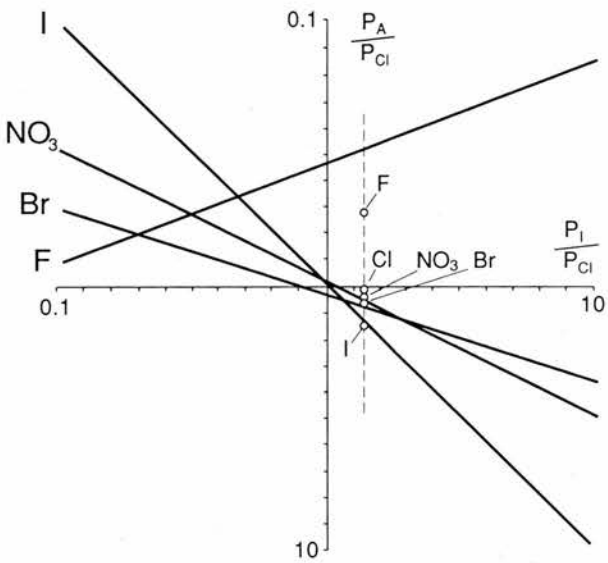


Fig. 4. Selectivity of the Ca-activated chloride channel for the halides and nitrate. Solid lines represent the selectivity isotherms taken from Wright and Diamond (1977). The isotherms represent permeability of the anions observed in a large number of different biological systems. The permeability ratio for each anion relative to chloride (P_A/P_{Cl}) is plotted on the ordinate with the permeability of iodide relative to chloride (P_I/P_{Cl}) on the abscissa. Intersections between the five isotherms represent the transitions among the seven permeability sequences of Wright and Diamond (1977).

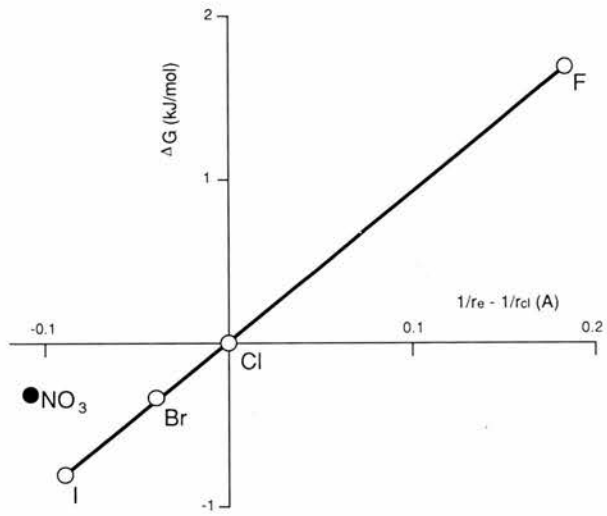


Fig. 5. Reuter and Stevens (1980) plot of free energy barriers for the anions as a function of the reciprocal of anionic radii. The energy difference ΔG for the rate-limiting barrier of each anion, relative to chloride, is plotted on the ordinate and the difference between the inverse of their crystal radii plotted on the abscissa. The line represents a fit with the linear term $a_1 = 9.1$ kJAmol^{-1} in Eq. (6).

on the abscissa. Seven different halide selectivity sequences can be drawn from this graph according to the intersection of the various isotherms. The halide selectivity sequence will vary according to the biological system and channel under test. The Ca-activated chloride channel affords a halide selectivity sequence of I > Br > Cl > F; i.e., sequence 1 of Wright and Diamond (1977). The ion selectivity of a channel is determined by both the ionic environment within the channel pore and by the interaction between the channel wall and ions passing through the channel. Using the extended Eisenman (1961, 1962; Eisenman & Horn, 1983) theory of Wright and Diamond (1977) the number of cationic binding sites within the channel can be estimated. Hydrated anions entering the channel are transferred from water to cationic sites in the channel wall. The ease with which an anion passes through the channel is therefore dependent on the difference between the anion hydration energy (ΔG_H) and the field strength of the cationic binding site (ΔG_{site}). The energy required to transfer 1 mol of anion from water to channel binding site is (Wright & Diamond, 1977)

$$\Delta G_{trans} = \Delta G_{site} - \Delta G_H \quad (2)$$

Assuming channel walls have fixed monopolar posi-

tively charged sites of radius, r with point positive charge q_+ the principal ion-site interaction can be represented by the term $nq_+q_-/(r_+ + r_-)$ where r_+ and r_- are the ionic radius (Å) of cationic monopoles comprising each site and touching each anion. Then taking q_- as -1 for all monovalent anions, assigning the appropriate proportionality constant for the usual units, and assuming the positively charged sites within channel walls consist of $-NH_3^+$, $>NH_2^+$, NH^+, N^+, residues, then r_+ can be taken as the radius of nitrogen, 1.5 Å

$$\Delta G_{site} = -1388nq_+/(r_- + r_+) \tag{3}$$

Using Pauling ionic radii and appropriate hydration energies (Wright & Diamond, 1977) the number of positive charges, nq, within the channel can be evaluated by

$$\Delta G = \Delta G_{trans}(A^-) - \Delta G_{trans}(Cl^-) \tag{4}$$

ΔG of anion A^- and Cl^- can be expressed in terms of the permeability ratio of anion A^- to Cl^- (Borman, Hamill & Sakmann, 1987)

$$\Delta G = RT \ln P_A/P_{Cl} \tag{5}$$

The number of positive charges within the channel that are in contact with the anion can therefore be calculated from the permeability ratios given in the Table. It can be seen from the Table that the values of nq vary widely from a low of 0.89 for NO_3 to a high of 2.15 for F.

Another explanation of the anion selectivity can be drawn from the theory of Reuter and Stevens (1980), which relates the "fluidity" of the channel to that of free water. Assuming the interaction between anion and water is entirely electrostatic (Buckingham, 1957), then the quantity influencing the anionic permeability would be the electric field around the anion, i.e., its radius and valence. In the case of a channel with only one rate-limiting barrier, the barrier height G will depend on the inverse of the ionic radius of the anion. This can be represented as a power series where the energy function G has been expanded about the reciprocal radius of Cl^- as the reference ion

$$G(1/r_A) = G(1/r_{Cl}) + a_1(1/r_A - 1/r_{Cl}) + a_2(1/r_A - 1/r_{Cl})^2 \tag{6}$$

This equation is related to relative permeabilities expressed in Eq. (5). Incorporating Eq. (5) into Eq. (6) affords

$$\Delta G = G(1/r_A) - G(1/r_{Cl}) = \frac{RT}{F} \ln \frac{P_{Cl}}{P_A} \tag{7}$$

Therefore, plotting ΔG as a function of $1/r_A - 1/r_{Cl}$ affords a physical interpretation of the coefficients of expansion (a_1). When the relationship is linear the coefficient a_1 can be used to indicate the "fluidity" of the channel water structure as compared to free water (Reuter & Stevens, 1980), and therefore gives an indication of the constraints placed on the diffusion of ions through the channel; this is illustrated in Fig. 5. In the *Ascaris* calcium-dependent chloride channel the halide anions afford a straight line that can be described by the linear portion of Eq. (6) with a coefficient a_1 of 9.1 kJÅmol^{-1}. NO_3 does not fit the linear function of the power Eq. (6), ΔG in this case is more positive than that predicted for an ion of its radius.

Discussion

As shown in a previous study (Thorn & Martin, 1987), the activity of the calcium-activated chloride channel of *A. suum* decreases upon depolarization. The profile of voltage dependence of this calcium-activated Cl channel differs from that found in other large conductance chloride channels which tend to be active only in the range ±30 mV about zero (Grey, Bevan & Ritchie, 1984; Young et al., 1984). Whereas the calcium-dependent Cl current in *Ascaris* remains active at potentials in excess of −150 mV (*data not shown*) and only rectifies at positive membrane potentials.

The channel is not especially selective between the anions tested in this paper. The permeability ratios of halides follow sequence 1 of Wright and Diamond (1977), namely I > Br > Cl > F, indicative of a low field strength cationic binding site. Selectivity sequence 1 is displayed by several large conductance Cl channels (Grey et al., 1984; Marty, Tan & Trautmann, 1984; Young et al., 1984). In addition, the halide selectivity sequence of the smaller (30 pS) chloride channel in rat hippocampal neurons (Franciolini & Nonner, 1987) also conformed to sequence 1. However, unlike the calcium-activated chloride channel in *Ascaris*, the small conductance chloride channel was more permeable to nitrate than iodide. This halide permeability sequence is in agreement with that measured for the whole muscle membrane (Del Castillo et al., 1964) using changes in *Ascaris* resting membrane potential upon substitution of anions for external chloride. This method afforded a halide permeability sequence of I > Br > Cl; however, NO_3 was found to be more permeable

than I. Using a similar methology Rheinhallt Parri et al. (1991) investigated the selectivity of the GABA operated channel of the somatic muscle cell of *Ascaris*. Unfortunately, large standard errors prevented full resolution of the data; however, NO_3, I and Br were all more permeable than Cl. Likewise a similar permeability sequence ($I > NO_3 > Br > Cl > F$) is displayed by a calcium-dependent chloride current in isolated cells from rat lacrimal glands (Evans & Marty, 1986).

It would appear that the calcium-dependent chloride channel of *Ascaris* is not simply a water-filled pore as the conduction sequence differs from the permeability sequence, a feature usually indicative of a binding site for permeant ions within the channel wall. In addition, Fig. 5 illustrates ΔG [Eq. (7)] plotted as a function of the reciprocal of ion size. The data for the halides are described by the linear term in Eq. (6); a simple linear relationship between ion size and ΔG usually indicates a nonselective channel pore (Reuter & Stevens, 1980). The linear term a_1 is 9.1 kJÅmol^{-1}, for the calcium-dependent chloride channel, a_1 being a measure of the "fluidity" of the channel water structure as compared to free water (Reuter & Stevens, 1980). Thus, the calcium-dependent chloride channel is relatively "fluid." However, stronger constraints are placed on the diffusion of water molecules in the calcium-dependent chloride channel compared to water diffusion in the acetylcholine receptor channel, in whose case a_1 is only 1.4 kJÅmol^{-1}, indicating a very "fluid" channel. However, GABA and glycine gated chloride channels in mouse cultured spinal neurones are less "fluid." Both channels place stronger constraints on the diffusion of water, affording a_1 values of 28.8 and 18.8 kJÅmol^{-1}, respectively (Bormann, Hamill & Sakmann 1987).

However, ΔG_{NO_3} is not described by the linear portion of Eq. (6). ΔG for NO_3 is more positive than expected for an ion of its radius. This would suggest NO_3 interacts with water more strongly than anticipated. However, this is not borne out by the low hydration energy ΔG_H of NO_3 (Wright & Diamond, 1977). Therefore, ΔG for NO_3 is perhaps more influenced by ΔG_{site} than the halides. In calculating ΔG several assumptions are made, the most important being that the anions are spherical and as such the electrostatic interaction between water, anion and their surroundings will depend on the inverse of the ionic radius of the anion (Wright & Diamond, 1977). This is clearly not the case for NO_3 which is a planar molecule (Pauling, 1960). The radius of the horizontal plane of the NO_3 would therefore be an overestimation of the radius of NO_3 if the molecule interacts with the channel cationic binding sites along the vertical plane. Such a reduction in radius would shift ΔG_{NO_3} to the right in Fig. 5 bringing it in line with the halides. This hypothesis is borne out by the estimation of nq, the number of cationic binding sites within the channel with which the anions interact. Two simple interpretations of these data can be offered. The first would be to suggest that certain binding sites are inaccessible to larger anions such as nitrate. The second interpretation takes into account the possibility of an anion of small ionic radius and, therefore, dense negative charge to induce dipole moments within the channel wall, thereby 'creating' additional binding sites as it passes through the channel pore.

The role of this channel remains open to question. The channel is active at -30 mV, the resting membrane potential (RMP) of the somatic muscle cell of *Ascaris*, (Del Castillo, 1964; Brading & Caldwell, 1971) and could therefore contribute to the maintenance of the RMP. The chloride concentration of the perienteric fluid within the body cavity of *A. suum* is maintained at a lower concentration (52 mM) than that of the surrounding environment (Hobson, Stephenson & Eden, 1952). Hobson et al. (1952) also demonstrated that chloride is transported across the body wall to the outside and that the active site of this transport is a feature of the muscle or hypodermis. A possible role for the calcium-dependent chloride current in *Ascaris* is, therefore, the transport of chloride across the bag region of the muscle cell. In addition, preliminary experiments conducted within our laboratory indicate that the channel is able to conduct organic acids that form the products of anaerobic respiration. A possible further role of this channel, therefore, is the removal of metabolic waste products from the muscle cell.

This work was supported by the Scientific & Engineering Research Council (S.E.R.C.).

References

Borman, J., Hamill, O.P., Sakmann, B. 1987. Mechanism of anion permeation through channels gated by glycine and γ-aminobutyric acid in mouse cultured spinal neurons. *J. Physiol.* **385**:243–286

Brading, A.F., Caldwell, P.C. 1971. The resting membrane potential of somatic muscle cells of *Ascaris lumbricoides*. *J. Physiol.* **27**:605–624

Buckingham, A.D. 1957. A theory of ion-solvent interaction. *Disc. of the Faraday Soc.* **24**:151–157

Caldwell, P.C., Ellory, J.C. 1968. Ion movements in somatic muscle cells of *Ascaris lumbricoides*. *J. Physiol.* **197**:75–76P

Del Castillo, J., DeMellow, W.C., Morales, T. 1964. Influence of some ions on the membrane potential of *Ascaris* muscle. *J. Gen. Physiol.* **48**:129–140

Eisenman, G. 1961. On elementary atomic origin of equilibrium

ionic specificity. *In*: Symposium on Membrane Transport and Metabolism. A. Kleinzeller and A. Kotyk, editors. pp. 163–179. Academic, New York

Eisenman, G. 1962. Cation selective glass electrodes and their mode of operation. *Biophys. J.* **2:**259–323

Eisenman, G., Horn, R. 1983. Ionic selectivity revisited: the role of kinetic and equilibrium processes in ion permeation through channels. *J. Membrane Biol.* **76:**197–225

Evans, M.G., Marty, A. 1986. Calcium-dependent chloride currents in isolated cells from rat lacrimal glands. *J. Physiol.* **378:**437–460

Franciolini, F., Nonner, W. 1987. Anion and cation permeability of a chloride channel in rat hippocampal neurons. *J. Gen. Physiol.* **90:**453–478

Goldman, D.E. 1943. Potential impedence and rectification in membranes. *J. Gen. Physiol.* **27:**37–60

Grey, P.T.A., Bevan, S., Ritchie, J.M. 1984. High conductance anion-selective channels in rat cultivated Schwann cells. *Proc. R. Soc. London B.* **221:**395–409

Hobson, A.D., Stephenson, W., Eden, A. 1952. Studies on the physiology of *Ascaris lumbricoides*. 2. The inorganic composition of the body fluid in relation to that of the external environment. *J. Exp. Biol.* **29:**22–29

Hodgkin, A.L., Katz, B. 1949. The effect of sodium ions on the electrical activity of the giant axion of the squid. *J. Physiol.* **108:**37–77

Jarman, M. 1959. Electric activity in muscle cells of *Ascaris* muscle. *Nature* **184:**1244

Martin, R.J. 1980. The effect of GABA on the input conductance and membrane potential of *Ascaris* muscle. *Br. J. Pharmacol.* **71:**99–106

Martin, R.J. 1985. GABA and piperazine-activated single channel currents from *A. suum*. *J. Physiol.* **354:**46P

Martin, R.J., Pennington, A.J. 1989. A patch-clamp study of dihydroavermectin on *Ascaris* muscle. *Br. J. Pharmacol.* **98:**747–756

Marty, A., Tan, Y.P., Trautmann, A. 1984. Three types of calcium-dependent channels in rat lacrimal glands. *J. Physiol.* **377:**293–325

Pauling, L. 1960. The Nature of the Chemical Bond. pp. 283–284. Cornell University, New York

Reuter, H. Stevens, C.F. 1980. Ion conductance and ion selectivity of potassium channels in snail neurones. *J. Membrane Biol.* **57:**103–118

Rheinallt Parri, H., Holden-Dye, L., Walker, R.J. 1991. Studies on the ionic selectivity of the GABA-operated chloride on the somatic muscle bag cells of the parasitic nematode *Ascaris suum*. *Exp. Physiol.* **76:**597–606

Rosenbluth, J. 1965*a*. Ultrastructural organisation of obliquely striated muscle fibres in *Ascaris lumbricoides*. *J. Cell Biol.* **25:**494–515

Rosenbluth, J. 1965*b*. Ultrastructure of somatic muscle cells in *Ascaris lumbricoides*. II. Intermuscular junctions, neuromuscular junctions, and glycogen stores. *J. Cell Biol.* **26:**579–591

Rosenbluth, J. 1967. Obliquely striated muscle. III. Contraction mechanism of *Ascaris* body muscle. *J. Cell Biol.* **34:**15–33

Thorn, P., Martin, R.J. 1987. A high conductance calcium-dependent chloride channel in *A. suum* muscle. *J. Exp. Physiol.* **72:**31–49

Wright, E.M., Diamond, J.M. 1977. Anion selectivity in biological systems. *Physiol. Rev.* **57:**109–156

Young, G.P.H., Young, J.D.E., Destipande, A.K., Goldstein, M., Koide, S.S., Cohn, Z.A. 1984. A Ca^{2+}-activated channel from *Xenopus laevis* oocyte membranes reconstituted into planar bilayers. *Proc. Natl. Acad. Sci. USA* **81:**5155–5159

Received 29 April 1992; revised 19 August 1992

J. exp. Biol. **173**, 75–90 (1992)
Printed in Great Britain © The Company of Biologists Limited 1992

VOLTAGE-ACTIVATED CURRENTS IN SOMATIC MUSCLE OF THE NEMATODE PARASITE *ASCARIS SUUM*

BY R. J. MARTIN, P. THORN, K. A. F. GRATION AND I. D. HARROW

Department of Preclinical Veterinary Sciences, R. (D.) S.V.S, Summerhall, University of Edinburgh, Edinburgh, EH9 1QH and *Animal Health Discovery, Pfizer Central Research, Sandwich, Kent, CT13 9NJ*

Accepted 3 August 1992

Summary

1. Voltage-activated currents in cell bodies of the somatic muscle cells of *Ascaris suum* were studied using a two-microelectrode voltage-clamp technique. Cells recorded from had resting membrane potentials around −35 mV and had input conductances in the range 1–10 μS.

2. In cells bathed in artificial perienteric fluid, depolarizing steps from a holding potential of −35 mV elicited outward currents at a threshold of −15 mV. These currents had inwardly directed inflections on the rising phase, suggesting the presence of more than one current. Hyperpolarizing steps did not activate current.

3. Tetraethylammonium (TEA^+, 69 mmol l^{-1}) blocked the outward currents and allowed a voltage-dependent inactivating Ca^{2+} current to be observed. The peak current–voltage relationship was U-shaped with a threshold around −15 mV and peak at +5 mV. The reversal potential of the Ca^{2+} current was estimated by extrapolation to be +45 mV.

4. The permeability of the voltage-activated outward currents was studied by examining reversal potentials of tail currents. The reversal potentials were linearly dependent on the logarithm of the extracellular potassium concentration if extracellular [K^+] was greater than 10 mmol l^{-1}. The Na^+/K^+ permeability ratio of the currents was 0.04.

5. Inactivation, seen as a decline following the peak of the K^+ current, was produced by maintained depolarization. The recovery from inactivation was complex and could be described by the sum of two exponentials with time constants of 0.67 s and 20.1 s. Steady-state inactivation of the K^+ currents was observed at a range of holding potentials. Only a proportion (34 %) of the total K^+ current was inactivated by holding potentials more positive than −20 mV.

6. Extracellular application of 5 mmol l^{-1} 4-aminopyridine (4-AP) selectively abolished an early fast component of the K^+ current (the peak). The 4-AP-sensitive current decayed quickly with a time constant of around 10 ms; a Boltzmann fit to its activation curve had a half-maximal activation voltage of +14 mV and a 'slope' of 10.5 mV. The 4-AP-resistant current decayed with a time constant of around 1 s; a Boltzmann fit to its activation curve had a half-maximal activation voltage of +29 mV and a 'slope' of 12 mV.

Key words: *Ascaris suum*, voltage-clamp, muscle, calcium currents, potassium currents.

7. Depolarization activates a Ca^{2+} current and two K^+ currents: the K^+ currents were separated into lower-threshold, fast-inactivating (I_a-like) and higher-threshold, slowly inactivating (I_k-like) currents.

Introduction

Ascaris suum is an intestinal nematode parasite of pigs and is capable of maintaining its position in the gut by means of forwardly directed waves of contraction. The somatic muscle cell of *Ascaris* consist of a contractile spindle region; a balloon-shaped structure, the bag which contains the nucleus; and a thin process known as the arm which passes to a nerve cord where it is electrically coupled to adjacent cells and where it receives excitatory and inhibitory synaptic inputs (Rosenbluth, 1963, 1965). DeBell *et al.* (1963) and Weisblat *et al.* (1976) have studied the electrophysiology of *Ascaris* body muscle cells and described three types of depolarizing potential recorded in the bag region of the muscle which are related to contraction. They described the 'spike potentials', the 'slow waves' and the 'modulation waves'. The spike potentials were of varying amplitude up to 30 mV, lasted 5–10 ms and behaved like Ca^{2+} spikes; the slow waves were up to 20 mV in amplitude and lasted 100–1000 ms; the modulation waves lasted several seconds, were up to 5 mV in amplitude but were directly associated with muscle contraction. The currents responsible for depolarization and repolarization of the cells have yet to be isolated and identified.

Muscle cells of *Ascaris* are large enough to allow a two-microelectrode voltage-clamp to be used to examine membrane currents (Martin, 1982). This technique has revealed the presence of a voltage-sensitive Ca^{2+} current and two K^+ currents that underlie the spike potential and are the subject of this paper.

Materials and methods

The preparation

Ascaris suum, approximately 20 cm in length, were obtained from the local slaughterhouse, maintained in Locke's solution at 32 °C and used within 4 days. An anterior section of the worm, 2 cm long, was cut along a lateral line and then pinned cuticle side down onto a layer of Sylgard in the experimental chamber. The gut was then removed, exposing the muscle cell bodies. The experimental chamber consisted of a central bath with a liquid capacity of 1.8 ml. The bath was surrounded by a water jacket through which water was circulated to maintain the preparation at 37 °C. The worm was viewed from above through a Bausch and Lomb zoom microscope and cross illuminated using a fibre-optic light source. The preparation was continuously perfused with a Shuco pump and, by means of a broken pipette, positioned near (500 μm) the cell recorded from, in order to accelerate solution changes. The flow rate for the total perfusion system was set at 8 ml min^{-1} and cleared the bath in 4.5 min when filled with blue dye. An interval of 7–15 min was therefore used after a change of solution and before recording.

Electrodes

Two micropipettes were placed in the bag region of the muscle cells in order to carry

out the two-microelectrode voltage-clamp experiments. The micropipettes were pulled on a David Kopf puller from filamented glass tubing (Clarke Electromedical Instruments GC 150F-15). The current micropipettes had a resistance of 4 MΩ and the voltage micropipette had a resistance of 11 MΩ. Both were filled with 3 mol l^{-1} potassium acetate. 3 mol l^{-1} magnesium sulphate was used to fill the micropipettes when reversal potentials were being measured.

Solutions

Initially artificial perienteric fluid (APF) was used which contained (mmol l^{-1}): NaCl, 23; sodium acetate, 110; KCl, 24; $CaCl_2$, 6; $MgCl_2$, 5; glucose, 11; Hepes, 5; pH 7.6 with NaOH. For recording Ca^{2+} currents, a solution with TEA^+ to block K^+ currents and a high Ca^{2+} concentration was used containing (mmol l^{-1}): TEACl, 69; calcium acetate, 69; potassium acetate, 24; magnesium acetate, 5; glucose, 11; pH 7.6 with maleic acid. In most of the experiments described here, a Ca^{2+}-free lanthanum solution based on *Ascaris* Ringer was used which contained (mmol l^{-1}): NaCl, 135; KCl, 3; $MgCl_2$, 15.7; glucose, 3; Tris, 5; EGTA, 0.5; LaCl, 1; pH 7.6 with maleic acid. The use of this type of low-Ca^{2+} solution is likely to abolish secondary channel currents produced as a result of entry of Ca^{2+} into the cell: one example of this type of channel current in *Ascaris* is the Ca^{2+}-activated Cl^- channel (Thorn and Martin, 1987). In order to modify the reversal potential of tail currents, Ca^{2+}-free lanthanum solutions were used in which sodium was substituted for potassium; they contained (mmol l^{-1}): NaCl, 0.1–138; KCl, 0.1–138 (total K^++Na^+=138); $MgCl_2$, 15.7; glucose, 3; Tris, 5; EGTA, 0.5; LaCl, 1; pH 7.6 with maleic acid.

Recording system

A Dagan 8500 voltage-clamp was used and all output was displayed on a Gould OS400 digital storage oscilloscope with an IEEE 488 interface. The gain on the amplifier was adjusted to 2500–5000 V/V and the phase lag was adjusted for each cell to give optimal recording. Data were recorded on a Racal Store Four DS tape recorder with a bandwidth of up to 2.5 kHz. The signal was played back into a Lectromed chart recorder or a Gould Series 6000 XY plotter to provide hard copy. All pulse regimes were controlled by a Digitimer D100. Stimulus input was provided by Digitimer DS2 isolated stimulators. Leak subtraction, where used, was performed by summation of two current responses to equal but opposite-polarity voltage steps. The current response to hyperpolarizing steps was linear in the range used and therefore represented the leak current.

It was possible to check the quality of the space-clamp in the bag region of the muscle cell by placing a third micropipette in the base of the bag, at a site near the junction with the spindle, while the other two micropipettes for the voltage-clamp were placed at the top of the bag. Under these conditions it was found that the third micropipette could record a voltage response that was 95 % of the command potential within 500 μs. In view of the particular anatomy of the muscle cells of *Ascaris* it is, however, likely that there may be poorly controlled regions of membrane: these were recognised as 'notches' of inward current which occurred at a relatively long but irregular time after the start of the depolarizing pulse, producing a very abrupt rise in the inward current–voltage

relationship. Such events led to the rejection of the muscle cell for recording: only currents from cells which showed adequate voltage control were analysed.

Data analysis

The peak amplitude and time to peak of current responses were measured from graphs of currents plotted against time. The limiting equivalent voltage sensitivity for the Ca^{2+} current was determined from the maximum slope of the plot of $\log_e$(peak Ca^{2+} current/maximum peak Ca^{2+} current) against voltage (Hille, 1984). A BBC microcomputer with a Unilab interface was used to digitize the currents. Sampling rates were adjusted between 1 kHz and 0.05 kHz, depending on the duration the sample. The rate of decay was then analysed using the BMDP P3R non-linear regression program. The best fits to the Boltzmann equation were obtained using the NAG subroutine E04CCF.

Results

This paper describes results from 49 successful voltage-clamp experiments. The resting membrane potentials of recorded muscle cells were around −35 mV with a mean input conductance of 2.4±0.18 μS (mean ± S.E., N=9) measured using 150 ms hyperpolarizing voltage pulses.

Depolarizing voltage steps from a holding potential of −35 mV elicited an outward current in cells bathed in APF solution (Fig. 1A). These currents rose to a peak within 20 ms and had an inwardly directed inflection in the rising phase: these inflections were not because of 'breakthrough' as a result of poor space-clamping because they occurred in most cells at regular intervals after the onset of the depolarizing pulse. After the peak current there was a slow decay. As the depolarizing steps were made more positive, the outward-current peak became more pronounced. Hyperpolarizing steps did not induce active currents (Fig. 1B). A plot of current amplitude 20 ms after the voltage step against the potential shows the current increasing non-linearly on depolarization but linearly on hyperpolarization (Fig. 1C). The linearity observed following hyperpolarization was subsequently used to allow for 'leakage' correction.

Inward currents

In five experiments, substitution of sodium in APF with 69 mmol l^{-1} tetraethylammonium (TEA^+) and 69 mmol l^{-1} calcium revealed an inward current activated by depolarizing voltage-clamp steps from a holding potential of −35 mV. This inward current was identified as a Ca^{2+} current on the grounds that the permeant cation was calcium in the high-Ca^{2+} TEA^+ solution. As further confirmation of the identity of the inward current, it was found that bath-application of lanthanum (using 1 mmol l^{-1} LaCl) as a calcium channel blocker rapidly abolished the inward current (not shown). The Na^+ channel blocker tetrodotoxin was not used because of its lack of effect in *Ascaris* (Jarman and Ellory, 1969). A family of Ca^{2+} currents evoked by increasing depolarizing steps and corrected for leakage is shown in Fig. 2A. The threshold for activation of the inward current was around −15 mV. More depolarized voltage-clamp steps increased the amplitude of the inward-current peak up to a value of about +5 mV and thereafter

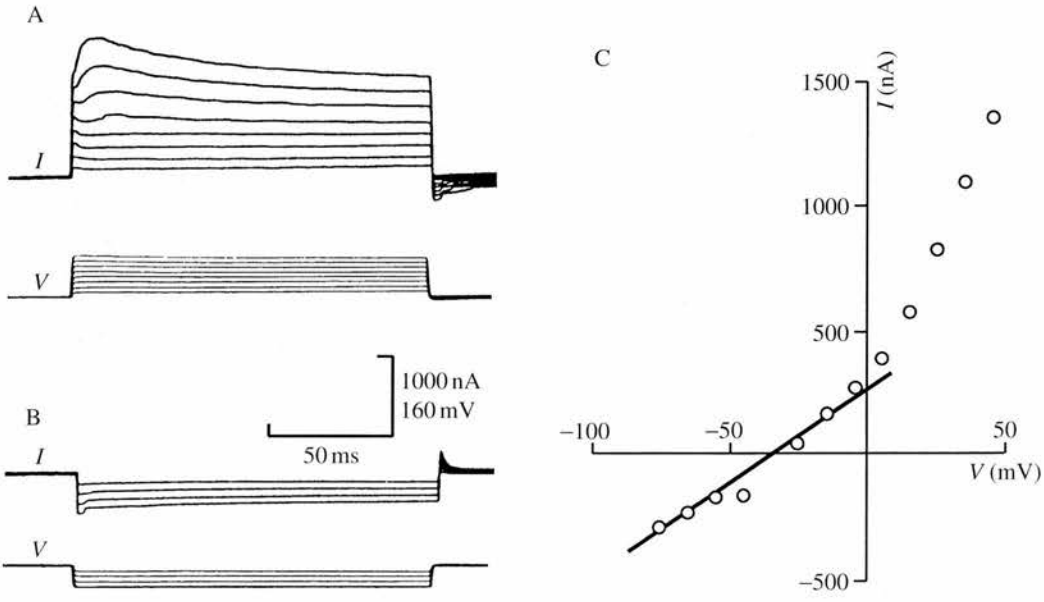


Fig. 1. Family of currents obtained from a cell under voltage-clamp bathed in APF. The current records are labelled *I* and voltage records are labelled *V*. The cell was stepped from a holding potential of −35 mV, in increments of 10 mV, to a series of step potentials (Sp). (A) Sp=−25 mV, −15 mV, −5 mV, 5 mV, 15 mV, 25 mV, 35 mV, 45 mV. (B) Sp=−45 mV, −55 mV, −65 mV, −75 mV, −85 mV, −95 mV, −105 mV. (C) Current–voltage plot from the same experiment as that of A and B. The peak current was measured 20 ms after the start of the step potential. The straight line illustrates the linear portion of the plot suitable for leakage correction.

decreased it with further depolarization; the time to peak decreased monotonically with increasing depolarization. At the most depolarized potentials, the peak of the inward current was followed by a small outward current which may be because of residual outward current not blocked by TEA^+. However, there was no evidence of any maintained current; at the end of the 150 ms pulses all the currents had inactivated and there was tail current on the return to the holding potential of −35 mV. The time constant for inactivation of the Ca^{2+} current was, therefore, less than 150 ms, the length of the voltage pulse. All the data from this cell relating peak inward current to voltage are shown in Fig. 2B. The maximum inward current was 411 nA, the extrapolated reversal potential was +45 mV and the limiting equivalent voltage-sensitivity (Hille, 1984) was 7.5 mV per e-fold increase in Ca^{2+} current.

The predicted Nernst Ca^{2+} potential with 69 mmol l^{-1} extracellular calcium and 1 μmol l^{-1} intracellular calcium is +140 mV, some 95 mV more positive than estimated here. Despite the theoretical prediction of +140 mV, many other authors report values as low as +40 mV to +70 mV, which they explain by the Ca^{2+} channels also being permeable to other monovalent ions (K^+) moving outwards through the Ca^{2+} channels (Reuter and Scholtz, 1977; Fenwick *et al.* 1982; Lee and Tsien, 1982).

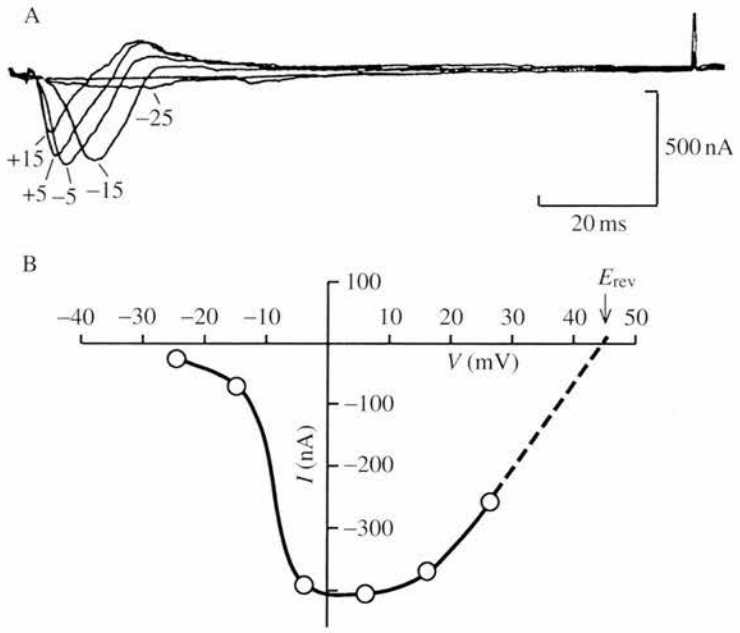


Fig. 2. (A) Leak-subtracted current–voltage relationship in a cell bathed in TEA^+ APF and 69 mmol l^{-1} Ca^{2+}. The cell was stepped from a holding potential of 35 mV to −25 mV, −15 mV, −5 mV, +5 mV, +15 mV and +25 mV; paired hyperpolarizing pulses were used for the leak subtraction procedure. Increased depolarizing steps increased and then decreased the inward current and decreased the time to peak current. A small outward current is also seen following the inward current. A capacitative current is seen at the end of the pulse but is not so apparent at the beginning because of the leak subtraction process used. (B) Peak Ca^{2+} current–voltage plot. Extrapolation of the plot gives an estimate of +45 mV for the reversal potential at 37 °C.

Effect of changing extracellular potassium concentration on the reversal potential of the tail current

The aim of this series of experiments was to examine the permeability of the outward current activated by depolarization. The experimental approach was to activate the currents and then to determine the reversal potentials of the tail currents at different potentials, in solutions of different potassium concentrations (Fig. 3A–D). Cells were bathed in Ca^{2+}-free lanthanum solutions to block Ca^{2+} currents (Meech and Standen, 1975; Thomas, 1984) and potassium was replaced by sodium. The experiments were carried out using a two-pulse voltage-clamp protocol: i.e. a holding potential of −35 mV, a prepulse potential of +55 mV for 10–20 ms to activate the outward current and a step potential to between −125 mV and +55 mV. The amplitude and duration of the tail current elicited during the step potential then allowed the reversal potentials of the current activated by depolarization to be determined.

Fig. 3A shows representative currents obtained from a cell bathed in 0.1 mmol l^{-1} potassium. Fig. 3B,C,D shows the currents obtained in 3 mmol l^{-1}, 30 mmol l^{-1} and

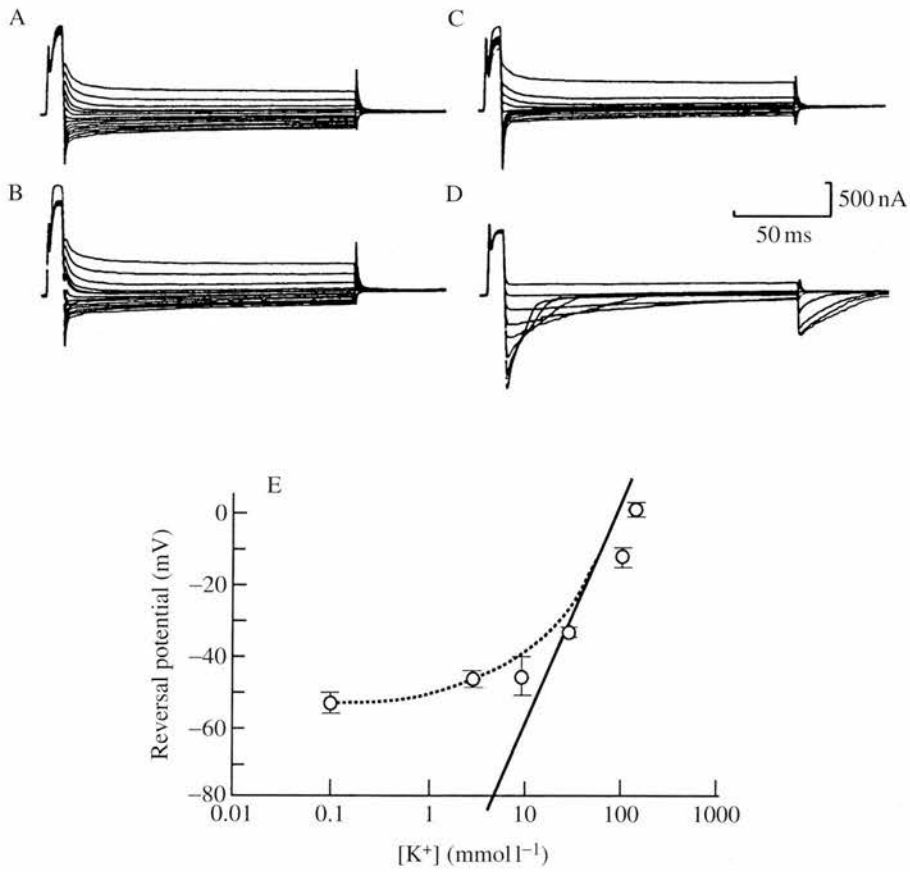


Fig. 3. Estimation of tail current reversal potentials in solutions of different K^+ concentration. A two-step protocol was used: the holding potential was −35 mV; the first step was to +55 mV for 10 ms to activate the current; the potential of the second voltage step was varied to determine the reversal potential of the tail current. In A, B and C the second steps were to −125 mV, −115 mV, −105 mV, −95 mV, −85 mV, −75 mV, −65 mV, −55 mV, −45 mV, −25 mV, −15 mV, −5 mV, 0 mV, +5 mV, +15 mV. In D the second steps were to −95 mV, −85 mV, −75 mV, −65 mV, −55 mV, −45 mV, −25 mV, −15 mV. (A) 0.1 mmol l^{-1} potassium lanthanum solution; (B) 3 mmol l^{-1} potassium lanthanum solution; (C) 30 mmol l^{-1} potassium lanthanum solution; (D) 138 mmol l^{-1} potassium lanthanum solution. The cell was bathed for 10 min in each solution before recording the currents at 37 °C. (E) The mean ± S.E. reversal potential, obtained from six experiments conducted in the same manner as the experiment illustrated in A, B, C and D is plotted as a function of log potassium concentration of the bathing solution. Reversal potentials were estimated from plots of tail-current amplitude against membrane potential. The points show linearity between 10 mmol l^{-1} and 138 mmol l^{-1} extracellular potassium, but at lower potassium concentrations the relationship was non-linear. The solid line on the graph was drawn according to the Nernst equation assuming an intracellular potassium concentration of 99.4 mmol l^{-1} (Brading and Caldwell, 1971). The dotted line was drawn using the constant-field equation with a Na^+/K^+ permeability ratio of 0.04.

138 mmol l^{-1} extracellular potassium, respectively. The reversal potential of the tail current moved in the depolarizing direction as extracellular potassium concentration increased. The means ± S.E. of reversal potentials were then plotted against log potassium concentration (Fig. 3E). The plot was essentially linear for extracellular potassium concentrations above 10 mmol l^{-1} but deviated below this concentration. The constant-field equation (Hille, 1984) for a channel current permeable to potassium and sodium predicts that:

$$E_{rev} = \boldsymbol{R}T/F \log_e \left(\frac{\beta[Na^+]_o [K^+]_o}{\beta[Na^+]_i + [K^+]_i} \right), \quad (1)$$

where E_{rev} is the reversal potential, $\boldsymbol{R}$, T and F have their usual meaning, $[Na^+]_o$ and $[Na^+]_i$ are the extracellular and intracellular sodium concentrations, $[K^+]_o$ and $[K^+]_i$ are the extracellular and intracellular potassium concentrations and β is the Na^+/K^+ permeability ratio. If the intracellular K^+ concentration is taken as 99.4 mmol l^{-1} (Brading and Caldwell, 1971) and β is set to zero then the reversal potential will be described by the Nernst equation shown by the solid line on the plot (Fig. 3E). If the intracellular sodium concentration is taken as 44.6 mmol l^{-1} (Brading and Caldwell, 1971) and β set to 0.04 then the constant-field equation predicts the relationship shown by the broken line on the plot (Fig. 3E).

These experiments are consistent with depolarization activating cation channel currents which are about twenty times more permeable to potassium than to sodium. The extracellular potassium concentration is around 20 mmol l^{-1} in *Ascaris* (Brading and Caldwell, 1971) and the reversal potential of the outward current is expected to be in the linear region of the plot (Fig. 3E) under physiological conditions. Subsequently in this paper the voltage-activated outward current is referred to as the K^+ current.

Recovery of K^+ current from inactivation

Prolonged depolarizing voltage steps produced a K^+ current which rapidly rose to a peak and then slowly declined. This decline was taken to indicate slow inactivation of the K^+ current during depolarization; at hyperpolarized potentials the inactivation would have to be removed to allow subsequent activation by depolarizing steps. In order to study the time course of recovery from inactivation, a two-step depolarizing protocol was used: the depolarizing steps were separated by intervals lasting up to 12 s at a holding potential of −35 mV (Fig. 4A). A delay of 1 min between each series of two depolarizing pulses was adequate to allow complete recovery of the K^+ current.

It can be seen from Fig. 4A that there is selective inactivation of an early component of the K^+ current (the peak), with the peak current amplitude of the second pulse recovering as the interpulse interval is lengthened. The time course of recovery from inactivation is shown in Fig. 4B, where the difference between the peak current and the steady-state current at the end of the second pulse was expressed as a percentage of the difference of first pulse: the value obtained represents the percentage recovery. The means ± S.E. of the recovery percentages obtained from six experiments were then plotted as a function of the interpulse interval (Fig. 4B). The points were then fitted by the equation:

$$R = 100 \times \{A[1 - \exp(-t/T_1)] + B[1 - \exp(-t/T_2)]\}, \quad (2)$$

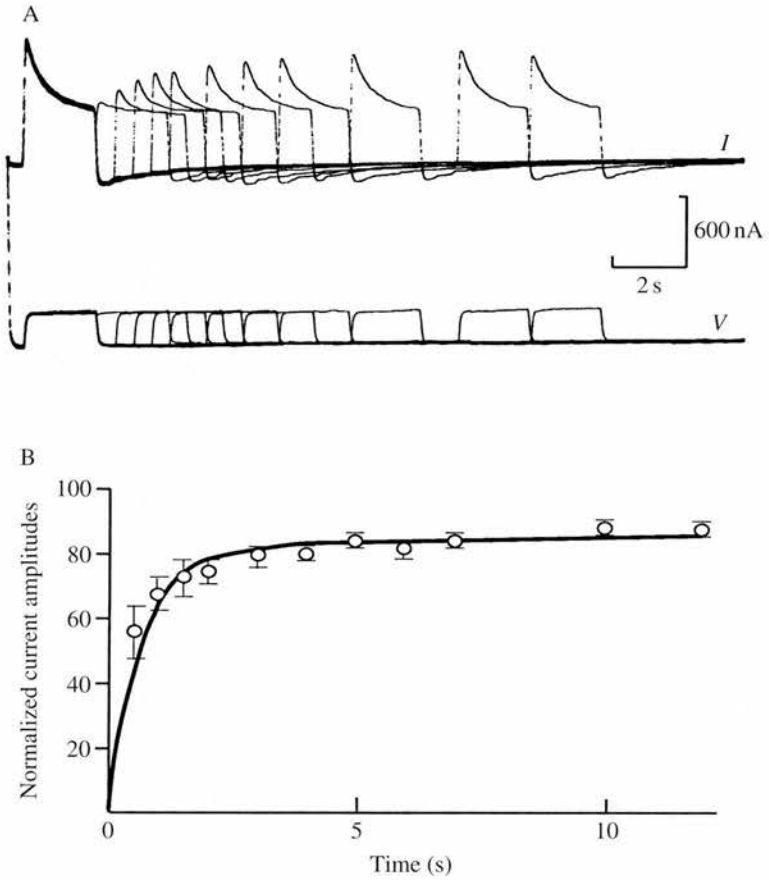


Fig. 4. Double-voltage-pulse estimation of the inactivation recovery time course. The cell was first stepped from a holding potential of −35 mV to a conditioning pulse of +55 mV; this was followed by a test pulse of +55 mV after increasing time intervals. The interpulse interval was measured as the time between the end of the conditioning pulse and the beginning of the test pulse. The interval was varied between 0 and 12 s. Ca^{2+}-free lanthanum solution. (A) Current (top) and voltage (bottom). The peak amplitude of the outward current activated by the test pulse was reduced at short interpulse intervals but showed a gradual recovery as the interpulse interval increased. (B) Plot of the difference between the peak current and steady-state current at the end of the test pulse expressed as a percentage of the same from the conditioning pulse. The means ± S.E. of the recovery percentages obtained from six experiments are plotted as a function of the interpulse interval. The points were fitted to the recovery equation (equation 2). A=0.825, T_1=0.67 s, B=0.087 and T_2=20.12, 37 °C.

where R is the percentage recovery, t is time, A and B are constants and T_1 and T_2 are the fast and slow time constants of recovery. T_1 was 0.67 s; T_2 was 20.1 s; A was 0.825 and B was 0.087 (line on Fig. 4B). Since A was large compared to B it follows that most of the recovery occurs in less than 2 s but full recovery was not observed after 12 s, the maximum test interval shown in Fig. 4B, since T_2 was 20.1 s.

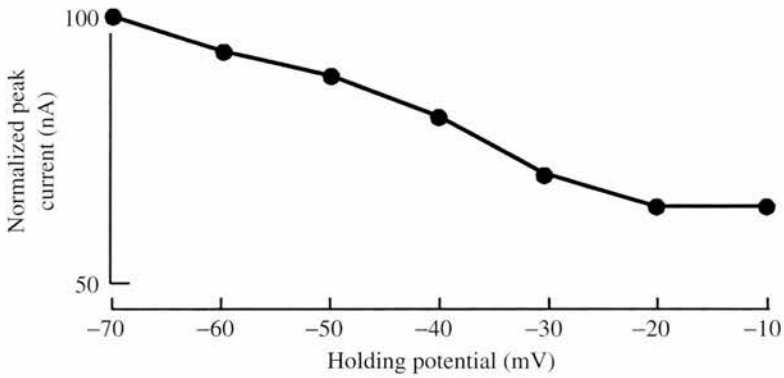


Fig. 5. Effect of holding potential on voltage-activated outward current in a single cell. Leak-subtracted current records; Ca^{2+}-free lanthanum solution; step potential +50 mV. Plot of the peak current amplitude as a percentage of the value obtained with a holding potential of −70 mV against holding potential. As the holding potential was reduced, the peak amplitude of the outward current was observed to decline, indicating that only a component of the outward current (34 %) was dependent on the holding potential.

Effect of holding potential on peak K^+ current amplitude

Steady-state inactivation was studied by holding cells at potentials between −70 mV and −10 mV and stepping to a potential of +50 mV. The amplitude of the peak K^+ current was reduced in all cells as the holding potential was made more depolarized. The effect of holding potential on K^+ current is plotted in Fig. 5 for a representative cell: the amplitude of peak K^+ currents at +50 mV obtained from different holding potentials was expressed as a percentage of the peak K^+ current obtained from a holding potential of −70 mV. It can be seen that the reduction in peak K^+ current, because of inactivation, was partial, since the current only declined by 34 % when very depolarized holding potentials (−20 mV) were used. Similar results were obtained from three other cells.

The selective effect of inactivation on the early component (the peak) of the K^+ current and the fact that only part of the K^+ currents may be inactivated by very depolarized holding potentials (Figs 4 and 5) suggest that the K^+ currents may be divided into two currents corresponding to an inactivating K^+ current and a non-inactivating K^+ current.

Effect of 4-AP on the outward current

A rapidly inactivating, transient K^+ current, known as I_a, and a slowly inactivating current, known as I_k, are prominent features of many other cells (e.g. Connor and Stevens, 1971; Neher, 1971; Kostyuk *et al.* 1981; Thompson, 1977; Belluzzi *et al.* 1985). The I_a currents of these cells are selectively blocked by the potassium channel antagonist 4-AP.

The effect of 5 mmol l^{-1} 4-AP on the K^+ currents of *Ascaris* was therefore examined using cells bathed in a lanthanum solution and given depolarizing steps to between −25 mV and +55 mV from a holding potential of −35 mV (Fig. 6A). The currents obtained in the presence of 4-AP showed an increase in the time to peak and a decrease in the peak amplitude (Fig. 6B). At a potential of +55 mV the amplitude of the current was

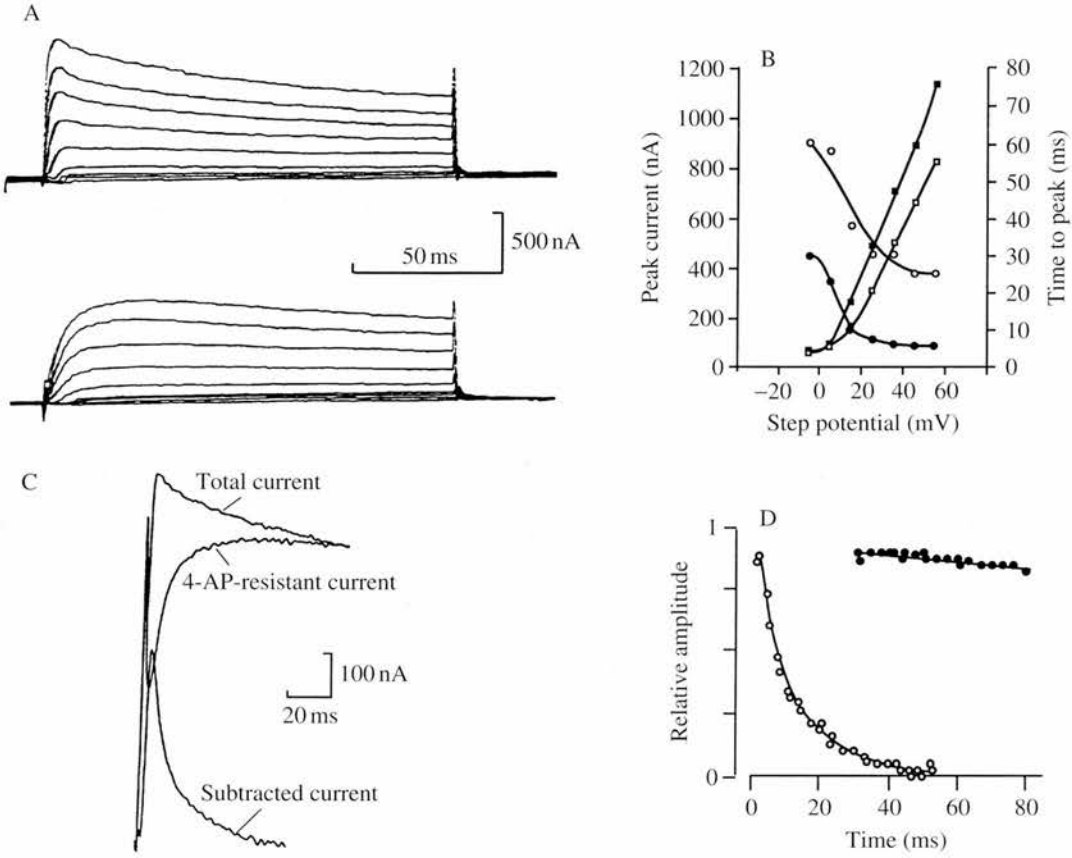


Fig. 6. Effect of 4-AP on leak-subtracted currents. (A) The upper set of currents is from a cell bathed in lanthanum solution and the lower set of currents is from the same cell bathed in 5 mmol l^{-1} 4-AP Ca^{2+}-free lanthanum solution. The holding potential was −35 mV and the cell was stepped to −25 mV, −15 mV, −5 mV, +5 mV, +15 mV, +25 mV, +35 mV, +45 mV and +55 mV. The currents in 4-AP show the loss of a fast component to the outward current, 37 °C. (B) Peak outward current and time to peak plotted against step potential before and after 5 mmol l^{-1} 4-AP. Time to peak before 4-AP, filled circles; after 4-AP, open circles. Peak amplitude before 4-AP, filled squares; after 4-AP, open squares. (C) Current records from a cell obtained with a step potential of +55 mV showing the 4-AP-sensitive current obtained by subtracting the 4-AP-resistant current from the control current. Upper trace, control in lanthanum solution; an initial capacitative surge is followed by a rapid rise of the current to a peak of 820 nA in 10 ms. Middle trace, in 5 mmol l^{-1} 4-AP lanthanum solution, shows the 4-AP-resistant current; the current shows a slow rise to a peak of 660 nA after 45 ms and the current decays with a rate constant of 1.1 s (fitted line). Lower trace, 4-AP-sensitive current obtained by subtraction. This current shows a rapid rise to a peak of 425 nA after 10 ms. (D) The decay of the 4-AP-sensitive current (open circles) is rapid with a time constant of 7.53 ms (fitted line) compared to the decay of the 4-AP-resistant current (filled circles; time constant for decay 1.1 s).

reduced to around 70 % of its original value; washing the preparation for 30 min did not reverse the effect of 4-AP.

The currents obtained after application of 5 mmol l^{-1} 4-AP were then subtracted from the control records to determine the 4-AP-sensitive current. Fig. 6C shows the currents at +55 mV. It can be seen that the 4-AP-sensitive current was a transient current which rose to a peak and decayed rapidly.

The rate of decay at +55 mV was described by fitting the 4-AP-sensitive current to the equation:

$$I = A\exp(-t/T), \tag{3}$$

where I is the current at time t, T is the time constant of decay and A is the current at time zero. T was 10.4 ms and A was 410 nA; similar results were obtained in six other cells. These results show that 4-AP was acting to block a fast transient component of the outward current. In order to illustrate the relative speed of inactivation shown by the 4-AP-sensitive current, the 4-AP-resistant current was also fitted by the decay equation (equation 3). It was found that the 4-AP-resistant current decayed with a time constant of 1.1s in the experiment illustrated in Fig. 6C. Similar results were obtained in eight other experiments. Thus, the 4-AP-sensitive current decayed at a rate two orders of magnitude faster than the 4-AP-resistant current at +55 mV.

Activation curves of 4-AP-sensitive and 4-AP-resistant currents

The peak amplitudes of the 4-AP-sensitive and the 4-AP-resistant currents were plotted against the step potential: all the data from the cell shown in Fig. 6, relating the peaks of the 4-AP-sensitive and 4-AP-resistant currents to voltage, are shown in Fig. 7A. The threshold for both currents was near −15 mV but between −15 mV and +25 mV the 4-AP-sensitive current peak was greater.

The activation characteristics of the two K^+ currents shown in Fig. 7A were analysed by estimating the conductance, g, at different depolarizations according to the relationship:

$$I = g(V - E_k), \tag{4}$$

where I refers to the peak current values, V is the step potential and E_k is the reversal potential; this equation assumes that the instantaneous current–voltage relationship is linear. The data were then fitted to the Boltzmann equation:

$$g = g_{max}/\{1 + \exp[(V_h - V)/k]\}, \tag{5}$$

where g is the conductance, g_{max} is the maximum conductance, V is the test potential, V_h is the 'half-activation' potential and k defines the slope. For the 4-AP-sensitive current the peak conductance was 5.3 μS, V_h was 14.1 mV and k was 10.5 mV; for the 4-AP-resistant current the peak conductance was 9.4 μS, V_h was 29.3 mV and k was 12.1 mV. The activation curve and the Boltzmann fit to the observations are shown in Fig. 7B: this figure is further evidence of the separate nature of the two K^+ currents and that the 4-AP-resistant current has a V_h which is 15 mV more positive than that of the 4-AP-sensitive current. The values of 10.5 mV and 12.1 mV for the slope, k, are similar to those obtained in other cells for potassium currents (e.g. squid axon, 12 mV, Hodgkin and Huxley, 1952; rat sympathetic neurone, 10 mV, Belluzzi *et al.* 1985). The values 10.5 mV and 12.1 mV

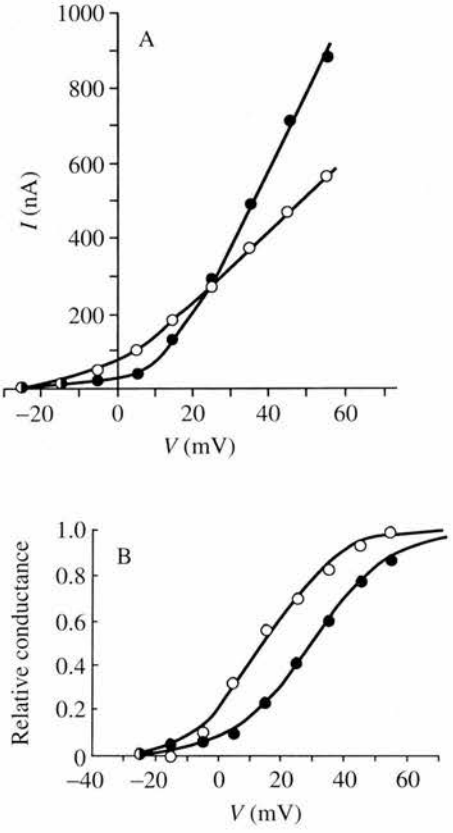


Fig. 7. (A) Peak current–voltage relationship for the 4-AP-sensitive (open circles) and 4-AP-resistant (filled circles) currents. Data from the experiment illustrated in Fig. 6A. (B) Activation curve for the 4-AP-sensitive and 4-AP-resistant currents fitted to Boltzmann equation; see text for further details.

in *Ascaris* for the slopes suggest that the gating charge for opening the 4-AP-sensitive channel is 24/10.5 (Hille, 1984), i.e. equivalent to 2.3 elementary charges and that for the 4-AP-resistant current is equivalent to 2.0 elementary charges.

Discussion

Our main conclusion is that a voltage-sensitive Ca^{2+} current and two K^+ currents can be isolated and observed in the soma of muscle cells of *Ascaris suum*. The large amplitude and relatively fast kinetics are consistent with these currents in combination generating the spike potentials described by Weisblat *et al.* (1976). Slower and smaller-amplitude currents which may underlie 'slow waves' and 'modulation waves' were not revealed in this study. It was pointed out in Materials and methods that low-Ca^{2+} solutions, as used in this study, were likely to abolish currents activated as a result of calcium entry. Thus, Ca^{2+}-activated channel currents could be present and be involved in the production of the slow waves and modulation waves.

Exogenous neural control and initiation of each spike potential at an initiation zone in the syncytium have been suggested for *Ascaris* (DeBell *et al.* 1963); the spikes were suggested to start at the syncytium and then to propagate actively or electrotonically *via* the arm to the rest of the muscle cell. The observations reported here show that the bag region (soma) possesses currents that could initiate spike potentials. It is therefore suggested that each muscle cell of *Ascaris* is capable of self-generated depolarizing activity and that the role of the electrical coupling at the syncytial region is to produce coordination of the depolarization of adjacent muscle cells for contraction of the body wall. The excitatory and inhibitory chemical synaptic inputs at the syncytium could speed or slow the depolarizations.

Ca^{2+} current

Two major types of Ca^{2+} current have been described in other cell types. There is a transient Ca^{2+} current which has been variously named low-threshold inactivating, LTI (see Kostyuk *et al.* 1988), transient (Bossu *et al.* 1985), low-voltage activated, LVA (Carbone and Lux, 1984), T (Fox *et al.* 1987) and type 1 (Narahashi *et al.* 1987). This current is transient and inactivates with a time constant in the region of 20 ms, may be activated at relatively negative potentials (−40 to −20 mV) but also requires relatively negative potentials (more negative than −40 mV) to remove inactivation. The second type of Ca^{2+} current seen in many cells decays slowly with a time constant of at least 1 s. It could be activated from less negative holding potentials than the transient current and has been referred to as high-threshold inactivating, HTI (Kostyuk *et al.* 1988), high-voltage activated HVA (Carbone and Lux, 1984) and L (Fox *et al.* 1987).

The Ca^{2+} current of *Ascaris* seen in our experiments had some but not all of the properties of both of these two major types of Ca^{2+} current: it inactivated but required a relatively depolarized potential for activation and was not inactivated by a holding potential of −35 mV. The current allows the production of a spike in *Ascaris* muscle cells with a resting membrane potential around −35 mV.

Little pharmacology has been done on the Ca^{2+} spikes of *Ascaris* but the report of Wann (1987) shows that the vertebrate Ca^{2+} antagonists verapamil and cinnarazine have little effect in *Ascaris*; the channel may therefore have a distinctive pharmacology.

K^+ currents

It has already been pointed out in this paper that two major types of K^+ current have been recognised in a wide variety of cells and that these types are referred to as I_a and I_k. The I_a is a transient current which significantly inactivates with time constants of 10–50 ms at holding potentials more depolarized than −40 mV (Connor and Stevens, 1971; Kostyuk *et al.* 1975; Thompson, 1977) and is usually blocked specifically by 4-AP (Connor and Stevens, 1971; Cook, 1988; but see Yeh *et al.* 1976; Ginsborg *et al.* 1991). The I_k current is a maintained current which is not significantly inactivated at holding potentials more depolarized than −40 mV (Connor and Stevens, 1971; Kostyuk *et al.* 1975; Thompson, 1977).

In this paper the K^+ current of *Ascaris* was separated into two components on the grounds that maintained depolarization and 4-AP selectively blocked a lower-threshold

(V_h=+14 mV) transient component (inactivation rate about 10 ms) but left a maintained current (inactivation rate constant about 1 s) which required greater depolarization (V_h=+29 mV) to produce activation. The 4-AP-sensitive current of *Ascaris* is therefore I_a-like and the 4-AP-resistant current is I_k-like.

The function of I_a currents as suggested by Connor and Stevens (1971) for neurones of *Anisodoris* is to serve as a damper on the interspike interval to space successive action potentials. This is also possible in *Ascaris* because inactivation of the I_a-like current appears to be complete at −20 mV (Fig. 5B). Activation occurs at potentials more positive than −30 mV (Fig. 7B) so that, at the steady state, only a small fraction of the channels may conduct in the narrow range of −30 mV to −20 mV. At the typical membrane potential of −35 mV, most of the I_a-like current would be inactivated. At the end of a Ca^{2+} spike the subsequent hyperpolarization removes inactivation of the I_a-like channel as well as closing the I_k-like channel and allowing the membrane to depolarize slowly again; the I_a-like current at this stage activates and slows the rate of depolarization until it becomes inactivated; the cell can then again reach threshold. Rates of recovery from inactivation are significant and have to be sufficiently rapid if the I_a-like current is going to behave in this manner. In this study most of the recovery of the transient current took place in less than 1 s but full recovery did not occur until after 12 s. Comparable recovery rates have been seen in *Archidoris* and *Anisodoris* neurones (Aldrich *et al.* 1979) and in the neural somata of *Helix pomatia* (Kostyuk *et al.* 1975; Heyer and Lux, 1976). This slow recovery from inactivation may permit the K^+ currents to contribute to the production of the 'slow waves' and 'modulation waves' of Weisblat *et al.* (1976). This effect and the effect of possible Ca^{2+}-activated channel currents are subjects for further investigation.

We are pleased to acknowledge the financial support of the SERC.

References

Aldrich, R. W., Getting, P. A. and Thompson, S. H. (1979). Inactivation of delayed outward current in molluscan somata *J. Physiol., Lond.* **291**, 507–530.

Belluzzi, O., Sacchi, O. and Wanke, E. (1985). A fast transient outward current in the rat sympathetic neurone studied under voltage-clamp conditions. *J. Physiol., Lond.* **358**, 91–108.

Bossu, J. L., Feltz, A. and Thomann, J. M. (1985). Depolarization elicits two distinct calcium currents in vertebrate sensory neurones. *Pflügers Arch.* **403**, 360–368.

Brading, A. F. and Caldwell, P. C. (1971). The resting membrane potential of the somatic muscle cells of *Ascaris lumbricoides*. *J. Physiol., Lond.* **217**, 605–624.

Carbone, E. and Lux, H. D. (1984). A low voltage-activated, fully inactivating Ca channel in vertebrate sensory neurones. *Nature* **310**, 501–502.

Connor, J. A. and Stevens, C. F. (1971). Voltage-clamp studies of a transient outward membrane current in gastropod neural somata. *J. Physiol., Lond.* **213**, 21–30.

Cook, N. S. (1988). The pharmacology of potassium channels and their therapeutic potential. *Trends pharmac. Sci.* **9**, 21–28.

DeBell, J. T., Del Castillo, J. and Sanchez, V. (1963). Electrophysiological of somatic muscle cells of *Ascaris lumbricoides*. *J. cell. comp. Physiol.* **62**, 159–177.

Fenwick, E. M., Marty, A. and Neher, E. (1982). Sodium and calcium channels of bovine chromaffin cells. *J. Physiol. Lond.* **331**, 599–636.

Fox, A. P., Nowycky, M. C. and Tsien, R. W. (1987). Kinetic and pharmacological properties

distinguishing three types of calcium channel in chick sensory neurones. *J. Physiol., Lond.* **394**, 173–200.

GINSBORG, B. L., MARTIN, R. J. AND PATMORE, L. (1991). On the sodium and potassium currents of a human neuroblastoma cell line. *J. Physiol., Lond.* **434**, 121–149.

HEYER, C. B. AND LUX, H. D. (1976). Control of the delayed outward potassium currents in bursting pacemaker neurones of the snail, *Helix pomatia*. *J. Physiol., Lond.* **262**, 349–382.

HILLE, B. (1984). *Ionic Channels of Excitable Membranes.* Sunderland, MA: Sinauer.

HODGKIN, A. L. AND HUXLEY, A. F. (1952). A quantitative description of membrane current and its application to conduction and excitation in nerve. *J. Physiol., Lond.* **117**, 500–544.

JARMAN, M. AND ELLORY, J. C. (1969). Effect of TTX on *Ascaris* somatic muscle. *Experientia* **25**, 507.

KOSTYUK, P. G., KRISHTAL, O. A. AND DOROSHENKO, P. A. (1975). Outward currents in isolated snail neurones. I. Inactivation kinetics. *Comp. Biochem. Physiol.* **51**C, 259–263.

KOSTYUK, P. G., SHUBA, YA. M. AND SAVCHENKO, A. N. (1988). Three types of calcium channels in mouse sensory neurones. *Pflügers Arch.* **411**, 661–669.

KOSTYUK, P. G., VESELOVSKY, N. S., FEDULOVA, S. A. AND TSYNDRENKO, A. Y. (1981). Ionic currents in the somatic membrane of rat dorsal root ganglion neurones. III. Potassium currents. *Neuroscience* **6**, 2439–2445.

LEE, K. S. AND TSIEN, R. W. (1982). Reversal of current through calcium channels in dialysed single heart cells. *Nature* **297**, 498–501.

MARTIN, R. J. (1982). Electrophysiological effects of piperazine and diethylcarbamazine on *Ascaris suum* somatic muscle. *Br. J. Pharmac.* **77**, 255–265.

MEECH, R. W. AND STANDEN, N. B. (1975). Potassium-activation in *Helix aspera* neurones under voltage clamp: a component mediated by calcium influx. *J. Physiol., Lond.* **249**, 211–240.

NARAHASHI, T., TSUNOO, A. AND YOSHI, M. (1987). Characterization of two types of calcium channels in mouse neuroblastoma cells. *J. Physiol., Lond.* **383**, 231–249.

NEHER, E. (1971). Two fast transient current components during voltage clamp on snail neurones. *J. gen. Physiol.* **58**, 36–53.

REUTER, H. AND SCHOLTZ, H. (1977). A study of the ion selectivity and kinetic properties of the calcium dependent slow inward current in mammalian cardiac muscle. *J. Physiol., Lond.* **264**, 17–47.

ROSENBLUTH, J. (1963). Fine structure of body muscle cells and neuromuscular junctions in *Ascaris lumbricoides*. *J. Cell Biol.* **19**, 82A.

ROSENBLUTH, J. (1965). Ultrastructure of somatic muscle cells in *Ascaris lumbricoides*. II. Intermuscular junctions, neuromuscular junctions and glycogen stores. *J. Cell Biol.* **26**, 579–591.

THOMAS, M. V. (1984). Voltage-clamp analysis of a calcium-mediated potassium conductance in cockroach (*Periplaneta americana*) central neurones. *J. Physiol., Lond.* **350**, 159–178.

THOMPSON, S. H. (1977). Three pharmacologically distinct potassium channels in moluscan neurones. *J. Physiol., Lond.* **265**, 465–488.

THORN, P. AND MARTIN, R. J. (1987). A high-conductance Ca-dependent chloride channel in *Ascaris suum* muscle. *Q. Jl exp. Physiol.* **72**, 31–49.

WANN, K. T. (1987). The electrophysiology of the somatic muscle cells of *Ascaris lumbricoides* and *Ascaridia galli*. *Parasitology* **94**, 555–566.

WEISBLAT, D. A., BYERLY, L. AND RUSSELL, R. L. (1976). Ionic mechanisms of electrical activity in somatic muscle of the nematode *Ascaris lumbricoides*. *J. comp. Physiol.* A **111**, 93–113.

YEH, J. Z., OXFORD, G. S., WU, C. H. AND NARAHASHI, T. (1976). Dynamics of aminopyridine block of potassium channels in squid axon membrane. *J. gen. Physiol.* **68**, 519–535.

Reprinted from Parasitology Today – *September 1993* *Vol. 9, No. 9*

Techniques

Patch-clamp and Chloride Channels in *Ascaris suum*

D.M. Dixon and R.J. Martin

Single-channel electrophysiology is an invaluable tool for the study of ion channels. However, it is a technique that has failed to attract widespread use by parasitologists. Here, Diane Dixon and Richard Martin outline the principles underlying single channel recording and highlight its uses in the discovery of a new and unusual chloride channel in the musculature of Ascaris suum.

A number of important anthelmintics act by gating ion channels, thereby altering the electrical properties of their target cells. In order to further our understanding of such antiparasitic agents, it is necessary to study their mechanism of action at the molecular level. This is made possible by electrophysiological techniques, particularly patch-clamp. This technique is now widely used in the study of transmembrane currents in mammalian neuronal and muscle cells. However, for several reasons, there is a dearth of information concerning, at the single-channel level, the functioning of the musculature and neuronal activity in parasites: (1) the patch-clamp technique is at its best when fresh parasite tissue is used, and this can sometimes be difficult to obtain regularly; (2) the cells of the nervous systems and the musculature are, in general, small, and are therefore inaccessible to the electrophysiologist; and (3) the technique is relatively new and complex compared to older and more established biochemical methodologies.

Why *Ascaris*?

Nevertheless, it is possible to overcome all of these difficulties. We chose to work on the nematode *Ascaris suum* which can be regularly and freshly obtained from our local abattoir. The musculature of *Ascaris* is suited to the patch-clamp technique as it is large and easily accessible. Initial experiments had involved the use of the two-microelectrode electrode voltage-clamp technique, but the limited resolution of this method led to the development of the preparation for single-channel recordings.

The patch-clamp technique depends on the ability to form a tight electrical seal between the edge of the recording pipette and the membrane under investigation. The electrical resistance between the membrane and the pipette tip needs to be larger than a giga ohm (10^9 Ω) in order to make successful recordings of the pico-amp currents (1 pA=10^{-12} A) produced by the opening and closing of single-ion channels in the membrane suspended across the pipette tip. It is essential, in order to obtain the giga-ohm seals required for single-channel recording, that the membrane under study is cleaned of extracellular matrix. The early experiments on *Ascaris* involved cleaning the surface of a flap preparation of the muscle tissue with collagenase. This was a simple procedure that entailed bathing a muscle flap preparation in a collagenase solution, the resulting debris was then washed off the cleaned tissue[1]. Subsequently this procedure was modified into a methodology for the production of spherical muscle vesicles (Box 1). The muscle membranes of the vesicles are complete, intact and very clean, allowing the regular formation of giga-ohm seals. Their size (averaging 25 μm in diameter) enables both whole cell and isolated patch experiments to be performed[2].

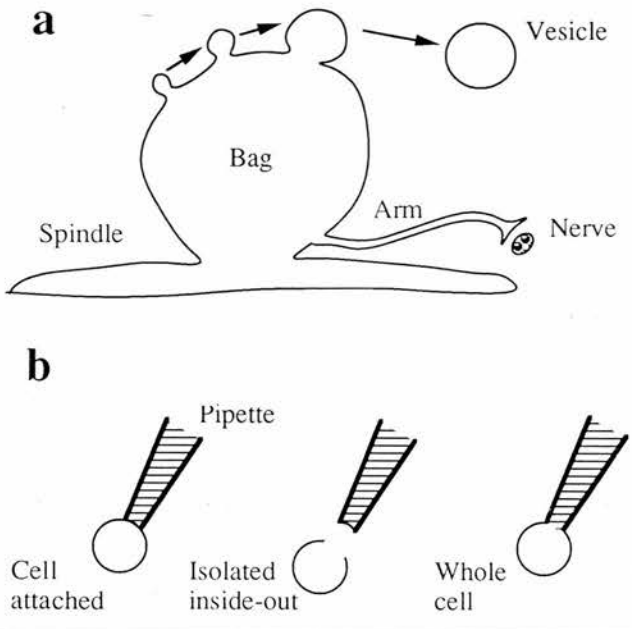
Experimental Possibilities

Once a piece of membrane has been electrically isolated, the experiment can continue in a variety of forms. A substantial proportion of published work involves the study of ligand-gated ion channels. For example, the action of avermectins on chloride channels and anthelmintics on the nicotinic acetylcholine channel are widely documented (for references, see Ref. 3). These studies entail the

© 1993, Elsevier Science Publishers Ltd, (UK) 0169–4758/93/$06.00

Box 1. Vesicle Formation

The ability to form a tight seal between pipette tip and membrane depends to a large extent on the membrane being clean of extracellular matrix. The technique most widely employed involves the enzymatic removal of the matrix. This procedure can be applied to most muscle preparations, for example it is used to disperse cardiac myocytes and to treat various skeletal muscle fibres. Here we discuss the procedure for the formation of clean vesicles from *Ascaris suum* muscle.



A small flap of body wall from *Ascaris suum* is pinned out, cuticle side down, and the gut removed. The preparation is then washed with extracellular solution and incubated for 10 min with collagenase solution (1 mg ml^{-1}). The muscle is then liberally washed with extracellular solution and incubated at 37°C. Approximately 1 h after enzyme treatment, the bag region of the muscle cell can be seen 'budding' (see Fig. part a). Once released, the vesicles are easily collected in a Pasteur pipette and transferred to the recording chamber.

Successful giga-ohm seals can be obtained with the clean membranes presented by the vesicles simply by pressing a fire polished patch pipette tip against the vesicle membrane and applying gentle suction. Once a giga-ohm seal is formed, the experiment can proceed in a variety of ways: the pipette can be left undisturbed in the cell attached mode; the pipette can be pulled away from the vesicle so forming an inside-out patch; or strong suction can be applied that bursts the membrane across the pipette tip leading to the whole-cell mode (see Fig. part b).

***(a)** Diagrammatic representation of a muscle cell from* Ascaris suum *showing the effect of treatment with enzyme solution.*

***(b)** Diagram of the various experimental methods available for the recording of single-channel currents from* Ascaris *muscle vesicles.*

analysis of the kinetics of channel currents. The mathematics involved can be quite complex, but the results give a uniquely detailed insight into the molecular states involved in the activation of the channel by both agonists and antagonists.

In addition, using isolated inside-out patches of membrane it is possible to record channel activity under a variety of intracellular ionic conditions. By introducing several different anions to the intracellular surface of the patch it is possible to build up a picture of channel permeability. Such studies involve a different type of analysis that utilizes the conductance and reversal potential of the permeant anions to probe the nature of the internal environment of the channel[4]. Using this methodology, we widened the scope of the work on *Ascaris* to examine a non-ligand-gated channel, namely the Ca-activated chloride channel (ie. a chloride channel that is dependent upon the presence of cytoplasmic Ca for opening) (Fig. 1).

Analyses of Single-channel Data

Single-channel currents are rectangular in appearance and approximately one pico amp in magnitude. The analysis of these single-channel currents takes two main forms: (1) the examination of the kinetics of channel opening; or (2) measurement of current amplitude and reversal potential.

Examination of open and closed times. This analysis is based on the distribution of the durations of single-channel events. The duration of the open or closed states of the channel is measured with computer techniques and analysed using a kinetic scheme.

An ion channel is either open (o) or closed (c) in the simplest analysis (Fig. 2a). The proportion of time the channel spends in the open state will depend on the rate constant for closure, α. Likewise the proportion of time the channel is closed depends on the rate constant for opening, β. For every second that the channel is open, it will shut α times, and for every second the channel is closed it will open β times. Therefore, it follows that the average time the channel spends in each particular state is the reciprocal of the rate constant that leads out of that state, ie. the mean open duration in milliseconds is $1/\alpha$. The rate of opening and closing are important characteristics of channel behaviour.

The distributions of open or closed times are exponential (this is illustrated for open times in Fig. 2b). An exponential curve describes the distributions of open and closed times in terms of a probability density function (*pdf*) :

$$pdf = \tau^{-1}.e^{-t/\tau}$$

where t is time (x axis), and τ is the time constant of the curve. It is the variable τ that determines the shape of the curve and is, on an exponential curve, numerically equal to the mean open time, $1/\alpha$. The same analysis can also be applied to the distributions of closed times.

However, in reality the kinetic behaviour of ion channels is rarely so simple. It is commonly the case that a single exponential will not adequately describe the observed data. That is to say the open-time histogram and the closed-time histogram can only be described mathematically by using multiple exponentials. In these cases, it is usual to fit several exponentials to the data using the method of maximum likelihood to produce values for the variables within the *pdf*. The number of exponentials required to fit the data is an indication of the number of states that the ion channel can exist in. For example, the *Ascaris* Ca-activated chloride channel displays complex channel kinetics[6]. The time distribution is best fitted by two exponentials and the closed-time distribution is fitted by three exponentials. The channel is therefore assumed to have two open states and three closed states.

Examination of the current amplitude and channel permeability. This second form of analysis measures the amplitude of the single-channel current

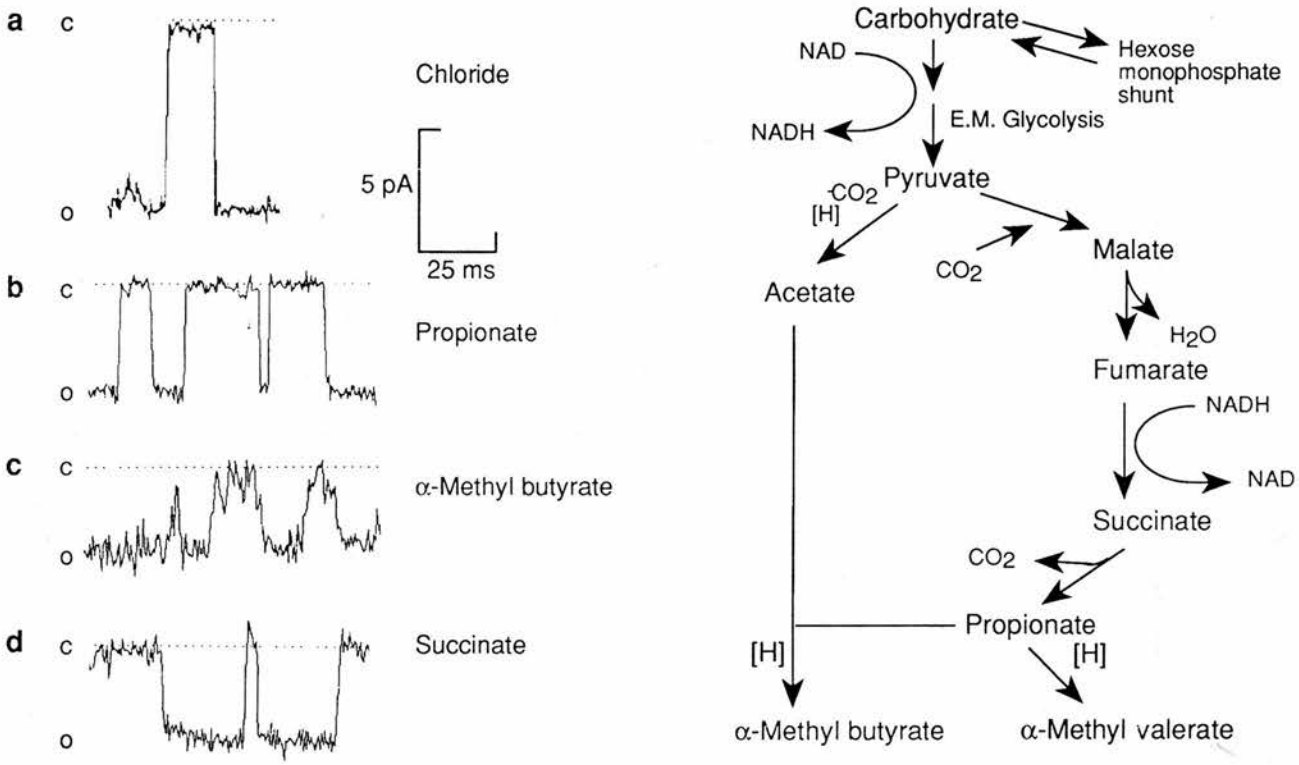


Fig. 1. Current records obtained from an inside-out patch of Ascaris *muscle (left) and a diagrammatical representation of the anaerobic metabolic pathway of* Ascaris *(right). Current records obtained when the channel is conducting: a, chloride; b, propionate; c, α-methyl butyrate; or d, succinate. The pipette solution (external solution) contained; 140 mM cesium chloride: 1 mM calcium acetate; 2 mM magnesium acetate and 10 mM HEPES, pH to 7.2 with cesium hydroxide. The bath solution (internal solution) contained: 140 mM cesium X; 1 mM calcium acetate; 2 mM magnesium acetate and 10 mM HEPES, pH to 7.2 with cesium hydroxide, where X is: a, chloride; b, propionate, c, α-methyl butyrate or d, succinate. The membrane potential is held at –50 mV in all examples. o and c denote open and closed states, respectively.*

and its relationship with membrane potential. Because the amplitude of single channel currents is relatively consistent from one opening to the next, the mathematics involved are simpler than those required for kinetic analysis. Using the same simple model as above (Fig. 2a), the channel can either be open or closed.

By altering the membrane potential it is possible to measure the current amplitude at various voltages. Amplitude histograms are drawn and the mean current at each voltage can be calculated (Fig. 3a). A current/voltage plot can be produced, the slope of which affords the conductance of the channel. The point at which the current/voltage plot crosses the x axis, ie. the point at which no net current is flowing across the patch, is

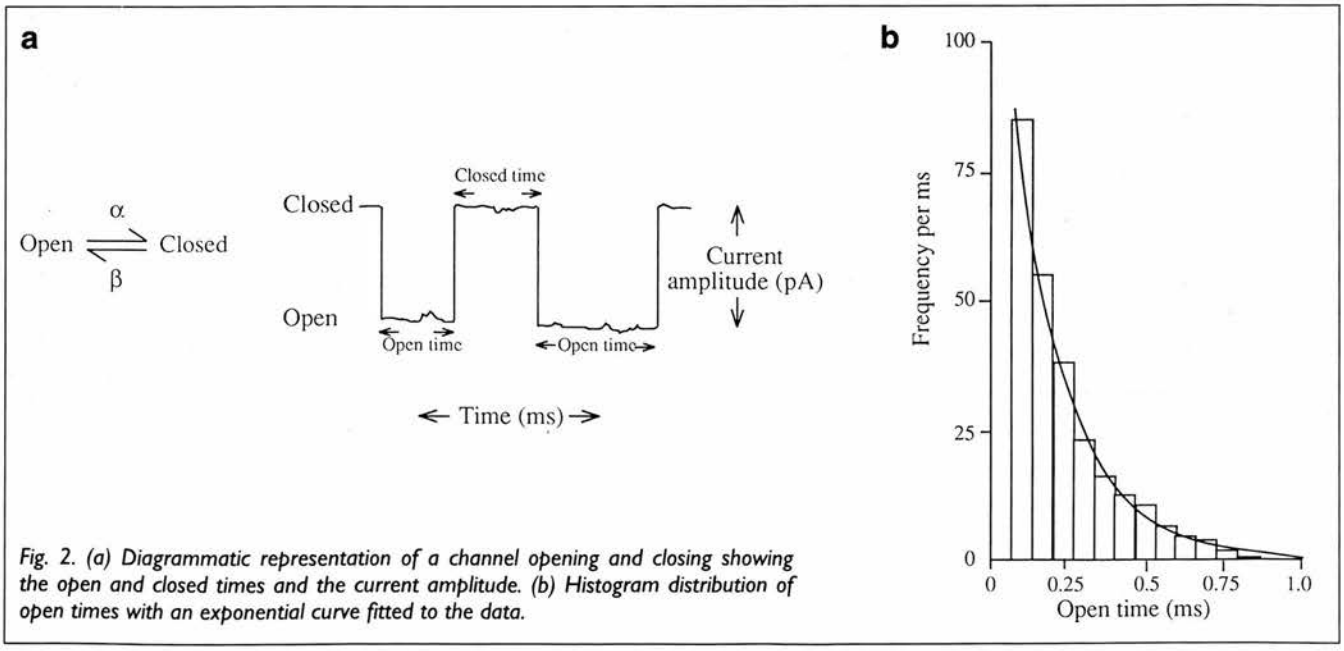


Fig. 2. (a) Diagrammatic representation of a channel opening and closing showing the open and closed times and the current amplitude. (b) Histogram distribution of open times with an exponential curve fitted to the data.

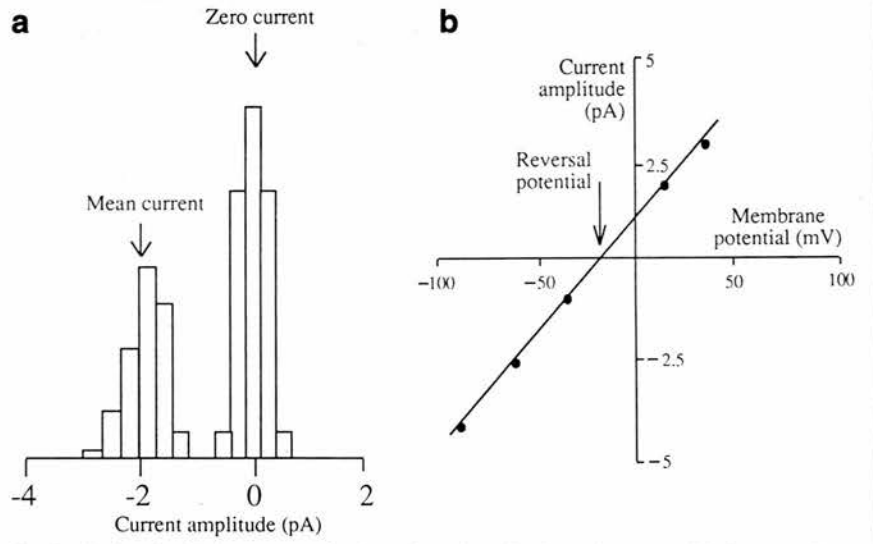


Fig. 3. (a) Amplitude histogram of a hypothetical single channel current. (b) Current-voltage graph for an anion selective channel with different species of anion on either side of the membrane. The slope of the graph is a measure of the single-channel conductance.

known as the reversal potential, E_{rev} (Fig. 3b).

The E_{rev} is dependent upon which ion is being conducted. Ion substitution experiments enable the calculation of permeability ratios between various permeant ion species. The E_{rev} is related to the permeability ratio (*Pr*) of two monovalent anions as follows:

$$E_{rev} = \frac{RT}{F} \log_e \left(\frac{[ion_1]_i + Pr[ion_2]_i}{[ion_1]_o + Pr[ion_2]_o} \right)$$

where R is the gas constant, T is absolute temperature and F is the Faraday constant, and where i and o denote ion concentrations on the intracellular (inside) and extracellular side (outside) of the membrane. If the internal concentration of ion_1 is zero, and the external concentration of ion_2 is zero, the equation simplifies to:

$$E_{rev} = \frac{RT}{F} \log_e \frac{Pr[ion_2]_i}{[ion_1]_o}$$

When such experiments are repeated for a wide variety of ions, a permeability sequence and a conductance sequence can be drawn up. The permeability sequence is a valuable source of information regarding the nature of the channel pore. For example the halide permeability sequence assembled for the Ca-activated chloride channel afforded information regarding the size of the channel pore and the number of cationic binding sites within it[4].

Ca-activated Chloride Channel

A detailed study of the permeability of a series of monocarboxylic acids revealed the channel was able to conduct all the aliphatic fatty acids within the series formate to heptanoate. Several of the fatty acids are important products of the anaerobic respiratory pathway of *Ascaris* (Fig. 1). Indeed the dicarboxylic acids formed as intermediate products of metabolism are also permeable. Previous studies[6] have shown the Ca-activated chloride channel is able to open fully at the resting membrane potential of *Ascaris*. Consequently, the muscle membrane is able, under normal membrane conditions, to remove products of metabolism from the inside of the cell. This is, to our knowledge, the first piece of work to show an ion channel that is capable of performing an excretory role in the muscle membrane. The widespread distribution of chloride channels throughout a diverse population of species could be an indication of the possible ubiquitous nature of such a channel. This work also highlights the usefulness of the electrophysiological technique in studying such systems.

Future Directions

Ascaris appears to be the only nematode parasite currently under study by single-channel electrophysiologists. As described above, it possesses a large musculature that favours such techniques. Unfortunately most nematodes remain too small for direct access by a patch pipette. However, with the advent of molecular biology techniques, access to the parasite nervous system is possible through a surrogate vehicle. The oocyte from the toad *Xenopus laevis* provides the perfect vehicle for such studies. Injection of purified parasite RNA into the oocyte results in the expression of nematode ion-channel proteins in the oocyt membrane. An avermectin-sensitive, glutamate-activated chloride current has recently been recorded from oocytes expressing *Caenorhabditis elegans* proteins[5]. The advent of molecular biological techniques cannot be underestimated: they represent the most important method available for the electrophysiological study of microscopic nematodes.

References

1 Martin, R.J. (1985) *Br. J. Pharmacol.* 84, 445–461
2 Martin, R.J., Kusel, J.R. and Pennington, A.J. (1990) *J. Parasitol.* 76, 340–348
3 Robertson, S.J. and Martin, R.J. (1993) *Br. J. Pharmacol.* 108, 170–178
4 Dixon, D.M., Valkanov, M. and Martin, R.J. (1993) *J. Membr. Biol.* 131, 143–149
5 Arena, J.P. *et al.* (1992) *Mol. Brain Res.* 15, 339–348
6 Thom, P. and Martin, R.J. (1985) *Q. J. Exp. Physiol.* 72, 31–49

Diane M. Dixon and Richard J. Martin at the Department of Preclinical Veterinary Sciences, Royal (Dick) School of Veterinary Sciences, Summerhall, Edinburgh, UK EH9 1QH. D.M. Dixon is currently at the Department of Physiology and Pharmacology, University of Strathclyde, 204 George Street, Glasgow, UK G1 1WX.

J. Membrane Biol. 138, 133–141 (1994)

The Journal of
Membrane
Biology
© Springer Verlag New York Inc. 1994

The Ca-Activated Chloride Channel of *Ascaris suum* Conducts Volatile Fatty Acids Produced by Anaerobic Respiration: A Patch-Clamp Study

M. Valkanov*, R.J. Martin, D.M. Dixon

Department of Preclinical Veterinary Sciences, R.(D.)S.V.S., Summerhall, University of Edinburgh, Edinburgh EH9 1QH, United Kingdom

Received: 22 June 1993/Revised: 6 August 1993

Abstract. Plasma membrane vesicles prepared from the bag region of the somatic muscle cell of the parasite *Ascaris suum* contain a large conductance, voltage-sensitive, calcium-activated chloride channel. The ability of this channel to conduct a variety of carboxylic acids, a number of which are products of anaerobic respiration, was investigated using the patch-clamp technique and isolated inside-out patches of muscle membrane. The channel has a conductance of 140 pS in symmetrical 140 mM chloride. Replacement of internal chloride with various carboxylic acids (140 mM) caused large hyperpolarizing shifts in the reversal potential. Permeability ratios, relative to chloride, were calculated for each acid. The relationship between permeability ratio and ionic size is inverse and linear predicting a pore diameter of 6.55 Å. This simple relationship was not observed between ionic size and conductance. Calculation of the transition state energy required to transfer a single methyl group from aqueous phase to the binding site afforded a value that was low but favorable, indicating a cationic binding site of low field strength. As the channel is able to open fully at the resting membrane potential of *Ascaris* and is permeable to fatty acids produced by anaerobic respiration, the possible role of this channel in the removal of metabolic products across the muscle membrane is discussed.

Key words: *Ascaris suum* — Chloride channels — Permeability — Fatty acids — Anaerobic respiration

* *Present address:* Central Laboratory of Biophysics, Bulgarian Academy of Sciences, Sofia, Bulgaria

Correspondence to: R.J. Martin

Introduction

In this study we have examined further the calcium-activated chloride channel currents in the muscle membrane of the porcine nematode parasite *Ascaris suum.* This channel is located on the body muscle membrane of *Ascaris* and is selective for anions, cations are not detectably permeant (Thorn & Martin, 1987; Dixon, Valkanov & Martin, 1993). Because of biophysical properties so far documented (Thorn & Martin, 1987; Dixon et al., 1993), it is difficult to assign this channel to any of the four categories described by Franciolini and Petris (1987). The maxi chloride channel, as defined by Franciolini and Petris, imposes a minimum conductance of 200 pS in symmetrical 150 mM Cl; the Ca-activated chloride current of *Ascaris* only reaches such a conductance in symmetrical 175 mM Cl. The *Ascaris* chloride current remains active at holding potentials in excess of −100 mV, whereas the maxi chloride currents tend to inactivate at potentials outside the range ±30 mV from zero. As the opening of the *Ascaris* chloride channels is dependent upon calcium, it is possible to put this channel in the ligand-activated category of chloride currents. However, the large conductance of the calcium-activated channel does not fall in line with the small conductances (<50 pS in 145 mM KCl in mouse cultured spinal neurons) normally displayed by the GABA and glycine receptor gated channels (Bormann, Hamill & Sakmann, 1987). The further category of background chloride currents includes channels that are likely to be open at the resting membrane potential of the cell. The resting membrane potential of *Ascaris* is low at −35 mV and the Ca-activated chloride channel is indeed active at this potential. Unfortunately, the other criteria of this category are a mild voltage dependence and a conductance of between 10–100 pS in symmetrical 150 mM Cl. Clearly, the calcium-acti-

vated chloride channel fails to fulfill either criterion (Thorn & Martin, 1987) as it is greatly affected by membrane potential and its conductance is double the upper limit of this category. Further investigations into the properties of this channel are therefore required.

In this paper we have studied the ability of the channel to conduct several aliphatic organic acids including acetate and propionate, both of which are formed in the mitochondria as products of carbohydrate metabolism (Fig. 1*A* and 1*B*). In turn, acetate and propionate are condensed to α-methyl butyrate and two units of propionate condense to form α-methyl valerate. These two branch chained, volatile, fatty acids are the major fermentation products of carbohydrate metabolism in *A. suum* (Saz & Weil, 1962). In addition to being found in muscle tissue, α-methyl butyrate and α-methyl valerate have also been isolated from perienteric fluid (Fig. 1*C*), where they constitute two thirds of all extracellular anions (Saz & Bueding, 1966). A mechanism, therefore must be available to the cell for the movement of these fatty acids across the muscle membrane. In this paper we have attempted to determine whether the calcium-activated chloride channel forms part of such a mechanism.

Materials and Methods

Preparation of Muscle Vesicles

A. suum, obtained from the local slaughterhouse, were maintained at 34°C in Locke's solution that was changed daily. The first 5 cm anterior region of the worm was discarded and the next 2 cm section of worm was taken and cut along one lateral line. The gut was removed and the resulting flap pinned out, cuticle side down, onto Sylgard in an incubation chamber at 37°C. The preparation was washed (three times) with extracellular solution, composition (in mM): NaCl, 35; NaAcetate, 105; KCl, 2; $MgCl_2$, 2; HEPES, 10; glucose, 3; ascorbic acid, 2; EGTA, 1; pH adjusted to 7.2 with NaOH. The washed flap was then incubated for 10 min with enzyme solution, composition (in mM): NaCl, 35; NaAcetate, 105; KCl, 2; $MgCl_2$, 2; HEPES, 10; glucose, 3; ascorbic acid, 2; collagenase, 1 mg/ml; pH adjusted to 7.2 with NaOH. Following enzyme treatment, the preparation was washed (three times) with extracellular solution and incubated in extracellular solution at 37°C. Approximately 1 hr after enzyme treatment, vesicles could be seen "budding off" from the bag region of the muscle cell membrane. The vesicles were harvested using a Pasteur pipette and transferred to the recording chamber.

Recording Setup

Microelectrodes were pulled to a resistance of 1–3 MΩ (Garner Glass 7052) and coated with Sylgard to improve frequency responses. Single channel recordings were made from inside-out patches of muscle membrane with seal resistances >1 GΩ. Currents were monitored using a LIST EPC7 current-voltage converter, viewed on an oscilloscope, digitized and recorded on Betamax tape. Prior to analysis, records were filtered at 1 kHz (3 dB) by an 8-pole Bessel-type filter.

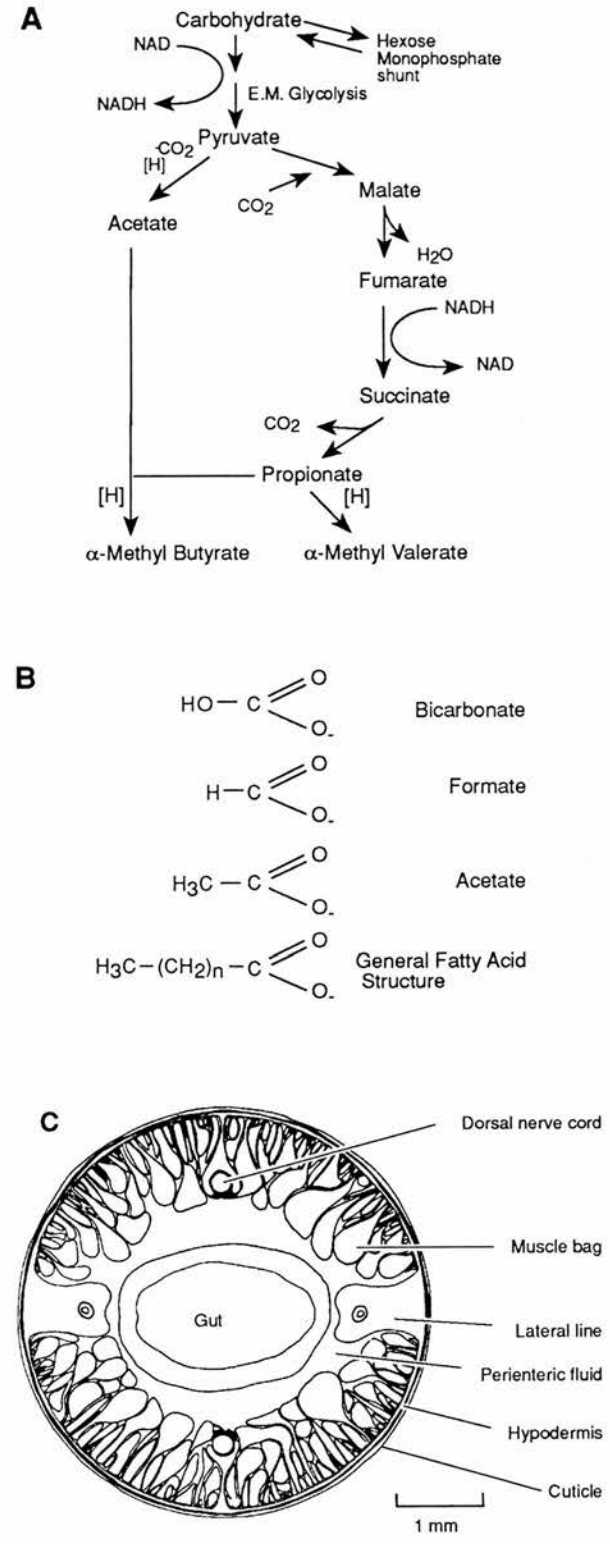


Fig. 1. (*A*) The anaerobic metabolism of carbohydrate in the muscle cells of *Ascaris suum*. (*B*) Diagramatic representation of the structures of the *n*-series carboxylic fatty acids. (*C*) Cross section through the body wall of *Ascaris*, illustrating the basic anatomy of the parasite.

Experimental Procedure

The experimental chamber was mounted on the stage of a Reichert-Jung Biostar inverted microscope. The vesicles were viewed at 200× magnification under phase contrast. All experiments were carried out at ambient temperature (15–22°C). The pipette solution remained constant throughout all experiments, composition (in mM): CsCl, 140; $Mg(Acetate)_2$, 2; $Ca(Acetate)_2$, 1; HEPES, 10; adjusted to pH 7.2 with CsOH. The bath solution was composed of (in mM): Test salt, 140; $Mg(Acetate)_2$, 2; $Ca(Acetate)_2$, 1; HEPES, 10; adjusted to pH 7.2 with CsOH, test ion being either chloride, bicarbonate, formate, acetate, propionate, butyrate, α-methyl butyrate (isovalerate), valerate (pentoate), caproate (hexoate), heptanoate. A high calcium concentration was used to ensure maximum activation of the channel currents (Thorn & Martin, 1987). All tested anions were supplied from Sigma: chloride and bicarbonate as cesium salts, the carboxylic acids were supplied as free acids.

For each patch, current records were obtained with chloride as bath test ion. The bath solution was then replaced with an alternative bath solution containing another test anion. In an additional series of experiments, records were obtained using each test ion in the initial bath solution, this solution was then exchanged for a bath solution containing chloride as test anion. This procedure ensured that it was the calcium-activated Cl channels that were present in the patch and that there was no contamination from other channels which may have been activated by the carboxylic acids.

The chamber was grounded using an agar bridge/AgCl electrode. In some experiments (with heptanoate) the pipette electrode was also encased in an agar jacket to ensure stability of junction potentials. Junction potentials were measured and taken into account in all calculations.

Analysis

Current records of at least 30 sec duration were made at fixed patch potentials between +100 and −100 mV and analyzed on an IBM PC2/70 computer using PAT, version 6.1 single channel analysis program (John Dempster, Strathclyde University). Current/voltage plots were constructed, and slope conductances and reversal potentials were determined from the region of the reversal potential to avoid errors incurred due to rectification of the current/voltage relationship. As an additional check on the stability of the current amplitudes, the potentials were revisited and the observations repeated. Each patch produced a very stable reversal potential but the slope conductance of the current/voltage plot sometimes reduced with time. If such a reduction occurred, the initial conductance value was recorded.

Determination of Permeability Ratios

In ion substitution experiments, the Goldman-Hodgkin-Katz equation (Goldman, 1943; Hodkgin & Katz, 1949) was used to calculate the relative permeability (P_A/P_{Cl}) of anion A with respect to Cl.

$$Erev = \frac{RT}{F} \times \ln \left\{ \frac{[Cl_i] + (P_A/P_{Cl})\,[A_i]}{[Cl_o] + (P_A/P_{Cl})\,[A_o]} \right\} \quad (1)$$

Subscripts i and o denote internal and external ion species, respectively, and R, T and F have their usual meanings.

In all calculations, the activities of the anions were taken into account (Robinson & Stokes, 1959). All the organic acids were >99% completely ionized at pH 7.2. Results are expressed as mean ± standard error of the mean (SEM).

Results

Vesicles were used within four hours of harvesting since the quality of the preparation began to deteriorate after this time i.e., the frequency of seal formation begins to decline and the vesicles become fragile.

The current/voltage relationship, with chloride as internal anion, was linear with a slope conductance of 144.3 ± 1.4 pS and a reversal potential of 0.03 ± 0.47 mV. Substitution of bath chloride with bicarbonate, formate, acetate, propionate, butyrate, α-methyl butyrate (isovalerate), valerate, caproate (hexanoate), valerate, caproate (hexoate) and heptanoate showed that all these ions could produce inward current at sufficiently negative patch potentials and, therefore, that they could move outwardly through the channel (Fig. 2).

Figure 3 illustrates the effect of replacing internal chloride with butyrate on the conductance and reversal potential of the calcium-activated chloride channel. The conductance in butyrate solution decreased at hyperpolarized potentials; however, at depolarized potentials the conductance increased to a value corresponding to that expected when the channel is conducting predominantly chloride. This effect was seen with all other replacement anions. Consequently, slope conductances were determined using currents recorded at membrane potentials about 10 mV more negative than the reversal potential for each respective anion.

All anions tested produced hyperpolarizing shifts in the reversal potential when they were substituted for chloride in the internal solution. Substitution of bath chloride with bicarbonate, formate, acetate and propionate caused hyperpolarizing shifts in the current/voltage plot for each anion, thereby producing a negative reversal potential between −7.6 ± 0.6 and −20.4 ± 0.3 mV, respectively (Table). Other larger anions produced hyperpolarizing shifts in the reversal potential greater than 25 mV. These anions were: butyrate; α-methyl butyrate (isovalerate); valerate; caproate (hexoate) and heptanoate which had reversal potentials ranging from −26.4 ± 0.92 to −66.2 ± 1.3 mV (Table).

Permeability ratios for each anion relative to chloride (P_A/P_{Cl}) were calculated from the reversal potential of each anion using Eq. (1) and were subsequently related to ionic size (Fig. 4*A*). Ionic size can be estimated in a variety of ways, one of the most common being the Stokes diameter. This method applies Stokes Law for macroscopic particles to particles of ionic dimensions. The original law relates the movement of a sphere through an ideal hydrodynamic continuum to the frictional resistance in terms of the dimensions of the particle and the viscosity (η) of the medium. For a spherical particle this is given by:

$$v = F/(6\pi\eta r)$$

Table. Values of a variety of physical constants for the permeable anions and data obtained during single channel experiments

Anion	Stokes diameter (Å)	Limiting equivalent conductance λ^0 ($cm^2 Int\Omega^{-1} equiv^{-1}$)	Reversal potential (mV)	Conductance (pS)	Relative Permeability (P_A/P_{Cl})	Number of patches
Chloride	2.41	76.4	0.03 ± 0.47	144.3 ± 1.4	1.06 ± 0.02	5
Bicarbonate	4.13	44.5	−18.1 ± 3.03	65.6 ± 12.0	0.50 ± 0.06	4
Formate	3.37	54.5	−7.6 ± 0.62	86.7 ± 3.8	0.74 ± 0.02	4
Acetate	4.48	40.9	−12.8 ± 1.13	68.4 ± 4.7	0.59 ± 0.03	3
Propionate	5.13	35.8	−20.4 ± 0.24	58.9 ± 2.2	0.44 ± 0.01	4
Butyrate	5.37	34.5	−26.4 ± 0.92	68.3 ± 11.9	0.35 ± 0.01	3
Valerate	5.51	33.4	−43.0 ± 2.54	30.3 ± 3.7	0.18 ± 0.02	4
α-Methyl butyrate	5.62	32.6	−36.3 ± 1.50	58.7 ± 15.8	0.24 ± 0.01	3
Caproate (hexoate)	5.97	30.8	−59.0 ± 0.58	29.1 ± 7.9	0.10 ± 0.01	3
Heptanoate	6.30	29.2	−66.2 ± 1.30	63.0 ± 9.3	0.07 ± 0.01	3

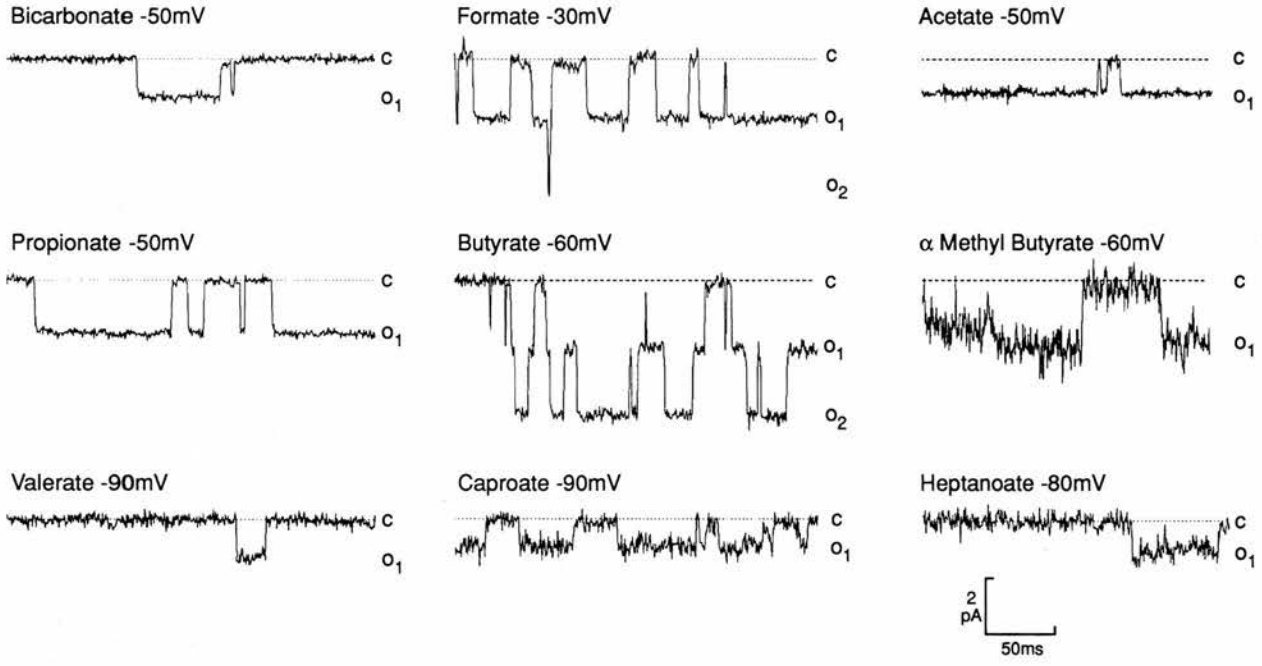


Fig. 2. Inward currents observed after replacement of the bath chloride with the test anion and isolated inside-out patches at the membrane potentials indicated. *C:* closed channel state. *O:* open channel state. Note that all these anions support inward currents at sufficiently negative patch potentials and that these anions may pass out through the channel.

where r = radius of sphere; v = velocity of sphere and F = Faraday constant. This can be applied to an ion whose radius is given by:

$$r = 1/(6\pi\eta u)$$

where u is the absolute mobility of the ion.

u can also be expressed in terms of the limiting equivalent conductivity:

$$r = |z|F^2/(6\pi N\eta^0\lambda^0)$$

where z = valency of the ion; λ^0 = limiting equivalent conductivity; η^0 = viscosity of the pure solvent and N = Avogadro number.

The limiting equivalent conductances are available for a wide variety of ions (Dippy, 1938; Robinson & Stokes, 1965), thereby enabling the calculation of r, the Stokes diameter of each ion (Table). The relationship between P_A/P_{Cl} and Stokes diameter was linear for all anions. It should be noted, however, that other workers use more complex analyses than described above (Bormann et al., 1987).

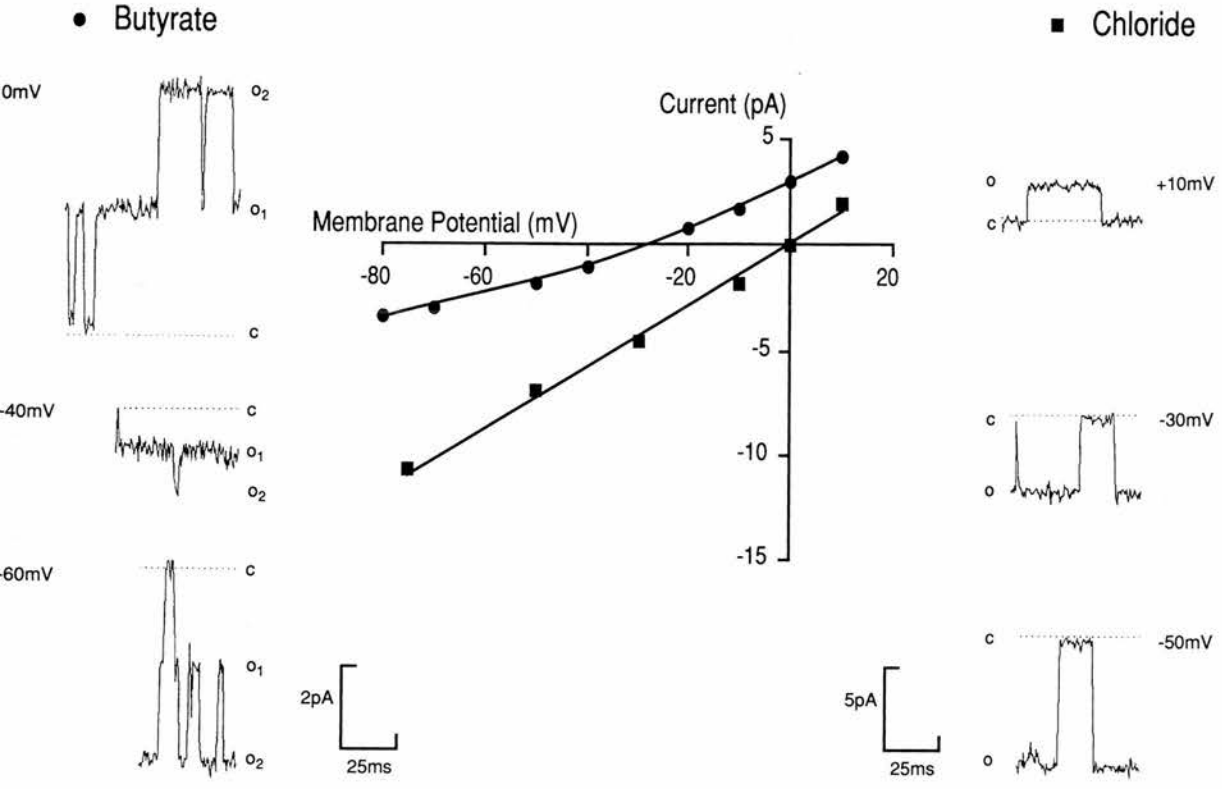


Fig. 3. Current/voltage relationship for symmetrical 140 mM chloride (squares) shown passing through the origin. The effect on the current/voltage relationship of replacing internal chloride with 140 mM butyrate is shown by the circles. The reversal potential shifts to −26 mV and the relationship is no longer linear, the conductance increases at potentials less negative than the reversal potential. Current records, obtained at the potentials indicated, are shown alongside the graph. *o* and *c* denote open and closed states, respectively. When butyrate was the internal anion, current records show the patch contained two channels denoted as o_1 and o_2. Currents are shown at a high time resolution to show the amplitude of the steps clearly.

Heptanoate, the seven carbon containing carboxylic acid, has a Stokes diameter of 6.30 Å and is measurably permeant. The diameter of the channel pore, therefore, must be greater than 6.30 Å. A simple linear regression fitted to the data intersects with the abscissa at 6.55 Å (Fig. 4*A*). This intersection provides an estimation of the effective diameter of the channel pore at its narrowest point. In addition to the Stokes diameter, an alternative measure of ionic size is the number of methyl groups within the organic acids. The relationship between P_A/P_{Cl} and the number of methyl groups in each acid is linear and shown in Fig. 4*B*. The intersect on the abscissa is 6.03, suggesting fatty acids with a total chain length greater than seven carbon atoms (six methyl groups) will not pass through the channel. Unfortunately, fatty acids longer than heptanoic are so lipophilic that the limit of solubility in aqueous solution is exceeded. Indeed, it is impossible to prepare aqueous solutions of sufficient concentration, of organic acids longer than nonoic acid.

In addition, the transition state energy (ΔG) between the binding site and the barrier peak (Andersen & Koeppell, 1992) can be expressed in terms of the permeability ratio of each acid relative to chloride

$$\Delta G = RT \ln (P_A/P_{Cl}) \quad (2)$$

The plot of ΔG against the number of methyl groups contained within each straight chained fatty acid (Fig. 5) can be described by two straight lines, whose slopes are a measure of the transition state energy change per methyl group for transfer from the aqueous phase to a binding site within the channel pore (Bormann et al., 1987; Murrell, Brown & Haydon, 1991). A least-squares regression through the points fitting the carboxylic acids, formate, acetate, propionate, butyrate and α-methyl butyrate, affords a slope of −0.609 kJmol^{-1}. The gradient of the second line describing the acids, valerate, caproate and heptanoate, is steeper at −1.157 kJmol^{-1}.

In addition to the hyperpolarizing shifts in the reversal potential, replacement of internal chloride with the respective anions also causes a reduction in slope

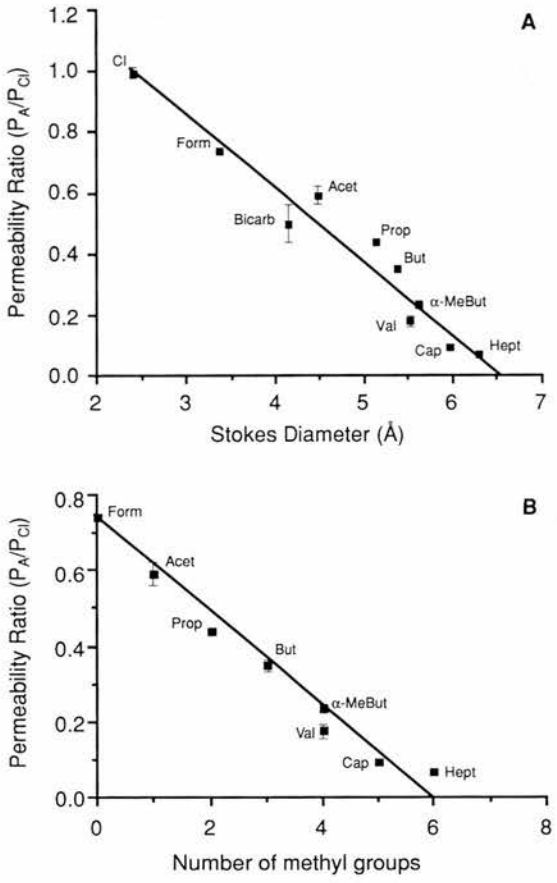


Fig. 4. (*A*) The relationship between permeability ratio and the Stokes diameter for each anion. The graph is fitted by a straight line described by the equation, $P_A/P_{Cl} = -0.25$ SD + 1.6, and cuts the abscissa at 6.55 Å. (*B*) The relationship within the aliphatic fatty acid chain. The graph is linear and crosses the abscissa at 6.03. Values are plotted as mean ± SEM (vertical bars). For the number of observations, *see* the Table.

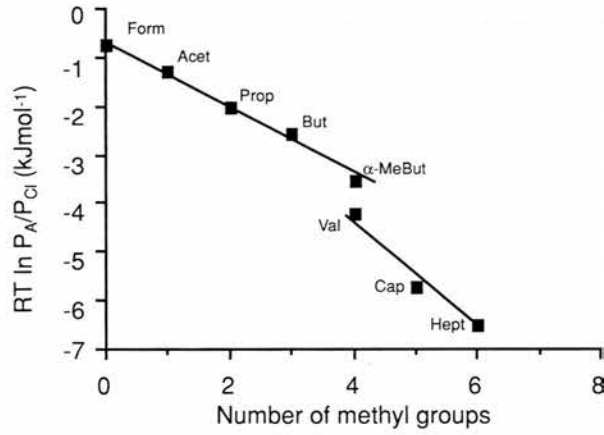


Fig. 5. Plot of ΔG, the energy required to move the fatty acid from an aqueous environment to the binding site within the channel pore ($RT \ln P_A/P_{Cl}$) against the number of methyl groups within the fatty acid chain. The slope of the individual lines affords an estimate of the transition state energy required to move a single methyl group from the bath solution to the binding site within the channel pore. The slope of the line fitting the acids, formate, acetate, propionate, butyrate and α-methyl butyrate, is -0.609 kJmol^{-1}. The gradient of the second line describing the acids, valerate, caproate and heptanoate, is steeper at -1.157 kJmol^{-1}.

conductance of the current/voltage relationships. Figure 6*A* shows the relationship between the slope conductance and the Stokes diameter for each anion. The relationship is linear with regard to chloride, bicarbonate, formate, acetate, propionate, valerate and caproate, which display conductances ranging from 144.3 ± 1.4 to 29.1 ± 7.9 pS (Table). Butyrate, α-methyl butyrate and heptanoate do not lie on the straight line graph; each has a conductance greater than expected for fatty acids of their ionic size, namely 68.3 ± 11.9; 58.7 ± 15.8 and 63.0 ± 9.3 pS, respectively. The relationship between conductance and the number of methyl groups within each acid (Fig. 6*B*) is also linear with the exception of butyrate, α-methyl butyrate and heptanoate. Again, all three anions display conductances greater than expected for their respective chain lengths.

Discussion

Size Limit for Permeant Ions

The relationship between permeability ratio and the Stokes diameter of each anion can be described by a straight line, the permeability ratio decreasing as the ionic diameter increases. Likewise, the relationship between P_A/P_{Cl} and the number of methyl groups in the fatty acid chain is also inverse and approximated by a straight line. This relationship is seen for a variety of other anionic and cationic channels (Bormann et al. 1987; McCleskey & Almers, 1985).

The pore size, as predicted from the graph of P_A/P_{Cl} *v*'s Stokes diameter, is 6.55 Å. The channel is therefore larger than the GABA and glycine receptor gated chloride channels of mouse cultured spinal neurons which have pore diameters of 5.6 and 5.2 Å, respectively (Bormann et al., 1987). However, a pore size of 6.55 Å is very much smaller than the lower limit of 20 Å predicted for the large conductance chloride channel found in rat cultured Schwann cells (Grey, Bevan & Ritchie, 1984).

Conductance

Butyrate, α-methyl butyrate (isovalerate) and heptanoate all show conductances that are greater than expected for anions of their size, whether their anionic size is de

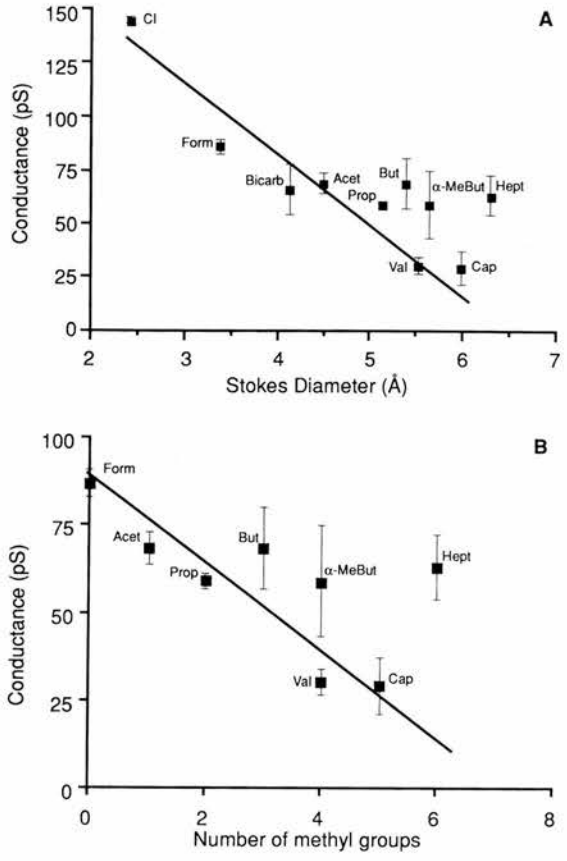
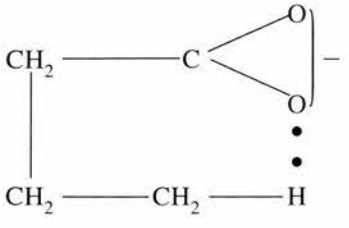


Fig. 6. (*A*) The relationship between conductance and the Stokes diameter for each anion. The graph can be described by a straight line with the exception of butyrate, α-methyl butyrate and heptoate. (*B*) The relationship between conductance and the number of methyl groups contained within the aliphatic fatty acid chain. The graph is linear, with the exception of butyrate, α-methyl butyrate and heptoate. Values are plotted as mean ± SEM (vertical bars). For the number of observations, *see* the Table.

scribed by Stokes diameter or the number of methyl groups in the fatty acid chain. In a paper to the chemical society in 1938, Dippy showed that butyric acid and α-methyl butyric acid have abnormally high dissociation constants as compared with other aliphatic fatty acids of the *n*-series up to nonoic acid. This observation was attributed to the ability of the terminal methyl group to associate with the oxygen of the carboxyl group thus:



This suggests that the secondary structures of butyrate and α-methyl butyrate are important in determining their conductance through the calcium-activated chloride channel. Heptanoic acid displays a normal dissociation constant, as measured by Dippy (1938), but in the light of the results obtained for butyrate and α-methyl butyrate, it is possible to assume that the secondary structure of a long chain fatty acid such as heptanoate could account for the abnormally high conductance of this fatty acid. Assuming all three fatty acids fold when in aqueous solution, then their ionic size, as perceived by the channel, may be smaller than that represented either by the Stokes diameter or the number of methyl groups within the chain.

Properties of the Channel-binding Site

The permeability sequence of the channel differs from the conductance sequence, a phenomenon usually ascribed to the presence of a binding site within the channel pore. Previous experiments investigating the permeability of the channel to other halides suggested between one and two cationic binding sites within the calcium-activated chloride channel (Dixon et al., 1993). The number of binding sites varied inversely with the size of the permeant anion. This same series of experiments also indicated that the internal environment of the calcium-activated chloride channel is relatively fluid compared to free water (Dixon et al., 1993). Unlike the relationship between the binding of *n* alcohols to a blockage site on the nicotinic acetylcholine gated channel of rat myocytes (Murrel et al., 1991), the graph of ΔG *vs.* the number of methyl groups cannot be described by a simple linear regression. The slope of the graph affords a transition state energy per methyl group for transfer from aqueous phase to the channel binding site. The observation that, in this case, the transition state energy for binding of the fatty acids is a curve indicates that ΔG for binding of individual methyl groups is dependent on the fatty acid presenting the methyl group to the binding site. It was possible, however, to fit two straight lines of good correlation (correlation coefficient >0.99) to the points on the graph, thereby affording two average values for the transition state energy per methyl group. The carboxylic acids, formate, acetate, propionate, butyrate and α-methyl butyrate, form the first straight line of slope -0.609 kJmol^{-1}, this value increases to -1.157 kJmol^{-1} for the line describing the relationship between valerate, caproate and heptanoate. It would appear, therefore, that the binding of the larger, more lipophilic acids to the channel wall is energetically more favorable than the binding of the smaller, less lipophilic acids. However, the larger energy change of -1.157 kJmol^{-1} is relatively low compared to the binding of *n*-alcohols to the blockage site on the nicotinic acetylcholine gated channel of rat

myotubes which afforded a standard transition state energy per methylene group of -3.3 kJmol^{-1}. This large energy change displayed by the *n*-alcohols is expected, as it is known that the environment of the binding site in the nicotinic acetylcholine channel is hydrophobic. The energy change involved in the move from an aqueous to a hydrophobic environment for increasingly lipophilic alcohols would therefore be large and favorable. If, in the case of the calcium-activated chloride channel, the difference between the aqueous environment surrounding the membrane and the environment within the channel is minimal, the energy change undergone by the fatty acid moving from aqueous phase to the binding site, although favorable, will be low. This being the case suggests that the environment within the channel is hydrophilic. The association, therefore, between permeant ions and the channel wall is not very strong.

Function of the Channel

The function of this channel, unlike its classification, is becoming easier to predict. The rectification displayed by the channel at depolarized potentials (Thorn & Martin, 1987) excludes an effective role in the repolarization of the cell that is attributed to other chloride currents (Owen, Segal & Barker, 1984; Geletyuk & Kazachenko, 1985). Other calcium-activated chloride currents have been found in rodent lacrymal glands (Findlay & Petersen, 1985; Marty, Tan & Trautmann, 1985; Evans & Marty, 1986) and in exocrine cells (Marty, Tan & Trautmann, 1985) where they appear to be involved in salt secretion. It is therefore of interest to note that the channel can conduct fatty acids involved in the anaerobic respiratory pathway of *A. suum*. Indeed, as stated above, the calcium-activated chloride channel is able to open at the resting membrane potential (-35 mV) of *Ascaris* muscle and is therefore able, under resting membrane conditions, to move intracellular anions across the muscle membrane to the perienteric fluid. At this potential, the chloride current flowing through a single channel is very low at -0.12 pA due to the ratio of internal to external chloride concentrations which in *Ascaris* muscle is 16.5:52.7 mM. Therefore, any anionic current flowing across the membrane at the resting membrane potential must be due to anions other than chloride. Unfortunately, it is experimentally very difficult to measure channel currents flowing across *Ascaris* muscle under normal physiological conditions, as the collagenase treatment required to obtain giga seals, results in the loss of membrane potential.

In addition, an increase in intracellular calcium concentration usually accompanies muscular activity, which in turn results in the formation of metabolic waste products that must be removed from the cell. Any increase in intracellular calcium would lead to an increase in the frequency of channel opening (Thorn & Martin, 1987), thereby facilitating the passage through the channel of the fatty acids that constitute metabolic waste. It is of interest to note that *Ascaris* eggs contain large amounts of the permeant acid α-methyl butyrate in the form of triglyceride (Tsang & Saz, 1973). This fatty acid plays an important role during development from egg to embryo. The eggs are unable to synthesize the fatty acid and must, therefore, absorb it from the perienteric fluid. In the light of the secretory role ascribed to other calcium-activated chloride channels, it is interesting to speculate on the possibility that this channel functions as a mechanism for the removal of metabolic substances across the muscle cell membrane. The internal pH of the intact muscle cells of *Ascaris*, as measured by hydrogen-selective microelectrodes, is 7.37 (Del Castillo et al., 1989). The low pKa values exhibited by the carboxylic acids ensure that the degree of ionization, at intracellular pH, is very high (>99%); consequently, a simple diffusion of the acids through the muscle membrane is unlikely. Indeed, the pH buffering power of *Ascaris* muscle appears to be high. Replacing the external sodium chloride in artificial perienteric fluid with sodium acetate only slightly reduced the internal pH to a new value of 6.93 (Del Castillo et al., 1989). If this channel does perform such an important physiological function, it will be necessary to establish whether muscle cells from other organisms also possess ion channels capable of conducting products of metabolism.

Once the volatile fatty acid metabolites have been excluded from the muscle, they accumulate in the perienteric space. Movement of the volatile fatty acids from the perienteric fluid through the cuticle of *Ascaris* to the outside has been observed by Sims et al. (1992). Although these authors suggested the possibility of an exchange process, the mechanism of the transport process across the cuticle was not identified. Our study raises the possibility that the transport process through the cuticle, like that through the muscle, may also involve a nonselective anion channel.

Considering the diversity of chloride channels, which are found in membranes as diverse as those of rat hippocampus (Franciolini & Nonner, 1987) and the bacterium *Escherichia coli* (Martinac et al., 1987), the description of a chloride current that does not fit comfortably in any contemporary classification is not altogether surprising. Our channel seems suited to transporting anions produced as a result of anaerobic respiration.

This work was financed by the Scientific and Engineering Research Council (S.E.R.C.). M. Valkanov was sponsored by The British Council.

References

Andersen, O.S., Koeppell, R.E. 1992. Molecular determinations of channel function. *Physiol. Rev.* **72(4):**S89–S158

Bormann, J., Hamill, O.P., Sakmann, B. 1987. Mechanisms of anion permeation through channels gated by glycine and γ-aminobutyric acid in mouse cultured spinal neurons. *J. Physiol.* **385:**243–286

Del Castillo, J., Rivera, A., Solorzano, S., Serrato, J. 1989. Some aspects of the neuromuscular system of *Ascaris*. *Q. J. Ext. Physiol.* **74:**1071–1087

Dippy, J.F.J. 1938. Chemical constitution and the dissociation constants of monocarboxylic acids. Part X saturated aliphatic acids. *J. Chem. Soc.* 1222–1227

Dixon, D.M., Valkanov, M., Martin, R.J. 1993. A patch-clamp study of the ionic selectivity of the large conductance, Ca-activated chloride channel in muscle vesicles prepared from *Ascaris suum*. *J. Membrane Biol.* **131:**143–149

Evans, M.G., Marty, A. 1986. A calcium-dependent chloride current in isolated cells from rat lacrymal glands. *J. Physiol.* **378:**437–460

Findlay, I., Petersen, O.I. 1985. Ach stimulates a Ca^{2+}-dependent Cl^- conductance in mouse lacrimal acinar cells. *Pfluegers Arch.* **403:**328–330

Franciolini, F., Nonner, W. 1987. Anion and cation permeability of a chloride channel in rat hippocampal neurons. *J. Gen. Physiol.* **90:**453–478

Franciolini, F., Petris, A. 1988. Chloride channels of biological membranes. *Arch. Biochem. Biophys.* **261:**97–102

Geletyuk, V.I., Kazachenko, V.N. 1985. Single Cl^- channels in molluscan neurons: Multiplicity of the conductance states. *J. Membrane Biol.* **86:**9–15

Goldman, D.E. 1943. Potential impedence and rectification in membranes. *J. Gen. Physiol.* **27:**37–60

Grey, P.T.A., Bevan, S., Richie, J.M. 1984. High conductance anion-selective channels in rat cultured Schwann cells. *Proc. R. Soc. B. London* **221:**395–409

Hodgkin, A.L., Katz, B. 1949. The effect of sodium ions on the electrical activity of the giant axon of the squid. *J. Physiol.* **108:**37–77

Martinac, B., Buechner, M., Delcour, A.H., Adler, J., Kung, C. 1987. Pressure sensitive ion channel from *Escherichia coli*. *Proc. Nat. Acad. Sci. USA* **84:**2297–2301

Marty, A., Tan, Y.P., Trautmann, A. 1984. Three types of calcium-dependent channel in rat lacrymal glands. *J. Physiol.* **357:**293–325

McCleskey, E.W., Almers, W. 1985. The Ca-channel in skeletal muscle is a large pore. *Proc. Nat. Acad. Sci. USA* **82:**7149–7153

Murrell, R.D., Brown, M.S., Haydon, D.A. 1991. Actions of *n*-alcohols on nicotinic acetylcholine receptor channels in cultured rat myotubes. *J. Physiol.* **437:**431–448

Owen, D.G., Segal, M., Barker, J.L. 1984. A Ca-dependent Cl^- conductance in cultured mouse spinal neurons. *Nature* **311:**567–576

Robinson, R.A., Stokes, R.H. 1965. Electrolyte Solutions. Butterworths, London

Saz, H.J., Bueding, E. 1966. Relationships between anthelmintic effects and biochemical and physiological mechanisms. *Pharmacol. Rev.* **18:**871–894

Saz, H.J., Weil, A. 1962. Pathway of formation of α-methyl valerate by *Ascaris lumbricoides*. *J. Biol. Chem.* **237:**2053–2056

Sims, S.M., Magas, L.T., Barsuhn, C.L., Ho, N.F.H., Geary, T.G., Thompson, D.P. 1992. Mechanisms of microenvironmental pH regulation in the cuticle of *Ascaris suum*. *Mol. Biochem. Parasitol.* **53:**135–148

Thorn, P., Martin, R.J. 1987. A high conductance Ca-dependent chloride channel in *Ascaris suum* muscle. *Q. J. Exp. Physiol.* **72:**31–49

Tsang, V.C., Saz, H.J. 1973. Demonstration and function of 2-methyl butyrate racemase in *Ascaris lumbricoides*. *Comp. Biochem. Physiol.* **45B:**617–623

J. Membrane Biol. 148, 41–49 (1995)

The Journal of
Membrane
Biology

© Springer-Verlag New York Inc. 1995

A Cl Channel in *Ascaris suum* Selectivity Conducts Dicarboxylic Anion Products of Glucose Fermentation and Suggests a Role in Removal of Waste Organic Anions

M.A. Valkanov*, R.J. Martin
Department of Preclinical Veterinary Sciences, R.(D.)S.V.S., Summerhall, University of Edinburgh, Edinburgh, EH19 3QA

Received: 28 February 1995/Revised: 22 June 1995

Abstract. The permeability of organic anions (produced from anaerobic fermentation of glucose) through a nonselective membrane Cl channel was examined. Single channel recording techniques were used to study the permeabilities of the anions: oxalate, succinate, oxaloacetate, malate, lactate and pyruvate in *Ascaris* muscle cell membranes. All of the anions, except malate, were found to be conducted through the channel. The relative permeability of most anions could be predicted from the component structure of the anions. The failure of the channel to conduct malate prevents an energy drain on the cell. These studies further the hypothesis that a Cl channel functions to transport waste organic anions across the cell membrane. This mechanism does not require specific exchange carriers for the anions. Channels with properties like the nonselective anion channels of *Ascaris,* are suitable for transport of carboxylic anions through cell membranes, down a concentration or potential gradient.

Key words: *Ascaris suum* — Cl channels — Permeability — Dicarboxylic acids — Anaerobic respiration

Introduction

In an anaerobic environment living cells produce energy by a process of fermentation in which molecules like glucose are oxidized. At the end of the process, one or more organic anions are excreted into the medium surrounding the cell as waste. The products that accumulate at the end of the process are often: lactate, acetate, propionate, butyrate and succinate. These anions, produced inside the cells, have to be removed through the cell membrane and so the question of how the anions cross the lipid barrier of the cell membrane is raised. An opportunity to examine aspects of this process is presented by a preparation of the parasitic nematode, *Ascaris suum.*

Adult *Ascaris* inhabit the small intestine of pigs in a low pO_2 environment and ferment glucose, Fig. 1, to produce energy and the carboxylic acids: acetic acid, propionic acid, succinic acid, butyric acid and α-methylbutyric acid (Bueding & Farrow, 1966; Saz & Bueding, 1966). The acids produced in the muscle cells, cross the cell membrane and accumulate in the surrounding perienteric fluid before further excretion across the cuticle of the parasite (Thompson et al., 1993). The flux of the organic anions across the muscle membrane is greater than the flux of sodium, the flux of potassium, or the flux of chloride, and appears to dominate the membrane potential (Ellory, 1967; Brading & Caldwell, 1971).

We have examined, using single channel recording techniques, properties of a high conductance Ca-activated Cl channel found in about 20% of patches made from muscle membranes of *Ascaris suum* (Thorn & Martin, 1987; Dixon, Valkanov & Martin, 1993; Valkanov, Martin & Dixon, 1994). The channel is a nonselective anion channel that can conduct simple monocarboxylic acid anions (acetate to heptanoate, including α-methylbutyric acid). We have suggested, as a result of the studies, that the Ca-activated Cl channel could function to transport organic anions across the cell membrane and that the membrane potential of the cell (−35 mV) would facilitate concentration of these anions outside. This mechanism does not require specific exchange carriers for the anions.

As a further test of this hypothesis, we now examine the permeability of the channel to the dicarboxylic anions: succinate, oxaloacetate and malate. Succinate is produced in mitochondria of muscle during glucose me-

* *Present address:* Institute of Biophysics, Bulgarian Academy of Sciences, Sofia, Bulgaria

Correspondence to: R.J. Martin

tabolism (Fig. 1) and is a major anion which is excreted from the muscle cell and accumulates in the perienteric fluid which surrounds the muscle cell. Malate and oxaloacetate are produced in muscle cytoplasm during glucose fermentation but they are not excreted and do not accumulate in the perienteric fluid. If malate or oxaloacetate leak out through this nonselective anion channel then there could be a substantial energy drain on the cell. In addition, we examine the permeability of the monocarboxylic acids lactate and pyruvate.

This paper, describes the results of experiments which show that the channel is able to conduct: succinate, lactate, pyruvate, oxaloacetate but not malate, and discusses the significance of the observations. We further suggest that channels with properties like the nonselective anion channels of *Ascaris,* are suitable for transport of carboxylic anions through cell membranes.

Materials and Methods

Preparation of Muscle Vesicles

Ascaris suum were obtained from the local slaughterhouse and maintained in Locke's solution at a temperature of 34°C. The Locke's solution was changed daily and the parasites discarded after 4–5 days. A 2-cm section of the worm, taken 5 cm from behind the head region, was cut along one of the lateral lines, the gut was removed and the body flap pinned, cuticle side down, onto Sylgard in a petri dish. The preparation was then washed with extracellular solution (mM): NaCl, 35; Na acetate, 105; KCl, 2; $MgCl_2$, 3; HEPES, 10; glucose, 3; ascorbic acid, 2; EGTA, 1; pH 7.2 with NaOH. The flap was then incubated in enzyme solution (collagenase, 1 mg ml^{-1} in EGTA-free extracellular solution) for ten min. The preparation was then washed well and incubated in extracellular solution at 37°C. After about 1 hr, vesicles could be seen budding off the bag region of the muscle cell. The vesicles were then collected with a Pasteur pipette and placed in the experimental chamber for recording.

Recording

The experimental chamber was mounted on an inverted microscope stage (Reichert-Jung Biostar) and the vesicles viewed at 200×. Experiments were carried out at room temperature (15–22°C). Except where stated in the results for the malate experiments, the pipette solution contained (mM): CsCl, 140; $Mg(Acetate)_2$, 2; Ca(Acetate), 1; HEPES, 1; adjusted to pH 7.2 with CsOH. The bath solution contained (mM): test salt, 140; $Mg(Acetate)_2$, 2; $Ca(Acetate)_2$, 1; HEPES, 1; adjusted to pH 7.2 with CsOH. A high concentration of Cs was used to block possible potassium currents. The test ion was: oxalate, succinate, oxaloacetate, malate, lactate and pyruvate. During some of the malate experiments, the bath and pipette solutions were reversed so that the malate was present in the pipette and Cl was the main anion in the bath. The bath solution with the test anion was initially exchanged for a solution with Cl to document the presence of active Ca-activated Cl channels; with the exception of malate, this control was unnecessary for all patches because the organic anion currents had easily recognized kinetics with long open-times. A high bath concentration of calcium was used to ensure activation of the Cl channels (Thorn & Martin, 1987). All the test anions were supplied by Sigma: Cl as a Cs salt and the carboxylic acids as free acids.

An agar Ag/Cl bath reference electrode was used. In the experiments with malate in the pipette, the pipette electrode was also encased in an agar jacket to ensure stability of junction potentials. Junction potentials were measured and taken into account in all calculations. Reversal potentials of the isolated patches are quoted conventionally with the outside membrane potential taken as zero and the inside membrane potential given relative to the outside.

Patch pipettes were made from capillary glass (Garner Glass 7092) and had resistances of 1–3MΩ and coated with Sylgard to improve frequency responses. Single-channel currents were recorded using the inside-out configuration and seal resistances were greater than 1GΩ. The currents were monitored with a List EPC-7 current-voltage amplifier and oscilloscope. The signal was filtered by an 8-pole Bessel filter (3dB, 1kHz) and recorded on DAT tape (converted Sony DTC 1000).

Analysis

Current records of at least 30-sec duration were made at fixed potentials between +100 and −100 mV and analyzed on an IBM PC2/70 computer using PAT 6.1 software (Dempster, Strathclyde University). Reversal potentials were determined, directly during recording, from the potential on the EPC-7 required to produce zero channel current — the potential at which the direction of the channel currents reversed. This method of determining the reversal potential permitted greater accuracy and precision and was better than interpolating between currents observed at more positive and more negative potentials. Current-voltage plots were drawn by eye but slope conductances were determined by least squares regression in the hyperpolarized region near the reversal potential to avoid errors due to rectification of the current-voltage plots. Each patch produced stable reversal potentials but the slope conductances sometimes reduced with time. If such a reduction occurred, the initial conductance was recorded.

Determination of Permeability Ratios of the Channel

The Ca-activated channel is only permeable to anions: the permeability of Cs in the presence of inorganic anions is negligible (Dixon et al., 1993) and in the presence of organic anions it is <0.07 (Valkanov et al., 1994). The Goldman-Hodgkin-Katz constant field equation (Goldman, 1943; Hodgkin & Katz, 1949) was used to calculate the relative permeability (P_A/P_{Cl}) of the monovalent or the divalent anions, A, from the single-channel current reversal potentials.

The general current equation for an anion given by constant field theory is:

$$I_A = \frac{F^2 Z_A{}^2 P_A V}{RT} \cdot \frac{[A]^o - [A]^i \exp(Z_A FV/RT)}{1 - \exp(Z_A FV/RT)} \tag{1}$$

where P_A is the permeability coefficient, Z_A is the valence, and $[A]^o$ and $[A]^i$ are the outside and inside activities, respectively of anion A.

At the reversal potential, E_{rev}, the net current in a perfectly selective anion permeable channel due to the flow of anions is zero; and when Cl is the only anion in the patch pipette and a monovalent anion A is the only permeant ion at the cytoplasmic surface of the membrane, the relative permeability P_A/P_{Cl} can be determined from:

$$P_A/P_{Cl} = \frac{[Cl]^o}{[A]^i} \cdot \exp(E_{rev} F/RT) \tag{2}$$

where R, T and F have their usual meaning and i denotes intracellular and o denotes extracellular concentrations.

When the anion A is divalent, the relative permeability was determined (Fatt & Ginsborg 1958) from:

$$P_A/P_{Cl} = \frac{[Cl]^o}{4[A]^i} \cdot \exp(E_{rev}F/RT) \cdot [\exp(E_{rev}F/RT) + 1] \quad (3)$$

In all calculations the activities of the anions were taken into account (Robinson & Stokes 1965). All the organic acids were at least 99% ionized at pH 7.2.

Results are expressed as mean ± SEM.

Determination of Anion Profiles and Mean Radii

The profile of each anion in this study was determined from space-filling models with the aid of ALCHEMY III software (TRIPOS Associates). Minimal energy conformations were obtained using TRIPOS' force field calculations and then side views and end on profiles obtained. The mean diameter of each anion was taken as the mean of the dimensions of a minimal rectangular box required to enclose the molecule (Hille, 1992).

Results

In a previous study (Valkanov et al., 1994) we had shown that monocarboxylic glucose fermentation products are permeant anions and pass through the Ca-activated Cl channel. Succinic acid, a dicarboxylic acid, is also produced in *Ascaris* muscle cells, Fig. 1, and accumulates outside the muscle cells in the surrounding perienteric fluid; it too might be expected to pass through the channel. We therefore decided to test the permeability of the channel to succinate and to a number of other appropriate dicarboxylic acids. Initially oxalate and then succinate, were selected for examination. Figure 2 shows the profiles of all the anions tested including oxalate and succinate.

Oxalate and Succinate

Figure 3 (oxalate and succinate) shows representative records of inward and outward currents through the channel, made using inside-out patches at positive and negative membrane potentials when the patch pipette contained 140 mM Cl and the bath anion was 140 mM oxalate or succinate. The channel supported inward and outward currents when either oxalate or succinate was present in the bath establishing that both of these anions are permeant and carry current.

The *I/V* plots of Fig. 4 (oxalate and succinate), show that the reversal potential for oxalate is near −3 mV and for succinate that it is near −15 mV. The slope conductance in the hyperpolarized region near the reversal potential of oxalate was 42pS and for succinate it was 41pS. The means ± SEM values for the reversal potentials and slope conductances are shown in the Table. Equation 3, was used to calculate the relative permeability of the anions. For oxalate P_A/P_{Cl} was 0.36 ± 0.01 (mean ± SEM, n = 3) for succinate it was 0.20 ± 0.01 (mean ± SEM, n = 4), Table. The profiles of these two anions, Fig. 2, show that succinate (mean diameter 5.5 Å) is larger than oxalate (mean diameter 4.5 Å,), and consistent with the lower permeability of succinate when compared to oxalate.

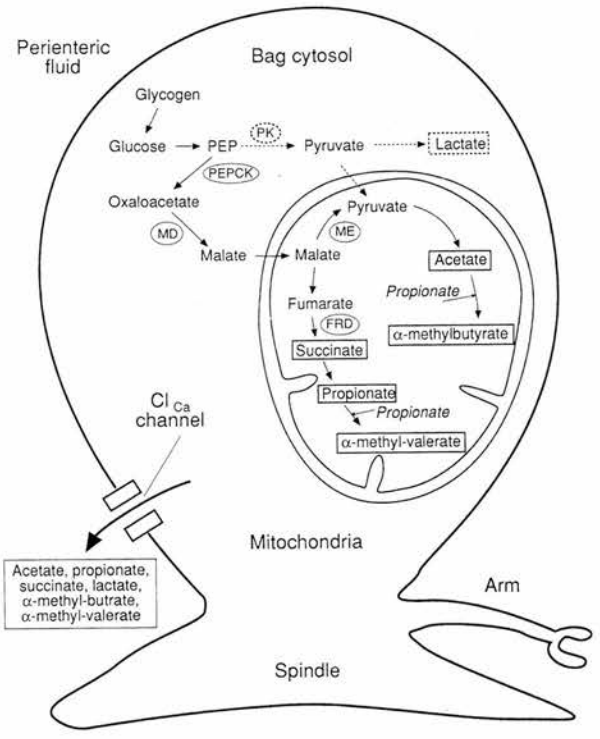


Fig. 1. Diagram of the glucose degradation pathway in *Ascaris* muscle, adapted from Saz, 1981, and Tielens and Van den Bergh, 1993. End products, which then accumulate in the perienteric fluid, are shown in boxes. PEP: phosho-enol pyruvate. PK: pyruvate kinase. PEPCK: phosho-enol pyruvate carboxy kinase. MD: malate dehydrogenase. ME: malic enzyme. FRD: fumarate reductase. The pathway outlined by the dashed arrows is absent or only present at a low level.

Oxaloacetate

We have seen that the simple dicarboxylic acids, oxalate and succinate, are permeant and support significant inward currents. The question of the permeability of other dicarboxylic acids like oxaloacetate, Fig. 1, that is part of the glucose fermentation pathway is then raised. If oxaloacetate is permeant and present in significant concentrations in muscle cytoplasm, then there could be an energy leak from the cell.

Figure 2 (oxaloacetate) shows the profile of oxaloacetate which has a mean diameter of 6.0 Å. It can be seen that the size of the end on profile is intermediate

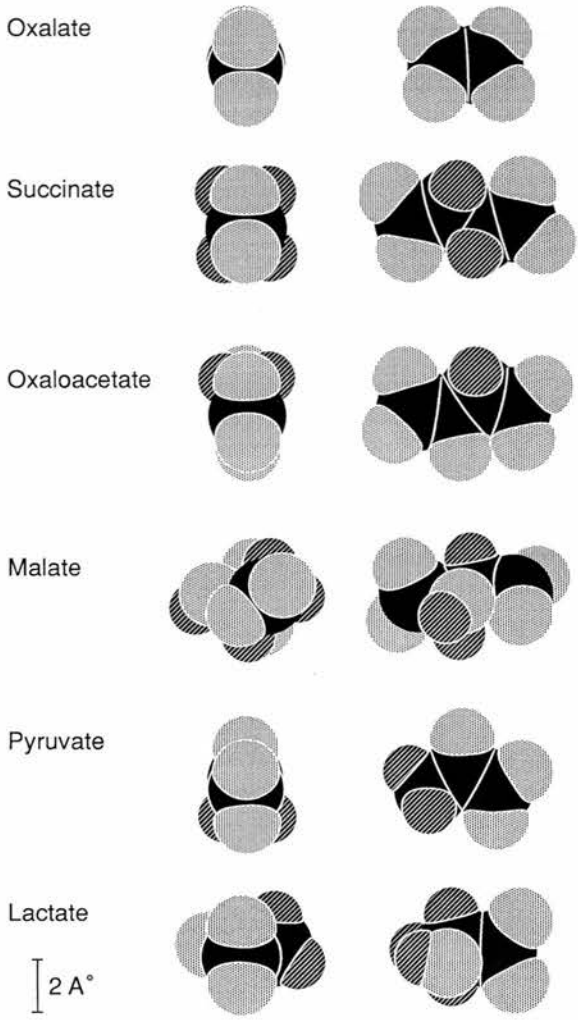


Fig. 2. Space filling models of oxalate, succinate, oxaloacetate, malate, pyruvate and lactate, end (left) and side (right) views.

between oxalate and succinate and if this profile determines relative permeability (Hille, 1992) then the oxaloacetate permeability would be expected to be between oxalate and succinate.

Figure 3 (oxalaoacetate) shows representative inward and outward current records and Fig. 4 (oxaloacetate) shows the *I/V* plot made from the same inside-out patch with 140 mM oxaloacetate present in the bath. The Table summarizes the mean ± SEM values for the reversal potential, slope conductance and P_A/P_{Cl}. The values for P_A/P_{Cl}, 0.32, together with the 64 pS slope conductance show that oxaloacetate is permeant and suggests that there could be a significant energy drain if oxaloacetate is available for diffusion from the cytoplasm. This point is considered further in the discussion.

The relative permeability of oxaloacetate, 0.32, is greater than succinate, 0.20, but less than oxalate, 0.36, and is consistent with the relative sizes of the end on profiles.

Malate

The mean diameter of malate is 6.5 Å. The end on profile of malate, Fig. 2, is greater than oxaloacetate and succinate, suggesting that malate would be less permeant than either of these other two anions. In our experiments (more than 50 patches) where malate replaced all the Cl in the bath, we consistently failed to detect the presence of inward channel currents. In an attempt to check if malate was directly gating the channel closed, experiments on four isolated patches, in symmetrical Cl and held at a potential of −20 mV, were carried out. In these patches, the addition of up to 120 mM malate in the bath failed to significantly reduce the probability of channel opening or change the amplitude of the channel currents. It appeared that the channel failed to conduct malate and conduct inward current.

We also reversed the location of the anions and carried out experiments on patches where the anion in the patch pipette was 140 mM malate and the bath anion was 140 mM Cl. In four patches at potentials ranging between +50 and −70 mV, only inward channel currents were recorded (Fig. 3, malate): the currents were only observed when the membrane was hyperpolarized and when the majority ion carrying the current was Cl. The *I/V* plot, Fig. 4 (malate) shows that the extrapolated reversal potential is near 0 mV. The Table shows mean ± SEM values. Interestingly, the calculated P_A/P_{Cl} for malate under these conditions is 0.5, but the channel fails to conduct an observable outward current. Malate appears to be able to enter the channel from the outside but does not conduct a current; this behavior may appear unusual but is explained by an ion binding to a site in the channel but having a low mobility in the channel (Gallacher, Maruyama, Petersen, 1984; Andersen & Koeppe, 1992). However malate may not enter the channel from the inside so easily since high concentrations of malate applied to the intracellular membrane surface did not block Cl channel currents.

Lactate and Pyruvate

In addition to the dicarboxylic acids above, the permeability of pyruvate and lactate were also examined. These anions might be produced during glucose fermentation, Fig. 1, and lactate has been reported in low concentrations in the perienteric fluid surrounding the muscle. Lactate has a larger mean diameter (5.5 Å) and end on profile than pyruvate (mean diameter, 5.2 Å), Fig. 2, and might be expected to be less permeant.

Figure 3 (pyruvate and lactate) shows representative

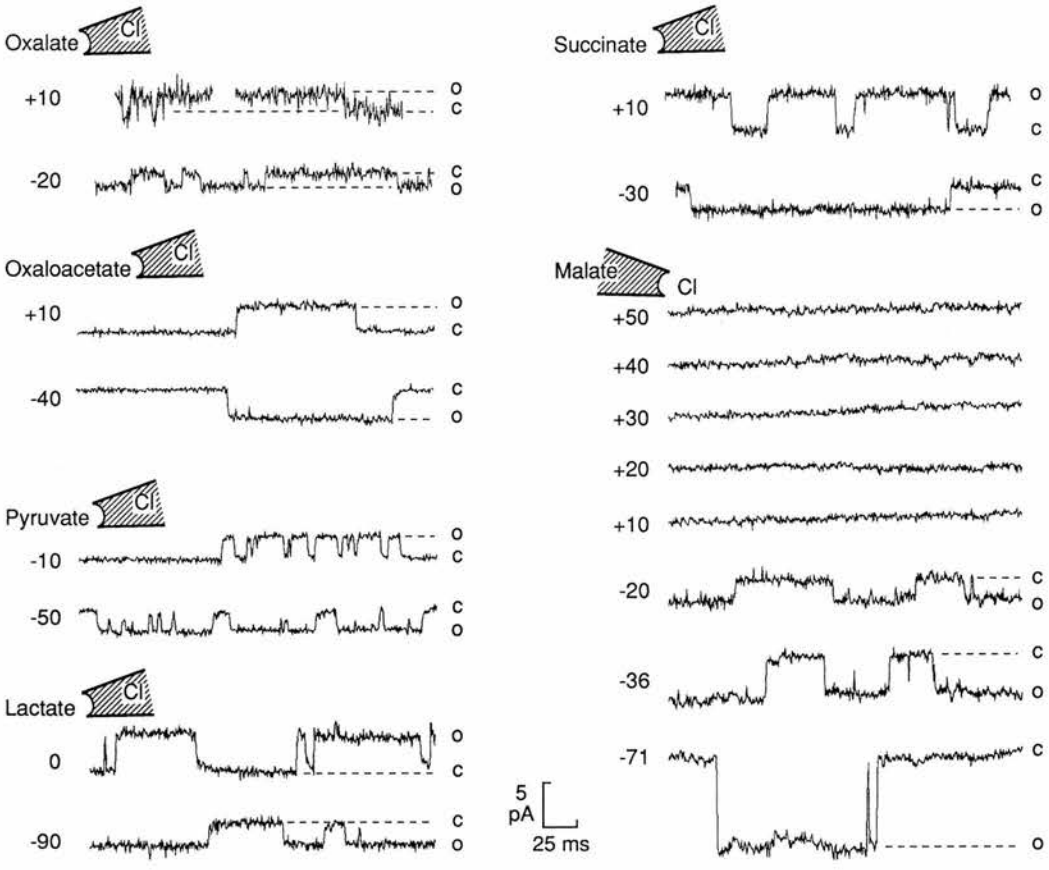


Fig. 3. Representative single channel currents from inside-out patch recordings. Inset: anion distribution. Trans-patch potentials are shown on the left of the current traces. *O:* open channel. *C:* closed channel; Oxalate: Pipette anion, 140 mM Cl; bath anion, 140 mM oxalate; Succinate: Pipette anion, 140 mM Cl; bath anion, 140 mM succinate; Oxaloacetate: Pipette anion, 140 mM Cl; bath anion, 140 mM oxaloacetate; Malate: Pipette anion, 140 mM malate; bath anion, 140 mM Cl; Pyruvate: Pipette anion, 140 mM Cl; bath anion, 140 mM pyruvate; Lactate: Pipette anion, 140 mM Cl; bath anion, 40 mM lactate.

inward and outward channel currents observed with pyruvate in the bath; the *I/V* plots for these patches is shown in Fig. 4. It can be seen that the reversal potential for pyruvate is near −30 mV and for lactate that it is more negative; the result demonstrates a lower relative permeability for lactate. The Table shows the mean ± SEM values of the reversal potentials, slope conductances and relative permeability of pyruvate and lactate.

Estimation of Transition Energies may be Made for Component Parts of the Organic Anions

In saturating barrier models of ion permeability with a one-ion pore, the relative permeability of an ion may be used to determine differences in transition energies between permeant anions transferring from the aqueous phase to a binding site in the channel (Bormann, Hamill & Sakmann, 1987; Andersen & Koeppell, 1992). Thus:

$$P_A/P_{Cl} = \exp[(G_A - G_{Cl})/RT], \quad (4)$$

where R and T have their usual meaning and $G_A - G_{Cl}$ is the difference in the transition energies for the anion A and Cl respectively. Even in multi-ion pores under 'constant offset energy' conditions the differences in transition energy barriers between two anions may be determined in the same way (Hille, 1975).

The difference $G_A - G_{Cl}$ between the energies for the anions observed in this study together with some of those reported by Valkanov et al., (1994) are plotted in Fig. 5: the graph shows $G_A - G_{Cl}$ against the number of methyl groups present and suggests that the component groups of the permeant anion behave additively to determine the transition energy of the whole anion. The line produced by the dicarboxylic acids oxalate and succinate is parallel to the plot formate to α-methylbutyrate. Both lines have least square slopes that afford a transition energy per methyl group from the aqueous phase to

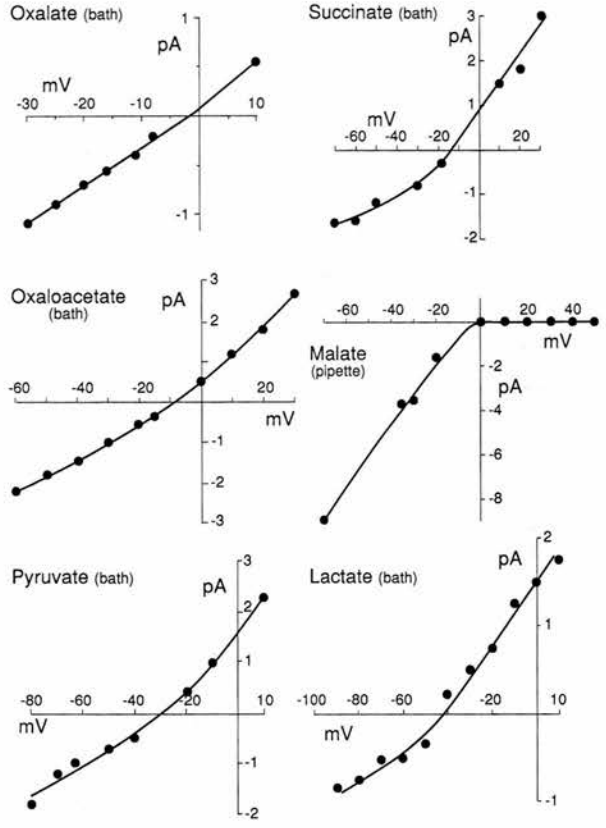


Fig. 4. Representative single channel *I/V* plots; Oxalate: E_{rev} – 3 mV; Slope conductance 44pS; Succinate: E_{rev} – 15 mV; Slope conductance 53pS; Oxaloacetate: E_{rev} – 8 mV; Slope conductance 55pS; Malate: Single channel *I/V* plot; E_{rev} 0.5 mV; note that malate was the anion in the pipette and that Cl was the anion in the bath. Pyruvate: E_{rev} – 30 mV; Slope conductance 50pS; Lactate: E_{rev} – 39 mV; Slope conductance 37pS.

the channel binding sites of –0.61 Kjmol^{-1}. The line oxalate-succinate is downwardly displaced from the formate to α-methylbutyrate plot by –1.9 Kjmol^{-1} suggesting that the extra carboxylic group increases the transition energy by that amount. The large transition energy of the $-COO^-$ group (compared to $-CH_2^-$ groups) can be explained by the greater dehydration energy (because of electrostatic interaction) that is required to permit translocation across the channel.

The downward displacement of pyruvate compared to acetate suggests that a –C=O group increases the transition energy by –1.5 Kjmol^{-1}. The downward displacement of lactate compared to acetate suggests that the addition of the –CHOH group increases the transition energy by –1.9 Kjmol^{-1}. The greater transition energy of lactate compared to pyruvate is not surprising because of the chiral carbon of lactate which makes the molecule of lactate larger than the molecule of pyruvate. It is pointed out however, that simple addition of the transition energies for the component groups of the anion does not predict accurately the observed relative permeability of malate or oxaloacetate; the failure may reflect the existence of selective ion binding sites within the channel.

Discussion

The Physiological Importance of the Permeability of the *Ascaris* Ca-Activated Cl Channel to Organic Anions

In a study of the membrane potential of *Ascaris* muscle based on the Goldman-Hodgkin-Katz voltage-equation, Brading and Caldwell (1971) showed that the relative permeability of the membrane to Cl is high (P_{Na}:P_K:P_{Cl} was 1:1:7); but the flux of organic anions is greater than the flux of sodium, the flux of potassium or the flux of chloride (Ellory, 1967), and appears to dominate the membrane potential (Brading & Caldwell, 1971).

In this paper and a previous paper (Valkanov et al., 1994), we have demonstrated the high permeability of the *Ascaris* Cl channel to carboxylic acids. This channel has a high density and is found in 20% of membrane patches in cluster of up to 15 channels per patch; these channels are active in recordings made from intact cells in a body flap preparation (Thorn & Martin, 1987). The high conductance (150 pS in symmetrical Cl) of the channel, the frequency with which it is observed and the fact it can be fully activated at the normal resting membrane potential, (–35 mV, Thorn & Martin, 1987) explains the permeability of the muscle membrane to both organic anions and Cl. The inward rectification shown by the channel in symmetrical Cl (Thorn & Martin, 1987) argues against a role in repolarization of the cell that is attributed to other Ca-activated Cl channels (Owen, et al. 1983; Geletyuk & Kazachenko, 1985).

Oxaloacetate

Oxaloacetate and malate are produced in *Ascaris* muscle cytoplasm during glucose metabolism (Saz, 1981; Tielens & Van den Bergh, 1993) but they do not accumulate in perienteric fluid. We found that malate was not normally conducted through the channel, but it was clear that oxaloacetate could be. With oxaloacetate having a conductance of 64pS and P_A/P_{Cl} of 0.32, the channel would permit extracellular accumulation of oxaloacetate. However this is not found to be the case in the whole animal.

The normal cytoplasmic concentration of oxaloacetate is relevant here: the cytoplasmic enzyme, malate dehydrogenase, rapidly reduces cytoplasmic oxaloacetate to malate (Saz, 1981). The cytoplasmic concentrations of oxaloacetate are therefore low. Another possible factor reducing oxaloacetate leak might be localization

Table. Mean + SEM values for the reversal potential, slope conductance and relative permeability of anions compared to Cl

Anion	W (Å)	H (Å)	L (Å)	D (Å)	E_{rev} (mV)	G (pS)	P_A/P_{Cl}	G_A/G_{Cl} (Kjmol-1)	Number of Patches
Oxalate	3.1	4.9	5.5	4.5	−5.6 ± 1.5	45.4 ± 2.0	0.36 ± 0.01	−2.50	3
Succinate	3.9	4.9	7.6	5.5	−17.2 ± 0.6	39.9 ± 12.4	0.20 ± 0.01	−3.94	4
Oxaloacetate	3.9	5.2	8.7	6.0	−7.4 ± 1.0	63.6 ± 13.1	0.32 ± 0.01	−2.79	5
Pyruvate	3.9	5.3	6.4	5.2	−29.3 ± 1.7	51.0 ± 10.9	0.32 ± 0.02	−2.79	5
Lactate	4.5	5.3	6.8	5.5	−33.5 ± 3.5	45.4 ± 12.6	0.27 ± 0.04	−3.21	4
Malate	4.8	6.3	8.5	6.5	0.1 ± 0.2	0	0.5 ± 0.01		5

Organic anion sizes (W: width; Height: height; L: length; D: mean dimensions). E_{rev}: reversal potential. *G:* slope conductance. P_A/P_{Cl}: relative permeability of the anion compared to Cl. G_A/G_{Cl}: transition energy. The correlation coefficient, *r*, between the relative permeability of all organic anions except malate and the slope conductance was 0.51.

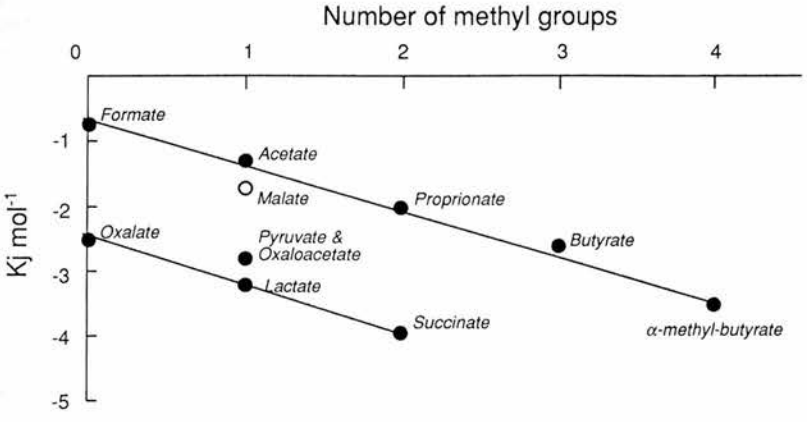


Fig. 5. Plot of the transition energies of anions determined from P_A/P_{Cl} values observed in this study and some from Valkanov et al. (1994) against number of methyl groups. The line fitted for the monovalent anions was obtained from a least squares fit of the points formate to α-methylbutyrate and the line for the divalent anions oxalate to succinate plotted parallel.

of metabolites as a result of the compartmentation of the glucose metabolic enzymes. However, a recent review on glucose metabolism in helminths, Tielens and Van den Berg (1993), suggests that compartmentation does not occur.

Malate

It is interesting that the mean diameter of malate, 6.5 Å, is near the limiting pore size of the Ca-activated channel, (6.6 Å Valkanov et al., 1994) suggesting that there is close contact between the malate anion and the walls of the channel. Malate did not enter and bind to the channel from the inside since experiments with malate in the bath failed to detect inward channel currents or to demonstrate evidence of blocking of Cl currents. When malate was placed in the patch pipette, the calculated P_A/P_{Cl} was 0.5 but the channel did not support current carried by malate. The observation is predicted if malate enters the channel from the outside and binds inside the channel (explaining the high relative permeability) but has low mobility in the channel (explaining the absence of malate current). In this respect, malate seems to behave in the same manner as rubidium in cation channels from mammalian exocrine acini (Gallacher et al., 1984). If binding to the channel site and mobility in the channel is not well related, it predicts and explains the poor correlation observed between the relative permeabilities and conductances of the other organic anions (Table, $r = 0.51$, and Valkanov et al., 1994). The ability of the Ca-activated chloride channel to prevent the movement of malate across the cell membrane would prevent an energy drain on the cell.

Lactate and Pyruvate

Very low levels of lactate have been detected in the perienteric fluid surrounding *Ascaris* muscle (Bueding & Yale, 1951) suggesting that a low level of excretion may occur through the channel. Pyruvate has not been reported in *Ascaris* perienteric fluid despite the fact that it is more permeant than lactate. *Ascaris* is not capable of forming significant quantities of cytoplasmic pyruvate, because the concentration of pyruvate kinase (which converts PEP to pyruvate) is very low (Saz, 1981). The level of cytoplasmic pyruvate appears to be very low and may only rise to 3.1 mM in mitochondria (Barrett & Beis, 1973). Thus, although the anion channel is permeable to lactate and pyruvate anions, significant loss may be prevented by low cytoplasmic levels.

The Physiological Function of Nonselective Anion Channels in a Number of Preparations may be the Membrane Transport of Carboxylic Acids Produced from Glucose Fermentation

The physiological functions of different types of Cl channels include: (i) GABA and glycine gated Cl channels which hyperpolarize and inhibit electrical activity in nerve and muscle cells (Bormann et al., 1987); (ii) Cl channels activated by osmotic stress and which may be involved in volume regulation (Worrell et al., 1989; Kubo & Okada, 1992); (iii) Cl channels which are spontaneously active and which contribute to the membrane potential and prevent hyperexcitability (Blatz & Magleby, 1983); (iv) Cl channels in parallel with ATP-dependent H^+ pumps involved in the maintenance of electroneutrality during acidification of intracellular organelles (Schmid, Burckhardt & Gogelein, 1989; (v) Cl channels involved in salt secretion (Findlay & Petersen, 1985; Marty, Tan & Trautmann, 1985). However, the function of a number of Cl channels remains unknown and in this group there is a group of nonselective anion channels with a relatively large (6.5 Å) pore. (Woodbury & Miles, 1973; Franciolini & Nonner, 1987).

The observations reported in this paper together with the report of Valkanov et al. (1994) demonstrate that the *Ascaris* Cl channel has a large pore (6.6 Å) and is permeable to both mono- and dicarboxylic acid products of glucose fermentation. The normal resting membrane potential of *Ascaris* muscle, around −35 mV (Martin, 1980), favors extracellular concentration of the organic anion products. Compared with ion channels known in animal cells and microorganisms (Hille, 1992), the Ca-activated Cl channel in *Ascaris* has the unusual property of conducting organic ions as a physiological substrates rather than an inorganic ion. Channels normally conducting organic anions are however, recognized in vacuolar membranes of plants (Hendrich & Marten, 1993).

It is usually assumed in vertebrate preparations that passage of most carboxylic acids across cell membranes is by simple diffusion of the uncharged protonated moiety. However, Woodbury and Miles (1973), who measured the resting membrane conductance of skeletal muscle using microelectodes, detected the presence of Cl channels with a pore cross section of 5.5×6.5 Å that was detectably permeable to butyrate and lactate. The existence of nonselective anion channels that have a large P_A/P_{Cl} for acetate (0.66) and propionate (0.5), has also been noted in rat hippocampal neuron membranes (Franciolini & Nonner, 1987) but the function was not identified. They too may conduct products of glucose fermentation.

In inner mitochondrial membrane preparations specific dicarboxylic acid and tricarboxylic acid carriers are recognized (Lehninger, 1965) but the presence of normally quiescent nonselective anion channels permeable to organic anions like acetate, propionate, and butyrate has been advocated (Galid & Baevis, 1986) and observed (Hayman, Spurway & Ashley, 1993). It seems possible that a function of large nonselective anion channels, could be to permit movement of carboxylic anions through lipid membranes.

This work was financed by the Scientific and Engineering Research Council (S.E.R.C.).

References

Andersen, O.S., Koeppell, R.E. 1992. Molecular determinants of channel function. *Physiol. Rev.* **72:**S89–S157

Barrett, J., Beis, I. 1973. The redox state of the free nicotinamide-adenine dinucleotide couple in the cytoplasm and mitochondria of muscle tissue from *Ascaris lumbricoides* (*Nematoda*). *Comp. Biochem. Physiol.* **44A:**331–340

Blatz, L.A., Magleby, K.L. 1983. Single voltage-dependent chloride-selective channels of large conductance in cultured rat muscle. *Biophys. J.* **43:**237–241

Bormann, J., Hamill, O.P., Sakmann, B. 1987. Mechanism of anion permeation through channels gated by glycine and γ-amminobutyric acid in mouse cultured spinal neurons. *J. Physiol. Lond.* **385:**243–286

Brading, A.F., Caldwell, P.C. 1971. The resting membrane potential of the somatic muscle cells of *Ascaris lumbricoides*. *J. Physiol. Lond.* **217:**605–624

Bueding, E., Farrow, G.W. 1956. Identification of succinic acid as a constituent of the perienteric fluid of *Ascaris* lumbricoides. *Exp. Parasitol.* **5:**345–349

Bueding, E., Yale, H. 1951. Production of α-methylbutyric acid by bacteria free *Ascaris* lumbricoides. *J. Biol. Chem.* **193:**411–423

Dixon, D.M., Valkanov, M., Martin, R.J. 1993. A patch-clamp study of the ionic selectivity of the large conductance, Ca-activated chloride channel in muscle vesicles prepared from *Ascaris* suum. *J. Membrane Biol.* **131:**143–149

Ellory, J.C. 1967. Ion movement in muscle cells of *Ascaris lumbricoides*. Ph.D Thesis, University of Bristol. UK

Fatt, P., Ginsborg, B.L. 1958. The ionic requirements for the production of action potentials in crustacean muscle fibers. *J. Physiol. Lond.* **142:**516–543

Findlay, I., Petersen, O.I. 1985. ACh stimulates a Ca^{2+}-dependent Cl-conductance in mouse lachrymal acinar cells. *Pfluegers Arch.* **403:**453–478

Francioloni, F., Nonner, W. 1987. Anion and cation permeability of a chloride channel in rat hippocampal neurons. *J. Gen. Physiol.* **90:**453–478

Galid, K.D., Baevis, A.D. 1986. Evidence for the existence of an inner membrane anion channel in mitochondria. *Biochem. Biophys. Acta* **853:**187–204

Gallacher, D.V., Maruyama, Y., Petersen, O.H. 1984. Patch-clamp study of rubidium and potassium conductances in single cation channels from mammalian exocrine acini. *Pfluegers Arch.* **401:**361–367

Geletyuk, V.I., Kazachenko, V.N. 1985. Single Cl^- channels in molluscan neurones: multiplicity of conductance states. *J. Membrane Biol.* **86:**9–15

Goldman, D.E. 1943. Potential impedance and rectification in membranes. *J. Gen. Physiol.* **27:**37–60

Hayman, K.A., Spurway, T.D., Ashley, R.H. 1993. Single anion chan-

nels reconstituted from cardiac mitoplasts. *J. Membrane Biol.* **136:**181–190

Hendrich, R., Marten, I. 1993. Malate induced feedback regulation of plasma membrane anion channels could provide a CO sensor to guard cells. *EMBO Journal.* **12:**897–901

Hille, B. 1975. Ionic selectivity, saturation, and block in sodium channels. A four-barrier model. *J. Gen. Physiol.* **66:**535–560

Hille, B. 1992. *Ionic Channels of Excitable Membranes.* S Sinauer Associates, Sunderland, MA

Hodgkin, A.L., Katz, B. 1949. The effect of sodium ions on the electrical activity of the giant axon of the squid. *J. Physiol.* **108:**37–77

Kubo, M., Okada, Y. 1992. Volume-regarded Cl- channel currents in cultured human epithelial cells. *J. Physiol.* **456:**351–371

Lehninger, A.L. 1965. The Mitochondrion: Molecular Basis of Structure and Function. Benjamen, Menlo Park, CA

Martin, R.J. 1980. The effect of γ-aminobutyric acid on the input conductance and membrane potential of Ascaris muscle. *Br. J. Pharmacol.* **77:**255–265

Marty, A., Tan, Y.P., Trautmann, A. 1984. Three types of calcium-dependent channel in rat lachrymal glands. *J. Physiol.* **357:**293–325

Owen, D.G., Segal, M., Barker, J.L. 1983. A Ca-dependent CP conductance in cultured mouse spinal neurones. *Nature* **311:**567–570

Robinson, R.A., Stokes, R.H. 1965. Electrolyte Solutions. pp. 571. Butterworths: London

Saz, H.J. 1981. Energy metabolism of parasitic helminths: adaptation to parasitism. *Ann. Rev. Physiol.* **43:**323–341

Saz, H.J., Bueding, E. 1966. Relationship between anthelmintic effects and biochemical and physiological mechanisms. *Pharmacol. Rev.* **18:**871–894

Schmid, A., Burckhardt, G., Gogelein, H. 1989. Single chloride channels in endosomal vesicle preparations from rat kidney cortex. *J. Membrane Biol.* **111:**265–275

Thompson, D.P., Ho, N.F.H., Sims, S.M., Barshuan, C.L., Thomas, E.M., Geary, T.G. 1993. Organic-acid excretion by *Ascaris suum* and *Haemonchus contortus:* Implications for microenvironmental pH regulation and drug absorption. *J. Cell. Biochem.* **S17C:**113

Thorn, P., Martin, R.J. 1987. A high conductance Ca-dependent chloride channel in *Ascaris suum* muscle. *Quart. J. Exp. Physiol.* **72:**31–49

Tielens, A.G.M., Van den Berg, S.G. 1993. Aerobic and anaerobic energy metabolism in the life cycle of parasitic helminths. *In:* Surviving Hypoxia. Mechanisms of Control and Adaptation. pp. 19–40. CRC Press, Boca Raton

Woodbury, J.W., Miles, P.R. 1973. Anion conductances of frog skeletal muscle. *J. Gen. Physiol.* **62:**324–353

Worrel, R., Butt, A.G., Cliff, W.H., Frizzel, R.A. 1989. A volume-sensitive chloride conductance in human colonic cell line T84. *Amer J. Physiol.* **256:**C1111–C1119

Valkanov, M.A., Martin, R.J., Dixon, D.M. 1994. The Ca-activate chloride channel of *Ascaris suum* conducts volatile fatty acids produced anaerobic respiration: a patch clamp study. *J. Membrane. Biol.* **137:**133–141

Effects of pH on a high conductance Ca-dependent chloride channel: a patch-clamp study in *Ascaris suum*

A. P. ROBERTSON* *and* R. J. MARTIN

Department of Preclinical Veterinary Sciences, R.(D.) S.V.S., Summerhall, University of Edinburgh, Edinburgh EH9 1QH

(*Received 2 November 1995; revised 6 February 1996; accepted 28 February 1996*)

SUMMARY

Plasma membrane vesicles prepared from the bag region of the somatic muscle cells of the parasitic nematode *Ascaris suum* contain high conductance, voltage sensitive, Ca-dependent chloride channels, suggested to be involved in the excretion of carboxylic acids produced by the anaerobic respiration of glucose (Valkanov, Martin & Dixon, 1994). The effect of altered pH on this channel was investigated using the patch-clamp technique and isolated inside-out membrane patches. Changes in pH had little effect on channel conductances and only a small effect on reversal potentials. Under control conditions (symmetrical pH 7·2) the channel had the highest probability of opening at ~ -35 mV (the resting membrane potential of the cell). At positive membrane potentials the probability of opening decreased. The Boltzmann equation was used to describe the relationship between membrane potential and probability of channel opening, and to calculate the effective gating charge. Reduction of external pH produced an increase in the probability of channel opening at hyperpolarized membrane potentials. An increase in internal pH caused a voltage-independent increase in the probability of channel opening and made the effective gating charge less negative. The effect of reducing internal pH was marked: the channel then opened most frequently at positive membrane potentials and the probability of opening at -35 mV was greatly reduced. The decrease in internal pH changed the polarity of the effective gating charge. A simple model was constructed to describe the effects of pH on channel gating.

Key words: patch-clamp, *Ascaris suum*, Cl^- channel, pH, effective gating charge.

INTRODUCTION

A preparation from the somatic muscle cells of the porcine parasitic nematode *Ascaris suum* has been developed which is suitable for electrophysiological study (Jarman, 1959; Martin, 1980). Previous studies have shown that the relatively low resting potential of the cell, ~ -35 mV, is insensitive to changes in the extracellular potassium concentration, but is dramatically affected by changes in extracellular chloride concentrations, thus demonstrating a relatively high chloride permeability (Del Castillo, De Mellow & Morales, 1964; Brading & Caldwell, 1971). Permeability ratios for K, Na and Cl of 1:4:7 respectively have been reported (Caldwell & Ellory, 1968). Patch-clamp studies on membrane vesicles prepared from the bag region of the somatic muscle cell have demonstrated the presence of 3 types of chloride channel. The largest and most commonly observed of these is a high conductance Ca-dependent chloride channel (140 pS in 140 mM Cl solution; Thorn & Martin (1987)). Previously, chloride channels have been assigned to 4 categories on the basis of their properties (Franciolini & Petris, 1987) however, the *Ascaris* Ca-dependent chloride channel does not readily fit in to any of these.

* Corresponding author.
Tel: 0131 650 6094. E-mail: alanr@lab0.vet.ed.ac.uk.

The ionic selectivity of the high conductance Ca-dependent chloride channel has been determined (Dixon, Valkanov & Martin, 1993; Valkanov, Martin & Dixon, 1994; Valkanov & Martin, 1995) and the ability of this channel to conduct the long-chain fatty acids, which are products of anaerobic respiration in *Ascaris*, has been demonstrated. This has led to the suggestion that the channel may be involved in the removal of these waste products from the cell (Valkanov *et al.* 1994).

In a review of muscle chloride channels, Bretag (1987) described several different channels where the conductance or gating was altered by changes in pH. Respiration in *Ascaris* muscles results in the production of protons and long-chain fatty acyl waste products (Saz & Weil, 1962). In this study we have looked at the effect of pH on the Ca-dependent chloride channel to gain a clearer insight into the mechanism of this channel's gating and its physiological function.

MATERIALS AND METHODS

Preparation of muscle vesicles

Specimens of *Ascaris suum* were collected from the local slaughter house at weekly intervals and maintained at 34 °C in Locke's solution (changed daily)

 Copyright © 1996 Cambridge University Press

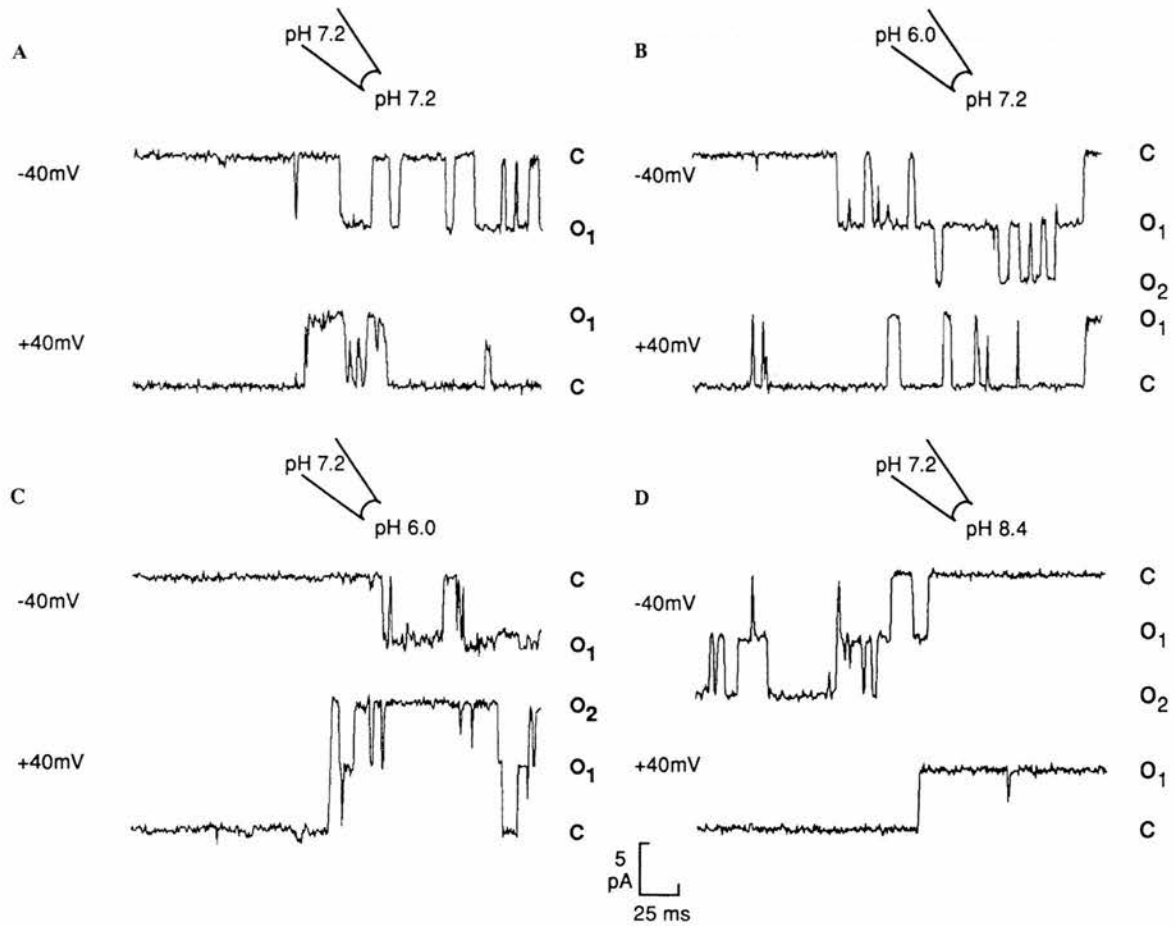


Fig. 1. Inward (−40 mV) and outward (+40 mV) currents in isolated inside-out patches under each of the experimental conditions. (A) Control; bath pH = 7·2, pipette pH = 7·2. (B) Bath pH = 7·2, pipette pH = 6·0. (C) Bath pH = 6·0, pipette pH = 7·2. (D) Bath pH = 8·4, pipette pH = 7·2.

for up to 4 days. The anterior 5 cm of the worm was discarded, the next 2 cm section of worm was removed and cut along one lateral line. The resulting flap was pinned cuticle side down onto Sylgard and the gut removed. The preparation was washed (3 times) with warm (37 °C) extracellular solution, composed of (mM): NaCl, 35; $Na(C_2H_3O_2)$, 105; KCl, 2; $MgCl_2$, 2; HEPES, 10; glucose, 3; ascorbic acid, 2; EGTA, 1; pH adjusted to 7·2 using NaOH. The washed flap was then incubated in enzyme solution (0·5 mg/ml collagenase in EGTA-free extracellular solution) for 10 min at 37 °C. Following enzyme treatment and 3 washes with extracellular solution the flap was incubated at 37 °C in extracellular solution. Approximately 1 h after collagenase treatment vesicles could be observed 'budding off' the bag region of the muscle cell membrane. The vesicles were harvested using a Pasteur pipette and transferred to the recording chamber.

Recording set-up

Patch pipettes with resistances of 1–3 MΩ (Garner glass 7052) and coated with Sylgard to improve frequency responses were used. Single-channel recordings were made using inside-out patches of muscle membrane with seal resistances > 1 GΩ. Currents were monitored using a LIST EPC-7 current–voltage converter, filtered at 1 kHz (3 dB) by an 8-pole Bessel-type filter, viewed on an oscilloscope (HITACHI VC-6025) and recorded on a Racal Thermionic Store Four FM tape recorder.

Experimental procedure

All experiments were carried out at room temperature (15–20 °C). Vesicles in the recording chamber were mounted on the stage of a Nikon TMS-PH3 inverted light microscope and viewed at ×200 magnification under phase-contrast. The chamber was grounded using an agar bridge.

The bath and pipette solutions were composed of (mM): CsCl, 140; $Mg(CH_3COO)_2$, 2; $Ca(CH_3COO)_2$, 1; HEPES, 10; adjusted to the desired pH with CsOH. Experiments were carried out with pipette solutions of pH (pH^o) 7·2 and bath solutions with pH (pH^i) at either 6·0, 7·2 or 8·4. The pHs of the bath solution and pipette solution were constant for each patch experiment. Using isolated inside-out membrane patches the pipette solution is in contact

with the extracellular surface of the membrane patch and the bath solution in contact with the intracellular surface of the membrane. Additional experiments involved a pipette solution pH of 6·0 and the bath solution pH of 7·2. For each patch, current records were obtained for potentials of −40, −30, −20, −10, +10 20, 30 and 40 mV.

Analysis

Records were analysed using an IBM PC2/70 computer and the PAT, version 6.1, single-channel analysis programme (John Dempster, Strathclyde University). Current–voltage plots were constructed to obtain slope conductances and reversal potentials of the currents. The probability of channel opening was calculated for each potential using the following equation:

$$P_{open} = (T_1 + 2T_2 + 3T_3, \ldots, + n \times T_n)/(n \times total\ time), \quad (1)$$

where P_{open} = probability of channel opening; T_n = time with n (and only n) channels open; n = the total number of channels in the patch; total time = duration of patch recording. T_n was calculated from the area under the peak of an all points current amplitude histogram corresponding to n (and only n) channels being open.

To minimize the effect of any rundown, a positive and then a negative potential was studied sequentially. A typical sequence was +40, −40, +10, −10, +20, −20, +30 and 30 mV. Only experiments where full sequences were obtained were used in the analysis. Channels opening to subconductance levels were classified as closed: only channel openings to the full conductance level were classified as open. Inspection of channel records revealed that subconductance levels were almost entirely absent at high values of P_{open}. At low P_{open} values (e.g. positive membrane potentials under control conditions) subconductance levels were more common; care was taken to avoid the opening of several channels to subconductance levels being interpreted as the opening of a smaller number of channels to the full conductance level.

Effective gating charge

The Boltzmann equation (2) was fitted by non-linear least squares regression to the P_{open}-voltage relationship with a FORTRAN program utilizing the NAG E04CCF subroutine, and was used to obtain values for the 'effective gating charge' of the channel under the various experimental conditions.

$$P_{open} = P_{max}/[1 + Exp\{(V_{half} - V)/V_{slope}\}], \quad (2)$$

where P_{max} is the maximum value of P_{open} (proportion of time the channel is open) allowed by the equation, V is the membrane potential in mV, V_{half} is the voltage at which the function is half its maximum value and V_{slope} is the slope factor. The 'effective gating charge' was calculated using:

$$effective\ gating\ charge = (kT/ze)/V_{slope}, \quad (3)$$

where k is Boltzmann's constant, T is absolute temperature on the Kelvin scale, z is the valence of the permeant ion and e is the elementary charge. kT/ze under experimental conditions was 24 mV (Hille, 1992).

Statistics

Statistical significance was assessed using analysis of variance. Additionally the reversal potential values for each experimental condition were compared with the control values using the Mann–Whitney test.

RESULTS

Vesicles were prepared daily and used within 5 h of enzyme treatment, after which time the preparation deteriorated to an extent where giga-seal formation was unlikely. Giga-seals were obtained from ~ 33 % of attempts with new patch pipettes but channel activity was detected in only ~ 25 % of all giga-seals. Not more than 15 % of seals displaying channels retained activity for long enough for sufficient recordings to be made.

Figure 1 shows representative channel recordings at −40 and +40 mV from patches under each of the experimental conditions examined. The records suggest that the proportion of time the channel is open is greater at hyperpolarized membrane potentials compared to positive membrane potentials except where there is a reduction in pH^i to 6·0. Under all experimental conditions the current–voltage relationship was linear (not shown) with, under control conditions (symmetric pH 7·2), a mean conductance of 149·0 pS and a mean reversal potential of 0·9 mV (Table 1). The changes in pH tested on each side of the membrane had no statistically significant effect on the conductance of the channel. For example pH 8·4/7·2 (intracellular/extracellular) gave a mean conductance of 146·0 pS and a mean reversal potential of 0·7 mV (Table 1). However, there was a small, but statistically significant ($0{\cdot}05 > P > 0{\cdot}02$), effect of pH on the reversal potentials using analysis of variance. Comparison of the values for each experimental condition using the Mann–Whitney test showed that only the condition $pH^0 = 6{\cdot}0/pH^i = 7{\cdot}2$ differed significantly from the control value ($P < 0{\cdot}05$).

Effect of pH on probability of channel opening

The effect of pH on the P_{open}-voltage relationship was highly significant, $P < 0{\cdot}0001$ when all data

Table 1. Mean conductance ± S.E.M. and mean reversal potential ± S.E.M. for each pH condition

(N = number of patch experiments.)

	Bath pH(pH^i)	Pipette pH (pH^o)	N	Mean conductance ± S.E.M. (pS)	Mean reversal potential ± S.E.M. (mV)
Control	7·2	7·2	5	149·0 ± 5·8	+0·9 ± 0·4
Intracellular acid	6·0	7·2	4	168·2 ± 4·5	+0·5 ± 0·4
Intracellular alkali	8·4	7·2	4	146·0 ± 9·0	+0·7 ± 0·2
Extracellular acid	7·2	6·0	4	139·3 ± 4·0	+2·2 ± 0·3

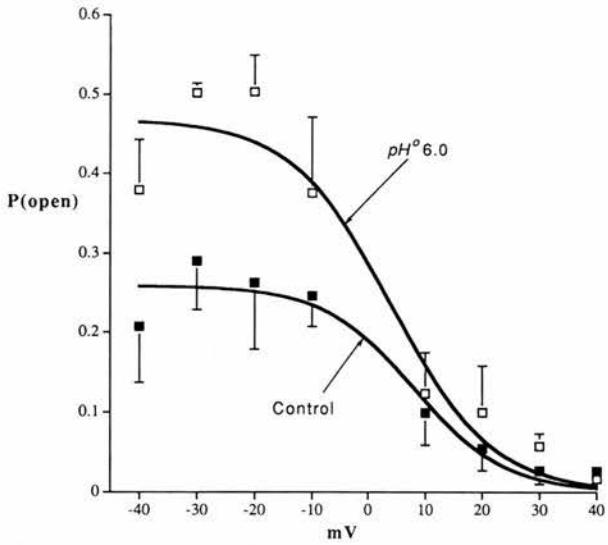


Fig. 2. Effect of acid pH^o on the P_{open}/membrane potential relationship. P_{open} values ± S.E.M. Control (■): pH^o 7·2, pH^i 7·2 ($n = 5$). Test (□): pH^o 6·0, pH^i 7·2 ($n = 4$). Lines of best fit were obtained for both data sets from the Boltzmann equation.

points were compared using analysis of variance. Figure 2 shows the mean P_{open} ± S.E.M. values when the pH at the extracellular surface of the membrane patch (pH^o) was reduced to 6·0. Control values are presented for comparison. The control plot shows that the channel is most likely to be open around the resting membrane potential of the cell, (−30 to −40 mV) with the mean P_{open} for −40 and −30 mV being 0·21 and 0·29 respectively. In contrast, P_{open} at +40 mV is much smaller with a mean value of 0·01. Previous studies have produced similar results for a symmetrical pH of 7·6 and a chloride concentration of ~ 175 mM (Thorn & Martin, 1987). The reduced pH^o produced a marked increase in P_{open} over the range of hyperpolarized membrane potentials tested: P_{open} −30 mV = 0·50 at $pH^o = 6·0$. There also appeared to be a small increase in P_{open} at most positive membrane potentials: pH^o7·2, P_{open} + 30 mV = 0·03; pH^o 6·0, P_{open} + 30 mV = 0·06. The slope of the line generated by the best fit to the Boltzmann equation showed that the effective gating charge was negative for both the control conditions and a reduced pH^o (Table 2).

The effects of an increase in pH at the intracellular surface of the membrane patch (pH^i) are shown in Fig. 3 with the control values presented for comparison. The slopes of the fits to the Boltzmann equation indicate no change in sign of the 'effective gating charge' associated with an increase in pH^i. However, the increase in pH^i produced a vertical shift in the P_{open}-voltage plot with P_{open} values at −30 mV and +30 mV of 0·29 and 0·03 respectively for $pH^i = 7·2$; and 0·35 and 0·07 for $pH^i = 8·4$.

Figure 4 shows the effect of reducing pH^i: Fig. 4A shows the values obtained for mean P_{open} when pH^i was reduced to 6·0. The mean P_{open} values for each of the potentials tested under the control conditions (symmetrical pH 7·2) are shown in Fig. 4B. The results show that a fall in pH^i produced a reduction in P_{open} at hyperpolarized potentials (pH^i 7·2 P_{open} at −30 mV was 0·29; pH^i 6·0 P_{open} at −30 mV was 0·03). At positive membrane potentials P_{open} is increased when pH^i is reduced: under control conditions P_{open} at +30 mV was 0·03; this rises to a P_{open} of 0·27 when $pH^i = 6·0$. The slope of the line obtained from the Boltzmann equation is positive (Table 2), indicating that the 'effective gating charge' had become positive when pH^i was reduced.

The effective gating charge and pH

Table 2 shows the values for the parameters of the Boltzmann equation obtained under the various pH conditions. The effective gating charge for the control conditions was −3·0 electron charges and is the minimum charge that is moved across the potential drop during the transition C⇔O. The estimate of the total charge will be low if the moveable charged groups in the channel travel only part of the way across the potential field. The results show that there is little change in the effective gating charge between the control conditions (−3 e) and reduced pH^o conditions (−2·7 e). The large change

Table 2. Values of P_{max}, V_{half} and V_{max} obtained from the Boltzmann fits and the 'effective gating charge' for each pH condition

	Bath pH (pH^i)	Pipette pH (pH^o)	P_{max}	V_{half}	V_{slope}	Effective gating charge
Control	7·2	7·2	0·26	8·0	−8·0	−3·0
Intracellular acid	6·0	7·2	0·34	2·6	13·1	+1·8
Intracellular alkali	8·4	7·2	0·36	18·9	−12·9	−1·9
Extracellular acid	7·2	6·0	0·47	4·0	−8·8	−2·7

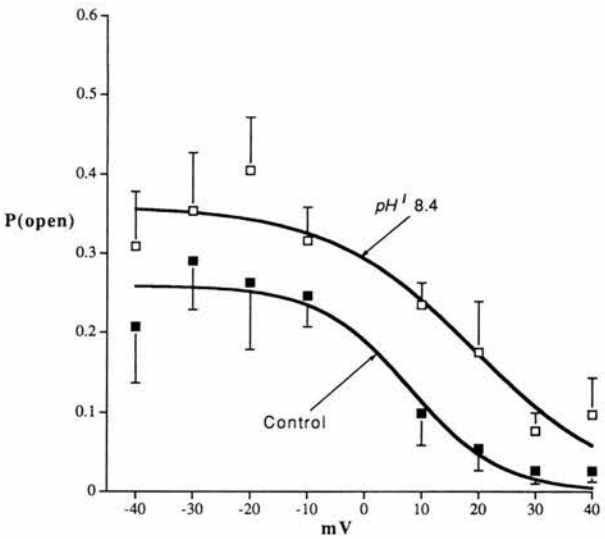


Fig. 3. Effect of alkali pH^i on the P_{open}/membrane potential relationship. P_{open} values ± S.E.M. Control (■): pH^o 7·2, pH^i 7·2 ($n = 5$). Test (□): pH^o 7·2, pH^i 8·4 ($n = 4$). Lines of best fit were obtained for both data sets from the Boltzmann equation.

associated with decreased pH^i, which gave an 'effective gating charge' of +1·8 e, may have been caused by the protonation of several amino acids on the gate of the channel protein.

V_{half} shifted from +8·0 mV (control) to +18·9 mV with the increased pH^i; decreased pH^i moved V_{half} along the voltage axis to +2·6 mV. Both of these horizontal shifts indicate a possible screening/neutralization of a negative surface charge on the intracellular face of the membrane (Hille, 1992). However, the negative movement of V_{half} from 8·0 mV (control) to 4·0 mV when pH^o was decreased cannot be explained by protons interacting with a negative surface charge on the extracellular face of the membrane: the increase in external [H^+] would produce a positive shift in V_{half} if protons were screening a negative surface charge.

Equation (2) also estimates the maximum values, P_{max}, of the P_{open} data sets. Under control conditions P_{max} was 0·26. Each of the experimental conditions shows increases in the value of P_{max}, when compared to the control. When the pH^i was reduced, P_{max} rose to 0·34; an increase in pH^i raised P_{max} to 0·36. A reduction of pH^o gave the largest increase in P_{max} to a value of 0·47.

DISCUSSION

The results show that changes in pH have no significant effect on single-channel conductances. The relationship between P_{open} and membrane potential, described by a Boltzmann equation, was significantly altered by changes in pH. The mechanisms involved in the pH sensitivity of this channel are considered and the physiological significance of the effects of pH is discussed.

Effect of pH on surface potential

Altered pH can lead to changes in surface charge that result in shifts in voltage dependence: negative shifts occur on increased extracellular pH and positive shifts occur on increased intracellular pH (Hille, 1992). For example, extracellular acidification to pH 4·5 leads to a +25 mV shift in the Na activation curve, whilst an increase in extracellular pH to 10 gives a −8 mV shift (Hille, 1968).

The significant positive shift in reversal potential on extracellular acidification in the *Ascaris* chloride channel (Table 1) implies that protons are altering the surface potential in a similar manner. The changes observed in V_{half} (Table 2) on altered pH^i are also consistent with proton concentration altering surface potential. The shift in V_{half} from the control value on reduced pH^o is not predicted by pH effects on surface potential; the shift in V_{half} implies that protons are interacting directly with the channel molecule.

Channel model and pH sensitivity of gating

Figure 5 shows a minimal model that explains the observed effects of pH on our *Ascaris* chloride

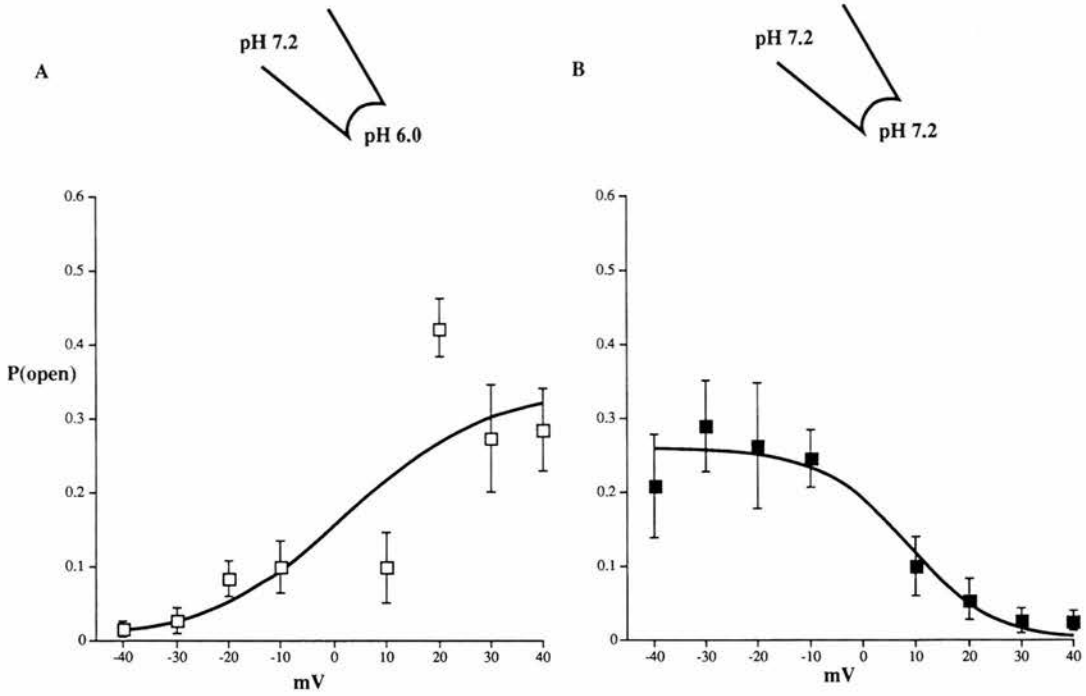


Fig. 4. (A) Relationship between mean $P_{open} \pm$S.E.M. and membrane potential with $pH^i = 6{\cdot}0$ ($n = 4$) (B) Relationship between mean $P_{open} \pm$S.E.M. and membrane potential under symmetrical pH 7·2 conditions ($n = 5$). Lines of best fit were obtained for both data sets from the Boltzmann equation.

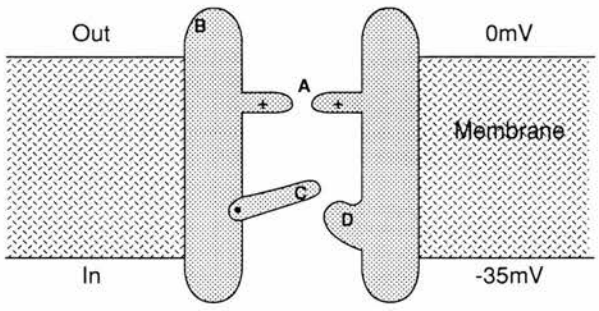


Fig. 5. A simple model of the Ca-dependent chloride channel under control conditions. (A) Selectivity filter of the channel. (B) Proton binding site on the extracellular surface of the channel molecule, proton binding increases P_{open}. (C) Voltage sensor or 'gate', under control conditions bears a charge of -3 e. Decreased pH^i causes binding of protons to imidazolium side-chains of histidine molecules which results in a change in the charge on the 'gate' to $+1{\cdot}8$ e. (D) Positively charged site, binds to a negative charge on channel 'gate' (site C).

channel. The selectivity filter (site A) may possess one or two cationic binding sites (Dixon *et al.* 1993); the lack of variation in the single-channel conductances suggests altered [H^+] has no effect on these sites within the pH range tested.

Extracellular acidification produced increases in P_{open} without affecting gating charge, indicating the presence of a site (site B) only approachable from the extracellular solution.

Under symmetrical pH 7·2 conditions the voltage sensor (site C) has an overall charge of -3 e (Table 2). Interestingly, the gating charge on *Torpedo* chloride channels is smaller, at $+1$ e (Hanke & Miller, 1983) whilst Na, Ca and K channels have larger gating charges of between $+4$ e and $+6$ e (Zagotta & Aldrich, 1990). The dramatic effects that changes in pH^i have on gating charge indicate that the voltage sensor are located intracellularly to the selectivity filter.

The charge on the voltage sensor is sensitive to pH^i (in the range 7·2 to 6·0) and becomes positive at pH 6·0. The *pKa* values of amino acids suggest that only histidine has the appropriate properties to achieve the change in gating charge; the *pKa*'s of other amino acids lie outside the pH range tested. It is therefore suggested that histidine is one of the constituent amino acids of the voltage sensor. The number of histidines that can be protonated is at least 5 (to allow for the change in gating charge from -3 e to $+2$ e); but probably more, for two reasons. First, if the voltage sensor only moves partway across the membrane electric field (as the channel opens) the measured gating charge is less than the actual number of charges present on the channel 'gate' (Hille, 1992). Secondly, studies on K^+ channels have shown that not all the charges on the voltage sensor contribute equally to the effective gating charge (Papazian *et al.* 1991; Logothetis *et al.* 1992).

Site D (Fig. 5) is required to explain the increase in P_{open} with the increase in pH^i. It is suggested that the site located at D normally contains a positively charged residue that forms an ion pair with one of the negative charges on the voltage sensor, similar to suggestions made for Na channels (Stühmer *et al.*

1989). The positively charged residue would lose its proton at high pH, facilitating the opening of the gate and explaining the observed increase in P_{open} at increased pH^i.

Limitations of the model

The above minimal model explains the effects of the pH values tested on the Ca-dependent chloride channel, but there are obvious limitations to this simple model. The Boltzmann model employed only allows for a single step between channel opening ⇔ closing, whereas previous studies have shown several open and closed states (Thorn & Martin, 1987) demonstrating that the gating process is more complex. Our model also shows the 'effective gating charge' located on a single 'gate' whereas, in K^+ channels, activation is brought about by 4 identical gating charges acting independently (Zagotta & Aldrich, 1980). The gating charges in the Ca-activated chloride channel may also act independently.

Physiological significance

Our results show that the Ca-dependent chloride channel is dramatically affected by changes in pH. At a symmetrical pH of 7·2 the channel has a relatively high P_{open} at the resting membrane potential of the cell; when the pH on the intracellular side of the membrane (pH^i) is reduced to 6·0 channel opening is virtually abolished. We have hypothesized that the protonation state of several histidine residues in the channel molecule play an important part in this pH sensitivity. It is interesting that one of the glycolytic enzymes (phosphofructokinase) in *Ascaris* muscle also displays pH sensitivity (Rao *et al.* 1987), due to the protonation of histidine residues present within the enzyme.

In *Ascaris* the anaerobic respiration of glycogen gives rise to carboxylic acids as waste products (Saz & Weil, 1962). The pH of the muscle cell cytoplasm is reported as 7·37 (Del Castillo *et al.* 1989), while the *pKa* values of the waste carboxylic anions have an upper limit of 4·7. At physiological pHs the waste carboxylic acids are $> 99{\cdot}2\,\%$ ionized suggesting that passive diffusion of the uncharged acid across the muscle cell membrane is an unlikely method of excretion. Under symmetrical (pH 7·2) conditions the Ca-dependent chloride channel is permeable to the waste carboxylic anions (Valkanov *et al.* 1994) and has its highest P_{open} around the resting membrane potential of the cell; these observations led to the hypothesis that the channel was responsible for the excretion of waste carboxylic anions (Valkanov *et al.* 1994). Anaerobic respiration in *Ascaris* also results in the production of protons which must be removed from the cell. The presence of an active ionic pump mechanism in the muscle cell has been suggested (Brading & Caldwell, 1971). If there is an active proton pump in the bag membrane, its action would lead to an increased pH^i and an increase in the ionized:unionized concentration ratio of carboxylic anions. In turn the raised pH^i favours opening of the Ca-dependent Cl channel. Thus the pH sensitivity of the channel may facilitate the excretion of waste anions.

A.P.R. was funded by a BBSRC Research Studentship.

REFERENCES

BRETAG, A. H. (1987). Muscle chloride channels. *Physiological Reviews* **67**, 618–714.

BRADING, A. F. & CALDWELL, P. C. (1971). The resting membrane potential of somatic muscle cells of *Ascaris lumbricoides*. *Journal of Physiology* **27**, 605–624.

CALDWELL, P. C. & ELLORY, J. C. (1968). Ion movements in somatic muscle cells of *Ascaris lumbricoides*. *Journal of Physiology* **197**, 75–76P.

DEL CASTILLO, J., DE MELLOW, W. C. & MORALES, T. (1964). Influence of some ions on the membrane potential of *Ascaris* muscle. *Journal of General Physiology* **48**, 129–140.

DEL CASTILLO, J., RIVERA, A., SOLORZANO, S. & SERRATO, J. (1989). Some aspects of the neuromuscular system of *Ascaris*. *Quarterly Journal of Experimental Physiology* **74**, 1071–1087.

DIXON, D. M., VALKANOV, M. & MARTIN, R. J. (1993). A patch-clamp study of the ionic selectivity of the large conductance, Ca-activated chloride channel in muscle vesicles prepared from *Ascaris suum*. *Journal of Membrane Biology* **131**, 143–149.

FRANCIOLINI, F. & PETRIS, A. (1988). Chloride channels of biological membranes. *Archives of Biochemistry and Biophysics* **261**, 97–102.

HANKE, H. & MILLER, C. (1983). Single chloride channels from *Torpedo* electroplax; activation by protons. *Journal of General Physiology* **82**, 25–45.

HILLE, B. (1968). Charges and potentials at the nerve surface: Divalent ions and pH. *Journal of General Physiology* **51**, 221–236.

HILLE, B. (1992). *Ionic Channels of Excitable Membranes*. 2nd Edn. Sinauer Associates, Sunderland, Mass.

JARMAN, M. (1959). Electric activity in muscle cells of *Ascaris* muscle. *Nature, London* **184**, 1244.

LOGOTHETIS, D. E., MOVAHEDI, S., SATLER, C., LINDPAINTER, K., NADAL-GINARD, B. (1992). Incremental reductions of positive charge within the S4 region of a voltage-gated K^+ channel result in corresponding decrease in gating charge. *Neuron* **8**, 531–540.

MARTIN, R. J. (1980). The effect of GABA on the input conductance and membrane potential of *Ascaris* muscle. *British Journal of Pharmacology* **71**, 99–106.

PAPAZIAN, D. M., TIMPE, L. C., JAN, Y. N. & JAN, L. Y. (1991). Alteration of voltage-dependence of *Shaker* potassium channel by mutations in the S4 sequence. *Nature, London* **349**, 305–310.

RAO, G. S. J., WARISO, B. A., COOK, H. W. H. & HARRIS, B. G.

(1987). Reaction of *Ascaris suum* phosphofructokinase with diethylpyrocarbonate. *Journal of Biological Chemistry* **262**, 14068–14073.

SAZ, H. J. & WEIL, A. (1962). Pathway of formation of α-methyl valerate by *Ascaris lumbricoides*. *Journal of Biological Chemistry* **237**, 2053–2056.

STÜHMER, W., CONTI, F., SUZUKI, H., WANG, X., NODA, M., YAHAGI, N., KUBO, H. & NUMA, S. (1989). Structural parts involved in activation of the sodium channel. *Nature, London* **339**, 597–603.

THORN, P. & MARTIN, R. J. (1987). A high-conductance calcium-dependent chloride channel in *Ascaris suum* muscle. *Quarterly Journal of Experimental Physiology* **72**, 31–49.

VALKANOV, M., MARTIN, R. J. & DIXON, D. M. (1994). The Ca-activated chloride channel of *Ascaris suum* conducts volatile fatty acids produced by anaerobic respiration: a patch-clamp study. *Journal of Membrane Biology* **138**, 133–141.

VALKANOV, M. & MARTIN, R. J. (1995). A Cl channel in *Ascaris suum* selectively conducts dicarboxylic anion products of glucose fermentation and suggests a role in removal of waste organic anions. *Journal of Membrane Biology* **148**, 41–49.

ZAGOTTA, W. N. & ALDRICH, R. W. (1990). Voltage-dependent gating of *Shaker* A-type channels in *Drosophila* muscle. *Journal of General Physiology* **95**, 29–60.

A non-nicotinic ACh receptor in muscle of *Ascaris suum*

R.J. Martin

Department of Preclinical Veterinary Sciences, University of Edinburgh, Edinburgh EH9 1QH

The anthelmintic levamisole activates nicotinic acetylcholine receptors (nAChRs) on muscle cells of the nematode parasite *Ascaris suum* (Martin, 1993). Nematode parasites exposed to levamisole show a spastic paralysis but they can recover with a loss of sensitivity to levamisole (Coles *et al.* 1975); after this recovery acetylcholine (ACh) still produces contraction. This observation can be explained if ACh activates other receptor types as well as the nAChRs activated by levamisole.

A two-microelectrode voltage-clamp technique (Martin *et al.* 1992) was used to examine voltage-activated K^+ currents in muscle cells of twenty-one *Ascaris* preparations. Figure 1 shows the typical inhibitory effect of ACh on K^+ currents in the presence of 100 μM tubocurarine to block nAChRs. All experiments with bath (1–100 μM) and ionophoretically applied ACh produced similar effects. In contrast, levamisole (1–30 μM) did not reduce the K^+ currents, nor did atropine (100 μM) antagonize the action of ACh (1–30 μM).

These observations suggest that an atropine-insensitive non-nAChR is also present in muscle of *Ascaris suum* that reduces K^+ currents; the receptor may permit recovery during levamisole therapy.

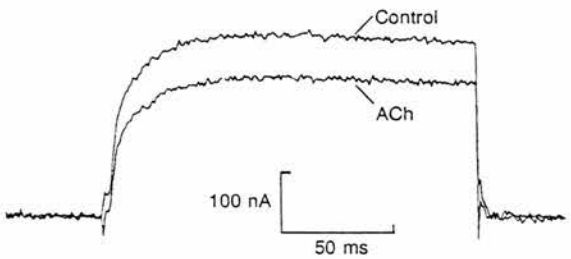


Fig. 1. Effect of ACh ionophoresis on K^+ currents activated by a step to +10 mV from a holding potential of −35 mV; 100 μM tubocurarine present. Solutions and technique as Martin *et al.* (1992).

REFERENCES

Coles, G.C., East, J.M. & Jenkins, S.N. (1975). *Gen. Pharmac.* **6**, 309–313.

Martin, R.J., Thorn, P., Gation, K.A.F. & Harrow, I.A. (1992). *J. Exp. Biol.* **173**, 75–90.

Martin, R.J. (1993). *Pharmac. Ther.* **58**, 13–50.

Altered myotube glutamine uptake associated with cell volume changes induced by aniso-osmotic exposure

Sylvia Y. Low, Michael J. Rennie and Peter M. Taylor

Department of Anatomy & Physiology, The University, Dundee DD1 4HN

Changes in cell volume associated with altered cell glutamine availability may be important signals for regulation of metabolic processes (e.g. protein and glycogen turnover) in skeletal muscle (Häussinger *et al.* 1993). In incubated skeletal muscle alterations in cell volume are associated with opposite changes in net glutamine release (Parry-Billings *et al.* 1991). We are investigating such phenomena in detail using cultured skeletal muscle exposed to different osmotic conditions.

Rat skeletal muscle myotubes in primary culture (330 mosmol kg^{-1}) were exposed for up to 60 min to media containing 60 mM NaCl with sucrose added to the required osmolarity (170, 330 and 430 mosmol kg^{-1}) before measurement of 50 μM L-[^{3}H]glutamine transport over 1 min. In preliminary experiments it was shown that these manoeuvres did not produce irreversible adverse effects. During hypo-osmotic exposure (Fig. 1) there was a rapid transient increase (reaching a maximum of ≈90 % after 2 min) of glutamine uptake associated with an increase in cell volume (measured using ^3H_2O with [^{14}C]mannitol as an extracellular marker). Exposure to hyperosmotic conditions (Fig. 1) resulted in a decrease in glutamine transport of ≈30 % which was maintained over 60 min.

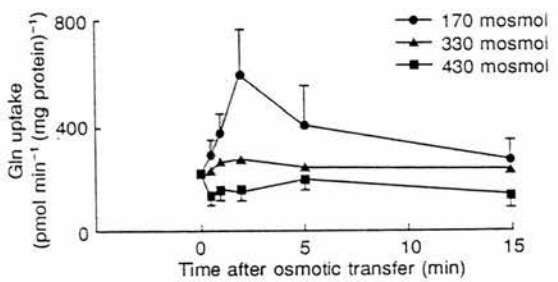


Fig. 1. Myotube glutamine uptake after osmotic transfer (mean value ± S.E.M. for five experiments).

The results show that muscle cell shrinkage (as occurs in disease or injury) may be associated with reduced unidirectional glutamine uptake; this may account in part for the lowered cell glutamine concentrations and increased net efflux of muscle glutamine characteristic of many catabolic states. In contrast, cell-swelling in skeletal muscle may have anabolic effects which are enhanced by associated increases in glutamine uptake and pool size (Rennie *et al.* 1986).

This work was supported by the UK Medical Research Council.

REFERENCES

Häussinger, D., Roth, E., Lang, F. & Gerok, W. (1993). *Lancet* **341**, 1330–1332.

influence of a mixed infection of *rtagia circumcincta* and *hostrongylus colubriformis*, and the ct of repeated oral dosage of febantel on pharmacokinetics of febantel in lambs

NDUYT, M. DEBACKERE, RCRUYSSE* & Q.A. McKELLAR**
*oep Farmacologie, Farmacie & Toxicologie. **Vakgroep ie. Parasitologie en Immunologie, Faculteit Diergenesskunde, plein 24, B-9000 Gent. ***Department of Veterinary acology, University of Glasgow Veterinary School, Bearsden Glasgow G61 1QH, UK*

duction

tel is a pro-benzimidazole anthelmintic which derives its ac- from the metabolites fenbendazole and oxfendazole (1). Its iacokinetic behaviour may be influenced by several factors was found that a moderate and to a lesser extent a heavy on with *Ostertagia circumcincta* or *Trichostrongylus formis* reduced the area under the plasma concentration– urve (AUC) of febantel and its metabolites in lambs (3, 4). ibs infected with a heavy infection of a resistant strain of *umcincta* the area under the curve was decreased by 26%. field conditions, lambs are normally parasitized with a infection of different nematodes, therefore in the present we investigated the pharmacokinetic parameters of febantel ts metabolites in lambs with a mixed infection of *O. cincta* and *T. colubriformis*. In the second part of this study, fluence of a previous treatment with febantel on its pharma- etics was studied.

rials and Methods

clinically health male, 5-month-old, parasite naive crossbred (Texel × Blue De Maine) were used. All the lambs were ad- tered Febantel (Rintal®, Bayer AG, Leverkusen, Germany) at a dose rate of 7.5 mg/kg bodyweight and plasma was col- as described previously (3). After a resting period of 4 weeks, mbs were allocated into two groups with four lambs in group five in group 2. Group 1 lambs were infected with a mixture 0,000 L3 *O. circumcincta* and 75,000 L3 *T. colubriformis* lar- Group 2 lambs were not infected. On day 28 after infection, e lambs were administered febantel orally at 7.5 mg/kg b.w. asma collected as above (3). Faecal egg counts, serum pepsino- eterminations and the measurement of febantel and its major olites were carried out as described in previous experiments The AUC was calculated using the trapezoidal rule (7).

lts

ebantel plasma concentrations were always very low and n a few samples did they exceed the detection limit. There 3.8% decrease for the AUC of the three metabolites in in- lambs in comparison with the AUCs in the same lambs be- nfection. The C_{max} values were higher and the t_{max} values er for all the metabolites in the parasitized animals. How- after repeated administration in the non-infected group was a decrease of 17% in total metabolite AUC following econd febantel administration compared to the first dose. For the same group the C_{max} and the t_{max} for all the metabolites were lower and shorter respectively on the second occasion.

Discussion

The most obvious finding in the parasitized lambs was that the bioavailability of febantel was markedly (4%) reduced. In particular the AUC of the oxfendazole and oxfendazole sulphone metabolites were reduced. The shorter t_{max} and lower C_{max} of the oxfendazole and oxfendazole sulphone metabolites and the 17% decrease of the total AUC of febantel and its metabolites after the second oral administration of febantel in uninfected lambs can perhaps be attributed to a possible effect of febantel or one of its metabolites on the liver mixed function oxidase and particularly on cytochrome P450. However this requires to be confirmed by *in vitro* metabolism studies.

Acknowledgements

The authors wish to thank Mr F. Vandekerkhove for the technical assistance. The helpful hand of Pharmacist E. Soenen, the laboratory work of Mrs M. Geerinck and Mr K Roels is fully appreciated. Thanks to Mrs E. Raulo-Roelens for typing this manuscript.

References

1. Delatour P. & Euzeby J. (1983) *Point Veterinaire*. **15**, 63–68.
2. Baggot J.D. & McKellar Q.A. (1994) *J Vet Pharmacol Therap.* (in press).
3. Debackere M., Landuyt J., Vercruysse J. & McKellar Q. (1993) *J Vet Pharmacol Therap.* **16**, 261–274.
4. Landuyt J., Debackere M., Vercruysse J. & McKellar Q. (1993) *Int J Parasitol* (submitted).
5. Landuyt J., Debackere M., Delbeke F. & McKellar Q. (1993) *Biomed Chromatog.* **7**, 78–81.
6. Berhen P., Dorny P. & Vercruysse J. (1987) *Am J Vet Res.* **48**, 664–669.
7. Gibaldi M. & Perrier D. (1975) *Pharmacokinetics*. (ed. James Swarbrick). Marcel Dekker, Inc. New York.

O9

Non-nicotinic acetylcholine receptors on nematode muscle may allow recovery of parasites from levamisole treatment

R.J. MARTIN
Department of Preclinical Veterinary Sciences, R.(D.)S.V.S., Summerhall, University of Edinburgh, EH9 1QH, UK

Introduction

Acetylcholine (ACh) is an excitatory transmitter of nematodes that is known to open, via a nicotinic receptor (nAChR), non-selective cation channels in the muscle membrane of parasitic nematodes, including *Ascaris suum* (1). Bath-application of ACh produces muscle depolarization and contraction.

The anthelmintic levamisole is a potent nicotinic agonist in nematodes and also opens the ACh channels (3, 4). However, levamisole is not just a simple agonist since it also produces open-channel block and desensitization. This means that recovery from levamisole therapy may occur, particularly if high concentrations are used.

Coles *et al.* (5). have described how levamisole produces contraction with spastic paralysis in nematode parasites and have pointed out that parasites may recover with loss of sensitivity to levamisole: after this recovery ACh may still produce contraction. This observation can be explained if ACh activates other receptor types as well as the nAChRs activated by levamisole.

We have examined the possibility that there may be an ACh receptor on *Ascaris* muscle that is homologous to the muscarinic receptor of vertebrates in addition to the nicotinic receptor already described.

Materials and Methods

A two-microelectrode voltage-clamp technique (6) was used to examine voltage-activated potassium currents in muscle cells of 21 *Ascaris* preparations.

Results

In these experiments it was shown that ACh produces a dose-dependent and reversible reduction of the potassium currents and that tubocurarine (100 μM) did not block the effect of ACh. In contrast levamisole (1–30 μM) did not reduce the potassium currents. Interestingly atropine (100 μM) did not antagonize the action of ACh as might be expected.

Discussion and Conclusions

These observations show that an atropine insensitive non-nAChR is present on *A. suum* muscle which would facilitate contraction and at which levamisole is not a potent agonist: this novel receptor may permit recovery during levamisole therapy and contribute to resistance.

References

1. Martin R.J. (1982) *Br J Pharmacol.* **77**, 255–265.
2. Pennington A.J. & Martin R.J. (1992) *J Exp Biol.* **154**, 201–221.
3. Robertson S. & Martin R.J. (1992) *Br J Pharmacol.* **108**, 170–178.
4. Martin R.J. (1993) *Pharmac Ther.* **58**, 13–50.
5. Coles G.C., East J.M. & Jenkins S.N. (1975) *Gen Pharmacol.* **6**, 309–313.
6. Martin R.J., Thorn P., Gration K.A.F. & Harrow I.A. (1992) *J Exp Biol.* **173**, 75–90.

O10

Occurrence of drug resistance in animal trypanosomiasis

S.M. ANIKA & B.M. ANENE
Faculty of Veterinary Medicine, University of Nigeria, Nsukka, Nigeria

Introduction

Animal production in the south eastern area of Nigeria which is endemic for trypanosomiasis is dependent largely on the use of trypanocides (1, 2). Reports from other parts of Africa indicate parasite resistance to trypanocides (3, 4) and resistance probably exists in Nigeria since cases of canine trypanosomiasis in the area rarely survive inspite of chemotherapy with trypanocides, usually diminazene aceturate. Drug-resistant strains of trypanosomes in Nigeria have only been partially investigated (5). We report here our preliminary findings from an investigation into the sensitivity to diminazene of isolates of *Trypanosoma brucei* from animals of the Nsukka area, south eastern Nigeria.

Materials and Methods

Blood samples from clinical cases presented to the University of Nigeria Veterinary Teaching Hospital (UNVTH) between August 1992 and March 1993 were examined for trypanosome infection. Giemsa-stained thin blood films were used to identify the trypanosome species (6). Each *T. brucei* isolate was tested by innoculating approximately 2.5×10^5 trypanosomes per ml of saline diluted infected blood into each of two rats. The tail blood was examined daily to establish the onset of parasitaemia. Treatment with a single dose of diminazene at 7 mg/kg i.p was carried out 3 days after the rat was parasitaemic and monitored for a total period of 100 days post treatment. If parasitaemia disappeared completely (i.e. no relapse), then the isolate was regarded as susceptible while it was considered resistant if after treatment there was a relapse. The potency of the batch of diminazene used was tested on an authenticated sensitive laboratory stock of *T. brucei*.

Results

The prepatent period of the isolates in the rats were 3–4 days. Of the 36 isolates (32 from dogs, 2 from goats and one each from horse and sheep) tested, 11 (30.6%) 10 of the dog isolates and the only isolate from the horse exhibited varying degrees of resistance (drug fastness and relapses) to diminazene. Two fascinating observations were recorded. Firstly, parasites persisted in the blood of a clinical canine case treated with diminazene at the dosage of 7 mg/kg, during re-examinations 12 days post treatment. When a repeat dose of the drug was administered, the dog subsequently developed fatal neurological manifestations. The infecting trypanosome was however susceptible to the drug when tested in the rat. Secondly an isolate also from the dog which was refractory to the initial dose of the drug was subsequently killed by a repeat dose of the drug. Relapses in the rats generally occurred at intervals of 9–36 days after diminazene treatment with a mean relapse interval of 24 ± SE 3.1 days. The control *T. brucei* (Gboko CT/70 NITR) was readily sensitive to the diminazene.

Discussion and Conclusions

The high prevalence rate of drug resistant strains of *T. brucei* (30.6%) recorded and reported cases from south western (5) and northern (4) areas of the country, suggest a widespread phenomenon. It is important to note that all the resistant isolates emerged from dogs and a horse which may be more frequently treated than sheep and goats which are largely food animals. The more frequent exposure of the parasites to trypanocides in the companion animals may explain in part the high frequency of isolation of resistant parasites in them. The fatal termination of the dog case in spite of treatment, by an isolate apparently sensitive to the drug in the rat, is also significant. This observation highlights the importance of the host–parasite interaction in the pathogenesis of drug resistance.

Acknowledgement

The study is supported by EEC Lomé III project for the control of animal trypanosomiasis in Nigeria.

References

1. Anene B.M., Chime A.B. & Anika S.M. (1991) *Br Vet J.* **147**, 275–282.

Oral Communications

diuretic activity in the batch of units under study was first confirmed. Head extracts, using Ringer solution or 15% TFA as a solvent, inhibited the fluid secretion by the Malpighian tubules: at a concentration of 0·3 head equivalents μl^{-1} (h.equiv μl^{-1}), secretion was slowed down by $62 \pm 11\%$ (mean value $\pm$ S.E.M.), $n = 7$, $P < 0{\cdot}05$, and $89 \pm 3\%$, $n = 4$, $P < 0{\cdot}05$, Student's paired t test, respectively. The 15% TFA extract of 40 000 heads was then run through several columns of a high performance liquid chromatography (HPLC) apparatus (Waters) using a linear acetonitrile (CH_3CN) gradient in order to try and purify peptide factors from the extract. During the first run (PrepPak DP C18, 0–80% acetonitrile) antidiuretic activity was recovered in the 10–20% CH_3CN fraction: fluid secretion was inhibited by $35 \pm 2\%$, $n = 10$, $P < 0{\cdot}05$, when applying the fraction to the tubules at a concentration of 0·1 h.equiv μl^{-1}. The fraction was then lyophilized and applied to the next column (PrepPak DP C4). A gradient of 0 to 50% CH_3CN was applied. A small but not statistically significant inhibition of secretion was caused by the 20–25% fraction, when applied to the tubules at a concentration of 0·5 h.equiv μl^{-1}. This fraction also contained the highest peak of absorption at the wavelength of 214 nm used during the run. The fraction was lyophilized and applied to the next column (Prep Nova Pak HR Phenyl, 0–50% CH_3CN, 0·1% TFA). During the third run several absorption peaks were still present. Antidiuretic activity was found in the 17–20% CH_3CN fraction, corresponding to the first absorption peak. At a 1·0 h.equiv μl^{-1} concentration it inhibited secretion by $33 \pm 9\%$, $n = 3$, $P < 0{\cdot}05$. All effects – from crude extracts to the fraction collected from the third column – were reversible.

The results indicate that peptides with direct inhibitory action on the Malpighian tubule are present in the head of the ant. To further purify and isolate a single peptide from the last fraction it will be run through a Nova Pak C8 column. The amino acid sequence will be determined in order to be able to synthesize the peptide and to elucidate, later on, the mechanism of interaction between the antidiuretic factor and the Malpighian tubules of *Formica polyctena*.

This work was supported by a B.O.F. grant (Bijzonder Onderzoeks Fonds) from the Limburgs Universitair Centrum.

REFERENCES

De Decker, N., Hayes, T.K., Van Kerkhove, E. & Steels, P. (1994). *J. Insect Physiol.* **40**, 1025–1036.

Petzel, D.H. & Conlon, J.M. (1991). *FASEB J.* **5**, A1059 (75th Annual Meeting, Atlanta, Georgia, April 21–25).

Spring, J.H., Morgan, A.M. & Hazelton, S.R. (1988). *Science* **241**, 1096–1098.

Spring, J.H. & Clark, T.M. (1990). *Progress in Comp. Endocr.* **342**, 559–564.

The Kostyuk technique for recording currents from isolated muscle bags of *Ascaris suum*

R.J. Martin and M.A. Valkanov

Department of Preclinical Veterinary Sciences, University of Edinburgh, Edinburgh EH9 1QH and Central Laboratory of Biophysics, Bulgarian Academy of Sciences

Large cells may be voltage-clamped and perfused extracellularly and intracellularly using a technique developed in Kostyuk's laboratory (Kostyuk *et al.* 1984). The technique uses a V-shaped micropipette with a small 20–30 μm hole in the tip and the isolated cells to be recorded from are drawn into the tip by suction. We have developed this technique for recording currents across the bag membrane of somatic muscle cells from *Ascaris suum*. Single severed collagenase isolated bags were mounted by drawing them into the recording tube permitting voltage clamp and intracellular and extracellular perfusion (Fig. 1*A*).

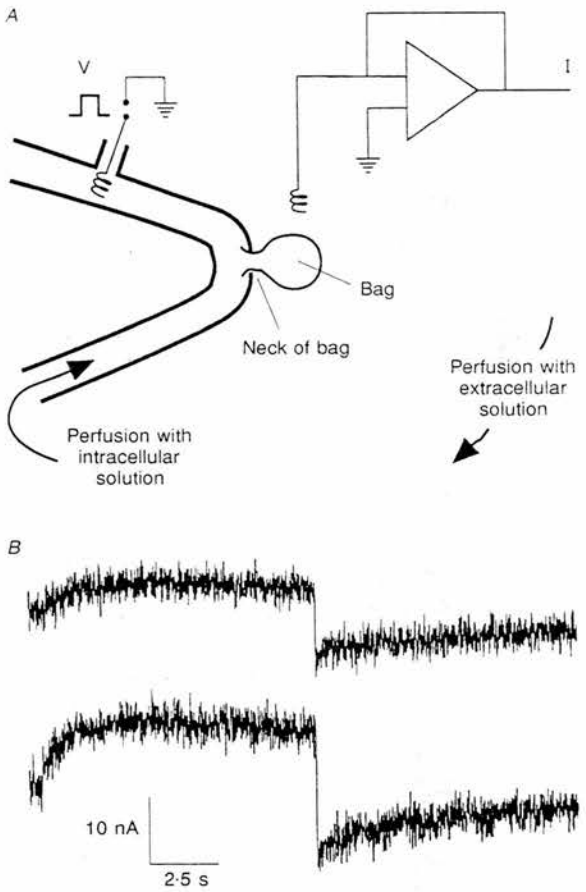


Fig. 1. *A*, diagram of isolated bag preparation under voltage clamp mounted in a V-micropipette. *B*, leak-corrected currents activated by step potential to +27 mV from holding potential −40 mV. Extracellular solution (mM): 135 caesium acetate, 19 BaCl, 10 TEA, 5 4-AP, 5 Hepes; pH 7·2 with CsOH. Intracellular solution (mM): 135 caesium acetate, 0·5 EGTA, 5 Hepes; pH 7·2 with CsOH. Top: control. Bottom: 50 μM ACh and 100 μM mecamylamine applied extracellularly.

Figure 1*B* shows examples of currents from a preparation bathed in symmetrical Cs^+ solutions with K^+ current blockers. The effect of ACh was to increase a slow voltage-activated current with a slow inward tail current. The current stimulated by ACh can be explained as a non selective cation current and may underlie the slow potential waves seen in *Ascaris* muscle preparations (Weisblat *et al.* 1976).

Supported by the Wellcome Trust.

REFERENCES

Kostyuk, P.G., Krishtal, O.A. & Pidoplichko, V.I. (1984). In *Intracellular Perfusion of Excitable Cells*, ed. Kostyuk, P.G. & Krishtal, O.A., pp. 35–51. John Wiley & Sons, Chichester.

Weisblat, D.A., Byerly, L. & Russel, R.L. (1976). *J. Comp. Physiol.* **111**, 93–113.

Dihydropyridine-sensitive charge movement in isolated crayfish (*Pacifasticus leniusculus*) neurons

E.R. Brown, A. Chrachri, I. Inoue* and I. Tsutsui†

*MBA Laboratory, Plymouth, *Institute for Enzyme Research, Tokushima University, Japan and †NIPS, Okazaki, Japan*

In vertebrate skeletal muscle, depolarization of the surface membrane releases Ca^{2+} from intracellular stores when Ca^{2+} influx is blocked. The L-type Ca^{2+} channel acts as a voltage sensor interacting directly with intracellular (sacroplasmic) Ca^{2+} release channels (measured as a voltage- and dihydropyridine (DHP)-sensitive charge movement). Where DHP-sensitive charge movement is absent, direct release of Ca^{2+} from intracellular stores does not occur (Inoue *et al.* 1994). We examined crayfish neurons that have prominent L-type Ca^{2+} currents (Chrachri, 1995) for the presence of DHP-sensitive charge movement.

Crayfish were decapitated after chilling to 4 °C for 1 h and the abdominal ganglia removed. Swimmeret motorneurons in the ganglia were labelled by backfilling overnight in 4% Lucifer Yellow in distilled water and dissociated in 8 mg ml^{-1} protease in crayfish ringer (CFR) for 1 h. Neurons were identified under UV and subjected to whole cell voltage clamp. The internal solution contained (mM): 174 caesium aspartate, 0·25 $CaCl_2$, 2·6 $MgCl_2$, 5 EGTA and 10 Hepes; pH 7·2. The external solution was CFR with 2 mM $BaCl_2$, 5 mM Co^{2+} and 2 μM TTX added to CFR to block L-type and Na^+ currents. After whole-cell capacity compensation and p/4 leak subtraction, charge/voltage relations (Q/V) were examined by integrating voltage-sensitive capacitive currents obtained during depolarizing voltage steps (Fig. 1). Results were plotted with Boltzmann functions (continuous lines in Fig. 1),

$$Q = Q_{max}/\{1 + \exp[-(V_m - V^*)/k]\},$$

where Q_{max} is the maximum value of Q, V^* is a voltage giving half Q_{max}, and k is a broadening factor.

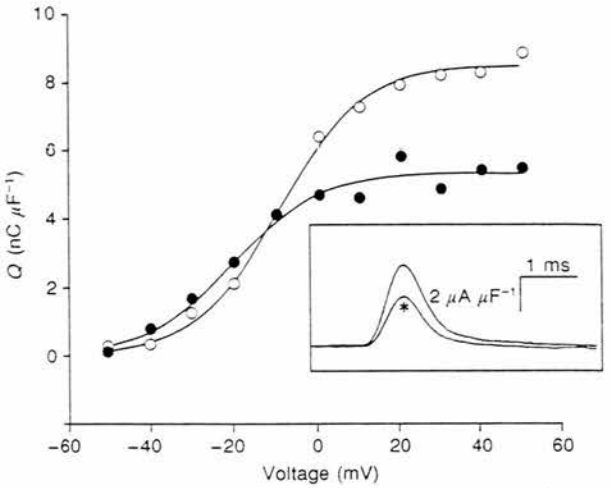


Fig. 1. Q/V relations before (○) and after (●) 5 μM nifedipine. Holding potential −70 mV, step depolarizations to values indicated. Inset, 'on' charge by depolarization to +50 mV before and after (*) nifedipine. Cell capacitance, 73 pF.

Q_{max} was 5·54 ± 0·91 nC μF^{-1} (mean ± S.E.M., $n = 5$). Addition of nifedipine significantly ($P < 0·05$, Student's t test) reduced Q_{max} to 2·6 ± 0·76 nC μF^{-1} (mean ± S.E.M., $n = 5$). We conclude that DHP-sensitive charge movement is present in these invertebrate neurons, as previously reported in vertebrate neurons (Shimahara *et al.* 1993).

Supported by the MBA and Monbusho UK–Japan exchange. E.R.B. is a BBSRC Advanced Fellow.

REFERENCES

Chrachri, A. (1995). *J. Exp. Biol.* **198**, 1483–1492.

Inoue, I., Tsutsui, I., Bone, Q. & Brown, E.R. (1994). *Proc. R. Soc. Lond.* B **255**, 181–187.

Shimahara, T., Bournaud, R. & Melliti, K. (1993). *Soc. Neurosci. Abstr.* **19**, 1332.

Effects of free radicals on the permeability of the nerve perineurium

Chris Strickland, Clare Parker, Neal Beamish and N. Joan Abbott

Physiology Group, Biomedical Sciences Division, King's College London, Strand, London WC2R 2LS

The perineurium is one component of the blood–nerve barrier (BNB), protecting the axonal microenvironment of the endoneurium. BNB permeability may increase under conditions of trauma, infection and inflammation (Olsson, 1990), but it is not clear whether the generation of oxygen free radicals plays a role. In this study we have examined the effects of free radicals on the potassium (K^+) permeability of the perineurium of the frog sciatic nerve.

The sciatic nerve was removed from stunned and pithed frogs (*Rana temporaria* or *R. pipiens*), and mounted in a

Experimental Physiology (1996), **81**, 909–925
Printed in Great Britain

EFFECTS OF ACETYLCHOLINE ON A SLOW VOLTAGE-ACTIVATED NON-SELECTIVE CATION CURRENT MEDIATED BY NON-NICOTINIC RECEPTORS ON ISOLATED *ASCARIS* MUSCLE BAGS

R. J. MARTIN AND M. A. VALKANOV*

*Department of Preclinical Veterinary Sciences, Royal (Dick) School of Veterinary Studies, Summerhall, University of Edinburgh, Edinburgh EH9 1QH, UK and *Institute of Biophysics, Bulgarian Academy of Sciences, Sofia, Bulgaria*

(MANUSCRIPT RECEIVED 13 MAY 1996, ACCEPTED 10 JULY 1996)

SUMMARY

Isolated muscle bags from the parasitic nematode *Ascaris suum* were prepared by collagenase treatment and dissection. Single bags were mounted in a V-shaped plastic pipette for voltage clamp application and intra- and extracellular perfusion. With 'physiological' intra- and extracellular solutions, depolarizing voltage steps from near the normal resting membrane potential, −40 mV, produced in leak-corrected currents, a slowly activating outward current at potentials more positive than −20 mV. At the end of the depolarizing pulse there was a slow inward tail current with a reversal potential near −20 mV. Hyperpolarizing voltage steps produced an outward current relaxation and an outward tail current with the same reversal potential. The observations can be explained by the presence in the bag of a non-selective cation channel current, I_{bcat}, that activates spontaneously at the holding potential; depolarization increases opening of the channel and hyperpolarization decreases opening. Bath-applied acetylcholine in concentrations greater than 10^{-7} M produced an increase in the amplitude of I_{bcat}. The effect of acetylcholine was not antagonized or prevented by 100 μM mecamylamine or 100 μM tubocurarine, suggesting the presence of a non-nicotinic acetylcholine receptor. Atropine (100 μM) had no detectable influence on the effect of acetylcholine but the FMRFamide peptide, PF_1, in concentrations >1 μM, reduced the amplitude of I_{bcat}. I_{bcat} was maintained when Cs^+ was used to replace intra- and extracellular cations, showing that the channels were permeable to Cs^+. It is concluded that the bag membrane possesses a slow voltage-activated non-selective cation channel current, I_{bcat}. The effect of acetylcholine in the presence of nicotinic antagonists indicates the presence of non-nicotinic acetylcholine receptors on the bag membrane. The effect of PF_1 indicates the presence of PF_1 receptors on the bag membrane.

INTRODUCTION

Nematode parasites continue to infect animals and man. One way of treating infections is to use a group of therapeutically related compounds: levamisole, pyrantel and morantel. These agents have a selective effect on the parasites, producing spastic paralysis. The drugs are known to exert a depolarizing effect on nematode muscle (Aceves, Erliji & Martinez-Marnon, 1970; Aubry, Cowell, Davey & Shevde, 1970) and to gate nicotinic acetylcholine channels on muscle (Harrow & Gration, 1985; Martin, Thorn, Gration & Harrow, 1992; Robertson, Pennington, Evans & Martin, 1994).

Resistance to a variety of anthelmintics, including the above nicotinic anthelmintics, is now recognized (Prichard, 1994) but explanations for the mechanisms of anthelmintic resistance remain to be elucidated. One form of resistance to nicotinic anthelmintics is the ability of some nematodes to recover from the effects of the anthelmintics despite the continued presence of the drug. Coles, East & Jenkins (1975) have described the effects of levamisole on

the pig intestinal nematode *Ascaris suum* and have reported that a proportion of these nematodes will recover from effects of levamisole despite the maintained presence of the drug. Interestingly, Coles *et al.* (1975) reported that *Ascaris* muscle in the recovered state will contract in response to injection/application of acetylcholine but will relax in response to other nicotinic anthelmintics. One interpretation of these observations is that there are two types of acetylcholine receptors on *Ascaris* muscle: one type, the nicotinic receptor, is lost during the long exposure to levamisole; the second type, a non-nicotinic receptor, escapes the effects of levamisole and remains to be stimulated by acetylcholine.

In vertebrate preparations, membrane ion channels may be activated by acetylcholine, which stimulates nicotinic or muscarinic receptors. The ion channels of nicotinic receptors are directly coupled and ligand gated as in *Ascaris*, but the ion channels associated with muscarinic receptors are indirectly coupled via G-proteins and are often coupled to voltage-activated channels (Kass & Freeman, 1993; Neer, 1994). In this study, we have examined the effects of acetylcholine on voltage-activated currents in *Ascaris* muscle to look for the presence of a second (non-nicotinic) type of acetylcholine receptor. We have used a V-shaped plastic pipette technique for application of voltage clamp and for intracellular perfusion (Kostyuk, Krishtal & Pidoplicho, 1984) to record voltage-activated currents from an isolated bag preparation of *Ascaris* muscle (Fig. 1). The advantages of this method are that: (1) it allows recording from a restricted region of the muscle cell (just the bag); (2) it permits control of the intra- and extracellular milieu of the cell; and (3) it allows a better space clamp than a two-microelectode voltage clamp (Martin *et al.* 1992), which is limited by the anatomy of the cell and electrical coupling between adjacent muscle cells (De Bell, Del Castillo & Sanchez, 1963; Del Castillo, Rivera, Solorzano & Serrato, 1989).

METHODS

Preparation of the isolated bags

Adult *Ascaris suum* were obtained from the local abattoir and maintained in Locke's solution at a temperature of 34 °C. The Locke's solution was changed daily and the *Ascaris* were used within 7 days. A 2 cm section of the worm, taken 5 cm behind the head region, was cut along one of the lateral lines. The gut was removed and the body flap pinned, cuticle side down, onto Sylgard® (Dow Corning) in a Petri dish. The flap preparation was then washed in extracellular solution.

The flap was incubated in enzyme solution (extracellular solution with added Sigma Type I collagenase, 0·2 mg/ml) for 10–15 min, washed and incubated for 1 h at 30 °C to achieve separation of the bag regions of the muscle cells. The preparation was then washed in extracellular solution to remove the collagenase and a fine pair of iris scissors used to make a cut, parallel to the flap, to separate the bag from the spindle region of the muscle cell (Fig. 1*A*). A single isolated bag was then sucked up into a carrier pipette, made from a fire-polished broken-tipped micropipette, using a Vernier screw to provide the fine control for suction. The isolated bag was then manipulated under a Nikon TMS inverted microscope (×40) into the orifice of a V-shaped plastic pipette using suction on the V-shaped pipette to pull the neck of the bag into, and seal, the orifice of the V-shaped pipette (Figs 1 and 2).

Recording system

We have used a V-shaped plastic pipette with a small orifice at the tip to make recordings of transmembrane currents under voltage-clamp conditions and to change extracellular and intracellular solutions from isolated bags of *Ascaris* muscle cells (Fig. 2*A*). The recording technique and electronic circuits have been described in detail (Kostyuk *et al.* 1984). The voltage-clamp circuit used in these experiments was made up in the Departmental Electronic workshop.

The principle of the recording technique was to mount an isolated bag in the 20 μm diameter hole located at the point of a V-shaped plastic pipette. After sealing the preparation in the hole, the potential

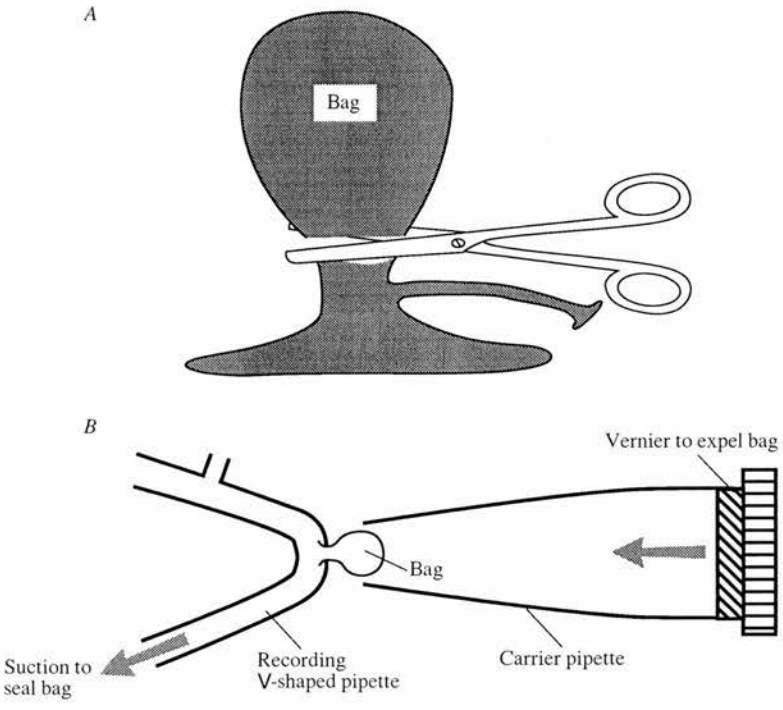


Fig. 1. Diagram of the preparation and mounting of the isolated bag preparation. *A*, a fine pair of iris scissors is used cut the bag from the spindle region of the muscle cell after treatment of the flap preparation with collagenase (0·25 mg/ml for 10 min). *B*, a carrier pipette, made from a fire-polished broken micropipette and fitted with a Vernier screw to control the uptake and expulsion of the isolated bag, is used to manipulate the isolated bag into the small orifice of the V-shaped pipette. Gentle suction on the V-shaped pipette by means of a syringe pulls the isolated bag into the orifice and increases the seal resistance.

across the bag was controlled by adjusting the potential within the V-shaped pipette. Sealing was measured by observing the current response to a standard voltage step and monitoring the decrease in the current as sealing took place. The transbag current was recorded with a virtual ground circuit that maintained the extracellular membrane and solution at earth potential. Experiments were carried out at room temperature, 15–25 °C.

The current–voltage (I–V) relationship of the recording system, in the absence of a preparation, was linear in the range −100 to 90 mV when holding at −40 mV. Outside this potential range there was some deviation from linearity that varied with the nature of the plastic of the V-shaped pipette and the size of the orifice. Recordings were therefore restricted to the linear current–voltage range.

The series resistance, R_s, between the stimulating electrode and the virtual ground observed without an isolated bag in the orifice of the V-shaped pipette was 100 kΩ. When an isolated bag was sealed with the help of suction into the orifice of the V-shaped pipette, the overall resistance between the intracellular stimulating electrode and the virtual ground circuit increased by two to ten times. The resistance of the isolated bag, R_m, could vary between 200 and 1000 kΩ. The transbag potential, V_o, under a stationary command potential, V_c, (Odipchuk & Timin, 1984) is given by:

$$V_o = \frac{V_c/R_m}{1 - R_s/R_m}. \quad (1)$$

The equation demonstrates that when R_s is equal to R_m, the control of the membrane potential is lost, and in these experiments V_o could vary between 10 and 50 % of V_c. In order to reduce the effect of a low R_m, we removed Ca^{2+} from the intracellular solution to reduce the opening of the Ca^{2+}-dependent Cl^-

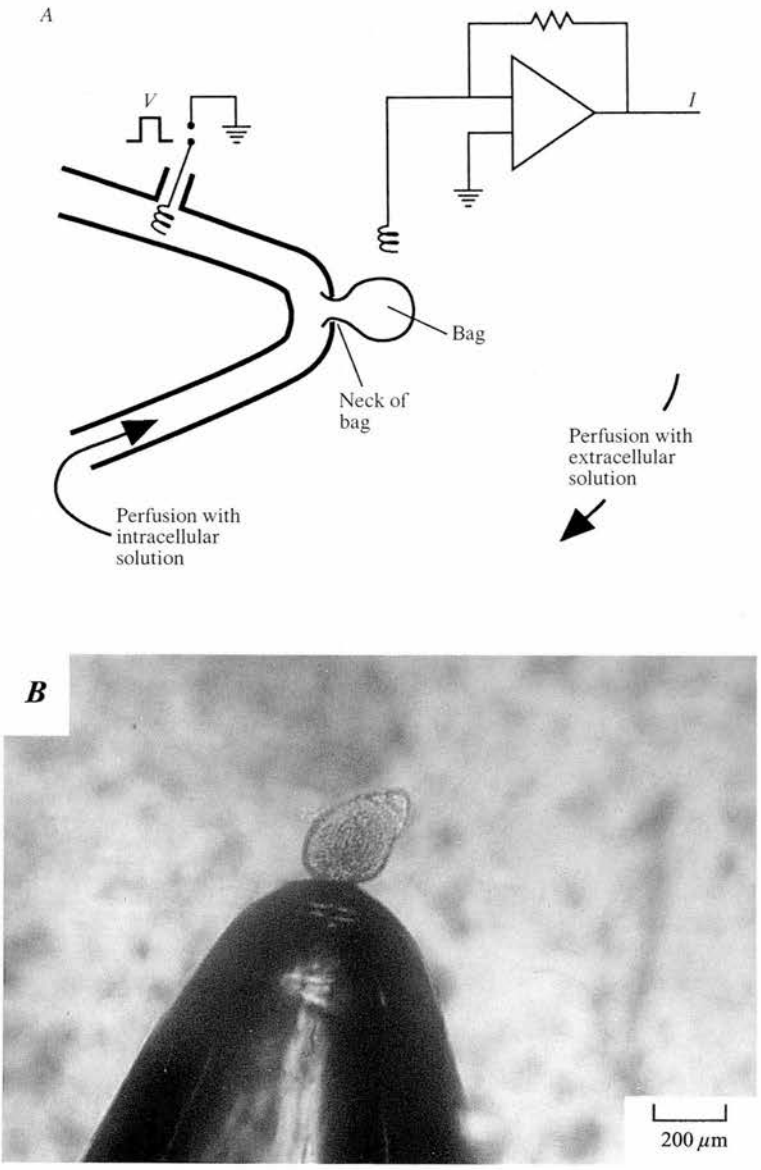


Fig. 2. Recording system and perfusion system. *A*, the voltage stimulus (V) was applied to the intracellular membrane via the micropipette. The transmembrane current (I) was recorded with a virtual ground circuit. Intracellular and extracellular perfusion was possible. *B*, photomicrograph of an isolated bag mounted in the V-shaped micropipette.

channels present in the bag membrane (Thorn & Martin, 1987). Glycogen is present in fresh *Ascaris* bags (Rosenbluth, 1965), so the cytoplasm of the bag can have a texture like jelly and increase R_s. In order to reduce the amount of glycogen, we used *Ascaris* after at least 2 days of maintenance in Locke's solution (starvation). We selected and made recordings from bags with an R_m of 400 kΩ or greater to give a maximum error of 25% in our measured voltages.

The time constant of the transient capacitative current following a step change in potential was in the range 100–500 ms. This time constant is determined by the product $R_m C_m$, where C_m is the capacitance of the bag; for the isolated bags, C_m was ~12·5 μF. The voltage-activated currents we investigated in this paper were slow, with time constants of ~2 s at room temperature, so we made no electronic correction for the membrane capacitative currents.

Voltage protocol

In most experiments we held the membrane potential near −40 mV, close to the normal resting membrane potential of the muscle cell. Voltage steps lasting 10 s, starting from −100 mV and increasing by 10 mV steps to +70 mV, were made every 120 s. The command potential was generated with a CED 1401 interface under the control of an IMB PS/2 model 70 386 computer and CED EPC software.

Leak- and capacitance-corrected currents

Current and voltage traces were filtered (3 dB, eight-pole Bessel at 1·5 kHz) and recorded permanently on tape, using a modified Sony DAT recorder, and on floppy disks. We carried out a leak and capacitance current correction procedure using the CED 1401 EPC software for current–voltage analysis that estimated and then subtracted a voltage step-scaled leak current. The current for scaling was measured from two 10 mV depolarizing steps and two hyperpolarizing steps from −40 mV for each individual *I–V* plot. The corrected current records display only the currents produced as a result of the conductance changes produced by voltage steps from the holding potential. If only one ion channel contributes to the current, the leak- and capacitance-corrected current corrected current is given by:

$$I = \Delta G_{V,h,t}(V - E_{rev}), \tag{2}$$

where $\Delta G_{V,h,t}$ is the change in membrane conductance of the voltage-sensitive channel current produced at time t by the voltage step to the potential V from a holding potential h. E_{rev} is the reversal potential of the channel. In all *I–V* plots, we measured the current 9·5 s after the start of the depolarizing pulse, to record steady-state current.

Solutions

The extracellular solution normally used to bathe the preparation contained (mM): NaCl, 123; KCl, 10; $MgCl_2$, 2; Hepes, 10; and glucose, 10; pH adjusted to 7·6 with NaOH. This solution was exchanged by steady gravity-driven perfusion when the effects of another solution were being tested or when effects of active substances were examined. The V-shaped pipette normally contained intracellular solution (mM): KCl, 135; and Hepes, 0·5; pH adjusted to 7·6 with KOH. 'Physiological' solutions are here defined as the use of the above extracellular solution in the bath and the above intracellular solution in the pipette. Intracellular solution was exchanged by steady perfusion of the V-shaped pipette when required. Cs^+-containing extra- and intracellular solutions were prepared by substituting Cs^+ for Na^+ and K^+ on an equimolar basis. Ba^{2+}-containing solutions were prepared by simple addition of BaCl to the normal extracellular solution described above.

Drugs

Acetylcholine, mecamylamine, tubocurarine, atropine, 4-aminopyridine (4-AP) and tetraethylamine (TEA) were purchased from Sigma. SPDNFLRamide (PF_1) was a gift from Dr T. Geary, Pharmacia and Upjohn, USA.

RESULTS

The results reported here are based on the analysis of observations on thirty-two isolated bag preparations. It was found that, once an isolated bag had been successfully located in the orifice of the V-shaped pipette, the seal resistance was very stable in the absence of perfusion. Perfusion was, however, sometimes associated with small changes – increases as well as decreases – in seal resistance. Recordings were rejected if the seal resistance changed by more than 25 %.

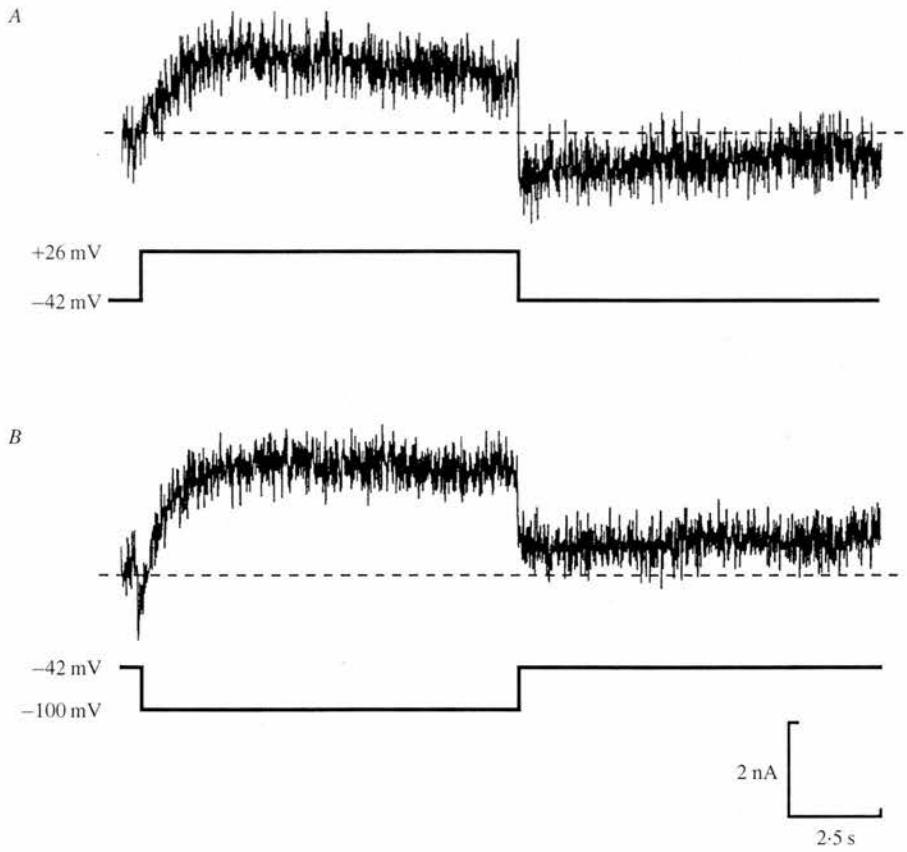


Fig. 3. Transbag currents following rectangular potential step from the holding potential. *A*, the depolarizing step from −42 to +26 mV results in a slowly developing outward current, which shows little inactivation, and then an inward tail current on repolarization. *B*, a hyperpolarizing step from −42 to −100 mV results in an initial inward current followed by an outward relaxation. At the end of the step potential, there is a steady outward tail current.

Voltage-clamp experiments reveal slow voltage-activated bag currents produced by depolarization and hyperpolarization

Figure 3*A* shows a representative example of the bag current produced by a depolarizing voltage step (from −42 to +26 mV). The depolarizing pulse produced an outward current that activated slowly over 2 s at +26 mV and showed little inactivation. At the end of the depolarizing pulse, there was a very slow inward tail current lasting longer than 10 s. Linear interpolation of the amplitude of the currents observed at the end of the positive pulse, +1·8 nA at +26 mV, and of the tail current on return to the holding potential, −1·0 nA at −42 mV, gives a value of −18 mV for the reversal potential of the current. The mean ± S.E.M. reversal potential for the current activated by depolarization estimated in this way was −21·6 ± 5·7 mV ($n = 9$).

Figure 3*B* shows the current trace observed after a hyperpolarizing pulse to −100 mV just after the depolarizing pulse of Fig. 3*A*. The current was initially inward following the

−100 mV step, and then it relaxed in an outward direction. At the end of the hyperpolarizing pulse there was a long, maintained outward tail current. The current at the end of the −100 mV step potential was +2·4 nA and on return to −42 mV it was 0·7 nA. Linear extrapolation of the current–voltage relationship yielded a value of −18 mV for the reversal potential of this current. In the other preparations, estimates of the reversal potentials of the tail currents produced by depolarization and hyperpolarization were also the same or similar, suggesting that the ionic basis for the current was identical.

In two-microelectrode voltage-clamp experiments on intact *Ascaris* muscle cells (Martin *et al.* 1992), the tail current following depolarization was found in ion-substitution experiments to be explained by a current permeable to both K^+ and Na^+, and the $Na^+ : K^+$ permeability ratio (α) was estimated assuming intracellular ion concentrations.

The relative $Na^+ : K^+$ permeability, α, of a cation channel was determined from the equation:

$$E_{rev} = \frac{RT}{F}\left(\frac{\alpha[Na^+]_o + [K^+]_o}{\alpha[Na^+]_i + [K^+]_i}\right), \quad (3)$$

where R is the molar gas constant, T the temperature in kelvin, F Faraday's number and E_{rev} the reversal potential. The subscript 'o' represents the extracellular molar concentration of Na^+ or K^+ ions and the subscript 'i' represents the intracellular molar concentration of the Na^+ or K^+ ions.

Using eqn (3) and the known intracellular and extracellular concentrations of Na^+ and K^+ ions in the experiments on the isolated bags, the permeability ratio for the current activated by depolarization was calculated to be 0·36 when E_{rev} was −22 mV. The voltage-activated bag current that is thus carried by Na^+ and K^+ ions is subsequently referred to as I_{bcat}.

Effect of acetylcholine on the voltage-activated bag currents

Acetylcholine is an excitatory neurotransmitter in nematodes that exerts some of its effects through nicotinic acetylcholine receptors on the bag membrane (Pennington & Martin, 1990). Figure 4*A* and *B* shows that the effects of acetylcholine (50 μM) on the voltage-activated bag currents were to increase the outward current seen during depolarization and to increase the size of the inward tail current. It is worth noting that effects of acetylcholine mediated via nicotinic ACh receptors are unlikely to show as voltage-activated currents because *Ascaris* nicotinic ACh receptors do not show significant voltage-sensitive opening following depolarization (Pennington & Martin, 1990). In addition, Fig. 4*C* shows that 100 μM mecamylamine, a potent nicotinic antagonist in *Ascaris* (Colquhoun, Holden-dye & Walker, 1991), does not antagonize the effect of acetylcholine on I_{bcat}. Extensive washing of the preparation only partially reversed the effect of acetylcholine (Fig. 4*D*). Complete *I–V* plots from these experiments are shown in Fig. 4*F*. In fourteen of nineteen preparations, the effect of acetylcholine was to augment I_{bcat}. The dose–response relationship of acetylcholine was not studied in detail, but it was observed that increases in concentration above 0·1 μM produced a dose-related increase in I_{bcat}. We also tested, in six bag preparations, the effects of the nicotinic anthelmintic levamisole in concentrations up to 300 μM. It was found that levamisole did not consistently enhance I_{bcat} and, in fact, at concentrations >100 μM, it reversibly reduced the bag input conductance and I_{bcat} (not shown).

We tested the effect of prior application of nicotinic antagonists on the action of acetylcholine and again found that the antagonists had little effect. Figure 5 shows the effect 10 μM acetylcholine on currents applied after 100 μM tubocurarine, a concentration known to block

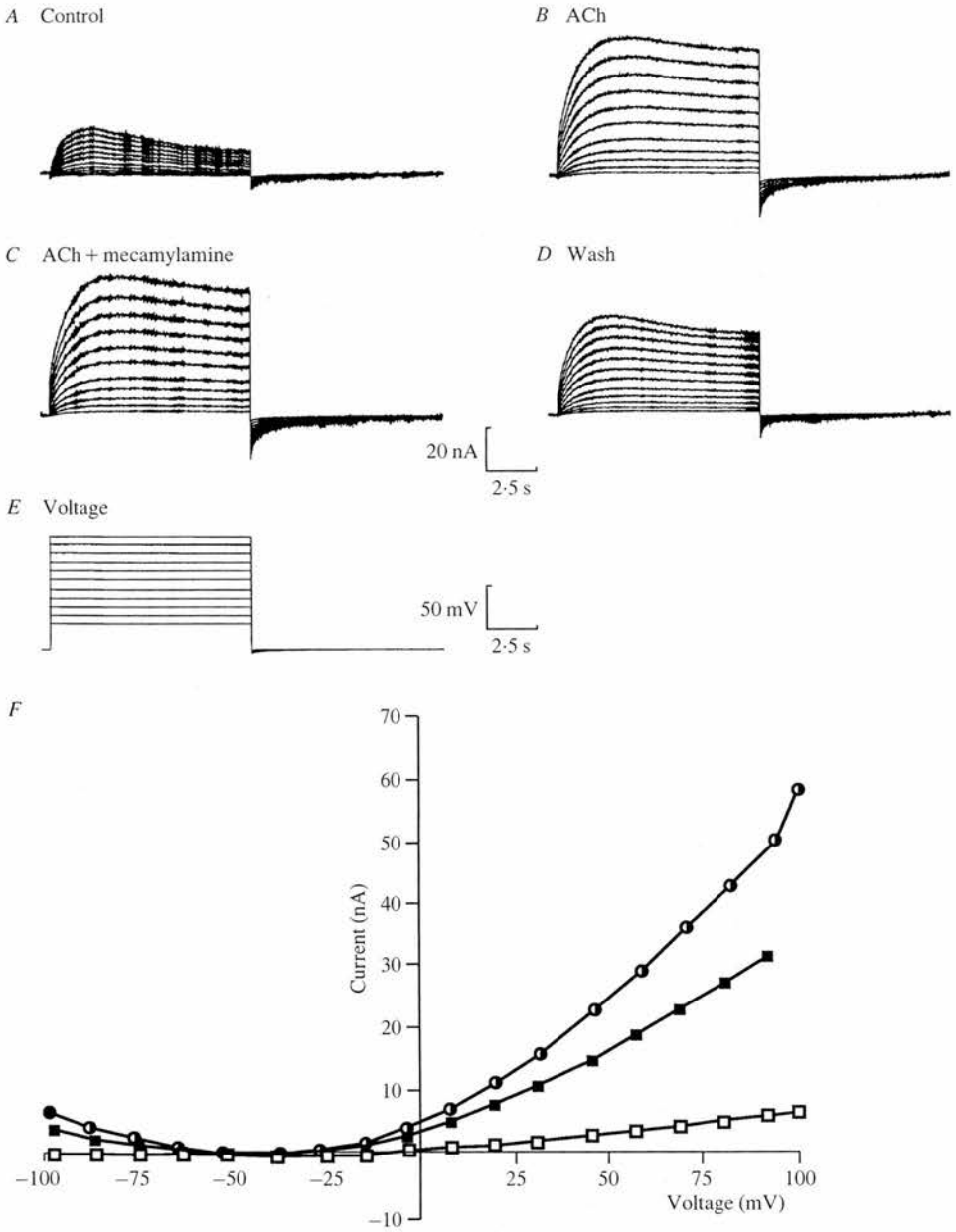


Fig. 4. Voltage-activated transbag currents produced by depolarizing voltage steps from a holding potential of −40 mV and the effect of acetylcholine. *A*, control transbag currents produced by depolarizing steps (*E*) repeated every 60 s. *B*, currents evoked by depolarizing pulses in the presence of 10 μM acetylcholine are bigger than control currents. *C*, currents evoked by the depolarizing pulses in the presence of 10 μM acetylcholine and 100 μM mecamylamine. *D*, current record evoked by depolarizing pulses after washing the preparation. The amplitudes of the currents are reduced compared with *B* and *C*. *F*, *I–V* plots, including currents produced by hyperpolarizing voltage pulses not shown in *A–E*. The control *I–V* plot (□) is increased in the presence of 50 μM acetylcholine (●) and the effect of acetylcholine is not antagonized following the addition of 100 μM mecamylamine (○). The current–voltage relationships in the presence of acetylcholine, and acetylcholine with mecamylamine, are superimposed (◑). The current amplitude was measured 9·5 s from the beginning of the step pulse. 'Physiological' intracellular and extracellular solutions were used. Holding potential, −40 mV.

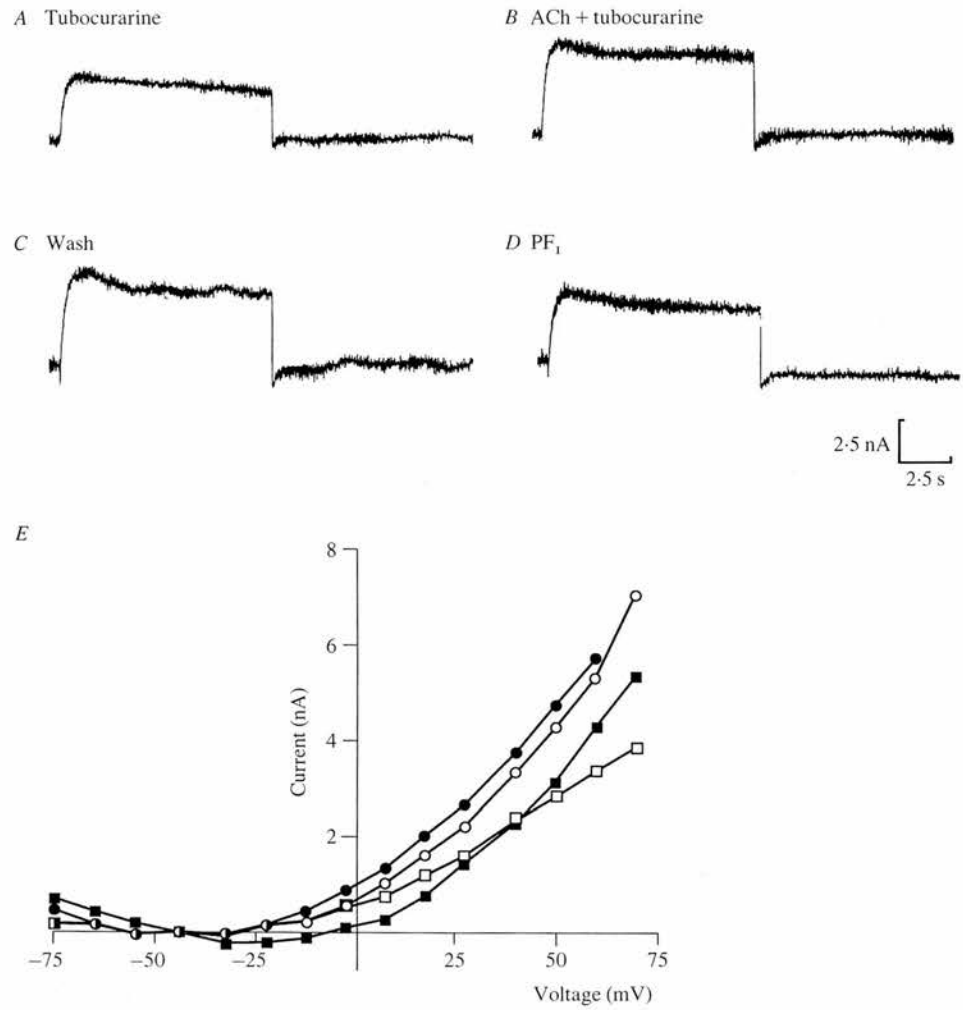


Fig. 5. Acetylcholine, applied after nicotinic antagonist, increases the voltage-activated transbag currents, but PF_1 decreases the voltage-activated current. 'Physiological' intra- and extracellular solutions were used. Holding potential, −40 mV; step potential, +26 mV. *A*, control current in the presence of 100 μM tubocurarine. *B*, current in the presence of 10 μM acetylcholine and 100 μM tubocurarine. *C*, wash current record. *D*, current response in 1 μM PF_1. *E*, full *I–V* plots of the voltage-activated current recorded 9·5 s after the start of the pulse and plotted against the step potential. □, 100 μM tubocurarine; ●, 10 μM acetylcholine and 100 μM tubocurarine; ○, wash; ■, 1 μM PF_1.

nicotinic receptors in *Ascaris* (Martin, 1982); Fig. 5*E* shows the *I–V* plots from these experiments. The lack of effect of the nicotinic receptor antagonists tubocurarine and mecamylamine shows that the effect of acetylcholine is mediated by a non-nicotinic receptor (Colquhoun *et al.* 1991). We therefore tested the antagonistic effects of the classic muscarinic antagonist, atropine, at 100 μM in four preparations, but found it to be without effect on the action of acetylcholine. We also tested the effects of application of 2 mM La^{3+}, a blocker of many Ca^{2+} channel currents, and found that it did not block or reduce I_{bcat} (4 preparations). The observation shows that I_{bcat} is not related to the voltage-activated Ca^{+} current, I_{Ca}, present in the intact muscle preparation (Martin *et al.* 1992).

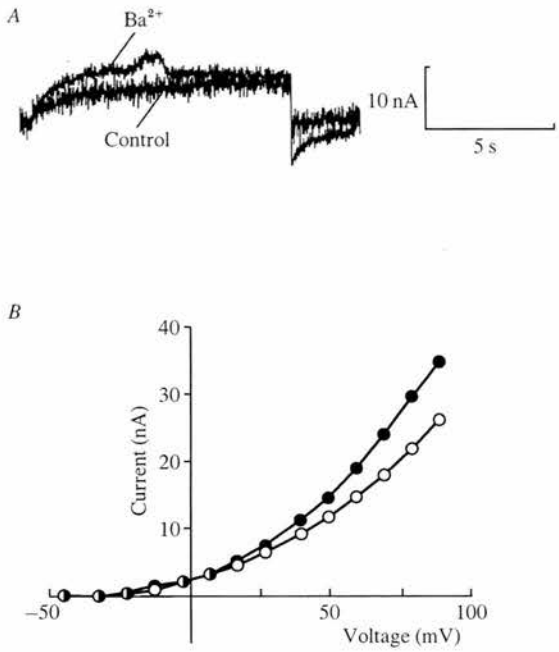


Fig. 6. Ba^{2+} increases the voltage-activated bag current. *A*, representative voltage-activated currents, showing the effect of addition of 6 mM Ba^{2+}. Holding potential, −40 mV; step potential, +40 mV. A transient outward current during the depolarizing pulse was seen in the presence of Ba^{2+}. *B*, full *I–V* plots of the voltage-activated current recorded 9·5 s after the start of the pulse and plotted against the step potential. ○, control; ●, 6 mM Ba^{2+}.

SDPNFLRFamide (PF_1) antagonizes the effect of acetylcholine on the voltage-activated bag current

PF_1 is an FMRFamide peptide that depresses the contractility of *Ascaris* somatic muscle and produces a non-Cl^--mediated hyperpolarization (Franks, Holden-dye, Williams, Pang & Walker, 1994; Bowman, Winterrowd, Friedman, Thompson, Klein, Davis, Maule, Blair & Geary, 1995). PF_1 also antagonizes the postsynaptic potentials produced by stimulating motoneurones (Franks *et al.* 1994). We tested the effects of PF_1 on I_{beat} in three preparations at concentrations between 0·5 and 3 μM and observed a depressent effect on I_{beat}. Figure 5*D* shows the depressant effect of 1 μM PF_1 on the voltage-dependent bag current following acetylcholine and Fig. 5*F* shows the *I–V* plots. In two of the three preparations tested, PF_1 reduced the voltage-dependent current in a dose-dependent manner at concentrations between 1 and 3 μM. It was also noticed that PF_1 significantly reduced the input conductance of the isolated bag preparations (not shown).

Effect of Ba^{2+} ions

The effects of Ba^{2+} ions on *Ascaris* muscle potentials have been examined by Weisblat, Byerly & Russel (1976). They observed that Ba^{2+} was able to stimulate the appearance of large regular depolarizing potential 'square waves'; the square waves appeared to arise from small potential 'slow waves' that were supported by cations, including Na^+. It was therefore of interest to investigate the effects on Ba^{2+} on I_{beat}.

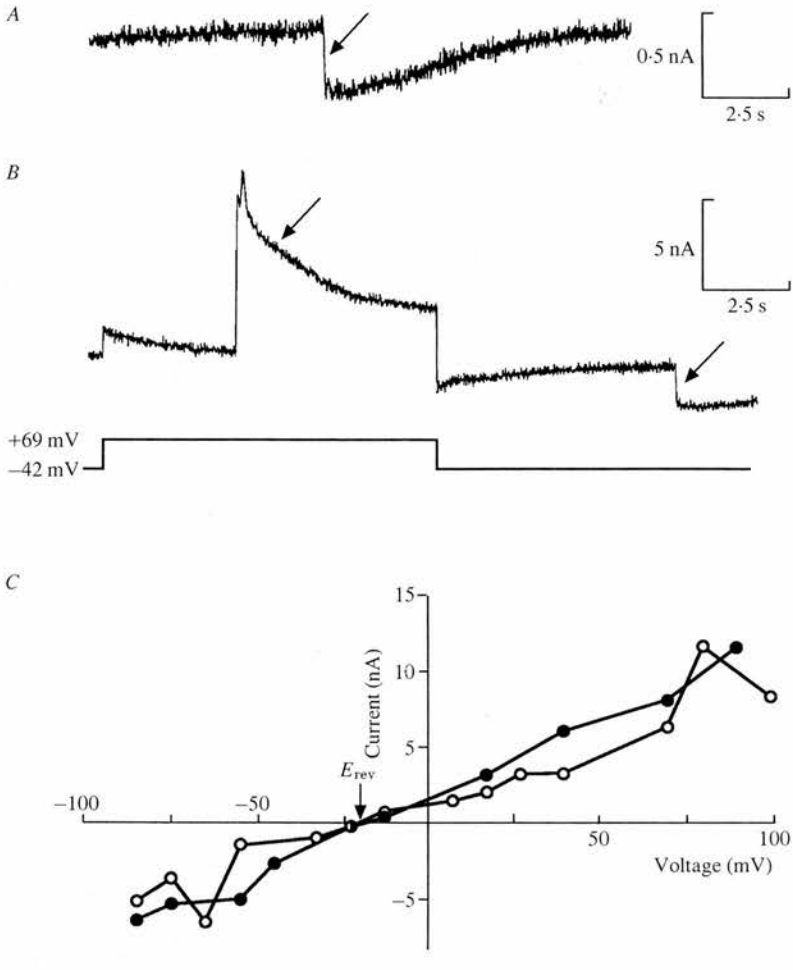


Fig. 7. Spontaneous bag currents produced after the application of 10 mM Ba^{2+} and the effect of acetylcholine. These spontaneous currents were observed in only one preparation. *A*, spontaneous inward current (arrow) at the holding potential, −40 mV. *B*, spontaneous current observed during a depolarizing step to +69 mV (left-hand arrow). Note that the direction of the current is outward but that the direction of the second current (right-hand arrow) is inward at −42 mV. *C*, plots of the peak amplitude of the spontaneous currents against the potential of the step voltage in the absence (○) and then the presence (●) of 50 μM acetylcholine. Note that the reversal potential of the spontaneous current was −18 mV in the presence or absence of acetylcholine, but the mean amplitude of the spontaneous current increased in the presence of acetylcholine.

We examined the effects of application of Ba^{2+} in concentrations from 2 to 19 mM (Ba^{2+} was added to the low-Ca^{2+} extracellular solutions). Figure 6 shows the typical enhancing effects of application of Ba^{2+} on I_{bcat} and on the *I–V* plots. It also shows the appearance of spontaneous currents that were observed in two preparations following the application of Ba^{2+}. In all nine experiments carried out, Ba^{2+} increased the amplitude of the current by between 15 and 90 % at potentials positive to +20 mV.

In one of the preparations, the addition of 4 mM Ba^{2+} to a preparation bathed in 'normal' solutions resulted in the appearance of spontaneous inward currents when the bag was held

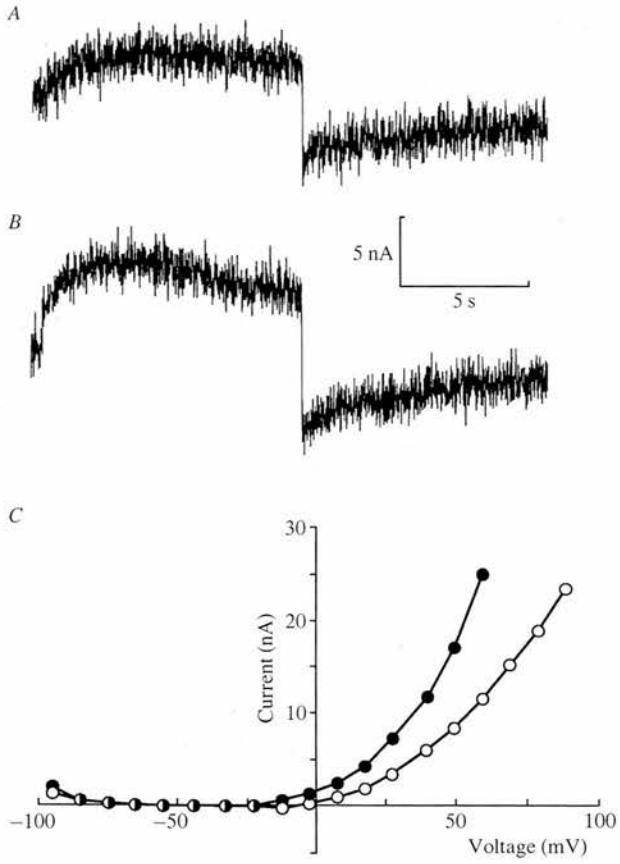


Fig. 8. Acetylcholine increases voltage-activated currents under conditions of K^+ channel block. Currents were activated by step potential to +27 mV from a holding potential of −40 mV. Extracellular solution (mM): caesium acetate, 135; BaCl, 19; TEA, 10; 4-AP, 5; and Hepes, 5; pH adjusted to 7·2 with CsOH. Intracellular solution (mM): caesium acetate, 135; EGTA, 0·5; and Hepes, 5; pH adjusted to 7·2 with CsOH. *A*, control. *B*, 50 μM acetylcholine in 100 μM mecamylamine applied extracellularly. *C*, *I–V* plots; current measured at 9·5 s after depolarization start. ○, control *I–V* plot; ●, *I–V* plot in the presence of 50 μM acetylcholine and 100 μM mecamylamine. Prolonged washing reduced but did not reverse the effect of acetylcholine (not shown).

at −40 mV (Fig. 7). These currents occurred approximately every 20 s and had a rapid rising phase, sometimes having a double peak, and then decaying in 10 s. Since the currents occurred spontaneously, it was possible to examine their *I–V* relationship. Figure 7*C* (○) shows that the reversal potential of the current was −18 mV, close to that of the voltage-activated I_{bcat}. The effect of bath-applied 50 μM acetylcholine on the amplitude of spontaneous currents was to increase it (Fig. 7*C*, ●). Although this effect of Ba^{2+} was observed in only one of our experiments, the properties of the spontaneous current (stimulated by Ba^{2+}, stimulated by acetylcholine, its reversal potential) were similar to I_{bcat}, suggesting a common ionic basis.

Effect of Cs^+ replacement on the voltage-dependent bag current

In order to test further the hypothesis that there is a voltage-dependent non-selective cation current in the bag membrane, we checked to see if Cs^+ ions would support currents under voltage-clamp conditions in the presence of K^+ channel blockers. Figure 8 shows a representative current trace and *I–V* plots of currents activated by different voltage steps with a holding potential of –40 mV in the presence of Cs^+ on both sides of the bag membrane. The presence of the K^+ channel blockers, 10 mM TEA, 4 mM 4-AP and 19 mM Ba^{2+} did not abolish the current. These observations are consistent with the presence of a slow voltage-dependent non-selective cation channel present in the bag membrane.

Figure 8 also shows, in the same preparation in symmetrically applied Cs^+, that the effect of 50 μM acetylcholine was to increase the amplitude of current and that prior application of 100 μM mecamylamine did not prevent the effect. In this experiment, repeated washing did not return the amplitudes of the current to control levels. The effect of 50 μM acetylcholine in three preparations was seen in preparations with either 100 μM mecamylamine ($n = 1$) or 100 μM tubocurarine ($n = 2$) present as a nicotinic antagonist.

DISCUSSION

Comparison with currents in the intact muscle preparation

We have shown in this paper that a slow non-selective cation bag current, I_{bcat}, is activated by depolarization to potentials more positive than –20 mV. This current results in a slow inward tail current on return to the holding potential, is resistant to 4-AP and TEA (10 mM), and is enhanced by acetylcholine and Ba^{2+}.

We have previously described (Martin *et al.* 1992) voltage-activated currents in intact muscle cells of *Ascaris*, in an experiment using a two-microelectrode voltage-clamp technique to record from a flap preparation. One of the currents identified (referred to as potassium current (I_K)-like) was resistant to 4-AP and required very high concentrations of TEA (69 mM) to block it. This current too could produce slow inward tail currents after depolarizing steps from holding potentials near the resting membrane potential. The reversal potential of its tail currents deviated from that predicted for a purely K^+-selective channel, with evidence of Na^+ permeability when extracellular K^+ was <10 mM; the $Na^+:K^+$ permeability ratio was estimated, assuming intracellular ion concentrations, to be around 0·04. A higher $Na^+:K^+$ permeability ratio would have obtained if the intracellular Na^+ concentration was higher than assumed or if the intracellular K^+ was lower than assumed. A higher $Na^+:K^+$ permeability ratio of 0·36 was found for I_{bcat}. In the isolated bag preparation, the intracellular ion concentration equilibrates with that found in the V-shaped micropipette and may provide a more secure estimate of the $Na^+:K^+$ permeability ratio.

The amplitude of the current in the intact preparation was, however, much larger than that recorded in the isolated bag preparation, but the properties of these two currents are similar, suggesting that they have the same basis. The larger size of the I_K-like current in the intact muscle preparation may be explained by the larger intact cell membrane contributing to the current and the higher temperature of the recordings made in the two-microelectrode voltage-clamp experiments.

The two other currents identified in the intact muscle preparation were the voltage-activated Ca^{2+} current, I_{Ca}, and an I_A-like current. We did not expect to see evidence of I_{Ca} in the isolated bag because we deliberately used low-Ca^{2+} conditions in our isolated bag experiments to avoid activation of large Cl^- channel currents (Thorn & Martin, 1987). We did not identify an I_A-like current sensitive to 5 mM 4-AP in the isolated bag preparations.

Function of I_{bcat}

One of the striking features of I_{bcat} is that it produces a slow inward tail current following depolarization. An inward tail current after depolarization is also seen in the intact muscle cell, even in Ca^{2+}-free conditions (see Fig. 4 of Thorn & Martin, 1987). Weisblat *et al.* (1976) have described, in intact *Ascaris* muscle cells, slow potential waves on which 'spike' potentials sit; the slow potential waves are 'supported' by Na^+, K^+, Mg^{2+}, Sr^{2+} and Ba^{2+} ions. The slow waves appeared to increase in amplitude and frequency when Ba^{2+} was added to the preparation and appear to be part of the intrinsic myogenic rhythm. Thus I_{bcat} may contribute to the generation of slow waves. It is interesting that the application of Ba^{2+} was seen in one preparation to generate a spontaneous inward current with properties not unlike that of I_{bcat}. This observation suggests that even an isolated muscle bag has the potential for generating rhythmic depolarization without an input from the nervous system.

Two types of cholinergic receptors

We have noted that acetylcholine will increase the amplitude of I_{bcat} and that the effect is mediated via a non-nicotinic receptor insensitive to atropine. Although the non-nicotinic acetylcholine receptor is not 'pharmacologically' like a muscarinic receptor, it could be 'physiologically' like the G-protein-coupled vertebrate muscarinic receptors (Neer, 1994). It has been observed before in invertebrate preparations that activities of simple agonists correlate with activities observed in vertebrate studies; but in contrast, activities of antagonists, which are often large and rigid molecules, do not correlate well between invertebrates and vertebrates (Duittoz & Martin, 1991). Presumably, agonist-binding sites may be preserved during evolution, but there is not the same selection pressure for the accessory binding sites of antagonists (Pax & Bennett, 1989) to be preserved. Futher evidence of a second type of cholinergic receptor is suggested by the observations of Segerberg & Stretton (1993). They reported that pilocarpine, a muscarinic agonist, in addition to acetylcholine, produces a dose-dependent depolarization of *Ascaris* muscle. They found that neither 100 μM tubocurarine, a nicotinic antagonist, nor 100 μM *N*-methyl-scopolamine, a muscarinic antagonist, consistently antagonized the pilocarpine response.

There is also biochemical evidence for the presence of non-nicotinic receptors in *Ascaris suum* muscle. Donahue, Masaracchia & Harris (1983) have observed that the effects of cholinergic agonists lead to an increase in the muscle levels of cAMP; Arevalo & Saz (1992) have observed that acetylcholine increases levels of phosphorylcholine, 1,2-diacylglyerides and phosphatidic acid, and have demonstrated the presence of phospholipase C activity. In vertebrate preparations, different muscarinic receptors (M1–M5) are directly or indirectly coupled to ion channels, or to adenyl cyclase, guanylate cyclase, phospholipase C or phospholipase A_2 by G-proteins (Kass & Freeman, 1993; Neer, 1994; Hall & Kotlikoff, 1995). Thus the effects of acetylcholine on I_{bcat}, mediated via a non-nicotinic receptor, along with the biochemical studies, suggest the presence of another type of muscle cholinergic

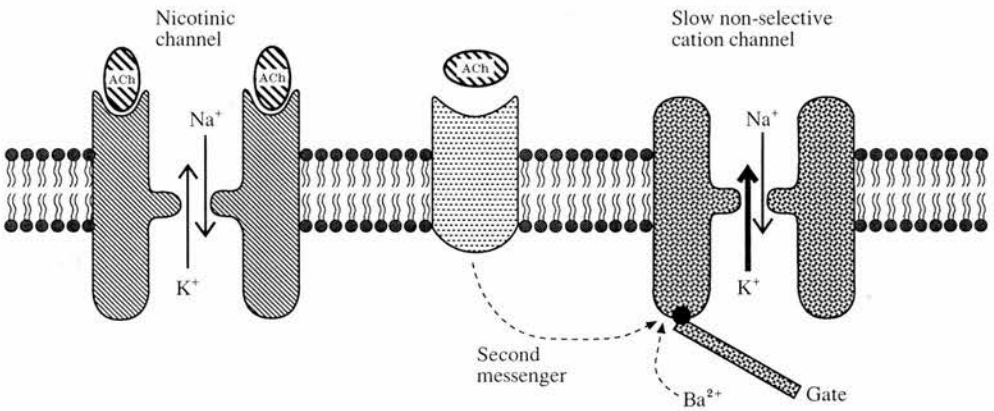


Fig. 9. Summary diagram shows the nicotinic acetylcholine receptor-operated channel and also the non-nicotinic acetylcholine receptor that increases the opening of a non-selective cation channel. The mechanism by which the non-nicotinic receptor activates the channel may involve second messengers because PF_1, whose action is mediated by NO, opposes the effect of acetylcholine (see Discussion).

receptor in *Ascaris* that is 'physiologically' but not 'pharmacologically' similar to vertebrate muscarinic receptors. Figure 9 is a summary diagram of the organization of the cholinergic receptors on the *Ascaris* bag membrane.

Resistance/recovery of nematodes after application of nicotinic anthelmintics

One form of resistance shown by parasitic nematodes to nicotinic anthelmintics is that of accommodation and recovery following long periods of exposure to an anthelmintic (Coles *et al.* 1975). The accommodation may be explained by nicotinic receptor inactivation as a result of continued exposure. These recovered nematodes no longer contract, but relax in response to high levels of levamisole or pyrantel, although they still contract in response to acetylcholine. The actions of acetylcholine and antagonist effects of levamisole on I_{bcat} seen in this study parallel effects on the recovered *Ascaris* preparations.

Again the explanation for these results is that, in addition to the nicotinic receptor on nematode muscle, there are non-nicotinic cholinergic receptors present on muscle that are not stimulated by high concentrations of nicotinic anthelmintics (Martin, 1993). This second cholinergic receptor may be related 'physiologically' to vertebrate muscarinic receptors.

Effects of PF_1

It was interesting that the FMRFamide PF_1 reversed the effect of bath-applied acetylcholine in this study. Bowman *et al.* (1995) have described the following: the inhibitory effects of PF_1 on *Ascaris* muscle flap contractility; the antagonist effect of PF_1 on the contraction produced by the nicotinic anthelmintic levamisole; and the hyperpolarizing action of PF_1 on muscle that is independent of extracellular Cl^-. The effect of PF_1 was also shown to be mediated via NO. Franks *et al.* (1994) have reported an antagonistic effect of PF_1 on muscle EPSPs evoked by electrical stimulation of motoneurones and suggested that the action of PF_1 was a presynaptic inhibition of acetycholine release. In this study, we have observed a direct antagonism of the effects of acetylcholine in the isolated bag preparation. The mode of action of PF_1 via NO

implies that the effect on I_{bcat} is mediated by guanylate cyclase and cGMP (Garthwaite, 1991; Moncada, Palmer & Higgs, 1991; Moncada & Higgs, 1993). This remains a subject for future study.

We are pleased to acknowledge the financial support of the Wellcome Trust, Grant 041617.

REFERENCES

ACEVES, J., ERLIJI, D. & MARTINEZ-MARNON, R. (1970). The mechanism of the paralysing action of tetramisole on *Ascaris* somatic muscle. *British Journal of Pharmacology* **38**, 602–607.

AREVALO, J. I. & SAZ, H. J. (1992). Effects of cholinergic agents on the metabolism of choline in muscle from *Ascaris suum*. *Journal of Parasitology* **78**, 387–392.

AUBRY, M. L., COWELL, P., DAVEY, M. J. & SHEVDE, S. (1970). Aspects of the pharmacology of new anthelmintics: pyrantel. *British Journal of Pharmacology* **38**, 332–344.

BOWMAN, J. W., WINTERROWD, C. A., FRIEDMAN, A. R., THOMPSON, D. P., KLEIN, R. D., DAVIS, J. P., MAULE, A. G., BLAIR, K. L. & GEARY, T. G. (1995). Nitric-oxide mediates the inhibitory effects of SDPNFLRFamide, a nematode FMRFamide-related neuropeptide, in *Ascaris suum*. *Journal of Neurophysiology* **74**, 1880–1888.

COLES, G. C., EAST, J. M. & JENKINS, S. N. (1975). The mechanism of action of the anthelmintic levamisole. *General Pharmacology* **6**, 309–313.

COLQUHOUN, L., HOLDEN-DYE, L. & WALKER, R. J. (1991). The pharmacology of cholinoceptors on the somatic muscle cells of the parasitic nematode *Ascaris suum*. *Journal of Experimental Biology* **158**, 509–530.

DE BELL, J. T., DEL CASTILLO, J. & SANCHEZ, V. (1963). Electrophysiology of the somatic muscle cells of *Ascaris lumbricoides*. *Journal of Cellular and Comparative Physiology* **62**, 159–177.

DEL CASTILLO, J., RIVERA, A., SOLORZANO, S. & SERRATO, J. (1989). Some aspects of the neuromuscular system of *Ascaris*. *Quarterly Journal of Experimental Physiology* **74**, 1071–1089.

DONAHUE, M. J., MASARACCHIA, R. A. & HARRIS, B. G. (1983). The role of cyclic AMP-mediated regulation of glycogen metabolism in levamisole-perfused *Ascaris* muscle. *Molecular Pharmacology* **23**, 378–383.

DUITTOZ, A. H. & MARTIN, R. J. (1991). Antagonist properties of arylaminopyridazine GABA derivatives at the *Ascaris* muscle GABA receptor. *Journal of Experimental Biology* **159**, 149–164.

FRANKS, C. J., HOLDEN-DYE, L., WILLIAMS, R. G., PANG, F. Y. & WALKER, R. J. (1994). A nematode FMRFamide-like peptide, SDPNFLRFamide (PF_1), relaxes the dorsal muscle strip preparation of *Ascaris suum*. *Parasitology* **108**, 229–236.

GARTHWAITE, J. (1991). Glutamate, nitric oxide and cell–cell signalling in the nervous system. *Trends in Neurosciences* **14**, 60–67.

HALL, I. P. & KOTLIKOFF, M. (1995). Use of cultured airway myocytes for study of airway smooth-muscle. *American Journal of Physiology* **268**, L1–11.

HARROW, I. D. & GRATION, K. A. F. (1985). Mode of action of the anthelmintics morantel, pyrantel and levamisole on muscle cell membrane of the nematode *Ascaris suum*. *Pesticide Science* **16**, 662–672.

KASS, R. S. & FREEMAN, L. C. (1993). Potassium channels in the heart: cellular, molecular, and clinical implications. *Trends in Cardiovascular Medicine* **3**, 149–159.

KOSTYUK, P. K., KRISHTAL, O. A. & PIDOPLICHO, V. I. (1984). Perfusion of isolated neurons fixed in plastic film. In *Intracellular Perfusion of Excitable Cells*, ed. KOSTYUK, P. K. & KRISHTAL, O. A., pp. 35–51. John Wiley & Sons, Chichester, New York, Brisbane, Toronto, Singapore.

MARTIN, R. J. (1982). Electrophysiological effects of piperazine and diethylcarbamazine on *Ascaris suum* somatic muscle. *British Journal of Pharmacology* **77**, 255–265.

MARTIN, R. J. (1993). Neuromuscular-transmission in nematode parasites and antinematodal drug-action. *Pharmacology and Therapeutics* **58**, 13–50.

MARTIN, R. J., THORN, P., GRATION, K. A. F. & HARROW, I. D. (1992). Voltage-activated currents in somatic muscle of the nematode parasite *Ascaris suum*. *Journal of Experimental Biology* **173**, 75–90.

MONCADA, S. & HIGGS, A. (1993). Mechanisms of disease: the L-arginine–nitric oxide pathway. *New England Journal of Medicine* **329**, 2002–2012.

MONCADA, S., PALMER, R. M. J. & HIGGS, E. A. (1991). Nitric oxide: physiology, pathology and pharmacology. *Pharmacological Reviews* **43**, 109–142.

NEER, E. J. (1994). G-proteins: critical control points for transmembrane signals. *Protein Science* **3**, 3–14.

ODIPCHUK, Y. V. & TIMIN, E. N. (1984). Electrical measurements on perfused cells. In *Intracellular Perfusion of Excitable Cells*, ed. KOSTYUK, P. K. & KRISHTAL, O. A., pp. 103–129. John Wiley & Sons, Chichester, New York, Brisbane, Toronto, Singapore.

PAX, R. A. & BENNETT, J. L. (1989). Effect of closantel on intrategumental pH in *Schistosoma mansoni* and *Fasciola hepatica*. *Journal of Parasitology* **75**, 169–171.

PENNINGTON, A. J. & MARTIN, R. J. (1990). A patch-clamp study of acetylcholine-activated ion channels in *Ascaris suum* muscle. *Journal of Experimental Biology* **154**, 201–221.

PRICHARD, R. K. (1994). Anthelmintic resistance. *Veterinary Parasitology* **54**, 259–268.

ROBERTSON, S. J., PENNINGTON, A. J., EVANS, A. M. & MARTIN, R. J. (1994). The action of pyrantel as an agonist and an open-channel blocker at acetylcholine-receptors in isolated *Ascaris-suum* muscle vesicles. *European Journal of Pharmacology* **271**, 273–282.

ROSENBLUTH, J. (1965). Ultrastructure of somatic muscle cells in *Ascaris lumbricoides*. II. Intermuscular junctions, neuromuscular junctions, and glycogen stores. *Journal of Cell Biology* **26**, 579–591.

SEGERBERG, M. A. & STRETTON, A. O. W. (1993). Actions of cholinergic drugs in the nematode *Ascaris suum*: complex pharmacology of muscle and motor-neurons. *Journal of General Physiology* **101**, 271–296.

THORN, P. & MARTIN, R. J. (1987). A high-conductance calcium-dependent chloride channel in *Ascaris suum* muscle. *Quarterly Journal of Experimental Physiology* **73**, 31–49.

WEISBLAT, D. A., BYERLY, L. & RUSSEL, R. L. (1976). Ionic mechanisms of electrical activity in the somatic muscle cell of the nematode *Ascaris lumbricoides*. *Journal of Comparative Physiology* **111**, 93–113.

[*From the Proceedings of the Physiological Society*, 26–27 *March* 1984
Journal of Physiology, **353**, 84*P*]

Single-channel currents in unfertilized mouse eggs

By K. P. Bland, C. Bountra, P. Georgiou, C. R. House and R. J. Martin*.
*Departments of Veterinary Physiology and *Veterinary Pharmacology, University of Edinburgh, Edinburgh EH9 1QH*

The presence of calcium channels in unfertilized mouse eggs is indicated by calcium action potentials evoked by depolarization (Georgiou, Bountra, Bland & House, 1984) and by inward calcium currents in voltage clamp experiments (Okamoto, Takahashi & Yamashita, 1977).

In order to examine these channels further, cell-attached patch recordings (Hamill, Marty, Neher, Sakmann & Sigworth, 1981) have been made from zona free mouse eggs. To facilitate giga-seal formation and to enhance the mean amplitude of single-channel currents, the solution bathing the egg and filling the patch electrode contained 80 mM-$SrCl_2$ as a replacement for NaCl. When the patch electrode was held near to 0 mV (transpatch potential is then about −90 mV), spontaneous inward currents were observed (Fig. 1).

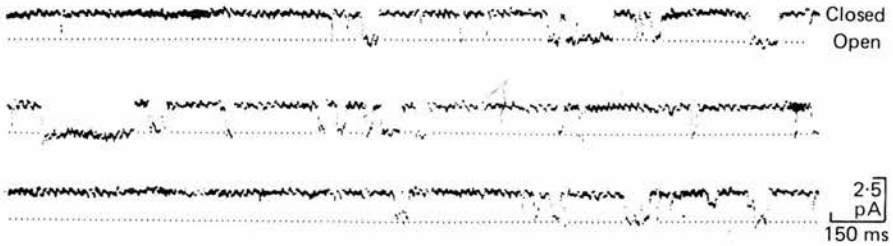


Fig. 1. Inward currents at a patch potential 12 mV more negative than the cell's resting membrane potential (filtered at −3 dB 100 Hz). The egg was bathed at 24 °C in a solution (pH 7·2) containing (mM): $SrCl_2$, 80; KCl, 5; $CaCl_2$, 1; $MgCl_2$, 1·2; glucose, 5·6; lactate, 20; buffered using Hepes, 5, and NaOH, 2·5. Methods of obtaining zona free eggs have been described by Georgiou *et al.* (1984).

At rest the channels were seen to open in bursts, as has been found in other preparations containing calcium channels (Reuter, 1983). The mean ± S.D. values of the amplitude of these channel currents were found to be 1·3 ± 0·5 pA ($n = 342$); probability of opening was 0·18. Furthermore channels open in synchrony with evoked action potentials.

Supported by the Wellcome Trust and Faculty of Veterinary Medicine, Edinburgh University. P. Georgiou is a Harriet Thomson scholar and C. Bountra is an M.R.C. scholar.

REFERENCES

Georgiou, P., Bountra, C., Bland, K. P. & House, C. R. (1984). *Q. Jl exp. Physiol.* **69**, 365–380.
Hamill, O. P., Marty, A., Neher, E., Sakmann, B. & Sigworth, F. S. (1981). *Pflügers Arch.* **391**, 85–100.
Okamoto, H., Takahashi, K. & Yamashita, N. (1977). *J. Physiol.* **267**, 465–495.
Reuter, H. (1983). *Nature, Lond.* **301**, 569–574.

Quarterly Journal of Experimental Physiology

If your library does not subscribe to this Journal, please ask them to do so.

Quarterly Journal of Experimental Physiology (1987) **72**, 483–492
Printed in Great Britain

SINGLE-CHANNEL CURRENTS FROM ZONA-FREE MOUSE EGGS

C. BOUNTRA AND R. J. MARTIN

Department of Preclinical Veterinary Sciences, R.(D).S.V.S., Summerhall, University of Edinburgh EH9 1QH

(RECEIVED FOR PUBLICATION 26 NOVEMBER 1986)

SUMMARY

Cell-attached patch recordings were made from zona-free mouse eggs to examine currents at the single-channel level; two types were identified. A channel with a mean conductance of 130 pS showed changes in reversal potential on dilution of the patch pipette solution consistent with a cation channel; the channel current persisted when the only cation in the pipette was K^+: it was concluded that this channel was permeable to K^+. The binomial distribution was used to describe the proportion of time 0, 1, 2, ..., n channels were open in multichannel recordings of the K^+ channel. Bursts of inward currents of about 1 pA, which showed voltage activation and could be recorded in the presence of CsCl and tetraethylammonium (TEA), were identified as Ca^{2+} channels.

INTRODUCTION

Voltage-dependent Ca^{2+} currents and Ca^{2+} action potentials in unfertilized eggs of mice and hamsters have been identified (Okamoto, Takahashi & Yamashita, 1977; Georgiou, Bountra, Bland & House, 1984). It has also been shown that Ca^{2+}-evoked opening of K^+ channels occurs in hamster and mouse eggs (Miyazaki & Igusa, 1981, 1982; Georgiou, Bountra, Bland & House, 1983). We have used the patch-clamp technique (Hamill, Marty, Neher, Sakmann & Sigworth, 1981) on zona-free mice eggs in an attempt to examine single ion channels. This paper describes properties of K^+ and Ca^{2+} channels which were identified.

METHODS

Egg donors

Mature female mice (balb-C strain) were used in this study. Mice were maintained under a fixed light–dark cycle (16 h light:8 h dark). Superovulation was induced by injecting intraperitoneally 10 international units of PMSG (Folligon, Intervet Labs Ltd, Cambridge) in the early evening followed by an intraperitoneal injection of 10 international units of HCG (human chorionic gonadotrophin, CG-2 Sigma Chemical Co., St Louis, U.S.A.) 48 h later. Animals were killed 15–18 h after the second injection and their oviducts placed in a dish containing a physiological solution (called normal) at room temperature (20–22 °C). The composition of the normal solution was (mM): NaCl, 120; KCl, 5; $MgCl_2$, 1·2; sodium lactate, 20; sodium pyruvate, 1; glucose, 5·6; HEPES, 5; NaOH, 3·2; pH, 7·4. Test solutions were produced by modification of the normal solution without sodium lactate, sodium pyruvate or glucose. 4 mM-Ca^{2+}/5 mM-K^+/2 mM-La^{3+} solution was produced by increasing $CaCl_2$ to 4 mM and adding 2 mM-$LaCl_3$. 10 mM-Ca^{2+}/5 mM-K^+ solution was produced by increasing $CaCl_2$ to 10 mM. 10 mM-Ca^{2+}/10 mM-TEA/125 mM-Cs^+ was produced by increasing $CaCl_2$ to 10 mM, adding 10 mM-TEA–Cl and replacing the NaCl and KCl with 125 mM-CsCl. 80 mM-Sr^{2+}/5 mM-K^+ solution was produced by replacing NaCl and $CaCl_2$with 80 mM-$SrCl_2$. 60 mM-Sr^{2+}/TEA/CsCl solution was produced by replacing the NaCl, KCl, $CaCl_2$ and $MgCl_2$ with 60 mM-$SrCl_2$ adding 10 mM-TEA-Cl and 10 mM-CsCl. 155 mM-K^+/EGTA solution was produced by replacing NaCl, $CaCl_2$ and $MgCl_2$

with 155 mM-KCl and adding 5 mM-EGTA. The pH was adjusted to 7·4 with either NaOH or KOH as appropriate. Eggs were removed from the oviducts and placed in normal solution containing hyaluronidase (1 mg ml^{-1}, type I-S, Sigma) for 5 min to remove the cumulus oophorus. Removal of the zona pellucida was achieved by transferring eggs (freed from the cumulus) into a normal solution containing protease, (1 mg ml^{-1}, type XIV, Sigma) for 10–15 min at room temperature.

Recording

An egg was transferred to a chamber (volume 5 ml) mounted on an inverted microscope (Biovert Reichert, Austria). The chamber contained a solid silver/silver chloride electrode in contact with a bathing solution. Patch electrodes were made from Hawksley microhaematocrit capillary tubes (Cat. No. 1604) and had resistances of 1–3 MΩ with outside diameters of 2 μm. The solution used to fill these patch pipettes varied with the aim of the experiment. The compositions of the solutions used are described earlier. La^{3+} was often added to the bathing solution in an attempt to promote sealing of the patch electrode to the egg membrane; the fact that there are microvilli on the surface of the egg limited the frequency of giga-seal formation; something like one-in-ten patches formed giga-seals.

Some of the recordings performed during the course of this study were obtained using a laboratory-made patch-clamp system (based on a Tele-dyne Philbric 1035 Op-Amp and a 1 GΩ (Welwyn) feed-back resistor. The remainder of the recordings were made with an EPC-7 patch-clamp system (List Electronic Instruments). Recordings were amplified and then filtered at 1 kHz (−3 dB). Inward currents are displayed downwards (negative); outward current are displayed upwards (positive).

A cell-attached patch was formed when a patch pipette was gently lowered on the surface of the zona-free egg and suction applied to help seal formation. The seal resistance between the pipette tip and membrane patch gradually increased and settled to levels between 0·5 and 2 GΩ. Higher resistance seals were not seen in this preparation, presumably as a result of the microvilli. The low seal resistances gave rise to large current pulses (20–80 pA for 40 mV) when the patch was depolarized through the patch pipette. To correct for this artifact a larger current pulse of the opposite polarity was subtracted from the current record during depolarization of the patch. Correction of the capacitative artifacts at the beginning and end of the artifact was limited.

In some cells a micro-electrode (30–80 MΩ) filled with 2 M potassium acetate was inserted into the egg for simultaneous potential recording and current injection. It was connected to the input of a high-impedance pre-amplifier (Dagan Model 8100 single-electrode system, Dagan Corp., U.S.A.). Current pulses from a Devices stimulator triggered by a Digitimer were passed by a bridge circuit between the barrel of the micro-electrode and bath electrode. This permitted measurement of input resistance and intracellular membrane potentials in some of the eggs; it also permitted current injection for changing membrane potential.

Data processing

Responses were monitored on an oscilloscope and recorded on a Racal Thermionic Store 4DS FM tape-recorder (slowest frequency response 1·25 kHz, −1 dB). These records were analysed with the aid of a Cromemco microcomputer programmed to measure channel open and closed times. The data were played back from the tape, sampled and digitized every 200 or 400 μs and continually monitored and adjusted for slow d.c. drifts. For single-channel patches an increase in current of greater than 70% of the unit channel current was recorded as a channel opening; after an opening, a decrease in the channel current to less than about 50% of the single-channel current was recorded as a channel closing. For each patch record, mean values, frequency histograms and the semilogarithmic plots of open and closed times were displayed and plotted by the microcomputer programs. Multichannel patches containing channels of the same type were analysed in a similar way to determine the proportion of time spent with at least 0, 1, 2, ..., n channels open.

RESULTS

Temperature increases channel current activity

One series of experiments was carried out to investigate the effect of temperature on channel opening. It was found that at room temperature (22 °C) the probability of channels being open was lower than at 35 °C; a rise in temperature was associated with a decrease

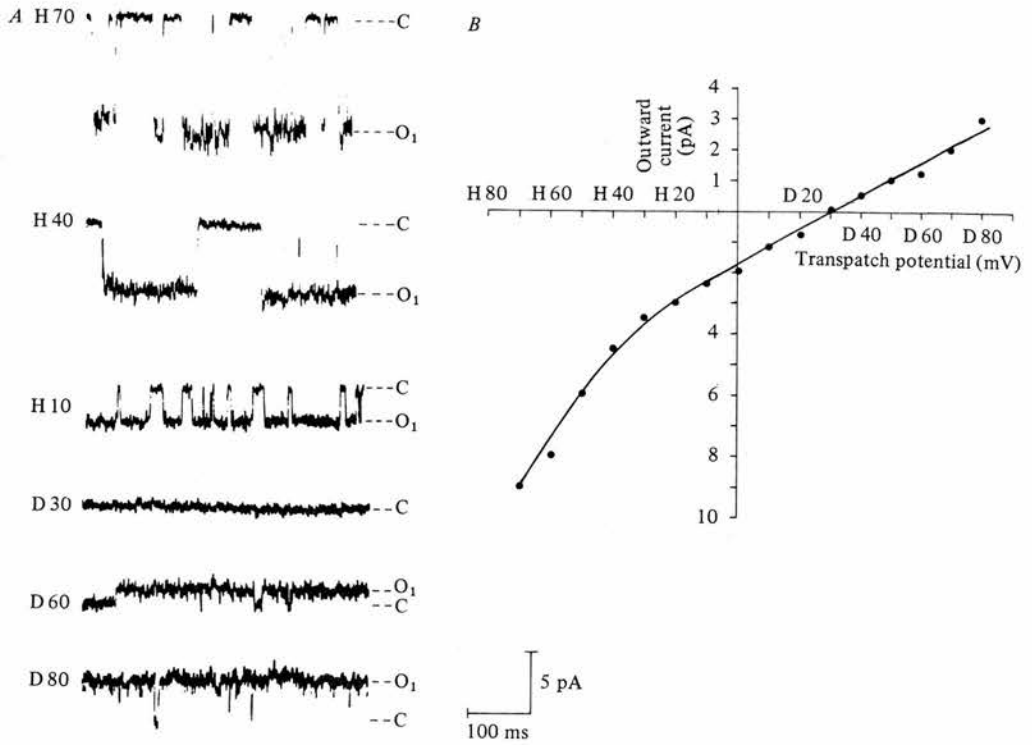


Fig. 1. *A*, channel records of the high-conductance K^+ channel at different patch-pipette potentials. The potential applied to the pipette is shown by the H or D number: H, hyperpolarizing; D, depolarizing. At H 70 p_{open} = 0·64; at H 10 p_{open} = 0·85. Pipette filled with 155 mM-K^+/EGTA solution. Egg bathed in 4 mM-Ca^{2+}/5 mM-K^+/2 mM-La^{3+} solution. Cell-attached patch. C = closed; O_1 = channel open. Upwards is outwards. *B*, current–voltage relationship. Note the pipette reversal potential is D 30 (−30 mV).

in mean open times. For example, in one preparation where outward channel currents were observed in a patch, the probability of a channel being open was 0·06 and there was a mean open time of 17·4 ms at 22 °C; at 35 °C the probability of channel opening was 0·21 and there was a mean open time of 5·6 ms. The increase in the probability of the channels being open at higher temperatures can be correlated with the lower input resistance which is seen at higher temperatures (Georgiou, Bountra & House, 1987). Subsequently, most experiments were done at room temperature.

High-conductance K^+ channels

High-conductance channels were observed in six cell-attached patches on eggs bathed in a solution containing 2 mM-$LaCl_3$ and 4 mM-$CaCl_2$ (4 mM-Ca^{2+}/5 mM-K^+/2 mM-La^{3+}). The increased Ca^{2+} and presence of La^{3+} promoted seal formation between the pipette and egg membrane. The patch pipette was filled with 155 mM-K^+/EGTA solution to reduce the Ca^{2+} concentration over the patch while maintaining a high K^+ concentration: the current–voltage relationship of these channels is illustrated in Fig. 1; to reverse the direction of the channel currents it was necessary to depolarize the patch by 30 mV. If these channels are K^+ channels and the K^+ concentration is equal on both sides of the membrane, then there is a low resting membrane potential of −30 mV in this egg. In six such experiments the mean potential applied to the pipette to obtain reversal of the currents was

-23 ± 8 mV (mean $\pm$ S.D.). The probability of the channel (Fig. 1) being open at a pipette potential of $+70$ mV was 0·64; the probability of the channel being open at the pipette potential of $+10$ mV was 0·85. Although this suggests that the channels are voltage sensitive, most patches did not display marked voltage sensitivity; in fact there was a statistically significant ($P < 0{\cdot}05$) positive correlation between patch potential and probability of opening in only two of the six patches examined.

Fig. 1*B* is a plot of the current–voltage relationship of the channels shown in Fig. 1*A*. The maximum slope of the plot suggests a channel conductance of 148 pS; it is, however, pointed out that there was evidence of rectification. In four other cell-attached patches, on four eggs bathed in 10 mM-Ca^{2+}/5 mM-K^+ solution, the corresponding slope conductances were 152, 140, 84 and 120 pS, respectively, giving an over-all mean of 129 pS. The large variability in the values obtained for the slope conductances is not easily explained. There are, however, large variations in estimates for the oocyte resting membrane potential; values between -23 mV and more negative than -65 mV have been reported (Okamoto *et al.* 1977; Georgiou *et al.* 1987). This variation, if real, may reflect differences in intracellular ion concentrations, giving rise to different K^+ channel conductances.

The above results give no conclusive information about which ion is passing through the high-conductance channel; it cannot be Na^+ because no Na^+ was present in the pipette solution; it is unlikely to be Ca^{2+} because the pipette contains only 10^{-9} M-Ca^{2+} (buffered with EGTA). The two possible remaining candidates, i.e. K^+ and Cl^- ions, were investigated.

It is predicted for a cation channel that dilution of the patch solution will produce a shift in patch reversal potential in the hyperpolarizing direction; this corresponds to a shift in the pipette reversal potential in the positive direction. In one group of experiments (seven cell-attached patches on seven eggs), the possibility that the channel currents were due to the movement of anions was ruled out: in these experiments the pipette solution (155 mM-K^+/EGTA) was diluted to 80, 50 or 25% with distilled water; the bathing solution in all these experiments was 4 mM-Ca^{2+}/5 mM-K^+/2 mM-La^{3+} and this was diluted to 80% in experiments in which the pipette filling solution had been diluted to 50 or 25%. The current–voltage relationship of channels observed in a cell-attached patch (pipette filled with 25% 155 mM-K^+/EGTA solution) is shown in Fig. 2*A*; the conductance was 49 pS and the pipette reversal potential was $+1$ mV. In another similar experiment the pipette reversal potential was $+5$ mV and the conductance was 40 pS. These two results suggested that the reversal potential of the channels in the patch was more negative when the pipette solution was diluted; such a shift would only be expected for a cationic channel. In an experiment in which the pipette solution was diluted to 50% the pipette reversal potential was -9 mV, and the conductance of the channel was 85 pS. When the patch pipette solution was diluted to 80%, similar results to those in the undiluted solutions were observed. In such experiments the pipette reversal potentials were -30, -32 and -36 mV and the maximum slope conductances of the channels were 125, 64 and 80 pS.

The K^+ concentration in the pipette solution was lowered by substituting it with Na^+ on an equimolar basis; this solution was based on low Ca^{2+} with 155 mM-K^+ and EGTA. The results of one such experiment are illustrated in Fig. 2*B*: the bathing solution was 4 mM-Ca^{2+}/5 mM-K^+/2 mM-La^{3+} (Fig. 2*B*) had a conductance of 125 pS; the pipette reversal potential obtained by extrapolation was $+4$ mV. In another similar experiment the pipette reversal potential was $+5$ mV and the channel conductance was 157 pS.

The above experiments showed that the effect of reducing the K^+ concentration in the patch solution was to shift the reversal potential of the patch in the hyperpolarizing

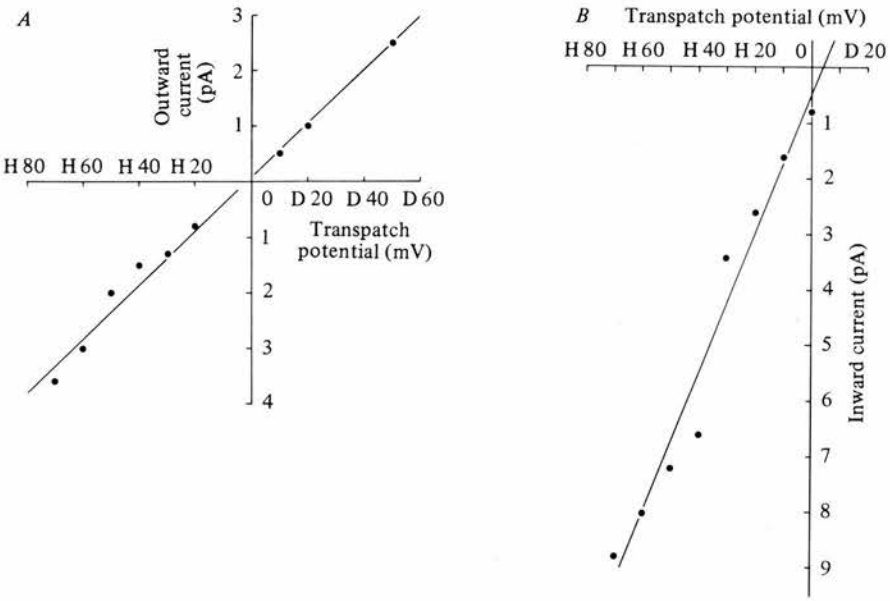


Fig. 2. *A*, current–voltage relationship of the high-conductance K^+ channel, pipette filled with diluted solution (25%) 155 mM-K^+/EGTA solution. Note that pipette reversal potential is +1 mV. Egg bathed in 4 mM-Ca^{2+}/5 mM-K^+/2 mM-La^{3+} solution. Cell-attached patch. *B*, relationship of the K^+ channel, pipette filled with 78 mM-KCl$^+$ 78 mM-Na^+/EGTA solution. Egg bathed in 4 mM-Ca^{2+}/5 mM-K^+/2 mM-La^{3+} solution.

direction. These observations lead to the conclusion that the high-conductance channel was selectively permeable to K^+.

Is the opening and shutting of K^+ channels described by the binomial distribution?

If n channels in a membrane patch have the same probability of opening and act independently of one another then the proportion of time $p(r)$, that 0, 1, 2, ..., n channels are open, should be described by the binomial distribution such that,

$$p(r) = \frac{n!}{r!(n-r)!} p^r (1-p)^{n-r}, \tag{1}$$

where n is the number of channels in the membrane patch, r is the number of channels open, and p is the probability that any channel is open. Fig. 3*A* illustrates multiple channel openings in a cell-attached patch at a pipette potential of −50 mV; the proportion of the total recording time that at least 0, 1, 2, ..., n channels were open was measured at different pipette potentials. The probability (p) of any channel opening could then be calculated as follows: let the proportion of the total recording time spent with at least 1, 2, ..., n channels open be T_1, T_2, ..., T_n; then,

$$p = \frac{(T_1) + (T_2) \ldots\ldots + (T_n)}{n}. \tag{2}$$

The fraction of time during which r channels and only r channels were open was calculated from the T values and plotted as bars in Fig. 3*B*. The binomial distribution was then used with the value of p to predict the proportion of time spent with only 0, 1, 2, ..., n channels open. The values for p at each pipette potential were 0·401 for −10 mV, 0·413

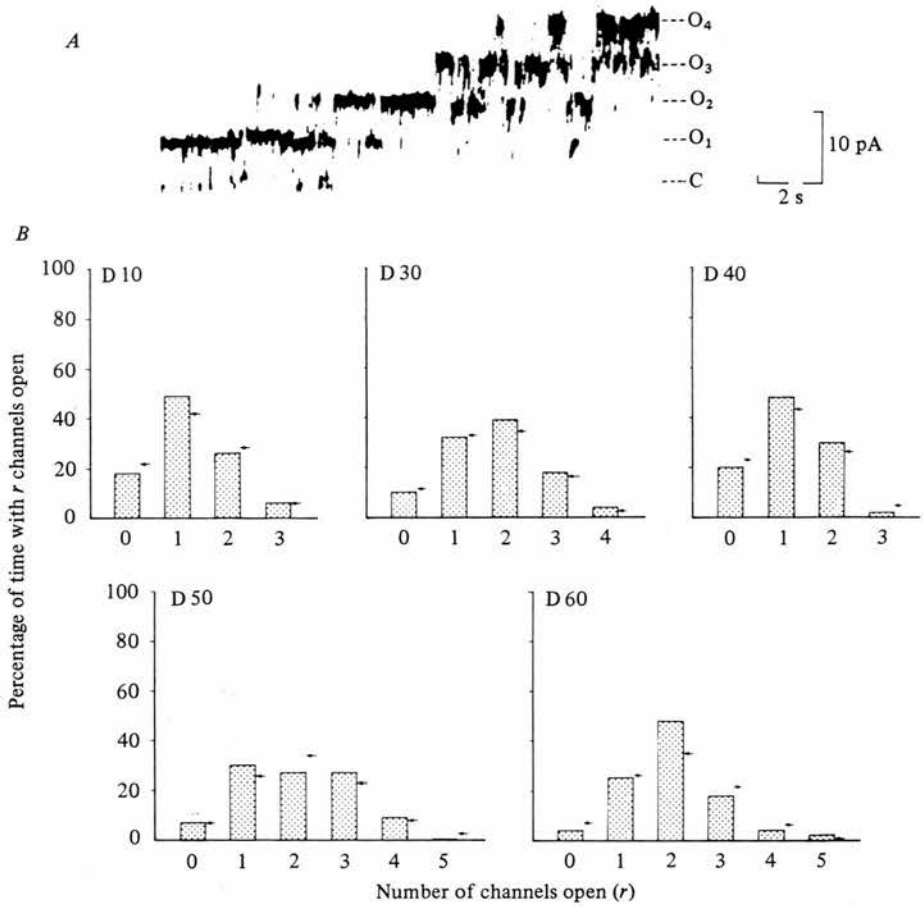


Fig. 3. *A*, multichannel cell-attached patch record of the high-conductance K^+ channel at a pipette potential of −50 mV. Pipette filled with 155 mM-K^+/EGTA solution. Egg bathed in 4 mM-Ca^{2+}/5 mM-K^+/2 mM-La^{3+} solution. Up to four channels can be seen to open here, although five were seen on a few occasions. C = closed; $O_1 \ldots O_4$ = 1, 2, 3 and 4 channels open, respectively. *B*, percentage of time *r* channels open (bars) and the predicted percentage times (arrows) from the binomial distribution.

for −30 mV, 0·378 for −40 mV, 0·402 for −50 mV and 0·393 for −60 mV. The distribution (Fig. 3 *B*) of the time spent with 0, 1, 2, ..., *n* channels open was approximately that expected if five channels were present under the patch. This is consistent with five channels opening independently and having the same probability of opening. The binomial distribution also described the opening of two other patches. However, in some patches the binomial could not predict adequately the distribution of the channels open. For example, in a patch record where two channels were seen to be open, one was seen to be open much of the time whereas the second channel opened very rarely; this implies that adjacent channels may not always have identical probabilities of opening. There are other precedents for K^+ channels behaving in this manner. It is interesting that observations made on an ATP-dependent K^+ channel in frog skeletal muscle found that the fit to the binomial was less good after isolated patches were exposed to ATP and that ATP reduced the probability of the channel being open (Spruce, Standen & Stanfield, 1987). The effect of ATP on K^+ channels has not been examined in oocytes.

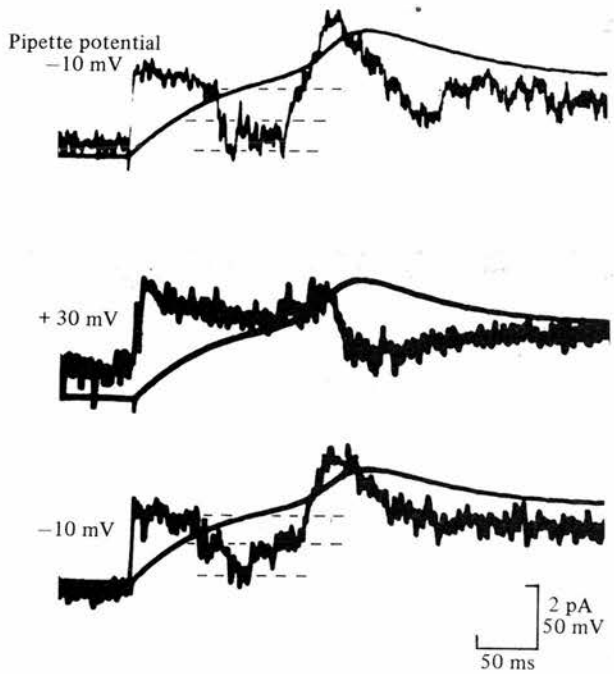


Fig. 4. Simultaneous cell-attached patch and intracellular potential records during injection of depolarizing current pulses through the intracellular pipette to produce a spike. The quiet trace is the intracellular potential; the noisy trace is the patch current record. Patch pipette filled with 60 mM-Sr^{2+}/TEA/CsCl solution. The cell was current clamped to a potential more negative than −50 mV. Note the opening of at least two channels when the patch pipette is at −10 mV but not at +30 mV. Egg bathed in 80 mM-Sr^{2+}/5 mM-K^+ solution.

Ca^{2+} channel currents recorded during depolarization with an intracellular electrode

It was possible to form a cell-attached patch on an egg and subsequently to impale it with an intracellular micro-electrode to current clamp the potential to values more negative than −50 mV. The passage of a depolarizing current pulse through the intracellular electrode then induced an action potential. An example of such an experiment is illustrated in Fig. 4. The quiet traces are the electrically evoked action potentials recorded by the intracellular electrode; the noisy traces are the patch currents recorded simultaneously. In the middle trace where the patch pipette potential was +30 mV, the depolarization of the cell to threshold was seen in the patch current as an outward current and the active rising phase of the action potential as an outward peak: these currents were interpreted as the result of resistive and capacitative coupling of the patch electrode to the cell (Fenwick, Marty & Neher, 1982). In the top and lower records the patch pipette potential was −10 mV; although the resistive and capacitative currents are still present, just prior to and during the rising phase of the action potential, there was a burst of inward channel currents. It is known that a Ca^{2+} current is responsible for the action current (Okamoto *et al.* 1977; Georgiou *et al.* 1984). The channel currents were interpreted as being due to activity of Ca^{2+} channels under the patch electrode which reached threshold when the pipette was at −10 mV but not at +30 mV. At least two channels were present and had amplitudes near 1 pA (80 mM-Sr^{2+} in the patch pipette). It was not possible to make estimates of mean open times.



Fig. 5. Depolarizing pulses above a threshold applied to the patch pipette can produce inward bursts of 1 pA Ca^{2+} channel currents. Left-hand trace shows the current record seen with a cell-attached patch depolarized by 30 mV; right-hand trace, same patch depolarized by 40 mV opens channels. Pipette filled with 10 mM-Ca^{2+}/10 mM-TEA/125 mM-Cs^{+} solution. Note that the current offset due to the low seal resistance was adjusted by subtracting a larger rectangular current pulse of the opposite polarity during the application of the depolarizing pulse to the patch pipette. Egg bathed in 10 mM-Ca^{2+}/5 mM-K^{+} solution.

Activation of Ca^{2+} channels by depolarizing pulses applied to the patch pipette

In order to investigate the voltage activation of Ca^{2+} channels, cell-attached patches were depolarized by applying negative pulses to the patch pipette; in the pipette was 60 mM-Sr^{2+}/TEA/CsCl solution to select for currents carried by Ca^{2+} channels. The effect of low seal resistances (0·5–2 GΩ) was corrected for by subtracting a large rectangular current pulse of the opposite polarity during depolarization of the patch pipette. In these experiments there was no intracellular micro-electrode in the egg, minimizing damage. Such an experiment is illustrated in Fig. 5. Notice that no inward channel currents were observed when the size of the depolarizing pulse applied to the patch was 30 mV. However, bursts of inward channel currents 1 pA in amplitude were observed when the depolarizing pulse was increased to 40 mV. These experiments indicate that the threshold for activation of these inward currents was 30–40 mV more positive than the transpatch potential. Similar results were obtained from four other patches. Effective mean open times for these channels were less than 6 ms, but estimates were limited by the resolution of the channels.

DISCUSSION

The experiments described here have indicated the presence in mouse eggs of at least two types of channel. They are: (1) a high-conductance (130 pS) K^{+} channel; (2) a voltage-activated Ca^{2+} channel which carried inward Sr^{2+} currents of *circa* 1 pA. It is pointed out that, in addition to these, other less well characterized channel types were occasionally seen; these channels had conductances of between 7·5 and 50 pS with pipette reversal potentials of between 0 and −50 mV.

K^{+} channels in mammalian eggs

Okamoto *et al.* (1977), using zona-free mouse eggs, have described an 'outward surge' current above a +50 mV membrane potential, possibly due to a K^{+} current. Igusa & Miyazaki (1983) and Georgiou *et al.* (1983) have described a Ca^{2+}-activated K^{+} conductance in hamster and mouse eggs which is thought to be involved in the production of the recurrent hyperpolarizing potentials seen during fertilization. The K^{+} channels described in

this paper could be observed at hyperpolarized potentials and were not activated exclusively by very depolarized potentials; they are unlikely to be responsible for the 'outward surge' current previously described. There remains the possibility that the 130 pS K^+ channel of the mouse is Ca^{2+} activated. The existence of high-conductance 'maxi-K^+' channels are recognized in other tissues where they are activated by depolarization and an increase in intracellular Ca^{2+} (e.g. muscle: Barrett, Magleby & Pallota, 1982; lacrimal gland: Findlay, 1984). A further study of the high-conductance K^+ channel in eggs is required to examine the combined influence of membrane potential and Ca^{2+}.

Density of Ca^{2+} channels in mouse eggs

Evidence for the existence of Ca^{2+} channels in mouse eggs was initially presented by Okamoto *et al.* (1977); under voltage clamp the maximum size of the Ca^{2+}–Sr^{2+} current they observed was 9·7 nA. The amplitude of a single Ca^{2+}–Sr^{2+} channel current in this study was about 1 pA. Using these two observations together with an estimate of the membrane surface area, it is possible to estimate the density of the Ca^{2+} channels if the channels are open all of the time. The egg membrane has a total capacitance of 660 pF (Georgiou *et al.* 1984) so that the actual surface area of the egg is calculated to be $6{\cdot}6 \times 10^{-4}$ cm^2 (specific membrane capacitance is 1 pF cm^{-2}). The Ca^{2+} channel density is then about 0·2 μm^{-2}; this density compares well with that obtained in rat cardiac cells (0·1–0·5 channels μm^{-2}; Reuter, Stevens, Tsien & Yellen, 1982). The typical patch pipette will record from a surface area of membrane of 5–10 μm^{-2} (Sakmann & Neher, 1983); therefore, it is likely that one to two Ca^{2+}–Sr^{2+} channels should be recorded with each cell-attached patch.

Conclusion

In conclusion, we have demonstrated that it is possible to apply the patch-recording technique to the mammalian egg cell and to record using cell-attached patch recordings. With this technique it was possible to identify K^+ channels and voltage-activated Ca^{2+} channels. Difficulties in obtaining high-resistance giga-seals were encountered, probably because of the presence of the microvilli on the surface of the membrane.

We are pleased to acknowledge the financial help of the Wellcome Trust and advice of Professor C. R. House and Dr P. Georgiou given during this study and preparation of the manuscript.

REFERENCES

Barrett, J. N., Magleby, K. L. & Pallota, B. S. (1982). Properties of single calcium-activated potassium channels in cultured rat muscle. *Journal of Physiology* **331**, 211–230.

Fenwick, E. M., Marty, A. & Neher, E. (1982). A patch-clamp study of bovine chromaffin cells and of their sensitivity to acetylcholine. *Journal of Physiology* **331**, 577–597.

Findlay, I. (1984). A patch-clamp study of potassium channels and whole cell currents in acinar cells of the mouse lacrimal gland. *Journal of Physiology* **350**, 179–197.

Georgiou, P., Bountra, C., Bland, K. P. & House, C. R. (1983). Calcium-evoked opening of potassium channels in hamster eggs. *Quarterly Journal of Experimental Physiology* **68**, 687–700.

Georgiou, P., Bountra, C., Bland, K. P. & House, C. R. (1984). Calcium action potentials in unfertilized eggs of mice and hamsters. *Quarterly Journal of Experimental Physiology* **69**, 365–380.

Georgiou, P., Bountra, C. & House, C. R. (1987). Intracellular and whole-cell recordings from zona-free hamster eggs: significance of leak impalement. *Quarterly Journal of Experimental Physiology* **72**, 105–118.

HAMILL, O. P., MARTY, A., NEHER, B., SAKMANN, B. & SIGWORTH, F. J. (1981). Improved patch clamp techniques for high resolution current recording from cells and cell free membrane patches. *Pflügers Archiv* **391**, 85–100.

IGUSA, Y. & MIYAZAKI, S. (1983). Effects of altered extracellular and intracellular calcium concentration on hyperpolarizing responses of the hamster egg. *Journal of Physiology* **340**, 611–632.

MIYAZAKI, S. & IGUSA, Y. (1981). Fertilization potential in golden hamster eggs consists of recurring hyperpolarizations. *Nature* **290**, 702–704.

MIYAZAKI, S. & IGUSA, Y. (1982). Ca-mediated activation of a K current at fertilization of golden hamster eggs. *Proceedings of the National Academy of Sciences of the U.S.A.* **79**, 931–935.

OKAMOTO, H., TAKAHASHI, K. & YAMASHITA, N. (1977). Ionic currents through the membrane of the mammalian oocyte and their comparison with those in tunicate and sea urchin. *Journal of Physiology* **267**, 465–495.

REUTER, H., STEVENS, C. F., TSIEN, R. W. & YELLEN, G. (1982). Properties of single calcium channels in cardiac cell culture. *Nature* **297**, 501–504.

SAKMANN, B. & NEHER, E. (1983). Geometric parameters of pipettes and membrane patches. In *Single-Channel Recording*, SAKMANN, S. & NEHER, E. New York, London: Plenum Press.

SPRUCE, A. E., STANDEN, N. B. & STANFIELD, P. R. (1987). Studies of the unitary properties of adenosine-5′-triphosphate-regulated potassium channels of frog skeletal muscle. *Journal of Physiology* **382**, 213–226.

[*From the Proceedings of the Physiological Society*, 19–20 *December* 1986
Journal of Physiology, **386**, 111*P*, 1987]

On the electrical properties of a human neuroblastoma cell-line (IMR-32)

By B. L. Ginsborg, R. J. Martin* and L. Patmore†. *Departments of Pharmacology and Preclinical Veterinary Sciences**, *University of Edinburgh and Department of Pharmacology†, Syntex Research Centre, Edinburgh*

We have looked at the electrical properties of the IMR-32 cell line (Tumilowicz, Nichols, Cholen & Greene, 1970) using conventional patch-clamp techniques. Our preliminary results show that these cells have neuronal properties. Voltage-activated inward sodium and outward potassium currents recorded from the whole cell are shown in Fig. 1. The sodium currents (*a*) displayed conventional activation and inactivation. Outward currents (*b*) were activated at around −10 mV; their amplitude increased, and time to peak shortened with increasing depolarization, and they declined slowly (*c*). These currents were reduced in a dose-dependent way in the presence of 4-AP (0·25–4 mM). Records from cell-attached patches are illustrated in (*d*) and (*e*); they correspond to channels of conductance of around 80 pS and of around 20 pS respectively. Note the inactivation in (*e*).

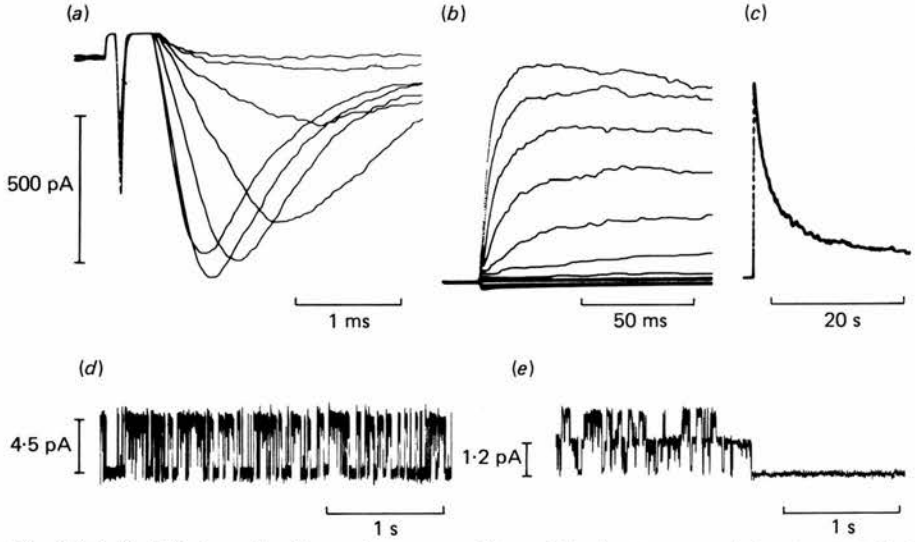


Fig. 1 (*a*)–(*c*). Whole-cell voltage-clamp recording with pipettes containing (mM), 1 $MgCl_2$, 10 HEPES, 2·5 $CaCl_2$, 11 EGTA; pH 7·2 and in (*a*) 140 CsCl, in (*b*) 95 KCl. Bath solution: 6 KCl, 10 HEPES, 1 $MgCl_2$; pH 7·4 at 20 °C and in (*a*) 145 NaCl and in (*b*) and (*c*) 266 sucrose and $CoCl_2$. (*a*) Holding potential (V_h) −80 mV and command potentials (V_c) −55 to −25 mV in 5 mV steps, pulses every 5 s. The first 0·5 ms of the trace should be disregarded. (*b*) $V_h = -40$ mV; $V_c = -70$ to +50 mV in 10 mV steps, pulses every 10 s. (*c*) $V_h = -60$ mV; $V_c = +30$ mV, 30 s pulse. (*d*)–(*e*) Cell-attached patch records with pipettes and bath containing (mM): 6 KCl, 145 NaCl, 1 $MgCl_2$, 2 $CaCl_2$, 10 HEPES; pH 7·4 at 20 °C. (*d*) Pipette potential −60 mV. (*e*) At beginning of record, pipette potential changed from +20 to −60 mV. Bath solutions all contained 5 mM glucose.

We thank Greig Duncan for preparing the cultures.

REFERENCE

Tumilowicz, J. J., Nichols, W. N., Cholen, J. J. & Greene, A. E. (1970). Definition of a continuous human cell line derived from neuroblastoma. *Cancer Res.* **30**, 2110–2118.

Journal of Physiology (1991), **434**, *pp.* 121–149
With 18 figures
Printed in Great Britain

ON THE SODIUM AND POTASSIUM CURRENTS OF A HUMAN NEUROBLASTOMA CELL LINE

BY B. L. GINSBORG, R. J. MARTIN* AND L. PATMORE†

*From the Department of Pharmacology and *Preclinical Veterinary Sciences, University of Edinburgh and †Department of Pharmacology, Syntex Research Centre, Edinburgh*

(*Received 19 April 1990*)

SUMMARY

1. The patch-clamp method was applied to the study of ionic currents activated by depolarization of undifferentiated IMR-32 human neuroblastoma cells. Whole-cell sodium and potassium currents and single potassium ion channel currents from cell-attached patches were investigated.

2. Cells had a mean resting potential of −38 mV and mean input resistance of 1·6 GΩ. Single action potentials were evoked under current clamp during the injection of depolarizing currents.

3. A voltage-dependent inward sodium current was observed which reversed at +44 mV. A Boltzmann fit to the activation curve gave a half-maximal activation voltage of −41·6 mV and a 'slope' of 3·9 mV. The steady-state inactivation curve had a half-maximal inactivation voltage of −81 mV and a 'slope' of 9·7 mV.

4. The time-dependent activation and inactivation of the current displayed classical Hodgkin–Huxley kinetics. Values for the time constants τ_m and τ_h of 0·16 and 0·63 ms were calculated for a voltage jump from −80 to −10 mV; τ_m and τ_h decreased as the step potential was changed from −30 to +20 mV.

5. Outward currents were activated in bathing solutions substantially free of anions and could thus be attributed to potassium ions. The tail current reversed in direction on repolarization to −60 mV when the potassium concentration in the bathing solution was increased from 6 to 30 mM. When the bathing solution contained 145 mM-potassium, and the patch pipette, 95 mM, a depolarization to −10 mV from a holding potential of −60 mV evoked an inward current.

6. Outward currents were examined by using voltage pulses which depolarized the cell to −20 mV, or more positive values, from a holding potential of −80 mV and by pulses which depolarized the cell to 0 mV, or to positive values, from a holding potential of −30 mV. A Boltzmann fit of typical activation data gave a half-maximal activation voltage of 17 mV and a 'slope' of 14 mV.

7. The time course of the rising phase of the current was described by a function of the form $A\{1-\exp[-(t-\delta t)/\tau]\}$, where δt varied between 1 and 4 ms and τ varied between 4 and 27 ms, decreasing with increasing depolarization. There was no evidence for a fast transient component.

MS 8428

8. The amplitude of outward currents was reduced by extracellular calcium ions, cobalt ions, tetraethylammonium and 4-aminopyridine.

9. During prolonged depolarization, the time course of the current could be described by the sum of two exponentially decaying components, with time constants of around 1 and 10 s. 4-Aminopyridine selectively reduced the slower component.

10. Single-channel currents were evoked by depolarization of cell-attached patches with electrodes containing normal extracellular solution. The most frequently encountered channel had a conductance of about 20 pS. Patches usually contained either no or several such channels; the activity of a single channel, however, could be recorded during the inactivation which occurred during prolonged depolarization.

11. A detailed study was made of records obtained from one cell in response to two different voltage jumps. With the 46 mV jump, bursts of openings of 26 ms average duration occurred, separated by interburst periods of 74 ms average duration; the 'open probability' was 0·26. With the 82 mV jump, bursts could not be distinguished; the open probability was 0·90.

12. If events shorter than 1 ms were disregarded, the probability density functions for open times were single exponentials with time constants of 8·5 ms for the 46 mV jump and 18 ms for the 82 mV jump. Two exponential components were required to describe the probability density function for the closed times with time constants of 1 and 70 ms for the 46 mV jump, and 1 and 10 ms for the 82 mV jump.

13. On the basis of these probability density functions, the whole-cell outward currents would be expected to be about six times larger for a voltage jump of 82 mV than for one of 46 mV and to rise at about twice the rate. This is consistent with what was observed.

INTRODUCTION

The human neuroblastoma cell line IMR-32 (Tumilowicz, Nichols, Cholen & Greene, 1970) has been the subject of various biochemical, pharmacological and differentiation studies (see e.g. Gupta, Notter, Felten & Gash, 1985; Clementi, Cabrini, Gotti & Sher, 1986; Sher, Gotti, Pandiella, Madeddu & Clementi, 1988). However, little is known of the electrical properties of these cells. Voltage-dependent inward and outward currents have been reported by Gotti, Sher, Cabrini, Bondiolotti, Wanke, Mancinella & Clementi (1987) and by Ginsborg, Martin & Patmore, (1987); Sher *et al.* (1988) have also demonstrated that calcium entry may be stimulated by depolarization, and Carbone, Sher & Clementi (1990) have given a detailed description of voltage-activated calcium currents. However, the sodium and potassium currents do not appear to have been investigated in detail, and the purpose of this paper is to provide a fuller account. We show that the undifferentiated IMR-32 cell can fire an action potential and can generate classical sodium and delayed-rectifier potassium currents (see e.g. Hille, 1984); the latter reflects the existence of voltage-sensitive channels of about 20 pS conductance.

METHODS

The experiments were done on about 120 cells between August 1985 and October 1987.

Cell cultures

The IMR-32 cell line was obtained from Flow laboratories and grown in 75 cm^2 culture flasks containing minimal essential medium (MEM) with Hanks salts and 25 mM-HEPES, 10% fetal calf serum, 100 i.u./ml penicillin and 100 μg/ml streptomycin at pH 7·35. Cells were grown at 37 °C until confluent and then transferred at a low density to 35 mm Petri dishes. No steps were taken

TABLE 1. Composition of solutions (mM)

	A	B	C	D	E	F
NaCl	145	145	6	121	—	10
KCl	6	6	145	30	6	110
$CaCl_2$	2	—	2	2	—	2·5
$MgCl_2$	1	1	1	1	1	1
EGTA	—	—	—	—	—	11
HEPES	10	10	10	10	10	10
Glucose	5	5	5	5	5	—
Sucrose	—	—	—	—	266	—
TTX	0·5 μM	0·5 μM	0·5 μM	0·5 μM	—	—

Solutions A–E were adjusted to pH 7·4 with NaOH. Solution F was adjusted to pH 7·2 with KOH. In some experiments $CoCl_2$ was added to the extracellular solution, as noted in the text. The free calcium concentration in the pipette solution F (whole-cell mode) was estimated as 0·1 μM, taking the value of 6·45 for $pK_{apparent}$ of Ca-EGTA at the ionic strength of the solution (Miller & Smith, 1984; D. J. Miller, personal communication).

EGTA, ethyleneglycol-bis-(β-aminoethylether)*N*,*N*′-tetracetic acid; HEPES, *N*-2-hydroxyethyl-piperazine-*N*′-2-ethanesulphonic acid; TTX, tetrodotoxin.

to induce morphological differentiation and such processes as were observed were less than 50 μm in length; the cells may therefore be regard as undifferentiated (cf. Gupta *et al.* 1985, who characterized differentiated cells as possessing neurites from 1·4 to 11 mm in length).

Solutions

The compositions of the extracellular solutions are listed in Table 1. In some experiments solution B was modified (B′) by the replacement of sodium by tetramethylammonium. For current-clamp recordings the pipettes were filled with solution (G) containing (mM): KCl, 100; $MgCl_2$, 1; $CaCl_2$, 1; EGTA, 11; HEPES, 10; pH adjusted to 7·2 with NaOH. The concentration of ionized calcium was calculated to be 3×10^{-8} M according to the routine kindly provided by Dr D. J. Miller (see Miller & Smith, 1984). For the recording of sodium currents under voltage clamp, potassium was replaced by caesium (140 mM), but the solution (H) was otherwise unchanged.

Drugs

Tetrodotoxin (TTX), tetraethylammonium chloride (TEA) and 4-aminopyridine (4-AP) were obtained from Sigma, dissolved in distilled water and diluted in the appropriate solution.

Electrical recordings

For electrical recordings the dishes containing the cells, bathed in a solution appropriate to the experiment to be done, as detailed below, were mounted on the stage of an inverted microscope. Currents and voltages were recorded by the whole-cell variation of the patch-clamp technique (Hamill, Marty, Neher, Sakmann & Sigworth, 1981) at room temperature (18–22 °C). The patch pipettes were pulled from Corning No. 7052 glass (1·55 mm o.d., 1·0 mm i.d.) and were fire-polished. The pipette resistances in free solution were between 1 and 3 MΩ. If the series resistance is taken as twice that in free solution (Marty & Neher, 1985) the voltage at the tip of the pipette

would differ from the command value by less than 6 mV for currents of up to 1 nA. Since currents in the present experiments were always smaller than 1 nA, resistance compensation was not employed. The values of voltages given in Results are uncorrected command values.

The patch pipette was tightly sealed onto the surface of the cell and the cell broken into by suction. The seal resistance before breaking into the cell was in the range 5–15 GΩ. After the cell was broken into, the input resistance, measured in a series of twelve cells (with 100 mM-K^+ in the pipette, solution G) was $1{\cdot}6 \pm 0{\cdot}7$ GΩ (mean ± S.D.) with a range of 0·8–3·0 GΩ. The EPC-7 amplifier (List electronics, Darmstadt, Germany), was used in the current-clamp mode (with the 1 GΩ feedback resistor), for recording resting membrane potentials and to allow constant-current pulses to be applied to the cell. It was used in the voltage-clamp mode to record voltage-activated currents. Voltage pulses were generated by a CED 1401 interface (Cambridge Electronic Design, Cambridge) under the control of an Apple II microcomputer. Cell capacitance, input resistance and the series resistance were determined from the current response to a 5 mV voltage-clamp pulse.

Data analysis

Electrical signals were recorded on magnetic tape with an FM tape-recorder (Racal Store 4D). Analog-to-digital and digital-to-analog conversions were performed at 12-bit resolution by means of the microcomputer and interface. Digitized records were stored on floppy disc for subsequent analysis. Sodium currents were usually recorded at 30 in/s and were replayed at 7·5 in/s, filtered with an 8-pole Bessel filter (−3 dB at 4 kHz) and digitized at 40 kHz; this is equivalent to 160 kHz sampling of the original recordings so that 6·4 ms of the original signal contained 1024 points. Correction for capacitance and leakage were made as described in Results and the corrected digital data transferred to the D–A converter of the CED 1401 interface (together with a suitable ramp to provide the time base) and thence to an analog plotter. Whole-cell outward currents were usually recorded at 7·5 in/s and, for analysis, replayed at the same speed, filtered with an 8-pole Bessel filter(−3 dB at 0·1 to 0·25 kHz) and digitized at 1–2·5 kHz. 'Hard copy' was produced either in the same way as described above for sodium current records or by sending the digital data to a digital plotter via the Easygraph programme provided by Edinburgh University Computing Service (EUCS) on its mainframe computer. Curves were fitted to the data by non-linear regression with the help of NAG (Numerical Algorithms Group, Oxford) minimizing routines E04JAF or E04CCF, also made available by EUCS.

Cell-attached patches

Standard techniques were used to obtain cell-attached patches (Hamill *et al.* 1981). Single-channel current records were made with the List EPC-7 amplifier (10 GΩ feedback resistor; List, Darmstadt, Germany) and recorded on magnetic tape at 7·5 ins/s (Racal Store 4). Channels were activated by depolarizing pulses; in general, responses to hyperpolarizing pulses consisted only of the capacitative and linear leakage components, and could therefore be used to correct the responses to depolarization in the same way as for whole-cell responses.

Data processing: preliminary test of stationarity

The tape was played back into the CED 1401 interface connected to a DCS 286 microcomputer under the control of PAT software (kindly provided by J. Dempster, Department of Physiology and Pharmacology, University of Strathclyde). Records were filtered with an 8-pole Bessel filter, −3 dB at 1 kHz and sampled at intervals of 100 μs. The PAT software produced files of open and closed durations which were inspected using the cusum technique (see Glasbey & Martin, 1986) to allow sections to be selected for stationarity. The cusum, S_j, for open times, say, is given by

$$S_j = \Sigma(X_i - X_m), \quad i = 1 \text{ to } j, \quad \text{for } j = 1, \ldots n, \tag{1}$$

where X_i is the rank order of the duration of the ith open period and X_m (which equals $n(n+1)/2$) is the mean rank. A random fluctuation about zero is expected for channels which show stationary behaviour. The significance of the deviation may be estimated by determining a test statistic, D_α, the maximum value of

$$|S_j|/\{1 + (\alpha - 1)j/n\}, \tag{2}$$

for $j = 1$ to n, and calculating

$$2\exp(-12\alpha D_\alpha^2/nX_m), \tag{3}$$

which is the approximate probability of obtaining a value larger than D_α for a sequence of random events. This test was applied for values of $\alpha = 9, 1, 1/9$ and the procedure was also applied to the closed times.

Probability density functions (PDFs)

PDFs for open and closed states were obtained from the selected single-channel data by the method of maximum likelihood (see Colquhoun & Sigworth, 1983), with the help of the NAG minimizing subroutine, E04CCF. The fitting procedure requires the selection of the minimum interval, t_m, that can be reliably observed. When this was set to a value below 0·9 ms, it was found that the open times were best fitted by a two-component PDF (time constants, τ'_o and τ_o, say) and the closed times by a three-component PDF (time constants, τ'_f, τ_f and τ_s, say). However, the components with the time constants τ'_o and τ'_f, which were smaller than t_m, dominated the PDFs and corresponded to unrealistically large numbers of 'missed' events; moreover, although the values of τ_o, τ_f and τ_s were relatively stable, values for τ'_o and τ'_f varied randomly with the choice of t_m. When t_m was set to 1 ms, the open times could be adequately fitted by a single exponential function with time constant close to τ_o and the closed times by the sum of two exponential functions with time constants close to τ_f and τ_s. Thus the PDFs for the open (4) and closed (5) times may be denoted:

$$(1/\tau_o)\exp(-t/\tau_o), \tag{4}$$

and

$$(a_s/\tau_s)\exp(-t/\tau_s)+(a_f/\tau_f)\exp(-t/\tau_f). \tag{5}$$

where $a_f = 1-a_s$. A rough check of the validity of the PDFs may be obtained by comparing the observed 'equilibrium' open probability, $p_{1\infty}$, say, i.e. the mean open time/(mean open time + mean closed time), with that predicted on the basis of the PDFs evidently given by

$$p_{1\infty} = \tau_o/(\tau_o+a_s\tau_s+a_f\tau_f). \tag{6}$$

As already shown by Sakmann & Trube (1984) in a somewhat different way, the predicted value of $p_{1\infty}$ depends on the PDFs of the open and closed times and is independent of the underlying kinetic model. The relative amplitudes and the time courses of the rising phases of the whole-cell currents that would be predicted on the basis of the PDFs were calculated as sketched below (cf. Sakmann & Trube, 1984, who cover some of the same ground; it may be noted that their eqn (24), p. 679, is defective).

The general form predicted from the PDFs for the time course of the open probability, $p_1(t)$, say, during the response to a voltage jump is given by

$$p_1(t) = p_{1\infty}-A\exp(-t/\tau_1)-B\exp(-t/\tau_2), \tag{7}$$

(see Colquhoun & Hawkes, 1977, 1981, 1982). A and B depend upon the initial conditions and the particular kinetic model, but τ_1 and τ_2 depend only on the PDFs. They are such that

$$\tau_1+\tau_2 = (\tau_o\tau_s+\tau_s\tau_f+\tau_f\tau_o)/(\tau_o+a_s\tau_s+a_f\tau_f) \tag{8}$$

and

$$\tau_1\tau_2 = \tau_o\tau_s\tau_f/(\tau_o+a_s\tau_s+a_f\tau_f). \tag{9}$$

For the kinetic model, $C_2 \rightleftharpoons C_1 \rightleftharpoons O$, if p_{10} and p_{20} denote the probability of states O and C_1, respectively at $t = 0$,

$$A = \{\tau_1 p_{1\infty}-p_{10}\tau_1(1-\tau_2/\tau_o)-p_{20}(a_f\tau_s+a_s\tau_f)\,p_{1\infty}\}/\{\tau_1-\tau_2\}, \tag{10}$$

and

$$B = p_{1\infty}-A. \tag{11}$$

If it is assumed that at $t = 0$, all the channels are in state C_2 then $p_{10} = p_{20} = 0$, and the time course shown in eqn (4) simplifies to

$$p_1(t) = p_{1\infty}[1-\{\tau_1\exp(-t/\tau_1)-\tau_2\exp(-t/\tau_2)\}/\{\tau_1-\tau_2\}]. \tag{12}$$

For the kinetic model $C_2 \rightleftharpoons O \rightleftharpoons C_1$, the expressions corresponding to eqns (10), (11) and (12) are:

$$A' = \{(\tau_1-\tau_f)\,p_{1\infty}-p_{10}\,\tau_2(\tau_1/\tau_f-1)-p_{20}(\tau_s-\tau_f)\,p_{1\infty}\}/\{\tau_1-\tau_2\}, \tag{13}$$

$$B' = p_{1\infty}-A' \tag{14}$$

$$p_1'(t) = p_{1\infty}[1-\{(\tau_1-\tau_f)\exp(-t/\tau_1)+(\tau_2-\tau_f)\exp(-t/\tau_2)\}/\{\tau_1-\tau_f\}]. \tag{15}$$

During the 46 mV depolarizations, it was possible to distinguish separate bursts of channel activation. The mean duration, t_b, of bursts predicted from the PDFs shown in eqns (4) and (5) are formally different for the two kinetic models. From the results of Colquhoun & Hawkes (1982) it may be shown that for the CCO model,

$$t_b = (1+\Phi^2 a_f/a_s)/\tau_o + \Phi^2 a_f \tau_s \tau_f / \{a_s(a_s+\Phi^2 a_f)(\tau_s-\tau_f), \quad (16)$$

where $\Phi = 1+\tau_f/\{a_f(\tau_s-\tau_f)\}$.

For the COC model,

$$t'_b = (\tau_o + a_f\tau_f)/a_s. \quad (17)$$

When τ_s is much greater than τ_f, which will be the case if bursts can be distinguished, Φ tends to 1 and eqn (16) reduces to eqn (17).

RESULTS

Resting and action potentials recorded under current clamp

In a series of fifty-two cells, where the patch pipette contained a high concentration of potassium (solution G, Methods), the resting potential had a mean of -38 ± 11 mV (mean $\pm$ S.D.) and ranged between -17 and -72 mV. The resting potentials of the majority of the cells (40) were between -30 and -60 mV; this range is similar to that reported for the mouse neuroblastoma, N1E-115 (-35 to -55 mV) by Moolenaar & Spector (1978). The values for IMR-32 cells are likely to be underestimates since the seal resistance was not often more than 5 times the cell input resistance, which could be as large as 3 GΩ (see Methods). Figure 1 illustrates an experiment in which the potential of a cell was hyperpolarized from its resting value of -42 mV to about -80 mV by passing an inward current of 30 pA (not shown) under current clamp. Responses were then observed to superimposed hyperpolarizing and depolarizing pulses of different amplitudes. Over the range of small current pulses (e.g. Fig. 1*a* and *b*) the voltage–current relation was linear, its slope corresponding to an input resistance of about 1·3 GΩ. With increasing depolarizations, the electrotonic potentials gave rise to local responses (e.g. Fig. 1*c*), and, at a threshold of between -45 and -35 mV, to an action potential (e.g. Fig. 1*d* and *e*) which was followed by a small undershoot. Only a single action potential occurred no matter how long or larger the current pulse, although on occasions the action potential was followed by a series of oscillations. The magnitude of the action potential increased with increasing stimulating current. In Fig. 1*d* the current was 75 pA and the action potential was 83 mV; in Fig. 1*e* the current was increased to 100 pA and the action potential amplitude rose to 92 mV. This corresponds to an input resistance of 0·36 GΩ at the peak of the action potential (as compared to the value 1·3 GΩ at -80 mV, mentioned above).

Voltage clamp

Sodium currents

As reported by Gotti *et al.* (1987), when the cell was under voltage clamp and the pipette contained a high concentration of potassium (solution G, Methods), the response to depolarization from a sufficiently negative holding potential consisted of a rapid inward followed by a sustained outward current. The sustained outward component was not seen if the potassium in the pipette was replaced with caesium (solution H, Methods); it could therefore be identified as a potassium current. The

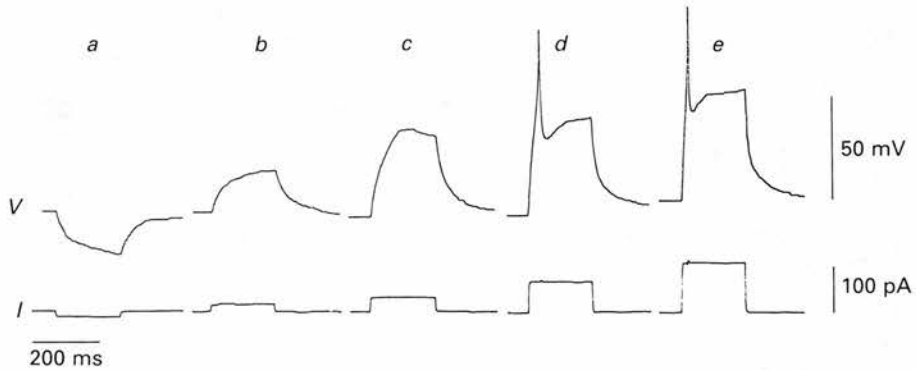


Fig. 1. Voltage responses (V) of IMR-32 cell to constant-current pulses (I). Resting potential, −42 mV; a steady inward current of about 30 pA was passed to set membrane potential to about −80 mV before applying current pulses. The extracellular solution (Table 1, solution A) contained 145 mM-Na^+ and pipette (solution G, Methods), 100 mM-K^+.

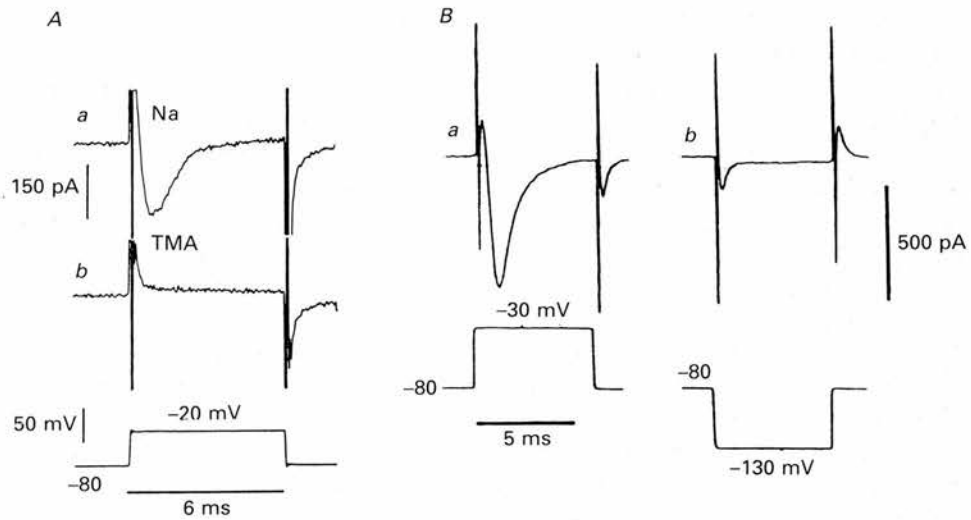


Fig. 2. Current responses of two different IMR-32 cells (A and B) to voltage steps applied under voltage clamp. Signals were recorded on magnetic tape at 60 in/s and replayed at $1\frac{7}{8}$ in/s into a pen recorder. The pipette contained 140 mM-CsCl (solution H, methods). A, effect of replacement of Na^+ by TMA^+; cell held at −80 mV and stepped to −20 mV for 6 ms. Aa, response in 145 mM-Na^+ (Table 1, solution A); Ab, abolition of transient inward current when Na^+ was replaced with 145 mM-TMA^+ (solution B′, Methods). B, comparison of responses to a depolarizing voltage step (a) and a hyperpolarizing voltage step of same amplitude (b) . Holding potential, −80 mV; pulse amplitude, 50 mV. Note that the response to a hyperpolarizing pulse consists only of symmetrical capacitative currents at the beginning and end of the pulse, together with a small steady inward current during the pulse. The extracellular solution (Table 1, solution B) contained 145 mM-Na^+ and no added Ca^{2+}.

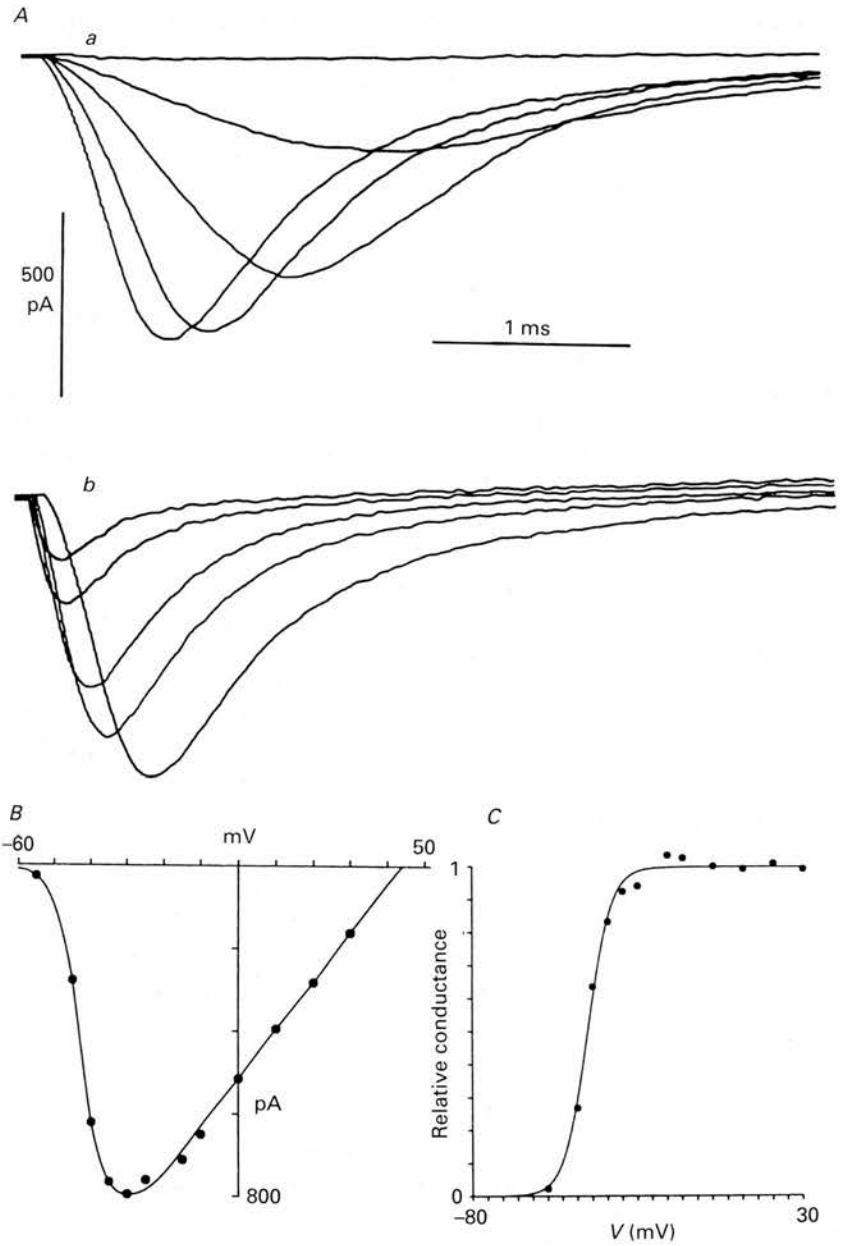


Fig. 3. Activation of inward current in a single IMR-32 cell by depolarizations of different amplitudes from a constant holding potential of −80 mV. The pipette contained 140 mM-CsCl (solution H, Methods); the extracellular solution (Table 1, solution A) contained 145 mM-Na^+. Individual responses were digitized and corrected for linear leakage and capacitative currents by proportional addition of the current evoked by a 25 mV hyperpolarizing pulse (cf. Fig. 2*B*). Records shown are averages of four to six individually corrected responses for each voltage step (not shown). The current transient during the rising phase of the voltage step has been blanked out and it should be noted that the initial 300 μs of record may not be reliable because of its critical dependence on the accuracy of correction. In *Aa*, responses are shown, in order of increasing amplitude, to depolarizing voltage steps of 25, 30, 40, 45 and 50 mV; in *Ab*, responses are shown, in

inward component could be suppressed by removal of sodium ions from the bathing solution or by the addition of 0·5 μM-TTX and could therefore be identified as a sodium current. Figure 2*Aa* shows an individual uncorrected pen record of the response of a cell held at −80 mV, and bathed in a sodium-containing solution (Table 1, solution *A*), to a 60 mV depolarizing pulse. The effect of replacement of the extracellular sodium with tetramethylammonium (solution B′, Methods) which clearly abolished the inward current, is shown in Fig. 2*Ab*.

Sodium currents were seen in over half the cells in which they were sought. Thus in a series of seventeen cells, thirteen showed active inward currents similar to those described here. The peak amplitudes ranged from 50 to 960 pA when the cell was held between −70 and −80 mV and depolarized by 60 mV; the amplitudes were not related to the size of the cell or to any other identifiable property.

Figure 2*Ba* shows another example of an uncorrected Na^+ current from a different cell, held at −80 mV and depolarized by 50 mV. Figure 2 *Bb* shows the effect of an equal hyperpolarization: the response evidently consists of approximately symmetrical capacitative currents at the beginning and end of the pulse and a small steady inward current during the pulse. The amplitude of such responses varied linearly with the amplitude of the hyperpolarizing voltage pulse and thus could be used to correct the sodium current records by proportional addition.

Activation of sodium current. A family of sodium currents evoked by increasing depolarizing steps from a holding potential of −80 mV and corrected for leakage and capacitative artifacts is shown in Fig. 3*A*. As can be seen in *Aa* the currents increased in peak amplitude with depolarization up to a value of about −25 mV and thereafter, as seen in *Ab*, decreased with a further increase in depolarization; the time to the peak of the current decreased monotonically with increasing depolarization. All the data from this cell relating peak current to voltage are shown in Fig. 3*B*. The maximum current was 800 pA and the extrapolated reversal potential was +44 mV.

The activation characteristics of the sodium currents shown in Fig. 3*A* were analysed by estimating the conductance (g) at different depolarizations according to the relation $I = g(V - E_{Na})$, where I refers to peak current values; this assumes that the instantaneous current–voltage relation is linear. The data were then fitted to the Boltzmann equation:

$$g = g_{max}/\{1 + \exp[(V - V_h)/k]\}, \quad (18)$$

where g is the conductance, g_{max}, the maximum conductance, V, the test potential, V_h, the 'half-activation' potential and k defines the slope. The peak conductance was 11·7 nS; as illustrated in Fig. 3*C*, V_h was 41·6 mV and k was 3·9 mV.

Steady-state inactivation. Inactivation of the sodium current was investigated by altering the holding potential and stepping the membrane potential to −20 mV (Fig. 4). A depolarization of the holding potential of the cell from −120 to −65 mV caused a progressive decrease in the amplitude of the inward current without any obvious

order of decreasing amplitude, to voltage steps of 55, 70, 80, 100 and 110 mV. *B* shows the relation between peak current and voltage derived from all the data for this cell. Curve drawn by eye: voltages were not corrected for the effect of pipette resistance (see Methods) and the maximum inward current may thus have occurred at a slightly more positive voltage (by up to 5 mV) than shown. *C*, 'Boltzmann' fit of the conductance–voltage relation (see text).

change in its time course. The normalized currents evoked from different holding potentials were plotted against those potentials (Fig. 4*B*). The data were fitted (cf. eqn. (18)) to:

$$I = I_{max}/\{1+\exp[(V_h - V)/k]\}, \tag{19}$$

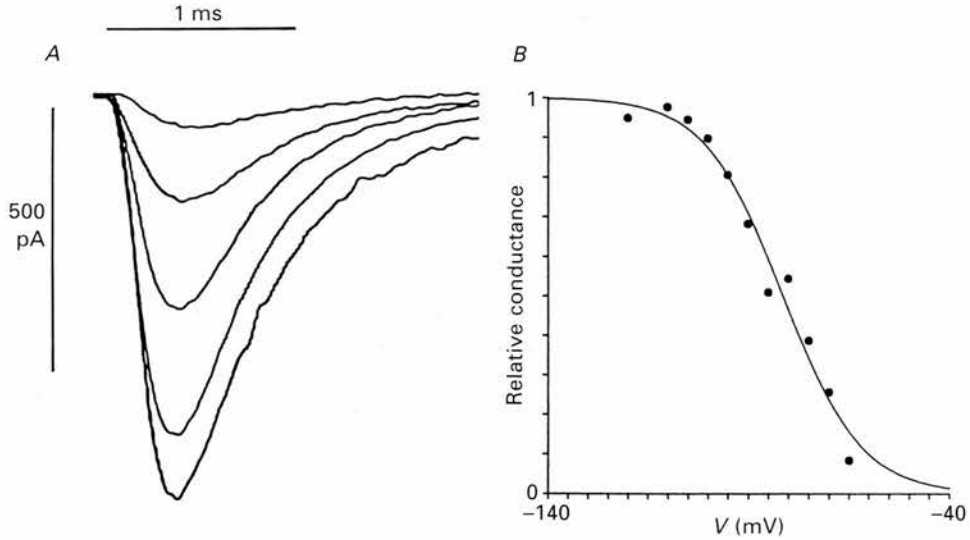


Fig. 4. Inactivation of sodium current at different holding potentials. Solutions as in experiment of Fig. 3. The cell was depolarized to −20 mV from various different holding potentials. In *A*, each record is the average of four to six individual responses corrected as described in the legend to Fig. 3. The holding potentials in order of increasing amplitude of responses were −65, −70, −85, −95 and −120 mV. *B*, Boltzmann fit of all the data from this experiment.

where I is the current, I_{max} is the maximum current, V_h is the voltage at which the current is half-inactivated, V is the membrane potential and k defines the slope. V_h was −81 mV and k was 9·7 mV. At the observed resting potentials of these cells the sodium current would be almost completely inactivated.

Time dependence of activation and inactivation of I_{Na}. In an attempt to see how far the observed sodium current was consistent with the classical model of Hodgkin & Huxley (1952) the time course of the currents evoked by various voltage jumps from −80 mV was compared with that given by the simplified equation:

$$I_{Na} = I\{1-\exp(-t/\tau_m)\}^3\exp(-t/\tau_h), \tag{20}$$

where τ_m and τ_h were estimated from the falling phase of the observed current by non-linear least-squares regression. The fitted values of τ_m and τ_h for the different currents analysed are shown in Fig. 5*B*. As pointed out by Belluzzi & Sacchi (1986), the time to peak predicted by eqn (20) is $\tau_m \ln(1+3\tau_h/\tau_m)$. A comparison of the predicted and observed values for the experiments illustrated in Fig. 3 is shown in Table 2. The observed times to peak decrease in much the same way as predicted, although the absolute values are 200–300 μs larger.

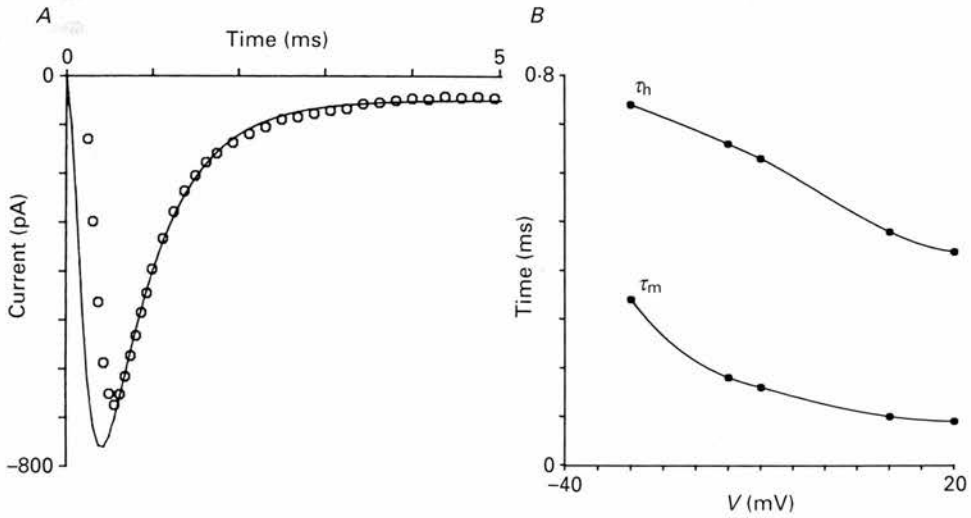


Fig. 5. Analysis of time course of sodium current. *A*, continuous curve shows the best fit of the form

$$I_{Na} = I\{1-\exp(-t/\tau_m)\}^3 \exp(-t/\tau_h),$$

to the falling phase (from 0·5 ms after start of the record) of the response to a voltage jump from −80 to −20 mV. ○, observed current. *B*, values of τ_m and τ_h estimated from best fits, as in *A*, to responses evoked by jumps from −80 mV to the different voltages. Curves drawn by eye.

TABLE 2. Comparison of observed and calculated times to peak sodium current

	Voltage (mV)				
	−30	−15	−10	10	20
Calculated time to peak (ms)	0·7	0·57	0·41	0·27	0·24
Observed time to peak (ms)	0·98	0·72	0·64	0·49	0·44

The model provided a good fit to the declining phase of the current. The rising phase is less well described but this is not surprising since its time course is critically dependent on the accuracy of the correction for capacitative current.

Potassium currents

In most experiments, outward currents were corrected by algebraic addition of a number of smaller currents evoked by appropriate hyperpolarizing pulses (Bezanilla & Armstrong, 1977). It was sometimes possible to correct by adding currents evoked by equal (but opposite) voltage jumps. This is illustrated in Fig. 6*A* from an experiment in which a cell was held at −60 mV, depolarized by 60 mV (*a*), and hyperpolarized by 60 mV (*b*). In *Ac*, the currents are superimposed to eliminate the capacitative artifact and the leakage current (including the passive linear current component). *Ad* shows the average of four such superimpositions. The initial inward deflection (1) shows the presence of a small sodium current which was absent when tetrodotoxin was added to the extracellular solution; '2' indicates the presence of a small outward tail-current.

In some experiments the capacitative artifact and the leakage currents were sufficiently small to make corrections unnecessary, and data processing was confined to averaging a number of uncorrected responses to depolarizing pulses. An example is shown in Fig. 6*B* in which sixteen responses were evoked at intervals of 10 s; the

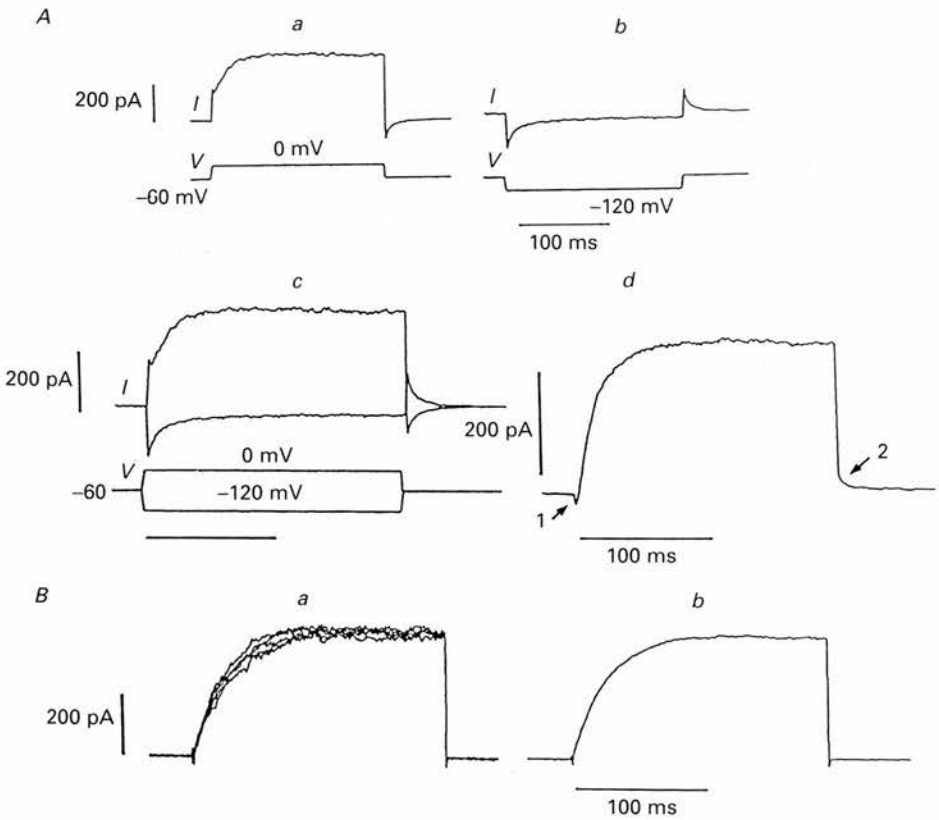


Fig. 6. Outward currents evoked by depolarization of IMR-32 cells. *A*, cell held at −60 mV depolarized to 0 mV (*a*) or hyperpolarized to −120 mV (*b*) during 200 ms voltage jumps. *I*, current (upward deflections in this and all other records correspond to outward currents); *V*, voltage (depolarization upward). In *Ac*, *a* and *b* are superimposed; *Ad* shows the average of the sum of four such pairs. The initial inward deflection (1) is presumably a sodium current; note the outward tail current (2). The resting potential of the cell was −62 mV. Extracellular solution as in Table 1, solution B, but without tetrodotoxin. *B*, cell held at −80 mV; currents evoked by 200 ms voltage jumps of 90 mV. *Ba*, individual, randomly fluctuating, responses; *Bb* shows the average of sixteen such responses. Voltage jumps applied at 10 s intervals. Extracellular solution as in Table 1, solution B.

five superimposed traces (responses to stimuli 1, 3, 5, 7 and 10) in Fig. 6*Ba* illustrate the random fluctuations in current which occur from stimulus to stimulus. The average of the set of sixteen responses is shown in Fig. 6*Bb*. In this experiment there was evidently no 'run-down', but it should be noted that stable current responses were not always obtained, even with high resistance seals, and 'run-down' was the usual reason for abandoning a cell.

Current–voltage relationships

In the experiment illustrated in Fig. 7, the extracellular solution contained no added calcium, and the usual NaCl content was replaced by sucrose. Inward cationic currents were thus eliminated, as was also the possibility of an outward current

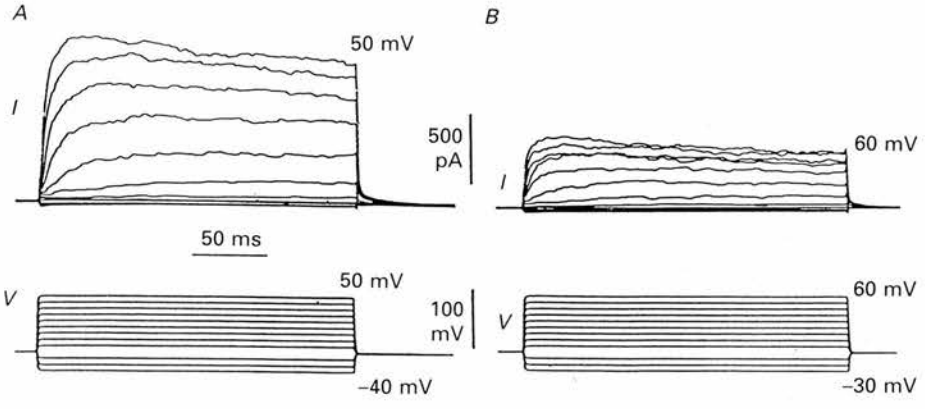


Fig. 7. Uncorrected current responses of cell bathed in low-chloride solution (28 mM; Table 1, solution E, but with 10 mM-$CoCl_2$) recorded with pipette containing high-chloride solution (112 mM; Table 1, solution F). Cell held at −40 mV (*A*) and −30 mV (*B*), hyperpolarized by 30 mV and depolarized by 90 mV in 10 mV steps during 200 ms voltage jumps. *I*, current; *V*, voltage.

carried by an influx of chloride ions. Families of responses to depolarizing and hyperpolarizing voltage steps from a holding potential of −40 mV are shown in *A*, and from a holding potential of −30 mV in *B*. In each set, the lowest current records, which cannot be distinguished from one another, show the responses to hyperpolarizations of 10, 20 and 30 mV. The very small inward currents are consistent with there being little, if any, sustained outward current at the holding potentials of −40 and −30 mV, and therefore little current to be suppressed by hyperpolarization. This was a general result, and there is thus no evidence for an M-current (see e.g. Adams, Brown & Constanti, 1982) in IMR-32 cells. The upper traces demonstrate that relatively large outward currents can be evoked at holding potentials as positive as −40 and −30 mV which inactivate to only a small degree during a 200 ms pulse. The results strongly suggest the presence of a delayed rectifier current, I_K.

Effects of high K^+ on currents

In Fig. 8*Aa*, with an extracellular concentration of potassium on 6 mM, the tail current (*t*, arrow) is outward; in *Ab* with 30 mM-extracellular potassium, the tail current (*t*, arrow) is inward, indicating that the equilibrium potential for the ion(s) carrying the current has changed from a level more negative than −60 mV to one less negative. In *B*, the concentration was raised from 6 mM (in *a*) to 145 mM (in *b*),

a concentration presumably greater than the intracellular value, since the recording electrode contained only about 100 mM-potassium; depolarization from −60 to −10 mV now caused an inward current. On repolarization to −60 mV the inward current increased further because of the increased driving force. From the current

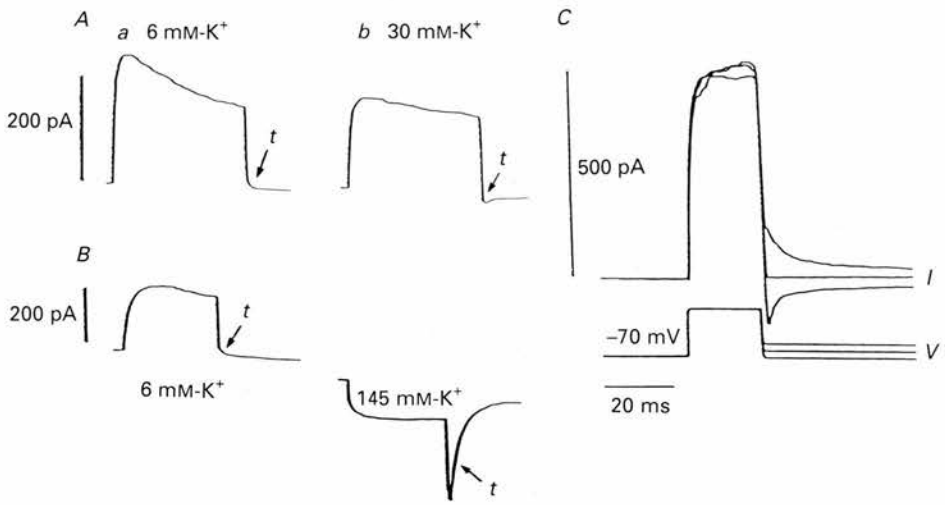


Fig. 8. Effect of an increase in extracellular potassium on currents evoked by depolarization. Records are averages of nineteen responses, corrected as in the experiment of Fig. 6*A*. *A*, cell held at −60 mV and depolarized to 0 mV during 200 ms voltage jump. In *Aa*, the extracellular potassium concentration was 6 mM (Table 1, solution A); in *Ab* it was increased to 30 mM (Table 1, solution D). Note the reversal of the direction of the tail current (arrow, *t*). *B*, cell held at −60 mV and depolarized to −10 mV for 200 ms. In *Ba* the potassium concentration was 6 mM (Table 1, solution A); in *Bb* it was increased to 145 mM (Table 1, solution C). Note the reversal of the current (see text). *C*, reversal potential for outward current in potassium concentration of 6 mM (Table 1, solution A). *I*, current; *V*, voltage. The cell was depolarized from a holding potential of −70 mV to +50 mV and repolarized to −40 mV to give an outward tail current, to −55 mV to give zero tail current and to −70 mV to give an inward tail current.

'jumps' which occurred at the end of the 50 mV voltage 'jumps', it is possible to infer that the depolarization caused a considerably greater increase in conductance, g say, in the higher external potassium. Thus g (at −10 mV) was 3·3 nS in 6 mM-potassium and 5·7 nS in 145 mM-potassium. A similar effect has been noted for I_K in other cells (see e.g. Dubois, 1981*a*; Sah, Gibb & Gage, 1988).

Reversal potential

Although a systematic study of the equilibrium potential for the tail current was not made, a range of values deduced from the direction of the current at different holding potentials may be given: −55 mV (1 cell, Fig. 8*C*), −60 mV (1 cell), −70 mV (1 cell), −80 to −85 mV (3 cells); six other cells had outward tail currents at −60 mV, and hence equilibrium potentials more negative than this value.

Activation of outward current

In the experiment of Fig. 9, the cell was held at −80 mV and depolarized by 10 mV steps from −30 mV up to +60 mV. A selection of corrected records is shown in *A*. The corresponding values of the conductances are plotted in *B* which also shows a

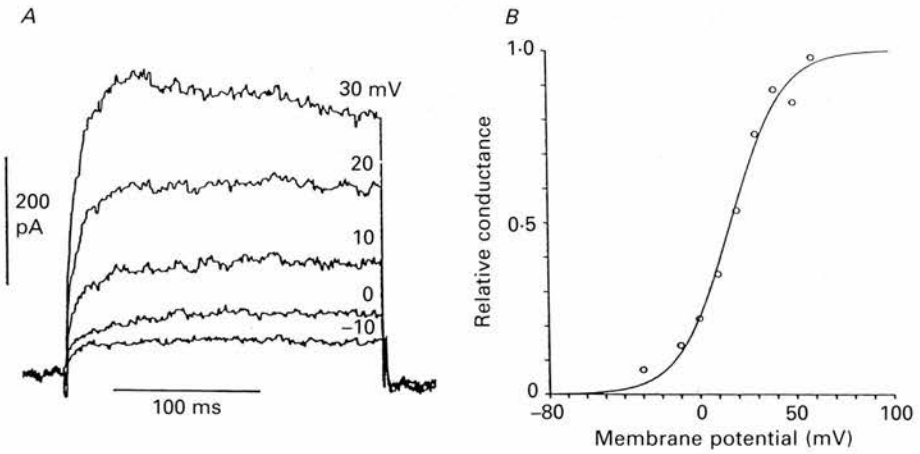


Fig. 9. Current responses of cell bathed in low chloride concentrations (8 mM; Table 1, solution E) recorded with a pipette containing high chloride (112 mM; Table 1, solution F). The cell was held at −80 mV, hyperpolarized to −110 mV and depolarized to +60 mV in steps of 10 mV during 200 ms voltage jumps. *A*, selection of corrected responses to indicated depolarizations. *B*, Boltzmann fit of data shown in *A* on assumptions that the 'instantaneous voltage–current' relation is linear and that the potassium equilibrium potential was −80 mV.

Boltzman curve, $g/g_{max} = 1/(1+\exp\{(V-V_h)/k\})$ where g_{max}, V_h and k were estimated from the data as described earlier. The value of k, 12·9 mV, is similar to that obtained in several other cells (e.g. squid axon, 12 mV, Hodgkin & Huxley, 1952; rat sympathetic neurone, 10 mV, Belluzzi, Sacchi & Wanke, 1985*b*; guinea-pig hippocampal cells, 13·6 mV, Sah *et al.* 1988). Values of 13 and 16 mV were obtained for V_h and of 19 and 13 mV for k in two other experiments which were less satisfactory than that illustrated.

Is there a transient voltage-dependent current, I_A?

As illustrated in Fig. 9, where the holding potential was −80 mV, depolarization did not evoke a rapid transient component of outward current corresponding to I_A which is a prominent feature in many other cells (e.g. Connor & Stevens, 1971; Neher, 1971; Kostyuk, Veselovsky, Fedulova & Tsyndrenko, 1981; Adams *et al.* 1982; Gustafsson, Galvan, Grafe & Wigstrom, 1982; Belluzzi, Sacchi & Wanke, 1985*a*). Although some degree of inactivation often occurred during 200 ms pulses, it did not appear to correspond to the presence of a classical I_A component. First, inactivation occurred even with holding potentials as positive as −40 mV; secondly, with such negative holding potentials as −80 or −90 mV, when an initial peak occurred it was prominent only when the cell was depolarized to 0 mV or beyond and increased with

increasing depolarization. Ypey & Clapham (1984) have described a delayed outward-rectifying potassium conductance with similar properties recorded from cultured mouse peritoneal macrophages. These properties do not correspond to those of classical I_A's, although, as has been pointed out by Rudy (1988), the distinction

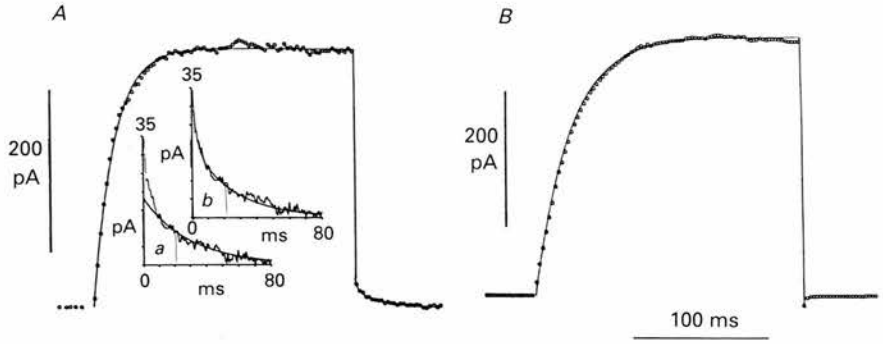


Fig. 10. Analysis of time course of currents shown in Fig. 6. *A* corresponds to Fig. 6*Ad*; holding potential, −60 mV. The line-fitting rising phase is:

$$312\{1-\exp[-(t-3{\cdot}1)/15{\cdot}6]\}.$$

The line fitting tail is:

$$15\exp(-t/2)+22\exp(-t/25).$$

○, experimental values; first point above baseline is at 9·4 ms after start of jump, after which points are at 2·4 ms intervals. Insets show tail current fits at greater resolution: *a* compares data with best single exponential fit, $18\exp(-t/30)$, disregarding first 10 ms of tail; *b* compares data with best double exponential fit as above. *B* corresponds to Fig. 6*Bb*; holding potential, −80 mV. The line-fitting rising phase is:

$$379\{1-\exp[-(t-2{\cdot}4)/26]\}.$$

○, experimental values at 2·4 ms intervals.

between I_A's and I_k's is somewhat blurred, now that a wide range of results is available.

Analysis of time course of currents

In the absence of inactivation, the time course of the rising phase of the outward currents evoked by depolarization could be fitted by the simple empirical relation:

$$I(t) = I_{max}\{1-\exp[-(t-\delta t)/t_1]\}, \tag{21}$$

where δt represents a 'delay' in activation, and t_1 an activation time constant. This relation has been used by Dubois (1981*b*) for the frog node of Ranvier, and provides a convenient way of comparing responses under different conditions. The values of δt were sensitive to the procedure used to correct for the initial capacitative artifact and cannot be regarded as reliable descriptors; the values of t_1 were, however, stable. Figure 10 shows the fitted course of the currents which have already been illustrated in Fig. 6; the particular values for δt and t_1 were 3·1 and 16 ms in *A* and 2·4 and 26 ms in *B*.

Where the current declined during the period of the relatively short depolarizing pulses (up to 300 ms), its time course could be fitted by a simple modification of eqn (21), namely,

$$I(t) = I_1'\{1-\exp[-(t-\delta t'/t_1')]\}\exp[-t/t_i], \tag{22}$$

where t_i may be regarded as a type of 'inactivation' time constant. There was little difference between the values of I_{max} and t_1, derived from fitting eqn (21) to the first 50 ms of the response and I_1' and t_1', derived from eqn (22) fitted throughout the whole time course of the depolarization. The rate of activation increased with increasing

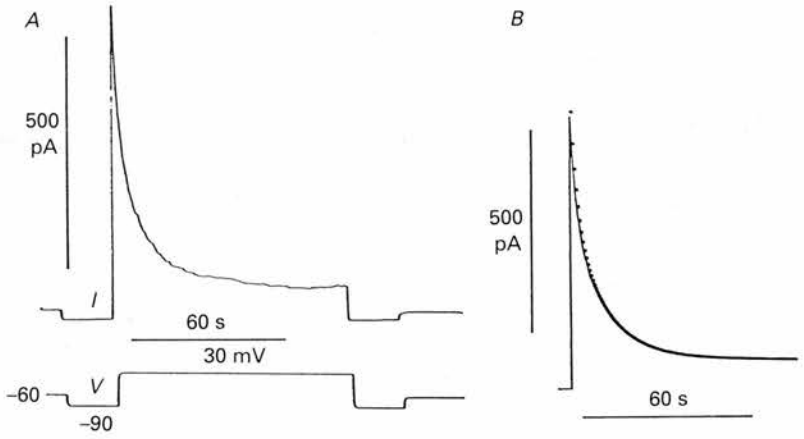


Fig. 11. Inactivation during prolonged depolarization. *A*, current (I) produced by 30 mV hyperpolarization followed by 120 mV depolarization (V). *B*, outward current compared with double exponential fit (t in s):

$$327\exp(-t/1{\cdot}8)+375\exp(-t/9{\cdot}9)+74\ pA.$$

The extracellular solution contained 5 mM- and the pipette 106 mM-potassium.

depolarization: in the experiment of Fig. 9, t_1 fell from 17 ms at 0 mV to 3·6 ms at +60 mV. For six cells which were depolarized to levels between −10 and +10 mV the value of t_1 was 18 ms (range 6–27 ms); for five cells depolarized to between +20 and +60 mV the mean value of t_1 was 8 ms (range 4–15 ms). Values for t_i ranged from about 0·5 to 2 s.

Tail current

The curves in Fig. 10*A* (inset) show fitted time courses of the tail current. As for the frog node of Ranvier (reviewed by Dubois, 1983) and the human T lymphocyte (Cahalan, Chandy, DeCoursey & Gupta, 1985, p. 215), the tail current was best described by the sum of two exponentially decaying components. A similar result was obtained in two other experiments.

Inactivation during prolonged depolarization

The inactivation of the outward current during prolonged depolarization was investigated in a series of experiments, illustrated in Fig. 11, in which a cell was first hyperpolarized to −90 mV, to remove inactivation, and then depolarized to different levels for a period of 90 s. The decline of the current could be fitted by the sum of two exponentially decaying components:

$$I(t) = a_f\exp(-t/t_f)+a_s\exp(-t/t_s), \tag{23}$$

with t_f around 1–2 s and t_s around 10 s; similar results were obtained from two other

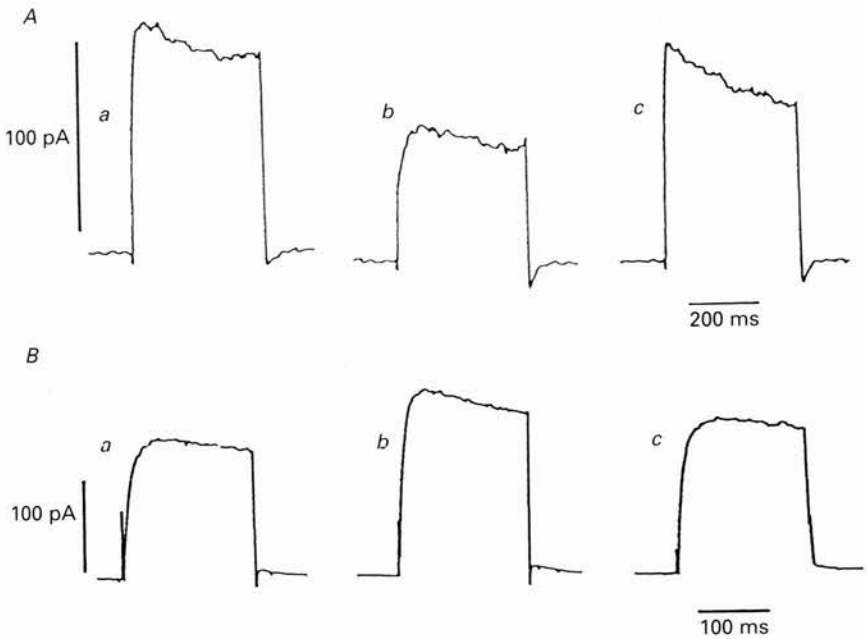


Fig. 12. Effect of calcium on currents. *A*, control responses (*a* and *c*) in 'calcium-free' solution (Table 1, solution B) and test response (*b*) in 2 mM-calcium (Table 1, solution A). *B*, a different cell, control responses (*a* and *c*) in 5 mM-calcium and test response (*b*) in 'calcium-free' solution. Both cells were held at −80 mV and depolarized to 0 mV.

TABLE 3. Inactivation of I_K during prolonged depolarization

Voltage jump	a_f(pA)	t_f(s)	a_s(pA)	t_s(s)
	Cell A			
−90 to −30	214	2·3	65	8·3
−90 to −10	227	1·6	171	7·1
−90 to 0	310	2·3	158	10
−90 to 30	327	1·8	375	9·9
	Cell B			
−60 to 30	423	1·7	236	10
	Cell C			
−60 to 30	485	1·5	325	7·9

cells. These values are within the range for inactivation time constants of delayed rectifier currents in other cells (see e.g. Rudy, 1988). Presumably the time constant, t_f, corresponds to the inactivation time constant, t_i, in eqn (22). Values for the amplitudes and time constants for three cells are shown in Table 3.

Effect of divalent cations

The possible existence of calcium-activated potassium currents was investigated by examining the effects of either adding or withdrawing calcium from the extracellular solution. As illustrated in Fig. 12, the presence of calcium reduced rather than enhanced the outward current. The inhibitory action of calcium was

shared by cobalt. Currents were reduced to between about 0·9 and 0·6 of their control values, in four experiments in which the calcium concentration was either 2 or 5 mM and three experiments with 4 mM-cobalt.

Actions of tetraethylammonium (TEA) and 4-aminopyridine (4-AP)

Although both TEA and 4-AP are known to block a variety of potassium channels, TEA is usually classified as a specific blocker of delayed rectifier potassium currents,

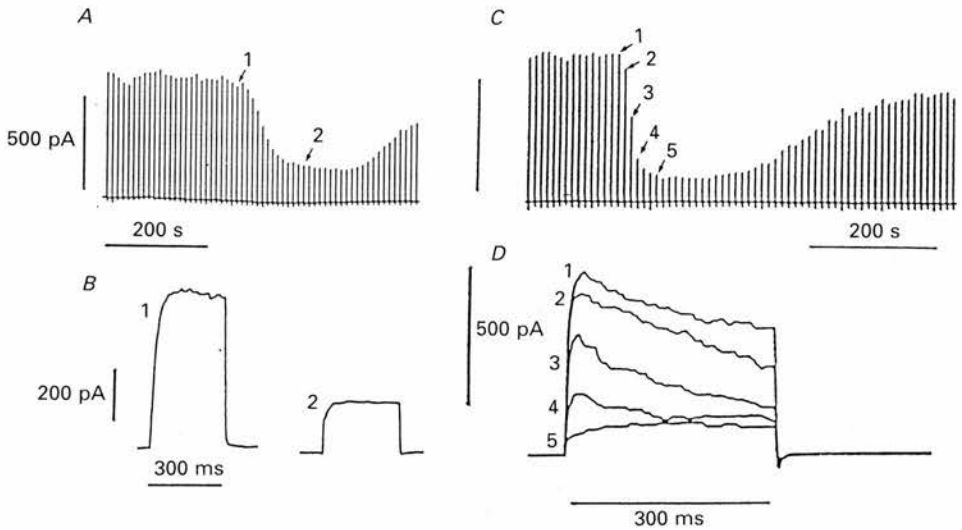


Fig. 13. Effects of TEA and 4-AP. *A*, TEA: responses, recorded on chart recorder, to 300 ms depolarization of 90 mV from holding potential of −70 mV followed by a hyperpolarization of 20 mV. TEA (10 mM) was added to perfusate (Table 1, solution A) at the beginning of record, and removed when outward current was reduced to its minimal value. *B*, individual outward currents at higher resolution, numbered as in *A*. Uncorrected records. *C*, 4-AP: responses, recorded on chart recorder, to 300 ms depolarization of 70 mV from holding potential of −60 mV, followed by an equal hyperpolarization. 4-AP (2 mM) was added to perfusate (Table 1, solution A) at the beginning of record, and removed when the outward current was reduced to its minimal value. *D*, individual outward currents at higher resolution, numbered as in *C*. Uncorrected records.

and 4-AP as a specific blocker of I_A's (see e.g. Cook, 1988). However, 4-AP has been found to block delayed rectifier currents in human T lymphocytes (DeCoursey, Chandy, Gupta & Cahalan, 1984), in mouse Schwann cells (Konishi, 1989) and in chick calcitonin cells (Kawa, 1988).

Both TEA and 4-AP were found to block the outward current in IMR-32 cells as illustrated in Fig. 13. The cells were successively depolarized, and 300 ms later, hyperpolarized, the sequence being repeated at intervals of 10 s. No effect was observed on the inward currents (which can just be seen as small deflections below the baseline with the low amplification used in Fig. 13) but the outward current was rapidly reduced by the addition of TEA to or 4-AP. Concentrations of TEA between

0·5 and 20 mM were investigated in six experiments. No effect was observed with 1 mM-TEA or less, but the results were not otherwise sufficiently consistent for quantitative analysis.

The action of 4-AP was examined in greater detail, as illustrated in Fig. 14. As first reported for the delayed rectifier current of the squid axon by Yeh, Oxford, Wu &

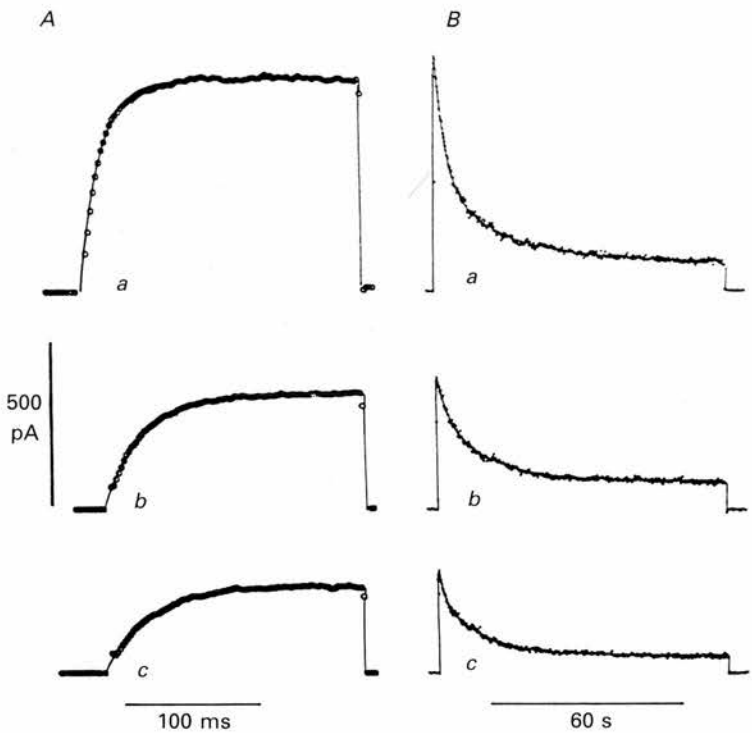


Fig. 14. Effect of 4-AP on activation and inactivation. Cell held at −60 mV and depolarized to 30 mV during either 200 ms (*A*) or 90 s (*B*) voltage jumps. Traces labelled *a* are responses in control solution (Table 1, solution A); traces labelled *b* and *c* are responses in 0·25 and 1 mM-4-AP respectively. In *A*, experimental values are shown at 2 ms intervals (omitting initial and final capacitative artifacts); fitted lines (t in ms):
for *a*, $695(1-\exp[(-t+1{\cdot}8)/14{\cdot}5])$ pA,
for *b*, $381(1-\exp[(-t+1{\cdot}8)/28{\cdot}7])$ pA,
for *c*, $289(1-\exp[(-t+2{\cdot}1)/33{\cdot}7])$ pA.
In *B*, fitted values at 1 s intervals are (t in s):
for *a*, $423\exp(-t/1{\cdot}7)+236\exp(-t/10)+87$ pA,
for *b*, $102\exp(-t/1{\cdot}7)+216\exp(-t/7{\cdot}1)+85$ pA,
for *c*, $95\exp(-t/0{\cdot}7)+191\exp(-t/10)+52$ pA.

Narahashi (1976), 4-AP can be seen to produce not only a concentration-dependent reduction in amplitude, of the outward current, but also a decrease in its activation rate. When the responses to prolonged depolarization were fitted according to eqn (23) (p. 137). It could be seen that the predominant effect of 4-AP was on the more rapidly inactivating component of the current. A summary of the effect of 4-AP on the amplitude of the outward current is given in Table 4.

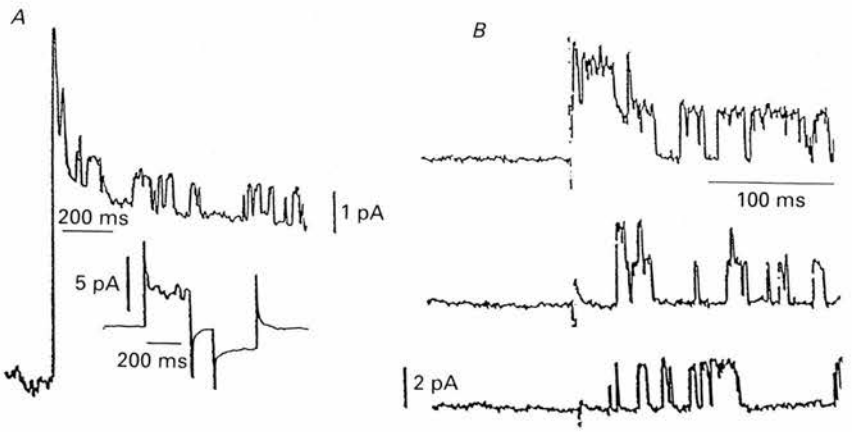


Fig. 15. Records of single-channel activity from cell-attached patches. *A*, uncorrected records from a patch held at resting potential and depolarized by 60 mV; shows responses to 60 mV depolarization (upward deflection) followed by 50 mV hyperpolarization at lower resolution. *B*, corrected records of outward currents from three different patches. In each case, the holding potential of patch was 20 mV hyperpolarized with respect to the resting potential; a depolarizing voltage-jump of 90 mV was then applied. Solution A (Table 1) was used in pipette and bath, but without tetrodotoxin. Records were filtered with an 8-pole Bessel filter, −3 dB at 1 kHz and sampled at intervals of 100 μs.

TABLE 4.

Concentration of 4-AP	Number of cells	Amplitude in 4-AP / Amplitude in control
0·25	5	0·58 ± 0·11 (S.E.M.)
1·0	6	0·40 ± 0·13 (S.E.M.)
4·0	1	0·32
10	1	0·32

Single-channel recording from cell-attached patches

Although a variety of different currents was seen (see e.g. Ginsborg *et al.* 1987), patches were usually quiescent when the trans-patch potential was equal to, or hyperpolarized with respect to the resting potential; when they were depolarized, patches displayed channel activity as shown in Fig. 15. The single-channel currents were of relatively large and uniform amplitude and it seemed appropriate to investigate their properties in greater detail.

Single-channel conductance

The single-channel conductance was determined by measuring single-channel currents activated by depolarizations to different levels. In the experiment illustrated in Fig. 16, the patch was hyperpolarized by 20 mV for several seconds before each period of depolarization by 50–90 mV. The slope conductance derived from Fig. 16*B* was 20 pS. Similar results were obtained from twenty different patches, the slope conductances falling within the range of 15–25 pS. Values within the same range

have been reported for a number of cells including the squid axon (17·5 pS originally observed by Conti & Neher, 1980, and 20 pS more recently by Llano, Webb & Bezanilla, 1988), murine N1E-115 neuroblastoma cells (20–25 pS, Misler & Falke, 1985), human (Decoursey *et al.* 1984) and murine lymphocytes (Lewis & Cahalan,

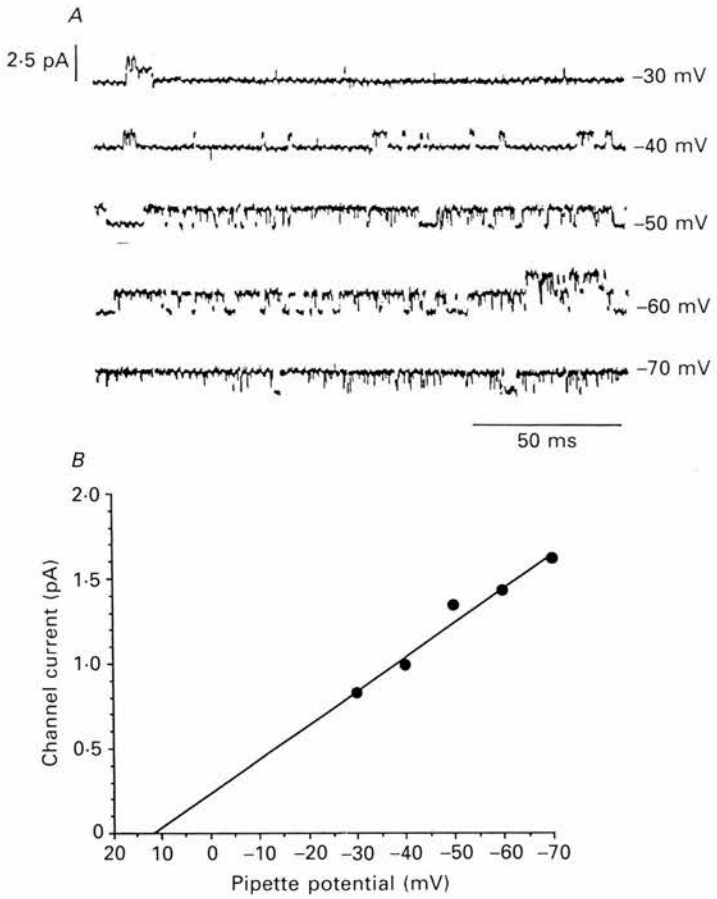


Fig. 16. Effect of membrane potential on single-channel currents. *A*, records are from the same patch which was first hyperpolarized by 20 mV for a few seconds and then depolarized by 50 mV to 90 mV, as indicated by values of final pipette potential given with each trace. *B*, plot of amplitude of channel current against pipette potential. Solution A (Table 1) was used in pipette and bath, but without tetrodotoxin. Records were filtered with an 8-pole Bessel filter, −3 dB at 1 kHz and sampled at intervals of 100 μs.

1988) (16–18 pS), *Xenopus* cultured spinal neurones (21 pS, Harris, Henderson & Spitzer, 1988, Fig. 3), cultured mouse peritoneal macrophages (16 pS, Ypey & Clapham, 1984), and cultured rat hippocampal neurones (15–20 pS, Rogawski, 1986). However, not all delayed rectifier channels have conductances close to 20 pS. Stansfeld & Feltz (1988) report values from 5 to 10 pS for dorsal root ganglion cells and Ypey, Ravesloot, Buisman & Nijweide (1988) values of the order of 100 pS for embryonic chick osteoblasts; (see Castle, Haylett & Jenkinson, 1989 for review).

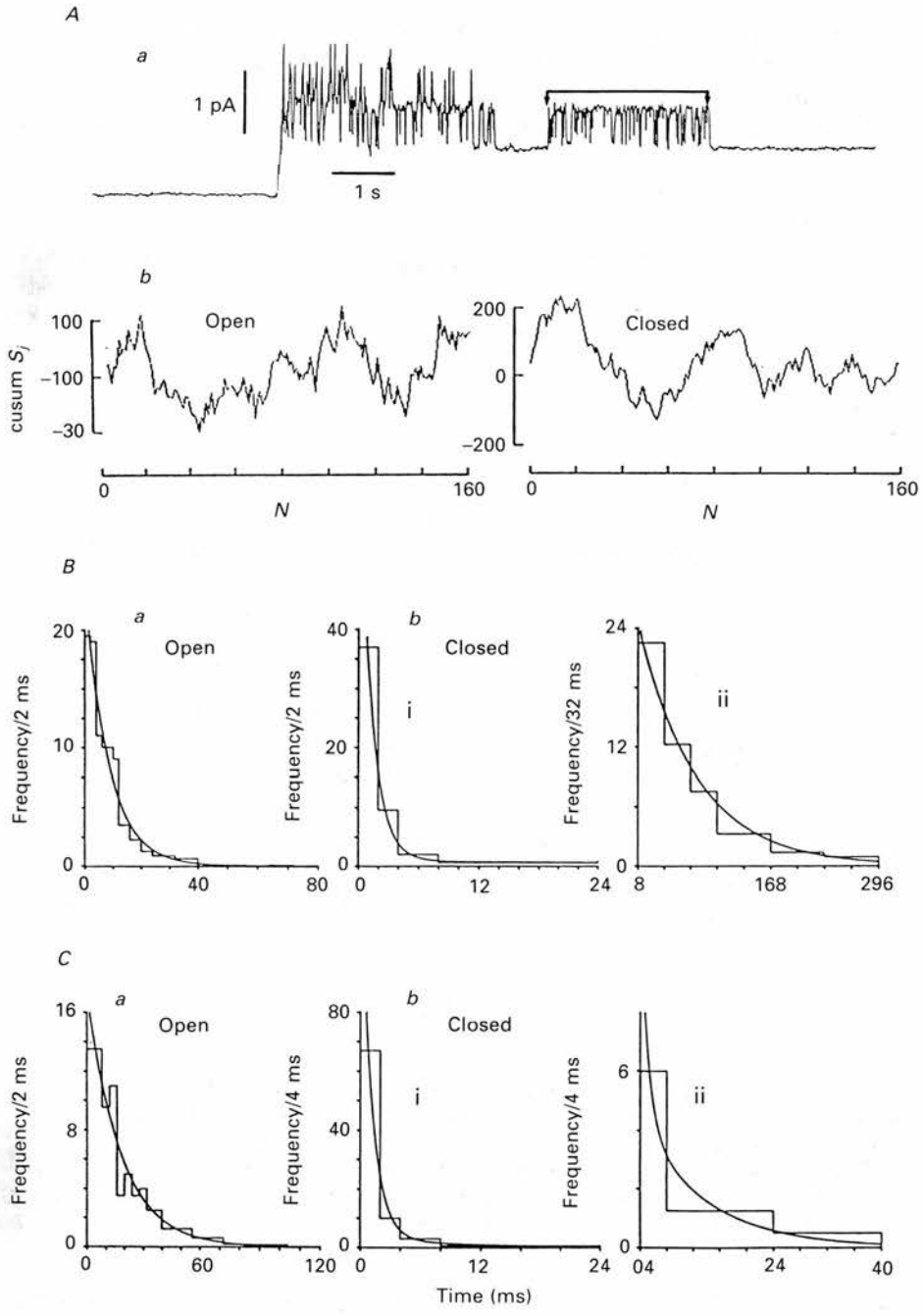


Fig. 17. Probability density functions of open and closed intervals (PDFs). *A*, selection of data: isolated cluster of single-channel activity (indicated by bar) tested for stationarity by cusum method (see text). Records were filtered with an 8-pole Bessel filter, −3 dB at 1 kHz and sampled at intervals of 100 μs. *B*, depolarizing voltage jump of 46 mV.

Kinetic analysis

When a patch was depolarized, and held at the depolarized level, single-channel behaviour which appeared to correspond to inactivation of whole-cell currents was observed. Thus the initial period of channel activity, which often contained simultaneous openings of several channels, was followed by alternate periods of 'silence' and of single openings. These were attributed to one and the same channel, for any given period, by analogy with the interpretation of the 'clusters of bursts' seen in patches of skeletal muscle endplates during desensitization by acetylcholine (Sakmann, Patlak & Neher, 1980). As illustrated in Fig. 17, this idea received some support from a cusum analysis (see Methods). A sample record is shown in Fig. 17*Aa* with the values of S_j (see eqn (1) plotted in Fig. 17*Ab* against N, the sequential number of either the opening (i) or closing (ii). It is immediately apparent that S_j does not deviate systematically from zero and the stationary behaviour of the events was confirmed by the significance test. Thus the probabilities of obtaining values of D_α (see eqn (3), for a random sequence, at least as large as those observed, for values of α of 9, 1 and 1/9, were 0·1, 0·93 and 1 for the open times, and 0·69, 1 and 0·94 for the closed times.

Probability density functions

The results from a patch depolarized by 46 and 82 mV were analysed in detail. Direct observations of the open probabilities for the 46 and 82 mV depolarizations were 0·26 and 0·89, respectively. The openings in response to the 46 mV depolarization were grouped into easily distinguishable bursts, the minimum interburst interval being 5 ms and the mean burst duration being 26 ms. From the PDFs illustrated in Fig. 17*B*, the mean values for the open times were 8·5 and 18 ms respectively for the 46 and 82 mV jumps (eqn (4), Methods). From the PDFs for the closed times (eqn (5), Methods) the values for a_s, τ_s, a_f and τ_f for the 46 and 82 mV jumps, were respectively: 0·41, 71 ms, 0·59 and 1·3 ms; 0·18, 9·9 ms, 0·82 and 1·1 ms. The predicted open probabilities (eqn (6), Methods) for the 46 and 82 mV jumps of 0·22 and 0·87 respectively are in reasonable agreement with those directly observed (0·26 and 0·89, see above). The predicted average burst duration for the 46 mV depolarization (eqn (17), Methods) of 22·6 ms is also in reasonable agreement with the directly observed value of 26 ms (see above).

A further test is provided by a comparison between the predicted and observed ratios of the steady (maximum) whole-cell currents, I_{max} say, evoked by stimuli corresponding to the 82 and 46 mV voltage jumps applied to the patch. If N is the total number of appropriate channels in the whole-cell membrane; g, the channel

---

a, histogram of open intervals in the range 0–80 ms with single exponential fit by maximum likelihood; time constant 8·5 ms. *b*, histograms of closed intervals in the ranges 0–24 ms (i) and 8–296 ms (ii); there was an additional interval of 593 ms. Superimposed fit (t in ms):

$$(0{\cdot}59/1{\cdot}26)\exp(-t/1{\cdot}26)+(0{\cdot}41/71{\cdot}4)\exp(-t/71{\cdot}4).$$

C, depolarizing voltage jump of 82 mV. *a*, histogram of open intervals in the range 0–120 ms; time constant, 18 ms. *b*, histograms of closed intervals in the ranges 0–24 ms (i) and 4–40 ms (ii). Superimposed fit (t in ms):

$$(0{\cdot}82/1{\cdot}13)\exp(-t/1{\cdot}13)+(0{\cdot}18/9{\cdot}9)\exp(-t/9{\cdot}9).$$

conductance; E_K, the potassium equilibrium potential; V, the potential to which the cell is depolarized; and $p_{1\infty}$, the equilibrium open probability at the potential V, then

$$I_{max} = Ngp_{1\infty}(V-E_K). \quad (24)$$

If the resting potential is taken as -40 mV and E_K as -70 mV, the predicted value of I_{max} (82)/I_{max} (46) is (0·87) (112)/(0·22) (76) = 5·8; if the resting potential is taken as -60 mV, the predicted ratio is 6·5. Experimentally, it was found that the whole-cell current ratio varied between 3·5 and 9 (three cells, see e.g. Fig. 7). Although the test is clearly not precise, the predictions and observations are not incompatible.

DISCUSSION

Sodium currents

The voltage-sensitive sodium currents evoked from the human neuroblastoma cell line IMR-32 are qualitatively similar to those that can be evoked from many other types of cell. The amplitudes are relatively small which partly reflects the small size of the cell, typically about 15 μm in diameter, and partly, presumably, a low channel density. Thus the maximum sodium conductance, that we have observed for the IMR-32 cell corresponds to about 2 mS/cm^2 which may be compared with values of 85 mS/cm^2 for the mouse neuroblastoma clone N1E-115 (Moolenaar & Spector, 1978) and 100 mS/cm^2 for rat sympathetic neurones (Belluzzi & Sacchi, 1986).

The method of estimating the time constants of activation and inactivation of the sodium current, τ_m and τ_h, allowed their determination over only a narrow voltage range and did not allow the separation of inactivation into slow and fast components. However, in so far as their values can be compared with other published results, τ_m and τ_h for IMR-32 neuroblastoma are within the range reported for other cells. Thus τ_m fell from 0·34 ms at -30 mV to 0·09 ms at 20 mV; the corresponding values for the rat sympathetic neurone, although at a slightly higher temperature, were 0·4 and 0·1 ms (Belluzzi & Sacchi, 1986). The value of τ_h for IMR-32 fell from 0·74 ms at -30 mV to 0·44 ms at $+20$ mV; the corresponding values for N1E-115, also estimated in a way which would not separate slow and fast inactivation, were 1 ms and 0·4 ms (Moolenaar & Spector, 1978).

Other features of activation and inactivation of the sodium current of IMR-32 cells are similar to those recently reported by Sah, Gibb & Gage (1988) for acutely dissociated hippocampal neurones. For both types of cell the maximum current occurs at a depolarization of -30 mV and with a time to peak, at this membrane potential, of about 1 ms. Also for both types of cell, about half the maximum conductance is inactivated at a holding potential around -80 mV and it requires depolarization to about -40 mV to activate half the available channels. The voltage sensitivity of activation is slightly greater for IMR-32 (k = 3·9 mV, eqn (18)) than for the hippocampal cells (k = 6·6 mV); for inactivation, the voltage sensitivities are almost identical.

Potassium currents

When depolarized, most cells generate a variety of outward potassium currents. These include transient voltage-dependent currents (I_A); a non-inactivating current (I_M); slowly inactivating voltage-dependent currents (I_K), and a number of different

calcium-dependent potassium currents. In the present investigation, it was found that the outward current of the undifferentiated IMR-32 cell was predominantly, if not exclusively, of the I_K variety (but see Gotti *et al.* 1987) as judged by the relatively depolarized holding potentials from which it could be evoked, by its slow rate of

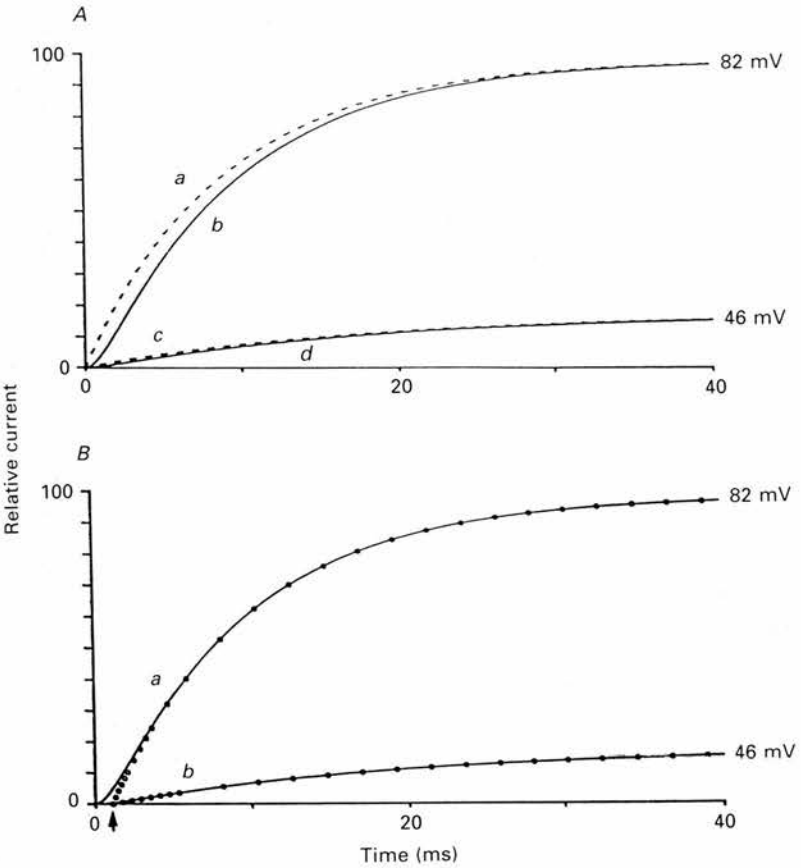


Fig. 18. Time course of rising phase of current predicted by PDFs according to the kinetic models COC and CCO. Ordinates are relative amplitudes of current. Upper curves correspond to a depolarizing jump of 82 mV and lower curves to 46 mV. In *A* the dashed lines correspond to the COC scheme. The continuous lines in both *A* and *B* correspond to CCO.
Aa (COC, 82 mV): $97{\cdot}4(1-0{\cdot}99\exp[-t/9{\cdot}0]-0{\cdot}01\exp[-t/1{\cdot}1])$.
Ab and *Ba* (CCO, 82 mV): $97{\cdot}4(1-1{\cdot}14\exp[-t/9{\cdot}0]+0{\cdot}14\exp[-t/1{\cdot}1])$.
Ac (COC, 46 mV): $16{\cdot}8(1-0{\cdot}99\exp[-t/17{\cdot}3]-0{\cdot}01\exp[-t/1{\cdot}2])$.
Ad and *Bb* (CCO, 46 mV): $16{\cdot}8(1-1{\cdot}07\exp[-t/17{\cdot}3]+0{\cdot}07\exp[-t/1{\cdot}2])$.
The circles in *Ba* correspond to $97{\cdot}4(1-\exp[(-t+1{\cdot}13)/9{\cdot}0])$, and in *Bb* to $16{\cdot}8(1-\exp[(-t+1{\cdot}18)/17{\cdot}3])$ (see text).

inactivation during prolonged depolarization, and by the effects of increasing the extracellular potassium concentration. It could be evoked in the virtual absence of calcium in the bathing solution and was thus not considered to be calcium dependent; it could be evoked in the virtual absence of anions and was therefore not

due to an influx of chloride ions. The absence of an inward current on hyperpolarization to −60 mV from a holding potential of −30 mV argues strongly against the existence of an I_M (see e.g. Brown, 1983, 1988) in IMR-32 cells.

Kinetic models

It seems highly likely that the '20 pS' channels described in the Results, which open on depolarization and have voltage-sensitive kinetics are those which underly the whole-cell currents. The kinetic models compatible with the single-channel PDFs presented in the Results, namely, closed ⇌ closed ⇌ open (C_2C_1O) and closed ⇌ open ⇌ closed (C_2OC_1) predict (eqns (12), (15) and (24); see legend for additional assumptions) the whole-cell currents illustrated in Fig. 18. It is clear that on account of the delayed rising phase of the current, the CCO model (continuous lines, Fig. 18*A*) provides a better fit to the observed form of the current. It is of further interest that, if the first few milliseconds are disregarded, the form of the empirical fit to the *observed* current (see eqn (21) $I(t) = I_{max}\{1-\exp[-(t-\delta t)/t_1]\}$, provides an excellent fit to the predicted currents (●, Fig. 18*B*) with values of δt (1·13 and 1·18, Fig. 18*B*) similar to those of the 'observed' delay terms (0·5–3·1 ms). Further qualitative support for the CCO model comes from the observation that two exponentially decaying components were required to describe the tail currents (see e.g. Fig. 10). The agreement between the experimental data and predictions based on the CCO model with the PDFs for the '20 pS' channels provides strong support for the idea that these channels underlie the whole-cell delayed rectifier current. As pointed out on p. 125, there was evidence for at least one extra term with time constant below 1 ms, corresponding to short-lived open and closed states that could not be properly resolved, in each of the PDFs. The additional terms to which they give rise will have very small time constants and would not affect the predictions based on the PDFs. Thus although the CCO model must be a simplification, it presumably represents an important part of the kinetic scheme (see e.g. Conti & Neher, 1980).

We thank Mr Greig Duncan and Miss Jackie O'Connell for preparing the cultures.

REFERENCES

Adams, P. R., Brown, D. A. & Constanti, A. (1982). M-Currents and other potassium currents in bullfrog sympathetic neurones. *Journal of Physiology* **330**, 537–572.

Belluzzi, O. & Sacchi, O. (1986). A quantitative description of the sodium current in the rat sympathetic neurone. *Journal of Physiology* **380**, 275–291.

Belluzzi, O., Sacchi, O. & Wanke, E. (1985*a*). A fast transient outward current in the rat sympathetic neurone studied under voltage-clamp conditions. *Journal of Physiology* **358**, 91–108.

Belluzzi, O., Sacchi, O. & Wanke, E. (1985*b*). Identification of delayed potassium and calcium currents in the rat sympathetic neurone under voltage clamp. *Journal of Physiology* **358**, 109–129.

Bezanilla, F. & Armstrong, C. M. (1977). Inactivation of the sodium channel I: sodium current experiments. *Journal of General Physiology* **70**, 549–566.

Brown, D. A. (1983). Slow cholinergic excitation – a mechanism for increasing neuronal excitability. *Trends in Neurosciences* **6**, 302–307.

Brown, D. A. (1988). M-Currents: an update. *Trends in Neurosciences* **11**, 294–299.

Cahalan, M. D., Chandy, K. G., DeCoursey, T. E. & Gupta, S. (1985). A voltage-gated potassium channel in human T lymphocytes. *Journal of Physiology* **358**, 197–237.

CARBONE, E., SHER, E. & CLEMENTI, F. (1990). Ca currents in human neuroblastoma IMR32 cells: kinetics, permeability and pharmacology. *Pflügers Archiv* **416**, 170–179.

CASTLE, N. A., HAYLETT, D. G. & JENKINSON, D. H. (1989). Toxins in the characterization of potassium channels. *Trends in Neurosciences* **12**, 59–65.

CLEMENTI, F., CABRINI, D., GOTTI, C. & SHER, E. (1986). Pharmacological characterization of cholinergic receptors in a human neuroblastoma cell line. *Journal of Neurochemistry* **47**, 291–297.

COLQUHOUN, D. & HAWKES, A. G. (1977). Relaxation and fluctuations of membrane currents that flow through drug-operated channels. *Proceedings of the Royal Society* B **199**, 231–262.

COLQUHOUN, D. & HAWKES, A. G. (1981). On the stochastic properties of single ion channels. *Proceedings of the Royal Society* B **211**, 205–235.

COLQUHOUN, D. & HAWKES, A. G. (1982). On the stochastic properties of bursts of single ion channel openings and clusters of bursts. *Philosophical Transactions of the Royal Society* B **300**, 1–59.

COLQUHOUN, D. & SIGWORTH, F. J. (1983). Fitting and statistical analysis of single-channel records. In *Single Channel Recording*, ed. SAKMANN, B. & NEHER, E., pp. 191–263. Plenum Press, New York and London.

CONNOR, J. A. & STEVENS, C. F. (1971). Voltage-clamp studies of a transient outward membrane current in gastropod neural somata. *Journal of Physiology* **213**, 21–30.

CONTI, F. & NEHER, E. (1980). Single channel recordings of K^+ currents in squid axons. *Nature* **285**, 140–143.

COOK, N. S. (1988). The pharmacology of potassium channels and their therapeutic potential. *Trends in Pharmacological Sciences* **9**, 21–28.

DECOURSEY, T. E., CHANDY, K. G., GUPTA, S. & CAHALAN, M. D. (1984). Voltage-gated K^+ channels in human T lymphocytes: a role in mitogenesis? *Nature* **307**, 465–468.

DUBOIS, J. M. (1981*a*). Simultaneous changes in the equilibrium potential and potassium conductance in voltage clamped Ranvier node in the frog. *Journal of Physiology* **318**, 279–295.

DUBOIS, J. M. (1981*b*). Evidence for existence of three types of potassium channels in the frog Ranvier node membrane. *Journal of Physiology* **318**, 297–316.

DUBOIS, J. M. (1983). Potassium currents in the frog node of ranvier. *Progress in Biophysics and Molecular Biology* **42**, 1–20.

GINSBORG, B. L., MARTIN, R. J. & PATMORE, L. (1987). On the electrical properties of a human neuroblastoma cell-line (IMR-32). *Journal of Physiology* **386**, 111*P*.

GLASEBY, C. A. & MARTIN, R. J. (1986). Exploratory and confirmatory plots of single-channel records. *Journal of Neuroscience Methods* **16**, 239–249.

GOTTI, C., SHER, E., CABRINI, D., BONDIOLOTTI, G., WANKE, E., MANCINELLI, E. & CLEMENTI, F. (1987). Cholinergic receptors, ion channels, neurotransmitter synthesis, and neurite outgrowth are independently regulated during the in vitro differentiation of a human neuroblastoma cell line. *Differentiation* **34**, 144–155.

GUPTA, M., NOTTER, M. D., FELTON, S. & GASH, D. M. (1985). Differentiation characteristics of human neuroblastoma cells in the presence of growth modulators and antimitotic drugs. *Developmental Brain Research* **19**, 21–29.

GUSTAFSSON, B., GALVAN, M., GRAFE, P. & WIGSTROM, H. (1982). A transient outward current in a mammalian central neurone blocked by 4-aminopyridine. *Nature* **299**, 252–254.

HAMILL, O. P., MARTY, A., NEHER, E., SAKMANN, B. & SIGWORTH, F. J. (1981). Improved patch-clamp techniques for high-resolution current recording from cells and cell-free membrane patches. *Pflügers Archiv* **391**, 85–100.

HARRIS, G. L., HENDERSON, L. P. & SPITZER, N. C. (1988). Changes in densities and kinetics of delayed rectifier potassium channels during neuronal differentiation. *Neuron* **1**, 739–750.

HILLE, B. (1984). Classical biophysics of the squid giant axon. *Ionic Channels of Excitable Membranes*, pp. 23–57. Sinauer Associates Inc., Sunderland, MA.

HODGKIN, A. L. & HUXLEY, A. F. (1952). A quantitative description of membrane current and its application to conduction and excitation in nerve. *Journal of Physiology* **117**, 500–544.

KAWA, K. (1988). Voltage-gated sodium and potassium currents and their variation in calcitonin-secreting cells of the chick. *Journal of Physiology* **399**, 93–113.

KONISHI, T. (1989). Voltage-dependent potassium channels in mouse Schwann cells. *Journal of Physiology* **411**, 115–130.

KOSTYUK, P. G., VESELOVSKY, N. S., FEDULOVA, S. A. & TSYNDRENKO, A. Y. (1981). Ionic currents in the somatic membrane of rat dorsal root ganglion neurons. III. Potassium currents. *Neuroscience* **6**, 2439–2445.

LEWIS, R. S. & CAHALAN, M. D. (1988). Subset-specific expression of potassium channels in developing murine T lymphocytes. *Science* **239**, 771–775.

LLANO, I., WEBB, C. K. & BEZANILLA, F. (1988). Potassium conductance of the squid giant axon. Single-channel studies. *Journal of General Physiology* **92**, 179–196.

MARTY, A. & NEHER, E. (1985). Potassium channels in cultured bovine adrenal chromaffin cells. *Journal of Physiology* **367**, 117–141.

MILLER, D. J. & SMITH, G. L. (1984). EGTA purity and the buffering of calcium ions in physiological solutions. *American Journal of Physiology* **246**, C160–166.

MISLER, S. & FALKE, L. (1985). Single 'delayed rectifier' potassium channel currents in neuroblastoma. *Biophysical Journal* **47**, 146a.

MOOLENAAR, W. H. & SPECTOR, I. (1978). Ionic currents in cultured mouse neuroblastoma cells under voltage-clamp conditions. *Journal of Physiology* **278**, 265–286.

NEHER, E. (1971). Two fast transient current components during voltage clamp on snail neurones. *Journal of General Physiology* **58**, 36–53.

ROGAWSKI, M. A. (1986). Single voltage-dependent potassium channels in cultured rat hippocampal neurons. *Journal of Neurophysiology* **56**, 481–493.

RUDY, B. (1988). Diversity and ubiquity of K channels. *Neuroscience* **25**, 729–749.

SAH, P., GIBB, A. J. & GAGE, P. W. (1988). Potassium current activated by depolarization of dissociated neurons from isolated hippocampal neurons. *Journal of General Physiology* **92**, 263–278.

SAKMANN, B., PATLAK, J. & NEHER, E. (1980). Single acetylcholine-activated channels show burst kinetics in the presence of desensitizing concentrations of agonist. *Nature* **286**, 71–73.

SAKMANN, B. & TRUBE, G. (1984). Conductance properties of single inwardly rectifying potassium channels in ventricular cells from guinea-pig heart. *Journal of Physiology* **347**, 641–657.

SHER, E., GOTTI, C., PANDIELLA, A., MADEDDU, L. & CLEMENTI, F. (1988). Intracellular calcium homeostasis in a human neuroblastoma cell line: modulation by depolarization, cholinergic receptors, and α-latrotoxin. *Journal of Neurochemistry* **50**, 1708–1713.

STANSFELD, C. & FELTZ, A. (1988). Dendrotoxin-sensitive K^+ channels in dorsal root ganglion cells. *Neuroscience Letters* **93**, 49–55.

TUMILOWICZ, J. J., NICHOLS, W. W., CHOLEN, J. J. & GREENE, A. E. (1970). Definition of a continuous human cell line derived from neuroblastoma. *Cancer Research* **30**, 2110–2118.

YEH, J. Z., OXFORD, G. S., WU, C. H. & NARAHASHI, T. (1976). Dynamics of aminopyridine block of potassium channels in squid axon membrane. *Journal of General Physiology* **68**, 519–535.

YPEY, D. L. & CLAPHAM, D. E. (1984). Development of a delayed outward-rectifying K^+ conductance in cultured mouse peritoneal macrophages. *Proceedings of the National Academy of Sciences of the USA* **81**, 3083–3087.

YPEY, D. L., RAVESLOOT, J. H., BUISMAN, H. P. & NIJWEIDE, P. J. (1988). Voltage-activated ionic channels and conductances in embryonic chick osteoblast cultures. *Journal of Membrane Biology* **101**, 141–150.

an obvious change in either activation kinetics or leak conductance.

In inside-out patches the unitary currents of 7 pS were reversibly blocked by Ca^{2+} with an IC_{50} of around 67 nM and a Hill slope of 1·5. No change in unitary conductance, or open times occurred, but long shut intervals increased. The rat EAG channel thus responds to 10–200 nM cytosolic Ca^{2+}. Channel blockade by Ca^{2+} suggests a mechanism which could, in neurones, reinforce excitation during the twin stimuli of membrane depolarization and intracellular Ca^{2+} elevation.

We are indebted to Professor D. Colquhoun (UCL, London) for advice, and help with computer software. The work was supported by grants from the Deutsche Forschungsgemeinschaft and the Wellcome Trust (to C.E.S.).

REFERENCES

Ludwig, J., Terlau, H., Wunder, F., Brüggemann, A., Pardo, L.A., Marquardt, A., Stühmer, W. & Pongs, O. (1994). *EMBO J.* **13**, 4451–4458.

Warmke, J.W., Drysdale R. & Ganetzky, B. (1991). *Science* **252**, 1560–1562.

Effects of temperature and cytoplasmic disruption on whole-cell membrane currents of rat bone marrow-derived mast cells

P.B. Hill, R.J. Martin and H.R.P. Miller

Departments of Preclinical Veterinary Sciences and Veterinary Clinical Studies, R(D)SVS, University of Edinburgh, Edinburgh EH9 1QH

In recent studies, rat mucosal type mast cells were shown to possess only a K^+-selective inwardly rectifying current (IR_K) with conventional whole-cell patch clamp techniques at room temperature (Lindau & Fernandez, 1986; McCloskey & Qian, 1994). To determine if these results were influenced by recording conditions, we compared whole-cell membrane currents obtained from rat bone marrow-derived mast cells (BMMCs) at various temperatures using the amphotericin B perforated-patch and conventional whole-cell voltage clamp techniques. Voltage steps were applied from −100 to +40 mV from a holding potential of −40 mV. Pipette solutions contained (mM): 137 KCl, 2·7 NaCl, 1 $CaCl_2$, 3 $MgCl_2$ and 10 Hepes, pH 7·3 (perforated patch) and 137 KCl, 2·7 NaCl, 0·1 $CaCl_2$, 1 $MgCl_2$, 10 Hepes and 1 EGTA, pH 7·3 (conventional whole-cell). The extracellular solution contained (mM): 137 NaCl, 2·7 KCl, 2 $CaCl_2$, 5 $MgCl_2$, 10 Hepes and 5·6 glucose, pH 7·3. Bath temperature was varied between room temperature (16–20 °C) and 37 °C with a Peltier device.

The IR_K current was present in rat BMMCs at all temperatures with both recording techniques. In contrast, an outwardly rectifying (OR) current at potentials more positive than −30 mV was only observed with the perforated patch method or if the bath temperature was increased to > 25 °C (Table 1). Lowering the extracellular Cl^- concentration to 50 mM reduced the conductance of the OR current from 2·7 ± 2·1 to 0·51 ± 0·53 nS (mean ± S.D., $n = 5$) and shifted its reversal potential by +31 ± 21 mV (mean ± S.D., $n = 5$). The chloride channel blocker DIDS decreased the OR current conductance from 2·7 ± 2·2 to 1·1 ± 1·5 nS (mean ± S.D., $n = 5$), also indicating that the OR current was carried by Cl^- ions.

Table 1. Percentage of BMMCs showing the OR current under various experimental conditions

	16–20 °C	25–37 °C
Cytoplasm disrupted: conventional WCR	0% ($n = 30$)	40% ($n = 5$)
Cytoplasm preserved: perforated patch	26% ($n = 91$)	68% ($n = 59$)

WCR, whole-cell recording.

The results indicate that detection of certain whole-cell currents depends upon experimental methodology. The effect of temperature and cytoplasmic disruption suggests that the OR_{Cl} current is dependent on a cytoplasmic messenger but it does not require stimulation of the cell with secretagogues for its activation. Activation of the current by depolarization suggests that it may contribute to the repolarization of the membrane potential that occurs following stimulation of mast cells with antigen, thus allowing sustained Ca^{2+} entry essential for exocytosis.

Supported by the Wellcome Trust.

REFERENCES

Lindau, M. & Fernandez, J.M. (1986). *J. Gen. Physiol.* **88**, 349–368.
McCloskey, M.A. & Qian, Y.X. (1994). *J. Biol. Chem.* **269**, 14813–14819.

Electrophysiological properties of human eosinophils

M. Tare, D.V. Gordienko, S. Parveen, C. Fenech, C. Robinson and T.B. Bolton

Department of Pharmacology and Clinical Pharmacology, St George's Hospital Medical School, Cranmer Terrace, London SW17 0RE

Despite intense interest in the biology of eosinophils and their putative roles in host defence, there is little information about how changes in the cell membrane electrical properties may influence their behaviour. In this study, the basic electrophysiological properties of freshly prepared human eosinophils were investigated.

Normodense eosinophils were prepared as described previously (Gordienko *et al.* 1995). Conventional whole-cell patch clamp technique was used to measure membrane potential, to estimate the passive electrical properties and to characterize whole-cell currents. After the cells were placed on glass coverslips they were superfused with standard

stine of experimentally infected pigs, slaughtered mainly 28 days post-infection. Muscle-flap preparations were made using a micro-scalpel and fine pins, and muscle cells prepared for cell-attached patch recordings of levamisole-activated currents (for method, see Robertson & Martin, 1993).

Our results from eight patches showed that levamisole activates a cation-selective channel (Fig. 1) with conductances between 36 and 46 pS and mean open times at −75 mV between 1·3 and 3·2 ms in levamisole-sensitive *O. dentatum*.

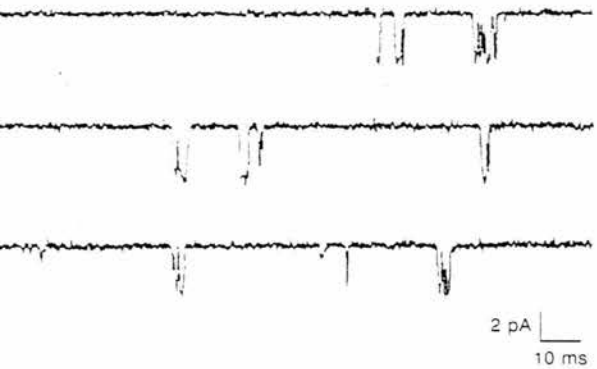


Fig. 1. Levamisole-activated channels. Vesicle-attached patch. Openings downwards. Patch-potential −75 mV, 10 μM levamisole in pipette. Main state −3·07 pA. Filter, −3 dB, 1·5 kHz, 8-pole Bessel.

Supported by the Wellcome Trust.

REFERENCES

rn, H., Roepstorff, A., Waller, P.J. & Nansen, P. (1991). *Vet. Parasitol.* **37**, 21–30.
ertson, S.J. & Martin, R.J. (1993). *Br. J. Pharmac.* **108**, 170–178.

comparison of whole-cell currents in isolated ucosal and connective tissue rat mast cells

. Hill, R.J. Martin and H.R.P. Miller

partments of Preclinical Veterinary Sciences and erinary Clinical Studies, R(D)SVS, University of inburgh, Edinburgh EH9 1QH

Subpopulations of mast cells with distinct biochemical and actional characteristics have been identified in rodents and n. Based on their anatomical locations, these cells are ignated mucosal mast cells or connective tissue mast cells l differ in terms of protease content, proteoglycan ntent, and response to secretagogues. Previous studies re shown that this heterogeneity also extends to their ctrophysiological properties: mucosal-type mast cells ssessed only a K^+-selective inwardly rectifying current (McCloskey & Qian, 1994), whereas connective tissue mast cells did not appear to have whole-cell currents unless stimulated with secretagogues or second messengers (Matthews *et al.* 1989). We recorded whole-cell currents in fifty-six rat bone marrow-derived mast cells (mucosal phenotype) and fifty-four rat peritoneal mast cells (connective tissue phenotype) using the amphotericin B perforated patch technique. Voltage steps were applied from −140 to +100 mV from a holding potential of −40 mV. The pipette solution contained (mM): 137 KCH_3SO_4 or KCl, 2·7 NaCl, 1 $CaCl_2$, 3 $MgCl_2$ and 10 Hepes; pH 7·3. The extracellular solution contained (mM): 137 NaCl, 2·7 KCl, 2 $CaCl_2$, 5 $MgCl_2$, 10 Hepes and 5·6 glucose; pH 7·3. Bath temperature was varied between room temperature (16–20 °C) and 37 °C with a Peltier device.

As previously reported, only the mucosal-type mast cells exhibited an inwardly rectifying K^+ current. However, in contrast to previous studies, we found that an outwardly rectifying chloride current could be demonstrated in both cell types. Important features of the current were: (1) activation at potentials more positive than −30 mV; (2) reduction in current amplitude and chloride conductance when the extracellular Cl^- concentration was reduced to 16·7 mM by substituting Na^+-isethionate for NaCl; (3) reversible blockade by the chloride channel blocker DIDS (20 μM); (4) dependence on temperature – the current could be elicited in a significant proportion of cells by increasing the bath temperature to > 25 °C; (5) dependence on a cytoplasmic component – the current was rarely observed when currents were recorded using the conventional whole-cell voltage clamp technique; (6) the current was more commonly observed and was greater in magnitude when peritoneal mast cells were incubated overnight in the presence of 10 ng ml^{-1} stem cell factor, an important survival factor for connective tissue mast cells; (7) the current could also be activated by a 33% decrease in extracellular osmolality.

The results show that an outwardly rectifying chloride conductance can be observed in both mucosal and connective tissue-type mast cells without stimulating the cells with secretagogues or intracellular second messengers. This current could help to maintain a negative membrane potential when mast cells degranulate, and may play a role in volume regulation.

Supported by the Wellcome Trust.

REFERENCES

McCloskey, M.A. & Qian, Y.X. (1994). *J. Biol. Chem.* **269**, 14813–14819.
Matthews, G., Neher, E. & Penner, R. (1989). *J. Physiol.* **418**, 131–144.

Pflügers Arch – Eur J Physiol (1996) 432:986–994
© Springer-Verlag 1996

ORIGINAL ARTICLE

P. B. Hill · R. J. Martin · H. R. P. Miller

Characterization of whole-cell currents in mucosal and connective tissue rat mast cells using amphotericin-B-perforated patches and temperature control

Received: 10 May 1996 / Received after revision: 4 July 1996 / Accepted: 8 July 1996

Abstract Rat mucosal type mast cells are thought to possess only a K^+-selective inwardly rectifying (IR_K) current in the resting state. We used rat-bone-marrow-derived mast cells (BMMCs) as a model of mucosal mast cells and recorded whole-cell membrane currents from cells perforated with amphotericin B. Under these conditions, both inwardly rectifying (IR) and outwardly rectifying (OR) currents were observed. The reversal potential and conductance of the IR current depended on the extracellular K^+ concentration, indicating that the channel was K^+ selective. The OR current was not affected by changes in extracellular K^+ concentration, but lowering extracellular Cl^- concentration reduced the conductance and shifted the reversal potential in a positive direction. The OR current was not affected by K^+ channel blockers, but was reversibly blocked by the chloride channel blocker 4,4'-diisothiocyanato-2,2'-stilbenedisulphonate (DIDS), again indicating a Cl^- conductance. The IR_K current was also detected in the majority of cells using the conventional whole-cell recording configuration at room temperature. In contrast, the OR_{Cl} current was only observed in 7% of recordings made at room temperature with the conventional whole-cell voltage-clamp mode, but was detected in 66% of cells if the bath temperature was increased and the integrity of the cell's cytoplasm was preserved by using the perforated-patch technique. Under similar conditions, the OR_{Cl} current was also present in rat peritoneal mast cells, a connective tissue phenotype previously thought to have no whole-cell currents in the resting state. The role of this current and factors affecting its activation are discussed.

P. B. Hill (✉) · R. J. Martin
Department of Preclinical Veterinary Sciences,
Royal (Dick) School of Veterinary Studies,
The University of Edinburgh,
Summerhall, Edinburgh, EH9 1QH, Scotland

H. R. P. Miller
Department of Veterinary Clinical Studies,
Royal (Dick) School of Veterinary Studies,
The University of Edinburgh, Scotland

Key words Mast cells · Whole-cell currents · K^+ channels · Cl^- channels · Inward rectifier

Introduction

Recent electrophysiological studies have suggested that mast cells can possess two types of ion channel that regulate the resting membrane potential: an inwardly rectifying K^+ (IR_K) current [18, 22, 28] and an outwardly rectifying Cl^- (OR_{Cl}) current [14]. The presence or absence of these currents depended on the phenotype of the mast cell (connective tissue or mucosal), and on the species from which the cells were derived. In mouse bone-marrow-derived mast cells (BMMCs), which can differentiate into different phenotypes, both currents were observed either concurrently or individually [14]. Rat BMMCs [22] and RBL-2H3 cells [18, 28], both mucosal phenotypes, only possessed the IR_K current in the resting state. In contrast, neither the IR_K nor the OR_{Cl} currents were present in resting rat peritoneal mast cells, an example of the connective tissue type [18, 22].

Other membrane currents have been described to occur in rat mast cells but only when various second messengers were included in the pipette solution or when the cell was stimulated with secretagogues. These messenger or ligand-activated channels include: Ca^{2+}-permeable channels [13, 20]; cation-selective channels [3, 13, 20]; outwardly rectifying K^+ channels [22, 28]; and outwardly rectifying chloride channels [2, 21, 27, 30]. These channels have been implicated in the process of degranulation, because their activity was only detectable following stimulation of the cells and not in the resting state.

The conventional whole-cell recording configuration, as used in the previous studies, causes dialysis of the intracellular milieu and loss of many cytoplasmic components including solutes and messengers [10, 26]; in addition the above-described experiments were performed at room temperature. To determine if these factors influenced the electrophysiological properties of mast cells, we measured whole-cell currents of mucosal and con-

nective tissue type rat mast cells at various temperatures using the amphotericin-B-perforated-patch technique. We report that an outwardly rectifying chloride current, previously described to occur only in rat mast cells stimulated with secretagogues, is present in both mucosal and connective tissue type mast cells in the resting state.

Materials and methods

Cell preparation

Male Wistar rats between 175 g and 200 g (Moredun Research Institute, Edinburgh, UK) were exsanguinated whilst deeply anasthetized with halothane and used as donors of bone marrow, peritoneal cells and for preparation of lymph node conditioned medium (LNCM). The preparation of bone-marrow-derived cultured mast cells and the production of LNCM have been described [6]. Briefly, femoral bone marrow cells from healthy rats were cultured at 2.5×10^5 to 5×10^5 cells/ml in Iscove's Modified Dulbecco's Medium (IMDM, Gibco-BRL, Paisley, UK) supplemented with 20% horse serum (Advanced Protein Products, Brierley Hill, UK), penicillin (100 IU/ml), and streptomycin (100 µg/ml). The cells were stimulated with batch-tested LNCM at 10–25% v/v, and re-fed every 2–5 days. The percentage of mast cells was determined by differential counts (400 cells) of Leishman's-stained cytocentrifuge preparations. Mature cultures (n = 12) ranging in age from 13 to 37 days and each containing more than 85% mast cells were used for these experiments, with consistent results. Cells taken at this stage of culture can be regarded as mature as judged by the degree of cytoplasmic granularity and in their content of the mucosal mast-cell-specific protease, rat mast cell protease-II [8].

Peritoneal mast cells were collected by peritoneal lavage with Hanks Balanced Salt Solution (HBSS) containing 2% fetal calf serum (FCS), penicillin/streptomycin and 10 units/ml heparin. Cells were washed twice, re-suspended in 30% Percoll and layered on top of a two-stage Percoll density step gradient consisting of 4 ml of 1.09 g/ml over 2 ml of 1.1 g/ml. After centrifugation at 500 g for 20 min, a pellet containing >95% mast cells was obtained. The cells were washed three times in HBSS and re-suspended at a concentration of 2×10^5 to 4×10^5 cells/ml in RPMI medium (Gibco-BRL) containing 10% FCS. Peritoneal mast cells were either used on the day of collection, or were incubated for 24–48 h in the presence or absence of 10 ng/ml recombinant rat stem cell factor ($rrSCF^{164}$), an important mast cell survival, growth and differentiation factor [5].

Solutions and reagents

For amphotericin-B-perforated-patch recording, the pipette solutions contained (in mM): 137 KCl or KCH_3SO_4, 2.7 NaCl, 1 $CaCl_2$, 3 $MgCl_2$, 10 HEPES (pH 7.3) and for conventional whole-cell recording (in mM): 137 KCl or KCH_3SO_4, 2.7 NaCl, 0.1 $CaCl_2$, 1 $MgCl_2$, 10 HEPES, 1 EGTA (pH 7.3). Mast cell Ringer was used as the extracellular solution and contained (in mM): 137 NaCl, 2.7 KCl, 2 $CaCl_2$, 5 $MgCl_2$, 10 HEPES, 5.6 glucose (pH 7.3). In some experiments, NaCl was replaced with KCl to make extracellular solutions containing 10, 50, 90, 137 or 165 mM KCl. Low Cl^- solutions containing 51 and 14 mM Cl^- were made by substituting Na acetate and K acetate for NaCl and KCl respectively, and a low Cl^- solution containing 16.7 mM Cl^- was prepared by substituting Na-isethionate for NaCl. Amphotericin B was obtained from Calbiochem, UK, and the channel blockers 4,4'-diisothiocyanato-2,2'-stilbenedisulphonate (DIDS), 4-aminopyridine, and tetraethylammonium chloride (TEA) were obtained from Sigma, Poole, UK. $rrSCF^{164}$ was kindly provided by Dr. Keith Langley of Amgen, Thousands Oak, Calif., USA.

Whole-cell recordings

For electrophysiological recording, mast cells were re-suspended in mast cell Ringer, plated onto glass coverslips, and incubated at 37°C for up to 7 h before being placed in the recording chamber. Both mast cell phenotypes adhered to untreated glass without need for further immobilization. Any contaminating macrophages in the preparations could be discerned by their large size and lack of cytoplasmic granularity. Perforated-patch recordings were performed using amphotericin B to permeabilize the membrane as described elsewhere [29]. Briefly, 2 µl of a 50 mg/ml stock solution of amphotericin B in dimethylsulphoxide (DMSO) (Sigma) was added to 0.5 ml of pipette solution to yield a final concentration of 200 µg/ml. Sylgard-coated pipettes were heat polished to resistances between 0.5 and 2.5 MΩ and their tips were filled to ≈150 µm with pipette solution free of amphotericin B. Pipettes were then back filled with the amphotericin B/pipette solution before being used immediately to obtain a gigaohm seal. Perforation of the membrane patch, as revealed by the appearance of slow capacitance transients, occurred within 5–25 min and recordings were only made when the access resistance fell to less than 25 MΩ. Capacitance transients were cancelled using capacitive cancellation circuitry on the amplifier which yielded the whole-cell capacitance and access resistance. Conventional whole-cell voltage-clamp recordings were performed as described [7], and the results were compared to those obtained with the perforated-patch technique.

Whole-cell voltage-clamp recording (in both configurations) was performed with a patch-clamp amplifier (EPC-7, List). The reference electrode was an Ag-AgCl wire which, in ion substitution experiments, was connected to the bath solution through an agar bridge containing 150 mM KCl. In control experiments, junctional potentials that developed at this interface were less than 1 mV and no corrections were made. When the KCl in the pipette solutions was replaced with KCH_3SO_4, large junctional potentials developed at the pipette solution/pipette electrode interface. These could not be cancelled using the pipette offset potential circuitry on the amplifier. To overcome this problem, a fine open-ended plastic tube containing 150 mM KCl in 5% agar was placed over the pipette electrode which acted as an agar bridge between the electrode and the pipette solution (modified from [1]). The zero-current potential before formation of the gigaohm seal was set to 0 mV. Voltage pulses of 200 ms duration were applied every second from –100 mV to +40 mV in 10-mV steps from the holding potential of –40 mV. In some experiments, this protocol was extended from –140 mV to +100 mV to accentuate the currents (see Results and legends). The voltage pulses and membrane currents were stored digitally on video tape and on a continuous pen recording. Currents were filtered at 2 kHz by an 8-pole Bessel filter, digitized with an analogue–digital converter (CED 1401, Cambridge, UK), and stored with the voltage pulses on a personal computer for later analysis. Current/voltage (I/V) relationships were generated and analysed with the CED voltage-clamp software in which currents were sampled at 1 kHz and averaged over a 20-ms period. In most cases, the currents were sampled in the middle of the 200-ms pulse. However, if there was evidence of time-dependent inactivation, the currents were sampled in the region of the peak. Leak currents determined from the linear range of the I/V curve were subtracted before calculating slope conductances using a least squares fit to data points between –140 mV to –100 mV and +80 mV to +100 mV. Due to the magnitude of inward currents in high-K^+ buffers, conductances in these conditions were calculated in the range –100 mV to –80 mV.

Bath temperature was varied between room temperature (16–20°C) and 37°C with a Peltier device (Firbank Electronics, UK). We found that, at 37°C, the stability of the pipette-membrane seal was unreliable, often resulting in breakdown of the preparation. We therefore increased the temperature of the extracellular solution in the recording chamber in approximately 5°C increments, and recorded the whole-cell currents at 25°C, 30°C and 37°C if possible. Each temperature change took approximately 2 min. For some of the statistical analysis, data acquired at the

three temperatures have been grouped and results reported for the range 25–37°C. Solution changes were made by perfusion and aspiration of the bath (chamber volume 4 ml) which took from 30 s to 2 min depending on flow rate. During solution exchange, the perfusate passed over the activated Peltier element before reaching the cells; the bath temperature typically decreased by 2–3 °C during this time but this did not affect the current recordings described here.

Statistical analysis

Conductances are expressed as mean ± SD. Comparisons between conventional whole-cell recordings and perforated-patch recordings were made by unpaired Student's *t*-tests. Conductances at room temperature (16–20°C) were compared to those in the range 25–37°C by paired or unpaired Student's *t*-tests, depending on whether recordings were obtained in both ranges from the same cell. Because of small group sizes with non-parametric distributions, conductances at each temperature increment were compared using Kruskal-Wallis and Mann-Whitney tests.

Results

Whole-cell currents in rat BMMCs

I/V relationships obtained from 79 rat BMMCs perforated with amphotericin B and warmed to temperatures between 25 and 37°C showed two types of voltage-dependent current. An inwardly rectifying (IR) current was rapidly activated by hyperpolarizing potential steps (Fig. 1A), and an outwardly rectifying (OR) current was seen in cells depolarized to positive potentials (Fig. 1B). At potentials between –100 mV and +40 mV, the OR currents were instantaneous and sustained, but at higher potentials the current exhibited time-dependent inactivation (see later). A total of 37 cells (47%) showed the inwardly and outwardly rectifying currents concurrently (Fig. 1C). An additional 15 cells (19%) showed only the outward current, and in 14 cells (18%) only the inward current was observed. In some cells (16%), no voltage-dependent currents were observed and the *I/V* relationship represented a basal leak conductance. Both the IR and OR currents were observed when recording with pipette solutions containing either KCl or KCH_3SO_4, suggesting that movement of Cl^- from the pipette into the cell was not responsible for induction of the currents.

The IR and OR conductances in the range of 25–37°C were 1.74 ± 1.1 nS (n = 41) and 2.21 ± 1.4 nS (n = 31) respectively. The capacitance of rat BMMCs was 4.8 ± 1.5 pF (mean ± SD, n = 116), but this did not correlate with the IR or OR conductances, suggesting that the currents were not directly dependent on membrane area. The mean leak conductance in the range of 25–37°C was 0.75 ± 0.62 nS (n = 53).

Ionic selectivity of the currents

The IR currents observed to occur in our rat BMMCs were very similar in appearance to those described to be present in RBL-2H3 cells [18, 28], rat BMMCs grown in the presence of interleukin-3 (IL-3) [22], and cultured mouse BMMCs [14], in which the currents were characterized as a K^+-selective inward rectifier. Our *I/V* curves were characterized by inward currents at potentials more negative

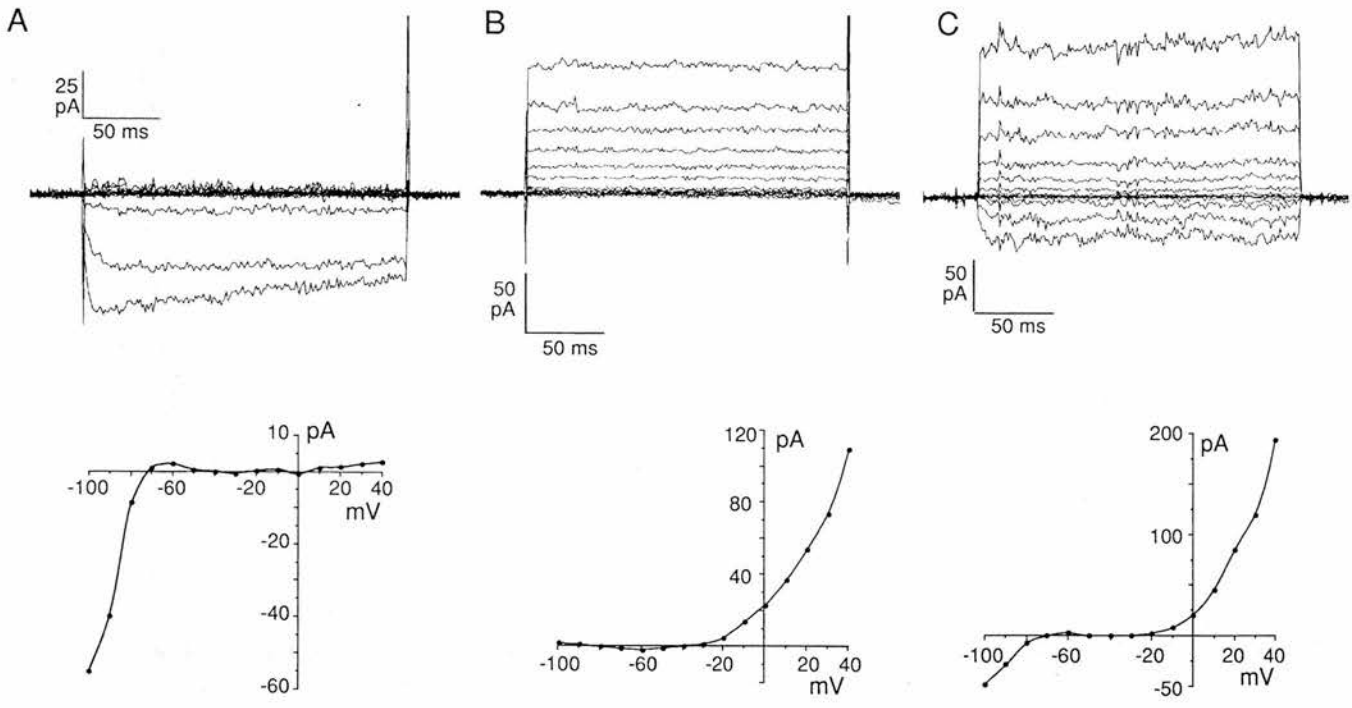


Fig. 1A–C Whole-cell membrane currents recorded from amphotericin-B-perforated rat bone-marrow-derived mast cells (BMMCs) with accompanying leak-subtracted current/voltage (*I/V*)relationships. Cells were clamped at a holding potential of –40 mV and voltage pulses of 200 ms duration were applied from –100 mV to + 40 mV in 10-mV steps at 1-s intervals. **A** Inwardly rectifying current. **B** Outwardly rectifying current. **C** Concurrent inwardly and outwardly rectifying currents

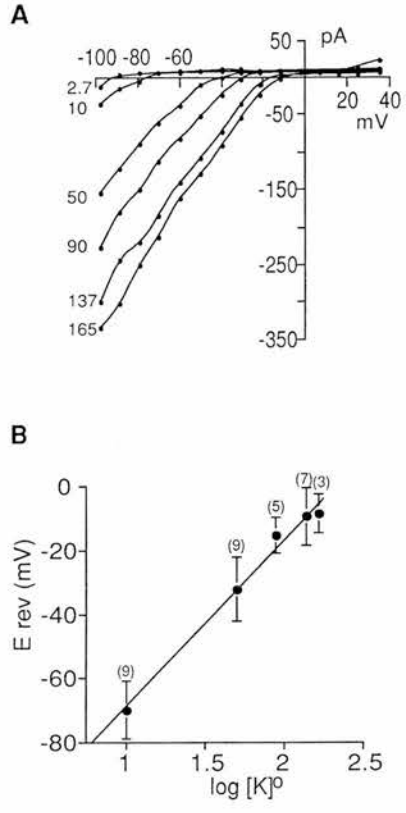


Fig. 2A, B Effect of extracellular K^+ concentration on inwardly rectifying currents. **A** Whole-cell *I/V* curves of a BMMC in six different concentrations of extracellular K^+. There is a positive shift in reversal potential as the extracellular K^+ increases from 2.7 mM to 165 mM. **B** Reversal potentials (*E rev*) plotted against $\log_{10}$ extracellular K^+ (mM). The line is a least-squares fit to the data. The slope of 52 mV/decade is close to that predicted for a K^+-selective membrane

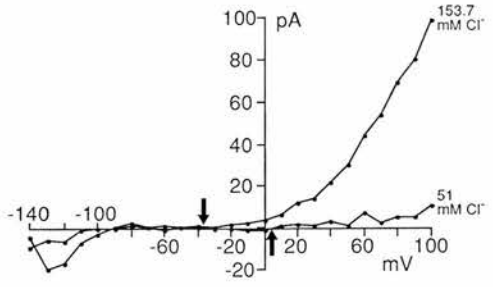


Fig. 3 Effect of extracellular Cl^- concentration on the outwardly rectifying current. When the extracellular Cl^- concentration is decreased from 153.7 mM to 51 mM by substituting Na-acetate for NaCl, the outwardly rectifying conductance is markedly decreased and the reversal potential shifts in a positive direction (*arrows*)

than the K^+ reversal potential and typically contained a region showing a small outward current just positive to the reversal potential, as shown in Fig. 1A. To investigate the proportion of cells showing the IR current, we first examined *I/V* relationships from 21 BMMCs in extracellular solutions containing 2.7 and 10 mM K^+. In mast cell Ringer (2.7 mM K^+) 15 cells (71%) showed the IR current, but when the extracellular K^+ was increased to 10 mM the current was present in all 21 cells (100%). When the extracellular K^+ was increased from 2.7 mM to 165 mM (with a corresponding decrease in the Na^+ concentration), the reversal potential of the *I/V* curves shifted in a positive direction (Fig. 2A). The linear relationship between reversal potential and log extracellular K^+ concentration with a least squares slope of 52 mV/decade indicates that the conductance is essentially K^+ selective (Fig. 2B). The slope conductance measured between –100 mV and –80 mV also increased with extracellular K^+ and was 1.48 ± 0.7 nS in 10 mM K^+(n = 9), 4.27 ± 1.4 nS in 50 mM K^+ (n = 9), 5.50 ± 2.3 nS in 90 mM K^+(n = 5), 6.24 ± 2.8 nS in 137 mM K^+(n = 7), and 5.8 ± 4.0 nS in 165 mM K^+(n = 3). An increase in conductance with increasing extracellular K^+ concentration also indicates that the current is predominantly carried by K^+ ions.

The OR current was not affected by changes in extracellular K^+ concentration. However, when the extracellular Cl^- concentration was reduced to 51 mM by substituting Na acetate for NaCl, the OR conductance decreased by 82 ± 8.5% (Fig. 3), from a mean of 2.7 ± 2.1 nS to 0.51 ± 0.53 nS (n = 5). In three cells bathed in extracellular solution containing 14 mM Cl^- the peak OR conductance was reduced to 0.24 nS in one cell and completely abolished in the other two cells. If cytosolic Cl^- was invariant during solution exchange, the shift in reversal potential predicted by the Nernst equation for a threefold decrease in extracellular Cl^- concentration would be 28 mV for a membrane selectively permeable to Cl^-. Reducing the extracellular Cl^- concentration from 153.7 mM to 51 mM resulted in a positive shift in the reversal potential of the OR current by 31 ± 21 mV (n = 5, Fig. 3 arrows). The deviation from theory resulting in a large standard deviation may reflect changes in intracellular Cl^- concentration occurring during the exchange (cytosolic Cl^- is not known in perforated-patch experiments and varies until a Donnan equilibrium is established between pipette and cell). The OR conductance was also decreased when Na isethionate was substituted for NaCl to yield an extracellular solution containing 16.7 mM Cl^- (3.39 ± 2.3 nS to 0.88 ± 1.2 nS, n = 4), and this effect was reversible on washout of the bath (Fig. 4B).

The OR current was not affected by 100 μM 4-aminopyridine or 25 mM TEA (not shown), but the OR conductance was reversibly decreased by the chloride channel blocker DIDS. Addition of 20 μM DIDS to the extracellular solution reduced the OR conductance by 69 ± 23% from a mean of 2.8 ± 2.0 nS to 1.0 ± 1.3 nS (n = 7). Figure 4C shows a typical experiment in which the OR conductance decreased after addition of 20 μM DIDS to the bath, but partially recovered after the blocker was washed out. All of these observations indicate that the OR currents in rat BMMCs are predominantly carried by Cl^- ions.

Dependence of the OR Cl^- conductance on bath temperature and cytoplasmic integrity

The OR chloride conductance has not been described previously to occur in rat mucosal type mast cells inves-

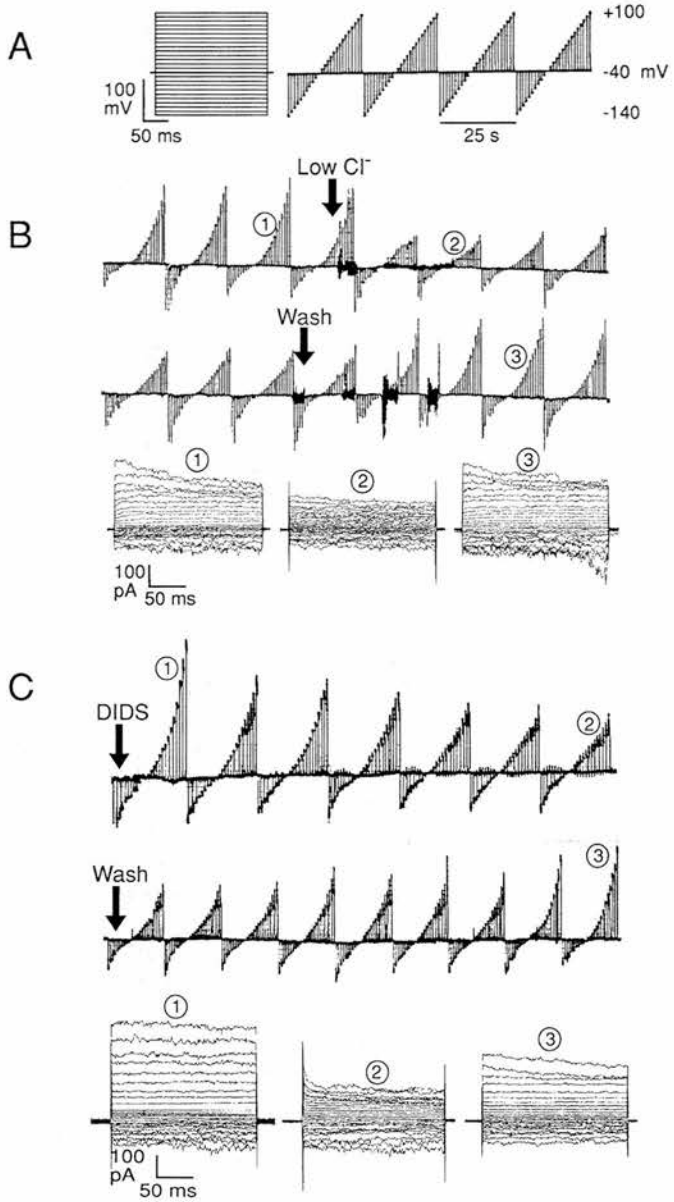


Fig. 4 Effect of extracellular Cl^- concentration and DIDS on whole-cell membrane currents in BMMCs. **A** The voltage step protocol. Cells were held at a holding potential of –40 mV and voltage pulses of 200 ms duration were applied from –140 mV to +100 mV in 10-mV steps at 1-s intervals. **B,C** Typical continuous pen recordings of the *I/V* relationships. Below each *trace* are the original superimposed currents evoked by the 25 voltage steps labelled by each *encircled number*. **B** Whole-cell currents in a BMMC after the mast cell Ringer (153.7 mM Cl^-) was exchanged for an extracellular solution containing Na-isethionate (16.7 mM Cl^-, *first arrow*). The outwardly rectifying (OR) current, showing time-dependent inactivation at potentials above +60 mV, is markedly reduced between *encircled number 1* and *encircled number 2*. At the *second arrow*, the bath was washed out with mast cell Ringer resulting in restoration of the current (*encircled number 3*). Noise indicates the time taken for solution exchange. Pipette solution contained KCH_3SO_4. **C** Effect of DIDS on the OR current. At the *first arrow*, 20 μM DIDS was added to the bath resulting in gradual diminution of the OR current. At the *second arrow*, the DIDS was washed out of the bath resulting in recovery of the OR current. Pipette solution contained KCl

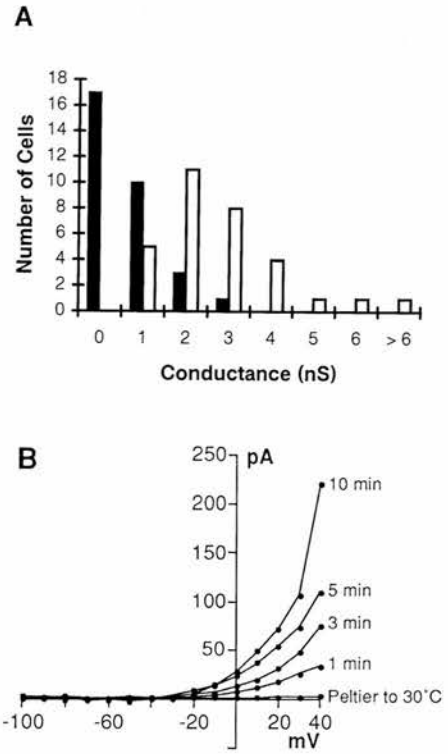


Fig. 5 **A** Perforated-patch experiments showing the effect of increasing bath temperature on 31 BMMCs that showed the OR chloride (OR_{Cl}) current at 25–37°C. The distribution of OR_{Cl} conductances at room temperature (16–20°C) is shown by the *black bars* and those between 25 and 37°C by the *white bars*. The shift of the distribution to the *right* indicates activation of the current by the rise in temperature. **B** Activation of the OR_{Cl} current in a cell warmed from room temperature to 30°C. *I/V* relationships are shown at intervals following activation of the Peltier device. The cell was clamped at a holding potential of –40 mV and voltage pulses of 200 ms duration were applied from –100 mV to + 40 mV in 10-mV steps. Leak currents were subtracted

tigated using conventional whole-cell recording techniques [18, 22]. We wished to determine if our results were influenced by recording conditions, so we compared 117 perforated-patch recordings obtained at room temperature (16–20°C) with our results at the warmer temperatures in the range of 25–37°C. At room temperature, 23% of amphotericin-B-perforated BMMCs displayed both IR_K and OR_{Cl} currents concurrently, with a further 49% showing only IR_K currents. In marked contrast to the results obtained at 25–37°C, only 3% of BMMCs displayed exclusively outward currents. Out of 117 cells, 25% appeared quiescent, displaying neither inward nor outward currents. The IR_K and OR_{Cl} conductances at room temperature were 1.22 ± 0.7 nS (n = 56) and 1.25 ± 0.9 nS (n = 20), respectively, both significantly lower than those recorded at 25–37°C (P<0.005). The difference between these results and those described earlier is primarily attributable to the increased proportion of cells showing OR_{Cl} currents at 25–37°C (26% at room temperature compared to 66% at 25–37°C). This effect is illustrated in Fig. 5A, which shows the effect of warming on the distribution of OR_{Cl}

Table 1 Effect of recording conditions on the OR_{Cl} conductance. The probability of observing the conductance increases as the conditions approach physiological. WCR - Whole cell recording

Parameter	Conventional WCR: cytoplasm disrupted		Perforated-patch recording: cytoplasm preserved	
Temperature	16–20 °C	25–37 °C	16–20 °C	25–37 °C
% Cells showing OR_{Cl}	7%	21%	26%	66%
Number cells showing OR_{Cl}	3/44	3/14	30/117	52/79
Mean conductance ± sd (nS)	0.87 ± 0.6 (n = 3)	0.69 ± 0.1 (n = 3)	1.25 ± 0.9 (n = 30)	2.21 ± 1.4 (n = 52)

conductances in 31 BMMCs that showed the OR_{Cl} current at 25–37°C.

The effect of warming on the OR_{Cl} current was also demonstrated in individual cells by monitoring the *I/V* relationships as BMMCs were warmed. Figure 5B shows the development of the OR_{Cl} current in a typical cell following activation of the Peltier device. The temperature at which the OR_{Cl} current developed varied from cell to cell; in most BMMCs, the current developed at either 25 °C (n = 20) or 30°C (n = 22), but in some cells the current only appeared at 37°C (n = 6). The median OR conductance also increased with each temperature increment but the difference between the three temperatures did not reach statistical significance, probably due to small group sizes. In cells that exhibited the OR_{Cl} current, the time from the start of warming to development of the peak conductance ranged from 132 to 696 s with a mean and SD of 309 ± 132 s (n = 21). These figures indicate that the OR_{Cl} conductance continues to increase even after the elevation of temperature has been completed. This delay would most likely arise if the current was dependent on a cytosolic factor. The OR current was typically stable for long periods, and in one cell it was monitored for 60 min without deterioration. However, we could not determine if the effect of warming was reversible because our Peltier device did not allow rapid cooling of the bath. Taken together, these results clearly indicate that detection of the OR_{Cl} current is more likely if the temperature of the cells is increased towards physiological values.

We then examined conventional whole-cell recordings from BMMCs to determine if maintenance of cytoplasmic integrity was also important for demonstration of the OR_{Cl} current. *I/V* relationships showed that 41 out of 44 BMMCs at room temperature (93%) displayed the IR_K current, with a mean slope conductance of 0.83 ± 0.5 nS (n = 22). A small OR conductance (0.87 ± 0.6 nS) was also present at room temperature in 3 out of 44 cells, but only in those experiments in which KCH_3SO_4 was used in the pipette solution (n = 13). When cells were warmed to 25–37°C, 3 out of 14 BMMCs showed some OR conductance but it was much lower than that measured in perforated-patch recordings (0.69 ± 0.1 nS).

A summary of the effects of temperature and cytoplasmic disruption on the activation of the OR conductance in BMMCs is shown in Table 1. The results clearly indicate that the OR_{Cl} current is dependent both on temperature and the degree of cytoplasmic integrity.

Whole-cell currents in rat peritoneal mast cells

The OR chloride current in rat BMMCs was similar to that described to occur in rat peritoneal mast cells (RPMCs) when cAMP was included in the pipette solution or when the cells were stimulated with secretagogues [2, 11, 21]. To determine if an OR_{Cl} could also be detected in resting RPMCs, we used the perforated-patch technique to obtain *I/V* relationships from cells at room temperature and in the range 25–37°C. Figure 6B shows the development of an OR current in an RPMC warmed to 25°C and the abrupt decrease in current amplitude and slope conductance following addition of 20 μM DIDS to the bath. In five similar experiments, 20 μM DIDS reduced the mean OR conductance by 53 ± 28% from 1.7 ± 0.96 nS to 0.75 ± 0.53 nS (n = 5). A similar effect was observed when RPMCs showing the OR conductance in mast cell Ringer were perfused with an extracellular solution containing 16.7 mM Cl^- (Fig. 6C), again indicating that the conductance was Cl^- selective. As in rat BMMCs, the expression of the OR_{Cl} current was variable and depended on recording conditions. Out of 40 RPMCs, 10 (25%) showed the OR current between 25 °C and 37°C, in contrast to 9 out of 55 cells (16%) from which recordings were made at room temperature. The slope conductance also increased with temperature from 1.15 ± 0.36 nS (n = 9) to 1.51 ± 0.86 nS (n = 10), although the difference did not reach statistical significance. The OR_{Cl} was also more commonly observed in RPMCs that had been incubated for ≥ 24 h with 10 ng/ml $rrSCF^{164}$. From 55 RPMCs recorded at room temperature, 12 cells had been incubated with $rrSCF^{164}$; the OR_{Cl} was present in 5 cells from this subgroup (42%) in contrast to 4 out of the remaining 43 cells (9%). The mean OR conductance was higher in the $rrSCF^{164}$ treated group (1.3 ± 0.4 nS vs 0.96 ± 0.23 nS) but again the difference was not statistically significant.

In accordance with previous reports [18, 22], we could not demonstrate a K^+-selective IR current in RPMCs under our experimental conditions. In three cells bathed in high-K^+ Ringer (50 mM), there was no change in conductance in the range –140 mV to –100 mV.

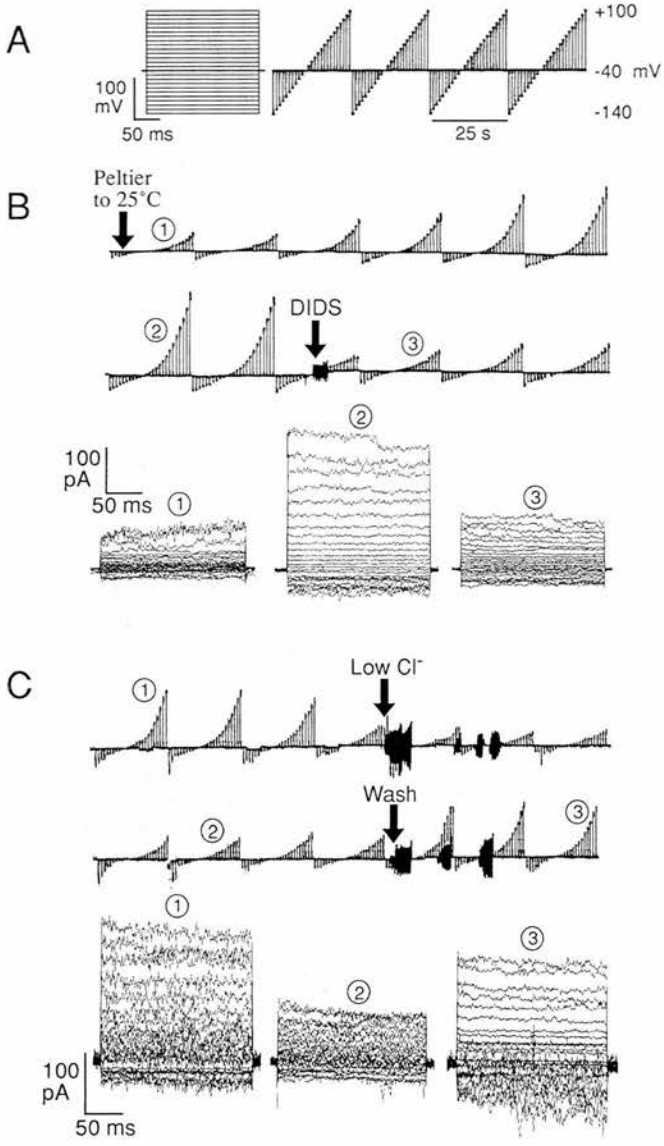


Fig. 6A–C Effect of temperature, DIDS and extracellular Cl^- concentration on whole-cell membrane currents in rat peritoneal mast cells (RPMCs). **A** The voltage step protocol. Cells were held at a holding potential of –40 mV and voltage pulses of 200 ms duration were applied from –140 mV to +100 mV in 10-mV steps at 1-s intervals. **B** After warming the cell to 25 °C (*first arrow*), an outwardly rectifying (OR) current develops that exhibits time-dependent inactivation at potentials greater than +60 mV (*encircled number 2*). At the *second arrow*, 20 μM DIDS was added to the bath resulting in a sudden diminution of the OR current (*encircled number 3*). Pipette solution contained KCH_3SO_4. **C** Whole-cell currents in an RPMC after the mast cell Ringer (153.7 mM Cl^-) was exchanged for an extracellular solution containing Na-isethionate (16.7 mM Cl^-, *first arrow*). The OR current is markedly reduced between (*encircled numbers 1* and *2*). At the *second arrow*, the bath was washed out with mast cell Ringer resulting in restoration of the current (*encircled number 3*). Noise indicates the time taken for solution exchange. Pipette solution contained KCH_3SO_4

Discussion

Activity of the OR_{Cl} in rat mast cells

In this study, we characterized whole-cell currents of rat BMMCs grown in the presence of cytokines derived from concanavalin-A-stimulated T-lymphocytes. These cells have not been studied electrophysiologically but they have been extensively characterized biochemically and immunologically and in all respects so far studied they are identical to intestinal mucosal mast cells [19, 23]. They may, therefore, represent a better model for electrophysiological studies of mucosal mast cells than RBL-2H3 cells [18] or mast cells grown in the presence of rat recombinant IL-3 [22]. In contrast to the latter studies, we report that rat BMMCs possess an OR_{Cl} in addition to the previously described K^+-selective inwardly rectifying (IR_K) current. This discrepancy may result from variations in cell phenotype; the additional growth factors and concanavalin A in the LNCM culture system could be necessary for expression of the outwardly rectifying chloride channel which was not observed to occur in either of the other cell types. However, this explanation seems unlikely because the OR_{Cl} was also present in RPMCs (an example of the connective tissue phenotype) and these cells were not exposed to the aforementioned factors.

A more likely possibility for the discrepancy described is the apparent dependency of the OR_{Cl} conductance on experimental conditions. We found that with the conventional whole-cell recording technique at room temperature (as used in previous studies) only 3 out of 44 BMMCs showed an OR_{Cl} current. However, when the integrity of the cell's cytoplasm was preserved using the perforated-patch technique, the OR_{Cl} current was readily demonstrable both in BMMCs (see Table 1) and RPMCs (Fig. 6). In addition, we found that increasing the bath temperature towards physiological values increased the proportion of cells that possessed the OR_{Cl} current, although the conductances were lower with the conventional whole-cell technique. These findings suggest that the OR_{Cl} may be dependent on an essential intracellular component that is leached out of the cell during conventional voltage-clamp recordings. A similar effect was recently reported for the immunoglobulin E (IgE) receptor-activated calcium conductance in rat mast cells, which could only be detected using perforated-patch recordings performed at 37°C [33].

The OR_{Cl} conductance observed in our experiments is similar to that induced in RPMCs when cAMP is included in the pipette solution [2, 27]. For example, the time course for development of the OR_{Cl} current in RPMCs following "break-in" is similar to that following warming of BMMCs or RPMCs; the shape of the *I/V* curve is similar in both cases; and both currents are blocked by 20 μM DIDS. In previous studies of RPMCs [27], it was concluded that in vivo a rise in intracellular cAMP following stimulation of the cells with secretagogues or antigen was responsible for activation of the OR_{Cl} current.

In our cells, neither secretagogues nor exogenous second messengers were required to elicit the current. This suggests that if cAMP is the "missing" cytosolic factor in conventional whole-cell recordings then only basal levels of the messenger are required to support the OR_{Cl} conductance.

The OR_{Cl} conductance in rat mast cells also shares certain similarities with a volume-regulated Cl^- conductance in T-lymphocytes [17]. In our experiments, the OR_{Cl} conductance was also observed when pipette KCl was replaced with KCH_3SO_4, suggesting that the current was not induced by movement of pipette Cl^- and osmotically obliged water into the cell during perforated-patch recordings. It was also concluded in previous studies that the cAMP-activated Cl^- current in RPMCs was not dependent on changes in cell volume [21].

However, cells subjected to perforated-patch recordings are very susceptible to small osmotic imbalances between cytosol and bath which could lead to activation of volume-regulated Cl^- channels. The effect of osmolarity on the activation of OR_{Cl} in BMMCs and RPMCs, and the relationship between the currents described here and in previous studies, therefore awaits further study.

Variation in expression of whole-cell currents

In the mouse BMMC system, the presence or absence of IR_K and OR_{Cl} currents in individual mast cells was interpreted as heterogeneity of ion channel expression [14]. We also found variation in the presence of the two currents in our cell populations, but we favour an alternative explanation to heterogeneity of ion channel expression. We suggest that a normal rat BMMC possesses the ion channels for both the IR_K and OR_{Cl} currents, and that the heterogeneous distribution of current patterns within the population results from extrinsic factors (i.e. experimental conditions) rather than intrinsic factors (i.e. restricted expression of ion channels). This is highlighted in Table 1, which shows the variation in expression of the OR_{Cl} conductance in BMMCs under different conditions. Likewise, the IR current was not detected in some cells in mast cell Ringer, but when the extracellular K^+ concentration was raised it was present in all cells tested. Hence, with both the OR_{Cl} and the IR_K, the lack of a detectable current did not reflect the lack of the appropriate ion channels. However, although we demonstrated the OR_{Cl} current in both BMMCs and RPMCs, the IR_K was only detectable in BMMCs. This may reflect true heterogeneity between the cell phenotypes as rat BMMCs and RPMCs have distinct biochemical and functional characteristics. However, the possibility still remains that the lack of the IR_K current may be an artefact of the isolation procedure, similar to that affecting IgE responses in freshly isolated RPMCs [32]. RPMCs undergo apoptosis on removal from the abdominal cavity, unless stimulated with the appropriate growth factors [5, 9], and the apparent influence of the cytokine $rrSCF^{164}$ on the OR_{Cl} current lends support to this hypothesis.

Physiological relevance of the IR_K and the OR_{Cl} currents in rat mast cells

Previous studies have shown that the IR_K is involved in regulation of the resting membrane potential [14, 18]. As seen in Fig. 1, the current is rapidly activated in BMMCs by hyperpolarizing potential steps, which in vivo would prevent further hyperpolarization. Note also the presence of the slight outward current "bump" in the IR_K *I/V* curve just positive to the reversal potential. This would tend to restore the resting membrane potential if the cell was slightly depolarized from the K^+ reversal potential. The IR_K current therefore provides a mechanism that would prevent excessive hyperpolarizations, and resist small depolarizations, of the cell. The lack of a detectable IR_K in RPMCs explains why the resting potential of these cells is close to 0 mV [18], but whether this accurately reflects the situation in vivo remains to be determined.

The OR_{Cl} current in our cells was only activated when the cell was depolarized to potentials more positive than –30 mV (Fig. 1B, C). This suggests that in vivo the OR_{Cl} current could be activated by large fluctuations in resting membrane potential or by depolarization, as occurs following stimulation of tumour mast cells following stimulation with antigen [12, 24, 31]. In RBL-2H3 cells, antigen-mediated depolarization is followed by a repolarization towards the resting membrane potential [15, 24], a process considered to be due to efflux of K^+ ions from the cell [16]. We suggest that the influx of Cl^- ions that follows activation of the OR_{Cl} [4] would also tend to repolarize the cell, thus restoring a negative membrane potential. The OR_{Cl} current in rat BMMCs could therefore serve two functions: (1) to regulate the resting membrane potential, as in mouse BMMCs [14] and (2) to counteract the depolarization of the cell during degranulation, thus maintaining the driving force for Ca^{2+} entry [21, 25].

Acknowledgements We thank Drs. A. MacDonald and M. Shipston for helpful advice, and Mrs. J. Vaagenes and Mrs. E. Thornton for technical support. This work was supported by a grant from the Wellcome Trust (038342/Z/93/Z/1.5B/PMC/RF)

References

1. Bormann J, Hamill OP, Sakmann B (1987) Mechanism of anion permeation through channels gated by glycine and gamma-aminobutyric acid in mouse cultured spinal neurones. J Physiol (Lond) 385:243–286
2. Dietrich J, Lindau M (1994) Chloride channels in mast-cells – block by DIDS and role in exocytosis. J Gen Physiol 104:1099–1111
3. Fasolato C, Hoth M, Matthews G, Penner R (1993) Ca^{2+} and Mn^{2+} influx through receptor-mediated activation of nonspecific cation channels in mast-cells. Proc Natl Acad Sci USA 90:3068–3072
4. Friis UG, Johansen T, Hayes NA, Foreman JC (1994) IgE-receptor activated chloride uptake in relation to histamine secretion from rat mast cells. Br J Pharmacol 111:1179–1183
5. Galli SJ, Zsebo KM, Geissler EN (1994) The kit-ligand, stem-cell factor. Adv Immunol 55:1–96
6. Haig DM, McMenamin C, Redmond J, Brown D, Young IG, Cohen SDR, Hapel AJ (1988) Rat IL-3 stimulates the growth

of rat mucosal mast cells in culture. Immunology 65:205–211
7. Hamill OP, Marty A, Neher E, Sakmann B, Sigworth FJ (1981) Improved patch-clamp techniques for high-resolution current recording from cells and cell-free membrane patches. Pflügers Arch 391:85–100
8. Hill PB, MacDonald AJ, Thornton EM, Newlands GFJ, Galli SJ, Miller HRP (1996) Stem-cell factor enhances immunoglobulin E-dependent mediator release from cultured rat bone-marrow-derived mast-cells – activation of previously unresponsive cells demonstrated by a novel ELISPOT assay. Immunology 87:326–333
9. Horigome K, Bullock ED, Johnson EM (1994) Effects of nerve growth-factor on rat peritoneal mast-cells – survival promotion and immediate-early gene induction. J Biol Chem 269:2695–2702
10. Horn R, Marty A (1988) Muscarinic activation of ionic currents measured by a new whole-cell recording method. J Gen Physiol 92:145–159
11. Janiszewski J, Bienenstock J, Blennerhassett M (1994) Picomolar doses of substance P trigger electrical responses in mast cells without degranulation. Am J Physiol 267:C138-C145
12. Kanner BI, Metzger H (1983) Crosslinking of the receptors for immunoglobulin E depolarizes the plasma membrane of rat basophilic leukemia cells. Proc Natl Acad Sci USA 80:5744–5748
13. Kuno M, Okada T, Shibata T (1989) A patch-clamp study: secretagogue-induced currents in rat peritoneal mast cells. Am J Physiol 256:C560-C568
14. Kuno M, Shibata T, Kawawaki J, Kyogoku I (1995) A heterogeneous electrophysiological profile of bone marrow-derived mast-cells. J Membr Biol 143:115–122
15. Labrecque GF, Holowka D, Baird B (1989) Antigen-triggered membrane potential changes in IgE sensitized rat basophilic leukemia cells: evidence for a repolarizing response that is important in the stimulation of cellular degranulation. J Immunol 142:236–243
16. Labrecque GF, Holowka D, Baird B (1991) Characterization of increased K^+ permeability associated with the stimulation of receptors for immunoglobulin E on rat basophilic leukemia cells. J Biol Chem 266:14912–14917
17. Lewis RS, Ross PE, Cahalan MD (1993) Chloride channels activated by osmotic stress in T lymphocytes. J Gen Physiol 101:801–826
18. Lindau M, Fernandez JM (1986) A patch-clamp study of histamine-secreting cells. J Gen Physiol 88:349–368
19. MacDonald AJ, Haig DM, Bazin H, McGuigan AC, Moqbel R, Miller HRP (1989) IgE-mediated release of rat mast-cell protease-II, beta-hexosaminidase and leukotriene-C4 from cultured bone marrow-derived rat mast-cells. Immunology 67:414–418
20. Matthews G, Neher E, Penner R (1989) Second messenger-activated calcium influx in rat peritoneal mast cells. J Physiol (Lond) 418:105–130
21. Matthews G, Neher E, Penner R (1989) Chloride conductance activated by external agonists and internal messengers in rat peritoneal mast cells. J Physiol (Lond) 418:131–144
22. McCloskey MA, Qian YX (1994) Selective expression of potassium channels during mast cell differentiation. J Biol Chem 269:14813–14819
23. McMenamin C, Haig DM, Gibson S, Newlands GFJ, Miller HRP (1987) Phenotypic analysis of mast cell granule proteinases in normal rat bone marrow cultures. Immunology 60:147–149
24. Mohr FC, Fewtrell C (1987) IgE receptor-mediated depolarization of rat basophilic leukemia cells measured with the fluorescent probe bis-oxonol. J Immunol 138:1564–1570
25. Mohr FC, Fewtrell C (1987) Depolarization of rat basophilic leukemia cells inhibits calcium uptake and exocytosis. J Cell Biol 104:783–792
26. Penner R, Pusch M, Neher E (1987) Washout phenomena in dialyzed mast cells allow discrimination of different steps in stimulus–secretion coupling. Biosci Rep 7:313–321
27. Penner R, Matthews G, Neher E (1988) Regulation of calcium influx by second messengers in rat mast cells. Nature 334:499–504
28. Qian YX, McCloskey MA (1993) Activation of mast cell K^+ channels through multiple G protein-linked receptors. Proc Natl Acad Sci USA 90:7844–7848
29. Rae J, Cooper K, Gates P, Watsky M (1991) Low access resistance perforated patch recordings using amphotericin B. J Neurosci Methods 37:15–26
30. Romanin C, Reinsprecht M, Pecht I, Schindler H (1991) Immunologically activated chloride channels involved in degranulation of rat mucosal mast cells. EMBO J 10:3603–3608
31. Sagi-Eisenberg R, Pecht I (1983) Membrane potential changes during IgE-mediated histamine release from rat basophilic leukemia cells. J Membr Biol 75:97–104
32. Taylor AM, Galli SJ, Coleman JW (1996) Stem-cell factor, the kit ligand, induces direct degranulation of rat peritoneal mast cells in vitro and in vivo: dependence of the in vitro effect on period of culture and comparisons of stem-cell factor with other mast cell-activating agents. Immunology 86:427–433
33. Zhang L, McCloskey MA (1995) Immunoglobulin E receptor-activated calcium conductance in rat mast cells. J Physiol (Lond) 483:59–66

/u/ere/par821 Sep10 ere – sps art A5 1 (X 0)

Electrophysiology of *Ascaris* muscle and anti-nematodal drug action

R. J. MARTIN, M. A. VALKANOV, V. M. E. DALE, A. ROBERTSON, *and* I. MURRAY

Department of Preclinical Veterinary Sciences, R.(D.)S.V.S., Summerhall, University of Edinburgh, Edinburgh, EH9 1QH, UK

SUMMARY

Three groups of anthelmintic drugs act directly and selectively on muscle membrane receptors of parasitic nematodes. These groups of anthelmintics are: (1) *The Nicotinic Agonists* (levamisole, pyrantel, morantel and oxantel) that act on acetylcholine receptors of nematode somatic muscle; (2) *The GABA Agonist*, piperazine, that acts on nematode muscle GABA receptors; and (3) *The Avermectins* that open glutamate gated Cl^- channels on nematode pharyngeal muscle. The electrophysiology and pharmacology of muscle and neuromuscular transmission the nematode parasite, *Ascaris suum*, is outlined and effects of anthelmintics that interfere with transmission described. Resistance to anthelmintics has appeared in some parasitic nematodes but the mechanisms of this resistance remain to be determined.

Key words: Electrophysiology, *Ascaris suum*, muscle, pharynx, levamisole, pyrantel, morantel, oxantel, piperazine, milbemycin, avermectins.

INTRODUCTION

One nematode parasite that is often used to study the mode of action of anthelminitic drugs is *Ascaris suum*, a large 30 cm nematode that can be recovered from the intestine of pigs. It has the advantage that it can be collected from the abattoir on a weekly basis and maintained in a warm saline solution for about five days. The large size of its muscle and nerve cells means that it is amenable to electrophysiological study. The electrophysiological actions of a number of anthelmintics, like levamisole, piperazine and avermectins have been studied using preparations from *Ascaris*.

This account outlines the electrophysiology and pharmacology of neuromuscular transmission in *Ascaris* and describes effects of anthelmintic drugs that act on its ion-channels.

THE ANATOMY AND PHYSIOLOGY OF THE SOMATIC NEUROMUSCULAR SYSTEM OF *ASCARIS*

The Nervous System

Goldshmidt (1908; 1909) recognized that there were only a small number of neurones present in *Ascaris* (about 250) and found that these neurones have the same structure and position in each animal. A similar organization is found throughout nematodes (White *et al.* 1976; White *et al.* 1986).

There are two main nerve cords that originate from a cranial pharyngeal nerve ring and run along the length of the body: the dorsal nerve cord and the ventral nerve cord (Fig. 1A). The cell bodies of all motor neurones are found in the ventral nerve cord and communicate with the dorsal nerve cord via commissures that contain one or two motor neurone axons, Fig. 1B.

The anatomy of the motorneurone system has been examined by Stretton *et al.* (1978). The commissures connecting the dorsal and ventral nerve cords form a pattern which repeats itself along the length of the body. The pattern consists of three right hand commissures and one left hand commissure; this pattern is used to define a segment. Fig. 1B illustrates one segment: there are 11 motor neurones present in the segment. In addition to the motorneurones, there are also interneurones present in the nerve cords. The 11 motorneurones of each segment are divided into 7 anatomical types according to the distribution of their axons and dendrites. Three of the motorneurones (DI, DE2 and DE3) occur only once in each segment, but the other four types (DE1, VI, V1 and DE3) occur twice in each segment.

The physiological role of each type of the motorneurone was also determined by Stretton *et al.* (1978) by selective electrical stimulation of single motorneurones and recording of the response in the muscle field of the motorneurone. This study showed that DI and VI were inhibitory and the DE1, DE2, DE3, V1 and V2 were, or were likely to be, excitatory.

Subsequently, histochemical studies demonstrated the presence of the enzyme choline acetyltransferase in the axons of DE1, DE2, DE3, V1 and V2, further supporting the view that acetylcholine is the excitatory transmitter in these neurones (Johnson & Stretton, 1985). Histochemical techniques have

 Copyright © 1996 Cambridge University Press

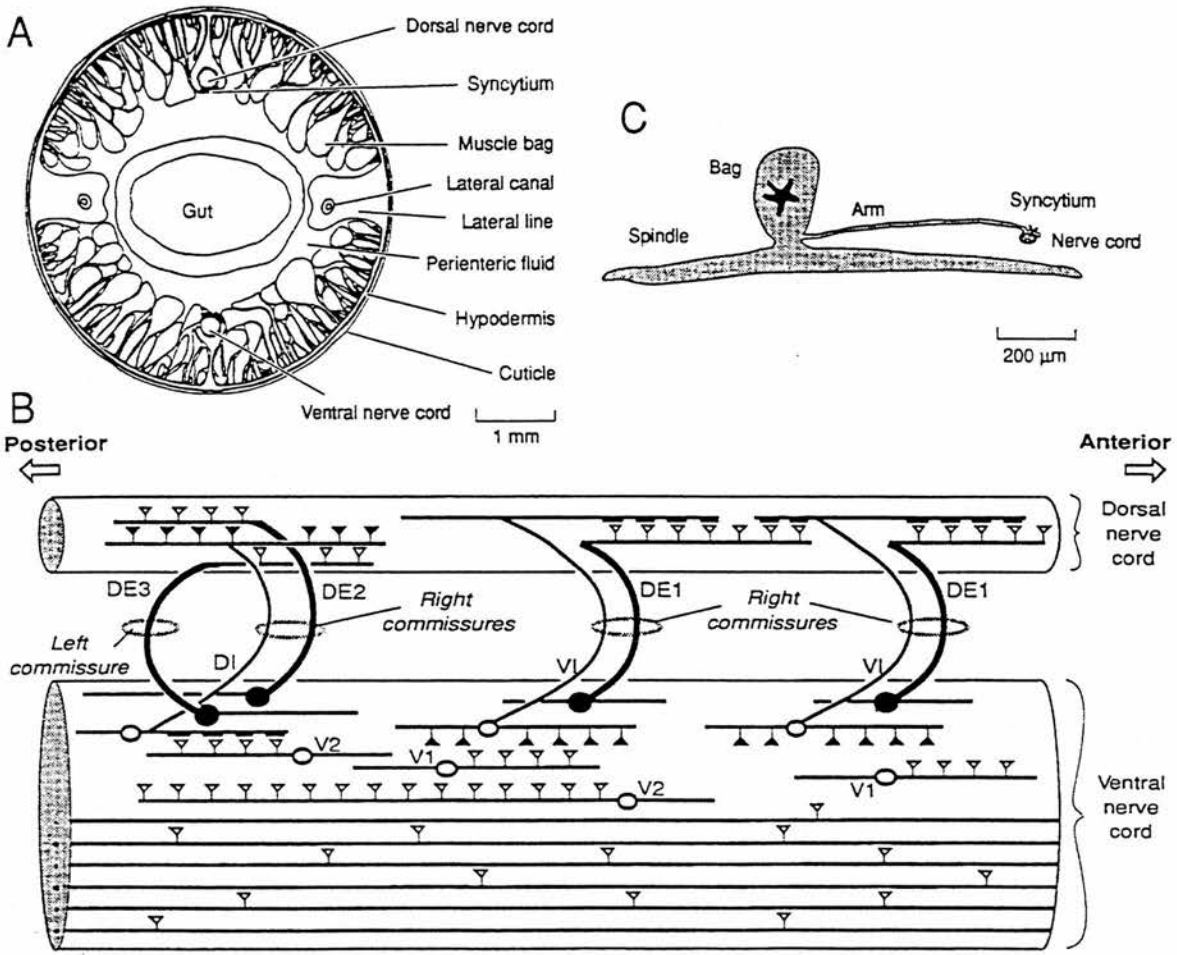


Fig. 1. Diagrams of the somatic neuromuscular structures of *Ascaris suum*. (A) Cross section through the anterior body wall. (B) Diagram of the anatomical organization of the dorsal and ventral nerve cord in one 'segment' of *Ascaris*. 11 motorneurones are present in each segment. 6 large interneurones run the length of the ventral cord. There are 7 anatomical types of motorneurones: dorsal excitatory, DE1, DE2 & DE3; dorsal inhibitory, DI; ventral inhibitory, VI; ventral excitatory, V1 & V2. All cell bodies of the motorneurones are in the ventral cord. (C) Diagram of the structure of a somatic muscle cell and the location of the neuromuscular junction at the syncytium.

also demonstrated GABA-immunoreactivity in the motor neurones, DI and VI (Johnson & Stretton, 1987; Guastella, Johnson & Stretton, 1991; Guastella & Stretton, 1991), a finding that is consistent with GABA being the inhibitory transmitter. In addition to the transmitters acetylcholine and GABA, it is likely that co-transmitters are also present in the motorneurones (Stretton *et al.* 1991). The most abundant are immunologically similar to FMRFamide. A number of these have been isolated from *Ascaris* and have been characterized (Stretton *et al.* 1991), the first was named AF1, *Ascaris* FMRFamide-like 1, (Cowden, Stretton & Davis, 1989), the second was named AF2 (Cowden & Stretton, 1993).

The anatomy of somatic muscle

Schneider (1895) was one of the earliest to describe the body muscle of *Ascaris* but the peculiar structure of the muscle cells with processes of the muscle cell passing to the nervous system rather than a process of the nervous system passing to the muscle cell meant that there was considerable debate about this between the early scientists (Goldschmidt, 1908, 1909; Cappe de Baillon, 1911).

Fig. 1A & C show the location and structure of *Ascaris* somatic muscle cells. Each cell is composed of: (1) the contractile spindle region which lies under the hypodermis; (2) the enlarged balloon-shaped structure which contains the nucleus and many glycogen granules and is referred to as the bag region; (3) the arm which usually arises at the base of the bag region and which is a thin process that passes from the muscle cell to the syncytium where it breaks up into a number of fine processes known as fingers. The neuromuscular junctions are formed between the longitudinal axons of the motorneurones and the syncytium by extensions of the longitudinal axons that break through the hypodermal chalice to approach the syncytium (Rosenbluth, 1965). There are two types of synaptic vesicles: 40 nM clear vesicles, clustered around the presynaptic membrane and dense-cored vesicles that are 80–100 nm in

u/ere/par821 Sep10 ere – sps art A5 3 (X 2)

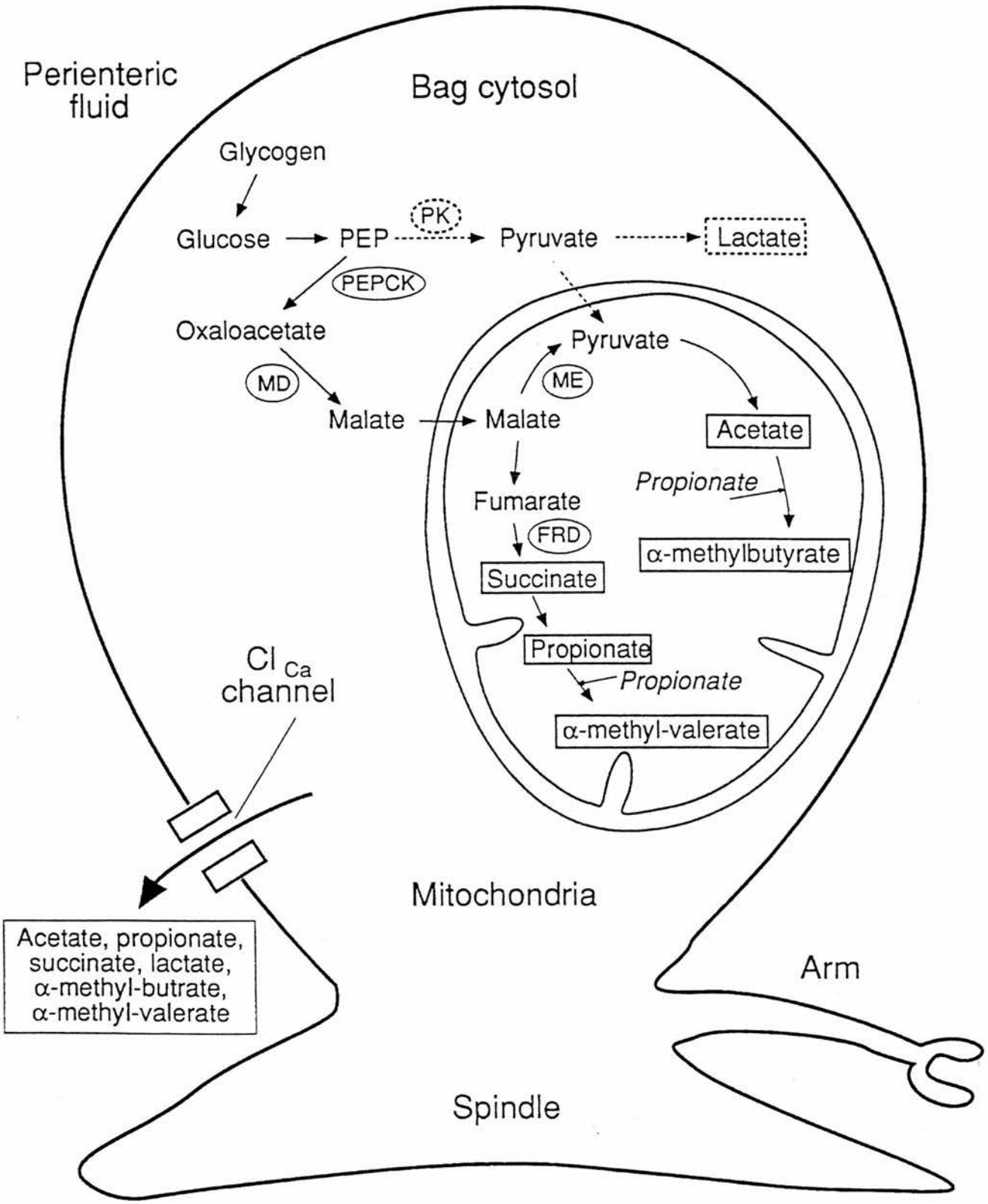


Fig. 2. Diagram of the breakdown pathway of glycogen in the cytoplasm and mitochondria in *Ascaris*. The end-products like succinate, propionate, acetate, α-methylbutyrate, α–methyl valerate are shown in a rectangular box outside the cell in the perienteric fluid and in a rectangular box at the original site of their production. PEP: phosho-enol pyruvate. PK: pyruvate kinase. PEPCK: phosho-enol pyruvate carboxy kinase. MD: malate dehydrogenase. ME: malic enzyme. FRD: fumarate reductase. The pathway outlined by the dashed arrows is absent or only present at a low level. One route for excretion through the muscle membrane is through the Ca-activated Cl^- channel.

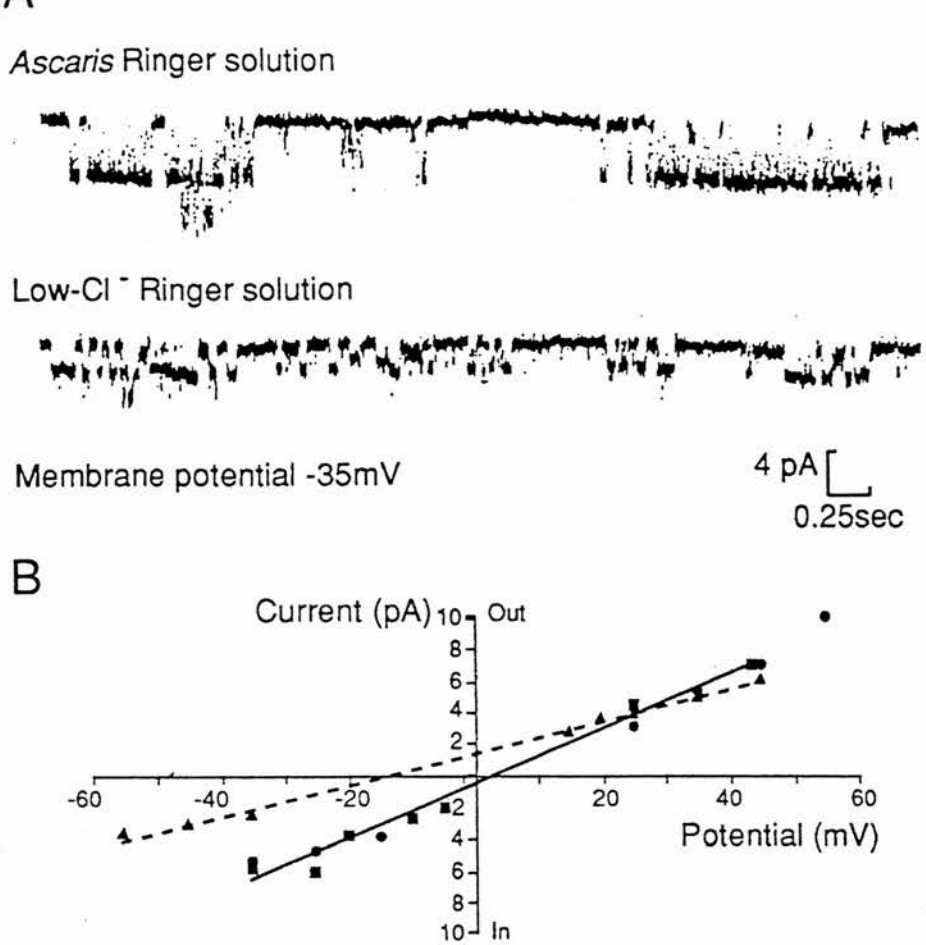


Fig. 3. Ca^{++}-activated Cl^- channel currents recorded in an isolated inside-out patch. (A) The top trace shows a recording at −35 mV in the presence of symmetrical Cl^- solutions; the lower trace shows channel currents recorded from the same patch and at the same membrane potential but after replacing the bath solution with a low-Cl^- solution. (B) the I/V plot shows the relationship between current amplitude and voltage in symmetrical Cl^- (▲) and in the presence of reduced bath-Cl^- (■ & ●). The reduced Cl^- causes a hyperpolarizing shift in the zero current potential and a reduction in the slope conductance of the channel. It shows that the channel conducts Cl^-.

diameter. Apart from regions in the head of *Ascaris*, only the dorsal muscles are connected to the dorsal nerve cord and only the ventral muscle is connected to the ventral nerve cord. This arrangement is a reflection of the fact that muscle contraction is only possible in the dorsal-ventral plane and that the dorsal muscle contracts while the ventral muscle relaxes and *vice versa*.

ELECTROPHYSIOLOGY OF SOMATIC MUSCLE

Membrane potential

Intracellular records of the membrane potential of *Ascaris* were made soon after the development of glass micropipettes (Jarman, 1959); he described a resting potential of about −30 mV on which was superimposed regular spike-like depolarizations. The ionic basis of the resting membrane potential was then investigated by Del Castillo, de Mello & Morales (1964) and Brading and Caldwell (1971). Both of these studies concluded that extracellular K^+ had little effect on potential in contrast to the effect of Cl^-. Brading & Caldwell (1971) suggested that an active pump, possibly moving carboxylic acids across the membrane, might explain the behaviour of the membrane potential.

Permeability of Ca^{++}-dependent Cl^- channels in the bag membrane and excretion of organic anions

The composition of the peri-enteric fluid, that surrounds the *Ascaris* muscle cells, has been examined by Hobson *et al.*, (1952*a*; *b*); Saz and Weil (1962); Tsang and Saz (1973). They showed that the peri-enteric fluid contains low concentrations of Cl^- but high concentrations of carboxylic acids (acetate, propionate, succinate, 2–methylbutyrate and 2–methylvalerate) that are produced inside the muscle cells from anaerobic fermentation of glucose (Fig. 2).

The bag membrane has been shown to contain a high density of Ca^{++}-dependent Cl^- channels that have conductances of 100 to 200 pS, (Fig. 3), (Martin

u/ere/par821 Sep10 ere – sps art A5 5 (X 4)

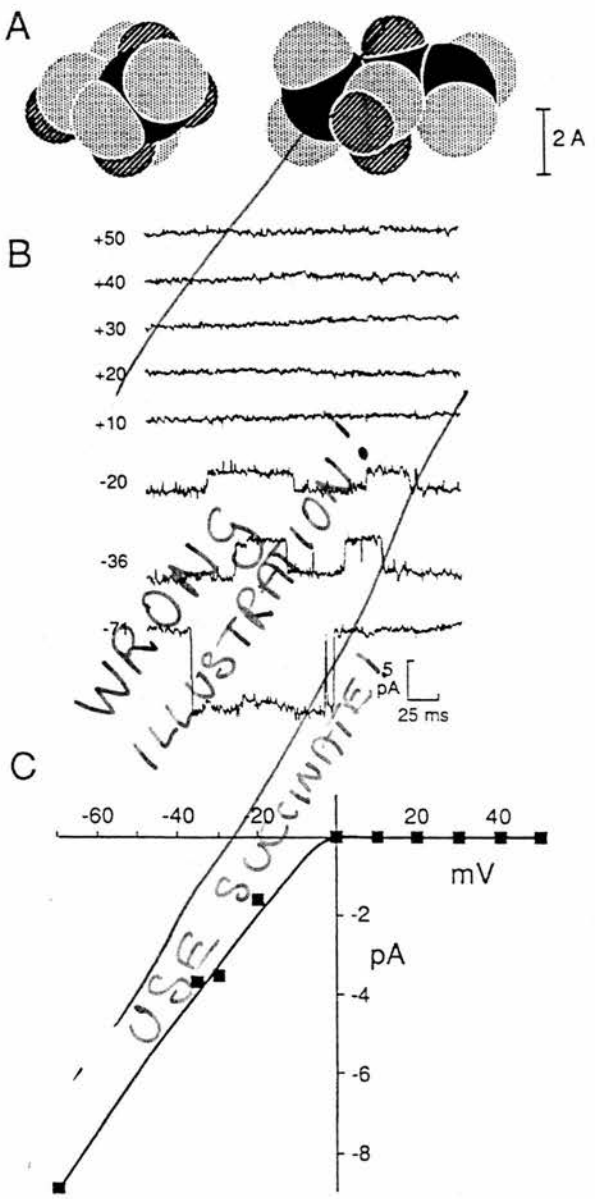


Fig 4. (A) Space-filling model of the end view and side view of succinate. (B) Isolated inside-out channel currents recorded with 140 mM Cl^- as the anion in the patch-pipette (at the extracellular surface of the membrane) and 140 mM succinate in the bath (at the cytoplasmic surface of the membrane). (C) I/V plot of the channel current amplitudes showing the zero current potential to be −15 mV. Note that succinate is able to carry current when the patch is sufficiently hyperpolarized. Such currents demonstrate permeability of succinate through the channel.

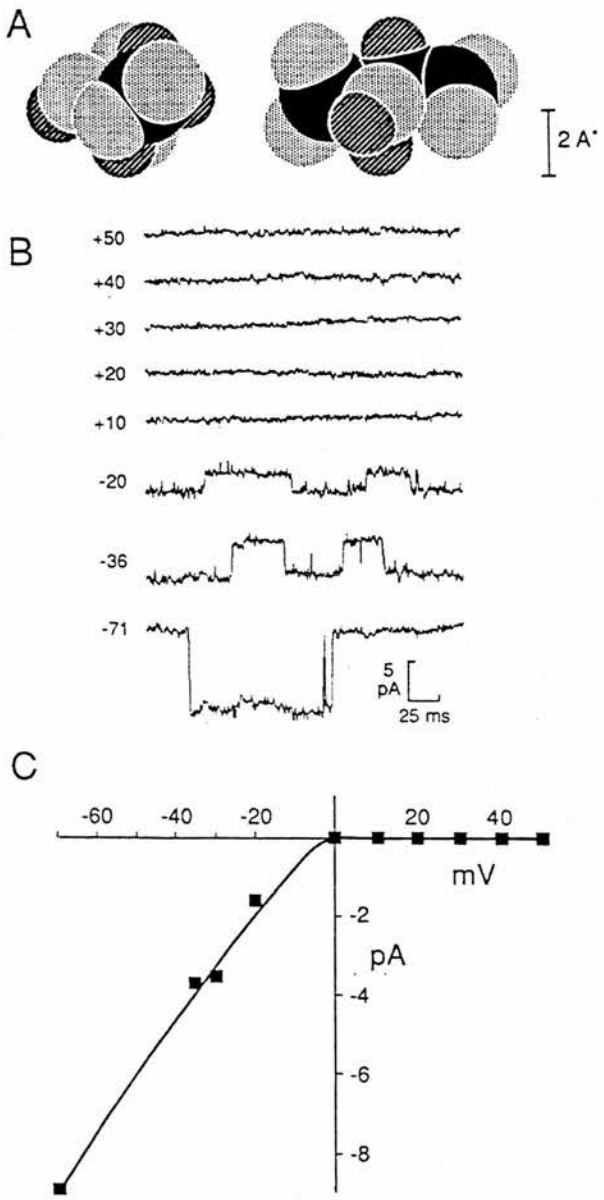


Fig. 5. (A) Space-filling model of the end view and side view of malate. (B) Isolated inside-out channel currents recorded with 140 mM malate as the anion in the patch-pipette (at the extracellular membrane surface) and 140 mM Cl^- in the bath (on the cytoplasmic surface of the membrane). (C) I/V plot of the channel current amplitudes. Note that malate is not able to carry current when the patch is depolarized. The lack of a malate currents at positive potentials demonstrates that malate does not permeate the channel.

et al. 1992). The density of these channels suggests that they are major contributors to the membrane potential. We have examined the permeability properties of this channel using single channel recording techniques (Valkanov, Martin & Dixon, 1994; Martin & Valkanov, 1995; Valkanov & Martin, 1995). The channel is a non-selective anion channel permeable to simple monocarboxylic anions (acetate to heptanoate, including α-methylbutyrate) with a pore diameter of around 6.5A °. We suggested as a result of these studies that the Ca^{++}-dependent Cl^- channel could be involved in the excretion of carboxylic anions across the bag membrane and that the resting membrane potential, −30 mV, would facilitate the concentration of organic acids outside the cell membrane. The proposed mechanism for excretion of carboxylic acids does not require any specific carrier system for the organic anions. It would, however, require some active excretion of protons or a counter anion to prevent the loss of potential as the organic anion is excreted.

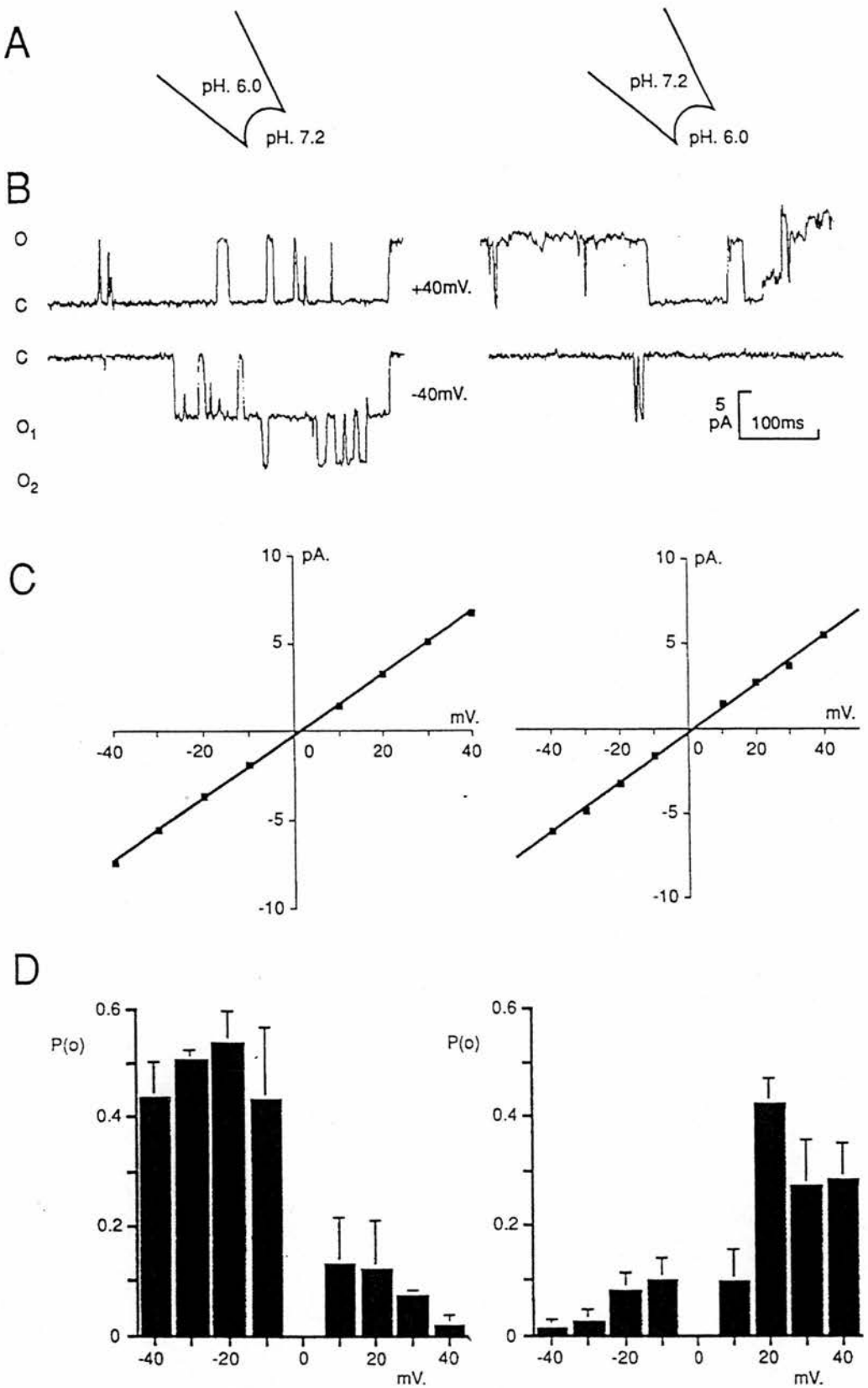


Fig. 6. Effect of reduced pH at the extracellular surface (right column of illustrations) and reduced pH at the cytoplasmic surface of the membrane (left column of illustrations). (A) Cartoon of the inside-out patch recording and the pH arrangement. (B) Representative traces of channel currents at +40 mV and −40 mV. (C) I/V plots of the channel currents. (D) Histogram of the probability of the channel being open at the different membrane potentials. Reduction of the extracellular pH had little effect on single channel conductance or on the effect of membrane potential on probability of opening and was similar to recordings made in symmetrical pH 7·2 (not shown). A

u/ere/par821 Sep10 ere–sps art A5 7 (X 6)

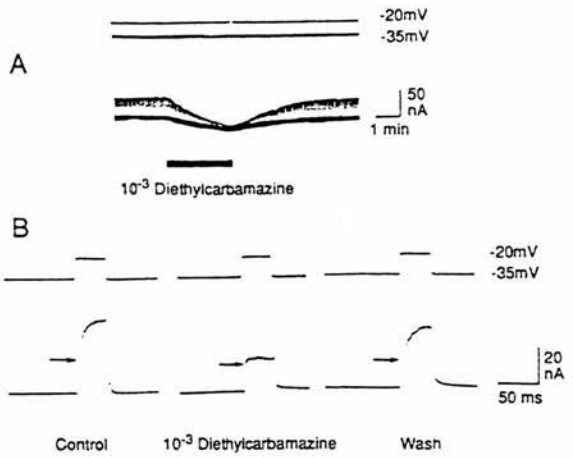


Fig. 7. Effect of diethylcarbamazine on the voltage-activated outward current of *Ascaris* muscle cells. (A) low time resolution recording; top, voltage steps to −20 mV from a holding potential of −35 mV; horizontal bar indicates the time of application of the diethylcarbamazine. (B) high- time resolution of the same events.

As a further test of this hypothesis, we have examined the permeability of the channel to the dicarboxylic anions: succinate, oxaloacetate and malate (Valkanov & Martin, 1995). Succinate is a major anion which is excreted from the muscle cell and it accumulates in the peri-enteric fluid. Malate and oxaloacetate are also produced in muscle cytoplasm during glucose fermentation but they are not excreted and do not accumulate in the peri-enteric fluid. If malate or oxaloacetate were to leak out of the cell then there would be a considerable energy drain on the cell. In addition, we have also examined the permeability of the monocarboxylic acids lactate and pyruvate.

Fig. 4 illustrates the currents that were recorded through the channel with succinate as the anion on the inside of the ion-channel and Cl^- on the outside of the channel; Fig. 5 illustrates the current recorded when malate was the anion on the outside of the membrane. From the reversal potentials, it is possible to determine the permeability of the test anion relative to Cl^- using the Goldman Constant field equation. It was found that all of the anions tested had a measurable permeability, but that only malate did not carry current through the channel. In *Ascaris*, the sarcoplasmic concentration of succinate and malate but not oxaloacetate, lactate or pyruvate may be significantly high (Tielens, 1994) because of activities of the intermediate enzymes. For example activity of malate dehydrogenase is high so that oxaloacetate concentrations in the cytoplasm are low. The properties of the channel, conducting monovalent anions with a Stokes diameter less the 6.5A ° and conducting succinate but not malate would permit excretion of acetate, propionate, succinate and α–methylbutyrate but not malate. Oxaloacetate, lactate, and pyruvate are not normally excreted in *Ascaris* and this may be explained by their low sarcoplasmic concentrations in *Ascaris*.

Because of the possible correlations between the activities of the Ca^{++}-activated Cl^- channel and pH, we chose to investigate the effect of pH on the activity of the channel (Robertson and Martin, 1996). Fig. 6 shows the effect on channel opening of reducing the pH on the cytoplasmic surface of the channel. It can be seen that an increase in H^+ concentration inside the muscle cell has no effect on the conductance of the channel but that the probability of the channel being open and the effect of membrane potential has reversed in polarity. This means that at the normal resting membrane potential of the bag, −35 mV, the channel opens less often when the intracellular pH is more acid and opens more when the intracellular pH is alkali. It means that if there is a proton pump excluding H^+ ions from the cell and increasing intracellular pH, the channel will open more frequently. Such a mechanism may be involved in the excretion of the carboxylic acid products of glucose metabolism.

Depolarizing potentials

The spontaneous depolarizing potentials that were first observed by Jarman (1959) were found to be myogenic in origin and appeared to arise from the syncytium (De Bell Del Castillo & Sanchez, 1963; De Bell, 1965). Three types of depolarizing potential have been distinguished by Weisblat & Russel (1976): (1) spikes of varying amplitude but up to 30 mV and 5–50 ms duration; (2) slow waves up to 20 mV in amplitude and lasting 100–100 ms; (3) a long lasting modulation wave up to 5 mV in amplitude, lasting 3–20 sec and associated with contraction.

The electrical activity of the adjacent muscle cell is correlated and is explained by electrical coupling due to tight junctions between muscle cell (De Bell *et al.* 1963; Del Castillo *et al.* 1989; Rosenbluth, 1965). The coupling allows adjacent muscle cells to synchronize depolarization and contraction.

The ionic basis of the spike potentials and slow-waves has been investigated using ion-substitution experiments by Weisblat, Byerly & Russel, (1976). It was found that Ca^{++} was required to support the

reduced intracellular pH had a dramatic effect on the membrane potential-probability of opening relationship and reversed the direction of its voltage sensitivity. The results were interpreted to indicate that the voltage-sensitive gate was pH sensitive and was accessible to protons from the cytoplasmic surface.

re/par821 Sep10 ere – sps art A5 8 (X 7)

Table 1. Single-channel conductances, mean open-times, and probability of being open of the channels activated by nicotinic anthelmintics.

Compound	Concentration (μM)	Conductance levels (pS)	Mean open-times (ms) at −75 mV	P open at −75 mV
Acetylcholine	1–10	25–35 & 40–50	1·96	0·03
Pyrantel	0·1–10	40 & 22	17·3	0·0057
Levamisole	1–10	32·9	1·47	0·0052
Oxantel	10	33·7	1·34	0·0014
Morantel	6	40 & 30	1·57	0·0076

spikes but that Na^+ or Ca^{++} was required for the slow waves. The currents responsible for spike potentials have been recorded by us using a two microelectrode voltage-clamp technique (Martin *et al.* 1992). Depolarization of the bag membrane results in activation of an inward Ca^{++} current and voltage-activated outward currents. Interestingly, part of the outward current may be blocked by 4–aminopyridine and by the anthelmintic diethylcarbamazine Fig. 7A and B (Martin, 1982).

ACETYLCHOLINE

Ascaris muscle has acetylcholine receptors

Baldwin & Moyle (1949) and then Norton & De Beer (1957) showed that bath application of acetylcholine produces contraction of *Ascaris* muscle strips, and they demonstrated the presence of acetylcholine receptors on muscle. Del Castillo, Del Mello & Sanchez, (1963) showed that the electrophysiological effect of acetylcholine was to produce depolarization and changes in spike frequency and amplitude. Originally it was reported by Del Castillo *et al.* (1963) that the acetylcholine receptors were only located at the syncytium region, but it was later shown, using focal application by ionophoresis, that there are also extrasynaptic nicotinic acetylcholine receptors located on the bag region of the muscle (Martin, 1982).

These extra-receptors on the bag region of the muscle were shown to be nicotinic since they were blocked by tubocurarine (Martin, 1982). Under voltage-clamp, ionophoresis of acetylcholine produces a current that has a reversal potential near 0 mV indicating that the acetylcholine nicotinic receptors are non-selective cation channels permeable to Na^+ and Ca^{++} (Martin, 1982; Harrow & Gration, 1985).

The patch-clamp technique has allowed single-channel currents activated by acetylcholine to be recorded using a vesicle preparation of the bag membrane (Pennington & Martin, 1990). The channels have at least two conductance levels, the main conductance is 40–50 pS and a smaller conductance is 25–30 pS. The mean open-times are around 2 ms (Table 1).

Pharmacology of the Ascaris *nicotinic acetylcholine receptor*

Membrane potential or contraction responses of *Ascaris* muscle to acetylcholine are blocked by tubocurarine but not atropine, so the acetylcholine receptors have been classified as nicotinic (Natoff, 1969; Rozhova, Malyutina & Shishov, 1980; Colquhoun, Holden-Dye & Walker, 1991). Further sub-classification of the receptor, on the basis of agonists potencies, suggests that the *Ascaris* receptor is pharmacologically similar to vertebrate ganglionic nicotinic receptors, but this sub-classification does not hold up when potencies of other nicotinic antagonists are examined. Mecamylamine, a ganglionic nicotinic antagonist and benzoquinonium, a neuromuscular nicotinic receptor antagonist, are both potent antagonists; the ganglionic antagonist hexamethonium and the neuromuscular nicotinic receptor antagonists, decamethonium and pancuronium are all weak antagonists. The detailed pharmacology of the *Ascaris* nicotinic receptor therefore differs from that of vertebrate nicotinic receptors. The nematode nicotinic receptor is best thought of as having its own (nematode) subtype (*e.g.* $nACh_n$ receptors). The selective agonist levamisole can be exploited therapeutically: it acts potently and selectively on the nematode nicotinic acetylcholine receptors but does not have potent effects on the nicotinic receptors of the host.

The nicotinic anthelmintics

Fig. 8 shows the chemical structure of the nicotinic anthelmintics. There are the imidazothiazoles (levamisole and butamisole); the tetrahydropyrimidines (pyrantel, morantel and oxantel), the quaternary ammonium salts (bephenium and thenium), and the pyrimidines (methyridine). These compounds act as agonists at nicotinic acetylcholine receptors of nematodes. Insoluble salts of pyrantel, morantel and oxantel are sold as oral preparations to prevent the active agent from leaving the gut and to minimize toxic effects on host receptors. They are therefore used against gastro-intestinal nematodes. Levamisole has less effect on host nicotinic receptors, and being partially unionized is well distributed in the

u/ere/par821 Sep10 ere – sps art A5 9 (X 8)

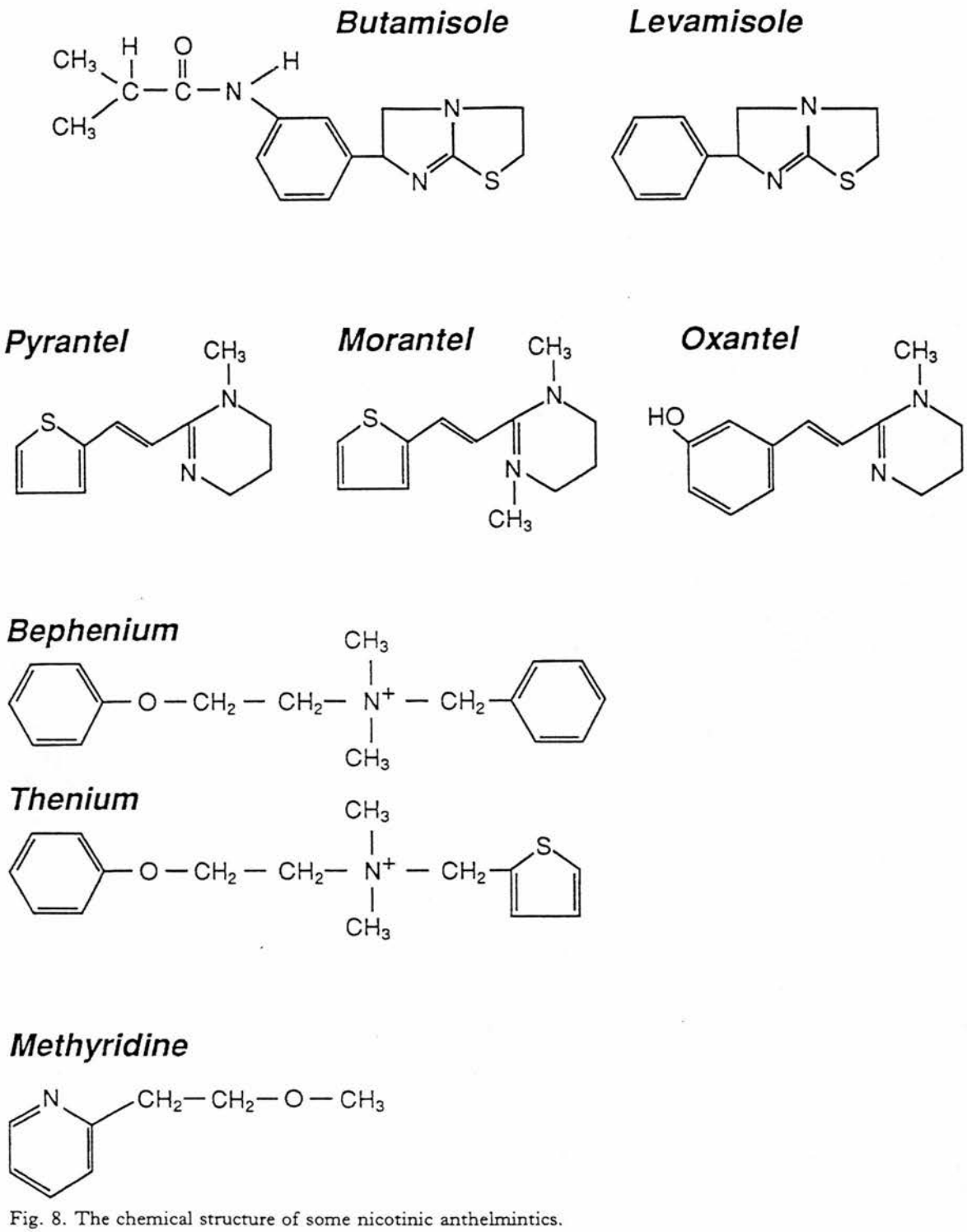


Fig. 8. The chemical structure of some nicotinic anthelmintics.

hosts body following oral administration or injection. Levamisole may be used to treat gastro-intestinal worms as well as lung worms. The electrophysiological effects of levamisole, pyrantel, morantel, and oxantel have been studied in greatest detail.

Intracellular potential and conductance effects of nicotinic anthelmintics

Bath application of tetramisole, the D,L-racemic mixture of which levamisole is the laevo-isomer, produces depolarization, an increase in spike frequency and contraction when applied to body flap preparations of *Ascaris* (Aceves, Erliji & Martinez-Marnon, 1970). Pyrantel and its analogues also produce depolarization, increased spike activity and contraction when bath applied to *Ascaris* muscle (Aubry *et al.* 1970).

The two-microelectrode current-clamp and voltage-clamp technique has been used to examine the effects of acetylcholine, levamisole, pyrantel, morantel (Martin, 1982; Harrow & Gration, 1985). These

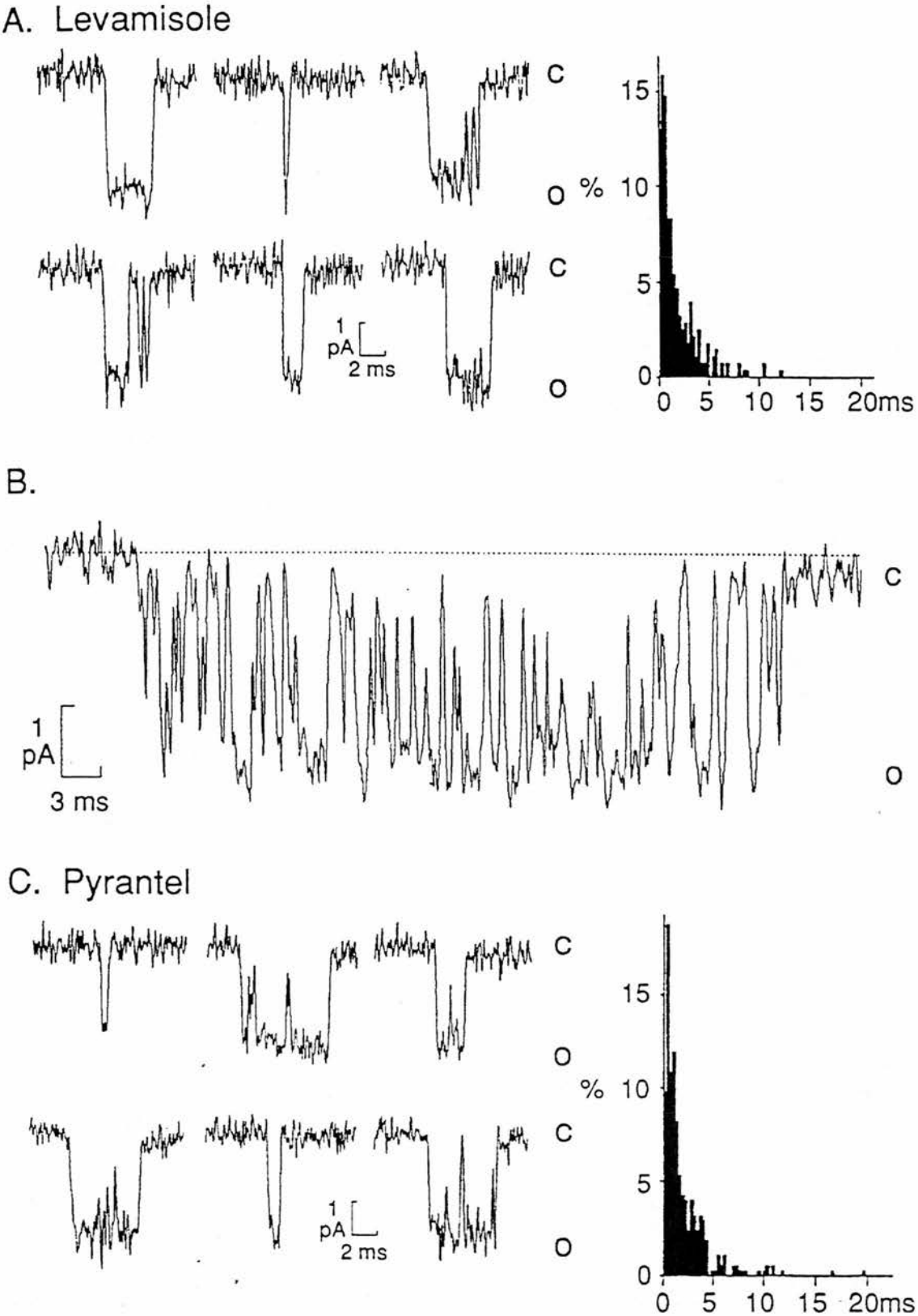


Fig. 9. Levamisole- and pyrantel- activated channel currents. (A) levamisole (10 μM) in the patch pipette activates the opening of fast non-selective cation channels in a cell-attached patch; c, closed state; o, open state. The distribution of the open times is shown in the histogram; the mean open time was 1·34 ms. (B) at higher levamisole concentrations (30 μM) levamisole produced a 'flickering open channel-block'. The dashed line indicate the level of the closed state. (C) pyrantel (0.1 μM) in the patch pipette activates the opening of fast non-selective cation channels in a cell-attached patch; c, closed state; o, open state. The distribution of the open times is shown in the histogram; the mean open time was 1.09 ms

Table 2. The blocking rate constants (k_{+B}), the unblocking rate constants (k_{-B}), and dissociation constants (K_B), for the nicotinic anthelmintics derived from an analysis of the channel currents using the simple open channel-block model at −50 mV & −75 mV

Constants	Levamisole	Pyrantel	Morantel	Oxantel
k_{+B} −50 mV	$2{\cdot}1 \times 10^7$ M^{-1} s^{-1}	$2{\cdot}2 \times 10^7$ M^{-1} s^{-1}	2×10^7 M^{-1} s^{-1}	$2{\cdot}4 \times 10^7$ M^{-1} s^{-1}
k_{+B} −75 mV	$3{\cdot}8 \times 10^7$ M^{-1} s^{-1}	$3{\cdot}1 \times 10^7$ M^{-1} s^{-1}	2×10^7 M^{-1} s^{-1}	$2{\cdot}4 \times 10^7$ M^{-1} s^{-1}
k_{-B} −50 mV	$2{\cdot}1 \times 10^3$ s^{-1}	$0{\cdot}8 \times 10^3$ s^{-1}	$0{\cdot}24 \times 10^3$ s^{-1}	$0{\cdot}44 \times 10^3$ s^{-1}
k_{-B} −75 mV	$1{\cdot}8 \times 10^3$ s^{-1}	$0{\cdot}6 \times 10^3$ s^{-1}	$0{\cdot}14 \times 10^3$ s^{-1}	$0{\cdot}16 \times 10^3$ s^{-1}
K_B −50 mV	123 μM	37 μM	12 μM	18·5 μM
K_B −75 mV	46 μM	20 μM	1 μM	7·5 μM

anthelmintics increase the input conductance and depolarize the membrane by opening non-selective cation channels which are permeable to Na^+ and K^+. Simultaneous application of acetylcholine and pyrantel showed that both agonists acted on the same nicotinic receptor (Harrow & Gration, 1985). The relative potency of the anthelmintics is: morantel = pyrantel > levamisole (Harrow & Gration, 1985).

In addition to the effects of the anthelmintics on the input conductance of the membrane, Harrow & Gration (1985) described the conductance dose-response curves for pyrantel and morantel as being bell-shaped. The concentration-effect relationship of pyrantel and morantel increases then decreases as the concentration of the anthelmintics is raised. One explanation for this phenomena is that of open channel-block (Colquhoun & Sakmann, 1985) by the anthelmintic. The nicotinic anthelmintics (including pyrantel and morantel) are large organic cations and could enter the nicotinic ion-channel from the outside; they try to pass through the channel pore like Na^+ or K^+ ions and produce block at narrow portion of the ion-channel. This block would be voltage-sensitive and increase with hyperpolarization of the membrane and concentration of the antagonists.

Single-channel currents activated by nicotinic anthelmintics

Initially, levamisole-activated single-channel currents, Fig. 9A were recorded from the muscle vesicle preparation (Robertson & Martin, 1993). The ion-channels were shown to be cation selective and to have similar kinetics to acetylcholine-activated channels at low levamisole concentrations (Table 1). The channels had mean open-times of 1.7 ms and had conductances in the range 20–45 pS. At higher concentrations of levamisole a flickering channel-block that increased on hyperpolarization was observed (Fig. 9B).

The channel-block produced by levamisole was described using a simple open channel-block model in which it is assumed that a single molecule of levamisole enters the open ion-channel and binds in a site within the channel pore, blocking it (Robertson & Martin, 1993):

$$C \underset{\alpha}{\overset{\beta'}{\rightleftharpoons}} O \underset{k-B}{\overset{k+B \cdot x_a}{\rightleftharpoons}} B$$

where C is the closed-state and O is the open-state of the channel, B represents the blocked-state with the anthelmintic occupying a block site in the channel pore. $\beta'\alpha$, k_{+B}, k_{-B} are rate constants and xa represents the anthelmintic concentration. β' is the opening rate of the channel and β' increases with concentration of the anthelmintic, α is the closing rate of the channel, k_{+B} is the blocking rate constant, and k_{-B} is the unblocking rate constant. The dissociation constant (K_B) for the anthelmintic binding to the block site is determined from the ratio k_B/k_{+B}. The lower the dissociation constant, the more potent the anthelmintic is as a channel-blocker.

The dissociation constant (K_B) of levamisole for the channel-block was 123 μM at −50 mV. Table 2 summarizes the kinetic parameters, including the association and dissociation rate constants of channel-block, that were measured at −50 mV and −75 mV (Robertson & Martin, 1993).

Pyrantel-activated channels (Fig. 9C) were then recorded using the same preparation and analytical technique (Robertson *et al.* 1994). The pyrantel-activated channels showed at least two distinguishable conductance levels: the main conductance level that was near 40 pS and the smaller conductance level that was near 22 pS. The pyrantel-activated channels showed a marked channel-block occurring at hyperpolarized potentials. The channel-block occurred more readily with pyrantel than with levamisole, and when the kinetics of the channel-block were analyzed in the same way as had been done for levamisole it was found that the dissociation constant, K_B, for pyrantel was lower than for levamisole (pyrantel K_B at −50 mV, 37 μM; levamisole K_B at −50 mV, 123 μM).

Table 1 summarizes properties of the channel currents activated by different nicotinic anthelmintics studied; it shows the conductances of the channels activated by acetylcholine and nicotinic anthelmintics, the mean open-times of the channels

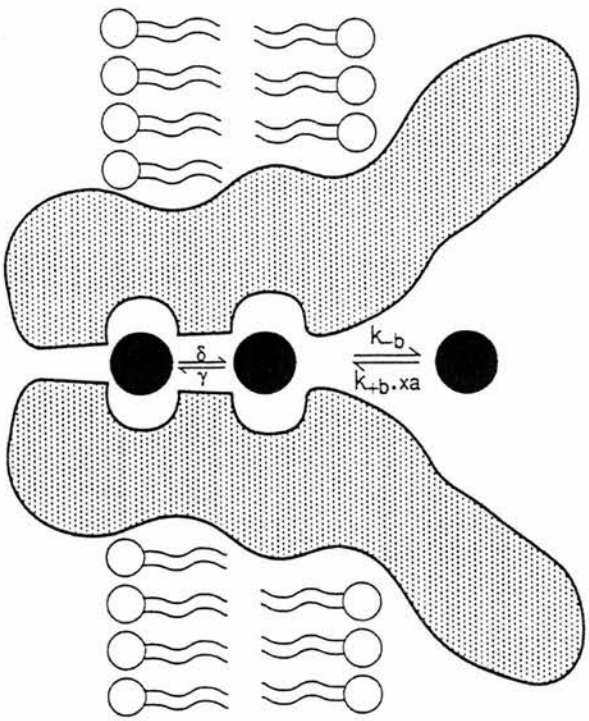


Fig. 10. Diagram of the two block site model used to describe the channel-block produced by morantel (Evans & Martin, 1996). It is assumed that a molecule of morantel at the extracellular entrance of the channel may enter and bind to a site near the entrance of the channel. The forward block rate is $K_{+B}.xa$, where xa is the molar concentration of morantel and k_{+B} is the rate constant M^{-1}. K_{-b} is the unblocking rate constant. The molecule of morantel, once bound may then proceed on to a second block site at a rate constant of γ and return from the second site to the first site at a rate of δ. Once a molecule of morantel has bound to the second block site, then the first block site may also be occupied by a second molecule of morantel. The nature of this block is that it shows a steep dose-response relationship with evidence of cooperativity. It is also possible to allow in the double block model to allow the rate at which the second molecule enters and leaves block site one to be different to when a single molecule of morantel enters an empty channel.

and the probability of the channel being open in the presence of the particular concentrations of anthelmintic. Table 2 shows values for the blocking rate (k_{+B}), unblocking rate (k_{-B}) and dissociation constant (K_B) derived using the same simple channel block model. The data were derived from Robertson & Martin (1993); Robertson *et al.* (1994); Dale & Martin (1995); Evans & Martin (1996).

Some general points may be made by examining the tables of the results. It can be seen that all the nicotinic anthelmintics produce channel-block, a form of self antagonism, and that levamisole is the least able to block its own channel. The channel-blocking ability of pyrantel is greater than levamisole: the greatest channel-block is produced by morantel (Evans & Martin, 1996).

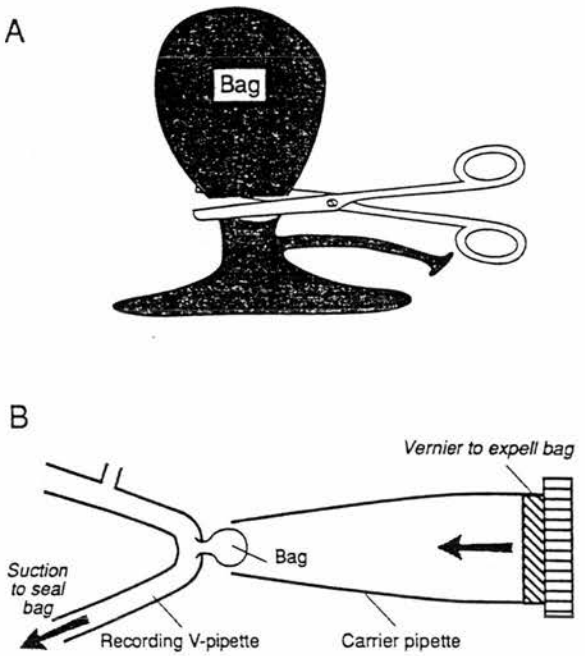


Fig. 11. (A) Diagram of the preparation and mounting of the isolated bag preparation for the Kostyuk voltage-clamp technique. After brief collagenase treatment, fine iris scissors were used to cut bags from the spindle region. (B) An isolated bag is then picked up in a manipulating pipette and placed with the neck in the mouth of the V-shaped pipette and sealed into the pipette by suction on the V-shaped micropipette.

It can also be seen that the least potent compound is oxantel which produced the lowest probability of opening even with high concentrations. The shortest mean open-times were observed with oxantel, 1·34 ms at −50 mV (Dale & Martin, 1995). Interestingly this compound is not effective therapeutically against Ascariasis but is used instead to treat *Trichuris* infections. Presumably the efficacy of oxantel against *Trichuris* but not against *Ascaris* is due to differences in the nicotinic receptors of the two species of nematode. Oxantel may be effective and produce opening of the *Trichuris* nicotinic acetylcholine receptor but is not so effective on the *Ascaris* receptor.

There may be more than one block site in the pores of Ascaris *nicotinic channels*

It has been usual to analyze properties of channel-blocking molecules by assuming that only one blocking ion enters and binds to a single site in the ion-channel pore. We found however, that when the properties of the ion-channel-block produced by morantel were analyzed in more detail (Evans & Martin, 1996) that the nature of the block could be better described by a multi-ion channel-block and that there is evidence of two block sites within the ion-channel. Fig. 10 illustrates a model we have proposed and used to describe the block produced by

u/ere/par821 Sep10 ere–sps art A5 13 (X 12)

morantel: it has the advantage of being able to explain more of the properties of the marked channel-block produced by morantel. Despite this, the simple channel-block model may be useful to allow a simple comparison of the degree of block produced by the different anthelmintics.

Non-nicotinic or 'muscarinic' cholinergic receptors in nematodes

In a number of vertebrate preparations, acetylcholine is able to alter the probability of voltage-dependent channel openings via G protein-coupled receptors. An action in nematodes, at receptors analogous to vertebrate muscarinic acetylcholine receptors modulating voltage-sensitive ion-channels, has yet to be fully reported.

There is biochemical evidence for the presence of 'muscarinic' receptors in *Ascaris suum* muscle: (i) Donahue, Yacob & Harris (1982) have observed that effects of cholinergic stimulation includes increases in levels of cyclic-AMP; (ii) Arevalo & Saz (1992) have observed that acetylcholine increases levels of phosphorylcholine, 1,2 diacylglycerides and phosphatidic acid and demonstrated the presence of phospholipase C activity. Donahue et al. (1982) and Arevalo & Saz (1992) did not distinguish between 'muscarinic' or 'nicotinic' cholinergic receptors

Kostyuk technique for recording voltage-dependent currents from the bag region of the muscle and effects mediated by cholinergic receptors

One problem with a two microelectrode voltage-clamp technique (Martin, 1982) for recording voltage-activated currents from *Ascaris* muscle effects of neurotransmitters is that is difficult to be certain that all the voltage-activated current produced is from the bag region muscle cell under clamp: the space-clamp is not likely to be perfect and some parts of the cell will escape the voltage-clamp. In addition, if we wish to study the effects of intracellularly-applied substances such as putative second messengers then they would have to be membrane permeable and be applied from the outside of the cell. To ameliorate these problems we have developed and applied the Kostyuk voltage-clamp technique to the isolated bag region of the muscle.

Large cells may be voltage-clamped and perfused intracellularly using a technique developed in Kostyuk's laboratory (Kostyuk, Krishtal & Pidoplicho, 1984). The technique consists of using a V-shaped glass or polythene tube/micropipette with a small 20–30 μm hole at the tip. The isolated cell to be recorded from is drawn onto the tip by suction producing a seal so that it is then possible to record voltage-clamp currents. To apply this technique for recording from *Ascaris* 'bags', we have used collagenase briefly to separate the 'bags' and then the bags are cut with fine iris scissors, Fig. 11A. The bags are then drawn up into the V-shaped micropipette for recording of bag currents during voltage steps, Fig 11B.

We have found that acetylcholine, in the presence of 100 μM tubocurarine or 100 μM mecamylamine, will increase slow voltage-dependent currents recorded using the Kostyuk technique even in absence of external calcium, Fig. 12. These voltage-activated currents have a long inward 'tail current' and have a reversal near -20 mV. The currents can be explained by the activation of another type of non-selective cation channel that appears to have much slower kinetics than the nicotinic channel and that appears to be slightly more selective for potassium than the nicotinic channel which has a reversal potential near 0 mV. Interestingly, we have found that the FMRFamide peptide PF1 (Geary *et al.* 1992) has the opposite effect on the current to acetylcholine and reduces this current. The properties of the voltage-dependent cation channel seem to be consistent with the properties of currents required to generate slow waves (Weisblat *et al.* 1976) and the effects of acetylcholine can be explained by the presence of another type of acetylcholine receptor on the muscle bag. Low concentration (< 10 μM) of atropine are not effective as an antagonist of the effects of acetylcholine so that the receptor is best referred to as a non-nicotinic receptor rather than a muscarinic receptor.

Resistance to anthelmintics

Previous studies on nematodes have shown that resistance to nicotinic anthelmintics may take two forms: (1) The selection of genetically resistant mutants with modified nicotinic acetylcholine receptors on muscle (Lewis *et al.* 1980, 1992). (2) Accommodation and recovery of parasites following long periods of exposure to the anthelmintics (Lewis *et al.*, 1980, 1992) and which may be explained by nicotinic receptor desensitization.

These resistant or recovered nematodes no-longer respond to the nicotinic anthelmintics but interestingly may still respond to acetylcholine (Coles, East & Jenkins, 1975). One explanation for these results is that, in addition to the nicotinic receptor on nematode muscle, there are other non-nicotinic cholinergic receptors present on muscle and which are not stimulated by the anthelmintics. This receptor may facilitate contraction by being coupled via G proteins to voltage-activated channel currents.

Pharmacology of the Ascaris *GABA receptor*

In addition to the extrasynaptic acetylcholine receptors on the bag region of the muscle cells, there are also extrasynaptic GABA receptors (Martin, 1980). The pharmacology to the extrasynaptic GABA

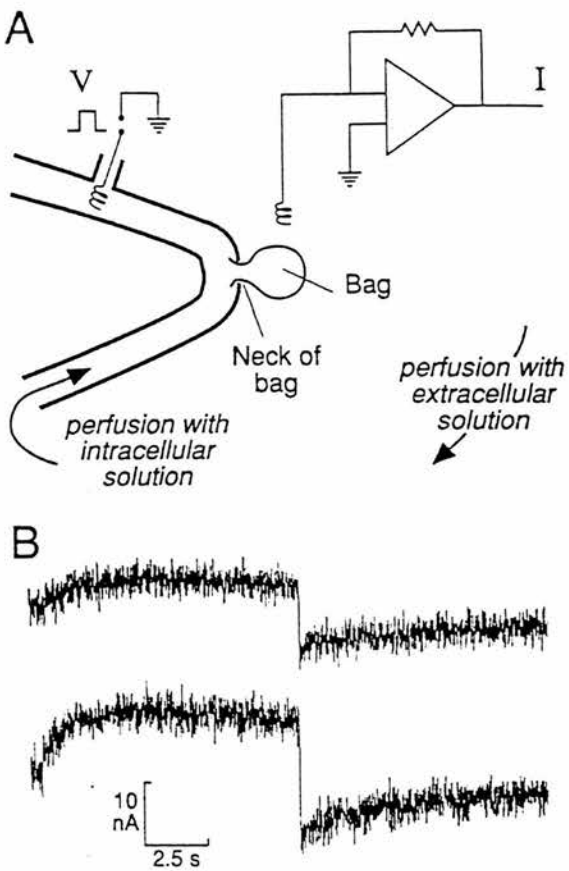


Fig. 12. (A) diagram of the Kostyuk voltage-clamp showing the V-shaped micropipette, the stimulation electrodes (V) and the recording of the current with the current voltage converter (I). Also illustrated is the ability to perfuse the isolated bag intracellularly or extracellularly. . (B) Leak-corrected currents activated by step potential to +27 mV from a holding potential −40 mV. Extracellular. solution (mM): Cs acetate, 135; BaCl, 19; TEA, 10; 4–AP, 5; HEPES, 5; pH 7·2 with CsOH. Intracellular. solution (mM): Cs acetate, 135; EGTA, 0·5, HEPES, 5; pH 7·2 with CsOH. Top: Control. Bottom: 50 μM ACh in 100 μM mecamylamine applied extracellularly.

receptor on *Ascaris* muscle has been examined with the two microelectrode current-clamp technique and the bath application of agonist and antagonists to examine the conductance-dose response relationship (Martin, 1980; Holden-Dye & Walker, 1988; Holden-Dye *et al.* 1988; 1989; Duittoz & Martin, 1989, 1990; Martin *et al.* 1995).

The relative potency of a range of GABA agonists have been determined by Holden-dye *et al.* (1989) the conductance dose-response relationships for of GABA agonists described by the Hill equation and the EC_{50}s determined by Duittoz & Martin (Martin, 1993) These observations showed that the agonist profile of the *Ascaris* receptor was similar to, but not identical to a vertebrate $GABA_A$ receptor.

In contrast it was found that vertebrate $GABA_A$ antagonists: bicuculline, securinine, pitrazepine, RU5135, dieldrin, and TBPS were weak or inactive (Martin, 1980; Holden-Dye *et al.* 1988; 1989; Martin *et al.* 1991). The potency of a series of arylaminopyidazine-GABA derivatives that act as competitive antagonists at vertebrate $GABA_A$ receptors as well as a the *Ascaris* GABA receptor do not show the same rank order potency (Duittoz & Martin, 1991 *a*, *b*). These differences further distinguish the *Ascaris* GABA receptor pharmacologically from vertebrate $GABA_A$ receptors and confirm the earlier suggestion (Martin, 1987) that there is different GABA receptor in nematodes, i.e. a $GABA_N$ receptor (not antagonized by pictrotoxin, N for nematodes).

The differences in the potencies of the arlyaminopyridazine-GABA derivatives at vertebrate $GABA_A$ receptors and *Ascaris* GABA receptors and the fact that these compounds are competitive antagonists at both types of receptor was interpreted to indicate that there are different accessory binding site on the *Ascaris* receptor (Duittoz & Martin, 1991 *b*). The study also indicated the action of novel arylaminopyridazine derivatives should be investigated with a view to examining further the structure activity of this series of compounds to find a more potent antagonist.

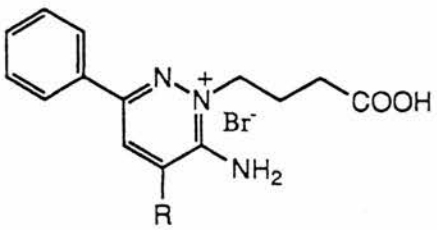
The structure-activity relationships of 35 novel derivatives of 2–(carboxypropyl)–3amino–4–methyl –6–phenyl pyridazine (SR 95103) were examined as GABA antagonists in the flap preparation of *Ascaris* using a two-microelectrode current-clamp technique (Martin *et al.* 1995). All but one of the potent antagonists displaced GABA dose-response curves to the right without reduction in the maximum response. The dissociation constants of the more potent competitive antagonists were described using a model which assumed that two molecules of GABA were required to open the ion-channel but that only one molecule of antagonist acted on each ion-channel. By exploring the structure activity relationship, the potency of the antagonist was increased from a K_B of 64 μM for SR 95103 to a K_B of 4·7 μM for NCS 281–93 [2–(3–carboxypropyl)–3–amino–4–phenylpropyl–6–phenyl pyridazine] (Table 3).

Possible therapeutic uses of GABA antagonists

Selective cholinergic agonists like levamisole, are used as anthelmintics and appear to work by acting as agonists on nematode muscle acetylcholine receptors (Harrow & Gration, 1985; Martin, 1993). Stimulation of the acetylcholine receptors produces depolarization and spastic paralysis of the nematode leading to its expulsion. Unfortunately resistance to therapy with these compounds is increasing, requiring higher concentrations of anthelmintic to be used (Sangster & Bjorn, 1995) or the change to a drug that has another mode of action. One way of increasing the effectiveness of a therapeutic regime

/u/ere/par821 Sep10 ere–sps art A5 15 (X 14)

Table 3. Derivatives modified in position 4



Compound	R	10*m*M % antagonism	0·1*m*M % antagonism	1*m*M % inhibition	K_B (μM)
SR 95103	CH_3	-	-	93 ± 3 (N = 5)	64 ± 13 (N =13)
SR 95132	C_6H_5	-	-	89 ± 3 (N = 5)	65 ± 20 (N = 9)
NCS 247-90	CH_3CH_2	-	-	95 ± 3 (N = 5)	55 ± 16 (N = 13)
NCS251-90	$C_6H_5CH_2$	-	24, 48 (N = 2)	99 ± 1 (N = 3)	31 ± 14 (N = 3)
NCS252-90	$(CH_3)_2CH$	-	-	81 ± 3 (N = 3)	-
NCS253-90	p-HO-$C_6H_5CH_2$	-	30, (N = 1)	91 ± 5 (N = 3)	-
NCS254-90	$C_6H_5CH_2CH_2$	-	56 ± 4 (N = 4)	97, 100 (N = 2)	11 ± 3 (N = 4)
NCS258-91	p-CH_3-$C_6H_4CH_2$	5, 11 (N = 2)	52, 42 (N = 2)	93,. 86 (N = 2)	-
NCS266-92	P-MeO-$C_6H_4(CH_2)_2$	0 (N = 1)	15, 38 (N = 2)	88, 97 (N = 2)	-
NCS267-92	m-Me)-$C_6H_4(CH2)2$	0, 0 (N = 2)	18, 35 (N = 2)	73, 93 (N = 2)	-
NCS268-92	4, 3-methylenedioxy	0, 0 (N = 2)	0, 0 (N = 2)	74, 58 (N = 2)	-
NCS281-93	$C_6H_5CH_2CH_2CH_2$	24, 10 (N = 2)	57, 50 (N = 2)	94, 96 (N = 2)	4·7 ± 0·7 (N = 11)
NCS282-93	$(C_6H_5)2CHCH_2$	11, 27 (N = 2)	75, 42 (N = 2)	73, 100 (N = 2)	Non-competitive

would be to add a selective GABA receptor antagonist along with the selective cholinergic agonist so that the two compounds could act in concert producing depolarization, contraction and spastic paralysis.

Further study of the structure activity relationships of arylaminopyridazines may permit the development of therapeutic approaches that can control nematode parasite resistant to other anthelmintic.

Piperazine

Piperazine has a heterocylic ring structure, Fig. 13, and is unlike GABA. Nonetheless, these two compounds act on the same receptor which is a ligand-gated Cl^- channel. GABA- and piperazine-activated channels have been recorded using cell-attached and isolated outside-out patches (Martin, 1985). Although the channels may have more than one conductance level, the most frequently observed was 22 pS for both agonists. However the mean open-time of the channels for piperazine was shorter, 14 ms, than that produced by GABA which produced channels that had mean open-times of 32 ms. GABA is more 10 to 100 times more potent than piperazine when conductance-dose responses are examined during bath application of the agonists (Martin, 1985). The difference in potency may be explained by the fact that higher concentrations of piperazine are required to produce the same opening rate as produced by GABA and that the average duration of the channel openings produced by piperazine is much shorter. The same probability of the channel being open can be achieved with lower concentrations of GABA than piperazine. Therapeutically however, GABA would be ineffective because it is not selective like piperazine and is in addition highly ionized and does not cross the cuticle and get access to the muscle receptors.

The avermectin receptor

The avermectins are a group of broad spectrum macrocyclic lactone antibiotic anthelmintics used to control nematode parasites in man and animals (Campbell & Benz, 1984). They are used to control onchocerciasis (river blindness) in humans and gastro-intestinal, cardiac and respiratory nematode parasites of domestic animals. The mode of action of the avermectins is to selectively paralyze the parasite by increasing muscle Cl^- permeability but the identity of the channel targeted by the avermectins has been controversial, see Arena (1994) for a recent review. Cloning of a GluCl–α and a GluCl–β subunit from the model soil nematode *Caenorrhabditis elegans* and co-expression of the subunits in *Xenopus* oocytes has led to the identification of an avermectin-sensitive glutamate-gated chloride ion-channel (Cully *et al.* 1994). The effects of avermectins, at low concentrations, are to potentiate the effect of glutamate, and at higher concentrations, the avermectins open the glutamate gated channel directly. The selective therapeutic effects of the avermectins might be explained by an action on a glutamate-gated Cl^- ion-channel that is present in parasitic nematodes but that it is not present in the host animal. One limitation of this hypothesis for the selective action of avermectins is that certain strains of collie dogs are sensitive to avermectins because they are thought to have a 'deficiency' in their blood brain barrier: this

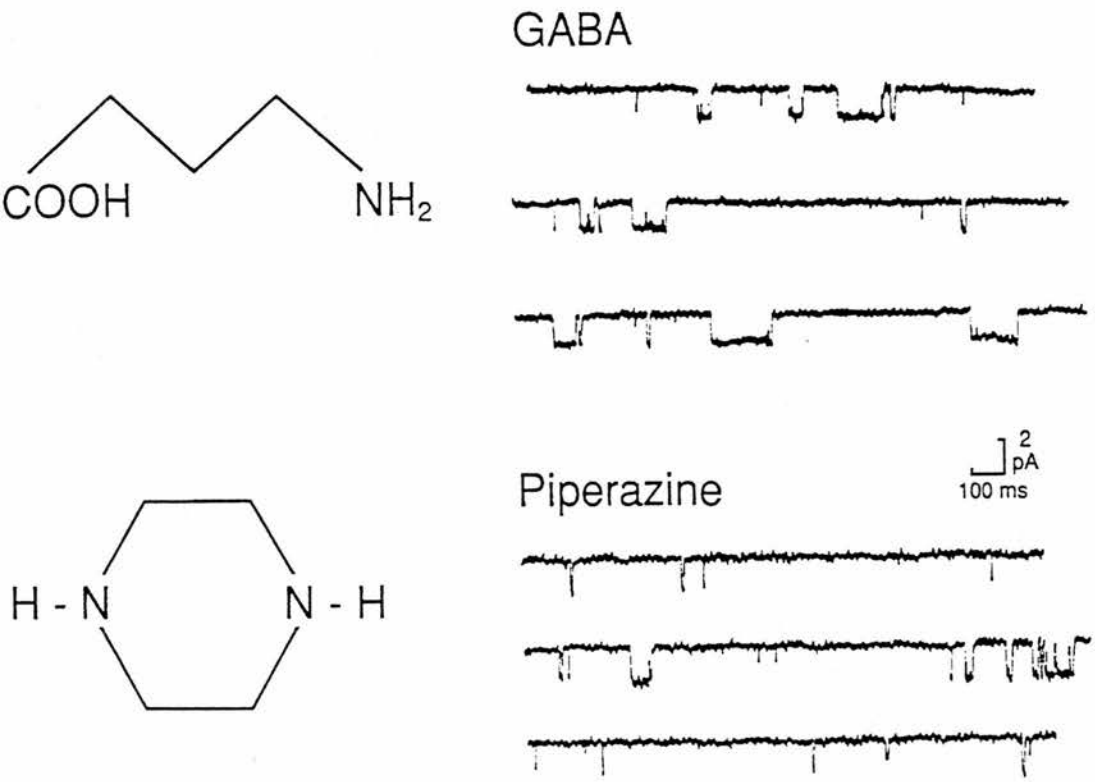


Fig. 13. Chemical structure of GABA and piperazine and their channel currents. Cell-attached patches. Transpatch potential −75 mV. Openings downwards. GABA: 3 μM GABA as the agonist in the patch pipette. Piperazine: 500 μM piperazine as the agonist. Effective mean open times: GABA 33 ms; piperazine 18 ms. Channel conductances 22 pS for both agonists.

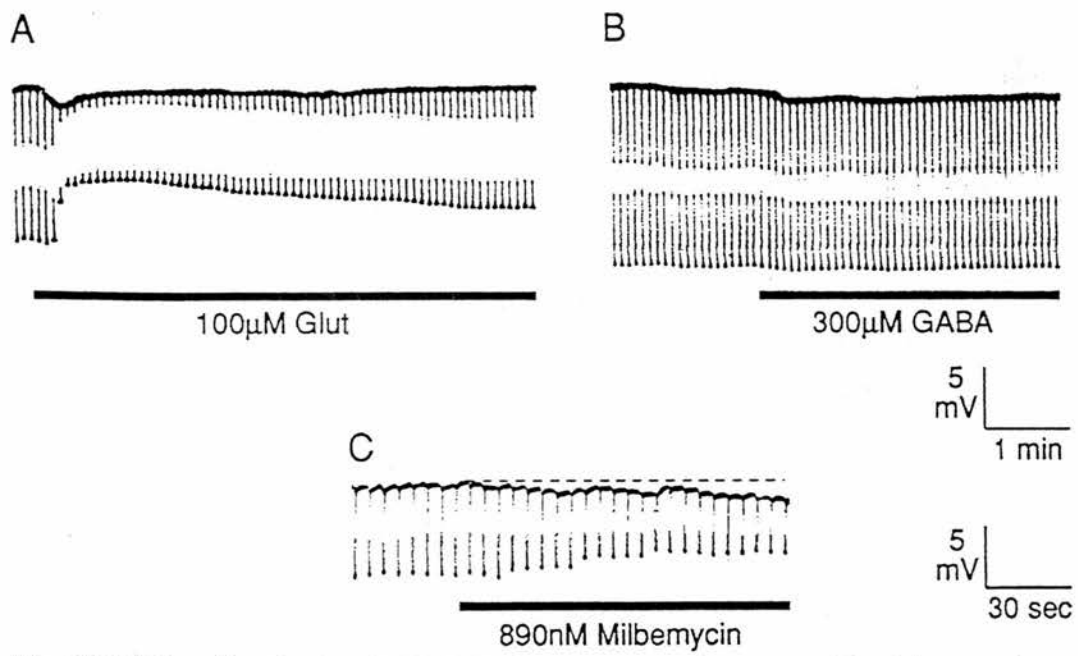


Fig. 14 (A) Effect of application of 100 μM L-glutamate on membrane potential and input conductance. Glutamate (applied during horizontal bar) produced a transient small hyperpolarization of 1 mV associated with an input conductance change from 157 μS to a peak of 429 μS (ΔG: 272 μS) desensitizing to 231 μS (ΔG: 74 μS) after 4 minutes. (B) After washing the preparation the input conductance of the pharynx returned towards control levels (142 μS) and the effect of 300 μM GABA was tested without effect (applied during the horizontal bar). The lack of effect of GABA was not due to desensitization because subsequent application of 100 μM L-glutamate increased the input conductance again (not shown). (C) Effect of 890 nM milbemycin D [different preparation to (A) and (B)] on the membrane potential and input conductance. Milbemycin slowly produced an increase in input conductance that was not reversed on washing (not shown).

/u/ere/par821 Sep10 ere–sps art A5 17 (X 16)

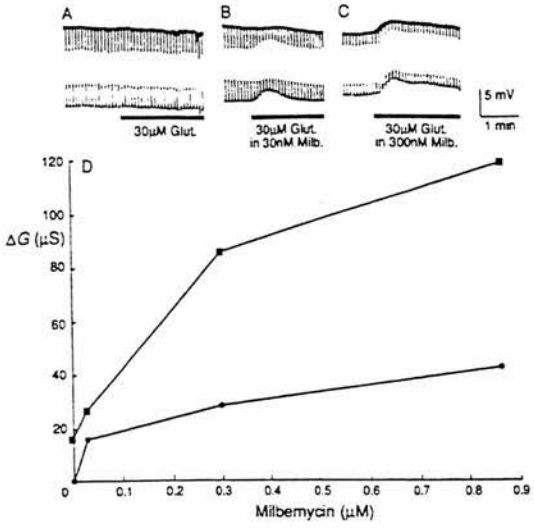


Fig. 15. Glutamate potentiation effects of milbemycin D. (A) Control 30 μM glutamate response, peak ΔG, is small, 16 μS. (B) In the presence of 30 nM milbemycin D the peak ΔG produced by 30 μM glutamate increased to 27 μS. (C) 300 nM milbemycin D increased the peak ΔG to 86 μS. In this particular preparation the glutamate response was a small depolarizing potential, indicating that the Cl-reversal potential was slightly depolarized relative to the membrane potential . (D) (■) plot of peak ΔG produced by 30 μM glutamate against milbemycin concentration; (●) plot of resting input conductance of the pharynx against milbemycin concentration. Results from the same experiment as (A), (B), & (C).

observation might suggest that there are avermectin sensitive Cl^- channels in the CNS of vertebrate hosts.

Molecular experiments using the *lacZ* marker suggest that the GluCl–β subunit of the glutamate channel is expressed in the pharynx of *C. elegans* pM4 muscle (Laughton, Wolstenholme & Lunt, 1995). The muscle is required for pharyngeal pumping/feeding and is known to receive an inhibitory motor neurone, M3, that is not likely to be GABAergic (Laughton *et al.* 1995) but glutamatergic (Avery, 1993). The location of the avermectin-sensitive glutamate-gated chloride channel, has been identified using a two microelectrode current-clamp technique (Martin, 1996) in *Ascaris* (Fig. 14). Experiments show that the pharyngeal muscle of this parasite possesses glutamate receptors that gate chloride channels and that are sensitive to the avermectin analogue milbemycin D.

Effect of glutamate

Fig. 15A shows effects of the application of 100 μM glutamate on *Ascaris* pharyngeal input conductance and membrane potential: glutamate produced a transient small hyperpolarization of 1 mV associated with an input conductance change from 157 μS to a peak of 429μS (ΔG: 272 μS) desensitizing to 231 μS (ΔG: 74 μS) after 4 minutes. The effect of glutamate but not GABA (Fig. 14B) in all preparations was to produce a reversible increase in input conductance associated with a small change in membrane potential; the membrane potential change was usually hyperpolarizing but in some preparations a small depolarizing potentials was observed. The glutamate induced increase in conductance is dose-dependent, and was fitted by the modified Hill equation with an ED_{50} of 60 ± 11 μM (mean $\pm$ S.E., n = 4). Zero-Cl^- solutions reversibly abolished the glutamate conductance responses and were used to demonstrate that the glutamate effect was mediated by a Cl^- channel (Martin, 1996).

Effect of milbemycin D

The effect of the ivermectin-analogue anthelmintic, milbemycin D, on the *C. elegans* avermectin-sensitive glutamate receptor expressed in *Xenopus* oocytes is to produce a potentiation of glutamate effects and to produce a slow irreversible increase in conductance of the membrane (Cully *et al.* 1994). The effects of milbemycin D on the input conductance of the *Ascaris* pharyngeal preparation is shown in the Figures 14C and 15A, B & C. In Fig. 14C, 890 nM milbemycin D slowly increased the resting conductance of the membrane from 353 μS to 857 μS and gave rise to a 2 mV hyperpolarization. Although milbemycin D mimicked the effect of glutamate on membrane potential and conductance, its effect as with the expressed receptor was not reversed on repeated washing. A potentiating effect of milbemycin D on the effects of glutamate was also seen: Figures 15A & B shows that 30 nM milbemycin D increased the peak ΔG produced by 30 μM glutamate from 16 μS to 27 μS and in Fig. 15C it is shown that 300 nM milbemycin D further increased the peak ΔG to 86 μS. In this particular preparation, the glutamate potential response was a small depolarizing potential, indicating that the Cl^- reversal potential was slightly depolarized relative to the membrane potential . The effect of milbemycin D concentration on the input conductance and the peak ΔG produced by 30 μM glutamate is plotted for this experiment in Fig. 15D: the Fig. emphasizes that the potentiation of glutamate was dose-dependent and that the potentiation increased as the effect of milbemycin on input conductance increased. The potentiation of the glutamate response by milbemycin D indicates that milbemycin and glutamate are interacting with the same channel and that the glutamate gated Cl^- channel described here is analogous to the *C. elegans* channel, expressed in *Xenopus* oocytes.

CONCLUSION

In this review we have outlined the electrophysiological properties of *Ascaris* muscle and described electrophysiological effects of anthelmintics whose

ere/par821 Sep10 ere – sps art A5 18 (X 17)

mode of action involves effects in membrane ion-channels. It is likely that some forms of resistance to anthelmintics will involve modification to of the properties of the target ligand-gated ion-channel.

ACKNOWLEDGMENT.

We are pleased to acknowledge the financial support of the Wellcome Trust.

REFERENCES

ACEVES, J., ERLIJI, D. & MARTINEZ-MARNON, R. (1970). The mechanism of the paralyzing action of tetramisole on *Ascaris* somatic muscle. *British Journal of Pharmacology* **38**, 602–7.

ARENA, J. P. (1994). Expression of *Caenorhabditis elegans* messenger-RNA in *Xenopus* oocytes: a model system to study the mechanism of action of avermectins. *Parasitology Today* **10**, 35–7.

AREVALO, J. I. & SAZ, H. J. (1992). Effects of cholinergic agents on the metabolism of choline in muscle from *Ascaris suum*. *Journal of Parasitology* **78**, 387–92.

AUBRY, M. L., COWELL, P., DAVEY, M. J. & SHEVDE, S. (1970). Aspects of the pharmacology of new anthelmintics: pyrantel. *British Journal of Pharmacology* **38**, 332–44.

AVERY, L. (1993). Motor-neuron m3 controls pharyngeal muscle-relaxation timing in *Caenorhabditis elegans*. *Journal of Experimental Biology* **175**, 283–97.

BALDWIN, E. & MOYLE, V. (1949). A contribution to the physiology and pharmacology of *Ascaris lumbricoides* from the pig. *British Journal of Pharmacology* **4**, 145–52.

BRADING, A. F. & CALDWELL, P. C. (1971). The resting membrane potential of the somatic muscle cells of *Ascaris lumbricoides*. *Journal of Physiology* (*London*) **217**, 605–24.

CAMPBELL, W. C. & BENZ, G. W. (1984). Ivermectin: A review of efficacy and safety. *Journal of Veterinary Pharmacology and Therapeutics* **7**, 1–16.

CAPPE DE BAILLON, P. (1911). Etude sur les fibres musculaires d' *Ascaris*. I. Fibres parietales. *Cellule* **27**, 165–211.

COLES, G. C., EAST, J. M. & JENKINS, S. N. (1975). The mechanism of action of the anthelmintic levamisole. *General Pharmacology* **6**, 309–13.

COLQUHOUN, D. & SAKMANN, B. (1985). Fast events in single-channel currents activated by acetylcholine and its analogues at the frog muscle end-plate. *Journal of Physiology* (*London*) **369**, 501–57.

COLQUHOUN, L., HOLDEN-DYE, L. & WALKER, R. J. (1991). The pharmacology of cholinoceptors on the somatic muscle-cells of the parasitic nematode *Ascaris suum*. *Journal of Experimental Biology* **158**, 509–30.

COWDEN, C. & STRETTON, A. O. W. (1993). AF2, an *Ascaris* neuropeptide - isolation, sequence, and bioactivity. *Peptides* **14**, 423–30.

COWDEN, C., STRETTON, A. O. W. & DAVIS, R. E. (1989). AF1, a sequenced bioactive neuropeptide isolated from the nematode *Ascaris suum*. *Neuron* **2**, 1465–73.

CULLY, D. F., VASSILATIS, D. K., LIU, K. K., PARESS, P. S., VANDERPLOEG, L. H. T. & SCHAEFFER, J. M. (1994). Cloning of an avermectin-sensitive glutamate-gated chloride channel from *Caenorhabditis elegans*. *Nature* **371**, 707–11.

DALE, V. M. E. & MARTIN, R. J. (1995). Oxantel-activated single-channel currents in the muscle membrane of *Ascaris suum*. *Parasitology*. **110**. 437–48.

DE BELL, J. T. (1965). A long look at neuromuscular junctions in nematodes. *Quarterly Reviews of Biology* **40**, 233–51.

DE BELL, J. T., DEL CASTILLO, J. & SANCHEZ, V. (1963). Electrophysiology of the somatic muscle cells of *Ascaris lumbricoides*. *Journal of Cellular & Comparative Physiology* **62**, 159–77.

DEL CASTILLO, J., DE MELLO, W. C. & MORALES, T. (1963). The physiological role of acetylcholine in the neuromuscular system of *Ascaris lumbricoides Archives International Physiologie Biochimie* **71**, 741–57.

DEL CASTILLO, J., DE MELLO, W. C. & MORALES, T. (1964). Influence of some ions on the membrane potential of *Ascaris* muscle. *Journal of General Physiology* **48**, 129–40.

DEL CASTILLO, J., RIVERA, A., SOLORZANO, S. & SERRATO, J. (1989). Some aspects of the neuromuscular system of *Ascaris*. *Quarterly Journal of Experimental Physiology and Cognate Medical Sciences* **74**, 1071–87.

DONAHUE, M. J., YACOUB, N. J. & HARRIS, B. G. (1982). Correlation of muscle-activity with glycogen-metabolism in muscle of *Ascaris suum*. *American Journal of Physiology* **242**, R514–R521.

DUITTOZ, A. H. & MARTIN, R. J. (1989). SR95103 acts as a GABA antagonist in *Ascaris suum* muscle. *British Journal of Pharmacology* **97**, 490P.

DUITTOZ, A. H. & MARTIN, R. J. (1990). Effects of the arylaminopyridazine-GABA derivatives, SR95103 and SR95531 on the *Ascaris* muscle GABA receptor: the relative potency of the antagonists in *Ascaris* is different to that at vertebrate GABAa receptors. *Comparative Biochemistry and Physiology C : Pharmacology Toxicology & Endocrinology* **98**, 417–22.

DUITTOZ, A. H. & MARTIN, R. J. (1991*a*). Effects of SR95103 on GABA-activated single-channel currents from *Ascaris suum* muscle. *Comparative Biochemistry And Physiology C-Pharmacology Toxicology & Endocrinology* **98**, 423–432.

DUITTOZ, A. H. & MARTIN, R. J. (1991*b*). Antagonist properties of arylaminopyridazine GABA derivatives at the *Ascaris* muscle GABA receptor. *Journal of Experimental Biology* **159**, 149–64.

GEARY, T. G., PRICE, D. A., BOWMAN, J. W., WINTERROWD, C. A., MACKENZIE, C. D., GARRISON, R. D., WILLIAMS, J. F. & FRIEDMAN, A. R. (1992). 2 FMRFamide-like peptides from the free-living nematode *Panagrellus redivivus*. *Peptides* **13**, 209–14.

GOLDSCHMIDT, R. (1908). Das Nervensystem von *Ascaris lumbricoides* und *Megalocephala*. Ein Versuch, in den Aufbau eines einfachen Nervensystems einzudringan, Zweiter Teil. *Zeitschrift fur wissenschaftliche Zoologie* **90**, 73–136.

GOLDSCHMIDT, R. (1909). Das Nervensystem von *Ascaris lumbricoides* und *Megalocephala*. Ein Versuch, in den Aufbau eines einfachen Nervensystems einzudringen, Zweiter Teil. *Zeitschrift fur wissenschaftliche Zoologie* **92**, 357–396.

GUASTELLA, J., JOHNSON, C. D. & STRETTON, A. O. W. (1991). GABA-immunoreactive neurons in the

/u/ere/par821 Sep10 ere–sps art A5 19 (X 18)

nematode *Ascaris*. *Journal of Comparative Neurology* **307**, 584–97.

GUASTELLA, J. & STRETTON, A. O. W. (1991). Distribution of H^3 GABA uptake sites in the nematode *Ascaris*. *Journal of Comparative Neurology* **307**, 598–608.

HARROW, I. D. & GRATION, K. A. F. (1985). Mode of action of the anthelmintics morantel, pyrantel and levamisole in the muscle cell membrane of the nematode *Ascaris suum*. *Pesticide Science* **16**, 662–72.

HOBSON, A. D., STEPHENSON, W. & BEADLE, L. C. (1952*a*). Studies on the physiology of *Ascaris lumbricoides*. I. The relation of total osmotic pressure, conductivity and chloride content of the body fluid to that of the external environment. *Journal of Experimental Biology* **29**, 1–21.

HOBSON, A. D., STEPHENSON, W. & EDEN, A. (1952*b*). Studies on the physiology of *Ascaris lumbricoides*. II. The inorganic composition of the body fluid in relation to that of the environment. *Journal of Experimental Biology* **29**, 22–9.

HOLDEN-DYE, L., HEWITT, G. M., WANN, K. T., KROGSGAARD-LARSEN, P. & WALKER, R. J. (1988). Studies involving avermectin and the 4-aminobutyric acid (GABA) receptor of *Ascaris suum* muscle. *Pesticide Science* **24**, 231–245.

HOLDEN-DYE, L., KROGSGAARD-LARSEN, P., NEILSEN, L. & WALKER, R. J. (1989). GABA receptors on the somatic muscle cells of the parasitic nematode, *Ascaris suum*: stereoselectivity indicates similarity to a GABA-type agonist recognition site. *British Journal of Pharmacology* **98**, 841–50.

HOLDEN-DYE, L. & WALKER, R. J. (1988). ZAPA, (Z)-3-[(amino iminomethyl)thio]-2-propenoic acid hydrochloride, a potent agonist at GABA receptors on the *Ascaris* muscle cell. *British Journal of Pharmacology* **95**, 3–5.

JARMAN, M. (1959). Electrical activity in the muscle cells of *Ascaris lumbricoides*. *Nature* **184**, 1244.

JOHNSON, C. D. & STRETTON, A. O. W. (1985). Localization of choline acetyltransferase within identified motoneurones of the nematode *Ascaris*. *Journal of Neuroscience* **5**, 1984–92.

JOHNSON, C. D. & STRETTON, A. O. W. (1987). GABA-immunoreactivity in inhibitory motor neurons of the nematode *Ascaris*. *Journal of Neuroscience* **7**, 223–35.

KOSTYUK, P. K., KRISHTAL, O. A. & PIDOPLICHO, V. I. (1984). Perfusion of Isolated Neurons Fixed in Plastic Film. In *Intracellular perfusion of excitable cells*. (eds. Kostyuk, P. K. & Krishtal, O. A. pp. 35–51. Chichester, New York, Brisbane, Toronto, Singapore: John Wiley and Sons.

LAUGHTON, D. L., WOLSTENHOLME, A. J. & LUNT, G. (1995). The beta subunit of the *C. elegans* inhibitory glutamate receptor is expressed in the pm4 pharyngeal muscle cells. *Worm Breeders Gazette* 14, 48.

LEWIS, J. A., WU, C.-H., LEVINE, J. H. & BERG, H. (1980). Levamisole-resistant mutants of the nematode *Caenorhabditis elegans* appear to lack pharmacological acetylcholine receptors. *Neuroscience* **5**, 967–89.

LEWIS, J. A., FLEMMING, J. T. & BIRD, D. (1992). Cloning nematode acetycholine receptor genes. In *Neurotox* '91, (ed. Duce, I. R.) pp. 155–164. London and New York: Elsevier Applied Science.

MARTIN, R. J. (1996). An electrophysiological preparation of *Ascaris suum* pharyngeal muscle reveals a glutamate-gated chloride channel sensitive to the avermectin analogue milbemycin D. *Parasitology* **112**, 247–52.

MARTIN, R. J. (1980). The effect of γ-aminobutyric acid on the input conductance and membrane potential of *Ascaris* muscle. *British Journal of Pharmacology* **71**, 99–106.

MARTIN, R. J. (1982). Electrophysiological effects of piperazine and diethylcarbamazine on *Ascaris suum* somatic muscle. *British Journal of Pharmacology* **77**, 255–65.

MARTIN, R. J. (1985). γ-aminobutyric acid- and piperazine-activated single channel currents from *Ascaris suum* body muscle. *British Journal of Pharmacology* **84**, 445–61.

MARTIN, R. J. (1987). The γ-aminobutyric acid receptor of *Ascaris* as a target for anthelmintics. *Biochemical Society Transactions* **17**, 61–5.

MARTIN, R. J. (1993). Neuromuscular-transmission in nematode parasites and antinematodal drug-action. *Pharmacology & Therapeutics* **58**, 13–50.

MARTIN, R. J., PENNINGTON, A. J., DUITTOZ, A. H., ROBERTSON, S. & KUSEL, J. R. (1991). The physiology and pharmacology of neuromuscular-transmission in the nematode parasite, *Ascaris suum*. *Parasitology* **102**, S41–S58.

MARTIN, R. J., THORN, P., GRATION, K. A. F. & HARROW, I. D. (1992). Voltage-activated currents in somatic muscle of the nematode parasite *Ascaris-suum*. *Journal of Experimental Biology* **173**, 75–90.

MARTIN, R. J., SITAMZE, J. M., DUITTOZ, A. H. & WERMUTH, C. G. (1995). Novel arylaminopyridazine-GABA receptor antagonists examined electrophysiologically in *Ascaris suum*. *European Journal of Pharmacology* **276**, 9–19.

MARTIN, R. J. & VALKANOV, M. A. (1995). A chloride channel in isolated muscle vesicles from *Ascaris suum* conducts products of anaerobic metabolism, suggesting a role in excretion of organic-anions. *Journal of Physiology* **482P**, 8.

NATOFF, I. L. (1969). The pharmacology of the cholinoceptor in muscle preparations of *Ascaris lumbricoides* cat. *suum*. *British Journal of Pharmacology* **37**, 251–57.

NORTON, S. & DE BEER, E. J. (1957). Investigations on the action of piperazine on Ascaris lumbricoides. *American. Journal of Tropical Medicine* **6**, 889–905.

PENNINGTON, A. J. & MARTIN, R. J. (1990). A patch-clamp study of acetylcholine-activated ion channels in *Ascaris suum* muscle. *Journal of Experimental Biology* **154**, 210–21.

ROBERTSON, S. J., PENNINGTON, A. J., EVANS, A. M. & MARTIN, R. J. (1994). The action of pyrantel as an agonist and an open-channel-blocker at acetylcholine-receptors in isolated *Ascaris suum* muscle vesicles. *European Journal of Pharmacology* **271**, 273–82.

ROBERTSON, S. J. & MARTIN, R. J. (1993). Levamisole-activated single-channel currents from muscle of the nematode parasite *Ascaris suum*. *British Journal of Pharmacology* **108**, 170–78.

ROBERTSON, A. P. & MARTIN, R. J. (1996). Effects of pH on the Ca-dependent chloride channel: a patch-clamp study in *Ascaris suum*. *Parasitology* **113**, 000–000.

ere/par821 Sep10 ere – sps art A5 20 (X 19)

ROSENBLUTH, J. (1965). Ultrastructure of somatic muscle cells in *Ascaris lumbricoides*. II. Intermuscluar junctions, neuromuscular junctions, and glycogen stores. *Journal of Cell Biology* **26**, 579–91.

ROZHOVA, E. K., MALYUTINA, T. A. & SHISHOV, B. A. (1980). Pharmacological characteristics if cholinoreception in somatic muscle of the nematode *Ascaris suum*. *General Pharmacology* **11**, 141–46.

SANGSTER, N. C. & BJORN, H. (1995). Levamisole resistance in *Haemonchus contortus* selected at different stages of infection. *International Journal for Parasitology* **25**, 343–8.

SAZ, N. J. & WEIL, A. (1962). A pathway of formation of alpha-methyl valerate by Ascaris lumbricoides. *Journal of Biological Chemistry* **237**, 2053–6.

SCHNEIDER, A. (1895). *Monograpie der Nematoden*. Berlin

STRETTON, A. O. W., COWDEN, C., SITHIGORNGUL, P. & DAVIS, R. E. (1991). Neuropeptides in the nematode *Ascaris suum*. *Parasitology* **102**, S107-S116.

STRETTON, A. O. W., FISHPOOL, R. M., SOUTHGATE, E., DONMOYER, J. E., WALROND, J. P., MOSES, J. E. R. & KASS, I. S. (1978). Structure and physiological activity of the motoneurons of the nematode *Ascaris*. *Proceedings of the National Academy of Sciences. USA* **75**, 3493–7.

TIELENS, A. G. M. (1994). Energy generation in parasitic helminths. *Parasitology Today* **10**, 346–52.

TSANG, V. C. & SAZ, H. J. (1973). Demonstration and function of 2-methyl-butyrate racemase in *Ascaris lumbricoides*. *Comparative Biochemistry and Physiology B* **45B**, 617–23.

VALKANOV, M. A. & MARTIN, R. J. (1995). A Cl channel selectively conducts dicarboxylic products from anaerobic glucose metabolism and indicates a role in transmembrane transport of waste organic anions. *Journal of Membrane Biology* **147**, 41–49.

VALKANOV, M. A., MARTIN, R. J. & DIXON, D. M. (1994). The Ca-activated chloride channel of *Ascaris suum* conducts volatile fatty-acids produced by anaerobic respiration – a patch-clamp study. *Journal of Membrane Biology* **138**, 133–41.

WEISBLAT, D. A., BYERLY, L. & RUSSEL, R. L. (1976). Ionic mechanisms of electrical activity in the somatic muscle cell of the nematode *Ascaris lumbricoides*. *Journal of Comparative Neurology* **111**, 93–113.

WEISBLAT, D. A. & RUSSEL, R. L. (1976). Propagation of electrical activity in the nerve cord and muscle syncytium of the nematode *Ascaris lumbricoides*. *Journal of Comparative Neurology* **107**, 293–307.

WHITE, J. G., SOUTHGATE, E., THOMPSON, J. N. & BRENNER, S. (1976). The structure of the ventral cord of *Caenorhabditis elegans*. *Philosophical Transactions of the Royal Society London, Series B* **275**, 298–327.

WHITE, J. D., SOUTHGATE, E., THOMPSON, J. N. & BRENNER, S. (1986). The structure of the nervous system of *Caenorhabditis elegans*. *Philosophical Transactions of the Royal Society of London, Series B* **314**, 1–340.

The Veterinary Journal 1997, **154**, 11–34

Review

Modes of Action of Anthelmintic Drugs

R. J. MARTIN

Department of Preclinical Veterinary Sciences, R.(D.)S.V.S., Summerhall, University of Edinburgh, Edinburgh EH9 1QH, UK

SUMMARY

Modes of action of anthelmintic drugs are described. Some anthelmintic drugs act rapidly and selectively on neuromuscular transmission of nematodes. Levamisole, pyrantel and morantel are agonists at nicotinic acetylcholine receptors of nematode muscle and cause spastic paralysis. Dichlorvos and haloxon are organophosphorus cholinesterase antagonists. Piperazine is a GABA (γ-amino-butyric acid) agonist at receptors on nematode muscles and causes flaccid paralysis. The avermectins increase the opening of glutamate-gated chloride (GluCl) channels and produce paralysis of pharyngeal pumping. Praziquantel has a selective effect on the tegument of trematodes and increases permeability of calcium. Other anthelmintics have a biochemical mode of action. The benzimidazole drugs bind selectively to β-tubulin of nematodes, cestodes and fluke, and inhibit microtubule formation. The salicylanilides: rafoxanide, oxyclozanide, brotianide and closantel and the substituted phenol, nitroxynil, are proton ionophores. Clorsulon is a selective antagonist of fluke phosphoglycerate kinase and mutase. Diethylcarbamazine blocks host, and possibly parasite, enzymes involved in arachidonic acid metabolism, and enhances the innate, nonspecific immune system.

KEYWORDS: Mode of action; anthelmintics; levamisole; dichlorvos; piperazine; avermectins; praziquantel; benzimidazoles; salicylanilides; clorsulon; diethylcarbamazine.

INTRODUCTION

Parasitic nematodes affect animals and man causing considerable suffering and poor growth. Effective anthelmintic drugs, used to treat and control these infestations, must have selective toxic effects on these parasites. Unfortunately with the increased use of these compounds, anthelmintic resistance has appeared and increased in frequency (Prichard, 1994). If resistance to a particular anthelmintic has occurred, it is likely that another anthelmintic with the same mode of action will also be ineffective although other anthelmintics with another mode of action, may still be effective. Clearly then, it is important to have an understanding of the mode of action of anthelmintics in order to inform the selection of effective therapeutic agents. This review describes modes of action of anthelmintic drugs (Table I).

NICOTINIC AGONISTS

Levamisole, butamisole, pyrantel, morantel, oxantel, bephenium and thenium

Fig. 1 shows the chemical structures of nicotinic anthelmintics. There are the imidazothiazoles (levamisole and butamisole); the tetrahydropyrimidines (pyrantel, morantel and oxantel); the quaternary ammonium salts (bephenium and thenium) and the pyrimidines (methyridine). These compounds act selectively as agonists at synaptic and extrasynaptic nicotinic acetylcholine receptors on nematode muscle cells (Fig. 2) and produce contraction and spastic paralysis. The electrophysiological effects of levamisole, pyrantel, morantel and oxantel have been studied in greatest detail.

1090-0233/97/040011-24/$12.00/0

© 1997 Baillière Tindall

Table I.
Summary table of the modes of action of anthelmintic drugs

	Generic drug name	*Examples of some U.K. & U.S.A. Trade Names*
Nicotinic agonists	levamisole	Nilverm
	butamisole	Styquin
	pyrantel	Strongid
	morantel	Paratect
	bephenium	
	thenium	Canopar
	methyridine	
Acetylcholinesterase inhibitors	haloxon	Mulitwurma
	dichlorvos	
GABA agonist	piperazine	Endorid.
GluCl potentiators	ivermectin	Ivomec
	abamectin	Enzec
	doramectin	Dectomax
	moxidectin	Cydectin
	milbemycin D	
Calcium permeability increase	praziquantel	Droncit
β-tubulin binding	thiabendazole	Thibenzole
	cambendazole	Equiben, Noviben
	oxibendazole	Loditac
	albendazole	Valbazen
	albendazole sulphoxide	Rycoben
	fenbendazole	Panacur
	oxfendazole	Systamex
	mebendazole	Telmin
	flubendazole	Flubenol
	febantel	Bayverm
	netobimin	Hepadex
	thiophanate	Wormalac, Nemafax
	triclabendazole	Fasinex
Proton ionophores	closantel	Flukiver
	rafoxanide	Flukanide, Ranide
	oxyclozanide	Zanil
	brotianide	In Flukombin and Vermadex
	nitroxynil	Trodax, Dovenix
	niclopholan	Bilevon, Distolon
	hexachlorophene	Coopaphene, Distodin
	dibromosalan	
	niclosamide	Yomesan
Inhibition of malate metabolism	diamphenethide	Coriban
Inhibition of phosphoglycerate kinase and mutase	clorsulon	In Ivomec Super
Inhibitor of arachidonic acid metabolism and stimulation of innate immunity	diethylcarbamazine	Caricide,Filaricide

Electrophysiological effects of nicotinic anthelmintics in nematodes

Intracellular recordings made with micropipettes from *Ascaris suum* body muscles have shown that bath application of tetramisole, the D/L racemic mixture of levamisole, produces mem-

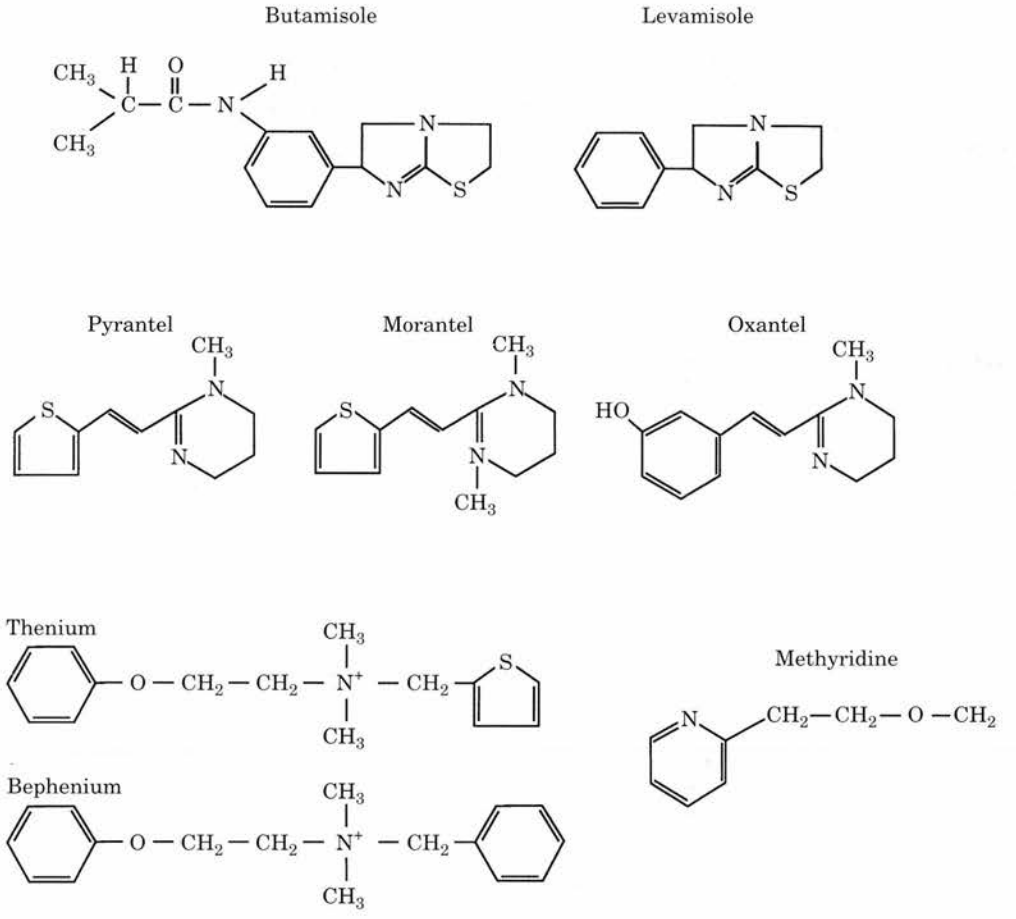


Fig. 1. Chemical structures of nicotinic anthelmintics.

brane depolarization, an increase in spike frequency and contraction (Aceves *et al.*, 1970). Pyrantel and its analogues also produce depolarization, increased spike activity and contraction when applied to *Ascaris* muscle (Aubry *et al.*, 1970) suggesting that these compounds have a common mode of action.

The two-microelectrode current-clamp and voltage-clamp techniques have been used to examine muscle membrane conductance changes in *Ascaris* produced by acetylcholine, levamisole, pyrantel and morantel (Martin, 1982a; Harrow & Gration, 1985). These anthelmintics have been shown to increase the membrane conductance and depolarize the membrane by opening non-selective cation ion-channels that are permeable to both Na^+ and K^+. Simultaneous application of acetylcholine and pyrantel showed that both agonists acted on the same nicotinic receptors, and the relative potency of the anthelmintics in bath application experiments was: morantel=pyrantel>levamisole>acetylcholine (Harrow & Gration, 1985).

In addition to effects of the anthelmintics on the membrane conductance of the muscle, Harrow and Gration (1985) described the conductance dose–response curves for pyrantel and morantel as being 'bell shaped'. The effect of this concentration–effect relationship is that the conductance-response increases then decreases as the concentration of the anthelmintics rises. One explanation for this phenomena is that of open channel block (Colquhoun & Sakmann, 1985) by the anthelmintic. Levamisole, pyrantel, morantel and oxantel are large organic cations, and could enter the nicotinic ion-channel from the outside and try to pass through the channel like Na^+ or K^+ ions but produce the block at the narrow region of the channel, the selectivity filter. This block would be voltage-sensitive and increase with hyperpolarization of the membrane and concen-

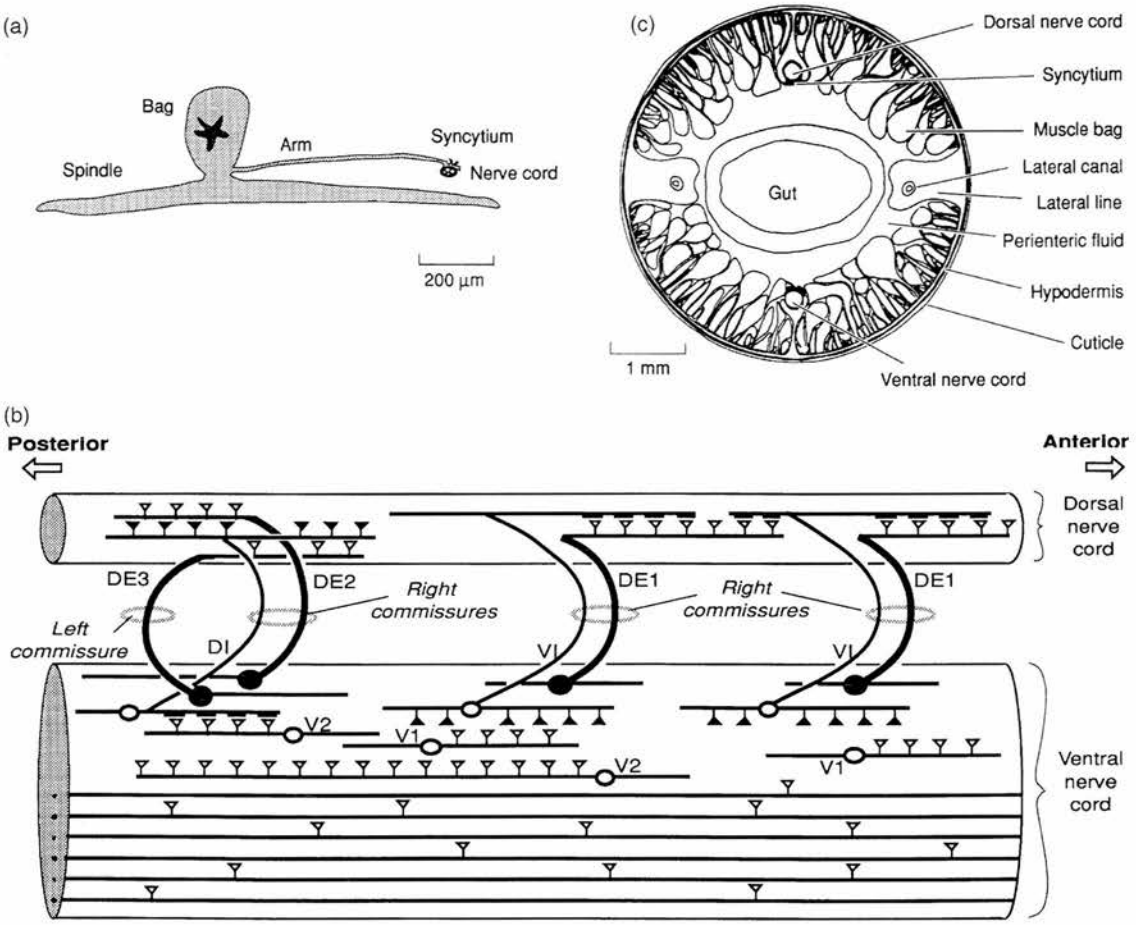


Fig. 2. Diagrams of the neuromuscular organization of nematode somatic muscle. (a) Diagram of a somatic muscle cell showing: the contractile spindle region; the balloon-shaped bag that contains the nucleus and glycogen granules; the arm which is a process of the muscle and reaches to one of the nerve cords where it divides into fingers that form an electrically-coupled complex with the fingers of adjacent muscle cells and collectively is known as the syncytium. The muscle cell possesses synaptic nicotinic acetylcholine receptors, and synaptic GABA receptors at the syncytial region and extrasynaptic acetylcholine and GABA receptors over the surface of the muscle. (b) Diagram of the dorsal and ventral nerve cord showing the cell represented in a segment. All the cell bodies of the motor neurones are contained in the ventral nerve cord. Each segment has three right-hand commissures and one left-hand commissure. Each commissure is made up of one or two axons or dendrites of the motor neurones that pass round the body to connect the ventral and dorsal nerve cord. Within each segment there are 11 motor neurones that are divided into seven anatomical types (DE1, DE2, DE3: dorsal excitatory motor neurones. DI: dorsal inhibitory motor neurones. VI: ventral inhibitory motor neurone. V1 & V2: ventral excitatory motor neurones. The remaining axons in the ventral nerve cord are intersegmental neurones. The excitatory motor neurones are cholinergic and the inhibitory motor neurones are GABAergic. (c) Diagram of a cross section of the body just caudal to the pharyngeal muscle. It shows the relative locations of the nerve cords, lateral lines, gut and muscle cells.

tration of the anthelmintic. This property of producing open channel block has been established using single-channel recording techniques (Robertson & Martin, 1993).

Single-channel currents activated by nicotinic anthelmintics

Initially, levamisole-activated channel currents [Fig. 3(a)] were recorded from the muscle vesicle preparation (Robertson & Martin, 1993) using the patch–clamp technique. The ion-channel currents activated by low levamisole concentrations were shown to carry cations and to have similar kinetics to acetylcholine-activated channels. The levamisole activated channels have a mean open time of 1.34 ms and a conductance in the range 20–45 pS. At higher concentrations of levamisole, a flickering open channel block that increases on hyper-

polarization is observed [Fig. 3(b)]. At −50 mV the dissociation constant for the channel block was 123 μM. In addition to the flickering block, clusters of openings were also observed at high levamisole concentrations where openings were separated by long (seconds) closed times: this clustering behaviour is similar to that assumed to be desensitization in vertebrates but was more voltage-sensitive and more prominent at hyperpolarized potentials in *Ascaris*.

Pyrantel-activated channels [Fig. 3(c)] have also been recorded using the same preparation (Robertson *et al.*, 1992). Pyrantel-activated channel showed at least two distinguishable conductance levels: the main conductance level was near 40 pS and the smaller conductance level was near 22 pS, suggesting the presence of more than one type of nicotinic receptor in the membrane. Again, the channels opened by pyrantel were shown to be permeable to monovalent cations and channel-block occurred at hyperpolarized potentials. The channel block occurred more readily with pyrantel than with levamisole as shown by the fact that the dissociation constant, K_B, for levamisole was higher than that of pyrantel (levamisole K_B at −50 mV 123 μM; pyrantel K_B at −50 mV 37 μM).

Table II summarizes the channel blocking properties of levamisole and pyrantel and, in addition, morantel and oxantel. Some general points may be made by examining Table II. It can be seen that all the nicotinic anthelmintics produce open channel-block, a form of self antagonism, and that levamisole is the least potent at blocking its own channel. The significance of the open channel block may relate to the ability of some nematodes to resist the effects of nicotinic anthelminitics: channel block may occur at such low anthelmintic concentrations that normal concentrations of anthelmintic are ineffective.

In *Ascaris*, the channel-blocking ability of pyrantel is greater than levamisole, but the greatest channel-block is produced by morantel with oxantel occupying an intermediate position between morantel and oxantel. The least potent agonist in *Ascaris* is oxantel which produces the lowest probability of channel opening even at high concentrations (Dale & Martin, 1995). Interestingly, oxantel is not effective therapeutically against ascariasis but is used instead to treat *Trichuris* infections. The efficacy of oxantel against *Trichuris* but not against *Ascaris* may be due to differences in the nicotinic receptors of the two species of nematode: oxantel may be effective and produce opening of the *Trichuris* nicotinic acetylcholine receptor but not so effective on the *Ascaris* receptor. The concentrations of oxantel and pyrantel along the intestine may also be a factor affecting efficacies of the drugs.

Non-nicotinic or 'muscarinic' cholinergic receptors in nematodes and resistance to anthelmintics

In a number of vertebrate preparations, acetylcholine is able to alter the probability of opening of voltage-dependent channels by acting via G-protein-coupled muscarinic receptors. An action in nematodes at acetylcholine receptors analogous to vertebrate muscarinic receptors, modulating voltage-sensitive ion channels has yet to be fully reported.

There is biochemical evidence for the presence of 'muscarinic' receptors in *Ascaris* muscle:

(1) Donahue *et al.* (1982) have observed that effects of cholinergic stimulation includes increases in levels of cyclic-AMP;
(2) Arevalo and Saz (1992) have observed that acetylcholine increases levels of phosphorylcholine, 1,2-diacylglycerides and phosphatidic acid, and demonstrated the presence of phospholipase C activity. Donahue *et al.* (1982) and Arevalo and Saz (1992) did not distinguish between 'muscarinic' or 'nicotinic' cholinergic receptors.

Previous studies on nematodes have shown that resistance to nicotinic anthelmintics may take two forms: (1) The selection of genetically resistant

Table II
Voltage sensitivity of dissociation constants of open channel block by the nicotinic anthelmintics

Membrane	*KB Levamisole*	$2K_B$ *Pyrantel*	K_B *Morantel*	K_B *Oxantel*
−50 mV	123 μM	37 μM	12 μM	18.5 μM
−75 mV	46 μM	20 μM	1 μM	7.5 μM
Voltage-sensitivity of K_B	e-fold every 20 mV	e-fold every 40 mV	e-fold every 22 mV	e-fold every 29 mV

K_B is the dissociation constant: the lower the concentration of this constant the more potent it is. At the concentration of the **K***B* the channel is blocked for 50% of its open time so the response would be reduced by a half.

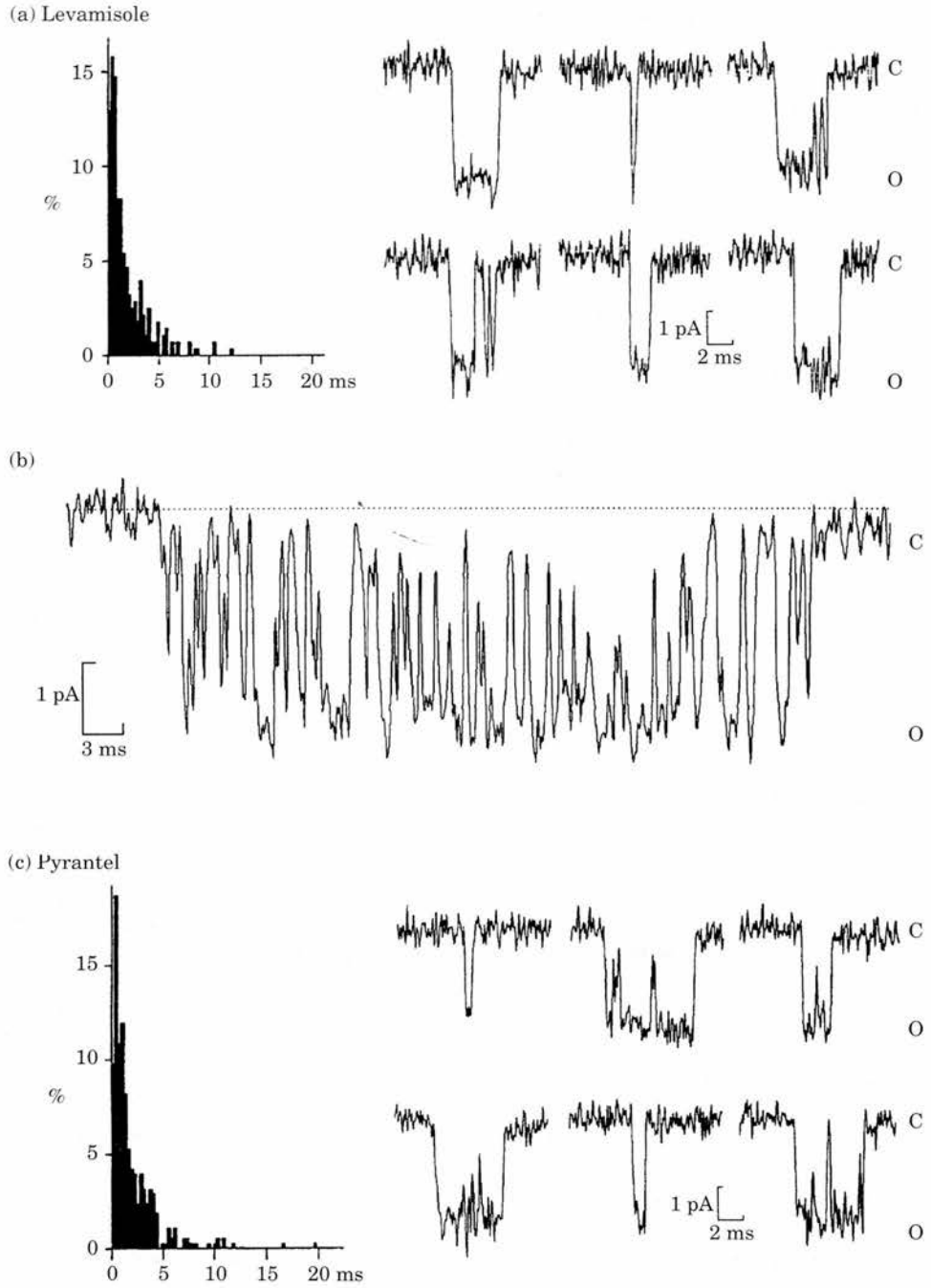


Fig. 3. Patch-clamp records of single-channel currents activated by levamisole. The patch-clamp technique allows the activity of single ion-channels in the membrane of the cell to be recorded as the channel opens and closes. Small (1×10^{-12} A) current pulses are recorded with this technique. The currents are rectangular in shape; C is the closed state and O is the open state. (a) Histogram of open-times and records of levamisole-activated single-channel currents. Cell-attached patches. Openings downward. Patch potential −75 mV; 10 μM levamisole in the patch pipette. Mean open time: 1.34 ms. (b) A flickering burst demonstrating channel block produced by 30 μM levamisole at −75 mV, cell-attached patch. The comb effect of the channel current is characteristic of a drug moving into and blocking the ion-channel. (c) Histogram of open-times and records of pyrantel-activated single-channel currents. Cell-attached patch; openings downward; patch-potential −75 mV; 0.1 μM micromolar pyrantel in the patch-pipette. Mean open-time: 1.09 ms. The pyrantel channel open times are on average slightly shorter than those of levamisole.

mutants with modified nicotinic acetylcholine receptors on muscle (Lewis *et al.*, 1980; Lewis *et al.*, 1992). (2) Accommodation and recovery of parasites after long periods of exposure to the anthelmintics (Lewis *et al.*, 1980; Lewis *et al.*, 1992), and which may be explained by nicotinic receptor desensitization.

These resistant or recovered nematodes no longer respond to the nicotinic anthelmintics, but interestingly, may still respond to acetylcholine (Coles *et al.*, 1975). One explanation for these results is that in addition to the nicotinic receptor on nematode muscle, there are other non-nicotinic cholinergic receptors present on muscle not stimulated by the nicotinic anthelmintics. Such receptors may facilitate contraction by being coupled via G-proteins to voltage-activated channels.

Genetics of resistance to nicotinic anthelmintics

The genetics of resistance to the anthelmintic levamisole has been studied in the laboratory using the small free-living soil nematode, *Caenorhabditis elegans*. Several hundred levamisole-resistant alleles have been identified that were isolated in several screens (Lewis *et al.*, 1980; Lewis *et al.*, 1992). The genes responsible for this resistance included: *lev-1, unc-29* and *unc-38* that encode the proteins subunits that make up the nicotinic ion channels of the nematode. In addition, other genes including: *unc-50, unc-63* and *unc-74* that are believed to be involved in receptor biosynthesis have been identified.

Only two strains of *lev-1* (×21 and ×61) were dominant when crossed over with wild-types (non-resistant) (Fleming *et al.*, 1994). The *lev-1* (×21) strain only involves mutation at a single amino-acid, replacing glutamic acid in the ion pore of the receptor ion channel (in alpha-7 at position 237) with a positively-charged lysine. This change is believed to be sufficient to change the ion channel from cationic to anionic, i.e., to convert the receptor from an excitatory channel to an inhibitory one. The *lev-1* (×61) strain contains the amino-acid leucine in the pore of the ion-channel (in alpha-7 at position 247): this point mutation is expected to produce increased desensitization and reduced affinity for levamisole, rendering levamisole less potent as an agonist.

The genetics of levamisole resistance in parasitic nematodes remains to be studied.

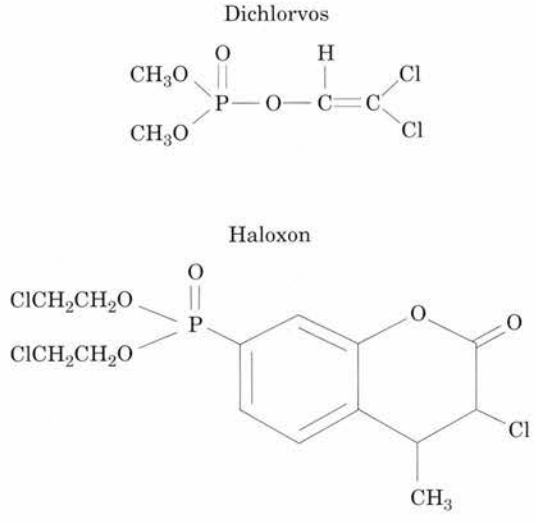


Fig. 4. Chemical structure of dichlorvos and haloxon.

ORGANOPHOSPORUS CHOLINESTERASE INHIBITORS

Dichlorvos, haloxon

Compounds like dichlorvos and haloxon are selective organophosphorus anti-cholinesterases (Fig. 4), and have an anthelmintic action, as well as an insecticidal, action. Dichlorvos and haloxon can control insect parasites, as well as helminth parasites. The mode of action of these compounds is to block the action of the parasite enzyme, acetylcholinesterase, leading to the excessive build up of the neurotransmitter, acetylcholine. This mode of action also predisposes towards toxicity in the host animal where acetylcholinesterase enzymes are also present. Because more selective combined anthelmintic+insecticidal agents (avermectins and milbemycin) are available, the organophosphorus compounds are now used less frequently.

The existence of cholinesterase, the enzyme that breaks down acetylcholine, was first described in *Ascaris* by Bueding (1952). The distribution of cholinesterase was described by Lee (1962) who used histochemical techniques. In the head region of *Ascaris*, most of the enzyme activity is associated with the contractile spindle region of the muscle and is in the extracellular matrix. Lee (1962) also described cholinesterase activity on the muscle arms near their endings on the nerve cords but not on the bag region of the muscle.

In *C. elegans*, three classes of acetylcholinesterase are recognized: class A, class B, and class C,

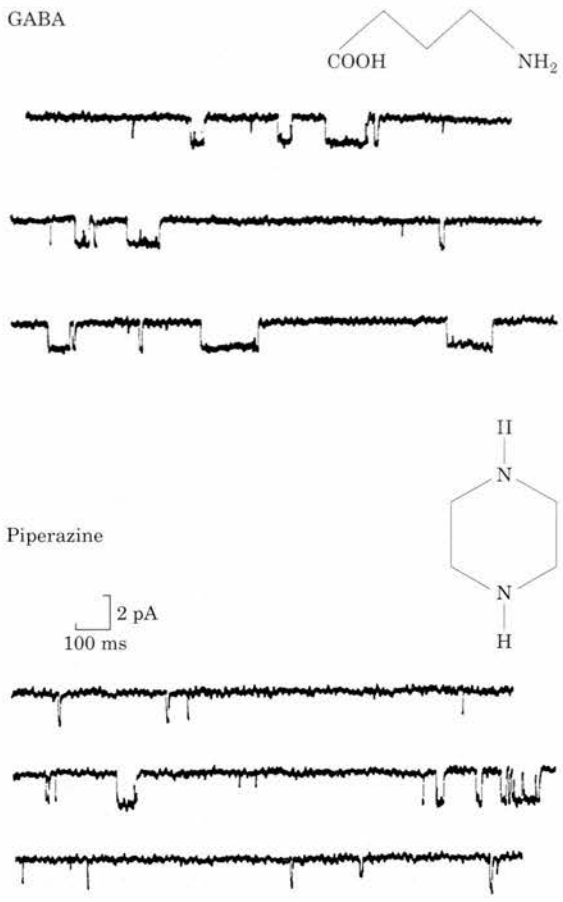


Fig. 5. The chemical structures of GABA and piperazine (left) and single-channel currents activated by them (right). Openings downward. Cell attached patches; −75 mV GABA channel mean open-times 32 ms. Piperazine mean-open times 18 ms. GABA 3μM. Piperazine 500 μM.

and are known to be products of three separate genes: *ace-1, ace-2 and ace-3* (Opperman & Chang, 1992). The three classes of acetylcholinesterase are separable by their solubility in Triton, their temperature stability and sensitivity to cholinesterase antagonists. In *C. elegans*, the major form is class B which is distributed in the head and body; classes A and C have a distribution biased towards the head. Extraction of the different classes for biochemical characterization has produced evidence that the enzyme may exist as a monomer, dimer and tetramer. Defects in the *ace-1, ace-2 and ace-3* genes suggest that the functions of the different classes are supplementary but that if there are defects in all of the genes, then elevated levels of acetylcholine occur in *C. elegans* and there is motor incoordination (Opperman & Chang, 1992).

Although acetylcholinesterase is responsible for the breakdown of acetylcholine and involved in motor action in nematodes, it is also secreted into the external environment in large quantities by *A. suum* and other parasitic nematodes. The function of the secreted acetylcholinesterase may be to reduce the effects of host acetylcholine in the intestine, perhaps decreasing mucosal glandular secretion by the host. The original hypothesis of a biochemical 'hold-fast' effect (reduced acetylcholine in the host intestine blocking peristalsis of the gut) has now been rejected. The identification of the function of secreted cholinesterase by parasitic nematodes, and the ability to antagonize this enzyme, may lead to the increased use of anticholinesterases in the future to facilitate removal of gut nematodes.

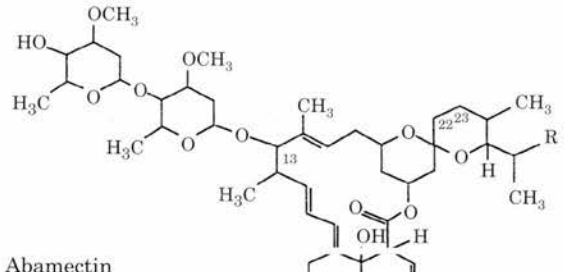
GABA AGONIST

Piperazine

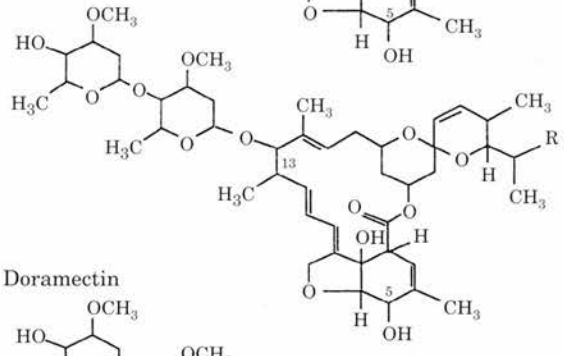
Piperazine has a heterocylic ring structure (Fig. 5), and unlike γ-amino-butyric acid (GABA), lacks a carboxyl group. However, these two compounds act on the same receptor that is a ligand-gated Cl^- channel found on the synaptic and extrasynaptic membrane of nematode muscle (Martin, 1980; Martin, 1982). Bath application of GABA or piperazine increases the opening of the muscle membrane Cl^- channels, hyperpolarizes the membrane potential, increases the membrane conductance and produces spastic paralysis. Piperazine appears to have a selective effect on large nematodes of the gastrointestinal tract, perhaps because the high CO_2 environment allows CO_2 to mimic the missing carboxyl group of piperazine. Piperazine appears less active against nematodes that occupy a high O_2 environment.

Piperazine- and GABA-activated channel currents (Fig. 5) have been recorded using cell-attached and isolated outside-out patches (Martin, 1985). Although the channels may have more than one conductance level, the most frequently observed is 22 pS for both agonists. However, the mean open time of the channels for piperazine was shorter, 14 ms, than that produced by GABA, which produced channels that had mean open times of 32 ms. GABA is more than 10–100 times more potent than piperazine when conductance dose–response relationships are examined during bath application of the agonists (Martin, 1985).

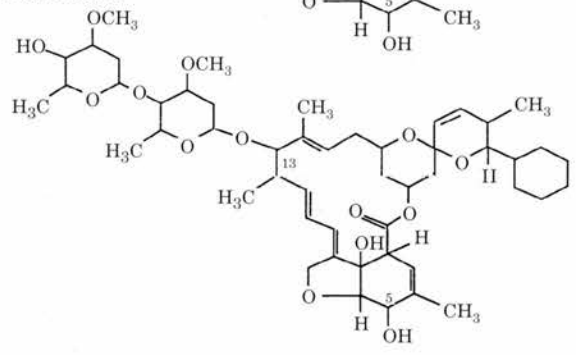
Ivermectin



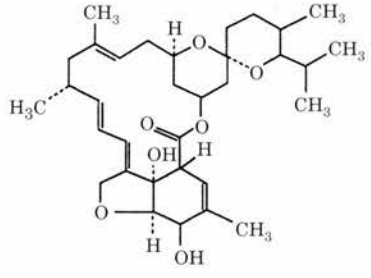
Abamectin



Doramectin



Milbemycin D



Moxidectin

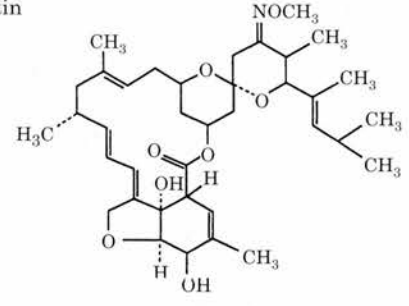


Fig. 6.

The difference in potency may be explained by the fact that higher concentrations of piperazine are required to produce the same opening rate of the channel as that produced by GABA, and that the average duration of the channel openings produced by piperazine is much shorter. The same probability of channel opening can be achieved with lower concentrations of GABA than piperazine. Therapeutically, however, GABA would be ineffective because it is not selective like piperazine and is highly ionized and does not cross the cuticle.

GLUTAMATE-GATED CHLORIDE (GLUCL) RECEPTOR POTENTIATORS

Ivermectin, abamectin, doramectin, milbemycin D, moxidectin

The avermectins (Fig. 6) are a group of broad-spectrum, macrocyclic, lactone antibiotic anthelmintics used to control nematode parasites in man and animals (Campbell & Benz, 1984), and assumed to have the same mode of action in both (Shoop *et al.*, 1995). They are used to control onchocerciasis (river blindness) in humans and gastrointestinal, cardiac and respiratory nematode parasites of domestic animals. The mode of action of the avermectins is to selectively paralyse the parasite by increasing muscle Cl^- permeability, but the identity of the channel targeted by the avermectins has been controversial, see Arena (1994) for a recent review. Cloning of a GluCl-α1 and a GluCl-β subunit from the model soil nematode *C. elegans*, and co-expression of the subunits in *Xenopus* oocytes, has led to the identification of an avermectin-sensitive GluCl ion-channel (Cully *et al.*, 1994). The effects of avermectins, at low concentrations, are to potentiate the effect of glutamate, and at higher concentrations, the avermectins open the glutamate-gated channel directly. The selective therapeutic effects of the avermectins could be explained by an action on a Glu Cl^-

Fig. 6. Chemical structure of avermectin and milbemycin anthelmintics. Ivermectin is at least 80% 22,23 dihydroavermectin B1a (R is sec butyl) and not more than 20% 22,23 dihydroavermectin B1b (R is isopropyl). Abamectin is at least 80% avermectin B1a (R is sec butyl) and not more than 20% avermectin B1b (R is isopropyl).

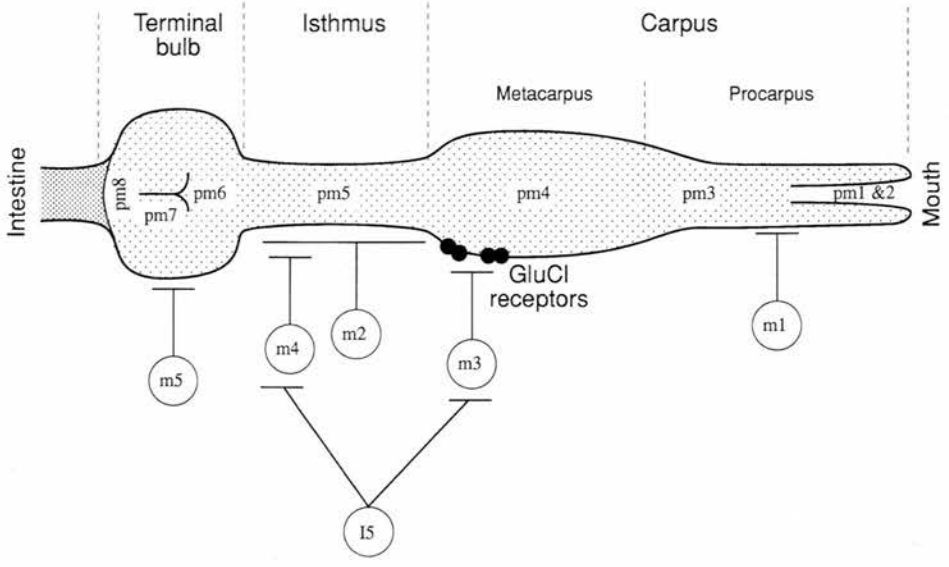


Fig. 7. Diagram of the pharyngeal muscle of *C. elegans* showing the location of the GluCl receptors on the *pm4* muscle cells that are innervated by the *m3* motor neurones. Also illustrated is the division of the pharyngeal muscle into the regions: terminal bulb; isthmus; carpus (subdivided into metacarpus and procarpus). The other motor neurones (*m1, m2, m4 & m5*) that innervate the muscle cells (*pm3, pm5, pm6, pm7*) are shown. The interneurones *I5* that inhibits *m3*, as well as *m4*, is shown. Adapted from Avery (1993).

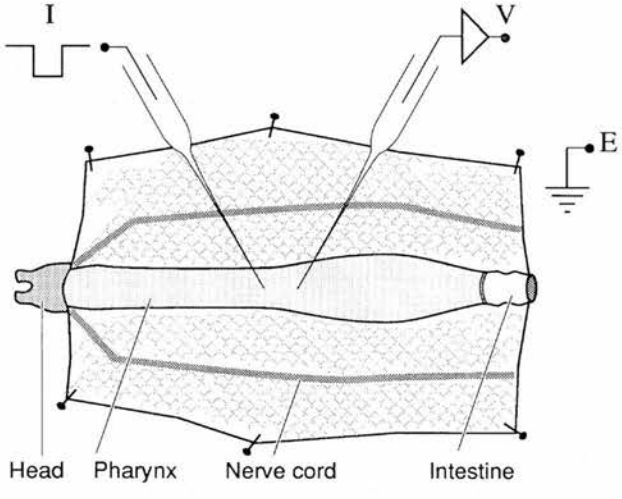


Fig. 8. Diagram of the preparation used to record the electrophysiological effect of glutamate and milbemycin D on the pharyngeal membrane potential and input conductance. Two micropipettes were inserted into the pharyngeal muscle: one was used to record membrane potential (V); the other was used to inject current (I).

ion-channel that is present in parasitic nematodes but not present in the host animal.

Molecular experiments using the *lacZ* marker suggest that the GluCl-β subunit of the glutamate channel is expressed in the pharynx of *C. elegans* pM4 muscle (Fig. 7) (Laughton *et al.*, 1995). The location of the GluCl-α1 subunit is not known. The pharyngeal muscle is required for feeding, and is known to receive an inhibitory motor neurone, M3 (Fig. 7), that is not likely to be GABAergic (Laughton *et al.*, 1995) but glutamatergic (Avery, 1993). The location of an avermectin-sensitive GluCl channel, has been identified using a two microelectrode current clamp technique (Martin, 1996) in the parasitic nematode, *A. suum* (Fig. 8). Experiments show that the pharyngeal muscle of this parasite possesses glutamate receptors that gate chloride channels and that are sensitive to the avermectin analogue milbemycin D.

Effect of glutamate

Fig. 9 shows effects of the application of milbemycin D and glutamate on *Ascaris* pharyngeal muscle input conductance and membrane potential: glutamate [Fig. 9(b)] produces a transient small hyperpolarization of 1 mV associated with an increase in membrane conductance. The effect of glutamate but not GABA [Fig. 9(c)] in pharyngeal *Ascaris* preparations is to produce a reversible increase in input conductance associated with a small change in membrane potential and to

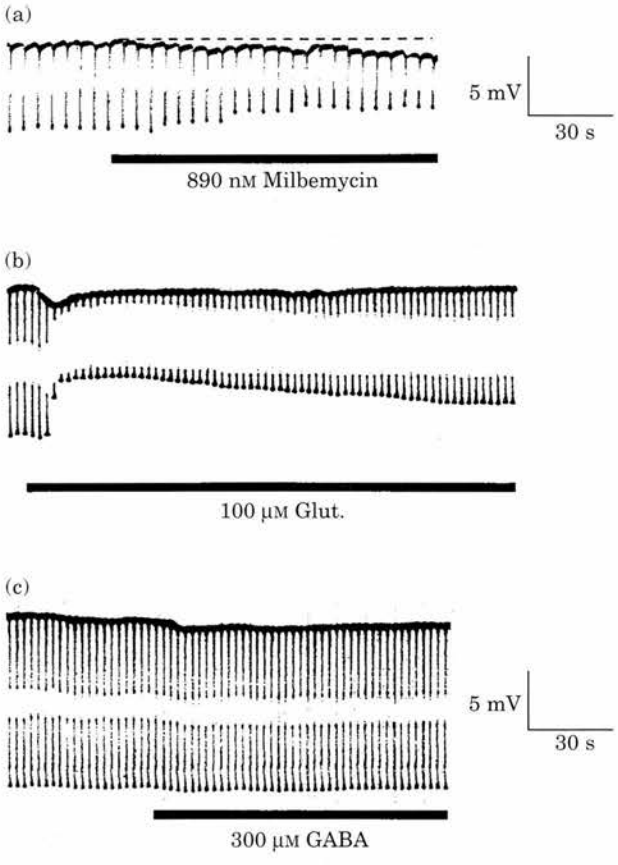


Fig. 9. (a) Effect of 890 nM milbemycin D on the membrane potential and input conductance. Milbemycin slowly produced an increase in input conductance that was not reversed on washing (not shown). (b) Effect of application of 100 μM L-glutamate on membrane potential and input conductance. Different preparation from (a). Glutamate (applied during horizontal bar) produced a transient small hyperpolarization of 1 mV associated with an input conductance change from 157 μS to a peak of 429 μS (ΔG: 272 μS) desensitizing to 231 μS (ΔG: 74 μS) after 4 min. (c) After washing the preparation the input conductance of the pharynx returned towards control levels (142 μS) and the effect of 300 μM GABA was tested without effect (applied during the horizontal bar). The lack of effect of GABA was not due to desensitization because subsequent application of 100 μM L-glutamate increased the input conductance again (not shown).

inhibit pharyngeal pumping that is part of the nematode parasite feeding process. Zero-Cl^- solutions were shown to abolish reversibly the glutamate-induced conductance responses (Martin, 1996) and were used to demonstrate that the glutamate effect was mediated by a Cl^- channels in *Ascaris*.

Effect of milbemycin D

The effect of ivermectin and milbemycin D, on the *C. elegans* avermectin-sensitive glutamate receptor expressed in *Xenopus* oocytes is to produce a potentiation of glutamate effects and to produce a slow irreversible increase in conductance of the membrane (Cully *et al.*, 1994). The effects of milbemycin D on the input conductance of the *Ascaris* pharyngeal preparation is to produce a small change in membrane conductance and to potentiate the effect of low concentrations of glutamate [Figs. (9a), 10(a), (b), (c) and (d)]. The location of the GluCl receptor or the avermectin binding α-subunit in the nematode remains to be explored fully. Recent molecular biological experiments with *C. elegans* on an ivermectin-resistant strain (*avr-15*) suggest that it is a GluCl-α2 subunit that is present in the pharyngeal muscle of *C. elegans* not the GluCl-α1 (review: Cully *et al.*, 1996). The location and function of the original GluCl-α1 subunit remains to be determined. However, the presence of more than one GluCl-α subunit indicates the presence of more than one site of action for the avermectins. It implies that the appearance of resistance to avermectins requires mutation of more than one gene.

In addition to effects on the pharyngeal muscle, ivermectin also has an effect on somatic muscle and opens non-GABA activated channels, and in addition, inhibits GABA-activated channels (Holden-Dye & Walker, 1990). Thus again it appears that the avermectins may have more than one site of action in parasitic nematodes.

INCREASED CALCIUM PERMEABILITY

Praziquantel

Fig. 11 shows the chemical structure of praziquantel. Praziquantel has a selective toxic effect on schistosome parasites, where its mode of action has been studied more extensively (Andrews *et al.*, 1983; Harnett, 1988) than in cestodes. Many actions of praziquantel may be explained by an increased Ca^{2+} permeability of parasite muscle and/or tegumental membranes. Fig. 12 is a diagram of the schistosome tegument and underlying muscle that illustrates the known sites where Ca^{2+} crosses into and between intracellular compartments, and therefore, the possible sites for praziquantel action.

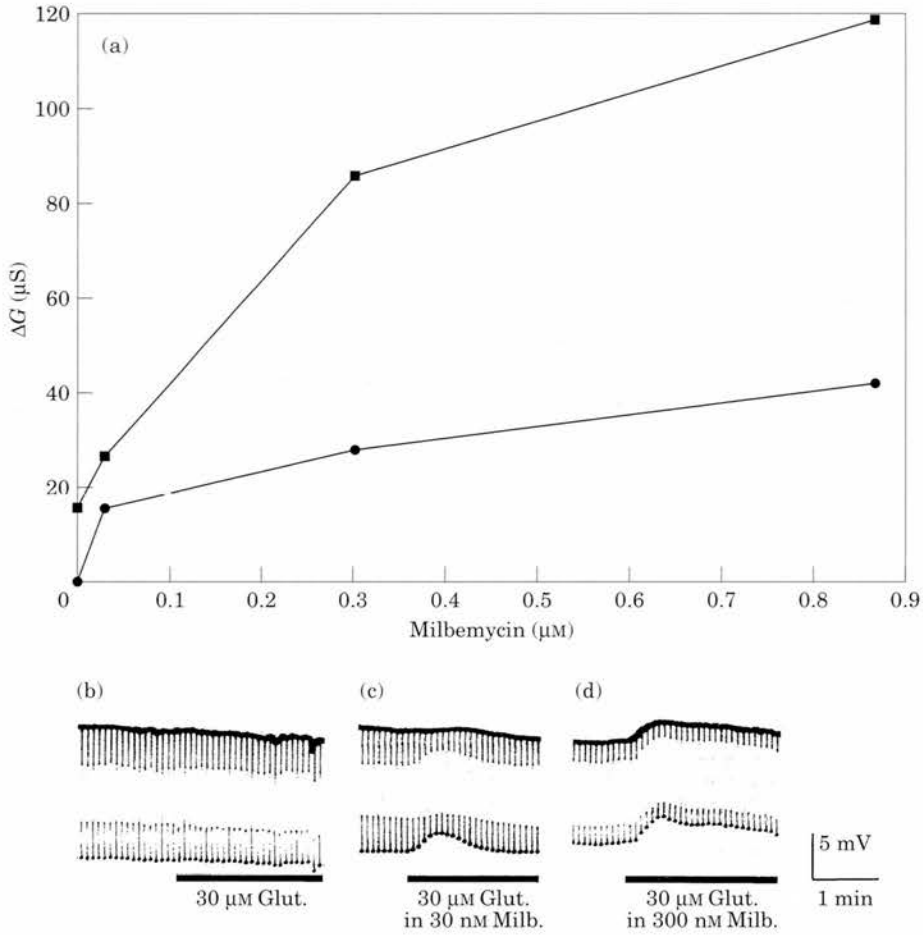


Fig. 10. Glutamate potentiation effects of milbemycin D. (a) (■) Plot of peak ΔG produced by 30 μM glutamate against milbemycin concentration; (●) plot of resting input conductance of the pharynx against milbemycin concentration. Results from the experiment illustrated in (b), (c) & (d).(b) Control 30 μM glutamate response, peak ΔG, is small, 16 μS. (c) In the presence of 30 nM milbemycin (D) the peak ΔG produced by 30 μM glutamate increased to 27 μS. (d) 300 nM milbemycin D increased the peak ΔG to 86 μS. In this particular preparation the glutamate response was a small depolarizing potential, indicating that the Cl-reversal potential was slightly depolarized relative to the membrane potential.

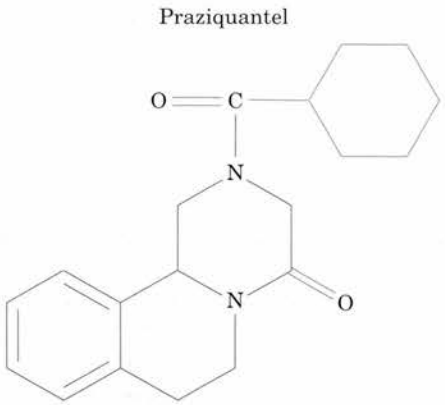


Fig. 11. Chemical structure of praziquantel.

Effect on Ca^{2+} permeability

Praziquantel is known to increase $^{45}Ca^{2+}$ influx across the schistosome tegument and to cause rapid muscle contraction of the parasite (Mehlhorn *et al.*, 1981). It is known that bathing the parasites in Ca^{2+}-free medium blocks the praziquantel induced contraction (Fetterer *et al.*, 1980; Wolde-Mussie *et al.*, 1982; Thompson *et al.*, 1984) but the effect of bathing the preparation in Ca^{2+}-free bath solution is not immediate, requiring more that 10 min to be effective. The effect of praziquantel on Ca^{2+} influx suggests that the sites of action are Ca^{2+} permeable ion channels in the membrane of the tegument and muscle cell (Blair *et al.*, 1994). The contractions in shistosomes are reversed if praziquantel is removed and may be

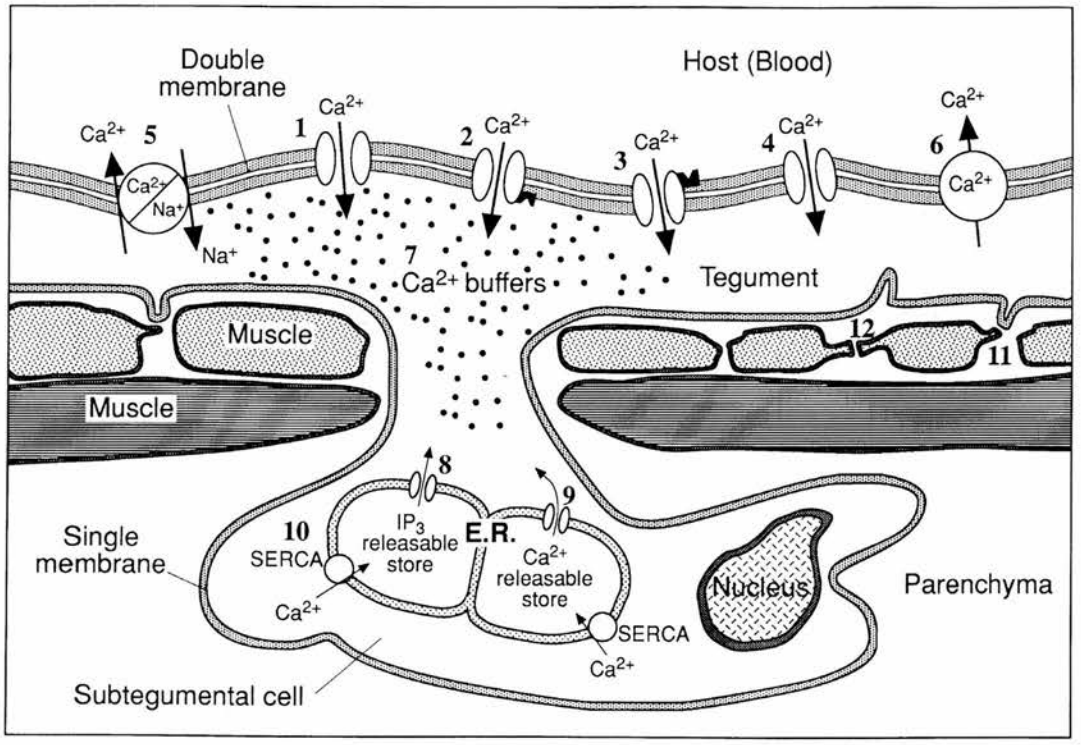


Fig. 12. Diagram of the structure of the body wall of *Schistosoma mansoni* showing the possible sites of action of praziquantel and mechanisms of Ca^{2+} transport into and out of the tegument. **1:** Voltage-activated Ca^{2+} channel. **2:** Intracellular messenger activated Ca^{2+} channel. **3:** Extracellular receptor operated Ca^{2+} channel. **4:** Non-selective cation channel also allowing entry of Ca^{2+}. **5:** Na^+/Ca^{2+} exchanger. **6:** Ca^{2+} ATPase pumping out Ca^{2+}. **7:** Intrategumental Ca^{2+} buffers. **8:** IP_3 releasable store from the sarcoplasmic reticulum. **9:** Ca^{2+} induced Ca^{2+} release channel (CICR channel). **10:** Ca^{2+} ATPase pump: sarcoplasmic endoplasmic reticulum Ca^{2+} (SERCA). **11:** Electrical junction between muscle cell and tegument. **12:** Electrical junctions between muscle cells. If praziquantel acts like caffeine it would act on site **9**. **13:** A proton pump may set up a pH gradient across the tegument and be required for normal function. A proton ionophore would upset this gradient and lead to the demise of the organism.

blocked by Mg^{2+}, or La^{3+} but not by Ni^{2+} Co^{2+} or the calcium-channel blocker D-600 (Fetterer *et al.*, 1980; Wolde-Mussie *et al.*, 1982). The application of a high K^+ solution to depolarize the schistosome preparation results in a rapid depolarization, but the application of praziquantel resultsin a slower onset depolarization. From these observations, it may be concluded that praziquantel somehow results in an increase in Ca^{2+} permeability across parasite membranes via channels that are not activated by depolarization. These channels must be pharmacologically different from those of the host animal or the praziquantel would affect the host animal.

Experiments on a snail smooth muscle preparation (Gardner & Brezden, 1984) have illustrated that caffeine mimics the effect of praziquantel in producing contraction, and that prior treatment of the muscle preparation with caffeine will eliminate the effect of praziquantel on the muscle preparation in Ca^{2+}-free solutions. These experiments suggest that caffeine and praziquantel share the same site of action.

In vertebrate smooth muscle preparations, caffeine acts to stimulate the opening of a large cation channel known as the CICR channel (calcium-induced calcium release channel) (Herrmann-Frank *et al.*, 1991) in the sarcoplasmic reticulum. This channel is activated by cytosolic rises in Ca^{2+}, adenosine triphosphate (ATP) and caffeine but is inhibited by Mg^{2+}. The CICR channel produces regenerative Ca^{2+} release from the sarcoplasmic reticulum following entry of Ca^{2+} through voltage-activated channels (Gregoire *et al.*, 1989). Large cation channels, which might be similar to the CICR channel, have been observed in the tegumental membrane of schistosomes (Day *et al.*, 1992).

Parasite antigen exposure

It has also been found that curative doses of praziquantel in infected animals results in antigens of schistosomes being exposed and binding and penetration of host antigen cells to the parasite after 17 h treatment (Harnett & Kusel, 1986; Brindley & Sher, 1987). The immune system of the host, therefore, plays an important role in the praziquantel-induced death of the parasite. One explanation for the exposure of the parasite antigen may be that increased cytosolic Ca^{2+} causes phospholipase C activation and then activation of protein kinase C (Berridge & Irvine, 1984; Sigiya & Furuyama, 1990). The phosphorylation of proteins by protein kinase C could then destabilize the tegument causing the observed vacuolation and antigen exposure (Wiest *et al.*, 1992). Once again the mode of action of praziquantel relates to an effect on Ca^{2+} permeability of the tegumental membranes. Praziquantel is used frequently to treat tapeworm infestations but less is known of the mode of action in this group of parasites. It is presumed that there is a common mode of action against trematodes and cestodes.

INHIBITION OF MICROTUBULE FORMATION, β-TUBULIN BINDING

Benzimidazoles: thiabendazole, cambendazole, mebendazole, fenbendazole, oxibendazole, oxfendazole, albendazole, albendazole sulphoxide, parbendazole, flubendazole, triclabendazole & prodrugs: netobimin, febantel, thiophanate

Fig. 13 illustrates the chemical structures of the benzimidazole anthelmintics and prodrugs. Prodrugs are converted to active benzimidazoles by metabolic processes in the host animal so that it is the active metabolites that are responsible for the anthelmintic action. Triclabendazole, the flukicidal compound, is assumed to act by the same mechanism as the other benzimidazoles but a clear explanation for its selective effect against fluke is not known (McKellar & Kinabo, 1991) but may be related to its high level of plasma protein binding.

β-tubulin binding

Mebendazole (Borgers *et al.*, 1975; Van den Bossche & De Nollin, 1973) and flubendazole (Van den Bossche & De Nollin, 1973) induce the loss of cytoplasmic microtubules of the tegumental and intestinal cells of cestodes and nematodes, and this is followed by loss of transport of secretary vesicles, a decreased glucose uptake and an increased utilization of stored glycogen. In *Ascaris*, mebendazole is taken up by pharyngeal and intestinal cells where it is found in the cytoplasmic fraction bound to proteins with molecular weights of about 50 and 100 kDa that represent monomers and dimers of tubulin. Our current understanding of the mode of action of the benzimidazoles thus started when it was recognized that the effect of mebendazole on *Ascaris* was to disrupt the microtubules of the intestinal cells producing an inability to take up glucose (Van den Bossche, 1972; Van den Bossche *et al.*, 1982). It was found that benzimidazole anthelmintic competed with the binding site for [H^3] colchicine on β-tubulin and that potency of the benzimidazole anthelmintics correlated with the dissociation constant for binding to nematode β-tubulin (Lacey, 1990; Sangster *et al.*, 1985).

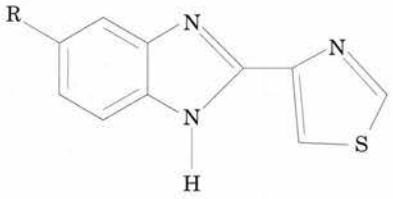
Microtubules are intracellular organelles that serve a variety of functions including movement of chromosomes during cell division; providing the structural skeleton to the cell; movement of intracellular particles including energy metabolites; and exocytosis. They are found in both animal, plant, fungi and some bacterial cells (Stryer, 1995).

Microtubules are composed of two 450 amino-acid proteins known as α-tubulin and β-tubulin. Fig. 14 is a diagrammatic representation of β-tubulin. It is composed of three domains: domain 1 is 34 kDa in size; domain 2 is 19 kDa in size and the tail is 2 kDa in size. There are GTP binding sites present which bind to sites I, II, III, and IV on the β-tubulin. The β-tubulin is folded so that the GTP-binding sites form a pocket.

Formation of microtubules

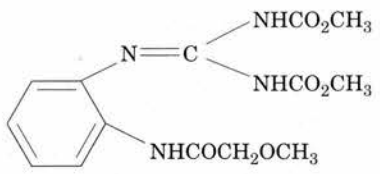
The formation of microtubules is a dynamic process (Fig. 14.) Formation involves the polymerization of tubulin at one end (the positive pole) and the depolymerization at the other end (the negative pole). The microtubules that form are made up of 13 tubulin molecule rings (6 α-tubulin+7 β-tubulin alternating with 7 α-tubulin+6 β-tubulin rings). Seventy-five to 85% of the mass of microtubules is composed of the tubulin proteins but in addition, microtubule-associated proteins (MAPs) are present stabilizing the structure. A number of factors favour polymerization including GTP, Mg^{2+}, and an increase in temperature (to 37°C). A decrease in temperature (to 4°C), the presence of Ca^{2+} or calmodulin will favour depoly-

BENZIMIDAZOLES



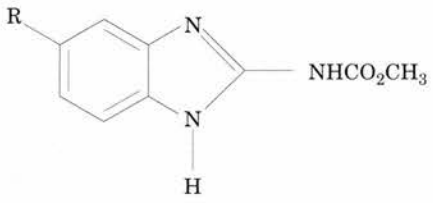
Thiabendazole: R = H—
Cambendazole: R = $(CH_3)_2CHOCONH$—

PRODRUG



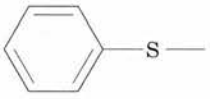
Febantel: converts to fenbendazole

BENZIMIDAZOLE CARBAMATES

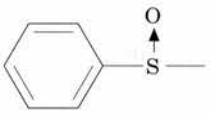


Oxibendazole: R = $CH_3CH_2CH_2O$—
Albendazole: R = $CH_3CH_2CH_2S$—

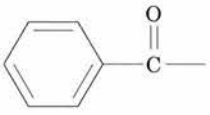
Fenbendazole: R =



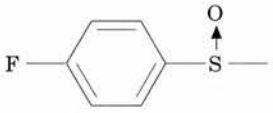
Oxfendazole: R =



Mebendazole: R =



Flubendazole: R =



TRICLABENDAZOLE

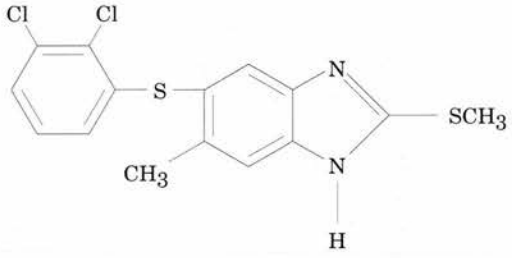


Fig. 13. Chemical structure of benzimidazoles, benzimidazole carbamates, prodrug febantel and the antifluke drug triclabendazole.

merization. Interestingly, α- and β-tubulin will polymerize into a number of shapes (rings and sheets) in addition to microtubules when *in vitro* preparations are made. The formation of microtubules may be inhibited by substances that bind to the leading edge (the positive pole) of polymerization. This process of inhibition is known as 'capping', and colchicine, vinblastine, vincristine, the mitotic inhibitors and benzimidazoles can do this by binding to β-tubulin molecules.

Thus the mode of action of the benzimidazole anthelmintics is the selective binding to nematode β-tubulin, and consequent inhibition of microtubule formation. The effects are, therefore, slower in onset than the anthelmintics that act as neurotransmitter agonists, and include slow onset

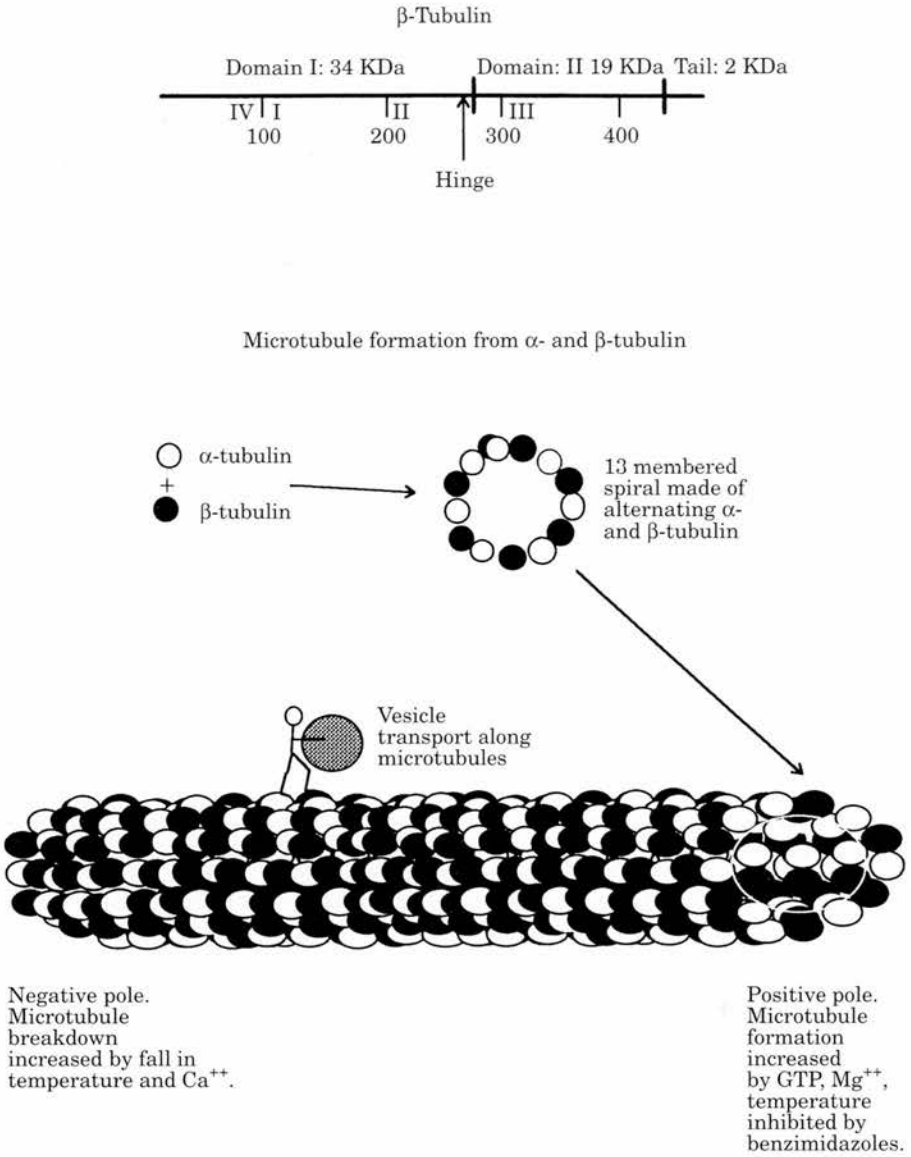


Fig. 14. Diagram of the 50 kDa β-tubulin protein. It consists of three domains that are separated by protease action. In the middle in a 'hinge' allowing the molecule to fold. The location of the amino acids 100, 200, 300 and 400 are shown. Below this is a diagram representing the formation of microtubules by α- and β-tubulin that polymerizes by forming a 13 membered hollow spiral. Each turn of the spiral allows the α- and β-tubulin to pack alternately along the length of the microtubule. Polymerization takes place at the positive pole where temperature and GTP Mg^{2+} and other factors favour microtubule formation. The formation of microtubules is inhibited by binding of benzimidazoles to β-tubulin to produce 'Capping' and inhibition of further microtubule formation. Breakdown occurs at the negative pole. The physiological function of the microtubules include intracellular transport via special proteins, kinesins or dynesins (here represented by the match-stick man).

starvation of the nematode (intestinal cell disruption) and an inhibition of egg production.

Genes for β-tubulin and resistance

In nematodes, two isotypes of β-tubulin have been identified: isotype I and isotype II which have separate genes (Guenette *et al.*, 1991; Guenette *et al.*, 1992; Lubega *et al.*, 1994). Each of these isotypes have alleles: up to six for isotype I; and up to 12 for isotype II. It is not known if the specific isotypes have different functions in the nematodes.

A reduction in the number of isotype alleles for β-tubulin is associated with the appearance of benzimidazole resistance (Roos *et al.*, 1995). Resistance is associated with a progressive loss of alleles of isotype 1 and a total loss of isotype 2 from the nematode population. A resistant population of *Haemonchus contortus* has been characterized by only the presence of a single β-tubulin allele referred to as allele 200. The appearance of resistance can be explained by a loss of susceptible phenotypes and the survival of a resistant phenotype and its increased representation in the remaining population.

In fungi, benzimidazole resistance is associated with the appearance of a different form of β-tubulin (Fujimura *et al.*, 1992; Jung *et al.*, 1992) which is characterized by the appearance of tyrosine instead of phenylalanine in position 200. Because mammalian β-tubulins have also tyrosine present in the 200 amino acid position (Lewis *et al.*, 1985) it is unlikely that benzimidazole resistance may be overcome by changes in drug chemistry. It would not be possible to design a selectively-toxic agent against the fungi because the fungi and host β-tubulins would both bind the benzimidazole to the same degree and so be toxic to both species. A similar phenomenon may occur with nematode parasites.

PROTON IONOPHORES: SALICYLANILIDES AND SUBSTITUTED PHENOLS.

Salicylanilides: closantel, rafoxanide, oxyclozanide, brotianide and substituted phenols: nitroxynil, niclopholan, hexachorophene dibromsalan & niclosamide

The pharmacology of a range of anti-fluke drugs have been reviewed (McKellar & Kinabo, 1991). In this section, the mode of action of the proton ionophores (often called oxidative phosphorylase uncouplers) are considered. The chemical structure salicylanilides and nitroxynil illustrates that each anthelmintic molecule possesses a detachable proton (Fig. 15). These molecules are very lipophilic and may shuttle protons across membranes, particularly the inner mitochondrial membrane. Fig. 16 represents the process by which ATP production occurs in the mitochondria, that is coupled to the proton gradient across the inner mitochondrial membrane. Oxidative phosphorylation may be summarized as electrons from NADH or FADH being conveyed through a series of protein complexes on the inner mitochondrial membrane. This process leads to protons being pumped out of the mitochondria matrix producing a proton motive force that is due to the pH gradient and transmembrane electric potential. ATP is synthesized when the protons flow back into the mitochondrial matrix through an enzyme complex. This process of oxidative phosphorylation takes place in the host animal (Stryer, 1995), as well as in the parasitic helminths (Van den Bossche, 1972; McKellar & Kinabo, 1991).

Lipid soluble substances that can carry protons may shuttle across the inner membrane of the mitochondria, and remove the proton gradient and uncouple oxidative phosphorylation so that the oxidation of NADH and FADH is no longer linked to the production of ATP and may carry on without its production. Fig. 15 shows the position of the proton that is able to dissociate from a variety of compounds. 2,4-Dinitrophenol, carbonyl-p-trifluoro-methoxyphenylhydrazone, (Stryer, 1995) and hexachlorophene, nitroxynil, oxyclozanide (Corbett & Goose, 1971; Edwards *et al.*, 1981b) are all lipophilic compounds that are capable of carrying protons across membranes, and therefore, may act to uncouple oxidative phosphorylation preventing the production of the proton gradient across the inner mitochondrial membrane.

The mechanism of action of the proton ionophores has been assumed to be to selectively uncouple oxidative phosphorylation in parasite mitochondria. Pax and Bennett (1989) have experimental evidence that the inner membrane of the parasite may not be the site of action of the proton ionophores. They observed that application of closantel to *Schistosoma mansoni and Fasciola hepatica* produces a fall in tegumental pH (6.8–6.5) when measured with an intracellular electrode, and that this change in pH occurred after 10 min and before any change in the production of ATP by the parasite. The intra-tegumental fall in pH was associated with a reduction in motility of the parasite and could explain the anti-parasitic action of closantel. It was concluded by Pax and Bennett (1989) that closantel was a membrane active molecule and that it may affect a number of biochemical and physiological processes. These processes are presumably sensitive to changes in intra-tegumental pH. Thus the site of action of the proton ionophores may include the tegument rather than just the mitochondria.

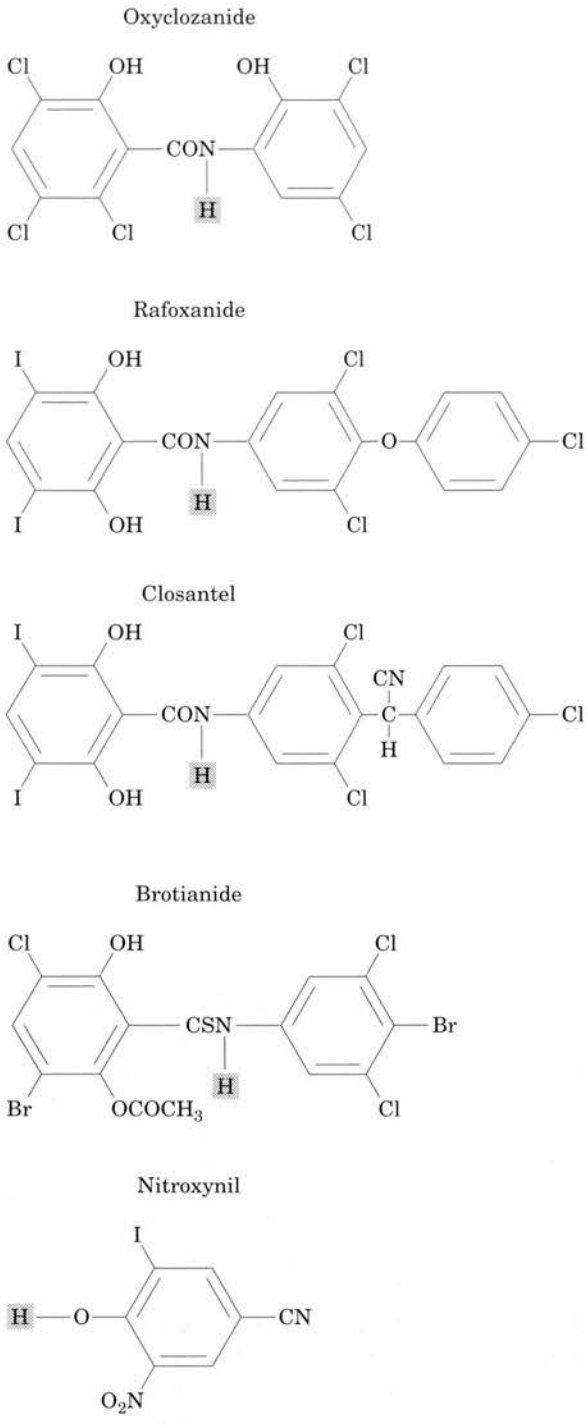


Fig. 15. Chemical structure of the salicylanilides oxyclozanide, rafoxanide & closantel and the DNP derivative nitroxynil. The location of the dissociating proton (H) is shown in the shaded box.

The anthelmintics that have the longest half-life in the body are the salicylanides and nitroxynil.

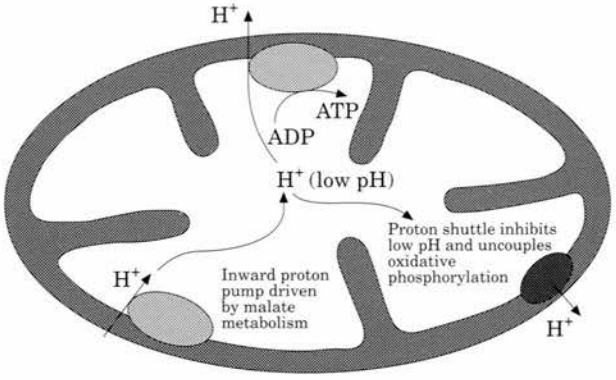


Fig. 16. Diagram of the mitochondria illustrating the inhibitory effects of an oxidative phosphorylase uncoupler on normal ATP production that is driven by the proton gradient inside the mitochondria and produced by tricarboxylic acid metabolism.

This is explained by their strong plasma protein binding which is more than 99% for the salicylanilides (Mohammed-Ali & Bogan, 1987) and 98% for nitroxynil (Alvinerie *et al.*, 1995). The selective anthelmintic action of these highly protein-bound anthelmintics may be explained, in part, by their effect against blood-sucking parasites, concentrating the anthelmintic in the parasite without the high tissue levels being produced in the host. The high level of protein binding may explain the selective effect of these agents, and the fact that well bled out carcasses have low tissue residue levels (McKellar & Kinabo, 1991). Thus the mode of action of this group of anthelmintic involves the selective delivery of the proton ionophores to the parasite because of the high level of plasma-protein binding.

DIAMPHENETHIDE

Diamphenethide (Fig. 17) is more active against immature *Fasciola hepatica* in the liver than the adult *Fasciola* in the bile ducts (Kendall & Parfitt, 1973). Diamphenethide is a prodrug that is deacetylated in the host's liver to an active form which is the monoamine and the diamine (Coles, 1976). The effects of the diamphenethide amine (active form) on *Fasciola in vitro* have been studied by Edwards *et al.* (1981a). These authors described how diamphenethide amine produces an elevation of malate concentrations, an intermediary breakdown product of glucose metabolism. They were not able to identify an action of diamphenethide on a particular enzyme in the glycolytic pathway but suggested that the effect on malate

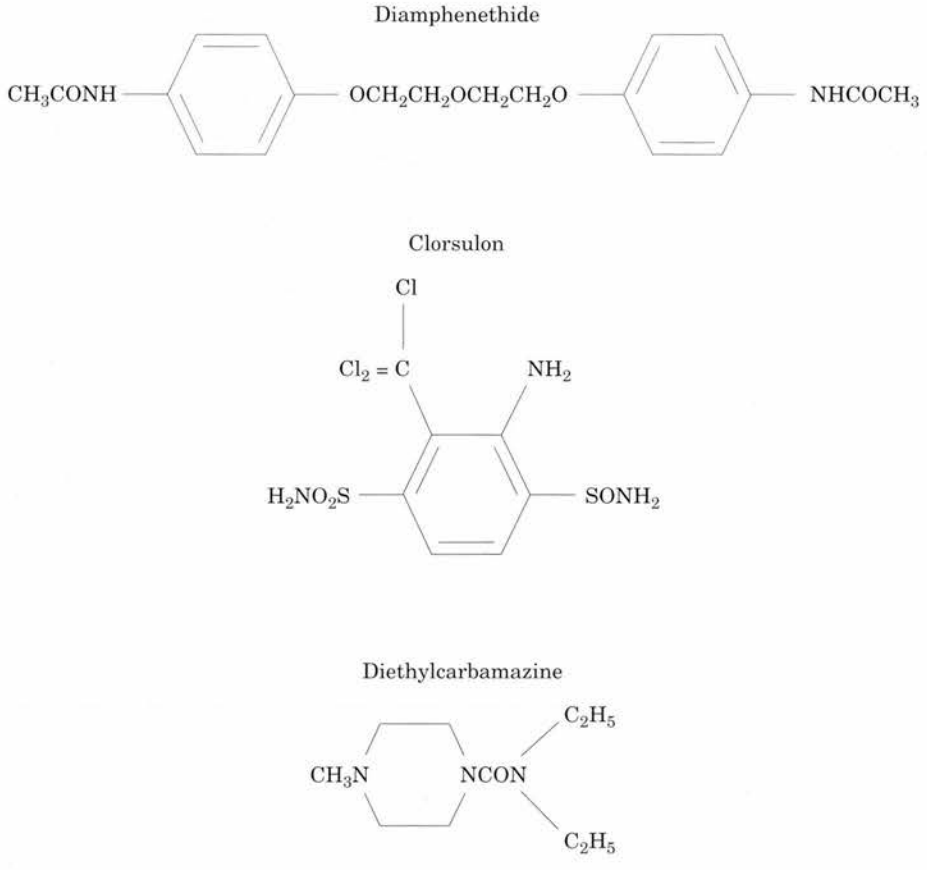


Fig. 17. Chemical structure of diamphenethide, clorsulon and diethylcarbamazine.

was likely to be a primary effect because it occurred early on and before the deterioration of the whole parasite. Interestingly, in the second paper of Edwards *et al.* (1981b) the effect of dopamine, a putative neurotransmitter in *Fasciola* had a protective effect against diamphenethide.

The action of diamphenethide remains to be defined in greater detail but the study of Edwards *et al.* (1981a) showed that its biochemical effects contrasted with the proton ionophore, oxyclozanide and appears to involve effects on malate metabolism in *Fasciola.*

INHIBITION OF PHOSPHOGLYCERATE KINASE AND MUTASE

Clorsulon

Clorsulon is 4-amino-6 trichloro ethenyl 1,3-benzenedisulphonamide (Fig. 17). Structurally, it is similar to 1,3-diphosphoglycerate (Schulman *et al.*, 1982) and consequently, inhibits the enzymes phosphoglycerate kinase (Schulman *et al.*, 1982) and phosphoglyceromutase (Schulman & Valentino, 1982) of *Fasciola* and inhibits the Emden–Meyerhoff pathways in fluke. As a result, there is a selective inhibition of glucose utilization, and acetate and propionate formation. The inhibition of the *Fasciola* phosphoglycerate kinase is competitive (Fig. 18) with a K_i of 0.29 mM: clorsulon competitively inhibiting the binding of ATP and 3-phosphoglycerate to the phosphoglycerate kinase. Schulman *et al.* (1982) suggested that the large group on the six position of clorsulon prevented the conformational change in the kinase enzyme required for activity. There was also a good correlation between the K_i values for antagonism of *Fasciola* phosphoglycerate kinase for a range of compounds related to clorsulon and the potency of these compounds as antifluke agents. This evidence supports the suggested mode of action.

The inhibition of *Fasciola* phosphoglyceromutase by clorsulon was studied by Schulman and

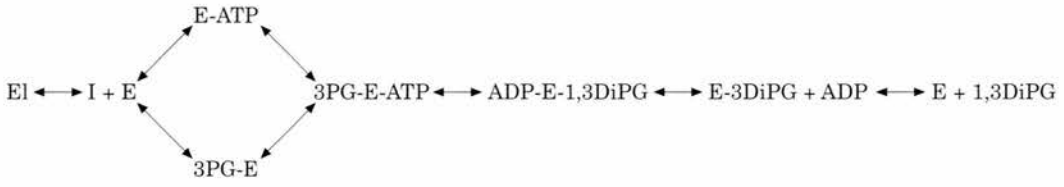


Fig. 18. Diagram of the competitive antagonism of phosphoglycerate kinase (E) of *Fasciola hepatica* by clorsulon (I). Diphosphoryl glycerate: DiPG. 3-Phosphoryl glycerate: 3PG.

Valentino (1982) who pointed out that this enzyme requires 2,3-diphosphoglycerate for activation and the close similarity of clorsulon to diphosphoglycerates could explain its inhibition of the mutase enzyme. These authors purified the enzyme and compared some of its properties with mammalian phosphoglyceromutase that were not inhibited by clorsulon. There appears to be no recent studies on the mode of action of this series of compounds although clinical trials and efficacy studies have been made.

DIETHYLCARBAMAZINE

The chemical structure of diethylcarbamazine a piperazine derivative is shown in Fig. 17. Electrophysiological experiments following bath application to *A. suum* of high concentrations of diethylcarbamazine have shown that it does not mimic the action of piperazine (Martin, 1985).

Effects of diethylcarbamazine

A major indication for diethylcarbamazine at low doses is as an anti-filarial drug; it is a good microfilaricide (including microfilariae of the dog heartworm, *Dirofilaria immitis*) but has limited macrofilaricidal effects. The limited action of diethylcarbamazine against some adult helminths (e.g. cattle lungworm, *Dictyocaulus*) requires nearly 10 times the dose of the prophylactic anti-filarial dose, and may therefore, involve another mode of action. This review covers the mode of action of low doses of diethylcarbamazine; little is known of the mode of action of high doses of diethylcarbamazine.

Most studies suggest that diethylcarbamazine has no direct action on filarial parasites (Johnson *et al.*, 1991). It appears to have no action at reasonable concentrations *in vitro*. In marked contrast to *in vitro* experiments, it is known that *in vivo* diethylcarbamazine is effective within 4 min following intravenous injection (Hawking & Laurie, 1949). The specific immune response does not appear to be involved because nude, athymic mice, infected with *Brugia pahangi*, showed a marked reduction in microfilariae following diethylcarbamazine treatment (Vickery *et al.*, 1986). Thus T cells and T-dependent responses (IgG and IgE) do not appear to be involved. The involvement of complement also seems unlikely because clearing of microfilaria from the nude mice by diethylcarbamazine was not inhibited by prior treatment with cobra venom factor treatment (Vickery *et al.*, 1986).

Effects on arachidonic acid metabolism may be the mode of action of diethylcarbamazine

Diethylcarbamazine has an antagonistic action of the metabolic enzymes that metabolize arachidonic acid, the products released as a result of phospholipase A_2 action on cell membranes. Fig. 19 illustrates the sites of action of diethylcarbamazine proposed by Maizels and Denham (1992). Although 5-lipoxygenase is often being cited as being inhibited by diethylcarbamazine, this may not be the case. In a mast cell line, conversion of 5-HPETE to leukotriene (LT)A_4 by LTA_4 synthetase was blocked by diethylcarbamazine (Mathews & Murphy, 1982). Razin *et al.* (1984) found that in mouse, 5-lipoxygenase conversion of arachidonic acid to 5-HPETE was not inhibited but that LTC_4 and LTA_4 production was inhibited.

Diethylcarbamazine also appears (Kanesa-Thasan *et al.*, 1991) to inhibit endothelial production by cyclo-oxygenase of prostaglandin (PG)I_2 (prostacyclin) and PGE_2 production but does not affect platelet production of thromboxane (TX)A_2 by cyclo-oxygenase and the 12-lipoxygenase products 12- and 15-HPETE. Interestingly, microfilariae also produce their own PGI_2 and PGE_2 and like endothelial cell of blood vessels, diethylcarbamazine also inhibits the microfilarial production (Kanesa-Thasan *et al.*, 1991). The co-administration of glucocorticoids, that are known to block phospholipase A_2 activity and the production of arachidonic acid (Fig. 19), together

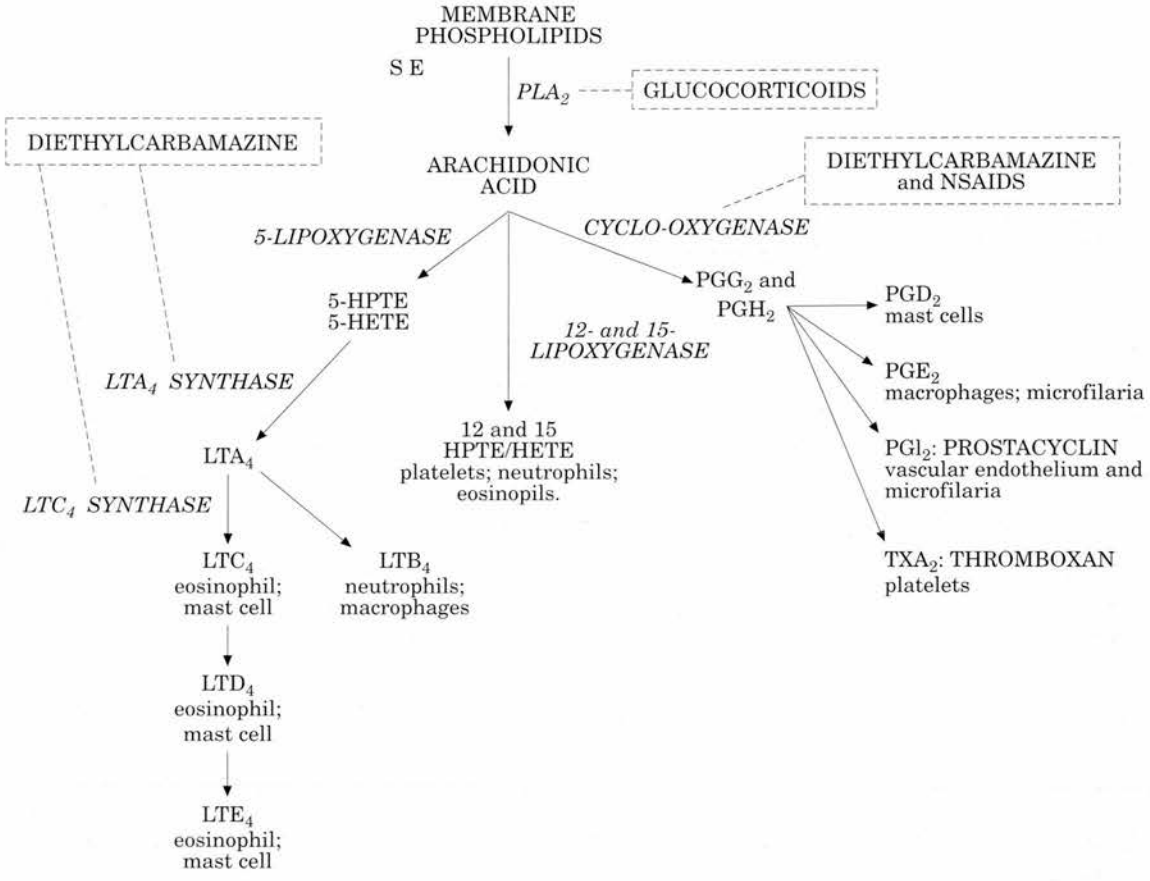


Fig. 19. Diagram of the production of the leukotrienes and prostaglandins via lipoxygenase or cyclo-oxygenase from arachidonic acid that is produced from membrane phospholipids as a result of phospholipase A_2 acidity. The inhibitory sites of action of glucocorticoids, non-steroidal anti-inflammatory drugs (NSAIDs) and diethylcarbamazine are shown. Diethylcarbamazine is shown inhibiting the action of LTA_4 synthase that converts 5-hydroperoxyeicosatetraenoic acids (5-HPETE) and 5-hydroxyeicosatetraenoic acids (5-HETE) to the leukotrienes LTA_4 and LTA_4 to LTC_4 in mast cells and eosinophils. Diethylcarbamazine is also shown inhibiting the cyclo-oxygenase enzyme that converts arachidonic acid to the prostaglandins PGG_2 and PGH_2. The subsequent production of PGD_2, PGE_2, PGI_2 & TXA_2 is also inhibited in the blood vessels and microfilaria.

with diethylcarbamazine, reduces the effect of diethylcarbamazine (Stingl *et al.*, 1988). Thus, diethylcarbamazine seems to inhibit production of PGI_2 and PGE_2 by microfilaria and endothelial cells. The normal level of production of PGI_2 and PGE_2 that produces a tonic dilation of blood vessels and inhibits aggregation of neutrophils and eosinophils is reduced by administration of diethylcarbamazine.

A plausible explanation of the mode of action of diethylcarbamazine is that this compound alters the metabolism of arachidonic acids in host endothelial cell and also in microfilariae that are susceptible to the action of diethylcarbamazine. There is then a vasoconstriction, amplified endothelial adhesion and immobilization of the microfilariae and cytotoxic activity by the host platelets and granulocytes. It appears that diethylcarbamazine activates an innate immune response rather than an adaptive immune response (Maizels & Denham, 1992). This mode of action can explain why diethylcarbamazine has no action *in vitro* against microfilariae and is effective in non-immune animals.

ACKNOWLEDGEMENTS

I am pleased to acknowledge the financial support of the Wellcome Trust who have supported my work on the electrophysiology of the piperazine,

nicotinic anthelmintics and the GluCl receptors of *Ascaris*.

REFERENCES

ACEVES, J., ERLIJI, D. & MARTINEZ-MARNON, R. (1970). The mechanism of the paralysing action of tetramisole on *Ascaris* somatic muscle. *British Journal of Pharmacology* **38,** 332–44.

ALVINERIE, M., FLOC'H, R. & GALTIER, P. (1995). Plasma protein binding of nitroxynil in several species *Journal of Veterinary Pharmacology and Therapeutics.* **14,** 170–3.

ANDREWS, P., THOMAS, H., POHLKE, R. & SEUBERT, J. (1983). Praziquantel. *Medical Research Reviews.* **3,** 147–200.

ARENA, J. P. (1994). Expression of *caenorhabditis elegans* messenger-RNA in *Xenopus* oocytes: a model system to study the mechanism of action of avermectins. *Parasitology Today* **10,** 35–7.

AREVALO, J. I. & SAZ, H. J. (1992). Effects of cholinergic agents on the metabolism of choline in muscle from *Ascaris suum. Journal of Parasitology* **78,** 387–92.

AUBRY, M. L., COWELL, P., DAVEY, M. J. & SHEVDE, S. (1970). Aspects of the pharmacology of new anthelmintics: pyrantel. *British Journal of Pharmacology* **38,** 332–44.

AVERY, L. (1993). Motor-neuron m3 controls pharyngeal muscle-relaxation timing in *Caenorhabditis elegans. Journal of Experimental Biology* **175,** 283–97.

BERRIDGE, M. J. & IRVINE, R. F. (1984). Inositol trisphosphate, a novel second messenger in cellular signalling transduction. *Nature* **312,** 315.

BLAIR, K. L., BENNETT, J. L. & PAX, R. A. (1994). *Schistosoma mansoni*: myogenic characteristics of phorbol ester induced muscle contraction. *Experimental Parasitology* **78,** 302–16.

BORGERS, M., DE NOLLIN, S., DE BRABANDER, M. & THIENPOINT, D. (1975). Influence of the anthelmintic mebendazole in nematode intestinal cells. *American Journal of Veterinary Research* **36,** 1153–66.

BRINDLEY, P. J. & SHER, A. (1987). The chemotherapeutic effect of praziquantel against Schistosoma mansoni is dependent on host antibody response. *Journal of Immunology* **136,** 215–20.

BUEDING, E. (1952). Acetycholinesterase in *Schistosoma mansoni. British Journal of Pharmacology* **7,** 563–6.

CAMPBELL, W. C. & BENZ, G. W. (1984). Ivermectin: a review of efficacy and safety. *Journal of Veterinary Pharmacology and Therapeutics* **7,** 1–16.

COLES, G. C., EAST, J. M. & JENKINS, S. N. (1975). The mechanism of action of the anthelmintic levamisole. *General Pharmacology.* **6,** 309–13.

COLES, G. C. (1976). The inactivity of diamphenethide against liver fluke in certain species of mammals. *Journal of Parasitology* **20,** 110–1.

COLQUHOUN, D. & SAKMANN, B. (1985). Fast events in single-channel currents activated by acetylcholine and its analogues at the frog muscle end-plate. *Journal of Physiology (London)* **369,** 501–57.

CORBETT, J. R. & GOOSE, J. (1971). The biochemical mode of action of the fasciolicides, nitroxynil, hexachlorophene, and oxyclozanide. *Biochemical Journal* **121,** 41.

CULLY, D. F., VASSILATIS, D. K., LIU, K. K., PARESS, P. S., VANDERPLOEG, L. H. T. & SCHAEFFER, J. M. (1994). Cloning of an avermectin-sensitive glutamate-gated chloride channel from *Caenorhabditis elegans. Nature* **371,** 707–11.

CULLY, D. F. WILKINSON, H. VASSILITIS, D.K. ETTER, A. & ARENA, J. (1996). Molecular Biology and Electrophysiology of Glutamate-gated Chloride Channels of Invertebrates. *Parasitology* **113,** SXXX–SYYY.

DALE, V. M. E. & MARTIN, R. J. (1995). Oxantel-activated single-channel currents in the muscle membrane of *Ascaris suum. Parasitology* **110,** 437–48.

DAY, T. S., BENNETT, J. L. & PAX, R. A. (1992). *Shistosoma mansoni:* patch-clamp study of a non-selective cation channel in the outer tegumental membrane of females. *Experimental Parasitology* **74,** 348–56.

DONAHUE, M. J., YACOUB, N. J. & HARRIS, B. G. (1982). Correlation of muscle-activity with glycogen-metabolism in muscle of *Ascaris suum. American Journal Of Physiology* **242,** R514–R21.

EDWARDS, S. R., CAMPBELL, A. J., SHEERS, M., MOORE, R. J. & MONTAGUE, P. E. (1981a). Studies of the effect of diamphenethide and oxyclozanide on the metabolism of *Fasciola hepatica. Molecular and Biochemical Parasitology* **2,** 323–38.

EDWARDS, S. R., CAMPBELL, A. J., SHEERS, M., MOORE, R. J. & MONTAGUE, P. E. (1981b). Protection of *Fasciola hepatica* against flukical action of the amine of diamphenethide in vitro. *Molecular and Biochemical Pharmacology.* **2,** 339–48.

FETTERER, R. H., PAX, R. A. & BENNETT, J. L. (1980). *Schistosoma mansoni:* characterization of the electrical potential from the tegument of adult males. *Experimental Parasitology* **49,** 353–65.

FLEMMING, J. T., SQUIRE, M., SATTELLE, D. B., LEWIS, J. A. (1994). Sequence Analysis of the lev-1 Dominant Alleles (x21, x61) Predict Alterations in the Ionic Selectivity of the Channel. *Worm Breeders Gazette.* **13,** 76.

FUJIMURA, M., OEDA, K., INOUE, H. & KATO, T. (1992). A single amino acid substitution in the β-tubulin gene of *Neurospora* confers both carbendazim resistance and diethofencarb sensitivity. *Current Genetics* **21,** 399–404.

GARDNER, D. R. & BREZDEN, B. L. (1984). The sites of action of praziquantel in a smooth muscle of *Lymnaea stagnalis. Canadian Journal of Physiology and Pharmacology.* **62,** 282–7.

GREGOIRE, G., LOIRAND, G. & PACAUD, P. (1989). Ca^{2+} and Sr^{2+} entry induced Ca^{2+} release from the intracellular Ca^{2+} store in smooth muscle cells of rat portal vein. *Journal of Physiology* **474,** 483–500.

GUENETTE, S., PRITCHARD, R. K., KLEIN, R. D. & MATLASHEWSKI, G. (1991). Characterization of a β-tubulin gene and β-tubulin gene products of *Brugia pahangi Molecular Biochemical Parasitology* **44,** 153–64.

GUENETTE, S., PRITCHARD, R. K. & MATLASHEWSKI, G. (1992). Identification of a novel *Brugia pahangi* β-tubulin gene (b2) and a 22-nucleotide spliced leader sequence on β1-tubulin mRNA. *Molecular Biochemical Parasitology* **50,** 275–284.

HARNETT, W. (1988). The anthelmintic action of praziquantel. *Parasitology Today* **4,** 144–6.

HARNETT, W. & KUSEL, J. R. (1986). Increased exposure of parasite antigens at the surface of adult male *Schistosoma mansoni* exposed to praziquantel in vitro. *Parasitology* **93,** 401–5.

HARROW, I. D. & GRATION, K. A. F. (1985). Mode of action of the anthelmintics morantel, pyrantel and levamisole in the muscle cell membrane of the nematode *Ascaris suum*. *Pesticide Science.* **16,** 662–72.

HAWKING, F. & LAURIE, W. (1949). Action of hetrazan on filariasis and onchocerciasis. *Lancet* **2,** 146–7.

HERRMANN-FRANK, A., DARLING, E. & MEISSNER, G. (1991). Functional characterization of the Ca^{2+} gated Ca^{2+} release channel of vascular smooth muscle sarcoplasmic reticulum. *Pflugers Archives 418,* 353–9.

HOLDEN-DYE, L. & WALKER, R. J. (1990). Avermectin and avermectin derivatives are antagonists at the 4-aminobutyric acid (GABA) receptor on the somatic muscle-cells of *Ascaris*—is this the site of anthelmintic action. *Parasitology* **101,** 265–71.

JOHNSON, P., MACKENZIE, C. D., DENHAM, D. A. & SUSWILLO, R. R. (1991). The effect of diethylcarbamazine on the *in vitro* serum-mediated adgerence of feline granulocytes to microfilariae of *Brugian pahangi. Tropical Medicine and Parasitology.* **39,** 291–4.

JUNG, M. K., WILDER, I. B. & OAKLEY, B. R. (1992). Amino acid alterations in the benA (β-tubulin) gene of *Aspergillus nidulans* that confer benomyl resistance. *Cell Motility and Cytoskeleton* **22,** 170–4.

KANESA-THASAN, N., DOUGLAS, J. G. & KAZURA, J. W. (1991). Diethylcarbamazine inhibits endothelial and microfilarial prostanoid metabolism *in vitro. Molecular and Biochemical Parasitology,* **49,** 11–20.

KENDALL, S. B. & PARFITT, J. W. (1973). The effect of diamphenethide of *Fasciola hepatica* at different stages of development. *Research in Veterinary Science* **15,** 37, 40.

LACEY, E. (1990). Mode of action of benzimidazoles. *Parasitology Today* **6,** 112–5.

LAUGHTON, D. L., WOLSTENHOLME, A. J. & LUNT, G. (1995). The beta subunit of the *C. elegans* inhibitory glutamate receptor is expressed in the pm4 pharyngeal muscle cells. *Worm Breeders Gazette* **14,** 48–.

LEE, D. L. (1962). The distribution of esterase enzymes in *Ascaris lumbricoides. Parasitology* **52,** 241–60.

LEWIS, J. A., WU, C. -H., LEVINE, J. H. & BERG, H. (1980). Levamisole-resitant mutants of the nematode *Caenorhabditis elegans* appear to lack pharmacological acetycholine receptors. *Neuroscience* **5,** 967–89.

LEWIS, J. A. FLEMMING, J. T. & BIRD, D. (1992) Cloning nematode acetycholine receptor genes. In *Neurotox '91,* ed. Duce, I. R. pp. 155–64. London and New York: Elsevier Applied Science..

LEWIS, S., LEE, M. G.-S. & COWEN, N. J. (1985). Five mouse tubulin isotypes and their regulated expression during development. *Journal of Cell Biology* **101,** 852–61.

LUBEGA, G. W., KLEIN, R. D., GEARY, T. G. & PRICHARD, R. K. (1991). *Haemonchus contortus:* the role of 2 beta tubulin gene subfamilies in the resistance to benzimidazole anthelmintics. *Biochemical Pharmacology* **47,** 1705–15.

MAIZELS, R. M. & DENHAM, D. A. (1992). Diethylcarbamazine (DEC): immunopharmacological interactions of an anti-filarial drug. *Parasitology* **105,** S49–S60.

MARTIN, R. J. (1980). The effect of γ-aminobutyric acid in the input conductance and membrane potential of *Ascaris* muscle. *British Journal of Pharmacology* **71,** 99–106.

MARTIN, R. J. (1982). Electrophysiological effects of piperazine and diethylcarbamazine on *Ascaris suum* somatic muscle. *British Journal of Pharmacology* **77,** 255–65.

MARTIN, R. J. (1985). γ-aminobutyric acid- and piperazine-activated single channel currents from *Ascaris suum* body muscle. *British Journal of Pharmacology* **84,** 445–61.

MARTIN, R. J. (1996). An electrophysiological preparation of *Ascaris suum* pharyngeal muscle reveals a glutamate-gated chloride channel sensitive to the avermectin analogue milbemycin D. *Parasitology* **147.**

MATHEWS, W. R. & MURPHY, R. C. (1982). Inhibition of leukotriene biosynthesis in mastocytoma cells by diethylcarbamazine. *Biochemical Pharmacology.* **31,** 2129–32.

MCKELLAR, Q. A. & KINABO, L. D. B. (1991). The pharmacology of flukicidal drugs. *British Veterinary Journal* **147,** 306–19.

MEHLHORN, H., BECHER, B., ANDREWS, R., THOMAS, H. & FRENKEL, J. R. (1981). In vivo and in vitro experiments on the effect of praziquantel on *Schistosoma mansoni*: a light and electron microscope study. *Arzneimittel Forschung* **31,** 544–54.

MELLANBY, H. (1955). The identification and estimation of acetylcholine in three parasitic nematodes (*Ascaris* lumbricoides, *Litomosoides carinii,* and the microfilariae of Dirofilaria repens). *Parasitology* **45,** 287–94.

MOHAMMED-ALI, N. A. K. & BOGAN, J. A. (1987). The pharmacodynamics of the flukicidal salicylanilides, rafoxanide, closantel and oxyclozanide. *Journal of Veterinary Pharmacology and Therapeutics* **10,** 127–33.

OPPERMAN, C. H. & CHANG, S. (1992). Nematode acetylcholinesterases–molecular-forms and their potential role in nematode behavior. *Parasitology Today* **8,** 406–11.

PAX, R. A. & BENNETT, J. L. (1989). Effect of closantel on intrategumental pH in *Schistosoma mansoni* and *Fasciola hepatica. Journal of Parasitology* **75,** 169–71.

PRICHARD, R. K. (1994). Anthelmintic resistance. *Veterinary Parasitology* **54,** 259–68.

RAZIN, E., ROMEO, L. C., KRILIS, S., LIU, F.-T. & LEWIS, R. A. (1984). An analysis of the generation and the secretion of preformed mediators from mouse bone marrow-derrived mast cells. *Journal of Immunology* **133,** 938–45.

ROBERTSON, S., J., PENNINGTON, A. J., EVANS, A. M. & MARTIN, R. J. (1992). Pyrantel activated single-channel currents in the nematode parasite *Ascaris*-suum. *British Journal of Pharmacology* **107,** P 154–.

ROBERTSON, S. J. & MARTIN, R. J. (1993). Levamisole-activated single-channel currents from muscle of the nematode parasite *Ascaris suum. British Journal of Pharmacology* **108,** 170–8.

ROOS, M. H., KWA, M. S. G. & GRANT, W. N. (1995). New genetic and practical implications of selection for

anthelmintic resistance in parasitic nematodes. *Parasitology Today* **11,** 148–50.

SANGSTER, N. C., PRITCHARD, R. K. & LACEY, E. (1985). Tubulin and benzimidazole-resistance in *Trichostrongylus colubriformis* (*Nematoda*). *Journal of Parasitology* **71,** 645–51.

SCHULMAN, M. D., OSTLIND, D. A. & VALENTINO, D. (1982). Mechanism of action of mk-401 against *Fasciola hepatica* -inhibition of phosphoglycerate kinase. *Molecular and Biochemical Parasitology* **5,** 133–45.

SCHULMAN, M. D. & VALENTINO, D. (1982). Purification, characterization and inhibition by mk-401 of *Fasciola hepatica* phosphoglyceromutase. *Molecular And Biochemical Parasitology* **5,** 321–32.

SIGIYA, H. & FURUYAMA, S. (1990). Sphingisine increases inositol trisphosphate in rat parotid acinar-cells by a mechanism that is independent of protein kinase C but dependent on extracellular calcium. *Cell Calcium* **11,** 469–75.

SHOOP, W. L., MROZIK, H. & FISHER, M. H. (1995). Structure and activity of avermectins and milbemycins in animal health. *Veterinary Parasitology* **59,** 139–56.

STINGL, P., PIERCE, P. F., CONNOR, D. H., GIBSON, D. W., STRAESSLE, T., ROSS, M. A. & RIBAS, J. L. (1988). Does dexamethasone suppress the Mazzotti reaction in parients with onchocerciasis. *Acta Tropica.* **45,** 77–85.

STRYER, L. 1995 *Biochemistry.* New York: W. H. Freeman and Company..

THOMPSON, D. P., PAX, R. A. & BENNETT, J. L. (1984). Microelectrode studies on the tegument and sub-tegumental compartments of male *Schistosoma mansoni*: an analysis of compartments of electrophysiological properties. *Experimental Parasitology* **58,** 314–15.

VAN DEN BOSSCHE, H. 1972 *Comparative Biochemistry of Parasites.* New York: Academic Press..

VAN DEN BOSSCHE, H., ROSHETTE, F. & HORIG, C. (1982). Mebendazole and related anthelmintics. *Advances in Pharmacology and Chemotherapy* **19,** 67–128.

VAN DEN BOSSCHE, H. & DE NOLLIN, S. (1973). Biochemical effects of mebendazole on *Trichinella spirales* larvae. *Journal of Parsitology* **59,** 970–6.

VICKERY, A. C., NAYAR, J. K. & TAMPLIN, M. L. (1986). Diethylcarbamazine on microfilariae of *Litomisoides carinii in vitro* and *in vivo. Zeitshrift fur Parasitenkunde* **72,** 805–13.

WIEST, P. M., LI, Y., OLDS, G. R. & BOWEN, W. D. (1992). *Schistosoma mansoni*: characterization of phosphoinositide response. *Experimental Parasitology* **74,** 38–45.

WOLDE-MUSSIE, E., VANDE-WAA, J., PAX, R. A., FETTERER, R. H. & BENNETT, J. L. (1982). *Schistosoma mansoni*: calcium efflux and the effects of calcium-free media on the responses of the electrical potential from the tegument of adult males musculature to praziquantel and other agents inducing contraction. *Experimental Parasitology* **53,** 270–8.

(Accepted for publication 21 June 1996)

Target sites of anthelmintics

R. J. MARTIN[1], A. P. ROBERTSON[1] *and* H. BJORN[2]

[1] *Department of Preclinical Veterinary Sciences, R.(D.)S.V.S., University of Edinburgh, Summerhall, Edinburgh EH9 1QH*
[2] *Department of Pharmacology and Pathobiology, Danish Centre for Experimental Parasitology, Royal Veterinary and Agricultural School, Bülowsvej 13, DK-1850 Frederiksberg C, Denmark*

SUMMARY

This paper reviews sites of action of anthelmintic drugs including: (1) levamisole and pyrantel, which act as agonists at nicotinic acetylcholine receptors of nematodes; (2) the avermectins, which potentiate or gate the opening of glutamate-gated chloride channels found only in invertebrates; (3) piperazine, which acts as an agonist at GABA gated chloride channels on nematode muscle; (4) praziquantel, which increases the permeability of trematode tegument to calcium and results in contraction of the parasite muscle; (5) the benzimidazoles, like thiabendazole, which bind selectively to parasite β-tubulin and prevents microtubule formation; (6) the proton ionophores, like closantel, which uncouple oxidative phosphorylation; (7) diamphenethide and clorsulon, which selectively inhibit glucose metabolism of *Fasciola* and; (8) diethylcarbamazine, which appears to interfere with arachidonic acid metabolism of filarial parasites and host. The review concludes with brief comments on the development of anthelmintics in the future.

Key words: acetylcholine receptor, levamisole, pyrantel, piperazine, ivermectin, praziquantel, benzimidazoles, closantel, diamphenethide, clorsulon, diethylcarbamazine.

INTRODUCTION

Anthelmintic drugs are used to control, prevent and treat nematode and trematode parasite infestations in both humans and domestic animals. They will continue to be used until effective vaccines are produced and/or hygiene standards have been improved. As anthelmintic drugs have been used continuously for parasite control, resistance has gradually developed and is now found in a number of parasite species against most of the anthelmintics (Prichard, 1994). This resistance occurs more frequently when the same anthelmintic agent has been used intensively and without good hygiene standards to assist control. If resistance to a particular anthelmintic occurs, it is likely that an anthelmintic that has the same mode of action will also be ineffective (cross-resistance). One reason for developing an understanding of the mode of action of anthelmintics is to enable selection of other anthelmintics that will be effective for therapeutic purposes. Another reason for pursuing the mode of action of anthelmintics is that we may be able to understand how parasites develop resistance to the anthelmintics.

There are two major modes of action of anthelmintics. There are the drugs that act on parasite membrane ion-channels and which usually have a more rapid therapeutic effect; the other group acts more slowly on a range of 'biochemical' target sites found in parasites. Table 1 summarizes the target site of anthelmintics that act on membrane ion-channels. The target ion-channels include: the excitatory nicotinic acetylcholine receptor on muscle of nematodes; the inhibitory γ-aminobutyric acid (GABA) receptor channel also present on nematode muscle; and the glutamate-gated Cl^- channel. Table 2 summarizes the modes of action of anthelmintics that act at more 'biochemical' target sites.

The target site (enzyme or ion-channel) of the anthelmintic may be present in the host animal as well as the parasite; it is usually pharmacologically distinct in the parasite in order to permit selective drug action. For example, the benzimidazole anthelmintics bind selectively to nematode β-tubulin to effect their action. β-tubulin is present in the host animal as well but is sufficiently different in its three dimensional protein structure in the mammalian host so that benzimidazole anthelmintics only bind to the nematode β-tubulin molecule. Other anthelmintics act on targets only present in parasites. The avermectins bind to a glutamate-gated Cl^- ion-channel that has only been found in certain invertebrates including nematodes. This permits the very selective toxic action of avermectins against nematode parasites without harming the host animal. Anthelmintics acting on a target protein only present in parasites are often favoured because of advantages of greater safety and selectivity.

This introductory review covers sites of actions of anthelmintic agents including the nicotinic acetylcholine channel of nematodes, the GABA channel, the glutamate-gated Cl^- channel and biochemical sites of action including β-tubulin and glycolytic enzymes. The review concludes with a brief comment on the future development of anthelmintics.

 © 1997 Cambridge University Press

Table 1. Ion-channel target sites of anthelmintic drugs

Target site (and parasite group)	Generic drug name
Nicotinic acetylcholine receptor (in nematodes) (Martin, 1993; Robertson & Martin, 1993; Evans & Martin, 1996)	Levamisole, butamisole, pyrantel, morantel, bephenium, thenium, methyridine
GABA receptors (in large intestinal nematodes) (Martin, 1985)	Piperazine
GluCl receptor (in nematodes and insect parasites) (Cully *et al.* 1996; Martin, 1996)	Ivermectin, abamectin, doramectin, moxidectin
Membrane calcium permeability (in cestodes and trematodes) (Redman *et al.* 1996)	Praziquantel

Table 2. Anthelmintic target sites other than ion-channels

Target site (and parasite group)	Generic drug name
β-tubulin (in nematodes)	Thiabendazole, cambendazole, oxibendazole, albendazole, albendazole sulphoxide
β-tubulin (in nematodes, cestodes and trematodes) (Roos *et al.* 1995)	Fenbendazole, oxfendazole, mebendazole, flubendazole, febantel, netobimin, thiophanate, triclabendazole
Proton ionophores (concentrated and effective against blood feeders: flukes, *Haemonchus contortus*, *Oestrus ovis*) (McKellar & Kinabo, 1991)	Closantel, rafoxanide, oxyclozanide, brotianide, nitroxynil, niclopholan, hexachlorophene, dibromosalan, niclosamide
Malate metabolism (in immature *Fasciola*) (Edwards *et al.* 1981*a*, *b*)	Diamphenethide
Phosphoglycerate kinase and mutase (in *Fasciola*) (Schulman *et al.* 1982*a*)	Clorsulon
Arachidonic acid metabolism and innate immunity of host (effective against filaria) (Maizels & Denham, 1992)	Diethylcarbamazine

Readers interested in details of the dosages and administration, uses (spectrum of action) and host toxicity, in humans are referred to the recent comprehensive text of Martindale (1996) and for equivalent data for animals are referred to the Compendium of Data Sheets for Veterinary Products (NOAH, 1997).

NICOTINIC ACETYLCHOLINE RECEPTORS

Somatic muscle cells of nematodes possess both synaptic and extrasynaptic nicotinic acetylcholine receptors. This has been shown, for example, by the experiments of Martin (1982) and Harrow & Gration (1985). These electrophysiological experiments involved the use of micropipettes placed intracellularly in muscle cells of the large nematode parasite of the pig, *Ascaris suum*. They showed that application of acetylcholine and the anthelmintics, levamisole, pyrantel and morantel (Fig. 1) resulted in the depolarization and increase in input conductance of the muscle membrane to sodium and potassium. The affects of acetylcholine were antagonized by the nicotinic antagonist tubocurarine. Subsequently patch-clamp studies, (Robertson & Martin, 1993; Robertson *et al.* 1994; Dale & Martin, 1995; Evans & Martin, 1996) have shown that the nicotinic anthelmintics open non-selective cation channels. Each channel is characterized by a particular conductance but the conductance varies between channels recorded from different patches in the range 19–60 pS. The mean open-time of the channels varies with the anthelmintic but is in the range of 0·5 ms to 2·5 ms. Thus with these electrophysiological experiments it has been possible to establish that the nicotinic anthelmintics have an action on a receptor with properties similar to but not identical with the nicotinic receptors in mammalian and vertebrate species. There must be pharmacological differences between the nicotinic receptors of nematodes and those of their host since levamisole is a selective agent producing depolarization and spastic paralysis of the nematode without a significant action on the host

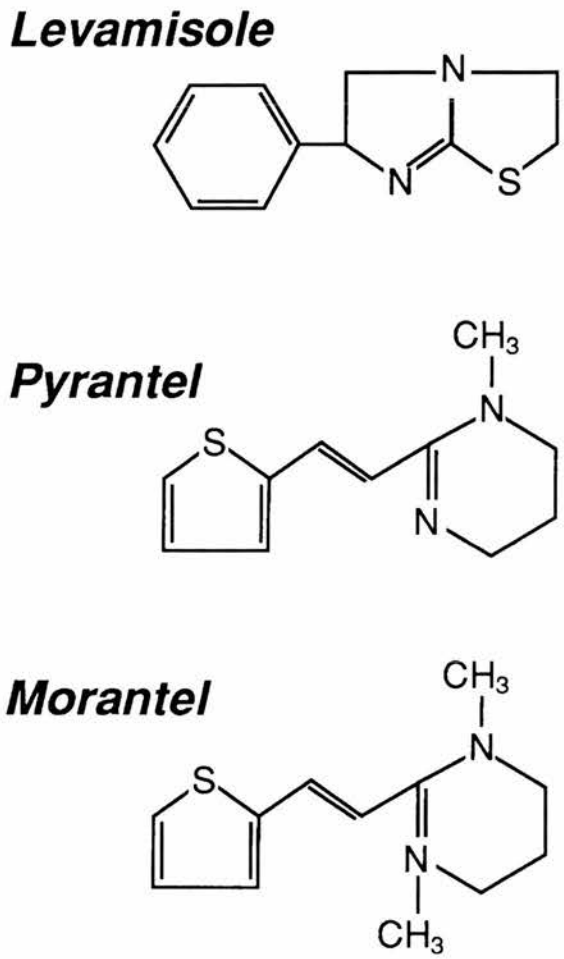


Fig. 1. The chemical structure of some nicotinic anthelmintics.

muscle. Thus the detailed pharmacology of the nematode nicotinic receptor must differ significantly from that of the host nicotinic receptors.

Structure of the nicotinic acetylcholine receptor ion-channel (nAChR)

The torpedo electric organ nicotinic receptor has been studied most extensively (Changeau, Devillers-Thiery & Chemouilli, 1996) because of its high concentration on the electric organ. It is a useful model for the nicotinic receptors of nematodes as well as higher species. The receptor-operated transmembrane ion-channel is made up of 5 subunits arranged around a central ion-channel like the staves of a barrel. Each subunit is made up of between 437–501 amino acids (Fig. 2). The five subunits of *Torpedo* are: 2α, 1β, 1γ and 1δ, (Fig. 3). The α-subunits of all nicotinic receptors, including nematodes, are believed to contain the ligand binding site and are characterized by the presence of two adjacent cysteines at positions 192 and 193 coupled by -SS- bonds (Fig. 2). Fig. 3A shows that each subunit of the channel is formed from an extracellular loop at the *N*-terminal, four lipophilic α-helical units, M1, M2, M3 and M4 and a short *C*-terminal section. There is also an intracellular loop between M3 and M4. The pore of the ion channel is lined by the M2 sections. The pore of the ion channel formed by the M2 regions forms three negatively charged rings (Fig. 4). There is an extracellular ring lined by glutamate and aspartate which are negatively charged amino acids. There is a middle ring which is narrower and believed to form the selectivity filter of the ion-channel. It too is lined by negatively charge amino acids. This time just glutamate is involved. On the more intracellular region of the pore, another ring is formed, known as the cytoplasmic ring. It also contains negatively charged amino acids. The middle negatively-charged ring forms a narrow selectivity filter, passing only positively charged cations through the ion pore. The nicotinic acetylcholine receptor thus is able to conduct sodium, potassium and to a lesser extent, calcium through the pore. Large cationic structures like local anaesthetics, or indeed the anthelmintics like levamisole, pyrantel and morantel are too large to pass through the channel. They may pass through the extracellular ring but become blocked at the middle ring. Once they reach this site they are capable of producing channel block. Voltage-sensitive channel block by the anthelmintics, levamisole (Robertson & Martin, 1993), pyrantel (Robertson *et al.* 1994), oxantel (Dale & Martin, 1995) and morantel (Evans & Martin, 1996), has been described for the nicotinic receptors of the nematode *Ascaris suum*. These anthelmintics are agonists and antagonists of the nematode *nAChR*.

Vertebrate neuronal nicotinic receptors may be composed of a pentameric structure like that of the *Torpedo* nicotinic receptor but it is believed that only α and β-subunits combine to produce the ion channel (McGehee & Role, 1995). However, there are currently 7 different types of neuronal α-subunit and 3 different β-subunits, each of which may combine in a variety of ways to produce a large number of subtypes of *nAChR*s (McGehee & Role, 1995). It is known that injection of cRNA encoding α- and β-subunits into *Xenopus* oocytes will produce functional nicotinic channels of the neuronal type. These channels have been studied with the patch-clamp technique and it has been shown that they are characterized by heterogeneity (Papke & Heineman, 1996; Papke *et al.* 1996). The channels recorded from in each patch may be separated into subtypes which have different conductances and mean open-times. The subtype may be produced by: variations of the stoichiometry of the subunits of the channel ($\alpha\beta\alpha\beta\beta$ *vs.* $\alpha\beta\alpha\beta\alpha$); variations in the subunit composition ($\alpha\beta_2\alpha\beta_2\beta_2$ *vs.* $\alpha\beta_3\alpha\beta_3\beta_3$ – the subscript here refers to the different β subunit structure not the stoichiometry); or variations in the arrangement of the pentameric channel (i.e. $\alpha\alpha\beta\beta\beta$ *vs.* $\alpha\beta\alpha\beta\beta$).

Studies on the soil nematode, *Caenorhabditis elegans*, have shown that three genes: *lev-1*, *unc-38*

ACH1

```
                1                  11                  21          *       31                  41
MSVCTLLISC  AILAAPTLGS  LQERRLYEDL  MRNYNNLERP  VANHSEPVTV  HLKVALQQII
           51                  61                  71          *       81                  91                 101
DVDEKNQVVY  VNAWLDYTWN  DYNLVWDKAE  YGNITDVRFP  AGKIWKPDVL  LYNSVDTNFD
                  111                 121          S---                   S          151                 161
STYQTNMIVY  STGLVHWVPP  GIFKISCKID  IQWFPFDEQK  CFFKFGSWTY  DGYKLDLQPA
                  171                 181                 191          SS     201                 211
TGGFDISEYI  SNGEWALPLT  TVERNEKFYD  CCPEPYPDVH  FYLHMRRRTL  YYGFNLIMPC
-------M1-  --          241         ----------  -M2-----261             272         ------
ILTTLMTLLG  FTLPPDAGEK  ITLQITVLLS  ICFFLSIVSE  MSPPTSEAVP  LLGIFFTCCM
-----M3---  ----        301         311         321         331         341
IVVTASTVFT  VYVLNLHYRT  PETHDMGPWT  RNLLLYWIPW  ILRMKRPGHN  LTYASLPSLF
                  351                 361                 371                 381                 391                 401
STKPNRHSES  LIRNIKDNEH  SLSRANSFDA  DCRLNQYIMT  QSVSNGLTSL  GSIPSTMISS
                  411                 421                 431                 441                 451         --------
NGTTTDVSQQ  ATLLILHRIY  HELKIVTKRM  IEGDKEEQAC  NNWKFAAMVV  DRLCLYVFTI
----M4----  ---         481
FIIVSTIGIF  WSAPYLVA
```

UNC-38

```
                                    191                 201
.....NSRV   AKRRAKNYPS  CCPQSAYIDV  TYYLQL...
```

Fig. 2. Amino-acid sequence of two α-subunits from *C. elegans*. Top: Amino acid sequence of an nAChR α-subunit (ACH1_CAEEL) from *C. elegans* determined from the gene sequence (Ballivet *et al.* 1996). During the synthesis of the receptor the signal sequence (*italics*) is cut off. The four putative membrane-spanning helical units M1, M2, M3 and M4 are indicated. The asterisk indicates an asparagine residue that is one site of high glycosylation. The region YDCC (tyrosine, aspartate, cysteine, cysteine) is the putative agonist binding site. The M2 region forms the putative pore region of the ion-channel. Bottom: Partial sequence of *unc-38* (Fleming *et al.* 1993 EMBL Accession Number: X98600) the α-subunit of *C. elegans* adult muscle receptor. Note that an extra amino acid proline separates the tyrosine (189) and the two cysteine (192, 193) amino acids. Deletion of the extra amino acid of *unc-38* (one from between tyrosine and the double cysteines) may remove the selective binding of levamisole and make the receptor like a mammalian receptor.

and *unc-29* of the 10–11 genes involved in levamisole resistance of this nematode (Table 3) encode the subunits of nicotinic ion-channels (Lewis *et al.* 1980; Fleming *et al.* 1997). Evidence for this is based on the homology of the *lev-1*, *unc-38* and *unc-29* amino acid sequences and the fact that when co-expressed in *Xenopus* oocytes they will produce functional channels gated by levamisole. Pairwise intranuclear injection of cDNA for *unc-38* along with *lev-1* is capable of producing functional channels (Fleming *et al.* 1997). Similarly, pairwise injection of *unc-38* with *unc-29* will also produce functional channels. This implies that the nicotinic receptor of *C. elegans* and perhaps that of nematodes could be comprised of varying combinations of subunits. An illustration of this varying structure which may make up the nicotinic channel is shown in Fig. 5: even in this illustration the number of possible arrangements is limited by maintaining the *unc-38* subunits, required for agonist binding, fixed in number and position. It is pointed out that other α subunits are also recognized in *C. elegans* including the subunit *ACh1* (also referred to as CE21, Ballivet *et al.* 1996) and have been cloned and expressed. Interestingly *ACh1* will express as a homo-oligomer in *Xenopus* oocytes and produce channels sensitive to nicotine but not levamisole. One explanation for the difference in the levamisole-sensitivity of channels produced with *unc-38* subunits in contrast to channels with *ACh1* subunits may relate to the addition of and extra amino acid at the putative agonist binding site between tyrosine (189) and cysteine (192) in *unc-38* which is not present in the levamisole insensitive *ACh1* subunit (Fig. 2).

It is believed that *unc-38* is required for the ligand-binding site. Evidence for this is based on the homology of *unc-38* with the α-subunit of torpedo and the fact that exclusion of *unc-38* from the pairwise cRNA injections into *Xenopus* oocytes results in the failure of expression.

It is known that the precise pharmacological profile of neuronal nicotinic receptors of vertebrates can vary with the molecular structure of the ion channel (Covernton *et al.* 1996). It varies with the molecular structure of the α-subunit and is also influenced by the β-subunit structure. It has been suggested that the agonist binding sites on nicotinic acetylcholine receptors may actually be on the interface between the α and β subunits (Karlin & Akabas, 1995). Thus in nematodes with the *unc-38*,

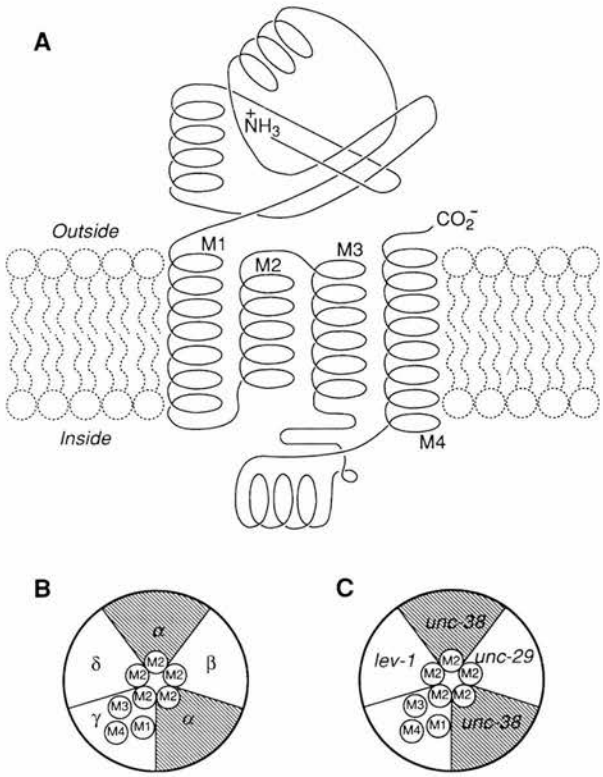


Fig. 3. The structure of the nicotinic channel. A: Diagram of the putative arrangement of the amino acid sequence in the membrane with the 4 α-helices M1, M2, M3 and M4 form transmembrane segments. There is a cytoplasmic loop between M3 and M4. B: The subunit arrangement of the *Torpedo* electric organ nicotinic receptor. Note that the M2 region forms the lining of the channel pore. C: A possible arrangement of the subunits *unc-38*, *unc-29*, *lev-1* that may make up the levamisole receptor. (Derived from Noda *et al.* 1983).

unc-29 and *lev-1* subunits, one could produce a variety of combinations of *unc-38* with *unc-29* and *lev-1* to produce the *nAChR* subtypes. Each of these particular combinations of ion channel will have slightly different pharmacological profiles and biophysical kinetics. It may be possible to separate out the properties of some of the individual combinations biophysically since they may have different conductance levels and mean open times.

We have examined the nicotinic receptor on *A. suum* muscle at the single channel level, using acetylcholine, levamisole, pyrantel and morantel as the agonists (Pennington & Martin, 1990; Robertson & Martin, 1993; Robertson *et al.* 1994; Evans & Martin, 1996). In all of these single channel studies, we have found that there is considerable variation in the conductance level of the channel observed between patch recordings. The conductance levels of the single channel currents have ranged between 15 pS at the lowest extreme up to 60 pS at the highest extreme. In some individual patch experiments it has been clear that more than one conductance level is present. The origin of this variability may be explained if we have different subunit combinations, some producing small conductance levels and others producing higher conductance levels. There are many other causes of variability. Our source of *Ascaris* varies dramatically and could easily influence the particular observations because factors like diet may alter the biophysical properties of the lipid membrane in which the ion channels site. To reduce this possibility, we have now conducted experiments on a smaller nematode, *Oesophagostomum dentatum* that may be infected from laboratory-maintained strains and produced in pigs under more controlled conditions. Our experiments on the nicotinic receptors of *O. dentatum* activated by levamisole also showed great variability. Fig. 6 shows an example of a channel recording at −75 mV where there are at least two amplitude current levels present. This implies that in this patch there are at least two different sub-types of nicotinic receptor, each may have a slightly different pharmacology, one channel type may be more resistant to opening by levamisole than the other. We have seen evidence suggesting that there are up to 4 nicotinic receptor subtypes present in *O. dentatum* (Martin *et al.* 1997). This heterogeneity may facilitate the development of anthelmintic resistance to nicotinic anthelmintics and perhaps other anthelmintics that act on membrane ion channels.

GABA AGONIST: PIPERAZINE

Piperazine is a heterocyclic ring without a carboxyl group. Despite this, it acts as a simple GABA agonist and gates open GABA receptors on the somatic muscle of nematodes (Del Castillo, De Mello & Morales, 1964; Corbett & Goose, 1971; Martin, 1985). It increases the Cl^- conductance of the muscle membrane leading to an increase in the membrane potential (a hyperpolarization) and a reduction in excitability. This leads to a relaxation of the body muscle and flaccid paralysis. Piperazine is effective against large intestinal nematodes and is potentiated by the presence of a high pCO_2. The CO_2 may interact with the heterocylic ring of piperazine and substitute for the carboxyl group of GABA.

AVERMECTINS

The avermectin anthelmintics (see Fig. 7) include ivermectin, abamectin, doramectin, and moxidectin, Their mode of action is to increase the Cl^- permeability of nerve and muscle membrane of invertebrates but the identity of the target ion-channel has been controversial (see Arena, 1994, for a review). The mode of action does not appear to be via GABA-gated Cl^- channels. Expression cloning experiments using *Xenopus* oocytes have suggested an action of avermectins on a glutamate-gated Cl^- (GluCl) channel (Cully *et al.* 1994). The channel is presumably a pentomer like that of the nicotinic

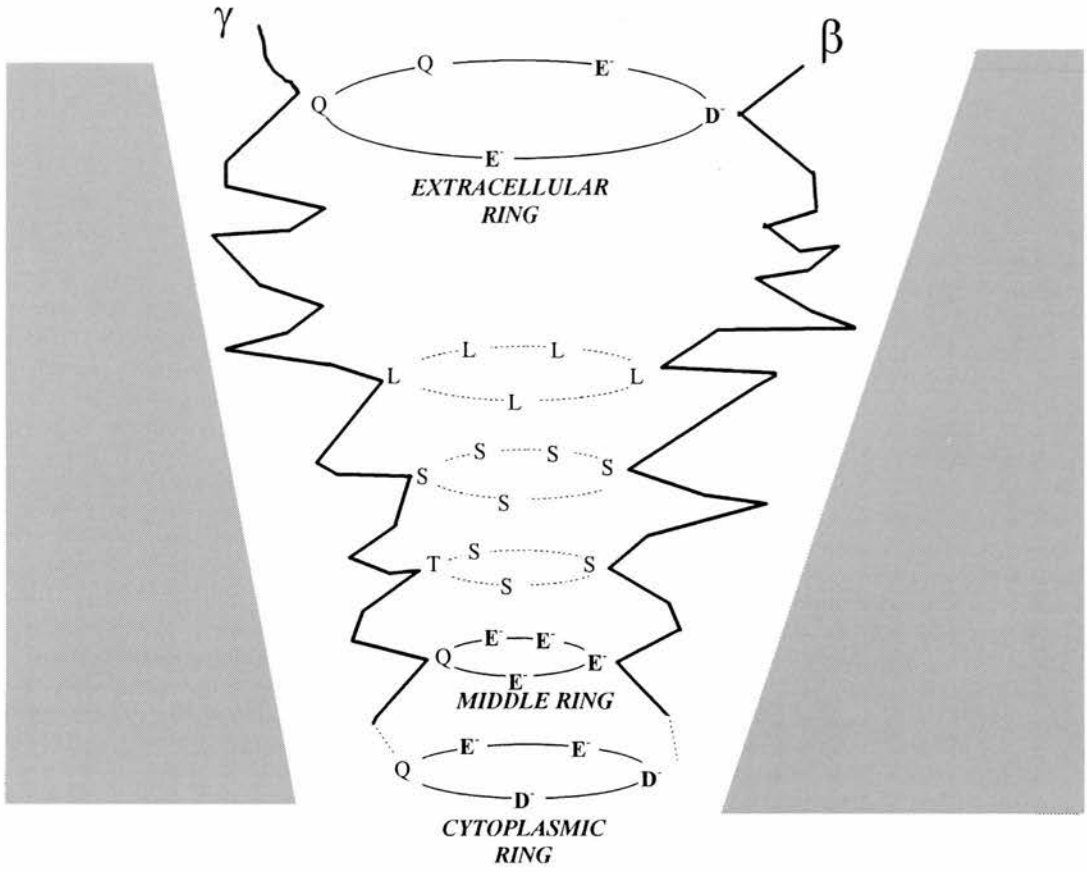


Fig. 4. The structure of the *Torpedo* nicotinic (derived from Revah *et al.* 1990). The organization of the pore of the nicotinic ion-channel showing: the presence of the outer extracellular ring lined with glutamate and aspartate amino acids; the middle ring which appears to act as a selectivity filter and is lined with glutamate amino acids forming a charged negative ring; the inner cytoplasmic ring lined with aspartate and glutamate amino acids.

Table 3. Genes responsible for levamisole resistance in *C. elegans* (Fleming *et al.* 1996)

Gene	Chromosome	Product
unc-38	I	α-subunit
unc-29	I	Non α-subunit
lev-1	IV	Non α-subunit
unc-74	I	Receptor expression
unc-50	III	Receptor expression
lev-8	X	Receptor expression
lev-9	X	Receptor expression
lev-10	I	Receptor expression
lev-11	I	Muscle specific Contraction defect
unc-22	IV	Muscle specific Contraction defect

Other *nAChR* subunit genes have been identified in the *C. elegans* genome. These subunits have not yet been demonstrated to be involved in levamisole resistance. They include: *ach1*, *ach2*, *ach3*, *deg-3*, *t09a5.3* and *ZC504*, *FO3F8.2*.

receptor but the equivalent of the M2 region which forms the ion channel pore of the *nAChR* channels is lined with positively charged sites so that the channel is selectively permeable to anions (Cl^-). The pentomer may be comprised of GluCl-α subunits which contain the glutamate binding site and the GluCl-β subunit that contains the ivermectin binding site.

The locations of the glutamate-gated chloride channel in nematodes were not determined by the expression studies of Culley *et al.* (1994). Molecular experiments using the *lac-Z* marker showed that the GluCl β-subunit of the glutamate channel was expressed in the pharyngeal muscle of *C. elegans* (Laughton, Wolstenholme & Lunt, 1995). The location of the GluCl-α subunit was not determined. As a result of these experiments, Martin (1996) used a two micro-electrode current clamp technique on the pharyngeal muscle of *A. suum*. These experiments demonstrated that the parasite possesses glutamate receptors that gate chloride channels and that this channel is potentiated by ivermectin analogues.

Fig. 8 shows the effect of application of glutamate on the pharyngeal muscle of *Ascaris* which is to produce a brief hyperpolarization and a reversible increase in conductance of the muscle. It also shows the effect of the application of milbemycin, an avermectin. Recent molecular experiments with *C. elegans* on an ivermectin resistance strain (*avr-15*)

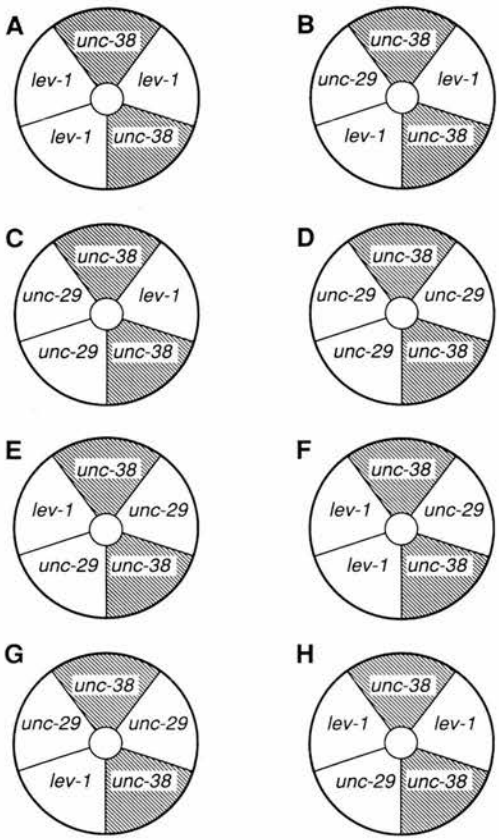


Fig. 5. Diagram of some possible subunit arrangments of *unc-38*, *unc-29* and *lev-1* subunits forming the nematode nAChR channel sensitive to levamisole. The *unc-38* is equivalent to the α subunit of vertebrate nicotinic channels. The *unc-29* and *lev-1* subunits are equivalent to vertebrate β subunits. The diagram shows that there are up to 8 different combinations possible if two *unc-38* subunits have to be maintained in the same relative position. If the conductance of the channel were altered only by the number of *unc-29* or *lev-1* subunits present in this scheme then 4 channel types would be distinguished on a basis of channel conductance. The diagram also illustrates that if the binding of the agonist molecule is at the interface of the *unc-38* subunit and an adjacent molecule then the binding of the agonist (including levamisole) will depend on subunit composition (derived from Martin *et al.* 1997).

suggests that it is a GluCl-α_2 subunit that is present in the pharyngeal muscle of *C. elegans*, not the GluCl-α_1 subunit (review, Cully *et al.* 1997). The location function and expression of the GluCl-α_1 remains to be determined. It does not appear to be present in the pharynx. The distribution of this subunit may help to determine other sites of action of the ivermectins.

CALCIUM PERMEABILITY: PRAZIQUANTEL

Praziquantel is used for the control of schistosomiasis and cestode infections. It has little action against nematode parasites. Its mode of action has been reviewed recently (Redman *et al.* 1996). Application of praziquantel to *Schistosoma mansoni* results in a slow depolarization of the tegument. Associated with the depolarization is an increase of influx of calcium (Fetterer, Pax & Bennett, 1980; Mehlhorn *et al.* 1981; Wolde-Mussie *et al.* 1982; Thompson, Pax & Bennett, 1984). The mode of entry of calcium is not known but Fig. 9 illustrates some possible routes. It is, however, known that its activity may be blocked by high concentrations of magnesium, lanthanum, nickel, and cobalt. The site of action of praziquantel appears to be the tegument of *Schistosoma* as application of praziquantel to isolated body muscle cells from *Schistosoma* has little effect. It is known that application of praziquantel to a muscle preparation from snails mimics the application of caffeine. In fact, prior application of caffeine to this snail muscle preparation pre-empts and abolishes the effect of praziquantel in low calcium extracellular solutions (Gardner & Brezden, 1984).

Thus it appears that the site of action of praziquantel may involve the same site as caffeine. Caffeine is known to act on a calcium-induced calcium release (CICR) channel in the sarcoplasmic reticulum of muscle. This channel releases a flood of calcium into the cytoplasm from the sarcoplasmic reticulum and is triggered by a smaller rise in cytoplasmic calcium produced through voltage-activated calcium channels in the cell (sarcolemma) membrane. The CICR channel of sarcoplasmic reticulum has a high conductance of several hundred pS and has some similarity to the large conductance channel in the tegument of *Schistosoma* (Day, Bennett & Pax, 1992).

It is also known that following the application of praziquantel through *S. mansoni* antigens are exposed that were not previously available to the host. As a result of this exposure, presumably by damage to the outer bilayer of the double bilayer of the tegument, host inflammatory cells move in to attack the schistosome. The exposure of the antigen may be a secondary effect of the elevated calcium since maintained calcium levels not only elevate the exposure of antigens but there is a blebbing of the schistosome membrane (Redman *et al.* 1996).

Most of the mode of action studies on praziquantel have involved *S. mansoni*. Less is known about the direct effect of praziquantel on cestode parasites. It is presumed the mode of action on both groups of parasite is the same.

BENZIMIDAZOLES: β-TUBULIN

The benzimidazole group of anthelmintics including thiabendazole, mebendazole and fenbendazole, are broad-spectrum anthelmintics which have an action against gastrointestinal nematodes and in some cases, at a higher concentration, actions against trematodes. Their mode of action is now known to involve binding to β-tubulin. β-tubulin along with

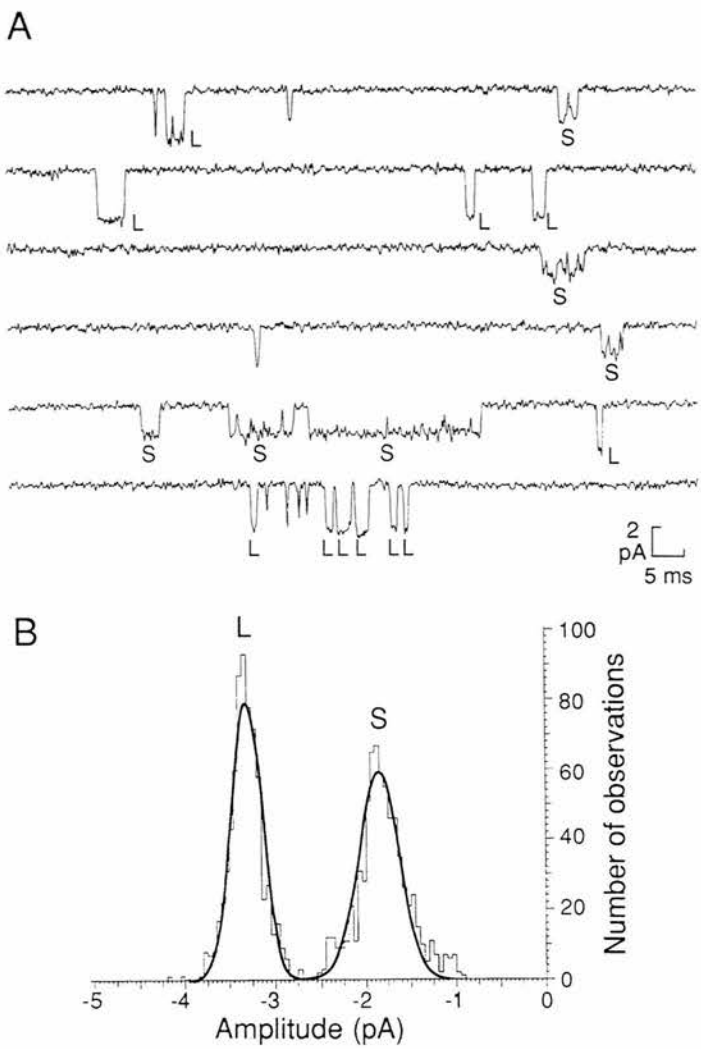


Fig. 6. A: Cell-attached patch recording at −75 mV showing a small (S) and larger (L) nAChR channel present. B: Amplitude histogram of open-channel amplitudes. Smaller conductance channel: mean current = −1·8 pA ± 0·2 (24·8 pS) labelled S in Fig. 5A. Larger conductance channel: mean current = −3·3 ± 0·2 pA (43·8 pS) labelled L in Fig. 5A). Histograms of the amplitudes of the open-channel currents were fitted with Gaussian distributions. 49% of the events were to the smaller amplitude, 51% were to the larger amplitude.

α-tubulin polymerizes to form microtubule structures inside the cells of nematodes and the host animal (Stryer, 1995).

The mode of action of the benzimidazoles started to be understood when it was realized that mebendazole given to *Ascaris* produced damage to the intestinal cells of the parasite. It was found that there was a loss of cytoplasmic tubules of both the intestinal cells and teguments of cestodes and nematodes (Van den Bossche & De Nollin, 1973; van den Bossche, Roshette & Horig, 1982). This was associated with a loss of transport of secretory vesicles and the failure of the intestinal cells to take up glucose. Thus following application of mebendazole, the parasite starved. It was found in *Ascaris* that mebendazole bound to cytoplasmic proteins that had a molecular weight of 50 kDa and 100 kDa which are monomers and dimers of tubulin. It was found that the benzimidazoles anthelmintics competed for the binding site on β-tubulin with colchicine, a substance known to block cell division in the metaphase (Sangster, Prichard & Lacey, 1985; Lacey & Gill, 1994). Microtubules serve a variety of intracellular functions including transport of cytoplasmic secretory vesicles (Stryer, 1995).

Structure and function of microtubules

Microtubules are formed in a dynamic process by the combination of two 450 amino acid proteins that are known as α-tubulin and β-tubulin (Stryer, 1995). The formation of the microtubules involves the polymerization of tubulin at one end, known as the positive pole, and the depolymerization at the other end, known as the negative pole. Microtubules that form are made up of thirteen tubulin molecule rings (6 α-tubulin plus 7 β-tubulin, alternating with 7 α-tubulin plus 6 β-tubulin rings). There are a number of factors which encourage polymerization and these factors include GTP, magnesium and an increase in

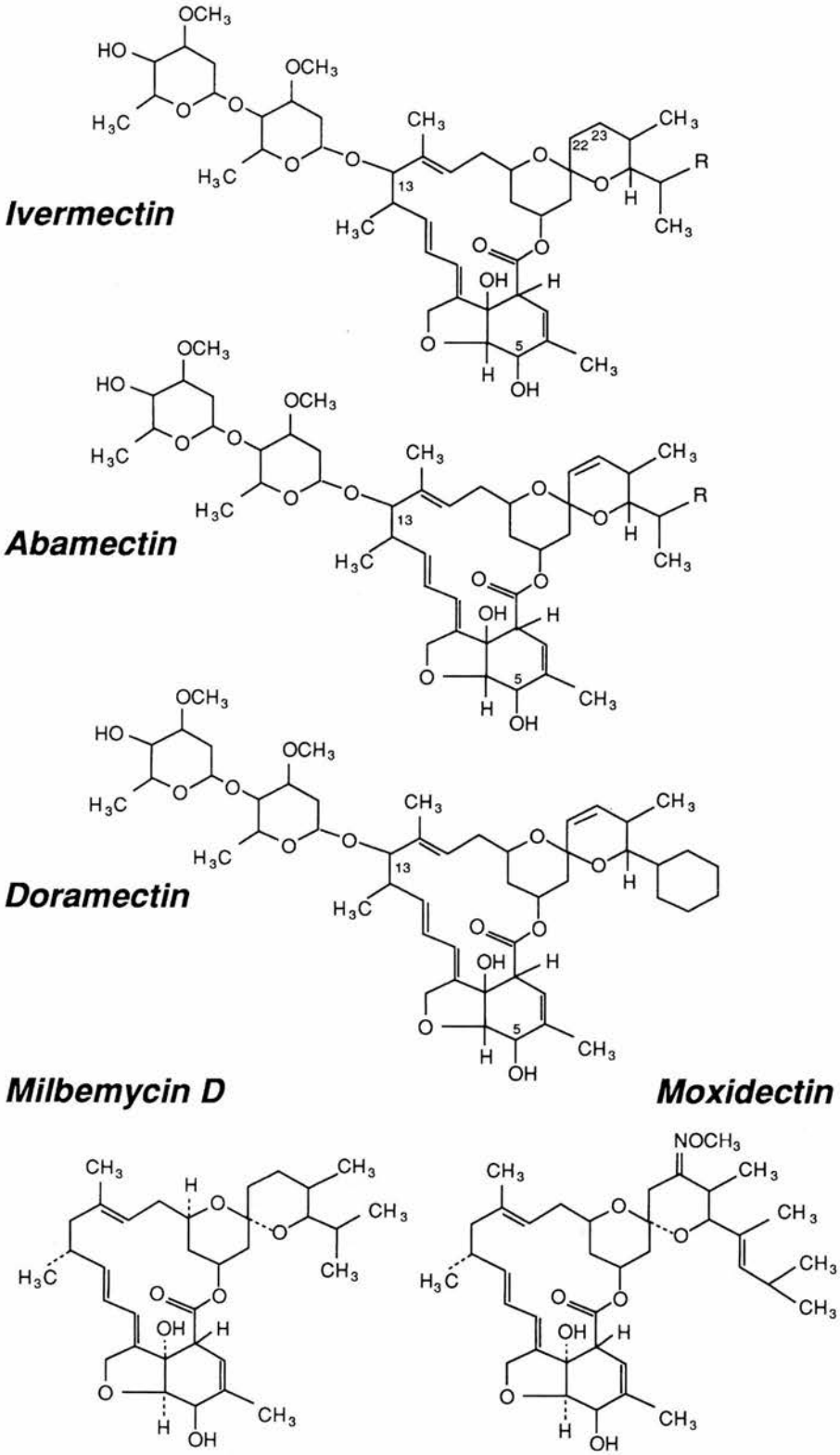


Fig. 7. The chemical structures of the avermectin anthelmintics.

temperature: a fall in temperature to 4 °C or the presence of calcium or calmodulin favours depolymerization. The formation of microtubules can be prevented or inhibited by substances that bind to the positive pole (the leading edge) of polymerization. This process is known as capping and it can be achieved by colchicine, vinblastine, vincristine, or the benzimidazoles, which do this by binding to β-tubulin molecules.

Thus we know that the mode of action of benzimidazole anthelmintics is to bind to nematode β-tubulin more selectively than the host microtubule β-tubulin. The onset of benzimidazole anthelmintic action is therefore slower than that of the anthel-

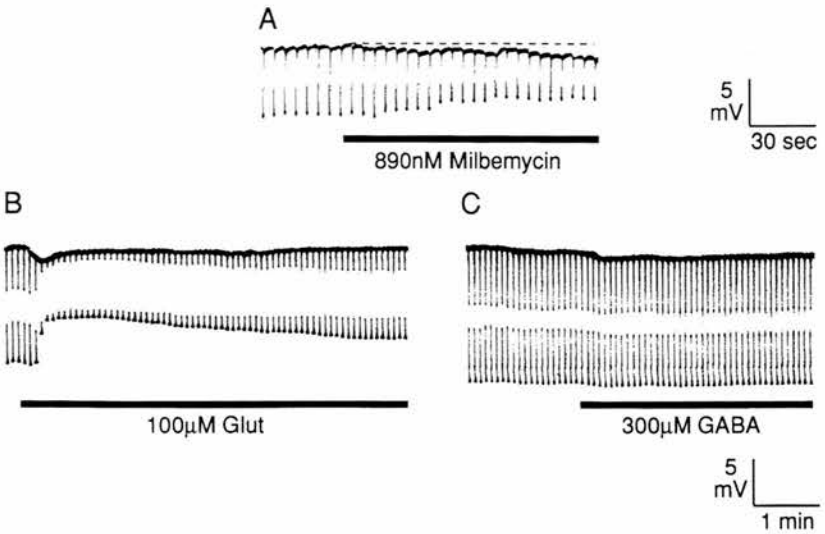


Fig. 8. A: Effect of 890 nM milbemycin D on the membrane potential and input conductance. Milbemycin slowly produced an increase in input conductance that was not reversed on washing (not shown). B: Effect of application of 100 μM L-glutamate on membrane potential and input conductance. Different preparation from B. Glutamate (applied during horizontal bar) produced a transient small hyperpolarization of 1 mV associated with an input conductance change from 157 μS to a peak of 429 μS (ΔG: 272 μS) desensitizing to 231 μS (ΔG: 74 μS) after 4 minutes. C: After washing the preparation the input conductance of the pharynx returned towards control levels (142 μS) and the effect of 300 μM GABA was tested without effect (applied during the horizontal bar). The lack of effect of GABA was not due to desensitization because subsequent application of 100 μM L-glutamate increased the input conductance again (not shown) (derived from Martin *et al.* 1995).

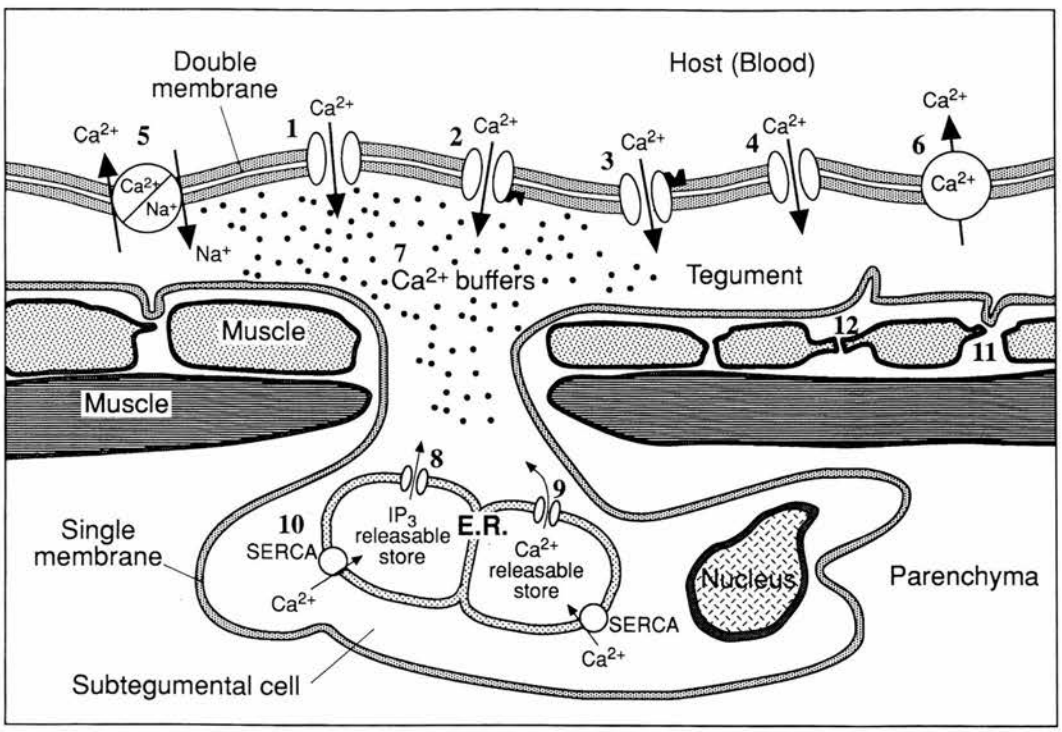


Fig. 9. Diagram of the structure of the body wall of *Schistosoma mansoni* showing the possible sites of action of praziquantel and mechanisms of Ca^{2+} transport into and out of the tegument. 1: voltage-activated Ca^{2+} channel. 2: Intracellular messenger activated Ca^{2+} channel. 3: Extracellular receptor operated Ca^{2+} channel. 4: Non-selective cation channel also allowing entry of Ca^{2+}. 5: Na^+/Ca^{2+} exchanger. 6: Ca^{2+} ATPase pumping out Ca^{2+}. 7: Intrategumental Ca^{2+} buffers. 8: IP_3 releasable store from the sarcoplasmic reticulum. 9: Ca^{2+}-induced Ca^{2+} release channel (CICR channel). 10: Ca^{2+} ATPase pump: sarcoplasmic endoplasmic reticulum Ca^{2+} (SERCA). 11: Electrical junction between muscle cell and tegument. 12: Electrical junctions between muscle cells. If praziquantel acts like caffeine it would act on site 9 (derived from Redman *et al.* 1996).

mintics that work directly on ion-channels. Benzimidazoles must produce starvation of the nematode by intestinal disruption and/or inhibition of egg production.

In *Haemonchus contortus*, two types of β-tubulin have been recognized: isotype 1 and isotype 2 (Roos, Kwa & Grant, 1995). These two isotypes have separate genes and have a number of alleles: there are up to six alleles for isotype 1 and up to 12 alleles for isotype 2. The function of the specific isotopes is not known in nematodes. Roos *et al.* (1995) has shown that there is a reduction in the number of isotype alleles for β-tubulin during the appearance of benzimidazole resistance. Observations made on the appearance of resistance of *H. contortus* showed that there was a progressive loss of alleles for isotype 1 and a total loss of alleles for isotype 2. Resistance may be explained by loss of susceptible phenotypes of the β-tubulin and the survival of resistance phenotypes. It is known that benzimidazole resistance in fungi is associated with the appearance of a different form of β-tubulin (Fujimura *et al.* 1992). It is characterized by the appearance of a tyrosine instead of phenylalanine in position 200 on the β-tubulin chain. Unfortunately, mammalian β-tubulins also have tyrosine at position 200 (Lewis, Lee & Cowen, 1985) so it is unlikely that benzimidazole resistance may be overcome by changes in the chemistry of the drug since the fungal benzimidazole has learned to mimic the host β-tubulin. If such a phenomenon occurs in nematode parasites, it would result in the inability of the benzimidazoles to exert a selective toxic effect.

PROTON IONOPHORES

The proton ionophores include the salicylanilides and substituted phenols (for a review see McKellar & Kinabo, 1991). They include closantel, rafoxanide, oxyclozanide and brotianide. They are a range of compounds that have anti-fluke action. Their mode of action is that of a proton ionophore which is usually called an oxidative phosphorylase uncoupler. Each of the salicylanilides or the substituted phenols contains a detachable proton group. The compounds are all very lipophilic so that they dissolve in the phospholipid membranes of cells and may shuttle across the membrane carrying protons. They do this particularly across the inner mitochondrial membrane and will reduce any proton gradient. Since a proton gradient is necessary for the production of ATP by mitochondria there is an inhibition of the energy production by the mitochondria following poisoning by the salicylanilide.

The selective mode of action of the series of compounds that act as oxidative phosphorylase uncouplers is believed to involve and to be associated with the very high plasma protein binding of these compounds which are effective therapeutically. The anthelmintics used in this way have a very long half-life of more than fourteen days. More than 95% of the salicylanilides are plasma protein bound. Thus the selective action of these anthelmintics may be explained by an action on blood-sucking parasites concentrating the anthelmintic in the parasite as it takes in high levels of plasma protein.

Pax & Bennett (1989) have examined the pH gradient across *S. mansoni* following treatment with salicylanilides. They were able to demonstrate an effect on the tegument of the parasite indicating that this may be a site of action for these anthelmintics. Thus mitochondria may not be the only site at which these compounds exert their effect.

MALATE METABOLISM

The compound diamphenethide is an agent that is effective against immature *Fasciola hepatica* in the liver but less effective against *Fasciola* in the bile ducts. Diamphenethide is deacetylated in the host liver to an active monoamine and diamine (Coles, 1976). The amine of diamphenethide has an action which produces an elevation of malate concentration in *Fasciola* (Edwards *et al.* 1981*b*). Malate is an intermediary break-down product of glucose in this parasite. It is known that dopamine, a putative neurotransmitter in *Fasciola*, has a protective effect against diamphenethide but the mode of action of a diamphenethide has yet to be defined in greaer detail (Edwards *et al.* 1981*a*).

PHOSPHOGLYCERATE KINASE AND MUTASE INHIBITION

Clorsulon is very similar in structure to 1,3-diphosphoglycerate and because of this it inhibits the enzymes phosphoglycerate kinase and phosphoglyceromutase of *Fasciola* (Schulman & Valentino, 1982; Schulman *et al.* 1982*a*). Thus it prevents the full breakdown of glucose by the Emden-Meyerhoff pathway and inhibits glucose utilization. The inhibition of the phosphoglycerate kinase was competitive with clorsulon inhibiting the binding of 3-phosphoglycerate and ATP to the kinase. Clorsulon thus has a dose-dependent inhibitory effect on immature and mature *Fasciola* (Schulman *et al.* 1982*b*).

ARACHIDONIC ACID METABOLISM AND INNATE IMMUNITY

Diethylcarbamazine is a piperazine derivative used in low doses as an anti-filarial drug. Although it has a good microfilaricidal action, it has limited macrofilaricidal action. Its action against some adult helminths requires nearly 10 times the prophylactic filarial dose and may involve another mode of action.

Although the structure of diethylcarbamazine might suggest it acts like piperazine, electro-

physiological studies following bath application to *A. suum* have shown that it does not mimic the actions of piperazine (Martin, 1982). It appears that there is little direct action on filariae when diethylcarbamazine is added to isolated parasites. It has quite marked *in vivo* effects in experiments in contrast to its *in vitro* effects. Following intravenous injection it produces an anti-filarial action within about 4 minutes (Hawking & Laurie, 1949). In mice that have had their immune system impaired genetically (nude, athymic mice) which are infected with *Brugia pahangi* there is a marked reduction in microfilariae following administration of diethylcarbamazine (Vickery, Nayar & Tamplin, 1986). These experiments show that T-cells and T-dependent responses (IgG and IgE) are not involved.

It is known that diethylcarbamazine has an antagonistic action on the metabolism of arachidonic acid which is produced from the breakdown of cell membranes under the influence of phospholipase A_2 (Maizels & Denham, 1992). It is often said that 5-lipoxygenase is the enzyme which is inhibited by diethylcarbamazine. But it has also been suggested that synthesis of LTA_4 by LTA_4-synthase from 5-HPETE is blocked by diethylcarbamazine in mast cells (Mathews & Murphy, 1982; Razin *et al.* 1984). Diethylcarbamazine is also believed to block production of PGI_2 (prostacyclin) by inhibition of endothelial cyclo-oxygenase (Kanesa-Thasan, Douglas & Kazura, 1991). It does not appear to have any effect on the production of thromboxane (TXA_2). Microfilariae also produce their own PGI_2 and PGE_2 and these too are inhibited by diethylcarbamazine during treatment (Kanesa-Thasan *et al.* 1991). It seems then that diethylcarbamazine inhibits production of PGI_2 and PGE_2 by both endothelial cells and microfilariae. These two eicosanoids are involved in the control of blood vessel tone and the inhibition of neutrophil aggregation and granulocyte aggregation.

Thus a reasonable explanation for the action of diethylcarbamazine at low doses to prevent microfilariae is that it alters the metabolism of arachidonic acids in the host endothelial cells and microfilariae. As a result of this, there is constriction of the blood vessels and aggregation of the host granulocytes and host platelets. Thus it appears that diethylcarbamazine activates an innate immune response rather than an adaptive response (Maizels & Denham, 1992). This mode of action could explain why diethylcarbamazine does not have an effect *in vitro* against the microfilariae and is not effective in non-immune animals.

FUTURE DEVELOPMENT OF ANTHELMINTICS

Continued economic losses in animal production and human disease due to parasites are still of concern to industrial chemists looking for new anthelmintic agents. The intensive use of drugs for the control of nematode parasites has and will continue to lead to the development of resistance. New anthelminitics are needed for the future but the huge costs associated with the development on new compounds and the small economic size of the market for anthelmintics will make future development slow. The limited market size and concerns over resistance and residues are reflected in the decrease in patent applications. With increased knowledge of parasite physiology, particularly the nicotinic acetylcholine receptors, the GABA receptors and the glutamate-Cl^- channel as examples, a directed rational search for new leads should be possible. Surveying natural substances (plant extracts and antibiotics) is also in an early stage with only a small fraction of the microbial ecosystem having been surveyed. Recently, the dioxapyrrolomycins as lead compounds for AC303630 (Hunt, 1994), the anthelmintic cyclodepsipeptide PF1022A (Martin *et al.* 1996) and paraherquamides (Schaeffer *et al.* 1990) have been reported. These show the continuing potential of such an approach. There remains a demand for new potent broad-spectrum anthelmintics which are effective against resistant parasites, harmless to the environment and can be cost-effective. Anthelmintics with different parasite target sites are to be expected in the future.

ACKNOWLEDGEMENTS

R. J. M. is pleased to acknowledge the financial support of The Wellcome Trust who have supported my electrophysiological work on the nicotinic anthelmintics and the glutamate receptors of *Ascaris*. H. B. is pleased to acknowledge the support of the Danish National Research Foundation.

REFERENCES

ARENA, J. P. (1994). Expression of *Caenorhabditis elegans* messenger RNA in *Xenopus*-oocytes: a model system to study the mechanism of action of avermectins. *Parasitology Today* **10**, 35–37.

BALLIVET, M., ALLIOD, C., BERTRAND, S. & BERTRAND, D. (1996). Nicotinic acetylcholine receptors in the nematode *Caenorhabditis elegans*. *Journal of Molecular Biology* **258**, 261–269.

CHANGEAU, J.-P., DEVILLERS-THIERY, A. & CHEMOUILLI, P. (1996). Acetylcholine receptor: An allosteric protein. *Science* **225**, 1335–1345.

COLES, G. C. (1976). The inactivity of diamphenethide against liver fluke in certain species of mammals. *Journal of Parasitology* **20**, 110–111.

CORBETT, J. R. & GOOSE, J. (1971). The biochemical mode of action of the fasciolicides, nitroxynil, hexachlorophene, and oxyclozanide. *Biochemical Journal* **121**, 41.

COVERNTON, P. J. O., KOJIMA, H., SIVILOTTI, L. G., GIBB, A. J. & COLQUHOUN, D. (1996). Comparison of neuronal nicotinic receptors in rat sympathetic neurones with

subunit pairs expressed in *Xenopus* oocytes. *Journal of Physiology (London)* **481**, 27–34.

CULLY, D. F., VASSILATIS, D. K., LIU, K. K., PARESS, P. S., VANDERPLOEG, L. H. T. & SCHAEFFER, J. M. (1994). Cloning of an avermectin-sensitive glutamate-gated chloride channel from *Caenorhabditis elegans*. *Nature* **371**, 707–711.

CULLY, D. F., WILKINSON, H., VASSILITIS, D. K., ETTER, A. & ARENA, J. P. (1996). Molecular biology and electrophysiology of glutamate-gated chloride channels of invertebrates. *Parasitology* **113**, S191–S200.

DALE, V. M. E. & MARTIN, R. J. (1995). Oxantel-activated single-channel currents in the muscle membrane of *Ascaris suum*. *Parasitology* **110**, 437–448.

DAY, T. S., BENNETT, J. L. & PAX, R. A. (1992). *Schistosoma mansoni*: patch-clamp study of a non-selective cation channel in the outer tegumental membrane of females. *Experimental Parasitology* **74**, 348–356.

DEL CASTILLO, J., DE MELLO, W. C. & MORALES, T. (1964). Mechanism of the paralysing action of piperazine on *Ascaris* muscle. *British Journal of Pharmacology* **22**, 463–477.

EDWARDS, S. R., CAMPBELL, A. J., SHEERS, M., MOORE, R. J. & MONTAGUE, P. E. (1981*a*). Protection of *Fasciola hepatica* against flukicidal action of the amine of diamphenethide *in vitro*. *Molecular and Biochemical Parasitology* **2**, 339–348.

EDWARDS, S. R., CAMPBELL, A. J., SHEERS, M., MOORE, R. J. & MONTAGUE, P. E. (1981*b*). Studies of the effect of diamphenethide and oxyclozanide on the metabolism of *Fasciola hepatica*. *Molecular and Biochemical Parasitology* **2**, 323–338.

EVANS, A. M. & MARTIN, R. J. (1996). Activation and cooperative multi-ion block of single nicotinic-acetylcholine channel currents of *Ascaris* muscle by the tetrahydropyrimidine anthelmintic, morantel. *British Journal of Pharmacology* **118**, 1127–1140.

FETTERER, R. H., PAX, R. A. & BENNETT, J. L. (1980). *Schistosoma mansoni*: characterization of the electrical potential from the tegument adult males. *Experimental Parasitology* **49**, 353–365.

FLEMING, J. T., BAYLIS, H. A., SATELLE, D. B. & LEWIS, J. A. (1996). Molecular cloning and *in vitro* expression of *C. elegans* and parasitic nematode ionotropic receptors. *Parasitology* **113**, S175–S190.

FUJIMURA, M., OEDA, K., INOUE, H. & KATO, T. (1992). A single amino acid substitution in the β-tubulin gene of *Neurospora* confers both carbendazim resistance and diethofencarb sensitivity. *Current Genetics* **21**, 399–404.

GARDNER, D. R. & BREZDEN, B. L. (1984). The sites of action of praziquantel in a smooth muscle of *Lymnaea stagnalis*. *Canadian Journal of Physiology and Pharmacology* **62**, 282–287.

HARROW, I. D. & GRATION, K. A. F. (1985). Mode of action of the anthelmintics morantel, pyrantel and levamisole on muscle-cell membrane of the nematode *Ascaris suum*. *Pesticide Science* **16**, 662–672.

HAWKING, F. & LAURIE, W. (1949). Action of hetrazan on filariasis and onchocerciasis. *Lancet* **2**, 146–147.

HUNT, D. A. (1994). 2-Arylpyrroles: novel uncouplers of ocidative phosphorylation. In: *Advances in the Chemistry of Insect Control III* (ed. G. G. Briggs), pp. 127–140. Cambridge, Royal Society of Chemistry.

KANESA-THASAN, N., DOUGLAS, J. G. & KAZURA, J. W. (1991). Diethylcarbamazine inhibits endothelial and microfilarial prostanoid metabolism *in vitro*. *Molecular and Biochemical Parasitology* **49**, 11–20.

KARLIN, A. & AKABAS, M. (1995). Towards a structural basis for the function of nicotinic acetylcholine-receptors and their cousins. *Neuron* **15**, 1231–1244.

LACEY, E. & GILL, J. H. (1994). Biochemistry of benzimidazole resistance. *Acta Tropica* **56**, 245–262.

LAUGHTON, D. L., WOLSTENHOLME, A. J. & LUNT, G. (1995). The beta subunit of the *C. elegans* inhibitory glutamate receptor is expressed in the pm4 pharyngeal muscle cells. *Worm Breeders Gazette* **14**, 48.

LEWIS, J. A., WU, C.-H., LEVINE, J. H. & BERG, H. (1980). Levamisole-resistant mutants of the nematode *Caenorhabditis elegans* appear to lack pharmacological acetylcholine receptors. *Neuroscience* **5**, 967–989.

LEWIS, S., LEE, M. G.-S. & COWEN, N. J. (1985). Five mouse tubulin isotypes and their regulated expression during development. *Journal of Cell Biology* **101**, 852–861.

MAIZELS, R. M. & DENHAM, D. A. (1992). Diethylcarbamazine (DEC): immunopharmacological interactions of an anti-filarial drug. *Parasitology* **105**, S49–S60.

MARTIN, R. J. (1982). Electrophysiological effects of piperazine and diethylcarbamazine on *Ascaris suum* somatic muscle. *British Journal of Pharmacology* **77**, 255–265.

MARTIN, R. J. (1985). γ-aminobutyric acid- and piperazine-activated single channel currents from *Ascaris suum* body muscle. *British Journal of Pharmacology* **84**, 445–461.

MARTIN, R. J. (1993). Neuromuscular transmission in nematodes and anthelmintic drug action. *Pharmacology and Therapeutics* **58**, 13–50.

MARTIN, R. J. (1995). An electrophysiological preparation of *Ascaris suum* pharyngeal muscle reveals a glutamate-gated chloride channel sensitive to the avermectin analogue milbemycin D. *Parasitology* **112**, 247–252.

MARTIN, R. J., HARCLER, A., LONDERSHAUSEN, M. & JESCHKE, P. (1996). Anthelmintic actions of the cyclic depsipeptide PF1022A and its electrophysiological effects on muscle cells of *Ascaris suum*. *Pesticide Science* **48**, 343–350.

MARTIN, R. J., ROBERTSON, A. P., BJORN, H. & SANGSTER, N. C. (1997). Heterogenous levamisole receptors: a single-channel study of nicotinic acetylcholine receptors from *Oesophagostomum dentatum*. *European Journal of Pharmacology* (in the Press).

MARTINDALE (1996). *The Extra Pharmacopoea*. 31st Edition. (ed. Reynold, J. E. F.), pp. 103–128. The Royal Pharmaceutical Society of Great Britain, London, England.

MATHEWS, W. R. & MURPHY, R. C. (1982). Inhibition of leukotriene biosynthesis in mastocytoma cells by diethylcarbamazine. *Biochemical Pharmacology* **31**, 2129–2132.

MCGEHEE, D. S. & ROLE, L. W. (1995). Physiological diversity of nicotinic acetylcholine receptors expressed by vertebrate neurons. *Annual Review of Physiology* **57**, 521–546.

McKELLAR, Q. A. & KINABO, L. D. B. (1991). The pharmacology of flukicidal drugs. *British Veterinary Journal* **147**, 306–319.

MEHLHORN, H., BECHER, B., ANDREWS, R., THOMAS, H. & FRENKEL, J. R. (1981). *In vivo* and *in vitro* experiments on the effect of praziquantel on *Schistosoma mansoni*: a light and electron microscope study. *Arzneimittel Forschung* **31**, 544–554.

NODA, M., TAKAHASHI, H., TANABE, T., TOYOSATA, M., KIKYOTANI, S., FUTUTANI, Y., HIROSE, T., TAKASHIMA, H., INAYAMA, S., MIYATATA, T. & NUMA, S. (1983). Structural homology of *Torpedo californica* acetylcholine receptor subunits. *Nature (London)* **302**, 528–532.

NOAH (1997). *Compendium of Data Sheets for Veterinary Products 1996–97*. Beccles, Suffolk. William Clowes Ltd.

PAPKE, R. L., BOULTER, J., PATRICK, J. & HEINMANN, S. (1996). Single channel currents of rat neuronal nicotinic acetylcholine receptors expressed in *Xenopus laevis* oocytes. *Neuron* **3**, 589–596.

PAPKE, R. L. & HEINEMAN, F. (1996). The role of the β_4-subunit in determining the kinetic properties of rat neuronal nicotinic acetylcholine α_4-receptors. *Journal of Physiology (London)* **440**, 95–112.

PAX, R. A. & BENNETT, J. L. (1989). Effect of closantel on intrategumental pH in *Schistosoma mansoni* and *Fasciola hepatica*. *Journal of Parasitology* **75**, 169–171.

PENNINGTON, A. J. & MARTIN, R. J. (1990). A patch-clamp study of acetylcholine-activated ion channels in *Ascaris suum* muscle. *Journal of Experimental Biology* **154**, 201–221.

PRICHARD, R. K. (1994). Anthelmintic resistance. *Veterinary Parasitology* **54**, 259–268.

RAZIN, E., ROMEO, L. C., KRILIS, S., LIU, F.-T. & LEWIS, R. A. (1984). An analysis of the generation and the secretion of preformed mediators from mouse bone marrow-derived mast cells. *Journal of Immunology* **133**, 938–945.

REDMAN, C. A., ROBERTSON, A. P., FALLON, P. G., MODHA, J., KUSEL, J. R., DOENHOFF, M. J. & MARTIN, R. J. (1996). Praziquantel: An urgent and exciting challenge. *Parasitology Today* **12**, 14–20.

REVAH, F., GALZI, J.-L., GIRAUDAT, J., HAUMONT, F., LEDERER, F. & CHANGEAUX, J.-P. (1990). The non-competitive blocker [H^3]chlorpromazine labels three amino acids of the acetylcholine receptor γ subunit: Implications for the α-helical organization of the regions MII and for the structure of the ion channel. *Proceedings of the National Academy of Sciences, USA* **87**, 4675–4679.

ROBERTSON, S. J., PENNINGTON, A. J., EVANS, A. M. & MARTIN, R. J. (1994). The action of pyrantel as an agonist and an open-channel blocker at acetylcholine-receptors in isolated *Ascaris suum* muscle vesicles. *European Journal of Pharmacology* **271**, 273–282.

ROBERTSON, S. J. & MARTIN, R. J. (1993). Levamisole-activated single-channel currents from muscle of the nematode parasite *Ascaris suum*. *British Journal of Pharmacology* **108**, 170–178.

ROOS, M. H., KWA, M. S. G. & GRANT, W. N. (1995). New genetic and practical implications of selection for anthelmintic resistance in parasitic nematodes. *Parasitology Today* **11**, 148–150.

SANGSTER, N. C., PRICHARD, R. K. & LACEY, E. (1985). Tubulin and benzimidazole-resistance in *Trichostrongylus colubriformis* (Nematoda). *Journal of Parasitology* **71**, 645–651.

SCHAEFFER, J. M., BLIZZARD, T. A., ONDEYKA, J. G., GOEGELMAN, R., SINCLAIR, P. J. & MROZIK, H. (1992). [^{3}H]Paraherquamide binding to *Caenorhabditis elegans*: studies on a potent new anthelmintic agent. *Biochemical Pharmacology* **43**, 679–684.

SCHULMAN, M. D., OSTLIND, D. A. & VALENTINO, D. (1982*a*). Mechanism of action of mk-401 against *Fasciola hepatica* – inhibition of phosphoglycerate kinase. *Molecular and Biochemical Parasitology* **5**, 133–145.

SCHULMAN, M. D., VALENTINO, D., CIFELLI, S. & OSTLIND, D. A. (1982*b*). Dose-dependent pharmacokinetics and efficacy of mk-401 against old, and young-mature infections of *Fasciola hepatica* in the rat. *Journal of Parasitology* **68**, 603–608.

SCHULMAN, M. D. & VALENTINO, D. (1982). Purification, characterization and inhibition by mk-401 of *Fasciola hepatica* phosphoglyceromutase. *Molecular and Biochemical Parasitology* **5**, 321–332.

STRYER, L. (1995). *Biochemistry*. New York. W. H. Freeman and Company.

THOMPSON, D. P., PAX, R. A. & BENNETT, J. L. (1984). Microelectrode studies on the tegument and sub-tegumental compartments of male *Schistosoma mansoni*: an analysis of compartments of electrophysiological properties. *Experimental Parasitology* **58**, 314–315.

VAN DEN BOSSCHE, H., ROSHETTE, F. & HORIG, C. (1982). Mebendazole and related anthelmintics. *Advances in Pharmacology and Chemotherapy* **19**, 67–128.

VAN DEN BOSSCHE, H. & DE NOLLIN, S. (1973). Biochemical effects of mebendazole on *Trichinella spiralis* larvae. *Journal of Parasitology* **59**, 970–976.

VICKERY, A. C., NAYAR, J. K. & TAMPLIN, M. L. (1986). Diethylcarbamazine on microfilariae of *Litomosoides carinii in vitro* and *in vivo*. *Zeitschrift für Parasitenkunde* **72**, 805–813.

WOLDE-MUSSIE, E., VANDE-WAA, J., PAX, R. A., FETTERER, R. H. & BENNETT, J. L. (1982). *Schistosoma mansoni*: calcium efflux and the effects of calcium-free media on the responses of the electrical potential from the tegument of adult males musculature to praziquantel and other agents inducing contraction. *Experimental Parasitology* **53**, 270–278.